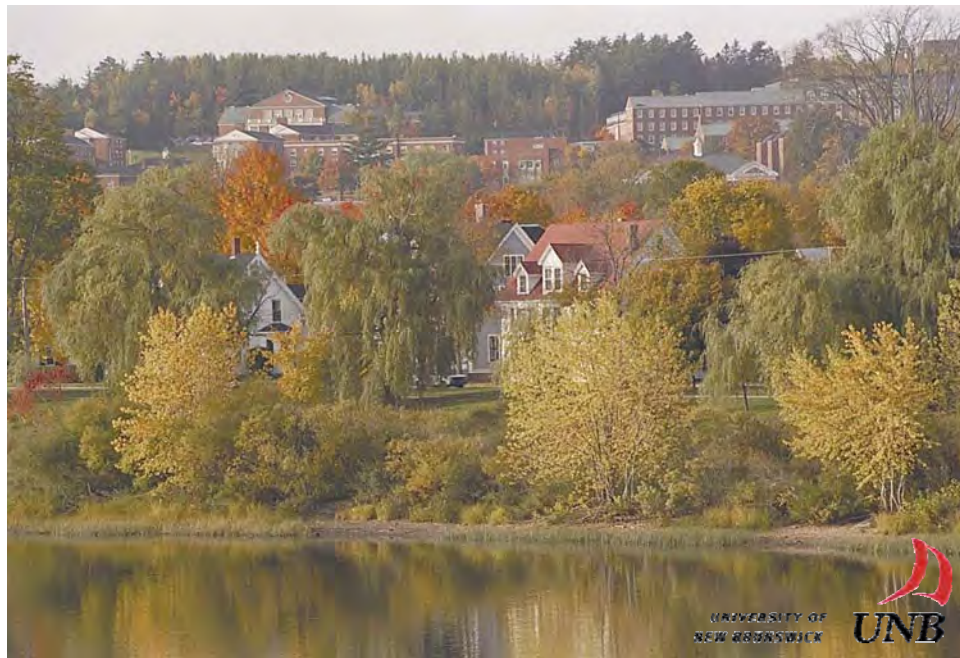




**PROCEEDINGS OF THE 24TH
INTERNATIONAL APPLIED GEOCHEMISTRY SYMPOSIUM
FREDERICTON, NEW BRUNSWICK, CANADA**



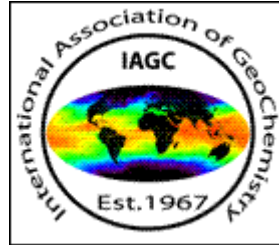
JUNE 1ST-4TH, 2009

EDITED BY

DAVID R. LENTZ, KATHLEEN G. THORNE, & KRISTY-LEE BEAL



VOLUME I



All rights reserved.
This publication may not be reproduced in whole or in part, stored in a retrieval system or transmitted in any form or by any means without permission from the publisher.

ISBN 978-1-55131-136-4

©2009 AAG

**PROCEEDINGS OF THE 24TH
INTERNATIONAL APPLIED GEOCHEMISTRY SYMPOSIUM
FREDERICTON, NEW BRUNSWICK
CANADA
JUNE 1ST-4TH, 2009**

EDITED BY

**DAVID R. LENTZ
KATHLEEN G. THORNE
KRISTY-LEE BEAL**

VOLUME I

TABLE OF CONTENTS

TECHNICAL EDITORS	XIII
DEEP SEARCH GEOCHEMICAL EXPLORATION METHODS	1
Exploration for deeply buried gold deposits in the Bendigo region, Victoria, Australia: regolith geochemistry of the Lockington area	3
<i>Dennis Arne¹, Emily House², Geoff Turner³, Keith Scott⁴, and Ed Dronseika⁵.....</i>	<i>3</i>
Fingerprinting mineral deposit types using iron-oxide chemistry: Application to till from Thompson, Manitoba, Canada	7
<i>Georges Beaudoin¹, Céline Dupuis¹, & Beth McClenaghan².....</i>	<i>7</i>
Indicator mineral signature of the Halfmile Lake Zn-Pb-Cu volcanogenic massive sulphide deposit, New Brunswick, Canada.....	11
<i>Gabriela Budulan¹, M. Beth McClenaghan², Michael A. Parkhill³, & Dan Layton-Matthews¹..</i>	<i>11</i>
Surface geochemical anomalies in northern Chile:.....	15
product of the extended metallogenesis of buried copper deposits.....	15
<i>Eion M. Cameron¹, Matthew I. Leybourne², Martin Reich³, & Carlos Palacios³</i>	<i>15</i>
Geochemistry of Archean sulfidic black shale horizons: combining data at multiple scales for improved targeting in VMS exploration	19
<i>John B. Chapman¹, Jan M. Peter¹, Daniel Layton-Matthews² & J. Bruce Gemmell³</i>	<i>19</i>
An investigation of partial extractions designed to solubilize Pb and Zn from soils using a complexation desorption mechanism	23
<i>Janice Chipman¹, John Murimboh¹, & Cliff Stanley².....</i>	<i>23</i>
3D GIS as a support for ore vectoring.....	27
<i>Eric. de Kemp¹, T.Monecke², E.M. Schetselaar¹, E.Girard³, K. Lauzière³, M.Sheshpari¹, J. Goutier⁴, G. Perron⁵, E. Grunsky¹, & G. Bellefleur¹.....</i>	<i>27</i>
Element Distribution Patterns and Mineral Discoveries using Biogeochemical Methods.....	31
<i>Colin Dunn¹, Robert Thompson², Robert Anderson³, & Alain Plouffe⁴</i>	<i>31</i>
Spatio-temporal geochemical dynamics of an acid rock drainage stream in the Yukon Territory: implications for mineral exploration.....	35
<i>Kristen B. Feige^{1,2}, Paul Gammon², & Danielle Fortin¹.....</i>	<i>35</i>
Soil mineralogy and geochemistry of surficial materials around the XY base-metal massive sulfide deposit, Selwyn Basin, Yukon	39
<i>P. Gammon, ^{1,2}, W. Goodfellow, ^{1,2}, J. Vaive¹, P. Pelchat¹, & K. Feige^{1,2}.....</i>	<i>39</i>
Application of ‘metals-in-soil-gas’ techniques to mineral exploration in exotic overburden	43
<i>Yuyan Gao¹, Mingqi Wang¹, and Yinhan Liu²</i>	<i>43</i>
In the beginning A personal retrospective of exploration geochemistry in the 1960s-1980s.....	47
<i>G.J.S Govett</i>	<i>47</i>
Controls on silver distribution in the Main Zone of the 2.68 Ga Hackett River Zn-Pb-Cu-Ag volcanogenic massive sulfide deposit, Nunavut, Canada.....	51
<i>Hannah L. J. Grant¹, Daniel Layton-Matthews¹, & Jan M. Peter²</i>	<i>51</i>
3-D element patterns above deeply buried mineralization: new evidence and insights into electrical dispersion	55
<i>Stewart M. Hamilton¹.....</i>	<i>55</i>

Lithogeochemical halos and vectors for ores in volcanic arcs and sedimentary basins	59
<i>Ross R. Large</i>	59
Groundwaters in mineral exploration.....	63
<i>Matthew I. Leybourne¹ & Eion M. Cameron²</i>	63
Soluble ionic gold in soils.....	67
<i>Melvyn J. Lintern¹, Chris G. Ryan², & Robert M. Hough¹</i>	67
Gold in pedogenic carbonate revealed	71
<i>Melvyn J. Lintern^{1,2}, Chris G. Ryan³ & Robert M. Hough¹</i>	71
Till indicator mineral and geochemical signatures of magmatic Ni-Cu deposits, Thompson Nickel Belt, central Canada	75
<i>M.B. McClenaghan¹, S.A. Averill², I.M. Kjarsgaard³, D. Layton-Matthews⁴, & G. Matile⁵</i>	75
Lithogeochemical exploration vectors for Au-rich volcanogenic massive sulfide deposits: Examples from the world-class Doyon-Bousquet-LaRonde mining camp, Abitibi Greenstone Belt, Canada..	79
<i>Patrick Mercier-Langevin¹, Benoît Dubé¹, & Mark D. Hannington²</i>	79
Application of field-portable x-ray fluorescence spectrometers in mineral exploration, with examples from the Abitibi Greenstone Belt	83
<i>Jan M. Peter¹, Patrick Mercier-Langevin², & John B. Chapman¹</i>	83
Exploration for Zn-rich mineralisation in semi-arid environments: an example from the Cobar region, NSW, Australia.....	87
<i>Keith M. Scott¹ & Angela N. Lorrigan²,</i>	87
Soil micro-layer, airborne particles, and pH: the Govett connection	91
<i>Barry W. Smee</i>	91
Robust 'organic' geochemistry identifies and vectors to deeply buried exploration targets.....	97
<i>D. A. Sutherland¹</i>	97
ORE-FORMING SYSTEMS: A GEOCHEMICAL PERSPECTIVE	101
Siderophile elements in the zonal structure of ore geochemical systems: exploration aspects	103
<i>G. Abramson¹</i>	103
Cassiterite-sulfide mineralization revealed by dispersion flows in Belaya Sopka Mountain (northeastern Russia).....	107
<i>Anna D. Ananchenko^{†1} & Svetlana R. Tikhomirova^{†1}</i>	107
Geochemical characterization of humic substances isolated from phosphatic pellets and their surrounding matrix, Ras-Draâ, Tunisia	111
<i>Aida Ben Hassen¹, Jean Trichet¹, Jean-Robert Disnar¹, & Habib Belayouni²</i>	111
Petrogenesis of dykes related to Cu-Au & base-metal Au-Ag occurrences, Mt. Freegold area, Dawson Range, Yukon Territory, Canada	115
<i>Thierry Bineli Betsi¹ & David R. Lentz¹</i>	115
The primacy of magma compositions in determining the Re and W contents of molybdenite.....	119
<i>Phillip L. Blevin¹</i>	119
RE minerals in Esfordi apatite- magnetite deposit, Central Iran	123
<i>Mohammad Boomeri¹, Kazuo Nakashima², & David R. Lentz³</i>	123
Numerical simulation of the sill-driven convective ore-forming system at Matagami, Quebec: implications for metal leach zones	127
<i>Patrick M. Carr¹, Lawrence M. Cathles III², & C. Tucker Barrie³</i>	127

Minerals exploration and supply: a worldwide perspective	131
<i>William X. Chávez, Jr.</i>	131
Mineralogical host phases for the PGE in magmatic Ni-Cu-PGE deposits at the Creighton Mine, Sudbury, Canada	135
<i>Sarah A.S. Dare¹, Sarah-Jane Barnes¹, Hazel M. Prichard², & Peter C. Fisher²</i>	135
Late Mesoproterozoic S-type Sargipali granite and tungsten-mineralization: Singhbhum-Orissa craton, India	139
<i>Sangita Chowdhury¹, David R. Lentz², & Saumitra Misra³</i>	139
Bimodal post-collision volcano-plutonic complex in the southern rim of the eastern flank of the Mongol-Okhotsk orogenic belt	143
<i>I.M. Derbeko¹, V.A. Ponomarchuk², D.L. Vyunov³, & S.K. Kozyrev³</i>	143
Petrographic characterization of propylitic alteration associated with porphyry Cu–Mo deposits in the Collahuasi District, Northern Chile: implications for mineral exploration	147
<i>Merline Djouka-Fonkwé¹, Kurt Kyser¹, H. Alan Clark¹, J. Christopher Oates², & Christian Ihlenfeld²</i>	147
Petrologic, geochemical characteristics, and age of skarn-related granitoids at the Mactung Tungsten Deposit, Yukon, Canada.....	151
<i>Ayalew. L. Gebru¹ & David R. Lentz¹</i>	151
Use of micro-XRF in the characterization of hydrothermal alteration: application to the subaqueous felsic dome-flow complex of the Cap d'Ours segment of the Glenwood rhyolite, Rouyn-Noranda, Québec	157
<i>Dominique Genna^{1,2}, Damien Gaboury^{1,2}, Lyndsay Moore¹, & Wulf Mueller¹</i>	157
Regional rock geochemistry of the Leninogorsk and Zyryanovsk VMS region (Rudny Altay Kazakhstan) - implications for genesis and exploration.....	161
<i>I. Goldberg¹, G. Abramson¹, V. Los², V. Nazarov³, & C. Haslam⁴</i>	161
Geochemistry and tectonics as an exploration tool for Circum-Pacific porphyry copper, gold, and molybdenum deposits: evidence from the Baguio District, Philippines	165
<i>Pete Hollings¹ & David R. Cooke²</i>	165
Metals distribution and correlations in polymetallic veins from Pingüino Indium-bearing deposit, Deseado Massif, Patagonia, Argentina	169
<i>Sebastián Jovic^{1,2}, Paula Liñan¹, Diego Guido^{1,2}, Gerardo Páez^{1,2}, Remigio Ruiz¹, & Isidoro Schalamuk^{1,2}</i>	169
Chemical compositions of carbonate minerals from Chehelkureh ore deposit, Iran: implications for evolution of base-metal mineralization	173
<i>Mohammad Maanijou¹, David R. Lentz², & Iraj Rasa³</i>	173
Rare earth element variations in volcanogenic massive sulfides, Bathurst Mining Camp, New Brunswick: evidence from laser-ablation ICPMS analyses of phosphate accessory phases	177
<i>Sean H. McClenaghan¹, David R. Lentz², & Wilfredo G. Diegor³</i>	177
Controls and consequences of intrusion-related Au deposition at the Morila Au Mine, SW Mali .	181
<i>Christopher R.M. McFarlane¹, Karen Grey¹, & David Lentz¹</i>	181
Syenite, lamprophyre, and carbonatite dykes of the Moose Creek Valley, Ice River Alkaline Complex, southeastern British Columbia, Canada: implications for REE potential	185
<i>Thomas R. Mumford¹, Dave R. Lentz¹, & Cliff S.J. Shaw¹</i>	185

Morphology of gold nanoparticles synthesised from gold chloride and gold cyanide complexes under evaporative conditions	189
<i>Ryan R. P. Noble¹, Elizabeth M. Grenik^{1,2}, Robert M. Hough¹, Melvyn J. Lintern¹, David J. Gray¹, Rob Hart², Peta Clode³, & John Murphy³</i>	189
Coupled Micro-XRF elemental mapping and LA-ICP-MS geochemistry of pyrites to decipher the cause of gold precipitation in quartz-sulfide gold-bearing veins, Poderosa-Pataz district, Peru.....	193
<i>Carlos Oré Sanchez¹ & Damien Gaboury^{1,2}</i>	193
IPGE (Os, Ir, Ru) are not in chromite	197
<i>Philippe Pagé¹, Sarah-Jane Barnes¹, Michael L. Zientek², Hazel M. Prichard³, & Peter C. Fisher³</i>	197
Aplitic dykes at the world-class Cantung tungsten skarn deposit: indicators of fluid flow and mineralizing processes	201
<i>Kirsten L. Rasmussen¹, David Lentz², & Hendrik Falck³</i>	201
Geochemistry and genesis of a mafic-ultramafic hosted VMS occurrence, Marathon, Ontario	205
<i>Marc L. Rinne¹, Peter N. Hollings¹, & Aubrey J. Eveleigh²</i>	205
The Middle River Gold deposit, NE New Brunswick, Canada: an example of an orogenic style gold system in the Brunswick Subduction Complex.....	209
<i>Sabine Schwarz¹, David Lentz¹, & James Walker²</i>	209
Gold mineralization in the Kakagi-Rowan Lake greenstone belt: a study of the Angel Hill Gold Zone	213
<i>Scott Secord¹ & Pete Hollings¹</i>	213
Rhenium in Canadian mineral deposits.....	217
<i>W. David Sinclair¹, Ian R. Jonasson¹, Rod V. Kirkham², & Art E. Soregaroli³</i>	217
Getting the scale right: links between metallogenesis, planetary degassing and the redox state of Earth's oceans?	221
<i>John L. Walshe¹</i>	221
⁴⁰ Ar- ³⁹ Ar geochronological constraints of the ore-bearing ductile shear zones at Hukeng tungsten deposit, Jiangxi Province	225
<i>Zhang Wei¹, Chen Maohong^{1,2}, Ye Huishou², & Yang Zongxi¹</i>	225
USING ISOTOPE GEOCHEMISTRY TO EXPLORE FOR RESOURCES	229
Isotopic studies and comparison of marbles in the Sambagawa metamorphic belt, central Shikoku, Japan and marbles from the Kumdy-Kol area of Kokchetav Massif, North Kazakhstan.....	231
<i>Zaure Bekmukhametova¹</i>	231
Cu Isotope Study of the Silver Bell Porphyry Cu Mine.....	235
<i>Molly Dendas¹, Ryan Mathur¹, & Spencer Titley²</i>	235
A geochronological based approach to characterize the setting of the Buffalo Head Hills kimberlite field, northern Alberta, Canada.....	239
<i>D. Roy Eccles¹, Art R. Sweet², Rob A. Creaser³, & Larry M. Heaman³</i>	239
Nature of $\delta^{18}\text{O}_{\text{quartz}}$ variation in a Slate-belt – hosted orogenic gold province, Nova Scotia, Canada: evidence for fluid: rock interaction	243
<i>Daniel J. Kontak¹, T. Kurt Kyser², & Rick J. Horne³</i>	243

Tracing progressive redox gradients and directions of hydrothermal flow using uranium and lithium isotopes	247
<i>Kurt Kyser, Majdi Geagea, Don Chipley, Paul Alexandre, Mark Raycroft, April Vuletich, & Rachel Schwartz-Narbonne</i>	
247	
The use of Cu isotope fractionation in low temperature ore systems as a geochemical exploration tool	251
<i>Ryan Mathur¹, Spencer R. Titley², Susan Brantley³, & Marc Wilson⁴</i>	
251	
Oxygen isotope zoning in subvolcanic, intrusion-centered submarine hydrothermal systems as a guide to VMS exploration	255
<i>Bruce E. Taylor¹, Greg Holk², Benôit Dubé³, & Alan Galley¹</i>	
255	
Exploration geochemistry, geochronology, and tracer isotopic data of copper mineralisation in dolomitic rocks, Dos Parecis Basin, Rondonia, Brazil	259
<i>Aldo Vásquez^{1,2}, Pedro Perez¹, & Angelo Aguilar¹</i>	
259	
The nature and significance of lithogeochemical and stable isotope alteration halos in the Hollinger-McIntyre gold deposit, Ontario, Canada.	265
<i>Gibran D. Washington¹, Mona C. Sirbescu², Kevin T. Jensen², & Edmond H. van Hees¹</i>	
265	

RECENT DEVELOPMENTS IN LITHOGEOCHEMICAL METHODS WITH EXPLORATION APPLICATIONS 271

Lithogeochemistry of central Victorian orogenic gold deposits, Australia	273
<i>Dennis Arne¹, Emily House², & Vladimir Lisitsin²</i>	
273	
Immobile Element Lithogeochemistry of felsic volcanic rocks hosting the Restigouche Volcanogenic Massive Sulfide Deposit, Bathurst Mining Camp, New Brunswick, Canada	277
<i>Amanuel Bein¹ & David R. Lentz¹</i>	
277	
Geological and geochemical evolution of the San Miguel skarn, Tandilia Belt, Buenos Aires Province, Argentina	281
<i>Raúl de Barrio¹, Mabel Lanfranchini^{1*}, Ricardo Etcheverry^{1,2}, Agustín Martín-Izard³, Mario Tessone¹, & María Paz¹</i>	
281	
Geochemistry of auriferous banded iron formation, northeastern Saharan metacraton, Egypt.....	285
<i>Ahmed M. El Mezayen¹, Talaat M. Ramadan², & Atef O. Abu Salem³</i>	
285	
Gold depletion and enrichment in basalt-covered areas in Central Victoria, Australia: key for mineral exploration	289
<i>I. Goldberg¹, G. Abramson¹, & V. Los²</i>	
289	
The application of quantitative automated mineralogy in enhancing geochemical data interpretation in mineral exploration and metallurgical processes	293
<i>Chris Gunning¹, Hugh de Souza¹, & Tassos Grammatikopoulos¹</i> ,	
293	
Provenance of the Upper Carboniferous sedimentary rocks, Maritime Basin, New Brunswick, Canada: a sedimentary geochemical approach.....	297
<i>M.M.N. Islam, David R. Lentz, & David G. Keighley</i>	
297	
Spatial geochemical trends of beach and dune sands from the Northeastern coast of Mexico: implications for provenance	301
<i>Juan Jose Kasper-Zubillaga¹, John S. Armstrong-Altrin¹, & Arturo Carranza Edwards¹</i>	
301	
The Chemistry of black shale and exploration for VHMS, Mount Read Volcanics, Western Tasmania	305
<i>Andrew W. McNeill¹</i>	
305	

Weathering-related rare earth element patterns in the regolith of the Cobar region, western New South Wales	309
<i>K.G. McQueen</i>	309
Lithogeochemical vectors to ore: a study of the Elura Zn-Pb-Ag deposit, Cobar, NSW, Australia	313
<i>K.G. McQueen¹ & M.A.I. Whitbread²</i>	313
Lithogeochemistry of the Quebrada Blanca Porphyry Cu Deposit, Atacama Desert, Northern Chile	317
<i>Tamara Moss & Cliff Stanley</i>	317
Classification of Igneous Rocks Using Lithogeochemistry Data, Essential Rock Mineralogy, and Projective Geometry in a.....	321
<i>Cliff Stanley</i>	321
Distal exhalative manganese enriched stratigraphy to carbonate-hosted zinc deposits, Adirondack Lowlands, New York State, U.S.A.	325
<i>Alex Tolson¹ & Norm Duke²</i>	325
Lithogeochemical analysis through the deformed volcanosedimentary sequence hosting the Boomerang massive sulfide deposits, Tulks Belt, Central Newfoundland	331
<i>Ryan M. S. Toole¹ & David R. Lentz¹</i>	331
Stratigraphic and geochemical interpretation of the Early Silurian Woodstock ferromanganese deposits, New Brunswick, Canada.....	335
<i>Bryan C. Way¹, David R. Lentz, & David G. Keighley</i>	335
Lithogeochemistry of the Meguma Supergroup, Nova Scotia, Canada: petrographic constraints, depositional environments and alteration haloes about sediment hosted hydrothermal mineral deposits	339
<i>Chris E. White¹ & Clifford R. Stanley²</i>	339
NEW AND OLD DISCOVERIES: GEOCHEMICAL EXPLORATION CASE STUDIES	343
Using regional geochemistry, geology, aeromagnetics, Landsat, and digital elevation models (DEM) to define favourable areas for porphyry-style mineralization in southwestern Alaska	345
<i>Eric D. Anderson¹, Robert G. Eppinger¹, & Karen D. Kelley¹</i>	345
Termitaria: its application as sample media to gold.....	349
<i>Emmanuel Arhin</i>	349
Exploration history and discovery of a new mineralization style, Freegold Mountain area, Dawson Range, Yukon Territory, Canada	353
<i>Thierry Bineli Betsi¹, Fabrizio Colombo², & David R. Lentz¹</i>	353
Evidence of 25-m of Vertical Metal Migration Over the High-Grade Perseverance Zinc Ore Body, Matagami, Quebec	357
<i>Lynda Bloom¹ & Charles Beaudry²</i>	357
Exploration stream sediment geochemistry of the Otago region, New Zealand	361
<i>Anthony B. Christie¹, & Richard Carver²</i>	361
A Hydrogeochemical Exploration Study at the Pebble Deposit, Alaska.....	365
<i>R.G. Eppinger¹, D.L. Fey¹, K.D. Kelley¹, S.M. Smith¹, & S.A. Giles¹</i>	365
Spectral, geochemical, and petrographic spatial analysis of the Maze Lake orogenic gold exploration project, Nunavut.....	369
<i>Anna Fonseca¹, Patrick Lengyel², & Cameron Rennie³</i>	369

Porphyry Copper Indicator Minerals (PCIMs) in glacial till samples from the giant Pebble porphyry Cu-Au-Mo deposit: exploration significance	373
<i>Karen D. Kelley¹, Robert G. Eppinger¹, Steven M. Smith¹, & David L. Fey¹</i>	373
Geochemical and mineralogical exploration of sandstones in the Lublin Carboniferous Basin, SE Poland	377
<i>Aleksandra J. Kozłowska¹ & Katarzyna L. Jarmolowicz-Szulc¹</i>	377
Target delineation by Fuzzy Logic approach at East-Kahang Porphyry Cu-Mo deposit, Central Iran	381
<i>Ahmad R. Mokhtari¹, Hooshang Asadi-Haroni¹, Seyed-Hassan Tabatabaei¹, & Somayeh Akbar¹</i>	381
Carlin-type gold geochemical patterns delineated by different-density data	385
<i>Lanshi Nie^{1,2,3} & Xueqiu Wang^{2,3}</i>	385
Organic and inorganic surface expressions of the Lisbon and Lightning Draw Southeast oil and gas fields, Paradox Basin, Utah, USA	389
<i>David M. Seneshen¹, Thomas C. Chidsey, Jr², Craig D. Morgan², & Michael D. Vanden Berg²</i>	389
An orientation soil survey at the Pebble Cu-Au-Mo porphyry deposit, Alaska	393
<i>Steven M. Smith¹, Robert G. Eppinger¹, David L. Fey¹, Karen D. Kelley¹, & S.A. Giles¹</i>	393
Ore deposit simulation and reserve estimation in Masjeddaghi epithermal gold mineralization – Azerbaijan - Iran	397
<i>Payam Soodishoar¹ & Maryam Hashemi²</i>	397
The application of litho-geochemistry for VMS exploration in the Sherridon Complex, northern Manitoba	403
<i>Sean A. Timpa¹, Lynda Bloom², & Johan D. Krebs³</i>	403
Orientation survey results at the Tameapa property in Sinaloa, Mexico	407
<i>Todd W. Wakefield¹</i>	407
Gold dispersion under pediplanation in desert terrains	411
<i>Bimin Zhang^{1,2,3}, Xueqiu Wang^{1,3}, Qinghua Chi^{1,3}, & Qingtian Lü²</i>	411
Structure and stratigraphy of the Key Anacon Main Zone and East Zone massive sulfide deposits, Bathurst Mining Camp, NB, Canada	415
<i>Joseph D.S Zulu¹, David. R. Lentz¹, & James A. Walker²</i>	415
URANIUM DEPOSITS: GEOCHEMICAL EXPLORATION TECHNIQUES TO CASE STUDIES.....	419
Fraser Lakes Zones A and B, Way Lake Project, Saskatchewan: geological, geophysical, and geochemical characteristics of basement-hosted uranium mineralization.....	421
<i>Irvine R. Annesley¹, Carol Cutford¹, Dave Billard¹, Richard T. Kusmirski¹, Ken Wasyliuk¹, Terrance Bogdan¹, Ken Sweet², & Chris Ludwig³</i>	421
Geochemical controls on uranium precipitation in calcrete palaeochannel deposits of Namibia ...	425
<i>R.J. Howell¹, A. Barnes, J. Grogan, & M. Dey</i>	425
Variability of U and some trace elements in ferromanganese nodules of the Clarion-Clipperton zone (Pacific Ocean) and mechanism of their formation.....	431
<i>V. M. Guliy¹ & O. M. Tysiachna¹</i>	431
Mineralogical, geochemical, and geochronological constraints in the Double S Zone uranium deposit, Lac Turgeon Granite, north shore of the St. Lawrence Seaway, Quebec, Canada	435
<i>Susan Kingdon¹, David Lentz¹, & Douglas Hall²</i>	435

Exploration strategies for Uranium deposits	439
<i>Kurt Kyser, Paul Alexandre, Paul Polito, Merline Djouka-Fonkwe, Majdi Geagea, & Yulia Uvarova</i>	439
Basement-hosted uranium oxides from Athabasca Basin: mineralogy, U/Pb dating, major and Rare Earth Element (REE) concentrations: comparison with U-oxides from deposits located in the vicinity of the unconformity.....	445
<i>Julien Mercadier¹, Michel Cuney¹, & David Quirt²</i>	445
Two contrasted types of Uranium mineralization in the "Cage" Uranium district, Nunavik, Quebec, Canada	449
<i>Jérémy Neto¹, Christian Marignac¹, Michel Cuney¹, Claude Caillat², & Jean Luc Lescuyer²</i>	449
Applying Pb isotopes in unconformity-type uranium exploration	453
<i>David Quirt¹</i>	453
Timing, chemistry, and implication of fluids in Canadian and Australian unconformity-related uranium deposits	457
<i>Antonin Richard, Michel Cathelineau, Michel Cuney, Marie-Christine Boiron, Donatienne Derome, & Cécile Fabre</i>	457
Petrological, geochemical, and isotopic evaluation of the Grenvillian uraniferous pink and white granitic pegmatites, Fort-Coulonge, Quebec.....	461
<i>Caroline Richer¹ & David R. Lentz¹</i>	461
Role of geochemistry in the search for Uranium deposits	465
<i>Samuel B. Romberger¹</i>	465
Mobility of Uranium and Radon associated with uranium roll front occurrences in the Horton Group of the Windsor area, Nova Scotia, Canada.....	469
<i>R.J. Ryan¹, A.M. O'Beirne-Ryan², D. Finlayson², & A. Parsons²</i>	469
QA/QC, verification and integration of multisource data for the Novoveska Huta and Kuriskova deposits in Eastern Slovakia.....	473
<i>Ravi Sharma</i>	473
A U-bearing hydrothermal vein system related to the strongly peraluminous, high heat producing North Pole Stream granitic suite, north-central New Brunswick Canada	477
<i>David A. Shinkle¹, David R. Lentz¹, & Steven R. McCutcheon²</i>	477
Diverse uranium mineralization in the Central Mineral Belt of Labrador, Canada: multiple styles and multiple questions	481
<i>Greg W. Sparkes¹ & Andrew Kerr¹</i>	481
Harvey: a volcanic-hosted Uranium occurrence at the edge of the Maritimes Basin.....	485
<i>José M. Texidor Carlsson¹ & Neil E. Downey¹</i>	485
Deep-penetrating geochemical exploration for hidden sandstone-type uranium deposits in the Turpan-Hami basin, northwestern China	489
<i>Xueqiu Wang^{1,2}, Shanfa Xu^{1,2}, Qinghua Chi^{1,2}, Bimin Zhang^{1,2}, & Lanshi Nie^{1,2}</i>	489
Vectoring potential of multi-element chemistry in unconformity-associated uranium deposits: major and trace element signatures of the McArthur River Uranium Deposit, Saskatchewan, Canada....	493
<i>Donald M. Wright</i>	493
Broad-based physicochemical paragenetic aspects of primordial uranium deposits of endogenic origin.....	497
<i>Igor A. Zotov¹ & Maksim V. Seredkin²</i>	497

NORTH ATLANTIC MINERALS SYMPOSIUM	501
Mass change constraints and hydrothermal alteration of felsic volcanic rocks that host the Restigouche Volcanogenic Massive Sulfide Deposit, Bathurst Mining Camp, New Brunswick, Canada	503
<i>Amanuel Bein¹ & David R. Lentz¹</i>	503
Results of 2008 exploration program Mount Pleasant Property: geochemistry, mineralogy, and deposit modeling of Sn-In and WO ₃ -MoS ₂ zones	507
<i>Trevor Boyd¹ & Gustaaf Kooiman¹</i>	507
The Nash Creek Zn–Pb–Ag deposit, Tobique –Chaleurs Zone, New Brunswick, Canada	511
<i>Derek Brown¹ & James Walker²</i>	511
The Williams Brook gold discovery – northern New Brunswick	515
<i>Heather Campbell¹ & Art Hamilton¹</i>	515
Age constraints and Grampian orogenesis of the Lower to Middle Ordovician Tyrone Igneous Complex, Northern Ireland	519
<i>Mark R. Cooper¹, Quentin G. Crowley^{2,3}, David M. Chew³, Steve P. Hollis⁴ & Stephen R. Noble²</i>	519
Molybdenum and tungsten mineralization associated with late-stage granitoid magmatism in the Appalachian Orogen of Newfoundland: an overview and a summary of recent developments.....	523
<i>Andrew Kerr¹, Tim van Nostrand¹, Lawson Dickson¹, & Edward Lynch²</i>	523
Distribution and geochemistry of Cu-rich massive sulfides at the Brunswick No. 12 Deposit, Bathurst Mining Camp, New Brunswick.	527
<i>Sean H. McClenaghan¹, David R. Lentz², & Erin M. Powe²</i>	527
Litho-geochemistry of Ordovician Sedimentary Rocks: Implications for VMS Exploration in the Bathurst Mining Camp (BMC), Canada	531
<i>Steven R. McCutcheon¹ & James A. Walker¹</i>	531
Evaluating Bromine Geochemistry as a Prospecting Tool For Potash in Western Newfoundland	535
<i>Jackie O' Driscoll¹, Robert Boehner², Lawrence Winter¹ & Roland Butler¹</i>	535
Mesothermal, auriferous quartz veins of the Golden Promise deposit, central Newfoundland: their setting and the nature of wall rock alteration	539
<i>Hamish Sandeman¹, Heather Rafuse¹, David Copeland² and Jeff Morgan³</i>	539
Cathodoluminescence: A tool to discriminate the tectonic history in gold-bearing veins in the Brunswick Subduction Complex, Canada.....	543
<i>Sabine Schwarz¹, David Lentz¹, & James Walker²</i>	543
Ireland's historic mine sites inventory	547
<i>Gerry Stanley¹, Eibhlin Doyle¹, Vincent Gallagher¹, Fionnuala Ni Mhairtin¹, & Jane Brogan²</i>	547
Metallogeny of the gold-enriched Cambro-Ordovician rocks in the Annidale area, south-central New Brunswick, Canada.....	551
<i>Kathleen G. Thorne¹, Susan C. Johnson², Malcolm J. McLeod², & Leslie R. Fyffe¹</i>	551
Early Devonian felsic volcanic rocks and associated Zn–Pb mineralization, Tobique–Chaleurs Zone, New Brunswick, Canada.....	555
<i>James A. Walker¹</i>	555
Sulfide petrology and geochemistry of the Key Anacon Main Zone and East Zone massive sulfide deposits, Bathurst Mining Camp, NB, Canada	559
<i>Joseph D.S. Zulu¹, David. R. Lentz¹, & James A. Walker²</i>	559

PREFACE

Dear IAGS 2009 participants,

It is with great pleasure that I welcome to you to Canada, New Brunswick, Fredericton, and the University of New Brunswick (UNB). The Association of Applied Geochemists (AAG) has a long and prestigious history with this being the 24th symposium organized to date. As many of you know, UNB hosted one of the first regional meetings of the association, back in 1976. Our group at UNB has grown in different ways since then, very much reflecting the growth of the discipline and the Society AAG. Together with the International Association of GeoChemistry (IAGC) and International Association of Geoanalysts, AAG has partnered to build a broad as possible IAGS meeting to meet the needs of industry, as well as those of research organizations, including universities and governments. This level of cooperation helped produce this cross disciplinary perspective, needed to build for the future of applied geoscience, from mineral exploration and development through to protecting the environment that we are intimately aware of. It is this same perspective that also helped build the environment for student's research to be highlighted at this meeting like never before, with generous sponsors, who helped make that feasible; it is in all our best interests to be fostering this critical interest in our research community, especially considering the demographic issues facing us in the near future. I'm hoping that this level of mutual cooperation and respect foster a new era of collaborations, as to do it alone is not a viable option. I personally thank all those contributors, reviewers, and editors for their submissions and excellence with the process of producing this diverse and in depth program and the derivative volumes produced here. It is always the team effort, which brings alive team spirit and team success that is the key to moving this monumentally forward, so kudos to my team for making this IAGS as best as it can be.

Dave Lentz,
IAGS Chair

TECHNICAL EDITORS
(Listed in alphabetical order)

Mark Arundell
U. Aswathanarayana
Roger Beckie
Chris Benn
Robert Bowell
Charles Butt
Bill Coker
Hugh deSouza
Sara Fortner
David Gladwell
Wayne Goodfellow
Eric Grunsky
William Gunter
Gwendy Hall
Jacob Hanley
Russell Harmon
David Heberlein
Brian Hitchon
Andrew Kerr
Dan Kontak
Kurt Kyser

David Lentz
Ray Lett
Matthew Leybourne
Steven McCutcheon
Beth McClenaghan
Nancy McMillan
Paul Morris
Lee Ann Munk
Dogan Paktunc
Roger Paulen
Ernie Perkins
David Quirt
Andy Rencz
David Smith
Cliff Stanley
Gerry Stanley
Nick Susak
Bruce Taylor
Ed Van Hees
James Walker
Lawrence Winter

DEEP SEARCH GEOCHEMICAL EXPLORATION METHODS

EDITED BY:

**WAYNE GOODFELLOW
GWENDY HALL
MATTHEW LEYBOURNE**

Exploration for deeply buried gold deposits in the Bendigo region, Victoria, Australia: regolith geochemistry of the Lockington area

Dennis Arne¹, Emily House², Geoff Turner³, Keith Scott⁴, and Ed Dronseika⁵

¹ioGlobal, 469 Glen Huntley Road, Elsternwick, Victoria 3185 AUSTRALIA (e-mail: dennis.arne@ioGlobal.net)

²Geoscience Victoria, Department of Primary Industries, GPO Box 4440, Melbourne, Victoria 3001 AUSTRALIA

³Exploration Management Services, PO Box 811, Strathfieldsaye, Victoria 3551 AUSTRALIA

⁴RSES, Australian National University and CSIRO Exploration & Mining, PO Box 136, North Ryde New South Wales 1670 AUSTRALIA

⁵Genalysis Laboratory Services, 15 Davison Street, Maddington, Western Australia 6109 AUSTRALIA

ABSTRACT: Soil surveys and blind tests conducted over the Lockington East Au (\pm As, \pm Sb) deposit, which lies 60 km northeast of Bendigo in northern Victoria, have demonstrated that soil samples can reveal the presence of geochemically anomalous basement at depths of 40 to 60 m beneath transported Murray Basin cover. A soil sampling protocol for Au exploration in northern Victoria in covered areas using aqua regia analysis of the A-horizon >1 mm size fraction for Au and As is recommended, followed by sampling of A2-horizon soils, generally at a depth of 10 to 20 cm. A2-horizon samples should be subjected to several partial extractions in order to yield useful results. A digestion using 0.1 M Na-pyrophosphate and analysed for Au, As and Sb by inductively coupled plasma mass spectrometry (ICP-MS): Fe, Mn and Ca analysed by ICP-optical emission spectroscopy (OES): and organic C analysed spectroscopically in the Na-pyrophosphate digestion extract is recommended. The data should either be normalised to Fe, Mn, C or Ca, as appropriate, or residuals calculated from regression analysis. A2- and B-horizon samples should also be subjected to aqua regia digestion and analysed for Au, As and Sb by ICP-MS and for Fe and Ca by ICP-OES in order to provide verification of the Na-pyrophosphate results. Again, the data must either be normalised or subjected to regression analysis in order to identify anomalous areas. A weak alkaline digestion analysed for Fe, As and Sb may also yield useful results, as would the use of 4M HCL at room temperature followed by analysis for As, Sb and Au. The use of BLEG analyses for Au and Ag on small (100 g) samples has not been demonstrated to be statistically significant in this study, but larger (i.e. 2 kg) BLEG samples may be useful at a reconnaissance scale. A minimum follow-up sample spacing of 50 m is suggested in order to generate multi-sample anomalies. Sampling toward the end of summer or in autumn prior to significant winter rainfall is recommended in order to maximise metal concentrations measured relative to analytical background, and to enhance potential anomalies. Soil pH should be determined on all soil samples (5:1 de-ionised water to soil mixture) and can also be used to verify areas of anomalous soil response. The resolution and accuracy of the results are such that preliminary drill targets can be defined using surface soil sampling.

KEYWORDS: *soil, partial extractions, gold, geochemistry*

INTRODUCTION

The discovery of buried gold mineralisation at Lockington under between 40 and 100 m of Murray Basin sedimentary cover was made in mid-2004 by Gold Fields Australasia Pty Ltd as a result of combined geophysical targeting and regional soil sampling. Further buried gold mineralisation has subsequently been discovered on the Lockington East group of exploration licences, approximately 3 km east of the original Lockington discovery. By late 2007, over

100,000 m of aircore and nearly 11,500 m of diamond core had been drilled to define disseminated pyrite and arsenopyrite Au mineralisation in Ordovician basement 45 km north of the Fosterville gold deposit.

Detailed soil traverses were undertaken by CSIRO over the Lockington deposit following its discovery to determine the optimal grain size fraction for sampling. In 2006 Geoscience Victoria initiated the Developing Gold Undercover program with the intention of aiding mineral explorers in their search for buried gold

deposits in Victoria (Figure 1). The Lockington discovery provided a timely opportunity to study the soil anomalies associated with buried gold mineralisation in northern Victoria, and to further refine sampling and analytical protocols. The results of these investigations are summarised in Arne *et al.*, (2009).



Fig.1. Location of the Lockington deposit in northern Victoria. The locations of a number of major central Victorian gold deposits are also shown.

GEOLOGICAL SETTING

The Lockington area lies in the Riverina Plains region of northern Victoria, 60 km northeast of Bendigo. Palaeozoic basement in this region is overlain by Late Cretaceous to Quaternary marine to terrestrial sediments of variable thickness. Depth of cover in the study area ranges from 40 m to more than 100 m, and is characterised by a regolith profile through rocks ranging in age from Ordovician to Tertiary. This profile is typical of the Riverina Plain in the Murray Basin and includes several extended periods of erosion. The basement consists of metamorphosed Ordovician mudstones, siltstones and sandstones that are typically weathered to an average depth of 15 m. These rocks belong to the Bendigo Structural Zone, which is well endowed with orogenic Au deposits further south, and are inferred to have similar mineralisation potential beneath the Murray Basin.

GEOCHEMICAL INVESTIGATIONS

Shallow (<10 cm) soil samples for particle size analysis were collected from an area over the Lockington deposit for separation into seven grain size fractions at CSIRO. These, along with a bulk soil sample, were analysed for Au and a suite of 18 other elements by ICP-OES and ICP-MS following an aqua regia digestion. Soil samples to test a range of partial extractions were collected by Geoscience Victoria at depths of 0-20 cm (A-horizon), 20-40 cm (A-B transition) and 40-60 cm (B-horizon) over the Lockington East deposit. Top soil and leaf litter were removed prior to sampling the A-horizon. The soil samples were sieved to less than 2 mm in the field and tested for the presence of pedogenic carbonate with dilute HCl. These samples were analysed by aqua regia digestion, bulk leach extractable gold (BLEG), a weak alkaline digestion containing dilute cyanide, a 4M HCl digestion and a 0.1 M Na-pyrophosphate digestion.

As a regional observation, arsenic is concentrated in the >1 mm soil fraction, and defines broad-scale anomalies in areas of shallow bedrock or residual soil. It has probably been adsorbed onto amorphous secondary Fe oxides, some of which have formed pisoliths. By contrast, Au is generally concentrated in the clay-sized fraction of transported soils.

Gold is elevated over buried mineralisation at Lockington East in the aqua regia digestions, and the pathfinder elements As and Sb are elevated in the Na-pyrophosphate (Figure 2), weakly alkaline and 4 M HCl digestions above buried Au mineralisation. However, the metals also show strong positive correlations with either aqua regia Fe or partially extracted Fe from the weak alkaline digestion. In addition, As and Sb in the Na-pyrophosphate extraction show a strong positive correlation with the amount of organic C in humic acids.

Soil anomalies present in the raw element data from a variety of extractions are attributed to the effects of metal scavenging onto the surfaces of either Fe oxides or humic/fulvic acids. These metal

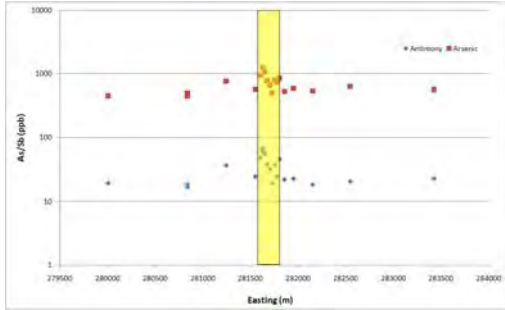


Fig. 2. As and Sb in Na-pyrophosphate digestion from A-horizon soil samples ~40 m above the Lockington East Au deposit. The position of the buried Au deposit is shown by the shaded rectangle.

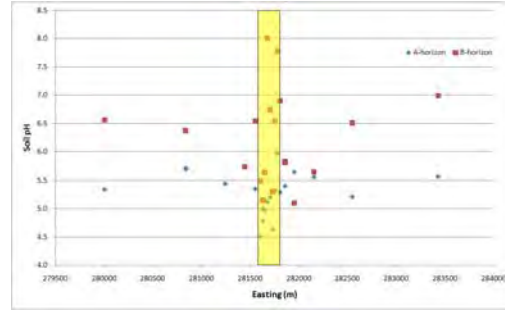


Fig. 3. Soil pH over the Lockington East Au deposit. The position of the buried Au deposit is shown by the shaded rectangle.

anomalies are associated with lower soil pH in the A-horizon and elevated pH in the B-horizon (Figure 3).

Soil anomalies over bedrock mineralisation are still apparent in some partial extraction data once corrected for the effects of scavenging, either by normalisation of metal data to Fe or organic C, or through the use of residuals from regressions through scatter plots of associated elements. The Au/Fe ratios from aqua regia digestion of A2-horizon samples, As/Fe ratios from aqua regia digestion of B-horizon samples, and Sb/C and As/C ratios from A2-horizon samples from the Na-pyrophosphate digestion all provided surface anomalies with hypergeometric probabilities less than 5%. The lowest hypergeometric probability (0.08%), and therefore the parameter least likely to be a random effect, is provided by Na-pyrophosphate Sb data normalised to both aqua regia Fe and spectroscopic organic C. A similar ratio from Na-pyrophosphate As data also provides a statistically acceptable hypergeometric probability if a slight degree of lateral dispersion is allowed (i.e. if a sample on either side of the vertical extension of bedrock Au mineralisation are included as “anomalous”).

The results of a blind test over a region with ~60 m of transported cover indicate that BLEG Au, and Na-pyrophosphate Sb/C and As/C provide a good indication of mineralised bedrock at depth.

Data from the Na-pyrophosphate partial extractions and estimates of organic C contained in humic and fulvic acids from spectroscopic determinations show poor reproducibility over time. Analysis of data from re-sampling in September 2007 show significantly lower results over bedrock mineralisation than the original orientation survey conducted in April 2007, although the general pattern appears to be preserved. Re-analysis of the duplicate field samples in the same batch indicates that this variation largely reflects seasonal variations in metal content of the soils, possibly related to rainfall patterns, but also includes a component of laboratory variation between batches.

CONCLUSION

Soil geochemistry using partial extractions has detected weakly mineralised basement below 40 to 60 m of transported cover in northern Victoria, Australia. Au, Sb and As are elevated in A-horizon soils following aqua regia, BLEG, weakly alkaline, 4 M HCl and Na-pyrophosphate digestions. These metals show a positive correlation with Fe and, in the case of the Na-pyrophosphate digestion, with organic C. Statistically valid anomalies remain for aqua regia Au, and Sb and As in Na-pyrophosphate following normalisation of the data for Fe and C content. They are also associated with lower pH in A-horizon soils and higher pH in B-horizon soils.

ACKNOWLEDGEMENTS

This project would not have been possible without the support of Gold Fields Australasia Pty Ltd.

REFERENCE

ARNE D.C., HOUSE, E., TURNER G., SCOTT, K.M,
AND DRONSEIKA, E. 2009. Exploration for

deeply buried gold deposits in northern Victoria: soil, regolith and groundwater geochemistry of the Lockington and Lockington East gold deposits. *Geoscience Victoria Gold Undercover Report 10*. Department of Primary Industries, Victoria. Available free from <http://www.dpi.vic.gov.au/minpet/store>

Fingerprinting mineral deposit types using iron-oxide chemistry: Application to till from Thompson, Manitoba, Canada

Georges Beaudoin¹, Céline Dupuis¹, & Beth McClenaghan²

¹Département de géologie et de génie géologique, Université Laval, Québec, QC G1V 0A6 CANADA
(e-mail: beaudoin@ggl.ulaval.ca)

²Geological Survey of Canada, 601 Booth Street, Ottawa, ON K1A 0E8 CANADA

ABSTRACT: Magnetite and hematite are common in a range of deposit types. These minerals form a range of partial to complete solid-solutions and they are resistant to supergene weathering. The compositional differences are used to construct discriminant diagrams that separate different deposit types. A first diagram using Ni+Cr vs. Si+Mg allows isolation of Ni-Cu-PGE deposits and Cr deposits from other deposit types. Similarly, the Al/(Zn+Ca) vs. Cu/(Si+Ca) is used to isolate Cu-Zn-Pb VMS deposits. Samples plotting outside the Ni-Cu-PGE and Cu-Zn-Pb VMS fields are discriminated using the Ni/(Cr+Mn) vs. Ti+V diagram that efficiently separate IOCG, porphyry, BIF, skarn and Fe-Ti-V deposits. The method is applied to magnetite and hematite separated from three till samples collected near the Thompson Ni-Cu massive sulfide deposits, Manitoba, Canada. Tests for heterogeneity of the till magnetite chemical composition show that sub-samples provide similar compositional ranges. Iron oxides chemical composition from till samples collected down-ice from the Pipe and South pits of the Thompson mine plot in part within the field of Ni-Cu massive sulfide deposits, demonstrating the potential of the method in mineral exploration in regions overlain by glacial sediments.

KEYWORDS: *magnetite, hematite, till, nickel, geochemistry, mineral*

INTRODUCTION

Iron oxides (hematite and magnetite) are common minerals found in magmatic and metamorphic rocks and can be major to accessory minerals in a range of mineral deposit types. The range in chemical composition of the various deposit type environments likely controls the chemical composition of iron oxides in mineral deposits, such that this compositional variety can be used to fingerprint mineral deposit types (Carew 2004; Gosselin *et al.* 2006; Beaudoin & Dupuis 2009).

In addition to their ubiquity in mineral deposits, magnetite and hematite have potential to be used for mineral exploration from heavy mineral separates because they are resistant to chemical weathering and mechanical abrasion during transport, an important feature of indicator minerals (Belousova *et al.* 2002). Because of their resistance to weathering, the iron oxides can be a useful indicator mineral in highly weathered terrains. Magnetite is present in all shield-derived tills and because of its magnetic

properties it can be easily recovered from surficial sediments. The <2.0 mm ferromagnetic fraction of till is routinely recovered from exploration samples during heavy mineral processing at commercial laboratories and set aside for archiving. In the Thompson Nickel Belt (TNB), for example, till samples contain between 1 and 80 g of magnetite per 10 kg, on average 8 g. This translates into 1000s of grains per 10 kg.

ANALYTICAL METHODS AND SAMPLE PREPARATION

Polished thin sections or iron oxides grains polished in epoxy mounts were analyzed using Université Laval CAMECA SX-100 5-WDS electron microprobe under a beam of 15 kV at 100 nA, using a range of natural and synthetic standards. After counting over the peak for 20 to 30 sec, background is measured on both sides for 10 sec. These settings yield minimum detection limits (mdl) as low as 20 ppm for elements such as K, Ca, Al, Si, Ti and Mg, 50 ppm for Mn, Cr and V, 200 ppm for Cu,

Zn and Ni. The optimized analytical routine allows analysis of one spot in less than 5 min.

The ferromagnetic fraction of the till samples was separated by standard methods by Overburden Drilling Management Ltd (ODM). Subsamples containing 22 to 110 randomly selected grains were prepared by ODM. To test for heterogeneity, two sets of 5 subsamples, from 2 till samples, were prepared from the 0.5-1.0 mm size fraction using a plastic riffle at Université Laval.

IRON OXIDE SIGNATURE OF MINERAL DEPOSIT TYPES

We have developed a series of discriminant diagrams that empirically allow discrimination of a range of deposit types. Some diagrams are useful to uniquely discriminate samples from one deposit type from all other types of deposits, whereas others distinguish fields that are characteristic for several deposit types. Because of compositional variation between grains and samples from a deposit, we compute the average composition of a deposit using non-parametric distribution modelling methods to take into account less than detection limit data (Helsel 2005).

The Ni+Cr vs Si+Mg diagram is efficient in separating the average composition of Ni-Cu-PGE deposits from other deposit types (Fig. 1). A podiform chromite deposit plots at high Ni+Cr values, but the high Cr in magnetite from podiform chromite deposits allows unambiguous identification.

Volcanogenic massive sulfide deposits (VMS) plot with a high probability within a distinct field in the Al/(Zn+Ca) vs. Cu/(Si+Ca) diagram (Fig. 2). This diagram is based on the compositional characteristics of magnetite in VMS that typically has high Zn, Ca and Si, and low Al. Magnetite from the unusual massive magnetite alteration zone at the Ansil deposit plots outside the VMS field (Fig. 2).

The Ti and V content are related to the deposit type, such that the sum of Ti+V is useful to discriminate between deposit

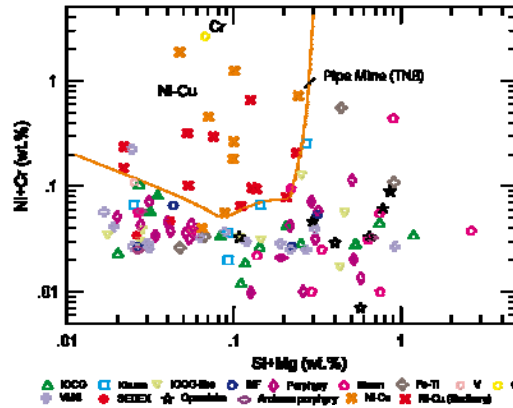


Fig. 1. Discriminant diagram to identify Ni-Cu massive sulfides and Cr deposits. The average composition for a deposit is shown.

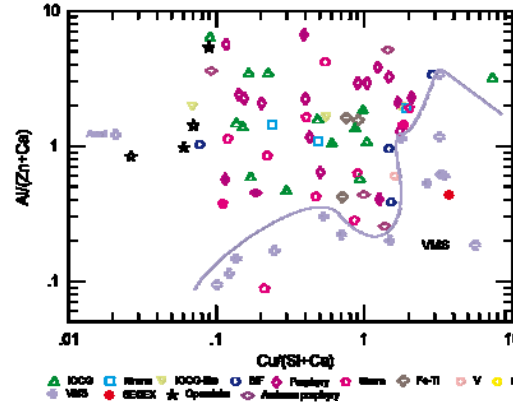


Fig. 2. Discriminant diagram to identify VMS deposits. The average composition for a deposit is shown. Ni-Cu massive sulfide deposits are not shown on this diagram.

types, in combination with Ni/(Cr+Mn) (Fig. 3). To avoid clutter, Ni-Cu-PGE deposits, identified using the Ni+Cr vs. Si+Mg diagram (Fig. 1) are not plotted because the Ni/(Cr+Mn) vs. Ti+V diagram does not discriminate for these deposits.

In the Ni/(Cr+Mn) vs. Ti+V diagram (Fig. 3), fields for IOCG, Kiruna, Cu-Mo-Au porphyry, V and Fe-Ti deposits are well defined. Hostrock magnetite from IOCG and porphyry deposits plot outside the respective fields for mineralization (Fig. 3). The Routivare deposit plots outside the field for Kiruna-type deposits. Several VMS deposits plot within the IOCG field, but VMS deposits are uniquely identified using the Al/(Zn+Ca) vs. Cu/(Si+Ca) diagram (Fig. 2). One Opemiska Cu-Au

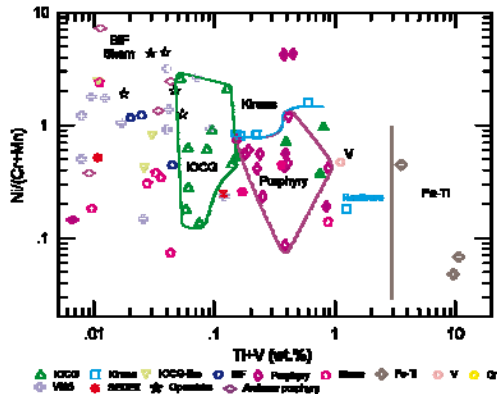


Fig. 3. Discriminant diagram to identify Fe-Ti, porphyry Cu-Mo-Au, Kiruna, and IOCG deposits. Filled symbols are for magnetite from hostrocks. The average composition for a deposit is shown. Ni-Cu massive sulfide deposits are not shown on this diagram.

vein plots within the IOCG field. Skarn display no characteristic compositional signature in the Ni/(Cr+Mn) vs. Ti+V diagram, but can be discriminated using a Ca vs. Ti+V diagram (not shown).

CASE STUDY: GLACIAL TILLS FROM THOMPSON

The Thompson Nickel Belt (TNB), Manitoba, Canada, is host to world class magmatic massive sulfide Ni-Cu-PGE deposits. The deposits subcrop beneath 2 to 30 m of glacial sediments and have been eroded by glaciers flowing SW and then W during the Wisconsin glaciation.

We report, here, results for three till samples from a large regional study (McClenaghan *et al.* 2009): 1) 05-MPB-08, from the south shoulder of the Thompson Mine South pit, contains abundant pentlandite and chalcopyrite; 2) 06-MPB-58, from a location 600 m west and down-ice (W) of the main ore zone at the Pipe Mine, contains sperrylite; 3) 06-MPB-61, from the west shoulder of the Pipe Mine open pit, 200 m W (down-ice) of the ore zone, contains sperrylite.

Magnetite and hematite grains from the ferromagnetic fraction of till samples 05-MPB-08, 06-MPB-58 and 06-MPB-61 were randomly selected by ODM. A total of 22 grains from sample 05-MPB-08, 69

grains from 06-MPB-58 and 110 grains from 06-MPB-61 were selected for analysis. To test the heterogeneity of the heavy mineral concentrates, five sub-samples of the 0.5-1.0 mm size fraction of till sample 06-MPB-58 and 06-MPB-61, labeled, each, A to E, were aliquoted using a plastic riffle and prepared for microprobe analysis (from 33 to 82 grains for each subsample).

The composition of magnetite and hematite selected by ODM from the three till samples is shown in Fig. 4. Although the composition of only one grain from sample 05-MPB-08 plots within the field of Ni-Cu deposits, the average composition of iron oxides from this sample plots within the field for Ni-Cu deposits. Four grains from sample 06-MBP-58 plot within the field for Ni-Cu deposits but the average composition for this sample plots outside the Ni-Cu deposits field (Fig. 4). Several grains and the average composition of sample 06-MPB-61 plot within the field of

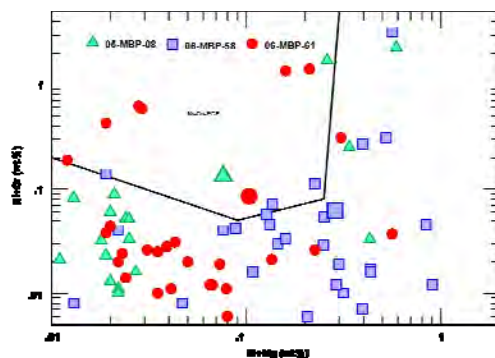


Fig. 4. Composition of magnetite and hematite grains from the till samples prepared by ODM. Larger symbol is the average composition for all analyses for each sample.

Ni-Cu deposits (Fig. 4).

These results are confirmed by comparison of five sub-samples from 06-MBP-58 and 06-MPB-61 (Fig. 5). A small proportion of each sub-sample of 06-MPB-58 plots within the Ni-Cu deposits field whereas the average of all sub-samples plots outside the Ni-Cu deposits field (Fig. 5A). Similarly, a number of grains and the average composition of each sub-samples from 06-MPB-61 plot within the field for Ni-Cu deposits (Fig. 5B).

DISCUSSION AND CONCLUSION

The chemical composition of iron oxides is useful to discriminate a range of mineral deposit types. Discriminant diagrams can be used to identify potential for specific mineral deposit types to occur in an area that has been glacially eroded using till. In this study, a small subset of the ferromagnetic fraction (50 grains, 0.5-1.0 mm size fraction) of a till has been shown to adequately display the compositional

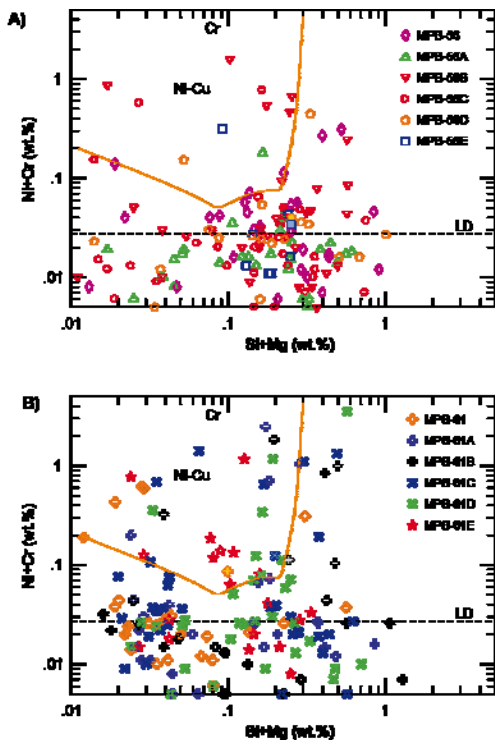


Fig. 5. Composition of 5 sub-samples from A) 06-MPB-58 and B) 06-MPB-61. Filled symbol is the average composition. The horizontal line LD shows the value for the combined detection limits of Ni+Cr, such that analyses that plot beneath this line are not significant.

range of iron oxides from that sample.

The TNB case study shows that iron oxides from till samples down-ice from Ni-Cu massive sulfides have a similar chemical signature to that in magmatic Ni-Cu deposits. Further testing of additional till samples from varying distances down-ice of the TNB would provide further insights into the TNB Ni-Cu deposit signatures and glacial transport distances.

ACKNOWLEDGEMENTS

We thank the DIVEX research network and the Geological Survey of Canada for their continued support for this research.

REFERENCES

- BEAUDOIN, G. & DUPUIS, C. 2009. Iron-oxide trace element fingerprinting of mineral deposit types; In: CORRIVEAU, L. AND MUMIN, H. (ed) *Exploring for Iron Oxide Copper-Gold Deposits: Canada and Global Analogues*, Short Course Volume, Geological Association of Canada Annual Meeting, Québec City, 107-121.
- BEAUDOIN G., DUPUIS C., GOSSELIN P., & JÉBRAK M., 2007. Mineral chemistry of iron oxides: application to mineral exploration In: ANDREW, C.J. (ed) *Ninth Biennial SGA Meeting. Society for geology Applied to Mineral Deposits*, Dublin, 497-500.
- BELOUSOVA, E.A., GRIFFIN, W.L., O'REILLY, S.Y., FISHER, N.I. 2002. Apatite as an indicator mineral for mineral exploration: trace-element compositions and their relationship to host rock type. *Journal of Geochemical Exploration*, **76**, 45-69.
- CAREW, M.J. 2004. *Controls on Cu-Au mineralisation and Fe oxide metasomatism in the Eastern Fold Belt, N.W. Queensland, Australia*. Unpublished PhD thesis, James Cook University, 308 p.
- HELSEL, D. 2005. *Nondetects and Data Analysis*. Wiley, New York, 250 p.
- MCCLENAGHAN, M.B., MATILE, G., LAYTON-MATTHEWS, D., & PYNE, M. 2009. Till geochemical signatures of magmatic Ni-Cu deposits and regional till geochemistry, Thompson Nickel Belt, Manitoba. *Geological Survey of Canada Open File 6005*, 116 p.

Indicator mineral signature of the Halfmile Lake Zn-Pb-Cu volcanogenic massive sulphide deposit, New Brunswick, Canada

Gabriela Budulan¹, M. Beth McClenaghan², Michael A. Parkhill³, & Dan Layton-Matthews¹

¹ Queen's University, Department of Geological Sciences and Geological Engineering, Kingston, ON K7L 3N6 CANADA (e-mail: gbudulan@nrcan.gc.ca)

² Geological Survey of Canada, 601 Booth Street, Ottawa, ON K1A 0E8 CANADA

³ New Brunswick Department of Natural Resources, Geological Surveys Branch, P.O. Box 50, Bathurst, NB E2A 3Z1 CANADA

ABSTRACT: Till and bedrock were sampled around the Halfmile Lake Zn-Pb-Cu volcanogenic massive sulphide (VMS) deposit, Bathurst Mining Camp as part of the Geological Survey of Canada's Deep search Targeted Geoscience Initiative-3. The purpose of this study is to document the till indicator mineral and geochemical signature of a VMS deposit. The deposit is hosted by the volcano-sedimentary sequence of the Ordovician Tetagouche Group. Epiclastic rocks, felsic pyroclastic rocks, crystal-rich felsic tuffs, quartz-feldspar porphyritic intrusions, intermediate and basic dikes, sulphides, and gossan are the main rock types found surrounding the Halfmile Lake deposit. A thin (<2 m) layer of silty sand, locally derived subglacial till covers most of the deposit area. The till contains 20-40% pebble to cobble sized clasts that are angular-subangular in shape. A preliminary set of indicator minerals identified in mineralized bedrocks include: chalcopyrite, pyrite, galena, sphalerite, ferro- and nonferromagnetic pyrrhotite, ilmenite, goethite, and beudantite. Indicator minerals identified in till include: chalcopyrite, pyrite, native gold, goethite, jarosite, and beudantite.

KEYWORDS: *indicator minerals, till geochemistry, VMS deposit, mineralogy, heavy mineral concentrate*

INTRODUCTION

The recovery of indicator minerals from till has become an important exploration method in glaciated terrain in the past 30 years and now include suites for detecting a variety of ore deposit types including diamonds, gold, Ni-Cu-PGE, porphyry Cu, massive sulphide and tungsten deposits (McClenaghan 2007). Indicator minerals are important as an exploration tool because their dispersal in surficial sediments may provide an exploration target much larger than the mineralized zone.

Till geochemistry and boulder tracing are well established exploration methods in Canada for base metals (McClenaghan 2007) however, there has been limited research on minerals that are effective in exploring for VMS deposits in glaciated terrain. To address this knowledge gap, the Geological Survey of Canada (GSC) has undertaken a study to document the indicator mineral and till geochemical

signature of the Halfmile Lake Zn-Pb-Cu VMS deposit.

Till and bedrock were sampled in 2007 around the Halfmile Lake Zn-Pb-Cu volcanogenic massive sulphide (VMS) deposit, Bathurst Mining Camp, New Brunswick (Fig. 1) as part of the Geological Survey of Canada's Deep search project, Targeted Geoscience Initiative-3 (2005-2010). This project is a collaborative effort between the Geological Survey of Canada, the New Brunswick Department of Natural Resources and Queen's University.

GEOLOGICAL SETTING

Bedrock Geology

The Halfmile Lake deposit consists of massive, breccia, and stockwork Zn-Pb-Cu sulfide mineralization hosted by volcanic and sedimentary rocks of the Ordovician Tetagouche Group (Mireku & Stanley 2006; Adair 1992). The main sulphide minerals in the deposit are

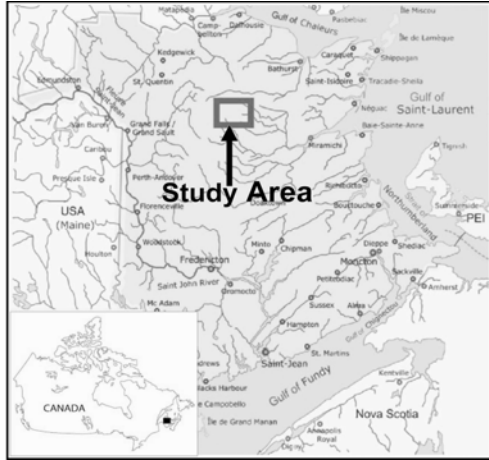


Fig. 1. Location of the study area in eastern Canada.

sphalerite, galena, chalcopyrite, pyrrhotite and pyrite (Adair 1992). Subcropping preglacial (Pliocene) gossan is preserved over parts of the deposit (Boyle 2003). Epiclastic rocks, interbedded fine-grained felsic pyroclastic rocks, crystal-rich felsic tuffs, quartz-feldspar porphyritic intrusions and intermediate and basic dikes are the main rock types hosting the Halfmile Lake deposit (McCutcheon & Walker 2001).

Surficial Geology

A thin (<2 m) layer of silty sand, grayish-yellow to yellowish-brown, locally derived subglacial till covers most of the deposit area. It is found on the lee sides of hills, usually in valleys, and may be Early Wisconsinan to pre-Late Wisconsinan in age (Parkhill & Doiron 2003). The till contains 20-40% pebble-cobble sized clasts that are angular-subangular in shape. Ice-flow indicators together with till fabric analyses, till clast provenance studies, till geochemistry, and the distribution of boulder erratics indicate that the dominant ice flow direction associated with this surface till was to the east (070°–110°) (Parkhill & Doiron 2003).

METHODS

Sampling

Forty eight bedrock (5 kg) samples were collected of ore and host rocks from surface outcrops and drill holes. Fifty six,

25 kg till samples were collected up-ice (west), overlying and up to 2 km down-ice (east) of the Halfmile Lake deposit from existing exploration trenches, hand dug holes and new backhoe trenches. Till samples were collected from the C-soil horizon or B-C-horizon.

Sample Preparation and Analysis

Bedrock and till samples were processed at Overburden Drilling Management Ltd. (ODM) in Ottawa to produce heavy mineral concentrates. Bedrock samples were milled to <2.0 mm and the <2.0 mm material was passed over a shaking table. The heavy mineral fraction was then further refined using heavy liquid separation in methylene iodide diluted to a specific gravity of 3.20. The resulting heavy mineral fraction was separated into a ferromagnetic and nonferromagnetic fraction. The non-ferromagnetic fraction was sieved into four size fractions: 0.18-0.25, 0.25-0.5, 0.5-1.0, 1.0-2.0 mm. The 0.25-0.5 mm fraction was further separated into <0.6, 0.6-0.8, 0.8-1.0, and >1.0 amps based on the paramagnetic properties of minerals to assist picking this very fine grained fraction. The 0.25-0.5, 0.5-1.0, 1.0-2.0 mm fractions were then examined for indicator minerals. Till samples underwent a similar sample processing procedure as the bedrock samples except that a larger weight was processed. Mineralized bedrock samples and all till heavy concentrates were micropanned to recover gold and sulphide minerals in the <0.25 mm fraction. Selected indicator mineral grains will be picked from bedrock and till samples to be photographed and analyzed by SEM, electron microprobe and laser ablation ICP-MS techniques.

Bedrock samples were analyzed at Actlabs using four acid digestion ICP-MS to determine major, minor and trace element concentrations.

The <0.063 mm fraction of till was analyzed by aqua regia and lithium metaborate fusion-nitric acid digestions ICP/ES and MS.

RESULTS

Mineral Identification in PTS

Several minerals have been identified in polished thin sections of various rock types including massive sulphide, gossan, intermediate crystal-lapilli tuff, and felsic ash tuff (Fig. 2). These minerals include: apatite, monazite, zircon, allanite, titanite, xenotime, magnetite, cassiterite, cobaltite-gersdorffite, rutile, ilmenite, goethite, sphalerite, galena, arsenopyrite, chalcopyrite, pyrite, and pyrrhotite. These minerals range in size from 20 µm to 250 µm and represent potential indicator minerals.

Bedrock Indicator Minerals

Sulphide minerals were recovered only in the 0.25-0.5 mm fraction because of their fine-grained nature in the bedrock. A preliminary set of indicator minerals include:

- 1) unweathered ore:
chalcopyrite, pyrite, galena, sphalerite, ferromagnetic and nonferromagnetic pyrrhotite, magnetite, ilmenite, goethite and beudantite;
- 2) gossan:
pyrite, galena, sphalerite, goethite, and beudantite; and
- 3) altered and mineralized host rocks:
chalcopyrite, pyrite, sphalerite, ferromagnetic and nonferromagnetic pyrrhotite, ilmenite, and goethite.

Till Indicator Minerals

A preliminary set of indicators identified in till immediately down-ice of the deposit and gossan include: chalcopyrite, pyrite, gold, goethite, jarosite and beudantite. Heavy mineral grain abundances

decrease down-ice (east) of the Halfmile Lake deposit (Fig. 3).

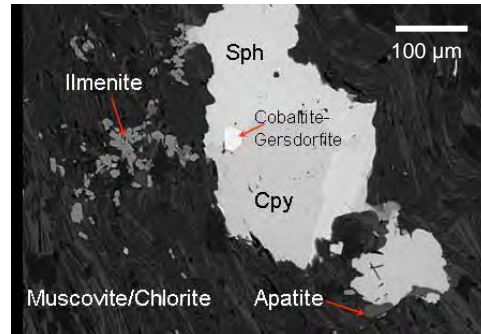


Fig. 2. SEM image of several minerals identified in PTS in a felsic volcanic rock.

IMPLICATIONS FOR EXPLORATION

The outcomes of this study are:

- a set of indicator minerals of a VMS deposit,
- till contains indicator minerals up to 750 m down-ice, and
- heavy mineral sampling methods are suitable in the Bathurst Mining Camp, especially areas covered by thick till.

ACKNOWLEDGEMENTS

Xstrata Zinc is thanked for providing access to the Halfmile Lake deposit and providing samples and geological information. The authors also thank J. Walker, H. Campbell, M. Desrosiers, J. Burns, and L.-P. Cyr for assistance with field work.

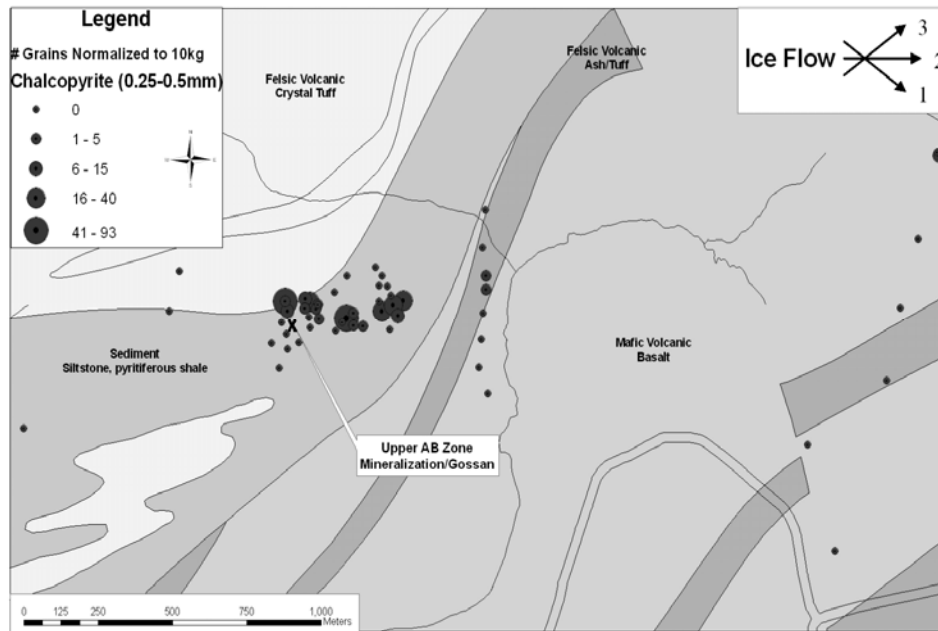


Fig. 3. Distribution of chalcopyrite grains in 0.25-0.50 mm fraction of till samples normalized to 10 kg sample weight. Bedrock geology from van Staal et al. 2003.

REFERENCES

- ADAIR, R.N. 1992. Stratigraphy, structure, and geochemistry of the Halfmile Lake massive-sulfide deposit, New Brunswick: *Exploration and Mining Geology*, **1**, 151–166.
- BOYLE, D.R. 2003. Preglacial weathering of massive sulfide deposits in the Bathurst Mining Camp: Economic geology, geochemistry, and exploration applications. In: GOODFELLOW, W.D., McCUTCHEON, S.R., AND PETER, J.M., (eds) *Massive sulphide deposits of the Bathurst Mining Camp, New Brunswick, and Northern Maine*: Economic Geology Monograph **11**, Society of Economic Geologists, 689–721.
- McCLENAGHAN, M.B. 2007. Till geochemical and heavy mineral exploration methods in glaciated terrain, *Exploration 07-Workshop 2: Exploration Geochemistry-Basic Principles and Concepts Short course Notes*, 23-32.
- McCUTCHEON, S.R., & WALKER, J.A. 2001. Volcanogenic massive sulphide deposits of the Bathurst Mining Camp: Geological Association of Canada-Mineralogical Association of Canada, Joint annual meeting, St. John's, Newfoundland, *Guidebook for Field trip B7*, 89.
- MIREKU, L.K. & STANLEY, C.R. 2006. Litho-geochemistry and hydrothermal alteration at the Halfmile Lake South Deep Zone, a volcanic-hosted massive sulphide deposit, Bathurst Mining Camp, New Brunswick: *Exploration and Mining Geology*, **15**, 177-199.
- PARKHILL, M.A., & DOIRON, A. 2003. Quaternary geology of the Bathurst Mining Camp and implications for base metal exploration using drift prospecting, In: GOODFELLOW, W.D., McCUTCHEON, S.R., AND PETER, J.M., (eds) *Massive sulphide deposits of the Bathurst Mining Camp, New Brunswick, and Northern Maine*. Economic Geology, Monograph **11**, Society of Economic Geologists, 631-660.
- VAN STAAL, C.R., WILSON, R.A., ROGERS, N., FYFFE, L.R., GOWER, S.J., LANGTON, J.P., McCUTCHEON, S.R., AND WALKER, L.A. 2003. A New Geological Map of the Bathurst Mining Camp and Surrounding Areas. A product of integrated geological, geochemical and geophysical data, In: GOODFELLOW, W.D., McCUTCHEON, S.R., AND PETER, J.M. (eds) *Massive sulphide deposits of the Bathurst Mining Camp, New Brunswick, and Northern Maine*. Economic Geology Monograph **11**, Society of Economic Geologists, New Brunswick, scale 1:100 000.

Surface geochemical anomalies in northern Chile: product of the extended metallogenesis of buried copper deposits

Eion M. Cameron¹, Matthew I. Leybourne², Martin Reich³, & Carlos Palacios³

¹Eion Cameron Geochemical Inc., 865 Spruce Ridge Road, Carp, ON CANADA (e-mail: eioncam@gmail.com)

²Ocean Exploration, GNS Science, Lower Hutt NEW ZEALAND

³Depart. de Geología, Facultad de Ciencias Físicas y Matemáticas, Universidad de Chile, Santiago CHILE

ABSTRACT: Work starting in 1999 showed saline-metal anomalies at the surface above copper deposits buried deeply beneath piedmont gravels. These were identified as a product of saline basement waters rising along fracture zones during earthquakes. A visit to the Radomiro Tomic copper mine, also in 1999, suggested that anomalies were a surface expression of a larger process where pulses of fluid expelled by dewatering of the forearc basin moved through deposits replacing some primary supergene minerals with atacamite, a copper oxychloride. This proposal proved controversial, since atacamite was considered a primary oxide. Recent work, mainly at the University of Chile, has shown: (a) salinities of fluid inclusions in atacamite are the same as local saline groundwater; (b) ³⁶Cl data indicate that atacamite could not have formed earlier than 1.5 Ma, contrasting with alunite dates showing primary supergene oxidation extended over the period 44 to 9 Ma; (c) U-Th dating of gypsum-atacamite intergrowths give Pleistocene ages of 237 ka for Chuquicamata, 127 ka for Spence and as low as 75 ka for other deposits. These recent ages for saline metasomatism of deposits and, by inference, for surface anomalies, show why anomalies can be readily recognized by soil surveys, rather than having been removed over time by erosion.

KEYWORDS: Chile, copper, atacamite, anomalies, Pleistocene

INTRODUCTION

Studies beginning in 1999 in the Atacama Desert identified saline-metal anomalies above copper deposits buried beneath thick piedmont gravel cover (Cameron *et al.* 2002, 2005). Anomalies formed as a result of basement fluids rising along fracture zones that cut the deposits and gravels. From the beginning it was apparent that more was involved in the process than simply the formation of anomalies. A visit to the Radomiro Tomic mine in 1999 suggested that the same saline fluids that had created the surface anomalies had substantially modified the initial supergene assemblage, including the formation of atacamite, a mineral that accounts for a substantial amount of the copper production of northern Chile.

THE ATACAMITE STORY

Supergene enrichment played a critical role in making northern Chile the world's prime copper-producing province. For copper porphyry deposits in the central

Atacama Desert supergene enrichment extended from 44 to 9 Ma, reaching a maximum at 21 to 14 Ma (Arancibia *et al.* 2006). Supergene oxidation required significant rainfall, and was terminated by the onset of hyper-aridity. The visit to the Radomiro Tomic open pit in 1999 showed a basement hill of supergene ore covered by piedmont gravels. The principal ore mineral at Radomiro Tomic is atacamite, $\text{Cu}_2\text{Cl}(\text{OH})_3$, found in many of the deposits of the region (Fig. 1). Both specifically for this deposit and for the region, atacamite was considered a primary product of supergene oxidation. But this was not possible given the geological relationships displayed in the pit. Atacamite is readily soluble in meteoric water (Woods & Garrels 1986) and would have been removed by the rainfall that accompanies supergene alteration and/or by stream waters that carried the gravels that bury the hill of ore. At this deposit, atacamite could not have formed prior to the

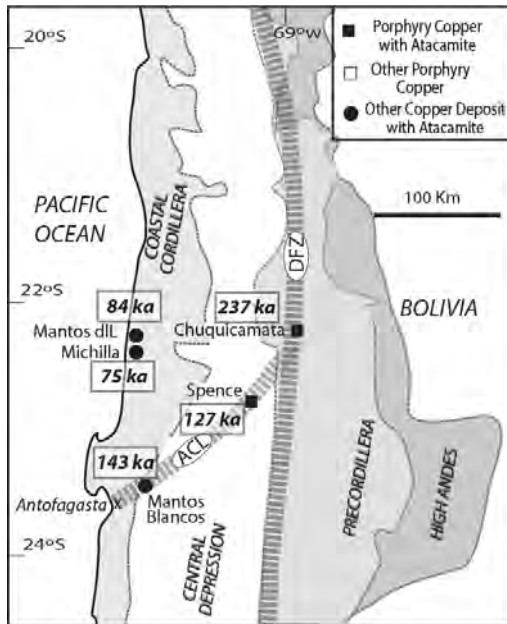


Fig. 1. Distribution of copper deposits in northern Chile including those containing atacamite in the oxide zone. DFZ is the Domeyko Fault Zone and ACL is Antofagasta–Calama Lineament. The land between the High Andes and the coast is the hyper-arid central Atacama Desert.

deposition of the gravels at c. 10 Ma. Further, atacamite-bearing upper and lower oxide zones are separated, immediately below the water table, by a zone lacking atacamite. When water dripping from the pit wall was tested with a conductivity meter, it proved to be meteoric. Later analyses showed the water to be rich in copper. A slow flow of this layer of meteoric water, 'floating' on deeper saline water, has removed atacamite from this zone.

Hydrogeochemical studies at the Spence deposit, also a hill of atacamite-bearing ore covered by gravel, showed that rising saline waters have caused primary supergene minerals, such as brochantite, to be replaced by atacamite. Episodic pumping caused by earthquakes forced the waters to the surface to create the saline-metal anomalies at Spence, at Radomiro Tomic, and elsewhere.

SALINITIES OF FLUID INCLUSIONS IN ATACAMITE

If atacamite has formed in recent times by rising saline groundwater, then fluid inclusion salinities should match that of saline groundwater at the sites. For the Mantos Blancos and Spence deposits salinities of inclusions in atacamite are the same as those measured in saline groundwater sampled from drill holes (Reich *et al.* 2008). The correspondence between groundwater and inclusion salinities is made more significant by the substantial difference in salinities between the two deposits: average values in NaCl_{eq} for Mantos Blancos water is 7.6 (n = 32), inclusions 8.4 (n = 49); Spence water 2.3 (n = 13), inclusions 2.7 (n = 43). Salinities of fluid inclusions in atacamite are coincident with that for gypsum supersaturation. TEM observations show an intimate association between atacamite and gypsum at the macro to nanometer scale.

Isotopic data for $\delta^2\text{H}$ vs. $\delta^{18}\text{O}$ for the saline waters at Spence established that these are formation waters of deep origin (Cameron & Leybourne 2005; Leybourne & Cameron 2006). The deep origin of these waters is also revealed by their high iodine content. Also, soil anomalies are linked to the waters by their high iodine content; up to 1.6% water-soluble iodine above the West Fault that cuts the Mansa Mina deposit, south of Chuquicamata. Concentrations of iodine are low in seawater and freshwater, because iodine is fixed by organisms, but reaches high levels in forearc fluids. Forearc sediments are rich in organic material, from which iodine is released during deep diagenesis. The Atacama Desert is the world's largest producer of iodine from surface deposits. These were thought to be atmospheric precipitates from marine aerosols. Feyn *et al.* (2007) have shown that the radiogenic isotope ^{129}I in this iodine is too low to be of seawater origin, but is consistent with 'old' iodine derived from Jurassic and Cretaceous sediments of the forearc that underlie the Atacama Desert.

DATING ATACAMITE

Reich *et al.* (2008) measured ^{36}Cl in atacamite from Mantos Blancos, Spence and three other deposits. These show low ^{36}Cl -to-Cl ratios (11×10^{-15} to 28×10^{-15}), comparable to previously reported ratios of deep formation waters. Further, ^{36}Cl -to-Cl ratios in atacamite correlate with U and Th concentrations in host rocks. This suggests that subsurface production of fissiogenic ^{36}Cl was in secular equilibrium with waters involved in atacamite formation. Because atacamite does not contain U or Th, production of ^{36}Cl is not continued once chlorine has entered the crystal structure; from that time the ^{36}Cl -to-Cl ratio decreases with age. The fact that measurable ^{36}Cl is present indicates that atacamite formation occurred less than 1.5 Ma ago (five times half-life of ^{36}Cl).

The intimate association between gypsum and anhydrite permitted a further refinement in dating. The U-series disequilibrium method is based on the natural fractionation of U and Th isotopes that lead to the preferential precipitation in authigenic minerals of parent nuclides over insoluble daughter products. The method has been successfully applied to obtain absolute ages of minerals that precipitate from aqueous solutions (e.g., gypsum, anhydrite, and halite), in a range between <10 and 350 ka. Only primary gypsum associated with atacamite in veins and veinlets, with no evidence of recrystallization or dissolution, was measured using the isochron approach of Luo & Ku (1991) that corrects for initial ^{230}Th contamination. Samples from five deposits all show Pleistocene ages, with Chuquicamata being the oldest, 237 ± 8 ka. Younger ages are obtained for Mantos Blancos, 143 ± 29 ka; Spence, 127 ± 29 ka; Mantos de la Luna; 84 ± 11 ka; and Michilla, 75 ± 0.4 ka. Chuquicamata and Spence are copper porphyry deposits, the others are stratiform copper deposits of the Coastal Cordillera (Fig. 1).

CONCLUSIONS

The metallogenic evolution of the copper porphyry deposits of the Atacama Desert included a long phase of supergene

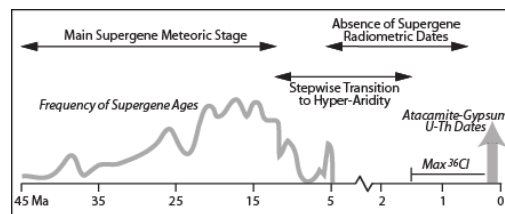


Fig. 2. Geochronology of supergene processes for copper deposits in northern Chile (modified from Reich *et al.* 2009).

enrichment extending from Eocene to Miocene time (Fig. 2). After several million years, many of these deposits experienced a second stage, during the Pleistocene, where saline forearc waters converted part of the initial oxide assemblage to atacamite, an important ore mineral. The second stage also involved stratiform copper deposits in the Coastal Cordillera. We infer that the formation of the saline-metal anomalies at the gravel surfaces above the deposits was synchronous with the rise of saline forearc fluids through the deposits, modifying the original supergene oxide assemblage to one containing atacamite. Near Mantos Blancos, Palacios *et al.* (2005) found a link between atacamite formation and surface anomalies. Green coloured salt efflorescence containing atacamite and chalcantite occur along the surface trace of major faults that cut deeply buried copper mineralization. A Pleistocene age helps explain why the anomalies can be readily recognized during soil surveys. Anomalies formed at an earlier time might have been removed or redistributed by surface erosion or rainfall. Indeed, climate played a critical role in the evolution of the deposits, the anomalies being part of their metallogeny. Rainfall in an arid to semi-arid climate during the first stage made possible supergene enrichment. Hyper-aridity during the second stage ensured the preservation of saline-metal anomalies and atacamite; with rainfall sufficient to cause recharge of meteoric water through gravels to the oxide zones, atacamite would have been dissolved. The Pleistocene age for the northern Chile anomalies provides a link with anomalies

above the Mike gold-copper deposit, Nevada. This deposit is covered by a thick sequence of Carlin Formation. Metal anomalies are located on the surface trace of a Pleistocene age fault that cuts both the deposit and the cover rocks (Cameron *et al.* 2005).

REFERENCES

- ARANCIBIA, G., MATTHEWS, S.J., & PEREZ DE ARCE, C. 2006. K-Ar and ⁴⁰Ar/³⁹Ar geochronology of supergene processes in the Atacama Desert, Northern Chile: tectonic and climatic relations. *Journal Geological Society London*, **163**, 107-118.
- CAMERON, E.M., LEYBOURNE, M.I., & KELLEY, D.L. 2002. Exploring for deeply-covered mineral deposits: formation of geochemical anomalies in northern Chile by earthquake-induced surface flooding of mineralized groundwaters. *Geology*, **30**, 1007-1010.
- CAMERON, E.M. & LEYBOURNE, M.I. 2005. Relationship between groundwater geochemistry and soil geochemical anomalies at the Spence copper porphyry deposit, Chile. *Geochemistry: Exploration, Environment, Analysis*, **5**, 135-145.
- CAMERON, E.M., HAMILTON, S.M., LEYBOURNE, M.I., HALL, G.E.M., & MCCLENAGHAN, B.E. 2004. Finding deeply-buried deposits using geochemistry. *Geochemistry: Exploration, Environment, Analysis*, **4**, 1-26.
- CAMERON, E.M., LEYBOURNE, M.I., & KELLEY, D.L. 2005. Exploring for deposits under deep cover using geochemistry. *Society of Economic Geologists Newsletter*, No. **63**, 5-15.
- CAMERON, E.M., LEYBOURNE, M.I., & PALACIOS, C. 2007. Atacamite in the oxide zone of copper deposits in northern Chile: Involvement of deep formation waters? *Mineralium Deposita*, **42**, 205-218.
- FEHN, U, MORAN, J.E., SNYDER, G.T. & MARAMATSU, Y. 2007. The initial 129I/I ratio and the presence of 'old' iodine in continental margins. *Nuclear Instruments and Methods in Physics Research*, Section B, **259**, 496-502.
- LUO S.D. & KU T.L. 1991. U-series isochron dating - a generalized method employing total-sample dissolution. *Geochimica et Cosmochimica Acta*, **55**, 555-564.
- LEYBOURNE, M.I. & CAMERON, E.M. 2006. Composition of groundwaters associated with porphyry-Cu deposits, Atacama Desert, Chile: Elemental and isotopic constraints on water sources and water-rock reactions. *Geochimica et Cosmochimica Acta*, **70**, 1616-1635.
- PALACIOS, C., GUERRA, N., TOWNLEY, B., LAHSEN, A. & PARADA, M. 2005. Copper geochemistry in salt from evaporate soils, Coastal Range of the Atacama Desert, northern Chile: an exploration tool for blind Cu deposits. *Geochemistry: Exploration, Environment, Analysis*, **5**, 371-378.
- REICH, M., PALACIOS, C., PARADA, M.A., FEHN, U., CAMERON, E.M., LEYBOURNE, M.I. & ZUNIGA, A. 2008. Fluid inclusion, groundwater geochemistry, TEM and 36Cl. Evidence for a genetic link between basinal brines and atacamite formation, Atacama Desert, Chile. *Mineralium Deposita*, **43**, 663-675.
- REICH, M., PALACIOS, C., VARGAS, G., LUO, S., CAMERON, E.M., LEYBOURNE, M.I., PARADA, M.A., & ZUÑIGA, A. 2009. Supergene enrichment of copper deposits since the onset of modern hyperaridity in the Atacama Desert, Chile. *Mineralium Deposita*, (in press).
- WOODS, T.L. & GARRELS, R.M. 1986. Phase relations in some cupric hydroxy minerals. *Economic Geology*, **8**, 1989-2007.

Geochemistry of Archean sulfidic black shale horizons: combining data at multiple scales for improved targeting in VMS exploration

John B. Chapman¹, Jan M. Peter¹, Daniel Layton-Matthews² & J. Bruce Gemmell³

¹Geological Survey of Canada, 601 Booth Street, Ottawa, ON K1A 0E8 CANADA
(e-mail: john.chapman@nrcan-mcan.gc.ca)

²Department of Geological Sciences and Geological Engineering, Queen's University, Kingston, ON K7L 3N6, CANADA

³ARC Centre of Excellence in Ore Deposits, University of Tasmania, Hobart Campus, Private Bag 126, Hobart, Tasmania 7001 AUSTRALIA

ABSTRACT: Metalliferous black shales are a common but minor component of many subaqueous volcanic successions. These shales are commonly drilled during volcanogenic massive sulfide (VMS) deposit exploration programs. Although ore metal enrichment can be determined by conventional assay methods, matrix dilution and post-burial hydrothermal and metamorphic processes may obscure information on the type and mechanism of metal addition to the shale. We used a combination of geochemical methods at a variety of scales to discriminate between VMS-prospective and VMS-barren horizons. In addition, element signatures associated with hydrothermal plume fallout were identified and used to determine relative direction to the palaeo-venting centre. Portable x-ray fluorescence (pXRF) analysers were used to identify and correlate prospective mineralized horizons within exploration drill cores. pXRF is a rapid and relatively inexpensive method of analysis that can deliver quantitative geochemical information at a cm-scale and help to identify intervals meriting further, more costly and time-consuming analyses. Subsequently, laser-ablation ICP-MS analysis of metal sulfides was used to constrain hydrothermal, hydrogenous and diagenetic end-member compositions, and to quantify element remobilization during post-burial alteration. These data were then used to refine the pXRF survey methodology and develop primary vectors toward potential concealed VMS deposits.

KEYWORDS: *black shale, VMS, exploration vectoring, LA-ICP-MS, portable XRF*

INTRODUCTION

Metalliferous sediments are a common component of modern ocean-floor sedimentary sequences, recording halos of metal dispersion from seafloor hydrothermal vent systems (Gurvich, 2006). Sulfidic black shales are also commonly present as intercalations in ancient subaqueous volcanic sequences, where each likely represents a significant hiatus in volcanic activity and deposition. These shale horizons form geophysical anomalies (conductors) that are routinely drilled during exploration for volcanogenic massive sulfide (VMS) base metal deposits.

Some horizons are enriched in ore metals and associated elements (e.g. Zn, Cu, Ag, Cd, Sn), whereas others are barren. However, element distributions in such rocks are commonly extremely

heterogeneous and identification of enriched horizons is therefore largely dependent on the assay interval selected. Identification of structurally repeated horizons and correlation of individual shale horizons between drill holes is commonly problematic. Even where horizons can be correlated, the variable dilution of hydrothermal signatures by terrigenous and hydrogenous shale matrix minerals hinders interpretation of metal sources, especially where drilling coverage is limited or element-enrichment is subtle. In addition, later hydrothermal and metamorphic redistribution may have modified any primary exhalative enrichment patterns.

The objectives of our study are to provide an accurate, precise, robust and cost effective framework within which sedimentary horizons can be assessed to

provide evidence of: a) the presence or absence of hydrothermal metal input; b) the type of hydrothermal activity recorded within, and prospectivity of, any one horizon; and c) the direction, along strike and down dip extent, and relative distance to the coeval venting centre (where a single horizon has been intersected more than once). This was achieved by the combination of geochemical analytical methods including: conventional whole-rock analysis, laser-ablation inductively coupled plasma mass spectrometry (LA-ICP-MS) and portable x-ray fluorescence (pXRF) analysers; each optimised for different spatial resolution, and with varying cost and sensitivity characteristics.

GEOLOGY AND MINERALOGY

Metalliferous sedimentary rock horizons occur as intercalated units between volcanic rocks of the 2.7 Ga Kidd-Munro assemblage (KMA) of the Abitibi sub-province, Canada (Hannington *et al.*, 1999). The shale horizons are widely distributed within the KMA and commonly occur as carbonaceous (graphitic) and/or sulfidic argillaceous shale units. Multiple horizons may be present in any one drillcore, representing both primary depositional stratigraphy and subsequent fold repetition.

Pyrite and pyrrhotite are the dominant sulfides in the shale horizons, with minor sphalerite, galena and chalcopyrite. Iron sulfides occur in six distinct textural habits: *Py1*, pyrite-rich laminae and framboids (sub-mm to 1 cm; primary chemical sedimentary); *Py2*, recrystallized and remobilized laminae and disseminations (early diagenetic); *Py3*, crustiform bands displaying growth textures and banding, commonly much disrupted (0.3 to 2 cm; early to late diagenetic); *Py4*, nodules displaying no internal fabric, and concretions displaying concentric zonation (0.5 to 4 cm; early to late diagenetic); *Py5*, metamorphic porphyroblasts, overgrowths and pressure shadows (0.2 to 3 cm; peak to post-peak metamorphic). Finally, *Py1* to *Py4* have been subject to variable late-stage alteration and replacement by secondary pyrrhotite.

GEOCHEMICAL ANALYSIS METHODS

Whole-rock geochemistry

The metal budget of any individual shale horizon reflects a variable admixture of materials with a number of end member compositions. Even where the sulfide component of a sample is >10%, conventional discrimination plots used to identify and quantify hydrothermal input such as Co/Ni ratio (e.g., Meyer *et al.*, 1990) or rare earth element plots (e.g., Johannesson *et al.*, 2006) are hindered in their application due to dilution by the non-sulfide silicate detrital minerals.

Principal component analysis (PCA) of bulk sample geochemical data has been used to identify element associations that reflect major source contributions. Plotting first and second principal components of whole rock geochemical data has identified three dominant element groupings: 1) hydrothermal – Ag, As, Bi, Cd, Cu, Hg, In, Mo, Ni, Pb, Sn, Te, Zn; 2) hydrogenous – Au, Ca, Cr, Mn, Pt, Sb, Sc, Ti, V; and 3) terrigenous – Al, Ba, Be, Ce, Cs, Dy, Er, Eu, F, Ga, Gd, Hf, Ho, La, Lu, Mg, Nb, Nd, Pr, Rb, Sm, Sr, Ta, Tb, Th, Tm, U, Y, Yb, Zr. Iron and S do not have eigenvalues consistent with the major PCA groupings, and their eigenvalues in the second principal component suggest that their abundance may in fact be due to water column, rather than hydrothermal, processes. Hence, absolute pyrite and pyrrhotite abundance are poor indicators of hydrothermal input to black shales.

Laser-ablation ICP-MS

In-situ LA-ICP-MS trace element analysis of Fe-sulfides of various textural types was used to investigate inter-element correlations and sulfide end-member compositions. Trace elements of putative hydrothermal origin showing significant enrichment in pyrite include Ag, Au, As, Bi, Cu, Pb, Sb, Sn, Ti and Zn, whereas Co, Ni, Mo, Se, Pt and Te enrichments are presumed to have a hydrogenous origin. Comparison of these element groupings with those determined from bulk chemical analyses highlights further the complex nature of element distributions and associations within the sulfide component

of the KMA black shale horizons. In general, the early, visibly included pyrite forms (Py1 to Py3) have the greatest trace element contents, and later, inclusion-free metamorphic pyrite (Py5 and pseudomorph pyrrhotite) contains the lowest trace element abundances.

A complication of the LA-ICP-MS technique is that few elements substitute stoichiometrically into the pyrite crystal lattice. Arsenic, Co and Ni demonstrate stoichiometric lattice substitutions, but many others are more commonly incorporated as non-stoichiometric substitutions, and as microinclusions of other sulfide minerals within pyrite (Deer *et al.*, 1992). Recrystallization, annealing and metamorphism will further exclude these trace elements from the pyrite structure (Large *et al.*, 2007). This is clearly seen in the variable transient signals of different elements during the laser ablation process. In a single ablation, elements such as As, Co, Ni and Sb commonly show distinct covariance with Fe, indicative of substitution within the pyrite lattice; however, elements such as Zn, Cd and Ag display sharp spikes in the transient LA-ICP-MS profile, indicative of their presence within sulfide microinclusions or as non-stoichiometric substitution within the pyrite. Other elements such as Cu, Pb and Bi show a mixed transient signal, most likely reflecting zonation within the pyrite grains. At present, it is not known if these elements are hosted within the pyrite, or whether minerals that host these elements form extremely fine dispersions that are not resolvable by the laser technique (~30 microns).

Portable XRF

Although not yet routine, the use of pXRF analysers both for rock outcrop and core elemental determinations is already showing much promise. Their analysis window is approximately 1 cm in diameter, such that pXRF instruments offer a compromise between the spatial resolution offered by micro-analytical techniques such as LA-ICP-MS, and the

bulk sample integration of traditional chemical analysis methods.

It is apparent from our pXRF analyses that at the scale of the analytical window, there are regular, reproducible, variations in element enrichments between sulfide accumulations (nodules, concretions, crusts) and shale matrix. Some of the largest base metal and associated element contents measured in the field (e.g. Zn ≈ 1.4 wt%; Cu ≈ 600 ppm; Mn ≈ 1 wt%; Cd ≈ 90 ppm; Hg ≈ 50 ppm) are in apparently (to the naked eye) sulfide-free shale. The majority of such enrichments appear to be due to the incorporation of disseminated, very fine-grained, Fe-rich sphalerite. In many instances this is not evident even when using a hand lens, and care must be taken not to overlook these cryptic enrichments.

Pyrite commonly displays distinctly different trace element abundances than the host shale matrix. Figure 1 demonstrates that elemental abundances can vary significantly even between adjacent sulfide masses. Element exclusion is greatest where the associated pyrite is strongly recrystallized or is of metamorphic origin, with “dirty” concretions and crustiform material showing the least deviation from matrix abundances.

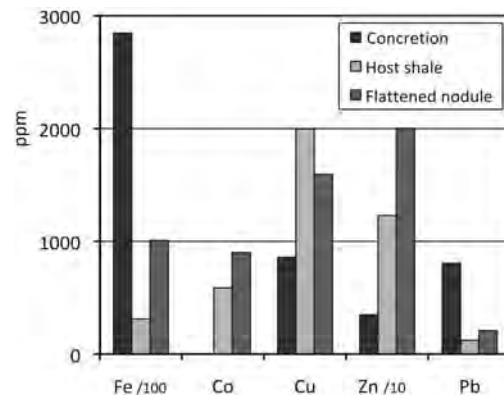


Fig. 1. Selected portable XRF element analyses for two pyrite masses and their shale host. The two masses, both ~2 cm in diameter, are within 5 cm of one another but display different trace element contents, both from one another and from their silicate host. The shale matrix analysis is taken between the two.

CONCLUSIONS

Hydrothermal geochemical signatures are recognized by the use of traditional whole-rock geochemical analyses. However, their intensity can vary greatly over narrow intervals; furthermore, they are difficult to quantify and are subject to significant sampling bias. These signatures are a result of elements being hosted in multiple mineral phases within a single horizon. In order to more effectively and efficiently rank areas meriting additional work in VMS exploration, it is essential to understand the sources, distribution, and mineralogical and paragenetic association of geochemical signatures observed in shale horizons.

Various analytical methodologies have been assessed with respect to better constraining geochemical anomalies. Traditional whole-rock methods can integrate signals from a wide core interval, but are relatively expensive (\$50+ per sample) and time-consuming. Laser-ablation ICP-MS analysis is a powerful tool for deconvolving sulfide chemistry and paragenesis, however, sample size is limited (making the technique prone to sampling bias), analysis costs are high, and lag times on data feedback are long. Portable XRF analysis is non-destructive and provides cost-effective and essentially instantaneous information on sample composition and can be performed on site, during a drill program, and so used to refine exploration targeting on the fly. Combination of the three approaches provides a comprehensive and powerful investigative methodology for elucidating element signatures in shale horizons, and opens the way for potential development of exploration vectoring protocols for application during routine core analysis.

ACKNOWLEDGEMENTS

We thank Xstrata Copper Canada, and in particular Gordon Maxwell, Louis Martin and Margie MacLeod, for their time and assistance during the course of this study.

REFERENCES

- DEER, W.A., HOWIE, R.A. & ZUSSMAN, J., 1992. *An Introduction to the Rock Forming Minerals*. Prentice Hall.
- GURVICH, E.G., 2006. *Metalliferous Sediments of the World Ocean*. Springer, New York.
- HANNINGTON, M.D., BARRIE, C.T. AND BLEEKER, W., 1999. The giant Kidd Creek volcanogenic massive sulfide deposit, western Abitibi Subprovince, Canada: preface and introduction. In: HANNINGTON, M.D. & BARRIE, C.T. (eds) *The Giant Kidd Creek Volcanogenic Massive Sulfide Deposit, Western Abitibi Subprovince, Canada*. Economic Geology Monograph 10. Economic Geology Publishing Company, Littleton, CO, 1-30.
- JOHANNESSON, K.H., HAWKINS JR., D.L. & CORTÉS, A., 2006. Do Archean chemical sediments record ancient seawater rare earth element patterns? *Geochimica et Cosmochimica Acta*, **70**, 871-890.
- LARGE, R.R., MASLENNIKOV, V.V., ROBERT, F., DANYUSHEVSKY, L.V. & CHANG, Z., 2007. Multistage sedimentary and metamorphic origin of pyrite and gold in the giant Sukhoi Log deposit, Lena Gold Province, Russia. *Economic Geology*, **102**, 1233-1267.
- MEYER, F.M., ROBB, L.J., OBERTHÜR, T., SAAGER, R. & STUPP, H.D., 1990. Cobalt, nickel, and gold in pyrite from primary gold deposits and Witwatersrand reefs. *South African Journal of Geology*, **93**, 70-82.

An investigation of partial extractions designed to solubilize Pb and Zn from soils using a complexation desorption mechanism

Janice Chipman¹, John Murimboh¹, & Cliff Stanley²

¹ Dept. of Chemistry, Acadia University, Wolfville, NS, B4P 2R6 CANADA (e-mail: 080629c@acadiau.ca)

² Dept. of Earth & Environmental Science, Acadia University, Wolfville, NS, B4P 2R6 CANADA

Abstract: Soil samples collected across the till-covered Northeast Zone of the Gay's River carbonate-hosted massive sulfide Zn-Pb deposit, Stewiacke, Nova Scotia, were analysed for metal concentrations using several partial leaches. This experiment was designed to determine the optimal reagent that solubilizes metals via a 'complexation desorption' mechanism, whereby ligands producing strong complexes 'encourage' desorption of metals from mineral(oid) surfaces. Several salinities of K-halide solutions were tested. Exploration accuracy and geochemical contrast were determined for each digestion using minimum hypergeometric probability and Student's t-test probability procedures. Pre- and post-digestion pH-pE conditions of soil samples illustrate that ambient pore water pH and pE conditions are strongly controlled by an Fe⁺²-Fe(OH)₃ buffer, and indicate that this buffer remains important even during digestion. Overall, partial digestion results were unsuccessful and did not accurately produce anomalous samples over 'anomalous sites', with high geochemical contrast. Nevertheless, the relative performances of the digestions can be related to the reagent behaviours and Pb- and Zn-complex stability constants. As a result, it is likely that the distribution of adsorbed Zn and Pb in soils at Gay's River does not have a geometry that conforms to an ideal vertical or up-dip element dispersion model.

Keywords: *partial digestion, complexation, desorption, geochemical exploration, MHP, MTP, pH, pE, digestion monitoring.*

INTRODUCTION

In many places on earth, mining companies have already discovered (mostly in the last 50 years) the majority of mineral deposits exposed at the surface. As a result, mineral deposits that have not been discovered are typically buried by some form of surficial material, such as gravel, till or volcanic ash. This exotic cover makes exploration for most buried mineral deposits expensive and difficult, because the chemistry of this overlying material is different from that in the mineral deposits or its host rocks.

Fortunately, ground waters dissolve and transport metals from mineral deposits at depth to the surface, where the metals adsorb onto the surfaces of organic matter and Fe- and Mn-oxy-hydroxide particles in the soil. Unfortunately, the adsorption of these ions contributes only a small amount of additional metal to the soil, resulting in marginally anomalous

concentrations of elements above mineralized zones.

Partial digestions can be used to specifically extract the labile component of an element concentration in a soil. Loosely bound metals can be solubilized using a leach that is not strong enough to dissolve mineral(oid) substrates or to solubilize background elements hosted within soil particles. Because the background element components are not digested by these extractions, high geochemical contrast between anomalous and background samples commonly exists.

Thus, one approach to the liberation of electrostatically-bound ions from soil particle surfaces involves the use of partial leaches containing complexing ligands (such as halide salt solutions). These liberate the adsorbed metals by forming complexes, thereby out-competing the adsorption surfaces for these metals.

METHOD

Thirty-two soil samples on a N-S traverse were collected from the brunisolic B-horizon (20 cm average depth) in May, 2008 over the drill-defined Northeast Zone of the Gay's River carbonate hosted massive sulfide (CHMS) Zn-Pb deposit, Stewiacke, Nova Scotia. This mineral target is buried by up to 10 m of exotic till and c. 10 m of gypsum, and so represents an ideal location to evaluate the exploration performance levels of partial digestions designed to extract labile elements from soil particle surfaces.

Potassium halide salt solutions were used to test a soil particle desorption mechanism involving preferential metal-ligand complexation. Samples of 0.5 g were immersed in 40 ml of reagent at STP and periodically agitated for 4 hours, filtered through a 0.45- μ m filter, and then analysed by ICP-MS. Results from a range of ligands of different ionic radii (F⁻, Cl⁻, Br⁻, I⁻) and concentrations (0.01 M, 0.1 M, 1 M) were obtained. A de-ionized water leach control and a commercial aqua regia digest were used for comparative purposes.

In addition, because all of these soils contain Fe(OH)_{3(am)} [the mineraloid ferrihydroxide], both before and after digestion (based on colour), the pH of each soil and the resulting solution after digestion were measured, along with the soluble iron concentration (Fe⁺²). Using these data and the equilibrium:

$$\text{Fe}^{+2}_{(\text{aq})} + 3 \text{H}_2\text{O} \rightleftharpoons \text{Fe}(\text{OH})_{3(\text{am})} + 3 \text{H}^+ + \text{e}^-$$
 which defines a corresponding mass action equation, the pE of the sample can be calculated:

$$\text{pE} = -3\text{pH} - \log \alpha_{\text{Fe}^{+2}} - \log K.$$

This equation allows determination of how the partial digestion affected the pH and pE of each soil sample, and determines which component, soil or reagent, most acted as a buffer during digestion.

RESULTS

A hypergeometric probability (HP) can be used to quantitatively measure the accuracy of a soil geochemistry program tested over a mineral deposit target with

known location (*i.e.* an orientation survey). This statistic, when applied to exploration samples using a specific threshold, yields the probability that the same number of anomalous samples, randomly located in space, will occur over the known anomalous sites with the same frequency as that observed in the orientation survey. The lower the HP (*e.g.* the minimum HP for any threshold; MHP), the less random the result, and the more likely that the observed anomalies are a result of non-random processes (*i.e.* the anomalous samples are not likely due to random noise, but are rather due to a true anomalous character in the soils).

The Student's t-test probability (TP) measures the geochemical contrast (essentially equivalent to precision) of an exploration method. This probability identifies the likelihood that anomalous and background concentrations, defined by a specific threshold, are derived from the same population by measuring the difference between the mean anomalous and background concentrations. The lower the TP (*e.g.* the minimum TP for any threshold; MTP), the more geochemical contrast and the more likely that random variations will not influence or change the results.

Because accuracy and geochemical contrast are both desirable traits for an exploration method, a combination of the MHP and the associated TP at the MHP-defined threshold defines the quality of the exploration method, in this case, the best ligand type and concentration of partial digestion for soils over the target CHMS deposit (Figs. 1, 2). Two different extractions for Zn and Pb have the best exploration accuracy scores (lowest MHPs) and associated acceptable geochemical contrast (TPs) at the MHP threshold.

For Zn, the most successful digestion appears to be 0.1 M KF. Unfortunately, all but two of the analyses for this digestion were at or below detection, and one above detection analysis occurs directly over the mineralized zone, resulting in an artificially low MHP. As a result, the best partial digestion for Zn is 1.0 M KF (Fig. 3),

because it has a low MHP and results are mostly sufficiently above the detection limit. In contrast, the most accurate partial digestion for Pb is 0.01 M KBr (Fig. 4).

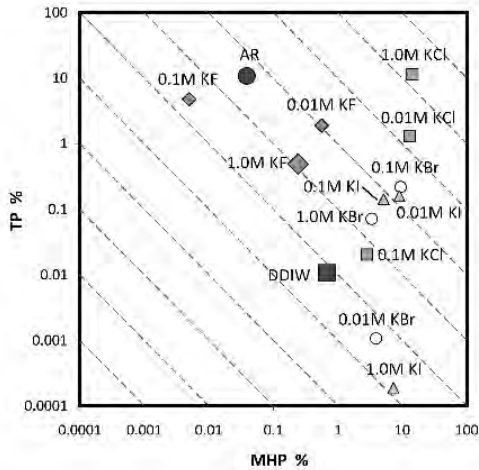


Fig. 1. Logarithmic scatterplot of MHP versus TP at the MHP threshold for Zn to identify the best partial digestion for detecting mineralization at the Gay's River CHMS Zn-Pb deposit, Nova Scotia. AR = Aqua regia; DDIW = distilled, de-ionized water.

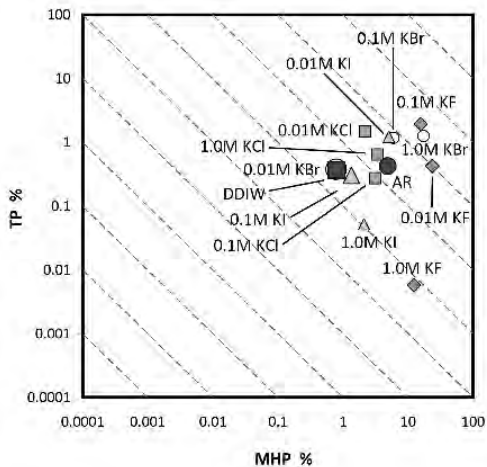


Fig. 2. Logarithmic scatterplot of MHP versus TP at the MHP threshold for Pb, analogous to Figure 1.

In the following graphs, the two best extractions for Zn and Pb are presented in traverses across the Northeast Zone at Gay's River. In these graphs, the dashed line represents the threshold that produces the lowest (most accurate) MHP for each element and digestion.

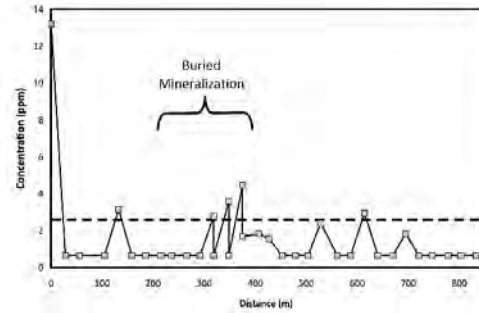


Fig. 3. A N-S soil traverse of Zn concentrations obtained using a 1.0 M KF salt solution partial extraction.

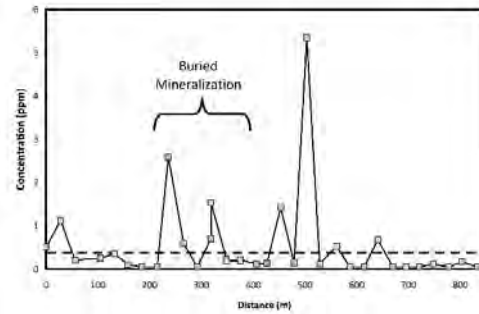


Fig. 4. A N-S soil traverse of Pb concentrations obtained via partial extraction using a 0.01M KBr salt solution.

DISCUSSION

Overall, the best geochemical accuracies for the partial extraction of Zn were obtained with KF salt solutions (MHPs = 0.56 %, 0.005 %, and 0.24 % for 0.01 M, 0.1 M, and 1.0 M KF, respectively; Fig. 1). The effectiveness of KF, over KCl, KBr, and KI, can be attributed to the higher stability constant of ZnF^+ ($\log K_{ZnF^+} = 1.15$) in comparison to the stability constants of the other Zn halides ($\log K_{ZnCl_3^-} = 0.50$, $\log K_{ZnCl^+} = -0.58$, and $\log K_{ZnI_2^0} = -1.69$).

Similarly, the best geochemical accuracies for the partial extraction of Pb were obtained with 0.01 M KBr, 0.1 M KI, and 1 M KI salt solutions (MHPs = 0.79 %, 1.3 %, and 2.1 %, respectively). The effectiveness of KI and KBr can be attributed to the relatively high stabilities of PbI_4^{-2} and $PbBr_3^-$ ($\log K_{PbI_4^{-2}} = 4.40$ and $\log K_{PbBr_3^-} = 3.00$). Although the stability of PbF_3^- ($\log K_{PbF_3^-} = 3.42$) is also relatively high, the extraction efficiency is probably affected by fluoride, which is a weak base,

resulting in a high pH that triggers formation of insoluble lead hydroxide.

A pH-pE diagram illustrating the stability fields of $\text{Fe}^{+2}_{(aq)}$, $\text{Fe}^{+3}_{(aq)}$ and $\text{Fe}(\text{OH})_{3(am)}$ is presented for the 0.01 M KF extraction in Figure 5. This describes the change in ambient pH and pE during digestion.

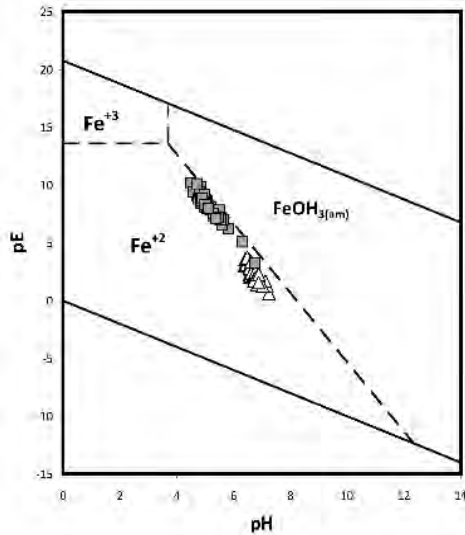


Fig. 5. A pH-pE diagram for the 0.01 M KF extraction. Grey squares represent the soil pH-pE conditions in equilibrium with distilled, de-ionized water (the ambient soil pH-pE conditions), whereas the open triangles represent the pH-pE conditions of the soil-reagent slurries after digestion.

Because most of these soils have similar soluble Fe concentrations, ambient soil sample pore water conditions plot close to a single line with slope of -3, corresponding to the Fe^{+2} - $\text{Fe}(\text{OH})_3$ stability boundary, and confirming the presence of $\text{Fe}(\text{OH})_3$ in the samples (Fig. 5). Because fluoride is a weak base, digestion with KF caused an increase in pH. In contrast, fluoride should not cause a change in pE. Nevertheless, the pE decreased during digestion, precisely because the Fe^{+2} - $\text{Fe}(\text{OH})_3$ buffer responded to the pH change imposed by the KF salt solution. As a result, both pH and pE changed significantly during digestion, pH because of the reagent, and pE because of a redox buffer in the soils.

These changes have significant effects on the solubility of metals in the KF solution. Firstly, the reduction in pE caused some reduction of $\text{Fe}(\text{OH})_3$ to Fe^{+2} , increasing the Fe concentration in the digestion and lowering the stability boundary between Fe^{+2} and $\text{Fe}(\text{OH})_3$. Secondly, the higher pHs resulted in less adsorption of Pb and Zn, and possibly the precipitation of Pb and Zn hydroxides, resulting in less Pb and Zn in solution and more concentrations below detection.

Clearly, knowledge of the redox changes and controls operating during digestion is critical in the interpretation of partial digestion results.

CONCLUSIONS

Partial extractions of KF, KCl, KBr, and KI solutions were tested over a buried CHMS Zn-Pb mineral deposit. Results indicate that these reagents were not very successful in detecting the location of mineralization, as MHPs were not low, indicating relatively random behaviour. Nevertheless, results do appear to behave in ways that suggest that these partial digestions did effectively solubilize adsorbed Pb and Zn from soil particle surfaces. This may suggest that transported ions adsorbed to soil particles above the Northeast Zone are irregularly distributed, and assumptions involving an ideal accumulation zone above or up-dip from this mineralization may not be valid for data interpretation.

ACKNOWLEDGEMENTS

This research was supported by NSERC Discovery Grant #'s 214602-312584 and 220302-217290 to the second and third authors, with contributions from the Acadia Centre for Microstructural Analysis in the K.C. Irving Environmental Science Centre at Acadia University, and via logistical support and access from Acadian Mining Corporation.

3D GIS as a support for ore vectoring

**Eric. de Kemp¹, T.Monecke², E.M. Schetselaar¹, E.Girard³, K. Lauzière³,
M.Sheshpari¹, J. Goutier⁴, G. Perron⁵, E. Grunsky¹, & G. Bellefleur¹**

¹ Geological Survey of Canada, 615 Booth Street, Ottawa, ON K1A 0E9 CANADA
(e-mail: edekemp@nrcan.gc.ca)

² Dep. of Geology and Geological Engineering, Colorado School of Mines, 1516 Illinois Street, Golden, CO 80401
UNITED STATES OF AMERICA

³ Geological Survey of Canada, 490, rue de la Couronne, Québec City, QC G1K 9A9 CANADA

⁴ Géologie Québec - Bureau de l'exploration géologique du Québec, Ministère des Ressources naturelles et de la
Faune, 70 boul. Québec, Rouyn-Noranda, QC J9X 6R1 CANADA

⁵ Mira Geoscience Limited, 310 Victoria, Suite 309, Westmount, QC H3Z 2M9 CANADA

ABSTRACT: Exploration for deep-seated mineral deposits in mature mining camps requires integration of large and heterogeneous data sets. Traditionally, geological, geochemical, and geophysical observations have typically been acquired independently and only within a restricted spatial context. Although methodological developments are still in progress, new 3D GIS technologies already provide powerful tools that can be used to integrate such heterogeneous data sets and to visualize, compare, and characterize geological relationships in a realistic environment. The present paper provides examples from the Noranda mining camp demonstrating the applicability of 3D GIS as a new tool in mineral exploration.

KEYWORDS: 3D GIS, Noranda, Horne Mine, Blake River Group, Mineral Exploration

INTRODUCTION

Mineral exploration in maturing mining camps is challenging as the likelihood of discovering new ore bodies at or close to surface diminishes over time (Fig. 1). Exploration for deep resources is accompanied by an increase in risk and exploration costs as deep targeting relies on limited data. Traditionally, exploration is conducted using one or two methods for near surface mineral detection, with a strong focus on testing geochemical or geophysical anomalies. A more sophisticated exploration strategy is required to locate hidden ore bodies, typically involving interdisciplinary data comparison and interpretation, with a strong focus on a team-based approach.

3D GIS provides a particularly useful method to address the challenges of deep mineral exploration as it permits spatial data analysis in a rigorous fashion (de Kemp 2007). Based on examples from the Noranda camp, one of Canada's most mature and economically important mining camps, the present paper highlights innovative approaches that can be

employed for deep exploration using 3D GIS.

GEOLOGICAL ENVIRONMENT

Massive sulfide exploration in the Noranda camp has traditionally focused on the delineation of intersections between favourable horizons and hydrothermal up-flow zones. In almost all cases, these up-flow zones coincide with synvolcanic structures that crosscut the local volcanic stratigraphy at high angle (Gibson & Galley 2007). Recognition of hydrothermal up-flow zones associated with massive sulfide ore bodies relies on detailed field investigations, supplemented by extensive geochemical surveys and structural, stratigraphic and volcanological analysis (Setterfield *et al.* 1995).

Recalculation of whole-rock geochemical data to normative corundum represents a particularly useful geochemical tool that can point to hydrothermal alteration zones. Normative corundum represents alkali imbalance in sub-alkaline rocks which is generally an indicator of Na depletion and K

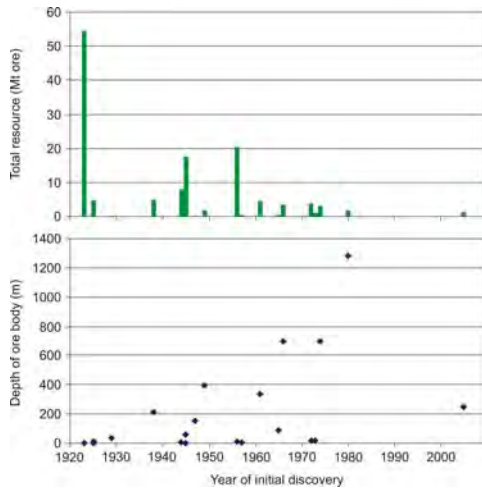


Fig. 1. Tonnage and depth diagram of historic massive sulphide discoveries in the Noranda camp (data from Gibson & Galley 2007).

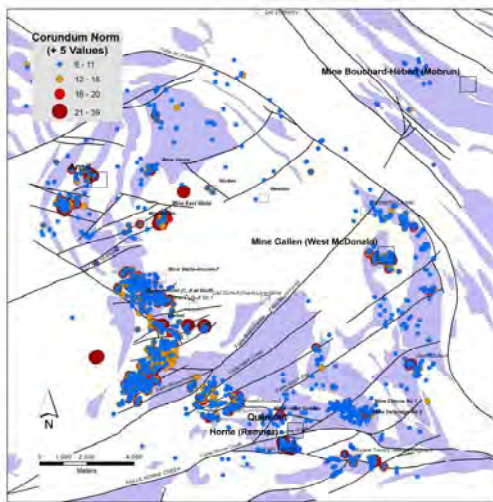


Fig. 2. Distribution of samples in the Noranda camp that are typified by >5 normative corundum values. Felsic volcanic rocks are given as shaded polygons.

enrichment (Grunsky 2007). A simple abundance and map distribution plot highlights the importance of high corundum values as a vector to mineralization (Fig. 2). However, 3D interpretation of the geological relationships has to be performed when data derived from drill holes are included in the analysis (Fig. 3). This is particularly important in the Noranda camp as there is a 40-60° easterly regional fold plunge

which can dramatically offset geochemical plots that are simply projected to surface.

3D GIS also provides the framework for placing geochemical data, lithological information, structural data, and interpreted geologic elements into one common environment (Fig. 3). Analysis of the data shows, for example, that corridors of high normative corundum values coincide with zones of dyke emplacement along early structures. Important hydrothermal up-flow zones such as the McDougall-Despina fault set (Setterfield *et al.* 1995) can be readily identified this way.

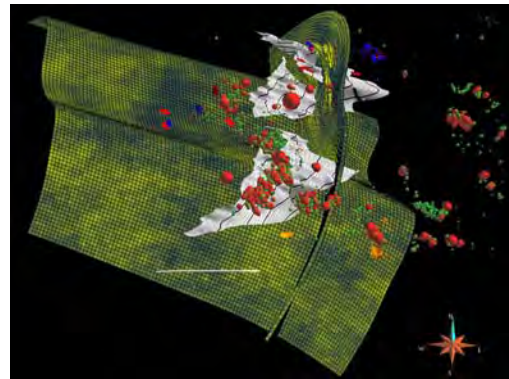


Fig. 3. 3D representation of the Noranda camp looking down plunge. The figure shows the distribution of ore bodies (orange) and a lithological simulation (green-yellow grid). The favourable horizon (white surface) is contoured at 1 km depth intervals. Variably sized spheres with >5 normative corundum values mark the location of alteration zones. Horizontal scale is 5 km at ground elevation (data from E-Sigeom, RNFQ, and Xstrata Copper).

At the scale of an individual deposit, 3D GIS can be used to visualize metal zonation patterns and their relationship to geological elements such as syn-volcanic intrusions (Fig. 4). 3D GIS also represents the tool of choice to examine the geometry of an ore body and to target drilling in areas of possible extensions.

MULTI-DATA INTERPRETATION

Visual correlation between geological, geochemical and geophysical data is

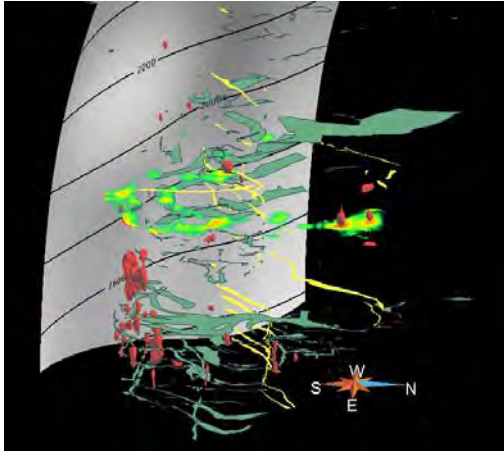


Fig. 4. Lower part of the Horne deposit depicting relationships between synvolcanic mafic dykes (green), late syenite dykes (yellow) and high grade Cu mineralization (red bodies). Structural contours are 200 feet.

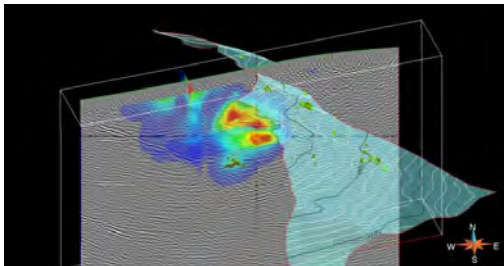


Fig. 5. Locations of massive sulfide ore bodies (green) at marker horizon (C-Horizon) along the Amulet high-resolution seismic line of Bellefleur *et al.* (2007). Intensity of chlorite alteration is superimposed (data from Xstrata Copper).

dramatically enhanced in a 3D GIS environment (Fig. 5). Particularly useful are high-resolution seismic surveys as these data increase the ability to interpret the degree of spatial continuity and the anisotropy directions of geological features observed in drill core and in surface outcrops. Based on geophysical surveys, a single key observation can be upscaled for at least several hundreds of metres.

GEOSTATISTICS

Kriging-based estimation techniques also represent an important toolset allowing the recognition of spatial distribution patterns

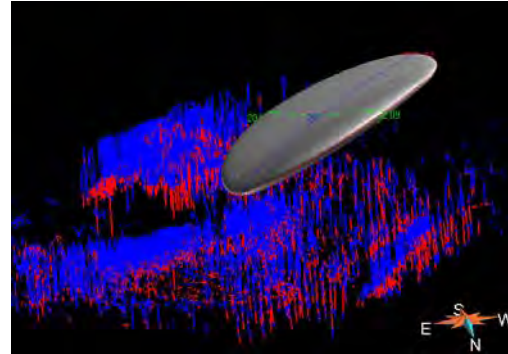


Fig. 6. 3D visualization of a UVW spheriogram in relation to a control drill hole data set. Red and blue intersections indicate the presence and absence of felsic volcanic rocks, respectively (data from Xstrata Copper).

(Figs. 6). Although these techniques have traditionally been used mostly by ore reserve engineers, the mineral exploration community can now take advantage of these powerful geospatial tools in the 3D GIS environment.

DEPOSIT ANALYSIS

The advantages of using 3D GIS technology at the deposit scale can be illustrated using the Horne deposit as an example. Integration of geologic and geochemical data reveals that zones of high Cu content are spatially related to syn-volcanic dykes that are interpreted to mark the locations of early structures (Fig. 7). In an exploration scenario, structural and stratigraphic interpretation combined with a simple visual inspection of the geological relationships could be employed to identify areas of high mineral potential.

INDUSTRY APPLICATION

3D GIS provides new and exciting opportunities for the mineral exploration community. Successful application of this technology, however, requires a change in exploration culture. To take advantage of this technology in the search for deep resources, a number of strategic decisions need to be made by exploration companies. These include:

- (1) Investing in 3D data management

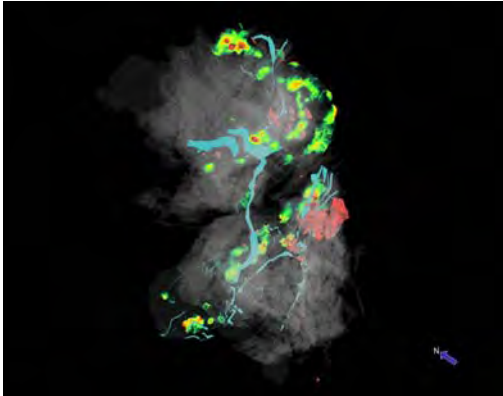


Fig. 7. Top view of the Horne deposit showing massive sulphides (transparent white), synvolcanic mafic dykes and sills (blue), and areas of high Cu grades (red).

through hiring and training of personnel as well as the acquisition of software and hardware.

(2) Development of a corporate 3D IT strategy to build multi-disciplinary 3D exploration teams.

(3) Establishing 3D training sets to define critical geological elements and geometrical relationships at the camp scale through integration of surface and subsurface lithological, geochemical, and geophysical data.

(4) Advancing geological knowledge through 3D cross domain data reconciliation and team-based data interpretation.

ACKNOWLEDGEMENTS

We thank Xstrata Copper for providing access to historical mine information. In particular, Louis Martin helped facilitating

modelling of the Noranda and Bathurst camps. The Horne model was developed with the assistance of Anastasia Vander Most and Susann Stolze. GSC contribution number 20080742.

REFERENCES

- BELLEFLEUR, G., DE KEMP, E., GOUTIER, J., & ALLARD, M. 2007. High-resolution 2D seismic imaging in the Noranda camp and implications for exploration. *Exploration 2007*, Toronto, Sept. 9 to 12, 2007.
- DE KEMP, E.A. 2007. 3-D geological modelling supporting mineral exploration. In: GOODFELLOW, W.D. (ed) *Mineral Deposits of Canada: A Synthesis of Major Deposit-types, District Metallogeny, the Evolution of Geological Provinces, and Exploration Methods*. Geological Association of Canada, Mineral Deposits Division Special Publication, **5**, 1051-1061.
- GIBSON H. & GALLEY A. 2007. Volcanogenic massive sulphide deposits of the Archean, Noranda District, Quebec. In: GOODFELLOW, W.D. (ed) *Mineral Deposits of Canada: A Synthesis of Major Deposit-types, District Metallogeny, the Evolution of Geological Provinces, and Exploration Methods*. Geological Association of Canada, Mineral Deposits Division Special Publication, **5**, 533-552.
- GRUNSKY, E.C. 2007. Geochemical data evaluation and interpretation. In Coker, W.B. (ed) *Exploration Geochemistry - Basic Principles and Concepts, Workshop 2, Exploration 07*, Toronto, 13-17.
- SETTERFIELD, T.N., HODDER, R.W., GIBSON, H.L., & WATKINS, J.J. 1995, The McDougall-Despina Fault Set, Noranda, Québec: Evidence for fault-controlled volcanism and hydrothermal fluid flow. *Exploration and Mining Geology*, **4**, 381-393.

Element Distribution Patterns and Mineral Discoveries using Biogeochemical Methods

Colin Dunn¹, Robert Thompson², Robert Anderson³, & Alain Plouffe⁴

¹Consulting Geochemist, 8756 Pender Park Drive, Sidney, BC V8L 3Z5 CANADA (e-mail: colindunn@shaw.ca)

²Consulting Geologist, 10915 Deep Cove Rd, Sidney, BC V8L 5P9 CANADA

³Geological Survey of Canada, 101-605 Robson St., Vancouver, BC V6B 5J3 CANADA

⁴Geological Survey of Canada, 601 Booth Street, Ottawa, ON K1A 0E8 CANADA

ABSTRACT: Studies over the past half century have greatly advanced the understanding of biogeochemical processes. Uranium biogeochemical anomalies identified 30 years ago are now known to contain multiple zones of rich U deposits. Mapping of multi-element patterns in southern British Columbia suggests that, among other elements, Tl and Hg may be biogeochemical pathfinder elements for Broken Hill-type Sedex deposits. The halogens in plants, too, may provide additional vectors toward base metal-mineralized areas. Opportunistic sampling during field mapping projects can add important focus for detailed exploration, and help trace the source of till anomalies. Molybdenum in cedar foliage has outlined the MAX Moly mine area and generated additional targets of similar magnitude of unknown origin. Investigation of one of these in southern BC has resulted in the discovery of low-grade mineralization in rocks exhibiting similar characteristics to the MAX Moly deposit. Moving forward, more emphasis on the distribution of volatile elements (e.g., Hg; halogens associated with fluid inclusions) as well as commodity elements, and an improved understanding of the role of bacteria in mobilizing metals should further entrench the role of biogeochemical methods for assisting in the exploration for mineral deposits.

KEYWORDS: *Biogeochemistry, Exploration, Uranium, Base Metals, Molybdenum*

INTRODUCTION

Over the past half century there have been significant developments in the understanding and application of biogeochemical methods to the search for buried mineral deposits – both deep and shallow. It is now apparent that depth of root penetration and relationship of plant chemistry to soil composition are not critical to obtaining subtle biogeochemical responses to deeply buried mineralization. Various processes invoked for explaining partial leach soil anomalies are equally relevant for explaining signatures of elemental anomalies in plant tissues. These include movement by diffusion, electrochemical cells, seismic pumping, artesian flow, and particularly bacterial movements. These processes are, however, somewhat modified and controlled by plant requirements and tolerances, so that the ‘barrier mechanisms’ identified by Kovalevsky (1979) come into play and need to be

considered when interpreting data from biogeochemical surveys.

Information from surveys conducted decades ago can now be viewed in light of subsequent exploration activities, and the value of biogeochemical surveys (when and where to use the techniques) can be more accurately assessed and applied using the rapidly-advancing analytical methodologies (e.g. ICP-MS) that are now widely available.

URANIUM

More than 30 years ago it became apparent that sandstones of the Athabasca Basin in Saskatchewan are host to significant deposits of uranium. Previous work elsewhere, primarily in the Colorado Plateau (Cannon 1964) and the former Soviet Union (Kovalevsky 1972), had shown that plants are capable of accumulating high concentrations of U. Surveys near the eastern margin of the Athabasca Group revealed an area of

about 10,000 km² within which U in spruce twigs consistently contained more than 10 times the normal background level of U in plant tissues (10 ppb U in dry tissue, Markert 1994; Dunn 2007), with far higher concentrations extending over several thousand km². This 'Wollaston Uranium Biogeochemical Anomaly' (Dunn 1982) is underlain by the Wollaston Domain that hosts 25% of global U production. Within this anomaly, where depth to the U-hosting Athabasca unconformity with the Wollaston Domain ranges from 0-300 m, detailed surveys over known mineralization showed a strong response in the vegetation. Over the McClean Lake deposit, at a depth of 150 m, U in spruce trees showed the classic Rabbit's Ears-type of response that has been attributed to electrochemical cells (Govett 1976). Over the 30 years since that discovery, within the Wollaston anomaly more than 16 U deposits have been discovered that contain more than 1 million lbs U₃O₈. The most recent of these is the Roughrider zone of Hathor Exploration Ltd. discovered in 2008, where drilling has intersected up to 23 m grading >11 % U₃O₈ at a depth of 300 m (<http://www.hathor.ca>). Currently, the CAMIRO Athabasca project is testing the surface signatures of many geochemical techniques, including vegetation, to known mineralization more than 400 m deep.

BASE METALS

The Geological Survey of Canada has a 'Targeted Geoscience Initiative' (TGI-3) program, which in south and south-central British Columbia helps stimulate base metal exploration activities. The terrain in much of this area is rugged, has variable thickness of till cover and is heavily forested, yet in light of past discoveries it remains highly prospective for various types of metal deposit. Of five known groups of Zn/Pb deposits within a cover sequence that mantles Palaeoproterozoic core gneiss, mineralization at Kingfisher and adjacent deposits comprises the only group below the tree-line. The widespread regional distribution of thin calcareous units that host these deposits lends

credence to the concept that similar mineralization may lie beneath the extensive area that is covered by a veneer of glacial deposits and dense forest.

As part of the TGI-3 program several biogeochemical surveys have been undertaken. A helicopter-supported survey was conducted over 700 km² that included the stratigraphic setting of the Kingfisher deposit and similar stratigraphic units that border Tsuius Creek, to collect 562 Douglas-fir tree tops at 1 km spacing.

Analysis of dry twigs revealed areas of Zn enrichment with associated elements (Cd, Tl and Mn) that show a spatial relationship to areas of Pb enrichment (with Fe, Hg, REE, Al, and Ti), especially south of Tsuius Creek. A strong Pb/Zn zonation is typical of Broken Hill-type Sedex mineralization. Of particular note were localized high Tl values.

Subsequent analysis of the ashed needles from these twigs confirmed the patterns established from the dry twigs. It served to enhance some signatures (notably Ag) and added a layer of data for the halogens, demonstrating a F association. Also from these additional analyses a pattern of Cd and B enrichments at Kingfisher was evident.

Follow-up ground studies involved the analysis of outer bark from western hemlock collected at 100 m sample spacing over the Tl anomaly south of Tsuius Creek. This permitted more clearly defining the extent of the Tl anomaly (600 m x 600 m) and its relationship to other trace elements. Figure 1 shows the Tl anomaly and the spatial relationship of Hg which appears to define a conjugate set of lineaments interpreted as leakage from structural weakness. The multi-element association at this locality suggests that Tl and Hg may be pathfinder elements to concealed base-metal mineralization.

In the Bonaparte Lake area of south-central BC, samples of outer bark from Engelmann spruce and lodgepole pine were collected on an opportunistic basis during the course of field mapping. Consequently, the sample distribution was uneven, but expedient and sufficient to

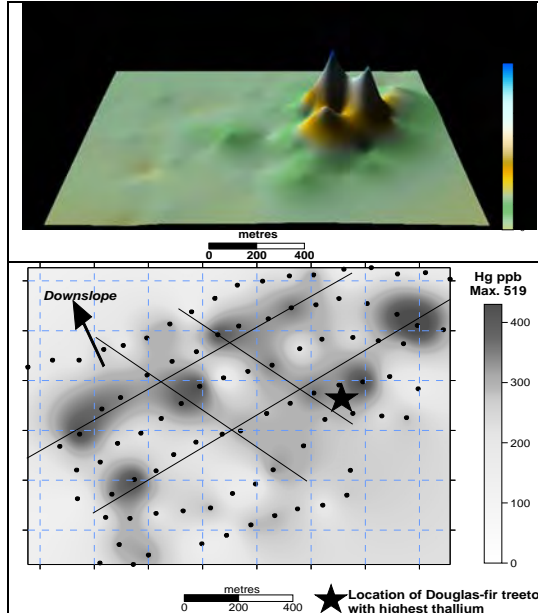


Fig. 1. Thallium (3D plot, viewed from south) and Hg in dry western hemlock bark – Tsuius Creek, BC (Dunn & Thompson 2009a).

provide indications of areas with potential concealed mineralization.

Five hundred samples were collected. The analytical data provided a basis for comparing and contrasting the geochemical signatures of the two types of bark and defining those elements that generated the same or similar signatures while establishing other elements that generated different distribution patterns because of tolerances to, or requirements for, those elements. Most elements generated similar distribution patterns attesting to the robustness of the biogeochemical method and reinforcing the significance of the signatures (Dunn & Anderson 2009). Elements that tended to show different patterns (e.g., Ba, Sr) were those that were significantly more concentrated in a particular sample medium. The pine bark was more enriched than the spruce in Ag, Al, Cd, La, Pb and Sb. Conversely, spruce was more enriched in Ba, Ca, Mn, Rb, Sr, and Zn.

Results from a recent till survey (Plouffe *et al.*, 2009) revealed unusually high concentrations of thorianite in the heavy mineral concentrates. Plots of thorianite-

related elements – Th, U, and REE – in the conifer bark samples indicate an area of subtle enrichment that is located up-ice from the proven direction of ice movement. This may help to more closely focus on the source of the thorianite. Multi-element signatures in the bark assisted, too in identifying known Cu mineral occurrences, delineating areas of Au enrichment and possibly PGE, as well as defining signatures characteristic of the principal plutonic and volcanic units. For example, there are significant increases in Ni, Cr and Co over known and concealed mafic to ultramafic units.

MOLYBDENUM

The MAX property lies near the north end of the Kootenay Arc in tightly folded, strongly sheared Palaeozoic metasedimentary rocks. The reported commodities are Mo, W, Pb, Zn and Cu. The area is heavily forested rugged terrain with outcrop largely obscured by a cover of till. Cedar foliage was collected along several traverses up the steep hillside toward known mineralization.

The location of the discovery outcrop was clearly outlined by Mo in cedar, and two additional Mo anomalies of unknown source and similar intensity were identified (Fig. 2). In mid-2008, Roca Mines drilled two drill holes, 100 m apart that targeted the northern biogeochemical anomaly. They reported “*Intense silicification, hornfelsing, locally strong quartz veining, and pervasive sericite alteration with trace molybdenite throughout...reminiscent of the MAX resource itself where the extent of a relatively minor molybdenite mineralized zone on surface lies atop a large-scale mineralized deposit currently being mined.*” Roca Mines press release, 12th August 2008 (www.rocamines.com).

CONCLUSIONS

(1) Examination of data from past biogeochemical surveys in context of subsequent discoveries has established their relationship to mineralization.

(2) Pathfinder and commodity element distribution patterns from recent surveys have delineated new targets for base

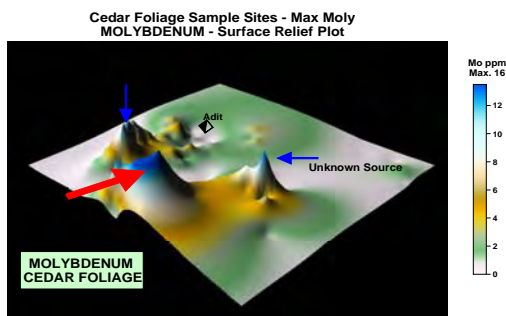


Fig. 2. 3D plot of Mo in cedar foliage. MAX Moly mine (Dunn & Thompson 2009b).

metals and other commodities, and resulted in new discoveries.

(3) It is anticipated that focus on volatile elements (especially halogens and Hg) and improved understanding of processes (notably bacteria) in mobilizing metals from depth will provide further successes for biogeochemical surveys.

REFERENCES

CANNON, H.L. 1964. Geochemistry of rocks and related soils and vegetation in the Yellow Cat area, Grand County, Utah, *United States Geological Survey Bulletin* **1176**, 127 p.

DUNN, C.E. 1982. The massive Wollaston Uranium Biogeochemical Anomaly in the boreal forest of Northern Saskatchewan, Canada. In: *Uranium Exploration Methods: Review of the NEA/IAEA Research and Development Programme, Paris, France, 1 - 4 June, 1982*, OECD Nuclear Energy Agency, 477-491.

DUNN, C.E. 2007. Biogeochemistry in Mineral Exploration. In: HALE, M. (ed) *Handbook of Exploration and Environmental Geochemistry* **9**, Elsevier, Amsterdam, 462 p.

DUNN, C.E. & ANDERSON, R.G. 2009. Biogeochemical surveys in the Bonaparte Lake area, south-central British Columbia (NTS 92P09 and 10). *Geological Survey Canada Open File*, **6149** CD-ROM

DUNN, C.E. & THOMPSON, R.I. 2009a. Investigations of base metal and gold biogeochemical anomalies in the Mabel Lake area, southern British Columbia (NTS 82L09 and 10), *Geological Survey Canada Open File*, **6147**, CD-ROM.

DUNN, C.E. & THOMPSON, R.I. 2009b. Biogeochemical signatures of the area around the MAX molybdenum mine. *Geological Survey Canada, Current Research* **2174**, CD-ROM.

GOVETT, G.J.S. 1976. Detection of deeply buried and blind sulphide deposits by measurement of H⁺ and conductivity of closely spaced surface soil samples. *Journal of Geochemical Exploration*, **6**, 359-382.

KOVALEVSKY, A.L. 1972. Biogeochemical prospecting for uranium deposits, *Journal Atomic Energy*, **33**, 647-652.

KOVALEVSKY, A.L. 1979. *Biogeochemical exploration for mineral deposits*. Oxonian Press Pvt. Ltd., New Delhi, 136 p.

MARKERT, B. 1994. Progress report on the element concentrations cadastre project (ECCP) of INTERCOL/IUBS, *International Union of Biological Sciences, 25th General Assembly, Paris*, 54 p.

PLOUFFE, A., BEDNARSKI, J.M., HUSCROFT, C.A., & MCCUAIG, S.J. 2009. Gold grain content of till in the Bonaparte Lake map area, south central British Columbia. *Geological Survey of Canada Open File* **6047**, CD-ROM.

ESS Contribution No. 20080669

Spatio-temporal geochemical dynamics of an acid rock drainage stream in the Yukon Territory: implications for mineral exploration

Kristen B. Feige^{1,2}, Paul Gammon², & Danielle Fortin¹

¹University of Ottawa, 140 Louis Pasteur Private, Ottawa ON K1N 6N5 CANADA (email: kfeige@NRCan.gc.ca)

²Geological Survey of Canada, 601 Booth St., Ottawa ON K1A 0E8 CANADA

ABSTRACT: Acid rock drainage (ARD) is a natural phenomenon known to occur via water-rock interactions at or near base-metal deposits. As part of the Geological Survey of Canada (GSC) TGI3 (Targeted Geoscience Initiative) Deep Search Project, this research aims to enhance our understanding of the surficial geochemical and biogeochemical processes that influence the mobility and dispersion of elements, and to evaluate their importance when using ARD stream geochemistry to detect subsurface mineralization. A sampling campaign was conducted at an ARD stream at the XY-deposit (Pb-Zn SEDEX (sedimentary exhalative) deposit), Howard's Pass area, Yukon Territory, during the summer of 2008. The watercourse was sampled across the spring-summer seasonal cycle for aqueous geochemistry, authigenic mineral precipitate geochemistry and mineralogy, and detrital components. Our results indicate that seasonal changes may lead to spatio-temporal variations in surficial processes that effect element dispersion, and thus these processes require further investigation to determine their importance when using ARD geochemistry to detect subsurface mineralization.

KEYWORDS: SEDEX deposit, Yukon Territory, acid rock drainage, mineral exploration vectors, groundwater.

INTRODUCTION

Acid rock drainage (ARD) is a natural phenomenon generated through the interaction of groundwaters and base-metal deposits, primarily, the oxidation and dissolution of Fe-sulphide minerals. The acid generated from these reactions is a strong agent of rock dissolution, and consequently ARD groundwaters carry with them a record of the rocks encountered along their flow path. Stream waters such as these may carry anomalous loads of dissolved base metals, which could potentially be used by the exploration industry to detect subsurface mineralization. Surficial geochemical and biogeochemical processes strongly influence element mobility and dispersion in ARD streams, especially in cold climates where extreme seasonal changes can lead to spatio-temporal variation in these processes. As such, this project aims to investigate the degree to which these processes are important when using ARD to detect subsurface mineralization. It is doing so by investigating a single stream with ARD

emanating off the "XY" SEDEX deposit, Howard's Pass, Yukon Territory.

GEOLOGICAL SETTING

The XY-deposit at Howard's Pass is a stratabound Pb-Zn deposit formed during the lower Silurian, hosted by a succession of carbonates, cherts and carbonaceous pyritic shales in a syncline structure that underlies Sugar Mountain and Yara Peak (Fig. 1; Morganti, 1979). The deposit is comprised of finely laminated sphalerite, galena, chalcopyrite, and pyrite. Tectonic deformation has left the bedrock highly fractured, which is inferred to control the flowpath of groundwaters emanating from the deposit (Jonasson and Goodfellow, 1986). During the spring, stream drainage from the deposit is fed mainly by snowmelt, while in the summer meteoric and groundwaters are important sources of runoff. A detailed description of the Howard's Pass XY-deposit can be found in Morganti (1979) and Goodfellow *et al.* (1983).

SAMPLING AND METHODOLOGY

The sampling campaign on the ARD stream was conducted between June and August, 2008. Samples of surface water and associated authigenic mineral precipitates and detrital sediment were collected on a daily basis. Samples were taken along the entire length of the ARD stream, ranging from an altitude of 1690 m.a.s.l. to approximately 1400 m.a.s.l. The temperature, pH, Eh, and DO were measured *in situ* using a pre-calibrated field multimeter (Eureka Manta multiprobe). Dissolved ferrous iron was measured colourimetrically on-site by the 1,10-phenanthroline method. The surface waters were filtered (0.45 µm pore size) and acidified with ultra-pure HNO₃ to a final concentration of 1% (v/v) for major and trace element analysis. Filtered, unacidified samples were also collected for major inorganic anions analysis. Sediments were collected daily. All samples were securely stored at 4 °C for up to four weeks prior to shipment to the GSC laboratories in Ottawa.

Major and trace element concentrations in the acidified samples were determined via ICP-MS (inductively coupled plasma mass spectrometry) and ICP-OES (inductively coupled plasma optical emission spectroscopy) at the GSC's Geochemistry Research Laboratory. Dissolved anion concentrations were measured by IC (ion chromatography) on the unacidified samples, also at the GSC's Geochemistry Research Laboratory. Characterization of the sediment mineralogy and texture by XRD (X-ray diffraction), SEM (scanning electron microscopy) and TEM (transmission electron microscopy) is ongoing.

RESULTS AND DISCUSSION

Interpretation of our hydrogeochemical results is complicated by the paucity of baseline data for ARD streams about the XY-deposit, which would allow us to identify "anomalous" metal concentrations. Baseline datasets for streams in the Selwyn Basin were compiled by Goodfellow (1983), however, these relate to alkaline to circumneutral streams,

precluding their use in our low pH system given the enhanced dispersion and mobility of base metals under acidic conditions.

Water samples collected during June have lower (4 to 44-fold lower) dissolved base metal concentrations (Table 1) relative to samples taken in August (Table 1), reflecting base flow dilution from the spring freshet. The spatial variation in authigenic mineral precipitates in ARD streams at the XY-deposit becomes increasingly visually apparent as the summer season progresses. Their bulk mineralogy and elemental composition is currently being analyzed, as well as their relationship with the stream microbial community. Such seasonal variation is likely a result of the temporal evolution of the stream hydrochemistry. These changes may be governed by the local hydrological conditions (fluctuations in groundwater flow and volume) and the underlying geology, both of which can contribute to base-flow dilution and acid-neutralization processes. The distribution of indigenous microorganisms can also influence the spatial evolution of ARD waters; for example, algal mats growing in ARD waters at MacMillan Pass, Yukon Territory, have been observed to concentrate Zn and Pb by one and five orders of magnitude, respectively, reflecting the ability of microorganisms to influence their local environment (Lawrence *et al.*, 1998). Together, the aforementioned surficial processes result in the spatial attenuation of dissolved base metals, through adsorption/coprecipitation reactions with authigenic mineral precipitates. Similar spatial variation has been reported for other ARD streams (Lee *et al.* 2002; Espana *et al.* 2006; Eppinger *et al.* 2007).

For mineral exploration purposes, spatio-temporal variations in ARD hydrochemistry may provide indicators to the location of an orebody; e.g., anomalous concentrations of dissolved base metals may suggest that the orebody is proximal to this anomaly. At XY, the highest concentrations of dissolved base

Table 1. Temporal variation in dissolved Zn (ppm) and Pb (ppb) concentrations for sites proximal to near-surface mineralization. Sampling locations distal to the near-surface mineralization were not accessible in June. See Figure 1 for reference to sampling location.

Sampling location	Zn (ppm)			Pb (ppb)		
	XY 5	XY 6	XY 7	XY 5	XY 6	XY 7
June 21/08	13.50	11.10	9.50	0.33	0.06	0.03
August 3/08	50.80	44.30	42.60	1.87	1.80	1.33
Concentration factor	4	4	4	6	30	44

Table 2. Spatial variation observed for select elements, moving from upper (1690 m.a.s.l.) to lower (1497 m.a.s.l.) reaches of the ARD stream. Concentrations are given in ppm for all elements, except Pb, which is in ppb.

Sampling location	pH	S	Mg	Al	Zn	Fe	Si	Ni	K	Na	Pb
S1	3.3	3503.7	996.4	847.5	475.3	303.1	29.1	15.3	4.3	1.9	10.7
XY2	3.4	1092.9	314.5	187.6	134.4	84.4	13.1	4.4	2.2	1.4	8.7
XY3	3.5	930.9	261.9	148.6	109.9	55.5	11.9	3.7	2.1	1.2	7.5
XY4	4.3	667.5	194.4	103.1	76.8	25.6	9.7	2.5	1.9	1.0	3.8
XY4.5	4.7	551.2	186.9	45.8	56.4	16.9	7.6	2.0	2.0	1.0	2.2
XY5	5.0	503.9	169.2	22.3	50.6	14.6	6.5	1.8	1.8	0.9	1.5

metals (Table 2) are found at the sampling location where the ARD waters first emanate from the skree (elevation 1690 m, sampling location “S1” in Fig. 1). However, this site is distal (>100 m vertically) to the orebody in comparison to other sites such-as “XY 4.5” (Fig. 1). These more proximal sites carry a dissolved metal load that is approximately 10-fold lower (Table 2). The lower dissolved Zn concentrations proximal to the near-surface mineralization are likely the result of preferential partitioning of Zn to biofilms, biominerals, and sediments under the local geochemical conditions along the flow path. Determining how one could identify the proximal sites as those closest to the orebody is part of ongoing research. This research includes analyzing biominerals and sediments to determine the extent to which temporal changes in the local hydrology and microbiology influence (or potentially mask) spatial changes in element mobility within the ARD stream.

CONCLUSIONS

The spatio-temporal variations observed at an ARD stream about the XY-deposit,

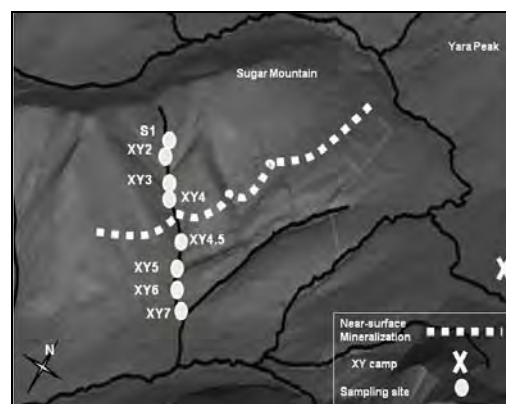


Fig. 1. Surface projection of the XY-deposit, Yukon Territory.

and other sites, suggest that a systematic understanding of these environments is required to maximize their use for mineral exploration. Static, single snap-shot measurements are insufficient for the establishment of baseline data from which anomalies related to potential subsurface mineralization can be detected, as these will generally not characterize the inherently dynamic nature of ARD systems. Without an intimate understanding of the surficial geochemical and biogeochemical processes influencing

the base metal concentrations in ARD systems, near-surface mineralization may go undetected by geochemical reconnaissance studies.

ACKNOWLEDGEMENTS

We thank the GSC and the TGI3 Deep Search program for funding this research, Selwyn Resources for their logistical support and permission to access the site during the field season, Andre Pellerin for his assistance in the field, and Judy Vaive and Pierre Pelchat for analyzing our water chemistry samples.

REFERENCES

- EPPINGER, R.G., BRIGGS, P. H., DUSEL-BACON, C., GILES, S.A., GOUGH, L.P., HAMMARSTROM, J.M., & HUBBARD, B.E. 2007. Environmental geochemistry at Red Mountain, an unmined volcanogenic massive sulphide deposit in the Bonnifield district, Alaska Range, east-central Alaska. *Geochemistry-exploration, environment, analysis*, **7**, 207 – 223.
- ESPANA, J.S., PAMO, E.L., PASTOR, E.S., ANDRES, J.R., & RUBI, J.A.M. 2006. The removal of dissolved metals by hydroxysulfate precipitation during oxidation and neutralization of acid mine waters, Iberian Pyrite Belt. *Aquatic Geochemistry*, **12**, 269 – 298.
- GOODFELLOW, W.D., 1983. Stream sediment and water geochemistry of the Howard's Pass (XY) Zn-Pb deposit and Nor Zn-Pb-Ba occurrence, Selwyn basin, Yukon and Northwest Territories, Geological Survey of Canada, Open File 845, p. 12.
- GOODFELLOW, W.D., JONASSON, I.R. & MORGANTI, J.M. 1983. Zonation of chalcophile elements about the Howard's Pass (XY) Zn-Pb deposit, Selwyn Basin, Yukon. *Journal of Geochemical Exploration*, **19**: 503 – 542.
- JONASSON, I.R. & GOODFELLOW, W.D. 1986. Sedimentary and diagenetic textures, and deformation structures within sulfide zone of Howards Pass (XY) Zn-Pb deposit, Yukon and Northwest Territories. In: *Mineral Deposits of Northern Cordillera*, Special Volume **37**, Canadian Institute of Mining and Metallurgy, 51-70.
- LAWRENCE, J.R., SWERHONE, G.D.W. & KWONG, Y.T.J. 1998. Natural attenuation of aqueous metal contamination by an algal mat. *Canadian Journal of Microbiology*, **44**: 825 – 832.
- LEE, G., BIGHAM, J.M. & FAURE, G. 2002. Removal of trace metals by coprecipitation with Fe, Al and Mn from natural waters contaminated with acid mine drainage in the Ducktown Mining District, Tennessee. *Applied Geochemistry*, **17**, 569 – 581.
- MORGANTI, J.M. 1979. *The geology and ore deposits of the Howards Pass area, Yukon and Northwest Territories: the origin of basinal sedimentary stratiform sulphide deposits*. Ph.D. thesis, University of British Columbia.

Soil mineralogy and geochemistry of surficial materials around the XY base-metal massive sulfide deposit, Selwyn Basin, Yukon

P. Gammon,^{1,2} W. Goodfellow,^{1,2} J. Vaive¹, P. Pelchat¹, & K. Feige^{1,2}

¹ Geological Survey of Canada, 601 Booth St., Ottawa, ON K1A 0E8 CANADA
(e-mail: pgammon@nrcan.gc.ca)

² Department of Earth Sciences, University of Ottawa, ON K1N 6N5 CANADA

ABSTRACT: Selwyn Resources' Howard's Pass deposits in eastern Yukon, Canada, contains 386 Mt of massive sulfide mineralization distributed across 13 individual deposits. As part of the Geological Survey of Canada's (GSC) TGI3 Deep Search Project, soil samples were collected across the 'XY' deposit with the aim of developing new exploration strategies that can discriminate such mineralisation from the high local background values. Earlier research demonstrated that Pb is an effective discriminator of the XY deposit. In this research, Pb and Zn from a hydroxylamine partial leach analysis of 'B' horizon soils discriminate the XY deposit. However, in contrast to many surveys that focus on the uppermost B horizon, this survey demonstrates that the least weathered portions of the B horizon soils are those that effectively discriminate the orebody location. This is likely due to the geochemical signature having a detrital and not hydrochemical origin. It seems likely that the dominant pyritic black shale clasts within the XY soils provide a substrate that is readily destabilised by pedogenesis, and which are then consequently soluble via this partial leach protocol. It is likely that the soil matrix strongly influenced the results of this partial leach experiment.

KEYWORDS: *soil sampling; mineral exploration, partial, leach, base metals, Yukon*

INTRODUCTION

The Selwyn Basin in the Yukon Territory of Canada hosts major SEDEX Zn-Pb sulphide deposits, the biggest being the relatively large (~90.4 Mt) deposits at Howard's Pass (XY), owned by Selwyn Resources (Morganti 1979; Goodfellow 2004). This research focuses on the surficial geochemical expression of the 'XY' deposit, one of the 13 known orebodies within the Howards Pass district.

Soil geochemistry is a common method in many mineral exploration programs. Generally the aim of soil sampling programs is to determine a surficial geochemical expression of the rocks underlying the soil and overburden. Any potential buried mineralization is then interpreted from geochemical departures from background values. In the Selwyn Basin the problem is the background values, which on the whole are very high due to an abundance of sulfidic black shales (Morganti 1979; Goodfellow 2004). The research question addressed herein

is: "what is the best soil sampling protocol for high background geological settings such as the Selwyn Basin?" We addressed this question using a suite of 'partial leach' geochemical protocols on soil sample transects across the XY deposit. We only report the results of a hydroxylamine partial leach here, which is designed to dissolve amorphous iron oxides within the sample.

GEOLOGICAL SETTING

The XY deposit is a stratiform Zn-Pb-dominated massive sulfide 'SEDEX' orebody (Goodfellow 2004). It is situated near the base of the Duo Lake Formation within the Road River Group (Morganti 1979). The Duo Lake Formation is comprised predominantly of carbonaceous, sulfidic shales, with subsidiary cherty and phosphatic components in the strata immediately surrounding the ore horizon (Goodfellow *et al.* 1983). The Duo Lake Formation is underlain by carbonates of the Rabbitkettle Formation, which outcrop in parts of the valley in

figure 1. This sedimentary package underwent multiphase deformation during the Laramide Orogeny.



Fig. 1. Photograph across the alpine terrain at XY, with a hummocky till plain in the foreground backed by the orebody-hosting 'Sugar Mountain'. The soil sample transect follows the black line, stopping at the end of soils and start of the scree slope. The XY orebody's surface projection is at the base of the mountain.

Surficial deposits at XY are dominated by tills and colluvium, which have been locally reworked by alluvial and glacio-fluvial processes (Figs. 1 & 2a). On the transect reported herein, the depth of overburden varies from negligible on mountain sides to at least 5 m thick in central parts of the till plain in central valley areas (unknown maximum thickness). In the section of the traverse the XY ore zone is c. 10 m thick, and occurs below c. 3 m of colluvial overburden (Fig. 2). Pedogenesis is generally restricted to minor to moderate horization that has produced predominantly brunisols (Canadian Soil Classification System, Agri-Canada 1998).

METHODS

One hundred metre-spaced soil samples on two traverse lines were collected in the summer of 2007 (here we report one of those lines, Fig. 1). At each site the B horizon was sampled in 15-cm thick intervals; dependent on the thickness of the B horizon, between one and three samples per site were collected. B

horizons at XY were generally pervasively red at the top transitioning to mottled red-brown in lower samples, indicating lower degrees of oxidation and weathering with increasing depth.

The partial leach protocol used a 2-h leach, using 40 ml of 0.25 M hydroxylamine hydrochloride in 0.1 M HCl at 60°C, on 1 g of the <63- μ m fraction (Cameron *et al.* 2004). This hydroxylamine leach is designed to dissolve secondary iron and manganese oxides. This relatively aggressive leach protocol will also dissolve phosphatic, calcareous and amorphous clay components, and will likely desorb any ions weakly bonded to other components.

RESULTS AND DISCUSSION

The partial leach results indicate that there was considerable dissolution of multiple phases, including iron oxides (Fe, Fig. 2D), clays (Al, Fig 2F), carbonates (Fig. 2E), and phosphates (Fig. 2H).

Phosphatic shales and carbonates are at the surface only in the lowest portion of the valley. This is reflected in peak Ca and P values being at alluvial sites 10 and 11, indicating that the phosphates and carbonates are likely sourced from local erosion. Furthermore, the Ca and P values are highest in the lowest, least-weathered portions of B horizons, suggesting that weathering has leached these relatively soluble components from the upper portions of the soil.

Overall, the Fe and Al values by this partial leach are high, suggesting that this partial leach aggressively dissolved these soils, irrespective of the soil facies. Despite the changes in red colouration, and SEM petrography indicating mineral authigenesis was predominantly in the uppermost B horizon sample, with minimal secondary mineral authigenesis in the lower B horizon samples, the partial leach extracted more Fe from samples lower in the B horizon. Aluminium dissolved by this partial leach was consistently high across all B horizon samples. This distribution of high Al and Fe dissolution suggests that the partial leach did not only dissolve

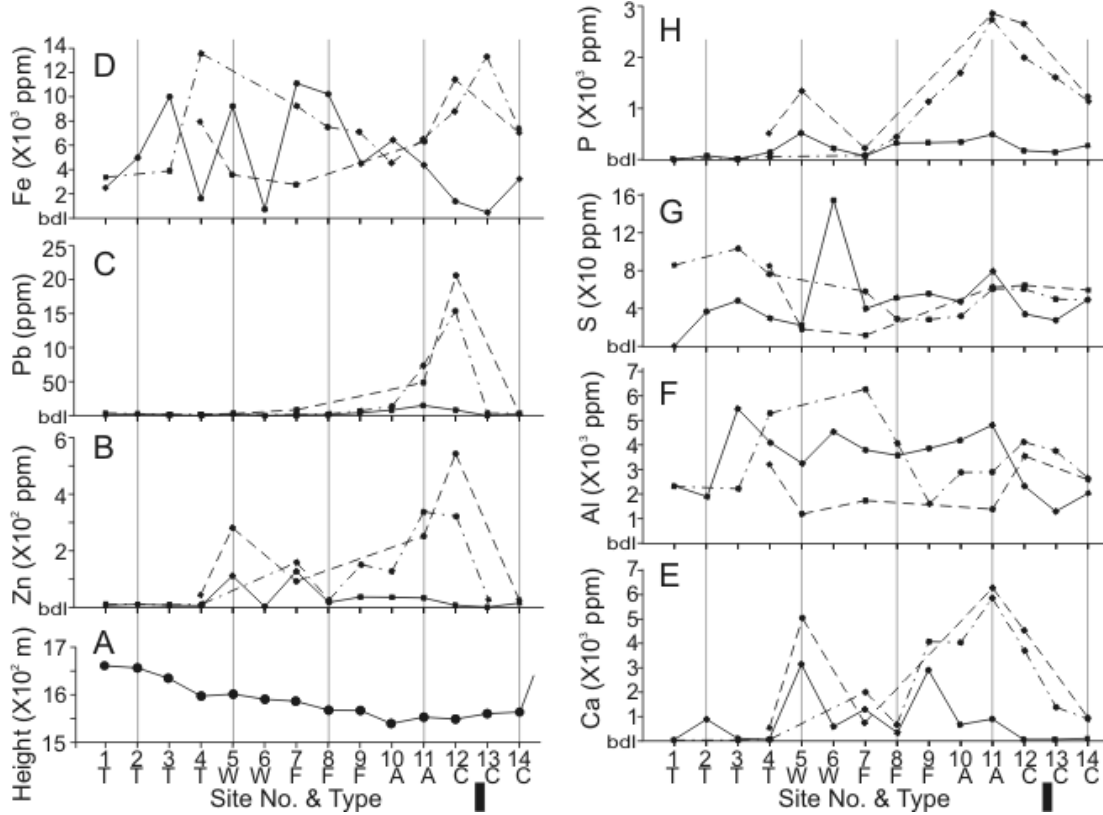


Fig. 2. Elevation (A) and chemical (B-H) crossplots against soil sample site number. Transect is south (left) to north (right). The different B horizon soil depths are given by different line characteristics: solid line = uppermost 15 cm of the B horizon; dashed-dotted line = 15-30 cm of the B horizon; dashed line = 30-45 cm of the B horizon. The XY orebody's surface projection is at the black bar. Gray lines in the background are to aid site projection across crossplots. The depositional characteristics of each soil site are: T – till; W – seasonally waterlogged till; F – fluviglacial till; A – alluvium; C – colluvium.

secondary B horizon clays and oxyhydroxides, but also some other Fe- and Al-bearing components of the soil. SEM, XRD, and heavy mineral analysis all failed to report sulfides in any B horizon sample. Hydrolytic oxidation of pyrite forms sulphuric acid, which would likely destabilise the metamorphic clay components of the shale clasts. This would likely make them, plus the ex-pyrite Fe, susceptible to dissolution during this partial leach, which may be the reason for the relatively high Al and Fe values reported for this leach. Thus the Al, Fe, and S geochemical signatures found in this partial leach procedure are likely a modified detrital signature rather than a secondary pedogenic signature.

Petrographic research is investigating the weathering paragenesis of these samples.

Previous research had demonstrated that Pb was a good pathfinder element for the XY orebody (Goodfellow *et al.* 1983). However, the processes by which the soil materials around the XY orebody had obtained their geochemical signature were previously unclear. In this partial leach experiment, a number of pathfinder elements (e.g. Zn and particularly Pb; Figs. 2B, 2C) clearly discriminate the orebody, but only in the lower B horizon samples. Pathfinder elements in the upper B horizon samples do not discriminate the orebody horizon. This again suggests that the geochemical signal is not derived from weathering-induced B-horizon mineral precipitation, but more likely from detrital

components leached by the hydroxylamine protocol. This contrasts with the many soil sampling protocols that emphasize the uppermost B horizon as the preferred sample medium. These soil sampling protocols are primarily attempting to access a hydrogeochemical record of the underlying rocks that may be contained within secondary soil minerals (e.g. Mann *et al.* 1998; Cameron *et al.* 2004). Essentially this hydroxylamine leach experiment has detected a detrital record of the underlying orebody, and not the hydrochemical record generally sought in a soil sample partial leach experiment. The detrital record was likely made soluble via this partial leach protocol through pedogenic weathering processes.

CONCLUSIONS

This research investigated the soil geochemistry over the XY deposit, Howard's Pass, Yukon Territory, using a hydroxylamine partial leach protocol. In this case study:

- (1) The XY deposit location was clearly discriminated using Pb and Zn from the high background values in lower B horizon soils, but not in upper B horizon soils. This finding contrasts the many protocols that emphasize the upper B horizon as the most appropriate for soil sampling.
- (2) The geochemical signature of the XY orebody within these soils is likely derived from detrital sources, not hydrochemical sources. A hydrochemical signature of the XY orebody was not isolated in these soils by this protocol. Perhaps a less aggressive partial leach protocol may be more suitable given the substrate type.
- (3) Substrate types and the pedogenic processes they prompt can influence the results in partial leach experiments.

ACKNOWLEDGEMENTS

We thank Selwyn Resources for their invaluable logistical and scientific support. André Pellerin, Samantha Murphy, and Muhder Khafaji were all excellent field assistants and companions.

REFERENCES

- AGRI-CANADA (1998). *The Canadian System of Soil Classification*. 3rd Edition. Ottawa, Agriculture and Agri-Food Canada.
- CAMERON, E. I., HAMILTON, S.M., LEYBOURNE, M. I.G., HALL, E.M., & MCCLENAGHAN, M.B. (2004). Finding deeply buried deposits using geochemistry. *Geochemistry: Exploration, Environment, Analysis*, **4**: 7-32.
- GOODFELLOW, W. D. (2004). Geology, genesis and exploration of SEDEX deposits, with emphasis on the Selwyn Basin, Canada. In: DEB, M. & GOODFELLOW, W.D. (ed) *Sediment-hosted Lead-Zinc Sulphide Deposits: Attributes and Models of Some Major Deposits of India, Australia and Canada*. Delhi, India, Narosa Publishing House, 24-99.
- GOODFELLOW, W.D., JONASSON, I.R., & MORGANTI, J.M. (1983). Zonation of chalcophile elements about the Howard's Pass (XY) Zn-Pb deposit, Selwyn Basin. *Journal of Geochemical Exploration*, **19**, 503-542.
- MANN, A.W., BIRRELL, R.D., MANN, A.T., HUMPHREYS, D. B., & PERDRIX, J.L. (1998). Application of the mobile metal ion technique to routine geochemical exploration. *Journal of Geochemical Exploration*, **61**: 87-102.
- MORGANTI, J. M. (1979). *The geology and ore deposits of the Howards Pass Area, Yukon and Northwest Territories: the origin of basinal sedimentary stratiform sulphide deposits*. Unpublished PhD thesis, University of British Columbia.

Application of 'metals-in-soil-gas' techniques to mineral exploration in exotic overburden

Yuyan Gao¹, Mingqi Wang¹, and Yinhan Liu²

¹China University of Geosciences, Beijing 100083 CHINA (email: mingqi@cugb.edu.cn)

²Institute of Geophysical and Geochemical Exploration, Langfang, Hebei 065000 CHINA

ABSTRACT: The use of ICP-MS combined with liquid collectors greatly improved the reliability of the 'Metals-in-soil-gas' (MSG) technique in the late 1990s. To date, the MSG technique has been successfully applied in various locations varying in: commodity type (e.g. gold, base metals and nickel), depth of burial, and climatic regimes (e.g. from semi-arid through to wet temperate). In this paper, three case studies are reported to illustrate the effectiveness of the technique. The results show that in MSG, a suite of chalcophile elements, similar to the association of commodity and pathfinder elements in the deposits, exhibit sharp anomalies above the known sulphide mineralization. Copper and Zn peaks can reach tens of thousands of ppb over a background of <100 ppb for Cu and <200 ppb for Zn. The authors suggest that the MSG technique can be used as a powerful tool for mineral exploration both in residual and exotic overburdens.

KEYWORDS: *Metals-in-soil-gas, gold, base metals, nickel, copper, mineral exploration*

INTRODUCTION

The 'metals-in-soil-gas' (MSG) technique, and advances therein, have been summarised by Wang *et al.* (2008). In the past few years, MSG geochemistry has been studied extensively with the support of the Chinese Geological Survey, Nature Science Foundation Committee (NSFC), and Program 863, Ministry of Science and Technology, China. The MSG technique was used to detect concealed mineralization including gold, base metals and nickel in China, although the process by which the metals migrate from deeply buried ore deposits to near-surface soil in gaseous form is controversial. Here, we report three case studies on base metal, nickel and copper mineralization buried beneath exotic overburden.

METHODS

A modified active method was used for collect 'gaseous' metals from soil air (Wang *et al.* 2008). The sampling device consists of a cone-shaped sampler, a special Millipore filter (0.45 μm), a liquid collector, and a battery-operated pump. The liquid collector comprises a high

density polyethylene bottle containing 15 ml of 3% HNO_3 prepared in a clean room with ultra-pure HNO_3 and deionized water. When sampling, the cone-shaped sampler is pushed 30-40 cm into the soil, and the 'Earth gas' is pumped through a silica gel tube and the Millipore filter to prevent coarse particles entering the liquid collector. The pumping lasts 2-3 minutes with a total of 3 litres of gas pumped through at each hole. At each sampling site, a composite of samples is collected from three holes at an interval of 2-3 meters to improve the sampling reproducibility.

All MSG samples, including blanks, were analysed by the IGGE (Institute of Geophysics and Geochemistry) Central Lab and the National Geological Lab using ICP-MS for 40 elements including Pb, Zn, Cu, Ag, Ni, Bi, Cd, Au, Mo, & W.

RESULTS

Jiaolongzhang base metal deposit, Gansu

Aeolian loess covers over 600,000 km^2 in China. Conventional surface geochemical techniques have not been successfully

employed in these areas. The Jiaolongzhang base metal deposit in western China is located in a loess-covered area. The 3600-m long by 200-m wide mineralized zones are covered by both loess (50-80 m) and tertiary red sandstone (20-50 m) (Ren *et al.* 1995; Wang *et al.* 2008). The blind ore bodies contain mainly Zn, Pb, Zn, and pyrite. The host rock is chlorite-quartz sandstone and limestone, and the main ore minerals are pyrite, sphalerite, galena and chalcopyrite. The bedrock comprises mainly intermediate and acidic marine volcanic rocks. Lead, Zn, Cu, Ag, Cd, Ag, Bi are highly enriched in the ore bodies, which are good indicators for an MSG survey.

Earlier research showed that a conventional soil (total decomposition) survey provided no anomaly and a 1M NH₄Cl partial leach for Pb and Zn produced only a one-point anomaly over the mineralization along Line 48 over Jiaolongzhang deposit. However, Cu, Pb, Sb, Bi in the MSG or geogas technique show sharp anomalies with double peaks over mineralization and the highest Cu, Pb, Zn concentrations can reach to over 1000 ng/L (Wang *et al.* 2008).

To understand the characteristics of the MSG response over the known mineralization zone, Lines 20, 28, 32, 40 and 48 were sampled in 2007. MSG signatures vary greatly with time, climate, devices and sampling team. Response ratios are calculated by dividing each sample value by the predetermined background value for that element under the same sampling conditions to reduce these errors.

Figure 1 shows MSG ratios for Cu, Pb, Zn, Ag, Cd, Ag and Bi along each profile: strong anomalies are evident over the ore bodies and Cu and Pb anomalies along different lines seem to be spatially associated with the known mineralized zone covered by thick transported overburden (Fig.1). The strong base metal MSG responses south of the mineralized zone along Lines 40 and 32 are as yet not

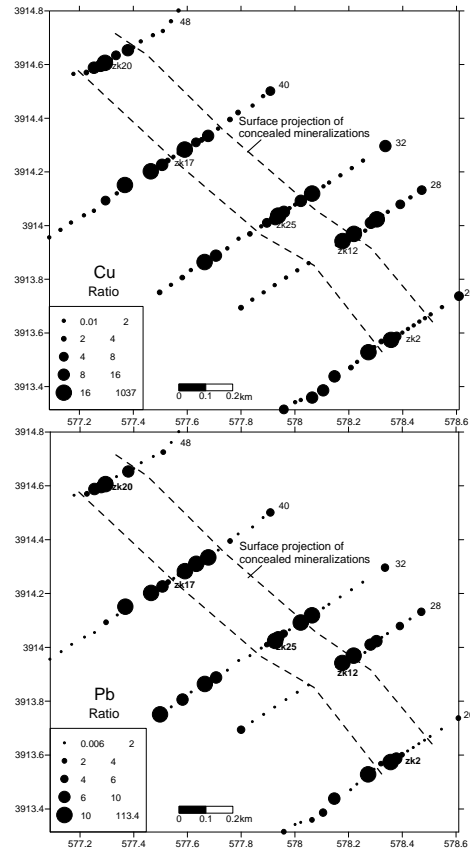


Fig. 1. MSG Cu and Pb signatures at the Jiaolongzhang base metal deposit, Gansu, China.

fully understood because the target area has not been defined by drilling.

Lashuixia Cu-Ni deposit, Qinghai

The Lashuixia Cu-Ni deposit in Qinghai has been mined for over 20 years and most of the known ore has now been excavated. Brownfields exploration using conventional geochemistry is not successful in locating concealed mineralization because most of the area is covered by quaternary sediments and a tertiary red layer. Moreover, the application of electrical geophysical techniques is difficult because of the highly conductive nature of clay cover. MSG techniques were used to test effectiveness of the method in this terrain and to define new targets for drilling.

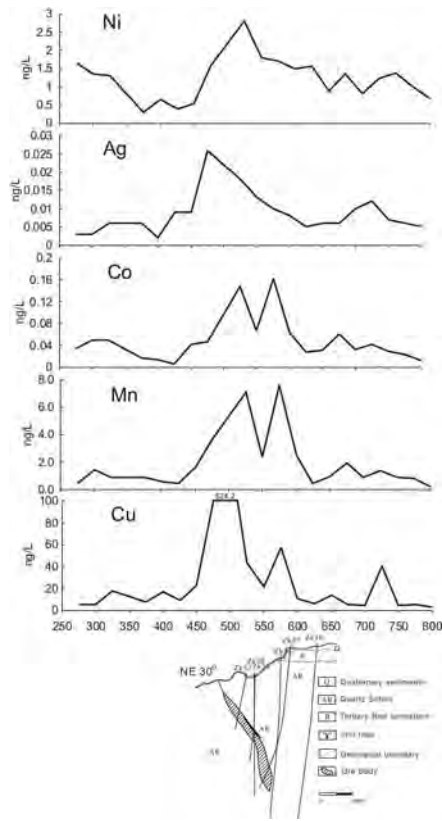


Fig. 2. MSG signatures of Cu, Mn, Co, Ag, & Ni along Line 204 of the Cu-Ni Lashuixia deposit, Qinghai.

Magmatic Cu-Ni ore bodies are hosted in quartz schist and partially in gneiss. The ore averages 4.2% Ni, 3.0% Cu, and 0.01-0.2% Co and contains a small amount of platinum group elements. The main minerals comprise violarite, pyrite, marcasite, chalcopyrite, quartz and plagioclase.

The MSG responses for Cu, Ag, and Ni along Line 204 are similar but that for Cu is particularly strong over mineralization (Fig. 2). Responses for Mn and Co are similar but their peaks occur to the north of the known ore bodies (Fig. 2). The results indicate the MSG technique can be useful in locating buried Cu-Ni mineralization.

An MSG grid survey was conducted to define potential targets; over 1500 samples were collected on a 50-m by 50-m grid. The MSG Cu and Ni responses

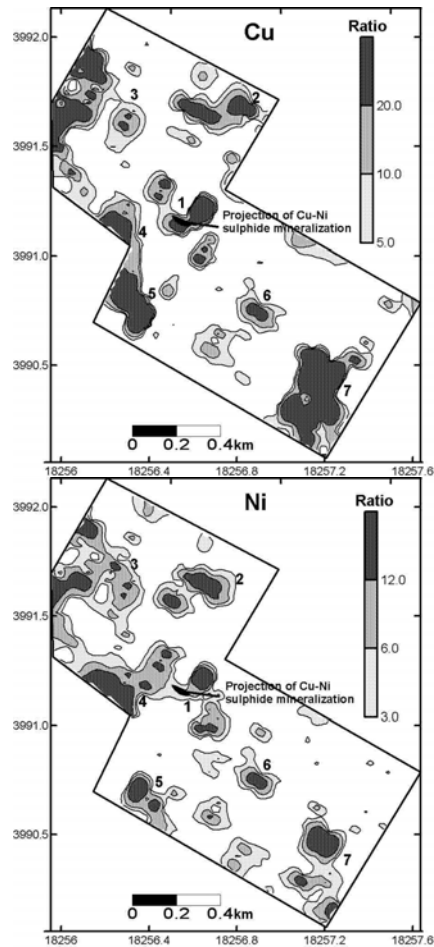


Fig. 3. MSG Cu and Ni contour maps at the Lashuixia case study area, Qinghai, China.

show only weak anomalies over the known Cu-Ni mineralization (Fig.3). The causes of this weak response likely are that (1) bedrock outcrops around known mineralization and (2) the soil cover is very thin, making it difficult to preserve the soil gas itself. However, several strong anomalies were delineated in an unknown area. Among these, Anomaly 4 is spatially adjacent to the known deposit and has the highest MSG response ratios, indicating potential for Cu-Ni mineralization.

Wangjiazhuang Cu deposit, Shangdong

The Wangjiazhuang Cu deposit is situated in Zouping County, Shangdong, China. The ore bodies are hosted in quartz diorite covered by 80 m of alluvium. The ore

averages 6.9% in Cu and consists of massive to disseminated sulphides including chalcopyrite and pyrite (Zhang *et al.* 2008). Thick quaternary cover prevents use of conventional geochemical methods although geophysical techniques played an important role in discovering the deposit.

A pilot MSG study along Line 15 was carried out to detect buried deposits in the area. Soils were also sampled to test the effectiveness of conventional geochemical techniques at several MSG sites. Elements in soil were determined by ICP-MS following the strong 4-acid (near total) digestion.

Strong, apical MSG anomalies were observed above the centre of the concealed main Cu ore bodies for Bi, Copper, Pb and Zn produced both apical and rabbit-ear anomalies over the known buried Cu mineralization. Silver yielded weak rabbit-ear anomalies at either side of the Cu orebodies (Fig. 4). However, in soil only the total concentrations of Ag, Cu, Pb, and Bi increase slightly.

CONCLUSION

These three case studies indicate that the MSG technique is indeed successful in showing strong responses over background in areas of base metal, Cu-Ni and porphyry Cu mineralization. All data support the contention that 'gaseous metals' do exist in soil gas and can be used as a practical tool for mineral exploration in areas covered both with residual and exotic overburden.

ACKNOWLEDGEMENTS

We would like to thank Program 863, the Ministry of Science and Technology and Geological Survey of China for their support of this research. Special thanks are due to Professor Zhang Qin and Ma Gengtian of the Centre Lab at IGGE and Mrs Hu Mingyue in the National Geological Lab for their assistance in sample analysis. We are also grateful to Gwendy Hall for the time spent in editing this paper.

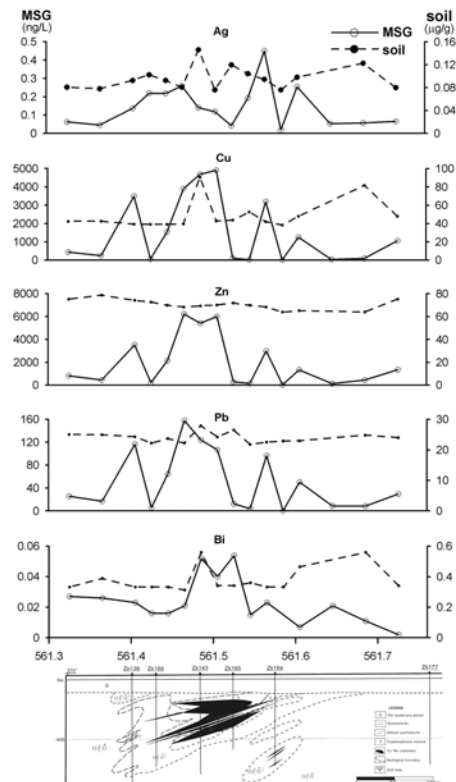


Fig. 4. MSG and soil signatures of Bi, Cu, Pb, Zn, Ag along Line 15 at the Wangjiazhuang porphyry Cu deposit, Shandong, China.

REFERENCES

- WANG, M.Q., GAO, Y.Y., & LIU Y.H. 2008. Progress in the collection of geogas in China. *Geochemistry: Exploration, Environment, Analysis*, **6**, 183-190.
- REN, T.X., YANG, S.P., LIU, Y.H. 1995. Characteristics of element dispersion and geochemical exploration for concealed ore deposits overlain by loess and red soil in eastern Gansu Province, China. *Journal of Geochemical Exploration*, **55**, 105-113.
- ZHANG, J., XU, Z.W., LI, H.Y., & YANG, X.N. 2008. The Mineralization Geochemistry of the Wangjiazhuang Copper Deposit in Zouping County, Shandong Province, and a Discussion on Its Genesis. *Geological Review*, **54**, 466-476.

In the beginning A personal retrospective of exploration geochemistry in the 1960s-1980s

G.J.S Govett

P.O Box 207, Moss Vale, NSW 2075 AUSTRALIA (email: penycoed@optusnet.com.au)

ABSTRACT: The discovery in the 1960s to early 1970s that rock geochemistry could be used to detect mineral deposits under 50-100 metres of post-mineralization rocks was probably one of the first indications that that geochemistry could be used for deep exploration. Some case histories from Cyprus and Canada are presented to illustrate this. The second important impetus to considering deep exploration was research into the mechanisms involved in the formation of anomalies. This led to the proposal of electrochemical models and the measurement of unconventional parameters such as pH, conductivity in water slurries of samples as well as measurement of elements in dilute leaches including water. These developments are illustrated by case histories from Canada and Australia.

KEYWORDS: *deep exploration, anomaly formation, halos, electrochemistry, sulfides*

INTRODUCTION

In an article in the Northern Miner in March 1973 I wrote, in part, that ".....geochemistry has been largely restricted to the search for near-surface deposits. Recent work at the University of New Brunswick suggests that this restriction is not necessarily valid – geochemical techniques can be developed to prospect for deeply buried deposits." (Govett 1973a). This is no longer a new idea as demonstrated by the Canadian CAMIRO project (Cameron *et al.* 2004) and Australian Cooperative Research Centres based at CSIRO (e.g., Butt *et al.* 2005; Anand 2009) that are developing geochemical methods for the problem of the thick cover.

Although much research at both UNB (University of New Brunswick) and UNSW (University of New South Wales) was on drainage and soils geochemistry, this paper will deal mostly with rock geochemistry and anomaly formation.

ROCK GEOCHEMISTRY IN CYPRUS

The sparse literature on element distribution in rocks around mineral deposits in the 1960s reported measurable concentrations for only a few metres from mineralization unless there was a

leakage halo. It was incomprehensible to me that large concentrations of metals in ore bodies would not leave an imprint on the enclosing rocks.

Research on the cupriferous massive sulfide deposits of Cyprus while working for the United Nations Development Program in 1967-68 resulted in one of the first regional rock geochemistry surveys published outside the USSR (Govett & Pantazis 1971). The sulfide deposits occur in a pillow lava and dyke sequence peripheral to the plutonic basic and ultrabasic rocks of the Troodos Massif. An outcrop length of about 550 km was sampled along 20 traverses at right angles to the strike over a total traverse length of 93 km.

There is a significant regional variation in trace elements: Cu decreases away from the Troodos Massif and Zn increases. Most of the known deposits lie in low Cu (<65ppm) zones with high Zn (>65ppm) and generally enhanced Co contents.

The difference in the element concentration in the vicinity of mineralization relative to background is small and single element anomalous patterns extend a maximum of several tens of metres from mineralization. Significant differences in

populations, however, can be detected as much as 135m stratigraphically above mineralization. LDF (linear discriminant functions) were calculated for a variety of combinations of Cu, Zn, Co and Ni and a program was developed to calculate discriminant scores for individual samples (Govett 1972).

THE UNIVERSITY OF NEW BRUNSWICK Rock Geochemistry

Following my appointment to the Department of Geology in September 1968 rock geochemical studies were undertaken on five Palaeozoic Zn-Pb (Cu) massive sulfide deposits in northern New Brunswick. A total of 115,000 analyses were performed on 13,000 rock samples from the environs of the Heath Steele B and ACD zones, BMS (Brunswick Mining and Smelting) No. 12, Caribou and Key Anacon sulfide deposits. In all cases significant anomalies were defined.

The variation in Pb and Zn contents in relation to the 50% probability line between anomalous and background conditions (calculated by LDF with Pb and Zn as variables) was essentially the same at BMS No. 12, Heath Steele ACD zone and the Caribou deposit, but at Heath Steele B zone the corresponding 50% probability line was at right angles to that at the other three deposits. Wahl (1978) concluded from these and other data that the Heath Steele B zone was a distal deposit whereas the others were proximal deposits. The major elements also define halos related to proximity to mineralization.

Goodfellow & Wahl (1976) investigated water-soluble Na, K, Ca, Mg, F, and Cl as well as pH and conductance at BMS No.12 and Heath Steele B zone. They found halos comparable to total Pb and Zn halos at both deposits.

On a regional scale (one sample per 5 km² over an area of 2,000 km²) in the Bathurst region of New Brunswick, the ore elements give the best patterns relating to mineralization (Govett & Pwa 1981). This is different from the mine scale where the major elements give the clearest anomalies.

Formation of Anomalies

An underlying theme in the majority of research projects was the problem of formation of anomalies. Sato & Mooney (1960) showed that the generation of self-potential patterns around sulfide bodies was due to Eh differences in solutions in contact with the orebody. Accordingly, some simple tank experiments were carried out that clearly indicated the possibility of an electrochemical mechanism for metal dispersion (Govett 1973b).

More sophisticated tank experiments led to electrochemical hypotheses on metal zoning in sulfides (Govett & Whitehead 1974) and a proposed model for the surface expression of ionic species that have migrated under the influence of electrical currents around a sulfide body (Govett 1976; Govett *et al.* 1976). The greatest concentrations were predicted to occur where the current density is greatest (at the margin of a conductor) with relatively low values over the conductor where the current density is least. The characteristic double peak was termed a "rabbit-ear anomaly" (Govett 1976).

Whitehead (1973) identified Mn halos in the iron formation overlying the Heath Steele B zone and showed that there were both vertical and lateral variations in Mn:Fe ratios. This was one of the first demonstrations of redox controlled dispersion that extended laterally on the paleo-seafloor for several km from the sulfide deposit.

At the White Lake Cu-Zn sulfide deposit (near Flin Flon, Manitoba) no geochemical signature had been obtained from conventional soil geochemistry. Where the deposit is overlain by 23m of barren rock and 8m of glacial overburden including an upper 1m of impermeable varved clay, a strong characteristic rabbit-ear H⁺ anomaly clearly indicates the location of the orebody, as predicted by the electrochemical model (Govett 1976).

THE UNIVERSITY OF NEW SOUTH WALES

In Australia a number of studies demonstrated extensive rock geochemical

halos similar to those of massive sulfides in Canada (e.g., Fedikow & Govett 1985).

The very thick and electrically highly conductive weathering residuum in Australia limited the use of conventional geochemical techniques. Nevertheless, the Elura Zn-Pb-Ag massive sulfide body in New South Wales showed trace element, H⁺ and conductance patterns in the A and B horizon soils over more than 100m of overburden similar to those found in Canada (Govett *et al.* 1984).

The last Govett PhD student from the UNB proposed a modification of the Govett electrochemical model (Smee 1983). This was adopted to interpret the results at Elura whereby the current density will be greatest at the base of the most conductive zone (which is at the base of the totally weathered zone at Elura). The current flow will be essentially horizontal before plunging vertically to the top of the margins of the sulfide body. Therefore, the greatest movement and concentration of cations will be at the base of the most conductive zone and at the margins of the sulfide body.

Cambro-Ordovician altered meta-rhyolitic pyroclastics are host to the Thalanga Zn, Pb and Cu massive sulfide deposit in Queensland (Govett & Atherden 1987). Beyond the sub-outcrop gossan zone mineralization is covered by up to 70 m of Tertiary horizontal terrestrial sandstones, conglomerates and siltstones (Campaspe beds).

Soil samples taken at a depth of 2-5 cm showed that where there is only one metre of Campaspe beds the anomalies are as expected: very strong Pb and Zn, distinct but low Cu, rabbit-ear conductance, and a triple peak H⁺. This pattern gradually changes with increasing thickness of Campaspe beds and where there is 50 m of Campaspe beds the Zn anomaly remains strong, there is no Pb anomaly, the Cu anomaly is distinct but low, and there is a well defined rabbit-ear H⁺ anomaly. EDTA-soluble Zn has exactly the same pattern as total Zn.

The interpretive dilemma at Thalanga is the same as at Elura and elsewhere, i.e., how to account for the surface anomaly.

The greatest movement and concentration of cations will be at the margins of the sulfide body along the base of the Tertiary Campaspe beds that are more conductive than the host rocks by virtue of their saline pore water. The presumption of upward diffusion of ions over great thicknesses of overburden to form surface anomalies that has been relied upon for so long is probably fatally flawed. It seems to be singularly unlikely that ions would move by diffusion in a straight vertical line to give surface anomalies immediately above an ore zone. Moreover, whatever the process, it has to be dynamic and continuing to give a precise anomaly in the top 2-5cm of soil overlying 50 m of Tertiary sediments that overlie the Thalanga sulfide deposit.

Long after the above work on electrochemical element migration described above was published, Hamilton (1998) pointed out that Govett (1976) and Bølviken & Løgn (1975) had described an electrolytic cell (which would not work as described) rather than a voltaic cell that should work. Hamilton was, of course, correct. I have passed over to him some unpublished data on Thalanga and I look forward to his interpretation of the dispersion patterns there.

ACKNOWLEDGEMENTS

Firstly, I must thank Dr W.D. Goodfellow for suggesting that I write this up. I wish to thank UNB Emeritus Professor A.L. McAllister for my appointment to the department of geology and for supporting my unconventional approach to academic research. I must also extend my gratitude to dozens of research students at UNB and UNSW whose own research underpinned anything that I may have achieved.

REFERENCES

- ANAND, R.R. 2009. Predictive geochemistry in areas of transported overburden: AMIRA P778: Predictive Geochemistry in Areas of Transported Overburden. IAGS abstract.
- BUTT, C.R.M., ROBERTSON, I.D.M., SCOTT, K.M., & CORNELIUS, M. (eds) 2005. *Regolith expression of Australian ore systems.*

- Cooperative Research Centre for Landscape Environments and mineral Exploration (CRC LEME)*; 423 p.
- BØLVIKEN, B. & LOGN, Ø. 1975. An electrochemical model for element distribution around sulphide bodies. In: I.L. Elliott & W.K. Fletcher (Editors), *Geochemical Exploration 1974*, Elsevier, Amsterdam, 631-648.
- CAMERON, E.M., HAMILTON, S.M., LEYBOURNE, M.L., HALL, G.E.M., & MCLENAGHAN, M. B. 2004. Finding deeply buried deposits using geochemistry. *Geochemistry Exploration, Environment, Analysis*, **4**; 7-32.
- FEDIKOW, M.A.F. & GOVETT, G.J.S. 1985. Geochemical alteration halos around the Mount Morgan gold-copper deposit, Queensland, Australia. *Journal of Geochemical Exploration*, **24**, 247-272
- GOODFELLOW, W.D. & WAHL, J.L. 1976. Water extracts of volcanic rocks – detection of anomalous halos at Brunswick No. 12 and heath Steele B-zone massive sulphide deposits. *Journal of Geochemical Exploration*, **6**, 35-59
- GOVETT, G.J.S. 1972. Interpretation of a rock geochemical exploration survey in Cyprus – statistical and graphical techniques. *Journal of Geochemical Exploration*, **1**, 77-102
- GOVETT, G.J.S. 1973a. Geochemists at UNB seeking deep prospecting methods. *The Northern Miner*, **March 8**, 31
- GOVETT, G.J.S., 1973b. Differential secondary dispersion in transported soils and post-mineralization rocks: an electrochemical interpretation. In: JONES, M.J (ed.) *Geochemical Exploration 1972*. Proceedings of the 4th International. Geochemistry Exploration Symposium, London., *Institution of Mining and Metallurgy*, 81-91.
- GOVETT, G.J.S. 1976. Detection of deeply buried and blind sulphide deposits by measurement of H⁺ and conductivity of closely spaced surface soil samples. *Journal of Geochemical Exploration*, **6**, 359-382.
- GOVETT, G.J.S. & ATHERDEN, P.R. 1987. Electrogeochemical patterns in surface soils -- detection of blind mineralization beneath exotic cover, Thalanga, Queensland, Australia. *Journal of Geochemical Exploration*, **28**: 201-218.
- GOVETT, G.J.S. & PANTAZIS, Th. M., 1971. Distribution of Cu, Zn, Ni and Co in the Troodos Pillow Lava Series, Cyprus. *Institution of Mining and Metallurgy Transactions, Section. B*, **80**: 27-46.
- GOVETT, G.J.S. & PWA, A. 1981. Regional reconnaissance exploration rock geochemistry for massive sulphides, New Brunswick, Canada. *Journal of Geochemical Exploration*, **15**, 139-158
- GOVETT, G.J.S. & WHITEHEAD, R.E.S. 1974. Origin of metal zoning in stratiform sulfides: a hypothesis. *Economic Geology*, **69**, 551-556.
- GOVETT, G.J.S., DUNLOP, A.C. & ATHERDEN, P.R. 1984. Electrogeochemical techniques in deeply weathered terrain in Australia. *Journal of Geochemical Exploration*, **21**, 311-331.
- GOVETT, G.J.S., GOODFELLOW, W.D., & WHITEHEAD, R.E.S., 1976. Experimental aqueous dispersion of elements around sulfides. *Economic Geology*, **71**: 925-940.
- HAMILTON, S.M. 1998. Electrochemical mass transport in overburden: a new model to account for the formation of selective leach geochemical anomalies in glacial terrain. *Journal of Geochemical Exploration*, **63**, 155-172.
- SATO, M. & MOONEY, H.M. 1960. The electrochemical mechanism of sulphide self-potentials. *Geophysics*, **25**, 226-249
- SMEE, B.W. 1983. Laboratory and field evidence in support of electrogeochemically enhanced migration of ions through glaciolacustrine sediment. *Journal of Geochemical Exploration*, **19**, 277-304.
- WAHL, J.L. 1978. *Rock geochemical exploration at the Heath Steele and Key Anacon deposits, New Brunswick*. PhD thesis, University of New Brunswick, Fredericton, New Brunswick.
- WHITEHEAD, R.E. 1973. Environment of stratiform sulphide deposition; variation in Mn:Fe ratio in host rocks at heat Steele Mine, New Brunswick, Canada. *Mineralium Deposita*, **8**, 148-160

Controls on silver distribution in the Main Zone of the 2.68 Ga Hackett River Zn-Pb-Cu-Ag volcanogenic massive sulfide deposit, Nunavut, Canada

Hannah L. J. Grant¹, Daniel Layton-Matthews¹, & Jan M. Peter²

¹Department of Geological Sciences and Geological Engineering, Queen's University, Kingston, ON, K7L 3N6 CANADA (email: granth@students.geol.queens.ca)

²Geological Survey of Canada, 601 Booth Street, Ottawa, ON, K1A 0E8 CANADA

ABSTRACT: The Main Zone of the Hackett River volcanogenic massive sulfide (VMS) deposit, within the Hackett River Greenstone Belt of the Slave Craton, is highly enriched in Ag. Of the total Ag, 79.4% is contained within Ag-rich freibergite (the Sb-bearing end-member), whereas chalcopyrite hosts 6.3% and galena 1.8%. Trace Ag-bearing minerals such as electrum, stephanite, acanthite and Bi-bearing sulfides host the remainder of the Ag and have a limited spatial distribution within the deposit. As constrained by the mineral assemblages, low-temperature and relatively oxidizing conditions favour partitioning of Ag into freibergite, whereas more reducing conditions favour partitioning of Ag into galena. At high temperatures (>250°C) and highly reducing conditions, Ag is enriched in Ag-Bi-Se-rich galena and other Bi-bearing sulfides whereas under less reducing conditions, Ag is concentrated in chalcopyrite. The principal controls on silver residence in the Hackett River Main Zone therefore are temperature, fluid redox conditions and the Bi and Sb content of the hydrothermal fluid available for coupled substitution with silver. The mineralization likely formed during sub-seafloor replacement of the host volcanic and volcanoclastic rocks with subsequent pervasive recrystallization of mineralization during amphibolite grade metamorphism. Deposit-scale zone refining resulting from dissolution of previously precipitated sulfides and subsequent re-precipitation due to interaction with circulating hydrothermal fluid is the most important control on the distribution of Ag.

KEYWORDS: *silver, VMS, freibergite, zone refining, redox*

INTRODUCTION

Volcanogenic massive sulfide (VMS) deposits are an important global resource for Ag. In Canada, VMS deposits are the principal source of Ag accounting for 52% of total production and 56% of measured and indicated reserves to 2006 (Lydon 2007). The Hackett River Zn-Pb-Cu-Ag VMS deposit is located within the Hackett River Greenstone Belt of the Slave Craton (Fig. 1) and is enriched in Ag (up to 3000 g/t). The Hackett River deposits rank at the 90th to 95th percentile for Ag grade in the global inventory of VMS deposits (Franklin et al., 2005). The Hackett River Main Zone (HRMZ) grades 127 g/t Ag, 0.30 wt. % Cu, 4.67 wt. % Zn, 0.75 wt. % Pb and 0.50 g/t Au for the stratigraphically higher massive sulfide lens and 65 g/t Ag, 0.91 wt.% Cu, 0.87 wt.% Zn, 0.11 wt.% Pb and 0.38 g/t Au for the stringer sulfides stratigraphically beneath the sulfide lens

(Wardrop 2006).

In this study, field, petrographic, bulk geochemical and mineral chemical data are presented with the aim of elucidating the mineralogical residence and spatial distribution of Ag within the HRMZ. A mass balance was calculated for Ag from electron microprobe analyses of sulfide minerals relative to bulk assays for the Main Zone deposit previously published by Wardrop (2006) for Sabina Silver Corporation.

GEOLOGICAL SETTING

The Hackett River VMS deposits are hosted within the Ignerit Formation and are part Yellowknife Supergroup within the Slave Craton. The Ignerit Formation consists of highly silicified felsic volcanic rocks of calc-alkaline affinity that are intercalated with discontinuous lenses of calc-silicate that are interpreted to be tuffs

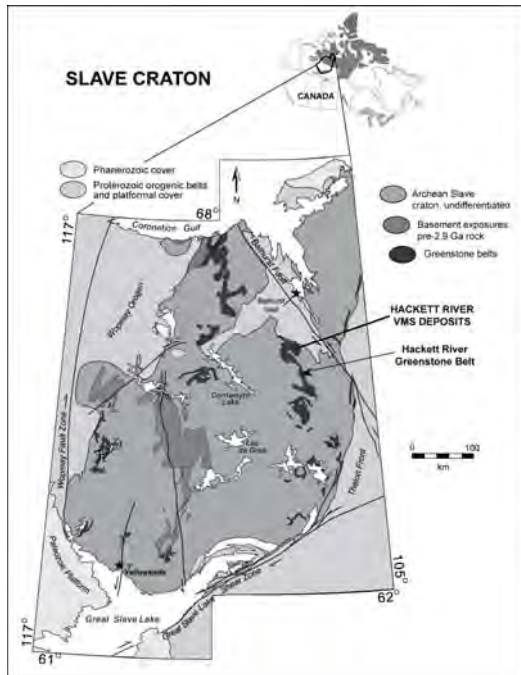


Fig. 1. Simplified geology of the Slave Craton and location of the Hackett River VMS deposits within the Hackett River Greenstone Belt (modified after Bleeker *et al.* 2007).

that have been carbonate altered and subsequently metamorphosed to amphibolite grade.

MINERALIZATION

The HRMZ consists of a semi-massive to massive sulfide lens with underlying copper-rich sulfide stringer mineralization. The deposit has been folded into an upright, relatively open south-plunging synform with a central barren massive pyrite and pyrrhotite core coincident with the NW-SE synformal axis through the approximate centre of the deposit. Our work indicates five different mineralization types within the HRMZ: 1) disseminated footwall sulfides of chalcopyrite, pyrrhotite and pyrite, 2) stringer mineralization containing chalcopyrite, Bi-Ag-Pb-bearing sulfides, pyrite, and pyrrhotite with trace galena and sphalerite, 3) pyrite-poor mineralization of sphalerite – pyrrhotite – chalcopyrite and freibergite [(Ag,Cu)₁₀(Fe,Zn)₂Sb₄S₁₃] located at the top of the stringer zone, 4) calc-silicate hosted sphalerite, pyrite, chalcopyrite, freibergite,

pyrrhotite, and galena, and 5) sphalerite-pyrite-galena and freibergite mineralization within the semi-massive to massive sulfide lens.

SILVER DISTRIBUTION

Compared to the bulk Ag content, 32% of the Ag in the HRMZ resides in type 5 mineralization with 31% of the Ag in type 4 and 29% within type 3 mineralization. The remainder of the Ag (8%) is hosted within type 2 stringer mineralization. Type 2 was split into subtypes 2a and 2b to differentiate between Cu and Cu-Bi enrichment, respectively.

Freibergite is the dominant host for Ag in the HRMZ, wherein Ag concentrations increase stratigraphically upwards with 99% of Ag hosted by type 5 mineralization (Table 1). Silver-bearing chalcopyrite contains 40% of the Ag in type 2a mineralization and 13% in type 3 where chalcopyrite contains up to 7.29 wt.%. Within both freibergite and chalcopyrite, Ag directly substitutes for Cu in the mineral lattice. Freibergite within the HRMZ is also consistently enriched in Ag (21.9 to 38.5%) compared to many other VMS deposits (e.g. Kidd Creek; Hannington *et al.* 1999, Heath Steele; Chen & Petruk 1980, Rosebery; Huston *et al.* 1996).

Silver occurs within galena by coupled substitution with Bi and to a lesser extent with Sb. Minor Ag-bearing minerals contribute significantly to the overall mass balance: matildite (AgBiS₂) and Bi-Ag-Pb sulfides of the lillianite-gustavite homologous series (Pb₃Bi₂S₆- PbAgBi₃S₆) are important Ag hosts within type 2b mineralization, whereas stephanite (Ag₅SbS₄) is an important host for Ag within types 2a and 3. Electrum was only documented in calc-silicate type 4 mineralization, where it has a high Ag:Au ratio of ~1.94:1.

DISCUSSION

The distribution of Ag within the HRMZ is a product of large-scale zone refining involving the redistribution by dissolution of lower temperature (<250°C) Pb-Zn-Ag

MINERAL	AG BUDGET (%)
Freibergite	79.4
Chalcopyrite	6.3
Galena	1.8
Electrum	3.4
Stephanite	3.6
Matildite	2.9
Bi-Ag-Pb sulfides	1.3
Other	1.3

Table 1. Mass balance of silver in minerals from the Hackett River Main Zone relative to the Ag bulk assays from Wardrop (2006).

minerals and reprecipitation of minerals by higher temperature (>300°C) hydrothermal fluids containing elements such as Cu, Se and Bi (Eldridge *et al.*, 1983). Minerals precipitated under the more reduced and higher temperature conditions (mainly chalcopyrite) were introduced into the HRMZ footwall stringer zone at the base of paragenetically earlier, lower temperature mineralization. A distinct high-temperature suite of Cu, Bi, Te, and Se is concentrated in the lower portion of the deposit and is particularly associated with the fluid upflow conduit (mineralization type 2b) where maximum temperatures and most reducing conditions occurred. Trace galena from mineralization type 2b contains up to 5 wt. % Se, 2.1 wt.% and 1.2 wt.% Ag. Incorporation of Se into galena is indicative of highly reduced conditions and is the only expression of elevated Se within the HRMZ. The mutual occurrence of Bi-Ag-Pb sulfides with the Se-Bi-Ag enriched galena also indicates precipitation from reduced, high-temperature (>300°C) fluids (e.g. Marcoux *et al.* 1996). Chalcopyrite is an important host for Ag only at higher temperatures, under more reducing conditions and in the lower portion of the HRMZ deposit.

The hydrothermal fluid migrated outwards and upwards from the higher-temperature stringer zone replacing an earlier low-temperature sulfide assemblage composed primarily of sphalerite and galena. The leading edge of this replacement is marked by a chalcopyrite mineralization front within mineralization type 3 at the base of the sulfide lens. Mineralization type 3 is a thin, <1 m reaction front separating mineral

assemblages that record a change in mineral precipitation conditions from high-temperature and more reduced to less reduced and cooler hydrothermal fluids stratigraphically up-wards. In addition to elements with a mutual lower temperature affinity (Pb, Zn, Sb, Cd and Hg), Ag released by the dissolution of earlier, lower temperature mineral assemblages was transported by evolving fluids upward during zone refining and reprecipitated in the upper and lateral parts of the HRMZ system.

An increase in oxidation state stratigraphically above mineralization type 3 is indicated by the presence of lesser amounts of pyrrhotite and chalcopyrite and increasing replacement of pyrrhotite by pyrite. Precipitation temperatures also decreased as shown by increasing amounts of sulfides stable only at lower temperatures (<250°C). The Ag content of galena decreases as the amount of Ag within freibergite increases. This is due to higher amounts of Bi within the hydrothermal fluid under more reduced conditions that increase the content of Ag in galena by coupled substitution with Pb (Amcoff 1984). Under more oxidizing conditions (and lower temperatures), the amount of Sb relative to Bi increases and Ag is preferentially incorporated into Sb-rich freibergite. This is also a reflection of increasingly more oxidized conditions stratigraphically higher in the HRMZ.

CONCLUSIONS

The major minerals that host Ag within the Main Zone deposit are freibergite, chalcopyrite and galena with trace Ag-bearing minerals such as electrum, stephanite, acanthite and Bi-bearing sulfides hosting the remainder of the Ag. Bulk Ag contents increase upwards and laterally within the HRMZ above mineralization type 3, and this is likely an artefact of zone refining and transport of Ag by increasingly oxidized and cooler fluids distally from the high temperature upflow zone. Low temperature and more oxidizing conditions favoured partitioning of Ag into freibergite in the upper portion of the HRMZ, and less oxidizing

conditions favoured galena as a host. At higher temperature, the most reducing conditions favoured Ag incorporation into Ag-Bi-rich galena (plus Se) and Bi-bearing sulfides or Ag-rich chalcopyrite under slightly less reducing conditions below the base of the massive sulfide lens.

ACKNOWLEDGEMENTS

We thank Sabina Silver Corporation for assistance and permission to undertake this study. The assistance of K. E. Venance during electron microprobe analyses performed at the Geological Survey of Canada Laboratories in Ottawa is gratefully acknowledged. Research grants awarded to the first author by the SEG Hugh E. McKinstry Fund, SEG Canada Foundation and the Mineralogical Association of Canada are also gratefully acknowledged.

REFERENCES

- AMCOFF, O. 1984 Distribution of Silver in Massive Sulfide Ores. *Mineralium Deposita*, **19**, 63-69.
- BLEEKER, W. & HALL, B. 2007 The Slave Craton: Geological and Metallogenic Evolution. In: GOODFELLOW, W.D. (ed.), *Mineral Deposits of Canada. A Synthesis of Major Deposit Types, District Metallogeny, the Evolution of Geological Provinces, and Exploration Methods*. Geological Association of Canada, Mineral Deposits Division, 849 - 880.
- CHEN, T.T. & PETRUK, W. (1980). Mineralogy and characteristics that affect recoveries of metals and trace elements from the ore at Heath Steele Mines, New Brunswick. *Canadian Institute of Mining and Metallurgy Bulletin*, **73**, 167-179.
- ELDRIDGE, C.S., BARTON, P.B., JR. & OHMOTO, H. 1983. Mineral textures and their bearing on formation of the Kuroko orebodies. *Economic Geology Monograph*, **5**, 241-281.
- FRANKLIN, J.M., GIBSON, H.L., & GALLEY A.G. 2005. Volcanogenic Massive Sulfide Deposits. In: HEDENQUIST J. W., THOMPSON, J. F., GOLDFARB, R. J., & RICHARDS J. P. (eds.), *Economic Geology 100th Anniversary Volume*. Economic Geology and the Bulletin of the Society of Economic Geologists, 523-560.
- HANNINGTON, M.D., BARRIE, C.T., & BLEEKER, W. 1999. The giant Kidd Creek volcanogenic massive sulfide deposit, western Abitibi Subprovince, Canada: preface and introduction. In: HANNINGTON, M.D. & BARRIE, C.T. (eds.), *The Giant Kidd Creek Volcanogenic Massive Sulfide Deposit, Western Abitibi Subprovince, Canada*. Economic Geology Monograph 10. 1-30.
- HUSTON, D.L., JABLONSKI, W., & SIE S. H. 1996. The distribution and mineral hosts of silver in eastern Australian volcanogenic massive sulfide deposits. *Canadian Mineralogist*, **34**, 529-546.
- LYDON, J.W. 2007. An Overview of the Economic and Geological Contexts of Canada's Major Mineral Deposit Types. In: GOODFELLOW, W.D. (ed.), *Mineral Deposits of Canada. A Synthesis of Major Deposit Types, District Metallogeny, the Evolution of Geological Provinces, and Exploration Methods*. Geological Association of Canada, Mineral Deposits Division, 3-48.
- MARCOUX, E., MOELO, Y., & LEISTEL, J.M. 1996. Bismuth and cobalt minerals as indicators of stringer zones to massive sulphide deposits, Iberian Pyrite Belt. *Mineralium Deposita*, **31**, 1-26.
- WARDROP. 2006. *Unpublished technical report on the Hackett River property, Nunavut, Canada*. Toronto, Canada; prepared for Sabina Silver Corp, 1109 p.

3-D element patterns above deeply buried mineralization: new evidence and insights into electrical dispersion

Stewart M. Hamilton¹

¹Ontario Geological Survey, 933 Ramsey Lake Road, Sudbury, ON, P3E 2G9 CANADA
(e-mail: stew.hamilton@ontario.ca)

ABSTRACT: Subsurface geochemical data from the Thalanga Pb-Cu-Zn prospect in Australia demonstrate that 'rabbit-ear' geochemical anomalies in areas of thick cover can have a distinct 3-D character extending from mineralization to ground surface. The pattern suggests dispersal in cover materials by 'redox-induced spontaneous polarization' at the edge of an inferred reduced chimney. Redox gradients at the margins of reduced chimneys are horizontal. Grains of semiconductive minerals in overburden will electrically polarize in these gradients developing negative poles in the positive redox direction, i.e. outward from the chimney. Voltages from multiple grain-dipoles configured end-on will be additive and a macroscopic, negative-outward electrical field will result. Current will move inward and in a donut-shaped current distribution will wrap downward toward ore and then outward from the reduced chimney in deeper areas where the redox gradient is weakest. Cations of ore-forming elements will be induced out of the reduced chimney and upward toward surface to complete the electrical circuit. Elements such as Pb and Cu will be partly attenuated as they move out of the reduced chimney. Zn, which has only one oxidation state will be attenuated least and will have the largest dispersion halo.

KEYWORDS: *Dipole, reduced chimney, SP, soil geochemistry, redox, Thalanga*

INTRODUCTION

In the 1960s and 1970s the use of soil geochemistry in mineral exploration led to the discovery of the now commonly observed twin-peak or 'rabbit-ear' geochemical anomaly (Govett 1976). From the time rabbit-ear anomalies were first described they were attributed to electrochemical processes but the theory proposed at that time could only adequately account for these features where deposits were buried under just a few metres of cover. However, subsequent case studies continue to demonstrate that such patterns and other evidence of electrochemical processes in soils persist as overburden thickens, even as the responses diminish in magnitude.

One of the early case studies with convincing evidence of electrochemical processes over deeply buried mineralization was carried out on the Thalanga Pb-Zn-Cu prospect in Queensland, Australia (Govett & Atherden 1987). That study showed strong rabbit-ear responses in surface soils in commodity elements and elevated H⁺ in

the same soils, despite the deposit being buried by up to 50 m of exotic cover. Previously unpublished subsurface geochemical data for one of the lines at Thalanga have become available that demonstrates the surface anomalies have a 3-dimensional character. This paper describes some of these data and interprets them in the context of recent ideas on electrochemical dispersion above ore deposits.

ELECTRICAL DIPOLES AND CURRENT DEVELOPMENT AROUND CONDUCTIVE ORE-BODIES

It was known for most of the last century that metallic ore bodies electrically polarize when in contact with country rock with non-uniform oxidative properties (Schlumberger 1920), and that this often results in measurable spontaneous electrical potentials (SP) on surface. Sato & Mooney (1960) argued that universally more oxidizing conditions above the water table result in the development of a cathodic pole to the upper portion of any metallic ore body that crosses it. The

upper ore becomes negatively charged due to the upward movement of electrons from reducing agents (electron donors) in groundwater at depth, toward oxidizing agents (electron acceptors) in the shallow environment. In order to maintain electrical neutrality a return current occurs in the groundwater electrolyte around the ore body. Current in the ore body occurs as electron movement and thus can only occur in ores that are electronic conductors or semi-conductors, such as pyrite or graphite. Current in the country rock is due to ionic conduction. This involves the movement of mass and charge with cations moving upward toward the cathodic part of the ore and anions toward the anodic part at depth (Fig. 1).

Sato & Mooney (1960) pointed out that the oxidation of the conductor itself cannot be responsible for the SP phenomenon because it would oxidize locally in the upper part of the ore-body where oxidizing agents are in direct contact with the ore and there would be no separation of charge and therefore no SP phenomenon. The redox reactions that produce SP therefore occur between reactants in the groundwater environment at the top and bottom of the ore body. This cathodically protects the upper part of the ore body from direct oxidation. Oxidation of the ore body can still occur (hence gossans) but results from local 'detached' oxidation which cannot produce SP.

LIMITATIONS OF THE DIPOLE MODEL

Natural electrical dipole development around electronic conductors in the earth is theoretically sound, supported by experimentation and well documented through 100 years of field observation. However the problem with it is that it only describes a subset of cases where SP occurs over ore deposits. It cannot account for cases where voltages exceed c. 500 mV (Sato & Mooney 1960) and these are not rare. There should also be no response at all over disseminated sulfides yet large porphyry deposits and other disseminated systems produce the largest SP responses so far documented

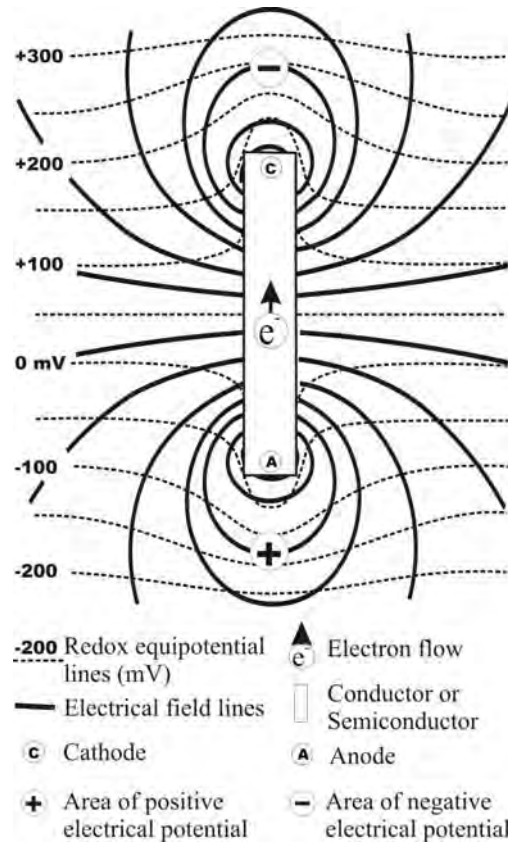


Fig. 1. Electrical dipole development around a conductor crossing redox equipotential lines. Positive current in the country rock (not shown) travels perpendicular to electrical field lines from the anode to the cathode (modified after Govett 1976 and Hamilton 1998).

with magnitudes commonly exceeding 500 mV (Corry 1985) and sometimes as high as several volts.

GEOCHEMICAL ANOMALIES WITH ELECTROCHEMICAL CHARACTER

In the 1970s, the dipole model was further developed to account for soil geochemical anomalies on surface above buried ore deposits (Govett 1976; Bolviken & Logn 1975). For the first time the current line and redox-equipotential distribution was illustrated (Govett 1976) and a modified version of that model is shown in Figure 1. This configuration was used to account for the existence of rabbit-ear geochemical anomalies in shallow soils. It was argued that the higher current densities at the top of the ore body would result in higher

concentrations of cations in soils on either side. In cases where thicker overburden cover was encountered, the vertical movement of cations to surface was explained by upward diffusion from these higher current areas. However, many subsequent studies have shown that this anomaly morphology is also characteristic of soil over deeply buried mineral deposits where it often exhibits discreet, high contrast anomalies that would not be expected to occur if diffusion were the vertical transport mechanism.

Govett & Atherden (1987) show Pb and Zn shallow soil geochemical data collected over the Thalanga Pb-Zn-Cu deposit. Four lines were sampled that represent burial depths of 0, 1, 30 and 50 m. The anomalies display a rabbit-ear pattern centred on the deposit regardless of overburden thickness. The magnitude of the anomalies diminishes with increasing cover and Pb diminishes more rapidly than Zn.

The Zn and Pb soil profiles for the Thalanga sample line with 50 m of cover are reproduced in Figures 2 and 3. The lower half of each figure, respectively, are previously unpublished data showing the subsurface Zn & Pb distribution in the Tertiary clastic sedimentary rocks (the Campaspe Beds) covering the deposit. Samples were collected in the early 1980s by rotary-air-blast (RAB) drilling and analysed by near-total digestion according to methods reported in Govett & Atherden (1987). The subsurface data were not published at that time for reasons of company confidentiality. They confirm what the surface transects had suggested, i.e. that the rabbit-ear morphology has a 3-dimensional character. This explains why the surface soil anomaly morphology remains largely intact, albeit of a lower magnitude, as overburden thickens.

REDOX-INDUCED SPONTANEOUS POLARIZATION

The 3-D results at Thalanga suggest that electrochemical processes are not only occurring in bedrock and basal overburden, but also throughout the entire sequence of cover materials to surface.

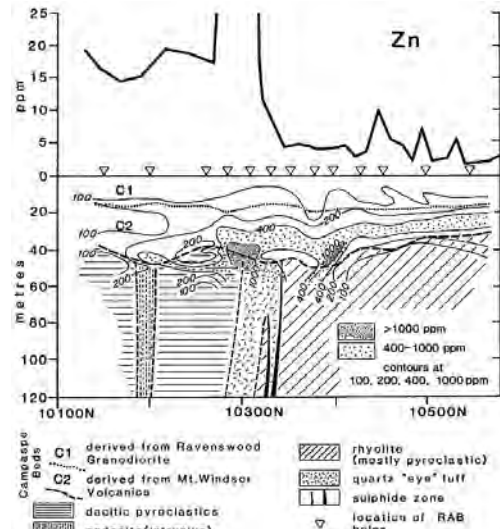


Fig. 2. Distribution of Zn in surface soils and in Campaspe beds overlying the Thalanga sulfide deposit (G. Govett, pers. comm. 2009).

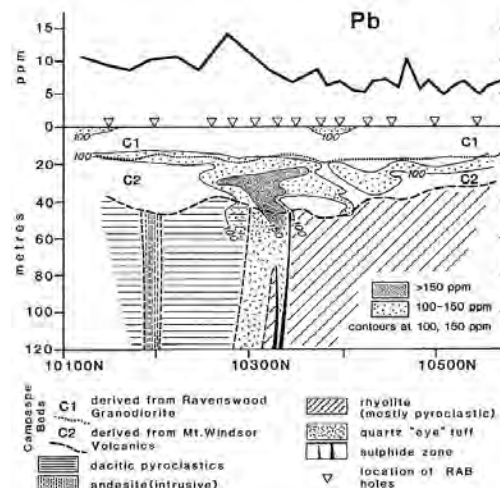


Fig. 3. Distribution of Pb in surface soils and in Campaspe beds overlying the Thalanga sulfide deposit (G. Govett, pers. comm. 2009).

Dipole development around a conductor immersed in an electrolyte with uneven oxidative properties is scale independent. Even tiny conductive or semi-conductive mineral grains in overburden will develop dipoles if there are redox differences across them. Almost all solids have some semi-conductive properties and therefore the nature of the conductive minerals is of less importance than the existence of a redox gradient. Large redox gradients in overburden contain polarisable minerals,

each of which will develop a tiny dipole with a negative electrical pole pointed toward the oxidizing end of the redox gradient. Since the dipoles are all pointed in the same direction and many are aligned end-to-end their voltages are additive in series resulting in a macroscopic electrical field with a negative (cathodic) end aligned toward the more oxidizing conditions. This has been referred to as redox-induced spontaneous polarization (Hamilton & Hattori 2008)

Reduced chimneys' have been documented over mineral deposits (e.g. Hamilton *et al.* 2004) and are inferred to occur almost everywhere. At Thalanga, the gossans and deep oxidative profile are evidence that oxidizing agents are being preferentially consumed over the ore, thereby forming a reduced chimney. At the margins of the chimney, redox-induced dipoles will be mostly sideways and negative-outward (Fig. 4), inducing cations to move inward and downward. Since the redox gradient at the edge of a reduced chimney is strongest on surface and diminishes with depth, the magnitude of the resultant horizontal dipoles also decreases. These weaker dipoles contribute to the inward current and further direct it downward. Farther down, near the oxidizing ore body, the redox contrast between the reduced chimney and the surrounding groundwater environment is low enough that no major dipoles form and the return current wraps upward to complete the electrical circuit.

As the return current moves outward

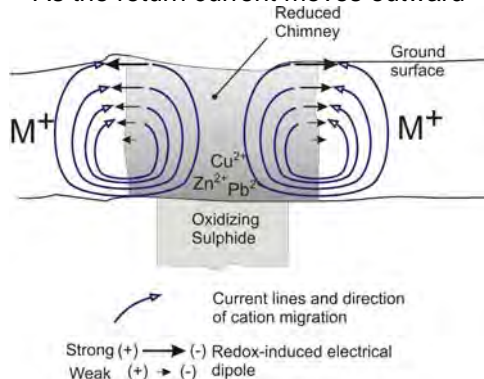


Fig. 4. Current distribution due to redox-induced spontaneous polarization at the margins of a reduced chimney.

and upward, the ore-related cations encounter increasingly oxidized conditions, which limit their mobility. Pb, the least mobile in oxidized environments, will attenuate first, followed by Cu. Zn, which has only one oxidation state, is not affected by the changing redox conditions and therefore travels the farthest and produces the largest dispersion halo.

ACKNOWLEDGEMENTS

I would like to thank Gerry Govett for providing Figures 2 and 3 and suggesting I write this paper. I would also like to thank Kagara Ltd, the current holders of the Thalanga prospect for agreeing to the publication of the subsurface data.

REFERENCES

- BØLVIKEN, B., & LØGN., O. 1975. An electrochemical model for element distribution around sulfide bodies. In: I. ELLIOT & K. FLETCHER (eds.), *Geochemical Exploration 1974*. Elsevier, Amsterdam, 631-648.
- CORRY, C.E. 1985. Spontaneous polarization associated with porphyry sulfide mineralization: *Geophysics*, **50**, 1020-1034.
- GOVETT, G.J.S. 1976. Detection of deeply buried and blind sulfide deposits by measurement of H⁺ and conductivity of closely spaced surface soil samples. *Journal of Geochemical Exploration*, **6**, 359-382.
- GOVETT, G.J.S. & ATHERDEN, P.R. 1987. Electrochemical patterns in surface soils – detection of blind mineralization beneath exotic cover, Thalanga, Queensland, Australia. *Journal of Geochemical Exploration*, **28**, 201-218.
- HAMILTON, S.M. 1998. Electrochemical mass-transport in overburden: a new model to account for the formation of selective leach geochemical anomalies in glacial terrain. *Journal of Geochemical Exploration*, **63**, 155-172.
- HAMILTON, S.M. & HATTORI, K.H. 2008. Spontaneous potential and redox responses over a forest ring. *Geophysics*, **73**(3), B67-B75.
- SATO, M., & MOONEY, H.M. 1960. The electrochemical mechanism of sulfide self-potentials. *Geophysics*, **25**, 226-249.
- SCHLUMBERGER, C. 1920. Essais de prospection électrique du sous-sol, *Comptes Rendes, Académie des Sciences*, **170**, 519-521.

Lithogeochemical halos and vectors for ores in volcanic arcs and sedimentary basins

Ross R. Large

CODES, University of Tasmania, Private Bag 126, Hobart, Tasmania 7001 AUSTRALIA
(email: ross.large@utas.edu.au)

ABSTRACT: Lithogeochemical halos and exploration vectors for a variety of volcanic- and sediment-hosted ore types are reviewed; including VHMS, SEDEX, BHT and orogenic gold deposits. Many deposits show two component halos; a regionally extensive distal halo which follows the favourable stratigraphy, and a more proximal cross-cutting texturally destructive halo immediately surrounding the deposit. For base metal ores the distal halos are defined by muscovite or carbonate alteration with Mn and Tl as the best pathfinder elements. For gold ores in sediments the distal halo is defined by pyrite and organic matter enrichment in the sediments and anomalous V, As, Mo, Se, Ni, Ag and Zn termed the VAMSNZ suite.

KEYWORDS: alteration, gold, VMS, sedex, VAMSNZ

VOLCANIC HOSTED MASSIVE SULFIDES

Volcanic-hosted massive sulfides (VHMS or VMS) have intense localised alteration zones and related halos that cut across the volcanic stratigraphy and provide obvious exploration targets. Mineralogical changes in both felsic and mafic volcanics involve proximal zoned alteration assemblages dominated by albite → sericite → carbonate → chlorite → quartz, and provide a clear vector to ores. Systematic compositional changes in key minerals, particularly sericite, chlorite and carbonate provide additional vectors. Use of the alteration box plot (Ishikawa AI versus CCPI) assists to discriminate diagenetic alteration from subtle to intense hydrothermal alteration, related to VHMS 1 (Gifkins *et al.* 2005; Fig. 1, Large *et al.* 2001a, b). Thallium and antimony are the best distal halo trace elements for the hanging wall of Zn-Pb-rich VHMS (Fig. 2), where they extend well beyond other halo indicators including Zn, Pb, S/Na₂O, Ba/Sr and Ishikawa AI.

SEDEX ZN-PB-AG DEPOSITS

Alteration halos may be regionally widespread, extending along the favourable stratigraphy for up to 15 km (Fig. 3). In the dolomite siltstone-hosted vent distal

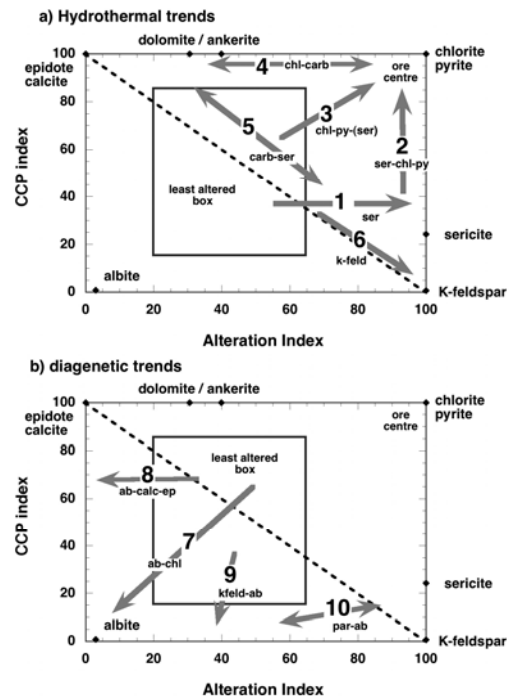


Fig. 1. Trends on the VHMS alteration box plot showing alteration related to (a) hydrothermal activity and (b) diagenesis.

SEDEX deposits of northern Australia (e.g., McArthur River, Century, Lady Loretta), the lithogeochemical halos extend several hundred meters into the overlying stratigraphy and several kilo-

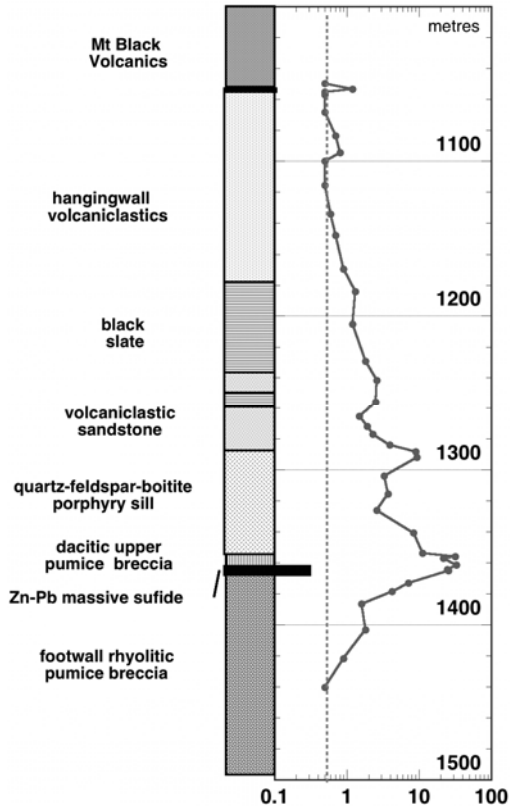


Fig. 2. Thallium halo to the Rosebery VHMS K-lens in drillhole 120R.

metres along the favourable stratigraphy away from the deposit (Broadbent *et al.* 2002; Large *et al.* 2001a, b; Large & McGoldrick 1998). The major mineralogical change in the alteration halo is the chemistry of the sedimentary and hydrothermal carbonate. Fe and Mn content of the carbonate commonly increases towards ore both across stratigraphy and along stratigraphy (Large *et al.* 2005). At Lady Loretta, the sedimentary carbonate zonation passing away from the deposits is, ore → Mn-siderite → Fe-Mn dolomite → dolomite. Century and McArthur river show similar patterns, although the siderite zone is absent at McArthur River. Turner (1990) and Goodfellow (2004) record similar zonation of carbonate minerals around the Tom and Jason deposits in the Selwyn Basin, Canada.

Chemical changes in sediments within the halo involve addition of FeO and MnO accompanied by depletion in MgO, CaO

and Na₂O. A SEDEX alteration index, based on these lithogeochemical changes, has been developed to assist mineral exploration (Large *et al.* 2000; Fig 4; Large & McGoldrick 1998). In sedimentary host rocks devoid of carbonate, the most common halo forming mineral is muscovite. Sullivan and the SEDEX deposits of the Anvil Camp in the Selwyn Basin all show widespread envelopes of muscovite alteration in the hangingwall sediments to ore (Carne & Cathro 1982; Lydon *et al.* 2000; Shanks *et al.* 1987). In addition to Mn, the other important lateral geochemical indicator that marks the favourable horizon, away from mineralisation is Tl. Thallium occurs at values of 100-1000 ppm through the Zn-Pb ores, and decreases systematically away from the deposit to values of less than 1ppm at distances of 1 to 20km along the favourable horizon (Large *et al.* 2000). Thallium is more useful as a geochemical vector than Zn and Pb because of its systematic spatial variations, compared with the erratic patterns shown by the latter. Other elements that may be enriched in the halo to SEDEX deposits are Ba, Hg, Sb, As, Ni, Bi and P (Leach *et al.* 2005). Carbon, oxygen and strontium isotopes of the calcareous sediments also hold potential as vectors to ore (e.g., Goodfellow 2000; Large *et al.* 2001a, b; Leach *et al.* 2005; Taylor *et al.* 2000).

BROKEN HILL TYPE (BHT) DEPOSITS

Walters *et al.* (2002) reports that alteration of meta-sediments and meta-volcanics surrounding BHT deposits is commonly defined by extensive zones of garnet spotting within the gneissic host rocks (e.g. Broken Hill, Cannington, Gamsberg). The ore lenses are commonly surrounded by quartz-Mn-garnet-rich zones that pass outwards into garnet spotted psammopelitic metasedimentary rocks. Rozendaal and Stumpfl (1984) record Mn-rich garnets over a distance of 1.5 km along strike from the Gamsberg deposit. The Mn content of garnet commonly increases towards the ore lenses. A characteristic package of altered metasediments and exhalites, including quartz gahnite rocks, thin

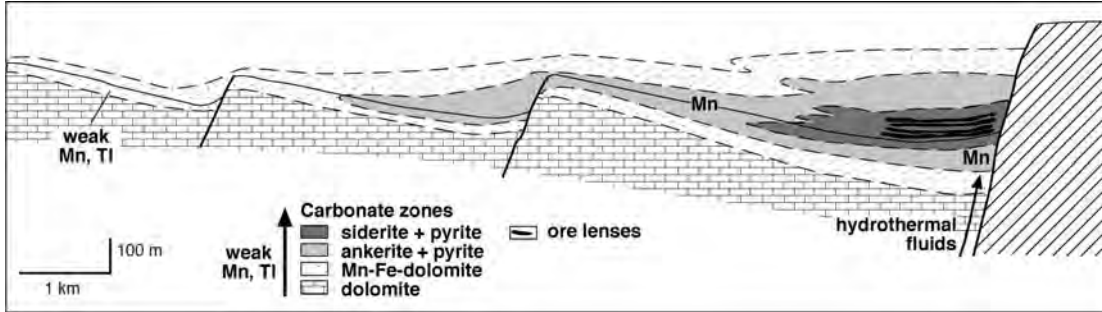


Fig 3. Regional stratiform alteration in dolomitic shales lateral to SEDEX Zn-Pb-Ag deposits.

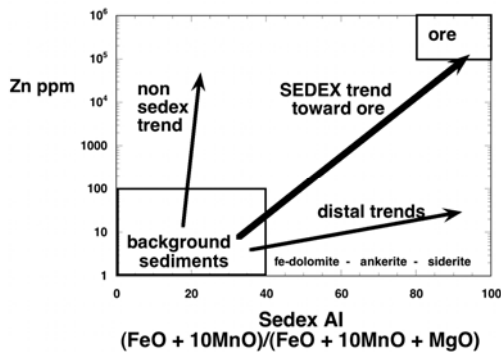


Fig. 4. Trends in sedex Al versus Zn.

banded iron formations and pegmatite with plumbian feldspar occurs along the favourable horizon away from the deposit (Walters *et al.* 2002). Geochemical studies show enrichment in Fe, Mn, K/Na ratio and Pb in the metasediments within the alteration halo, and depletion in Na, P, Ba and in some cases Ca, Mg and Al (Plimer 1979; Walters *et al.* 2002).

OROGENIC AU-AS DEPOSITS

Our recent research has defined two types of lithochemical halos related to sediment-hosted orogenic and Carlin type gold deposits. The first is a distal stratiform zone of regionally extensive carbonaceous sediments defined by anomalous V, As, Mo, Se, Ni, Ag and Zn, known as the VAMSNZ suite of elements. These define a lithochemical halo that may extend tens of kilometres along the favourable stratigraphy away from orogenic Au-As deposits. This suite of elements is concentrated, with gold, in organic matter and associated diagenetic pyrite, during sedimentation and diagenesis in anoxic to

euxinic environments (Large *et al.*, 2007). The second halo is more focussed around the gold deposit, and relates to fluid movement and gold up-grading associated with metamorphism and deformation. The inner zone is characterised by elevated As and Au, and the outer zone by carbonate spotting and muscovite alteration. This proximal halo varies from 50 to 200 m thick.

REFERENCES

- BROADBENT, G.C., ANDREWS, S.J., & KELSO, I.J. 2002. A decade of new ideas; geology and exploration history of the Century Zn-Pb-Ag deposit, northwestern Queensland, Australia. *Special Publication (Society of Economic Geologists U.S.)*, **9**, 119-140.
- CARNE, R.C. & CATHRO, R.J. 1982. Sedimentary exhalative (sedex) zinc-lead deposits, northern Canadian Cordillera. *Canadian Institute of Mining and Metallurgy, Bulletin*, **75**, 66-78.
- GIFKINS, C., HERRMANN, W., & LARGE, R.R. 2005. *Altered Volcanic Rocks: a guide to description and interpretation*. Centre of Ore Deposit Research, University of Tasmania. 286 p.
- GOODFELLOW, W.D. 2000. Sedimentary basinal fluid compositions, anoxic oceans and the origin of sedex Zn-Pb deposits: *Abstract Volume (Geological Association of Canada)*, **25**, unpaginated.
- GOODFELLOW, W.D. 2004. Geology, genesis and exploration of SEDEX deposits, with emphasis on the Selwyn Basin, Canada. In: MIHIR, D. & GOODFELLOW, W.D. (eds.), *Sediment-hosted lead-zinc sulphide deposits; attributes and models of some major deposits in India, Australia and Canada*, Narosa Publishing House, New Delhi, India, 24-99.
- LARGE, R.R. & MCGOLDRICK, P.J. 1998. Lithochemical halos and geochemical

- vectors to stratiform sediment hosted Zn-Pb-Ag deposits, 1. Lady Loretta Deposit, Queensland. *Journal of Geochemical Exploration*, **63**, 37-56.
- LARGE, R.R., BULL, S.W., & MCGOLDRICK, P.J. 2000. Litho-geochemical halos and geochemical vectors to stratiform sediment hosted Zn-Pb-Ag deposits Part 2 HYC deposit McArthur River, Northern Territory. *Journal of Geochemical Exploration*, **68**, 105-126.
- LARGE, R.R., GEMMELL, J.B., & PAULICK, H. 2001a. The Alteration box plot - a simple approach to understanding the relationship between alteration mineralogy and litho-geochemistry associated with volcanic-hosted massive sulfide deposits. *Economic Geology*, **96**, 957-971.
- LARGE, R.R., ALLEN, R.L., BLAKE, M.D. & HERRMANN, W. 2001b. Hydrothermal alteration and volatile element halos for the Rosebery K lens volcanic-hosted massive sulfide deposit, western Tasmania. *Economic Geology*, **96**, 1055-1072.
- LARGE, R., BULL, S., MCGOLDRICK, P., & WALTERS, S. 2005. Stratiform and stratabound Zn-Pb-Ag deposits in Proterozoic sedimentary basins, Northern Australia. *Economic Geology 100th Anniversary Volume*, 931-963.
- LARGE, R.R., MASLENNIKOV, V., ROBERT, F., DANYUSHEVSKY, L.V., & CHANG, Z. 2007. Multistage sedimentary and metamorphic origin of pyrite and gold in the giant Sukhoi Log deposit, Lena gold province, Russia. *Economic Geology*, **102**, 1233-1267.
- LEACH, D.L. *et al.* 2005. Sediment-hosted lead-zinc deposits; a global perspective. *Economic Geology 100th Anniversary Volume*, 561-608.
- LYDON, J.W., PAAKKI, J.J., ANDERSON, H.E., & REARDON, N.C. 2000. An overview of the geology and geochemistry of the Sullivan deposit. In: LYDON, J.W., HOY, T., SLACK, J.F. & KNAPP, K. (eds.), *The Geological Environment of the Sullivan Deposit, British Columbia, Geological Association of Canada, Mineral Deposits Division, Special Publication*, **1**, 505-522.
- PLIMER, I.R. 1979. Sulphide rock zonation and hydrothermal alteration at Broken Hill, Australia. *Transactions of the Institution of Mining and Metallurgy. Section B: Applied Earth Science*, **88**, 161-176.
- ROZENDAAL, A. & STUMPFL, E.F. 1984. Mineral chemistry and genesis of Gamsberg zinc deposit, South Africa. *Transactions of the Institution of Mining and Metallurgy. Section B: Applied Earth Science*, **93**, B161-B175.
- SHANKS, W.C., III, WOODRUFF, L.G., JILSON, G.A., JENNINGS, D.S., MODENE, J.S., & RYAN, B.D. 1987. Sulfur and lead isotope studies of stratiform Zn-Pb-Ag deposits, Anvil Range, Yukon: Basinal brine exhalation and anoxic bottom-water mixing. *Economic Geology*, **82**, 600-634.
- TAYLOR, B.E., TURNER, R.J.W., LEITCH, C.H.B., WATANABE, D.H., & SHAW, D.R. 2000. Oxygen and hydrogen isotope evidence for the origins of mineralizing and alteration fluids, Sullivan Pb-Zn mine and vicinity, British Columbia. In: Lydon, J.W., Hoy, Trygve, Slack, J.F. & Knapp, K. (eds.), *The Geological Environment of the Sullivan Deposit, British Columbia, Geological Association of Canada, Mineral Deposits Division, Special Publication*, **1**, 652-672.
- TURNER, R.J.W. 1990. Jason stratiform Zn-Pb-barite deposit, Selwyn Basin, Canada (NTS 105/01). Geological setting hydrothermal facies and genesis. In: ABBOTT, J.G & TURNER, R.J.W. (eds.), *Mineral Deposits of the Northern Canadian Cordillera: International Association on the Genesis of Ore Deposits. Field Trip 14, Guidebook*, 137-175.
- WALTERS, S., SKRZECZYNSKI, B., WHITING, T., BUNTING, F., & ARNOLD, G. 2002. Discovery and geology of the Cannington Au-Pb-Zn deposit, Mount Isa Eastern Succession, Australia; development and application of an exploration model for Broken Hill-type deposits. *Special Publication (Society of Economic Geologists U.S.)*, **9**, 95-118.

Groundwaters in mineral exploration

Matthew I. Leybourne¹ & Eion M. Cameron²

¹*Ocean Exploration, GNS Science, Lower Hutt NEW ZEALAND*

(e-mail: m.leybourne@gns.cri.nz)

²*Eion Cameron Geochemical Inc., 865 Spruce Ridge Road, Carp, ON CANADA*

ABSTRACT: Groundwater is an important medium for geochemical exploration of many different styles of mineralization, including porphyry copper, volcanogenic massive sulfide (VMS), sandstone uranium, and gold. Groundwater recharges to depth, resulting in greater likelihood of interacting with buried mineralization than media used in surface geochemical methods, and thus providing a three-dimensional perspective. Advances in the understanding of ore formation processes, water-rock interaction and element transport/attenuation in the secondary environment are enhancing the efficacy of groundwater geochemical exploration. This paper describes key techniques and methodologies for sampling, analysis and interpretation of groundwater geochemical data, and provides two different approaches for use by industry: routine exploration and research approaches. New advances in analytical methods are providing new isotopic systems and improving the cost and speed of traditional isotopic techniques, which can greatly aid in interpretation of water sources, water-rock reactions and fingerprinting of ore sources. Case studies are presented for the use of groundwater geochemistry around a porphyry copper deposit in the hyperarid Atacama Desert of Chile, and VMS mineralization in a mature mining camp in Canada. This paper also summarizes key elemental associations for successful utilization of aqueous geochemistry in mineral exploration. The most successful aqueous-phase indicators of mineralization are those that are ore-associated and mobile in solution.

KEYWORDS: *groundwater, mineral exploration, deposit types, isotopes*

INTRODUCTION

Because many surface and near surface mineral deposits have been discovered, the challenge for mineral exploration is to find new, more deeply buried deposits, particularly in areas where thick cover exists and in mature mining camps (Cameron *et al.* 2004). Groundwater is proving to be a powerful mineral exploration medium because: 1) advances in analytical methods, in particular ICP-MS and, more recently MC-ICP-MS (multi-collector) have greatly lowered detection limits and have the potential to revolutionize the use of isotopes in geochemical exploration; 2) groundwaters recharge to depth so that there is potential to penetrate deeply into the earth's crust, so that unlike surficial geochemical methods, groundwater geochemistry offers the potential to explore into the third dimension and detect deeply buried mineralization; 3) groundwaters are chemically reactive with mineralization and host rocks, in particular where waters

are O₂-bearing; 4) groundwater flows away from the site of mineralization, providing a potentially broader exploration target than litho-geochemistry; 5) there is little sample preparation; and 6) for many species of interest in geochemical exploration, background concentrations are low, enhancing anomaly contrast.

Groundwater geochemistry is also proving to be a key tool in the interpretation of geochemical data from weak leaches of soils (Cameron *et al.* 2004). One of the difficulties of soil weak leaches is that interpretation of the results is hampered by poor understanding of metal-migration mechanisms (Goldberg 1998; Cameron *et al.* 2004). For example, recent work in the Atacama Desert of northern Chile has indicated that seismic pumping of groundwaters interacting with mineralization is a viable mechanism for producing significant anomalies in soils and gravels over porphyry copper mineralization (Cameron *et al.* 2002; Cameron *et al.* 2004) (Fig. 1).

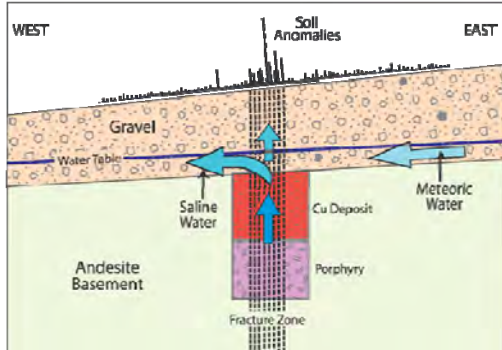


Fig. 1. Conceptual model for dispersion via groundwater flow after water-deposit interaction. This model also indicates the formation of soil geochemical anomalies from seismic pumping of groundwater.

Geochemical techniques for mineral exploration rely on the development of anomalies in the regional geochemical background. Critical to development of effective exploration strategies is an understanding of the mechanisms of anomaly development in different settings and for different sample media. In contrast to surface geochemical anomalies (dominated by mechanical dispersion), groundwater geochemical anomalies fundamentally develop by hydromorphic dispersion.

KEY CONSIDERATIONS

In some environments, such as northern Chile or parts of Australia, grid drilling is common, ideal for the purposes of groundwater geochemical exploration. Groundwater geochemistry is also practical in areas where domestic or agricultural wells already exist, and from springs and seeps that represent groundwater return to surface (indeed, stream waters generally represent shallow groundwater discharge). Groundwater from exploration drill holes provides additional data to litho-geochemistry; groundwater flow may provide geochemical vectors to mineralization even in an apparently barren hole. Sampling techniques range from simple down-hole bailers to complicated straddle-packer systems; the choice depends to a great extent on the objectives of the sampling program and the nature of the

hydrology.

A geochemical anomaly develops in groundwater by flow through mineralization; interpretation is greatly enhanced where there is information regarding the local and regional hydrology (Carey *et al.* 2003; Leybourne & Goodfellow 2003; Gilliss *et al.* 2004). Interpretation of hydrology is simplified in regions dominated by porous flow in unconfined aquifers, and significantly more complicated where flow is fracture-dominated, or where significant density contrasts between different groundwater flow systems exist (Carey *et al.* 2003).

A full understanding of groundwater geochemistry requires analysis and interpretation of the major ion composition. Major ions permit classification and interpretation of water type, mixing, evaporation, water-rock reaction and recharge. Although the major ion chemistry of waters in a hydrogeochemical survey should be interpreted and considered in conjunction with the trace metal data, owing to the complexities of water-rock reactions, cation exchange reactions and formation of secondary minerals, the major element chemistry of water should be used with great caution as an exploration guide in the absence of other (i.e., deposit-diagnostic) chemical data.

The degree to which a water sample will be anomalous with respect to proximal or distal mineralization depends on the solubility of the species that reflect that style of mineralization under the prevailing pH, Eh, and salinity conditions. Ideally, the geochemical explorationist would like any sample medium to have anomalies in all species that define the style of mineralization. In reality, this is rarely, if ever, the case. However, although waters and sediments will not necessarily have anomalies in all the relevant elements, it is important to understand why this is the case and avoid the temptation to include elements that are not diagnostic of the style of mineralization.

Traditionally, stable and radiogenic isotopes have not been used in routine mineral exploration programs. Use of

isotopes has been hampered by cost, additional requirements for sampling and perceived difficulties in data interpretation. Although this underutilization of isotopes in exploration is unlikely to change for large exploration programs, there are applications that warrant their incorporation. The light stable isotopes (e.g., O, H, S) can greatly assist in the interpretation of water sources, mixing and water sulfide interaction (Cameron & Leybourne 2005; Leybourne & Cameron 2006; Leybourne *et al.* 2006) (Fig. 2). In addition, advances in analytical methods in terms of detection limits, sample throughput and lower costs are such that some isotope systems may become as routine as ICP-MS elemental analyses are today. Isotopes of potential use in mineral exploration include the traditional stable isotopes (O, H, C, S), radiogenic isotopes (Pb, Sr), and non-traditional isotope systems, such as Fe, Se and Cu.

CONCLUSIONS

The following recommendations can be made with respect to the use of groundwater geochemistry in mineral exploration. There is a continued need for better integration of real aqueous geochemical data and thermodynamic modeling programs, in particular the incorporation of kinetic thermodynamics and adsorption to Mn and clay minerals. In addition, the thermodynamic databases for saline waters (greater than seawater) are limited with respect to most of the trace metals of interest to exploration. Accurate hydrological models are needed in a study area in order to connect surface aqueous geochemistry to groundwater flow and metal sources. In new areas or new styles of mineralization, orientation studies are important, in particular with a view to determining the elemental associations that are diagnostic of that style of mineralization. In these kinds of studies, emphasis should be placed on characterization of groundwaters (via wells, springs), surface waters and partial leaches of stream (and groundwater suspended) sediment. Determine the type of sampling apparatus to be used; routine

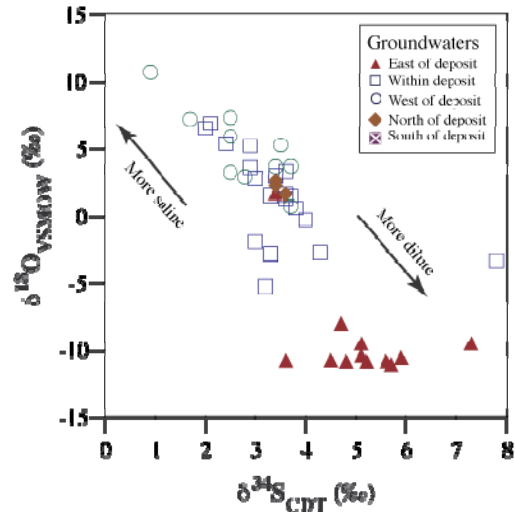


Fig. 2. Stable isotopes of S and O in groundwaters, Spence porphyry Cu deposit, Chile. These data are consistent with mixing between deep saline waters and regional dilute meteoric waters.

exploration may only require a flow-through bailer, whereas, more detailed studies will likely need some form of down-hole pump or straddle-packer system, particularly in fractured-rock media to provide optimal understanding of the redox state of the groundwater system. If resources permit, isotopic analyses can prove invaluable. In particular, Pb isotopes can be used to fingerprint metal sources and S isotopes (in both SO_4^{2-} and HS^- , as appropriate) can provide vectors to mineralization. Analytical methods are rapidly advancing in terms of technology and more rapid and cost-effective techniques. It is likely that isotopic analyses, such as Pb and S, will become cheap and routine in a small number of years. One of the great advantages of collecting groundwater samples during exploration is that the data is also critical in establishing local and regional geochemical baselines should the program be successful in finding mineralization and the decision made to initiate mining.

REFERENCES

- CAMERON, E.M., HAMILTON, S.M., LEYBOURNE, M.I., HALL, G.E.M., & MCCLENAGHAN, B. 2004. Finding deeply-buried deposits using

- geochemistry. *Geochemistry: Exploration, Environment, Analysis*, **4**, 7-32.
- CAMERON, E.M. & LEYBOURNE, M.I. 2005. Relationship between groundwater chemistry and soil geochemical anomalies at the Spence copper porphyry deposit, Chile. *Geochemistry: Exploration, Environment, Analysis*, **5**, 135-145.
- CAMERON, E.M., LEYBOURNE, M.I., & KELLEY, D.L. 2002. Exploring for deeply covered mineral deposits: Formation of geochemical anomalies in northern Chile by earthquake-induced surface flooding of mineralized groundwaters. *Geology*, **30**, 1007-1010.
- CAREY, M.L., MCPHAIL, D.C., & TAUFEN, P.M. 2003. Groundwater flow in playa lake environments: impact on gold and pathfinder element distributions in groundwaters surrounding mesothermal gold deposits, St. Ives area, Eastern Goldfields, Western Australia. *Geochemistry: Exploration, Environment, Analysis*, **3**, 57-71.
- GILLISS, M.L., AL, T.A., BLOWES, D.W., HALL, G.E.M., & MACLEAN, B. 2004. Geochemical dispersion in groundwater from a weathered Cu-Zn deposit in glaciated terrain. *Geochemistry-Exploration Environment Analysis*, **4**, 291-305.
- GOLDBERG, I.S. 1998. Vertical migration of elements from mineral deposits. *Journal of Geochemical Exploration*, **61**, 191-202.
- LEYBOURNE, M.I. & CAMERON, E.M. 2006. Composition of groundwaters associated with porphyry-Cu deposits, Atacama Desert, Chile: Elemental and isotopic constraints on water sources and water-rock reactions. *Geochimica et Cosmochimica Acta*, **70**, 1616-1635.
- LEYBOURNE, M.I., CLARK, I.D., & GOODFELLOW, W.D. 2006. Stable isotope geochemistry of ground and surface waters associated with undisturbed massive sulfide deposits; constraints on origin and water-rock reactions. *Chemical Geology*, **231**, 300-325.
- LEYBOURNE, M.I. & GOODFELLOW, W.D. 2003. Processes of metal solution and transport in ground waters interacting with undisturbed massive sulfide deposits, Bathurst Mining Camp, New Brunswick. In: GOODFELLOW, W.D., McCUTCHEON, S.R., & PETER, J.M. (eds.), *Massive Sulphide Deposits of the Bathurst Mining Camp, New Brunswick, and Northern Maine*, Economic Geology Monograph, **11**, 723-740. Society of Economic Geologists, Inc.

Soluble ionic gold in soils

Melvyn J. Lintern¹, Chris G. Ryan², & Robert M. Hough¹

¹CSIRO Exploration & Mining, P.O. Box 1130, Bentley, 6102 AUSTRALIA
(e-mail: mel.lintern@csiro.au)

²CSIRO Exploration and Mining, c/o CMSE, Bayview Avenue, Clayton, VIC3168 AUSTRALIA

ABSTRACT: Mobile Au in soil has been postulated for many years. It has been used by the mineral exploration industry in areas of transported overburden as a vector towards buried deposits. Until now, the nature of this mobile Au has not been known or investigated. Soil samples from a colluvial area above the Bounty Deposit (Yilgarn Craton, Western Australia) investigated by analytical techniques including laser ablation inductively coupled mass spectrometry (LA-ICP-MS) and synchrotron x-ray fluorescence (SXRF) combined with X-ray absorption spectrometry (XAS) have allowed us to map the 'invisible' Au in these soils and suggests that at least some of it occurs in an ionic form.

KEYWORDS: *gold, synchrotron XRF, mineral exploration, ionic gold, Yilgarn Craton*

INTRODUCTION

For centuries Au was thought to be an inert (noble) metal dissolving only in highly aggressive solutions such as aqua regia or cyanide. However, over time it was postulated that metallic Au could also be dissolved in the natural environment by ligands such as thiosulphate, halogens and certain organic ions (Ong & Swanson 1969; Boyle 1979; Gray & Lintern 1998).

Recently, it has been shown that Au in soil can be dissolved using deionised water, the most benign of lixiviants (Gray *et al.* 1999). The reason for this is not clear: either (i) Au occurs in a soluble form within the soil, and/or (ii) deionised water is dissolving an adsorbed ligand in the soil such as cyanide that subsequently dissolves metallic Au. Notwithstanding these uncertainties, use has been made of this previously recognised soluble Au characteristic in soil by mineral exploration and analytical companies, to provide a possible vector towards mineral deposits.

The study of natural Au in soil has been hampered by low concentrations, typically in the ppb range. Investigating the presence of metallic ions has been made more difficult with very few traditional techniques that may be used (e.g. polarography, high voltage electrophoresis and ion chromatography). At the low concentrations of Au in soil, these

techniques may not have practical application at all. Here, we make use of SXRF to map Au in soil and demonstrate that some of the Au is ionic in form.

METHOD

Soil samples were collected systematically down a 2 m deep colluvial soil profile located over Au mineralisation at the Bounty Gold Deposit (Yilgarn Craton, Western Australia), prior to mining. Bulk samples were analysed by ICP-AES, ICP-MS and XRD and further sub-sampled and analysed to ensure that they contained detectable Au prior to detailed analysis by LA-ICP-MS, SXRF and x-ray adsorption near edge spectrometry (XANES).

Samples from the entire profile were analysed for 'soluble' Au using deionised water, iodide (0.1M KI) and cyanide (2000 ppm KCN) in a sequential digest using activated carbon to precipitate the Au (details of method found in Lintern & Butt (1992)).

Two samples from the soil profile were randomly separated into very small sub-samples (a few millimetres across) and analysed after *aqua regia* digestion to assess the heterogeneous nature of the Au distribution. Replicate sub-samples were analysed to assess the likelihood of finding Au in other soil particles using LA-

ICP-MS and SXRF. Based on low Au concentration variation for these sub-samples, further sub-samples of the remaining bulk material were mounted in epoxy resin to form discs (c. 2.5 cm in diameter) and polished for LA-ICP-MS, SXRF and XANES analyses

RESULTS

Water- (up to c. 20% of total Au), iodide- (c. 90%) and cyanide-soluble Au (100%) were recorded in all samples down the soil profile. Although the bulk sample Au-Ca correlation is strong down-profile, there is no correlation at the scale of soil particles. Soil particles with high Ca do not necessarily correspond with those high in Au. Critically, Au was present in all soil particles and the standard deviation in the results was acceptable with respect to the aims of the experiment. The results suggest that any soil particle of similar size from the two bulk samples may be investigated. We considered that Au concentrations were high enough (c. 600 ppb) and of sufficiently low variability (<20 % RSD) for the next stage of analysis by LA-ICP-MS and SXRF.

The Au and Ca LA-ICP-MS data for samples from the profile at Bounty indicate the following:

- (1) Au is highly variable but the samples containing the most bulk sample Au register the highest raw counts by LA-ICP-MS.
- (2) Sharp maxima suggest that some Au is particulate, and is not confined to one specific soil particle or location in the soil profile.
- (3) Ca concentrations are less variable and lack sharp maxima, suggesting that the distribution of calcite and/or dolomite is more uniform than Au.
- (4) Peaks in Ca and Au are uncorrelated.

SXRF maps reveal Au distributed throughout the specimen, with Au accumulations in certain areas. Gold is clearly associated with Br in some areas and potentially with other halides (which were not determined). XANES analysis suggests Au(I) speciation. Other areas of higher Au and Br show no correlation with each other.

The results confirm the hypothesis that some of the Au is ionic. This ionic Au appears to be associated with Br but other halogens or evaporites may also be present and play a role in complexing the Au. The results do not preclude the possibility that water is dissolving a ligand in the soil which in turn is dissolving and complexing other Au in the sample. Some Au in the soil appears to be metallic in form as nanoparticles.

Both inorganic and organic processes may be involved with Au mobilisation and precipitation. In laboratory studies, water and 0.1 M KI solutions are capable of dissolving substantial proportions of the Au in the profile at Bounty, although there are important differences in the Au dissolution response to the two lixiviants down-profile. Iodide-dissolved Au is closely correlated with total Au, whereas the proportion of water-soluble Au is greater (relative to iodide and total Au) near the top of the profile. This difference may reflect the relative ratios of ionic and non-ionic Au present in the sample. More water-soluble Au occurs near the surface and may be related to a greater mass of active plant roots, more micro-organisms or higher concentrations of organic compounds.

CONCLUSIONS

For many years, mineral explorers have been using soluble Au as vectors to mineralisation. The results described here may partly explain the nature of this soluble Au and increase our understanding of the processes that lead to its formation.

ACKNOWLEDGEMENTS

We thank Robert Gordon and Steve Heald of the Advanced Photon Source, Chicago; and David Gray, Nathan Reid, David Lentz and Gwendy Hall for commenting on earlier versions of the abstract.

REFERENCES

- BOYLE, R.W. 1979. Chemistry, mineralogy and geochemistry of gold (chapter II). The geochemistry of gold and its deposits.

- Geological Survey of Canada Bulletin*, **280**, 584 p.
- GRAY, D.J. 1998. The aqueous chemistry of gold in the weathering environment. CSIRO Division of Exploration Geoscience, Perth, Restricted Report EG4R, 65 pp. (Reissued as *Open File Report 38*, CRC LEME, Perth, 1998), 65.
- GRAY, D.J., LINTERN, M.J., & LONGMAN, G.D. 1990. Chemistry of gold in some Western Australian Soils. CSIRO Division of Exploration Geoscience, Perth, Restricted Report 126R, 62p. (Reissued as *Open File Report 68*, CRC LEME, Perth, 1999)
- LINTERN, M.J. & BUTT, C.R.M. 1992. The distribution of gold and other elements in soils and vegetation at Zuleika, Western Australia. CSIRO Division of Exploration Geoscience, Perth, Restricted Report 328R, 95 pp. (Reissued as *Open File Report 52*, CRC LEME, Perth, 1998)
- ONG, H.L. & SWANSON, V.E. 1969. "Natural organic acids in the transportation, deposition and concentration of gold." *Quarterly of the Colorado School of Mines* **64**, 395-425.

Gold in pedogenic carbonate revealed

Melvyn J. Lintern^{1,2}, Chris G. Ryan³ & Robert M. Hough¹

¹CSIRO Exploration & Mining, P.O. Box 1130, Bentley, WA6102 AUSTRALIA

(e-mail: mel.lintern@csiro.au)

²Curtin University of Technology, Department of Applied Geology, Bentley, WA6102 AUSTRALIA

³CSIRO Exploration and Mining, c/o CMSE, Bayview Avenue, Clayton, VIC3168 AUSTRALIA

ABSTRACT: Calcrete is an important sampling medium used for Au exploration in Australia and elsewhere. Until now, the form of the Au has not been identified *in situ* in calcrete even though concentrations have been in the hundreds of ppb. We present images generated using data derived from synchrotron X-ray fluorescence and X-ray adsorption near edge spectrometry that show the distribution of Au in pedogenic carbonate samples and demonstrate its correlation with Br. The images also show an association between Au and organic material in the carbonate sample that supports a previously proposed mechanism of Au accumulation in pedogenic carbonate that has been shown to occur through vegetation.

KEYWORDS: gold, vegetation, mineral exploration, Au-Br, calcrete

INTRODUCTION

Pedogenic carbonate of various forms (generically described as calcrete or caliche) has been sampled and analysed to locate Au mineralisation in Australia (Edgecombe 1997; Lintern *et al.* 1997; Lintern 2001; Drown 2003) and elsewhere. Trace amounts of Au are concentrated in calcrete occurring close to mineralisation and surficial regolith carbonates may even be anomalous for Au where mineralisation is buried beneath transported overburden (Bristow *et al.* 1996; Lintern 2007). The strong correlation of Au with alkaline earth metals (Ca, Mg, and Sr) in soil profiles is unexpected given the very different chemistries of Au to these elements and suggests that the processes leading to their co-location in the soil profile are similar. However, despite its importance to mineral exploration, various difficulties (e.g. the low concentrations) have hampered research on the detailed nature of the Au in calcrete.

METHOD

Samples were collected from a 2-m deep trench excavated prior to mining from the Bounty Gold Deposit in Western Australia. Bulk soil samples were analysed by ICP-

AES, ICP-MS and XRD, and further sub-sampled and analysed to ensure that they contained Au prior to detailed analysis by LA-ICP-MS, SXRF (synchrotron X-ray fluorescence) and μ XANES (X-ray adsorption near edge spectroscopy). Two samples from the trench were randomly divided into very small sub-samples (a few millimetres across) and analysed after *aqua regia* digestion to assess the heterogeneous nature of the Au distribution. Replicate sub-samples were analysed by ICP-MS to assess the probability of finding future Au in unanalysed soil particles using LA-ICP-MS and SXRF. Large sub-sample Au concentration variation would indicate a low probability of finding Au in other soil particles from the sample. As analytical variability for these sub-samples was low, further sub-samples of the remaining bulk material were mounted in epoxy resin to form polished discs (c. 2.5 cm in diameter) for LA-ICP-MS, SXRF and XANES analyses.

A LSX-200 Plus Laser Ablation System (CETAC Technologies, Omaha, Nebraska, USA), using a Nd:YAG laser with a wavelength of 266 nm, was used for the analyses. A spot size of 100 μ m was selected. Sufficient volume of ablated

material was required for Au to be detected. A 'trough' 100 μm wide and 2.5 cm long was left as the laser was tracked across the diameter of the discs.

SXRF imaging and XANES analysis were made at the PNC/XOR beamline at the Advanced Photon Source, Argonne National Laboratory (Heald. *et al* 2007) using photon energies of 17.0 and 12.5 keV for SXRF imaging and 11.8 to 12.1 keV for XANES analysis. XANES analysis across the Au L₃ edge used steps of 5 eV (from 11.82 – 11.89 keV), 0.5 eV (from 11.89-11.97 keV) and 0.07 k (from 11.97-12.1 keV) with a one second dwell per step.

SXRF imaging data were projected onto elemental images using the Dynamic Analysis method (Ryan 2000; Ryan & Jamieson 1993) in the GeoPIXE software package, which uses a standardless analysis approach (Ryan *et al.* 2005). The Dynamic Analysis method constructs a matrix transformation to deconvolute or 'un-mix' overlapping element lines and background to reconstruct separated elemental images with strong discrimination against interferences caused by overlapping lines and detector artefacts, such as tailing and escape peaks. In this work, it enabled the separation of Au L lines from interferences from W (L β , γ overlap with Au L α , β), Zn (K β overlap with Au L α), Yb (L γ overlap with Au L α), As (K α tails interfere with Au L α ; K β close to Au L β) and Br (K α tails interfere with Au L β). Spectra were extracted from selected regions of images and least squares fitted using GeoPIXE in order to verify in detail the accuracy of the deconvolution and the identification of important features such as the Au distribution.

RESULTS

The results show that Au is distributed throughout the specimens and ionic Au is partly associated with a root void and possibly filaments (rootlets) within the specimen. This is the first direct evidence for ionic Au in any regolith material and is consistent with Au mobilisation within the rhizosphere. Natural ionic Au species in

the weathered environment have only ever been reported before as dissolved Au in groundwaters or pore waters and as remnant Au-containing minerals. Ionic Au has been identified before in conjunction with so-called 'invisible' Au in arsenopyrites (e.g., Cabri *et al.* 2000; Xiaoqing & Zhonggang 2002).

XANES analyses show that ionic Au commonly occurs around cores of Au⁰ suggesting a dissolution-precipitation process, i.e. previously accumulated Au has been dissolved and is then dispersed into the surrounding soil; current observations are a snapshot of active processes. Gold is in part correlated with Br. However, the significance of the Br-Au association is unclear since other 'evaporites' such as chloride, sulphate or iodide that were not determined may be more significant. The Au-Br association may represent i) a simple Au bromide molecule, ii) a Au chloride molecule (with minor Br correlated with Cl), iii) a halogenated Au-organic complex or iv) a precipitation zone where saturation has been reached for a variety of salts that may include separate Au and Br ionic complexes. Any Au complex must be stable enough to survive the harsh and changing conditions in soil.

CONCLUSIONS

The results confirm the importance of biotic influences in the control of Au mobilisation in soil. Importantly, the results support the role that vegetation is playing in the formation of Au in calcrete anomalies by creating conditions in the rhizosphere that cause the precipitation of Au.

ACKNOWLEDGEMENTS

We thank Robert Gordon and Steve Heald of the APS, Chicago, David Gray and Ryan Noble (CSIRO), and David Lentz and Gwendy Hall (Organising Committee, 24th IAGS 2009) for improving earlier versions of this abstract.

REFERENCES

BRISTOW, A.P.J., LINTERN, M.J., & BUTT, C.R.M. 1996. Geochemical expression of concealed

- gold mineralization, Safari Prospect, Mt Celia, Western Australia. *CRC LEME Report 13R/Exploration and Mining Report 281R*. 58p. (Reissued as Open File Report **104**, CRC LEME, Perth, 2001).
- CABRI, L.J., NEWVILLE, M., GORDON, R.A., CROZIER, E.D., SUTTON, S.R., MCMAHON, G., & JIANG, D. 2000. Chemical speciation of gold in arsenopyrite. *Canadian Mineralogist*, **38**, 1265-1281.
- DROWN, C.G. 2003. The Barns Gold Project. *Quarterly Earth Resources Journal of Primary Industries and Resources South Australia*, **28**, 4-9.
- EDGEcombe, D. 1997. Challenger gold deposit. *Mines and Energy Resources South Australia Quarterly Journal*, **4**, 8-11.
- HEALD, S.M., CROSS, J.O., BREWE, D.L., & GORDON, R.A. 2007. The PNC/XOR X-ray microprobe station at APS sector 20: Proceedings of the 14th National Conference on Synchrotron Radiation Research - SRI 2007. *Nuclear Instruments and Methods in Physics Research Section A*, **582**, 215-217.
- LINTERN, M.J. 1997. Calcrete sampling for gold exploration. *Mines and Energy Resources South Australia Quarterly Journal*, **5**, 5-8.
- LINTERN M.J. 2001. Exploration for gold using calcrete - lessons from the Yilgarn Craton, Western Australia. *Geochemistry: Exploration, Environment, Analysis*, **1**, 237-252.
- LINTERN, M.J. 2007. Vegetation controls on the formation of gold anomalies in calcrete and other materials at the Barns Gold Prospect, Eyre Peninsula, South Australia. *Geochemistry: Exploration, Environment, Analysis* **7**, 249-266.
- RYAN, C.G. 2000. Quantitative trace element imaging using PIXE and the nuclear microprobe. *International Journal of Imaging Systems and Technology*, **11**, 219-230.
- RYAN C.G. & JAMIESON D.N. 1993. Dynamic analysis: on-line quantitative PIXE microanalysis and its use in overlap-resolved elemental mapping. *Nuclear Instruments and Methods in Physics Research Section B*, **77**, 203-214.
- RYAN, C.G., ETSCHMANN, B.E., VOGT, S., MASER, J., HARLAND, C.L., VAN ACHTERBERGH, E., & LEGNINI, D. 2005. Nuclear Microprobe - Synchrotron synergy: towards integrated quantitative real-time elemental imaging using PIXE and SXRF. *Nuclear Instruments and Methods in Physics Research Section B* **231**, 183-188.
- XIAOQING Z. & ZHONGGANG W. 2002. Gold occurrence and ore genesis, Yata micro-disseminated gold deposit, Guizhou, Southwest China. *Chinese Journal of Geochemistry*, **21**, 370-373.
- YANG, B.X., RIVERS, M., SCHILDKAMP, W., & ENG, P.J. 1995. GeoCARS microfocussing Kirkpatrick-Baez mirror bender development. *Review of Scientific Instruments*, **66**, 2278.

Till indicator mineral and geochemical signatures of magmatic Ni-Cu deposits, Thompson Nickel Belt, central Canada

M.B. McClenaghan¹, S.A. Averill², I.M. Kjarsgaard³,
D. Layton-Matthews⁴, & G. Matile⁵

¹ Geological Survey of Canada, 601 Booth Street, Ottawa ON, K1A 0E8 CANADA
(email: bmcclena@nrcan.gc.ca)

² Overburden Drilling Management Ltd., 107-15 Capella Ct, Ottawa, ON, K2E 7X1 CANADA

³ Consultant, 15 Scotia Place, Ottawa, ON, K1S 0W2 CANADA

⁴ Department of Geological Sciences, Queen's University, Kingston, ON, K7L 3N6 CANADA

⁵ Manitoba Geological Survey, 360-1395 Ellice Avenue, Winnipeg, MA, R3G 3P2 CANADA

ABSTRACT: The Geological Survey of Canada conducted a study around the ultramafic-associated Ni-Cu deposits in the northern Thompson Nickel Belt, Manitoba, Canada to document the indicator mineral and geochemical signatures of the deposits in till. Samples used in this study include archived till collected in 1996 and till and bedrock samples collected in 2005 and 2006. Ni-Cu mineralization indicator minerals identified in the study include pentlandite, pyrrhotite, sperrylite, chalcopyrite, pyrite, millerite and arsenopyrite. Indicators of potentially fertile ultramafic intrusions include chromite, Cr-diopside, forsterite, enstatite and Cr-corundum. Till geochemical pathfinder elements identified in this study include Ni, Cu, Pd, Pt, Co, As, Cd, Ag, Sb, Bi, Se, S, and Te. Six anomalous till samples from remote locations outside the Belt contain significant elevated concentrations of pathfinder elements and warrant further investigation. The Laurentide Ice Sheet flowed SW across the belt and subsequently W and exploration along the belt and in the surrounding terranes should consider both the older southwest and younger westward ice flow events when interpreting and following up till mineralogical and geochemical results.

KEYWORDS: *indicator minerals, till geochemistry, pathfinder elements, Ni-Cu exploration*

INTRODUCTION

Few case studies have been published for magmatic Ni-Cu-PGE deposits and even fewer that document the indicator mineral signatures of this deposit type. The Geological Survey of Canada (GSC) through its Targeted Geoscience Initiative 3, in collaboration with the Canadian Mining Industry Research Organization (CAMIRO) and the Manitoba Geological Survey (MGS) collected and analyzed a suite of bedrock and till samples from around the Thompson and Pipe ultramafic Ni sulfide deposits in the north part of the Thompson Nickel Belt (TNB), northern Manitoba, Canada (Fig. 1). The objective of the study was not to define the dispersal trains from each deposit. Instead sample sites were selected to characterize the geochemical and mineralogical signature of Ni-Cu mineralization at the deposit- and camp-scale at varying

distances down-ice and to define background.

GEOLOGICAL SETTING

The TNB is a 10 to 35 km wide belt of variably reworked Archean basement gneisses and Early Proterozoic cover rocks along the NW margin of the Superior Craton (Zwanzig *et al.* 2007). It hosts several world-class magmatic Ni-Cu deposits that have been strongly structurally and metamorphically modified. Nickel sulfide mineralization is associated almost exclusively with, or localized within, ultramafic bodies within the lower part of the Proterozoic rocks (Bleeker & Macek 1996). Primary (i.e., non-supergene) ores are dominated by pyrrhotite, pentlandite, pyrite, and millerite. Chalcopyrite, magnetite and ferro-chromite are ubiquitous minor phases (Layton-Matthews *et al.* 2007)

The most recent glaciation, during the Wisconsin, resulted in ice that flowed SW from an ice centre in Keewatin and then W from ice centred in Hudson Bay (Klassen 1986) (Fig. 1). Both ice flow events eroded and transported metal rich debris from the TNB deposits. In general, till across the region is thin (<3 m thick) and has a silty sand matrix. As the Laurentide Ice Sheet melted back 7800 years BP, the region was inundated by glacial Lake Agassiz for approximately 100 years, during which time rhythmically-bedded clay and silt were draped over bedrock and till, in places up to 40 m thick. As a result, the region is a flat lying clay plain comprising a relatively low relief, poorly drained landscape dominated by organic deposits with few bedrock outcrops. The TNB is the source of a well developed indicator mineral dispersal train best defined by Cr-diopside content in till that extends up to 300 km southwest of the Belt (Matile & Thorleifson 1997). The elevated Cr-diopside abundances in till overlying the TNB are accompanied by local occurrences of chalcopyrite, hercynite, chromite and loellingite in till proximal to the Ni deposits.

METHODS

Bedrock (5 kg) and till samples (15 kg) were collected across the northern TNB in 2005 and 2006, most closely spaced around the Thompson and Pipe Ni-Cu deposits. Till samples collected in 1996 (Matile & Thorleifson 1997) were re-analyzed as part of this study. Bedrock samples were collected from various lithologies within or adjacent to the TNB, and mineralized and unmineralized ultramafic intrusions. Till samples included sites at varying distances down-ice (SW and W) of the Thompson and Pipe mines. The <0.063 mm fraction of till was analyzed using aqua regia and lithium borate fusion/nitric acid digestions and inductively coupled plasma emission and mass spectrometry (ICP-ES/MS) techniques. Gold, Pt, Pd were determined by fire assay/ICP-MS. Bulk till and crushed bedrock samples were processed using a combination of tabling and heavy

liquid separation to produce ferro- and non-ferromagnetic heavy mineral concentrates. Indicator minerals were examined and counted in the 0.25 to 2.0 mm portion of the concentrates. Electron microprobe analyses were completed for chromite and olivine from till and bedrock, in addition to Cr-diopside, olivine and Cr-corundum from till samples.

INDICATOR MINERAL RESULTS

A well developed indicator mineral signature (1000s to 10,000s of grains) occurs in till proximal (<1 km) to sulfide mineralization. Ni-Cu mineralization indicator minerals include pentlandite, pyrrhotite, sperrylite, chalcopyrite, pyrite, millerite, arsenopyrite and loellingite. Of these minerals, chalcopyrite and sperrylite are the most likely to survive glacial transport and subsequent surficial weathering (Averill 2007) and thus will be the most useful for regional exploration. Indicators of potentially fertile ultramafic intrusions include chromite, Cr-diopside, forsterite, enstatite, and Cr-corundum. Chromite and Cr-diopside (> ~1% wt.% Cr₂O₃) in till are most abundant in till samples proximal to mineralization. Mineral abundance patterns for chromite, Cr-diopside, forsterite, and enstatite also indicate that some of these grains are derived from ultramafic rocks east of the TNB, some of which may warrant further investigation for their potential to host Ni-Cu mineralization.

The composition of chromite in bedrock ranges from ferrochromite (FeCr₂O₄) with >60 wt.% Cr₂O₃ to Cr-rich magnetite (Fe(Fe,Cr)₂O₄) with >10 wt.% Cr₂O₃. A second trend ranges from magnesian chromite ((Fe,Mg)(Cr,Al)₂O₄) with >60 wt.% Cr₂O₃ to spinel *sensu stricto* (MgAl₂O₄). A striking feature of the magnetite trend chromites is their elevated Zn content (>2 to 18 wt.% ZnO) that is restricted in occurrence to mineralized bedrock at the Thompson, Birchtree and Pipe mines and proximal (<500 m) till samples. Zn-rich chromite was expected as other researchers have reported its presence in TNB deposits (e.g., Paktunc & Cabri 1995), as well as other magmatic Ni-Cu deposits around the world (e.g.,

Peltonen & Lamberg 1991). The cause of Zn enrichment in chromite in the TNB ores is likely related to the high grade of metamorphism that has affected the belt. The Thompson mine is at the highest metamorphic grade (granulite) of all the deposits in the belt and so the most Zn-rich chromites are expected here. Ongoing research is focusing on determining potential source(s) of the Zn in the chromites and identifying other trace elements that may fingerprint chromite associated with mineralization through laser ablation ICP-MS studies and on olivine chemistry.

The bedrock source of the 10s to 100s of Cr-diopside grains in till across the region has not yet been found. In spite of the predominance of pyroxenites and peridotites in the TNB, remnants of primary Cr-diopside are scarce because most rocks have been metamorphically and metasomatically altered such that serpentine has replaced olivine and orthopyroxene and amphibole, chlorite, talc and carbonate has replaced clinopyroxene. Because the Cr-diopside source is unknown, their compositional range and relationship to Ni-mineralization cannot be determined.

TILL GEOCHEMICAL RESULTS

Ni-Cu ores in the TNB are dominated by pentlandite, pyrrhotite, pyrite and millerite (Burnham *et al.* 2003; Layton-Matthews *et al.* 2007) and thus local metal-rich till is Ni-rich (up to 3760 ppm). Till samples that contain the highest Ni contents also contain up to 50,000 pentlandite grains/10 kg in the 0.25-0.5 mm fraction. Till with elevated Cu values (215 ppm) at the Thompson and Pipe mines contain up to 2500 chalcopyrite grains/10 kg. TNB ore also contains Te, As, Sb, Co, Cd, Se and Bi-bearing mineral species, which are likely the source of elevated concentrations of these elements in till proximal to the deposits. A variety of PGE minerals occur in the ores, thus, it is likely that PGE minerals are the source of the elevated Pd (up to 98 ppb) and Pt (up to 13 ppb) concentrations in till. Sperrylite grains were recovered from nine till

samples collected near the Thompson and Pipe mines. The full suite of till pathfinder elements for Ni-Cu deposits in the TNB include Ni, Cu, Pt, Pd, Co, As, Ag, Cd, Sb, Bi, S, Se, and Te (McClenaghan *et al.* 2009). Using these pathfinder elements, six anomalous till samples in remote locations collected as part of the 1996 regional survey were identified. These samples are new exploration targets as they may indicate the presence of previously unknown Ni-Cu mineralization.

IMPLICATIONS FOR EXPLORATION

- Till mineralogy and geochemistry are useful Ni-Cu exploration methods in the TNB. Exploration should consider both the older SW and younger W ice flow events when interpreting till data.
- Elevated chromite and Cr-diopside (> ~1% wt.% Cr₂O₃) abundances combined with the presence of Ni-Cu sulfide minerals are strong indicators of potential Ni-Cu mineralization. Elevated Zn content (>2 wt.% ZnO) in chromite is only found in strongly mineralized rocks and is the strongest indicator for mineralization other than the actual ore minerals. Zn content in chromite from Ni-deposits in regions with lower metamorphic grade might be considerably lower and this feature thus does not have universal application.
- Chalcopyrite and sperrylite are the most useful metallic indicator minerals identified as they are the most likely to survive glacial transport and surficial weathering.
- Till geochemistry of <0.063 mm fraction is a useful tool for Ni exploration in the TNB and surrounding region. Pathfinder elements include Ni, Cu, Pd, Pt, Co, As, Cd, Ag, Sb, Bi, Se, S, and Te.
- Several multi-element (Ni, Cu, Pt, Pd, Co, Cr, As) anomalies occur in till samples in remote locations SW and W of the TNB that suggest presence of mineralized bedrock and warrant further exploration.
- For Ni exploration in the TNB and surrounding areas, till samples in thin drift areas can be collected from the flanks of bedrock outcrops, and from till exposures in road cuts and along lake shorelines and river banks. In areas of thicker cover, backhoe trenching and overburden drilling

could be utilized to obtain till below the potentially thick clay cover.

- Indicator mineral techniques are one of the main exploration methods for gold and diamonds in glaciated terrain. This case study has documented indicator minerals for Ni-Cu deposits. These minerals can be used in tandem with gold and diamond indicators to assess the mineral potential of broad regions and at local scales.

ACKNOWLEDGEMENTS

GSC funding was provided under the Targeted Geoscience Initiative 3 (2005-2010). The 2005 field season was funded by CAMIRO Project 04E01 and MGS. J. Macek (MGS) is thanked for sharing his bedrock geology knowledge of the TNB and assisting with sampling. M. Doherty (ALS Chemex) and T. Lane (CAMIRO) assisted with the planning and sampling in 2005. Vale-Inco is thanked for providing access, confidential information, samples, and assistance with fieldwork.

REFERENCES

AVERILL, S.A. 2007. Viable indicators in surficial sediments for two major base metal deposit types: Ni-Cu-PGE and porphyry Cu. In: Exploration 07 Workshop 3: *Indicator Mineral Methods in Mineral Exploration*, 33-42.

BLEEKER, W. & MACEK, J. 1996. Evolution of the Thompson nickel belt, Manitoba: setting of Ni-Cu deposits in the western part of the Circum Superior Boundary zone. Field Trip Guidebook A1. Geological Association of Canada, 44 p.

BURNHAM, O.M. *et al.* 2003. Geology, stratigraphy, petrogenesis, and

metallogenesis of the Thompson Nickel Belt, Manitoba: *Final Report for CAMIRO Project 97E-02*.

- KLASSEN, R.W. 1986. Surficial geology of north-central Manitoba. Geological Survey of Canada, *Memoir* **419**, 57 p.
- LAYTON-MATTHEWS, D., LESHER, C. M., BURNHAM, O. M., LIWANAG, J., HALDEN, N.M., HULBERT, L., & PECK, D. 2007. Magmatic Ni-Cu-platinum group element deposits of the Thompson Nickel Belt. In: GOODFELLOW, W. (ed.), *Mineral Deposits of Canada: A Synthesis of Major Deposit Types, District Metallogeny, the Evolution of Geological Provinces and Exploration Methods*. Geological Association of Canada, Special Volume **5**, 409-432.
- MATILE, G.L.D. & THORLEIFSON, L.H. 1997. Till geochemical and indicator mineral reconnaissance of northeastern Manitoba. Manitoba Energy and Mines, Open File 97-3.
- MCCLENAGHAN, M.B., MATILE, G., LAYTON-MATTHEWS, D., & PYNE, M. 2009. Till geochemical signatures of magmatic Ni-Cu deposits and regional till geochemistry, Thompson Ni Belt, Manitoba. *Geological Survey of Canada, Open File* **6005**.
- PELTONEN, P. & LAMBERG, P. 1991. Chromian spinel in Svecofennian ultramafic intrusions: compositional evolution during fractional crystallization, cooling, regional metamorphism and alteration. *Geological Survey of Finland, Special Paper* **12**, 23-31.
- ZWANZIG, H.V., MACEK, J.J., & MCGREGOR, C.R. 2007. Lithostratigraphy and geochemistry of the high-grade metasedimentary rocks in the Thompson Nickel Belt and adjacent Kiseynew Domain, Manitoba: implications for nickel exploration. *Economic Geology*, **102**, 1197-1216.

Lithogeochemical exploration vectors for Au-rich volcanogenic massive sulfide deposits: Examples from the world-class Doyon-Bousquet-LaRonde mining camp, Abitibi Greenstone Belt, Canada

Patrick Mercier-Langevin¹, Benoît Dubé¹, & Mark D. Hannington²

¹Geological Survey of Canada, 490 rue de la Couronne, Québec, QC, G1K 9A9 CANADA
(e-mail: pmercier@nrcan.gc.ca)

²University of Ottawa, 140 Louis Pasteur, Ottawa, ON, K1N 6N5 CANADA

ABSTRACT: The Doyon-Bousquet-LaRonde mining camp contains some of the best examples of Au-rich VMS deposits worldwide in terms of size and grade. These deposits are associated with tholeiitic to transitional mafic to intermediate rocks and transitional to calc-alkaline felsic rocks of the Bousquet Formation that define a continuous rather than a bimodal trend. The ore lenses are associated with two principal types of alteration assemblages that locally coexist: 1) a neutral propylitic quartz, biotite, Mn-rich garnet and sericite assemblage represented by gradual gains in MnO and losses in Na₂O and, 2) an aluminous assemblage comprising mainly aluminosilicates and quartz marked by an intense leaching of all major oxides. The characterization of each unit using immobile element ratios helps define the stratigraphy and target the most fertile horizons, whereas the presence and intensity of one or the two alteration assemblages provide effective vectors to ore.

KEYWORDS: gold-rich, volcanogenic massive sulfide, alteration, vectors, Abitibi

INTRODUCTION

Gold-rich volcanogenic massive sulfide deposits (VMS) represent a prime exploration target as they commonly contain very large amounts of Au combined with significant quantities of base metals. Some of the world's best examples of Au-rich VMS deposits in terms of size and grade are located in the Doyon-Bousquet-LaRonde (DBL) mining camp in the Blake River Group of the Abitibi Subprovince (Fig. 1).

The VMS deposits of the DBL camp are associated with diverse styles of alteration assemblages that may coexist within the same deposit (Dubé *et al.* 2007). The variations in alteration style and intensity towards the numerous deposits and ore lenses of the DBL camp can be mapped using lithogeochemistry, which represents a powerful tool in characterizing prospective areas and stratigraphic horizons, and in vectoring towards mineralized zones, as discussed in the following sections.

GEOLOGICAL SETTING

The Doyon-Bousquet-LaRonde (DBL) mining camp deposits (~25 Moz Au) are hosted by the 2699-2697 Ma Bousquet Formation. The Bousquet Formation is part of the Blake River Group of the Southern Abitibi Greenstone Belt and comprises mainly intermediate to felsic, coherent and flow-brecciated volcanic rocks of transitional to calc-alkaline magmatic affinity cut by a synvolcanic tholeiitic to calc-alkaline polyphase intrusion (Mooshla pluton) and by mafic sills and dikes (Lafrance *et al.* 2003; Mercier-Langevin *et al.* 2007a). The Bousquet Formation now forms a steeply dipping, south-facing homoclinal sequence (Fig. 1). The main deformation event is responsible for some transposition and was accompanied by upper greenschist facies metamorphism that overprinted the primary hydrothermal assemblages (Dubé *et al.* 2007; Mercier-Langevin *et al.* 2007a).

The Au-rich polymetallic VMS deposits of the Doyon-Bousquet-LaRonde mining camp (Westwood, Ellison, Bousquet 1 and

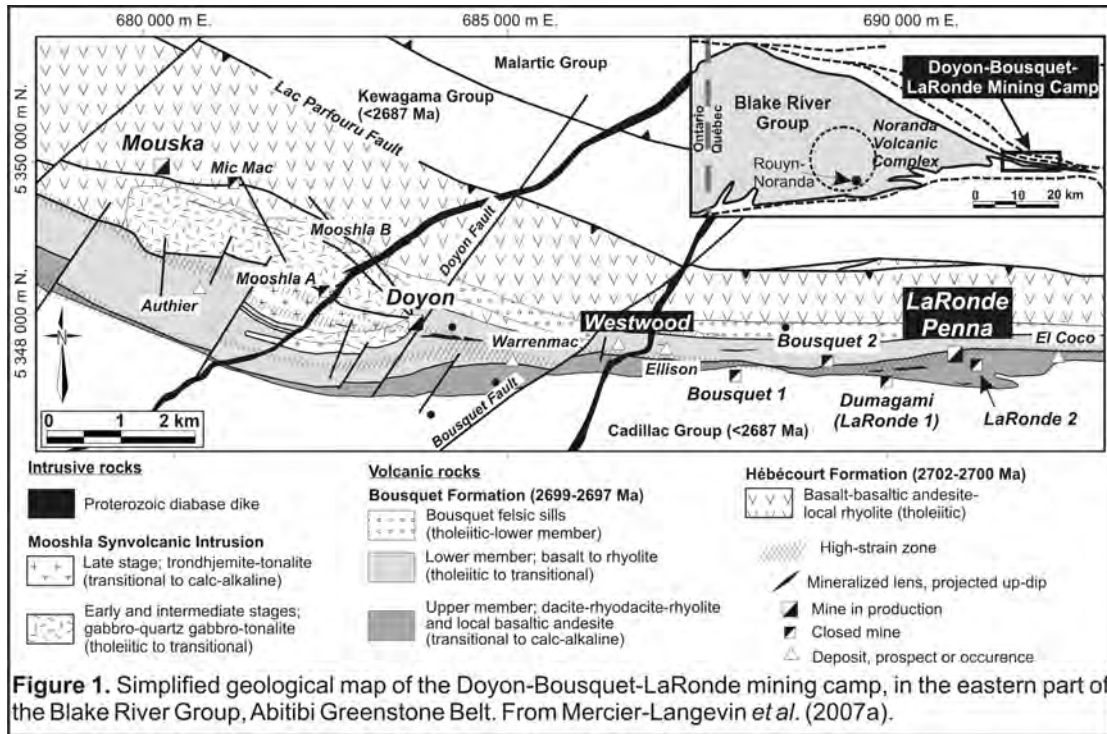


Figure 1. Simplified geological map of the Doyon-Bousquet-LaRonde mining camp, in the eastern part of the Blake River Group, Abitibi Greenstone Belt. From Mercier-Langevin *et al.* (2007a).

2, Dumagami and LaRonde Penna; Fig. 1) consist of semimassive to massive sulfide ore lenses that formed on different stratigraphic horizons (stacking), in part by subsea-floor replacement of felsic flow breccia and mafic to intermediate sills and in part by exhalative activity during a single protracted synvolcanic hydrothermal event (Dubé *et al.* 2007; Mercier-Langevin *et al.*, 2007a).

The VMS mineralization of the DBL camp are associated with wide zones of discordant to semi-conformable neutral or propylitic, intermediate and advanced argillic style alteration that are thought to be the result of gradual mixing between seawater and magmatic fluids (Dubé *et al.* 2007; Mercier-Langevin *et al.* 2007a) generated in an intermediate setting between back-arc basin and volcanic arc environments (Mercier-Langevin *et al.* 2007b).

LITHOGEOCHEMISTRY
Host Rocks Signature

The mafic to intermediate and tholeiitic to transitional rocks of the Bousquet Formation are characterized by moderately enriched chondrite-normalized LREE and MREE patterns, flat HREE profiles and negative Nb, Ta, Zr, and Hf

anomalies. The felsic transitional to calc-alkaline rocks of the Bousquet Formation are characterized by high incompatible element contents, enriched LREE and flat HREE profiles, pronounced negative Nb, Ta, and Ti anomalies, and positive Zr and Hf anomalies (Fig. 2). These profiles can be compared to FI- and FII-type rhyolites of Leshner *et al.* (1986) (Fig. 2), highlighting the prospectivity of calc-alkaline felsic-bearing volcanic sequences for VMS, including those that are Au-rich. Contrary to many VMS-bearing sequences, the Bousquet Formation defines a continuous rather than a bimodal magmatic trend.

Each unit of the Bousquet Formation can be distinguished using ratios of hydrothermally immobile elements, helping define the stratigraphy in strongly altered, mineralized, and highly-strained areas of the DBL camp and target the most fertile stratigraphic horizons. The use of detailed lithogeochemistry helped demonstrate that the main polymetallic ore horizon of the Westwood deposit is at the contact between two distinct rhyolites and a basaltic-andesite unit, which is the lateral equivalent to the main ore horizon of the LaRonde Penna deposit (20 North lens, ~50 Mt) located about 5 km to the east, highlighting the potential for Au-rich

massive sulfide lenses in the western portion of the Bousquet Formation.

Alteration Zones and Vectors

The Au-rich VMS deposits of the DBL camp are associated with upper greenschist facies metamorphic assemblages that are derived from widespread synvolcanic hydrothermal alteration. There are two main styles of alterations developed in the vicinity of the ore lenses in the DBL camp: 1) a neutral or propylitic assemblage and, 2) an aluminous assemblage. These two assemblages can coexist within the same deposit as shown at the LaRonde Penna mine (Fig. 1). Along the 20 North lens, neutral alteration is associated with Au-Zn-Cu-Ag mineral-

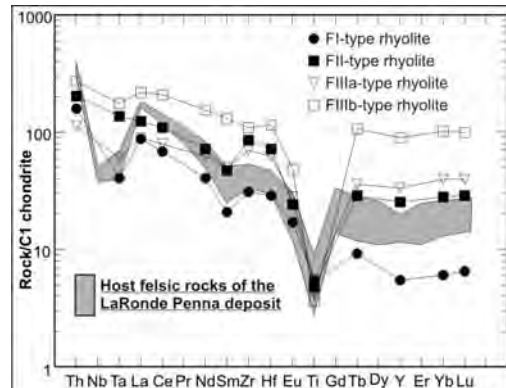


Figure 2. Chondrite-normalized REE-HFSE diagram of Archean F-type rhyolites against the pattern of the LaRonde host felsic rocks. From Mercier-Langevin *et al.*, 2007b).

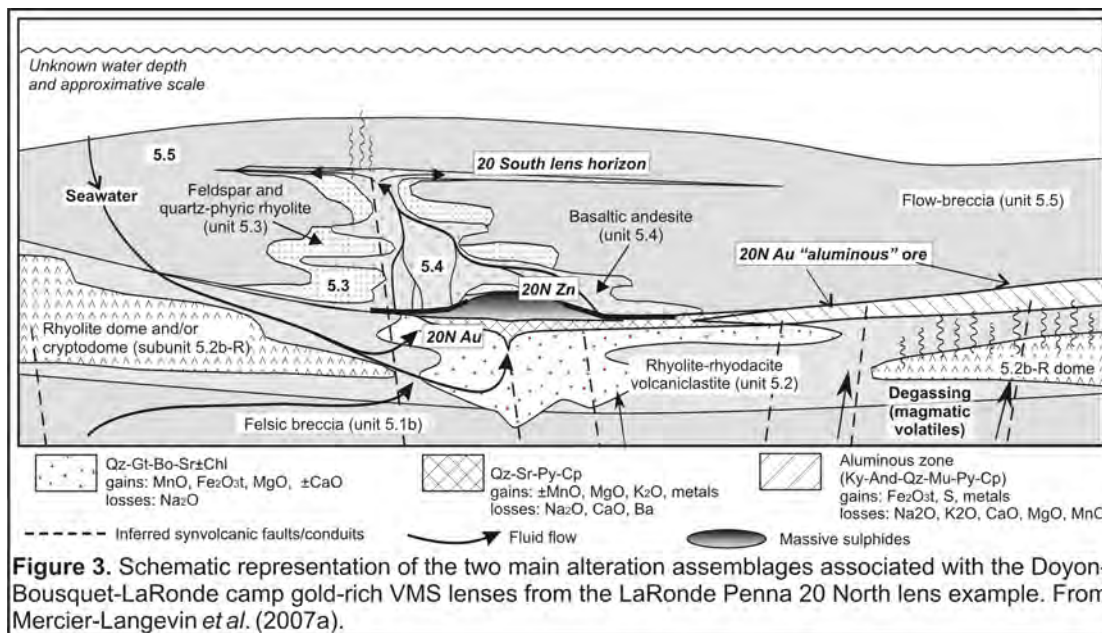


Figure 3. Schematic representation of the two main alteration assemblages associated with the Doyon-Bousquet-LaRonde camp gold-rich VMS lenses from the LaRonde Penna 20 North lens example. From Mercier-Langevin *et al.* (2007a).

ization that gradually (laterally) evolves toward an aluminous alteration and a Au- and Cu-rich zone (Fig. 3). In other areas, the neutral alteration can be distal and give way to aluminous alteration proximal to the ore, which is the case at Bousquet 1 and Bousquet 2 (Fig. 1).

The neutral alteration is mainly characterized by increasing enrichments in MnO, Fe₂O₃^(t), and MgO and losses of Na₂O (Fig. 3) towards the ore in association with the presence of a quartz,

biotite, Mn-rich garnet, sericite±chlorite, epidote and chloritoid (Dubé *et al.* 2007). In the transition zone, the Mn-rich garnet is gradually replaced by staurolite towards more aluminous alterations zones. The aluminous alteration zone is characterized by strong to total leaching of all oxides except Al₂O₃, Fe₂O₃^(t), and SiO₂ associated with the presence of aluminosilicates in a quartz-rich matrix that is the metamorphic equivalent of an advanced argillic alteration (Dubé *et al.* 2007).

CONCLUSIONS

Gold-rich polymetallic VMS deposits such as those hosted by the Bousquet Formation represent a very attractive exploration target. Lithogeochemistry is a key tool in mapping units and tracing hydrothermal vectors towards the ore in the DBL camp. Some key geochemical features are summarized here:

- (1) The Au-rich VMS deposits of the DBL camp are associated with felsic, transitional to calc-alkaline volcanic and volcanoclastic rocks of the FI- and FII-type;
- (2) Although ore zones are stacked in the stratigraphy, the main ore lenses are located along a key horizon at the contact between two distinct rhyolites and a basaltic-andesite unit;
- (3) The two main alteration assemblages of the DBL camp (neutral and aluminous) are characterized mostly by gains in MnO and losses in Na₂O, respectively, and by intense leaching of most oxides.

REFERENCES

- DUBÉ, B., MERCIER-LANGEVIN, P., HANNINGTON, M.D., LAFRANCE, B., GOSSELIN, P., & GOSSELIN, P. 2007. The LaRonde Penna Au-rich volcanogenic massive sulfide deposit, Abitibi, Quebec: Mineralogy and geochemistry of alteration and implications for genesis and exploration. *Economic Geology*, **102**, 633-666.
- LAFRANCE, B., MOORHEAD, J., & DAVIS, D. 2003. Cadre géologique du camp minier de Doyon-Bousquet-LaRonde. *Ministère des Ressources naturelles, de la Faune et des Parcs du Québec, ET2002-07*, 43 p.
- LESHER, M., GOODWIN, A.M., CAMPBELL, I.H., & GORTON, M.P. 1986. Trace-element geochemistry of ore-associated and barren, felsic metavolcanic rocks in the Superior Province, Canada. *Canadian Journal of Earth Sciences*, **23**, 222-237.
- MERCIER-LANGEVIN, P., DUBÉ, B., HANNINGTON, M.D., DAVIS, D.W., LAFRANCE, B., & GOSSELIN, G. 2007a. The LaRonde Penna Au-rich volcanogenic massive sulfide deposit, Abitibi greenstone belt, Quebec: Part I. Geology and geochronology. *Economic Geology*, **102**, 585-609.
- MERCIER-LANGEVIN, P., DUBÉ, B., HANNINGTON, M.D., RICHER-LAFLÈCHE, M., & GOSSELIN, G. 2007b. The LaRonde Penna Au-rich volcanogenic massive sulfide deposit, Abitibi greenstone belt, Quebec: Part II. Lithogeochemistry and paleotectonic setting. *Economic Geology*, **102**, 611-631.
- MERCIER-LANGEVIN, P., DUBÉ, B., LAFRANCE, B., HANNINGTON, M., GALLEY, A., MOORHEAD, J., & GOSSELIN, P. 2007c. Metallogeny of the Doyon-Bousquet-LaRonde mining camp, Abitibi greenstone belt, Quebec. In: GOODFELLOW, W.D. (ed.), *Mineral Deposits of Canada: A synthesis of Major Deposit-Types, District Metallogeny, the Evolution of Geological Provinces, and Exploration Methods*. Geological Association of Canada, Mineral Deposits Division, Special Publication No.5, 673-701.
- MERCIER-LANGEVIN, P., WRIGHT-HOLFELD, A., DUBÉ, B., BERNIER, C., HOULE, N., SAVOIE, A., & SIMARD, P. 2009. Stratigraphic setting of the Westwood-Warrenmac ore zones, Westwood Project, Doyon-Bousquet-LaRonde mining camp, Abitibi, Quebec. *Geological Survey of Canada, Current Research*, in press.

Application of field-portable x-ray fluorescence spectrometers in mineral exploration, with examples from the Abitibi Greenstone Belt

Jan M. Peter¹, Patrick Mercier-Langevin², & John B. Chapman¹

¹Geological Survey of Canada, 601 Booth Street, Ottawa, ON, K1A 0E8 CANADA
(e-mail: jpeter@nrcan.gc.ca)

²Geological Survey of Canada, 490 rue de la Couronne, Québec, QC, G1K 9A9 CANADA

ABSTRACT: Field-portable x-ray fluorescence analyzers (PXRF) are being increasingly utilized in geological and geochemical applications. Benefits include: non-destructive, in situ or ex situ analysis, simultaneous multi-element (ca. 25) quantitative and/or semiquantitative determinations, portability, excellent detection limits for many elements, high sample throughput, and low cost per analysis. Their usability has been improved by technological developments (x-ray tubes, sensitive detectors, data reduction algorithms), that have increased the spectrum of elements that can be analyzed, the quality of the data, rate of data acquisition, convenience, and user experience. We have recently incorporated the use of hand-held and bench-top PXRF in our activities, and present here two case studies of their application in the Abitibi Greenstone Belt, one is chemostratigraphic mapping of volcanic units, and the other is discrimination between black shales that have a hydrothermal component and those that are barren.

KEYWORDS: *portable x-ray fluorescence spectrometry, portable xrf, geochemistry, chemostratigraphy, Abitibi*

INTRODUCTION

PXRF have been greatly improved over the last few decades such that they now can find far-reaching application in the fields of geology and geochemistry. Herein, we review features of currently available PXRF, discuss their benefits and limitations, and give practical suggestions and guidelines for their selection and use in mineral exploration. Finally, we present two case-studies from our recent work in the Abitibi Greenstone Belt in Ontario and Quebec, Canada.

THEORY & INSTRUMENTS

In energy dispersive x-ray fluorescence spectrometry, a sample is bombarded by x-rays that cause the atoms within the sample to fluoresce (i.e., give off their own characteristic x-rays) and this fluorescence is then measured, identified and quantified. The energy of the x-rays identify the elements present in the sample and, in general, the intensities of the x-ray lines are proportional to the concentration of the elements in the sample, allowing quantitative chemical

analysis. Details of the method can be found in Van Grieken and Markowicz (2002).

Recently, miniaturized, x-ray tubes have largely replaced previously used radioisotope sources for most applications as these provide higher x-ray fluxes, shorter count times, and better precision.

Silicon positive intrinsic negative (SiPIN) detectors are most commonly used today, and these convert incoming x-ray signals to voltage that is proportional to the energy of the incoming x-rays; these voltages are then sorted by a multichannel analyzer and fed to a miniature computer. Their energy resolution is too low to permit detection and quantification of many of the key light elements (LE; Mg, Al, Si). There are recent improvements that place the analytical path in a vacuum rather than air (most presently available PXRF). Because low energy x-rays generated by LE are attenuated in air, its removal maximizes the x-rays that are detected.

Silicon drift detectors (SDD) are now available in some PXRF; they have a higher energy resolution and count rates,

making them much more suitable for measurement of LE in an air path.

Hand-held PXRF are available in a lightweight pistol form. Bench-top PXRF are slightly larger and heavier, and have a more powerful tube than most hand-held PXRF, which provides better precisions and detection limits for many elements. There are numerous accessories available for PXRF. There are several manufacturers of PXRF models that are optimized for geological and geochemical applications.

ANALYTICAL ELEMENT SELECTION

Geological and geochemical applications of PXRF generally require multi-element analysis; however, the more elements that are included within an analytical test, the greater the likelihood of problems such as peak overlaps or interferences, and manufacturers typically will provide machine calibrations for 20-30 elements in a particular analytical mode (see below). Our instruments have been calibrated for a range of elements for characterization of lithological units, different mineralization types and associated hydrothermal alteration, and other geochemical exploration vectors.

CALIBRATIONS & ANALYTICAL MODES

Fundamental Parameters (FP) are universal standardless, factory built-in calibration programs that describe the physics of the detector's response to pure elements, correction factors for overlapping peaks, and a number of other parameters to estimate element concentration while theoretically correcting for matrix discrepancies (e.g., Figura 1987). FP should be used for accurately measuring samples of unknown chemical composition in which concentrations of light and heavy elements may vary from ppm to high percent levels.

Compton Normalization (CN) is an "internal" standard, in which spectra are normalized to the Compton peak, which is produced by incoherent backscattering of the source radiation and is present in every sample. The intensity of the incoherent radiation backscatter reflects

both the composition of LE in the sample matrix as well as the overall concentration of detectable elements (Nielson & Sanders 1983). LE-dominant matrices produce a larger Compton peak, so this method provides the best results for measurement of sub-percent concentration of heavy elements in samples composed mainly of LE.

Our instruments have 4 analytical modes, with the first two being most useful as they are relatively insensitive to sample matrix composition.

1) Process Analytical: employs FP and should be used for analysis of "ore grade or style" mineralization with some gangue; this provides "assay" level data and typical detection limits (DL) of 0.5 wt%.

2) "Soils": employs CN and should be used for analysis of soils, rocks, and other materials with a predominantly LE matrix; gives "geochem" level data at DL varying between 1 and 100 ppm.

3) Empirical Analysis: uses reference standards to establish an empirical calibration line (Piorek & Rhodes 1988) and can be useful for samples where all major elements present cannot be analyzed. The standards should be matrix-matched and contain a range of element concentrations bracketing the desired level of quantification.

4) "Analytical" or "Alloys": employs FP and should be used for native metals and provides typical DL of 0.1-0.5%.

POTENTIAL APPLICATIONS

PXRFs are well-suited to myriad applications within the entire exploration, mining, and remediation cycle. Among these are: 1) geological surface and underground mapping; 2) geochemical exploration (rock, soil and stream sediment surveys); 3) determination of metal contents of mineralized samples, mineral identification during prospecting and logging of drill core and cuttings; 4) mining and mineral processing grade control; and 5) environmental baseline and monitoring studies.

SELECTED EXAMPLES

PXRF analyses were used to assist in

distinguishing between different volcanic units of the Chibougamau area on the basis of high field strength elements (HFSE; Ti, Zr, Y), and to characterize the base metal contents of mineralization intersected in drillcore in the footwall of the Lemoine VMS deposit, Quebec (Fig. 1). Two major units can be recognized on the basis of HFSE contents: high Ti-low Zr, and high Zr-low Ti. PXRF Zr abundances are very similar to ICP-ES determinations of fewer selected samples, but an applied correction factor of 1.5 was necessary for PXRF Ti to match ICP values. However, data for both methods readily distinguished the units. The Cu-Zn-enriched nature of mineralization is correctly identified by both methods.

PXRF analyses of sulfidic black shales intercalated with volcanic rocks of the Kidd-Munro Assemblage were used to differentiate between sedimentary horizons that contain a hydrothermal component and those that do not; characterization of the element enrichment suite and metal abundance data of the former are being used to vector toward concealed hydrothermal vent sites and mineralization. Figure 2 depicts geochemical profiles for Cu and Zn in 3 drillcores situated stratigraphically along 2.3 km of strike length and located about 8 km north of the Kidd Creek Zn-Cu-Pb-Ag mine, Ontario, as determined by hand-held and bench-top PXRF. The figure shows that of the 3 broadly spaced

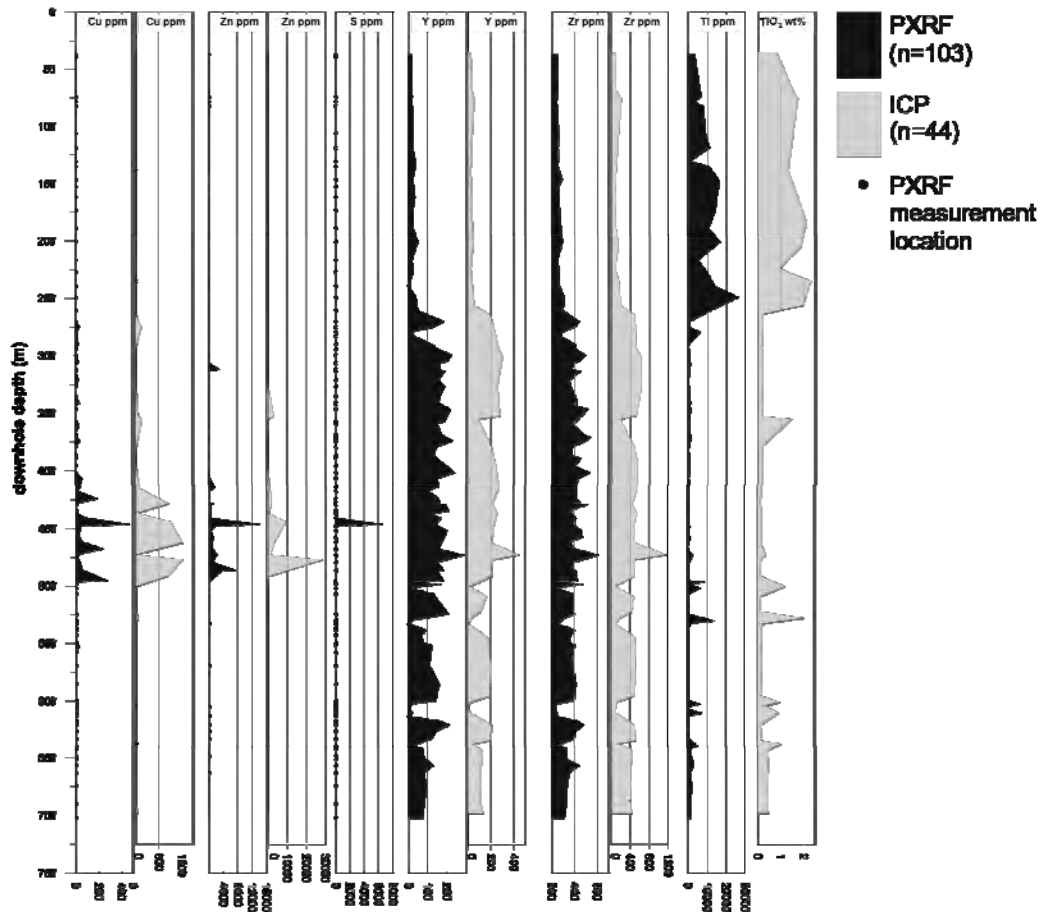


Fig. 1. Downhole log of selected element abundances in a part of drillcore LEM-40 from the footwall of the Lemoine VMS deposit, Chibougamau, Quebec as determined by conventional ICP and hand-held portable x-ray fluorescence spectrometer.

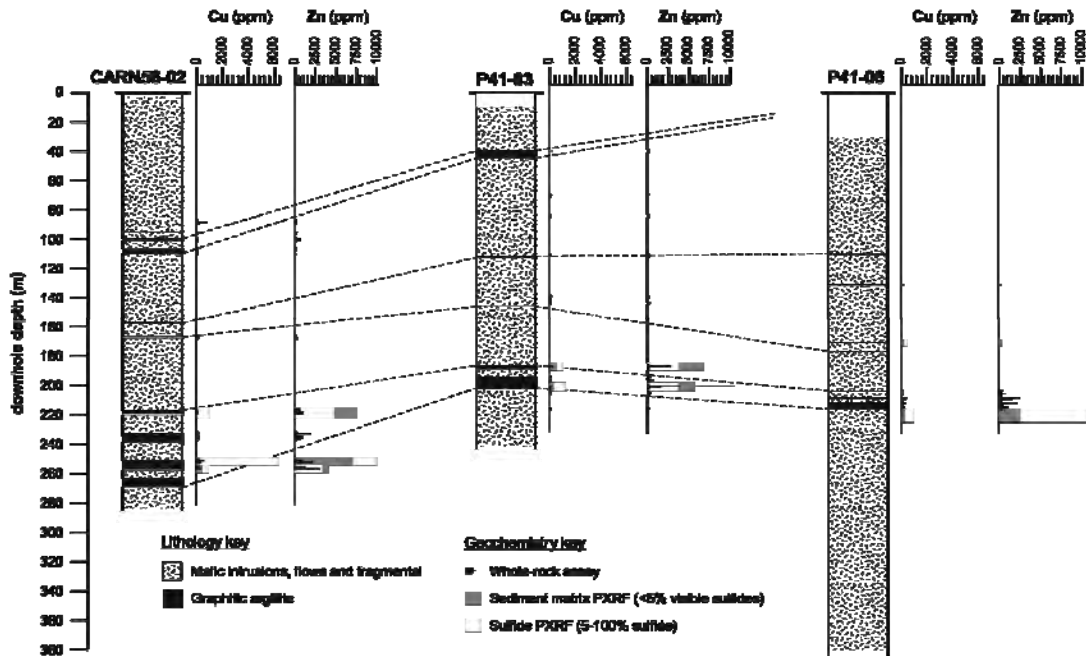


Fig. 2. Fence diagram of downhole Cu and Zn abundances in sulfide modules, concretions, crusts and laminae and matrix of graphitic argillite intersections in three drillcores 2.6 km apart and 8 km north of the Kidd Creek mine, as determined by bench-top and hand-held PXRF.

argillite-bearing intervals, only the stratigraphically lowermost contains a hydrothermal signature and the upper 2 are barren. Within this horizon, diagnostic decoupled distribution of Cu and Zn is not evident in conventional assay data but is clearly recognized in PXRF analyses. Vectoring along this lower horizon may guide further exploration.

CONCLUSIONS

PXRFs provide rapid, low cost, non-destructive, quantitative and/or qualitative multi-element analyses of many different sample media that require little or no sample preparation and instrument calibration for many applications. The two example presented here illustrate the use of PXRF in mapping rock units and mineralized zones, and this can empower the user to make on-the-fly decisions to optimize sampling strategy in order to

minimize analytical costs or maximize operational effectiveness.

REFERENCES

- FIGURA, P.M. 1987. Standardless quantitative X-ray fluorescence analysis using stored calibration constants. *American Laboratory*, **19**(2), 156-164.
- NIELSON, K.K., & SANDERS, R.W. 1983. Multi-element analysis of unweighed biological and geological samples using backscatter and fundamental parameters. *Advances in X-Ray Analysis 1983*, **26**, 385-390.
- PIOREK, S. & RHODES, J.R. 1988. A new calibration technique for X-ray analyzers used in hazardous waste screening. In: *Proceedings of the 5th National Conference on Hazardous Waste and Hazardous Materials, April 19-21, Las Vegas, Nevada*, 428-433.
- VAN GRIEKEN, R.E. & MARKOWICZ, A.A. (eds.). 2002. *Handbook of X-ray Spectrometry, Second Edition, Revised and Expanded*, Marcel Dekker, New York, 2002, 1016 p.

Exploration for Zn-rich mineralisation in semi-arid environments: an example from the Cobar region, NSW, Australia

Keith M. Scott¹ & Angela N. Lorrigan²,

¹ RSES, Australian National University and CSIRO Exploration & Mining, PO Box 136, North Ryde, New South Wales 1670 AUSTRALIA

(e-mail: keith.scott@csiro.au)

² OZ Minerals, 31 Queen Street, Melbourne, Victoria 3000 AUSTRALIA

ABSTRACT: Detailed examination of soil fractions in the Endeavor Mine area in the Cobar region reveals that the coarse (>2 mm) and magnetic fractions are hematite- and maghemite- rich and consistently elevated in Ag, As, Fe, Pb and Sb and depleted in Al, Ca, Cd, Cu, K, Na and Zn relative to the fine (<63 µm) clay-goethite-rich fraction. Phosphorus and S are also generally elevated in the fine soil fraction. Recognition of this separation can be used to understand the significance of areas of Pb anomalism in pisoliths relative to partial leach Zn anomalies within the region. Despite the concentration of Zn into the fine soil fraction, the time involved in sample preparation would generally preclude its systematic use in regional exploration programs for Zn-rich mineralisation. However, other studies in the region suggest that the proportion of fine material in this semi arid region is generally 35-50% so that whole soil results may be used with caution.

KEYWORDS: *soil, geochemistry, mineralogy, Zn-Pb deposits, Cobar region.*

INTRODUCTION

Zinc-Pb-rich Cobar-style deposits occur in Palaeozoic metasediments of the Cobar region, NSW, Australia. Weathering has affected the region since at least the Tertiary. The Cainozoic weathering has extended to depths of about 60–80 m with residual soil generally <2 m thick. However 15–20 m sequences of colluvial cover commonly occur throughout the region with sequences locally >60 m thick in palaeovalleys (Chan *et al.* 2004). Lags in the region tend to be composed of quartz, lithic and ferruginous nodules/fragments (Dunlop *et al.* 1983), with maghemite a common component in the latter (Lorrigan 2000, 2005).

At the Endeavor (formerly Elura) Mine (43 km NNW of Cobar), the main lens of the Elura Zn-Pb-Ag orebodies is subcropping with a small patch of gossanous float present in an essentially flat landscape. There Pb in saprolite (>50 ppm in an area 1.4 x 1.0 km) and lag (>50 ppm in an area 2.5 x 1.6 km) define the underlying mineralisation. However Zn in soil is anomalous for >1 km to the southwest of the main lens (Lorrigan

2005). Similarly, at Wagga Tank (130 km south of Cobar), Pb >30 ppm in 1-2 mm soil material (in an area at least 200 x 200 m) readily defines subcropping mineralisation, whereas Zn anomalism in the same material is less coherent (Scott *et al.* 1991). The Hera Zn-Pb-Cu-Au-Ag deposit (80 km SE of Cobar), occurs under thin colluvial cover. Broad Pb anomalism occurs in surficial soils along traverses across the deposit, especially in the coarse and magnetic fractions (>100 ppm for 600 m; Scott 2006). Zinc anomalism (>40 ppm for 550 m) is also present in the coarse soil fraction but not in the magnetic fraction. Thus, how Zn occurs in soils in the semi-arid Cobar region needs to be understood.

This study documents the chemistry and mineralogy of soil fractions adjacent to the Endeavor Mine area to evaluate how best to use soils in regional exploration in western NSW.

SAMPLES AND METHODS

Approximately 3 kg of soil was collected from 0–15 cm at 4 sites in the Endeavor Mine area. Background residual soils

were collected at two sites located about 2 km north of the Endeavor headframe on Poon Boon Station. Soils developed on transported material that gives rise to the Bengacchah Zn anomaly (in bedrock 2.6 km SSW of the subcropping main lens) were also sampled at two locations.

Four surficial soils were collected from along a traverse across the projected position of the blind Northern Pods mineralisation (450 m below surface). This traverse was originally made to conduct a partial leach study over the Northern Pods, with samples 138538 and 138539 being soils with low mobile metal ion (MMI) response 250 m east of samples 138440 and 138441 which are directly over the mineralisation and show anomalous MMI response.

Soil samples were wet sieved into (a) 2–4 mm, (b) 1–2 mm, (c) 0.5–1 mm, (d) 250–500 μm , (e) 125–250 μm , (f) 63–125 μm and (g) <63 μm fractions. A ferruginous/magnetic fraction (m) was also prepared from the 2–4 mm fraction. Soil fractions were crushed, digested with $\text{HNO}_3/\text{HCl}/\text{HF}/\text{HClO}_4$ and then analysed by Inductively Coupled Plasma Optical Emission Spectrometry (ICP-OES) for Al, Ca, Cu, Fe, K, Mn, Na, P, S and Zn. Inductively Coupled Plasma Mass Spectrometry (ICP-MS) was used to determine Ag, As, Cd, Pb and Sb because of the lower detection limits by this method. The mineralogy of selected samples was determined by qualitative X-ray diffractometry.

RESULTS

Surficial soils developed upon transported material (Bengacchah) have <1% coarse material (>2 mm) and about 50% finer than 63 μm whereas the residual soils tend to have several percent coarse material and <40% fine material. Quartz in soils in transported material (Bengacchah) also tends to be more rounded than elsewhere.

Examination of soil fractions coarser than 250 μm indicates that they contain a substantial amount of magnetic material. The proportion of magnetic to non-magnetic (lithic) material generally

decreases with decreasing grain size. The mineralogy of the coarse and fine soil fractions suggests that coarser fractions contain hematite, goethite and maghemite. The <63 μm fraction is richer in clay minerals (muscovite/illite and kaolinite) and contains goethite as the only Fe oxide.

Chemical analysis shows that the coarse (>2 mm) and magnetic fractions are consistently richer in Ag, As, Fe, Pb and Sb than the fine (<63 μm) fraction which is richer in Al, Ca, Cd, Cu, K, Na and Zn. Phosphorus and S are also generally elevated in the fine soil fraction. However, high S (>600 ppm) occurs associated with elevated Ca in the coarse fraction in the Bengacchah area, reflecting the presence of gypsum. Iron contents are lowest in material sized between 63–250 μm but slightly more abundant in the fine fraction. This suggests that Fe is dominantly present in hematite and maghemite in the coarse soil material and present mainly as goethite in the finest material. The concentration of Pb in the coarse and magnetic fractions and Cu and Zn in the finest soil fraction should be noted.

Table 1 shows that in samples 138462 and 139464 (Bengacchah) and 138540 and 139541 (Northern Pods area), Zn and Cd are elevated in all soil fractions, with the values in the fine (<63 μm) fraction at least double those in corresponding samples from the Poon Boon area. (High Zn in the coarse fraction of 138462 is due to soil nodules composed of calcite and gypsum.) Sulfur also tends to be more abundant in all four Northern Pods samples than in the Poon Boon samples. Lead is slightly elevated in the coarse and magnetic fractions of the Northern Pods or Bengacchah samples relative to Poon Boon (background) samples.

DISCUSSION AND RECOMMENDATIONS FOR SOIL SAMPLING

As indicated above, Pb is preferentially concentrated in coarse and magnetic soil fractions, with Zn concentrated in the finer soil fraction. Dunlop *et al.* (1983) also observed this separation of Pb and Zn in

Table 1. Geochemistry of surficial soil fractions, Endeavor Mine area.

Location	Sample	Fraction	Ca ppm	Cd ppm	Cu ppm	Fe %	Pb ppm	S ppm	Zn ppm
Bengacchah (transported)	138462	>2 mm	5520	0.4	27	27.00	72	3400	220
		<63 µm	1760	0.3	47	3.95	37	260	220
		Magnetic	560	0.2	26	39.80	84	250	59
	138464	>2 mm	1270	0.1	21	29.60	71	690	43
		<63 µm	1330	0.2	41	4.10	39	260	150
		Magnetic	410	<0.1	27	41.70	91	200	39
Poon Boon (background)	138466	>2 mm	470	<0.1	25	23.20	50	100	42
		<63 µm	1890	<0.1	42	4.05	33	200	79
		Magnetic	540	<0.1	24	30.70	52	100	36
	138468	>2 mm	740	<0.1	18	36.20	61	140	23
		<63 µm	2140	<0.1	48	4.40	29	230	73
		Magnetic	640	0.1	22	43.70	72	110	36
Northern Pods- barren	138538	>2 mm	470	<0.1	17	46.00	84	310	13
		<63 µm	2660	<0.1	52	4.10	40	420	72
		Magnetic	450	<0.1	19	51.30	97	290	12
	138539	>2 mm	480	<0.1	16	38.90	86	280	12
		<63 µm	1790	<0.1	44	3.85	41	410	59
		Magnetic	410	<0.1	19	51.80	89	250	13
Northern Pods- mineralised	138540	>2 mm	500	0.2	20	36.80	68	200	66
		<63 µm	1610	0.8	43	4.40	36	390	460
		Magnetic	610	0.2	24	44.10	81	170	87
	138541	>2 mm	1370	0.1	25	35.20	62	230	69
		<63 µm	2970	0.3	48	4.40	36	330	200
		Magnetic	850	<0.1	21	38.80	68	150	77

drainage channel soils about the Endeavor Mine site. Furthermore, they found that Pb >50 ppm (with only low Zn) in 1-2 mm pisoliths from stream channels defined an anomaly for 5 km about the Elura orebody whereas the soil auger anomaly (Bengacchah) with Pb >50 ppm extends approximately 1.3 km SW of the Elura orebody in a palaeochannel. Such features of the Bengacchah anomaly are consistent with mechanical dispersion, probably from the wall alteration about the top of the Elura orebody (Govett *et al.* 1984; Lorrigan 2005) which formed a topographic high during the early Tertiary

(Gibson and Pain 1999). Ferruginous, coarse Pb-rich Bengacchah anomaly material would have been deposited over a relatively short interval in a palaeochannel and subsequently covered by later depositional material. However ferruginous material (commonly pisoliths) in the current stream channels reflects material transported and reworked over the period since the Tertiary. Thus the anomalous Pb in surficial coarse and magnetic soil fractions from the Bengacchah and Northern Pods area represents Tertiary to present mechanical dispersion.

Zinc is elevated in the fine (<63 µm) soil fractions relative to coarse and magnetic soil fractions but high values (>100 ppm) are found in the fine fraction of surficial soils in the Bengacah area and immediately above the 450 m-deep Northern Pods mineralisation. Fine material from soils 250 m east of the latter are not so enriched. This suggests that the Zn is not particularly mobile, possibly reflecting derivation from a very local source, possibly siderite up dip from the Northern Pods and Bengacah.

Although Zn contents are highest in the fine fraction of the soils, the time needed to prepare such a soil fraction makes its use impractical. However, because fine generally makes up 35-50 % of the whole soil in the Endeavor, Hera and Wagga Tank areas, it may be able to be used directly. For example, Zn ≥150 ppm occurs in the highly anomalous samples above Northern Pods mineralisation relative to <40 ppm in a sample 250 m away. However, one would need to determine details of the soil size distribution in other areas being explored.

REFERENCES

CHAN, R.A., GREENE, R.S.B., HICKS, M., LE GLEUHER, M., MCQUEEN, K.G., SCOTT, K.M., & TATE, S.E. 2004. Regolith architecture and geochemistry of the Byrock area, Giralbone region, north-western NSW. *CRC LEME Open File Report* **159**. 71p.

- DUNLOP, A.C., ATHERDEN, P.R., & GOVETT, G.J.S. 1983. Lead distribution in drainage channels about the Elura zinc-lead-silver deposit, Cobar, New South Wales, Australia. *Journal of Geochemical Exploration* **18**, 195-204.
- GOVETT, G.J.S., DUNLOP, A.C., & ATHERDEN, P.R. 1984. Electrochemical techniques in deeply weathered terrain in Australia. *Journal of Geochemical Exploration*, **21**, 311-331.
- LORRIGAN, A.N. 2000. Distribution of the Elura lag anomaly. In McQueen, K.G. & Stegman, C.L. (eds) *Central West Symposium Cobar 2000 Extended Abstracts*. CRC LEME, Perth, 51-54.
- LORRIGAN, A.N. 2005. Elura Zn-Pb-Ag deposit, Cobar district, NSW. In BUTT, C.R.M., ROBERTSON, I.D.M., SCOTT, K.M. & CORNELIUS, M. (eds.), *Regolith Expression of Australian Ore Systems*. CRC LEME, Perth, 143-145.
- GIBSON, D. & PAIN, C. 1999. Landform units on the Elura Mine Lease. *CRC LEME Report* **113R**, 7p. + 2 maps.
- SCOTT, K.M. 2006. Soil characteristics at the Hera Au-Cu-Zn-Pb-Ag deposit, Nymagee region, NSW. CRC LEME Restricted Report 241R/CSIRO, *Exploration & Mining Report* **P2006/517**, 75p.
- SCOTT, K.M., RABONE, G., & CHAFFEE, M.A. 1991. Weathering and its effect upon geochemical dispersion at the Wagga Tank deposit, N.S.W., Australia. *Journal of Geochemical Exploration*, **67**, 413-426.

Soil micro-layer, airborne particles, and pH: the Govett connection

Barry W. Smee

4658 Capilano Rd., North Vancouver, B.C., V7R 4K3 CANADA (e-mail: bwsmee@geochemist.com)

ABSTRACT: Geochemical research in the 1960s and 1970s produced exploration methods that could be used to quickly explore large areas from the air using the Barringer-developed AIRTRACE collection and analytical system. Geochemical patterns seen from the analyses of dust from the soil-air interface, known as the soil micro-layer, were thought to be connected to the electrogeochemical model developed by Govett and his students in the early 1970s. This theory was closely linked to H⁺ release from oxidizing sulfide bodies. Additional studies from the '70s to the present by the author have shown that the measurement of pH and detection of pH-related patterns from the soil micro-layer may detect mineralization through appreciable cover and can be done in the field in real time at little expense. Two examples from this research are shown.

KEYWORDS: *Airtrace, pH, soils, micro-layer, electrogeochemistry, deep exploration.*

INTRODUCTION

The late 1960s and early 1970s saw the introduction of innovative research into geochemical processes that remain at the forefront of applied geochemical technology after nearly forty years. The leading research school at that time was Imperial College in London under the direction of John Webb. His students defined 'thinking outside the box' in applied geochemistry. The following retrospective connects a few of these ideas and offers a simple method for mineral exploration through cover that was ultimately distilled from this work.

AIRBORNE GEOCHEMISTRY

One of the more interesting aspects that appear to have been disfavored or at least lost in the last forty years was the work of W. Beauford and J. Barber at Imperial College, and G. Curtin at the USGS on the release of heavy metals to the atmosphere from plants. Much of this work was published later in the 1970s (Beauford *et al.* 1977; Curtin *et al.* 1974), but had caught the eye of Tony Barringer, one of the leading thinkers in mineral exploration technology in the late 1960s. Barringer had also been introduced to work done on the soil-air interface (the soil micro-layer) that had been shown to be a

zone of accumulation of ions. Some of this work was published in the later 1970s (Barringer 1977).

Barringer, ever on the lookout for methods to explore ground quickly (he was the inventor of the proton precession magnetometer, Input Airborne EM system, the Airborne mercury analyzer, the COSPEC airborne gas analyzer amongst many other technologies) thought that if one could collect airborne particles in an aircraft as it flew close to the ground and analyze them for many elements, one could then marry airborne geophysics and geochemistry in one aircraft. Barringer was granted patents on the method itself, which he called AIRTRACE, and on the particle collection method and the method of analyses of the particles (Barringer 1973a, b).

The AIRTRACE system was mounted on either a fixed wing or helicopter equipped with 'aerodynes' that ingested airborne particles and concentrated this dust on sticky tape that was inside the aircraft. The tape was advanced to a clean position for every five seconds of flight and a record number placed on the tape and the flight path camera film so that the location of the dust spot could be located on the ground.

This tape was analyzed in the Barringer laboratory in Toronto using the first ICP-

ES and the first laser ablation system on which Barringer held a patent for many years.

Microscopic examination of ablated particles showed that only the outer layer of dust particles was consistently being vaporized. Barringer knew that AIRTRACE was collecting the particles from the soil micro-layer: the location of ion accumulation in the soil.

This was recognized as being similar to a weak or selective extraction. Very often, the pattern of element responses over mineralization was 'double-peak' in form and restricted to the immediate vicinity of the deposits. A few published results illustrate these 'donut' (plan) or 'rabbit-ear' (profile) anomalies (Barringer 1977).

THE LINK TO ELECTROGEOCHEMISTRY

The reason for these patterns was not known. However the 1973 paper by Gerry Govett on electrogeochemical transport of ions was very timely. Govett proposed that ions might move through surface cover in response to a natural electrical force created by oxidizing sulfides. Further research both in the laboratory and the field confirmed that this was not only possible, but measurable, and produced in profile a 'rabbit-ear' pattern (Govett 1976). Govett & Chork, (1977) showed that this pattern was being controlled by hydrogen ion movement. This work was in part funded by Barringer Research who saw the 'potential' for explaining the AIRTRACE patterns. Govett showed that the techniques are applicable in an arid environment (Govett *et al.* 1984).

I studied the electrogeochemical phenomena in the laboratory and field while at the Geological Survey of Canada as part of my Ph.D. work under Govett. The field study area selected was in the varved clay belt of Northern Quebec over a VMS deposit covered by between 5 m and 30 m of till, varved clay and organic material. The varved clay was thought at the time to be a complete mask to geochemical movement.

Fortunately the Hudson Bay lowland-derived varved clay is alkaline and Ca-rich and provided an ideal substrate in which

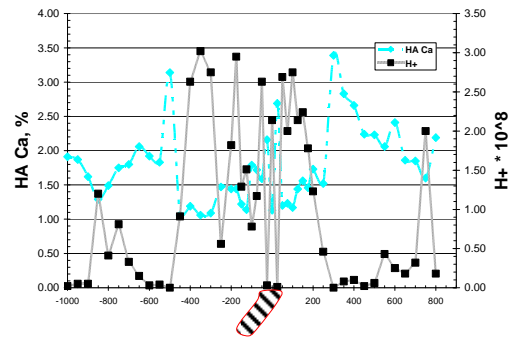


Fig. 1. Profile from the top of varved clay over a VMS deposit in Northern Quebec showing the relationship between H⁺ concentration and aqua regia soluble Ca. (adapted from Smee 1983).

to detect hydrogen ion anomalies. This work showed that not only did the surface soil produce a clear hydrogen ion response above and down dip from the VMS, but also moved the pH-sensitive elements (Ca and Fe) in response to changing pH conditions as shown in Figure 1 (Smee 1983). In the case of calcite, for a pH of <7 the Ca becomes mobile and may move in solution over time. Once the alkaline conditions are re-established, the Ca precipitates as calcite.

This movement of pH-sensitive elements, and Ca particularly has been used by me with success for the past 25 years as a routine exploration tool (Smee 1998, 1999, 2003) and has led to the discovery of several sulfide bodies. The use of a field pH meter and a bottle of water as a primary exploration method in alkaline terrain appears to be too easy to be true. However one can produce remarkable data with these simple tools and a drop of 10 % HCl.

USING PH TO HIGHLIGHT TARGETS THROUGH COVER IN ARID AREAS

Alkaline soil conditions exist in most semi-arid to arid conditions. Oxidizing sulfides should produce a change in pH in the surface soil as confirmed by Hamilton *et al.* (2004), and especially in the soil micro-layer where an upward moving front of H⁺ accumulates, as shown nearly 40 years ago. If this soil micro-layer is sampled



Fig. 2. Sampling the soil micro-layer in acid conditions. See text for analytical method.

(Fig. 2), slurried with distilled water and the pH measured, the response should be obvious.

However experience has shown that other factors such as a break-in-slope or a water-bearing structure can produce single-peak anomalies. These are somewhat confusing when attempting to interpret a soil survey.

The actual pattern in alkaline soils related directly to oxidizing sulfides should include two variables: positive H^+ surrounded by an increase in Ca concentration where the mobilized calcite re-precipitates. Both of these variables can be detected by initially measuring the soil slurry pH, then by adding a drop of 10 % HCl, stirring the solution for about 10 seconds and taking the pH again.

Soils of lower pH (high H^+ molar concentration) have mobilized the Ca and therefore the soil slurry will be relatively unbuffered. The addition of HCl to the solution will immediately drop the pH in these samples where calcite has been removed, but will have little effect where calcite been precipitated. These buffered soils should be on the edge of the low pH (high H^+). The pattern from an oxidizing sulfide should therefore be an H^+ high and surrounded by a small or no change in H^+ concentration when HCl has been added.

Plotting a variable that is significant when small is rather difficult. The method developed to clearly highlight the areas of calcite precipitation on a chart or plan map involves some manipulation. To do this, the acidified H^+ in moles (converted from pH) is subtracted from the non-acidified H^+ . The least differences are the areas of calcite precipitation. The inverse difference (1/difference) is calculated and plotted. This variable produces positive peaks which are far more pleasing to the eye. For ease these are called Inverse Difference Hydrogen (IDH) anomalies.

Two examples are shown: one from the porphyry copper-gold Hugo South Oyu Tolgoi area, Mongolia and one from a quartz reef hosted gold deposit south of the Bulyanhulu mine, Tanzania, Africa. Figures 3a-d over Line 475800 N at the

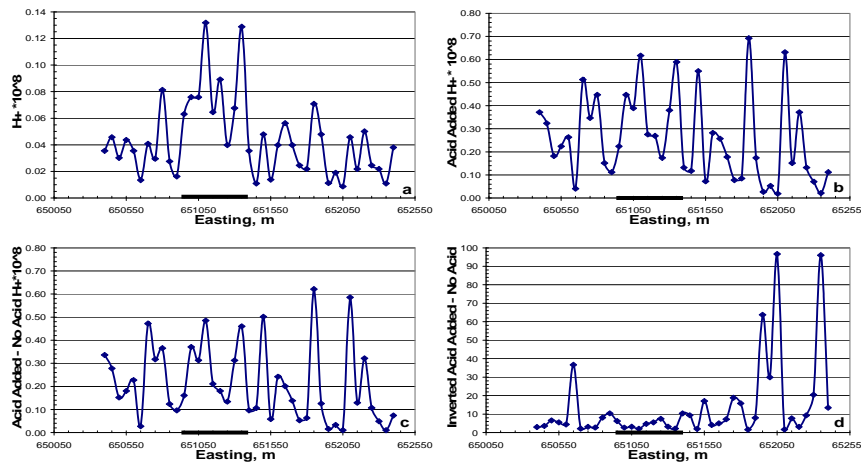


Fig. 3. Profiles of the step-wise handling of the pH data illustrated by Line 475800 N of the Hugo South Cu-Au deposit

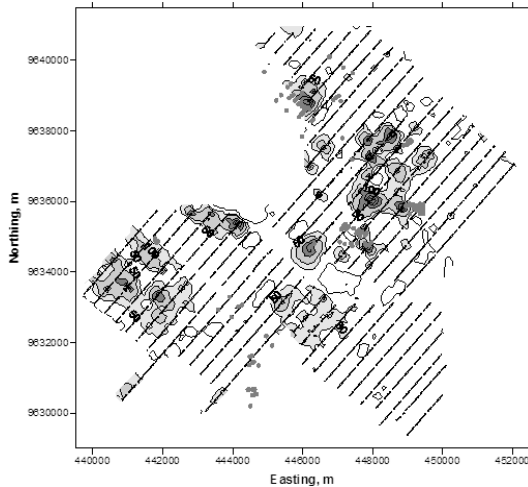


Fig. 4. Plan view of IDH in soils over extension of mineralized horizon from Bulyanhulu Tanzania. Dots are drill locations. The interpretation of soil pH was done after the drilling was completed.

south end of Hugo South shows the step-wise progression of data handling to produce both the H^+ and IDH patterns in profile. The acid peak surrounded by the calcite halo is easily seen. The thick black line at the bottom of each figure is the surface projection of the mineralization. Figure 3a is the H^+ moles $\times 10^8$ from the soil micro-layer. Figure 3b is the acidified soil slurry converted to H^+ moles $\times 10^8$. Figure 3c is acidified H^+ minus original H^+ . Figure 3d is the inverted difference from 3c. (IDH). Calcite is absent over the projection of mineralization and H^+ anomaly, but occurs outboard from the mineralization. Alluvium thickness c. 40 m.

The Tanzanian example in Figure 4 is a plan contour map of the IDH anomalies together with drill holes shown as dots. There is sparse to no outcrop with much of the area covered by fluvial and alluvial deposits. The drill holes were positioned using geological mapping and geophysics rather than the pH survey. The predominance of holes shows the location of gold mineralization. The soil IDH shows the areas of mineralization in many instances, and other areas which have yet to be tested by drilling.

This inexpensive technique was developed because of imaginative and

multi-disciplinary thinking nearly 40 years ago.

ACKNOWLEDGEMENTS

I would like to thank Ivanhoe Mines and Mr. Dale Sketchley for assisting in the collection of the soil samples and allowing the data over Oyu Tolgoi to be released. Barrick Gold collected the information and allowed the data from Bulyanhulu South to be shown. Tony Barringer showed me that doing what other people have done will result in finding what other people have found. Gerry Govett inspired the initial research and has remained a mentor over the years.

REFERENCES

- BARRINGER, A.R. 1973a. Method and apparatus for geochemical surveying. 1973a: *US Patent No. 3759617*.
- BARRINGER, A.R. 1973b. Method and apparatus for sensing substances by analyses of adsorbed matter associated with atmospheric particles. *US Patent No. 3768302*.
- BARRINGER, A.R. 1977. AIRTRACE - an airborne geochemical exploration technique. *USGS. Prof. Pap. 1015*, 231-251.
- BEAUFORD, W., BARBER, J., & BARRINGER, A.R. 1977. Release of particles containing metals from vegetation into the atmosphere. *Science*, **195**(4278), 571-573.
- CURTIN, G.C., KING, H.D., & MOSIER, E.L. 1974. Movement of elements into the atmosphere from coniferous trees in subalpine forests of Colorado and Idaho. *Journal of Geochemical Exploration*, **3**, 245-263.
- GOVETT, G.J.S. 1973. Differential secondary dispersion in transported soils and post-mineralization rocks: an electrochemical interpretation. In: M.J. JONES (ed.), *Geochemical Exploration 1972: Proc. of the Fourth IGES, London*, 81-91.
- GOVETT, G.J.S. 1976. Detection of deeply buried and blind sulfide deposits by measurement of H^+ and conductivity of closely spaced surface soil samples. *Journal of Geochemical Exploration*, **6**, 359-382.
- GOVETT, G.J.S. & CHORK, C.Y. 1977. Detection of deeply buried sulphide deposits by measurement of organic carbon, hydrogen ion and conductance in surface soils. In: *Prospecting in Areas of Glaciated Terrain, Helsinki. Institution of Mining and Metallurgy, London*, 49-55.

- GOVETT, G.J.S., DUNLOP, A.C., & ATHERDEN, P.R. 1984. Electrogeochemical techniques in deeply weathered terrain in Australia. *Journal of Geochemical Exploration*, **21**, 311-331.
- HAMILTON S.M., CAMERON E.M., McCLENAGHAN M.B., & HALL, G.E.M. 2004. Redox, pH and SP variation over mineralization in thick glacial overburden. Part II: field investigation at Cross Lake VMS property. *Geochemistry: Exploration, Environment, Analysis*, **4**, 45-58.
- SMEE, B.W. 1982. Laboratory and field evidence in support of the electrogeochemically enhanced migration of ions through glaciolacustrine sediment. *Journal of Geochemical Exploration*, **19**, 277-304.
- SMEE, B.W. 1998. A new theory to explain the formation of soil geochemical responses over deeply covered gold mineralization in arid environments. *Journal of Geochemical Exploration*, **61**, 149-172.
- SMEE, B.W. 1999: The effect of soil composition on weak leach solution pH: a potential exploration tool in arid environments. *Explore*, **102**, 4-7.
- SMEE, B.W. 2003. Theory behind the use of soil pH measurements as an inexpensive guide to buried mineralization, with examples. *Explore*, **118**, 1-19.

Robust 'organic' geochemistry identifies and vectors to deeply buried exploration targets

D. A. Sutherland¹

1. Activation Laboratories Ltd., 1336 Sandhill Drive Ancaster, ON, L9G 4V5 CANADA
(e-mail: dalesutherland@actlabsint.com)

ABSTRACT: Surficial soil surveys use pathfinder elements that have been shown to be useful as a predictive geochemistry in determining the location of exploration targets. Innovative analytics have been developed to similarly use organic compounds as a complementary exploration tool. Soil Gas Hydrocarbons (SGH) is based on a weak leach extraction of near-surface samples followed by an analysis having the sensitivity to detect the minute but unique organic hydrocarbons that bacteria have leached and metabolized from interaction with mineral deposits at depth. These compounds are not gaseous but migrate from depth with the electrochemically induced mass flow from the oxidation and reduction reactions in REDOX cells developed over buried targets. Surficial samples act as collectors of the over 160 specific heavier hydrocarbons that are grouped into chemically related 'pathfinder' classes that have dispersed to the surface. The expected order of dispersion or 'geochromatography' of these classes is able to vector to the location of buried exploration targets. Specific combinations of the classes identify the target type even at over 500 metres in depth. SGH is a dual purpose deep penetrating predictive geochemistry that can both locate and identify blind uranium, gold, SEDEX, VMS, nickel, and copper mineral targets, kimberlite pipes and petroleum sources.

KEYWORDS: SGH, hydrocarbons, partial extraction, deep penetrating organic geochemistry

INTRODUCTION

The use of 'organic' geochemical surveys for exploration has historically been confined to C1 to C4 compounds in the carbon series (methane, ethane, propane, butane) that are gases. However, the alteration of these signals by the biosphere and the effects of barometric pressure and precipitation on gas flux reduce their use in delineating buried targets. An alternative to these light compounds are relatively heavy hydrocarbon compounds that have been hypothesized to be present but at much lower concentrations. With customized lab instrumentation, a method has been developed to prove the existence and use of these heavier hydrocarbons in surficial samples for exploration. This relatively new geochemistry entitled 'Soil Gas Hydrocarbons' (SGH) represents a breakthrough in analytics as it has been able to obtain the higher level of sensitivity required to characterize the hydrocarbon signature related to mineral targets to a reporting limit of one part-per-trillion for

over 160 targeted compounds. The large suite of compounds is able to be subdivided into groups of chemically related organic compound classes. Each class has different solubilities, molecular weights, partition coefficients, etc., and thus they disperse through the overburden at different rates and can be observed at different distances from a buried target through the process of 'geochromatography' as measured by the analysis of near-surface samples. The observation of these dispersal patterns allows accurate vectoring to the location of blind deposits. The specific classes of compounds detected over a target have been associated with the organic signature developed from different mineral types and are thus 'pathfinder' classes that can identify the type of mineralization at depth.

METHOD

Originally only B-horizon surficial soil samples were collected for SGH surveys. Research by the Ontario Geological

Survey (OGS) and the Geological Survey of Canada (GSC) has indicated that the upper B-horizon soil resulted in a higher SGH signal and is thus probably the most ideal sample. In additional research it has been shown that other soil horizons, humus, peat, lake-bottom sediments and even snow are also collectors of the hydrocarbons targeted in this method. A fist-sized sample (c. 500 g) from a transect or grid design consisting of at least 50 regularly spaced sample locations that extend into background areas is best. Samples need no special preservation for shipping.

Samples are dried in temperature-controlled rooms kept at 40°C. The fraction that falls through a 60-mesh sieve (<250 µm) is collected and used for analysis.

A 0.5-g aliquot is analysed from the homogenized sample using an aqueous leach to target and extract weakly bound hydrocarbons from the surface of the sample particles or grains.

Samples are analysed using gas chromatography coupled with mass spectrometry (GC-MS). This instrument separates the organic hydrocarbons in the extract with a very high resolution fused silica capillary column prior to mass spectrometric detection. Acquisition parameters have been customized to detect the target list of 162 hydrocarbons with the sensitivity required to obtain 1 part-per-trillion reporting limits which represents an innovation in these analytics.

Specialized chromatographic deconvolution and integration software further isolates and accurately measures the mass ion responses for the specific hydrocarbons targeted. An external standard calibration method is used to compare the responses of these hydrocarbons to known response factors from a series of n-alkanes to obtain semiquantitative results. Concentrations are reported in an Excel spreadsheet without any statistical modifications.

DISCUSSION

In several research surveys samples have

been collected in duplicate from different soil horizons or of different sample types (e.g. peat and underlying wet soil). It has been found that the variation in results between different sample media including various soil types, glacial till, lake-bottom sediments, peat, and humus is minor to the extent that different sample types can be collected within the same sample survey. The variability of including different sample types is minor compared to the loss of data from missed locations as the hydrocarbon signature is independent of sample type.

The SGH compounds targeted are robust to general sampling, shipping and sample preparation procedures, largely due to the lower volatility of the higher molecular weight compounds. The technique is also robust to cultural activities, even to the extent that successful analysis and interpretation has been done from roadside right-of-way samples.

RESULTS

Several member mining companies of the Canadian Mineral Industry Research Organization (CAMIRO) sponsored a two-year research project in 1997 (CAMIRO 97E04). SGH organic signatures were tested and used to successfully locate nine of the ten targets that were blindly submitted to the lab from study areas known to be difficult for geochemical surveys. The targets studied included copper, gold, nickel, uranium and volcanic massive sulfide (VMS) deposits. SGH was also able to display a 'deep penetrating' nature as it located the McArthur River uranium deposit that was in excess of 500 m in depth.

In 2001, a second CAMIRO research project (01E02) was initiated. The objective of this project was to investigate the source of these hydrocarbons, and to further investigate the ability of this geochemical technique to discriminate between barren and ore-bearing conductors. This project was sponsored by additional mining companies and government agencies and extended into a third year. The project included other

target types of SEDEX, kimberlite and Olympic Dam type targets which were used to define new SGH geochemical signature templates. Microbiological lab experiments were independently conducted to investigate whether the hydrocarbons measured by SGH were related to bacterial activity. A consortia of bacteria were grown directly on various samples of ore, were extracted, and then analysed by SGH. It was discovered that the hydrocarbons were released in the death-phase of the bacteria presumably after eventual cell membrane rupture. A similar set of hydrocarbons were found in ore samples as well as surficial soil samples over the mineralization. Thus the SGH results from surficial samples were shown to be directly influenced by the bacterial activity on the ore at depth and reflected the type of mineralization. This confirmed earlier research where it was observed that the SGH signature from pulverized VMS shelf specimens representing modern black smoker and older Mattabi and Kidd Creek deposits matched exceptionally well in their SGH VMS signature and also to the signature detected in surficial soils over VMS deposits from geographically different locations.

During the CAMIRO 01E02 project, seven surveys were submitted from over kimberlite pipes. Research defined the SGH signature and studied the dispersion of the anomalous compound classes of hydrocarbons as shown in the following figures. With SGH, kimberlites are distinguished using higher molecular weight classes of compounds. In Figure 1, the heaviest pathfinder class of polyaromatic hydrocarbons moves through the overburden at the slowest rate and thus forms a halo anomaly that is dispersed to the greatest distance from the kimberlite as shown by the dotted oval. Figure 2 illustrates a slightly lighter kimberlite pathfinder class of alkylated-biphenyls that disperses less and forms the halo anomaly shown by the dashed oval. Figure 3 of branched-alkanes moves through the overburden more easily and forms the tight halo anomaly

that definitively shows the edge of the outer rim of the kimberlite pipe as the boundary of a REDOX cell. Together these classes accurately vector to the target location. The mix of classes found identifies the target as a kimberlite pipe.

From independent research, SGH appears to be an excellent tool for identifying reduced areas or REDOX cells in overburden (S. Hamilton, OGS, pers. comm. 2004).

CONCLUSIONS

The majority of the hydrocarbons detected by this geochemical technique have been proven to originate from bacteriological activity at depth. The heavier SGH compounds are robust and thus a wide variety of sample types may be used which is valuable in sampling in difficult Canadian environments. SGH is able to

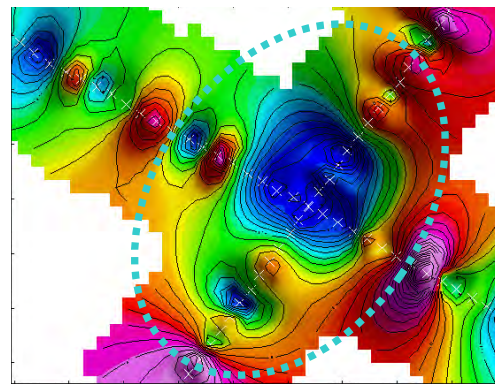


Fig. 1. Tertiary kimberlite pathfinder class.

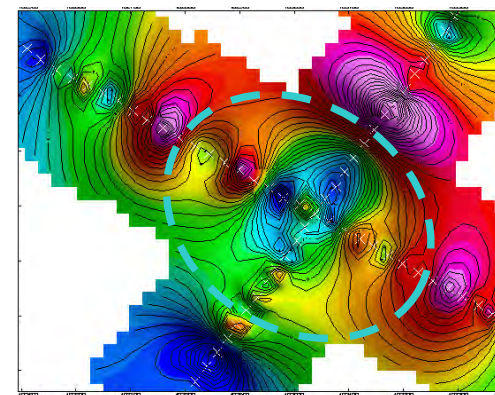


Fig. 2. Secondary pathfinder class.

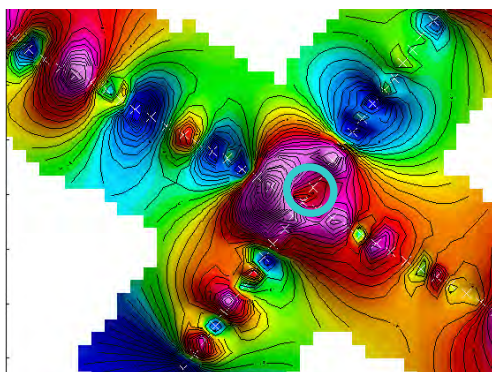


Fig. 3. Primary kimberlite pathfinder class.

locate the vertical projection of a target through geochromatographic vectoring of the various hydrocarbon pathfinder classes. The mix of the hydrocarbon classes detected is able to identify the type of mineralization at depth. It has been shown to be a deep penetrating geochemical technique that is able to discriminate between barren and ore-bearing conductors, and magnetic anomalies, prior to the planning of expensive drilling programs and thus reducing exploration costs. The SGH data from over 400 targets has been interpreted since 2004, thus thoroughly testing the various mineral templates used to confirm the identity of the buried target for a wide variety of commodities.

ACKNOWLEDGEMENTS

CAMIRO research projects 97E04 and 01E02, sponsor participants: Cameco Corporation, Outokumpu, Western Mining Corporation, Inco, Cominco, BHP-Billiton, Rio-Algom, Barrick Gold, Newmont, Noranda, Anglo American, Codelco, HBED, Xstata, Ontario Geological Survey, Alberta Geological Survey, Manitoba Geological Survey, and the Ontario Mineral Exploration Technologies Program (OMET). The independent consultants for CAMIRO 01E02 included Dr. Ronald Klusman, Dr. Gordon Southam, Dr. Joel Leventhal, Dr. Stewart Hamilton and Dr. Barbara Sherwood-Lollar. Geosoft kindly donated training and software to these projects. Mapping of SGH signatures were conducted using Geosoft Oasis Montaj.

REFERENCES

- GOVETT, G.J.S. & ATHERDEN, P.R. 1987. Electrogeochemical patterns in surface soils – Detection of blind mineralization beneath exotic cover, Thalanga, Queensland, Australia. *Journal Geochemical Exploration*, **28**, 201-18.
- GOVETT, G.J.S., GOODFELLOW, W.D., & WHITEHEAD, R.E.S. 1972. Experimental aqueous dispersion of elements around sulfides. *Economic Geology*, **71**, 925-40.
- HALL, G.E.M., HAMILTON, S.M., MCCLENAGHAN, & CAMERON, E.M. 2004. Secondary geochemical signatures in glaciated terrane. SEG 2004 abstracts "Predictive Mineral Discovery Under Cover", September 27, 2004 Perth, Australia.
- HAMILTON, S. Electrochemical mass-transport in overburden: a new model to account for the formation of selective leach geochemical anomalies in glacial terrain. *Journal Geochemical Exploration*, **63**(3), 155-172.
- ILCHIK, R.F., BRIMHALL, G.H., AND SCHULL, H.W. 1986. Hydrothermal maturation of indigenous organic matter, Alligator Ridge gold deposits, Nevada: *Economic Geology*, v. 81, p. 113-130.
- JANUSZCZAK, N., HAMILTON, S.M, HATTORI, K., SADER, J., SOUTHAM, G., BRAUNEDER, K., & DONKERVORT, L. Advances in soil geochemical exploration methods for areas of glacial cover. *9th International Kimberlite Conference, Extended Abstract No. 91KC-A-00109*, 2008.
- KELLEY, D.L., CAMERON, E.M., & SOUTHAM, G. Secondary geochemical dispersion through transported overburden. *SEG 2004 abstracts "Predictive Mineral Discovery Under Cover", September 27, 2004 Perth, Western Australia*.
- KESLER, S.E., GEREDENICH, M.J., & STEININGER, R.C. 1990. Dispersion of soil gas around micron gold deposits. *Journal Geochemical Exploration*, **38**, 117-132.
- KLUSMAN, R.W., SAEED, M.A., & ABU-ALI, M.A. 1992. The potential use of biogeochemistry in the detection of microseepage of petroleum. *American Association Petroleum Geologist*, **76**, 851-63.
- KLUSMAN, R.W. *Soil Gas and Related Methods for Natural Resource Exploration*. John Wiley & Sons Ltd, ISBN 0-471-93892-0.
- SUTHERLAND, D.A. AND HOFFMAN E., Soil Gas Hydrocarbons – A dual purpose geochemical exploration method for the location and identification of buried mineral and petroleum targets. *Abstracts West Pacific Geophysics Meeting*, Beijing, China (2006) AGU, 87(36)

ORE-FORMING SYSTEMS: A GEOCHEMICAL PERSPECTIVE

EDITED BY:

**JACOB HANLEY
DAN KONTAK
PETE HOLLINGS**

Siderophile elements in the zonal structure of ore geochemical systems: exploration aspects

G. Abramson ¹

¹*Iteresources Pty Ptd, Level 2, 49-51 York st., Sydney, NSW, 2000 AUSTRALIA
(e-mail: gabramson@ionex.com.au)*

ABSTRACT: The elements of the iron group (Co, Ni, Mn, Cr, Ti, V, and Sc) have specific features of distribution in ores and wall rock as follows:

- These elements are localized mainly in the outer zones of the nuclear parts of ore geochemical systems of different ranks (ore bodies, ore deposits, ore regions), frequently forming sub-annular structures.
- Within the limits of the positive anomalies of the ore-forming elements the siderophile elements are in the anomalously lowered (sometimes in the sub-background) concentrations.
- These regularities are fractal, i.e. occur at all scales of ore objects - from the regional to the local.
- In the barren anomalies (in zones with dispersal mineralization) the regular distribution of iron group elements is not observed.

Detailed mineralogical studies have shown that pyrite of different generations is the main form containing siderophile elements, and their zonal distribution is connected both to the position of wall rock pyritization zones and to the concentration changes of these elements within the pyrites.

The presentation on sections, plans and 3-D models provides examples of the distribution of siderophile element.

KEYWORDS: *exploration, geochemical, system, siderophile, anomaly*

INTRODUCTION

A model of an ore geochemical system has been developed (Goldberg et al, 2003), which can be applied to ore entities of various categories: ore bodies, deposits and ore regions. The nuclear section of the system contains a zone of accumulation of the principal ore and associated elements. The peripheral areas contain zones of depletion of ore-forming elements. Anomalies of siderophile elements (Ni, Co, Mn, Ti, V, Cr), which are the subject of this paper, are located on the periphery of the nuclear sections of these systems.

In areas of accumulation of ore-forming elements the siderophile elements, as a rule, form zones of lower concentrations relative to the background concentration. Experience shows that these zones most probably contain ore bodies and deposits

of commercial significance. Examples are given below which illustrate the behaviour of siderophile elements in ore objects of various ranks and types of mineralisation.

MAYSKOE AU-AS DEPOSIT (RUSSIA)

This deposit is located in the north-east of Russia and belongs to a gold-arsenic type of low-sulphide formation (Abramson et al, 1980). It lies within a carbonaceous terrigenous rock of Triassic age and is associated with a dome-shaped uplift in a node of intersecting faults of various directions. The ore bodies consist of zones of silicification and kaolinization with veinlet-disseminated sulphide mineralisation. Gold is present in the form of finely-dispersed dissemination in arsenopyrite and pyrite. As an example, Figure 1 illustrates the distribution of Au and Mn in connection with commercial ore

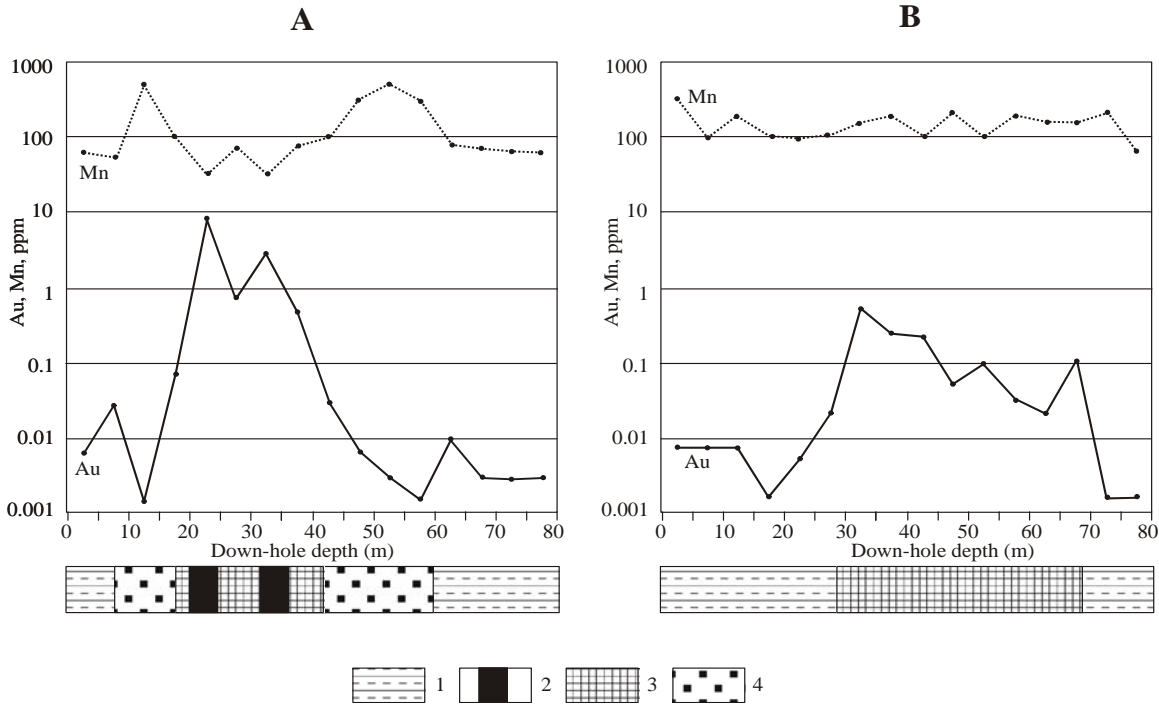


Fig.1. Distribution of Au and Mn in haloes of commercial ore bodies (A) and in a zone of barren disseminated mineralisation (B). Mayskoe deposit. Russia. 1. Black shale. 2. Ore body. 3. Zone of mineralisation. 4. Zone of pyritization

bodies (A) and a zone of disseminated mineralisation (B). Clear differences can be seen in the distribution of Mn in these two cases. In the first case (Fig. 1A) manganese comprises relatively low concentrations in the ore-bearing zone and ore bodies, while accumulating in the external pyritization zones. The distribution curve for gold shows the level of accumulation of this metal in the ores and haloes. The zone of disseminated mineralisation (Fig. 1B) is marked by elevated concentrations of gold and weak, undifferentiated haloes of Mn. A similar pattern of distribution can be seen in the case of Co and Ni (Abramson & Zhabin 1991).

BENDIGO GOLD FIELD (AUSTRALIA)

Bendigo is a classic example of a low-sulphide gold-quartz deposit located in a folded sequence of sandstone and shale of the Cambrian-Ordovician age (Ramsay *et al.* 1998; Goldberg *et al.* 2007). Regional soil geochemistry covers an area of ~4,000 km². Sampling Grid 5x5 km. 134 samples were collected as can be seen in Fig. 2, titanium anomalies form sub-

annular structures. Moreover, in the zone of the Bendigo deposit titanium forms areas with relatively low concentrations (depletion zones) and accumulates in its peripheral sections at a considerable distance from the centre of commercial mineralisation.

PROMEZHUTOCHNOE AU-AG DEPOSIT (RUSSIA)

This example shows possible mineral forms of occurrence of siderophile elements in ores and ore-surrounding zones.

The deposit is located in north-eastern Russia and belongs to a gold-silver type of sulphide-deficient formation (Abramson *et al.* 1993). It lies within a black-shale rock mass of the Upper Triassic. They consist of quartz breccias and veins of quartz of a colomorphic texture. Ore mineralisation includes low-grade gold, electrum and a small quantity of sulphides (< 0.1%). The average gold content in the ore bodies is 10 ppm, Ag >100 ppm. In the lateral sections of the ore bodies and at some distance from them there are zones of pyritization. The geochemical features of

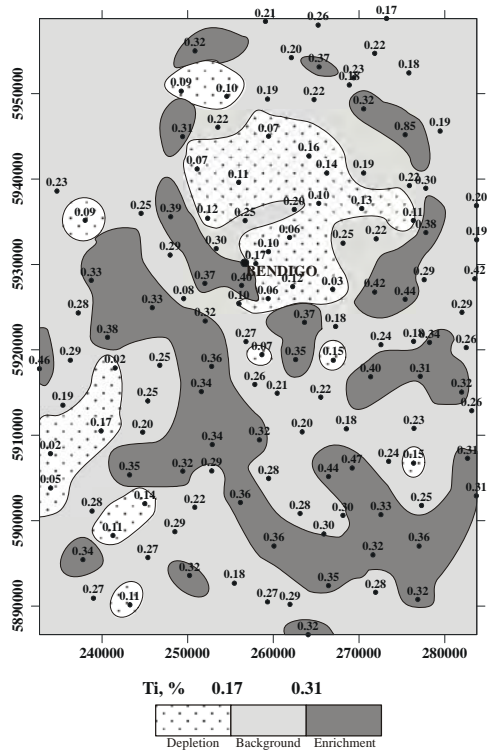


Fig.2. Distribution of Ti in rock. Bendigo Gold Field, Victoria. Australia.

the deposit were studied on the basis of geochemical sampling of trench walls and deep bore cores. The vertical zonalities of the ore bodies is characterised by rapid petering out of gold as the depth increases, and an accumulation of tungsten and tin. An important part is played by elements of the siderophile group: Co, Ni and Mn. Their distribution is characterised by low (relative to background levels) concentrations at the ore level of the ore-bearing structures and a constant increase in concentration in relation to depth and on the flanks of the ore bodies. Because the ore bodies crop out at the surface, the distribution of elements in the upper sections is not discussed here.

An investigation of mineral fractions in ores and ore-adjacent areas carried out jointly with I.M. Shulgina (Abramson *et al.* 1993) has shown that pyrite of various generations is the main concentrator of Co, Ni and Mn (Table 1). The distribution of these elements is linked mainly with the quantity of pyrite concentration in ores and

Table 1. Concentration of Co, Ni and Mn in minerals and pyritization zones (ppm) of the Promezhutochnoe deposit.

Minerals	Ni	Co	Mn
Pyrite	160	70	1650
Limonite	70	45	650
Antimonite	10	none	300
Miargyrite	10	none	240
Pyritization zones	170	60	2100

Table 2. Distribution of main ore minerals in the Promezhutochnoe deposit (% , ppm).

Zones	Minerals (%)			
	Pyrite	Limonite	Antimonite	Miargyrite
Upper-middle	0.03	1.2	3	0.07
Middle	~1	-	0.7	-
Bottom	7	-	-	-

ore-adjacent areas (Table 2).

CONCLUSIONS

The material obtained from this investigation shows:

- (1) Despite the individual features of formation of the deposits and differences in ore composition and morphology, a general pattern of distribution of elements of the siderophile group can be observed. They accumulate in the peripheral areas of ore objects (the nuclear parts of ore geochemical systems) of different categories, often forming a picture of concentric zonalities.
- (2) Pyrite of various generations is the main mineral form of occurrence of the siderophile elements.
- (3) Siderophile elements can serve as a reliable indicator for determining the commercial significance of an anomaly and its spatial location within commercial ore mineralisation.

ACKNOWLEDGEMENTS

I should like to express my gratitude to Issai Goldberg, who provided very useful advice to me in the preparation of this paper.

REFERENCES

ABRAMSON, G.J., GRIGORIAN, S.V., & GRIGOROV, S.A. 1980. Results of an investigation of the geochemical halos at one Au deposit. *Lithochemical method of exploration of*

- endogenetic deposits*. Moscow, IMGRE, 16-22 (In Russian).
- ABRAMSON, G.J. & ZHABIN A.G. 1991. Recommendations for the use of geochemical methods in exploration for gold deposits. Moscow, IMGRE. (In Russian).
- ABRAMSON, G.J., KASUSHKIN, A.V., & SHULGINA, I.M. 1993. A geological and geochemical model as a reflection of structure of the anomaly field of an ore object. *Applied aspects of geochemical research*. Moscow, IMGRE, 29-50 (In Russian).
- GOLDBERG, I.S., ABRAMSON, G.J., HASLAM, C.O., & LOS, V.L. 2003. Depletion and enrichment of primary haloes: their importance in the genesis of and exploration for mineral deposits. *Geochemistry: Exploration, Environment, Analysis*, **3**, 281-293.
- GOLDBERG, I.S., ABRAMSON, G.J., HASLAM, C.O., & LOS, V.L. 2007. Depletion and enrichment zones in the Bendigo gold field: a possible source of gold and implications for exploration. *Economic Geology*, **102**, 745-753.
- RAMSAY, W.R.H., BIERLEIN, F., PARNE, D.C., & VANDERBERG, A.H.M. 1998. A review of turbidite-hosted gold deposits, central Victoria. Regional setting, styles of mineralisation and genetic constraints. *Ore Geology Reviews*, **13**, 131-151.

Cassiterite-sulfide mineralization revealed by dispersion flows in Belaya Sopka Mountain (northeastern Russia)

Anna D. Ananchenko^{†1} & Svetlana R. Tikhomirova^{†1}

¹ Federal State Unitary Scientific-Production Enterprise Aerogeologia
(<http://www.aerogeologia.ru/>; s.tikhomirova@g-to-g.com)
2/8, Academician Volgin Street, Moscow, 117071 RUSSIAN FEDERATION
† Deceased

ABSTRACT: Lithochemical mapping on *dispersion flows* in northeastern Russia (4000 km²) established precious metal, cassiterite-sulfide, polymetallic, lead-zinc, copper-molybdenum, and other types of mineralization. Spectral assays of the *dispersion flows* identified complex point, linear, and areal geochemical anomalies that required systematization. The assays underwent statistical processing to calculate the local geochemical background and make a quantitative estimate of the mineral potential throughout the studied territory based on *dispersion flow productivity*. The high *total dispersion flow productivity* led to the selection of several sites for detailed study. Geological examination confirmed the geochemist presence of numerous types of mineralization, including cassiterite-sulfide ore within Belaya Sopka Mt. (White Hill Mt., 100 km²), where, besides a high tin concentration, the potential also exists for mineable contents of lead, zinc, copper. Plots, portrayed on a space image, of *total dispersion flows productivity* and *secondary halo productivity* revealed the importance of superimposition of linear and ring structures which may aid in selection of target areas for exploration and setting a high priority for field studies in few areas of 3 km².

KEYWORDS: *dispersion flows, cassiterite-sulfide, Belaya Sopka Mt., northeastern Russia*

INTRODUCTION

In 1974–1982 geochemical mapping on *dispersion flows* throughout an area of 4000 km² in northeastern Russia (Fig. 1) was conducted by a team of the Aerogeologia Expedition. The supervisor of the geochemical investigations, Anna D. Ananchenko, was at that time a senior geochemist of Aerogeologia and PhD researcher at the Chair of Geochemistry at the Moscow State University.

The theoretical basis for the development of geochemical methods in Russian exploration practice was the 1909 work by V. I. Vernadsky on the universal *dispersion, migration, and concentration* of chemical elements and the teaching of *mineral deposit field dispersion* in conjunction with the *quantitative interpretation of geochemical anomalies* in the basic practical works of N.I. Safronov (1936, 1957), who was a geophysicist and geochemist who experienced Soviet government repression.

TECTONICS AND METALLOGENY

The studied area is part of the Okhotsk-Chukotka Volcanogenic Belt (OChVB). The OChVB is an elongated structure on the border between two folded provinces: Verhoyan-Chukotka (Mesozoic) and Koryak-Kamchatka (Cenozoic). The metallogeny of the Penzhinsky sector of the OChVB is characterized by three main types of mineralization: plutonic (gold-sulfide-quartz, gold-rare-metal, lead-zinc), volcanic (copper-molybdenum, polymetallic, gold-quartz), and telethermal (mercury, mercury-antimony). The main metallogenic feature of the OChVB was its high prospectiveness for precious metal deposits (Shilo & Babkin 1978; and others). Prospecting practice has determined that epithermal deposits, which formed in hydrothermal systems related to volcanic activity, are characterized by fine-grained gold (0.05–0.2 mm) and cassiterite. Minerals may be encountered in samples removed from a local source larger than 100 km² (Lugov

Makeev *et al.* 1972). The gold dust fraction lost during panning ranged up to 150–200 grains, a possible loss of 25–100% (Krutous 1976). Mineral search on dispersion flows proved to be an effective exploration method in poorly studied northeastern Russia.

Eastern and Western Projects

At several stages of the geochemical mapping (1:50,000) spectral assays on dispersion flows within the Eastern and Western Project areas (Fig. 1) revealed numerous occurrences. Below is an example of the mineralization discovered during the Western Project (Fig. 2). *Dispersion flow* samples were collected from clay-sand stream sediments. Sampling followed a grid that provided an observation density of 2–4 geochemical samples per km² (Solovov 1965). *Secondary dispersion halos* in sites were sampled by taking fine fractions from eluvial or diluvial deposits 15–20 cm beneath the surface. Depending on the features of the promising areas, testing was carried out on a 200/250 x 40/50 m or 100 x 20 m grid. Field processing of the samples consisted of drying and screening the sampled material through a sieve (–1 mm). The final weight of one dried sample was about 100–150 g.

Geochemical Halos of Western Project

During the Western Project, a total of 3000 grab samples were assayed by using the rapid spectral method to determine 32 elements and chemical adsorption to determine gold. Spectral assay data were processed in order to determine the distribution of 24 elements. Background (C_i) values were calculated using Lognormal Statistics software.

Anomalous concentrations of associated elements were established for five local areas (Fig. 3a). Revealed within the 100-km² Belaya Sopka Mt. area was a combined anomaly with up to 2 g/t Ag, 0.6 g/t Au, 0.1% Pb, 0.2% Zn, 0.003% Sn, 0.002% Bi, and 0.015% As.

Twenty three catchment basins were identified by dividing each elementary stream into several intervals containing

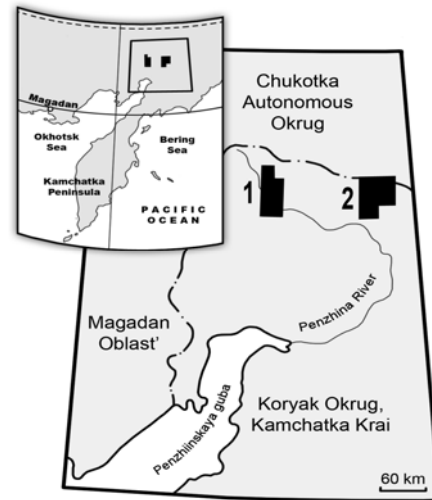


Fig. 1. Eastern (1) and Western (2) Project areas, Koryak Okrug, Kamchatka Krai (North), northeastern Russia.

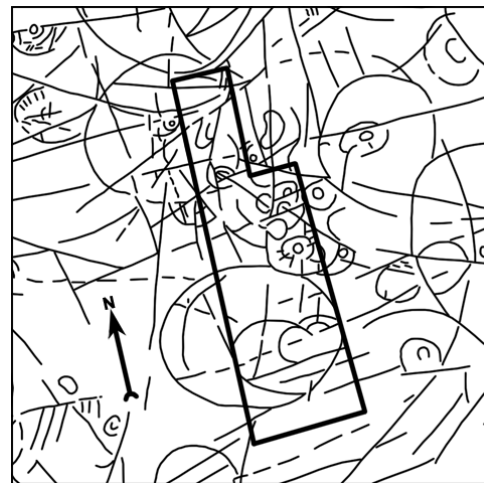


Fig. 2. Western Project limit (1600 km²) on interpreted satellite image (1:1,200,000), Penzhina River sector of the OChVB.

sample points. The position of the initial points (R_0) was clearly defined in almost all cases. Location of finite points (R) for some cases required a correction (λ'), which depends on the local slope effect (α) and the ratio between the size of the catchment area at the initial (S_R) and final (S_R) points. The required corrections were made using productivity diagrams and equations from Solovov & Shvarov (1980).

Equations (Solovov 1965) calculated the *dispersion flow productivity* (P'_x) and the *total dispersion flow productivity* (P'_Σ).

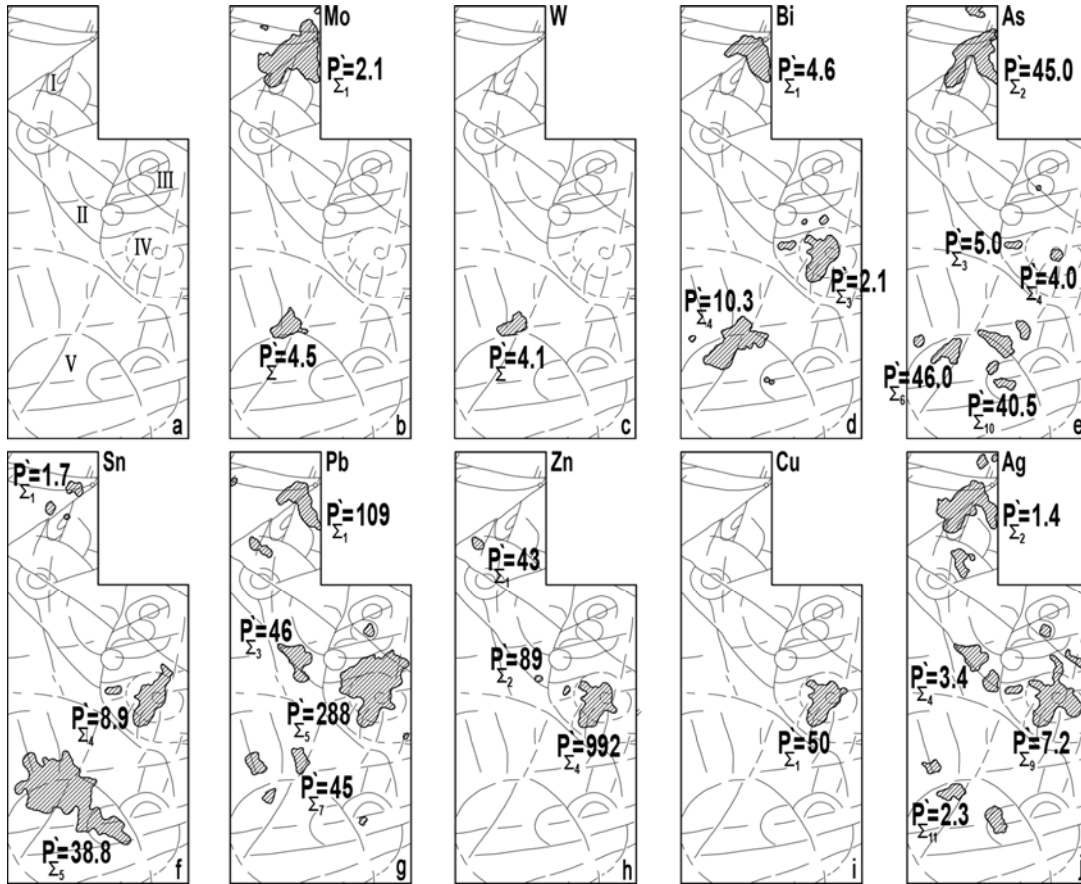


Fig. 3. Mineralization linked to the ring structures: I – Urkuveem (Mo with Ag and Bi, greisen type), II – Keyukveem (polymetallic), III – Kitivelgin (Au, arsenic-antimony association), IV - Belaya Sopka (Sn, cassiterite-sulfide association), V – Shestakovka (Sn with Ag and Bi, cassiterite-silicate association). Total productivities (P_{Σ} , $m^2\%$) for more promising catchment areas (outlined) and/or linear and ring structures are numbered.

High productivity of dispersion flows (P'_x) for the major associated elements (Sn, Pb, Zn, Cu) that are typical for cassiterite-sulfide mineralization have been established for the Belaya Sopka Volcano-Plutonic Structure that made the like-named mountain range a high, first-priority target (Ananchenko 1982).

Geological Confirmation

Calculation of P'_x showed that Sn has the highest productivity in three catchment basins. This fact has allowed definition of a site (2.5 km^2) for detailed investigation. Examination was accompanied by control grab, chip, channel, and technological sampling. Testing in a grid of $200 \times 40 \text{ m}$ identified anomalies with the following

maximum concentrations: 0.1% Pb ($C'_i = 0.03\%$), 0.2% Zn ($C'_i = 0.007$), 10 g/t Ag ($C'_i = 0.6 \text{ g/t}$), 0.08% Sn ($C'_i = 0.001\%$).

Mineralization was represented by quartz-chlorite-carbonate-sulfide veins with visible chalcopyrite, galena, sphalerite, pyrrhotite, cobaltite, limonite and malachite. Fractures filled by veins are identified on aerial photos as one submeridional zone up to 20 m thick and 500 m long. The northeastern linear system represented by a shear zone containing veinlets with arsenopyrite, bismuthine, gold and silver sulfosalts. Twelve veins that differ in extent and intensity of mineralization were discovered, with some veins yielding 3 wt. % Sn, 3 wt. % Cu, and up to 250 g/t Ag.

CONCLUSIONS

The geochemical investigations have taken on a far greater significance due to the discovery of numerous deposits in inaccessible Koryak Okrug. The Serebryany and Bich Au-Ag occurrences were discovered in 1975-1976. Panning and geochemical mapping revealed the Chuvanka and Os'minog (Au-Ag, Cu-Mo) occurrences. The Left Urkuveem Pb-Zn occurrence was established in 1978 and the Burnyi (Sn-Cu-Ag) and Sulfidnyi (Cu-Ag) occurrences were evaluated in the early 1980s.

ACKNOWLEDGEMENTS

Many people contributed to sampling and initial processing of a vast amount of dispersion flow data: Lazareva Z.A., Meretskov S.G., Shavurin S.A., Kotov S.Yu., Kuks K.R., Kuks K.A., Kuznetsova T.G., Pavlova V.E., and Shmakov S.G.[†] Valuable comments were given by Kostenko N.P., Plyashkevich L.N., Yakymenko E.L., and others. Sonin, I.I.[†], who was chief of the team at Aerogeologia and Solovov A.P.[†] gave invaluable help. Thanks to all who assisted. The second author participated in works in 1981-1983.

REFERENCES

ANANCHENKO, A.D. 1982. *Geochemical investigations during the group geological mapping of 1: 50 000 scale in the North-East of the U.S.S.R. Methodology and results*. PhD dissertation. Chair of Geochemistry, Moscow State University, Moscow, 256

- KRUTOUS, V.I. 1976. Study of the shapes, numbers, and terms of the fine gold concentrations in the Yano-Kolyma gold bearing belt. *Magadan*, 250.
- LUGOV, S.F., MAKEEV, B.F., & POTAPOVA, T.M. 1972. Mechanism of development and location of the North-East USSR tin-ore deposits. Moscow, *Nedra*, 360.
- SAFRONOV, N.I. 1936. On the question of "dispersing halos" of mineral deposits and their using during the search and exploration. *Problems of Soviet Geology*, **4**, 302-323
- SAFRONOV, N.I. 1957. The form of the state of dispersed elements in nature and their searching importance. In: *Geochemical search for ore deposits*. Moscow, Gosgeoltekhizdat, 52-61.
- SHILO, N.A., BABKIN, N.B., & BELYI, V.F. 1978. East-Asian system of marginal volcanic belts, features of the structure, magmatism and metallogeny. In: *Proceedings of the Academy of Sciences of the U.S.S.R., Geological Series*, **2**, 24-31.
- SOLOVOV, A.P. 1952. On the question of estimation of mineralization on the results of the metallometric surveys. *Subsoil Exploration*, **4**, 48-50.
- SOLOVOV, A.P. 1965. Lithochemical methods of searching on the secondary dispersion halos and dispersion flows. In: *Instruction on the geochemical methods for searching of ore deposits*. Moscow, Nedra, 43-95.
- SOLOVOV, A.P. & SHVAROV Y.V. 1980. Estimation of mineralization on the lithochemical dispersion flows. *Exploration and Protection of Subsoil*, 25-30

Geochemical characterization of humic substances isolated from phosphatic pellets and their surrounding matrix, Ras-Draâ, Tunisia

Aida Ben Hassen¹, Jean Trichet¹, Jean-Robert Disnar¹, & Habib Belayouni²

¹ ISTO, Institut des Sciences de la Terre d'Orléans, Rue de Saint-Amand, Bâtiment Géosciences, BP 6759, 45067 Orléans Cedex 2 (email: aidabenhassen@yahoo.fr)

² Département des Sciences de la Terre, Faculté des Sciences de Tunis, Université Tunis El Manar, 1060, Tunis TUNISIE

ABSTRACT: Humic substances (HS) were extracted from pellets (phosphatic grains 10-500 µm size) and their surrounding matrices (< 50 µm), collected from Ras-Draâ deposit (Tunisia). Before, extraction, TOC content was measured using Rock-Eval pyrolysis. The HS were characterized by various geochemical analyses: CHONS elemental analysis, Fourier-transformed infrared spectroscopy (FTIR) and solid-state ¹³C CPMAS NMR. The chemical extraction of the HS from both fractions according to the IHSS (International Humic Substances Society) procedure, indicates a higher abundance of extractable humic compounds within pellets (~70% of TOC) and a variable but lower extraction yield in matrices (~18% of TOC). The elemental composition of extracted HS shows high H/C and S/C ratios in both fractions indicating that these HS originated from marine aliphatic OM. This planktonic origin was confirmed by spectroscopic analyses of HS (FTIR and solid-state ¹³C CPMAS NMR) that show a predominance of aliphatic structures and O-containing functional groups. The Rock-Eval pyrolysis applied to total OM confirms the marine planktonic origin of the phosphatic OM but it exposes its low degree of diagenetic evolution. Despite the homogeneity in their origin, pelletal and matricial OM give critical differences which are indicators of allochthonous origin of these pellets - faecal pellets - within their related sediments.

KEYWORDS: *humic, phosphatic, extraction, pyrolysis, pellets*

INTRODUCTION

Several investigators of the organic matter (OM) associated to sedimentary phosphatic deposits (Sandstrom 1982; Belayouni 1983; Belayouni & Trichet 1983; Nathan 1990; Ben Hassen 2003, 2007) have already highlighted the importance of studying this organic content within phosphorites for understanding the phosphatogenesis.

These Early works, mainly for ca. thirty years ago, provided information about the nature and the origin (mainly marine planktonic) and the low degree of diagenetic evolution of this OM. Moreover, all these studies concluded the quantitative importance of extractable HC in the OM associated to phosphorites. But these works were performed on bulk phosphorites. Thus, it seems to us that a comparative study of the specific composition and properties of the OM of pellets and of their surrounding sediments

separately, can help to understand the mechanisms of phosphatogenesis. Our study aimed to carry geochemical characterization of OM in both fractions and to draw some relevant conclusions on the genesis of the Ras-Draâ ore pellets.

GEOLOGICAL SETTING

The Ras-Draâ ore mine is located between Tozeur and Nefta, in southern Tunisia. This deposit is a natural continuity of the great Gafsa-Metlaoui phosphatic basin (Fig. 1).

During the paleocene, the phosphatized basin was a marine gulf open to the sea on both sides of an emerging land mass, the Kasserine island (Cayeux 1896, 1941; Sassi 1974).

The phosphatic series, about ~ 50 m thick, and of Paleocene-Eocene age, consists of ten phosphatic layers (Sassi 1974) interbedded with non- or poorly phosphatized strata with various facies

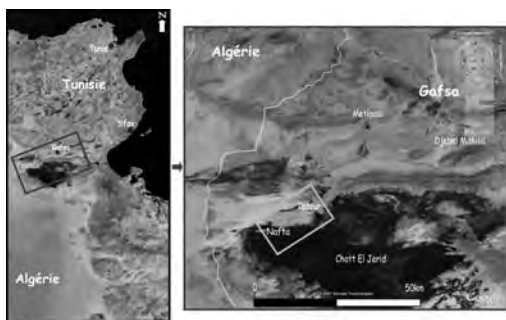


Fig. 1. Location map of the Ras-Draâ phosphate ore deposit in the Gafsa-Métlaoui basin, Tunisia (source: www.earth.google. fr).

(shales, marls, cherts, limestones).

EXPERIMENTAL

The studied samples were collected from the Ras-Draâ mine. The phosphatic grains (pellets) were separated from their exogangue (matrix) by granulometric fractionation after hand-processing the bulk samples under water.

For the analysis we selected pellets whose size lie between 100 and 500 μm (with 28 to 38% of P_2O_5) and matrix samples defined by a grain size < 50 μm (less phosphatized with $\text{P}_2\text{O}_5 \sim 7\%$).

Humic (HA) and fulvic acids (FA) and Humin (HU) were isolated utilizing the standard method recommended by the International Humic Substances Society (IHSS). Their amounts were obtained by quantifying carbon in each fraction and in each step of the fractionation procedure.

The study of HS extracted from both fractions (pellets and matrices) was performed by various geochemical analyses: CHONS elemental analysis, Fourier-transformed infrared spectroscopy (FTIR) and solid-state ^{13}C CPMAS NMR.

RESULTS AND DISCUSSION

The main results of the quantitative extraction of HS and of geochemical analyses of extracted organic fractions are:

- (1) The Total Organic Carbon (TOC) content (Table 1), given by the Rock-Eval pyrolysis, varies between 0.30 % and 1.62 % in phosphatic pellets and between 1.22 % and 4.05 % in their adjacent matrices.
- (2) The characterization of the OM

Table 1. HS yields and Rock-Eval pyrolysis data on pellets and matrices from the CI à CVIII layers of the Ras-Draâ deposit. ns : non significant values.

	AF (%)	AH (%)	HU (%)	TOC (%)	Tmax (°C)
CI Pellets	13,59	50,45	35,96	1,26	ns
CII Pellets	12,92	68,58	18,50	1,48	ns
CIII Pellets	7,67	73,62	18,70	0,40	421
CIV Pellets	16,21	73,39	10,40	0,30	427
CV Pellets	5,34	79,07	15,59	0,49	427
CVI Pellets	6,17	85,57	8,26	0,68	422
CVII Pellets	11,84	68,12	20,03	0,57	421
CVIII Pellets	17,03	55,82	27,15	1,62	ns
CI Matrice	2,48	4,46	93,06	2,41	ns
CII Matrice	4,23	6,46	89,31	2,14	ns
CIII Matrice	6,52	32,03	61,45	1,22	410
CIV Matrice	8,87	14,85	76,27	3,24	419
CV Matrice	2,00	23,23	74,77	3,10	413
CVI Matrice	1,90	10,81	87,29	3,82	419
CVII Matrice	2,78	7,08	90,14	4,00	417
CVIII Matrice	7,07	4,42	88,51	2,57	ns

contained in the two fractions (pellets and matrices) by RE pyrolysis concludes, on one hand, to the planktonic origin of the OM (Type II), in both fractions, and, on the other hand, to a low degree of maturity of the pelletal and matricial OM (RE Tmax < 430 °C) (Table 1).

(3) The HS yields from the pelletal and matricial OM (Table 1) shows a high content of humic compounds isolated from pellets (humic carbon up to 75% of TOC) and a lower one in adjacent sediments (humic carbon less than 21% of TOC), along with the higher content of HU (low mature kerogen) in surrounding sediments and the lowest in the pellets.

(4) The OM appears to be essentially of marine planktonic origin, as deduced from: (i) elemental analysis (the atomic ratios O/C and H/C values of 0.15 and 1.29 % in HA and 0.40 and 1.55% in FA, respectively, indicate that these humic compounds originated from marine aliphatic organic matter); (ii) FTIR analysis of humic materials (Fig. 2. spectra obtained for HA show these humics are rich with aliphatic structures which is

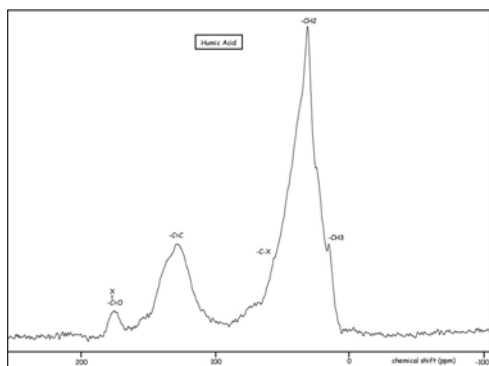


Fig. 2. ¹³C solid state NMR spectrum of a HA extracted from phosphatic pellets collected from Ras-Draâ phosphatic sediments.

typical of algal material); (iii) solid-state ¹³C CPMAS NMR (Figure 3 spectra obtained for HA show a strong aliphatic carbon peak at 0-50 ppm, indicating abundant oxygen-bearing aliphatic structures within these organic components).

CONCLUSIONS

This comparative study of OM in phosphatic pellets and their surrounding matrix provided information about the origin (essentially planktonic) and the low degree of diagenetic evolution of this OM in both fractions. Moreover, this study confirms the abundance of extractable humic compounds in the OM associated to phosphatized samples. The bulk OM within the pellets is essentially humic whereas the OM within the matrix of these pellets is different: it is not humic but a low mature kerogen. With regards to the age of the pellets, such high concentrations of HS in Ypresian phosphatic sediments imply an excellent preservation of the OM within the phosphatic grains. In contrast, the matricial OM differ by the nature of the diagenetic evolution that it has undergone. The nature of this matricial OM is quite usual for an ypresian age, epicontinental, never buried over a maximum of 150 m depth, sedimentary layer.

One explanation can be given for these differences: pellets though to be foreign bodies whose diagenetic story has been quite different, and independent, of that of their embedding sediment. These bodies

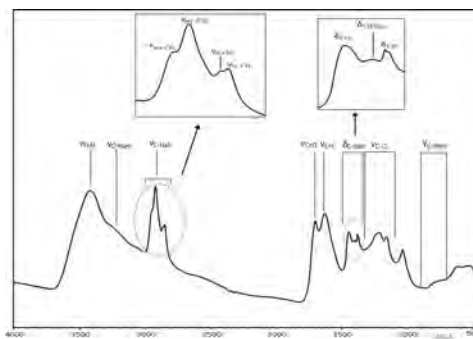


Fig. 3. FTIR spectrum of a HA extracted from phosphatic pellets collected from Ras-Draâ phosphatic sediments.

have been demonstrated to have derived from fish feces (Ben Hassen 2007) and their OM has been ingested by planktivorous fishes.

REFERENCES

- BELAYOUNI, H. 1983. Etude de la matière organique dans la série phosphatée du bassin de Gafsa-Métlaoui (Tunisie). *Application à la compréhension des mécanismes de la phosphatogenèse*. Thèse de Doctorat es-Sciences, Université d'Orléans. France.
- BELAYOUNI, H. & TRICHET, J. 1983. Preliminary Data On The Origin And Diagenesis Of The Organic Matter In The Phosphate Basin Of Gafsa (Tunisia), In: BJØROY *et al.* (eds.), *Advances In Organic Geochemistry 1981*. John Wiley And Sons, 328-335.
- BEN HASSEN, A. 2003. *Etude Pétrographique Et Minéralogique Préliminaire D'une Série Phosphatée Tunisienne*. Rapport Diplôme d'Etudes Approfondies, Université d'Orléans. France.
- BEN HASSEN, A. 2007. *Données Nouvelles Sur La Matière Organique Associée Aux Séries Du Bassin Phosphaté Du Sud-Tunisien (Gisement De Ras-Draâ) Et Sur La Phosphatogenèse*. Thèse De Doctorat, Université d'Orléans. France.
- CAYEUX L. 1896. Note Préliminaire Sur La Constitution Des Phosphates De Chaux Du Sénonien Du Sud De La Tunisie. *Comptes Rendus De l'Académie Des Sciences, Paris*, 273-276.
- CAYEUX L. 1941. Les Phosphates De Chaux Sédimentaires De France (France Métropolitaine Et d'Outre-Mer). **Tome I**. Imprimerie Nationale, Paris.
- NATHAN, Y. 1990. Humic substances in phosphorites: occurrence, characterization and significance. In: NOTHOLT, A.J.G. &

- JARVIS, I. (eds.), *Phosphorite Research and Development*, Geological Society Special Publications, **52**, 49-58.
- SANDSTROM, M.W. 1982. *Organic Geochemistry Of Phosphorites And Associated Sediments*. Phd Thesis, Australian National University, Canberra.
- SASSI, S. 1974. *La sédimentation phosphatée au Paléocène dans le sud et le centre-ouest de la Tunisie*. Thèse de Doctorat es-Sciences, Université de Paris-Orsay, France.

Petrogenesis of dykes related to Cu-Au & base-metal Au-Ag occurrences, Mt. Freegold area, Dawson Range, Yukon Territory, Canada

Thierry Bineli Betsi¹ & David R. Lentz¹

¹Department of Geology, University of New Brunswick, 2 Bailey Drive, Fredericton NB, E3B 5A3 CANADA
(e-mail: dlentz@unb.ca)

ABSTRACT: Dykes spatially associated with porphyry-like Cu and base-metal Au-Ag occurrences in the Mt. Freegold area (northern Canadian Cordillera) range from mafic (basaltic andesite) to felsic (rhyolite) units. Major and trace elements, as well as O and H isotope data, are consistent with magmas from both the crust and the mantle that evolved through crystal fractionation, crustal assimilation, and mixing processes. Dykes typically display much lower HREE relative to LREE, i.e., high La/Yb and high Sr/Y, which may at the first glance suggest an adakite-like signature. However assessments on other parameters such as Mg#, Na₂O, and Cr contents do not attest their adakitic affinity. The plagioclase-hornblende association and the lack of pyroxene are indicative of a water-rich source magma and support the high pressures (1.95 & 3.4-3.7 kb) derived from hornblende geobarometry. Zircon ²⁰⁶Pb/²³⁸U weighted ages reveal that dykes were emplaced from Jurassic (188 Ma) through to Middle Cretaceous (104-109 Ma) and Late Cretaceous (75.2 Ma). This suggests that mineralization may also have occurred at different times.

KEYWORDS: Cordillera, fractionation, mixing, calc alkaline, adakite

INTRODUCTION

The Dawson Range in the Canadian Cordillera hosts several deposit types that belong to the Dawson Range Au-Cu-(Mo) Belt portion of the Tintina Au Province. The geology of the area (Fig. 1) consists of the Devonian-Permian Yukon-Tanana Terrane intruded by the Upper Triassic to Early Jurassic Big Creek Metaplutonic Suite and Granite Batholith, as well as the Early Cretaceous Dawson Range Batholith. This terrane also hosts Middle to Late Cretaceous volcanic rocks and related dykes of the Mount Nansen and Carmacks groups, respectively (Carlson 1987). Mineralization is thought to be spatially and genetically associated with these dykes. The goal of this study is to provide a complete petrologic and geochemical data set to enable a better understanding of the petrogenesis of different dyke sets found in the area, referred to as the Northern Freegold Resources (NFR) Freegold Mountain project, and establish a petrologic link between them.

PETROLOGY

Dykes of the Dawson Range range from mafic to felsic aplitic and porphyritic bodies, which include: basaltic andesite, latite, andesite, trachyte, dacite, and rhyolite. Aplitic bodies are fine-grained, equigranular to sub-equigranular, whereas porphyritic dykes display phenocrysts of variable size in either a sugary or intergranular groundmass. Major minerals

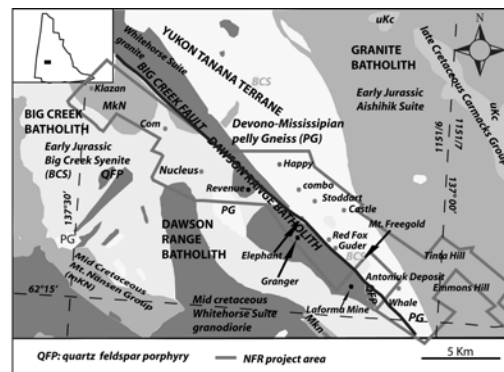


Fig.1. Location and geology of the Dawson Range, Yukon, and NFR claim boundaries (after Pautler 2006).

may be consistent with a magma mixing process. In the Rb versus Y+ Nb diagram (Fig. 4), dykes plot in the upper part of the I-type volcanic arc field overlapping into the syn-collisional. The position in the upper part of the volcanic arc field is consistent with mature arc rocks derived from the mantle, whereas the overlapping in the syn-collision field portrays once again the melting of crustal pelitic rocks or their incorporation in the melting process. Dykes are depleted in Rb, Th, and U, but slightly enriched in Cs. The depletion in Rb may suggest little or no crustal contribution during magma genesis and evolution, whereas the Cs content that is out of range of mantle values, testifies to the assimilation of crustal rocks. The $\delta^{18}\text{O}$ values from quartz grains and wall rock samples range from 6 to 10 ‰ (VSMOW) and are characteristic of igneous rocks with both mantle and crustal contribution. Wall rocks are depleted in D and δD values range from - 166 to -122 ‰ (VSMOW), which are beyond the range of magmatic isotopic values. These δD values may largely be a result of post-crystallization exchange between the rocks and heated meteoric ground water.

Chondrite-normalized REE patterns show that all types of dykes are depleted in HREE relative to LREE (Fig. 5). Also dykes display high Sr/Y (ave. 86 ppm) and La/ Yb (up to 80 ppm) ratios.

These characteristics may suggest geochemical characteristics similar to adakites and may also infer garnet-bearing and plagioclase- free sources. (Drummond & Defant 1990). However, others parameters such as the Mg# (ave.< 0.3), Na₂O < 3.5 wt.%, and Cr < 30 ppm are not consistent with an adakitic affinity. As pointed out by Richards & Kerrich (2007), other processes, likely fractionation of minerals that preferentially partition Y and HREE, may have contributed to high Sr/Y and La/Yb ratios. Hornblende, as well as zircon, apatite, and titanite are able to fractionate HREE relative to LREE and probably accounted for the observed pattern. Geobarometry of

hornblende in accordance with the calibration of Hammarstrom & Zen (1986) yielded pressures of 1.95, 3.4, & 3.6 to

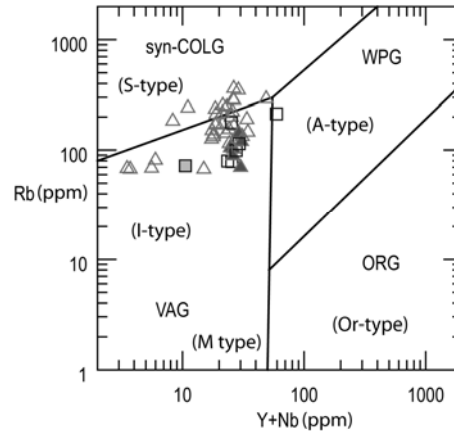


Fig. 4. Y+Nb vs. Rb (ppm) plot showing that dykes are mature arc rocks derived from the mantle, and from melting of crustal pelitic rocks or their incorporation in the melting process.

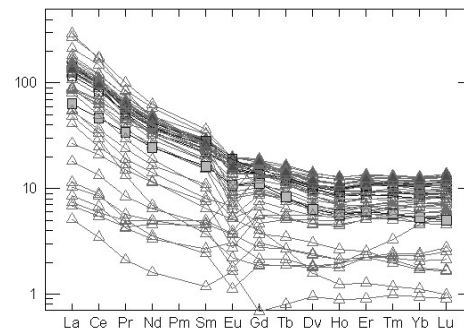


Fig. 5. C1 chondrite-normalized REE patterns showing the low HREE relative to LREE, suggesting a garnet-bearing and plagioclase-free source, as well as an adakitic-geochemical composition.

3.7kb. This is indicative of two magma chambers feeding the dykes, with one dacitic dyke deriving from the shallow chamber whereas, latitic, andesitic, and another dacitic dyke were derived from the deep chamber. Thermal ionisation mass spectrometry (TIMS) zircon U-Pb ages from mineralized quartz-feldspar rhyolitic dykes and those closely associated to the mineralization reveal that dykes range in age from Lower Jurassic (188 Ma) to Early Cretaceous (75.2 Ma) with most of them displaying Middle Cretaceous ages (104-109 Ma).

CONCLUSIONS

This study shows that:

- (1) Dawson Range's dykes were derived from both mantle and crustal sources. Melting of the rock sources gave rise to water-rich magmas that consequently crystallized over significant depths;
- (2) Dawson Range's dykes are a calc-alkaline suite that may have evolved through AFC and mixing processes, giving rise to a few samples that only partially fit the adakitic criteria;
- (3) While it has been thought that felsic dykes are only associated with the Middle Cretaceous Mount Nansen magmatic event in the Dawson Range, it appears that the Late Cretaceous Carmack's event also generated felsic dykes;
- (4) The Jurassic, Middle Cretaceous, and Late Cretaceous ages of dykes spatially associated with the mineralization suggests that the mineralization age may be extended beyond the unique Late Cretaceous age assigned to mineralization (Smuk *et al.* 1999).

ACKNOWLEDGEMENTS

We thank Yukon Geological Survey (YGS), Northern Freegold Resources (NFR), and NSERC for funding & logistical support.

REFERENCES

- ANNEN, C., BLUNDY, J.D., & SPARKS, R.S.J. 2006. The genesis of intermediate and silicic magmas in deep crustal hot zones. *Journal of Petrology*, **47**, 505-539.
- CARLSON, G.G. 1987. Geology of Mount Nansen (115-1/3) and Stoddart Creek (115-1/6) map areas Dawson Range, Central Yukon. *Indian and Northern Affairs Canada, Northern Affairs, Yukon Region, Open File 1987-2*.
- DRUMMOND, M.S. & DEFANT, M.J. 1990. A model for trondhjemite-tonalite-dacite genesis and crustal growth via slab melting: Archean to modern comparison. *Journal of Geophysical Research*, **95**, 21503-21521.
- HAMMARSTROM, J.M. & ZEN, E. 1986. Aluminum in hornblende: an empirical igneous geobarometer. *American Mineralogist*, **71**, 1297-1313.
- MOORE, G.M. & CARMICHAEL, I.S.E. 1998. The hydrous phase equilibria (to 3kbar) of an andesite and basaltic andesite from western Mexico: constraints on water content and conditions of phenocrysts growth. *Contributions to Mineralogy and Petrology*, **130**, 304-319.
- PAUTLER, J. 2006. *Evaluation Report on the Freegold Project, NTS 115/3, 6 & 7, Latitude 62°18'N, Longitude 137°12'W, Whitehorse Mining District, Yukon*, 108p.
- PETFORD, N. 2003. Rheology of granitic magmas during ascent and emplacement. *Annual Review of Earth and Planetary Sciences*, **31**, 399-427.
- RICHARDS, J.P. & KERRICH, R. 2007. Adakite - like rocks; their diverse origins and questionable role in metallogenesis. *Economic Geology*, **102**, 537-576.
- SMUK, K.A., WILLIAMS-JONES, A.E., & FRANCIS, D. 1997. The Carmacks hydrothermal event: an alteration study in the southern in the southern Dawson Range, In: *Yukon Geology 1996, Exploration and Geological Services Division, Yukon Region, Indian and Northern Affairs, Canada*, 92-106.

The primacy of magma compositions in determining the Re and W contents of molybdenite

Phillip L. Blevin¹

¹NSW Department of Primary Industries, PO Box 344, Hunter Regional Mail Centre, 2320, NSW, AUSTRALIA.
(e-mail: phillip.blevin@dpi.nsw.gov.au)

ABSTRACT: The Re contents of molybdenites from intrusion related ore deposits in eastern Australia are strongly negatively correlated with the degree of compositional evolution of the associated granitoids. Conversely, the tungsten content and Se/Te ratio of molybdenites (as analysed by LAM-ICP-MS) are positively correlated, indicating that the composition of the magmatic sources is a primary control on the abundance of these elements in molybdenite. In this regard, the siderophile/lithophile trace element geochemistry of the molybdenites parallel the broader gradation from Cu dominated to Sn-Mo-W dominated mineralization with increasing magmatic compositional evolution. Reconnaissance studies indicate that relative oxidation state of the Mo- versus Sn-mineralised magmatic suites do not affect these relationships. While whole rock analytical data indicates that Mo behaves incompatibly in oxidised intermediate to felsic magmas and compatibly in reduced magmas, the behaviour of Re appears compatible in both cases. These results have applications for exploration, ore genesis and Re-Os dating.

KEYWORDS: molybdenite, rhenium, granite, ore deposit, fractionation

INTRODUCTION

Molybdenite is the only common concentrator and economic source of Re. This is because MoS₂-ReS₂ effectively comprises a solid solution. The association of Re with Mo in this manner suggests that Mo and Re may also behave similarly during magmatic processes.

The Re content of unaltered hydrothermal molybdenites range from fractions of parts per million to percent values although a range of atomic Re/Mo values between 10⁻³ to 10⁻⁶ is most common (Terada *et al.* 1971; Newberry 1979a; Ishihara 1988). Numerous studies have dealt with aspects of Re in molybdenite including the documentation of Re contents in natural samples; correlation of Re content with conditions of molybdenite formation such as *f*S₂ and T (Terada *et al.* 1971); inter- and intra-deposit and inter-regional comparative studies (Morgan *et al.* 1968; Terada *et al.* 1971; Giles & Schilling 1972; Ishihara 1988); the relationship between Re contents and polytypism in molybdenite (Ayres 1974; Newberry 1979b); the effects

of post-crystallisation alteration (Newberry 1979a; McCandless *et al.* 1993); and even as evidence for metamorphic origin for low Re molybdenite (Stein 2006). A common conclusion of many earlier studies was that the Re/Mo ratio in molybdenites was a function of crystallisation temperature (Terada *et al.* 1971).

Giles and Schilling (1972) showed that the Re contents of molybdenite from porphyry Cu deposits was significantly higher (mean = 720 ppm) than those from porphyry Mo systems (mean = 50 ppm) while Re contents of molybdenites from greisens and pegmatites tended to be relatively low (Morgan *et al.* 1968). Newberry (1979a) noted that a strong inverse relationship existed between Re content (of molybdenites) and the Cu grade in several ore deposits. Despite the number of these studies little attention has been paid to the possibility that primary magmatic compositional controls, such as those which influence the ore element ratios (Cu:Mo:Sn:W etc.) observed in these deposits may also be an important control on the Re content of molybdenites.

MOLYBDENITES IN EASTERN AUSTRALIA

Molybdenite is a widespread and common mineral in hundreds of small deposits, disseminations and showings associated with the Palaeozoic granites of eastern Australia. Data exists on the geology of these deposits (Weber *et al.* 1978); the Re content of molybdenites (Riley 1967; Morgan *et al.* 1968; Blevin & Jackson 1998); the distribution of molybdenite polytypes (Ayres 1974), and the chemistry of Mo-mineralized granites (Blevin & Chappell 1992). Molybdenite occurs in veins, pipes, skarn and greisen style Mo, W-Mo±Bi and Cu-Mo deposits, as an accessory in Cu and/or Au deposits, and in trace amounts in Sn deposits. In eastern Australia molybdenite is mainly associated with oxidized, medium- to high-K I-type granites (Blevin & Chappell 1992) in addition to porphyry Cu-Au systems. Molybdenum dominant deposits are generally small and are not generally overprinted by high temperature potassic alteration, or lower temperature supergene overprints. Phyllic alteration is commonly present. Post crystallisation alteration of molybdenite, where present, is usually represented by ferrimolybdate.

METHODS AND RESULTS

Analytical Procedures

Rhenium contents of molybdenites have been derived from two sources: the literature (see above) where most Re concentration data was obtained by solution analysis and neutron activation; and by *insitu* LAM-ICP-MS (Blevin & Jackson 1998). In the later study molybdenites were analysed in 100 micrometer thick sections using a UV laser ablation microprobe at Macquarie University. In the absence of suitable sulfide reference materials, standardisation was performed using the silicate reference material NIST SRM 610. Differences in ablation yields were corrected by internal standardisation using Mo. The elements analysed were Si, Ti, Cr, Fe, Ni, Cu, Zn, As, Se, Zr, Nb, Mo, Pd, Ag, Sn, Sb, Te, W, Re, Au, Pb, and Bi. The elements Re, W, Se, and Te were found to be highly correlated with Mo. In

some cases Bi and Sn showed good correlations although most Bi was located in inclusions of galenobismutite, cosalite, and ikunolite that were common in most molybdenites analysed. The high degree of correlation of Re, W, Se, and Te strongly suggested that they comprise substitutions within the molybdenite lattice, rather than inclusions. Calculated Re concentrations using this method agreed well with previous analytical work on other molybdenites from these deposits, and with electron microprobe microanalysis of the laser analysed crystals.

Results

The relative degree of fractionation undergone by the medium- to high-K granite magmas of eastern Australia can be monitored by the concentration of Rb, which is incompatible in granitic magmas during fractionation, and by the ratios Rb/Sr and K/Rb. This relationship holds also for low-K granites which have low Rb contents and high K/Rb values (>300). Atomic Re/Mo ratios of molybdenites and the degree of fractionation of the related granites are strongly negatively correlated. The highest atomic Re/Mo value was from the Mt Morgan, Cadia and Yeoval Cu-Au deposits while lower Re/Mo molybdenites are associated with Mo-dominant or Sn-dominant mineralizing systems which are related to chemically more evolved granites. Molybdenite from scheelite skarn deposits occupies an intermediate position between Cu- and Mo-dominant granites both in terms of the Re/Mo ratio of the molybdenite and the degree of evolution of the related granite (at least in terms of Rb/Sr). Tungsten contents in the molybdenites are correlated in exactly the opposite way to that of Re. The Se/Te ratio increases from Cu-dominated to Mo and Sn dominated mineral systems.

DISCUSSION

Rhenium contents are low in molybdenites associated with reduced Sn-mineralized granites, and in molybdenites associated with the ilmenite-series granites of Japan. Ilmenite-series granites obtained their

reduced character through incorporation of crustal carbon either via assimilation of reduced sediments or mixing with magmas derived at least in part from those sources containing reduced sediment (Ishihara 1981). The average Re content of reducing marine sediments is ~50 ppb (with a range of 2 - 127 ppb; Koide *et al.* 1986) which is significantly above crustal and mantle averages. If ilmenite-series granites have attained their reduced character through the incorporation of reduced sedimentary materials, then it may be speculated that molybdenites related to these rocks could be expected to have higher Re contents than those related to granites derived from more purely igneous protoliths. The ilmenite-series granites of Japan tend to have lower K/Rb than magnetite-series granites, and are generally more felsic (Ishihara & Terashima 1992). In this regard, the difference observed in Re contents between molybdenites of the magnetite and ilmenite-series may alternatively be reconciled with the degree of compositional evolution of the associated magmas rather than to their relative oxidation states. The observed regional variation in Re contents of molybdenites in eastern Australia (e.g. between Tasmania and the mainland) can also simply be explained by the Tasmanian granites being generally more felsic and compositionally evolved.

Behaviour of other elements in molybdenite are highly consistent with ore element ratios in associated mineral deposits and strongly suggest that their control is dominantly that of their availability in the associated magmas at the time of hydrothermal fluid exsolution and transport.

Implications for Re-Os dating

The comparison of the Re content of a molybdenite with its structural polytype has been proposed as a method for assessing the viability of samples for Re-Os dating. "3R" molybdenite has been assumed to grow via a screw dislocation mechanism triggered by the incorporation of Re during crystallisation. Low Re "3R"

molybdenites are assumed to have lost Re during post crystallisation processes and are thus unviable for Re-Os dating. The results of this study have shown that W and probably Bi and Sn can substitute in significant amounts into molybdenite. The structural mismatch between these elements and the molybdenite lattice is much higher than that for Re suggesting that these elements may also be responsible for the triggering of the 3R polytype formation.

CONCLUSIONS

- (1) Re contents of unaltered molybdenites are primarily a function of the composition of the related ore magma.
- (2) LAM-ICP-MS studies indicate that other elements, in particular W, can substitute into the molybdenite lattice and can also be interpreted in terms of magma composition.
- (3) Re/W and Se/Te ratios in molybdenites are sensitive indicators of the ore element assemblages of the associated mineral deposits, and of the degree of compositional evolution of the associated magma.
- (4) Low Re molybdenite in granite related Sn-W-Mo mineral systems are not the result of post crystallisation leaching of Re, nor are they evidence for a metamorphic origin (cf. Stein 2006).

ACKNOWLEDGEMENTS

Published with the permission of the Director, Geological Survey of New South Wales, NSW Department of Primary Industries.

REFERENCES

- AYRES, D. 1974. Distribution and occurrence of some naturally-occurring polytypes of molybdenite in Australia and Papua New Guinea. *Journal of the Geological Society of Australia*, **21**, 273-278.
- BLEVIN, P.L. & CHAPPELL, B.W. 1992. The role of magma sources, oxidation states and fractionation in determining the granite metallogeny of eastern Australia. *Transactions of the Royal Society of Edinburgh*, **83**, 305-316.
- BLEVIN, P.L. & JACKSON, S. 1998. Potential Applications of LAM-ICP-MS technology in

- economic geology: a preliminary study of molybdenite and pyrite. *Geological Society of Australia Abstracts*, **49**, 44.
- GILES, D.L. & SCHILLING, J.H. 1972. Variation in rhenium content of molybdenite. 24th *International Geological Congress*, **10**, 145-152.
- ISHIHARA, S. 1981. The granite series and mineralization. *Economic Geology 75th Anniversary Volume*, 458-484.
- ISHIHARA, S. 1988. Rhenium contents of molybdenites in granitoid-series rocks in Japan. *Economic Geology*, **83**, 1047-1051.
- ISHIHARA, S. & TERASHIMA, S. 1992. K/Rb ratio of two contrasting magma series of the neogene plutonic belts in Japan. In: GUANGZHI, T (ed.), *Petrogenesis and mineralization of granitoids*. Science Press, Beijing, 23-33.
- KOIDE, M., HODGE, V. F., YANG, J., STALLARD, M., GOLDBERG, E., CALHOUN, J., & BERTINE, K. 1986. Some comparative marine chemistries of rhenium, gold, silver and molybdenum. *Applied Geochemistry*, **1**, 705-714.
- MCCANDLESS, T.E., RUIZ, J. & CAMPBELL, A.R. 1993. Rhenium behaviour in molybdenite in hypogene and near surface environments: Implications for Re-Os geochronometry. *Geochimica et Cosmochimica Acta*, **57**, 889-905.
- MORGAN, J.W., LOVERING, J.F., & FORD, R.J. 1968. Rhenium and non-radiogenic osmium in Australian molybdenites and other sulphide minerals by neutron activation analysis, *Journal of the Geological Society of Australia*, **15**, 189-194.
- NEWBERRY, R.J.J. 1979a. Polytypism in molybdenite (II): relationship between polytypism, ore deposition, alteration stages and rhenium contents. *American Mineralogist*, **64**, 768-775.
- NEWBERRY, R.J.J. 1979b. Polytypism in molybdenite (I): a non-equilibrium impurity-induced phenomenon. *American Mineralogist*, **64**, 758-767.
- RILEY, G.H. 1967. Rhenium concentration in Australian molybdenites by stable isotope dilution. *Geochimica et Cosmochimica Acta*, **31**, 1489-1497.
- STEIN, H.J. 2005. Low-rhenium molybdenite by metamorphism in northern Sweden: Recognition, genesis, and global implications. *Lithos*, **87**, 300-327.
- TERADA, K., OSAKI, S., ISHIHARA, S., & KIBA, T. 1971. Distribution of rhenium in molybdenites from Japan. *Geochemical Journal*, **4**, 123-141.
- WEBER, C.R., PATERSON, I.B.L., & TOWNSEND, D.J. 1978. Molybdenum in New South Wales. Geological Survey of New South Wales. *Mineral Resource Series* 43

RE minerals in Esfordi apatite- magnetite deposit, Central Iran

Mohammad Boomeri¹, Kazuo Nakashima², & David R. Lentz³

¹Geology Department, University of Sistan and Baluchestan, Zahedan IRAN
(e-mail: boomeri@hamoon.usb.ac.ir)

²Department of Earth and Environmental Sciences, Faculty of Science, Yamagata University, Yamagata JAPAN.

³Department of Geology, University of New Brunswick, PO Box 4400, Fredericton, NB, E3B5A3 CANADA

ABSTRACT: The stratabound Esfordi REE-P iron deposit is located in an Upper Precambrian volcanogenic complex. It is one of the more than 45 iron deposits in the Bafq area. The deposit has been petrologically investigated for textural relations, mineralogy, and mineral composition. This deposit is highly P-rich with local pegmatitic apatite veins. The main mineral assemblage in the Esfordi deposit is magnetite and apatite that is associated with Fe-Mg calcic pyroxene and actinolite. RE-bearing minerals are mainly apatite, monazite, allanite, and parisite. F.g. pink apatite occurs interstitial to granular apatite and magnetite crystals. Huge euhedral pyramidal and prismatic crystals of apatite are also abundant. Analysis shows these are fluor-apatite with F contents between 2.68 and 4.87 wt%. RE minerals were mainly formed along apatite grain boundaries and within veinlets. RE minerals are very rich in light REE (Ce, La, Nd, & Pr).

The deposit has similarities to Kiruna-type deposits. The Kiruna-type deposits are thought to have crystallized from volatile-rich iron oxide magmas derived by immiscibility in calc-alkaline to slightly alkaline parental magmas. The skarn assemblage, one head crystals of apatite, late RE minerals and veining around the Esfordi deposit indicate that hydrothermal process were definitely active at a later stage.

KEYWORDS: *Central Iran, Esfordi, apatite-magnetite, RE minerals*

INTRODUCTION

Esfordi apatite-magnetite deposit is located in 35 km northeast of Bafq city, in Central Iran. The Bafq is an important mining district and hosts several Iron deposit (about 2000 million tonnes) and a few Zn-Pb, U, Mn, and REE anomalies. The Esfordi deposit is the most rare-earth elements (REE)-rich and most P-rich member of these iron deposits. Choghart (200 million tonnes) and Chadormalu (400 million tonnes) iron deposits are now operating for iron, while Esfordi deposit (17 million tonnes with 30 % Fe oxide, 14 wt% P₂O₅, and about 2 wt% REE) is now operating for P. In addition, economic grade for REE is quite high relative to other rare elements, because their extraction as pure elements requires a higher technology than for other elements (Mariano 1989). Although, the Esfordi deposit is not comparable to giant REE deposits, such as Bayan Obo (China) and Mountain Pass (USA) carbonatite deposits (Kanazawa & Kamitani 2006) with respect

to the size and grade, but it appears to be a valuable REE deposit, because the mining is by inexpensive open-pit methods.

This paper identifies the RE minerals and presents preliminary information on mineral composition and geological and mineralogical features of the deposit. Chemical composition of minerals was determined by a wave length dispersive electron probe microanalyzer (EPMA), an automated JEOL JXA-8600 Superprobe, at Yamagata University.

GEOLOGICAL SETTING

The mineralized district is restricted by two main strike-slip faults of Kubanan to the east and Posht e Bdam to the west (Fig. 1a). The host rocks are a thick sequence of Upper Precambrian-Cambrian rhyolite, tuff, alkali granite, syenite, mafic dykes, magnetite, dolomite, gypsum, limestone, black shale, and sandstone. The Upper Precambrian-Cambrian sequence is overlain unconformably by Mesozoic and

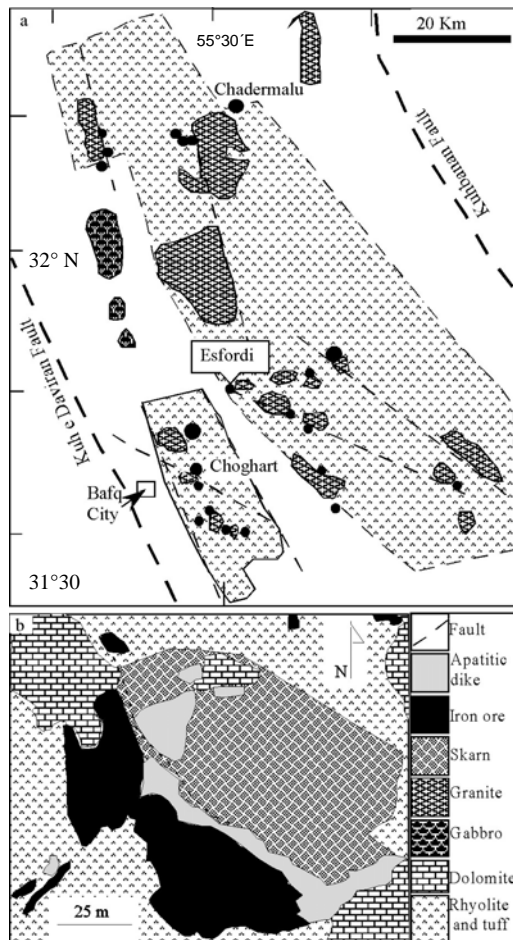


Fig. 1. a) Upper Precambrian-Cambrian Bafq metallogenic province in Central Iran (modified from NISCO 1980. b) a simple geology map of the Esfordi P mine (modified after Jami *et al.* 2007).

younger formations. The felsic igneous rocks are calc-alkaline and alkaline series magmas. The nature of the volcanism in the area can be interpreted as a signature of extensional tectonic setting such as arc/back-arc basin complexes. On the other hand, black shale and thick sequence of limestone and dolomite are similar as those of formed in intracontinental and passive continental margins. Ramezani & Tucker (2003) reported that the granitic intrusions and felsic volcanic rocks were formed in an active continental margin.

DISCUSSION & CONCLUSIONS

The ores appear to be a part of a thick

dolomitic layer that occurs on top a thick volcanic sequence dominated by acid pyroclastic rocks (Fig. 1b). The mine area is spherical in shape with a diameter of 500 metres, depth of 100 metres and spread across 20 hectares. It comprises of iron ore and phosphatic rocks of igneous type associated with actinolite, diopsidic pyroxene, quartz, feldspar, and carbonates. The ore can be divide into magnetite-rich, apatite-rich, apatite dyke, actinolite-rich and felsic pyroclastic horizons (Fig. 1b). Apatite occurs as microcrystalline red rocks with more than 90 wt % apatite, euhedral pyramidal and prismatic crystals of apatite (up to 15 cm length and 10 cm diameter) and pink powder interstitial to magnetite and granular apatite crystals. The analyzed apatites are fluor-apatites with F contents between 2.68 and 4.87 wt%. Amphibole occurs as long tabular and fibrous crystals and it is the most abundant skarn mineral. The analyzed amphibole classify as actinolite with Mg/(Mg +Fe) between 0.63 to 0.82. Calcic pyroxene occurs as tabular and prismatic long crystals. This mineral appears to be an earlier phase, because it was cut by amphiboles. It is diopsidic in composition, with the hedenbergite component ranging from 23 to 26 %. Garnet occurs as euhedral isotropic minerals and it is associated with apatite in actinolite-rich horizon. Although actinolite and diopsidic pyroxene are the most common silicates found in the deposit, garnet is a rare phase. Garnet classify as pure andradite (andradite end member is > 90 %). Common RE minerals in Esfordi are monazite, allanite, and parasite (Table 1). There are also other phases with briotholite composition. RE minerals were mainly formed along apatite and actinolite grain boundaries and within fractures (Fig. 2). Large size RE minerals (mainly as allanite) are associated with apatite-actinolite assemblage (Fig. 2b), whereas f.g. RE minerals (mainly as monazite) are associated with pure apatite samples (Fig. 2c). RE minerals are highly enriched in light REE such as Ce, La, Nd and Pr (Table 1). Apatite contains a few

Table 1. EPMA of RE minerals from the Esfordi deposit, Bafq, Iran.

Minerals	Allanite		Monazite		Parisite	
	Max	Min	Max	Min	Max	Min
SiO ₂ wt%	33.29	31.29	28.17	26.92	3.34	0.00
TiO ₂	0.82	0.23	0.00	0.00	0.06	0.00
Al ₂ O ₃	9.90	7.54	0.02	0.00	0.50	0.00
Fe ₂ O ₃	23.98	20.85	0.30	0.00	1.86	0.37
MnO	0.21	0.12	0.07	0.03	0.07	0.00
MgO	0.67	0.28	0.01	0.00	0.62	0.00
CaO	10.78	9.60	0.98	0.30	18.23	17.36
P ₂ O ₅	0.00	0.00	0.00	0.00	1.56	0.06
Ce ₂ O ₃	13.86	9.84	36.93	36.42	26.05	22.78
La ₂ O ₃	6.31	4.59	16.87	12.55	8.78	8.28
Pr ₂ O ₃	2.20	0.92	5.43	4.11	3.64	3.14
Nd ₂ O ₃	3.54	1.80	11.74	7.27	9.43	8.42
Gd ₂ O ₃	0.86	0.55	3.01	2.60	2.99	2.67
F	0.18	0.10	0.70	0.53	3.17	2.21
Sm ₂ O ₃	0.43	0.01	1.56	0.03	1.20	0.93
Eu ₂ O ₃	0.21	0.07	0.71	0.05	0.67	0.43
Dy ₂ O ₃	0.14	0.00	0.09	0.00	0.83	0.18
ThO ₂	0.13	0.00	1.48	0.00	0.22	0.05
Total	98.5	95.3	101.0	98.1	76.9	69.2
Si	3.29	3.16	0.96	0.94		
Ti	0.06	0.02	0.00	0.00		
Al	1.15	0.89	0.00	0.00		
Fe	1.81	1.58	0.01	0.00		
Mn	0.02	0.01	0.00	0.00		
Mg	0.10	0.04	0.00	0.00		
Ca	1.14	1.04	0.04	0.01		
Ce	0.51	0.36	0.55	0.54		
La	0.23	0.17	0.25	0.19		
Pr	0.08	0.03	0.08	0.06		
Nd	0.13	0.06	0.17	0.11		
Gd	0.03	0.02	0.04	0.04		
F	0.03	0.02	0.05	0.04		
Sm	0.02	0.00	0.02	0.00		
Eu	0.01	0.00	0.01	0.00		
Dy	0.00	0.00	0.00	0.00		
Th	0.01	0.00	0.03	0.00		

percent REE in its composition. However, the main part of REE may be from apatite as it is main mineral of the deposit and apatite-rich horizons contain high-grade REE ore.

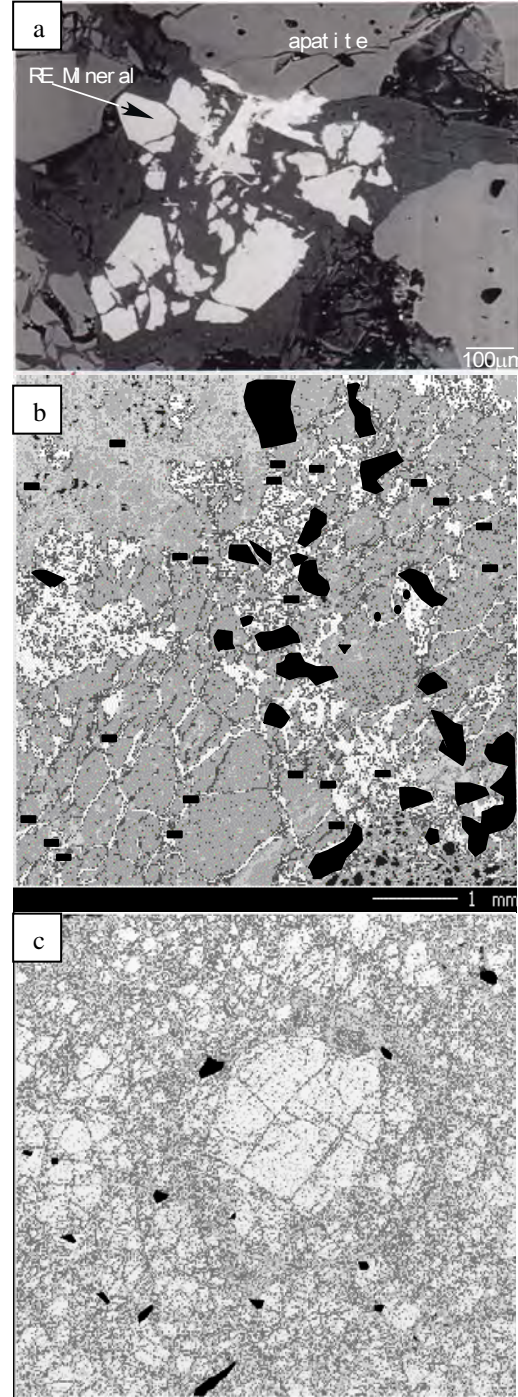


Fig. 2. SEM-BSE image and EPMA maps from Esfordi deposit. a) White crystals in fractures are REE minerals. b). RE minerals (sketched by black colour) are interstitial to actinolite (gray parts). c) RE minerals (black) and apatite (white) EPMA map.

REE ores are mainly associated with

carbonatite, alkaline, and pegmatitic rocks, associated hydrothermal systems, and placer environments. The Esfordi deposit is a Kiruna-type deposit. Several hypotheses have been examined to explain the origin of Kiruna-type deposits. The idea of an iron-oxide melt solidified into ore was first introduced by Geijer (1910). The Kiruna-type iron ores also introduced as hydrothermal deposits by Sillitoe & Burrows (2002). Recently, most REE mineralization associated with Kiruna-type systems is interpreted to be hydrothermal in origin. The skarn assemblage, one head crystals of apatite, late REE-rich minerals and veining around the Esfordi deposit indicate that hydrothermal process were definitely active at a late stage. Fluid inclusion studies on the Esfordi deposit by Jami *et al.* (2007) indicate three types of hydrothermal fluids. The hydrothermal fluids have probably remobilized REE from apatite and formed LE minerals at these late stages.

REFERENCES

- GEIJER, P. 1910. Igneous rocks and iron ores at Kiirunavaara, Lausavaara, and Toulluvaara, Sweden. *Economic Geology*, **5**, 699-718.
- JAMI, M., DUNLOP, A.C., & COHEN D.R. 2007. Fluid inclusion and stable isotope study of the Esfordi apatite-magnetite deposit, Central Iran. *Economic Geology*, **102**, 1111-1128.
- KANAZAWA, Y. & KAMITANI, M. 2006. Rare earth minerals and resources in the world. *Journal of alloys and compounds*, **408-412**, 1339-1343.
- MARIANO, A.N.1989. Economic geology of Rare earth elements. In: LIPIN, B.R., & MCKAY, G.A. (eds.), *Geochemistry and mineralogy of rare earth elements*. Reviews in Mineralogy, **21**, 309-337.
- NISCO (National Iranian Steel Corporation), 1980. Report on result of search and evaluation works at magnetic anomalies of the Bafq iron ore region during 1976-1979. *Unpublished internal report*, 260 p.
- RAMEZANI, J. & TUCKER R.D. 2003. The Saghand region, Central Iran: U-Pb geochronology, petrogenesis and implications for Gondwana tectonics. *American Journal of Science*, **303**, 622-665.
- SILLITOE, R.H. & BURROWS. D.R. 2002. New field evidence bearing on the origin of the EL Laco magnetite deposit, northern Chile. *Economic Geology*, **97**, 1101-1109.

Numerical simulation of the sill-driven convective ore-forming system at Matagami, Quebec: implications for metal leach zones

Patrick M. Carr¹, Lawrence M. Cathles III², & C. Tucker Barrie³

¹Xstrata Exploration, 500, boulevard Industriel, Matagami, QC, J0Y 2A0 CANADA
(e-mail: pcarr@xstratazinc.ca)

²Cornell University, Ithaca, NY, 14853 USA

³C.T. Barrie and Associates, 29 Euclid Avenue, Ottawa, ON, K1S 2W2 CANADA

ABSTRACT: VMS districts are typically ~40 km in diameter and contain about a dozen regularly spaced Cu-Zn orebodies; in these districts, typically one or two of the deposits contain more than half of the district's resources. We numerically investigate this deposit size and spatial distribution through two-dimensional finite element modeling of the convection above the Bell River sill in the Matagami district, Quebec, Canada. The zinc transport across the seafloor is dominated by those hydrothermal plumes driven by the strong horizontal gradient in temperature alongside the vertical portion of the retreating 350°C isotherm of the edges of the cooling intrusion. Convection occurs both above the sill and along its underside, and metal is extracted from both sides of the cooling sill.

KEYWORDS: VMS deposits, sill-driven convection, numerical models, metal depletion, thermal mixing zones

INTRODUCTION

In most VMS districts, one or two large deposits dominate a camp full of smaller deposits (e.g., Horne Mine, Noranda; Matsumine, Kuroko; Matagami Lake Mine, Matagami). We use finite element simulation of hydrothermal convection and associated chemical processes in attempt to explain this spatial distribution.

Thermally-driven convection in porous media has been simulated since Lapwood (1948) and has become increasingly complex and realistic. No models to our knowledge have systematically investigated the number and size of deposits that might form above a sill, nor have any modeled a system that would permit significant flow on the side and under the intrusive heat source.

MODEL BASICS

We simulate these systems using standard finite element techniques (e.g., Baker 1983) for solutions to the porous media conservation equations of mass, momentum, and energy on a rectilinear mesh using a code called BasinLab (Manning *et al.* 1987).

We deliberately keep the simulations as

simple as possible, and many assumptions and simplifications are included. Of particular note, rock permeability is taken to be a constant, modified only as a function of temperature in which it is elevated between 275 and 375°C and depressed at higher temperatures. This simulates thermal cracking (Lister 1974) and reproduces observed seafloor vent temperatures (Von Damm *et al.* 1983; Kelley *et al.* 2002).

Simulation results are shown here in terms of zinc metal vented into the ocean by hydrothermal fluid saturated with respect to zinc sulfide, the concentration of which increases exponentially with temperature (capped at 14.5 ppm at 400°C). The specific relation is similar to the one given by Large (1992), and is calibrated to end-member concentrations derived from seafloor observations (Seyfried *et al.* 2003). Details of the calculations are outlined in Carr *et al.* (2008).

MATAGAMI MODEL

The Matagami VMS district is located in western Quebec in the Archaean Abitibi green-stone belt and comprises primarily

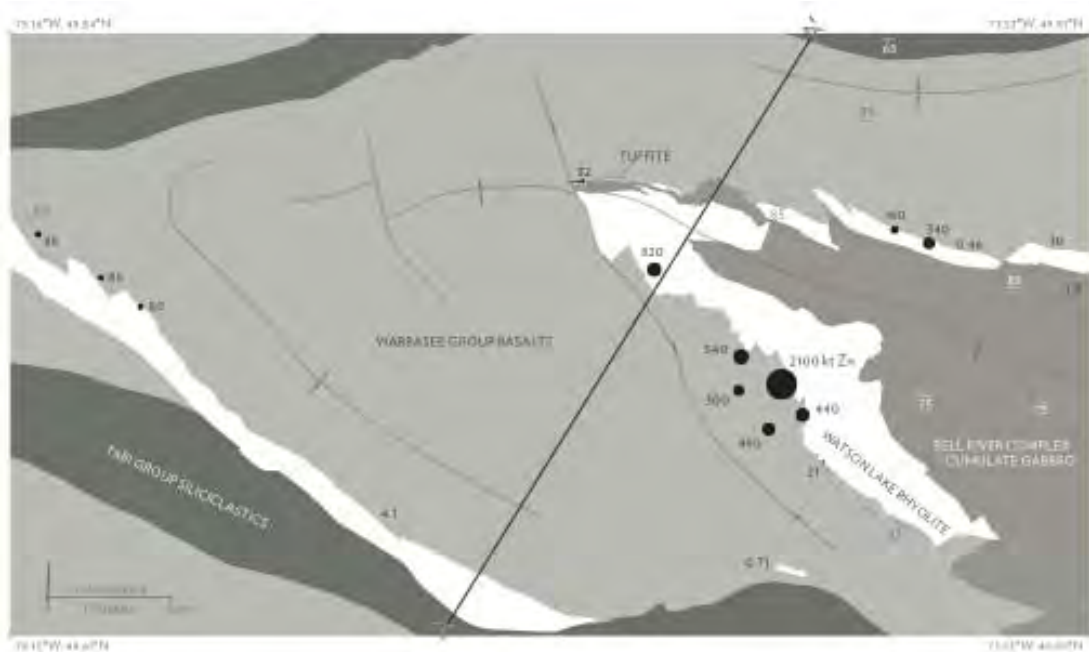


Fig. 1. Regional geology of the Matagami area (after Sharpe 1968) showing the tonnage of zinc metal at known deposits. Cross section A–A' is shown in Fig. 2

tholeiitic volcanics and intrusions formed in a back arc or continental rift zone. The regional geology is shown in Figures 1 (map) and 2 (cross-section A–A').

Most of the deposits are conformable with the Key Tuffite, a silicified tuff with a thickness ranging from 0.3 to 20 m, and traceable throughout the camp.

The footwall units below the ore horizon include the Watson Lake Rhyolite and the Bell River Complex intrusion. Both have U–Pb dates of ~2724 Ma (Mortensen 1993), and the Bell River Complex is considered to be the heat source which drove the hydrothermal circulation that created the ore deposits.

The hanging wall is composed of intermediate to mafic volcanics, beginning with the Wabasse Group basalts. Upsection are some interfingered rhyolites and small tuffaceous units, followed by hundreds of meters of massive basalt.

For the simulation, we reconstruct cross section A–A' to the time of ore deposition assuming conservation of rock volume and a sharp anticlinal postmineralization fold. The reconstructed sill has a thickness of 6.5 km at its centre thinning to a feather

edge over 30 km and a flat top. At the simulation of intrusion, the top of the calculation domain is the Watson Lake Rhyolite; 50,000 years after intrusion 100-m-thick strata at 2°C are added at 10,000 year intervals. All strata have a base permeability of 10^{-15} m^2 (1 millidarcy).

Figure 3 shows the metal transported across the numerical seafloor folded back onto cross section A–A'. Figure 4 shows zinc addition and depletion in the domain.

The evolution of the simulation (Carr *et al.* 2008, their Figure 12) shows that the vent site farthest from the cell center develops first, at 700 years after intrusion. Weak convection cells develop over the center of the sill, but most of the high-temperature venting occurs where the circulation is driven by the edge of the cooling sill. Venting of 300°C fluid continues for 135,000 years.

DISCUSSION

One of the most interesting aspects of the simulations is the way in which the convection cell that forms at the edge of the sill subsequently induces the formation of convection cells above the sill. Although

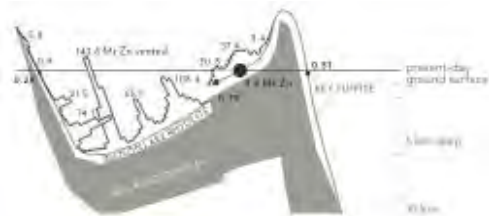


Fig. 2. Cumulative flux across the seafloor folded back onto the Key Tuffite horizon from cross section A–A' in Figure 2. Tonnages in bold are the known deposits from the camp.

Rayleigh convection forms above the centre of the sill, it is overprinted by the later and larger (from double to an order of magnitude more Zn metal) hydrothermal plumes driven by the horizontal gradient at the vertical boundary created as the sill cools toward the centre. Since we maximize permeability at 325°C, these plumes approximately follow this isotherm.

This edge convection cell creates significant flow along the side of the cooling 350°C isotherm, and, because of the geometry of the Bell River Complex, along the underside of the sill. Since metals are leached where pore water is heated, this creates leach zones along the underside as well as along the top of the sill.

Since these plumes are not Rayleigh convection, this phenomenon is not permeability dependent. We can, however, temper the magnitude by decreasing permeability with depth. A sufficiently steep exponential decay in permeability will result in a system dominated by the Rayleigh convection generated along the sill top, and various linear decay functions will systematically decrease the contribution of metal from the underside of the sill.

Changes in the geothermal gradient can have the same effect as changes in the permeability. Brikowski & Norton (1989) model a similarly shaped sill, but in a mid-ocean ridge environment. The increased temperature in the host rock (the gradient is ~200°C/km) means that the horizontal gradient created by the intrusion, and therefore the contribution of the edge convection cell, is much less.

We use a much lower gradient, 21°C/km. This may even be high—pore water convection driven by previous intrusive activity is likely to have cooled the area (*c.f.* Fehn *et al.* 1983).

CONCLUSION

In VMS systems in tectonic environments which have sufficiently low geothermal gradients and sufficiently constant permeability with depth, we would expect to see metal leaching at the underside and through the intrusion as well as along the top surface.

ACKNOWLEDGEMENTS

This material is based on work supported by NSF grant 9811143 and CAMIRO grant 96E01, with additional support from Noranda Exploration. Paul Manhardt provided solver core maintenance and coding support, and Jenn Adams was essential to the convergence of the simulations.

REFERENCES

- BAKER, A.J. 1983. *Finite Element Computational Fluid Mechanics*. Hemisphere, New York.
- BRIKOWSKI, T. & NORTON, D. 1989. Influence of magma chamber geometry on hydrothermal activity at mid-ocean ridges. *Earth and Planetary Science Letters*, **93**, 241-255.
- CARR, P.M., CATHLES, L.M., & BARRIE, C.T. 2008. On the size and spacing of volcanogenic massive sulfide deposits within a district with application to the Matagami District, Quebec. *Economic Geology*, **103**, 1395-1409.
- FEHN, U., GREEN, K.E., VON HERZEN, R.P., & CATHLES, L.M. 1983. Numerical models for the hydrothermal field at the Galapagos spreading center. *Journal of Geophysical Research*, **88**, 1033-1048.
- KELLEY, D.S., BAROSS, J.A., & DELANEY, J.R. 2002. Volcanoes, fluids, and life at mid-ocean ridge spreading centers. *Annual Review of Earth and Planetary Sciences*, **30**, 385-491.
- LAPWOOD, E.R. 1948. Convection of a fluid in a porous medium. *Mathematical Proceedings of the Cambridge Philosophical Society*, **44**, 508-521.
- LISTER, C.R.B. 1974. On the penetration of water into hot rock. *The Geophysical Journal*

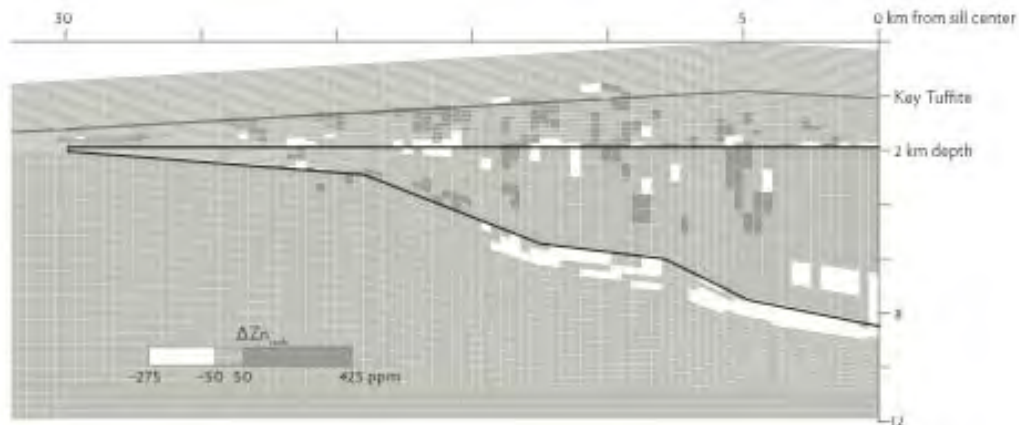


Fig. 3. Cumulative extraction and deposition of zinc at the end of the simulation. The algorithm assumes local chemical equilibrium.

of the Royal Astronomical Society, **39**, 465-509.

MANNING, R.A., MANHARDT, P.D., ORZECOWSKI, J.A., CATHLES, L.M., & BAKER, A.J. 1993. A parallel 3-D geologic basin modeling code. *Technical Report for the SIAM Conference on Mathematical and Computational Issues in the Geosciences, Knoxville*.

SEYFRIED, W.E., JR., SEEWALD, J.S., BERNDT, M.E., DING, K., & FOUSTOUKOS, D.I. 2003. Chemistry of hydrothermal vent fluids from the Main Endeavor Field, northern Juan de

Fuca Ridge: geochemical controls in the aftermath of June 1999 seismic events. *Journal of Geophysical Research*, **108**, 2429-2452.

VON DAMM, K.L., GRANT, B., & EDMOND, J.M. 1983. Preliminary report on the chemistry of hydrothermal solutions at 20°N, East Pacific Rise. In: RONA, P.A., BOSTROM, K., & SMITH, K.L., JR. (eds.) *Hydrothermal Processes at Seafloor Spreading Centers*. Plenum, New York, 369-389.

Minerals exploration and supply: a worldwide perspective

William X. Chávez, Jr.

*Minerals Engineering Department, New México School of Mines, Socorro, New México U.S.A.
(email: wxchavez@nmt.edu)*

Abstract: The current economic “downturn” in the consumption of mineral commodities has changed the manner in which companies and countries attempt to guarantee a secure supply of mineral resources. Although minerals exploration as yet comprises traditional, greenfield-style ore search, many companies now emphasize brownfield exploration efforts because the economics of expanding current mine operations is generally much more advantageous than developing a start-up mine.

Current stockpiles of base metals, aluminum, and ferrous products indicate that mine production has not yet been restricted enough so as to allow consumption of metals to reach an equilibrium with mine production. Even given this observation, some companies and countries are increasing metals production from mines so as to exert greater influence on the economics of a particular metals commodity; this is true for major and intermediate mining companies, and countries with substantial base metal or ferrous mineral resources.

Property acquisitions represent an alternative to the risks associated with traditional exploration, and available to companies and countries with sufficient cash-on-hand or with joint-venture partners. Because many mineral properties are substantially undervalued, acquisitions represent an economically-favorable manner of securing future mineral resources, allowing companies and state entities to prepare for the next upswing in mineral commodity demand; in addition, acquiring future resources provides some measure of economic security in that a source of minerals commodities is essentially guaranteed.

Although future minerals exploration will continue to involve high-risk frontier and novel geographic regions, the conservative nature of the mining and minerals supply businesses dictates that more traditional and pragmatic methods will be applied to ore search.

Keywords: *mineral exploration, supply, mine start-up*

BACKGROUND

Although worldwide exploration for ferrous, base-, and strategic metals has slowed substantially, the production of these metals has not slowed concomitantly; exploration for, and in some regions, production of, base- and precious metals is presently increasing. Because the consumption – and hence, production – of ferrous-, base-, and many strategic metals has been limited by economic considerations in the greatest consuming nations, most notably China, India, Russia, and the United States, metal stockpiles continue to increase or have stalled at a metastable equilibrium, pushing producers into mine closures or restriction of mine production, with important exceptions.

Current stockpiles of base- and ferrous metals are so great as to require that

mines slow significantly their metals production if an equilibrium between metals supply and consumption demand is to be established. World copper stockpiles, for example, contain so much refined metal that they represent the annual production from several world-class copper mines; in this case, the equivalent of the current annual copper production from the combined Collahuasi-Quebrada Blanca Districts of northern Chile, representing about one-seventh of the total copper production from Chile. Similarly, zinc stockpiles represent nearly a year of metal production from the Cloncurry District of northern Australia - as well as a substantial amount of primary lead production. The fact that stockpiles continue to grow or are just reaching a quasi- equilibrium state, even with mine closures and production decreases,

means that mine production has yet to adjust substantially to worldwide base metals demand.

Restriction of metals production by operating mines will likely be necessary for several years as consumption from current metal stockpiles catches up with stockpiled inventories and mine production. Even recent copper purchases by China have only slightly drawn down stockpiles, and are reflected in modest increases in short-term copper prices. The obvious global crisis has also stemmed demand, although precious metal markets are moving ahead, albeit sluggishly.

PRODUCTION & EXPLORATION VS. ACQUISITION CONSIDERATIONS

Counter to the necessity of temporarily decreasing base metals production are new mine openings that have been undertaken because some producers expect to gain financial advantage by having new mines ready to replace closed or reduced-output mines, to supply to local metals markets, or to keep prices depressed so as to place an economic *force majeure* on struggling producers. For example, CODELCO, the Chilean state mining company, continues to mine as-usual with the hope of maintaining a significant advantage in overall costs for copper production; MMC Norilsk Nickel, the world's leading nickel and PGE producer, also expects to maintain nickel production, but only in its mines in Russia, having closed all of its nickel mines in Australia and limiting production from other non-Russian mines. This action has had ramifications for other nickel producers, who can not compete with the greater grades and lower labour costs of Russian mines. Precious metal mines, especially those of gold, have generally fared better than base metals as consumers purchase gold as a hedge commodity.

The decreased value of holdings in minerals properties has meant that even large mining companies are considered to be available as potential sources of metal resources – via takeover - by both well-funded companies and as-yet well-funded

nations. This means that it is more expedient with respect to economies of investment and of time to purchase mineral resources – and the companies that hold them – than to engage in the laborious, expensive, and risky ventures of minerals exploration. Consequently, many mineral properties that might otherwise languish due to insufficient financing (or interest) on behalf of mining companies may now see some re-activation of exploration as they are taken-over by entities with capital to spend on property evaluation. Another benefit of this practice is that some marginal properties may receive greater exploration attention, with the idea of establishing better or new resource models for future metal mines.

Besides the observation that some countries and companies that have available cash are preparing for the next demand-driven upswing in required minerals production by acquiring mineral properties, there is also the opportunity by money-flush organizations to negotiate commitments from local to national governments for minerals supplies in exchange for development of infrastructure. This is a barter-style agreement that is of particular interest to commodity-rich or potentially-rich developing nations, whose own economies can not support development of necessary infrastructure, and whose technical support and labor pools may not have the background to design and construct significant development projects. The upside here is that countries receive needed infrastructure, often designed and built by the resource-requiring company or country. Downsides to this type of minerals-for-development swap is that in many cases the infrastructure is provided only in those mineral-rich geographic regions that are of direct interest to the mineral-receiving beneficiary (for example, as has happened in the past in Bolivia, México, the D.R.C., Zambia, Botswana), and that such development projects may be postponed or delayed indefinitely if economic conditions and the value of a particular commodity warrant such. As an example, the agreement between various

Chinese metals companies and the Democratic Republic of the Congo, involving development of infrastructure in return for commitments of significant quantities of base metals, has been put in abeyance until base metal values improve to the point where development of mines and their associated infrastructure is economically more advantageous than simply buying base metals from available providers.

Because so many mineral properties are currently undervalued, property acquisition represents a very favorable avenue of insuring future metals supply; this option is available only to those companies or countries with substantial cash reserves or those willing to engage in joint-venture arrangements in order to share risks and benefits. China, Russia, and India have each shown the initiative of acquiring either specific mineral properties or a specific commodity in order to satisfy national interests. For example, China has acquired properties or companies that would help assure supplies of copper, nickel, tantalum-niobium, and iron; Russia continues to seek expansion of its nickel and PGE reserves through the purchase of foreign assets, and India has attempted to acquire copper resources through a tender for ASARCO. Forward actions such as these allow countries to gain greater control on certain commodities supplies to greater extents than otherwise permitted through domestic-only production, as well as securing and satisfying domestic requirements of metals.

It is apparent that the need for a secure supply of mineral commodities is currently driving some countries, and forward-thinking companies, to continue to acquire, prospect for, evaluate, and enter into feasibility studies of, potential near-term mining properties. In some cases, properties are being prepared for immediate production by either completing construction of mining infrastructure or by expansion of existing mine and mill capacities. The idea is to have a property ready to increase production or to be put into production when commodity prices rebound, and to do so more quickly than

care-and-maintenance mines. Although quite risky, the current undervalued nature of such acquisitions represents a substantial potential for economic and security-of-supply gains by the investing countries and companies.

FUTURE EXPLORATION

Future exploration efforts, necessary to maintain detailed knowledge of the location, size, and concentrations of metals resources, will necessarily emphasize under-explored and frontier regions. Exploration in geologically-, geographically-, and socially-challenging areas will consume substantial amounts of time and money in defining potentially productive metallogenic regions; for example, targets being considered include: epithermal precious metal systems in shallow waters of the southwest Pacific; base- and precious metal occurrences in the Himalaya regions, notably large (and to-date, low-grade) porphyry systems; extensions of known metallogenic belts into the northern Andes, notably Colombia; highly prospective areas within conflict regions (for example, Tethys Belt countries). Some very prospective areas may be deemed too risky because of state-imposed taxes/royalties or inconsistent legal bases (e.g., Mongolia, the D.R.C., central Asia, Bolivia, Venezuela) or continued social-economic or security difficulties (e.g., East African Rift region, some Latin America countries, Himalaya – Tethys region). As such, and given the conservative nature of minerals exploration and mining companies, the overall exploration picture will almost certainly result in companies investing the bulk of their resources in and around known districts, retreat prospects, and relatively safe greenfield terrains rather than in novel frontier regions.

Mineralogical host phases for the PGE in magmatic Ni-Cu-PGE deposits at the Creighton Mine, Sudbury, Canada

Sarah A.S. Dare¹, Sarah-Jane Barnes¹, Hazel M. Prichard², & Peter C. Fisher²

¹Canadian Research Chair in Magmatic Metallogeny, Science de la Terre, Université du Québec à Chicoutimi, 555 Bld. de l'Université, Saguenay, PQ, G7H 2B1 CANADA (e-mail: sasdare@hotmail.com)

²School of Earth and Ocean Sciences, Cardiff University, Main Building, Park Place, Cardiff, CF10 3YE UK

ABSTRACT: Magmatic Ni-Cu sulfide ores may contain platinum-group elements (PGE) that are recoverable as by-products of mining these ores. It is of interest to understand which minerals host the PGE for two reasons: 1) to efficiently extract the PGE; 2) to understand the petrogenesis of the ores. The distribution of PGE from magmatic Ni-Cu-PGE deposits at the Creighton Mine, Sudbury, Canada has been investigated. A PGE mass balance has been carried out by comparing whole rock PGE concentrations to the sum of solid solution concentrations of PGE in base metal sulfides (BMS) and the associated PGM. Calculations show that the BMS host the majority of Ru and Pd (80-95%) and Os (65%), but Ir, Rh, Pt and Au are absent from the BMS. In contrast, Ir, Rh and Pt are hosted by sulfarsenide-bearing PGM within the BMS. These comprise irarsite (IrAsS)-hollingworthite (RhAsS) cores, containing some Pt, Os and Ru, and Ni-cobaltite (NiCoAsS) rims. Pentlandite is the main host for Pd because Pd diffuses from nearby Cu-rich phases into early-forming coarse-grained pentlandite. Pd-bearing PGM (michenerite PdBiTe), Pt-bearing PGM (sperrylite PtAs₂) and Au (electrum AuAg) are present but rare.

KEYWORDS: Ni-Cu-PGE deposit, sulfides, Sudbury, Laser-Ablation ICPMS, PGM

INTRODUCTION

It is well known that magmatic sulfides collect PGE and can form magmatic ore deposits (e.g., Merensky Reef, Bushveld, Republic of South Africa; Noril'sk, northern Siberia, Russia; Sudbury, Ontario Canada). It is necessary to determine which mineral phases host the PGE in order to: 1) efficiently extract the PGE and 2) better understand the petrogenesis of the ores. A number of processes may control the distribution the PGE in a magmatic sulfide ore deposit, including fractional crystallization of monosulfide solid solution (mss) from a base metal-rich sulfide liquid, direct crystallization of PGM from fractionated sulfide liquid, exsolution of PGM during sulfide cooling, and remobilization of PGE by reworking of the sulfides by late magmatic and/or hydrothermal fluids, deformation and metamorphism (see Barnes *et al.* 2008 for references).

Earlier studies of PGE distribution in magmatic sulfides have used microprobe, SIMS and micro-PIXE (e.g. Cabri *et al.*

2003). However, for many of the PGE, the concentrations in ores from Ni-Cu-PGE deposits were less than detection limit. laser ablation ICPMS (LA-ICPMS) offers three advantages over these techniques, namely: 1) lower detection limits (ppb level), 2) accessibility, and 3) time-resolved analysis.

LA-ICPMS has been used to determine the *in-situ* PGE content of base metal sulfides from PGE-rich reefs (e.g., Ballhaus *et al.* 2001; Holwell *et al.* 2007; Godel *et al.* 2008; Barnes *et al.* 2008). These studies demonstrate that all of the PGE, except Pt together with Au, are predominantly hosted by sulfides in solid solution and that pentlandite is a major carrier for Pd. The distribution of PGE in Ni-Cu-rich PGE deposits is less well-known. Huminicki *et al.* (2005) lasered sulfides from Copper Cliff Mine, Sudbury and calculated that the sulfides carried very little PGE and thus PGE were hosted mainly by PGM. We are furthering the study of Sudbury by investigating the distribution of PGE from Creighton Mine.

GEOLOGICAL SETTING AND SAMPLES

Ni-Cu-PGE mineralization at Sudbury is zoned with respect to Cu and PGE as a result of fractional crystallization from a base metal sulfide liquid, but metamorphism, fluids and deformation also affected these ore deposits (e.g., Farrow & Lightfoot 2002 and authors therein). The two main styles of mineralization are: 1) Fe-Ni-rich pyrrhotite ores (with minor pentlandite and chalcopyrite) in embayments along the base of the complex in noritic/gabbro-noritic (contact ores) and 2) Cu-Pt-Pd-Au-rich chalcopyrite ores (with minor pentlandite, pyrrhotite and PGM) forming veins and stockworks in the country rock below the complex (footwall ores). Creighton Mine, on the southern margin of the complex, is one of the largest contact-style deposits.

We have analysed 14 samples of contact-style ore from Creighton Mine comprising disseminated ores (< 30% sulfides), inclusion-bearing ores (containing fragments of the norite) and massive ores (> 80% sulfides). The ores contain on average 75% pyrrhotite, 17% pentlandite and 8% chalcopyrite. Chalcopyrite content varies from 0-25%.

ANALYTICAL METHODS

Whole rock and LA-ICPMS analyses were carried out at Université du Québec à Chicoutimi (UQAC). Sulfur was determined by combustion and IR analysis. Ni and Cu were determined by atomic absorption spectrophotometry after aqua regia digestion. Gold and PGE were determined by Ni-sulfide fire assay followed by Te co-precipitation followed by ICPMS.

We used a Thermo X7 ICPMS coupled to a New Wave Research 213 nm UV laser to determine the PGE and Au in the sulfides. Other chalcophile metals (Ag, As, Bi, Cd, Co, Cu, Fe, Ni, Pb, Re, Sb, Se, Sn, Te and Zn) were also monitored. Analytical conditions were: beam size of 80 µm; laser pulse rate of 10 Hz; laser output power of 0.3 mJ/pulse to ablate the sulfide for 60s after a 20s gas blank was collected. Sulfide standards were used to

calibrate analyte sensitivities and to monitor data quality. Detection limits were: 3-10 ppb for Os, Ir, Rh, Pt and Au and 20-30 ppb for Ru and Pd. A typical time-resolved spectrum for LA-ICPMS analysis is shown in Figure 1. The PGM were located on a Zeiss SMT S360 SEM at Cardiff University using a magnification of x50. PGM were qualitatively analyzed with INCA ENERGY EDX system.

PGE MASS BALANCE

In order to establish which base metal sulfide minerals host the PGE at the Creighton Mine we calculated a mass balance following the method of Barnes *et al.* (2008). We used the whole rock PGE content, the concentration of PGE in each sulfide and the mass fraction of each sulfide phase in the ore to determine the proportion (wt. %) of each PGE hosted by the sulfides in solid solution.

At the Creighton Mine, the sulfides host the majority of Ru and Pd (80-95%) and Os (65%) but Ir, Rh, Pt and Au are not hosted by the sulfides. Pyrrhotite and

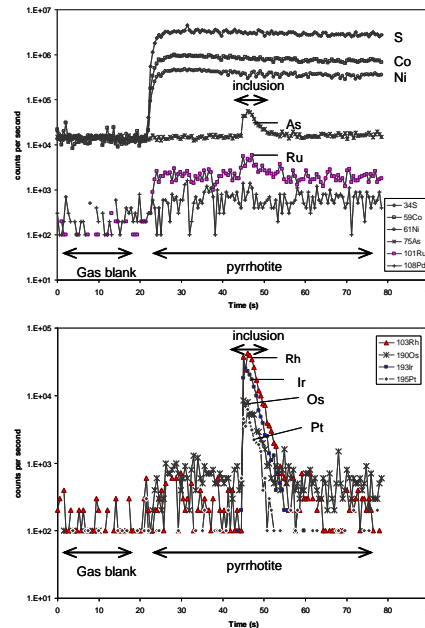


Fig. 1. Time-resolved spectrum for the LA-ICP-MS analysis of PGE in pyrrhotite. After 20s of gas blank the laser is turned on for 60s. Pyrrhotite contains only Os-Ru but a peak in the signal for Ir-Rh-Pt (Os) and As occurs where a PGM inclusion is encountered.

pentlandite host Ru and Os in equal proportions. Pentlandite is the main host of Pd (1 ppm) but chalcopyrite also contains some Pd (0.6 ppm); in contrast, pyrrhotite contains none. This indicates pentlandite exsolved from an Os-Ru rich mss, together with pyrrhotite. The origin of Pd in pentlandite is discussed below.

PGM

The PGM study reveals that sulfarsenide minerals are very common in the ores. They account for the Ir, Rh and Pt 'missing' from our calculated sulfide mass balance. These sulfarsenide minerals are euhedral and zoned in PGE (Fig. 2). They have an irarsite (IrAsS) surrounded by hollingworthite (RhAsS) core and a Ni-cobaltite (CoAsS) rim that contains some Rh (3 wt. %). The PGM cores also contain minor amounts of Pt (6 wt. %) and Os-Ru (1 wt%).

The sulfarsenides are small (5-20 μm) and the PGM cores are typically 1 – 5 μm . They are hosted almost entirely within the base metal sulfides, mainly in pyrrhotite and pentlandite but also in chalcopyrite. We estimate that the cobaltite equilibrated at 550-600°C. The PGM cores either crystallized from the sulfide melt or exsolved > 550°C from the sulfides during cooling.

Sperrylite (PtAs_2), electrum (AuAg) and michenerite (PdBiTe) are rare. Michenerite was observed to infill fractures in amphibole indicating that some Pd can be remobilized during metamorphism and deformation.

TEXTURAL LA-ICPMS STUDY OF Pd IN PENTLANDITE

In order to investigate why pentlandite is enriched in Pd compared to pyrrhotite we used the LA-ICP-MS to measure Pd in three different textures of pentlandite shown in Figure 3.

In all cases, the amount to Pd in pentlandite decreases from coarse grained (0.5 – 2.5 ppm) to veinlets (0.2 – 1 ppm) to flames (< 0.2 ppm). Also, coarse-grained pentlandite in chalcopyrite-rich ores (10 – 25% Ccp) are richer in Pd (1 – 2.5 ppm) than those (0.5 ppm Pd) in

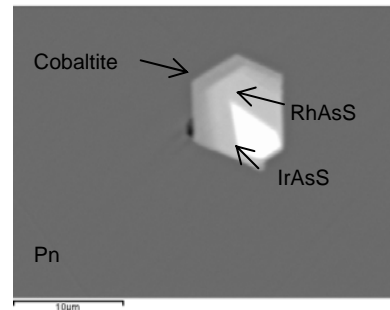


Fig. 2. Back-scattered electron image of a euhedral, zoned sulfarsenide hosted in pentlandite (Pn). Inner core (white) is irarsite (IrAsS), outer core (pale grey) is hollingworthite (RhAsS), rim (dark grey) is Rh-bearing Ni-cobaltite.

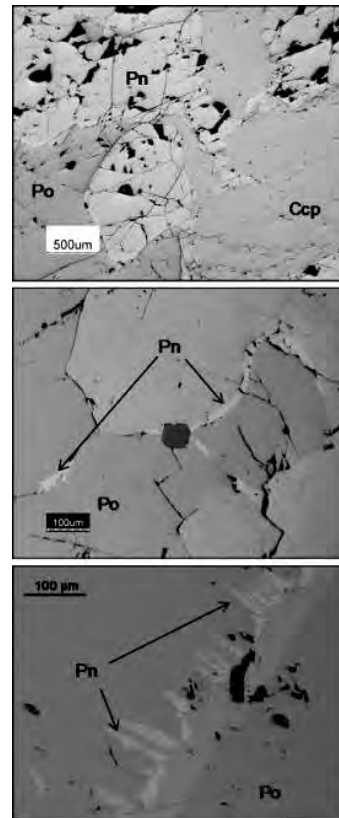


Fig. 3. Coarse grained pentlandite (Pn), often associated with chalcopyrite (Ccp), b) fine to medium-grained pentlandite aligned in veinlets along the pyrrhotite (Po) grain boundaries and c) exsolution flames of pentlandite in pyrrhotite.

chalcopyrite-poor ores (< 10% Ccp).

We propose that Pd diffuses from trapped Cu-rich phases into pentlandite during/after its exsolution from mss.

Chalcopyrite-rich pyrrhotite ores provided more Pd to diffuse into pentlandite than chalcopyrite-poor ores because Pd partitions into the Cu-rich liquid during sulfide fractionation. Most of the diffusion occurred early, when the coarse grained pentlandite formed, before the pentlandite veinlets and flames exsolved from mss.

CONCLUSIONS

- (1) Base-metal sulfides host the majority of Ru, Pd and Os in solid solution but contain no Ir, Rh and Pt.
- (2) Pyrrhotite and pentlandite exsolve from mss with equal proportions of Os and Ru.
- (3) Pyrrhotite does not contain Pd whereas pentlandite is enriched in Pd (up to 2.5 ppm).
- (4) Pd diffuses from Cu-rich phases into nearby pentlandite that formed early (i.e. coarse grained).
- (5) Sulfarsenide-bearing PGM are zoned with respect to Ir, Rh, Pt, Co, Ni and As (irarsite, hollingworthite, Rh-bearing cobaltite) and probably exsolved from the base-metal sulfides during cooling.
- (6) Only a minor amount of Pd is remobilized into PGM (michenerite) during deformation and metamorphism.

ACKNOWLEDGEMENTS

We thank Vale-Inco for partially funding the project and with thanks to the technical support from Creighton Mine and the Exploration groups from Vale and Vale-Inco. We also thank D. Savard and R. Cox for their support with whole rock and LA-ICPMS analyses. This work was partially funded by the Canadian Research Chair in Magmatic Metallogeny.

REFERENCES

- BALLHAUS, C. & SYLVESTER, P. 2001. Nobel metal enrichment processes in the Merenkys Reef, Bushveld Complex. *Journal of Petrology*, **41**, 545-561.
- BARNES, S.J., PRICHARD, H.P., COX, R.A., FISHER, P.C., & GODEL, B. 2008. The location of the chalcophile and siderophile elements in platinum-group elements ore deposits (a textural, microbeam and whole rock geochemical study): Implication for the formation of ore deposits. *Chemical Geology*, **248**, 295-317.
- CABRI, L.J., SYLVESTER, P., TUBRETT, M., PEREGOEDOVA, A., TUBRETT, M., & LAFLAMME, J.H.G. 2003. Comparison of LAM-ICP-MS and micro-PIXE results for palladium and rhodium in selected samples of Noril'sk and Talnakh sulfides. *The Canadian Mineralogist*, **41**, 321-329.
- FARROW, C.E.G. & LIGHTFOOT, P.C. 2002. Sudbury PGE revisited: Toward an integrated model. In: CABRI, L.J. (ed.), *The geology, geochemistry, mineralogy and mineral beneficiation of platinum group element 2002*. Canadian Institute of Mining, Metallurgy and Petroleum, Special Volume, **54**, 273-297.
- GODEL, B., BARNES, S.J., & MAIER, W.D. 2008. Platinum-group elements in sulphide minerals, platinum-group minerals, and whole-rocks of the Merenkys Reef (Bushveld Complex, South Africa). *Journal of Petrology*, **48**, 1569-1604.
- HOLWELL, D.A. & McDONALD, I. 2007. Distribution of platinum-group elements in the Platreef at Overysel, northern Bushveld Complex: a combined PGM and LA-ICP-MS study. *Contributions to Mineralogy and Petrology*, **154**, 171-190.
- HUMINICKI, M.A.E., SYLVESTER, P.J., CABRI, L.J., LESHER, C.M., & TUBRETT, M. 2005. Quantitative mass balance of platinum-group elements in the Kelly Lake Ni-Cu-PGE deposit, Copper Cliff Offset, Sudbury. *Economic Geology*, **100**, 1631-1646.

Late Mesoproterozoic S-type Sargipali granite and tungsten-mineralization: Singhbhum-Orissa craton, India

Sangita Chowdhury¹, David R. Lentz², & Saumitra Misra³

¹Department of Geology, University of Calcutta, Kolkata-700019, INDIA
(e-mail: sanggeol@live.in)

²Department of Geology, University of New Brunswick, Fredericton, NB, E3B 5A3 CANADA
³Indian Institute of Geomagnetism, New Panvel, Navi Mumbai- 410 218, INDIA

ABSTRACT: The Sargipali granitoid pluton, intrusive into the western part of Singhbhum Group of metasediments lying at the northern, eastern, and western margins of the Singhbhum-Orissa craton, eastern India, is spatially and temporally associated with co-genetic tungsten-bearing calc-silicate skarn. Geochemical features imply that the granites are highly evolved. Petrographic and geochemical considerations point towards a monazite and Zr fractionated low temperature S-type granite that was emplaced at ~0.96 Ga (CHIME monazite age) post-dating the sedimentation of Gangpur Group of rocks at ~1.7 Ga and syngenetic Pb-Cu sulfide mineralization in this area at ~1.69 Ga. The emplacement of the pluton was age equivalent to the final phase of deformation and metamorphism of the area. The REE data suggest that the foliated variety of the pluton might have generated by partial melting process whereas the composition of the main massive variety was mostly dominated by variable source rock composition.

KEYWORDS: *Singhbhum-Orissa craton, Singhbhum Group supracrustals, Peraluminous S-type granite, Geochemistry, Monazite age*

INTRODUCTION

The Singhbhum-Orissa craton of the eastern Indian shield, a granite-greenstone terrain of Archaean age (~3.6-3.1 Ga) having an areal extent of ~ 40,000 sq. km., is unconformably overlain by a supracrustal sequence of Mesoarchaeon age (~3.12-3.09 Ga), known as the Singhbhum Group along the northern, western and eastern margins of the craton (Saha 1994; Misra 2006). This supracrustal cover, also described as Singhbhum Mobile Belt, is intruded by a number of small younger granitoid plutons of various ages. Among them a less known granitoid body that is intrusive into the mobile belt metasediments to the west in and around Sargipali, Sundergarh District, Orissa, is economically important because it is spatially and temporally associated with the tungsten-bearing calc-silicate skarn. The granitoid pluton also has intruded a Pb-Cu ore body (Fig.1), but shows no genetic relationship with the sulfide ores.

A considerable amount of work has

been undertaken in this region mostly aimed at the economic aspects of the Pb-Cu deposits (Sarkar, 1974; Chowdhury 2002). Although most primary tungsten deposits in the world are spatially and genetically related to granitoids, the granitoids and tungsten-bearing calc-silicate skarns of Sargipali area have received little recognition so far. It is, therefore, clear that the necessity exists to investigate the granitoid in more detail to gain better evaluation on the possible chemical properties of the magma that perhaps gave rise to the associated W-bearing skarns. Also no attempt had been made to establish age data of the granites. Therefore, the petrology, mineralogy, geochemistry, and a new monazite U-Th-total Pb age data of the Sargipali granitoid body were obtained, in an attempt to evaluate the genesis and tectonic setting of evolution of this pluton, and its possible relationship to W.

GEOLOGICAL SETTING

The Sargipali granitoid pluton occurs

within a metasedimentary assemblage of pelitic, psammitic, and calc-silicate units of the Gangpur Group.

The regional structure of the Gangpur Group is represented by an easterly plunging reclined fold (F_1), which co-axially refolded into an antiform (F_2). A later generation gentle F_3 fold with N-S trending vertical axial planes, however, has overprinted these F_1 and F_2 folds. The present study area lies on the southern limb of the regional fold. The granitoid pluton intruded along the fold axis of the late generation cross fold (F_3) (Fig. 1).

The granitoid pluton is mostly massive, with some isolated off-shoots of the pluton in the east show foliation in the NW-SE direction with moderate dips towards SW (Fig.1), which is parallel to the schistosity of the country-rock metapelites. Pegmatites and pegmatitic quartz veins occur in metasediments, spatially associated with the granites.

PETROLOGY & GEOCHEMISTRY

The underformed massive variety of granitoid pluton is leucocratic, white, very coarse to medium grained showing hypidiomorphic granular texture. A pink coloured, coarse porphyritic granitoid variety is also recognized locally. A white-coloured granitoid material locally occurs in fractures of the porphyritic variety of the pluton indicating a late phase of granitic activity. Both the massive and foliated varieties of the granitoid pluton consist predominantly of quartz, K-feldspar, and plagioclase (An_8 to An_{10}) with muscovite, tourmaline, biotite, chlorite, garnet, monazite, zircon, apatite, titanite fluorite, scheelite, galena, chalcopryrite, and ilmenite as common accessories. Secondary minerals formed via alteration are epidote and sericite.

In the CIPW normative Ab-An-Or diagram, the Sargipali granitoid is a 'granite' (Fig. 2a). This granite is characterized by high normative corundum (avg. 4%), therefore is strongly peraluminous (Fig. 2b).

The Harker variation plots do not show any significant correlations of oxides such as Al_2O_3 , Na_2O , CaO , MgO , P_2O_5 , and FeO^T with SiO_2 , only K_2O shows

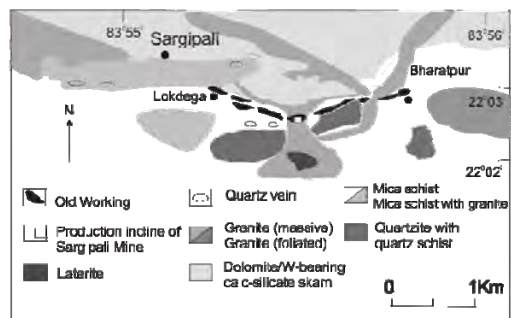


Fig. 1. Geological map of the area around Sargipali (modified after Ghosh *et al.* 1999)

decreasing trend with increasing SiO_2 . The SiO_2 content (>74 wt%), molar A/CNK ratios (>1.2), K_2O/Na_2O ratios (~ 2), and presence of accessory minerals like muscovite, biotite, garnet and ilmenite in the pluton suggest that the Sargipali granite is S-type in nature. In the Rb – (Y+Nb) (Fig. 3a), Nb–Y, Ta–Yb, and Rb–(Yb+Ta) trace-element discrimination diagrams, all varieties of Sargipali granites plot mostly in the syn-collision granite (syn-COLG) field after Pearce (1996), which is consistent with S-type granite characteristics.

The granite as a whole are rich in incompatible elements (Rb, Y, Nb, Ga), but poor in compatible elements (Sr, Cr, V). The rocks are remarkably rich in Rb (>300 ppm) and depleted in Sr (~ 35 ppm). This readily defines them as being highly evolved. However, increasing of SiO_2 , and decreasing of TiO_2 , FeO^T , K_2O , Th, Zr and LREE from foliated to massive variety indicate that foliated granite may represent a higher degree of partial melting, and considerably less evolved than massive granite (cf. Bogaerts *et al.* 2003). Low Zr (4-90 ppm) is indicative of low temperature of this highly silicic felsic magma (Lentz & Suzuki 2000). The positive correlation of Zr with TiO_2 probably imply that Zr fractionated from the initial melt with time.

In C1 chondrite-normalised REE plots (Fig. 3b), the foliated granites ($\sum REE \sim 200$ ppm) show strongly fractionated LREE and flat HREE with $(Ce/Yb)_N \sim 50$. The massive granites are relatively very low in REE (9 to 34 ppm), showing relatively flat to highly variable LREE and

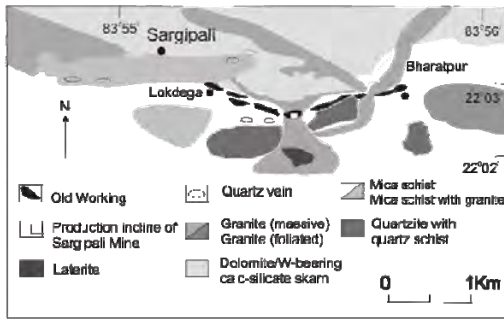


Fig. 1. Geological map of the area around Sargipali (modified after Ghosh *et al.* 1999)

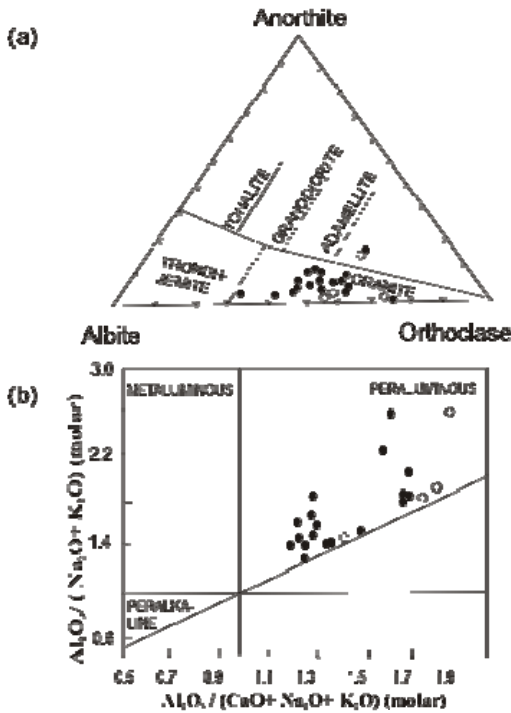


Fig. 2. Plot of Sargipali granitoid in (a) CIPW normative Ab-Or-An diagram (after Barker 1979), and (b) Shand's classification of granites, based on Al-saturation index. Symbols: filled circles - massive granite, open circles - foliated granite.

relative enrichment of HREE. The $(Ce/Yb)_N$ ratios of this granite is ~ 5 . The fractionated LREE and flat HREE pattern of the foliated granites perhaps indicate low T partial melting dominating chemistry of this granite or extensive low T fractionation. The REE pattern of the massive granite is heterogeneous and perhaps suggestive of source-dominated chemistry of these granites. The low REE may be due to the fractionation of LREE-

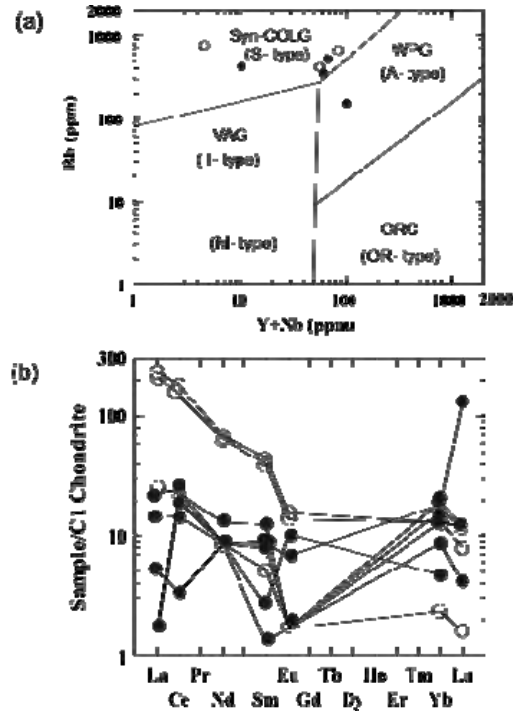


Fig. 3. Sargipali granitoid showing (a) updated Rb vs Y+Nb discrimination plots (after Pearce 1996) and (b) CN REE systematics. Symbols are same as in Figure 2

enriched accessory minerals like monazite and HREE enriched zircon and apatite that take up all the REEs.

Broad correlation between igneous composition, skarn type, spatial association, and respective metal contents indicates that the granite is associated with W skarns. Both the varieties of granite are W-bearing. The concentration of W (avg. 500 ppm) in granite is very high compare to the associated skarns (W \sim 300 ppm). In terms of major- and trace-element chemistry, the Sargipali granite is comparable to averages of world S-type granitoids associated with W skarns. Like many other W-bearing granites, the Rb/Sr ratio of Sargipali granite is high (> 4), while unlike other W-Sn deposit related granites, W is concentrated in both early and late intrusive stages.

GEOCHRONOLOGY

The monazite U-Th-Pb CHIME ages of massive and foliated granites (one sample each) were calculated from microprobe data (after Montel *et al.* 1996). The

foliated and massive granite yield Th-U total Pb weighted mean age of 974 ± 6 Ma and 959 ± 6 Ma, respectively. These age data indicate that the Sargipali granite has post-dated the sedimentation of the host Gangpur Group of rocks at ~ 1.70 Ga (Sarkar 1980) and syngenetic Pb-Cu sulfide mineralization at ~ 1.69 Ga (Ghosh *et al.* 1999). This pluton is time correlative with the last phase of deformation of the present area, and final phase of shearing along the Singhbhum Shear zone that is situated mostly along the boundary of the Singhbhum-Orissa craton to the south and the Singhbhum Group of metasediments in the north, and related to metamorphism at ~ 1.0 Ga.

CONCLUSIONS

- (1) The granite pluton, which intruded the Singhbhum Group of metasediments to the west near the Sargipali area, is of two broad types, i.e., an undeformed massive granite and pegmatite system in the west and foliated granite along the east margin.
- (2) Both of these granite phases are highly evolved, strongly peraluminous muscovite-, garnet-, monazite-, zircon-, and ilmenite- bearing low T S-type syncollisional granites. The massive variety is more evolved than the foliated one.
- (3) Both the massive and foliated granites are spatially and temporally associated with the tungsten-bearing calc-silicate skarn, which is likely formed by this evolved pluton.
- (4) Monazite dating suggests that the Sargipali granite pluton is ~ 0.96 - 0.97 Ga, post dating the sedimentation of the host Gangpur Group of rocks (~ 1.70 Ga) and syngenetic Pb-Cu sulfide mineralization (~ 1.69 Ga). It is time equivalent to the final phase of deformation in the Sargipali area as well as the movement along the Singhbhum Shear Zone, and related metamorphism at ~ 1.0 Ga.

ACKNOWLEDGEMENTS

Financial support for this research was provided by NSERC Discovery grant (DL).

Douglas Hall supervised monazite age analyses at UNB, Canada.

REFERENCES

- BARKER, F. 1979. Trondhjemite: definition, environment and hypothesis of origin, in Trondhjemites, Dacites and related rocks. F. BARKER (ed.). Elsevier Scientific Publishing Co., 1-12.
- BOGAERTS, M., SCAILLET, B., LIEGEOIS, J.P., & VANDER A.J. 2003. Petrology and geochemistry of the Lyngdal granodiorite (Southern Norway) and role of fractional crystallisation in the genesis of Proterozoic ferro-potassic A-type granites. *Precambrian Research*, **124**, 149-184.
- CHOWDHURY, S. 2002. The Sargipali sulfide deposit of Orissa, India: its atypical lead-high character and genesis. *Journal Nepal Geological Cong. Society*, **27** (Special Issue), 11-24.
- GHOSH, S., THORPE, R.I., & GHOSH, A.K. 1999. Lead and sulphur isotope geochemistry of galena from Sargipali sulphide deposit, Sundergarh, Orissa –Implications for ore genesis. *Indian Journal of Earth Science*, **26**, 1-12.
- LENTZ, D.R. & SUZUKI, K. 2000. A low F pegmatite-related Mo skarn from the southwestern Grenville Province, Ontario, Canada: Phase equilibria and petrogenetic implications. *Economic Geology*, **95**, 1319-1337.
- MISRA, S. 2006. Precambrian chrono-stratigraphic growth of Singhbhum-Orissa craton, eastern Indian shield: An alternative model. *Journal Geological Society of India*, **67**, 356-378.
- MONTEL, J.M., FORET, S., VESCHAMBRE, M., NICOLLET, C. & PROVOST, A. 1996. Electron microprobe dating of monazite. *Chemical Geology*, **131**, 37-53.
- PEARCE, J.A. 1996. Sources and settings of granitic rocks. *Episodes*, **19**, 120-125.
- SAHA, A.K. 1994. Crustal evolution of Singhbhum-North Orissa, eastern India. *Geological Society of India memoir*, **27**, 341p.
- SARKAR, S.C. 1974. Sulfide mineralization at Sargipali, Orissa. *India. Economic Geology*, **69**, 206-217.
- SARKAR, S.N. 1980. Precambrian stratigraphy and geochronology of Peninsular India. A review. *Indian journal of Earth Science*, **7**, 12-26.

Bimodal post-collision volcano-plutonic complex in the southern rim of the eastern flank of the Mongol-Okhotsk orogenic belt

I.M. Derbeko¹, V.A. Ponomarchuk², D.L. Vyunov³, & S.K. Kozyrev³

¹ Institute of Geology and Nature Management, Far East Division, Russian Academy of Sciences, 1, Relochniy, Blagoveshchensk, 675000 RUSSIA (e-mail: derbeko@mail.ru)

² Institute of Geology and Mineralogy, Siberian Division, Russian Academy of Sciences, 3, Akademika Koptyuga, Novosibirsk, 630090 RUSSIA

³ "Amurgeologia" open joint-stock company, 15, Chudinovsky, Blagoveshchensk, 675014 RUSSIA

ABSTRACT: In the southern rim of the eastern flank of the Mongol-Okhotsk orogenic belt a bimodal volcano-plutonic complex of trachybasalt-rhyolite composition was being formed 119-97 Ma ago. The occurrence of the rocks of the complex is bounded by the structures of the Anikinsky "threshold" (120 meridians) in the west of the area and by the Bureya-Jiamusi terrane in the east. The rocks are enriched in Ba, Sr and Pb at low Ta, Nb, Ti concentrations and a high value of Zr/Hf (34-52) ratio. They are characterized by quite a narrow range of isotope compositions of ⁸⁷Sr/⁸⁶Sr (0.7057-0.7065) at T_{Nd}(DM-2st)=975-1047 Ma and this may be indicative of a substantial homogeneity of a melting substratum and a crustal component of the beginning of the Late Riphean. Such characteristics bring those rocks closer to the Late Paleozoic-Early Mesozoic bimodal associations of the Central-Asian rift system. There is an assumption that the formation of the rocks is related to collision processes that resulted in the closure of the eastern flank of the Mongol-Okhotsk basin and there was also an effect of the plume source.

KEYWORDS: *bimodal complex, collision, orogenic belt*

INTRODUCTION

By the present time the models of geodynamic settings for a number of regions of the North-Asian continent combining the action of deep plumes and riftogenesis have been worked out (see. Magma types 2006). A significant part in formation of magmatic complexes accompanying riftogenesis belongs to the sources of different nature and to characteristics of the continental crust contaminated by those complexes. These very data accounted for the formation of a contrasting volcanism which is widely developed in the zone of the Central-Asian fold belt. The paper considers a bimodal volcano-plutonic complex of the end of the Late Cretaceous. It is spatially located within the continuation of the formations with similar composition which compose the Central-Asian fold belt.

GEOLOGICAL SETTING

Along the southern margin of the Mongol-Okhotsk orogenic belt (the north-western

flank of the Amur continent) the bimodal occurrences form separate volcanic fields from 2 to 180 km² (Fig. 1) within the area extended for 600 km with the width from 50 to 300 km. In the south their extent is actually bounded by the river Amur valley (Zhang Hong *et al.* 2000) and in the east by the structures of the Bureya-Jiamusi terrane. In the west they disappear at the point of the belt wedging (120 meridians) and subsequently reappear in the rim of the western branch of the Mongol-Okhotsk belt with the age of the Early MZ and older (Magma types 2006). The origin of the bimodal rock complexes in the rim of the western branch of the Mongol-Okhotsk belt is attributed to collision between the North-Asian and Sino-Korean continents (Magma types 2006).

Collision processes in this region involving large-scale intraplate processes have been completed by the beginning of the Early Cretaceous (190 Ma) by the closure of the Paleoasian ocean and a significant western part the Mongol-Okhotsk basin (Magma types 2006). In

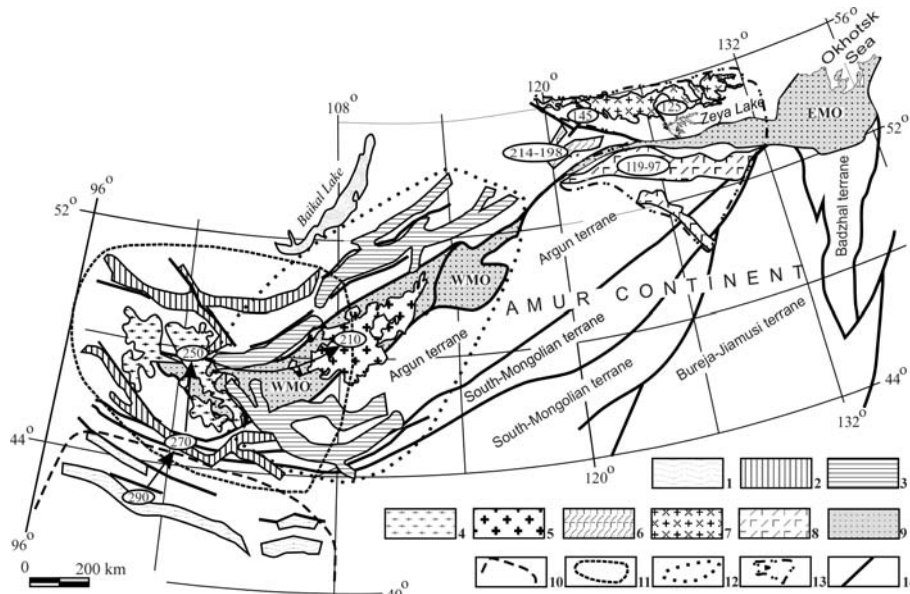


Fig.1. Structural-tectonic sketch map of volcano-plutonic complex and plutonic complex of the Late Paleozoic-Mesozoic within the rim of the Mongol-Okhotsk orogenic belt. Central Asian rift system to the west from 120° meridian, modified from Yarmolyuk et al, 2002: bimodal and alkaline-granitic rocks of the Late Carboniferous – Early Permian -1, Permian -2; bimodal basalt-comendite and alkaline granites -3; granitoids: Permian -4, Early Mesozoic -5. Collisional alkaline – moderately alkaline volcano-plutonic complexes -6. Subalkaline – normal granitoids Late Mesozoic -7. Field spread of bimodal volcano-plutonic complex of the end of the Early Cretaceous -8. Mongol-Okhotsk orogenic belt (Parfenov *et al.* 1999) -MO. Boundaries of the Mongolian Plume's projection in time: Late Carboniferous–Early Permian -10, Permian -11, Early Mesozoic -12 (from Magma types 2006), towards the end of the Early Cretaceous by authors' data -13. Tectonic contacts -14.

that time in the east within the Mongol-Okhotsk basin terrigenous rocks continued to accumulate. About 130 Ma ago continental volcano-plutonic complexes began to form: at the beginning calc-alkali andesite complexes and, then, bimodal trachybasalt – rhyolite ones in the belt's rim. A sequence of the formation of the bimodal complex's cover facies is as follows (from the bottom to the top): trachyandesite basalts, trachyandesites, tuffogenic-sedimentary rocks; rhyolites, rhyodacites, trachyrhyolites, perlites, tuffs and ignimbrites, interlayers of trachyandesites and tuffogenic sedimentary rocks; trachyandesites, andesites. The total thickness is up to 500 m. The complex comprises the bodies of the subvolcanic and vent fennel facies, and comagmatic plutonic rocks: subalkaline granites – leucogranites, granodiorites, quartz diorites, quartz monzonites.

Age

According to geochronological data obtained by Rb-Sr, U-Pb, ⁴⁰Ar/³⁹Ar methods the following sequence is revealed: trachyandesite basalts, trachyandesites -119, 115, 100, 97 Ma; rhyolites -117, 115 Ma; andesites -105.9 Ma. The age of subalkaline granites of the complex is 118 Ma (⁴⁰Ar/³⁹Ar, Sorokin & Ponomarchuk 2002). It can be said that magmatic activity (119-97 Ma) extinguished in the very beginning of the Late Cretaceous. The bimodal composition of the complex's rocks is accounted for two ranges of SiO₂ concentration: I – 52-67 wt.% - trachyandesite basalts, trachyandesites, andesites. Their high alkalinity is related to the presence of potassic feldspar, red-brown biotite in matrix and sanidine in phenocrysts. These are moderately low magnesia, moderately low titaniferous rocks with Al₂O₃=16.0-17.3 wt.% of the high potassic calc-alkali series. II - 72-78

wt.% - rhyolites, trachyrhyolites, perlites with normal, rarely, moderate alkalinity, $Al_2O_3=11.1-13.9$ wt.%, low magnesia, low titaniferous belong to the high potassic calc-alkaline series. All the varieties are enriched in LREE. In $(La/Yb)_n$ ratio the values 10-20 predominante, $(La/Sm)_n=2.9-6.0$, and the fractionation level of heavy lanthanoids is lower: $(Gd/Yb)_n=0.6-3.4$. Eu minimum in basic-medium rocks is not distinct ($Eu/Eu^*=0.70-0.86$) but in acid rocks it is deeper ($Eu/Eu^*=0.33-0.70$). By the bimodal character, A-type granitoids development and a number of geochemical features (sharp Nb, Ta, Ti minimums, and the maximums in Ba, Rb, Th, K concentrations) and also by the ratio of $Zr/Hf=34-52$ in basic and medium varieties the rocks of the complex are close to some occurrences in the western flank of the Mongol-Okhotsk orogenic belt which form a part of the North-Mongolian – West-Transbaikalian rift zone (Vorontsov *et al.* 2007). The rocks of the complex under consideration are characterized by quite a narrow range of isotope compositions at rather slight variations of $^{87}Rb/^{86}Sr$ (0.7057-0.7065) that may be indicative of an affinity of the source for petrochemically different occurrences. A relatively wide is the range of values of $\gamma_{Nd}(T)=(-0.6)-(-3.3)$ at $T_{Nd}(DM-2\sigma)=975-1047$. These data indicate that there is a substantial affinity between substratum of melting and crustal component of the beginning of the Late Riphean. It is mentioned above that there is similarity between some geochemical features of the rocks of the complex under study and that of the Late Paleozoic-Mezozoic Central-Asian rift system. On $^{87}Rb/^{86}Sr - \gamma_{Nd}(T)$ diagram the field of figurative points of this complex fits in the composition fields of the Early- Late Mesozoic intraplate magmatic rocks of the Central Asia (Fig. 2).

But still there are some differences between those rocks: the presence of rocks with normal alkalinity (they predominate in a group of acid rock varieties) in the described complex, low

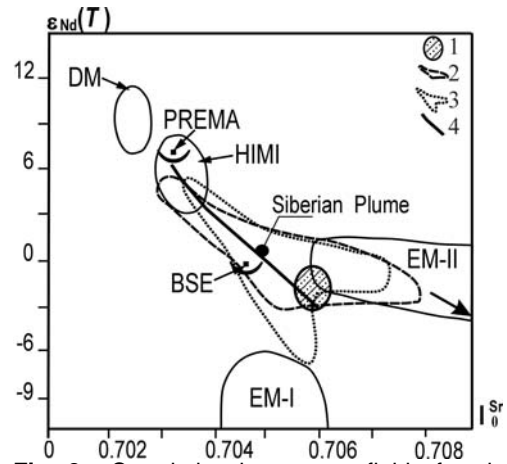


Fig. 2. Correlation between a field of rocks' compositions of the bimodal complex and the fields of intraplate magmatic rocks in the Central Asia and typical magma sources by primary isotope compositions of Sr and Nd. Fields of rocks: explore bimodal complex -1, Early Mesozoic -2 and Late Mesozoic -3 of Central Asia. Correlation trend of basalt composition of the bimodal series of the Early Mesozoic Mongol – Transbaikalian region (Yarmolyuk *et al.* 2002) -4. At drawing of the diagram we used the data from the work (Magma types, 2006). PREMA and BSE values (Zindler & Hart 1986), Siberian plume (Sharma *et al.* 1992).

concentrations of highly-charged elements such as Nb, Ta, Zr, Hf. Such features bring them closer to the products of subduction origin. The studied structures are confined to the zones of the rocks with the age of (130-120 Ma) that are compared with the products formed under subduction conditions (Gordienko *et al.* 2000). Taking into account a proximity of their ages we presume that the rocks of the bimodal complex intruded into continental crust warmed up by subduction processes and this resulted in partial mixing and inheritance of the subduction rocks' features by the occurrences of the bimodal complex.

Geodynamic model

In the west of the Mongol-Okhotsk belt the rocks of a bimodal series constitute a part of the Early Mesozoic North-Mongolian – West-Transbaikalian rift zone. For this zone a quite precise geodynamic model has been worked out (Magma types

2006). It lies in the parallel existing conditions of collisional compression and in a plume impact on a site being under the conditions of collisional compression. On the discrimination rocks of the complex in question is plotted at a direct proximity from the points determining a position of those characteristics for the Siberian plume (Sharma 1992). It is also combined with the fields of the Late Mesozoic intraplate magmatic occurrences, of the Central Asia and overlaps the lower part of a correlation trend of basalts of the bimodal series of the Late Mesozoic Mongol–Transbaikalian Region.

On the diagrams showing tectonic settings (Pearce 1996) the figurative points of acid rocks are concentrated within the fields of post-collision (syn-collision) or at the boundary of collision – intraplate conditions. For the rocks of acid - medium composition the field of the Island arcs' basalts with a shift and their partial location in the field of the continental rift basalts is determined. To establish a probability of a plume impact on the Late Mesozoic magmatic process in the region the following calculation was used (Fitton *et al.* 1997): $\epsilon_{\text{Nb}} = 1.74 + \log(\text{Nb}/\text{Y}) - \log(\text{Zr}/\text{Y})$. Positive ϵ_{Nb} values indicating an impact of the plume source are characteristic of basic-medium rocks. For the acid rock varieties ϵ_{Nb} value is (-1.4) - (1.5). The diagnostic features are also: a moderate enrichment of the rocks in LREE; ratios of $(\text{La}/\text{Sm})_n > 1.8$ and $(\text{Ce}/\text{Yb})_n > 7$ (Schilling *et al.*, 1983; LeRoe *et al.*, 1983), being 2.9-5.7 and 11.6-25.5 for basic – medium rocks, respectively.

CONCLUSIONS

119-97 Ma ago, along the south margin of the eastern flank of the Mongol-Okhotsk orogenic belt a bimodal volcano-plutonic complex of subalkaline – normal petrochemical series was being formed. At the present stage of its study one may presume that the petrochemical and geochemical characteristics of rocks are the evidence that its formation was going on under the collisional conditions at the impact of a plume source. Its impact manifested itself stronger at forming of

basic-medium rocks while at the formation of acid rocks a leading part belonged to the crustal melt sources.

REFERENCES

- FITTON, J.G. *et al.* 1997. Thermal and chemical structure of the Iceland plume. *Earth and Planetary Science Letters*, **153**, 197-208.
- GORDIENKO, I.V. *et al.* 2000. Upper Amur volcano-plutonic belt East Asia. *Geology & Geophysics*, **41**, 1655-1669.
- LE ROEX, A. P. *et al.* 1982. Ferrobasalts from the Spiess Ridge segment of the Southwest Indian Ridge. *Earth and Planetary Science Letters*, **60**, 437-451.
- Magma types and their sources in the Earth's history. 2006. Moscow: IGEM RAS.
- PARFENOV, L.M., POPEKO, L.I., & TOMURTOGOO, O. 1999. Problems of tectonics of Mongol-Okhotsk orogenic belt. *Geology of the Pacific Ocean*, **18**, 24-43.
- PEARCE, J. 1996. Sources and settings of granitic rocks. *Episodes*, **24**, 956-983.
- SCHILLING, J.-K. *et al.* 1983. Petrologic variations along the Mid-Atlantic Ridge from 29°N to 73°N. *American Journal of Science*, **283**, 510-586.
- SHARMA, M., BASU, A.R., & NESTERENKO, G.V. 1992. Temporal, Sr-, Nd- and Pb-isotopic variations in the Siberian flood basalts: implications for the plume-source characteristics. *Earth and Planetary Science Letters*, **113**, 365-381.
- SOROKIN, A.A. & PONOMARCHUK, V.A. 2002. Umlekan-Ogodzha Early Cretaceous magmatic belt: duration of magmatism. *Geochimica et Cosmochimica Acta*, **66**, 15^a, A728.
- VORONTSOV, A.A. *et al.* 2007. Sources of magmatism and geodynamics of formation of the Early Mesozoic North-Mongolian – West-Transbaikalian rift zone. *Petrology*, **15**, 37-60.
- YARMOLYUK, V.V. *et al.* 2002. Tectono-magmatic zoning, sources of magmatic rocks and geodynamics of the Early Mesozoic Mongol-Transbaikalian region. *Geotectonics*, **4**, 42-63.
- ZHANG HONG *et al.* 2000. The dynamic background of Mesozoic volcanic activity in northern part of Daxing'anling Mts. (China). *Geology of the Pacific ocean*, **19**, 109-117.
- ZINDLER, A. & HARRIS, S. 1986. Chemical geodynamics. *Annual Reviews of Earth and Planetary Science*, **14**, 493-571.

Petrographic characterization of propylitic alteration associated with porphyry Cu–Mo deposits in the Collahuasi District, Northern Chile: implications for mineral exploration

Merline Djouka-Fonkwé¹, Kurt Kyser¹, H. Alan Clark¹, J. Christopher Oates², & Christian Ihlenfeld²

¹*Department of Geological Sciences and Geological Engineering, Queen's University, Kingston, ON, K7L 3N6 CANADA (email: merlinefonkwe@geol.queensu.ca)*

²*Geochemistry Division, Anglo American plc, 20 Carlton House Terrace, London, SW1Y 5AN UNITED KINGDOM*

ABSTRACT: The Collahuasi district is a major porphyry Cu–Mo sub-province in northern Chile. Late Eocene-early Oligocene mineralization in the district involved hydrothermal alteration of the Permo-Triassic Collahuasi Group granodiorites, diorites, andesites, dacites and voluminous rhyolites, which had previously experienced regional sub-greenschist metamorphism. Hydrothermal alteration mapping represents an indispensable and effective technique in prospecting for hydrothermal deposits, but in low-grade metamorphic terrains, recognition of key minerals, particularly those associated with subtle propylitic alteration, is hampered by their resemblance to metamorphic mineral assemblages (the “green rock” dilemma). Distinguishing propylitic alteration from “background” metamorphism is also a challenge using geochemistry because petrographic criteria for recognizing subtle propylitic alteration, particularly in felsic rocks, are poorly defined. However, specific features of the petrography of outcrop mafic and felsic samples from the Collahuasi district do distinguish rocks with varying degrees of propylitic alteration, the latter representing a key boundary of the mineralizing system in porphyry Cu–Mo deposits, from background rocks that resemble propylitically altered rocks in outcrop. The mineralogical criteria, which differ for each rock type, are useful in refining the geochemical changes associated with propylitic alteration, aid in defining the location and extent of porphyry Cu–Mo systems in similar terrains.

KEYWORDS: *Collahuasi District, porphyry Cu–Mo deposit, petrography, propylitic alteration, sub-greenschist metamorphism*

INTRODUCTION

Porphyry Cu–Mo deposits and other hydrothermal deposits are commonly associated with characteristic hydrothermal alteration patterns (Lowell & Guilbert 1970) that may be far more extensive than the ore zone, thereby providing a much larger target for exploration. Consequently, identification and mapping of hydrothermal alteration have become important techniques in exploring for porphyry Cu–Mo deposits at both regional and local scales.

Mineralization-related alteration processes induce changes in mineralogical compositions as well as textural and chemical changes of the host-rocks in the environs of ore deposits, including those at depth. Distal to the deposits, the impact on the host-rocks is

subtle, and identification of the chemical changes and alteration minerals is difficult, due to their typically fine-grained nature. Moreover, in many terrains, alteration is further obscured because similar mineral assemblages may form as products of regional low-grade metamorphic processes. Methodologies that identify hydrothermally altered-rocks associated with mineralization include multispectral remote sensing (Sabins 1999) and lithogeochemistry (Urqueta *et al.* 2005). However, these methods rarely differentiate subtle hydrothermal effects, such as propylitic alteration that marks the outer boundary of the system, from regional low-grade metamorphic mineral assemblages.

This study uses microscopic observations to discriminate propylitic

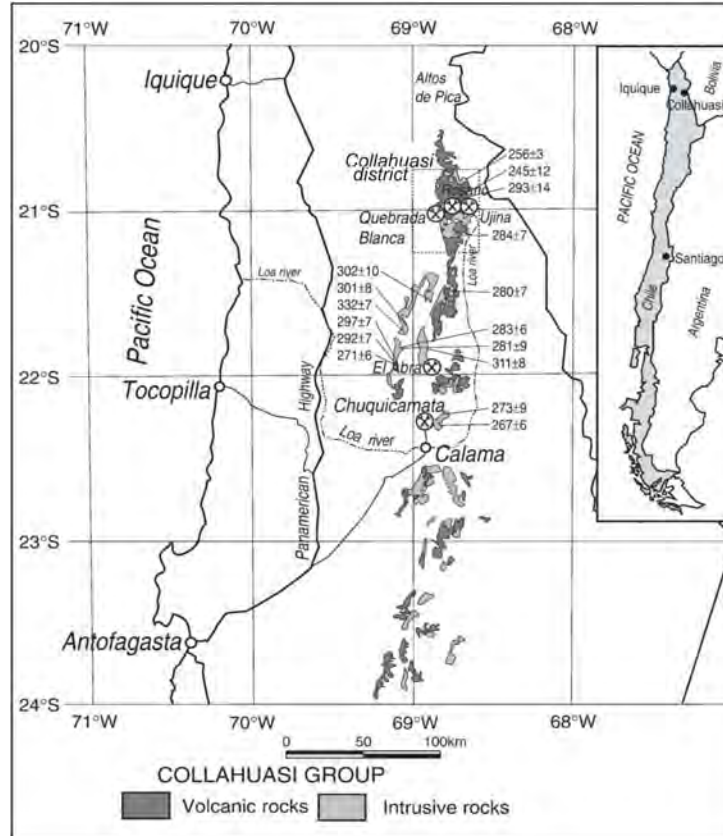


Fig. 1. Location map of the Collahuasi district (outlined) and geographic distribution of the outcrops of main igneous units of the Collahuasi Group in northern Chile. Ages for granitoids from the region are also shown (from Munizaga *et al.* 2008 and references therein).

alteration minerals from assemblages characteristic of regional very low-grade metamorphism in the porphyry Cu–Mo deposit-rich Collahuasi district of northern Chile. Propylitic alteration is normally directly associated with potassic alteration that accompanies Cu mineralization. Proper identification of propylitically-altered rocks relative to “background” regional rocks that appear to be the same in the field is therefore of value delineating of potentially fertile areas. The aim of this study is to evaluate the usefulness of petrography as an effective tool to refine exploration strategies for porphyry Cu–Mo deposits in the Collahuasi district.

GEOLOGY OF THE COLLAHUASI DISTRICT

The Collahuasi district occupies an area of 1250 km² in the Andes of northern Chile, between 20°45’S–21°07’S, 68°75’W–

68°20’W (Fig. 1). It belongs to the most important porphyry Cu–Mo belt in Chile (Maksaev *et al.* 2007). The porphyry Cu–Mo deposits are associated mainly with granodiorite to quartz monzonite plutons of late Eocene-early Oligocene age, which intruded igneous, volcanic and sedimentary rocks of the Permo-Triassic Collahuasi Group (Masterman 2003; Munizaga *et al.* 2008). The north-trending Domeyko and Loa faults bound the rocks of the Collahuasi Group. To the west, Jurassic sedimentary rocks of the Quehuita Formation and Cretaceous volcanic and sedimentary rocks of the Cerro Empexa Formation unconformably overlie the rocks of the Collahuasi Group. Voluminous Neogene ignimbrites and lavas occur in the eastern part of the district.

Prior to the hydrothermal alteration associated with mineralization in the

Collahuasi district, regional low-grade metamorphism affected most parts of northern Chile. To the west of the Collahuasi district, in the Coastal Cordillera, regional metamorphism is interpreted to be prehnite–pumpellyite to lower greenschist facies and is characterized by the epidote–chlorite–actinolite–titanite–K-feldspar–quartz–calcite–prehnite–pumpellyite association (Fuentes *et al.* 2005; Oliveros *et al.* 2006)

PETROGRAPHIC OBSERVATIONS

Petrographic observations were made on polished thin sections, for 313 outcrop samples. Average sample spacing was one sample per 1 km² within a radius of 15 km or less from the known porphyry Cu–Mo deposits, and one sample per 2 km² outside this area. Five rock types are distinguished in the district: andesites, diorites, granodiorites, dacites, rhyolites and sandstones. Rhyolites and dacites dominate in the zone of known porphyry Cu–Mo deposits. Sandstones are much less common and were not studied.

Low-Grade Regional Metamorphism

The low-grade regional metamorphism is interpreted to be sub-greenschist facies, according to the metamorphic facies definition of Turner (1981). This metamorphism is non-destructive, with preservation of primary textures. Characteristic metamorphic minerals in diorites, granodiorites and andesites are chlorite, epidote and sericite. Chlorite has a dark-green colour and replaces hornblende and biotite along grain margins. Epidote, colourless to pale-yellow, alters hornblende. Plagioclase is moderately sericitized. Calcite is observed in rare cases, mainly as veinlets. In rhyolites and dacites, the effects of greenschist metamorphism are much more subtle, with limited modification of original minerals. Sericite selectively replaces feldspars and is found as disseminations in the groundmass.

Propylitic Alteration

In diorite, granodiorite and andesites, propylitic alteration is characterized by

abundant epidote, chlorite, carbonates and albite. This propylitic assemblage is similar to the original definition of propylitic alteration, which was described in intermediate to mafic rocks (Coats 1940; Creasey 1959; Rose & Burt 1979) and propylitic alteration minerals in some key porphyry Cu deposits (e.g., Creasey 1966; Lowell & Guilbert 1970; Norman *et al.* 1991). In contrast to greenschist metamorphism in the Collahuasi district, propylitic alteration has a pervasive character wherein alteration minerals are distributed throughout the rocks with partial or total destruction of original textures. Plagioclase, are altered to aggregates of calcite, chlorite, epidote, and minor albite and sericite. Chlorite, epidote and calcite also replace hornblende and biotite, but the chlorite is light- to medium- green and the epidote pinkish- to greenish- yellow.

Propylitically-altered rhyolites and dacites are characterized by widespread aggregates of calcite disseminated in the groundmass and replacing feldspars, leading to partial to complete destruction of the rock textures. Scarce albite is also observed. In ferromagnesian deficient rocks (felsic rocks), calcite and albite are most likely to form as products of propylitic alteration, as chlorite and epidote need an Fe- and Mg-rich environment to develop. Propylitic alteration is attributed to H₂O- and CO₂-rich, low temperature (200-350°C) fluids (Reed 1997), which cannot transport the Fe and Mg necessary for the formation of chlorite and epidote when reacting with felsic rocks. Thus, the mineral assemblages of propylitic alteration are strongly related to the lithology and original mineralogical composition of the rock.

CONCLUSIONS

The diagnostic mineralogy of sub-greenschist metamorphism and propylitic alteration of altered plutonic and volcanic rocks associated with porphyry Cu–Mo deposits in the Collahuasi district is summarized in Table 1. Chlorite and epidote originating from regional meta-

Table 1. Diagnostic mineralogy of greenschist metamorphism and propylitic alteration of associated with porphyry Cu–Mo deposits in Collahuasi district.

		Diagnostic minerals for propylitic alteration	Diagnostic minerals for sub-greenschist metamorphism
Rock type	Granodiorites Diorites Andesites	Chlorite, Epidote, Carbonates, Albite	Chlorite, Epidote, Sericite, Rare carbonate veinlets
	Rhyolites Dacites	Carbonate, Albite	No carbonates Minor sericite
Mode of occurrence of the alteration minerals		Abundant and disseminated in the rock with destruction of original textures	Incipient depending on the mineral, preservation of the primary igneous textures

morphism versus propylitic alteration display different habits and colours that relate to their distinct chemical compositions. For felsic rocks in which mafic minerals are absent or rare, the mineral assemblage calcite and albite is considered as typical for propylitic alteration. The habit of carbonates, widespread and disseminated in the groundmass, is diagnostic of propylitic versus “background” alteration with the former originating from the addition of magmatic CO₂.

REFERENCES

COATS, R. 1940. Propylitization and related types of alteration on the Comstock Lode. *Economic Geology*, **35**, 1-16

CREASEY, S. C. 1959. Some phase relations in hydrothermally altered rocks of porphyry copper deposits. *Economic Geology*, **54**, 351-373.

FUENTES, F., FÉRAUD, G. AGUIRE, L., & MORATA, D. 2005. ⁴⁰Ar/³⁹Ar dating of volcanism and subsequent very low-grade metamorphism in a subsiding basin: example of the Cretaceous lava series from central Chile. *Chemical Geology*, **214**, 15-177.

LOWELL, J.D., & GUILBERT, J.M. 1970. Lateral and vertical alteration–mineralization zoning in porphyry ore deposits. *Economic Geology*, **65**, 373-408.

MAKSAEV, V., TOWNLEY, B., PALACIOS, C., &

CAMUS, F. 2007. Metallic ore deposits. In: MORENO T. & GIBBONS W. (eds.), *The Geology of Chile*. The Geological Society, London, 179-199.

MASTERMAN, G.J. 2003. *Structural and geochemical evolution of the Rosario Cu-Mo porphyry deposit and related Cu-Ag veins, Collahuasi district, northern Chile*. PhD thesis, University of Tasmania, Tasmania, Australia.

MUNIZAGA, F., MAKSAEV, V., FANNING, C.M., GIGLIO, S., YAXLEY, G., & TASSINARI, C.C.G. 2008. Late Paleozoic–Early Triassic magmatism on the western margin of Gondwana: Collahuasi area, Northern Chile. *Gondwana Research*, **13**, 407-427.

NORMAN, D.K., PARRY, W.T., & BOWMAN, J.R. 1991. Petrology and Geochemistry of Propylitic Alteration at Southwest Tintic, Utah. *Economic Geology*, **86**, 13-28.

OLIVEROS, V., FÉRAUD, G. AGUIRE, L., FORNARI, M., & MORATA, D. 2006. The Early Andean Magmatic Province (EAMP): ⁴⁰Ar/³⁹Ar dating on Mesozoic volcanic and plutonic rocks from the Coastal Cordillera, northern Chile. *Journal of Volcanology and Geothermal Research*, **157**, 31-330.

REED, M. H. 1997. Hydrothermal alteration and its relationship to ore fluid composition. In: BARNES, H.L. (ed.), *Geochemistry of hydrothermal ore deposits*, 3rd ed., J. Wiley & Sons, Inc., New York, 173-235.

ROSE, A.W. & BURT, D.M. 1979. Hydrothermal alteration. In: BARNES, H.L. (ed.), *Geochemistry of hydrothermal ore deposits*, 2nd ed., J. Wiley & Sons, Inc., New York, 173-235.

SABINS F.F. 1999. Remote sensing for mineral exploration. *Ore Geology Reviews*, **14**, 157-183.

TURNER, F.J. 1981. *Metamorphic petrology: mineralogical, field, and tectonic aspects*, 2nd ed., Hemisphere Publishing Corporation Washington New York London.

URQUETA, E., KYSER, K., CLARK, A., STANLEY, C., & OATES, C. 2005. Rosario & District Mineralization, Alteration and Geochemistry: Vectors to Ore. *22nd International Geochemical Exploration Symposium* September 19-23, 2005, Perth, Australia.

Petrologic, geochemical characteristics, and age of skarn-related granitoids at the Mactung Tungsten Deposit, Yukon, Canada

Ayalew. L. Gebru¹ & David R. Lentz¹

¹Dept. of Geology, University of New Brunswick, Fredericton, NB, E3B 5A3 CANADA (email: d835v@unb.ca)

ABSTRACT: Three granitic rocks types occur adjacent to the Mactung pyroxene skarn-related tungsten mineralization hosted by metamorphosed calcareous rocks. All the granitic rocks are peraluminous with ASI ranging from 1.05 to 1.6. Trace elements, such as Ba, Rb, Th, Sr, Ce, Zr, Nd, Pb, Rb, and La, strongly differentiate the three groups of intrusions. The biotite granite and the plagiogranite appear to have an arc-like affinity. The leucogranite depicts both S- and crustal A-type affinity. However, due to their low content of Zr, REE, and Na/Ka, and higher Rb, they may be classified as fractionated S-type granites. Ar-Ar dating of micas and U-Pb dating of zircons indicate at least two magmatic episodes at Mactung, at about 92.1 and 97.6 Ma for the younger leucogranite and the older biotite granite, respectively. The oldest and deepest intrusive phase is most intimately associated with the main stage W (Cu-Bi-Au) mineralization.

KEYWORDS: *Yukon, Mactung, Geochemistry, Geochronology, Granitoids,*

INTRODUCTION

Mactung is located in the Yukon Territory, in northwestern Canada, NE of Whitehorse, the capital of Yukon. The area is known for its large tungsten skarn deposit (33 Mt at 0.9% WO₃, using 0.5% cut-off grade). The deposit lies near the border of the Yukon and NWT, and is centred at about 63° 17' N latitude and 130° 10' W longitude.

There is general agreement on the magmatic origin of the deposit, although the role of the adjacent granite pluton in mineralization processes has been disputed. For instance, Atkinson *et al.* (1986) stated the circular Mactung leucogranitic pluton's proximity to the skarn is accidental. Selby *et al.* (2003) determined that the Mactung intrusion is a late granite (92.1± 0.2 Ma), based on dating of zircon by U-Pb methods, compared to a mineralization age of 97.5 ±0.5 Ma (Re-Os isochron age of molybdenite in quartz veins).

GEOLOGICAL SETTING

All rocks of the area belong to the sedimentary sequence of the Selwyn basin of late Proterozoic to Mississippian age (Abbott *et al.* 1986), and are on a

major NW-SE facies boundary. The sedimentary rocks have undergone low-grade regional metamorphism prior to contact metamorphism.

Supracrustal rocks at Mactung may be grouped into three major types: Upper, Middle, and Lower Metasedimentary rocks (Fig. 1). The Upper Metasedimentary rocks consist of dark limestone, chert, black shale, and conglomerate and are correlated to the Devonian-Mississippian Earn Group. The Middle Metasedimentary rocks consist of calcareous black shale, graptolitic black shale, and pelite belonging to the Due Lake Fm; dolostone (now talc-tremolite rock) and calcareous-pelites belonging to the Rabbitkettle Fm; pelites belonging to the Hess River Fm, and carbonate-rich layers belonging to the Sekwi Fm. The Lower Metasedimentary rocks belong to the Vampire Fm and are comprised of biotite schist and biotite-chlorite-muscovite schist. Tungsten ore, skarn, and calc-silicate alteration are associated with the lower carbonate layer overlying the Vampire Fm., and in an upper calcareous pelite belonging to the Rabbitkettle Fm, separated from each other by a barren 100m thick strongly hornfelsed pelite belonging to the Hess

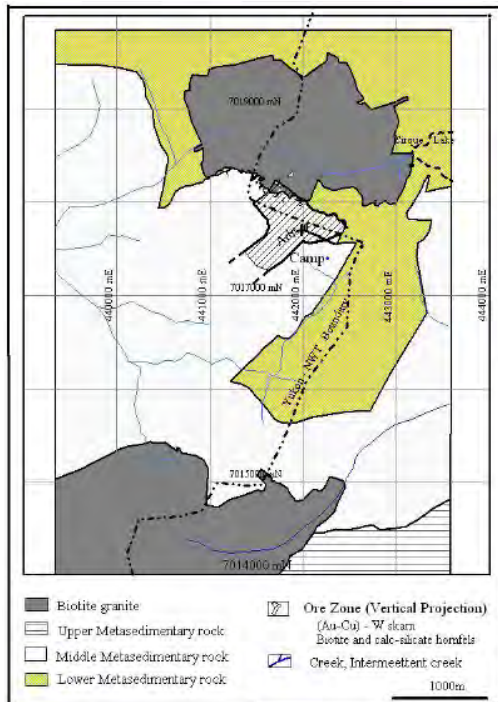


Fig. 1. Local Mactung Geology (Yukon-NWT). further south, a number of prominent aplitic dykes occur. Porphyritic granites similar in colour to that of the biotite granite, and leucogranite were intersected in drill holes. In places, these granites become richer in calcic plagioclase with lower amounts of biotite giving the rocks a lighter colour.

River Fm.

Two biotite granite stocks occur south and north of the Mactung tungsten deposit. The northern granite is porphyritic, composed of quartz, feldspar, biotite, muscovite, and tourmaline. Accessory minerals are apatite, epidote, rutile, titanite, and zircon. It is cut by a late generation of quartz veins that are typically molybdenite bearing. Quartz veinlets of 0.2-1.2cm, similar to those found in the ore zone biotite hornfels, were found in partially assimilated biotite hornfels xenoliths, near the southern contact zone of the northern granite. These xenoliths are hornfelsed and the veins in them do not cross the granite-hornfels boundary and hence are considered to be of an early generation. The southern granite is medium grained and equigranular in texture and is

mineralogically similar to the northern stock. Leucocratic granite, composed of feldspars, quartz, muscovite, tourmaline, garnet, apatite, epidote, and rare dark biotite, occurs as a smaller intrusion within the porphyritic biotite granite, dominating the peripheral part. Granitic dykes that are similar in composition to the leucocratic granite crop out to the north. In the southern part of the area, in the valley south of the camp and

GEOCHEMICAL COMPOSITION

All of the samples from the three rock types have SiO₂ greater than 68%; the highest values occurring in leucogranite (72-75%). Using the Middlemost's classification diagram, the plagiogranite plots within the granodiorite field, and the remaining intrusions plot in the granite field. Selected trace-element plots are presented in Figure 2. These plots show a scattered relationship between the leucogranite and the biotite granite and do not define coherent trends, implying they are not cogenetic. The leucogranite shows variability in the trace-element contents, possibly due to local magma interaction with host rocks, and subsequent chemical modification. Increasing muscovite and tourmaline contents close to host rocks may support this suggestion. The composition of biotite granite appears homogeneous suggesting either that there was little interaction with host rocks during emplacement or that the primary magma interacted with the country rocks, but had homogenized well prior to final emplacement and solidification.

All the rocks are peraluminous with ASI in the range of 1.05-1.1 for plagiogranite; 1.1-1.2 for porphyritic biotite granite, and 1.2-1.6 for leucogranite.

The biotite granite and the plagiogranite appear to have an arc-like I-type affinity. The leucogranite depicts both S- and crustal A-type affinity (Fig. 3a, b). However, the leucogranite has low values of Zr, REE, and Na/K, and higher Rb. Such features are characteristic of very fractionated S-type granites. Based on the Whalen *et al.* (1987) discrimination

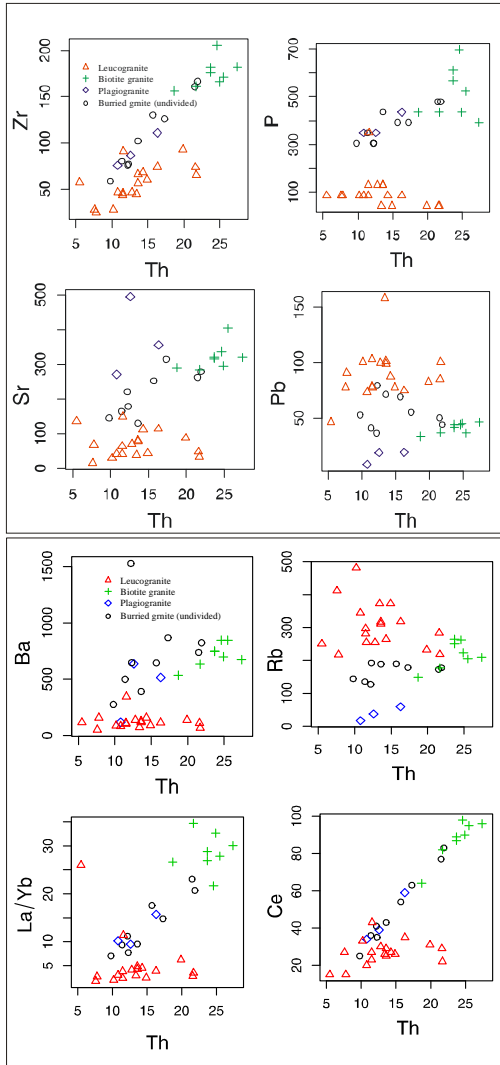


Fig. 2. Thorium variation diagram (ppm) versus selected trace-elements (ppm).

diagram (Fig. 4c, d), plots of the leucogranite entirely fall within the “I+S” field, strengthening the S-type classification of the leucogranite. The petrogenetic difference between the biotite granite and the leucogranite is also reflected in their REE composition. The average La, Ce, Nd, Sm, Eu, Tb, Yb, Lu, and Σ REE content of the leucogranite is 12.8, 26.8, 5.2, 3.2, 0.6, 0.7, 3.6, 0.6, 53.4, and that of the biotite granite is 49.5, 87.6, 25.3, 5.0, 1.3, 0.5, 1.8, 0.3, 171.1, respectively. The REE values in 0.6, 0.5, 2.0, 0.3, and 86.2 in the order plagiogranites are 23.8, 44.0, 12.0, 2.9,

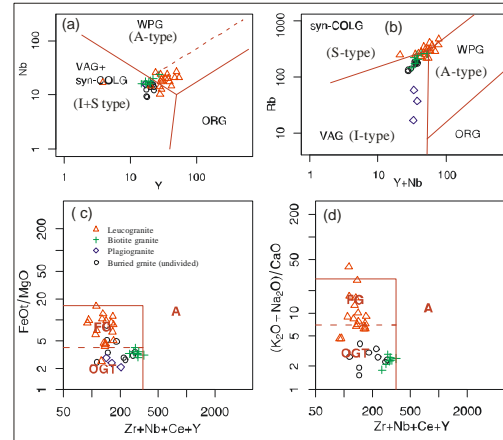


Fig. 3. Empirical geotectonic discrimination diagrams: (a, b) after Pearce *et al.* (1984); (c, d) after Whalen *et al.* (1987)

above. REE values of the biotite granite suggest a possible continental crust magma derivation.

Based on zircon saturation geothermometry, the plagiogranite formed near a liquidus of about 740°C; porphyritic biotite granite from a melt of 800°C, and leucogranite from a melt of 720°C. Pressure for the emplacement of granitoids of Mactung maybe deduced from the skarn minerals. Analysis of sphalerite co-existing with pyrrhotite and pyrite using SEM-EDS for S, Cd, Mn, Fe and Zn at the UNB laboratory gave 33.26, 1, 0.54, 10.3, and 54.32 %, respectively. This amounts to about 18.04 mole% FeS in sphalerite yielding a pressure estimate of about 2kb.

GEOCHRONOLOGY

Mineral grains of biotite and muscovite were separated from ten samples representing biotite granite, leucogranite, aplitic dyke, granite dyke, biotite hornfels, amphibole-pyroxene skarn, and biotite schist (Vampire Fm), lower ore zone biotite, and pyrrhotite-bearing skarn. They were age dated using the Ar-Ar method at the University of Toronto. Five granitic samples were later dated using U-Pb on zircons at University of British Columbia.. Summary of the estimated ages are given in Table 1.

Interaction between late-stage alteration processes, possibly related to the

Table 1. Ar-Ar and U-Pb age dates for Mactung granitoids

Lithology	Easting (m)	Northing (m)	Ar-Ar age (Ma)	U-Pb age (Ma)
Aplitic dyke	441501	7015976	94.0±0.5Ma (bt)	97.2 ± 0.2
Granitic dike	442733	7017826	92.9±0.4 Ma (mu) 95.3±0.4Ma (mu)	97.1 ± 0.3
Biotite granite	440026	7015106	-	97.2 ± 0.2
Biotite granite	442806	7018033	95.6 ±0.3Ma (mu) 94.0±0.3Ma (bt) 91.8±0.4 Ma (bt)	97.1 ± 0.1
Leucogranite	442806	7018033	93.3±1.2Ma (mu)	*92.1 ± 0.2
Biotite granite (near skarn)	441839	7018089	98.1±2 Ma (mu) 95.1 ±0.8 Ma (bt)	97.6 ± 0.2
Biotite hornfels	441889	7018110	97.1±1.9Ma (bi)	-
Amph-Pxn skarn	441910	7018082	127±20 Ma (Amph with pxn core)	127.1 20
Biotite schist (Vampire Fm):	441979	7017724	95.7±0.4 Ma (bt)	-
Biotite bearing skarn (Ore zone)	442117	7017731	90.7±3.1 Ma (bt)	-

* Interpreted from Selby *et al.* (2003)

leucogranite magmatic episode, and biotite granite is evident from occurrence of distinct plateaus of at least two important ages; for instance in felsic granitic dyke (MAC-165), based on muscovite grains step heating, two plateaus of low and high temperatures, representing corresponding ages of 92.9 ± 0.4 Ma and 95.3 ± 0.4 Ma, are recognized. This sample was seen to contain biotite richer portions in the field. U-Pb age dating on zircons also revealed an older age attributable to biotite granite. Overprinting of similar younger age is seen in biotite crystals from biotite granite, where a lower age of 91.8 ± 0.4 Ma indicates resetting until the cessation of plutonism. Another observable feature of the Ar-Ar dating is the closeness between biotite ages of biotite granite and biotite hornfels. Zircon grains separated from two samples of the biotite granite near the contact and away from the contact gave U-Pb dates of 97.6 ± 0.2 and 97.1 ± 0.1 Ma, respectively.

CONCLUSIONS

(1) Based on the geochemistry and age dating of the granitoids, at least two episodes of magmatism of different sources are evident at Mactung: the first episode, possibly from the melting of the crust, formed the biotite granite – the main

intrusion near the skarn and further south. The second episode resulted in the emplacement of leucogranite peripheral to the biotite granite and probably originated from the fusion of sediments followed by extensive crystal fractionation.

(2) The biotite granite is similar in age and composition to those of the Tungsten suite intrusions of the Nahanni area, including that of the Cantung Granite, the causative intrusion for tungsten mineralization at Cantung. The leucogranite is similar in age to those of the youngest part of the Tombstone suite, lying northwest of Mactung and those occurring all the way into Alaska. These granite types are known for porphyry-type gold (W-Mo).

(3) Based on these new results, the U-Pb ages of 92.1 ± 0.2 Ma determined by Selby *et al.* (2003) represents the latest magmatic episode (leucogranite) instead of the main ore-forming magmatic episode (biotite granite). The 97.5 ± 0.5 Ma Re-Os age dates on molybdenite determined by Selby *et al.* (2003) are identical to our U-Pb age dating on zircon crystals of porphyritic biotite granite, which is the main intrusion phase at Mactung, linked to W (Cu-Bi-Au) skarn. However, mineralizing fluids began separating during emplacement of this deeper coarsely porphyritic granite, based on the mineralized breccia fragments locally hosted by this granite and associated dykes.

ACKNOWLEDGEMENTS

We thank NA Tungsten Corp. for covering field work expenses, and for permission to carry out this research on its property. Argon-Argon dating of biotite and U-Pb dating of zircons were possible through the generous grants of the Geological Surveys of the Yukon and North West Territories.

REFERENCES

ABBOT J.G., GORDEY, S.P., & Templeman-Kluit, D.J. 1986. Setting of stratiform, sediment hosted lead zinc deposits in Yukon and northeastern British Columbia, In: MORIN, J.A. (ed.), *Mineral Deposits of the Northern Cordillera*. Canadian Institute of Mining and

- Metallurgy Special Volume **37**, 1-18.
- ATKINSON, D. & BAKER, D.J. 1986. Recent developments in the geologic understanding of Mactung, In: MORIN, J.A. (ed.), *Mineral Deposits of the Northern Cordillera*. Canadian Institute of Mining and Metallurgy Special **37**, 234-244.
- PEARCE, J., HARRIS, N.B.W., & TINDLE, A.D. 1984. Trace element discrimination diagrams for the tectonic interpretation of granitic rocks. *Journal of Petrology*, **25**, 956-983.
- SELBY, D., CREASER, R.A., HEAMAN, L.M., & HART, C.J.R. 2003. Re-Os and U-Pb Geochronology of the Clear Creek, Dublin Gulch, and Mactung Deposits, Tombstone Gold Belt, Yukon, Canada: absolute timing relationships between plutonism and mineralization. *Canadian Journal of Earth Science*, **40**, 1839-1852.
- WHALEN, J.B., CURRIE, K.L., & CHAPPELL, B.W. 1987. A-type granites: geochemical characteristics, discrimination and petrogenesis. *Contributions to Mineralogy and Petrology*, **95**, 407-419.

Use of micro-XRF in the characterization of hydrothermal alteration: application to the subaqueous felsic dome-flow complex of the Cap d'Ours segment of the Glenwood rhyolite, Rouyn-Noranda, Québec

Dominique Genna^{1,2}, Damien Gaboury^{1,2}, Lyndsay Moore¹, & Wulf Mueller¹

¹ Université du Québec à Chicoutimi (UQAC), ² Laboratoire de métallogénie expérimentale et quantitative (LAMEQ) 555, boul. de l'Université, Chicoutimi, QC, G7H 2B1 CANADA (e-mail: dominique.genna@uqac.ca)

ABSTRACT: Hydrothermal alteration is important in the vectoring of mineralization in volcanic terrains. However, geochemical analyses of these alterations are often based on bulk rock analyses and are unrepresentative. For example, in the context of a subaqueous felsic dome-flow complex such as those found in the Abitibi greenstone belt, the breccia facies is omnipresent and the glassy matrix, more porous than the fragments, better records the passage of hydrothermal fluids. The development of a new analytical methodology using micro-XRF enables separate studies of alteration of the matrix versus the fragments with respect to major element composition. Twelve elements are mapped on windows considered sufficiently homogenous and representative of each sample. An average is then calculated for the analyzed area and yields a nearly complete analysis (with the exception of loss on ignition). In the field, a sufficiently uniform sampling mesh allows the determination of spatial distribution of alteration. The application of this method has been tested successfully on samples from the Cap d'Ours complex of the Glenwood rhyolite in the Rouyn-Noranda region of Québec. The use of micro-XRF offers new perspectives in the treatment of hydrothermal alteration such as variations of chemical elements in minerals, calculation of normative minerals on homogeneous areas and mapping of compositional zonation in minerals.

KEYWORDS: *hydrothermal alteration, Micro-XRF, volcanogenic mineralization, felsic complex, Blake River Group*

INTRODUCTION

The study of hydrothermal alteration is of major interest in the understanding and subsequent exploration of volcanogenic mineralizing systems and, therefore, is relatively well documented (Franklin *et al.* 2005). Bulk analytical methods to characterize the alteration, such as X-ray fluorescence, are fairly effective for homogeneous rock samples. However, in volcanic complexes where alteration is heterogeneous (such as volcanic breccias), it becomes important to analyze fragments and matrix separately because of differing porosities. This is especially problematic in subaqueous felsic dome-flow complexes, which have a strong economic potential for volcanogenic massive sulphide deposits, where brecciated facies are omnipresent. It is to account for such problems that the proposed method was developed.

GEOLOGICAL PARAMETERS

Regional Geology

The field area selected for the development of this methodology was the Cap d'Ours segment of the Glenwood rhyolite, located in the Blake River Group (BRG) in the Abitibi greenstone belt. Pearson & Daigneault (2009) interpret the BRG as the result of a large complex of nested and sequential calderas, which correspond to the successive collapses of the Misema, New Senator and Noranda calderas (Fig. 1).

Local Geology

The Cap d'Ours is largely composed of fragmentary Filla rhyolitic lavas and forms the eastern boundary of the Glenwood rhyolite at the south-eastern margin of the New Senator caldera (Fig. 1). Field work conducted during the summer of 2008 led to the interpretation of the Cap d'Ours as remnants of a subaqueous felsic dome-

flow complex (Fig. 2). The abundance of brecciated facies, the favourability of type FIIIa rhyolites for VMS mineralization (Gaboury & Pearson 2009), disseminated mineralization (fine pyrite replacement +/- chalcopyrite and trace gold), hydrothermal alteration and the low degree of deformation and metamorphism (sub-greenschist) of the study area provide an ideal environment to conduct this newly proposed analytical technique on hydrothermally altered volcanic rocks.

METHODOLOGY

Hydrothermal alteration of the Cap d'Ours is typified by silica, chlorite, sericite, epidote and carbonate phases. In order to quantify the intensity of alteration within the volcanic edifice, a new approach was adopted for both sampling and analyses.

The increased porosity of the matrix of the brecciated facies facilitated circulation of hydrothermal fluids and recorded a much better expression of hydrothermal alteration, necessitating separate analyses of both matrix and fragments for each sample. The composition of the rhyolitic fragments is relatively constant for both major and trace elements and is the least altered material. Sampling at 50 m intervals provided a mesh sufficiently uniform to be representative. Fragments and matrix were collected for all breccias sampled.

Geochemical analyses were conducted on unpolished thin sections 30 μm thick using micro-XRF – EDAC Eagle III mapping at the l'Université du Québec à Chicoutimi (UQAC). Use of the micro-XRF permits analyses of major element compositions with a relatively fast, non-destructive, *in situ* method through points or maps. The parameters (Table 1) were selected in order to optimize the speed and quality of the results on the basis of micro-probe analyses of chlorite.

Over 160 analyses were conducted using 58 thin sections. Twelve elements were mapped on a minimum of three areas per thin section. The windows of analysis correspond to areas of 64 x 50 pixels (1.7 x 1.3 mm) and were considered sufficiently homogeneous to be representative of the sample. The composition was determined using a time analysis of 800 ms per pixel and an average was calculated using the area analyzed. The method provides a nearly complete chemical analysis, with the exception of loss on ignition.

Table 1. Micro-XRF analysis parameters.	
Map size	64 x 50 pixels (1.7 x 1.3 mm)
Limit - kV	20
μA	200
Dwell (time/point)	800

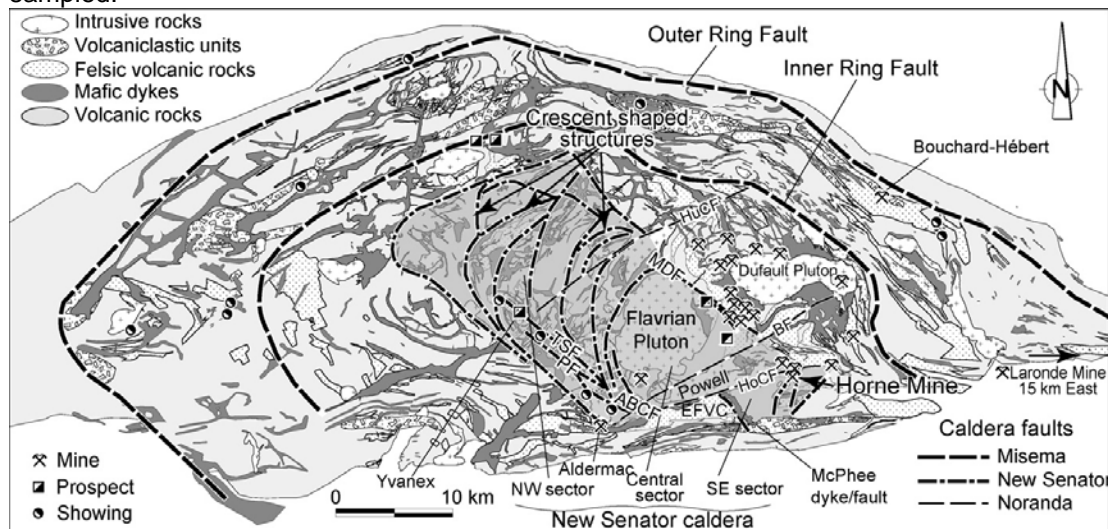


Fig. 1. Structure and geometry of the Blake River megacaldera complex (modified from Pearson & Daigneault 2009). The Cap d'Ours area is located 2km south of the VMS Horne Mine.

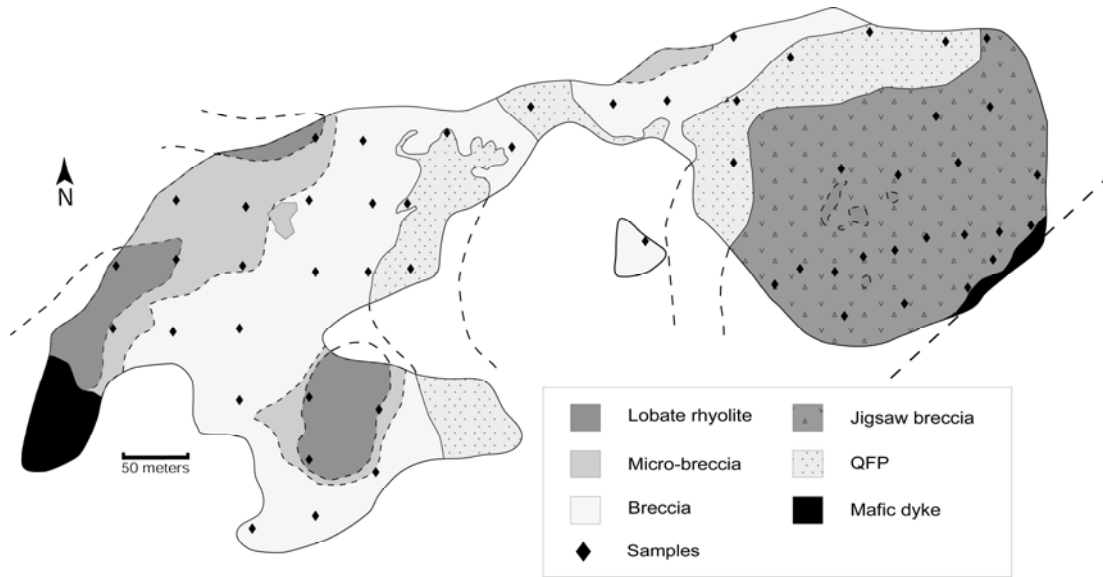


Fig. 2. Interpretative volcanic facies mapping of the Cap d'Ours segment of the Glenwood rhyolite (Genna & Moore 2008).

RESULTS

Sampling at 50 m intervals provided a sufficiently uniform mesh to represent the spatial zonation of the hydrothermal alteration of the Cap d'Ours. The mass balance calculations (not presented here) are used to highlight a leaching of MgO, Na₂O and SiO₂ in the eastern part of the complex, while the west is more enriched in these elements. Figure 5 illustrates the distribution of SiO₂ and shows a significant silicification of the glassy matrix in the west part of the outcrop, proximal to the inferred vent of the complex. An increase in alteration can also be correlated with proximity to mineralized zones.

In addition to micro-XRF analyses, 13 samples were analyzed by X-Ray Fluorescence (XRF) (ALS Chemex) to compare major element results. Although some discrepancies were observed, the difference between XRF and micro-XRF was relatively consistent and it is therefore possible to establish a correction factor for each element.

The range of possible uses for micro-XRF in application to the analysis of hydrothermal alteration is significant: elemental variations in minerals (e.g., Fe and Mg in chlorite), calculation of

normative minerals in a homogeneous area, mapping the compositional zonation of minerals, etc.

CONCLUSIONS: ADVANTAGES AND LIMITS

Application of this method within the Cap d'Ours segment of the Glenwood rhyolite has identified distinct distributions of alteration associated with a low-temperature hydrothermal system. The ability of this method to detect diffuse alteration will make micro-XRF analyses a powerful tool in exploration.

Advantages: 1) consistent and valid results despite a semi-quantitative

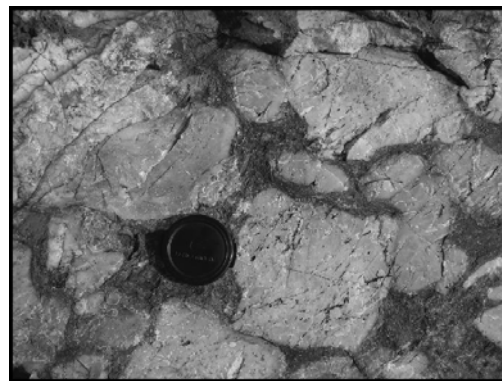


Fig. 3. Photograph of brecciated facies of the Cap d'Ours (lens cap is 43 mm).

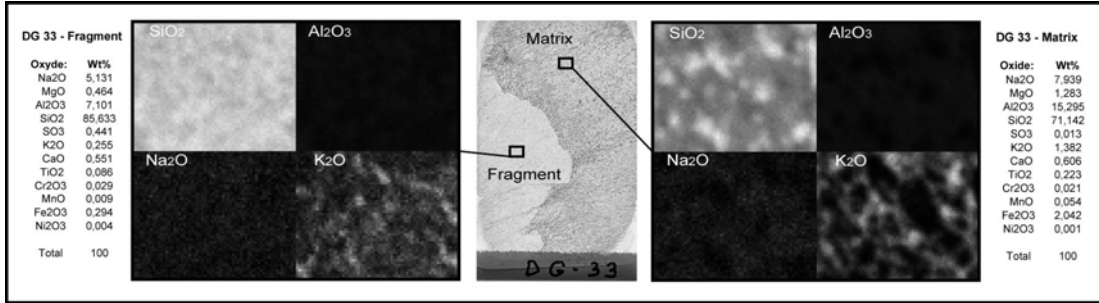


Fig. 4. Example of elemental mapping of both fragments and matrix with average composition of analyzed areas at left and right margins, respectively.

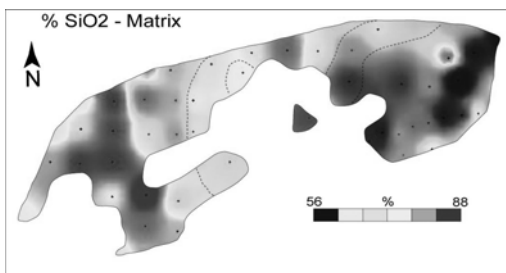


Fig. 5. Distribution of SiO₂ in glassy matrix.

method; 2) direct link between mineralogy, texture and chemical composition; 3) fast acquisition and data processing with low-cost analysis.

Limitations: 1) uniformity and representativeness of the analyzed area; 2) quantification of light elements (e.g. Mg); and 3) inability to obtain levels of

volatiles. These limitations can be overcome easily by dedicated calibrations, optimization of the analytical window size and normative mineral calculations for volatile estimation.

REFERENCES

- FRANKLIN, J.M., GIBSON, H.L., JONASSON, I.R., & GALLEY, A.G. 2005. Volcanic Massive Sulfide Deposits. *Society of Economic Geology – 100th Anniversary Volume*, 523-560.
- GABOURY, D. & PEARSON, V. 2008. Rhyolite geochemical signatures and association with volcanogenic massive sulfide deposits: Examples from the Abitibi belt, Canada. *Economic Geology*, **103**, 1531-1562.
- PEARSON, V. & DAIGNEAULT, R. 2009. An Archean megacaldera complex: The Blake River Group, Abitibi greenstone belt. *Precambrian Research*, **168**, 66-82.

Regional rock geochemistry of the Leninogorsk and Zyryanovsk VMS region (Rudny Altay Kazakhstan) - implications for genesis and exploration

I. Goldberg¹, G. Abramson¹, V. Los², V. Nazarov³, & C. Haslam⁴

¹Interresources Pty Ltd, Level 2, 49-51 York Street, Sydney, NSW 2000 AUSTRALIA
(e-mail: igoldberg@allegiance-mining.com.au)

²Academy of Mineral Resources, Nazyrbaya Batyra, 146/11, Almaty KAZAKHSTAN

³JSC "Kazzinc", Promyshlennaya, 1, Ust-Kamenogorsk KAZAKHSTAN

⁴Trident Energy Ltd, Suite 3, Level 15 Wawkner Centre, 449 St. Kilda Rd Vic 3004

ABSTRACT: The Rudny Altay VMS province extends over 500 km along the north-eastern border of Kazakhstan. The deposits are now largely depleted and this aim, the "Kazzinc" has commenced exploration work based on IONEX technology, which involves mapping of polar geochemical systems. The work is being conducted in several stages, the first stage include 20,000 km² a regional geochemical survey (5 x 5 km) in Leninogorsk and Zyryanovsk ore regions, which are content the main resources in Rudny Altay. Geochemical survey has shown, that all deposits are localised into enrichment zones of ore forming elements (nuclear systems). Depletion zones of these metals have been identified on the periphery of the enrichment zones. The sizes of the Leninogorsk geochemical system constitutes 8000 km², and Zyryanovsk system – 6000 km². Titanium is formed enrichment zones on the external boundaries of the nuclei of these systems. The formation of such systems is associated with the huge-scale mobilization metals from rocks. These studies have shown that, with IONEX technology, indentifying and then appraising geochemical systems is a first step in regional mineral exploration. In the case of the Leninogorsk and Zyryanovsk regions this technology has enabled to reduce the area for further exploration by about 80%

KEYWORDS: *geochemistry, Rudny Altai, depletion, enrichment, anomaly*

INTRODUCTION

The Rudny Altay pyrite-polymetallic province (VMS deposits) which includes the Leninogorsk and Zyryanovsk ore regions, located along the north-eastern border of Kazakhstan (Fig 1). Total reserves Zn, Pb and Cu in of the Leninogorsk and Zyryanovsk ore regions sums to 43 million tonnes of metals. The deposits are now largely depleted and this aim, the "Kazzinc" has commenced exploration work in the Leninogorsk and Zyryanovsk ore regions using IONEX technology. (Goldberg et al., 2003, Goldberg et al., 2007). The work is being conducted in several stages. The first stage included a regional geochemical survey on area of 20 000 km², scale - 1:500,000 (5X5 km) with sampling, including 800 rock samples. It is the first time that a geochemical survey has been carried out in Rudny Altay on such a

scale. Based on these data, the following aspects are discussed: geochemical pattern of zinc and titanium distribution, the source of the metals, and the criteria of evaluation of potential areas.

THE GENERAL GEOLOGICAL SETTING

The Rudny-Altay volcanic arc is a Devonian bimodal suite of volcanic rocks. The Rudny Altay Block is separated by the Irtysh dip-sited shear zone on the west from Kalba and the North-Eastern shear zone on the East from Gorny Altay (Fig1). Down to a depth of about ten kilometres the territory of the region has a distinct two-layer structure. The lower layer (S₂-D₁) consists of highly dislocated and metamorphosed sandstones and greenschist rocks. Higher up lie the rocks of the upper layer. It is presented volcanogenic-sedimentary formation (D₁-D₃). The main deposits are linked spatially

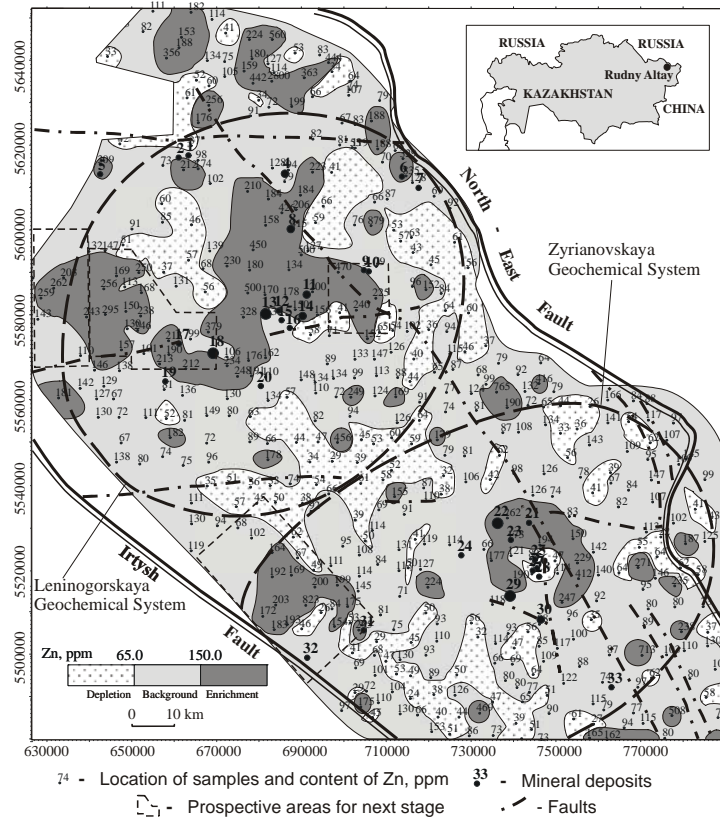


Fig. 1. Distribution of Zn in rock in in Leninogorsk and Zyryanovsk regions.

to this formation. The youngest rocks consist of carbonate-terrigenous deposits (D_3-C_1), rocks of gabbro-granodiorite-granite formation (C_2-C_3) and granites (P_1). The total area formed by granites is approximately 30%. Quaternary deposits cover approximately one third of the area.

THE GEOCHEMICAL SYSTEMS OF THE LENINOGORSH AND ZYRYANOVSK ORE REGIONS

The analysis of rock samples was conducted in the chemical laboratory in Ust-Kamenogorsk, Kazakhstan. by inductively coupled plasma mass spectrometry, and the equipment used was an ELAN-6100 (US) mass spectrometer. In the present abstract the distribution of two elements: zinc (as the basic ore-forming element) and titanium (of the siderophile element) is examined. The sensitivity of the analysis is 5 ppm for Zn and 0.05% for Ti. The analytical results for Zn and Ti are presented on contoured

maps at scale of 1:500,000. The contour intervals used for each element were based on the statistical cumulative graphs of distribution (Figs. 1 and 2).

Distribution of Zn, (Fig.1)

The distribution of zinc over the area is characterised by considerable heterogeneity. Anomalous concentrations of Zn (enrichment and depletion zones) cover approximately 35% of the study area.

Enrichment zones: within the study area there are several enrichment zones: two, Leninogorsk and Zyryanovsk, contain most of the know VMS deposits. Both are proximal to intersection of major regional fault. In Leninogorsk ore region the total area of the enrichment zone is approximately 2,400 km². In the Zyryanovsk region area of enrichment is approximately 1,300 km².

Depletion zones: In the Leninogorsk region the depletion zones are located

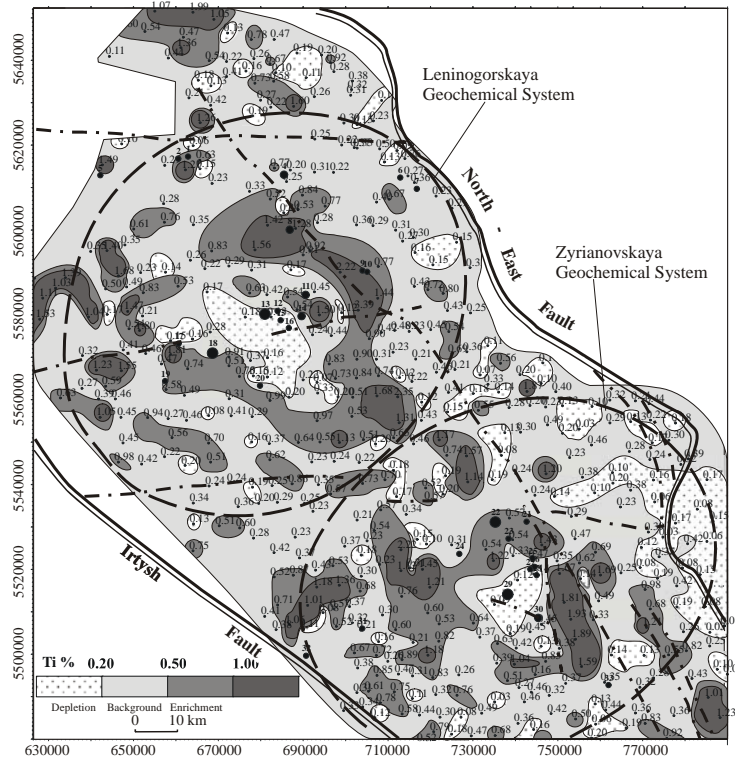


Fig. 2. Distribution of Ti. in rock in in Leninogorsk and Zyryanovsk regions (see Fig.1).

around the enrichment zones. To the north and north-east they are immediately contiguous, while to the south-east and south they are situated at a distance of 10-20 km, forming a semicircle around the central enrichment zone. The total area of depletion in this region is approximately 2,400 km².

In the Zyryanovsk region the depletion zones are located primarily in the form of individual anomalous areas 10-20 km wide surrounding the enrichment zone to the south-west and north-east. They are situated at a distance of approximately 10 km from the enrichment zone, essentially forming a ring-like structure. The total area of depletion is 1,300 km².

Distribution of Ti (Fig. 2)

In the Leninogorsk ore region the main titanium enrichment zone forms a horsehoe-shaped anomaly around the zinc enrichment zones. The size of the internal area is about 900 km². At its centre there is a depletion zone of 450

km². The majority of deposits are inside this zone or on its periphery.

The diameter of this external ring-like structure centered round the main group of deposits of the Leninogorsk region is 80-90 km.

To the west of this ring-like structure, on the boundary of the area, there are several enrichment local anomalies of Ti around enrichment zones of Zn and Pb. In the Zyryanovsk region all the main deposits, are surrounded by a ring-shaped zone of Ti enrichment of 5-10 km in width. The internal part of the area of the ring-like anomaly mainly comprises a depletion zone of about 150 km².

CONCLUSIONS

1. Implication for ore genesis

This regional-scale geochemical survey has defined two main polar geochemical systems: the Leninogorsk and Zyryanovsk. The main VMS deposits are localised in zones of enrichment of the ore-forming elements. The depletion zones of the ore-forming elements

surround the enrichment zones. The geochemical ore systems have a shape close to isometric. The area of the Leninogorsk system is approximately of 8000 km² and the Zyryanovsk system - about 6000 km². The enrichment zones of Ti define the external borders of the nuclei of these systems.

The geochemical data shows that: 1. The main enrichment zones coincide with rocks of the volcanogenic-sedimentary sequence (D₁-D₃) which are the host all of the VMS deposits. However, the enrichment zone of ore forming elements also represented in younger rocks, including P₁. 2. An enormous redistribution of the ore forming elements throughout the regional rock mass, including post-Devonian rock.

2. Implication for exploration

These studies have shown that, with IONEX technology, indentifying and then appraising geochemical systems is a natural first step in regional mineral exploration. If a number of geochemical systems are defined, the quantum of metal depletion in the depletion zones is the key parameter in allocating priority among those geochemical systems. In second phase of exploration a closer

sample spacing is employed over only the enrichment zone of the selected geochemical system, as such systems are fractal.

In the case of the Leninogorsk and Zyryanovsk regions this technology has enabled the client to reduce the area for further exploration by about 80%

REFERENCES

- GOLDBERG, I.S., ABRAMSON, G.J., & LOS, V.L. 2003. Depletion and enrichment of primary haloes: their importance in the genesis of and exploration for mineral deposits: *Geochemistry, Exploration, Environment, Analysis*, **3**, 281-293.
- GOLDBERG, I.S., ABRAMSON, G.J., HASLAM C.O., & LOS, V.L. 2007. Depletion and enrichment zones in the Bendigo Gold Field: a possible source of gold and implications for exploration. *Economic Geology*, **102**, 745-753.
- POPOV V.V., STUCHEVSKY N.I., & DEMIN, U.I. 1995. *Polymetallic ore deposits of Rudny Altai, Moscow*, 420 p. (In Russian).
- SHERBA, G.N. 1983. Polymetallic massive sulfide deposits of Rudny Altai. In: IVANOV, S.N. (ed.), *Massive sulphide deposits of the USSR*: Moscow, Nauka Publishing House, 87-148 (In Russian).
- SMIRNOV V.I. (edited). 1977, *Ore Deposits of the USSR*, **2**, Pitman Publishing, London, San Francisco.

Geochemistry and tectonics as an exploration tool for Circum-Pacific porphyry copper, gold, and molybdenum deposits: evidence from the Baguio District, Philippines

Pete Hollings¹ & David R. Cooke²

¹Geology Department, Lakehead University, 955 Oliver Rd, Thunder Bay, ON, P7B 5E1 CANADA
(e-mail: peter.hollings@lakeheadu.ca)

²CODES, The Australian Research Council's Centre for Excellence in Ore Deposits, University of Tasmania, Private Bag 79, Hobart, 7001, Tasmania AUSTRALIA

ABSTRACT: Pliocene and Pleistocene magmatic rocks of the Baguio District, Philippines, that are spatially and temporally associated with mineralisation can be broadly subdivided into an intermediate to felsic suite of mineralised low- to medium-K intrusions, some of which have adakitic affinities, and a suite of mafic to intermediate, medium-K to shoshonitic hornblende-phyric dykes. The geochemical and isotopic characteristics of the dykes are consistent with primitive mantle-derived melts that underwent minimal crustal contamination as they ascended through the arc crust. In contrast, the intermediate to felsic suite has been contaminated by young arc crust, suggesting ponding and fractionation within shallow-crustal magma chambers. Eastward-directed subduction of the Scarborough Ridge along the Manila Trench is associated with flattening of the downgoing slab. Magmas generated from the downgoing ridge can account for the isotopic recharge of the Pliocene sub-arc mantle, as well as the generation of the primitive melts and adakitic rocks found within the Baguio District. The interaction between primitive mafic melts and the more felsic calc alkaline rocks has generated fertile magmas that were highly productive for porphyry copper and epithermal gold mineralization.

KEYWORDS: *Porphyry Cu-Au, Philippines, Ridge subduction, adakites*

INTRODUCTION

The circum-Pacific region hosts spectacular examples of porphyry Cu-Au, Cu-Mo, and related epithermal Au-Ag deposits. The Andean margin of South America contains some of the world's largest porphyry Cu-Mo deposits, and also some significant Cu-Au systems. Giant Cu-Mo systems also characterise SW USA and NW Mexico. The SW Pacific region is well-endowed with porphyry Cu-Au deposits. Tertiary or Quaternary oceanic island arcs host porphyry systems in the Philippines, Indonesia, and PNG. Significant Cu-Au porphyries also occur in Alaska, Canada, and Central America. Some segments of the Pacific rim are poorly endowed with porphyry deposits (e.g., New Zealand, Japan), but do contain important epithermal gold deposits. The ore deposits are most commonly associated with calc-alkalic magmatism. Cu-Au porphyry intrusions can be low-K (e.g., Batu Hijau, Indonesia),

medium-K (e.g., Baguio, Philippines), high-K (e.g., Grasberg, Indonesia) or alkalic in composition (e.g., Galore Creek, British Columbia).

Most of the youngest porphyries in the circum-Pacific region (e.g., Baguio and Mankayan districts, Philippines; Ok Tedi and Grasberg, New Guinea; El Teniente and Rio Blanco, Chile) have been exposed in arc segments that have undergone rapid uplift and exhumation. It has also been demonstrated that in the last 20 m.y., the formation of giant porphyry copper-molybdenum and copper-gold deposits in the circum-Pacific region has been closely associated with subduction of aseismic ridges and seamount chains, and (or) collision with oceanic plateaus beneath oceanic island and continental arcs (e.g., porphyry Cu-Mo deposits in central Chile, Cu-Au porphyries and giant high sulfidation deposits in northern Peru and Central America; porphyry and epithermal

deposits in northern Philippines; Cooke *et al.* 2005).

Studies of the host rocks to giant porphyry copper deposits in Central and Northern Chile have shown that there are recognizable changes in the geochemistry of the volcanic rocks prior to mineralizing events (Skewes & Stern 1995; Kay *et al.* 1999; Hollings *et al.* 2005). These include abrupt increases in the La/Yb ratios of volcanic rocks associated with mineralization, which have been interpreted to indicate a rapid change in the tectonic environment, likely associated with the subduction of an aseismic ridge. This study investigates those relationships in the island arc system of the Philippines.

THE BAGUIO DISTRICT

The Baguio District of the Philippines represents a complex tectonic setting sandwiched between two oppositely dipping subduction zones and associated with the subduction of the Scarborough Ridge (Fig. 1). The district is located in the Central Cordillera of Luzon within the Western Luzon arc. It records the evolution from Cretaceous - Eocene marginal basin sedimentation and volcanism, to shallow marine sedimentation, followed by construction of a calc-alkaline magmatic arc above the Manila Trench in the Middle Miocene. The Northern Luzon segment of the archipelago has experienced seamount subduction/obduction, collision, arc-flipping and ophiolite emplacement since the Cretaceous. The district represents one of the world's premier mineral provinces with >35 million ounces of gold and 2.7 million tonnes of copper contained in epithermal (e.g., Antamok; Sawkins *et al.*, 1979; Acupan, Cooke *et al.*, 1996), porphyry (e.g., Santo Tomas II; Imai 2001) and skarn resources (e.g., Thanksgiving; Callow 1967). The Mankayan district, approximately 70 km to the north, contains an additional 37 million ounces of Au and 8 Mt Cu in porphyry and epithermal deposits that formed at the same time as those in the Baguio district (Chang *et al.* submitted), highlighting the extraordinary fertility of this part of northern Luzon.

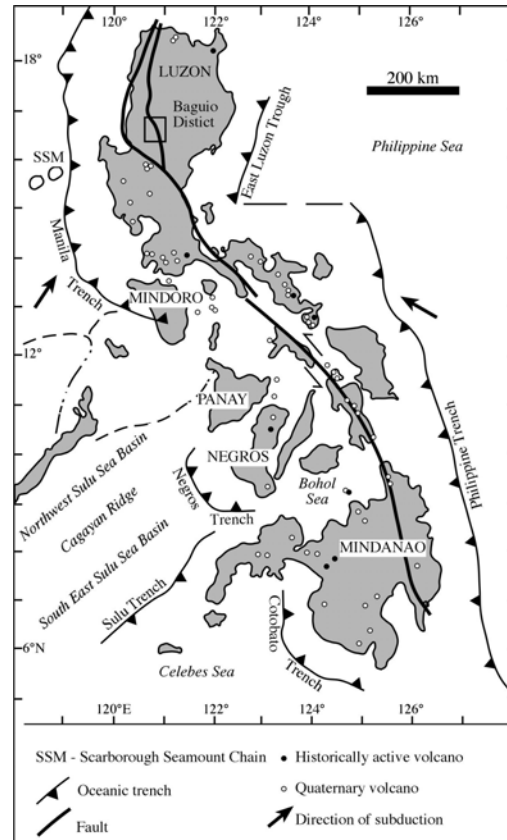


Fig. 1. Map of the Philippines showing submarine trenches, Philippine Fault and relative motion of Philippine and Eurasian plates (arrow). Solid circle = historically active volcano, open circle = Quaternary volcano. Modified after Mitchell and Leach (1991).

The Miocene stratigraphy in the Baguio District has been intruded by a series of Pliocene rocks. The hornblende-phyrlic Mafic Dike Complex intruded the central part of the Baguio District at 4.5 – 4 Ma (Waters *et al.* submitted). The complex is characterized by dense clusters of coarsely hornblende phenocrystic dikes with evidence for multiple injections. Several Pliocene to Pleistocene dioritic intrusive complexes are associated with porphyry copper-gold mineralization in the Baguio district. The Black Mountain Intrusive Complex includes the Black Mountain quartz diorite and the Mexico Diorite, as well as andesite dykes that have yielded ages of between 3.14 and 2.78 Ma (Waters *et al.* submitted; Sweet *et al.* 2008). Other Pliocene intrusive rocks

include the ~2 Ma Santo Tomas II-Bumolo-Clifton Cluster and the ~1 Ma Ampucao-Hartwell-Balatoc Cluster (Waters *et al.* submitted).

The dyke complex forms a coherent suite of basaltic through to evolved andesitic compositions, plot on a calc-alkaline to high-K calc-alkaline trend and show a narrow range of La/Sm_n ratios (1.4-3.1; Fig. 2). Younger Pliocene samples typically have higher La_n/Sm_n ratios with a peak in values around 3 Ma. Similarly the SiO₂ contents show a slight increase in younger samples, but also a spike at around 3 Ma. The trend to more felsic samples implies either a change in the nature of the mantle source or simply progressive fractionation of the same relatively shallow level magma chamber.

CONCLUSIONS

Unlike Central Chile, the tectonic complexity and gaps in the igneous record between 17 and 5 Ma obscures the signal of igneous fertility in the Baguio District. However, La/Yb ratios do show an increase in host rocks that predate and are coeval with mineralization. Published data for igneous rocks associated with porphyry mineralization in the Batu Hijau district also shows an increase in La/Yb ratios at the time of mineralization with ratios increasing to levels comparable to those in the Baguio district (Garwin 2000). This implies that in oceanic arc systems changes in the tectonic setting resulting in crustal thickening appear to be associated with mineralization events. The thinner crust beneath island arcs compared to that below continental arcs results in more subdued geochemical signatures of crustal thickening. Radiogenic isotopic data from rocks coeval with mineralization in the Baguio District can be interpreted to indicate that more primitive magmas were emplaced immediately prior to mineralization and may have acted as a heat or metal source. The data implies that in oceanic arc systems changes in the tectonic setting resulting in crustal thickening appear to be associated with mineralization events.

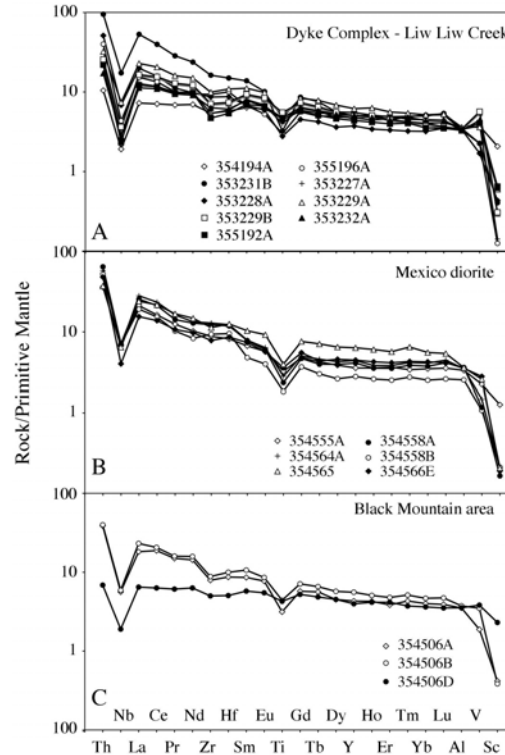


Fig. 2. Representative primitive mantle-normalized diagrams for samples from the Baguio District. Normalising values of Sun and MacDonough (1989).

ACKNOWLEDGEMENTS

This study was undertaken as part of Australian Mineral Industry Research Association (AMIRA) project P765—“Geochemical and Geological Halos in Green Rocks and Lithocaps”. Additional financial support was provided by a Natural Sciences and Engineering Research Council (NSERC) Discovery Grant to Hollings. The authors gratefully acknowledge logistical support from Anglo American personnel in the Philippines.

REFERENCES

CALLOW, K.J. 1967. The geology of the Thanksgiving mine, Baguio district, Mountain Province, Philippines. *Economic Geology*, **60**, 251-268.

CHANG, Z., HEDENQUIST, J., WHITE, N *et al.* Exploration tools for linked porphyry and epithermal deposits: Example from the Mankayan intrusion-centered Cu-Au district, Luzon, Philippines. *Economic Geology*, in review.

- COOKE, D.R., HOLLINGS, P., & WALSH, J. 2005. Giant porphyry deposits – characteristics, distribution and tectonic controls. *Economic Geology*, **100**, 801-818.
- COOKE, D.R., MCPHAIL, D.C., & BLOOM, M.S., 1996. Epithermal gold mineralization, Acupan, Baguio district, Philippines: geology, mineralization, alteration and the thermochemical environment of ore deposition. *Economic Geology*, **91**, 243-272.
- GARWIN, S.L. 2000. *The setting, geometry and timing of intrusion-related hydrothermal systems in the vicinity of the Batu Hijau porphyry copper-gold deposit, Sumbawa, Indonesia*. Unpublished PhD thesis, University of Western Australia, Perth, Australia.
- HOLLINGS, P., COOKE, D.R., & CLARK, A. 2005. Regional geochemistry of Tertiary volcanic rocks in Central Chile: implications for tectonic setting and ore deposit genesis. *Economic Geology*, **100**, 887-904.
- KAY, S.M., MPODOZIS, C., & COIRA, B. 1999. Neogene magmatism, tectonism and mineral deposits of the central Andes. In: SKINNER, B.J. (ed), *Geology and ore deposits of the Central Andes*. Society of Economic Geologists Special Publication, **7**, 27-59.
- MITCHELL, A.H.G. & LEACH, T. M. 1991. *Epithermal gold in the Philippines. island arc metallogenesis, geothermal systems and geology*. Academic Press Geology Series, London.
- SAWKINS, F.J., O'NEILL, J.R., & THOMPSON, J.M. 1979. Fluid inclusion and geochemical studies of vein gold deposits, Baguio District, Philippines. *Economic Geology*, **74**, 1420-1434.
- SKEWES, M.A. & STERN, C.R. 1994. Tectonic trigger for the formation of late Miocene Curich breccia deposits in the Andes of central Chile. *Geology*, **22**, 551-554.
- SUN, S.-s. & McDONOUGH, W.F. 1989. Chemical and isotopic systematics of oceanic basalts: implications for mantle composition and processes. In: SAUNDERS, A.D. & NORRIS, A.J. (eds.), *Magmatism in the ocean basins*. Geological Society, Special Publication **42**, 313-345.
- SWEET, G., WATERS, P., BAKER, M., HOLLINGS, P., & COOKE, D.R. 2008. The Black Mountain porphyry Cu-Au deposit, Baguio, Philippines. *Australasian Institute of Mining and Metallurgy, PACRIM Congress 2008, The Pacific Rim: Mineral Endowment, Discoveries & Exploration Frontiers*, Gold Coast, 451-456.
- WATERS, P.J., GONZALES, R.I., & COOKE, D.R. Geological setting and mineral deposits of the Baguio Mineral District. *Economic Geology*, in review.

Metals distribution and correlations in polymetallic veins from Pingüino Indium-bearing deposit, Deseado Massif, Patagonia, Argentina

Sebastián Jovic¹⁻², Paula Liñan¹, Diego Guido¹⁻², Gerardo Páez¹⁻²,
Remigio Ruiz¹, & Isidoro Schalamuk¹⁻²

¹Instituto de Recursos Minerales-Universidad Nacional de La Plata, La Plata ARGENTINA

²CONICET (e-mail: sebastianjovic@yahoo.com.ar)

ABSTRACT: The Pingüino deposit is characterized by the presence of In-rich polymetallic vein mineralization that represents an atypical epithermal occurrence for the low sulfidation epithermal mineralization from the Deseado Massif, Patagonia, Argentina. Polymetallic veins display high In, Zn, Pb, Ag, Cd, Au, As, Cu, Sn, W, and Bi values that are represented by complex sulfide mineralogy. This mineralization is developed in two main stages: an early Cu-Au-In-As-Sn-W-Bi stage, where indium is associated mainly with Sn mineralogy (ferrokesterite, stannite and cassiterite), and a late Zn-Pb-Ag-In-Cd-Sb stage with highest indium values related mainly with Zn (Fe-rich sphalerite).

KEYWORDS: *metals distribution, indium, Deseado Massif, Argentina*

INTRODUCTION

The Deseado Massif (DM) is located in the Santa Cruz province of the southern Argentinean Patagonia (Fig. 1). It is characterized by the presence of low sulfidation (LS) epithermal deposits that are genetically related to a complex long-lived (30 Ma) Jurassic bimodal magmatic event associated with tectonic extension. The DM is an important Au-Ag producer with four mines (Cerro Vanguardia, Martha, San José and Manantial Espejo) and it is the subject of intense prospecting activities. Mineralization consists of quartz veins, vein stockworks and hydrothermal breccias mainly hosted in Jurassic volcanic rocks. Metalliferous minerals in the quartz veins are commonly less than 1% in volume, mainly pyrite, native gold, electrum, argentite, native silver, Ag-sulfosalts, hematite, sphalerite, galena and chalcopryrite. The geochemical signature is characterized by anomalous precious metals, Au-Ag (Guido *et al.* 2005).

In recent years, some atypical epithermal occurrences (different to LS type) have been found in the DM. Mina Martha for example, is a Ag-rich deposit with a Ag:Au ratio of 1000:1 and high contents of base metals, and has been

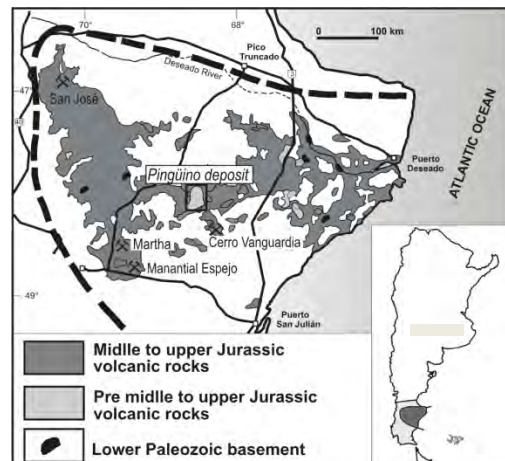


Fig 1. Deseado Massif geological map with Pingüino deposit location. (Guido *et al.* 2005).

defined as a intermediate sulfidation (IS) deposit (Gonzalez Guillot *et al.* 2004). The Pingüino deposit is another atypical epithermal deposit in the DM (Guido *et al.* 2005). It is located in the central part of the province, 40 km northwest from Cerro Vanguardia mine (Fig. 1) and is characterized by the presence of two vein types, early polymetallic sulfide-rich veins and late quartz-rich Ag-Au veins. The polymetallic veins show anomalous contents of Zn, Pb, Ag, In, Au, Cu, Cd, Sn,

Table 1. Summary of geochemistry analyses of polymetallic sulfide veins from Pingüino deposit.

Stage	Values	In	Au	Ag	Cu	Pb	Zn	Sn	Bi	Cd	As	Sb	W
PS ₁		ppm	ppm	ppm	wt.%	wt.%	wt.%	ppm	ppm	ppm	wt.%	ppm	ppm
Ivonne vein	Ave.	49.6	2.77	45.5	0.41	0.13	1.27	1267	93.9	61.7	1.00	66.5	55.2
n = 45	Max.	159.4	8.07	237.0	2.47	0.30	6.10	5961	390.8	338.2	4.41	509.1	740.0
	Min.	3.4	0.01	2.6	0.01	0.01	0.02	7	0.8	3.6	0.02	1.4	0.2
PS ₂													
M. Centro vein	Ave.	161.8	0.74	156.3	0.14	3.65	10.81	153	5.3	848.5	0.40	87.0	2.4
n = 100	Max.	1184	1.34	684.0	5.99	19.30	32.95	564	30.1	14900	1.28	634.8	25.2
	Min.	5.25	0.10	14.5	0.01	0.16	0.08	23	0.1	6.0	0.07	5.0	0.1

Sb, As, W, and Bi, classifying it as an indium-bearing polymetallic deposit.

The occurrence of indium-minerals is very rare in general, and indium substitutes in base metal sulfide minerals for elements with similar ionic radii. The most common In-bearing minerals are: sphalerite where In is substituting for Zn and Fe, stannite, kesterite and cassiterite where In is replacing Sn and Fe (Shwarz-Schampera & Herzig 2002).

The aim of this contribution is study the metals distribution, and specifically the indium distribution into the polymetallic mineralization stages from the Pingüino deposit sulfide veins.

PINGUINO DEPOSIT

The Pingüino veins, occupy more than 30 fault controlled structures. They have a NW and ENE strike and are hosted in Triassic continental sedimentary rocks and lower Jurassic epiclastic and volcanoclastic rocks, and are spatially related to lower Jurassic subvolcanic dioritic intrusions, basaltic sills and andesitic porphyries (Jovic *et al.* 2005).

Polymetallic Mineralization

The polymetallic veins are poorly exposed at surface and are characterized by the presence of gossans with remnants of breccias with quartz matrix and oxidized sulfide clasts. Hypogene polymetallic mineralization is characterized by the presence of massive and banded sulfide veins and sulfide breccias up to 13 m thick. This mineralization is developed in

two main stages. The early stage (Ps₁) is characterized by a complex paragenesis composed of pyrite, arsenopyrite, chalcopyrite, cassiterite, stannite, ferrokesterite, and minor sphalerite, galena, wolframite, bournonite, tetrahedrite, freibergite, argentotenantite, Ag-Pb-Bi sulfosalts (aramayoite, owyheeite, giesenita, ourayita), lillongite, enargite, and quartz, that is best represented in the Ivonne vein. During the second stage (Ps₂), Ps₁ minerals were replaced by Fe-rich sphalerite, galena, ferrokesterite, Ag-Pb sulfosalts and minor chalcopyrite, pirrotine, marcasite and tetrahedrite. The Ps₂ is best developed in the Marta Centro vein (Jovic *et al.* 2005; Crespi 2006).

Sampling and Geochemical Analysis

Hypogene veins zones between -30m to -120m depth from the Ivonne and Marta Centro veins were studied. These veins are 1000m and 700m in length and average 3m and 7m in thickness respectively and were drilled up to -400m. Representative samples were analyzed at Acme Analytical Laboratories (Chile-Canada) by instrumental neutron activation analyses (INAA), inductively coupled plasma-optical emission spectroscopy (ICP-OES), and inductively coupled plasma-mass spectrometry (ICP-MS). The studied Ps₁ samples are from the Ivonne vein (n=45) and Ps₂ from the Marta Centro vein (n=100). The average, maximum and minimum values of major (Zn, Pb, Cu, As), and trace element

Table 2. Correlation matrix for metals in Ps₁ from polymetallic sulfide veins at Pingüino deposit.

	In	Au	Ag	Cu	Pb	Zn	Sn	Bi	Cd	As	Sb
Au	0.67										
Ag	0.70	0.69									
Cu	0.67	0.66	0.84								
Pb	0.67	0.59	0.77	0.64							
Zn	0.40	-0.08	0.35	0.18	0.48						
Sn	0.77	0.82	0.64	0.54	0.63	-0.03					
Bi	0.67	0.69	0.83	0.63	0.50	0.22	0.52				
Cd	0.60	0.33	0.57	0.38	0.83	0.71	0.49	0.27			
As	0.31	0.61	0.50	0.24	0.34	0.02	0.34	0.59	0.23		
Sb	0.77	0.80	0.81	0.72	0.62	0.07	0.76	0.74	0.38	0.48	
W	0.50	0.71	0.41	0.47	0.52	-0.17	0.82	0.34	0.26	0.08	0.67

contents (Au, Ag, Sb, Bi, Sn, In, Cd, W) are listed in Table 1.

Ore Geochemistry

The ore geochemistry indicates the presence of high values of Cu, Au, As, Sn, W, Bi, Zn, Pb, Ag, In, Cd, and Sb in the polymetallic veins. Major and minor element associations reflect the two different mineralogical assemblages: the Ps₁ assemblage is characterized by anomalous values of Au, Cu, Sn, Bi, As and W, whereas the highest values of Zn, Pb, In, Ag, Cd and Sb are present in Ps₂ (Table 1). Ps₁ shows high correlations between Ag-Pb-Bi-Sb, Ag-Cu-Sb, Au-Sn-Sb-W and In-Sn-Sb (Table 2) while in Ps₂ the highest correlations are between In-Zn-Cd, In-Sn and Ag-Pb-Sb (Table 3).

DISCUSSION

Anomalous values of Au, Cu, Sn, Bi, As, and W in the Ps₁ indicate the precipitation of high temperatures minerals and metals that are represented by a complex mineralogy. The correlation between Ag-Pb-Bi-Sb suggests the presence of different Ag-Pb-Bi sulfosalts; correlation between Ag-Cu-Sb is associated with freibergite, argentotenantite, and tetrahedrite, while Sn-W is related to wolframite and cassiterite, and In-Sn-Sb with ferrokesterite, stannite and cassiterite. In Ps₂ the In and Cd, are present in the Fe-rich sphalerite (Crespi 2006) showing a high correlation between In-Zn-Cd; the correlation between In-Sn is associated with ferrokesterite. The presence of Ag-Pb sulfosalts is

responsible for the high correlation between these elements.

Indium concentrations in the polymetallic veins show a wide range (3.4 to 1184ppm In, Table 1). Based on the correlation coefficients of ore geochemistry, significant Indium (up to 1184 ppm) is related to the Ps₂ mineralization stage and closely associated with Fe-rich sphalerite, but also with ferrokesterite. There are important In anomalies in Ps₁ (up to 159.4 ppm) that are related to the Sn minerals, cassiterite, ferrokesterite and stannite (Crespi 2006).

CONCLUSIONS

The presence of high values of Cu, Au, As, Sn, W, Bi, Zn, Pb, Ag, In, Cd and Sb in the polymetallic veins from the Pingüinodeposit, represents an atypical geochemical signature for the epithermal deposits from the DM.

The distribution of the metals in the veins is represented by two mineralization stages: an early Ps₁ characterized by the presence Sn sulfides, Ag-Pb-Bi sulfosalts, Ag-Cu sulfosalts with the highest concentration of Cu, Au, As, Sn, W and Bi, and a late Ps₂ that shows the highest values of Zn, Pb, Ag, In, Cd and Sb with Fe-rich sphalerite, galena and Ag-Pb sulfosalts.

Indium is associated with both stages, but is concentrated in Ps₂ related mainly with Zn (Fe-rich sphalerite) and minor association with Sn (ferrokesterite). For Ps₁, Indium is associated with Sn, present

Table 3. Correlation matrix for metals in Ps₂ from polymetallic sulfide veins at Pingüino deposit.

	In	Au	Ag	Cu	Pb	Zn	Sn	Bi	Cd	As	Sb
Au	0.06										
Ag	0.19	0.21									
Cu	-0.07	0.00	-0.02								
Pb	0.17	-0.03	0.74	-0.09							
Zn	0.77	0.21	0.27	-0.16	0.39						
Sn	0.71	-0.03	0.46	-0.03	0.35	0.58					
Bi	0.56	0.06	0.09	0.39	-0.01	0.35	0.36				
Cd	0.80	0.26	0.23	-0.09	0.22	0.82	0.67	0.44			
As	0.05	-0.08	0.22	-0.09	0.37	0.17	0.10	0.01	0.11		
Sb	0.07	-0.02	0.81	-0.10	0.89	0.27	0.33	-0.09	0.16	0.37	
W	0.28	-0.03	0.07	0.38	-0.01	0.10	0.25	0.31	0.12	0.03	-0.01

in the Sn sulfides and oxides (ferrokesterite, stannite and cassiterite).

REFERENCES

- CRESPI, A. 2006. Estudi mineralògic dels dipòsits del massís de el Deseado (Argentina). *Universidad de Barcelona. Barcelona, España*
- GONZALEZ GUILLOT, M., DE BARRIO, R., & GANEM, F. 2004. Mina Martha, un yacimiento epitermal en el Macizodel Deseado, provincia de Santa Cruz. *VII Congreso de Mineralogía y Metalogenia, Córdoba, 1*, 199-204.
- GUIDO, D., JOVIC, S., & SCHALAMUK, I. 2005. A new metallogenic association (Sn-Cd-In-Zn-Ag-Au) in the Deseado Auroargentíferous province, Deseado Massif, Patagonia, Argentina. *Mineral Deposit Research: Meeting the Global Challenge. Beijing, China, 2*, 965-968.
- JOVIC, S., GUIDO, D., SCHALAMUK, I., MELGAREJO, J., & PROENZA, J. 2005. Mineralogía de veta Ivonne, depósito Cerro León: ¿Paragénesis de alta temperatura en la Provincia Auroargentífera del Deseado? *XVI Congreso Geológico Argentino, La Plata, 2*, 257-262.
- SCHWARZ-SCHAMPERA, U. & HERZIG, P. 2002. *Indium. Geology, Mineralogy, and Economics*. Springer-Verlag, Berlin, 257 p.

Chemical compositions of carbonate minerals from Chehelkureh ore deposit, Iran: implications for evolution of base-metal mineralization

Mohammad Maanijou¹, David R. Lentz², & Iraj Rasa³

¹Dept. of Geology, Faculty of Science, Bu-Ali Sina University, Hamedan IRAN (e-mail: mohammad@basu.ac.ir)

²Dept. of Geology, University of New Brunswick, P.O.Box 4400, Fredericton, NB E3B 5A3 CANADA

³Dept. of Geology, Faculty of Earth Sciences, Shahid Beheshti University, Tehran IRAN

ABSTRACT: The Chehelkureh Cu deposit is located NW of Zahedan (SE of Iran). Several stocks and dykes with granodiorite to quartz monzodiorite composition intruded the Eocene turbidites, and locally converted them to hornfels. Hypogene alteration consists of chloritization, carbonatization, silicification, kaolinization, sulfidization, and sericitization. Electron microprobe (EPMA) data show that carbonate compositions in the Chehelkureh deposit range from dolomite to ankerite, siderite, and magnesite. Replacement textures are present and oscillatory zoning apparently occurred during crystal growth in response to changes in temperature and composition of hydrothermal fluids. Temperatures derived from the ankerite-siderite geothermometer are 450° to 250°C and generally consistent with those from fluid inclusions and oxygen isotopes. The MnO and SrO contents of carbonate minerals in samples are up to 5.4 wt% and 0.2 wt%, which indicate at least parts of these carbonates were from hydrothermal fluids with an igneous origin, consistent with carbon isotopes results.

KEYWORDS: *chemical composition, carbonates, EPMA, Chehelkureh Ore Deposit, Iran*

INTRODUCTION

Chehelkureh is an ancient copper mine in Kuh-e-Lunka area, located 120 km NW of Zahedan (SE of Iran) at the longitude of 060°07'28.8" E and latitude of 30°14'9.3" N. The Kuh-e-Lunka area is in the eastern part of Dasht-e-Lut, located near the border with Pakistan and Afghanistan (Maanijou 2007). The Chehelkureh ore field consists of numerous lenses and veins with irregular shapes. In spite of high contents of base metals, with an average of 4.1% Cu+Zn+Pb, and Ag (average 22 ppm), they are poor in Au (average 0.14 ppm in 45 samples).

Carbonate mineralization is present in many hydrothermal deposits including base-metal veins and mesothermal gold deposits. In the Chehelkureh deposit, carbonate minerals occur in all host, altered and mineralized rocks. The ubiquitous occurrence of these minerals makes them potential indicators of changes in physical and chemical parameters during the evolution of the hydrothermal system. In this study we use chemical compositions of carbonates to

investigate the evolution of mineralization in Chehelkureh ore deposit.

GEOLOGICAL SETTING

The area is underlain by a sequence of Eocene intercalated greywackes, siltstones, and shales that host the ore deposit, and is bordered to the west by Cretaceous ophiolitic mélangé and to the east by Middle Eocene limestones (Valeh & Saeedi 1989). The Chehelkureh ore field is of complex shape with numerous, irregular lenses and veins. The ore field has an overall strike of N23°W and is displaced by faults striking roughly E-W (Maanijou *et al.* 2006). Several stocks and dykes of granodiorite to quartz monzodiorite and granite have intruded the sedimentary sequence of the area; they are oriented parallel to the major NW-SE fault set (Fig. 1).

The fault-fill mineralization includes quartz, dolomite, ankerite, siderite, calcite, molybdenite, pyrrhotite, arsenopyrite, pyrite, chalcopyrite, sphalerite, galena, selenian galena, marcasite, ilmenite, and rutile (Maanijou 2007).

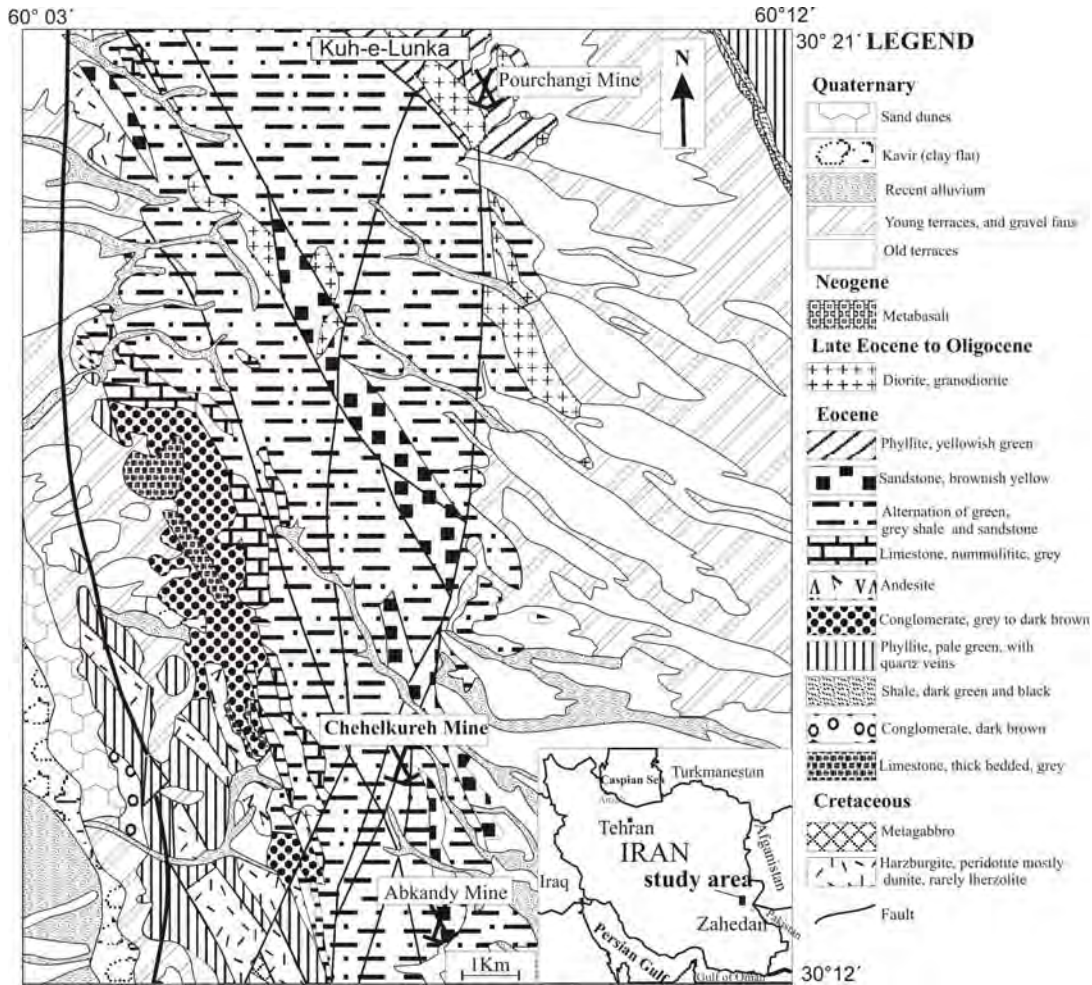


Fig. 1. Regional geological map of Chehelkureh polymetallic ore deposit (modified from Valeh & Saeedi 1989).

ANALYTICAL METHODS

One hundred samples were collected from drillholes, consisting of different lithologies, alteration, and mineralization. Polished thin sections were made from 70 samples of Chehelkureh rocks. Carbonates were analyzed for K, Na, Ca, Mg, Fe, Mn, Pb, Zn, Y and Sr using a JEOL-733 electron microprobe at the University of New Brunswick. An accelerating voltage of 15 kV with a beam current of 30 nA was applied (1µm beam) for a maximum count-time of 30 seconds.

CARBONATE OCCURRENCE AND PARAGENESIS

The carbonates typically occur as fine

grains disseminated throughout the matrix of greywackes and shales (turbidites), and as veins and veinlets. Veins and veinlets consist of coarser anhedral to subhedral carbonates with subordinate quartz in the center. Carbonate minerals also occur as complex intergrowths of siderite, magnesite, ankerite, and dolomite that contain abundant inclusions of quartz, chlorite, rutile, and pyrite. Most of the siderite and some of the ankerite were apparently consumed by sulfidation to pyrite, chalcopyrite, and other sulfides. There is also zoning in carbonates, which can be seen in veins and (or) at the scale of an isolated grain.

Oscillatory zoning apparently occurred during crystal growth in response to

changes in hydrothermal fluids (Fig. 2). Ca, Mg, and Fe mapping show the relative distribution of these elements in the grain. This compositional variation is attributed to episodic fluctuation in the temperature and composition of fluids in the Chehelkureh deposit.

CHEMICAL COMPOSITION OF CARBONATES AND CONCLUSIONS

The most important feature of mineral chemistry in carbonates of Chehelkureh deposit is the large range in the $\text{FeCO}_3:\text{MgCO}_3$ ratio which can indicate large variations in chemistry of hydrothermal fluids. Compositions extend along the magnesite-siderite join, from 22 to 72 mole% FeCO_3 (Fig. 3). Dolomite and ankerite compositions extend between 0 to 27 mole% FeCO_3 .

The major components CaO and MgO in dolomite have a minimal range indicative of very small variation in $\text{Ca}/(\text{Ca}+\text{Mg}+\text{Fe})$ ratios, whereas the minor elements such as SrO and MnO have a wide variation. Therefore trace components in carbonate minerals can be used as discriminant parameters to determine the origin of the carbonate rocks (cf. Yang & LeBas 2004). Compositional variation of carbonate minerals from Chehelkureh on the basis of MnO or SrO (wt%) versus $[\text{Ca}/(\text{Ca}+\text{Mg}+\text{Fe})]$ (atoms per formula unit, a.f.u.) diagrams (Fig. 4) show that the MnO and SrO contents in dolomite-ankerite are higher than those in siderite-magnesite and accessory calcite.

Calcite, ankerite, and dolomite in carbonates formed by hydrothermal fluids from mantle devolatilization usually contain higher MnO than SrO, indicating that Mn activity is relatively higher in the fluids (Yang & Le Bas 2004). Carbonates in veins and disseminated grains from Chehelkureh contain up to 5.4 wt% MnO and up to 0.2 wt% SrO, which suggests an igneous origin. Anovitz & Essene (1987) calibrated an ankerite-siderite geothermometer by fitting the Fe-Mg distribution constant (K_D) data for natural assemblages. Temperatures derived from the ankerite-siderite composition geothermometer in Chehelkureh deposit are generally consistent with those from fluid inclusions and oxygen stable isotope and are 450° to 250°C.

Ion microprobe analyses of *in situ*

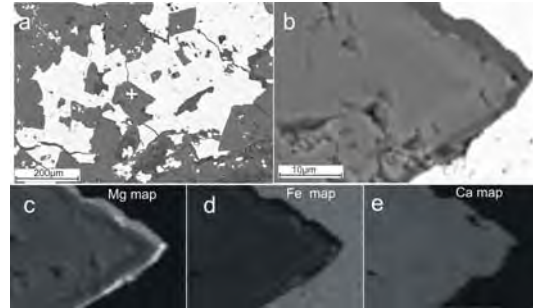


Fig. 2. EPMA back-scattered electron images of a polished section from Chehelkureh deposit. a) carbonate in a mineralized vein with chalcopyrite; b) larger image of carbonate grain marked by + in previous image, c), d) and e) are in turn compositional Mg, Fe and Ca images of that grain.

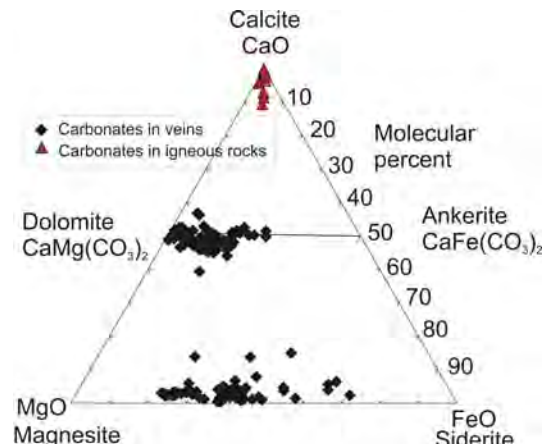


Fig. 3. Ternary plot of carbonate composition (EMP, mol%) in the Chehelkureh ore deposit.

accessory calcite grains in granites indicate relatively low Sr (120 to 660 ppm), negligible Rb and $^{87}\text{Sr}/^{86}\text{Sr}$ ratios equal to or higher than those of coexisting plagioclase (White *et al.* 2005). Sr content in the calcite of the Chehelkureh granitoids is relatively low. The ubiquitous nature of accessory calcite documented in this study implies late-magmatic growth or subsolidus replacement of igneous phases.

Mineral chemistry of carbonates of mineralized veins in the Chehelkureh ore deposit show that at least some of these carbonates were deposited from hydrothermal fluids of igneous origin, which is consistent with carbon isotopes results (Maanijou 2007).

REFERENCES

- ANOVITZ, L.M. & ESSENE, E.J. 1987. Phase equilibria in the system $\text{CaCO}_3\text{-MgCO}_3\text{-FeCO}_3$. *Journal of Petrology*, **28**, 389-414.

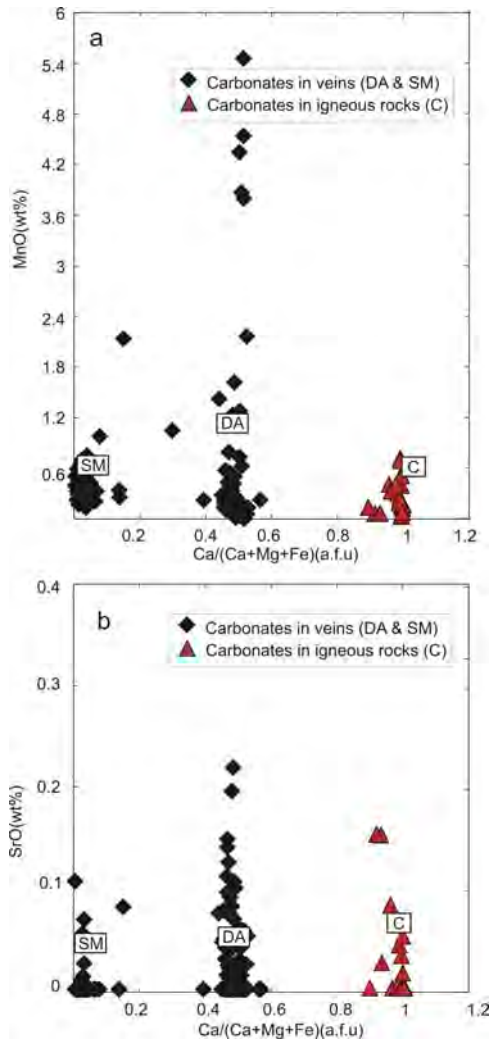


Fig. 4. Compositional variation of carbonate minerals from Chehelkureh on the basis of a) MnO (wt%) versus $[Ca/(Ca+Mg+Fe)]$ (atoms per formula unit, a.f.u.) diagram and b) SrO (wt%) versus $[Ca/(Ca+Mg+Fe)]$ a.f.u. diagram showed that there are three main groups: dolomite-ankerite (DA), siderite-magnesite (SM), and accessory calcite in igneous rocks (C).

MAANIJOU, M. 2007. *Geochemistry, origin of ore fluids, and formation of Chehelkureh copper deposit (NW of Zahedan)*. Ph.D. Thesis, Shahid Beheshti University, Tehran (in farsi with english abstract).

MAANIJOU, M., LENTZ, D., RASA, I., & ALETAHA, B. 2006. Petrography, Geochemistry and Geotectonic Environment of Arc-Related Granitoids in the Chehelkureh area, Southeast Iran: Implications for the Formation of the Polymetallic Ore Deposit in the Region. *12th IAGOD, Moscow*, 4 p.

VALEH, N. & SAEEDI, A. 1989. Geological map of Chehel Kureh. *Geological Society of Iran*, Sheet **8050**.

YANG, X.M. & LE BAS, M.J. 2004. Chemical composition of carbonate minerals from Bayan Obo, Inner Mongolia, China, implications for petrogenesis. *Lithos*, **72**, 97-116.

WHITE, A.F., SCHULZ, M.S., LOWENSTERN, J.B., VIVIT, D.V., & BULLEN, T.D. 2005. The ubiquitous nature of accessory calcite in granitoid rocks: Implications for petrogenesis. *Geochimica et Cosmochimica Acta*, **69**, 1455-1471.

Rare earth element variations in volcanogenic massive sulfides, Bathurst Mining Camp, New Brunswick: evidence from laser-ablation ICPMS analyses of phosphate accessory phases

Sean H. McClenaghan¹, David R. Lentz², & Wilfredo G. Diegor³

¹Geological Surveys Branch, New Brunswick Department of Natural Resources, P.O. Box 50, Bathurst, NB, E2A 3Z1 CANADA (e-mail: Sean.McClenaghan@gnb.ca)

²Department of Geology, University of New Brunswick, Fredericton, NB, E3B 5A3 CANADA

³Department of Earth Sciences, Memorial University of Newfoundland, St. John's, NF, A1B 3X5 CANADA

ABSTRACT: Chondrite-normalized REE profiles for massive sulfides exhibit a prominent positive Eu anomaly, with $(Eu/Eu^*)_N$ averaging 4.7, that correlates positively with Sn, Se, In, Co, Sc, and $(La/Lu)_N$, suggesting a hydrothermal influence on the enrichment of LREE and Eu. *In situ* analyses (n=112) of apatite, reveal elevated contents of Y, Sr, and REE with Σ REE contents averaging 1549 ppm. REE profiles for apatite display a prominent enrichment in Eu, with anomalies averaging 19 (as high as 222), that correlates with Sr and ratios of U/Th. REE profiles for xenotime (n=58) exhibit small positive Eu anomalies, averaging 3.4, broadly consistent with hydrothermal and diagenetic varieties of xenotime. Monazite analyses (n=140) exhibit enrichment in LREE and a prominent negative Eu anomaly, with $(Eu/Eu^*)_N$ averaging 0.52, consistent with a detrital signature that may mask hydrothermal components in massive sulfides of the Bathurst Mining Camp.

KEYWORDS: Rare-Earth-Elements, Phosphate, Bathurst Mining Camp, Volcanogenic Massive Sulfide, Laser Ablation ICP-MS

INTRODUCTION

The potential application of rare-earth elements (REE) as a hydrothermal tracer was originally investigated by Graf (1977), who first reported positive Eu anomalies in Algoma-type iron formation associated with volcanogenic massive sulfides (VMS) of the Bathurst Mining Camp (BMC), New Brunswick, Canada. It was also known that some REE, in particular Eu and the light rare earth elements (LREE), could be enriched in massive sulfides (Fig. 1), as well as their cogenetic stockwork sulfide complexes. Since then, similar REE variations have been reported in many ancient VMS deposits. Furthermore, measurements on hydrothermal fluids emanating from modern VMS systems on the seafloor have shown positive Eu anomalies, as well as LREE enrichment (Michard 1989).

Recent work (Peter & Goodfellow 2003) has documented the distribution of REE in iron formations of the BMC. Despite what is currently known of trace-element behaviour in exhalative sedimentary

systems (Gale *et al.* 1999; Spry *et al.* 2000) and footwall alteration zones (Lentz & Goodfellow 1996), there are few REE studies on massive sulfides. Moreover, mineralogical controls on REE distribution in zone-refined VMS deposits remain enigmatic. Elucidation of controls on REE distribution may enhance base-metal exploration in volcanic terrains.

GEOLOGICAL SETTING

VMS deposits of the BMC occur within a Middle-Ordovician bimodal volcanic and sedimentary sequence in the northern Appalachians of New Brunswick, Canada (Goodfellow & McCutcheon 2003). Volcanic rocks were emplaced between 472 and 455 Ma within an intra-continental back-arc basin (the Tetagouche-Exploits basin) at the eastern margin of the proto-Atlantic (Iapetus) Ocean (van Staal *et al.* 2003).

Syngenetic massive sulfides are largely concentrated along several prominent horizons corresponding to discrete breaks in volcanism, which are marked by the

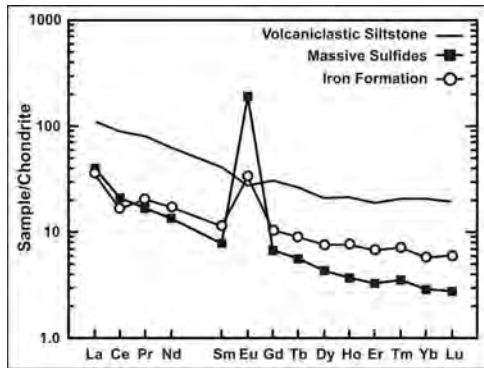


Fig. 1. Chondrite-normalized REE profiles for massive sulfides in the BMC.

accumulation of tuffaceous sedimentary rocks and locally Algoma-type iron formation (Peter & Goodfellow 2003).

Closure of the Tetagouche–Exploits basin by northwest-directed subduction from the Late Ordovician to Silurian led to incorporation of the back-arc terrain into the Brunswick subduction complex, accompanied by polyphase deformation and dominantly greenschist facies metamorphism (van Staal *et al.* 2003).

BULK GEOCHEMISTRY

Massive sulfides generally contain small quantities of REE compared to volcanic and sedimentary lithotypes; Σ REE contents average 33 ppm ranging from 0.93 to 263 ppm. Overall, Σ REE contents are strongly controlled by volcaniclastic material incorporated in massive sulfides during seafloor sedimentation. Consequently, there is a strong Σ REE correlation with Al_2O_3 ($r'=0.83$), TiO_2 ($r'=0.76$), Nb ($r'=0.82$), Th ($r'=0.87$), Y ($r'=0.86$), and Zr ($r'=0.73$).

Chondrite-normalized REE profiles (Fig. 1) for massive sulfides exhibit a prominent enrichment in LREE and Eu. The enrichment of LREE over the HREE is substantiated by strong positive Σ REE correlations with La, Ce, Pr, Nd and Sm, and a $(\text{La}/\text{Lu})_N$ ranging widely from 0.15 to 387. Europium anomalies are distinctly positive with $(\text{Eu}/\text{Eu}^*)_N$ averaging 4.7, but vary widely, ranging from 0.21 to 36. Minor negative Eu anomalies occur in semi-massive sulfides, due to dilution by volcaniclastic material. A positive

correlation of $(\text{Eu}/\text{Eu}^*)_N$ with Sn ($r'=0.43$), Se ($r'=0.32$), In ($r'=0.35$), Co ($r'=0.33$), and La/Lu ($r'=0.47$) suggests a degree of hydrothermal enrichment of LREE and Eu. Furthermore, a correlation between Σ REE and P_2O_5 ($r'=0.63$) indicates that hydrothermal REE signatures are strongly controlled by phosphate accessory phases.

MINERAL CHEMISTRY

Monazite

Monazite occurs as anhedral to subhedral masses associated with phyllosilicate-rich domains in massive sulfides. Masses display simple concentric zoning, a primary core, and commonly show fracturing and healing involving later generations of monazite growth that are likely a product of metamorphism (Fig. 2a).

Monazite has an average formula, $(\text{REE}_{0.89}\text{Y}_{0.03}\text{Th}_{0.03}\text{Ca}_{0.02}\text{Si}_{0.01})\text{P}_{1.01}\text{O}_4$ with REE dominated by La, Ce, and Nd, and notable contents of Y (1.5% Y_2O_3), Th (3.3% ThO_2) and U (0.19% UO_2). Chondrite-normalized REE profiles (Fig. 3) display a distinct enrichment in LREE with prominent negative Eu anomalies, which are broadly consistent with known profiles of monazite in metamorphosed terrains (Spear & Pyle 2002). The LREE contents of monazite have fairly restricted compositions dominated by Ce averaging 29.8% Ce_2O_3 and behaving sympathetically with contiguous LREE, exhibiting a positive correlation with La ($r'=0.61$), Nd ($r'=0.46$), and Pr ($r'=0.38$). Overall, Σ REE contents average 61.1%, ranging from 55.4 to 67.6% REE_2O_3 and display a negative correlation with Th ($r'=-0.86$), Ca ($r'=-0.85$), Y ($r'=-0.75$), and Pb ($r'=-0.54$). Trace-element contents of monazite masses are variable with primary cores that are depleted in LREE and enriched in Y and Th; whereas, late rims and healed fractures of monazite possess the higher contents of LREE. Raw count data for single spot laser-ablation ICP–MS analyses of monazite display sympathetic zoning of Th, U, and most REE, with Eu displaying sharp signal spikes corresponding with the ablation of monazite rims. The presence of distinctive

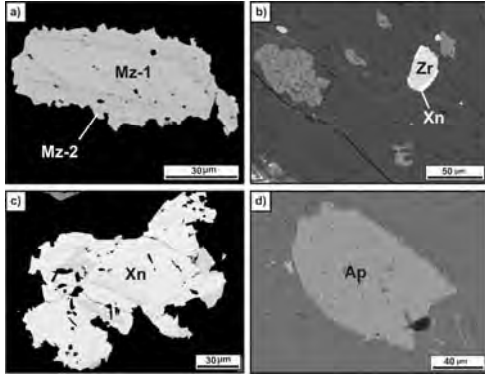


Fig. 2. SEM-BSE images of phosphate minerals in massive sulfides, (a) detrital monazite grain with a metamorphic rim, (b) detrital zircon grain with a xenotime rim, (c) complex zonation of a xenotime mass, and (d) apatite mass with a syntaxial overgrowth

spikes in Eu relative to LREE and HREE within monazite rims implies mobility of Eu during syn-metamorphic deformation.

Xenotime

Xenotime is the least abundant accessory mineral, occurring chiefly as small (<10 µm) overgrowths on detrital zircon grains (Fig. 2b). Zircon grains are likely detrital in origin based on their equant sub-rounded character and the deflection of a composite S_0/S_1 foliation, which is penetrative throughout the sulfide sections. Rare masses of xenotime can exhibit complex rhythmic (concentric) and irregular intergrowth zoning (Fig. 2c).

Analyses of xenotime provide an average formula, $(Y_{0.69}REE_{0.28})P_{1.01}O_4$ with contents of Y_2O_3 ranging from 34.5 to 42.6%; Y exhibits a positive correlation with Er ($r'=0.80$) and Yb ($r'=0.80$). Compositional zonation of xenotime varies as a function of REE content, with marked enrichment of MREE and Th in the core of xenotime masses and correspondingly higher $(Gd/Yb)_N$, averaging 2.3. In contrast, xenotime rims are enriched in Y and HREE, with lower ratios of $(Gd/Yb)_N$ averaging 1.0. Chondrite-normalized REE profiles (Fig. 3) display a characteristic “dogleg” pattern (Spear and Pyle, 2002) with enrichment in HREE relative to LREE and La, Ce, and Pr largely below the detection limits of the electron microprobe.

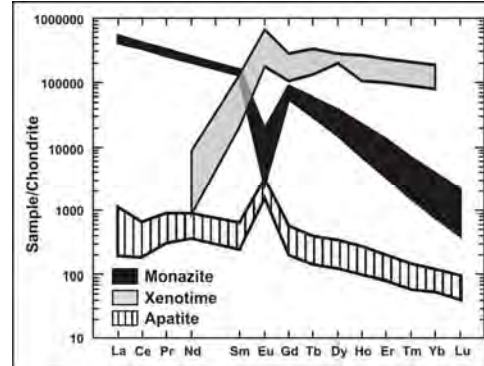


Fig. 3. Chondrite-normalized REE profiles for phosphate minerals in massive sulfides, BMC.

Profiles also exhibit small positive Eu anomalies, with values of $(Eu/Eu^*)_N$ averaging 3.4, and exhibiting a positive correlation with U ($r'=0.44$). Unlike monazite, xenotime has limited amounts of the actinide-series elements with ThO_2 averaging 0.33% and exhibiting a positive correlation with U ($r'=0.75$) and SiO_2 ($r'=0.61$). This suggests coupled substitution as thorite, $ThSiO_4$ or huttonite, $(Th,U)SiO_4$, which are isostructural with xenotime. Contents of REE, Th and U are broadly consistent with documented signatures for hydrothermal and dia-genetic varieties of xenotime (Spear & Pyle 2002); whereas, igneous varieties typically possess much higher contents of U and Th, and prominent negative Eu anomalies.

Apatite

Apatite is the most abundant phosphate mineral in exhalative sedimentary rocks of the BMC (Peter & Goodfellow 2003). Apatite occurs as fine- to medium-grained anhedral masses (Fig. 2), commonly 50 to 100 µm in diameter with rare masses reaching 1 mm in size. A composite S_0/S_1 foliation is deflected around apatite grains with the development of phyllosilicate- and quartz-rich pressure shadows. Extensive solution transfer during D_1 has led to continuous growth of apatite masses, resulting in syntaxial overgrowths that truncate the S_0/S_1 foliation and pre-deformation grain boundaries marked by distinct inclusion trails (Fig. 2).

Analyses revealed a fluor-apatite composition with an average formula,

$\text{Ca}_{5.02}\text{P}_{2.94}\text{O}_{11.9}(\text{F}_{1.02},\text{Cl}_{0.002})$. Overall, Y and REE account for the largest amount of elemental substitution into fluor-apatite. Contents of Y average 510 ppm, exhibiting a positive correlation with ΣREE ($r'=0.65$), in particular Ho ($r'=0.92$). ΣREE contents in apatite average 1549 ppm with values as high as 24,038 ppm. Contents of Eu average 295 ppm (range from 7.8 ppm to 1554 ppm) and exhibit a positive correlation with Sr ($r'=0.50$) and to a lesser degree the MREE. Chondrite-normalized REE profiles display a prominent enrichment in Eu, with anomalies $(\text{Eu}/\text{Eu}^*)_{\text{N}}$ averaging 19.0 (as high as 222), suggesting high temperature ($>250^\circ\text{C}$) and/or low pH hydrothermal conditions. Chondrite-normalized HREE contents exhibit a consistent decrease in abundance with increasing atomic number producing a negative slope with $(\text{Gd}/\text{Yb})_{\text{N}}$ averaging 5.8 and ranging from 0.70 to 24.7. Chondrite-normalized LREE generally increase in abundance with atomic number with $(\text{La}/\text{Sm})_{\text{N}}$ averaging 0.64, but exhibit considerably higher variability, ranging from 0.02 to 3.5. REE profiles can also exhibit small negative $(\text{Ce}/\text{Ce}^*)_{\text{N}}$ anomalies likely imparted during the mixing of hydrothermal fluids with seawater at or near the seafloor.

CONCLUSIONS

Contents of REE in massive sulfides from the BMC are strongly controlled by the abundance of and REE concentrations in phosphate minerals, specifically apatite, xenotime and monazite. Strong positive Eu anomalies in apatite, account for the anomalous Eu signatures of exhalative sulfides; whereas REE in monazite masses are largely reflective of detrital sources and may mask hydrothermal signatures. Limited release of mobile trace elements (LREE and Eu) during greenschist facies metamorphism has partly modified REE profiles for VMS deposits of the BMC.

ACKNOWLEDGMENTS

Electron-microprobe analyses were conducted with the assistance of Douglas Hall (UNB). Laser-ablation ICP-MS

analyses were performed at MUN and facilitated by Paul Sylvester and Mike Tubrett. This project was funded by an NSERC-CRD grant to David Lentz and the NB Department of Natural Resources.

REFERENCES

- GALE, G.H., DABEK, L.B., & FEDIKOW, M.A.F. 1999. The application of rare earth element analyses in the exploration for volcanogenic massive sulfide type deposits. *Exploration and Mining Geology*, **6**, 233-252.
- GOODFELLOW, W.D. & MCCUTCHEON, S.R. 2003. Geologic and genetic attributes of volcanic sediment-hosted massive sulfide deposits of the Bathurst Mining Camp, northern New Brunswick – a synthesis. *Economic Geology Monograph*, **11**, 245-302.
- GRAF, J.L. 1977. Rare earth elements as hydrothermal tracers during the formation of massive sulfide deposits in volcanic rocks. *Economic Geology*, **72**, 527-548.
- LENTZ, D.R. & GOODFELLOW, W.D. 1996. Intense silicification of footwall sedimentary rocks in the stockwork alteration zone beneath the Brunswick No. 12 massive sulphide deposit, Bathurst, New Brunswick. *Canadian Journal of Earth Sciences*, **33**, 284-302.
- MICHARD, A. 1989. Rare earth element systematics in hydrothermal fluids. *Geochimica et Cosmochimica Acta*, **53**, 745-750.
- PETER, J.M. & GOODFELLOW, W.D. 2003. Hydrothermal sedimentary rocks of the Heath Steele Belt, Bathurst Mining Camp, New Brunswick: Part 3. Application of mineralogy, mineral chemistry and bulk compositions to massive sulfide exploration. *Economic Geology Monograph*, **11**, 417-434.
- SPEAR, F.S. & PYLE, J.M. 2002. Apatite, monazite and xenotime in metamorphic rocks. In: KOHN, M.J., RAKOVAN, J. & HUGHES, J.M. (eds.), *Phosphates – geochemical, geobiological, and materials importance*. *Reviews in Mineralogy & Geochemistry*, **48**, 293-335.
- SPRY, P.G., PETER, J.M., & SLACK, J.F. 2000. Meta-exhalites as exploration guides to ore. *Reviews in Economic Geology*, **11**, 163-201.
- VAN STAAL, C.R., WILSON, R.A., ROGERS, N., FYFFE, L.R., LANGTON, J.P., MCCUTCHEON, S.R., MCNICOLL, V., & RAVENHURST, C.E. 2003. Geology and tectonic history of the Bathurst Supergroup, Bathurst Mining Camp and its relationship to coeval rocks in southwestern New Brunswick and adjacent Maine – a synthesis. *Economic Geology Monograph*, **11**, 37-60.

Controls and consequences of intrusion-related Au deposition at the Morila Au Mine, SW Mali

Christopher R.M. McFarlane¹, Karen Grey¹, & David Lentz¹

¹Geology Department, University of New Brunswick, 2 Bailey Drive, Fredericton, NB, E3B 5A3 CANADA
(e-mail: crmm@unb.ca)

ABSTRACT: The Morila Au deposit, southern Mali, is interpreted as a Paleoproterozoic intrusion-related gold system. Morila is hosted by immature volcanoclastic rocks that contain abundant fine-grained hypabyssal mafic intrusions that appear to have served as the main chemical traps for subsequent Au mineralization. Early low-grade Au mineralization was synchronous with ductile shearing and biotitization of the host rocks. This package was subsequently tectonically imbricated and contact metamorphosed under low-pressure amphibolite facies conditions. The main pulse of Au mineralization occurred after peak contact metamorphism and is associated with albitisation and low-T K-metasomatism along a NE-trending brittle fracture zone. Scheelite, as well as Bi-Te, Au-Sb, and Au-Ag alloys accompany auriferous arsenopyrite. A model involving magmatic-hydrothermal fluids derived from variably contaminated magmas generated from re-melting of metasomatized sub-arc mantle lithosphere appears to best satisfy the temporal, petrological, and geochemical constraints on Au mineralization.

KEYWORDS: West Africa, intrusion-related, gold, Birimian, Mali

INTRODUCTION

The >7 Moz Morila Au deposit, Mali, is an enigmatic member of a continuum of Au deposits now described across the West African Craton (Fig. 1). In contrast to more traditional shear zone-hosted and stockwork deposits, hydrothermal alteration and brittle structures at Morila are cryptic and there are no apparent lithological controls on mineralization.

Through the integration of field, microscopic, geochemical, and isotopic datasets we have identified Morila as a paleoproterozoic example of an intrusion-related Au system (IRGS, e.g., Hart 2007).

GEOLOGICAL SETTING

The host rocks to Morila are regionally equivalent to the Mesoproterozoic Birrimian basin and belt sequences exposed across the West African craton in Senegal, Mali, Cote d'Ivoire, Ghana and Burkina (Feybesse *et al.* 2006).

Regional Geology

The metasedimentary (volcanoclastic) sequence hosting Morila was deposited between 2160 to 2135 Ma, based on the

provenance of inherited zircon grains in metasediments in the immediate hangingwall of the deposit (Armstrong 2006). Nd-isotope model ages of ca. 2300 Ma for the same rocks attest to the juvenile nature of the Birimian crust in the area. This syn-rift period of sedimentation was associated with coeval emplacement of locally porphyritic hypabyssal mafic to intermediate dykes and sills, and was broadly coincident with the appearance of a series of juvenile island arc terranes that were subsequently amalgamated during the short-lived Eburnean Orogeny (ca. 2105-2090 Ma).

Deformation during the Eburnean Orogeny was regionally extensive. Exhumed paragneisses in Ghana record an early (2130-2105 Ma) high-temperature flat-lying ductile D1 phase of Eburnean deformation and metamorphism followed by broadly northeast-southwest directed folding and thrusting during a poorly-constrained D2 event (~2100 Ma?).

The final D3 phase of deformation is associated with a change to a transpressional kinematic regime. Whereas structures associated with

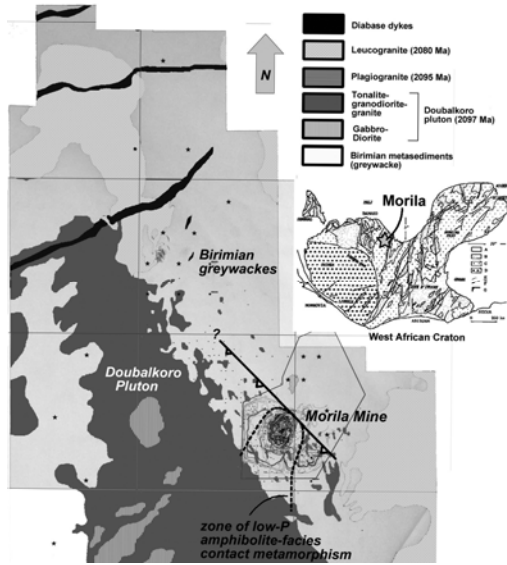


Fig. 1. Regional geology surrounding the Morila Au Mine, southern Mali. The deposit is hosted by immature Birimian metasediments and is proximal to a large composite post-Eburnean D2 pluton (Doubaikoro) and within a localized low-P contact aureole.

Eburnean D2 and D3 are well documented at Morila, evidence for early high-temperature ductile D1 deformation remains poorly documented.

In addition to the earliest syn-rift phase of hypabyssal magmatism, the host Birimian volcanoclastic rocks were intruded by a suite of syn- to post-Eburnean D2 plutons ranging in composition from diorite to granite. These magmas are calc-alkaline to alkaline (locally lamprophyric) and were emplaced as composite laccolithic plutons with associated dyke swarms. These composite plutons and dykes contain a variety of enclaves, xenoliths, and hybridized margins against host metasediments that record the effects of assimilation, contamination, and subsequent differentiation (AFC processes) of hybrid magmas.

A unique feature at Morila is the occurrence of locally abundant nebulous leucocratic veins that invade strongly foliated biotitized schists (Fig. 2).

Rather than partial melts derived from in-situ anatexis (i.e., leucosomes) these veins are trondhjemitic and represent distal magmatic injections from nearby

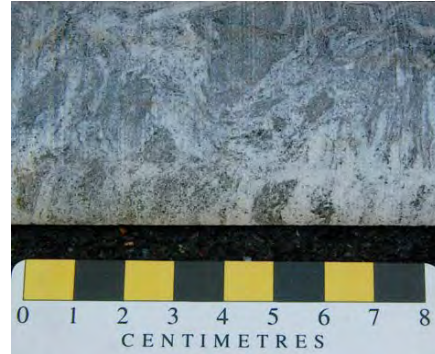


Fig. 2. Nebulous leucocratic veins representing magmatic-hydrothermal injections into hydrothermally-altered metasediments.

plutons.

Local Geology

A 10-20 m thick zone of low-grade disseminated Au mineralization (Fig. 3) broadly coincides with a sub-horizontal high-strain zone (Morila Shear Zone; MSZ) characterized by biotite schists with a sub-horizontal foliation that contains boudinaged and transposed milky white quartz veins, shallowly-plunging sheath folds, and translucent-grey quartz augen. The MSZ is locally proto-mylonitic to mylonitic as defined by elongate and rotated plagioclase porphyroclasts set in a very fine-grained matrix of dynamically recrystallized quartz and feldspar. Rather than a continuous through-going shear zone, the MSZ is now characterized by a network of anastomosing high-strain zones that may have been imbricated during Eburnean D2 or D3 deformation. Whereas biotite schists are the predominant lithology in the MSZ, dismembered, transposed, and metamorphosed enclaves of porphyritic mafic and intermediate intrusions are locally identifiable. Several lithogeochemical transects through the ore zone revealed elevated Cr, Ni, and V in ore zones suggesting a mafic protolith to the bulk of the mineralization.

The bulk of the Au mined at Morila was contained within a much narrower linear zone hosted within the MSZ. This north-northeast trending high-grade axis (HGA) was characterized by average Au grades >10 g/t with local intersections >100 g/t.

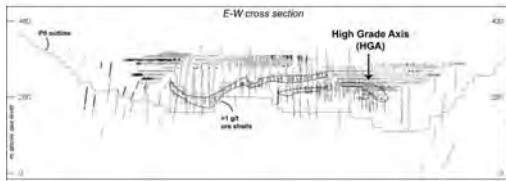


Fig. 3. E-W cross section through Morila showing the sub-horizontal attitude of the low-grade ore zones and the location of the HGA.

Mineralization along the HGA is contained primarily as Au blebs in post-D2 arsenopyrite porphyroblasts that overprint the main biotite foliation (MSZ, Fig. 4).

In addition to Au, a variety of Au-Sb, Au-Ag and Bi-Te alloys accompanied post-D2 arsenopyrite precipitation. Au and Bi-Te alloys are also locally concentrated in the biotite-rich margins of tonalite dykes that were contaminated by the host sediments. These alloys also appear to be concentrated within the HGA and are locally associated with disseminated scheelite and F-apatite. The latter also occur in late-stage veins that cross-cut weakly foliated granodiorite stocks that lie immediately beneath the HGA. A combination of BSE and CL imaging reveals that precipitation of these post-D2 sulfides and alloys occurred within a micro-porosity network that records dissolution-precipitation reactions involving quartz, plagioclase (albitised), and pyrrhotite (Fig. 5).

These textural observations suggest that the bulk of the mineralization at Morila was precipitated following low-P contact metamorphism and under relatively low fluid pressure conditions (i.e., no significant hydrofracturing).

CONCLUSIONS

The rocks at Morila record an intimate interplay between magmatism, contact metamorphism (and metasomatism), deformation, and mineralization. The spatial, temporal, and textural associations between contaminated post-D2 intrusions, contact metamorphism, and polymetallic post-D2 mineralization strongly suggests an intrusion-related origin for Morila. Other controls on Au mineralization include:

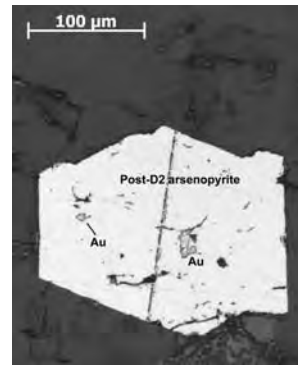


Fig. 4. Au blebs in post-tectonic arsenopyrite porphyroblast.

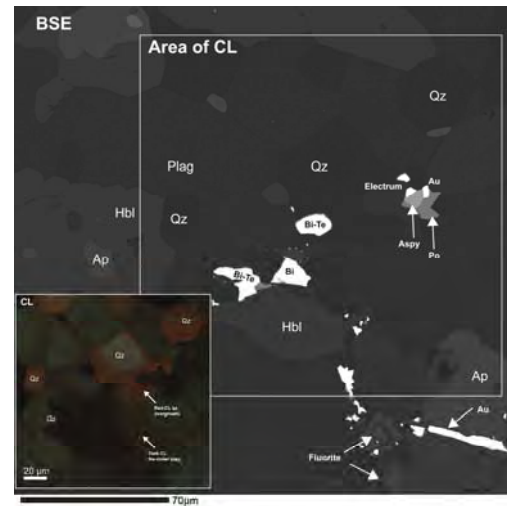


Fig. 5. SEM-BSE image showing Au, electrum, native Bi and BiTe alloys precipitated in an annealed amphibolite-facies metabasalt layer. The inset CL image reveals alloys and sulfides in contact with new generations of quartz (red) and plagioclase (dark) that records dissolution-precipitation reactions isolated along the grain boundaries of a previous annealed matrix.

- (1) Localization of Au precipitation in metabasaltic horizons.
- (2) Focusing of hydrothermal fluids below relatively impermeable greywacke hangingwall.
- (3) transfer of metals in high-T magmatic-hydrothermal veins.

Regionally, three magmatic processes are envisioned to have ultimately controlled mineralization at Morila: 1) re-melting of metasomatized lithospheric mantle during crustal-scale regional transpression; 2)

contamination and hybridization of magmas by relatively fertile immature rift-related sediments, and; 3) episodic magmatism and magma recharge over a ca. 10 Myr period following the waning phases of Eburnean D2.

ACKNOWLEDGEMENTS

We thank Paul Harbidge and Ken King (Randgold Resources Ltd), Tom Gell, and Sue Winkler (AngloGold Ashanti Ltd.), and the Government of Mali, for their support over the course of this project.

REFERENCES

ARMSTRONG, R. 2006. A Geochronological

Investigation of the Morila Gold Mine, Mali. PRISE (ANU, Research School of Earth Sciences) report #A03-220.

FEYBESSE, J.-L. *et al.* 2006. The paleoproterozoic Ghanaian province: Geodynamic model and ore controls, including regional stress modeling. *Precambrian Research*, **149**, 149-196.

HART, C.J.R. 2007. Reduced intrusion-related gold systems. In: Mineral deposits of Canada: A Synthesis of Major Deposit Types, District Metallogeny, the Evolution of Geological Provinces, and Exploration Methods. *Geological Association of Canada, Mineral Deposits Division, Special Publication No. 5*, 95-112.

Syenite, lamprophyre, and carbonatite dykes of the Moose Creek Valley, Ice River Alkaline Complex, southeastern British Columbia, Canada: implications for REE potential

Thomas R. Mumford¹, Dave R. Lentz¹, & Cliff S.J. Shaw¹

¹*Department of Geology, University of New Brunswick, PO Box 4400, Fredericton, NB, E3B 5A3 CANADA
(e-mail: thomas.mumford@unb.ca)*

ABSTRACT: The Ice River Alkaline Complex (IRAC) of southeastern BC is a well preserved bimodal Devonian-Carboniferous intrusion comprised of mafic-ultramafic and syenitic intrusive phases. Within the Moose Creek Valley there is an abundance of syenite, lamprophyre, and carbonatite dykes. The syenite dykes can be subdivided into three groups: nepheline syenite – nephelinolite group, syenite – monzodiorite group, and an alkali feldspar granite dyke. Two types of lamprophyres are present: sannaite and damtjernite, as well as calcio- and ferrocarnatites. Isotopic evidence suggests that the sannaite lamprophyres and syenite dykes are related to the partial melting of a depleted mantle source, the syenites are temporally related to the IRAC, and the ferrocarnatite displays an isotopically distinct signature.

KEYWORDS: *dykes, alkaline, carbonatite, syenite, lamprophyre*

INTRODUCTION

The Ice River Alkaline Complex (IRAC) in the western Main Ranges of the Canadian Rocky Mountains is a 29 km² J-shaped intrusion which comprises nepheline syenite and layered mafic sub-complexes intruded by a diverse swarm of dykes: syenitic, lamprophyric, and carbonatitic. Numerous geological investigations into the IRAC have resulted in a wide range of calculated ages, ranging from 165 to 459 Ma (Locock 1994). By focusing on the late dyke phases, it may be possible to constrain the age of the final period of magmatism associated with the IRAC, and provide insight into the parental source.

GEOLOGICAL SETTING

The IRAC is hosted in folded and faulted sedimentary rocks of Cambrian to lower Ordovician age (Currie 1975). These units are the slaty-limestone of the McKay Group (Cambro-Ordovician), massive limestone of the Ottertail Formation (Cambrian), and the sheared argillaceous rocks of the Cambrian Chancellor Formation (Allan 1914, Aitken & Norford 1967).

The IRAC was emplaced in a passive

margin setting, in the facies transition between shallow water carbonates and deeper water shales. During the Laramide orogeny (Cretaceous-Paleocene), the IRAC and host rocks were thrust approximately 200 km to the east, along a west-dipping décollement surface (Gabrielse 1991). During transport the IRAC acted as a relatively competent mass, whereas the host strata were mildly to strongly sheared (Currie 1975; Locock 1994). However, units near the margin of the IRAC, such as syenitic and lamprophyric dykes intruding the Ottertail Formation, are strongly deformed—often exhibiting boudinaged structures. The IRAC and host rocks have been regionally metamorphosed to prehnite-pumpellyite facies (Currie 1975).

Geology of the IRAC

The IRAC can be divided into four intrusive subunits, in order of emplacement these are: (1) an older feldspar-free layered mafic sub-complex (LMSC), (2) a large carbonatite lens, (3) a zoned nepheline syenite sub-complex (ZSSC), and (4) a dyke suite consisting of syenitic dykes, carbonatites, and alkaline

lamprophyres, as well as sodalite-bearing veins which cross-cut units of the complex and the host strata (Allan 1914; Currie 1975). The entire complex contains numerous veins, schlieren, and pegmatitic patches.

The feldspar-free LMSC consists of rhythmically layered sequences of: jacupirangite, ijolite, mela-ijolite, melanite ijolite, urtite, and wollastonite urtite (Currie 1975). These units are characterized by a lack of feldspar, and the presence of accessory primary calcite. Contacts between units are gradational, and grain size can vary widely within units.

The ZSSC consists of melano-leucocratic miaskitic nepheline syenite, with smaller quantities of sodalite syenite, peralkaline nepheline syenite pegmatites, zeolite syenite, and eudialyte syenite (Currie 1975; Locock 1994). The syenite sub-complex forms a roughly zoned, elliptical mass, which changes outwards from a pale green sodalite syenite core, to a leucocratic nepheline syenite, to a margin of melanocratic nepheline syenite.

Distribution of Dykes

The most pervasive late igneous feature in the eastern portion of the IRAC is the syenitic dyke swarm. The number of syenitic dykes is at least an order of magnitude greater than the lamprophyric dykes, and at least two orders of magnitude greater than the carbonatitic dykes. In its current orientation the syenitic dyke swarm displays a distinct NNW-trend, and the majority of the dykes dip southwest at moderate angles (35-65°), but shallow and near vertical dykes are observed. The dykes are typically light grey, fine-grained to pegmatitic, and range in width from 20 cm to >5 m. The exposed lateral extent of these dykes varies from a few metres to more than 200 m, where they typically either pinch out, or are covered in talus. Within the eastern portion of the IRAC, the syenitic dyke swarm cross-cuts the LMSC, ZSSC, and intrudes the Ottertail Formation. Within the dyke swarm, up to three different cross-cutting relationships have been observed

at a single outcrop, with contacts varying from sharp boundaries to diffuse margins.

Numerous aphanitic to fine-grained sannaite lamprophyres have been observed. They are dark grey to greenish, range in width from 15 cm to 3 m, and cross-cut the ZSSC, LMSC and Ottertail Formation. The lamprophyres all trend between ESE to WNW.

The contacts between lamprophyres and the IRAC range from planar to very irregular. The lamprophyres typically exhibit a chilled margin. However, at both the hand sample and thin-section scale, a sannaite lamprophyre sample exhibits a cusped boundary against a nepheline syenite dyke, indicative of two partially molten materials. Lamprophyre dykes cross-cutting syenitic dykes have also been observed.

Several carbonatite dykes/dykelets were observed; typically varying in width from 10 cm to 1.25 m, and from fine-grained to pegmatitic. The dykes generally have irregular contacts, and carbonatite dykes in the LMSC display evidence of a phlogopite-rich fenitization halo extending 1 to 5 m into the host rocks. There were no observed contacts between carbonatitic dykes and the syenitic dykes or lamprophyres, therefore no unambiguous order of relative emplacement can be determined for these units.

Petrography

Based on mineralogical and textural similarities (supported by geochemistry), the rocks of the syenitic dyke swarm can be subdivided into three groups: (1) nepheline syenite – nephelinolite group (NS-N), (2) syenite – monzodiorite group (SM), and (3) an alkali feldspar granite dyke.

The rocks of the NS-N dyke group range from nepheline syenite to sodalite-bearing nephelinolite. The primary phases in the NS-N dyke group are k-feldspar and nepheline, with variable abundances of amphibole, plagioclase, phlogopite, calcite, sodalite, titanite, cancrinite, apatite, clinopyroxene, zircon, chlorite, quartz, pyrochlore, and opaque phases.

The rocks of the SM dyke group range from mica syenite to mica rich nepheline-bearing monzodiorite. All observed SM dykes intrude the Ottertail Formation. The SM dyke group is characterized by a foliation (with exceptions) defined by the arrangement of kfs, pl, and white mica, also containing variable abundances of amp, ne, phl, cal, ttn, cpx, zrn, ep, qtz, and opaque phases.

All lamprophyres have been classified as sannaite lamprophyres, except an ultramafic damtjernite. The sannaite lamprophyres contain kfs, amp ± cal, cpx, phl, ap, pl, sodalite, ms, ttn, ep, white mica, chl, zrn, and opaque phases. The coarse-grained damtjernite consists of phenocrystic phlogopite, with groundmass calcite, alkali feldspar, and apatite.

Based on mineralogy the carbonatitic dykes have been classified as calciocarbonatites and ferrocarnatites; composed of cal ± kfs, phl, chl, ne, sodalite, and monazite.

Geochemistry

Overall the syenitic dykes are characterized by moderate silica contents (48 – 66 wt.%), CaO < Na₂O, low P₂O₅ (< 0.19 wt.%), TiO₂ (< 1.02 wt.%), MnO (< 0.3 wt.%), and a strong negative correlation between Al₂O₃ and MgO. Although generally enriched, the syenites have a wide range in ΣLREE (100–1970 ppm) and ΣHREE + Y (10–234 ppm) concentrations. The dykes range between peraluminous to peralkaline, with a subordinate number that are metaluminous. The dykes do not have strong europium anomalies; all Eu/Eu* values fall within 1.00±0.26. Relative to the SM group and alkali feldspar granite dyke, the NS-N group is characterized by lower silica contents (37–54 wt.%), enrichment in CaO, K₂O, Sr, and lower concentrations of Zr, Hf, U, Th, and Ta. The NS-N group is compositionally akin to the ZSSC, and are interpreted to be the result of periodic tapping of the ZSSC during formation.

The sannaite lamprophyric dykes are characterized by low silica (< 46 wt.%), CaO > Na₂O, low P₂O₅ (< 1.09 wt.%), and

strong negative correlation of MgO with SiO₂ and Al₂O₃. The ΣREE range between 337 – 507 ppm, and the (La/Yb)_{pm} values range between 22-32, indicating moderate LREE enrichment.

The carbonatites have a wide range in ΣLREE (150–25600 ppm) and ΣHREE + Y (60–1690 ppm) concentrations, and (La/Yb)_{pm} values range from 4 – 275, indicating weak to very strong LREE enrichment.

Sm-Nd and Rb-Sr isotopes

Sm-Nd isotopic data for the SM – NS-N syenite groups and sannaite lamprophyres are indistinguishable ($\epsilon_{Nd}=2.5$ to 4.0; based on an age of 368 Ma). Using the Rb-Sr data, the sannaite lamprophyres ($^{87}Sr/^{86}Sr_{368} = 0.70334 - 0.70392$) and NS-N dykes ($^{87}Sr/^{86}Sr_{368} = 0.70328 - 0.70431$) are also inseparable; however, the representative sample of the SM group is slightly lower ($^{87}Sr/^{86}Sr_{368} = 0.70291$).

As the sannaites have moderate to high Mg# (27-54), Nb/U (26-48), and no xenoliths (all consistent with minimal crustal contamination) they can be used to assess the nature of the mantle source. Regardless of the variation between groups, the low $^{87}Sr/^{86}Sr_{368Ma}$ values suggest that the sannaites (and syenites) were derived from partial melting in the mantle, and the ϵ_{Nd} values indicate that the mantle source was depleted relative to bulk earth.

The Sm-Nd data were used to create an isochron, which was used to derive and age (Fig. 1). The calculated age, 369±19 Ma, is in excellent agreement with the known age of the complex, 368±4 Ma (Parrish *et al.* 1987). This age is also consistent with our preliminary LA-ICP-MS zircon U-Pb dating of dykes in the SM and the NS-N groups.

Monazite crystals within the ferrocarnatite sample were dated using CHIME U-Th-Pb, and an age of 165±8 Ma was calculated. This age was used to evaluate the Sm-Nd ($\epsilon_{Nd} = -6.0$) and Rb-Sr ($^{87}Sr/^{86}Sr_{165} = 0.71061$) data; these values are considerably different than the syenites and the sannaites. The high initial $^{87}Sr/^{86}Sr$ and low ϵ_{Nd} indicate that the

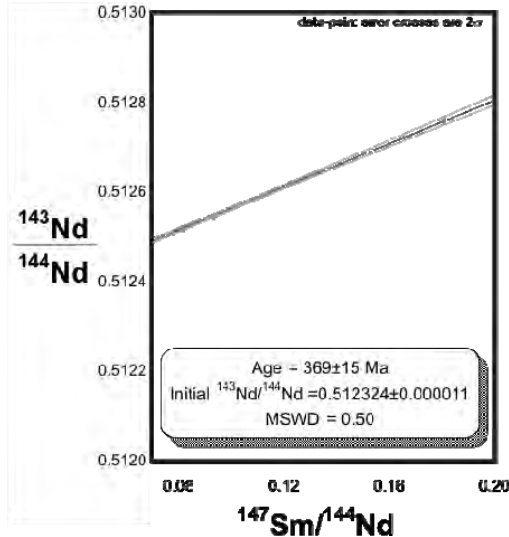


Fig. 1. Four point Sm-Nd isochron of the syenitic dykes (SM and NS-N groups).

carbonatite was derived from either a crustal source, or an enriched mantle source contaminated by crustal rocks, e.g., Ottetail Formation ($^{87}\text{Sr}/^{86}\text{Sr}_{165 \text{ Ma}} = 0.71206$, $\epsilon_{\text{Nd}} = -23$; Locock 1994).

CONCLUSIONS

- (1) The syenitic dyke swarm of the Moose Creek Valley can be subdivided based on mineralogy and geochemistry, into three groups: SM, NS-N, and an alkali feldspar granite dyke.
- (2) Isotopic data suggests that the sannaite lamprophyres and syenitic dykes are related to the same parental magma.
- (3) The SM and NS-N dykes are temporally related to the IRAC.
- (4) The ferrocarnatite is both isotopically and temporally distinct from the IRAC.
- (5) The carbonatites appear to have the

highest REE potential in the IRAC. However, as some REE-rich carbonatite dykes are related to separate magmatic event that occurred prior to the décollement, an undiscovered carbonatite body with REE potential may exist to the west.

ACKNOWLEDGEMENTS

We thank Eagle Plains Resources Ltd. for field area access, geochemical analyses, and financial support, specifically Jarrod Brown. Funding for this research was also provided by NSERC Discovery grants to D. Lentz and C. Shaw.

REFERENCES

- AITKEN, J.D. & NORFORD, B.S. 1976. Lower Ordovician Survey Peak and Outram Formations, southern Rocky Mountains of Alberta. *Bulletin of Canadian Petroleum Geology*, **15**, 150-207.
- ALLAN, J.A. 1914. Geology of field map-area, B.C. and Alberta. *Geological Survey of Canada, Memoir 55*, Ottawa, ON.
- CURRIE, K.L. 1975. The geology and petrology of the Ice River Alkaline Complex, British Columbia. *Geological Survey of Canada Bulletin 245*, Ottawa, ON.
- GABRIELSE, H. 1991. Structural Styles. In: GABRIELSE, H. & YORAT, C.J. (ed.), *Geology of the Cordilleran Orogen in Canada*. Geological Survey of Canada, Ottawa, ON, 81-98.
- LOCOCK, A.J. 1994. *Aspects of the geochemistry and mineralogy of the Ice River alkaline intrusive complex, Yoho National Park, British Columbia*. MSc thesis, University of Alberta, Edmonton, Alberta.
- PARRISH, R.R., HEINRICH, S., & ARCHIBALD, D. 1987. In: *Radiogenic Age and Isotopic Studies: Report 1*, Geological Survey of Canada, Paper **87-2**, 33-37.

Morphology of gold nanoparticles synthesised from gold chloride and gold cyanide complexes under evaporative conditions

Ryan R. P. Noble¹, Elizabeth M. Grenik^{1,2}, Robert M. Hough¹, Melvyn J. Lintern¹, David J. Gray¹, Rob Hart², Peta Clode³, & John Murphy³

¹CSIRO Exploration and Mining, 26 Dick Perry Avenue, Kensington, WA 6151 AUSTRALIA
(e-mail: ryan.noble@csiro.au)

²Centre for Materials Research, Curtin University of Technology, GPO Box U1987, Perth, WA 6845 AUSTRALIA

³Centre for Microscopy, Characterisation and Analysis, University of Western Australia, 35 Stirling Hwy, Crawley, WA 6009 AUSTRALIA

ABSTRACT: Single crystal, gold micro- and nano-particles were formed by evaporation of aqueous chloroauric acid and gold potassium cyanide. Gold crystal morphologies varied slightly with reaction time and temperature. In nearly all treatment combinations some micro and nano gold triangles and hexagons with face-centred cubic crystal system were present. Nanoparticles of Au were commonly observed in the 60-200 nm diameter size range. Characterization was conducted by UV-Vis spectroscopy, scanning electron microscopy with energy dispersive x-ray spectroscopy, transmission electron microscopy and confocal microscopy. The abundance of Au particles was low. However, the results of this work indicate that these morphologies are commonly and rapidly formed by evaporation, do not require bacteria, and have similar size distribution as those found naturally near a Au deposit in Western Australia. The results indicate that the formation of these natural crystals takes place very quickly (i.e., in a few hours or days). The inorganic process of groundwater evaporation is likely to be the major driving force for the formation of true secondary Au deposits in the vadose zone, particularly in arid and semi-arid regions of the world.

KEYWORDS: *gold, nano, particle, supergene, inorganic, Yilgarn Craton*

INTRODUCTION

Nano-particulate Au, with constrained morphology, has potential application in numerous fields. Bio-sensing, catalysis and optics (Shankar *et al.* 2004) are making use of nano-particulate noble metals.

Synthesis in solution of these nanoparticles has commonly used chloroauric acid, a reductant and a capping agent, with more recent developments utilizing organic ligands (Bi *et al.* 2008; Tan *et al.* 2003). The use of bacteria has also been associated with the formation of micro- and nano-particulate Au (Lengke *et al.* 2006; Southam & Beveridge 1994; Reith *et al.* 2006). Common gold crystal shapes (e.g., triangles and hexagons) have consistently been observed with these methods.

Recent work has identified populations of micro- and nano-particulate Au in natural supergene Au deposits (Hough *et*

al. 2008; Noble *et al.* in press). Natural supergene or secondary gold deposition occurs through weathering of the primary hypogene gold deposit and associated dissolution of the gold from the host quartz or sulfide primary minerals. The gold is remobilized in solution, transported and then redeposited via precipitation at a later stage.

Understanding the formation of micro- and nano-particulate gold may lead to a better understanding of supergene Au deposits, as well as the distance travelled and environmental conditions of mobilized Au (Noble *et al.* in press). This work has investigated the use of evaporation as the major process to form the Au morphologies observed. The influence of pH and ligand type on Au morphological variation has also been assessed.

MATERIALS AND METHODS

Experiments were conducted with

treatments varying in Au concentration, temperature of reaction, temperature of evaporation, time, organic additives and pH. The reagents used were: H₂AuCl₄ (Ajax); AuCl₃ (Alfa Aesar); KAuCN₂ (Johnson Matthey); millipore water (< 18 ohm); 0.1M HCl and 0.1M NaOH for pH adjustment of AuCl₃; 0.1M HNO₃, and 0.1M KOH for pH adjustment of KAuCN₂. In brief, 10 mL of Au-bearing solution was pipetted into a glass vial. The solution was then subjected to the various treatment parameters mentioned previously. Following this, 0.4 mL of the solution was pipetted onto glass slides (and carbon coated copper grids for Transmission Electron Microscopy - TEM) and left to evaporate at room temperature or on a hot plate at approx. 120°C in a fume hood. To confirm the absence of bacteria the slide was stained with SYTO[®] 9 green fluorescent nucleic acid stain.

UV-Vis absorbance of the solutions was measured on a Varian Cary 50 Spectrophotometer from 400-1000 nm at the initial introduction of solutions and at the end of the experiment.

Scanning electron microscopy (SEM; Philips XL-40) with an energy dispersive x-ray spectrometer (EDS) was used to obtain large scale images using the backscatter electron (BSE) detector and compositional data (EDS), operating at 30 kV. Field emission scanning electron microscopy (FESEM) images were collected on a model Zeiss 1555 VP-FESEM. An accelerating voltage of 3kV was used; this was adjusted to 1kV for some images to obtain true surface images during secondary electron imaging. For sample preparation the glass slides used previously, were subject to a thin carbon coating and were fixed on the edges using carbon tape.

TEM images were collected on a JEOL 2011 model at Curtin University Centre for Materials Research, Bentley, Australia.

SYTO[®] 9 stained fluorescence was imaged using a Leica TCS SP2 AOBS multiphoton confocal microscope.

RESULTS AND DISCUSSION

Single crystal, gold micro- and nano-

particles were formed by evaporation of aqueous chloroauric acid and gold potassium cyanide. Micro- and nano- gold triangles and hexagons with face centred cubic crystal morphology were observed. Nanoparticles of Au were commonly observed in the 60-200 nm diameter size range. Typical Au particles formed from AuCl₃ solutions are shown in Fig. 1. The experiments indicate that time in solution at a given temperature or pH condition did not greatly change the observed morphologies. Higher temperatures did result in fewer observed triangles.

In comparison to AuCN, AuCl₃ consistently produced greater numbers of Au triangles and hexagons. As expected, the more concentrated solutions produced greater numbers of Au particles. The dilute 5 ppm Au solutions were used for a more realistic comparison to natural solutions, although concentrations were still 2-3 orders of magnitude greater than those measured in the Golden Virgin pit, the site of naturally occurring particulate Au observed by Hough *et al* (2008).

The various experiments found populations of single crystal, Au particles. Sizes ranged from 20 µm to 60 nm. Numerous other Au-ligand salts were also present in varied morphologies.

The initial experiments conducted using H₂AuCl₄ and AuCN indicate that the particulate Au is not present in the solution, but is formed as a result of the concentration during evaporation. Later experiments with AuCl₃ solutions are similar to previous work in the area of materials science where nano-particles were shown to form in the solution as Au colloids formed with a resulting change in the solution colour as the reaction progresses, with colour controlled by the size of the colloidal Au (Shankar *et al.* 2004). Using evaporation as the mechanism of formation and the more acidified conditions similar to that of the southern Yilgarn groundwater environment, the absorption did not change during the experiments, indicating the Au is not colloidal during this time and formed after the solution was placed on the slide as a result of evaporation.

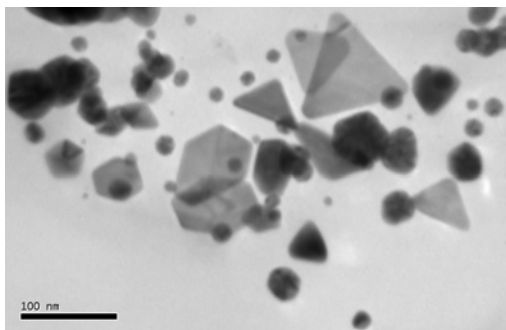


Fig. 1. Typical shapes of nanoparticulate gold formed from these experiments.

The size and nature of these Au populations is highly relevant to our understanding of partial extraction results of gold bearing regolith materials where interpretations of what Au is being extracted is key to the origin and exploration significance of the Au anomaly detected. It also supports a mechanism of colloidal transport of Au during supergene processes.

CONCLUSIONS

The results of this work indicate that triangular and hexagonal morphologies are commonly and rapidly formed by evaporation, do not require bacteria, and have similar size distribution as those found naturally near a Au deposit in Western Australia. The inorganic process of groundwater evaporation is potentially the driving force for the formation of transported Au deposits in the vadose zone, particularly in arid and semi-arid regions of the world.

ACKNOWLEDGEMENTS

Michael Verrall and Greg Hitchen (CSIRO) assisted in SEM work. The National Measurement Institute allowed use of the absorbance spectrophotometer. Western

Australia Centre for Microscopy for access to facilities. Funding for this work was provided by CRC LEME and CSIRO Minerals Down Under Flagship program.

REFERENCES

- BI, Y.P. & LU, G.X. 2008. Morphological controlled synthesis and catalytic activities of gold nanocrystals. *Materials Letters*, **62**, 2696-2699.
- HOUGH, R. M., NOBLE, R.R.P., HITCHEN, G.J. *et al.* 2008. Naturally occurring transparent gold nanoplates and particles. *Geology*, **36**, 571-574.
- KAMAT, P.V. 2002. Photophysical, photochemical and photocatalytic aspects of metal nanoparticles. *Journal of Physical Chemistry. B*, **106**, 7729-7744.
- LENGKE, M.F., FLEET, M.E., & SOUTHAM, G. 2006. Morphology of gold nanoparticles synthesised by filamentous cyanobacteria for gold(1)-thiosulfate and gold(III)-chloride complexes. *Langmuir*, **22**, 2780-2787.
- NOBLE, R.R.P., HOUGH, R.M., & GRENIK, E.M. *in press*. Natural and experimental clues to understand the transport and deposition of supergene gold in Western Australia. Explore.
- REITH, F., ROGERS, S. L., MCPHAIL, D. C., & WEBB, D. 2006. Biomineralization of Gold: *Biofilms on Bacterioform Gold*. *Science*, **313**, 233-236.
- SHANKAR, S.S., RAI, A., ANKAMWAR, B., SINGH, A., AHMAD, A., & SASTRY, M. 2004. Biological synthesis of triangular gold nanoparticles. *Nature Mater.* **3**, 482-488.
- SOUTHAM, G. & BEVERIDGE, T.J. 1994. The in-vitro formation of placer gold by bacteria. *Geochemica Cosmochemica Acta*, **58**, 4527-4530.
- TAN, Y., DAI, X., LI, Y., & ZHU, D. 2003. Preparation of gold, palladium and silver nanoparticles by the reduction of their salts with a weak reductant – potassium bitartrate. *Journal of Materials Chemistry*, **13**, 1069-1075.

Coupled Micro-XRF elemental mapping and LA-ICP-MS geochemistry of pyrites to decipher the cause of gold precipitation in quartz-sulfide gold-bearing veins, Poderosa-Pataz district, Peru

Carlos Oré Sanchez¹ & Damien Gaboury^{1, 2}

¹ Université du Québec à Chicoutimi (UQAC), ² Laboratoire de métallogénie expérimentale et quantitative (LAMEQ), 555, boul. de l'Université, Chicoutimi, G7H 2B1 CANADA (e-mail: carlos.ore@uqac.ca)

ABSTRACT: The geochemistry of pyrite associated with visible gold particles was studied by micro-XRF mapping and in situ LA-ICP-MS analysis to unravel metal enrichments and relationships in the quartz sulfide veins of the Poderosa-Pataz gold district in Peru. Element mapping in pyrite surrounding gold grains ranging from 0.01 to 0.15 mm revealed the systematic enrichment of As around or very close to visible gold accumulation. These As-enrichment zones define discordant rims and corridors overprinting pyrite grains. LA-ICP-MS spot analyses, performed in and outside the As-enrichment, indicate that As is enriched by factors up to 2000X in association with gold. In As-rich zones, Au, Ag, Hg and Sb are enriched 10X whereas Zn, Cu, Cd, In and Sn are depleted by the same factor. The electrochemical precipitation of gold is proposed as the main mechanism because of the intrinsic link between gold grains and As-enrichment in pyrites. Secondary pyrite transformation by hydrothermal fluids with elevated As and Au, Ag, Hg and Sb have induced change in semiconducting properties of the pyrite grains resulting in the precipitation of “invisible gold” and accumulation of gold particles during the last stage of the hydrothermal fluid circulation.

KEYWORDS: *Micro-XRF, LA-ICP-MS, pyrite, gold, Peru*

INTRODUCTION

The association between gold and pyrite is very common for most hydrothermal gold deposits. Gold can occur as “invisible gold” in arsenic-rich pyrite and arsenopyrite, as well as visible accumulations along the pyrite grain boundaries and as fracture filling and inclusions in pyrite. The cause of gold precipitation in association with pyrite has significant implications for ore genesis and mineral exploration. In this paper, we present the results of a detailed study of gold-pyrite relationships from various quartz sulfide gold-bearing veins from the Poderosa-Pataz district. This district, located in the Eastern Andean Cordillera of Northern Peru, produced > 6 M oz of gold in the past ~100 years from more than 30 veins hosted by the 330-327 Ma calc-alkaline granodiorite-diorite Pataz batholite (Haeberlin *et al.* 2004).

METHODOLOGY

Textural association between pyrite and

gold were studied in 96 polished sections from 20 different veins covering 2500 m of vertical elevation and 13 km laterally in the district. From these samples, 30 pyrite-gold relationships, on 17 polished sections were studied in detail using an EDAX Eagle III micro-XRF at UQAC. Detailed images of Mo, Ag, Sb, Cr, Fe, Co, Ni, Cu, As and Pb element distribution in pyrites with resolution of about 50 µm were produced over sample areas as large as 1 cm x 1 cm around visible gold grains (Fig. 1). The four most representative polished sections were studied by LA-ICP-MS at UQAC to obtain quantitative analyses of Ag, As, Au, Bi, Cd, Co, Cu, Ga, Ge, Hg, In, Mo, Ni, Pb, Sb, Se, Sn, Te, Th, Tl, W, U, and Zn. A total of 155 spot analyses, with spot diameter of 50 µm, were performed in pyrite grains close to visible gold particles. Analytical parameters and apparatus specifications are given in Gaboury & Graham (2004). The MASS-1 (Wilson *et al.* 2002; Tubrett *et al.* 2003) was used as a calibration standard for quantitative analyses. The data were

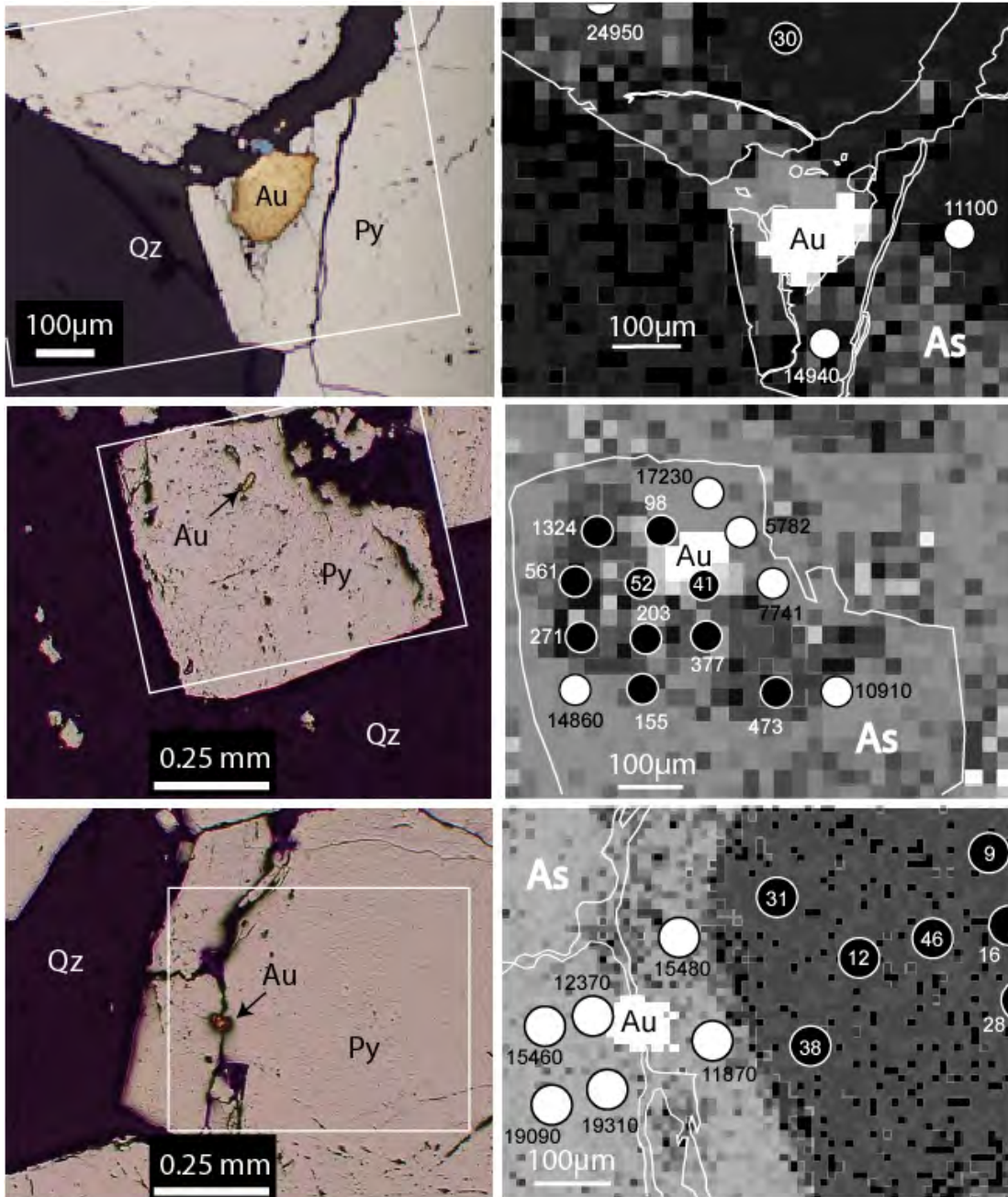


Fig. 1. Left side: microphotographs of visible gold occurrences in relation to pyrite crystals. Right side: related micro-XRF elemental mapping of As and spot location of LA-ICP-MS analyses with As values (ppm). The exact location of the micro-XRF map is indicated by the white square on the microphotographs (left side). On right side images, the light grey pixels indicate a relative enrichment of As in pyrites. For reference, the white contorted lines are the pyrite crystal borders. White and black spots are As-rich and As-poor portions of pyrites respectively. Note the discordant aspect of the As-enrichment corridors relative to the pyrite crystals and the sharp transition from As-poor and As-rich zones indicated by the LA-ICP-MS analytical As values.

reduced using the Thermo Plasmalab software version 2.5.5. Blank signal was

collected during 30s and ablation signal during 90s hence providing a time-

resolved signal. Calculation areas on the ablation signal were selected by considering consistency of As and Au signals. Sparks of Au-Ag signal related to inclusions were not included in the calculation. Analytical precision based on replicate analysis of the MASS-1 is better than 10%.

RESULTS

Under the microscope, gold forms visible particles ranging in size from 0.01 to 0.15 mm. Based on 839 observations of gold grains, it is established that visible gold occurs mostly 1) as fracture filling and inclusions in pyrite and at the interface between pyrite crystals (86%); 2) at the contact between pyrite and other sulfides (8%) such as arsenopyrite and chalcopyrite; and 3) in gangue minerals (6%).

The most striking outcome of the micro-XRF elemental mapping is the systematic association of visible gold with enrichment of As in pyrite (Fig. 1). Four dominant geometries are observed: 1) aureoles surrounding gold particles occurring as inclusions and along microfractures in pyrite; 2) rims developed at the interface along pyrite grains; 3) rims along boundaries of single pyrite crystals; and 4) as discordant corridors overprinting aggregated pyrite grains.

Quantitative LA-ICP-MS analyses were performed according to the subdivision between As-rich and As-poor portions of pyrite grains as revealed by micro-XRF maps. Suites of elements can be distinguished relative to As-enriched zones in pyrites (Fig. 2): 1) Au, Ag, Hg, and Sb are enriched by a factor of about 10 relative to As-poor zones; 2) Pb, Bi, and Co are slightly enriched; 3) Ni, Se, Mo, Ge, Te and Ga remain constant; and 4) Zn, Cu, Cd, In and Sn are depleted. Spatially, the transition from As-enriched to As-poor zones in pyrite is very sharp (Fig. 1). In these examples, the bimodal

distribution of As is clearly evidenced by factors of enrichment up to 2000 relative to the background levels in pyrite.

DISCUSSION

There is an intrinsic association between visible gold accumulation and zones of As-enrichment in pyrites. These spatial relationships may be explained by the electrochemical precipitation model of Moëller & Kersten (1994). The model implies that a small difference in electrical potential, due to As enrichment, induces electrochemical precipitation and accumulation of gold. Arsenic zoning in pyrite is well documented for gold deposits and commonly occurs as oscillatory concentric bands. They are interpreted as the result of fluctuation of fluid composition and physico-chemical conditions during pyrite growth (e.g., Belcher *et al.* 2004). In our case, the As-zoning clearly overprints pyrite crystals and aggregates and appears controlled by anisotropies such as fractures and grain boundaries. The precipitation of “visible gold” is hence related to a secondary change in pyrite composition induced by later hydrothermal fluids. These later fluids in addition to As, were also enriched in Au, Ag, Hg and Sb.

CONCLUSION

The electrochemical precipitation of gold is considered here the main mechanism for gold precipitation. Such a mechanism can be viewed as a filter to extract gold in solution, even in low concentration, during hydrothermal fluid flow in the veins. It can also be considered as independent of physico-chemical condition variations, hence accounting for the vertically and laterally extensive gold mineralization in the prolific Poderosa-Pataz district. The most important contribution of our study lies in the fact that the As enrichment is not a primary feature of pyrite growth but

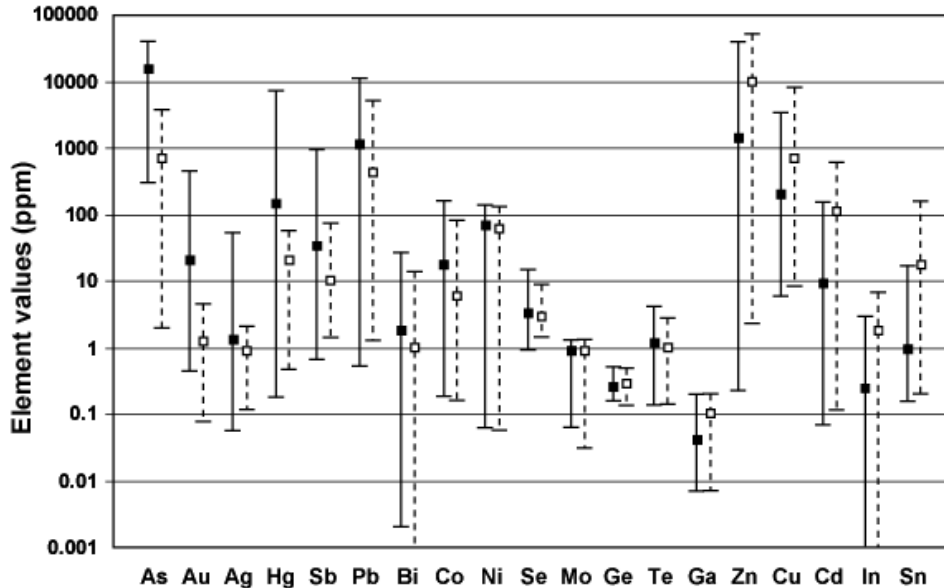


Fig. 2. Elemental range (line) and average (square dots) for LA-ICP-MS spot analyses in As-rich zones (black square: n = 96) and As-poor zones (open square and dashed line: n = 59) in pyrites. The order of elements follows the proposed suites of element behaviour relative to As enrichment (see text).

was rather induced by secondary fluid circulation. This conclusion highlights the critical role of arsenic for precipitating gold with pyrite even as a later overprint.

ACKNOWLEDGEMENTS

This is part of an ongoing PhD thesis by the first author. Funding is from Poderosa SA mining company (Peru) and NSERC grant to D. Gaboury. P. Bédard, R. Cox and D. Savard helped with the apparatus and data reduction.

REFERENCES

BELCHER, R.W., ROZENDAAL, A., & PRZYBYLOWICZ, W.J. 2004. Trace element zoning in pyrite determined by PIXE elemental mapping: evidence for varying ore-fluid composition and electrochemical precipitation of gold at the Spitskop deposit, Saldania Belt, South Africa. *X-Ray Spectrometry*, **33**, 174-180.

GABOURY, D. & GRAHAM, S. 2004. In-situ trace elements by LA-ICP-MS in metamorphosed pyrites as pathfinder for hydrothermal conditions. *Geochimica et Cosmochimica Acta*, Abstract of the 13th annual V.M.

Goldschmidt Conference Copenhagen, Denmark, June 5-11, 2004, A303.

HAEBERLIN, Y., MORITZ, R., FONBOTÉ, L., & COSCA, M. 2004. Carboniferous Orogenic Gold deposits at Pataz, Eastern Andean Cordillera, Peru: Geological and Structural Framework, Paragenesis, Alteration, and ⁴⁰Ar/³⁹Ar Geochronology. *Economic Geology*, **99**, 73-112.

MÖLLER, P. & KERSTEN, G. 1994. Electrochemical accumulation of visible gold on pyrite and arsenopyrites surfaces. *Mineralium Deposita*, **29**, 404-413.

TUBRETT, M., MIKOVA, J., SYLVESTER, P.J., & KOSLER, J. 2003. Trace element composition and homogeneity of MASS-1 sulfide calibration standard In: 5th International Conference on the Analysis of Geological and Environmental Materials, Rovaniemi. 9-11 June 2003 (<http://www.gsf.fi/geoanalysis2003/>)

WILSON, S.A., RIDLEY, W.I., & KOENIG, A.E. 2002. Development of sulfide calibration standards for the laser ablation inductively-coupled plasma mass spectrometry technique. *Journal of Analytical Atomic Spectrometry* **17**, 406-409.

IPGE (Os, Ir, Ru) are not in chromite

Philippe Pagé¹, Sarah-Jane Barnes¹, Michael L. Zientek²,
Hazel M. Prichard³, & Peter C. Fisher³

¹ Canadian Research Chair in Magmatic Metallogeny, Sciences de la Terre, Université du Québec à Chicoutimi (UQAC), 555 bld de l'Université, Saguenay, PQ, G7H 2B1 CANADA (e-mail: ppage@uqac.ca),

² U.S. Geological Survey, Spokane, Washington U.S.A

³ School of Earth and Ocean Sciences, Cardiff University, Main Building, Park Place, Cardiff, CF10 3YE UK

ABSTRACT: The correlation between Cr and IPGE (iridium-group platinum-group elements; Os, Ir, Ru, \pm Rh) and the similarity in the IPGE contents of chromitites from different settings suggest that the IPGE should partition into chromite. Experiments have shown that IPGE partition into spinel under oxidizing conditions. We have analyzed the IPGE in natural chromites using LA-ICPMS and can show that these elements are all below detection levels. Mass balance calculations show that chromite does not control the IPGE budget. Exsolution of IPGE from chromite in plutonic rocks is not a viable mechanism since we obtained similar results for chromite in lavas. IPGE are undetectable in chromite probably because they do not enter the chromite structure at geologically-realistic oxygen fugacities.

KEYWORDS: chromitite chromite, IPGE, PGM, oxygen fugacity, Laser-Ablation ICP-MS

INTRODUCTION

The well-known association between chromitite deposits and IPGE (Os, Ir, Ru, \pm Rh) enrichments (Page *et al.* 1982a, b; Stockman & Hlava 1984), as well as the similar IPGE contents between mantle chromitites and crustal chromitites (Fig. 1), have led researchers to suggest that IPGE partition into chromite. The fractionation of IPGE from Pt and Pd by chromite is used in petrogenetic modelling of stratiform PGE deposits.

This hypothesis has been reinforced by experimentalists who demonstrate that under oxidizing conditions ($fO_2 > FMQ+2$; FMQ: Fayalite-Magnetite-Quartz buffer) these elements can partition into spinel (Capobianco & Drake 1990; Capobianco *et al.* 1994; Richter *et al.* 2004; Homolova *et al.* 2008). However, laurite ([Ru, Os, Ir] S_2) and IPGE alloys are commonly present as small, discrete grains included within the chromites (Prichard *et al.* 1981; Stockman & Hlava 1984). Thus, there is some debate as to whether the IPGE enrichment of chromitites is due to partitioning of these elements into chromite or due to pre- to syngenetic laurite and/or alloys now included within chromite.

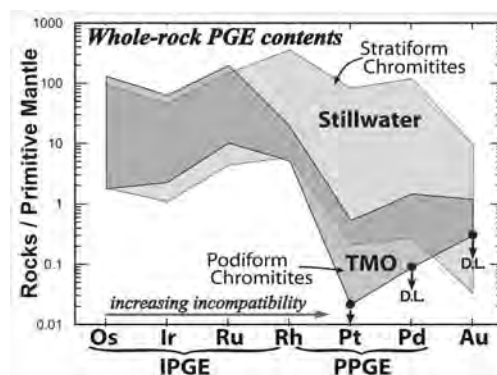


Fig. 1. Primitive mantle (PM) normalized whole rock PGE profiles for stratiform chromitites from the Stillwater Complex and for podiform chromitites from the mantle section of Theftord Mines Ophiolite (TMO). Note the similarity between IPGE contents of chromitites from these different tectonic settings. D.L.= detection limit.

The main purpose of this work is to determine the IPGE contents of chromites from mantle podiform chromitites, from crustal stratiform chromitites and from various types of lavas. The analyses have been carried out by laser ablation inductively coupled plasma mass spectrometer (LA-ICPMS) which allows *in-situ* determination of trace elements in chromite.

STUDIED SAMPLES

We analyzed chromites from 1) podiform chromitite deposits from the mantle section of the Thetford Mines Ophiolite (TMO), southern Québec Appalachians (Canada); 2) stratiform chromitite seams found within the Stillwater Complex, Montana (USA). In addition, we also analyzed chromite in lavas from different tectonic settings in order to: 1) verify whether the IPGE solubility in chromite could be related to geological setting and 2) eliminate recrystallization effects related to slow cooling which could be responsible for exsolution of the IPGE from chromite to form PGM (platinum-group minerals). The lavas we have analyzed to date are two boninites, (one from Bonin Island and the other from TMO), and a MORB from East Pacific Rise (Pagé 2001, 2006).

METHODOLOGY

Chromite major and minor element composition was determined by microprobe. The IPGE contents of chromite were determined at UQAC by a LA-ICPMS (Thermo X7 ICP-MS coupled to a New Wave Research 213 nm UV laser, 80 µm spot diameter, 10 Hz pulse rate, 0.3 mJ/pulse power). In addition to the IPGE other elements were monitored to control the nature of ablated material and the presence of included phases.

Whole rock Cr, Al, Mg, Fe, Co, Ni, Mn, V, Zn, and Sc of chromitites were determined by INAA; whole rock Ti and Ga were determined by XRF, and whole rock PGE were determined by Ni-sulfide fire assay followed by Te co-precipitation with ICP-MS finish.

RESULTS

Many inclusions of PGM were detected during ablation of chromite (Figs. 2 & 3). However, apart from the included PGM, the chromites do not contain any IPGE (detection limits for PGE: Os= 8.9 ppb, Ir= 3.0 ppb, Ru= 43.2 ppb, Rh= 15.9 ppb; Fig. 3).

A mass balance calculation was used to better understand the extent to which the IPGE are controlled by chromite. First, we

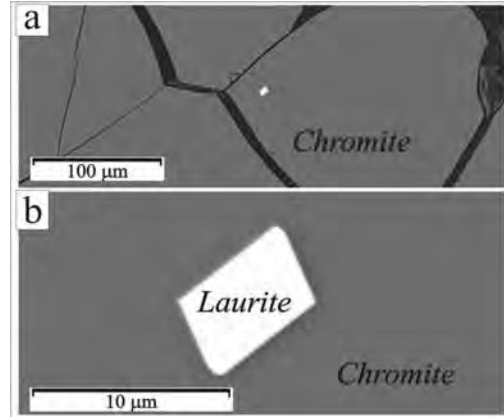


Fig. 2. Backscatter electron images of a laurite grain included within a chromite from Stillwater chromitite H. b) enlargement of transient LA-ICPMS signal shown in a).

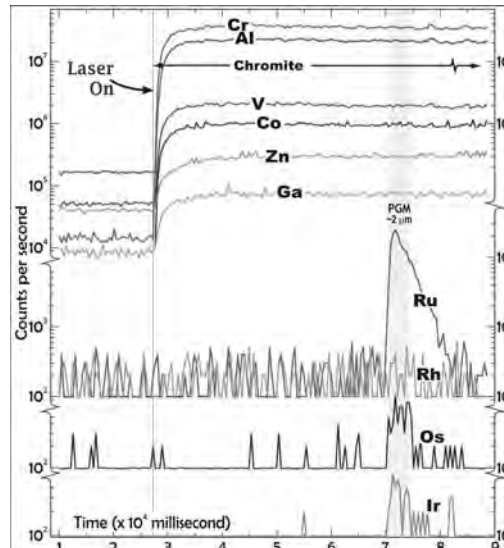


Fig. 3. Graph showing Cr, Al, V, Co, Zn, Ga, Ru, Rh, Os, and Ir profiles from a laser ablation analysis of chromite with counts per second vs time. Apart from a small Ru (\pm Os, \pm Ir)-bearing PGM inclusion (diameter \sim 2 µm), the chromites do not contain IPGE. Chromite sample is from a podiform chromitite from TMO.

calculated the weight fraction of chromite (F_{Chr}) in samples using the concentration of Cr_2O_3 in the whole-rock and in the chromite. Then, we evaluated the weight fraction of the different elements i from the whole rock that is present in the chromite and controlled by it using the equation:

$$F_{Chr}^i = 100 * (C_{Chr}^i * F_{Chr}) / C_{WR}^i \quad (1)$$

where F_{Chr}^i = % of element i in the whole-rock accounted for by the chromite, C_{Chr}^i = concentration of element i in the chromite, and C_{WR}^i = concentration of element i in the whole-rock (Table 1). Since IPGE were found to be less than detection levels, we used our LLD as the maximum IPGE content in the chromite. The calculations show that IPGE are not controlled by chromite.

In view of the presence of laurite and/or alloys, it can be concluded that these phases control IPGE abundance in chromitites.

DISCUSSION

One explanation to explain why IPGE are not detectable in chromite from plutonic rocks could be that the IPGE exsolve from chromite to form discrete PGM (now included within the chromite). However, if this were the case, it does not account for the source of sulphur found in the PGM (e.g., laurite). Nor does it explain the presence of Pt-bearing PGM, or composite PGM+silicate inclusions within chromite. Furthermore, if the IPGE are not detectable in chromite from plutonic rocks because of their exsolution to form PGM, they should be detectable in chromite from lavas but are not. It is most likely that the IPGE, at realistic oxygen fugacities, do not enter the chromite structure. This invalidates the results obtained from high oxygen fugacity partitioning experiments. Calculated oxygen fugacities from olivine-chromite pairs (Ballhaus *et al.* 1990) range from $0.61 < FMQ < +1.92$ for Stillwater chromitites, and from $-0.74 < FMQ < -0.05$ for TMO chromitites; these values are well below those reported from experiments that studied IPGE partitioning into chromite.

Chromite crystallization from a melt, or its re-equilibration with a melt, creates an even more reduced boundary layer at the crystal-melt interface as a consequence of the incorporation of Cr^{3+} and Fe^{3+} relative to divalent ions. The reduced conditions trigger the precipitation of IPGE minerals on the surface of crystallizing chromite that can be later on entrapped during chromite growth (Finnigan *et al.* 2008).

Table 1. Maximum proportion in % of WR IPGE accounted for by the chromite.

	Os	Ir	Ru	Rh	F_{Chr}
<i>Stillwater stratiform chromitites (n = 29)</i>					
Min	2.5	1.8	5.2	4.4	8.3
Max	27.0	19.0	29.0	49.7	97.3
Ave	11.0	7.9	15.6	22.4	65.7
<i>TMO podiform chromitites (n = 9)</i>					
Min	1.7	1.2	3.6	74.8	37.9
Max	61.2	17.4	40.2	133	86.7
Ave	24.0	7.6	20.2	111	62.6
<i>Various lavas</i>					
MORB	-	5.8	85.8	40.9	0.72
BONb	-	-	15.7	7.7	0.48
TMOb	-	9.8	33.1	10.2	0.36

CONCLUSIONS

We have evaluated the IPGE (Os, Ir, Ru, \pm Rh) content of chromite grains from chromitites and lavas in various tectonic settings using LA-ICPMS.

- (1) The concentrations of these elements in chromite are below detection limits. This cannot be attributed to the exsolution of IPGE from chromite to form PGM in slow cooling environments since similar results are obtained from chromite in rapidly cooled lavas.
- (2) Consideration of whole rock and chromite IPGE analyses, when combined in a mass balance calculation, shows that chromite does not control the IPGE budget.
- (3) IPGE solubility in chromite is favoured only at unrealistically high oxygen fugacity. In natural systems, chromite crystallization creates a reduction front that seems to trigger the precipitation of IPGE-bearing minerals on the chromite surface, in the boundary layer between the growing chromite and the surrounding melt (Finnigan *et al.* 2008).

ACKNOWLEDGEMENTS

J.H. Bédard, J.-M. Schroetter, A. Tremblay, and V. Bécu (INRS-ETE) are thanked for their help with mapping, and collecting samples during PP's PhD. P.L. Bédard, D. Savard and R.A. Cox (UQAC) are also thanked for their assistance with

the laboratory work and laser analysis. This work was funded by the Canadian Research Chair in Magmatic Metallogeny.

REFERENCES

- BALLHAUS, C., BERRY, R.F., & GREEN, D.H. 1990. Oxygen fugacity controls in the Earth's upper mantle. *Nature*, **348**, 437-440.
- CAPOBIANCO, C.H. & DRAKE, M. 1990. Partitioning of ruthenium, rhodium, and palladium between spinel and silicate melt and implications for platinum-group element fractionation trends, *Geochimica et Cosmochimica Acta*, **54**, 869-874.
- CAPOBIANCO, C.H., HERVIG, R.L., DRAKE, M. 1994. Experiments on crystal/liquid partitioning of Ru, Rh and Pd for magnetite and hematite solid solutions crystallised from silicate melt. *Chemical Geology*, **113**, 23-43.
- FINNIGAN, C.S., BRENNAN, J.M., MUNGALL, J.E., & McDONOUGH, W.F. 2008. Experiments and Models Bearing on the Role of Chromite as a Collector of Platinum Group Minerals by Local Reduction. *Journal of Petrology*, **49**, 1647-1665.
- HOMOLOVA, V., BRENNAN, J.M., McDONOUGH, W.F., & ASH, R. 2008. Olivine- and spinel-silicate melt partitioning of platinum group elements (PGEs) as a function of oxygen fugacity. *Geological Association of Canada / Mineralogical Association of Canada, Abstracts with program*, 74 p.
- PAGÉ, P. 2001. *L'origine de la distribution des teneurs en EGP dans les faciès mantelliques océaniques et ophiolitiques (exemples de la Faille Transformante Garrett, Pacifique sud et du massif de North Arm Mountain, Complexe Ophiolitique de Bay of Islands, Terre-Neuve, Canada)* M.Sc. thesis, Laval University, Québec, 414 p.
- PAGÉ, P. 2006. *Pétrogenèse de l'ophiolite de Theftford Mines, Québec, Canada, avec un accent particulier sur les roches du manteau et les chromitites*. Ph.D. thesis, Institut National de la Recherche Scientifique, Québec, PQ, Canada, 282 p.
- PAGE, N.J., CASSARD, D., & HAFFTY, J. 1982a. Palladium, Platinum, Rhodium, Ruthenium, and Iridium in chromitites from the Massif du Sud and Tiébaghi Massif, New Caledonia. *Economic Geology*, **77**, 1571-1577.
- PAGE N.J., PALLISTER J.S., BROWN M.A., SMEWING, J.D., & HAFFTY, J. 1982b. Palladium, platinum, rhodium, ruthenium and iridium in chromite-rich rocks from the Semail ophiolite, Oman. *Canadian Mineralogist*, **20**, 537-548.
- PRICHARD, H.M., POTTS, P.J., & NEARY, C.R. 1981. Platinum group element minerals in the Unst chromite, Shetland Isles. *Transaction of the Institution of Mining and Metallurgy (section B: Applied Earth Sciences)*, **90**, B186-B188.
- RIGHTER, K., CAMPBELL, A.J., HUMAYUN, M., & HERVIG, R.L. 2004. Partitioning of Ru, Rh, Pd, Re, Ir, and Au between Cr-bearing spinel, olivine, pyroxene and silicate melts. *Geochimica et Cosmochimica Acta*, **68**, 867-880.
- STOCKMAN, H.W. & HLAVA, P.F. 1984. Platinum-group minerals in Alpine chromitites from south-westren Oregon. *Economic Geology*, **79**, 491-508.

Aplitic dykes at the world-class Cantung tungsten skarn deposit: indicators of fluid flow and mineralizing processes

Kirsten L. Rasmussen¹, David Lentz², & Hendrik Falck³

¹University of British Columbia, 6339 Stores Road, Vancouver, BC, V6T 1Z4 CANADA
(e-mail: krasmusse@eos.ubc.ca)

²University of New Brunswick, 2 Bailey Drive, Box 4400, Fredericton, NB, E3B 5A3 CANADA

³Northwest Territories Geoscience Office, 4601-B 52nd Ave, P.O. Box 1500, Yellowknife, NT, X1A 2R3 CANADA

ABSTRACT: The Cantung mine (NWT) is one of the world's highest grade tungsten skarn deposits. At least six episodes of magmatism are evident underground: two unaltered and differentiated plutonic phases; three sets of highly differentiated felsic dykes emplaced mainly sub-parallel to folded bedding and affected by sporadic potassic ± white mica alteration; and a late set of extremely differentiated aplites that are pervasively calcic-metasomatized ± late white-mica alteration, and emplaced parallel to sub-vertical normal faults. Elevated grades of tungsten are empirically related to the aplite dykes. These late dykes originated from residual melt enriched in incompatible elements that evolved in a large, inwardly-crystallizing magma chamber. Due to an increase in volatile concentration with magma evolution, magmatic overpressuring initiated and propagated sub-vertical fractures into overlying rocks. Melt crystallized along the fractures by pressure-quenching and metal-rich magmatic fluid was brought into contact with reactive calcareous wallrocks to form tungsten skarn and a calcic magmatic fluid gradient that led to pervasive calcic metasomatism of the late aplites. The evolved and altered nature of the aplites reveals the existence of a large magmatic system at depth and provides information on the processes responsible for mineralization. These distinct aplites may be a useful tool for exploration.

KEYWORDS: *tungsten, skarn, aplite, Cantung, Cordillera*

INTRODUCTION

The northern Canadian Cordillera is one of the most well-endowed (richest) tungsten districts in the world (e.g., Dick & Hodgson 1982). The highest grade tungsten deposit in this district is the Cantung mine, a world-class tungsten skarn with recent reserve estimates of 2.9 Mt at 1.21%WO₃ indicated and 0.73 Mt at 0.74%WO₃ inferred (Clow *et al.* 2006), and over 4.6 Mt at 1.6%WO₃ removed prior to temporary mine shut-down in 2003 (Rasmussen 2004).

During mine operation from 1962-1986, researchers and mine geologists noted an empirical relationship between felsic dykes, or "aplites" and the localization of higher grade ore; this observation led to the hypothesis that the dykes may have played an important role in the formation of the deposit and perhaps could be used for exploration as indicators of tungsten-bearing fluid pathways (Atkinson 1984). However, this idea was not tested until

2003, due to a 15-year mine closure from 1986 to 2001.

GEOLOGICAL SETTING

Regional Geology

All of the significant tungsten deposits in the northern Cordillera are associated with intermediate to felsic, sub-alkaline plutons and batholiths of mid-Cretaceous age (e.g., Hart *et al.* 2004). This magmatism was emplaced well inboard of the ancestral North American margin, in a late- to post-collisional environment undergoing decompression-assisted partial melting of continental crust (e.g., Mair *et al.* 2006). Most of the intrusions associated with tungsten are very small, weakly to moderately peraluminous, K-feldspar-phyric to megacrystic, ilmenite- and biotite-bearing monzogranites (e.g., Hart *et al.* 2004). The Cretaceous magmatic rocks have intruded a thin veneer of Paleozoic, passive continental margin rocks, underlain by a thick

package of Proterozoic extension- or rift-related sediments that are in turn believed to be resting on thinned North American Archean to Paleoproterozoic basement.

Local Geology

Country rocks in the Cantung mine area consist of rocks typical of the Selwyn Basin, including turbiditic sandstone, deepwater limestone, chert, shale, and dolostone. Two ore-bearing calcareous units of the Sekwi Formation are bound by argillaceous rocks. In mine terminology, the “Swiss Cheese Limestone” (SCL) is a calcareous siltstone with chert nodules. The “Ore Limestone” (OL) conformably overlies the SCL, and is a pure, coarsely crystalline marble up to 50m thick.

Local strata were folded into a large NW-SE-trending syncline, and then refolded into a smaller, NE-SW trending overturned anticline that gently plunges to the northeast (Armstrong *et al.* 1983). Figure 1 is a generalized NW-SE section through the local geology. Five mine-scale, steeply dipping, brittle, NE-trending faults with small displacements cut the country rocks, intrusions, and skarn (Cummings & Bruce 1977).

Intrusive rocks at Cantung consist of the “Mine Stock”: a laterally extensive and flat-topped, biotite monzogranite with a fine-grained apical phase underlying the mineralization and local apophyses (inset; Fig. 1). The Mine Stock and country rock are cut by several pulses of aplitic to pegmatitic dykes. Although large quartz feldspar porphyry dykes are seen at the surface, the focus here is on dykes found underground. Quartz ± minor scheelite-chalcopyrite-biotite-tourmaline-powellite veins are sporadically exposed underground as sub-horizontal or bedding-concordant veins; a series of high-grade tungsten-mineralized, en-echelon quartz veins are exposed cutting the SCL in the floor of the Open Pit. Late lamprophyre dikes cut all the intrusions and the skarn.

Tungsten mineralization at Cantung is developed in two zones (Fig. 1). The Open Pit hosts anhydrous garnet-diopside skarn in the domed upper limb of the

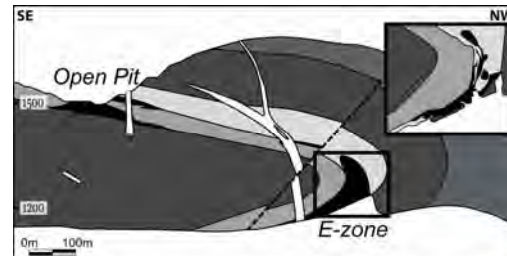


Fig. 1. General cross-section through the Cantung mine with upper right inset detailing typical E-zone geometry; ore zones are black and intrusive phases (including the underlying Mine Stock) are white (modified after Hodgson 2000).

recumbent fold (e.g., Crawford 1963). The underground E-zone ore is hosted within the OL in the hinge zone and the lower limb of the recumbent fold (Fig. 1). Although both anhydrous and hydrous skarn facies are found in the E-zone, the highest tungsten grades are associated with amphibole-pyrrhotite and biotite skarns. Skarn geometry in both zones includes irregularly shaped massive pods or lenticular wavy bands, is controlled by fractures, faults, and bedding planes, and is focused along the contacts of the OL.

Felsic Magmatic Episodes

There are six main textural, mineralogical, and morphological variations of felsic intrusions underground at Cantung:

- 1) medium-grained, K-feldspar megacrystic, hypidiomorphic-granular, biotite monzogranite (distal to skarn);
- 2) apical, fine- to medium-grained, sparsely K-feldspar-phyric, hypidiomorphic-granular, biotite monzogranite with minor secondary muscovite (proximal to skarn);
- 3) shallowly dipping, <20cm thick, fine-grained, sparsely K-feldspar megacrystic, biotite-rich monzogranite dykes with foliated biotite;
- 4) moderately dipping, <0.5m thick, fine-grained, biotite-poor, hypidiomorphic-equigranular monzo- to syeno-granite dykes;
- 5) moderately-dipping, <0.5m thick, fine-grained and foliated to pegmatitic, leucocratic, tourmaline-muscovite-garnet bearing, leucocratic dykes; and

6) syn-mineralization, steeply dipping, <0.25m thick, white, aplite dykes with tonalitic to dioritic chemistry.

All dyke sets are present as marginal phases to the Mine Stock proximal to skarn. Phase 6 dykes crosscut all other felsic dyke phases.

Structure

There are a few main structural trends that the underground dykes follow: (a) emplacement of phases 3, 4, and 5 predominantly sub-parallel to folded bedding planes near the apical Mine Stock (phase 2), or upper portions of the mine; (b) 115°-295°: emplacement of phases 4 and 5 sub-parallel to bedding in the lower recumbent fold limb (Fig. 2), or lower portions of the mine; and (c) 040°-220°: emplacement of phase 6 sub-parallel to the 5 mine-scale normal faults (Fig. 2), throughout the mine near the Mine Stock margins. Phase 6 dykes also offset other dykes and bedding in a normal sense.

Alteration

Several types of alteration in the intrusive phases are apparent from sample staining, petrography, geochemistry, and electron-probe microanalytical work. The main intrusive phases (1 & 2) are essentially unaltered, but phase 2 contains minor secondary muscovite; anorthite content in plagioclase is An_{41-45} , but approaches An_{49-55} (phase 2). Dyke phase 3 is similarly unaltered (An_{44}), except for cm-wide, bleached margins consisting of plagioclase (An_{56}) and quartz. Dyke phase 4 has been affected by early patchy to pervasive potassic alteration resulting in very fine-grained consertal and intergranular K-feldspar, and rare pale brown biotite veinlets or ragged grains. Several examples of dyke phases 4 and 5 also have very fine-grained, secondary white-green mica veins and plagioclase pseudomorphs.

Tonalitic phase 6 dykes are quartz- and plagioclase-rich (An_{43-49} ; up to An_{96-98} near skarn), and have undergone calcic metasomatism with replacement of K-feldspar by plagioclase and destruction of biotite. Dioritic phase 6 dykes are quartz

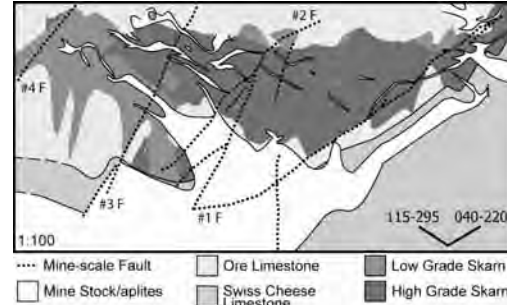


Fig. 2. Level plan showing the empirical relationship between high-grade skarn and dykes; two dominant trends of dykes, apophyses, and faults are apparent (Cantung Internal Files, 1981).

poor (<10%) and have also undergone pervasive calcic metasomatism, resulting in alteration of plagioclase (90-100%) to a range of compositions on the intra-grain scale (An_{39-98}), destruction of K-feldspar and biotite, and formation of minor epidote-group minerals, titanite, and apatite. The dioritic dykes are mineralized with calcite-titanite-pyrrhotite-chalcopyrite veinlets ± disseminated scheelite (5-90%) ± disseminated pyrrhotite (up to 40%). White-mica and calcite overprint the calcic mineral assemblage in all dioritic dykes.

Differentiation

Relatively low Ti/Zr ratios for the Mine Stock (~14-15) indicate a well-differentiated magma source. However, even lower Ti/Zr (~7-13) in the dykes, particularly phase 6, suggests that they originated from more evolved magmas. This differentiation is interpreted to have occurred gradually from normal magma crystallization processes.

INTERPRETATION

The felsic intrusive phases at Cantung provide information on a large and evolving magmatic system at depth. A highly differentiated, sub-horizontal magma body (phase 1) was emplaced into recumbently folded sedimentary rocks, accompanied by a finer-grained apical phase (phase 2) located near the fold hinge zone. A deeper source magma continued to evolve, crystallizing inward to form increasingly differentiated melts

enriched in incompatible elements, which were mainly emplaced sub-parallel to folded beds (phases 3, 4, & 5). Bleaching along the phase 3 dyke margins is due to interaction with calcic country rocks, and potassic alteration affecting phases 4 and 5 dykes is explained by pulses of hot magmatic fluids along the relatively permeable dykes. Extreme differentiation in the residual melt, due to a high degree of crystallization in the magma source region, led to an increase in fluid pressure. The resultant magma overpressuring resulted in the initiation and propagation of sub-vertical fractures and subsequent injection of highly differentiated melt and metal-rich magmatic fluid. A calcic fluid gradient developed between the aplite melt (phase 6) crystallizing by pressure-quenching, and calcareous country rocks reacting with magmatic fluid to form tungsten skarn, leading to pervasive calcic metasomatism of the aplites. Late white-green mica +/- calcite alteration affecting most dyke phases could be the result of interaction between the calcic fluids and minor influx of the last magmatic fluids.

The emplacement of extremely differentiated melts in association with high-grade tungsten skarn necessitates the existence of a large magmatic system at depth, capable of sequestering incompatible elements through normal crystallization processes prior to the main mineralization event. The aplites represent the most evolved melt extruded from the source magma, and as such their recognition has the potential to be a powerful tool in future exploration for tungsten mineralization at Cantung.

ACKNOWLEDGEMENTS

We thank North American Tungsten Corp., Dave Tenney, Bill Mann, Dan Kontak, and David Pattison for assistance. Funding for this project was provided by

the NWT Geoscience Office, the Aurora Research Institute Research Assistant Program, and the University of Calgary.

REFERENCES

- ATKINSON, D. 1984. Comments and observations on Cantung geology with comparison to Mactung based on March 19-22, 1984 mine visit. *Amex Northwest Mining Company Ltd. Inter-office memorandum*, 6 p.
- ARMSTRONG, D.W., HARRIS, F.R., KERRIGAN, J.E., KIEHN, O.A., & JOHNSON, R.E. 1983. Technological Assessment Report of Canada Tungsten Mining Corporation Ltd., Tungsten, NWT, Canada. *Amex engineering and management services company*, 184p.
- CRAWFORD, W.J.P. 1963. *Geology of the Canada Tungsten Mine, SW District of Mackenzie, Canada*. MSc thesis, University of Washington, Seattle, Washington.
- CUMMINGS, W.W. & BRUCE, D.E. 1977. Canada Tungsten - Change to underground mining and description of mine-mill procedures. *CIM Bulletin*, **70**, 94-101.
- DICK, L.A. & HODGSON, C.J. 1982. The MacTung W-Cu(Zn) contact metasomatic and related deposits of the northeastern Canadian Cordillera. *Economic Geology*, **77**, 845-867.
- HART, C.J.R., MAIR, J.L., GOLDFARB, R.J., & GROVES, D.I. 2004. Source and redox controls on metallogenic variations in intrusion-related ore systems, Tombstone-Tungsten Belt, Yukon Territory, Canada. *Transactions of the Royal Society of Edinburgh: Earth Sciences*, **95**, 339-356.
- HODGSON, C.J. 2000. Exploration potential at Cantung Mine, District of Mackenzie, NWT. *Andean Engineering*, 26p.
- MAIR, J.L., HART, C.J.R., & STEPHENS, J.R. 2006. Deformation history of the northwestern Selwyn Basin, Yukon, Canada: implications for orogen evolution and mid-Cretaceous magmatism. *GSA Bulletin*, **118**, 304-323.
- RASMUSSEN, K.L. 2004. The aplitic dykes of the Cantung Mine: petrography, geochemistry, and implications for the mineralization process. *University of Calgary, Calgary, Alberta*.

Geochemistry and genesis of a mafic-ultramafic hosted VMS occurrence, Marathon, Ontario

Marc L. Rinne¹, Peter N. Hollings¹, & Aubrey J. Eveleigh²

¹Department of Geology, Lakehead University, Thunder Bay, ON, P7B 5E1 CANADA
(e-mail: mrinne1@lakeheadu.ca)

¹Department of Geology, Lakehead University, Thunder Bay, ON, P7B 5E1 CANADA

²MetalCORP Ltd., 129 W. Frederica Street, Thunder Bay, ON, P7E 3V8 CANADA

ABSTRACT: The Big Lake volcanogenic massive sulphide (VMS) occurrence in the Schreiber-Hemlo belt of the Superior Province near Marathon, Ontario was discovered in March 2006. It is hosted in a mafic-ultramafic metavolcanic sequence lacking felsic volcanic or volcanoclastic rocks, as a surface of mineralisation and hydrothermal alteration currently defined over a plan area of approximately 0.5x0.5 km, subparallel to and 5-50 m below the base of a large ultramafic cumulate complex. Several arguments point to an overturned sequence, where VMS sulphides are stratigraphically above the ultramafic cumulates. Among other possibilities, a genetic relationship between these cumulates and the VMS is implied.

KEYWORDS: *volcanogenic massive sulphide, Superior Province, ultramafic, exploration geochemistry, Schreiber-Hemlo greenstone belt*

INTRODUCTION

The Big Lake Cu-Zn-Ag-Au volcanogenic massive sulphide (VMS) occurrence is hosted in mafic-ultramafic strata of the Schreiber-Hemlo greenstone belt near Marathon, Ontario (Fig. 1). This VMS is unusual in that it is one of a few documented VMS occurrences in sequences lacking felsic volcanic or volcanoclastic rock.

Three dimensional modeling and interpretation of whole-rock geochemical data were used to describe the setting and genesis of the occurrence, with the aim of clarifying how VMS mineralisation can occur in settings lacking felsic volcanic rock. Results of these models and geochemical data are presented here.

GEOLOGICAL SETTING

Regional Geology

The Wawa subprovince is a volcano-plutonic assemblage of 2.88-2.72 Ga rocks (Percival *et al.* 2006) accreted to the southern part of the Superior Province during the end of the Kenoran Orogeny, ca. 2.69 Ga. Extending approximately 1000 km from NE Minnesota to just south of James Bay, the Superior Province is

bounded to the north by the metasedimentary Quetico Subprovince and to the southeast by the Kapuskasing Structural Zone.

Local Geology

The Heron Bay assemblage is located in the southeast portion of the Schreiber-Hemlo Greenstone Belt of the Wawa Subprovince, south of the Hemlo Fault Zone and east of the Coldwell alkalic complex (Fig. 1). Mafic to ultramafic metavolcanic rocks of the Pulpwood-Playter Harbours sequence, located between the Pukaskwa and Heron Bay plutons, are host to the Big Lake VMS occurrence. The recently identified Big Lake Ultramafic Complex (BLUC) forms a prominent part of this host sequence, as an E-W striking sill-like body comprising laterally continuous sequences of ultramafic cumulates 200-350 m thick. The Big Lake VMS occurrence underlies the eastern margin of the BLUC (Fig. 1).

METHODS AND RESULTS

Scale of Study

Leapfrog software was used to generate lithological contacts and chemical

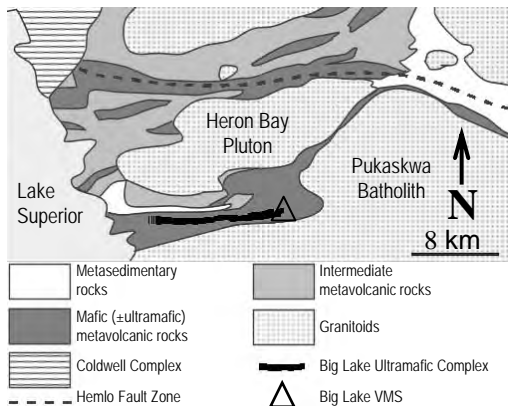


Fig. 1. Part of the Schreiber-Hemlo Greenstone Belt, showing the location of study. Modified after Polat *et al.* (1998).

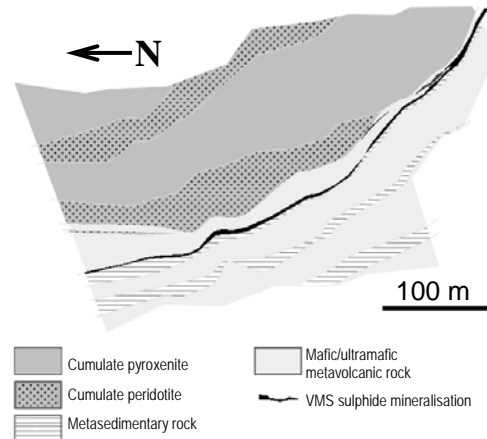


Fig. 2. Representative lithological section through the Big Lake Ultramafic Complex and Big Lake VMS occurrence.

distributions of the Big Lake VMS occurrence. Most modeling was restricted to 53 diamond drill holes over a plan area approximately 500 x 500 m and 400 m deep. Data used were compiled from MetalCORP assay and whole-rock sampling data, including 99 whole-rock metavolcanic samples and 60 whole-rock ultramafic cumulate samples.

Mineralisation and Lithostratigraphy

VMS mineralisation at Big Lake consists of stringer-textured to semi-massive pyrrhotite, chalcopyrite, and sphalerite, in decreasing order of abundance, at up to 80% sulphides by volume over a few metres. Best-mineralised intervals contain ~6 % Cu and ~2 % Zn weighted over five to ten metres, with significant enrichment in Au, Ag, and other metals.

The VMS sulphides define a broadly conformable sheet 5-50 m below the base of the BLUC. This synformal surface of mineralisation generally coincides with the transition from ultramafic cumulates and strongly foliated metavolcanic rocks to an underlying sequence of metavolcanic rocks and interflow metawacke and metasilstone rocks (Fig. 2). Sphalerite-pyrrhotite mineralisation in hydrothermal veins was also observed within the BLUC several km west of this study area.

Hydrothermal Alteration

Hydrothermal alteration, as defined by

chemical alteration indices or visual estimation in hand sample, is restricted to a few metres above visible sulphide mineralisation and may be a function of limited permeability in a flow-dominated setting, or some degree of tectonic shortening. The alteration mineral assemblages consist of chlorite, biotite, and anthophyllite, in decreasing order of abundance, and lack an appreciable zoning or strict relationship to metal contents. Veined talc was observed in some intensely altered intervals, though this may be of regional metamorphic origin.

Least-altered metavolcanic samples have Na₂O and MgO contents of 1.8-4.0 wt. % and 4-25 wt. %, respectively, whereas strongly altered samples (having greater than 30% hydrothermal minerals by volume, in dense net-textured veins, in places obscuring primary textures) contain less than 1.5 wt. % Na₂O and 11-23 wt. % MgO.

Whole-Rock Geochemistry

All samples plot in the basalt to alkaline basalt fields of the Zr/TiO₂ vs. Nb/Y diagram of Pearce (1996) (Fig. 3). The Nb/Y ratios define two distinct groups: (1) tholeiitic metavolcanic rocks structurally underlying VMS mineralisation; and (2) more alkaline ultramafic cumulates and metavolcanic rocks above VMS

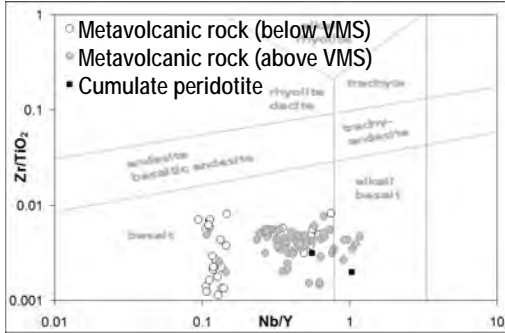


Fig. 3. Zr/TiO₂ vs. Nb/Y in rocks of the Big Lake VMS host sequence. Note two distinct sample populations. Fields are from Pearce (1996) after Winchester & Floyd (1977).

mineralisation.

Trace element patterns also differ between these two groups (Fig. 4). Samples above the VMS have weakly fractionated REE (La/Yb_{cn}=2-8), unlike underlying rocks with a nearly flat REE profile (La/Yb_{cn}= 1-2). Though absolute Nb concentrations are similar in both sample sets, structurally underlying rocks show weak negative Nb anomalies (Nb/Nb* = 0.4-0.9), and generally undepleted Th, Zr, and Hf, whereas overlying rocks show relatively undepleted Nb (Nb/Nb* = 0.6-1.3) and have relative depletions in the other HFSE.

The trace element patterns in Figure 4 are similar to komatiites of the Kidd-Munro assemblage, whose negative HFSE were interpreted by Wyman (1999) to be a result of contamination by other HFSE-depleted rock. If Big Lake volcanic rocks are plume-derived, their negative HFSE depletions could similarly be explained by country arc rock contamination in lavas or parent magma chambers.

Deposit Models

Given that olivine-compatible elements such as Mg or Co are likely to be most concentrated in the first olivine crystals to form an olivine cumulate, assays through two cumulate peridotite units of the BLUC reveal trends that are consistent with a downward younging direction (Fig. 5).

We did not encounter any evidence for assimilation of VMS sulphides by the BLUC. Given an overturned sequence, it

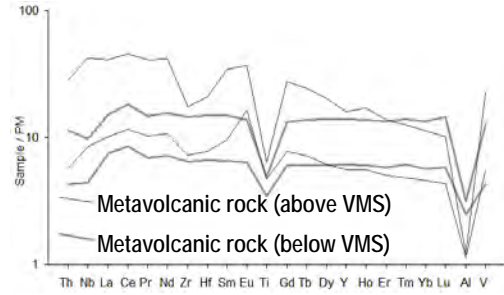


Fig. 4. Representative primitive mantle normalised trace element patterns of metavolcanic rocks structurally above and below VMS mineralisation. Normalising values are from Sun and McDonough (1989).

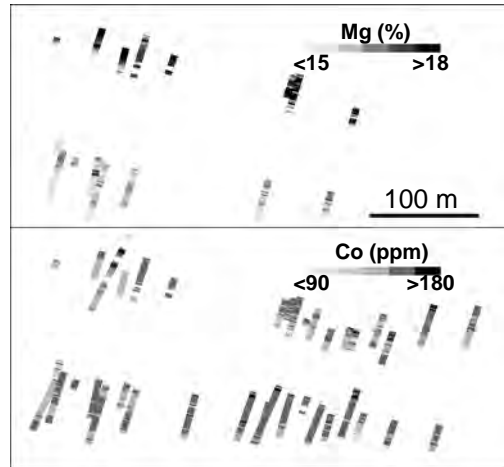


Fig. 5. View along strike of cumulate peridotites at Big Lake shows Mg and Co contents are highest at tops and gradually decrease down hole.

is possible that the BLUC is a shallow heat source directly responsible for VMS mineralisation, as was suggested by Barrie *et al.* (2001) for the Empire cumulate komatiite flow and Terminus VMS occurrence of the Kidd-Munro assemblage. This model is supported by the spatial relationship between VMS sulphides and the lower surface (stratigraphic top) of the BLUC, and by the occurrence of VMS sulphides within the BLUC several km west of the study area, implying a genetic relationship between the BLUC and VMS.

CONCLUSIONS

The Big Lake VMS occurrence is hosted in mafic-ultramafic metavolcanic rocks of

the Schreiber-Hemlo Greenstone Belt, in a setting lacking felsic volcanic or volcanoclastic rock. Modeling of lithology and chemical distributions yields the following conclusions:

- (1) The VMS sulphides define an anastomosing sheet subparallel to and 5-50 m below of the base of the BLUC;
- (2) Hydrothermal alteration involved Na depletion and Mg addition, and visibly altered rock is restricted to within a few metres above visible sulphide mineralisation, but not below;
- (3) BLUC peridotite chemostratigraphy, downward-fining cumulate flows, and asymmetry of hydrothermal alteration suggest the local host sequence to the VMS is overturned;
- (4) A plausible model for the Big Lake occurrence involves a genetic relationship between BLUC cumulates and VMS sulphides, similar to VMS occurrences of the Kidd-Munro assemblage summarized by Barrie *et al.* (2001). This would be the first such documented occurrence outside of the Abitibi subprovince, and illustrates the potential for similar occurrences above large ponded cumulates.

ACKNOWLEDGEMENTS

We thank MetalCORP Ltd. and the Ontario Centres of Excellence for their continued support of this project. The study was also supported by a Society of

Economic Geologists student research grant and an NSERC PGS-M scholarship.

REFERENCES

- Barrie, C., Erendi, A., & Cathles, L. 2001. Paleosea-floor volcanic-associated massive sulfide mineralization related to a cooling komatiite flow, Abitibi Subprovince, Canada. *Economic Geology*, 96, 1695-1700.
- Percival, J., McNicoll, V., & Bailes, A. 2006. Strike-slip juxtaposition of ca. 2.72 Ga juvenile arc and >2.98 Ga continent margin sequences and its implications for Archean terrane accretion, western Superior Province, Canada. *Canadian Journal of Earth Sciences*, 43, 895-927.
- Polat, A., Kerrich, R., & Wyman, D. 1998. The late Archean Schreiber-Hemlo and White River-Dayohessarah greenstone belts, Superior Province: collages of oceanic plateaus, oceanic arcs, and subduction-accretion complexes. *Tectonophysics*, 289, 295-326.
- Sun, S. & McDonough, W. 1989. Chemical and isotopic systematics of oceanic basalts: implications for mantle composition and processes. In: Saunders, A. & Norry, M. (ed.), *Magmatism in the Ocean Basins*. Geological Society Special Publication, 313-345.
- Wyman, D. 1999. A 2.7 Ga komatiite, low Ti tholeiite, arc tholeiite transition, and inferred proto-arc geodynamic setting of the Kidd Creek deposit: evidence from precise trace element data. *Economic Geology Monograph*, 10, 511-528.

The Middle River Gold deposit, NE New Brunswick, Canada: an example of an orogenic style gold system in the Brunswick Subduction Complex

Sabine Schwarz¹, David Lentz¹, & James Walker²

¹ University of New Brunswick, Department of Geology, Fredericton, NB, E3B 5A3 CANADA
(email: s.vetter@unb.ca)

² Geological Surveys Branch, Department of Natural Resources-Minerals, Bathurst, NB, E2A 3Z1 CANADA

ABSTRACT: The Middle River Gold (MRG) deposit is the largest of several genetically related Au-Sb-As occurrences hosted within the Brunswick Subduction Complex (BSC), NB (Canada). Mineralization and related alteration at MRG is localized in a shear zone cutting Middle Ordovician grey shale, siltstone, chert, and subalkaline to alkaline basalts. Mineralizing hydrothermal fluids were localized along late tectonic ductile to brittle shear zones that formed auriferous sulfide-bearing quartz-carbonate veins. Sulfide mineralization can be divided into three types; a) arsenopyrite-pyrite, b) sphalerite-galena-tetrahedrite-bismuthinite-chalcocopyrite, and c) Hg-argentite-electrum. Early sulfides consist of euhedral arsenopyrite and pyrite, which exhibit deformation textures. The cores of pyrite (<3 mm) exhibit dissolution, whereas the rims are faceted; data obtained by EPMA show four zones of variable gold content at constant As values. Arsenopyrite shows similar characteristics with only three different zones (core and rim are Au-rich). Fractures within arsenopyrite and pyrite are filled with sphalerite, galena, bismuthinite, chalcocopyrite, and tetrahedrite. Later Hg-Au-Ag-bearing fluids are responsible for mineralized quartz veins along microfractures. Sulfur isotopic data of arsenopyrite and pyrite have an average $\delta^{34}\text{S}$ of 8.0 ± 0.4 ‰ and one pyrite grain with -3.3 ‰ $\delta^{34}\text{S}$; the higher values are similar to the sulfides hosted within the California Lake Nappe (BSC).

KEYWORDS: *sulfides, Brunswick Subduction Complex, hydrothermal, orogenic gold, Northern Miramichi Highlands*

INTRODUCTION

The Brunswick Subduction Complex (BSC) is best known as the host sequence to world class, syngenetic volcanogenic massive sulfide deposits of the Bathurst Mining Camp (BMC) hosting deposits such as the giant Brunswick No. 12 VMS deposit (>300 Mt of massive sulfides). Less well known are the syntectonic, precious-metal breccia and (or) vein deposits/occurrences in the BSC. The shear zone-hosted Middle River gold deposit (MRG) is the most significant of these and has returned assays of up to 7.44 g/t Au over 6.5 m (DDH MR-05-06).

Gold mineralization at MGR has been delineated by trenching and diamond drilling over a strike length of >500 m and is open below 276 m. Visible gold has not been observed, so it is assumed that Au occurs as submicroscopic inclusions and (or) as refractory gold in sulfides.

Several stages of mineralization have

been recognized, all of which can be related to the tectonic evolution of the BSC (van Staal 1994). Repeated hydrofracturing during episodic tectonic events resulted in the development of multi-stage veins and alteration.

The purpose of this paper is to describe the gold-bearing sulfide-carbonate-quartz veins of the MRG in order to compare this deposit with similar styles of gold mineralization in the region.

GEOLOGICAL SETTING

The MRG area is within the BMC and characterized by three thrust-bound nappes, each containing rocks assigned to different stratigraphic units, specifically: the Miramichi Group, the Tetagouche Group (Tomogonops and Little River formations), and the California Lake Group (Boucher Brook Formation). The Miramichi Group consists of upward-fining sedimentary rocks that are in (dis-)

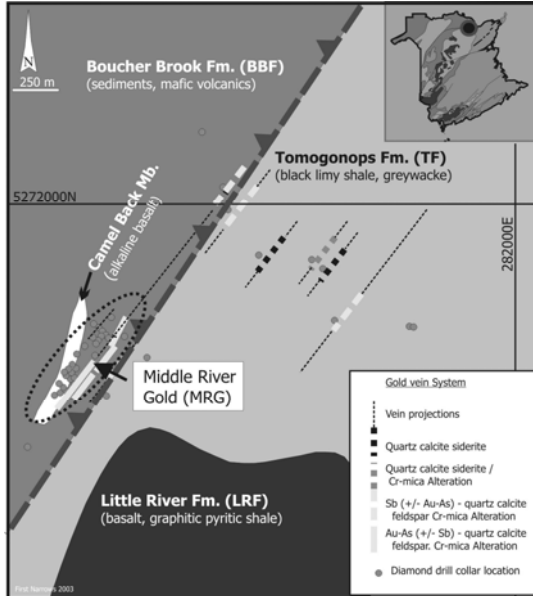


Fig. 1. Geological map of the Middle River Gold (MRG) deposit, including the characterization of the veins projected to the surface from drill data (Gummer 2004).

conformable contact with the overlying Tetagouche Group. The Tetagouche Group is divided into four formations of which only the Little River (LRF) and the Tomogonops formations (TF) are present in the MRG deposit area (Fig. 1). The LRF is characterized by dark grey to black shale, siltstone, and chert that are interlayered with subalkaline to alkaline pillow basalts (Camel Back Member). The TF consists of a coarsening-upward grey, thin- to medium-bedded, calcareous siltstone, shale, lithic (quartz) wacke, and non-calcareous coarse-grained sandstone and conglomerate (Langton 1996).

The Boucher Brook Formation is the upper-most unit in the California Lake Group and consists of grey shale, siltstone, chert, alkalic basalt, and minor peralkaline felsic volcanic rocks including the alkaline basalt of the Camel Back Member (Fig. 1).

The BSC (part of the Dunnage tectonic Zone) formed in Late Ordovician to Early Silurian (i.e., during the Salinic Orogeny), and contains the accreted and subducted remnants of the Middle to Late Ordovician Tetagouche–Exploits back-arc basin. Consequently, the rocks of the BSC have

undergone poly-phase brittle- to ductile deformation resulting in intense thrust tectonics prevalent in this type of setting. Exhumation of the BSC began during the main stage Salinic Orogeny (Early Silurian) and led to the deposition of Silurian sedimentary rocks. The ongoing orogenesis resulted in a polyphase deformed and regionally developed lower- to middle-greenschist grade metamorphism followed by exhumation to near the current structural level.

METHODS AND RESULTS

This investigation relied on petrographic analysis of polished sections using reflected light and the scanning electron microscopy (SEM) and electron microprobe (EPMA) analyses to identify minerals and to document the distribution of gold. The mineralized zone is coincident with a distinct bleached alteration zone that contains fine- to coarse-grained, subhedral arsenopyrite and pyrite in quartz-carbonate veins.

In the MRG deposit, five vein types are recognized (Types I through V). Type II arsenopyrite-pyrite-gold veins are linked to D₁ deformation via sericitization (⁴⁰Ar/³⁹Ar age date 435±3Ma, unpublished data) and carbonatization of the mafic volcanic and adjacent sedimentary host rocks. This mineralization is manifested by increasing Fe₂O₃* and a relative decrease in SiO₂, K₂O, and Al₂O₃ in whole-rock analyses. The color change of the rocks, from a dark grey-green to a beige-yellow, is coincident with the mineralization.

The five vein phases, three of which are sulfide-bearing, can be differentiated into: Type I - early quartz-carbonate, Type II - arsenopyrite-pyrite-quartz-carbonate, Type III - sphalerite-galena-tetrahedrite-bismuthinite-chalcopryrite, Type IV - Hg-argentite-electrum, and Type V – late, metal-barren quartz-carbonate veins.

Type I veins are folded, off set and are the earliest vein type, as they are cut by all other veins. Type II veins, 1-5 cm width with arsenopyrite and pyrite (90%) in a quartz-calcite gangue, are associated with the main stage of sulfide-electrum mineralization. Type III and Type IV veins

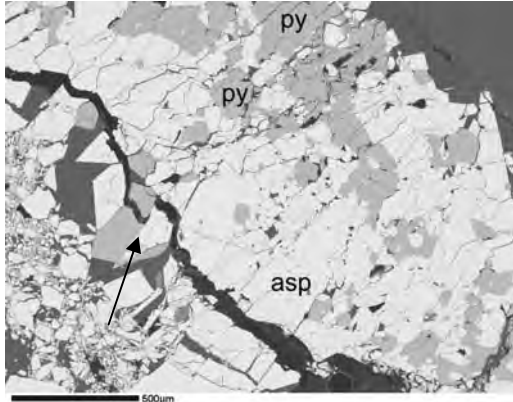


Fig. 2. SEM backscattered electron image of a Type II vein containing euhedral to cataclastically brecciated arsenopyrite (asp), pyrite (py), quartz, and calcite. A thin Type IV quartz vein showed a SEM-EDAX analysis of a very fine-grained mineral mass rich in Hg-Au-As vein (arrow).

occur as microfractures in arsenopyrite and pyrite (Type II), and their relative paragenetic relationship is uncertain. Type V quartz-carbonate veins are the youngest vein type, as they cut all other vein types. Type V veins have no recognizable associated alteration and they offset the foliation, as well as all earlier vein types (I to IV).

This study focused on the sulfide-bearing, types II to IV veins (0.5-2cm wide) and on the fine- to coarse-grained disseminated sulfides in the host rocks.

In Type II veins arsenopyrite is situated along the walls of the vein, with pyrite overgrowths and as vein fill. Wider veins contain angular to subrounded host rock fragments. These veins contain euhedral arsenopyrite (≤ 4 mm) and pyrite (≤ 3 mm) (Fig. 3). Both minerals have Au enriched rims and cores with an intermediate zone devoid of detectable Au.

Microfractures cutting sulfides of Type II veins are cored with anhedral galena, sphalerite, bismuthinite, tetrahedrite, and chalcopyrite in a quartz-calcite gangue. Tetrahedrite also occurs as thin coatings on arsenopyrite and pyrite. These grains and their coatings are too small to be analyzed by EPMA. The microveins (Type IV) appear in sulfides of Type II veins and consist of small (0.1-0.5 mm) anhedral

grains of argentite, electrum, and an undeterminable Hg mineral, in a quartz gangue. SEM-EDAX analyses of these fine grains show element peaks for Hg, Au, and Ag, but the grains are too small for precise determination of the mineral phase.

Sulfur Isotopes

Sulfide grains sampled from the Type II veins in the high gold zones from two drill cores were prepared for sulfur isotope analysis. Pyrite samples (n=5) have average $\delta^{34}\text{S}$ of 8.0 ± 0.5 ‰ and a range of 7.6 - 8.3 ‰, whereas arsenopyrite (n=4) averages 7.9 ± 0.5 ‰ and ranges between 7.3 - 8.4 ‰ (Fig. 3).

One sample of euhedral pyrite collected from a zone of disseminated sulfide coincident with a high-grade gold zone gave a $\delta^{34}\text{S}$ value of -3.3 ‰ (Fig. 3). Similar S isotope data have been reported from the BB Formation, Caribou mine, and other base-metal deposits in the area (Fig. 3).

CONCLUSIONS

The MRG mineralization can be related to the orogenic gold deposit model summarized by Groves *et al.* (2005):

- (1) Type II vein sulfides (arsenopyrite and

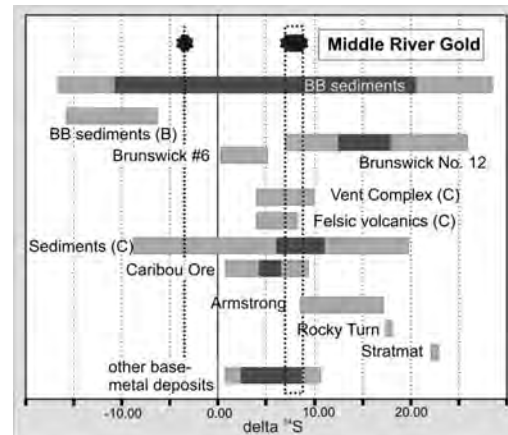


Fig. 3. Sulfur isotopic data for the MRG deposit compared to published data for sedimentary rocks and base-metal and gold deposits in the BSC. (BB=Boucher Brook Fm, B=Brunswick Mine area, C=Caribou Mine, data from Tupper 1960; Lentz *et al.* 1996; Goodfellow & McCutcheon 2003).

pyrite) have Au-rich cores and rims separated by an Au-poor zone. The Au zoning is interpreted to equate to hypozonal As-Au mineralization. At MRG this mineralization occurred during the main phase of the Salinic Orogeny.

(2) Microfractures cutting arsenopyrite and pyrite in Type II veins are infilled by base-metal sulfides (galena, sphalerite, bismuthinite, tetrahedrite, and chalcopyrite). The Cu, Bi, Zn, and Pb that formed these phases were likely scavenged from the VMS bodies and associate sulfide-bearing rocks in the area. The sulfide phases in Type III veins are characteristic of assemblages in orogenic epizonal Sb-Au mineralization.

(3) Mercury-Au-Ag rich (Type IV) veins are interpreted to represent epithermal, near surface mineralization subsequent to the orogenic mineralization and probably formed during the exhumation of the Brunswick Subduction Complex.

(4) The $\delta^{34}\text{S}$ values for arsenopyrite and pyrite in Type II veins might be linked to the strataform VMS deposits of the BSC. In particular, the $\delta^{34}\text{S}$ values are similar to those for the Caribou Mine (located in the California Lake Group [Spruce Lake Formation] above a felsic intrusion). The negative $\delta^{34}\text{S}$ value returned from one pyrite probably reflects biogenic S or reduced seawater sulfate from the Iapetus back-arc basin (Lentz *et al.* 1996).

4) Based on dating ($^{40}\text{Ar}/^{39}\text{Ar}$) of alteration-related sericite at 435 ± 3 Ma, the MRG mineralization is inferred to be associated with and, therefore, generated during the D₁ deformation of the BSC accretionary wedge system. Thus, mineralization at MGR can be described as being similar to the metamorphogenic orogenic gold style.

ACKNOWLEDGEMENTS

We thank the Department of Natural Resources for the funding of this project and their staff for research support. Additional funding was provided with a NSERC Discovery grant to DL.

REFERENCES

- GOODFELLOW, W.D. & McCUTCHEON, S.R. 2003. Geologic and genetic attributes of volcanic sediment-hosted massive sulfide deposits of the Bathurst mining camp, northern New Brunswick; a synthesis. *Economic Geology Monograph*, **11**, 245-301.
- GROVES, D.I., GOLDFARB, R.J., ROBERT, F., & HART, C.J.R. 2003. Gold deposits in metamorphic belts; overview of current understanding, outstanding problems, future research, and exploration. *Economic Geology*, **98**, 1-29.
- GUMMER, P. 2004. http://www.uno.ca/middle_river/.
- LANGTON, J.P. 1996. Relative age, stratigraphic position, and provenance of new sedimentary formations in the eastern Bathurst Camp, New Brunswick. In: CARROLL, B.M.W., (ed.), *New Brunswick Department of Natural Resources and Energy - Current Research*, **96-1**, 61-71.
- LENTZ, D.R., Goodfellow, W.D., & Brooks, E. 1996. Chemostratigraphy and depositional environment of an Ordovician sedimentary section across the Miramichi Group-Tetagouche Group contact, northeastern New Brunswick. *Atlantic Geology*, **32**, 101-122.
- TUPPER, W.M. 1960. Sulfur Isotopes and the origin of the Sulfide Deposits of the Bathurst-Newcastle Area of Northern New Brunswick. *Economic Geology*, **55**, 1676-1707.
- VAN STAAL, C.R. 1994. Brunswick subduction complex in the Canadian Appalachians; record of the Late Ordovician to Late Silurian collision between Laurentia and the Gander margin of Avalon. *Tectonics*, **13**, 946-962.

Gold mineralization in the Kakagi-Rowan Lake greenstone belt: a study of the Angel Hill Gold Zone

Scott Secord¹ & Pete Hollings¹

¹Lakehead University, 955 Oliver Rd. Thunder Bay ON, P7B 3W2 CANADA (e-mail: ssecord@lakeheadu.ca)

ABSTRACT: The Angel Hill Gold Zone is a recent discovery in Houston Lake Mining's West Cedartree Gold Project near Sioux Narrows, Ontario. The mineralised zone spans the contact between the ultramafic and gabbroic units of the Kakagi Gabbro Sill. Highest gold values occur in a zone of alteration up to 20 m either side of a 5 cm wide fault which runs parallel to the contact between the ultramafic and gabbro units of the sill. The gold zone was studied using petrographic techniques and SEM-EDS to assess the nature of mineralization and alteration, whereas down-hole geochemistry was used to determine mobility and fluid characteristics. Gold occurs as micron-size free gold, but predominantly as sylvanite and petzite within and rimming pyrite grains. However, not all pyrite contains gold, as both barren and fertile phases have been identified, suggesting a multistage fluid evolution. Alteration within the gold zone consists of serpentinite, carbonate, fuchsite and quartz, thus involving aqueous-carbonic fluids. Results to date have helped to define and characterise similar areas of mineralization determined through field mapping at the property-scale.

KEYWORDS: Archean, lode-gold, Superior Province, alteration, fuchsite

INTRODUCTION

The Kenora Mining District has historically been one of Ontario's leading gold producing areas. Houston Lake Mining Inc. has discovered a new gold occurrence, the Angel Hill Gold Zone (AHGZ), at their West Cedartree Gold Project (WCGP) near the township of Sioux Narrows, Ontario, near Lake of the Woods. The AHGZ is one of four known gold occurrences within the WCGP and is hosted in an altered peridotite at its contact with a gabbro of the Kakagi Gabbro Sill. The AHGZ has been exposed over 300 metres by mechanical trenching along a roughly north north-west trending zone. The AHGZ is considered to represent an example of Archean lode gold or mesothermal vein-type mineralisation. This project will analyze in detail the alteration associated with gold mineralization in order to help define a continuation of the zone.

GEOLOGICAL SETTING

Regional Geology

The WCGP is located in the western arm of the Savant Lake-Crow Lake greenstone

belt of the Wabigoon subprovince of the Superior Province (Card & Ciesielski 1986).

Local Geology

The WCGP is dominated by three main lithologies (Fig. 1): the Snake Bay formation of the Rowan Lake Group, the Emm Bay formation of the Kakagi Lake Group, and the Kakagi Sill (a gabbro and ultramafic intrusion). The Snake Bay formation conformably underlies the Emm Bay formation and is composed of greenschist grade mafic metavolcanic rocks and comprise interlayered massive, pillowed and porphyritic flows as well as tuff and lapilli tuff. The rocks are fine- to medium-grained and composed of plagioclase feldspar, chlorite, amphibole (tremolite and hornblende), quartz, muscovite, carbonate (calcite and ankerite) and talc. The Emm Bay formation is composed of intermediate to felsic lapilli tuffs, pyroclastic debris flows and lapilli tuffs. The rocks have a fine-grained texture and are composed chiefly of chlorite, plagioclase, quartz, and muscovite. Intruding these two volcanic suites is the Kakagi Gabbro Sill. The

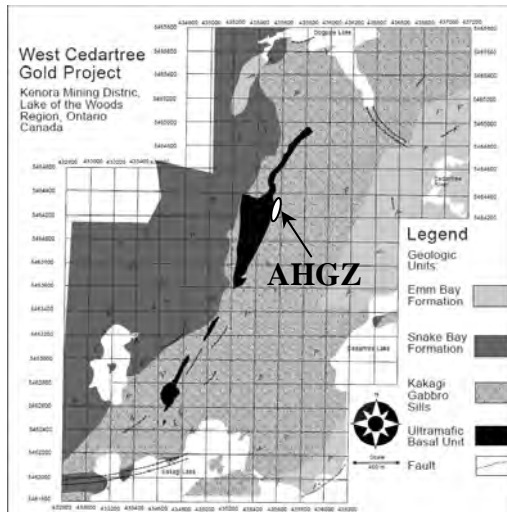


Fig. 1. Property map of the WCGP with outline of the AHGZ indicated.

intrusive contact is somewhat variable, but is generally sharp with well-defined margins. The sill is composed of an ultramafic basal unit that grades upwards into a differentiated gabbro away from the contact with Snake Bay formation. The ultramafic unit is an altered peridotite composed primarily of chlorite altered clino- (augite) and ortho- (hypersthene) pyroxene and highly serpentinised olivine with minor carbonate. The gabbro is composed chiefly of amphibole (tremolite with minor hornblende), plagioclase (albite), pyroxene (augite with minor hypersthene), mica (muscovite with minor biotite), chlorite, and quartz.

Methods

Field mapping at the property scale was performed over two summers at the WCGP (Fig. 1). Sampling was conducted throughout the property, across the gold zone and also from diamond drill holes. Scanning electron microscopy was performed at Lakehead University using an SEM-EDS JEOL 5900 equipped with an Oxford energy dispersion system with a resolution of 139eV. The backscatter electron detector (BSE) was used in order to locate and analyze gold phases and gangue phases associated with the mineralisation. Analyses were done using the following operating condition:

accelerating voltage of 20kV, a beam current of 0.475 pA and a beam width of less than 0.2 micrometres. Standardization was done using samples from the Lakehead University Instruments Lab's standard library. Whole-rock geochemical data was obtained using X-ray fluorescence and inductively coupled plasma mass spectrometry at the Geoscience Laboratory at GeoLabs in Sudbury, Ontario. Trace elements, including the REE and HFSE, were analyzed at the Geoscience Laboratories using a Perkin-Elmer Elan 9000 ICP-MS following a variation on the protocol described by Burnham & Schweyer (2004) and Tomlinson *et al.* (1998).

The Angel Hill Gold Zone

Drilling of the AHGZ has outlined a resources estimate of 106,400 tonnes grading 2.97 g/t (Cutting & Anthony 2005). The mineralised zone straddles the contact between the gabbro hanging wall and ultramafic footwall, which are separated by a zone of brittle deformation about 5 cm wide. The fault zone is filled with quartz and carbonate and a zone of alteration extends about 20 metres into the hangingwall and footwall. Footwall alteration is characterised by intense carbonatization with augite altered to carbonate and chlorite, hypersthene altered to chlorite and minor carbonate, olivine altered to serpentine and magnetite, and interstitial feldspars altered to muscovite. Slight silicification has occurred with a concomitant increase in the abundance of sulfides, chiefly pyrite with minor pyrrhotite. Hanging wall alteration, also characterized by intense carbonatization, consists of plagioclase extensively altered to mica and minor chlorite, augite altered to carbonate, and hypersthene altered to chlorite and carbonate. The secondary amphibole present is predominantly tremolite. Quartz flooding is evident, as well as an increase of matrix carbonate.

The main zone, as mentioned above, is a fault with quartz veining. The zone occurs in the ultramafic suite of the intrusion, as reflected by its texture and

events: (1) alteration of mafic phases to carbonate and felsic phases to micas; (2) influx of quartz and carbonate with the associated formation of fuchshite and deposition of gold +/- sulfides; (5) The nature of the gold mineralization suggests a protracted history of veining and alteration.

ACKNOWLEDGEMENTS

I would to thank Grayme Anthony and Dean Cutting at Houston Lake Mining Inc for their generous time and support. I would like to also thank NSERC for their generous support as well.

REFERENCES

BURNHAM, O.M. & SCHWYER, J. 2004. Trace

Element Analysis of Geological Samples by ICP-MS at the Geoscience Laboratories: Revised Capabilities Due to Improvements to Instrumentation. In: *Summary of Field Work and Other Activities 2004*. Ontario Geological Survey Open File Report **6145**, 54-1 to 54-20.

CARD, K.D. & CIESIELSKI, A. 1986. Subdivisions of the Superior Province of the Canadian Shield. *Geoscience Canada*, **13**, 5-13.

CUTTING D. & ANTHONY, E.G. 2005. Exploration summary and mineral resource estimate for the Angel Hill Gold Zone: West Cedartree Gold Project. Houston Lake Mining, 495 p.

TOMLINSON, K.Y. *et al.* 1998. Refinement of Hafnium (Hf) and Zirconium (Zr) analysis by improvement in the sample digestion procedure. *Ontario Geologic Survey, Miscellaneous Paper*, **169**, 189-192.

Rhenium in Canadian mineral deposits

W. David Sinclair¹, Ian R. Jonasson¹, Rod V. Kirkham², & Art E. Soregaroli³

¹Geological Survey of Canada, 601 Booth Street, Ottawa, ON, K1A 0E8 CANADA
(e-mail: sinclair@nrcan.gc.ca)

²1786 Golf Club Drive, Delta, BC, V4M 4E2 CANADA

³1376 West 26th Avenue, Vancouver, BC, V6H 2B1 CANADA

ABSTRACT: Rhenium is one of the most widely dispersed elements in the earth's crust and minerals in which rhenium is a major constituent are rare. It is similar geochemically to molybdenum and is concentrated primarily in molybdenite in granite-related deposits, particularly porphyry deposits, which are the principal industrial source of rhenium. Molybdenites from porphyry Cu and Cu-Au deposits have the highest contents of rhenium, typically ranging from 200 to 2000 ppm Re, although some (e.g., Ajax West, Mitchell) contain more than 3000 ppm Re. Molybdenites from porphyry Mo deposits generally contain much less rhenium, on the order of 100 ppm Re or less. Elevated contents of rhenium, ranging from 0.5 to 100 ppm, are also present in sediment-hosted Cu deposits, which are the second most important source of rhenium. Our data indicate that sediment-hosted Cu deposits in Canada, such as Redstone (NWT), have comparable rhenium contents and represent significant rhenium resources.

KEYWORDS: *rhenium, molybdenite, porphyry copper, sediment-hosted copper, Canada*

INTRODUCTION

Rhenium is a rare metal with total world production in 2007 estimated at about 50 tonnes. The principal industrial applications of rhenium are in high-temperature alloys used in jet engines and in platinum-rhenium catalysts used in the petroleum industry. In recent years, the demand for rhenium has increased and prices have risen to more than US\$10,000 per kg. In late 2008, rhenium was the sixth most expensive traded element (www.lipmann.co.uk/facts/expensive.html)

Rhenium abundance in most rocks is measured in parts per billion or less and minerals in which it is a major constituent are rare. It is similar geochemically to molybdenum, which it commonly accompanies through magmatic and related hydrothermal stages, and is concentrated in molybdenite associated with various types of granite-related deposits. Molybdenites with some of the highest concentrations of rhenium are associated with porphyry Cu and Cu-Au deposits, which are the primary industrial source of rhenium. Rhenium can also be concentrated by low-temperature

hydrothermal and diagenetic processes. Elevated levels of rhenium are present in sediment-hosted Cu deposits at Dzhezkazgan in Kazakhstan and in the Kupferschiefer of Poland and Germany, and these deposits are the second most important source of rhenium production. Rhenium is also recovered as a byproduct from in situ leaching of sandstone-hosted uranium deposits in Uzbekistan.

Rhenium in molybdenite has been studied by various authors (e.g., Giles & Schilling 1972; Stein *et al.* 2001; Berzina *et al.* 2005). Rhenium data in this paper are from a study of more than 150 Canadian and some foreign deposits (Jonasson *et al.* in prep.).

RHENIUM IN PORPHYRY DEPOSITS

Rhenium content of molybdenite from porphyry deposits varies widely and appears to be inversely related to the molybdenum content (Fig. 1). Molybdenites from porphyry Cu-Au deposits have the highest Re contents, typically on the order of thousands of ppm Re and ranging as high as 8170 ppm Re (Mitchell) and 4609 ppm Re (Kemess South). Re-in-

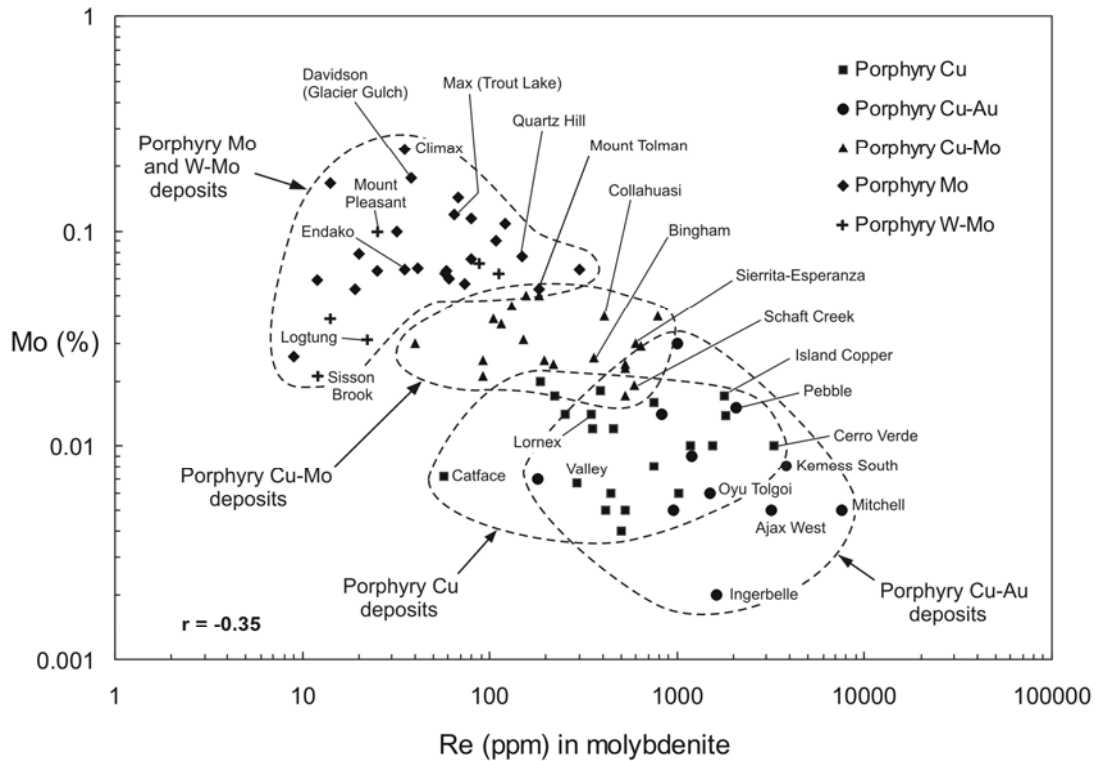


Fig. 1. Rhenium content of molybdenite versus Mo grade of Canadian and selected foreign porphyry deposits.

molybdenite contents of foreign porphyry Cu-Au deposits are also high, averaging about 1500 ppm at Oyu Tolgoi in Mongolia and as much as 2070 ppm Re in the Pebble deposit in Alaska.

Molybdenites from porphyry Cu deposits have Re contents that range from 59 ppm (Catface) to as high as 1863 ppm in the Island Copper deposit. The latter is notable for its rhenium production; during its operation from 1971 to 1994, the Island Copper mine produced about 27 t Re (Perelló *et al.* 1995). In foreign porphyry Cu deposits, the rhenium content of molybdenite is as high as 3200 ppm Re (e.g., Cerro Verde, Peru).

Re-in-molybdenite contents from Canadian porphyry Cu-Mo deposits range from 13 ppm Re (Whiting Creek) to 590 ppm Re (Schaft Creek). In foreign deposits, Re contents in molybdenites from most porphyry Cu-Mo deposits, excluding anomalous occurrences in northern Greece, are on the order of 200

to 800 ppm Re, e.g., Bingham, Utah (360 ppm Re), Sierrita-Esperanza, Arizona (600 ppm Re) and Collahuasi, Chile (410 ppm Re). Molybdenites from some porphyry-type Cu-Mo occurrences in northern Greece (Kirki, Melitena and Maronia) have exceptionally high Re contents that range from 7260 ppm to 42,100 ppm (Melfos *et al.* 2001). Such high contents of Re in molybdenite are atypical for porphyry deposits.

Rhenium contents in molybdenites from Canadian porphyry Mo and W-Mo deposits typically fall in the range of 10 to 100 ppm Re, e.g., Endako (35 ppm Re), Max-Trout Lake (65 ppm Re), Sisson Brook (12 ppm Re). Rhenium contents in molybdenites from foreign deposits are similar, e.g., Climax, Colorado (35 ppm Re), although they range as high as 149 at Quartz Hill, Alaska and 182 ppm Re at Mount Tolmin, Washington.

RHENIUM IN SEDIMENT-HOSTED COPPER DEPOSITS

Sediment-hosted copper deposits are the second most important source of rhenium after porphyry deposits. The rhenium content of deposits at Dzhezkazgan (Kazakhstan) averages 1.4 ppm Re (Hitzman *et al.* 2005), and the Lubin and Mansfeld-Sangerhausen deposits in the Kupferschiefer of Poland and Germany average 1.1 and 21 ppm Re, respectively. The mineralogy of rhenium in these deposits is not well understood, but Re appears to be concentrated in sulfide- and organic-rich sections that also carry elevated levels of Mo and PGEs. Average values of samples analyzed by us from sediment-hosted copper deposits and occurrences in Canada include 32 ppm Re in the Redstone deposit, NWT, 35 ppm at Lochaber Lake, NS and 29 ppm Re at Cape Dorchester, NB.

GRADE-TONNAGE CHARACTERISTICS OF RHENIUM-BEARING DEPOSITS

Rhenium grades of molybdenite-bearing deposits have been calculated based on the MoS₂ content of each deposit and assuming that Re is contained primarily in molybdenite. Calculated Re grades versus tonnages of Canadian and selected foreign deposits are plotted in Figure 2. Rhenium grades for porphyry deposits fall mainly in the range of 0.01 to 0.3 g/t Re, although a few deposits have higher grades ranging up to more than 0.6 g/t Re. The highest grades are in porphyry Cu deposits such as Cerro Verde (0.55 g/t Re) and porphyry Cu-Au deposits such as Mitchell (0.63 g/t Re) and Pebble (0.52 g/t Re); the lowest grades are in porphyry W-Mo deposits such as Logtung (0.01 g/t Re) and Sisson Brook (0.003 g/t Re). Rhenium grades of most porphyry Mo deposits are

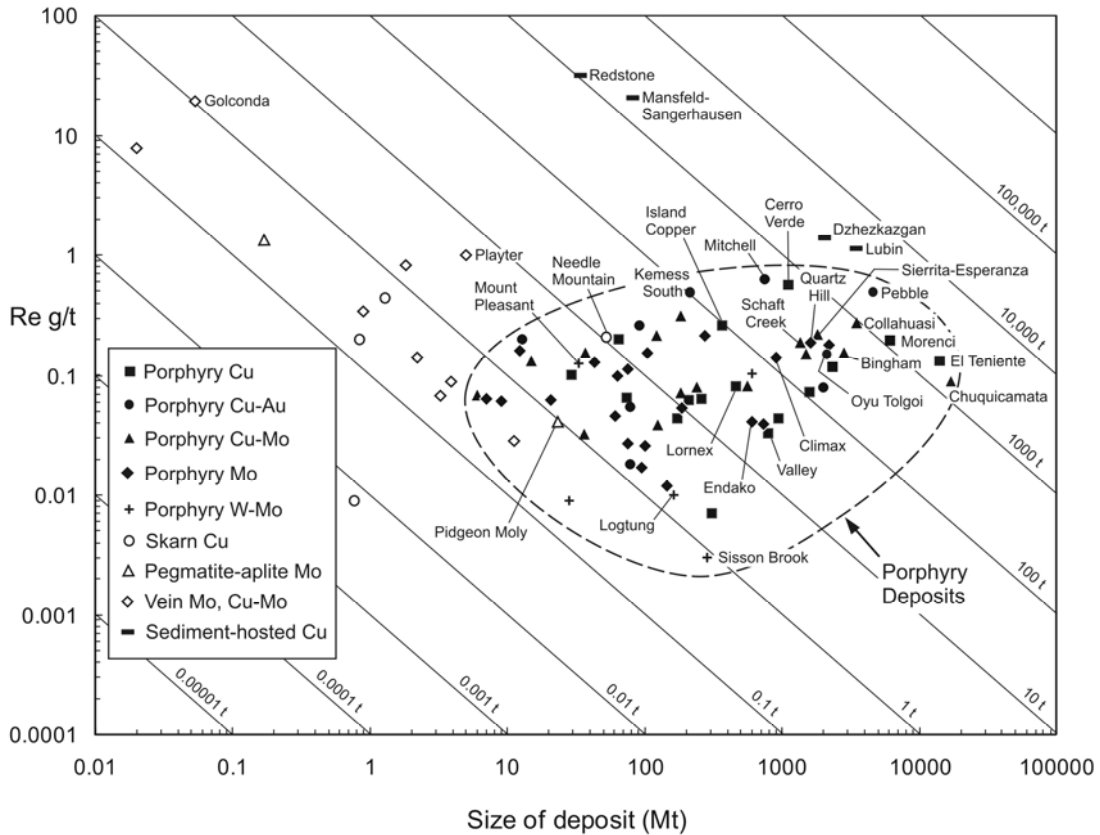


Fig. 2. Rhenium grade versus tonnage for Canadian and selected foreign deposits. Diagonal lines represent tonnes of contained rhenium.

within the range of 0.02 to 0.2 g/t Re, and are indistinguishable from Re grades of other types of porphyry deposits. This suggests that no appreciable differences exist between the overall rhenium contents of Mo-dominant porphyry deposits and Cu-dominant porphyry deposits of comparable tonnage. Variations in Re content of molybdenite in porphyry deposits are due primarily to simple mass balance phenomena; because all the Re in a deposit is taken up by molybdenite, the less molybdenite in a deposit, the higher its Re content, and vice versa.

Because of the large size of porphyry deposits, their total Re contents can be considerable, e.g., Pebble contains as much as 4000 t Re. Only large sediment-hosted Cu deposits such as in the Kupferschiefer and at Dzhezkazgan contain larger resources of rhenium.

Lesser but in some cases significant amounts of rhenium are present in other types of deposits such as skarn deposits (e.g., Needle Mountain-Gaspé Copper), pegmatite-aplite deposits (e.g., Pidgeon Moly) and vein deposits (e.g., Playter, Golconda).

CONCLUSION

Although porphyry Cu and Cu-Au deposits are likely the most important potential source of rhenium in Canada, other types of deposits including sediment-hosted Cu deposits and some vein deposits also represent potential sources.

ACKNOWLEDGEMENTS

Numerous colleagues assisted with sample collection and analysis. Bob Anderson contributed funds for sample

analysis through the GSC's Targeted Geoscience Initiative (TGI-3). Holly Stein (AIRIE) provided unpublished data on the Oyu Tolgoi deposit.

REFERENCES

- BERZINA, A.N., SOTNIKOV, V.I., ECONOMOU-ELIOPOULOS, M. & ELIOPOULOS, D.G. 2005. Distribution of rhenium in molybdenite from porphyry Cu-Mo and Mo-Cu deposits of Russia (Siberia) and Mongolia. *Ore Geology Reviews*, **26**, 91-113.
- GILES, D.L. & SCHILLING, J.H. 1972. Variation in rhenium content of molybdenite. *Report of the 24th Session, International Geological Congress*, **24**, (10), 145-152.
- HITZMAN, M., KIRKHAM, R., BROUGHTON, D., THORSON, J., & SELLEY, D. 2005. The sediment-hosted stratiform copper ore system. *Economic Geology 100th Anniversary Volume*, 609-642.
- JONASSON, I.R., SINCLAIR, W.D., KIRKHAM, R.V., & SOREGAROLI, A.E. (in prep.). Rhenium in Canadian mineral deposits. *Geological Survey of Canada*, Open File.
- MELFOS, V., VOUDOURIS, P., ARIKAS, K., & VAVELIDIS, M. 2001. Rhenium-rich molybdenites in Thracian porphyry Cu±Mo occurrences, NE Greece: *Bulletin of the Geological Society of Greece*, **34**, 1015-1022 (in Greek with English abstract).
- PERELLÓ, J.A., FLEMING, J.A., O'KANE, K.P., BURT, P.D., CLARKE, G.A., HIMES, M.D., & REEVES, A.T. 1995. Porphyry copper-gold-molybdenum deposits in the Island Copper cluster, northern Vancouver Island, British Columbia. In: SCHROETER, T.G. (ed.), *Porphyry Deposits of the Northwestern Cordillera of North America*. Canadian Institute of Mining, Metallurgy and Petroleum, Special Volume **46**, 214-238.
- STEIN, H.J., MARKEY, R.J., MORGAN, J.W., HANNAH, J.L., & SCHERSTEN, A. 2001. The remarkable Re-Os chronometer in molybdenite: how and why it works. *Terra Nova*, **13**(6), 479-486.

Getting the scale right: links between metallogenesis, planetary degassing and the redox state of Earth's oceans?

John L. Walshe¹

¹CSIRO Exploration and Mining, PO Box 1130, Bentley, WA 6102 AUSTRALIA (e-mail: john.walshe@csiro.au)

ABSTRACT: The mineral systems that created the major mineral deposits and provinces of Earth were thermo-chemical engines with roots deep in the mantle if not to the core. Anhydrous fluids, both strongly oxidizing and strongly reducing, are intrinsic, originate in the deep-Earth, and may be linked to Earth degassing. The chemical evolution of mineral systems within the crust reflects interactions of deep-Earth anhydrous fluids with the Earth's hydrous outer layers. These interactions generated the chemical gradients required to promote/sustain metal transport and/or deposition within the crust. To appreciate the size of these systems it is necessary to integrate information across a wide range of scales within mineral provinces and consider links with other Earth phenomena, particularly redox related phenomena of the Earth's mantle, crust, hydrosphere and atmosphere. Potential links between gold mineralization at ~ 2.7 to 2.63 Ga and the evolution of the hydrosphere are explored.

KEYWORDS: *mineral systems, mantle fluids, chemical gradients*

INTRODUCTION

Metal deposits within the Earth are rare and accumulations of high grade, large tonnage deposits are much more so. In contrast, models of formation of metal deposits are based on relatively common processes that operate within the middle to upper crust, hydro- and bio-sphere; metamorphism, basin dewatering, devolatilization of magmas, sea floor metamorphism, and meteoric fluid circulation. So why are metal deposits rare? Here it is argued that metal deposits and provinces are a product of thermo-chemical systems that have their roots in the deep mantle if not the core. Production of metal deposits and provinces through Earth history reflects the constraints of deep-Earth degassing, the trans-crustal and mantle architecture that controlled fluid release, the nature of the crustal interactions and tectonic controls on fluid focusing mechanisms in the mid to upper crust. Planetary degassing links mineral systems to many other Earth redox - related phenomena of the mantle, crust, hydrosphere and atmosphere. Understanding the crust - mantle links is the key to developing mineral systems models that are independent of commodity or traditional classification

schemes and provide robust explanations of the spatial and temporal distribution of deposits and provinces.

WHY METALLOGENIC PROVINCES AND EPOCHS?

The extant models provide little guide to understanding why some arcs of the circum Pacific are well endowed with Cu and Au deposits and others are not or why some Proterozoic basins of the Australian Craton are well endowed with base metal deposits but most are not. Why are quartz veins in Paleozoic slate belts mostly barren but a few richly endowed with gold? Existing models provide little guide as to why the porphyry Cu deposits of Chile formed in a few short pulses of a few million years despite the existence of an active convergent margin over 100s of millions of years.

Does the rarity of major metal accumulations in both space and time reflect the low probability of certain combinations of common processes of the crust including processes of preservation /denudation of the crust? Is it possible that we yet to understand some key elements of mineral systems that operate at length scales and time scales yet to be

appreciated?

**THE ROOTS OF MINERAL SYSTEMS:
HOW DEEP?**

The commonly observed spatial association of mineral deposits and provinces with old cratonic margins, cross-arc structures or tears in slabs and association of metallogenesis with times of plate re-orientation, slab-rollback and slab-faulting are important architectural and dynamic factors that suggest at least some fluids in mineral systems may originate at depths much greater than 10s of kilometres commonly assumed.

Au provinces are associated with crustal-penetrating structures, commonly traceable for 1000s kilometres across the Earth's surface. In the Eastern Yilgarn, Western Australia tomographic studies have identified "architecture" at depths >100 km that may have provided pathways for deep-Earth fluids. Given that aspect ratios (length to depth) of systems can be expected to be of the order of 1:1 then the depth of mineral systems could conceivably be 100s to 1000s of kilometres (Fig. 1). The distance from the surface of the Earth to the core is approximately 3000 km making it conceivable that some components in mineral systems originate in the lower mantle, if not the core of the Earth. Mantle tomography studies (e.g., van der Hilst & K arason 1999) have identified structures in the lower mantle that may provide pathways for fluids to migrate from the lower mantle/core to the Earth's outer layers.

**CHARACTERISTICS OF DEEP - EARTH
ANHYDROUS FLUIDS: LEARNINGS FROM
ARCHEAN AU DEPOSITS**

Studies of ~2.65 Ga gold systems in the Yilgarn Craton, Western Australia, have emphasised the interaction of intrinsically reduced ($\text{CH}_4 \pm \text{H}_2 \pm \text{N}_2 \pm \text{HCl}$) and oxidized ($\text{CO}_2 \pm \text{SO}_2$) anhydrous fluids as well as hydrous fluids in deposit formation. Carbonate veins have $\delta^{13}\text{C}$ between -4 and -6 ‰, typical of mantle values and primary sulfate have $\delta^{34}\text{S}$ of ~ 8 to 12 ‰,

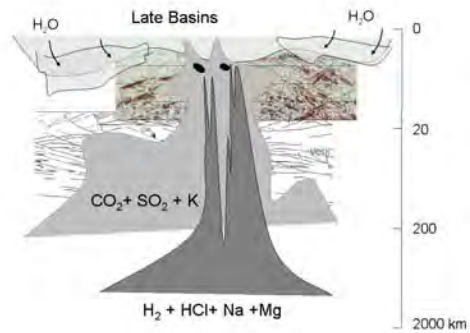


Fig. 1. Anhydrous fluids, oxidized and reduced, are intrinsic to mineral systems, originating in the deep-Earth.

consistent with precipitation from mantle/magmatic $\text{SO}_2 - \text{CO}_2$ fluids with mantle S ($\delta^{34}\text{S} \text{ SO}_{2(g)} \sim 0 \text{ ‰}$). The noble gas signature of CO_2 - rich fluids confirms the involvement of magmatic fluids that contained a mantle component ($^{40}\text{Ar}/^{36}\text{Ar} \leq 21000$ and $^{20}\text{Ne}/^{22}\text{Ne}$ of 7- 11). In contrast CH_4 - dominated fluid inclusions have much lower ^{36}Ar concentrations (sub-ppb) and exceptional noble gas signatures ($^{40}\text{Ar}/^{36}\text{Ar}$ of $\leq 50,000$; $^{20}\text{Ne}/^{22}\text{Ne} = 8.5 - 10$ and $^{21}\text{Ne}/^{22}\text{Ne}$ of ≤ 0.55), that indicate a deep-Earth abiogenic origin (Walshe & Kendrick 2009).

The ultimate source of $\text{CO}_2 \pm \text{SO}_2$ fluids was probably the sub-continental lithosphere as evidenced by the SO_2 discharge during island arc volcanism. The occurrence of oxidized fluids in late Archean gold deposits similar in character to oxidized fluids in magmatic - hydrothermal deposits of the circum-Pacific is consistent with argument that the upper mantle has been oxidized through much of Earth history. Possible sources of reduced fluids include serpentinisation reactions in the deep crust or mantle wedge. Thermodynamic studies, and inclusion mineralogy of diamondiferous kimberlites and lamproites suggest hydric fluids could dominate in the Earth at depths greater than 300 - 400 km. The Earth's core may well be the dominant reservoir of hydrogen (Williams & Hemley 2001). A core-mantle involvement in metallo-genesis, possibly linked to mantle overturn and plumes of

hydric fluids from the D^{II}- layer, provides an attractive explanation for the large-scale temporal pattern of metallogenic epochs.

THE ROLE OF MANTLE VOLATILES IN METALLOGENESIS

Metal transport and deposition capacities of mineral systems are closely linked to propagation of redox and related physico-chemical gradients (pH, aH₂, aHCl, aH₂S, aSO₂, aCO₂, aCH₄, aH₂O, etc) within mineral systems. For metals transported in solution, the rate of mineralization is a product of 3 factors (see Fig. 2);

1. Fluid(s) velocity
2. Changes in metal solubility with respect to physico-chemical parameters controlling solubility: P, T, redox, etc
3. Gradients in physico-chemical parameters (change with respect to distance)

Redox gradients in Au systems of the Yilgarn Craton, Western Australia have been mapped across gold lodes and at camp to district scales using C and S isotopes combined with alteration studies. These gradients can be related to the interplay of oxidized and reduced anhydrous fluids sourced from the mantle or lower crust (Fig. 1), as defined by stable and radiogenic isotopes, with aqueous fluids of crustal origin. Chemically contrasting fluids, particular fluids of contrasting redox state appear intrinsic to productive mineral systems.

LINKS BETWEEN EARTH DEGASSING, GOLD AND THE REDOX STATE OF LATE ARCHEAN OCEANS

One implication of Earth – degassing models of metallogenesis is that there should be links between the formation of the Earth’s resources, secular changes in architecture and geochemistry of the planet over some 4.5 billion years of evolution and phenomena such as mass extinction events, global anoxia, and atmospheric evolution.

The variation of δ¹³C, Δ³³S in sedimentary sulfides and phenomena

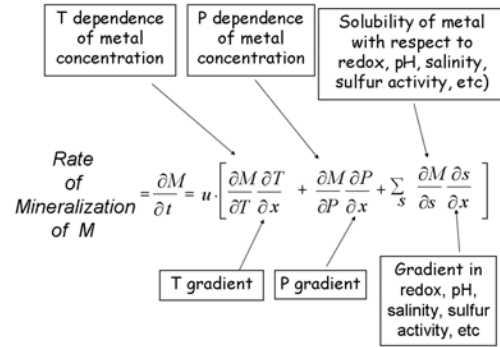


Fig. 2. Mathematical description of mineralization (after Phillips 1990).

such as banded iron formation are sensitive indicators of redox variations in the Earth’s hydrosphere and atmosphere and may be used to map the impact of deep-Earth degassing on Earth’s outer layers. From Figure 3 the levels of CH₄ ± H₂ and CO₂ ± SO₂ fluctuated in the hydrosphere/atmosphere prior to ~ 2.7 with H₂ dominating post ~ 2.5 Ga. Formation of Late Archean Au deposits, at ~ 2.7 to 2.63 Ga, can be interpreted as one manifestation of planetary degassing of highly reduced volatiles that impacted on the hydrosphere and atmosphere from ~ 2.7 to ~ 2.5 Ga as evidenced by a decline in BIF deposition after ~ 2.7 Ga and an excursion in Δ³³S. Peaks in deposition of BIFs prior to ~ 2.7 Ga could be taken as times of higher ratio of SO₂ - CO₂ / CH₄ - H₂ in the volatile flux. Increasing δ³⁴S of seawater in the Late Archean from near zero to ~ +10 ‰ at 2.5 Ga could reflect hydrothermal recycling of SO₂ from mantle de-volatilization fixed in the crust as sulphate.

The rate of H₂ escape from the upper atmosphere and thus oxygenation from decomposition of H₂O vapour is directly dependent on the density of H₂ at the critical level of escape. It may be that the Great Oxidation Event from ~ 2.4 Ga to ~ 2.0 Ga reflects elevated H₂ in the hydrosphere / atmosphere during much of this period.

CONCLUSIONS

Major mineral deposits and provinces may

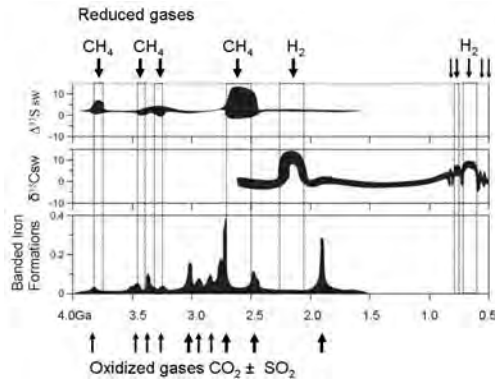


Fig. 3. Indicators of redox variations in the Earth's hydrosphere and atmosphere. Dominance of $\text{CH}_4 \pm \text{H}_2$ defined from $\Delta^{33}\text{S}$ anomalies, H_2 from $\delta^{13}\text{C}$ anomalies and $\text{CO}_2 \pm \text{SO}_2$ from banded iron formations. Data from Canfield (2005), Holland (2005), & Melezhik *et al.* (2005).

be considered one manifestation of planetary degassing and products of thermo-chemical engines with roots in the deep mantle. Studies of Yilgarn gold deposits, Western Australia, are providing insights into the nature of deep-Earth fluids and possible links to the evolution of the Late Archean hydrosphere and atmosphere.

ACKNOWLEDGEMENTS

The study of Archean gold deposits was financially supported by the Predictive Mineral Discovery Cooperative Research Centre (pmd²CRC) and MERIWA (Mineral and Energy Research Institute of Western Australia), Projects 358 and 377. The

support of SIGMC (Gold Fields) is acknowledged and the contributions of Peter Neumayr, Klaus Petersen and Tony Roache. Many friends and colleagues have contributed to the broader conversation re Earth degassing and mineral systems.

REFERENCES

- CANFIELD, D.E. 2005. The early history of atmospheric oxygen: Homage to Robert M. Garrels. *Annual Reviews Earth Planetary Science*, **33**, 1-36.
- HOLLAND, H.D. 2005. Sedimentary mineral deposits and the evolution of Earth's near-surface environments. *Economic Geology*, **100**, 1489-1509.
- MELEZHNIK, V.A., FALICK, A.E., HANSKI, E.J., KUMP, L.R., LEPLAND, A., PRAVE, A.R., & STRAUSS, H. 2005. Emergence of the aerobic biosphere during the Archean-Paleoproterozoic transition: Challenges of future research. *GSA Today*, **15**, 4-11.
- PHILLIPS, O.M. 1990. Flow controlled reactions in rock fabrics. *Journal of Fluid Mechanics*, **212**, 263-278.
- VAN DER HILST, R.D. & KÁRASON, H. 1999. Compositional heterogeneity in the bottom 1000 kilometers of Earth's mantle: Toward a hybrid convection model. *Science*, **283**, 1885-1888.
- WALSHE, J.L. & KENDRICK, M.A. 2009. Links between planetary degassing, gold and the redox state of Late Archean Oceans? 19th V.M. Goldschmidt Conference - Challenges to Our Volatile Planet, 2009.
- WILLIAMS, Q. & HEMLEY, R.J. 2001. Hydrogen in the deep Earth. *Annual Reviews Earth Planetary Science*, **29**, 365-418.

⁴⁰Ar-³⁹Ar geochronological constraints of the ore-bearing ductile shear zones at Hukeng tungsten deposit, Jiangxi Province

Zhang Wei¹, Chen Maohong^{1,2}, Ye Huishou², & Yang Zongxi¹

¹China University of Geosciences, Beijing, 100083 CHINA (email: zhangwei-china@live.cn)

²Institute of Mineral Resources, Chinese Academy of Geological Science, Beijing, 100037 CHINA

ABSTRACT: The Hukeng tungsten deposit is a large-scale quartz vein-type tungsten deposit, which is located at Wugong Mountain, west Jiangxi Province. Massive structure and banded structures occur widely in the ore-bearing quartz veins. Detailed field work and petrographic research reveal that these banded quartz veins are actually ductile shear zones, with quartzitic mylonite reflecting plastic deformation microstructures. ⁴⁰Ar/³⁹Ar dating of neoform sericite folia from mylonite in the EW- and NW-trending shear zones yield a plateau age of 144.1±1.5 Ma and 140.3±1.0 Ma, respectively and yield an isochron age of 144.6±3.6 Ma and 139.6±2.4 Ma, respectively. The Ar-Ar dating reveals that ductile shear deformation occurred after vein petrogenesis. The banded quartz veins were formed by the ductile shear of massive quartz veins. The formation mechanism of the ductile shear may be related to sidelong intrusion of the later magmatic emplacement.

KEYWORDS: Quartzs-veins-type tungsten deposit; banded structure; ductile shear zone; ⁴⁰Ar-³⁹Ar dating; Hukeng, Jiangxi

INTRODUCTION

The Hukeng tungsten deposit is a large-scale quartz vein-type tungsten deposit, which was discovered in 1950. At that time it was considered a small-scale deposit according to the proven reserves. After 50 years of mining and exploration, it is now recognized as a large-scale tungsten deposit. It didn't attract many researchers' attention, so there has been minimal research on it (Liu *et al.* 2004). In order to offer some useful information to direct exploration at depth and outside part of the ore deposit, we examined the mechanisms of formation of the ductily sheared quartz veins in terms of geological characters and chronology.

Regional Geology

The Hukeng Tungsten deposit is located at Wugong Mountain, which is situated along the central part of the north margin of the South China Caledonian fold belt (Tang *et al.* 1991). The Wugong Mountain area experienced multiple stages of magmatism and tectonic activity, therefore it possesses a unique rock association with a complicated structure style.

A great deal of research indicates that

the Wugong Mountain area is a typical Mesozoic metamorphic core complex (Lou *et al.* 2002), which consists of three-layers model: the baseottom is metamorphism-magma nuclear and ductile shear detachment zone; the middle part is shear fold zone; the top part is an unmetamorphic cover sequence.. Studies about its formation mechanism indicated that plate collision caused granite remelting, strong magmatic diapirism resulted in crustal uplift and formation of an extensional gliding nappe (Liu *et al.* 2003).

Local Geology

The research area consists of mica schist, mica-quartz schist, phyllitic quartz schist, gneiss, and granulite, which belong to Sinian Laohutang and Likeng formations. The overall sequence is inclined to S-SE with dips of 25° to 40°. In the main mining area, strata occur parallel to the contact between strata and intrusion, such that the interface formed a good geochemical barrier; this lead to the ore-bearing fluid enrichment and participation in the original joints (ore-hosting structure).

The ore-bearing rock body is the

Hukeng granite stock, which was the product of third stage Yanshanian intrusions that were invasion of early Yanshanian epoch covered by the Laohutang Formation rock. This muscovite granite's outcrop area is 14 km² and the stock's shape is irregular in space. The lithology of rock mass is muscovite granite. WO₃ in rock mass ranges from with a content of 160 to 1100 ppm, with $\times 10^{-6}$ and the average of level is $563 \text{ ppm} \times 10^{-6}$, which is 75 times the compared with average WO₃ content of granite from the Yanshanian Period. Thus we believe that this specialized granite is the source of the ore-bearing fluid.

The Hukeng granite stock was predominated by S-type granites which was enriched in SiO₂ and K, ascribed to K-high calc-alkaline series. The trace elements and REE analysis show that the intrusion has undergone full evolutionary differentiation. The fluids were participated in the forming process of the Hukeng granite intrusion, and the siliceous melts severely interacted with fluids enrich in volatile, which can provide conditions for the migration and enrichment of the ore-forming elements (Liu *et al.* 2008).

A fine-grained muscovite granite dyke with EW strike direction intruded into the Hukeng granite stock. It is gray with a fine-grained texture and massive structure. Constituent minerals consist of quartz, potassium feldspar, plagioclase, and muscovite. Accessory minerals contain garnet, fluorite, pyrite etc. Alteration in the fine-grained muscovite granite include greisenization and silicification.

Main faults in the area include the NE striking Hukeng-Zhangzhuang fault, the Xijialong-Yashan fault and the NW-trending Hukeng-Xijialong fault (Fig.1). The Hukeng tungsten deposit doesn't have the typical five layers model which is common in other tungsten deposit in south Jiangxi Province. The width of the single ore-bearing quartz veins is about dozens of centimetres and the average grade of WO₃ is lower than 1%. Constituent minerals in the quartz veins consist of wolframite, scheelite, pyrite. Accessory minerals contain sphalerite, copper pyrites,

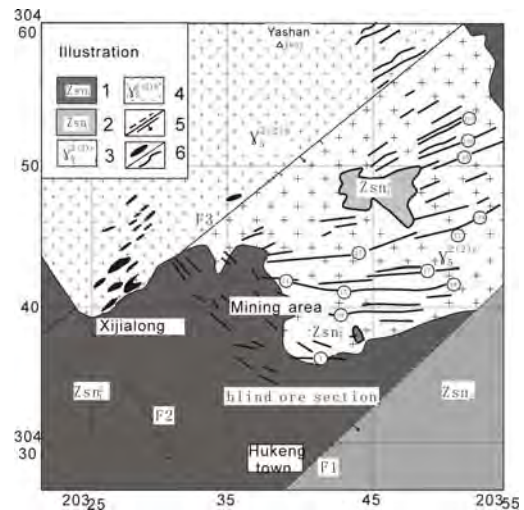


Fig. 1. General geological map of the Hukeng tungsten deposit, South China. 1-Schist, gneiss, and migmatite of Sinian Laohutang Formation; 2-Schist and gneiss of the Sinian Likeng Formation; 3-Third-stage Early Yanshanian muscovite granite; 4-Second-stage Early Yanshanian muscovite granite; 5-inferred large fault(s); 6- network and large vein structure of tungsten quartz veins.

molybdenite.

⁴⁰Ar-³⁹Ar age dating

Field and laboratory work suggests that banded quartz veins are actually the results of ductile shear movement and accordingly, the banded ores are quartzitic mylonite. The banded quartz veins have the typical character of mylonite, minerals' grain diameter become smaller (from normal 1-5cm to 20-30 μ m), i.e., grain-size reduction. Transposition foliations and lineations were generated during deformation. Heterogeneous ductile shearing of the granite occurred next to quartz veins. In order to confine the age of the ductile shear activity, sericite generated by the shearing were sampled. Results of our analysis appear below (Figs.2, 3). The sericite was generated by the ductile shear activity, so they don't contain any radiogenic Ar from the granite or hydrothermal muscovite, which were formed during earlier mineralizing episode. The age of sericite (140.3-144.1 Ma) indicates the blocking temperature age of shear deformation. The age difference between the two samples may

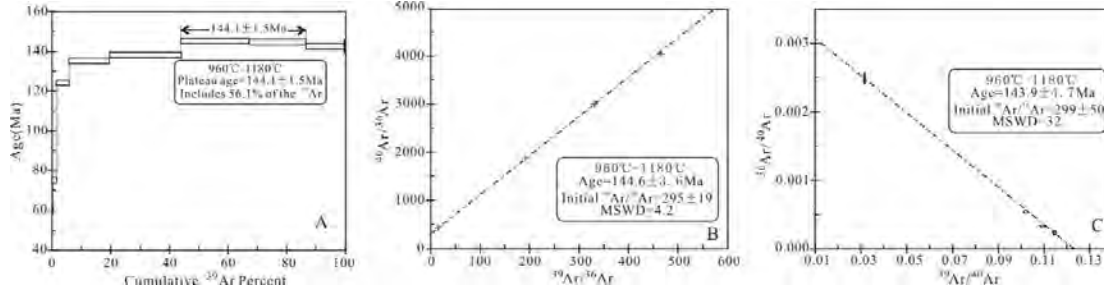


Fig. 2. The step heating Ar-Ar plateau age (A), isochron age (B), and inverse isochron age (C) for sericite folia from mylonite of the EW-trending ductile shear zone.

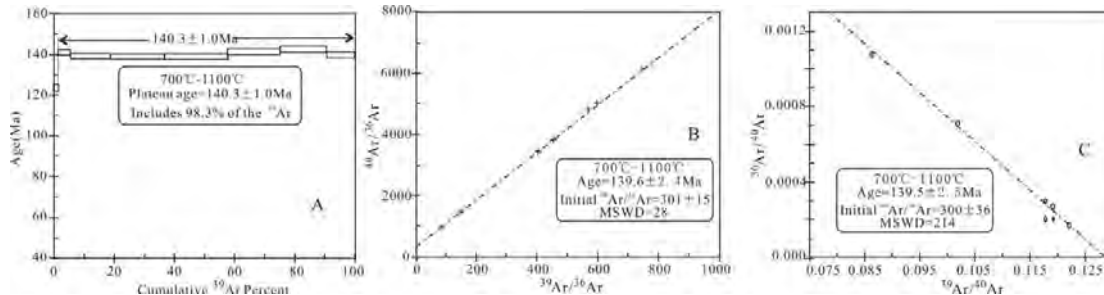


Fig. 3. The step heating Ar-Ar plateau age (A), isochron age (B), and inverse isochron age (C) for sericite folia from mylonite of NW-trending ductile shear zone.

only reflect the error difference, but also relate to the character of inhomogenous cooling in shear zone.

DISCUSSION

Time sequence between diagenesis, mineralisation and ductile shear activity. According to our field observations, the ductile shear zone is mainly developed in the ore-bearing quartz veins and seldom appear in the granite. This phenomenon indicates that the quartz veins, also the original joints, are the zone of relative weakness. The degree of shear deformation intensifies from the quartz veins' centre to both margins. In additionally ore minerals in the quartz veins are disaggregated and locally elongated in the stretching direction. All the macroscopic vein formation and growth features reveal that mineralisation happened before ductile shear activity.

The age of sericite (⁴⁰Ar/³⁹Ar, 140-144 Ma) also illustrates that the ductile shear activity was later than ore genesis (Zircon SHRIMP U-Pb, 152 Ma) (Liu *et al.* 2008) and mineralisation (Re-Os, 147-150 Ma) (Liu *et al.* 2008). It offers indirect and

complementary information to infer the later age of ductile shearing.

Mechanism of Ductile Shear Movement

The formation of the ductile shear is probably related to the extensional deformation of Wugong mountain metamorphic core complex. Wu *et al.* (2001) found that the Hukeng super-unit rock intrude along the south part of the shear detachment zone of the Wugong mountain metamorphic core complex. It indicates that the magmatic emplacement happened after the detachment movement. Liu *et al.* (2008) obtained the zircon SHRIMP U-Pb age from the medium- to coarse-grained muscovite granite, which belongs to the Hukeng super-unit rock. It is about 151.1 Ma, which means that extensional detachment preceded emplacement. So the later vein-parallel ductile shearing is unrelated to the earlier episode of extensional deformation.

Comparing the kinematic characteristics of the ductile shear zone and main fault zone in the mining area, there is a genetic relationship. Field mapping reveals that there was another intrusive episode after the ore-bearing granite was emplaced. It

may account for the ductile deformation. In addition, the direction of magmatic emplacement can be resolved mathematically into two components. This is a perfect kinematic model that explains the orientations of ore-bearing quartz veins in different directions (NW, EW) with both having left-lateral shear sense. Therefore, the ductile shear movement was likely the result of later magma emplacement.

Evolutionary Series of Metallogenic Structure

Based on the geological character, kinematic model, and formation age of ductily sheared, ore-bearing quartz veins, we can establish the petrogenetic evolutionary of the metallogenic structure: emplacement of medium- to coarse-grained muscovite granite (152 Ma) massive quartz veins formed along original joints (main mineralization period, 147 to 150 Ma) fine- to coarse-grained felsic dyke emplacement. Massive quartz veins suffered from ductile shearing resulting in heterogeneously deformed, banded quartz veins (140 to 144 Ma) second period of massive quartz precipitated in brecciated fault zone overprinting the former banded quartz veins with brittle fragments of the quartz veins.

ACKNOWLEDGEMENTS

The project is sponsored by the National

Major Fundamental Research Program of China (Grant No.2007CB411407; No.2007CB411405). Thanks are due to Tong Fusheng, Liu Zhiping and Qin Jianyun for providing supports in the field. I thanks David Lentz for constructive comments and suggestions.

REFERENCES

- LIU, J. *et al.* 2008. Re-Os dating of molybdenite from the Hukeng tungsten deposit in Wugongshan area, Jiangxi Province, and its geological implications[J]. *Acta Geologica Sinica*, **82**(11), 1576-1583.
- LIU, J. *et al.* 2008. Zircon LA-ICPMS U-Pb dating of Hukeng granite in Wugongshan area, Jiangxi Province and its geochemical characteristics[J]. *Acta Petrologica Sinica*, **24**(8), 1813-1822.
- LIU, X. 2003. Discussion of the structure problem in Wugongshan Region in Western Jiangxi province[J]. *Journal of East China Geological Institute*, **26**(3), 249-253.
- LIU, ZH.P. 2004. The occurrence law of the big vein belt and deep exploring direction in Hukeng Tungsten mine[J]. *China Tungsten Industry*, **19**(6), 30-33.
- LOU, F. SH. *et al.* 2002. The Mesozoic Wugongshan granitic domal extensional tectonics and petro-geochemistry[J]. *Geological Bulletin of China*, **21**(4/5), 264-269.
- TANG, J.F. *et al.* 1991. *Tectonic deformation and geological survey of Wugongshan metamorphic terrane*[M]. Wuhang: China University of Geosciences Press, 1-24.
- WU, F.J. *et al.* 2001. Basic features and age of the extensional gliding nappe structure of Wugongshan magmatic thermal dome in Jiangxi[J]. *Jiangxi Geology*, **15**(3), 161-165.

USING ISOTOPE GEOCHEMISTRY TO EXPLORE FOR RESOURCES

EDITED BY:

**ED VAN HEES
KURT KYSER
BRUCE TAYLOR**

Isotopic studies and comparison of marbles in the Sambagawa metamorphic belt, central Shikoku, Japan and marbles from the Kumdy-Kol area of Kokchetav Massif, North Kazakhstan

Zaure Bekmukhametova¹

¹Kazakh-British Technical University, 05000, Tolebi 59, Almaty KAZAKHSTAN (e-mail: zaureb31@yahoo.com)

ABSTRACT: Carbon and oxygen isotope studies were carried out on marbles occurring in epidote amphibolite masses from the Tonaru and Iratsu areas of the Sambagawa metamorphic belt, Japan and the Kumdy-Kol area of the Kokchetav Massif, Kazakhstan to compare them and to elucidate their origin. Based on the results of carbon and oxygen isotope analyses, marbles from the Tonaru and Iratsu areas were probably precipitated from sea water as their $\delta^{13}\text{C}$ values corresponds to those of marine carbonates. In contrast, $\delta^{13}\text{C}$ values of diamond-bearing dolomitic marbles from the Kumdy-Kol area corresponds to mantle carbon and their origin can be interpreted as having been derived from magmatic or deep-seated carbonates.

KEYWORDS: carbon, oxygen, isotopic, analysis, marble

INTRODUCTION

Marbles occur in many regional and contact metamorphic terrains in the world and isotopic studies of marbles have been carried out and report by many authors. Carbon isotope studies of marbles can be useful, in many cases, to reveal the origin of carbonates because differences in carbon isotope ratios of marbles can reflect different origins.

Carbon and oxygen isotope analyses were carried out on marbles occurring in the epidote amphibolite masses from the Iratsu and Tonaru areas of the Sambagawa metamorphic belt, central Shikoku, Japan and on diamond-bearing dolomitic marbles from the Kumdy-Kol site of the Kokchetav Massif, to compare them and to elucidate their origin.

MARBLES FROM THE SAMBAGAWA METAMORPHIC BELT, JAPAN

The Sambagawa metamorphic belt of central Shikoku is part of the intermediate high-pressure metamorphic belt in Japan. Marbles examined in this study were collected from Iratsu (samples Ta-01~Ta-14) and Tonaru (samples Ta-15~Ta16), as well as and epidote amphibolites masses from each area representing metamorphosed layered gabbro

complexes, which were subjected to the Sambagawa metamorphism of epidote amphibolite facies (Banno *et.al.* 1976; Takasu & Makino 1980). The marbles occur in lenticular form, about 1m maximum in width, intercalated concordantly or subconcordantly in the host epidote amphibolite, and composed mainly of calcite, diopside, hornblende and epidote with subordinate amounts of chlorite, muscovite, albite, quartz, and sphene.

According to Wada *et al.* (1984), the marbles from the Sambagawa metamorphic belt are isotopically classified into two groups. The first group comprises marbles in epidote amphibolite masses and the second includes marbles from the crystalline schists and from the marginal parts of the epidote amphibolite masses. These marbles were collected from the Hadeba, Fujiwara and Matsuno areas. Hadeba and Fujiwara areas belong to the high-grade portion of the garnet zone or the transitional part between the garnet and albite-biotite zones. In both areas, the marbles occur in lenticular form, about 3-40 cm in width. These marbles are composed mainly of calcite, graphite, diopside, tremolite and zoisite with subordinate amounts of chlorite,

muscovite, albite, quartz and sphene.

MARBLES FROM THE KOKCHETAV MASSIF, KAZAKHSTAN

The Kokchetav Massif of northern Kazakhstan is a very large, fault-bounded metamorphic complex of Late Proterozoic-Paleozoic protolith age, surrounded by the Caledonian rocks of the Ural-Mongolian fold belt. The Kokchetav UHP and HP belt runs NW-SE extending at least 150 km long and 17 km wide. This massif has attracted much interest since the discovery of metamorphic diamonds. It is the first locality where microdiamonds were found within metamorphic rocks derived from crustal material.

Diamond-bearing rocks within the Zerendin series include garnet-biotite gneiss, garnet-kyanite-muscovite-quartz schist, marble and eclogite. These kinds of rocks can be traced for a distance of about 100 km.

Marbles examined in this study were collected from the Kumdy-Kol area of the Kokchetav Massif I (samples Ku 1-Ku-3). Ogasawara *et al.* (2000) divided metacarbonate rocks from the Kumdy-Kol area of Kokchetav Massif into diamond-bearing dolomite marbles and diamond-free dolomitic marbles. Diamond-bearing dolomitic marble has been described as pyroxene-carbonate-garnet rock (Sobolev & Shatsky 1990) and as diamondiferous carbonate rock (Vavilov & Shatsky 1993). These two types of carbonate rocks were collected from an outcrop and a waste deposit at the Kumdy-Kol area. Ogasawara *et al.* (2000) also divided metacarbonate rocks from Kumdy-Kol area into diamond-bearing dolomite marbles and diamond-free dolomitic marbles. The differences in mineral assemblages in both types of marbles are explained by the local heterogeneity of the fluid compositions (Sobolev & Shatsky 1990).

Diamond-bearing Marbles:

Diamond-bearing marbles show granoblastic texture and this type of carbonate contains abundant microdiamond with or without graphite.

The mineral assemblage of diamond-bearing marble is mainly garnet and clinopyroxene with interstitial calcite and phlogopite. Accessory minerals include rutile and titanite, chlorite, quartz, K-feldspar and kyanite. The diamonds are cubo-octahedral, 12 μm in size on average and occur in zircons. They also occur in garnet with euhedral graphite (c.50 μm across) as inclusions. Graphite occurs on the surface of diamond crystals, and as secondary crystals ($\leq 300 \mu\text{m}$) in intergranular areas.

Diamond-free Marbles

These marbles show equigranular granoblastic texture, and according to Ogasawara *et al.* (2000), are characterized by the absence of graphite and diamond. They consist mainly of Mg-calcite + dolomite + forsterite + diopside + Ti-clinohumite. Garnet is replaced by symplectite of diopside, spinel and Mg-calcite, plus minor amounts of pyrrhotite, pyrite and chalcopyrite.

Two types of marbles occur as small, lenticular, banded or vein-like bodies within garnet-pyroxene and tremolite-chlorite-bearing quartzites, plagioclase gneisses, garnet-biotite and biotite gneisses of the Zerendinsk rocks series. Their field relation are not well known, but the features of these rocks suggest that two rock types probably were subjected to UHP metamorphic rocks at the same P-T conditions (Sobolev & Shatsky 1990, Ogasawara *et al.* 2000).

SAMPLES AND EXPERIMENTS

Carbon and oxygen isotope compositions of sixteen marbles from epidote amphibolites of the Sambagawa metamorphic belt and of three diamond-bearing marbles from the Kumdy-Kol area of Kokchetav Massif were measured. Powdered calcite from the marbles was decomposed by 100 percent phosphoric acid at 60°C to obtain carbon dioxide gas for isotopic analyses. Isotopic measurements were carried out using a triple-collector mass spectrometer (Finnigan MAT Delta E). All data are given in terms of a conventional expression in

Table 1. Isotopic composition of calcite in marbles collected from epidote amphibolite masses of the Sambagawa metamorphic belt, central Shikoku.

Sample	$\delta^{13}\text{C}$	$\delta^{18}\text{O}_{\text{PDB}}$	$\delta^{18}\text{O}_{\text{SMOW}}$
Iratsu area			
Ta-01	1.2	-15.2	15.2
Ta-02	1.3	-15.6	14.9
Ta-03	0.6	-14.5	15.9
Ta-04	3.6	-16.2	14.2
Ta-05	2.2	-12.6	17.9
Ta-06	3.4	-12.2	18.3
Ta-07	1.0	-15.0	15.5
Ta-08	-0.2	-16.6	13.8
Ta-09	1.8	-13.9	16.6
Ta-10	1.3	-17.9	12.4
Ta-11	0.0	-12.7	17.8
Ta-12	1.6	-16.4	14.0
Ta-13	-0.9	-16.4	14.0
Ta-14	0.6	-14.2	16.3
Tonaru area			
Ta-15	0.3	-16.0	14.5
Ta-16	-1.8	-18.1	12.3

per mil unit relative to PDB for $^{13}\text{C}/^{12}\text{C}$ and SMOW for $^{18}\text{O}/^{16}\text{O}$ ratios $\delta(\text{‰}) = (\text{R}(\text{sample})/\text{R}(\text{standard}) - 1) \times 1,000$, where R is the ratio in a sample and the standard.

The standard deviation of several independent analyses for the same material is about 0.05 and 0.1 ‰ for $\delta^{13}\text{C}$ and $\delta^{18}\text{O}$, respectively.

Carbon and oxygen isotope compositions of calcite in marbles collected from the Sambagawa metamorphic belt are given in Table 1. For calcites from 16 selected marbles from Iratsu and Tonaru areas of the Sambagawa metamorphic belt, we obtained $\delta^{13}\text{C}_{\text{PDB}}$ values that range from -1.8 to +3.6 ‰ and $\delta^{18}\text{O}_{\text{SMOW}}$ values of +12.3 to +17.9 ‰.

Carbon and oxygen isotope compositions of calcite in marbles collected from the Komdy-Kol area of the Kokchetav Massif are given in Table 2. $\delta^{13}\text{C}_{\text{PDB}}$ values of calcites of diamond-bearing marbles from the Kokchetav Massif are distinctly lower than those from the Iratsu and Tonaru areas, and fall in the range of mafic and ultramafic rocks between -5.2 to -8.4 ‰ with $\delta^{18}\text{O}_{\text{SMOW}}$

Table 2. Isotopic composition of calcite in marbles collected from the Komdy-Kol area of Kokchetav Massif

Sample	$\delta^{13}\text{C}_{\text{PDB}}$	$\delta^{18}\text{O}_{\text{PDB}}$	$\delta^{18}\text{O}_{\text{SMOW}}$
Ku-1	-5.2	-13.2	17.2
Ku-2	-8.4	-13.7	16.8
Ku-3	-6.4	-16.7	13.7

values of +13.7 to +17.2 ‰.

CONCLUSIONS

Based on our analyses, we conclude that the marbles from the Sambagawa metamorphic belt and those from the Kokchetav Massif have different origins.

Carbon and oxygen isotopic analyses show that marbles from the Iratsu and Tonaru areas in the Sambagawa metamorphic belt have $\delta^{13}\text{C}_{\text{PDB}}$ values close to zero, similar to most marine carbonates. These data suggest that these marbles have precipitated from sea water.

Taking into account the negative $\delta^{13}\text{C}_{\text{PDB}}$ values of marbles from the Komdy-Kol area, we propose a different origin from the marbles in the Sambagawa metamorphic belt. The origin of the Komdy-Kol marbles is interpreted as rocks derived from magmatic or deep-seated carbonates. The difference in mineral assemblage in diamond-bearing and diamond-free marbles from the same outcrop and deposit at the Kumdy-Kol area in the Kokchetav Massif is explained by local heterogeneity of the fluid composition and by the differences in CO_2 condition.

ACKNOWLEDGEMENTS

I wish to express many thanks to professor Akira Takasu of Shimane University, Japan, who was my supervisor during my stay in Japan for his support, teaching and useful suggestions. I also wish to thank professor Seto for his help to carry out isotopic analyses of my samples and Dr. Sampei for his helpful comments.

REFERENCES

BANNO, S. & YOKOYAMA, K., IWATA, O., &

- TERASHIMA, S. 1976. Genesis of epidote amphibolite masses in the Sanbagawa metamorphic belt of central Shikoku. *Geological Society of Japan*, **82**, 199-210.
- OGASAWARA, Y. & OHTA, M. *et al.* 2000. Diamond-bearing and diamond-free metacarbonate rocks from Kumdy-Kol in the Kokchetav Massif, northern Kazakhstan. *The Island Arc*, **9**, 400-416.
- SHATSKY, V.S., SOBOLEV, N.V., & VAVILOV, M.A. 1995. *Diamond-bearing metamorphic rocks of the Kokchetav Massif (northern Kazakhstan)*. *Ultrahigh-Pressure Metamorphism*. Cambridge University Press, Cambridge, 425-455.
- SOBOLEV, N.V. & SHATSKY, V.S. 1990. Diamond inclusions in garnets from metamorphic rocks. *Nature*, **343**, 742-746.
- TAKASU, A. & MAKINO, K. 1980. Stratigraphy and geologic structure of the Sambagawa metamorphic belt in the Bessi district, Shikoku, Japan-reexamination of the recumbent fold structures. *Chikyu Kagaku*, (Earth Science), **34**, 16-26.
- WADA, H. & ENAMI, M. 1984. Isotopic composition of marbles in the Sanbagawa metamorphic terrain, central Shikoku. *Japan Geochemical Journal*, **18**, 61-73.

Cu Isotope Study of the Silver Bell Porphyry Cu Mine

Molly Dendas¹, Ryan Mathur¹, & Spencer Titley²

¹Juniata College, 1700 Moore St, Huntingdon, PA USA
(email: dendamm06@juniata.edu)

²University of Arizona, Gould-Simpson Building #77, 1040 E 4th St., Tucson, AZ, 85721 USA

ABSTRACT: Silver Bell is a typical porphyry Cu deposit of the American southwest that has experienced intense weathering and remobilization of Cu during supergene processes. Cu isotope analyses of hematite, goethite, and jarosite from the leached cap, and chalcopyrite, cuprite, and chalcocite from the enrichment blanket at the Silver Bell Mine in Arizona reveal correlations between isotopic compositions and Cu concentrations of the minerals. Leach caps contain significantly lower amounts of Cu than enrichment blankets, and lighter Cu isotopic compositions, averaging -6.9‰. In contrast, the enrichment blankets contain heavier isotopic compositions averaging 5.4‰, therefore indicating that a rough mass balance exists between the two isotopic reservoirs. Isotopic fractionation of Cu is substantial during the leaching process, and could be used as an exploration tool.

KEYWORDS: *Cu isotopes, leaching process, Cu fractionation, supergene*

INTRODUCTION

The goal of this project is to find a geochemical correlation using Cu isotopes between leach caps and enrichment blankets. Leach caps have significantly lower amounts of Cu than found in enrichment blankets. As water reacts with chalcopyrite (CuFeS_2) found in the primary porphyry and previously leached rocks, Cu is taken into solution and as oxidation produces, creates sulfuric acid. When the ground waters reach the water table, chalcocite (Cu_2S) precipitates from solution, enriching the crust in Cu (Mathur *et al.* 2005).

GEOLOGICAL SETTING

The Silver Bell Mine is located thirty-five miles northwest of Tucson, at an elevation from 2,500 to 3,000ft. The mine consists of four open-pits and is located on 19,000 acres of land (Titley 1994).

The Silver Bell Mine area consists of dipping units that are composed of dacite porphyry, alaskite and monazite. The rock ages span the Paleozoic, Mesozoic and Cenozoic periods. The Paleozoic wall rocks consist of quartzite, siltstone and altered limestone. The carbonate rocks are exposed along the contact between the host rock and intrusions, and host the

principal skarn ores in the district. Along the western side of the district, carbonate and other types of rocks have been moved downward by faults, making a basin that has been filled with gravel deposits (Lopez 1995). The thickness of the Paleozoic beds cannot be determined because of faulting and dilation from sills. The Mesozoic host rocks consist of well-sorted and bedded arkose exposed at the southwest corner of the area. Some minor siltstone and conglomerate can also be seen. The Cenozoic intrusive rocks consist of post-mineral, mid-Tertiary andesite and hornblende dykes (Graybeal 1982).

METHODS

Samples were handpicked from both drill cores and directly from the mine pit. The

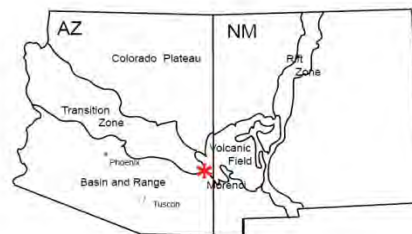


Fig. 1. Map of Arizona

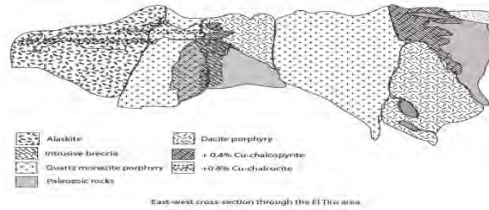


Fig. 2. Cross Section of the Silver Bell Porphyry Cu Mine.

drill core samples were selected from different lithologies to get a representation of the area. In addition, we examined mineralized skarns for evidence of leaching between layers. Minerals from drill cores were crushed and handpicked. Chemical and mineralogical analyses of the ores were conducted on a Scanning Electron Microscope (SEM) and through X-Ray Diffraction (XRD). SEM reveals the mineral replacements throughout the samples, whereas XRD reveals mineralogy. Each of the sections was scanned for places where Cu enrichment could be documented. Minerals were picked for isotopic analysis from each of the samples and confirmed by XRD and SEM.

The rock samples were cut and polished into thin sections to be used on the SEM at Juniata College. The SEM was used for petrographic textural analysis.

Samples were prepared for Cu isotope analysis on the Multicollector Inductively-Coupled Plasma Mass Spectrometer (MC-ICPMS) at University of Arizona. The Cu-rich samples were loaded and dissolved in pure HNO₃ and the Cu-poor samples were loaded and dissolved in a mixture of HCl and HNO₃. Chromatographic separation of the Fe and Cu ions was deemed necessary for the Cu-rich samples. The diluted solutions were injected into the MC-ICPMS using a microconcentric nebulizer. Samples were run numerous times to increase precision. The Cu isotope ratios are reported in conventional per mil notation, relative to the NIST 976 standard. Mass bias was also accounted for by bracketing methods with the NIST 976 standard.

DISCUSSION

The measured Cu isotope ratios vary from -14‰ to 9‰. This range shows that Cu isotope fractionation is significant during supergene leaching and enrichment.

Textural analysis revealed that there have been multiple leach events as recorded in previous studies (Titley 1995). For instance, in the SEM images and analysis of the samples, chalcocite can be seen as a replacement of pyrite. This is evidenced by formation of Cu mineral pseudomorphs after cubic pyrite. Evidence of replacement was seen in many of the samples.

In order to quantify the degree of Cu enrichment, and the number of leach events, we compared the magnitude of Cu isotope fractionation between the enrichment blanket and the leached cap. Relative to primary, hypogene ores, with a $\delta^{65}\text{Cu}$ value of near 0‰, the Cu isotope fractionation in the enrichment blanket averages 6‰, and in the leach cap, -7‰. The data demonstrate that the degree of isotopic fractionation is large, and its magnitude may correlate with the extent of leaching, as implied in Figure 3.

CONCLUSIONS

Leach caps have a significantly lower amount of Cu than in enrichment blankets due to downward migration and precipitation of leached copper in the form of chalcopyrite (CuFeS₂) chalcocite (Cu₂S) and cuprite (CuO).

In the leached cap, hematite is most abundant, followed by jarosite, goethite and malachite. The data from XRD and SEM also reveals that chalcocite is most

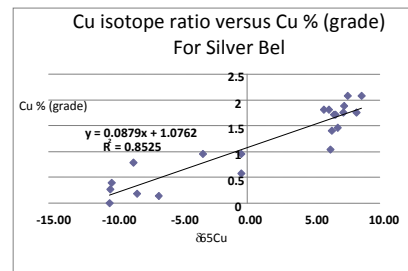


Fig. 3. Cu isotope ratio versus the Cu grade for Silver Bell Mine, Arizona.

abundant followed by cuprite and hematite in the leach cap. This mineralogy can be seen in transition through SEM textures. Samples show replacement of the pyrite by chalcocite, typically found in porphyry Cu deposits.

In the leach cap, the Cu isotopes are lighter than those in the enrichment blanket. Near the surface, the isotopes are extremely low, to about -14‰. Deeper in vertical profile at about 300 feet, the enrichment blanket contains a heavier isotope signature around 8‰. This pattern is observed throughout the drill core. The hypogene mineralization is near 0‰ and therefore, there has been fractionation of copper isotopes in the chalcopyrite during dissolution. This fractionation is seen because the hypogene ores are distinctly different than leach cap and enrichment minerals.

Samples included hematite (Fe_2O_3), goethite ($\text{FeO}(\text{OH})$), and jarosite ($\text{KFe}^{(\text{III})}_3(\text{OH})_6(\text{SO}_4)_2$) from the leach cap and chalcopyrite (CuFeS_2), chalcocite (Cu_2S), and cuprite (Cu_2O) from the enrichment blanket.

REFERENCES

- GRAYBEAL, F.T. 1982. Geology of the El Tiro area; Silver Bell mining district, Pima County, Arizona. *Advances in Geology of the Porphyry Copper Deposits: Southwest North America*. University of Arizona Press, Tucson, AZ.
- LOPEZ, J.A. & TITLEY, S.R. 1995. Outcrop and Capping Characteristics of the Supergene Sulfide Enrichment at North Silver Bell, Pima County, Arizona. In: PIERCE, W. & BOLM, J.G. (eds.), *Porphyry copper deposits of the American Cordillera: Arizona Geological Society Digest*, **20**, 424-435.
- MATHUR, R., RUIZ, J., TITLEY, S., LIERMANN L., BUSS, H., & BRANTLEY, S.L. 2005. Cu isotopic fractionation in the supergene environment with and without bacteria. *Geochimica et Cosmochimica Acta*, **69**, 5233-5246.
- TITLEY, S. 1994. Silver Bell Porphyry Copper Deposit, Silver Bell Mountains, Pima County, Arizona. *U.S. Geological Survey Circular* **1103-B**, 77-88.
- TITLEY, S. 1995. Geological Summary and Perspective of Porphyry Cu Deposits. In: *Southwestern North America; Porphyry Cu Deposits of the American Cordillera*. Arizona Geological Society Digest, **20**, 6-20.

A geochronological based approach to characterize the setting of the Buffalo Head Hills kimberlite field, northern Alberta, Canada

D. Roy Eccles¹, Art R. Sweet², Rob A. Creaser³, & Larry M. Heaman³

¹Energy Resource Conservation Board, Alberta Geological Survey, Edmonton, AB CANADA
(email: roy.eccles@ercb.ca)

²Natural Resources Canada, Geological Survey of Canada, Calgary, AB CANADA

³Department of Earth & Atmospheric Sciences, University of Alberta, Edmonton, AB CANADA

ABSTRACT: Chronological studies of kimberlite-host rocks in the diamondiferous Buffalo Head Hills kimberlite field of north-central Alberta facilitate new interpretation of the nature, timing and sequence of kimberlite eruptions in northern Alberta. Three different emplacement episodes are recognized in association with volcanic and intrusive activity: Late Cretaceous (~88-81 Ma) Smoky Group equivalent intra- and extra-crater facies, Late Cretaceous and Paleocene (~81 and ~64 Ma) intrusion of sills or dykes, and Paleocene (~60 Ma) Paskapoo Formation equivalent intra-crater facies. These specific periods of magmatism correspond to characteristic intra-field features such as spatial distribution, rock classification and diamond content.

KEYWORDS: Alberta, Buffalo Head Hills kimberlite field, Geochronology, Palynology, Kimberlite emplacement setting

INTRODUCTION

Kimberlite in the Western Canadian Sedimentary Basin (WCSB) has been referred to as 'Class 2 kimberlite' (Skinner & Marsh 2004). A distinct classification is required because these bodies differ from the classical South African carrot-shaped vertical intrusions known as 'pipes', in that Class 2 kimberlites contain large volumes of volcanoclastic rocks deposited in shallow (<500 m in depth) saucer-shaped craters with feeder zones that are often difficult to locate.

The preservation of near-surface to exposed kimberlitic bodies in the Buffalo Head Hills kimberlite field of northern Alberta (Fig. 1) provides an opportunity to contribute to the setting in which Class 2-type kimberlites are emplaced. This information will enhance our ability to model and evaluate known Class 2 kimberlite deposits, and to discover new fields of kimberlite within the WCSB.

Geochronological (radiogenic isotope and palynological) results are used here to understand the kimberlite-host rock relationships in the Buffalo Head Hills kimberlite field, and to provide new philosophy on the timing and distribution

of kimberlitic magmatism in the northern Alberta portion of the WCSB.

BACKGROUND

The Buffalo Head Hills kimberlite field is located approximately 350 km north of the city of Edmonton in north-central Alberta. The field was discovered in 1997 by Ashton Mining of Canada Inc., EnCana Corporation and Pure Gold Minerals Inc.

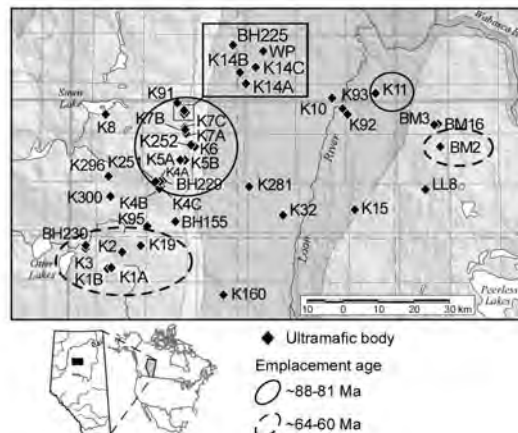


Fig. 1. Spatial location of ~88-81 Ma and ~64-60 Ma ultramafic rocks in the Buffalo Head Hills kimberlite field.

and is currently being explored by Diamondex Resources Ltd., Shore Gold Inc. and Grizzly Diamonds Ltd. This field of 41 known kimberlitic bodies has large near-surface geophysically-inferred kimberlite dimensions (up to and possibly >45 ha), potential economic grades (up to 55 carats per hundred tonnes; K252 kimberlite) and a high ratio of diamondiferous kimberlite to barren hybrid kimberlite-ultrabasic bodies (28 of the 41 occurrences contain diamond; e.g., Skelton *et al.* 2003; Eccles *et al.* 2008).

Examination of drill cores from 21 volcanic bodies provided kimberlite and host rock materials for two separate, but collaborative geochronological studies to understand the timing and distribution of kimberlite magmatism.

(1) Eccles *et al.* (2008) examined kimberlite cores for fresh macroscopic phlogopite and groundmass perovskite and reported robust Rb-Sr (four- to five-point isochrons) and U-Pb (individual ²⁰⁶Pb/²³⁸U grain data, linear regression, and weighted average ²⁰⁶Pb/²³⁸U) age determinations, respectively, for 12 bodies.

(2) Sweet *et al.* (in prep.) assembled a continuous bedrock section that spans vertically over 560 m to establish the chronostratigraphy and paleoenvironments across the Early Cretaceous (Albian) to Paleocene (Selandian) time-interval most critical for determining the relationship between the configuration of the sedimentary basin and the kimberlite eruptions.

These studies reported two distinctive events: one broadly coeval Turonian to Campanian (~88-81 Ma) volcanism-sedimentation, and the other, a younger Paleocene (~64-60 Ma) eruptive event. Three different emplacement settings are represented, the combination of which defines a complex kimberlite field characterized by tabular, often stacked kimberlite layers of varying ages (Fig. 2).

LATE CRETACEOUS SMOKY GROUP EQUIVALENT INTRA- AND EXTRA-CRATER FACIES

The oldest volcanism in this field is

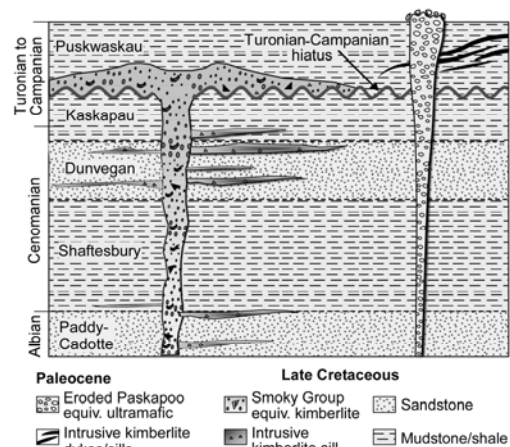


Fig. 2. Cartoon cross-section to depict the complex relations between Late Cretaceous and Paleocene volcanoclastic and intrusive kimberlite in northern Alberta.

recorded by a cluster of Late Cretaceous kimberlites interpreted to be emplaced coevally with Smoky Group host strata. Nine kimberlites yield Coniacian to Campanian ages of between 88 ± 5 Ma (U-Pb perovskite, K5A) and 81.2 ± 2.3 Ma (Rb-Sr phlogopite, K252). The ~88-81 Ma volcanic rocks are bona fide kimberlite (Eccles *et al.* 2004), the majority of which are located in the northwestern part of the field and correspond to a group of diamondiferous bodies, K14, K91 and K252 (Fig. 1), that have the highest diamond contents reported to date for this kimberlite field; these kimberlites have estimated diamond contents of between 12 and 55 carats per hundred tonnes (Skelton *et al.* 2003; Hood & McCandless 2004).

It is difficult to prove these kimberlites are coeval with deposition of Smoky Group sedimentary rocks because an extensive Turonian (in part or in whole) through Early Campanian hiatus, representing approximately nine million years of missing strata, coincides with emplacement. These kimberlites were either covered by post-event Santonian and Campanian strata, or exhumed to outcrop or subcrop beneath glacial deposits. Kimberlite morphologies of this group are complex because their emplacement is controlled by

paleotopography associated with the hiatus (possibly related to tectonic uplift), and subsequently modified as part of a Late Cretaceous landscape that was transgressed by marine waters.

LATE CRETACEOUS AND PALEOCENE INTRUSIVE SILLS AND DYKES

A second emplacement setting is intrusive and occurs as both Late Cretaceous and Paleocene volcanic rocks penetrated significantly older sedimentary rocks.

The Campanian (~81 Ma) K252 kimberlite, which has previously been interpreted as having volcanoclastic textures (Boyer 2005), is reinterpreted here to have, at least partially (i.e., the lower portion of this body), an intrusive origin. The discovery of 'peperitic' textures at an upper kimberlite-mudstone contact provides physical evidence that some of the K252 kimberlite layers were injected as sills into Albian and Cenomanian aged strata (~105 Ma to ~95 Ma). The 'peperite', which is defined by the disintegration of magma intruding and mingling with unconsolidated or poorly consolidated, typically wet sediments (White *et al.* 2000), is characterized by blocky and fluidal textures that include kimberlite-mudstone mingling, fines-depleted elutriation features, and thermally and mechanically-altered mudstone. Jigsaw-fit in-situ fragmentation and mineralized mudstone are also observed at the kimberlite-mudstone contact.

The importance of defining settings for Late Cretaceous volcanic activity in this region is emphasised by new geochronological data that show the two kimberlites with the highest diamond estimates to date, K14 and K252, are included in a 14-point Rb-Sr phlogopite isochron age of 81.5 ± 0.8 Ma (MSWD=0.25).

A much younger intrusive event is associated with the BM2 kimberlite, where Early Paleocene (6-fraction U-Pb perovskite weighted average of 63.5 ± 0.7 Ma) hypabyssal kimberlite intruded into Albian and possibly Cenomanian host rocks. This interpretation is supported by

the high thermal maturity indices of palynomorphs derived from the mudstone located directly adjacent to the kimberlite intrusion.

PALEOCENE PASKAPOO EQUIVALENT INTRA-CRATER FACIES

The youngest eruptive event is of Paleocene age (~60 Ma) whereas the youngest preserved host rocks capping the Buffalo Head Hills are of Campanian age (~78 Ma). In this instance, the only record of now eroded latest Campanian through Paleocene host rocks is provided by sedimentary xenoliths preserved in the truncated intra-crater facies ultramafic bodies (e.g., K1 body).

Selandian Rb-Sr ages of 59.6 ± 2.8 Ma and 60.3 ± 0.8 Ma were determined for the K1A and K19 bodies, respectively; these bodies occur in the southwestern part of the field and are either barren of diamond or have the poorest diamond results within this field (Hood & McCandless 2004; Fig 1). Mineralogical (e.g., amphibole, sanidine) and geochemical evidence (e.g., flatter chondrite-normalized REE pattern versus the steep profile of typical kimberlite) enticed Eccles *et al.* (2008) to conclude that these rocks are better referred to as hybrid kimberlite-ultrabasic rocks.

DISCUSSION AND CONCLUSIONS

This new account of the nature, timing and sequence of volcanic eruptions in the Buffalo Head Hills kimberlite field is made possible by improved age determinations. In summary, three different volcanic settings are recognized in the Buffalo Head Hills kimberlite field: Late Cretaceous Smoky Group equivalent intra- and extra-crater facies, Late Cretaceous and Paleocene intrusive sills and/or dykes, and Paleocene Paskapoo Formation equivalent intra-crater facies. Collectively, these episodes define a kimberlite complex characterized by tabular kimberlite layers of varying ages.

In addition to geological modelling, geochronological data has significant implication for diamond exploration. A northern Alberta 'diamond window' occurs

at ~88-81 Ma (Eccles *et al.* 2008) and appears to be prevalent at ~81 Ma.

Because of their proximity (~ 770 km) and similar Class 2 kimberlite designation, some discussion of the similarities and dissimilarities between the Buffalo Head Hills and Fort à la Corne fields is warranted. Both fields are dominated by primary pyroclastic, volcanoclastic and resedimented volcanoclastic kimberlite, and have large, multi-aged bodies. Hence, a favourable consequence to diamond explorers is that the inter- and extra-crater morphologies of Class 2 kimberlite in the WCSB could cover vast areas.

The Fort à la Corne field is significantly older (Albian) than the Buffalo Head Hills field in northern Alberta. However, the intrusion of Campanian (~81 Ma) kimberlite into the Albian Peace River Formation, which is stratigraphically equivalent to Fort à la Corne's Pense and Joli Fou kimberlite deposits, represents the first chronological link between the two fields and raises some enticing notions. As drilling in Alberta has only penetrated depths of about 250 m, it will be interesting to see if deeper exploratory drilling can discover Mannville aged kimberlite in northern Alberta (i.e., equivalent to Fort à la Corne's Cantuar kimberlite). Conversely, it will be interesting to see if any kimberlite layers at Fort à la Corne are intrusive in nature.

A significant dissimilarity between the Buffalo Head Hills and Fort à la Corne fields is the presence of intrusive kimberlite sills and/or dykes in northern Alberta. We propose that intrusive volcanism might occur in the Buffalo Head Hills when: 1) material from an earlier eruption forms a cap-rock at the top of the emplacement pathway and forces subsequent younger eruptions to either break through the now solid cap or penetrate outwards into preferential zones of weakness, and/or 2) the eruption(s) are

orceful enough to erupt both vertically and horizontally as the magma nears and breaches the surface.

We further speculate that intrusive kimberlite is preferentially injected into and/or directly adjacent to continental clastic wedges that are representative of major sea level low stands in the WCSB. To resolve the complex issues discussed here, grid-based drilling and large geochronological databases are required.

REFERENCES

- BOYER, L.P. 2005. *Kimberlite volcanic facies and eruption in the Buffalo Head Hills, Alberta*. M.Sc. thesis. University of British Columbia.
- ECCLES, D.R., HEAMAN, L.M., LUTH, R.W., & CREASER, R.A. 2004. Petrogenesis of the Late Cretaceous northern Alberta kimberlite province. *Lithos*, **77**, 435-459.
- ECCLES, D.R., CREASER, R.A., HEAMAN, L.M., & WARD, J. 2008. Rb-Sr and U-Pb geochronology and setting of the Buffalo Head Hills kimberlite field, northern Alberta. *Canadian Journal of Earth Sciences*, **45** (5), 513-529.
- HOOD, C.T.S. & MCCANDLESS, T.E. 2004. Systematic variations in xenocryst mineral composition at the province scale, Buffalo Hills kimberlites, Alberta, Canada. *Lithos*, **77**, 733-747.
- SKELTON, D., CLEMENTS, B., MCCANDLESS, T.E., HOOD, C. AULBACH, S., DAVIEW, R., & BOYER, L.P. 2003. The Buffalo Head Hills kimberlite province, Alberta. In KJARSGAARD, B.A. (ed.), *Slave Province and Northern Alberta Field Trip Guidebook*. Geological Survey of Canada, Miscellaneous Publication G-293.
- SKINNER, E.M.W. & MARSH, J.S. 2004. Distinct kimberlite pipe classes with contrasting eruption processes. *Lithos*, **76**, 183-200.
- SWEET, A.R., BOYCE, K., & ECCLES, D.R. In prep. Palynological constraints on kimberlite emplacement models: chronostratigraphy of host rock and clastic xenoliths, Buffalo Head Hills, Alberta.
- WHITE, J.D.L., MCPHIE, J., & SKILLING, I.P. 2000. Peperite: a useful genetic term. *Bulletin of Volcanology*, **62**, 65-66.

Nature of $\delta^{18}\text{O}_{\text{quartz}}$ variation in a Slate-belt – hosted orogenic gold province, Nova Scotia, Canada: evidence for fluid: rock interaction

Daniel J. Kontak¹, T. Kurt Kyser², & Rick J. Horne³

¹Department of Earth Sciences, Laurentian University, Sudbury, ON, P3E 2C6 CANADA
(e-mail: dkontak@laurentian.ca)

²Department of Geological Sciences, Queen's University, Kingston, ON, K7L 3N6 CANADA

³Acadian Mining, Halifax, 1969 Lower Water Street, Halifax, NS, B3J 2R CANADA

ABSTRACT: Vein quartz systems in the Meguma gold districts formed during flexural-slip folding of the bedded sandstone-siltstone sequence. Structural studies indicate the concordant (e.g., stratabound, saddle) and discordant (e.g., en echelon) veins represent a single hydrothermal event, but absolute age dating indicates veins formed during regional deformation (410 Ma) and widespread plutonism (380 Ma). Detailed sampling of all vein types at two deposit sites, constrained to 410 and 380 Ma, indicate similar $\delta^{18}\text{O}$ values (+15 to +16‰). Thus, fluids of similar $\delta^{18}\text{O}$ values were generated at widely different times in the same terrane from different processes. A compilation of $\delta^{18}\text{O}_{\text{quartz}}$ data for 14 gold districts arranged in their stratigraphic order indicates an upward increasing trend of $\delta^{18}\text{O}_{\text{quartz}}$. This observed trend can be modeled to result from increasing fluid:rock ratio if an increasing component of chlorite occurs in the wall rock, that is commensurate with the nature of the known composition variation of the stratigraphy up section.

KEYWORDS: *orogenic gold, oxygen isotopes, Meguma Group, Nova Scotia.*

INTRODUCTION

The Meguma Group, Nova Scotia, hosts over 60 past producing gold districts with historic production of >1 M oz. However, recent exploration activity has delineated resources of 0.6-1 M oz at several locations. The Meguma area has been the focus of many studies over the past century and a variety of models proposed for its origin spanning from syngenetic or exhalative, early- to late-stage metamorphic and intrusion-related. Debates on the origin of these and similar slate-belt - hosted vein deposits focused on the origin of the quartz veins and their age of emplacement. Recent structural studies of several gold districts (Horne & Culshaw 2001; Horne & Jodrey 2002) indicate that vein emplacement occurred during the later stages of fold tightening of the host rocks. In this paper, we present results for $\delta^{18}\text{O}_{\text{quartz}}$ determined for vein samples collected from two well characterized gold districts separated in time by about 30 Ma, compare these data to our earlier studies (Kontak & Kerrich

1995) and model an observed vertical variation of $\delta^{18}\text{O}_{\text{quartz}}$ based on sampling of 14 districts. These data provide further confirmation that: (1) veins in a given deposit represent deposition from a single, isotopically-homogeneous vein-forming fluid; (2) that the source of this fluid is external to the Meguma Group; and (3) that the calculated $\delta^{18}\text{O}_{\text{H}_2\text{O}}$ value of the vein-forming fluids reflect variable amounts of fluid:rock interaction.

GEOLOGICAL SETTING

The study area lies within the Meguma Terrane of southern Nova Scotia. The terrane is dominated by the metaturbiditic rocks of the Lower Paleozoic Meguma Group that were intruded at 380 Ma by meta- to peraluminous granitoid bodies. The Meguma Group has a sandstone-rich lower part and siltstone-rich upper part. Deformation and accompanying greenschist to amphibolite grade regional metamorphism occurred at 410-400 Ma. This deformation produced open, upright, northeast-trending folds with shallowly

plunging fold axes. Gold districts occur throughout the lower, sandstone dominant part of the stratigraphy and there is no apparent stratigraphic control, however, the gold districts are localized to structural domes.

DEPOSIT AREAS, VEIN FEATURES & AGE OF FORMATION

Gold districts occur at or proximal to fold hinges where quartz vein density increases dramatically. Vein types include bedding-concordant (i.e., bedding parallel, saddle reefs) and discordant types (en echelon, conjugate) and their mutually cross cutting relations indicate a single vein-forming event. All vein types are observed to contain gold. Horne & Culshaw (2001) argue that the layered Meguma Group rocks were deformed by a flexural-slip fold mechanism and that vein formation was associated with this process. In addition, vein formation also involved periodic fluid overpressures. Importantly, Morelli *et al.* (2005, and references therein) showed that vein formation occurred twice, once at 408 Ma and again at 380 Ma. Veins are dominated by Qtz-Carb-Sulfides (Fe-As) lesser silicates, and other sulfides (Zn Pb, Cu, Bi, Te). A regional zonation of vein mineralogy reflects district proximity to 380 Ma intrusions (Newhouse 1936; Smith & Kontak 1986). Wall rock alteration (e.g., silica, sericite, carbonate, sulfide, tourmaline) is present, but variably developed.

NATURE OF VEIN FORMING FLUIDS

Previous fluid inclusion and isotopic (Sri, $\delta^{18}\text{O}$, δD , $\delta^{13}\text{C}$, $\delta^{34}\text{S}$; Kontak *et al.* 1996; Kontak & Kerrich 1997) studies indicate that fluids were mixed aqueous-carbonic ($X_{\text{CO}_2} = 0.1-0.3$), exotic to the Meguma Group, and record variable amounts of fluid:rock interaction. Whereas C and S are dominantly wall rock derived, O isotopic data indicate an external reservoir with subsequent modification.

SAMPLING, ANALYTICAL PROCEDURES

Detailed sampling of all vein types was

done in two deposits, The Ovens and Dufferin, where earlier mapping (Horne & Culshaw 2001; Horne & Jodrey 2002) constrains the nature of veins collected. Oxygen was extracted from quartz separates using the BrF_5 technique and isotopic measurements performed using a Finnigan MAT 252 mass spectrometer at Queen's University, Kingston, Ontario. All values are reported using the δ notation in per mil (‰) relative to V-SMOW (Vienna standard mean ocean water, $\delta^{18}\text{O}$) and have a precision of ± 0.1 ‰ based on repeated analyses of standards.

ANALYTICAL RESULTS

$\delta^{18}\text{O}_{\text{quartz}}$ results for the two deposits are very similar regardless of vein types with averages of $+15.7 \pm 0.6$ ‰ (1σ , $n=11$) for Dufferin and $+15.2 \pm 0.9$ ‰ (1σ , $n=15$) for The Ovens. In addition, there is limited spread in the data for each area despite different vein types having been analyzed. Thus, although veins are classified based on structural type and appearance (e.g., laminated vs. non-laminated, saddle vs. limb, stratabound vs. discordant), the $\delta^{18}\text{O}_{\text{quartz}}$ values are the same. In addition, fluid inclusions are similar in quartz from the two areas, with low-salinity (i.e., <6-8 wt% NaCl_2 equiv.) aqueous-carbonic ($X_{\text{CO}_2} = 0.1-0.3$) types dominant.

DISCUSSION

Several issues are discussed below in order to assess to assess the nature and source of the vein-forming fluids.

$\delta^{18}\text{O}$ of Vein-Forming Fluid

The $\delta^{18}\text{O}$ values for vein-forming fluids for the two areas sampled are assessed using the $\Delta^{18}\text{O}$ (quartz- H_2O) and inferred temperature of vein formation (350-400°C; Fig. 1). The range of $\delta^{18}\text{O}_{\text{H}_2\text{O}}$ values is +9 to +12‰ for quartz deposition at 350-400°C. An alternative interpretation is that the variation in $\delta^{18}\text{O}_{\text{quartz}}$ reflects deposition from a fluid of uniform $\delta^{18}\text{O}$, but over a temperature range of about 50°C, as constrained by $\delta^{18}\text{O}_{\text{quartz}}$ values; it is not possible to discriminate between these models. Regardless, the vein fluids had a

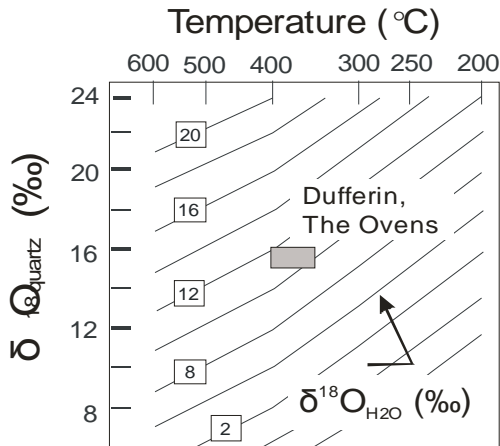


Fig. 1. A plot of $\delta^{18}\text{O}_{\text{Quartz}}$ versus $T(^{\circ}\text{C})$ with isopleths for $\delta^{18}\text{O}_{\text{H}_2\text{O}}$ values of fluids calculated using fractionation equation of Matsuhisa *et al.* (1979). The box outlines the inferred $\delta^{18}\text{O}_{\text{H}_2\text{O}}$ values for vein fluids at The Ovens and Dufferin.

uniform $\delta^{18}\text{O}_{\text{H}_2\text{O}}$ value of +9 to +12‰. Importantly, the data indicate that a fluid of similar $\delta^{18}\text{O}$ value can be generated by events separated by 30 Ma within the same geological terrane.

Regional Variation of $\delta^{18}\text{O}_{\text{Quartz}}$

Analyses of quartz veins from 14 gold districts indicates that there is a limited range in their $\delta^{18}\text{O}$ values for all vein types in an individual deposit, but a systematic enrichment in $\delta^{18}\text{O}_{\text{H}_2\text{O}}$ values is noted when data are arranged stratigraphically in the Meguma Group (Fig. 2), with one deposit area (West Gore) having extreme enrichment. The most primitive $\delta^{18}\text{O}_{\text{H}_2\text{O}}$ values occur for deposits at the base of the stratigraphy, with the lowest of these (+9.5‰) for a deposit (Beaver Dam, BD) proximal a 375 Ma granitic intrusion. The observed vertical variation in $\delta^{18}\text{O}_{\text{H}_2\text{O}}$ values might be explained by: (1) fluid cooling, (2) fluid mixing, or (3) fluid contamination. The first scenario is eliminated based on previous work indicating that there was no systematic cooling of fluids up section or a change in mineralogy. Case two is discounted, as there is no evidence, such as variable fluid salinity, to indicate fluid mixing occurred. To address contamination of the vein fluid,

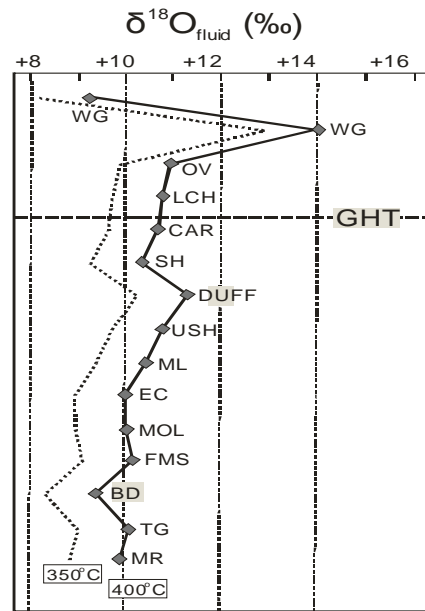


Fig. 2. Plot of $\delta^{18}\text{O}_{\text{H}_2\text{O}}$ values (350° and 400°C) for gold districts versus stratigraphic position in the Meguma Group. GHT is the contact between the sandstone dominant Goldenville Fm. And overlying shale dominant Halifax Fm.

we have modeled fluid:rock interaction using appropriate equations in Taylor (1978) and using a primary fluid of +9‰ (see Fig. 2) and an initial whole rock value of +12‰ (Meguma Group value; Longstaffe *et al.* 1980). The calculations indicate that the ^{18}O enrichment of the fluid is possible if a model rock composition contains chlorite and the infiltrating fluid is at 400-500°C. Such a composition is a proxy for the observation of an increasing shale component in Meguma Group higher in the stratigraphy along with a general decrease in metamorphic grade.

SUMMARY AND CONCLUSIONS

Meguma gold-quartz vein deposits were emplaced during regional metamorphism (408 Ma) and peraluminous magmatism (380 Ma) in conjunction with fold tightening of the Meguma Group rocks. Sampling of two well-constrained vein systems formed at these times with the structural features, vein mineralogy and fluid chemistry have identical $\delta^{18}\text{O}_{\text{Quartz}}$ and

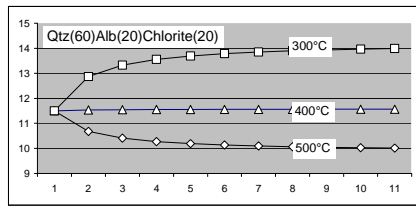


Fig. 3. Plot of fluid:rock ratio versus calculated $\delta^{18}\text{O}_{\text{altered rock}}$ for interaction of fresh rock of known modal composition ($\delta^{18}\text{O} = +12\text{‰}$) with fluid of $\delta^{18}\text{O} = +9\text{‰}$. Note that a $T > 500^\circ$ is required in order for the fluid to increase its $\delta^{18}\text{O}$ value.

indicate $\delta^{18}\text{O}_{\text{H}_2\text{O}}$ values of +9 to +12‰ for 350-400°C, and suggest a metamorphic fluid. Integration of these data with the $\delta^{18}\text{O}_{\text{quartz}}$ data for twelve other Meguma deposits indicates a gradual vertical enrichment in $\delta^{18}\text{O}$, that is interpreted to have resulted from fluid:rock interaction of a fluid of an initial $\delta^{18}\text{O}_{\text{H}_2\text{O}}$ of +9‰ with chlorite-bearing metasedimentary rocks. These conclusions are consistent with other chemical data indicating that the fluids responsible for vein formation are exotic to the Meguma Group.

ACKNOWLEDGEMENTS

This work was funded when the senior author was at the Nova Scotia Department of Natural Resources. Isotopic analyses were also supported by an NSERC Discovery grant to Kyser.

REFERENCES

HORNE, R. & CULSHAW, N. 2001. Flexural-slip folding in the Meguma Group, Nova Scotia. *Journal of Structural Geology*, **23**, 1631-1652.

HORNE, R. & JODREY, M. 2002. Geology of the Dufferin gold deposit (NTS 11D/16), Halifax County. *Nova Scotia Department Natural Resources, Report of Activities 2001*, 51-68.

HORNE, R.J. & PELLY. 2007. Geological transect of the Meguma Terrane from centre Musquodoboit to Tangier. *Nova Scotia Department Natural Resources, Report of Activities 2001*, 71-89.

KONTAK, D.J. & SMITH, P.K. 1989. Sulphur isotopic composition of sulphides from the Beaver Dam and other Meguma Group-hosted gold deposits, Nova Scotia: implications for genetic models. *Canadian Journal of Earth Sciences*, **26**, 1617-1629.

KONTAK, D.J., SMITH, P.K., & HORNE, R.J. 1996. Hydrothermal characterization of the West Gore Au-Sb deposit, Meguma Terrane, Nova Scotia. *Economic Geology*, **91**, 1239-1262.

KONTAK, D.J. & KERRICH, R. 1997. An isotopic (C, O, Sr) study of vein quartz and carbonate from Meguma gold deposits, Nova Scotia, Canada. *Economic Geology*, **92**, 161-180.

LONGSTAFFE, F, SMITH, T.E., & MUELENBACHS, K. 1980. Oxygen isotope evidence for the genesis of Upper Paleozoic granitoids from southwestern Nova Scotia. *Canadian Journal of Earth Sciences*, **17**, 132-141.

MATSUMIYA, Y., GOLDSMITH, J.R., & CLAYTON, R.N. 1979. Oxygen isotopic fractionation in the system quartz-albite-anorthite-water. *Geochimica et Cosmochimica Acta*, **43**, 1131-1140.

MORELLI, R.M., CREASER, R., SELBY, D., KONTAK, D.J., & HORNE, R.J. 2005. Rhenium-Osmium geochronology of arsenopyrite in Meguma Group gold deposits, Meguma Terrane, Nova Scotia, Canada: Evidence for multiple gold-mineralizing events. *Economic Geology*, **100**, 1229-1242.

NEWHOUSE, W.N. 1936. A zonal gold mineralization in Nova Scotia. *Economic Geology*, **31**, 805-831.

SMITH, P.K. & KONTAK, D.J. 1987. Meguma gold studies: some basic observations. *Mines and Minerals Branch Report of Activities for 1987, Part A., Nova Scotia Department of Mines and Energy, Report 87-5*, 69-72.

TAYLOR, H.P., Jr. 1978. Oxygen and hydrogen isotope studies of plutonic granitic rocks. *Earth & Planetary Science Letters*, **38**, 177-210.

Tracing progressive redox gradients and directions of hydrothermal flow using uranium and lithium isotopes

Kurt Kyser, Majdi Geagea, Don Chipley, Paul Alexandre, Mark Raycroft, April Vuletich, & Rachel Schwartz-Narbonne

Dept Geological Sciences & Geological Engineering, Queen's University, Kingston, ON CANADA
(e-mail: kyser@geol.queensu.ca)

ABSTRACT: Uranium isotopes fractionate as a result of nuclear volume effects such that $^{238}\text{U}/^{235}\text{U}$ ratios vary as a function of uranium oxidation state, being highest in reduced species such as U^{4+} in uraninite. The $\delta^{238}\text{U}$ values of uranium minerals from volcanic-, metasomatic-, unconformity-, sandstone- and calcrete related uranium deposits worldwide vary by 1.5 ‰ and can be used to indicate sources of uranium. Uraninites with reset ages caused by later recrystallization events have low $\delta^{238}\text{U}$ values as a result of mobilization of ^{235}U during interaction with later fluids. Thus, uranium isotopes provide information about source and redox history of the uranium in the deposits.

Lithium isotopes do not fractionate as a result of redox reactions, but ^7Li is preferentially partitioned into the fluid phase, whereas ^6Li prefers sites in alteration minerals such as micas. The $^7\text{Li}/^6\text{Li}$ ratios of mica and chlorite in alteration zones around uranium deposits are higher and decrease to lower values with distance from the ore relative to background mica in the Athabasca Group sandstones. In barren areas, high ratios are rare and background ratios are dominant. When used together, the isotopic composition of uranium and lithium can be utilized to refine both the genesis of uranium deposits and as exploration tools.

KEYWORDS: Fluid flow path, redox, isotopes

INTRODUCTION

Variations in the isotopic composition of uranium in uranium ores have only been reported in deposits from Gabon, where natural reactors went critical 2 billion years ago, thereby altering the $^{238}\text{U}/^{235}\text{U}$ ratio from that reported for all other natural samples (Naudet & Renson 1975; Bros *et al.* 1993). New ICP-MS technologies (Anbar *et al.* 2002) and advances in our understanding of how nuclear structure in the isotopes of some heavy elements can affect bonding have suggested that variations, albeit small, in uranium isotope ratios might occur as a result of redox reactions. These variations occur because nuclei with an odd number of neutrons, such as ^{235}U , have a smaller nucleus relative to nuclei with an even number of neutrons such as ^{238}U , and this difference will result in different bond strengths related to the different sizes of the nuclei. This effect results in differences in $^{238}\text{U}/^{235}\text{U}$ ratios between phases having different bond types, such as those

involving uranium with different oxidation states.

Uranium is a redox sensitive element, with most naturally occurring uranium either as U^{+4} or U^{+6} . Theory would indicate that ^{235}U should be preferentially retained in oxidized phases, such as dissolved U^{+6} , whereas ^{238}U should be preferentially partitioned into reduced species like uraninite (Bigeleisen 1996; Schauble 2007). Thus, most uranium deposits except those associated with high temperature processes should have small variations in their $^{238}\text{U}/^{235}\text{U}$ ratios as a result of the extent that a pool of uranium is reduced from U^{+6} to U^{+4} .

As predicted from the nuclear size effect on the distribution of uranium isotopes, Sterling *et al.* (2007) and Weyer *et al.* (2008) report a total variation of 1.5 ‰ in the $^{238}\text{U}/^{235}\text{U}$ ratios decreasing in the order from black shales > basalts, > seawater, > banded iron formations (BIFs). The black shales reflect preferential reduction by organic matter of ^{238}U from seawater,

basalts reflect reducing, high-temperature environments and BIFs reflect the preferential adsorption of ^{235}U from seawater by Fe-oxides (Weyer *et al.* 2008). Bopp *et al.*, (2008) report that $^{238}\text{U}/^{235}\text{U}$ ratios in sandstone-type uranium ores are greater than magmatic uranium ores by 1 ‰, but no explanation for this difference was proposed other than a reflection of different redox conditions.

In marked contrast to the chemical behaviour of U, Li is not redox sensitive so that variations in its isotopic composition will not reflect the redox process associated with deposits. However, the 17% mass difference between the ^6Li and ^7Li is significant so that fractionation of Li as it changes bonding environment should be substantial. The light isotope ^6Li preferentially enters solid phases, so that the $^7\text{Li}/^6\text{Li}$ ratio in a hydrothermal fluid should increase upstream, as should the ratios in the alteration minerals that result from this fluid (Millot *et al.* 2007). The $^7\text{Li}/^6\text{Li}$ ratio in alteration minerals should increase towards the deposit along the flow path of the mineralizing fluid (Millot & Negrel 2007). Thus, Li isotopes might be indicators of the direction of fluid flow in mineralizing systems.

RESULTS

Uranium Isotopes

The $^{238}\text{U}/^{235}\text{U}$ ratios of uranium minerals from volcanic-, metasomatic-, unconformity- and sandstone-related uranium showings and deposits worldwide measured by multi-collector ICP-MS indicate a total variation in $\delta^{238}\text{U}$ values of 1.5 ‰, with the $^{238}\text{U}/^{235}\text{U}$ ratio varying as a function of type of uranium deposit (Fig. 1).

Because of the high temperatures involved in magmatic- and metasomatic-related uranium deposits, variations in their $^{238}\text{U}/^{235}\text{U}$ ratios should be minimal, unless later alteration has resulted in mobilization of uranium. The calcrete deposits measured so far (Fig. 1) are known to have uranium derived from a near-by igneous source, and they have $^{238}\text{U}/^{235}\text{U}$ ratios in carnotite consistent with such a source. Metasomatic-related

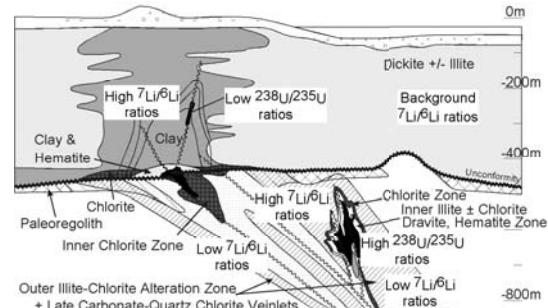


Fig. 1. $^{238}\text{U}/^{235}\text{U}$ ratios, expressed as $\delta^{238}\text{U}$ values, of uraninite ores from different classes of uranium deposits. Within the unconformity-related deposits, complex-type deposits have the lowest $^{238}\text{U}/^{235}\text{U}$ ratios whereas simple types have higher ratios. Also shown is the range of $^{238}\text{U}/^{235}\text{U}$ ratios in basalts/granites and sediments.

deposits also have $^{238}\text{U}/^{235}\text{U}$ ratios consistent with a dominantly igneous-related source.

Unconformity-type uranium deposits, as well as sandstone-hosted deposits, should be zoned in their $^{238}\text{U}/^{235}\text{U}$ ratios as a result of two processes. In the first process, the $^{238}\text{U}/^{235}\text{U}$ ratios in the first uraninite precipitated should be greatest and should decrease as the ^{238}U is preferentially removed from the fluid. This process will result in a gradient of $^{238}\text{U}/^{235}\text{U}$ ratios such that we would expect the highest ratios distal from the redox centre and within the redox centre we would expect lower ratios (Fig. 2). The other process that could affect the ratios would involve mobilization of uranium by later fluids. If these fluids are oxidizing, as they must be to mobilize the ore, we would expect ^{235}U to be preferentially partitioned into the fluid phase. Indeed, in some basement-hosted deposits, uraninite with the lowest apparent ages have the lowest $\delta^{238}\text{U}$ values as a result of ^{235}U being preferentially mobilized into secondary fractures. This ^{235}U could then be absorbed by iron oxides and other phases or precipitated as secondary minerals, resulting in $^{238}\text{U}/^{235}\text{U}$ ratios that decrease away from the ore zone. This uranium is extractable using a weak acid leach and can be used to vector into high-grade ore, and should be applicable to all

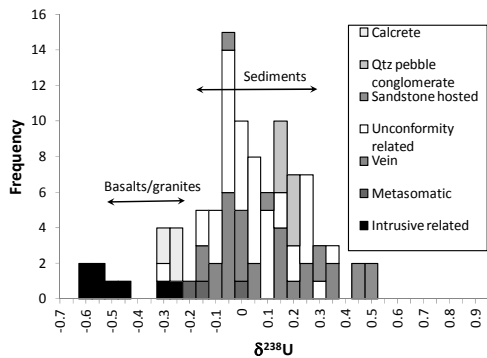


Fig. 2. General alteration and geologic features of basement- and sandstone-hosted uranium deposits showing distributions in U and Li isotope ratios.

uranium deposit types.

Lithium Isotopes

The ⁷Li/⁶Li ratios in muscovite and chlorite alteration proximal and distal to uranium deposits in the western Athabasca Basin and in barren systems in the eastern Athabasca Basin are highest in the ore zone and decrease in the basement rocks and lower Athabasca Group sandstones further away from the mineralized zone. In barren areas, high ratios are rare and background ratios are dominant. We interpret lower ⁷Li/⁶Li ratios to reflect the ingress of hydrothermal fluids associated with alteration and mineralizing events and the highest ratios as the down-stream portions of these systems, that have become enriched in ⁷Li. If valid, ⁷Li/⁶Li ratios would indicate where in the hydrothermal systems the muscovite and chlorite alteration is located because fluids associated with the ore forming process involve the highest degree of interaction with rocks to become enriched in ⁷Li.

CONCLUSIONS

²³⁸U/²³⁵U ratios, expressed as δ²³⁸U values, of uraninite ores from different classes of uranium deposits vary widely. These variations reflect a combination of the source of the uranium, the efficiency of the redox environment in which the minerals were precipitated and the degree that uranium was previously removed from the mineralizing fluid. Therefore, uranium

isotopes can be used to refine the critical processes in the generation of uranium deposits, as well as indicate proximity to an ore forming environment.

⁷Li/⁶Li ratios in muscovite and chlorite associated with uranium mineralizing events are distinct from background ratios, with the lowest values reflecting the beginning of hydrothermal alteration systems whereas the highest values are indicative of the terminal flow of hydrothermal fluids. Together, these two systems can be used to vector to ore-forming environments. Identification of proxies in elemental concentrations for these two isotope systems might result in an effective exploration tool as a vector for uranium deposits, particularly those in sedimentary basins.

ACKNOWLEDGEMENTS

We thank Cameco Corp., Uravan Minerals, Strateco Resources and the Royal Ontario Museum for samples used in this study.

REFERENCES

- ANBAR, A.D., ARNOLD, G.L., RYE, R., & WEYER, S. 2002. Iron isotopes in an Archean Paleosol; Abstracts of the 12th annual V. M. Goldschmidt conference. *Geochimica et Cosmochimica Acta*, **66**(15A), 18.
- BIGEISEN J. 1996. Temperature dependence of the isotope chemistry of the heavy elements. *Proceedings of the National Academy of Sciences*, **93**, 9393-9396.
- BROS, R., TURPIN, L., GAUTHIER-LAFAYE, F., HOLLIGER, P., & STILLE, P. 1993. Occurrence of naturally enriched (super 235) U; implications for plutonium behaviour in natural environments. *Geochimica et Cosmochimica Acta*, **57**, 1351-1356.
- KYSER, T.K., CHIPLEY, D., VULETICH, A., & ALEXANDRE, P. 2008. Variations in ²³⁸U/²³⁵U ratios in natural uranium ore minerals from sedimentary basins; Abstracts of the 18th annual V. M. Goldschmidt conference. *Geochimica et Cosmochimica Acta*, **72**(12), A508.
- MILLOT, R. & NEGREL, P. 2007. Multi-isotopic tracing (delta (super 7) Li, delta (super 11) B, (super 87) Sr/ (super 86) Sr) and chemical geothermometry; evidence from hydro-geothermal systems in France. *Chemical Geology*, **244**, 664-678.

- MILLOT, R., NEGREL, P., & SANJUAN, B. 2007. Lithium isotopes in geothermal systems; Abstracts of the 17th annual V. M. Goldschmidt conference. *Geochimica et Cosmochimica Acta*, **71**(15S), A667.
- NAUDET, R. & RENSON, C. 1975. Resultats des analyses systematiques de teneurs isotopiques de l'uranium. Results of systematic analyses of isotopic content of uranium. In: *Le phenomene d'Oklo--The Oklo phenomenon* International Atomic Energy Agency, Vienna, Austria (IAEA).
- SCHAUBLE, E.A. 2007. Role of nuclear volume in driving equilibrium stable isotope fractionation of mercury, thallium, and other very heavy elements. *Geochimica et Cosmochimica Acta*, **71**, 2170-2189.
- STIRLING, C.H., ANDERSEN, M.B., POTTER E.-K., & HALLIDAY, A.N. 2007. Low-temperature isotopic fractionation of uranium. *Earth and Planetary Science Letters*, **264**, 208-225.
- WEYER, S., ANBAR, A.D., GERDES, A., GORDON, G.W., ALGEO, T.J., & BOYLE, E.A. 2008. Natural fractionation of (super 238) U/ (super 235) U. *Geochimica et Cosmochimica Acta*, **72**, 345-359.

The use of Cu isotope fractionation in low temperature ore systems as a geochemical exploration tool

Ryan Mathur¹, Spencer R. Titley², Susan Brantley³, & Marc Wilson⁴

¹Juniata College, Huntingdon, PA USA (e-mail: mathur@juniata.edu)

²University of Arizona, Tucson, AZ USA

³Pennsylvania State University, State College, PA USA

⁴Carnegie Museum of Natural History, Pittsburgh, PA USA

ABSTRACT: On the surface of the earth highly weathered deposits are characterized by Fe-oxides that represent the weathered remnants of sulfide mineralization, it is difficult to find and assess potential enrichment at depth. In order to assess the importance of leaching and enrichment of mineral deposits, Cu isotope geochemical analyses of leach cap and enrichment minerals can provide important information about current and past supergene processes. We examine copper isotope fractionation in actively weathering soils, epithermal, porphyry copper and massive sulfide deposits from around the world. A distinct pattern of isotopically depleted weathered/leached minerals at the surface and isotopically enriched enrichment exists for all types of deposits. Patterns of isotopic fractionation and the magnitude of isotopic fractionation might suggest where the deposit could be located as well as the degree of weathering history (i.e., few vs. multiple leach events). Because the patterns of copper isotope fractionation are identical regardless of geologic environment, copper isotope analysis provides a technique for understanding supergene processes worldwide.

KEYWORDS: *Cu isotopes, porphyry copper, supergene*

INTRODUCTION

Understanding supergene processes and their impact on any deposit type is essential for mineral assessment. The degree or amount of weathering of porphyry copper deposits, massive sulfide deposits, or any sedimentary-related deposits will directly impact the concentration of metals found in the deposit. Conventional dating of supergene minerals indicates that weathering occurs over the span of millions of year, whereas some deposits show little evidence of supergene activity when drilled at depth.

In this contribution, the fractionation of Cu isotopes during the aqueous low temperature reactions aids in identification of the minerals involved in weathering and the extent of weathering in area.

The supergene environment is an ideal place to document the effects of copper isotope fractionation in the weathering cycles of ore deposits. As is the case with light stable isotopes (O, S, N, and C) copper isotopes are thought to fractionate due to quantum mechanical effects

associated with different vibrational frequencies associated with bonding (Seo *et al.* 2007). Models predicting fractionation of copper isotopes at both high temperatures (>300°C of ca. 0.5‰) and low temperatures (<50°C with approximately 3‰ fractionation) have been recently constructed (Seo *et al.* 2007). If multiple stages of low temperature leaching (progressive weathering of enrichment blankets) occurred; copper isotope fractionation in the leached caps and enrichment blankets could be on the order of several tens per mil. Other causes that could impact the degree of fractionation such as crystallography, pH, Eh, and temperature of these isotopes have been and are currently being investigated by (Wall *et al.* 2007). In this study, we focus on the copper isotope composition of the residual reactants and the products of sulfideweathering in nature.

GEOLOGICAL SETTING

Weathering of sulfide-rich rocks from

porphyry copper deposits, massive sulfide deposits and sulphide-bearing black shale from around the world provide global and diverse geologic perspectives of the utility of Cu isotope fractionation as an exploration tool.

In general, the emplacement processes of the ore deposits results in the development of intensely shattered (permeable) rock volume through which hydrothermal fluids flow, depositing both sulfide and silicate minerals, but most importantly in the context here, pyrite (FeS₂) and chalcopyrite (CuFeS₂). When the primary system is unroofed or exposed at or near the surface, and above a lowered water table, oxidizing waters and biogenic activity generate acid from the decomposition of pyrite. The acidic and oxidizing solutions dissolve copper sulphides (like chalcopyrite) and move copper in solution down to a level where free oxygen is diminished, generally considered the top of the water table. Progressive neutralization of the supergene fluids through hydrogen consumption in reaction with host rocks forms supergene silicate alteration minerals and chalcocite.

The processes result in the separation of levels in the supergene profile, the zone of *oxidation* downwards grades into a zone of *leaching*, then into a zone of *enrichment*.

During soil generation, the breakdown of rock to soil mimics the general supergene process described above with the oxidation of rock, formation of clays and the generation of oxide minerals.

METHODS

Samples are from drill core, hand specimens, or augered core. The samples are composed of oxide or sulfide for the ore deposit samples. The soil samples are mixtures of oxides and silicates. Approx. 0.05g of powdered sample material was dissolved in aqua-regia over night at 200°C and dried on a hot plate at 40°C. Cu was separated from the matrix through ion exchange chromatography (IEC) as outlined in Mathur *et al.* (2005) without the use of hydrogen peroxide. To ensure all of

the Cu was recovered, gravimetric yields were checked for IEC samples and only samples with >90% yield are reported.

The samples purified with IEC were diluted to approximately 100 ppb Cu. These samples were injected into a Multicollector Inductively-Coupled-Plasma mass spectrometer (MC-ICPMS, Micromass Isoprobe at the University of Arizona and Neptune at Washington State University) in low resolution mode using a microconcentric nebulizer to increase sensitivity for the samples with lower concentrations of copper. The nebulizer flow was adjusted so that the intensity of the ⁶³Cu beam remained constant at 2 volts. Both on and off peak blank corrections were applied to the data and yielded the same result.

Copper isotope ratios are reported in the familiar delta notation:

$$\delta^{65}\text{Cu} (\text{‰}) = \left\{ \left(\frac{\left(\frac{^{65}\text{Cu}}{^{63}\text{Cu}} \right)_{\text{sample}}}{\left(\frac{^{65}\text{Cu}}{^{63}\text{Cu}} \right)_{\text{standard}}} \right) - 1 \right\} \cdot 1000 \quad (1)$$

where the standard was the NIST 976 Cu standard. Two blocks of 25 ratios are reported as an average for each run. Within each run, the measurement error for $\delta^{65}\text{Cu}$ was less than 0.01‰ for all analyses.

A major concern surrounding isotope data obtained during analysis is the measurement error associated with mass fractionation within the instrument owing to variations in operating conditions (e.g. Marechal *et al.* 1999). In order to constrain the errors associated with copper isotope analyses on our instrument, we compared all of the copper ratios to the NIST 976 copper standard (eq. 1) using standard-sample-standard bracketing. The 2 σ error for the variation of the standard for eight analytical sessions was observed to be \pm 0.14‰.

DISCUSSION

Figure 1 plots all of the data from the ore deposits. Notice that primary high

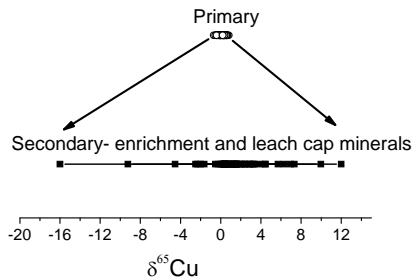


Fig. 1. Plot of $\delta^{65}\text{Cu}$ values for primary and secondary copper minerals. Data taken from Mathur *et al.* (2009), Aseal *et al.* (2007), Markl *et al.* (2005), Mathur *et al.* (2005), Larson *et al.* (2003), and this study.

temperature mineralization has a relatively tight cluster of $\delta^{65}\text{Cu}$, whereas enrichment and leach cap minerals span over 28‰. Thus, aqueous low temperature geochemical reactions result in large variations of the Cu isotope composition in rocks.

Three different isotope reservoirs characterize the weathering process in ore deposits:

- (1) High temperature, primary mineralization
- (2) Leached rock
- (3) Enriched rock

Each reservoir possesses a distinct isotopic signature. Several studies have demonstrated the impact of oxidation during weathering of primary sulphides. The oxidized product favours the heavy isotope, whereas the reduced residual material favours the lighter isotope. The relationship leads to the generation of distinct leach cap, enrichment and primary isotope signatures portrayed in Figure 2.

The data provides two general types of information: an indication of the degree of weathering in an area and the types of Cu minerals that weathered to generate the Cu isotope signatures present.

In order to quantify the degree of leaching that occurred during weathering, the following expression is used:

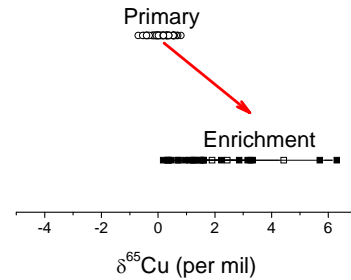


Fig. 2. Plot of primary chalcocopyrite and secondary chalcocite data taken from the same sources as Figure 1.

$$\Delta = \delta^{65}\text{Cu}_{\text{secondary Cu mineral}} - \delta^{65}\text{Cu}_{\text{primary Cu mineral}} \quad (2)$$

In theory, greater values of $\Delta^{65}\text{Cu}$ indicate greater degrees of leaching because each leach involves oxidation and reduction reactions that increase the fractionation of copper isotopes between secondary copper minerals. The equation could compare the primary sulfideto the leach cap value (this is what is done with the Marcellus soil sample) to obtain a value that indicates the degree of weathering. Both assume that leached Cu from the leach cap migrated downward without any lateral loss of Cu (for instance Cu rich waters laterally migrating to form exotic Cu deposits or that the groundwaters drained into a larger body of water). The values reported are the average copper isotope signature of each reservoir; in order to fairly assess the degree of leaching within a deposit, larger sampling sizes are necessary. Nonetheless, Mathur *et al.* (2005) modelled this behaviour with Rayleigh fractionation trends and positive Δ values further demonstrated that sequential leaching during weathering can lead to highly fractionated Cu isotope ratios in productive porphyry copper systems as demonstrated in Table 1.

The $\Delta^{65}\text{Cu}$ values greater than 1 correlate with deposits that have well developed enrichment blankets, whereas deposits with lower values such as Butte,

Table 1. Results from Mathur *et al.* (in print), Borg *et al.* (2009), and this study.

Deposit	$\Delta_{\text{secondary-primary}}$
Chuquicamata, Chile	1.85‰
El Salvador, Chile	2.33‰
Collahuasi, Chile	2.49‰
Morenci, USA	2.1‰
Butte, USA	0.38‰
Sliver Bell, USA	5.14‰
Skorpion, Nambia	0.60 ‰
Marcellus Soils	0.43‰

Skorpion and the Marcellus soils correlate with areas that have not experienced much secondary copper enrichment.

In order to develop larger $\Delta^{65}\text{Cu}$ values, reactions involving large fractionation factors or multiple leach events are necessary. Experimental work from Kimball *et al.* (in print) and Wall *et al.* (2007) defined fractionation factors during the oxidative dissolution of several Cu sulfides. The dissolution of chalcocite generated the largest fractionation factor with values at 2.5 to 3.6 in comparison to 0.8 to 1.6 for the other 7 sulfide analyzed. Thus, larger degrees of Cu isotope separation between the three isotopic reservoirs could indicate the construction and destruction of chalcocite enrichment blankets.

The exploration potential resides in the ability to find leach caps with lighter isotopic compositions that could indicate areas of leaching, or chalcocite samples that have heavier isotope compositions that correlate with multiple cycles of enrichment.

CONCLUSIONS

In summary, the dataset indicates:

- (1) Leach cap expressions on the surface reflect what could be beneath in these porphyry copper systems.
- (2) Cu isotope compositions of chalcocite from enrichment blankets or Fe-oxides

from leach cap minerals could indicate the degree of leaching.

- (3) The copper isotope composition of waters actively weathering copper minerals could have distinctly heavy copper isotope signatures and indicate areas where highly enriched ore exist.

ACKNOWLEDGEMENTS

This material is based upon work supported by the National Science Foundation under Grant No. CHE-0431328. We would like to thank Asarco, Codelco and Phelps Dodge for permission to sample and financial support.

REFERENCES

- A SEAL, D. MATTHEWS, A., BAR-MATTHEWS, M., & HALICZ, L.. 2007. Copper isotope fractionation in sedimentary copper mineralization (Timna Valley, Israel). *Chemical Geology*, **243**(3-4), 238-254.
- KIMBALL, B., *et al.* (in print) Copper isotope fractionation in acid mine drainage. *Geochimica et Cosmochimica Acta*
- LARSON, P.B. *et al.* 2002. Cu isotopes; tracing metal sources in ore deposits. *Geochimica et Cosmochimica Acta*, **66**(15A), 432.
- MARKL, G., LAHAYE, Y., & SCHWINN, G. 2006. Copper isotopes as monitors of redox processes in hydrothermal mineralization. *Geochimica et Cosmochimica Acta*, **70**(16), 4215-4228.
- MATHUR, R. *et al.* 2005. Cu isotopic fractionation in the supergene environment with and without bacteria. *Geochimica et Cosmochimica Acta*, **69**(22), 5233-5246.
- MATHUR R., *et al.* (in print) Exploration potential of Cu isotope fractionation in Porphyry Copper deposits. *Journal of Geochemical Exploration*.
- SEO, J.H., LEE, S.K., & LEE, I. 2007. Quantum chemical calculations of equilibrium copper (I) isotope fractionations in ore-forming fluids. *Chemical Geology*, **243**, 225-237.
- WALL, A., HEANEY, P., MATHUR, R. 2007. Insights into copper isotope fractionation during the oxidative phase transition of chalcocite, using time-resolved synchrotron X-ray diffraction. *Geochimica Cosmochimica Acta*, **77**, A1081.

Oxygen isotope zoning in subvolcanic, intrusion-centered submarine hydrothermal systems as a guide to VMS exploration

Bruce E. Taylor¹, Greg Holk², Benôit Dubé³, & Alan Galley¹

¹Geological Survey of Canada, Ottawa, ON, K1A 0E8 CANADA (btaylor@nrcan.gc.ca)

²Department of Geological Sciences, California State University, Long Beach, CA, 90840-39002 USA

³Geological Survey of Canada, Québec, QC, G1K 9A9 CANADA

ABSTRACT: Oxygen isotope mapping (previous and on-going) about four sub-volcanic intrusive centers in Canada (Clifford-Ben Nevis and Sturgeon Lake, Ontario; Noranda, Quebec; and Snow Lake, Manitoba) and in Sweden (Kristineberg), among others, has revealed a number of systematics that can be applied to the exploration of volcanic-associated massive sulfide (VMS) deposits. Isotope analysis acquired of >2500 whole-rock samples, plus >600 analyses from the literature, has facilitated mapping of paleo-hydrothermal systems covering from 84 km² (Snow Lake) to 525 km² (Noranda), with sample densities (samples/km) of 1.5 (Clifford-Ben Nevis) to 10.6 (Snow Lake). In simple systems, VMS deposits occur in isotopically "normal" rocks, between semi-conformable zones of low- and high- $\delta^{18}\text{O}$ values representing, respectively, the high-temperature reaction zone, and either later, hanging wall alteration during waning hydrothermal activity, or unaltered, post-VMS rocks. Recognition of both zones provides a means of assessing an area, and an exploration vector. Discordant alteration along synvolcanic faults provides a local exploration guide. Superposition of single-phase systems by successive magmatic emplacement and hydrothermal activity leads to multi-phased alteration, higher water/rock ratios and more productive areas. An apparent, positive correlation between district VMS tonnage, and aerial extent of synvolcanic intrusions and low $\delta^{18}\text{O}$ zones, suggests a means of quantitative terrane assessment.

KEYWORDS: *Subvolcanic, VMS, exploration, oxygen isotopes, hydrothermal system*

INTRODUCTION

Volcanic-associated massive sulfide (VMS) deposits that form at or near the seafloor in submarine, magmatic-centred hydrothermal systems contain altered rocks whose oxygen isotope characteristics provide a robust fingerprint of economic import. The application of oxygen isotope mapping to delineate large magmatic-centered hydrothermal systems has been described by a number of authors since the classic work of H. P. Taylor and co-workers (e.g., H. P. Taylor 1974). With few exceptions (e.g., Criss *et al.* 2000; Cathles 1993; Criss & Taylor 1983), however, the areas covered and the sample densities involved in these studies were necessarily restricted. A GSC-CAMIRO project (Galley *et al.* 2002) and current TGI-III Abitibi project (GSC-Quebec-Ontario) have afforded comparative study of several complex sub-marine magmatic-hydrothermal

systems on a sufficiently large scale that some new important, general aspects have emerged. Additionally, oxygen isotope techniques used to detect, delineate and quantify submarine hydrothermal systems offer an advantage over more classical lithogeochemical techniques because the record of isotopic alteration can survive to anatexis.

GEOLOGICAL SETTING

Three mineralized districts in Canada containing trondhjemitic to tonalitic subvolcanic complexes of variable size have been iso-topically mapped: Snow Lake, Manitoba (84 km²); Sturgeon Lake, Ontario (175 km²); and Noranda, Quebec (>525 km²); and one in Sweden: Kristineberg mine area, Skellefte district (90 km²). The Clifford stock, a sub-volcanic intrusion without known associated VMS deposits in the Clifford-Ben Nevis townships, Ontario (160 km²),

west of Noranda, originally selected as a control case, is now known to post date enclosing volcanic rocks by ca 10 Ma (Piercey *et al.* 2008). Current studies in the Blake River Group extend our knowledge eastward from Noranda (2704-2699 Ma), to the highly fertile Doyon-Bousquet-LaRonde Au-rich VMS district (2699-2695 Ma; McNicoll *et al.* 2008). The derived general isotopic systematics apply, in spite of differences in metamorphism, deformation, and magmatic and hydrothermal complexity.

ANALYTICAL METHODS

Representative hand samples, free of mega-scopic veining and weathered surfaces were analyzed for their oxygen isotope compositions using standard fluorination procedures employing BrF₅ (Clayton & Mayeda 1963; Taylor 2004), yielding ca.100 μmole-sized samples of CO₂ for isotope-ratio mass spectrometry in a Finnigan MAT252 mass spectrometer. The oxygen isotope data are reported using standard δ-notation in permil (‰), relative to V-SMOW. The routine value for NBS-28 obtained in the GSC-LSI laboratory (Ottawa) is 9.5 ‰. The precision of δ¹⁸O values reported for whole-rock samples in this study is better than 0.2 ‰.

The sample densities (samples/km²) for areas not highly-strained are: Clifford-Ben Nevis (1.5), Noranda (1.8), and Sturgeon Lake (2.6). Areas with marked folding, high strain, synvolcanic faults, and intrusive contacts are best sampled locally with closer spacing (e.g., Snow Lake, 10.6 samples/km²). Availability of outcrop and drill core determines uniformity of sample coverage.

RESULTS AND DISCUSSION

The plot of δ¹⁸O versus the integrated, water/rock ratio (e.g., Criss & Taylor 1986) in Figure 1 graphically describes isotopic alteration of two model rock types, andesite (A, primary δ¹⁸O = 6.0 ‰) and rhyolite (R, primary δ¹⁸O = 7.0 ‰), simply modeled by feldspar-seawater (δ¹⁸O_{SW} = 0.0 ‰), over a wide range of water/rock

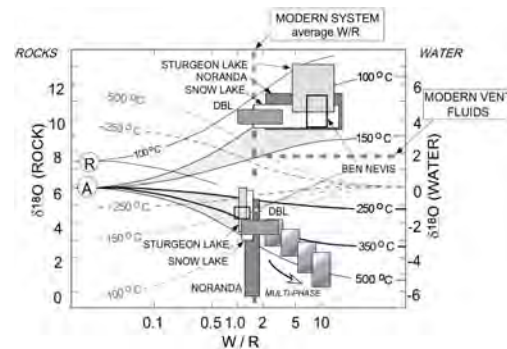


Fig. 1. Water/rock reaction diagramme illustrates fields of mapped high- and low-temperature isotopic alteration (see text) for rhyolites (R) and andesites (A) districts studied (DBL = Doyon-Bousquet-LaRonde). Solid and dashed curves: evolution of rock and water, respectively. Multi-phase reaction history of the central Noranda district, shown schematically, generally corresponds to intrusive history. Approximate δ¹⁸O of modern high-temperature submarine vent fluid and estimated W/R after Shanks *et al.* (1995) and Bowers & Taylor (1985), respectively.

ratios at water/rock ratios of ca. 1 to 2 (e.g., see Shanks *et al.* 1995) to yield the average isotopic compositions for low- and high-temperature altered rocks shown for each district. The fields of data in Figure 1 corresponds to those used to map zones of high- and low δ¹⁸O, i.e., areas of low- and high-temperature alteration, respectively. Differences in plotted positions of data fields reflect significant contrasts in the hydrothermal and non-hydrothermal alteration histories in each area. In Noranda, for example, altered rocks bear the effects of multiple, superposed hydrothermal systems.

Marked differences in whole-rock δ¹⁸O values are acquired during water/rock interaction due to variation in temperature (Fig. 1). Contour maps of whole-rock δ¹⁸O record cumulative paleo-heat and fluid flow.

Isotopic mapping of five selected areas in Canada and Sweden has indicated that the isotopic zones (δ¹⁸O <6‰ and >9‰; separate fields, Fig. 1) are not fully coeval. Values of δ¹⁸O ≥9‰ in hanging wall rocks largely indicate waning temperature and fluid flow, and post-date much of the high

temperature ($\delta^{18}\text{O} < 6.0 \text{‰}$), reaction zone alteration. Relative timing of hydrothermal activity and hanging-wall deposition is a key factor in recorded vertical isotopic gradient.

Paired high-low $\delta^{18}\text{O}$ patterns can provide a regionally applicable exploration guide: VMS deposits are located in 'normal' isotopic zones, between conformable low- and high- $\delta^{18}\text{O}$ zones (Fig. 2A-C). Discordant zones of isotopic alteration mark up-flow, typically along syn- volcanic faults, beneath VMS deposits.

SUMMARY

Key features of the selected districts (Fig. 3) include: Noranda: composite, multiphase high-temperature zone above Flavrian intrusive complex; VMS deposits associated with up-flow zones; Sturgeon Lake: single hydrothermal phase, area eventually emergent resurgent Biedelman Bay tonalite post-dated hydrothermal activity; Snow Lake: two magmatic cycles, each with hydrothermal systems; regionally metamorphosed; Kristineberg: two principal magmatic-hydro-thermal phases, regionally metamorphosed; Ben Nevis: younger, upright stock; single hydrothermal phase; no known VMS deposits.

ACKNOWLEDGEMENTS

The late Adrian Timbal provided

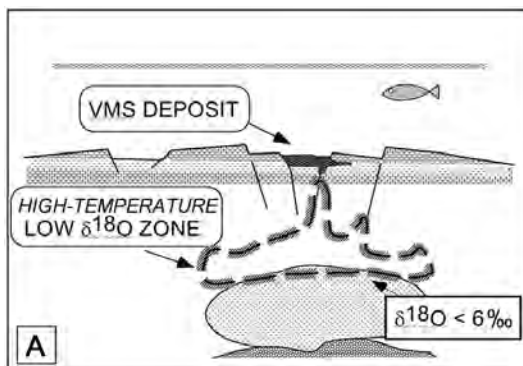


Fig. 2a. Schematic cross section of simple magmatic-centred hydrothermal system. Rocks within high-temperature (e.g., >350 °C) reaction zone are characterized by low values of $\delta^{18}\text{O}$.

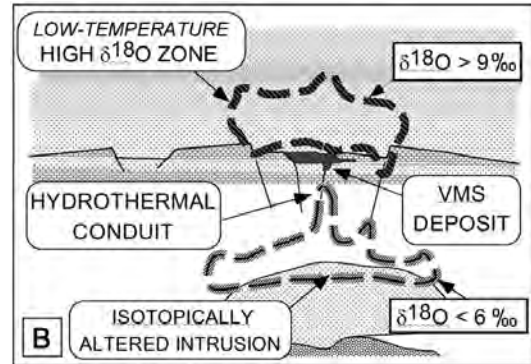


Fig. 2b. Where deposition continues post-VMS, cooling, fluids from the buried hydrothermal system can produce high- $\delta^{18}\text{O}$ zones in the hanging wall above up-flow conduits.

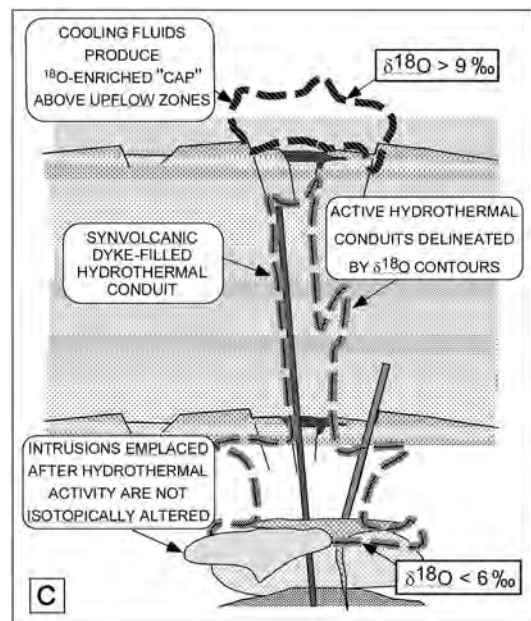


Fig. 2c. Successive intrusive episodes associated with hydrothermal activity can produce compound zones of isotopically altered rocks. The outer O-isotope isopleth is the youngest feature of the reaction zone, and the high $\delta^{18}\text{O}$ zone in the hanging wall, the youngest alteration feature overall. Post-hydrothermal intrusions usually lack oxygen isotope alteration.

invaluable analytical assistance during the GSC-CAMIRO project.

REFERENCES

CATHLES, L.M. 1993. Oxygen isotope alteration in the Noranda mining district, Abitibi

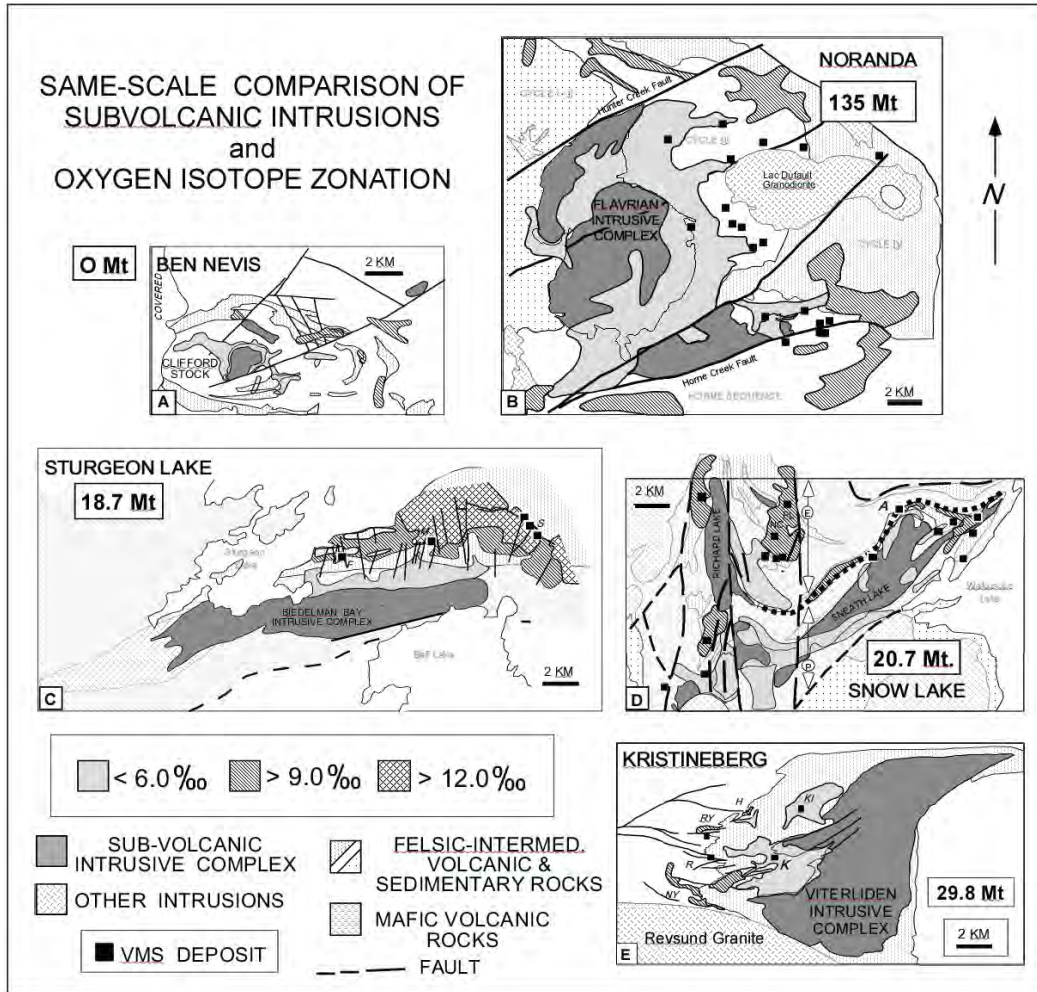


Fig. 3. The shapes of oxygen isotope zones associated with alteration about sub-volcanic intrusive complexes in a sub-marine environment reflect the local strain, yet still retain zoning systematics. Sizes of intrusions and high-temperature zones correlate approximately with total district tonnage of VMS

- greenstone belt, Quebec. *Economic Geology*, **88**, 1483-1511.
- CLAYTON, R.N. & MAYEDA, T. 1963. The use of bromine pentafluoride in the extraction of oxygen from oxides and silicates for isotopic analysis. *Geochimica et Cosmochimica Acta*, **27**, 43–52.
- GALLEY, A. *et al.* 2002. Database for CAMIRO project 94E07: Inter-relationships between subvolcanic intrusions, large-scale alteration zones and VMS deposits. *Geological Survey of Canada Open File 4431*.
- HOLK, G.J., TAYLOR, B.E., & GALLEY, A.G. 2008. Oxygen isotope mapping of the Archean Sturgeon Lake caldera complex and VMS-related hydrothermal system, Northwestern Ontario, Canada. *Mineral. Dep.*, **43**, 623-640.
- MCCNICOLL, V. *et al.* 2008. New U-Pb geochronology from the TGI-3 Abitibi/Plan Cuivre project: Implications for geological interpretations and base metal exploration. *Geological Association of Canada-Mineralogical Association of Canada Abstracts*, **33**, 110 p.
- PIERCEY, S.J. *et al.* 2008. Syn-volcanic and Younger Plutonic Rocks from the Blake River Group: Implications for Regional Metallogenesis. *Economic Geology*, **103**, 1243-1268.
- TAYLOR, B.E. 2004. Fluorination Methods in Stable Isotope Analysis. In: DEGROOT, P.A.(ed.), *Handbook of Stable Isotope Techniques*, **1**, Elsevier, Amsterdam, 400-472.

Exploration geochemistry, geochronology, and tracer isotopic data of copper mineralisation in dolomitic rocks, Dos Parecis Basin, Rondonia, Brazil

Aldo Vásquez^{1,2}, Pedro Perez¹, & Angelo Aguilar¹

¹Codelco-Chile. Exploration Division, Huérfanos 1270, Santiago, CHILE.

²AMEC Internacional (Chile) S.A. Américo Vespucio 100, 2nd floor, Santiago CHILE

(e-mail: aldo.vasquez@amec.com)

ABSTRACT: The Rondonia and Dos Parecis basins formed during the Neo-Proterozoic. Both are located in the south-western part of the Amazon Craton, Brazil. The Dos Parecis Basin is composed of two parallel sub-basins: Basin of Colorado in the north and Pimenta Bueno Basin in the south. A dolomitic layered unit crops out in the northern limit of the Colorado Basin and hosts copper sulphides, mainly chalcocite. The highest copper concentrations are found in white dolomites (4,137 ppm Cu on average), contained in primary chalcocite, and in copper and manganese oxides. The dolomitic unit has the highest concentrations of manganese (0.56% to 2.6% MnO). Surficial oxidation has produced anomalous concentrations of copper in soils (51 ppm to 98 ppm), and barium and manganese anomalies within 40 m to 160 m of the mineralised outcrops. The copper concentration in the fine fraction of stream sediments sampled from creeks cutting mineralisation varies downstream with anomalies not exceeding 135 ppm at 500 m to 1,000 m from the source.

Lead isotope ratios in chalcocite suggest a radiogenic lead contribution from the upper crust and give a Pb-Pb age of 800 Ma. In addition, chalcocite in dolomites has a high initial $^{87}\text{Sr}/^{86}\text{Sr}$ ratio, which is consistent with a high Rb/Sr ratio source typical of upper crustal rocks. The isotopic ratios in carbonates showed very low initial values of $^{87}\text{Sr}/^{86}\text{Sr}$ compared with the ratios for sea water from the Neo-Proterozoic to Permian; however, $^{87}\text{Sr}/^{86}\text{Sr}$ ratios of mineralised dolomitic carbonates have higher radiogenic isotope ratios than pure carbonates. There is a depletion of ^{13}C and ^{18}O in carbonates relative to normal sea carbonates, with values of $\delta^{13}\text{C}$ (PDB) between -5 and -4‰ and $\delta^{18}\text{O}$ (SMOW) between 23 and 25‰. The dolomites suffered a compositional change by reaction with an external source of fluid that affected their isotopic compositions as well as produced mineralisation.

KEYWORDS: exploration, copper, isotopy, dolomites, Rondonia.

INTRODUCTION

This work forms part of an effort to understand and to explore for the copper mineralisation discovered on the limits of the Dos Parecis Basin, Brasil. The mineralisation is associated with a unique dolomitic layer and corresponds to the presence of copper sulphides, mainly chalcocite. The study zone is located in the State of Rondonia, Brasil, 180 km to the south-east of the city of Ji-Parana.

This study sets forth the major conclusions resulting from geochemical exploration. Details of the complete exploration work are found in Aguilar *et al.* (2002).

GEOLOGICAL SETTING

Several large basins began to form during the Neo-Proterozoic on the Amazon Craton including the Rondonia Basin and Dos Parecis Basin. The Dos Parecis Basin is located on the southeast portion of the Amazon Craton, and is made up of magmatic and metamorphic rocks and by a Proterozoic to Cenozoic sedimentary and volcanic cover (Almeida *et al.* 1977).

REGIONAL GEOLOGY

The large sedimentary basins trend NW and contain extensive deposits. Sedimentation occurred from the Neo-Proterozoic to Mesozoic. The Dos Parecis Basin (Siqueira 1989; Pedreira & Bahia 2000) is comprised of marine and

continental volcanic deposits in two parallel sub-basins, one called the Colorado Basin in the south, and the other, the Pimenta Bueno Basin, in the north. Both basins are separated by paleo- to neoproterozoic rocks from the Guaporé Polycyclic Orogenic Belt. The oldest rocks of this belt comprise a large variety of orthogneiss and paragneiss, metavolcanic and metasedimentary rocks. Basic and acid igneous rocks, volcanic and intrusive, form also part of the youngest rocks of this belt (Scandolaro 1999) (Figs. 1 and 2).

LOCAL GEOLOGY

The set of sedimentary rocks deposited in the Colorado Basin and the Cuenca Pimenta Bueno Basin during the Palaeozoic gave rise to the Dos Parecis Basin (Pinto Filho *et al.* 1977). The Colorado Basin shows the following stratified units: a) basal conglomerate; b) dolomitic unit (DU); c) sandstones, siltstones and micaceous lutites; and d) red micaceous feldspar sandstones. The DU contains three units: a sedimentary breccia, a white dolomitic unit, and a pink dolomitic layer. The white dolomitic layer is the unit containing copper sulphide mineralisation, almost exclusively consisting of chalcocite, although covellite and digenite have also been identified. The carbonate rocks are correlated with the dolomitic layers in the Cacoal Formation of Palaeozoic defined by Siqueira (1989). The rocks of the Cacoal Formation are widely distributed in southern part of the Rondonia State and form part of the base of Dos Parecis Basin (Figs. 1 and 2).

The dolomitic rocks were affected by an alteration process evidenced by a bleaching of the rock at its base (Jones & Rehnfeldt 2001). The primary copper mineralisation is associated solely with the bleached portion of this dolomitic layer. Occasionally traces of copper oxides are observed in the basal conglomerate.

EXPLORATION GEOCHEMISTRY

Samples of rocks, core samples, stream sediments, panned semi-concentrate and

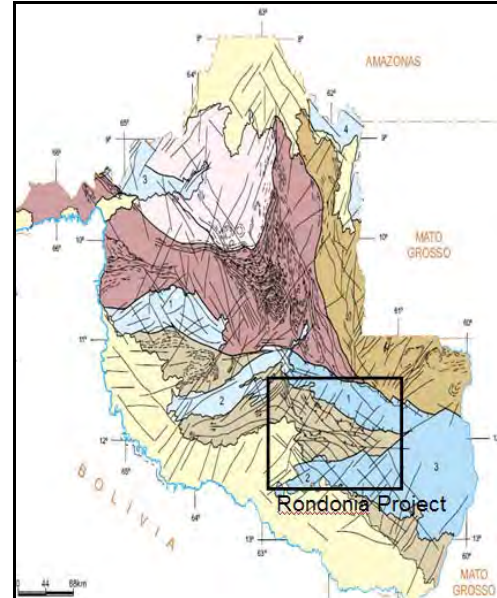


Fig. 1. Geology of the Rondonia State, Brazil.



Fig. 2. Legend for map shown in figure 1.

soil samples were collected to study the supergene dispersion patterns related to the mineralisation on the surface. Other samples were collected for stable and radiogenic isotopic analysis to determine the ages of granitoid rocks and mafic dykes cropping out in the area, and to characterise the sources of mineralising fluids and their interaction with the host rocks.

Geochemical analyses were done at Geosol Laboratory in Belo Horizonte, Brazil and consist of multi-element determinations through plasma spectrometry (ICP-AES) and Au through fire assay on 30 g of sample or using aqua regia digestion and atomic absorption. The sample digestion was done with aqua regia, or through a multi-acid digestion with hydrofluoric acid. The geo-chronology and stable isotope analyses were performed at the University of Sao Paulo.

ROCK GEOCHEMISTRY

The highest copper concentrations are contained in white dolomites (4,137 ppm on average) where primary chalcocite and copper and manganese oxides occur. No concentrations of interest in Au, Ag, Pb and Zn were detected in the dolomites. The dolomitic unit shows the highest concentrations in Mn (0.56% to 2.6%).

The basal conglomerate unit shows high and variable copper concentrations (142 ppm to >5,000 ppm). The high concentrations are due to the presence of copper oxides in fractures filling spaces between clasts. Copper oxides are observed where white, mineralised dolomite overlies the conglomerate.

Basement rocks contain locally high copper concentrations (1,529 ppm maximum). This unit locally has copper sulphides and oxides. Mafic dykes and basement rocks do not show anomalous concentrations of Au, Ag, Cu, Pb, Zn or Mo.

SOIL GEOCHEMISTRY

Anomalous Cu concentrations in soil samples taken from the B horizon (60 cm to 90 cm) occurs between 40 m and 160 m from the mineralised outcrops with sample concentrations between 51 ppm and 98 ppm, and local maximum values up to 2,580 ppm along with barium and manganese anomalies.

STREAM SEDIMENT GEOCHEMISTRY

Samples of drainage sediments and pan concentrates of heavy minerals were collected. Chemical analysis was undertaken on the fine fraction (-270# and

+400#), on the coarse fraction (-35# y +65#) of stream sediments and on whole-pan concentrates. Sediments in creeks cutting the non-mineralised sedimentary rocks contain copper concentrations between 7 ppm and 17 ppm in the coarse fraction; 21 ppm to 25 ppm in the fine fraction and variable concentrations between 34 ppm and 108 ppm in the whole-pan concentrates. Anomalous values for stream sediment samples containing detritus with copper oxides range from 51 ppm to 145 ppm in the fine fraction and 44 to 830 ppm in the pan concentrates. Copper concentration in the coarse fraction varies from 19 ppm to 39 ppm, up to anomalous values of 193 ppm and 290 ppm. The observed copper concentrations in the fine fraction, related to the distance downstream from the mineralised outcrops, is 39 ppm to 77 ppm between 0 and 500 m; 99 ppm to 135 ppm between 500 and 1000 m; 90 ppm between 1000 and 2500 m and less than 53 ppm at distances greater than 2500 m.

GEOCHRONOLOGY AND TRACER ISOTOPES

Lead, Sr, C and O isotope compositions were measured in carbonates of the dolomitic unit and in chalcocite concentrate. U-Pb and K-Ar radiometric dates were obtained from basement rocks and mafic dykes. The analysis were undertaken and The University of Sao Paulo under supervision of Professor C. Tassinari (Tassinari 2002).

GEOCHRONOLOGY

Maximum ages obtained from the basement rock samples correspond to a biotite and amphibole syenite (sample 1031) at $1,527.6 \pm 4.5$ My (U/Pb in zircons).

The basement rocks are cut by mafic dykes with epidote and biotite which showed the ages in Table 1.

The ages obtained for the basement rocks and mafic dykes show a maximum age that corresponds to the beginning of sedimentation at approximately 900 Ma.

Table 1. K/Ar ages in Mafic dykes.

Sample	Age (My)	Mineral
1019	1.042,7 ± 25,2	K-feldspar
1019	919,0 ± 16,2	whole rock
1030	955,5 ± 15,5	K-feldspar
1030	902,3 ± 16,4	whole rock

TRACER ISOTOPES

The lead isotope analyses of chalcocite concentrates gave the isotopic compositions shown in Figure 2.

The Pb isotope ratios are consistent with young mineralisation (less than 800 My), Neo-Proterozoic to Palaeozoic and are similar to lead isotope ratios of epigenetic mineralisation. This suggests a radiogenic lead contribution from the upper crust. The isotopic curves generated by the plumbo-tectonic model of Zartman and Doe (1980) show that the isotopic ratios are below 800 Ma and correspond to crustal values.

The Sr isotopes show high initial ⁸⁷Sr/⁸⁶Sr ratios in chalcocites, consistent with a high Rb/Sr ratio source. These high ratios are typical of upper crustal rocks. The isotopic ratios in carbonates showed very low initial ⁸⁷Sr/⁸⁶Sr values compared with ratios for sea water from the Neo-Proterozoic to Permian. Thus, fluid interaction affected the carbonates producing Rb and Sr remobilisation. Comparatively, the Sr isotope ratios of mineralised dolomitic-carbonates in the study area show higher radiogenic ratios than pure carbonates. It is likely that a fluid interacted with the carbonates leading to higher ⁸⁷Sr/⁸⁶Sr ratios.

The dolomites are depleted in ¹³C and ¹⁸O relative to normal marine carbonates, having values of δ¹³C_(PDB) between -5 and -4‰ and δ¹⁸O_(SMOW) between 23 and 25‰. This could confirm a change of isotopic composition of carbonates produced by an external fluid.

CONCLUSIONS

The white dolomitic unit show high copper concentrations due to the presence of copper sulphides, consisting almost exclusively of chalcocite. No anomalous

Table 2. Lead isotope ratios in chalcocite.

Sample	²⁰⁶ Pb/ ²⁰⁴ Pb	²⁰⁷ Pb/ ²⁰⁴ Pb	²⁰⁸ Pb/ ²⁰⁴ Pb
1026A	19,048	15,674	38,638
1026B	19,086	15,710	38,749
NB 18-13A	18,916	15,672	38,493
NB 18-13B	18,976	15,699	38,630

concentrations were found for Au, Ag, Pb, and Zn.

The basal conglomerate unit shows high and variable copper concentrations where secondary copper oxides formed as products of alteration of the overlying white dolomitic rocks.

(1) The copper concentration threshold for soil samples ranges from 54 ppm to 63 ppm.

(2) Expected copper concentrations in the fine fraction of stream sediments in creeks cutting mineralised outcrops do not exceed 135 ppm at 500 m to 1,000 m downstream.

(3) The lead isotope ratios indicate an upper crustal source for the lead and are consistent with mineralization at 800 Ma. Tracer isotopes in carbonates and chalcocite concentrates indicate that an external fluid altered the dolomitic unit changing its isotopic composition as well as deposited copper mineralisation.

ACKNOWLEDGEMENTS

We thank the Codelco Exploration Division for permitting this publication and allowing the comprehensive study, for which they provided fund and logistic support to carry out the exploration in this unrecognised and unexplored area of the planet. We thank the team for all discussions and conclusions.

REFERENCES

- AGUILAR, A, FAUNDEZ, P., MENDEZ, A., PEREZ, P., VASQUEZ, A., & VIEGAS, E. 2002. Proyecto Rondonia. *Internal Publication, Codeco Chile*.
- ALMEIDA F.F.M.; BRITO NEVES, B.B.; & FUCK, R.A. 1977. Porvincias estruturais brasileiras. In: *SBG, Simposio de Geologia do Nordeste*, **8**, Campina Grande, Atlas, 363-391.

- JONES C.E. & REHNfeldt, J. 2001. Proyecto Nova Brasilândia, Rondonia Brasil, Resultados del Proceso de Due Diligence. *Internal Report Codelco Chile*.
- PEDREIRA, A.J. & BAHIA R.B.C. 2000. Sedimentary Basins of Rondônia State, Brazil: Response to The Geotectonic Evolution of the Amazonic Craton. In: *Revista Brasileira de Geociências*.
- PINTO FILHO, F.P.; FREITAS, A.F. DE; MELO, C.F. DE; ROMANINI, S.J. Projeto Sudeste de Rondonia. Relatório Final. Porto Velho: CPRM, 1977. 4v.il. Convenio DNPM/CPRM.
- SCANDOLARA, J. E. *et al.* 1999. Geologia e Recursos Minerais do Estado de Rondônia. *Texto Explicativo do Mapa Geológico do Estado de Rondônia*. CPRM.
- SIQUEIRA, L.P. 1989. *Bacia dos Parecis*. *Boletim de Geociências da Petrobrás*.
- TASSINARI, C. 2002. Relatório Interpretativo dos dados isotópicos. Proyecto Nova Brasilândia – Parecis. *Internal Report, Codelco*.
- ZARTMAN, R.E. & DOE, B.R. 1981. Plumbotectonics, The Model. *Tectonophysics*.

The nature and significance of lithogeochemical and stable isotope alteration halos in the Hollinger-McIntyre gold deposit, Ontario, Canada.

Gibran D. Washington¹, Mona C. Sirbescu², Kevin T. Jensen²,
& Edmond H. van Hees¹

¹Wayne State University, Detroit, MI USA (midas@wayne.edu)

²Central Michigan University, Mt. Pleasant, MI USA

ABSTRACT: Two distinct mineralizing fluids formed the Hollinger-McIntyre-Coniaurum (HMC) deposit. The earliest fluid was associated with emplacement of a disseminated Cu-Au-Mo zone in the Pearl Lake Porphyry (PLP). The alteration pattern of the felsic rocks in the PLP is characterized by increased concentrations of K₂O, Au, Cu, Mo, W, and Sn, and K/Al, Sericite / Chlorite (SCI) and Sericite Alteration Indexes and the removal of CaO, relative to nearby “unaltered” rocks. The H₂O-CO₂-NaCl mineralizing fluid that altered the PLP had a temperature between 340° and 390°C, and a $\delta^{18}\text{O}_{\text{water}}$ composition of 11.7 to 12.7 ‰.

The H₂O-CH₄-CO₂-NaCl mineralizing fluid that deposited gold in and above the Hollinger Shear Zone (HSZ) had an estimated temperature of 290°C and a $\delta^{18}\text{O}_{\text{water}}$ of 4.6 ‰. This gold-bearing fluid was associated with increased concentrations of As, CO₂, and CO₂/CaO and removal of Na₂O from rocks in and above the HSZ. The isotopic composition of the auriferous fluid is similar to that of fluids that formed the Giant and Colomac deposits. Formation of the HMC Cu-Au-Mo and Au deposits by two geothermal systems with chemically distinct fluids has important implications for geochemical exploration efforts in the Porcupine Mining Camp and elsewhere.

KEYWORDS: *Hollinger, McIntyre, gold, mesothermal, lithogeochemical, alteration, stable isotope*

INTRODUCTION

Formation of mesothermal gold deposits is best studied in giant systems where geological conditions were optimal. The Hollinger-McIntyre-Coniaurum (HMC) is a giant deposit, located in the Porcupine Mining Camp of northeastern Ontario, that produced 891 metric tons of gold (31.4 million troy ounces) making it the largest mesothermal gold deposit in North America.

Two important, unanswered questions about mesothermal gold deposits include: (1) are they zoned chemically? and (2) was more than one mineralizing event involved in their formation? Studies of the Kolar gold field in India and the Sigma mine in Quebec found that gold fineness increased with depth. The occurrence of ankerite proximal to and calcite distal to gold veins in the HMC deposit has also been noted.

Studies of the Giant, Sigma, Dome, and Ptarmigan gold deposits found that they

have complex fluid histories (van Hees *et al.* 1999; Gray & Hutchinson 2001; Shelton *et al.* 2004; Olivio *et al.* 2006; van Hees *et al.* 2006).

The lithogeochemistry of wall rocks in the Hollinger-McIntyre-Coniaurum (HMC) deposit has not been fully explored. The objective of this study was to characterize the lithogeochemical alteration of the wall rocks and the stable isotope geochemistry of the veins in order to: (1) test if the HMC deposit is zoned chemically; (2) determine how many mineralizing events were involved in forming the HMC deposit; and (3) identify fluid pathways involved in formation of the HMC gold deposit.

GEOLOGICAL SETTING

The HMC deposit occurs in the Archean-age Abitibi Greenstone Belt of northeastern Ontario, Canada. The deposit is hosted by the Tisdale assemblage of metavolcanic rocks that vary in composition from ultramafic at the

base (Hershey Lake Formation), to felsic at the top (Gold Center Formation) of the sequence. A number of younger felsic rocks, including the Pearl Lake Porphyry (PLP), have intruded these rocks. The east end of the PLP hosts Cu-Au-Mo mineralization that has been interpreted to be an Archean porphyry copper deposit formed at $2,672 \pm 10$ Ma (Re/Os age), synchronous with the intrusion of late albitite dikes (Corfu *et al.* 1989; Ayer *et al.* 2003).

The Tisdale rocks were deformed by two tectonic events that resulted in superposition of east-west isoclinal folds on older north-south open folds. Five camp- to regional-scale faults, including the Hollinger Shear Zone (HSZ), have offset all these rocks. The HSZ is a reverse fault (~140 m offset) that passes through the Hollinger-McIntyre mine, strikes 57° , dips 65° S, extends to a depth of >1,500m and formed synchronous with the east-west folds. Most gold mineralization in the HMC deposit is associated with rocks in and above the HSZ.

The Abitibi greenstone belt has been metamorphosed to greenschist grade except where amphibolitic rocks are found adjacent to granite plutons and some gold deposits (Jolly 1978; Thompson 2005).

The HMC deposit has four alteration mineral assemblages that grade from the background greenschist facies to quartz-albite-ankerite-sericite proximal to individual veins (Smith & Kesler 1985). Studies of the HMC mine area have shown that higher concentrations of As, Ba, CO_2 , Rb, K_2O , and As occur near gold-bearing zones (Whitehead *et al.* 1981). Specifically, either the CO_2/CaO molar ratio, or a combination of K_2O and As concentrations can be used to discern "mineralized" from "barren" zones.

Wall rocks in the HMC deposit have $\delta^{13}\text{C}$ values that range from -0.5 to -3.9 ‰ and $\delta^{18}\text{O}$ values that range from 9.7 to 14.2 ‰ (Kerrick & Hodder 1982). Quartz and carbonate in quartz-tourmaline-ankerite veins have $\delta^{18}\text{O}$ values that range from 10.6 to 17.6 ‰ and 11.4 to 14.3 ‰, respectively (Wood 1991).

ANALYTICAL METHODS

Rock samples collected from archived core, mine workings and outcrop were pulverized, homogenized, then analyzed using four-acid dissolution (SGS Lab, Toronto) to determine the near-total lithochemical composition (cassiterite, rutile, monazite, zircon, sphene, gahnite, chromite and barite are partially dissolved). Gold analyses were done by Fire Assay with Atomic Absorption finish on 30g samples and have a detection limit of 5 ppb.

The $\delta^{13}\text{C}$ and $\delta^{18}\text{O}$ analyses were performed on vein carbonate by the University of Waterloo stable isotope lab.

RESULTS AND DISCUSSION

Sericite/chlorite alteration index (SCI) and the CO_2/CaO molar ratios (Figs. 1 and 2, respectively) are plotted on north-south cross-sections through the HMC deposit. The highest abundance of sericite occurs in the felsic intrusive rocks such as the Pearl Lake Porphyry (Fig. 1), whereas the highest CO_2/CaO molar ratio occurs in and above the Hollinger Shear Zone (Fig. 2). These two geochemically distinct trends are mimicked by a number of the other elements. Addition of Au (Fig. 3) K_2O , Cu, Mo, W, and Sn, and the removal of CaO. High K/Al and Sericite Alteration Indexes have similar distributions as the SCI index, and follow the felsic rocks. The addition of As and CO_2 , and the removal of Na_2O mimic the CO_2/CaO ratio by following rocks in and above the HSZ.

The association of the SCI alteration pattern with the Pearl Lake Porphyry and other felsic rocks is interpreted to indicate that they acted as a fluid conduit and permitted the vertical movement of the fluids through the fractured rocks in order to form the Cu-Au-Mo deposit.

The CO_2/CaO anomaly appears to indicate that Au deposits associated with the HSZ were formed by fluid that moved up along the HSZ, rather than by fluid moving through the felsic rocks.

The low $\delta^{18}\text{O}_{\text{cc}}$ composition of vein carbonate in the PLP (Fig. 4) indicates that fluids reacted with the felsic wall rocks as they passed through them. The

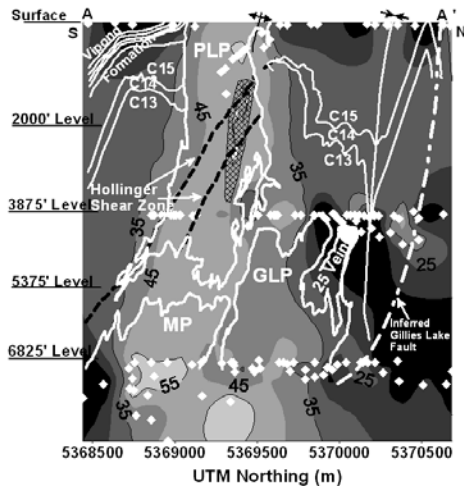


Fig. 1. Kriged and contoured cross-section of sericite / (sericite + chlorite)*100 Index (plotted in percent) along A - A' on McIntyre grid line 3500E through the HMC deposit. White diamonds indicate sample locations. Specific rock units such as C15 are labeled with abbreviations. The Cu-Au zone is indicated cross-hatching.

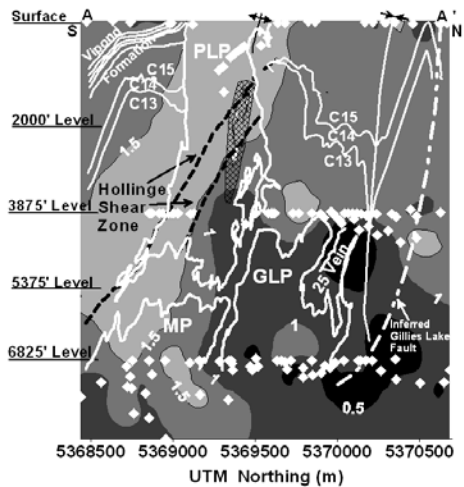


Fig. 2. Kriged cross-section of CO₂/CaO molar ratio along A - A' on McIntyre grid line 3500E through the HMC deposit has been modified by hand to reflect section geology. White dots indicate sample locations.

decrease in $\delta^{18}\text{O}_{\text{Cc}}$ from 14 to 12 ‰, as fluids moved up the HSZ, is also consistent with the mineralizing fluid reacting with the wall rock and implies a low water / rock ratio.

Coupling fluid inclusion

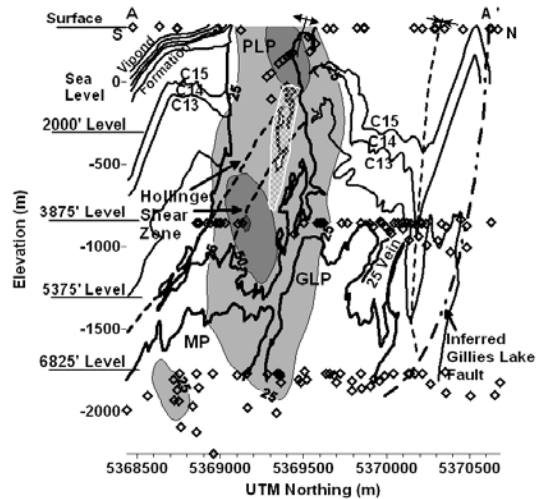


Fig. 3. Kriged and contoured cross-section of Au along A - A' on McIntyre grid line 3500E (white = 0-24 ppb, grey = 25-49 ppb, medium grey = 50-74 ppb, dark grey = 75+ ppb). Diamonds indicate sample locations.

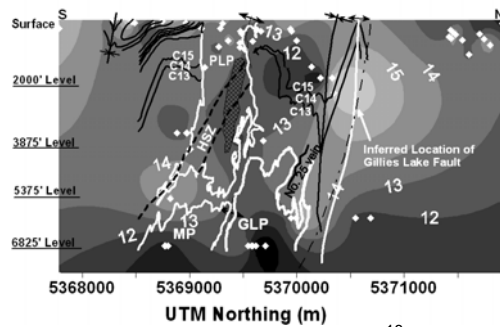


Fig. 4. Kriged cross-section of $\delta^{18}\text{O}_{\text{Cc}}$ along McIntyre grid line 3500E through the HMC deposit. White dots indicate sample locations.

temperature measurements with $\delta^{18}\text{O}_{\text{Cc}}$ values permits $\delta^{18}\text{O}_{\text{water}}$ of the mineralizing fluids to be determined. The McIntyre Cu-Au-Mo and Au fluids have distinctly different fluid compositions (Fig. 5), indicating that the mineralized zones were formed by two different hydrothermal systems. The compositions of the fluids that formed the HMC Au-bearing veins are comparable to those that deposited Au in the Giant and Colomac mines.

Failure to recognize that two distinct mineralizing fluids were involved in the formation of the HMC deposit resulted in at least two different alteration patterns being lumped together. Exploration carried

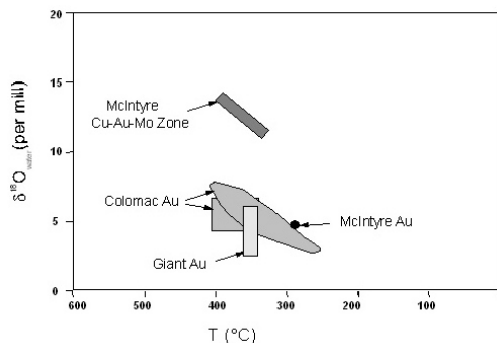


Fig. 5. Stable isotope composition of fluids that formed the Au and Cu-Au mineralization in the HMC mine. Comparative data is from the Giant and Colomac deposits (Shelton *et al.* 2004).

out using a single rather than two distinct geochemical models could be problematic.

SUMMARY

The results indicate:

- (1) two chemically distinct fluids formed Cu-Au-Mo and Au mineralization in the HMC Deposit.
- (2) Cu-Au-Mo and Au mineralizing fluids followed different hydrothermal conduits.
- (3) Failure to recognize deposits that were formed by complex fluid histories could result in unique geochemical model with a low probability of success being used to exploration for new deposits.

ACKNOWLEDGEMENTS

We thank the former Pamour Porcupine Mines and Placer Dome Canada Ltd. for permission to sample and financial support. Drs. Larry Lemke and Carl Freeman helped plot and interpret the data. Stable isotope analyses were provided by Mr. Bob Drimmie at the University of Waterloo. Bruce Taylor is thanked for his review of an earlier version of the manuscript.

REFERENCES

AYER, J.A., BARR, E., BLEEKER, W.C. *et al.* 2003. New geochronological results from the Timmins area: Implications for the timing of late-tectonic stratigraphy, magmatism and gold mineralization. *Ontario Geological Survey Summary of Field Work 2003*, 33 p.

CORFU, F., KROUGH, T.E., KWOK, Y.Y., & JENSEN, L.S. 1989. U-Pb zircon geochronology in the southwestern Abitibi greenstone belt, Superior Province. *Canadian Journal Earth Sciences*, **26**, 1747-1763.

GRAY, M.D. & HUTCHINSON, R.W. 2001. New Evidence for Multiple Periods of Gold Emplacement in the Porcupine Mining District. *Economic Geology*, **96**, 453-476.

JOLLY, W.T. 1978. Metamorphic history of the Archean Abitibi Belt. *Geological Survey of Canada Paper*, **78-10**, 63-78.

KERRICH, R. & HODDER R.W. 1982. Archean Lode Gold and Base Metal Deposits: Evidence for Metal Separation into Independent Hydrothermal Systems, *Geology of Canadian Gold Deposits: Canadian Institute of Mining and Metallurgy*, 144-160.

OLIVO, G.R., CHANG, F., & KYSER, T.K. 2006. Formation of the auriferous and barren North Dipper veins in the Sigma Mine, Val d'Or, Canada; constraints from structural, mineralogical, fluid inclusion, and isotopic data. *Economic Geology*, **101**, 607-631.

SHELTON, K.L., MCMENAMY, T.A., VAN HEES, E.H., & FALCK, H. 2004. Deciphering the Complex Fluid History of a Greenstone-Hosted Gold Deposit: Fluid Inclusion and Stable Isotope Studies of the Giant Mine, Yellowknife, Northwest Territories, Canada. *Economic Geology*, **99**, 1643-1663.

SMITH, T.J. & KESLER, S.E. 1985. Relation of fluid inclusion geochemistry to wallrock alteration and lithological zonation at the Hollinger-McIntyre gold deposit, Timmins, Ontario. *Canadian Institute of Mining Bulletin*, **78**, 35-46.

THOMPSON, P.H. 2005. A New Metamorphic Framework for Gold *Exploration-Kirkland Lake Area, Western Abitibi Greenstone Belt: Discover Abitibi Initiative*, Open File Report **6205**, 104 p.

VAN HEES, E.H., SHELTON, K.L., MCMENAMY, T.A., ROSS, L.M. JR., COUSENS, B.L., FALCK, H., ROBB, M.E., & CANAM, T.W. 1999. Metasedimentary influence on metavolcanic-rock-hosted greenstone gold deposits: Geochemistry of the Giant mine, Yellowknife, Northwest Territories, Canada. *Geology*, **27**, 71-74.

VAN HEES, E.H., SIRBESCU M-L., WASHINGTON, G.D., BENDA, K.J., SHELTON, K.L., FALCK, H., & TRENAMAN, R.T. 2006. Genesis of the Ptarmigan Gold Deposit: is it of magmatic affinity?. In: A.D. ANGLIN, H. FALCK, D.F. WRIGHT & E.J. AMBROSE (eds.), *Gold in the Yellowknife Greenstone Belt, Northwest*

- Territories*, GAC-MDD Special Pub. No.3, 270-285
- WHITEHEAD, R.E., DAVIES, J.F., CAMERON, R.A., & DUFF, D. 1981. Carbonate, alkali and arsenic anomalies associated with gold mineralization, Timmins Area. *Misc. Publication*, 318-333.
- WOOD, P.C. 1991. The Hollinger-McIntyre gold-quartz vein system, Timmins, Ontario: Geological characteristics, fluid properties and light stable isotope geochemistry. *Ontario Geological Survey Open File Report 5756*, 289 p.

**RECENT DEVELOPMENTS IN LITHOGEOCHEMICAL METHODS WITH
EXPLORATION APPLICATIONS**

EDITED BY:

**JAMES WALKER
CLIFF STANLEY
NICK SUSAK**

Lithochemistry of central Victorian orogenic gold deposits, Australia

Dennis Arne¹, Emily House², & Vladimir Lisitsin²

¹*ioGlobal, 469 Glen Huntley Road, Elsternwick, VIC 3185 AUSTRALIA (e-mail: dennis.arne@ioGlobal.net)*

²*Geoscience Victoria, Department of Primary Industries, GPO Box 4440, Melbourne, VIC 3001 AUSTRALIA*

ABSTRACT: Whole-rock geochemical data from almost 900 fresh drill core and underground samples taken from seven central Victorian orogenic gold deposits confirm the presence of distinct alteration haloes around the deposits. Using carbonate C analyses, thin section petrography, carbonate staining methods and TIR-NIR-SWIR hyperspectral imaging, primary ferroan carbonate alteration can be traced for up to several hundred metres away from gold mineralisation in meta-sedimentary rocks that are unaffected by post-mineralization metamorphism. A narrower and less distinct phyllic alteration zone can be identified using geochemical molar ratios in fresh samples or SWIR analysis. This zone extends from 70 m to 100 m beyond gold mineralisation. The phyllic halo generally overlaps a primary sulfidic alteration halo characterised by disseminated pyrite in areas distal to mineralized structures and arsenopyrite in areas proximal to mineralized structures. The extent of the sulfidic halo can be traced for up to 70 m – 90 m away from gold mineralization using low-level analysis of pathfinder elements, such as S, Au, As and Sb. A preliminary assessment of a further 650 whole-rock analyses of weathered rock suggests that secondary dispersion of chalcophile indicator elements exceeds that defined by primary dispersion haloes.

KEYWORDS: *lithochemistry, orogenic gold, central Victoria*

INTRODUCTION

A major study of primary and secondary geochemical dispersion around seven central Victorian gold deposits has been conducted by Geoscience Victoria as part of the 3-year, \$9 million Developing Gold Undercover initiative of the Victorian government. The major purpose of this work is to document the style and extent of wallrock alteration associated with central Victorian gold deposits to aide mineral explorers drilling through Cenozoic sedimentary cover in the Gold Undercover initiative area (Fig. 1). The study has been broken into two components: primary alteration and secondary dispersion effects. This paper mainly summarise the results of the investigation into primary alteration haloes at Bendigo, Ballarat, Castlemaine, Costerfield, Maldon, Fosterville and Wildwood. Preliminary results from a study of secondary dispersion using outcrop and soil samples will also be presented, along with a summary of hyperspectral analysis of representative diamond drill core.

GEOLOGICAL SETTING

The geochemical study covers selected gold deposits and occurrences in the western Lachlan Fold Belt. Most of the gold deposits studied in this report lie within the Bendigo Zone of the western Lachlan Fold Belt (Bendigo, Ballarat, Castlemaine, Maldon and Fosterville). A recent assessment of undiscovered gold endowment of the Bendigo and Stawell structural zones is provided by Lisitsin *et al.* (2007, 2009). Overviews of the regional geology, including summaries on gold metallogeny, are provided in VandenBerg *et al.* (2000) and Birch (2003). A recent detailed description of gold deposit models relevant to this study is provided by Moore (2007).

GEOCHEMICAL INVESTIGATIONS

Methodology

Nearly 900 fresh diamond drill core samples were collected from multiple drill holes along two or more cross sections through each of the deposits under investigation. Field determinations for ferroan carbonate were made on all fresh

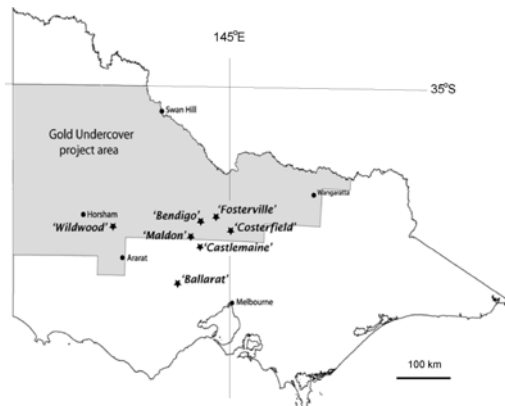


Fig. 1. Geoscience Victoria Developing Gold Undercover initiative area (shaded) showing the locations of the gold deposits discussed in this report.

samples. An additional 650 outcrop, shallow diamond drill core, aircore, soil auger (C-horizon only) and open pit samples were also collected from around the deposits, with the exception of Maldon. All samples were submitted for analysis of Al, Ca, Fe, K, Mg, Mn, Na, P, S, Zn, Au, Ag, As, Bi, Co, Cu, Mo, Ni, Pb, Rb, Sb, Se, Sr, Te (fresh samples only), Ba, Ti, W, Zr and, in a limited number of fresh samples, carbonate C, Hg, Pd & Pt.

Analytical and quality control details are summarised in Arne *et al* (2008). Gold was determined by fire assay, and major elements by ICP-OES following a four-acid digestion, with the exception of fresh drill core samples from Wildwood, which were analysed by lithium borate fusion and XRF. Trace elements were determined by ICP-MS. Refractory elements (W, Zr, Ba and Ti) were analysed by pressed powder XRF.

Jaw crusher splits were returned for hyperspectral analysis and were placed into plastic chip trays and sent to the CSIRO Hylogging Group in North Ryde, New South Wales, for analysis using HyChipsTM. Representative drill core from each of the study areas was scanned in its entirety using a HyloggerTM. Diamond drill core from Ballarat was also scanned using thermal infrared radiation (TIR) in order to assess the potential for mapping ferroan carbonate alteration patterns. The initial interpretation of the hyperspectral results

was undertaken by AusSpec International.

RESULTS

The results of this investigation generally support previous descriptions of primary wallrock alteration surrounding central Victorian gold deposits but, in addition, provide estimates of the lateral extent of alteration as well as practical geochemical threshold values. With the exception of deposits within the Stawell corridor that are associated with basaltic structural domes (i.e., Wildwood), primary geochemical dispersion around sediment-hosted central Victorian gold deposits can be characterized in terms of three overlapping alteration haloes:

(1) A sulfidic halo is characterized mostly by elevated S, Au, As and Sb. It extends further than suggested by previous alteration studies, and is defined by the development of disseminated hydrothermal pyrite and, to a lesser extent, arsenopyrite. Gold deposits of the Costerfield stibnite domain (i.e., Fosterville and Costerfield) can be differentiated from Au-As orogenic deposits by a greater primary dispersion of anomalous As and higher threshold values for Sb, as well as by the presence of slightly elevated concentrations of Hg (>0.01 ppm). Other chalcophile elements at variably elevated levels within the sulfidic alteration halo include Mo, Se, Bi, Pb and Cu.

(2) A poorly defined zone of phyllic alteration, which is characterized by a drop in the albite saturation index and an increase in the muscovite saturation index (when normalized to the Al content of the sample), either coincides with or lies within the sulfidic alteration halo. Absolute changes in K and Na concentrations in meta-sedimentary host rocks are dominated by lithological changes, and so the use of molar ratios is required to adequately define this zone by litho-geochemistry. This zone is not recognized in contact-metamorphosed deposits such as Maldon.

(3) Ferroan carbonates define the largest alteration halo associated with orogenic gold mineralization in central Victoria. They are most abundant adjacent to

mineralized structures, but can be detected up to 200 m away from mineralised structures, where the ferroan carbonate co-exists with regional metamorphic chlorite. The easiest method of detecting this halo in fresh core is by the use of carbonate staining techniques. Ferroan carbonate alteration can also be detected using carbonate C analyses, allowing the halo to be defined using the carbonate saturation index or Pearce Element Ratios, as well as through the use of thin-section petrography. Carbonate alteration appears to be accompanied by enrichments in Mn and Sr, and, at some deposits, Ca. The carbonate zone is also absent at contact-metamorphosed deposits.

The interpretation of litho-geochemical data from basaltic structural domes is complicated by lithological changes associated with the transition from basalt to overlying siliciclastic rocks, as well as by the polydeformed nature of the host sequence. Ferroan carbonate alteration is well developed, and low-level Au enrichment extends for a considerable distance away from zones of economic interest. Arsenic and Sb/Al anomalies are restricted to within approximately 10 m of mineralized zones. Sericite alteration is indicated by Na depletion and K enrichment in basalt within 20 to 40 m of mineralized zones. A number of other elements, including Mn, P, S, Zn, Mo, Cu, Se and Ba, are variably enriched within the rocks hosting Au mineralization, but it is not clear whether elevated concentrations of these elements are a product of syn-sedimentary exhalative activity or result from later hydrothermal alteration.

A preliminary interpretation of both new and historical surface rock and soil geochemical data suggests that Au, As and Sb are the most effective pathfinder elements in the supergene environment and that extensive secondary dispersion haloes can be recognized. Base metals, which are only rarely enriched in wallrocks within primary alteration haloes (Arne *et al.* 2008), correlate with Fe and Mn in weathered material due to scavenging.

Hyperspectral data

The phyllic alteration zone coincides with a subtle but consistent shift in the dominant AIOH peak in the short-wave infrared spectrum (~2210 nm) to slightly lower wavelengths, consistent with an inner white mica-ferroan carbonate mineral assemblage. A preliminary analysis of hyperspectral data over the visible to near infrared range suggests that ferroan carbonates may be detected but not reliably quantified. However, TIR data allow calcite and ferroan carbonate to be distinguished, and may also detect increasing Fe content in ferroan dolomite as mineralized structures are approached.

CONCLUSIONS

Recognition of the alteration haloes surrounding orogenic gold deposits in central Victoria provides a vector toward mineralized structures. The largest halo is defined by minor amounts of ferroan carbonate co-existing with regional metamorphic chlorite. Both the amount of ferroan carbonate and its iron content increases with proximity to the mineralized structures, whereas chlorite decreases to create a bleached appearance in fresh diamond drill core. Levels of Mn and Sr become elevated approaching gold mineralization while low-level elevated concentrations of S, Au, As and Sb accompany ferroan carbonate alteration. Levels of Au, As and Sb increase dramatically close to mineralization, and are accompanied by a drop in the albite saturation index and an increase in the ratio of the muscovite saturation index to Al. The presence of ferroan carbonate and changes in white mica composition can be determined by hyperspectral methods. Major deposits are associated with broad secondary dispersion haloes characterized by elevated Au, As and Sb.

ACKNOWLEDGEMENTS

It would not be possible to carry out a project of this scope without the assistance of the Victorian mineral exploration and mining industry. The following companies have provided access to diamond drill core material:

AGD Operations, Alliance Resources, Ballarat Goldfields (now Lihir Gold), Bendigo Mining, Castlemaine Goldfields, and Perseverance Corporation (now Northgate Minerals). This paper is published with the permission of the Director, GeoScience Victoria.

REFERENCES

- ARNE, D.C., HOUSE, E., & LISITSIN, V. 2008. Lithogeochemical haloes surrounding central Victorian gold deposits: Part 1 – Primary alteration systems, *Geoscience Victoria Gold Undercover Report 4*. Department of Primary Industries, Victoria
- BIRCH, W.D. (ed.). 2003. *Geology of Victoria*, Geological Society of Australia (Victorian Division) Special Publication **23**, 842 p.
- LISITSIN, V., OLSHINA, A., MOORE, D.H., & WILLMAN, C.E. 2007. Assessment of undiscovered mesozonal orogenic gold endowment under cover in the northern part of the Bendigo Zone. *Geoscience Victoria Gold Undercover Report 2*, Department of Primary Industries, Victoria.
- LISITSIN, V.A., OLSHINA, A., MOORE, D.H., & WILLMAN, C.E. 2009. Assessment of undiscovered mesozonal orogenic gold endowment under cover in the northern part of the Stawell Zone (Victoria). *Geoscience Victoria Gold Undercover Report 13*. Department of Primary Industries, Victoria.
- MOORE, D.H. 2007. Classifying gold deposits in central and western Victoria. *Geoscience Victoria Gold Undercover Report 1*, Department of Primary Industries, Victoria.
- VANDENBERG, A.H.M. *et al.* 2000. The Tasman Fold Belt System in Victoria – Geology and mineralisation of Proterozoic to Carboniferous rocks. *Geological Survey of Victoria Special Publication*. Department of Natural Resources and Environment.

Immobile Element Lithogeochemistry of felsic volcanic rocks hosting the Restigouche Volcanogenic Massive Sulfide Deposit, Bathurst Mining Camp, New Brunswick, Canada

Amanuel Bein¹ & David R. Lentz¹

¹*Department of Geology, University of New Brunswick, 2 Bailey Drive, Fredericton, NB,, E3B 5A3 CANADA
(email: u3x30@unb.ca)*

ABSTRACT: Altered volcanic rocks that host the Restigouche volcanogenic massive sulfide deposit in the Bathurst Mining Camp (BMC) consist of effusive and volcanoclastic rhyodacitic-dacitic volcanic rocks of tholeiitic–transitional, transitional, transitional-calc-alkaline magmatic nature. The rocks are characterized by evenly distributed volcanic facies and moderate to intense hydrothermal sericite, chlorite, carbonate, and silica alteration types. Lithogeochemical techniques such as binary plots of immobile elements and immobile element ratios are used to classify the various volcanic rocks into 7 groups and geological data from core logging confirmed that the geochemical classification is consistent and geologically meaningful. The study characterized geochemically unique units A, B, C, D, E, F, and G with distinctive Zr/TiO₂, Zr/Nb, Nb/Y, Zr/Th, TiO₂/Y, and TiO₂/Nb ratios. Temporal evolution of dominantly felsic volcanism from tholeiitic-transitional (unit B) to calc-alkaline (unit C) is demonstrated on the basis of Zr/Y ratio plot and chemostratigraphic relationships between the units.

KEYWORDS: *Restigouche, massive sulfide, immobile elements, binary plot, Zr/TiO₂*

INTRODUCTION

The Restigouche massive sulfide deposit is located in the northwestern part of the Bathurst Mining Camp (BMC), 60 km west of the city of Bathurst, northern New Brunswick. The property is currently controlled by Blue Note Mining and the company reports show that the deposit has an estimated reserve of 1.3 Mt grading 6.53% Zn, 5.05% Pb, and 99.6g/t Ag as of 2007 (Art Hamilton, Pers. Communication).

The present study was commenced in September 2008 in order to define the geological and lithogeochemical characteristics of the volcanic rocks hosting the Restigouche deposit. Geological mapping at 1:500 scale and drill core logging were performed at the Restigouche open pit mine site and the provincial drill core storage facility in Madran. Preliminary petrographic data from 8 diamond drill cores in combination with lithogeochemical data have been utilized to discern the volcano-stratigraphy characteristics and the effects of alteration overprinting due to hydrothermal activity

associated with formation of the deposit.

GEOLOGICAL SETTING

Regional Geology

The Bathurst Super Group comprises tectonically juxtaposed and internally imbricated nappes of the Fournier, California Lake, Tetagouche, and Sheephouse Brook groups. Collectively these units are interpreted to represent remnants of the Middle Ordovician ensialic-ensimatic Tetagouche–Exploits back-arc basin which formed by rifting of the Arenig-Caradoc Popelogan arc.

In the BMC the majority of the massive sulfide deposits occur in Late-Middle Ordovician volcano-sedimentary units of the California Lake and Tetagouche groups that disconformably overlie Cambro-Ordovician sedimentary rocks of the Miramichi Group (van Staal *et al.* 2003). Mineralized horizons of the California Lake and Tetagouche groups are dominantly made up of consanguineous calc-alkaline felsic volcanic rocks that were produced by melting of old, possibly sialic, infracrustal

rocks (Whalen *et al.* 1998).

The California Lake Group consists dominantly of volcanic rocks that occur in three major nappes, which are referred as the Canoe Landing Lake, Spruce Lake, and Mount Brittain, each off these nappes contains rocks assigned to formations of the same name (Rogers *et al.* 2003). The Restigouche volcanogenic massive sulfide deposit is hosted in the Mount Brittain Formation (MB) that according to Rogers *et al.* (2003) predominantly composed of feldspar- and minor quartz-porphyrific dacitic to rhyolitic rocks that are divided into MB1 and MB2 suites on the basis of petrographic and geochemical differences. Gower (1996) reported that the Mount Brittain Formation dominantly consists of felsic feldspar-crystal, lithic tuffs that conformably (?) overlie sedimentary rocks of the Miramichi Group on a northern limb of a regional anticlinorium. The Restigouche deposit occurs at the contact between feldspar crystal-poor (footwall) and feldspar crystal-rich (hanging wall) sequences. The apparent absence of feldspars in the crystal-poor footwall rocks might be attributed to pervasive feldspar-destructive hydrothermal alteration of the footwall (Gower 1996).

Local Geology

The Restigouche deposit is hosted by a sequence of effusive massive felsic flows and related autoclastic felsic breccias, volcanoclastic material (tuffaceous sedimentary) and feldspar-quartz-lithic lapilli tuffs. Intense chlorite alteration and accompanying silica alteration are well developed in footwall rocks immediately below massive sulfides, whereas pervasive sericitic and subordinate chloritic alteration, characterize the hanging wall. The strong silica alteration is characterized by relatively hard siliceous volcanic units with 5-30cm chert layers. Siderite occurring as rims on feldspar grains and on felsic lithic fragments, and siderite spots (<1-4mm in diameter) are common. The volcanic rocks that host the massive sulfide lens are strongly pyritiferous with disseminated <1-3mm anhedral to euhedral pyrite grains as well

as veins and veinlets and 0.5-10 cm aggregated pyrite patches. Fine-grained (<1mm) disseminated sphalerite and galena in both the hanging wall and footwall rocks are spatially associated with the massive sulfide. Minor chalcopyrite occurs in pyrite-rich stockwork below the sulfide lens and is associated with intense silica-altered zones below the exhalative massive sulfides.

Litho-geochemical Analysis

Litho-geochemical study of the volcanic sequence at the Restigouche deposit is based on XRF analysis of 123 diamond drill core samples, of these 80 are from 4 cores that were sampled to assess unit-controlled chemo-stratigraphic variation. Binary plots and ratios of immobile elements are used to discriminate the altered volcanic units. On the basis of Zr/TiO₂, Zr/Nb, Zr/Y, Nb/Y, Zr/Th, TiO₂/Y, and TiO₂/Nb the rhyodacitic-dacitic with subordinate rhyolitic and minor andesitic-trachy-andesitic volcanic rocks that host the Restigouche deposit are classified into seven geochemically distinct units of A, B, C, D, E, F, and G (Table 1). Units of A, B, C, D, E, and F are in ascending stratigraphic order whereas the stratigraphic position of unit G is yet to be defined. The Restigouche massive sulfide horizon occurs between units A-D and A-E.

Based on TiO₂/Al₂O₃ vs. Zr/Al₂O₃ plot, 5 separate populations; A, B, C, D and E with average Zr/TiO₂ = 0.041, 0.083, 0.110, 0.048, and 0.042 are recognized (Fig. 1). This classification is supported by other immobile-element ratios used in this study (Table 1; Figs. 2 to 4).

On the basis of Nb/Al₂O₃ vs. Y/Al₂O₃ unit A has Nb/Y=0.3 (Fig. 2). On Zr/Al₂O₃ vs. Nb/Al₂O₃ plot characterization of another unit G with Zr/Nb ratio of 8.19 is made (Fig. 3). The discrete grouping of samples from unit F is observed on TiO₂/Al₂O₃ vs. Nb/Al₂O₃, TiO₂/Al₂O₃ vs. Y/Al₂O₃ and Zr/Al₂O₃ vs. Th/Al₂O₃ diagrams. The clustering of unit F on the TiO₂/Al₂O₃ vs. Zr/Al₂O₃ plot (Fig. 1) is interpreted to be a primary feature of this unit (Fig. 4).

On the Zr/Al₂O₃ vs. Y/Al₂O₃

Table 1. Selected immobile element ratios of volcanic units (A-G) recognized at the Restigouche deposit.

		A	B	C	D	E	F	G
Zr/TiO ₂	Average	0.0414	0.0830	0.1100	0.0483	0.0423	0.0610	0.0715
	STD	0.0015	0.0070	0.0287	0.0032	0.0013	0.0022	0.0192
Zr/Nb	Average	14.23	14.77	19.01	15.07	14.22	15.13	8.19
	STD	0.77	1.43	2.31	0.79	0.66	1.12	0.78
Zr/Y	Average	12.11	4.45	7.98	6.80	8.72	4.48	4.98
	STD	26.76	0.73	1.36	2.86	3.89	0.88	1.19
Nb/Y	Average	0.912	0.300	0.420	0.457	0.613	0.299	0.616
	STD	2.152	0.031	0.052	0.216	0.273	0.066	0.167
Zr/Th	Average	9.64	10.56	32.30	13.03	12.84	10.60	7.94
	STD	2.43	2.53	8.45	4.09	4.45	2.07	1.91
TiO ₂ /Y	Average	299.56	54.29	82.16	140.11	206.46	73.58	87.77
	STD	679.78	11.39	41.14	52.34	93.02	14.64	77.25
TiO ₂ /Nb	Average	343.79	179.38	200.69	313.47	336.42	248.01	140.62
	STD	15.52	24.72	119.53	27.59	16.50	15.74	110.61

STD=standard deviation.

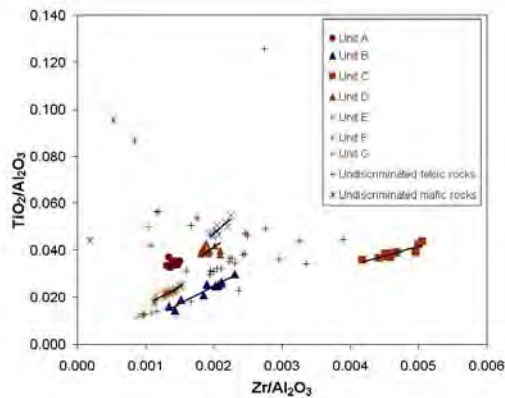


Fig. 1. TiO₂/Al₂O₃ vs. Zr/Al₂O₃ plot showing distinct clusters of the geochemically distinct volcanic units A, B, C, D, and E.

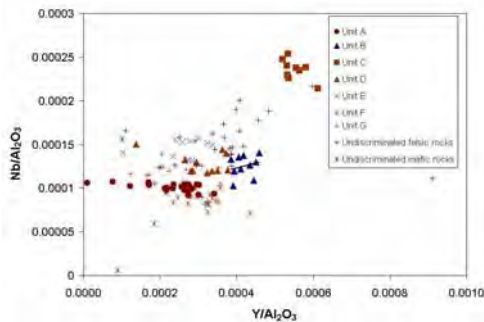


Fig. 2. Nb/Al₂O₃ vs. Y/Al₂O₃ plot marks that unit B represents a group of geochemically related volcanic rocks. Average Nb/Y ratio for units A, B, C, D, E, F and G is 0.912, 0.3, 0.42, 0.457, 0.613, 0.3, and 0.616, respectively.

discrimination diagram tholeiitic-transitional, transitional and transitional-calc-alkaline magmatic nature of the volcanic rocks is demonstrated, showing

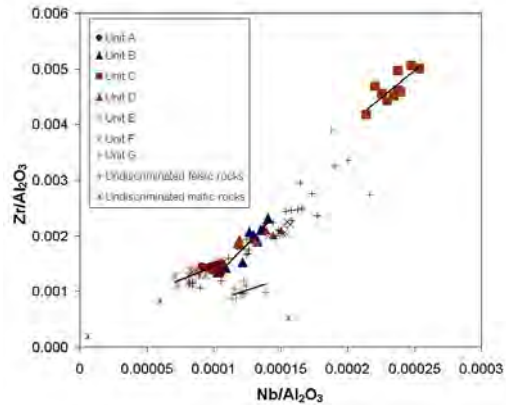


Fig. 3. Zr/Al₂O₃ vs. Nb/Al₂O₃ plot confirms that unit G is separate and geochemically unique. Trend lines for units B, C, F, and G are shown in figure. Zr/Nb ratios for units B, C, D, E, and G are 14.77, 19.01, 15.07, 14.22, 15.13, 14.23, and 8.19 respectively.

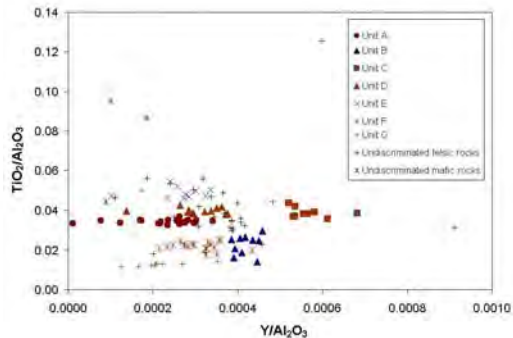


Fig. 4. TiO₂/Al₂O₃ vs. Y/Al₂O₃ plot showing geochemical association of unit F rocks. TiO₂/Y ratio for unit F is 73.58.

that tholeiitic-transitional unit B is overlain by calc-alkaline unit C (Fig. 5).

Several samples labelled as “undiscriminated samples” on the binary plots are widely scattered on figure 1. Most of these samples were collected from areas adjacent to chemostratigraphic contacts. The spurious nature of these data may reflect the effect of mixed-source sampling.

CONCLUSIONS

This study has revealed that;

- (1) The altered volcanic sequence that hosts the Restigouche deposit is dominantly made up of rhyodacitic/dacitic massive flows and related autoclastic breccias and volcanoclastic ash (tuffaceous

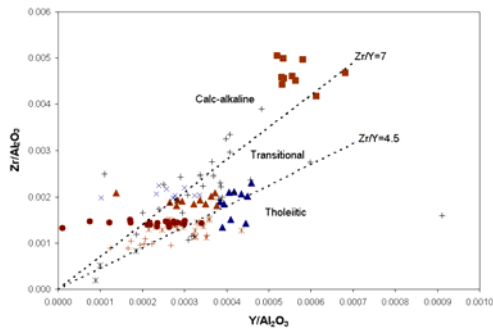


Fig. 5. Zr/Al₂O₃ vs. Y/Al₂O₃ plot showing tholeiitic-transitional, transitional, and transitional-calc-alkaline nature of the volcanic rocks that host the Restigouche massive sulfide deposit. Zr/Y boundary ratios for the trends that divide the tholeiitic-transitional and transitional-calc-alkaline fields are 4.5 and 7, respectively.

sedimentary rock) and quartz-feldspar-lithic tuff. Within this package seven geochemically distinct units are recognized.

(2) The Mount Brittain Formation is made up of tholeiitic-transitional, transitional, and transitional-calc-alkaline dominantly felsic volcanic units and have similar magmatic nature that is recognized elsewhere in felsic volcanic rocks of the BMC.

(3) Temporal evolution of felsic volcanism from transitional (unit B) to calc-alkaline (unit C) is supported by chemostratigraphic relationships between units A and B. Thus, the processes responsible for formation of the volcanic rocks hosting the Restigouche deposit are

associated with episodic felsic volcanism that produced volcanologically similar, but geochemically distinct rocks.

ACKNOWLEDGEMENTS

We acknowledge Blue Note Mining and NB Department of Natural Resources for their assistance and support during the course of the study.

REFERENCES

- GOWER, S.J. 1996. Geology, lithogeochemistry and mineral occurrences in the Portage Brook area, northwestern Bathurst Mining Camp, New Brunswick. New Brunswick Department of Natural Resources and Energy, Minerals and Energy Division, *Mineral Resource Report 96-1*, 13-43.
- ROGERS, N., VAN STAAL, C.R., MCNICOLL, V. & THERIAULT, R. 2003. Volcanology and tectonic setting of the northern Bathurst Mining Camp: Part 1. Extension and rifting of the Popelogan Arc. *Economic Geology Monograph*, **11**, 157-179.
- VAN STAAL, C.R., WILSON, R.A., ROGERS, N., *et al.* 2003. Geology and tectonic history of the Bathurst Supergroup, Bathurst Mining Camp, and its relationships to coeval rocks in southwestern New Brunswick and adjacent Maine: a synthesis. *Economic Geology Monograph*, **11**, 37-60.
- WHALEN, J.B., ROGERS, N., VAN STAAL, C.R., LONGSTAFFE, F.J., JENNER, G.A., & WINCHESTER, J.A. 1998. Geochemical and isotopic (Nd, O) data from Ordovician felsic plutonic and volcanic rocks of the Miramichi highlands: petrogenetic and metallogenic implications for the Bathurst Mining Camp. *Canadian Journal of Earth Sciences*, **3**, 237-252.

Geological and geochemical evolution of the San Miguel skarn, Tandilia Belt, Buenos Aires Province, Argentina

Raúl de Barrio¹, Mabel Lanfranchini^{1*}, Ricardo Etcheverry^{1,2}, Agustín Martín-Izard³, Mario Tessone¹, & María Paz¹

¹Instituto de Recursos Minerales (INREMI), FCNyM-UNLP, calle 64 N° 3, (1900), La Plata ARGENTINA (e-mail: debarrio@inremi.unlp.edu.ar)

²Consejo Nacional de Investigaciones Científicas y Técnicas (CONICET) ARGENTINA

³Departamento de Geología, Universidad de Oviedo SPAIN

ABSTRACT: The San Miguel skarn deposit is located in the Tandilia Belt, in the southern part of the Buenos Aires province in Argentina. It has developed in an igneous metamorphic complex, which exhibits a long geological evolution and is associated with a Proterozoic granitic magmatism.

The main mineral assemblages identified in the San Miguel deposit are: (1) Plagioclase ± clinopyroxene ± garnet formed during prograde metasomatic endoskarn development, (2) clinopyroxene ± garnet ± wollastonite ± vesuvianite, formed by metasomatic processes in marbles, and (3) amphibole > epidote ± quartz ± chlorite ± titanite, resulting from hydrous retrograde alteration of skarn.

The San Miguel deposit is classified as calcic skarn. Sulfide mineral deposition was not recognized in surface exposures.

KEYWORDS: *San Miguel Skarn, Buenos Aires Province, Argentina.*

INTRODUCTION

The San Miguel skarn is located 43km south of Tandil city, Buenos Aires Province, eastern Argentina (Fig. 1). It represents an isolated occurrence within the Tandilia Belt.

Previous geological work is scarce. The San Miguel skarn was discovered by Villar Fabre (1956). During the sixties, Villar Fabre & Quartino (1966), and Quartino & Villar Fabre (1967) conducted petrological studies of this deposit, defining skarn mineral facies.

The present study is part of a regional investigation program for the characterization of hydrothermal alteration processes in the Tandilia Belt, carried out by the research group of the Instituto de Recursos Minerales of the University of La Plata. As a result of that work, a magmatic-hydrothermal system with interesting geological features is recognized at the San Miguel skarn.

GEOLOGICAL SETTING

Regional Geology

The Tandilia Belt constitutes the southern

sector of the Río de La Plata Craton, together with Martín García Island and the western border of Uruguay. It comprises a complex igneous metamorphic association, which exhibits an extensive evolution during two main regional geotectonic events in southern South America: The Transamazonian Cycle (Paleoproterozoic ≈2200-1800 Ma) and the Brazilian Cycle (Neoproterozoic ≈900-570 Ma).

The Precambrian basement represented by the Buenos Aires Complex (Marchese & Di Paola 1975) comprises the oldest rocks in the Tandilia Belt. It is made up of tonalitic gneisses, granitic migmatites, amphibolites and scarce marbles, all of which are intruded by Proterozoic granitic bodies. These rocks form extensive hills of low relief, where lithological contacts are hardly ever observed due to the extensive Quaternary cover. Nevertheless, numerous quarries were developed in the region with the purpose of rock exploitation, allowing us to observe stratigraphic relationships between the different units. A Proterozoic-Lower

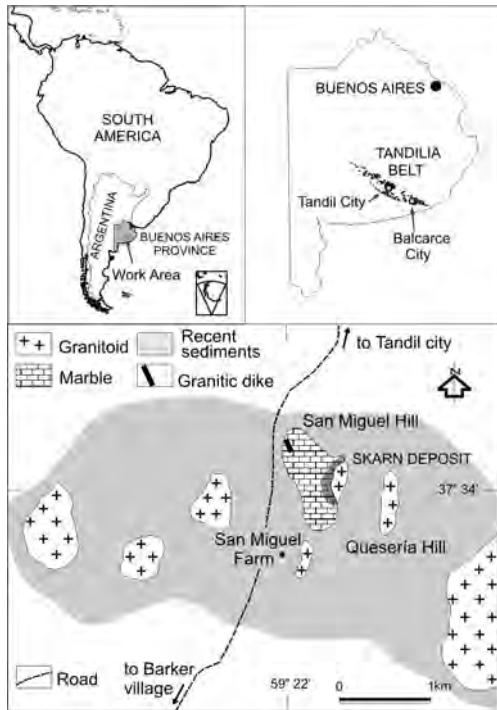


Fig. 1. Local geological map and geographic location of the San Miguel area.

Paleozoic sedimentary sequence (limestones, quartzites, and pelites), and a Quaternary cover complete the stratigraphic column.

Precambrian carbonate rocks were only recognized in two places: San Miguel quarry, located between the cities of Tandil and Barker, and Punta Tota quarry (Delpino & Dristas 2007), near Balcarce city, 100 km southeast of San Miguel. The San Miguel skarn was developed by the intrusion of granites and Punta Tota skarn is related to pegmatites that were segregated from garnet migmatite. Carbonate rocks at San Miguel skarn are mainly calcitic in composition. By contrast the marbles of Punta Tota are dolomitic in composition and form thin beds intercalated in amphibolites, constituting the upper part of a stratified basement sequence.

No geochronological data is available for the San Miguel granitic rocks; nevertheless, granitoids of similar mineralogical and petrological features, outcropping in neighboring areas, were dated by the SHRIMP method and

indicated a Paleoproterozoic age (Cingolani *et al.* 2002). They form part of a granitic series formed by several isolated bodies. This multiple granitic complex seems to correspond to the same tectonic event, syn-to-post tectonic with respect to the Transamazonian Cycle. They form a collisional belt where crust thickening linked with anatexis processes occurred, which in turn generated local acid volcanism and relevant mylonitic zones (Dalla Salda *et al.* 2005).

LOCAL GEOLOGY

Surface exposures of the San Miguel skarn deposit occur isolated over a 4000 m² area, surrounded by intruding Proterozoic granitoid outcrops. The San Miguel skarn is mainly hosted by the Precambrian marbles of the Buenos Aires Complex.

Marbles are whitish grey in colour. They occur in the form of irregular elongated bodies, several metres in length. The grain size varies from a few millimetres to 7cm, representing different recrystallization stages. Dark green diopside crystals are abundantly disseminated within the marble. Also, scarce tremolite, epidote, and other accessory minerals were recognized.

Granitoids are tonalitic to granitic in composition; they have granular hypidiomorphic to saccharoid microgranular texture. They are composed of plagioclase (An₃₂₋₃₈), microcline, quartz, diopside, tremolite, titanite, and apatite. Granitoids develop sub-horizontal lenses, and irregular elongated bodies, up to 1m wide which are intercalated within the marbles. In addition, granitic veins and veinlets a few millimetres to 10cm thick, cut the marble, following a chaotic pattern.

MINERAL GEOCHEMISTRY

Electron microprobe analyses were performed using a Cameca Camebax SX-100 at the Departamento de Geología, Universidad de Oviedo, Spain. Operating conditions were a 15 to 20 kV accelerating voltage, beam current of 15 to 20 mA, and beam size of 1 to 2 µm. Natural standards were certificated by MAC (Micro Analysis

Consultants Ltd., United Kingdom). The analyses were performed on pyroxene and garnet crystals of exoskarn facies. Microprobe data obtained from pyroxene shows a wide composition variation that fluctuates between 53-80 wt.% Di, 20-47 wt.% Hd, and minor amounts of Jo (0.05-0.36 wt.%). Furthermore, mineral garnet composition ranges between 68-99 wt.% Grs, 0-20 wt.% Ad, 0-8 wt.% Alm, and 0-0.75 wt.% Prp. These significant changes are mainly linked to the variations in the magmatic fluid composition of the system, where Fe, Mg, Al, and Si contents show an erratic behaviour, whereas Ca values remain constant.

GEOLOGICAL AND GEOCHEMICAL EVOLUTION

According to mineralogical textures, alteration mineral assemblages, geochemical analysis, structural relationships, and field observations, a sequential magmatic-hydrothermal evolution was defined at San Miguel Skarn.

1-Marble was firstly intruded by numerous pinkish, small granite veins, up to 2cm thick, developing an initial metasomatic stage represented by incipient reaction along cleavage and fissure planes of large calcite crystals. The calc-silicate mineral assemblage developed in marble is constituted by diopsidic clinopyroxene ± wollastonite, during which Ca enrichment began in the plagioclase of igneous rocks.

2- The increasing size of granitic intrusions, up to 1m thick, caused calcareous xenolith digestion, and a stronger reaction with the marble, generating magma hybridization (Fig. 2). Compositional and textural changes took place in igneous rocks, allowing endoskarn formation. This process was induced by high contents of CO₂ in the system that provoked some depletion in the aqueous phase activity of the granitic magma. Thus, the incorporation of a large amount of carbonate material in this magma allowed anhydrous calc-silicate mineral formation (pyroxene-garnet).

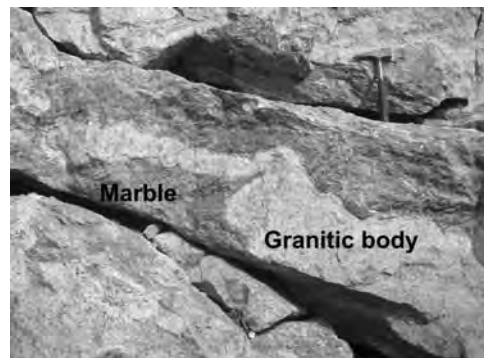


Fig. 2. Granitic intrusion in marble of San Miguel skarn.

Tonalitic-granodioritic facies subsequently show an increase of CaO of between 9.1 and 10.9 wt.%, and a depletion of SiO₂, reaching 56.4-58.8 wt.% (after Villar Fabre & Quartino 1966) towards the contact zone. Petrographically, a depletion of modal quartz and an increase of Ca contents in plagioclase are observed in an endoskarn mineral assemblage consisting of plagioclase ± diopside ± garnet ± titanite.

In addition, metasomatism of the marbles produced an exoskarn mineral association within the xenoliths, and also towards the contact with granitic rocks (several centimetres thick). This exoskarn paragenesis represents an advanced metasomatic stage. It is constituted by massive aggregates of diopside ± grossular ± wollastonite ± vesuvianite. It comprises < 1cm long, dark green prismatic clinopyroxene crystals, up to 4cm in length, isotropic reddish brown garnet, and 2cm long, white fibrous wollastonite that forms reaction rims surrounding garnet cores (Fig. 3).

3- Retrograde metamorphic processes, linked to hydrothermal fluid circulation, finally produced a new mineral assemblage constituted mainly by tremolite-actinolite > epidote ± chlorite ± quartz ± sericite ± titanite ± hematite. The amphibole appears as green fibrous crystals over clinopyroxene and other anhydrous minerals.

CONCLUSIONS

(1) The singular occurrence of

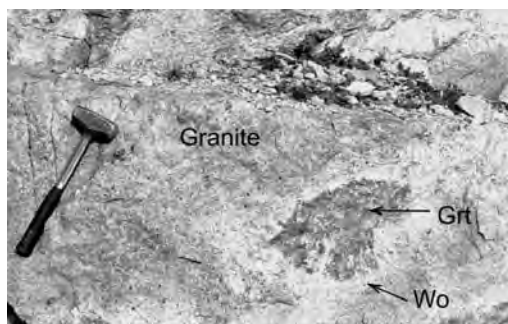


Fig. 3. Garnet aggregate surrounded by wollastonite rim, within granitic rocks.

Precambrian carbonate rocks in the San Miguel area allowed the formation of an isolated skarn deposit related to the Proterozoic magmatic hydrothermal activity and associated with the granite intrusions. Similar processes occurred at the Punta Tota skarn. These deposits at the present time constitute the only two skarns recognized in the Tandilia Belt of Buenos Aires Province.

(2) The San Miguel deposit is classified as calcic skarn (Ca and Ca-Mg (-Fe)-silicates). Sulfide mineral deposition was not recognized in the retrograde alteration facies, at least not in surface exposures.

REFERENCES

CINGOLANI, C.A., HARTMANN, L.A., SANTOS, J.O.S., & MCNAUGHTON, N.J. 2002. U-Pb SHRIMP dating of zircons from the Buenos Aires Complex of the Tandilia Belt, Río de La

Plata Craton, Argentina. *XV Congreso Geológico Argentino*, La Plata, **1**, 149-154.

DALLA SALDA, L., DE BARRIO, R.E., ECHEVESTE, H.J., & FERNÁNDEZ, R.R., 2005. El basamento de las Sierras de Tandilla. In: DE BARRIO, R.E., ETCHEVERRY, R.O., CABALLÉ, M.F., & LLAMBIAS, E. (eds), *Geología y Recursos Minerales de la Provincia de Buenos Aires. XVI Congreso Geológico Argentino*, La Plata, Relatorio, **31-50**.

DELPINO, S.H. & DRISTAS, J.A. 2007. Dolomitic marbles and associated calc-silicates, Tandilia belt, Argentina: Geothermobarometry, metamorphic evolution, and P-T path. *Journal of South American Earth Sciences*, **23**, 147-175.

MARCHESE, H.G. & DI PAOLA, E.C. 1975. Reinterpretación estratigráfica de la perforación Punta Mogotes N° 1, provincia de Buenos Aires. *Revista de la Asociación Geológica Argentina*, **30**, 17-44.

QUARTINO, B. & VILLAR FABRE, J. 1967. Geología y petrología del basamento de Tandil y Barker, provincia de Buenos Aires, a la luz del estudio de localidades críticas. *Revista de la Asociación Geológica Argentina*, **22**, 223-251.

VILLAR FABRE, J. 1956. Descripción geológica de la Hoja 33q, Barker (provincia de Buenos Aires). *Dirección Nacional de Minería. Unpublished report*.

VILLAR FABRE, J. & QUARTINO, B. 1966. Exomorphic and endomorphic effects from marble-contaminated granite contacts in the "San Miguel" quarry, Barker, Province of Buenos Aires, Argentina. *American Journal of Science*, **264**, 310-320.

Geochemistry of auriferous banded iron formation, northeastern Saharan metacraton, Egypt

Ahmed M. El Mezayen¹, Talaat M. Ramadan², & Atef O. Abu Salem³

¹Geology Dept, Al Azhar Univ., Cairo, EGYPT

²National Authority for Remote Sensing and Space Sciences, Cairo, EGYPT

(e-mail: ramadan_narss2002@yahoo.com)

³The Geological Survey of Egypt, Cairo, EGYPT

ABSTRACT: The present article presents and discusses the results of geochemical studies on the Archean banded iron formation (BIF) and their host rocks in East Oweinat district. The study area lies in the southern part of the Western Desert of Egypt and is underlain by the north eastern part of Saharan metacraton. Detailed mapping reveals intercalation of the Archean gneisses with thick (0.5-100 m) layers of BIF. Lithogeochemical analyses of the BIF for major- and trace-elements show that: SiO₂ and Fe₂O₃ are the two most abundant oxides, varying from 37.02 to 60.3% and 32.5 to 61.06% respectively. Also, 20 bedrock samples from the BIF were analyzed for gold using Atomic Absorption. The results of these analyses revealed that gold contents range from 3.75 up to 6.18 g/t. The Atomic Absorption data were confirmed by Fire Assay that returned gold values from 0.3 up to 3.47 g/t. The recognition of gold-bearing BIF makes the southern and southeastern parts of the study area promising territories for further exploration.

KEYWORDS: *Owieinat, Archean, Early Proterozoic, Banded Iron Formation, felsic granulites*

INTRODUCTION

The East Oweinat district is located in the southwestern part of the Western Desert of Egypt and is bounded by Latitudes 22°00' and 22°15' N and by Longitudes 25°35' and 26°05' E (Fig. 1). The area is underlain by the north eastern part of Saharan metacraton of Abdelsalam *et al.* (2002). Several authors stated that the high grade gneiss and migmatite terrane in the basement, west of the Nile, are part of a Pre-Pan- African continental plate (Richter & Schandelmeier 1990, Khattab *et al.* 2002). Several authors discussed the gold mineralization associated with the Banded Iron Formation (BIF) in the central Eastern Desert of Egypt.

El Shimi & Soliman (2002) were the first recognize gold mineralization in association with BIF in the central Eastern Desert of Egypt. Botros (2004) classified the gold deposits of Egypt into three types, i.e., I) stratabound deposits, II) non-stratabound deposits hosted in igneous metamorphic rocks and III) placer gold deposits. He subdivided the stratabound deposits into three main types: gold-

bearing Algoma-type BIF, gold-bearing tuffaceous sedimentary rocks and gold-bearing volcanogenic massive sulfide deposits.

This study focuses on the geochemistry of the BIF. This work also attempts to document the lithologic and structural controls of the BIF in East Oweinat district using Landsat ETM+ and Radarsat imagery complimented by field studies (Figs. 2 to 4).

GEOLOGICAL SETTING

The study district is mainly underlain by metamorphic Archean to Early Proterozoic and Neoproterozoic rocks. These are intruded by Late Precambrian granodiorites and biotite granites that have sharp intrusive contacts with host rocks and are uncomfortably overlain by the Gilf Formation (Paleozoic), Abu Ras Formation (Mesozoic) and Quaternary sediments (Fig. 4). The Archean to Early Proterozoic rocks are medium- to high-grade metamorphic rocks that include felsic granulites, garnet-quartz-feldspathic gneisses and quartzo-

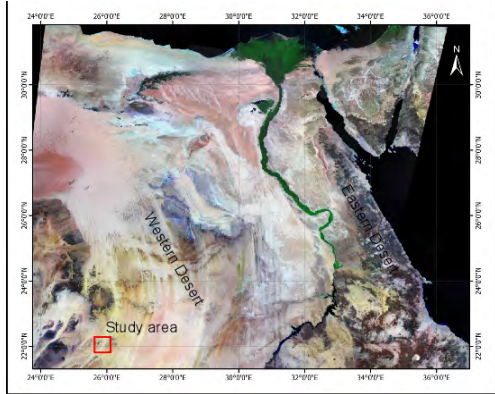


Fig. 1. Landsat TM image showing the study area (red box in southwest corner is the study area), western Desert Egypt.

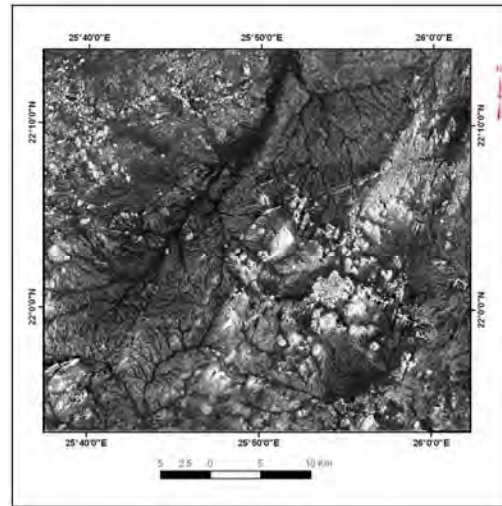


Fig. 3. RADARSAT-1 image for the study area outlined in Fig. 1

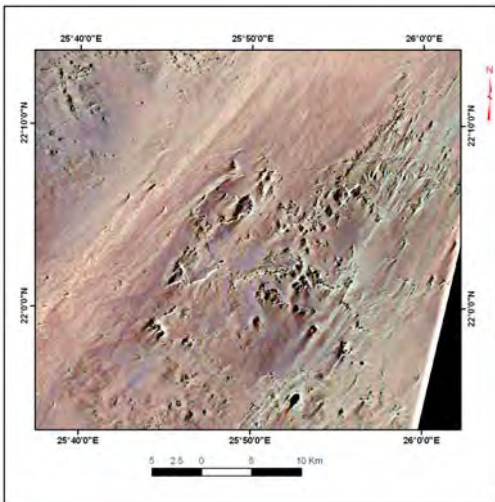


Fig. 2. Landsat TM image (Bands 7,4,2) for the study area outlined in Fig. 1

these beds ranges from 0.5 to 100 m and strike lengths have been traced for up to approximately 4 km. The BIF in NNE-SSW is generally thinner (average 5 m) than that of the other trends. The beds end abruptly by fault displacement or are obscured by thick sand sheets. Radarsat images reveal subsurface structures such as folds and faults that control the distribution of the BIF in the study area (Fig. 3).

Microscopically, the BIF is composed mainly of iron oxide rich bands that alternate with microcrystalline silica bands, quartz, chert and jasper. The ratios of these constituents are different from one sample to another. Occasionally, the samples contain sulfides, garnet and graphite.

Complete chemical analyses for major oxides and trace elements of 6 representative samples of BIF were carried out using XRF technique. The analyses reveal the following:

- SiO_2 and Fe_2O_3 are the two most abundant oxides. They vary from 37.02 to 60.3% and 32.5 to 61.06% respectively.
- $(\text{K}_2\text{O}+\text{Na}_2\text{O})$, MnO and P_2O_5 occur in very low concentrations.

The graphical representation of the average chemical composition for the trace elements of the BIF in this study are

feldspathic gneisses. Detailed mapping shows that the gneisses are intercalated with thick (≤ 100 m) horizons of BIF.

MINERALIZATION

The southern part of the study area (Fig. 4) is characterized by a large volume of BIF and associated gold mineralization. Here the BIF is hosted in the gneissic rocks and form ridges and isolated hills. The BIF horizons are strongly folded and faulted. These units generally strike E-W or NE-SW with dips of N 45° to NW 60° . Locally, some bands strike NNE-SSW and NW-SE with dips of NNW 40° and NE 60° , respectively. Generally, the thickness of

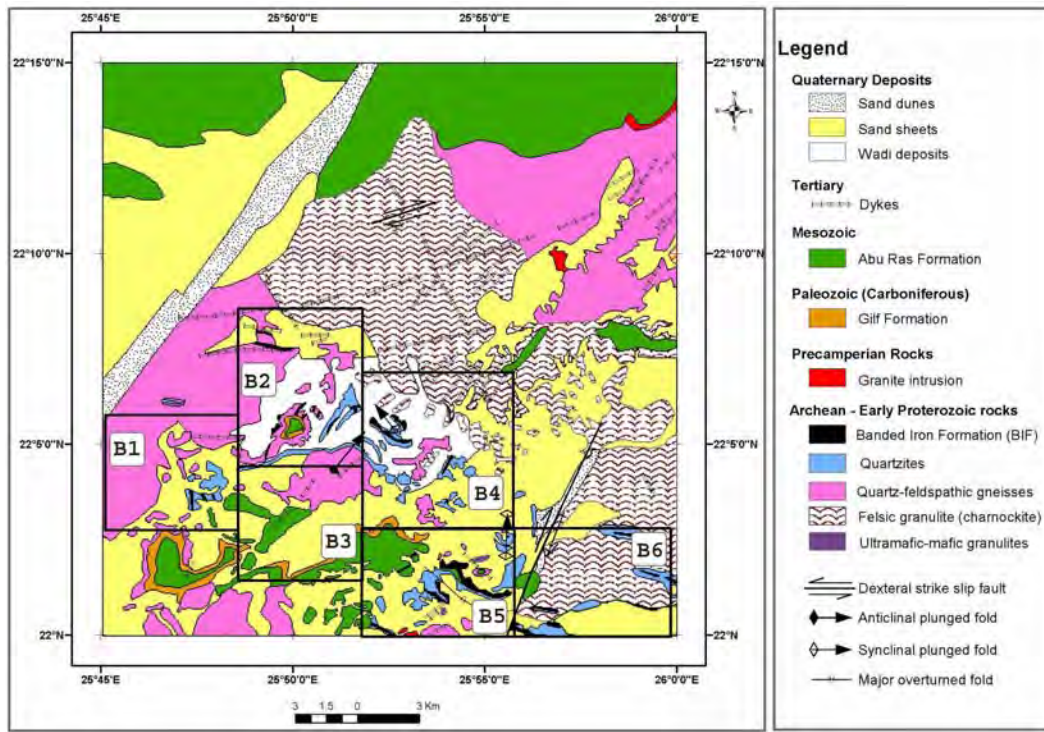


Fig. 4. Geological map for the study area (Modified after Khattab *et al.* 2002), B1 - B6 are promising areas

compared to typical Algoma type and Lake Superior type BIFs (Fig. 5) and shows that the samples in this study are similar to Superior type BIF. It is of particular interest to note that although the BIF in the study area have significant strike length and thicknesses, other field relations particularly the host rocks make them akin to the Lake Superior BIF. Twenty samples from the investigated BIF (areas B1-B6 on Fig. 4) were analyzed for gold, silver and other trace elements using Atomic Absorption. The results of these analyses revealed that gold contents range from 3.75 to 6.18 g/t. The Au is associated with arsenic and silver, where As and Ag contents range from 5.67 to 84 ppm and from 5.58 to 20.9 g/t respectively. The anomalous gold results were checked by Fire Assay analysis which confirmed that gold contents range from 0.3 to 3.47 g/t.

CONCLUSIONS

The study area is underlain by metamorphic Archean to Early Proterozoic and Neoproterozoic rocks. The Archean to Early Proterozoic rocks are represented by medium- to high-grade metamorphic rocks, including felsic granulites, garnet quartz-feldspathic gneisses and quartzo-feldspathic gneisses. Detailed mapping reveals intercalation of these gneisses with thick (up to 100 m), horizons of BIF. Radarsat imagery reveals subsurface structures such as folds and faults control the distribution of the BIF in the study area. The chemical analyses for major oxides and trace elements of the studied BIF reveal that: SiO_2 and Fe_2O_3 are the two most abundant oxides and vary from 37.02 to 60.3% and 32.5 to 61.06% respectively. Fire Assay analysis confirms the elevated gold content of the BIF returning values between 0.3 and 3.47 g/t. Therefore, the southern and southeastern parts of the region located in areas B1, B2, B3, B4, B5,

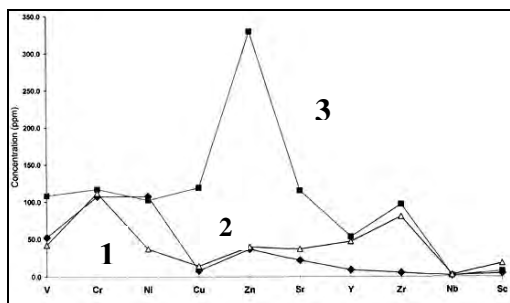


Fig. 5. Binary diagram showing the concentration of the average trace elements of the BIFs in the studied area (1), Lake Superior type (2) and Algoma type (3).

and B6 (Fig. 4) are promising for further Au exploration.

REFERENCES

ABDELSALAM, M.G., LIEGEOIS, J.P., & STERN, R.J. 2002. The Sahara Metacraton. *Journal of African Earth Sciences*, **34**, 119-136.

BOTROS, N. S. 2004. A new classification of the gold deposits of Egypt. *Ore Geology Reviews*, **25**, 1-37

EL SHIMI, K.A. & SOLIMAN, A.A. 2002. Gold mineralization associated the banded iron formation in the central Eastern Desert of Egypt; first record. *Annals of the Geological Survey, Egypt*, **25**, 281-299.

KHATTAB, M.M, *et al.* 2002. Al Oweinat Banded Iron Formation (SW Egypt) distribution and related gold mineralization. *Annals of Geological Survey, Egypt*, **25**, 343-364

RICHTER, A. & SCHANDELMIEIR, H. 1990. Precambrian basement Inliers of Western Desert, Geology, Petrology and Structural Evolution. In: SAID, R. (ed.), *The Geology of Egypt*, A. A. Balkema, 1990, 185-200.

Gold depletion and enrichment in basalt-covered areas in Central Victoria, Australia: key for mineral exploration

I. Goldberg¹, G. Abramson¹, & V. Los²

¹Interresources Pty Ltd, Level 2, 49-51 York St, Sydney, NSW 2000 AUSTRALIA
(e-mail: igoldberg@ionex.com.au)

²Academy of Mineral Resources, Nasarbaya Batyra, 146/11. Almaty KAZAKHSTAN

ABSTRACT: The problem of exploration for gold and other mineral deposits hidden under basalt in the Central Victoria gold province is part of the general problem of searching for concealed deposits. For bedrock areas we have demonstrated the effectiveness of identifying conjugate zones of ore element depletion and enrichment. Collectively, the enrichment and depletion zones constitute a unified ore geochemical system. A good correlation exists between the dimensions of the zone depleted in the ore-forming elements and the amount of those elements in the associated enrichment zone. Structurally similar geochemical systems have been identified by us in regions overlapped unconformably by basalts such as the southern part of Central Victoria. Here, a regional geochemical survey (over an area of 12 000 km²) using registration of metal-organic forms of gold and other metals in soil by the selective extraction of fulvate-humate (MPF method), we have identified geochemical systems similar to those in the Bendigo gold field. Mapping of geochemical systems, including enrichment and depletion zones of mobile forms of metals could be a key criterion for assessing the favourability of a region, in particular areas covered by basalt.

KEYWORDS: Gold, depletion, enrichment, cover basalt area

INTRODUCTION

Geochemical exploration in areas covered by blankets of consolidated or unconsolidated material is difficult at best. The Central Victoria gold province, Australia is a typical example. In the northern part of this province, where Ordovician host rocks crop out a considerable number of gold deposits are known, including the two largest goldfields at Bendigo and Ballarat (Fig. 1). No gold deposits are known in the southern part of the Central Victoria gold province where Ordovician host-rocks are unconformably overlain by post mineralization basalts.

Currently, an evaluation of the basalt covered area is being carried out by the geochemical group "Interresources Pty Ltd" using IONEX technology. This technology is based on mapping polar geochemical systems of various scales (Goldberg *et al.* 2003). Such systems include zones enriched and zones depleted in ore-forming elements. There is a linear relationship between the size of the depletion zone and the quantity of ore

metals in the deposit. This correlation is the principal criterion for assessing the potential of enrichment zones.

In covered areas IONEX technology involves investigating the distribution of mobile metals in soil. Depending on the environment, various geoelectrochemical methods are used: CHIM, selective extraction of fulvate-humate (MPF), TMGM and MDE (Antropova *et al.* 1992).

The present paper provides new data for the distribution of organic forms of gold in soil (MPF method) in the southern part of the Bendigo-Ballararat zone. The study area covers 12 000 km², most of which is covered by Tertiary basalts (Fig. 1).

GEOCHEMICAL SYSTEMS OF BENDIGO GOLDFIELD

The Bendigo-Ballararat zone is notable as the most productive gold mining region in Victoria, and includes the giant Bendigo goldfield as well as the large goldfields of Maldon, Castlemaine, and Fosterville.

The Bendigo-Ballararat zone lies between the Avoca and Mount William faults and

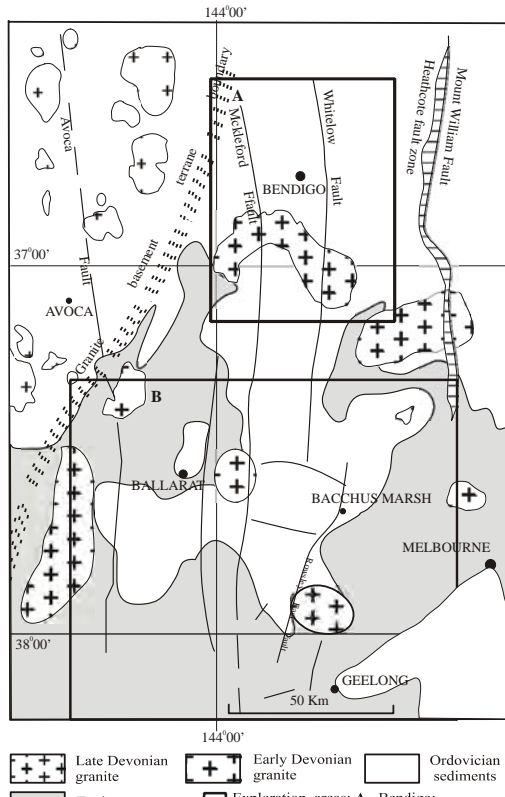


Fig. 1. Simplified geological map of Bendigo - Ballarat Zone, Victoria, Australia (Geology after Morand *et al.* 1995)

has a width averaging about 100 km (Vandenberg *et al.* 2000). The zone is characterized by north-south regional structural grain (Fig. 1).

The northern part of the Bendigo-Ballararat zone consists of an Ordovician flysch sequence which has been complexly deformed and intruded by late Devonian granitoids. In the south-western part of the study area Tertiary basalt overlies much of the Ordovician sedimentary sequence. Practically all known goldfields and mineralized zones have been discovered in areas where Ordovician sedimentary rocks crop out.

In the Bendigo area the distribution of gold and associated elements was studied in bedrock samples over an area of 3,750 km² (Fig.2).

The Bendigo goldfield is located within an enrichment zone of approximately 100 km² that has an average of 14 ppb Au. To the north a depletion zone underlying an

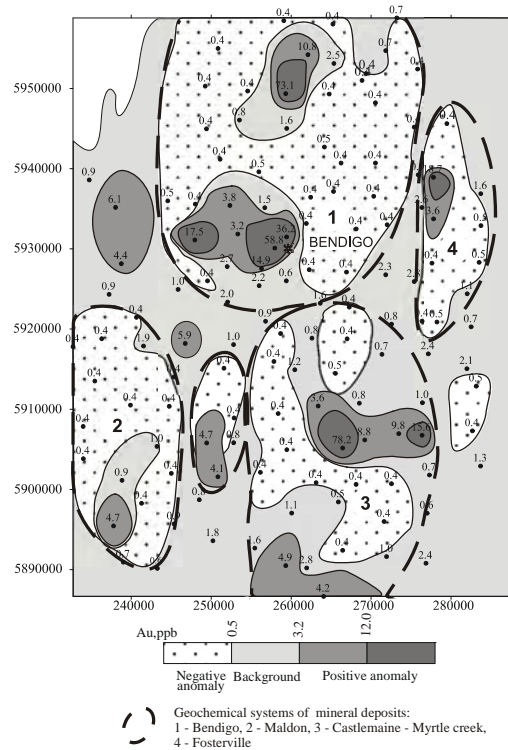


Fig. 2. Distribution of gold in rock and geochemical systems in Bendigo region Victoria. The area of this figure is outlined by box A on Fig. 1.

area of some 700-800 km², has an average gold content of less than 0.5 ppb. Together, the enrichment and depletion zones constitute a geochemical system which covers an area of more than 1000 km² (Goldberg *et al.* 2007).

A key criterion for the evaluation of a promising area is the approximately linear relationship between the area of the depletion zone and the amount of gold contained in the deposit (Fig. 3).

THE GEOCHEMICAL SYSTEM IN BASALT-COVERED AREAS

The 586 soil samples analyzed by the MPF method were collected in the southern part of the Bendigo-Ballararat zone a 12 000 km² area predominantly covered by Tertiary basalt (Figs. 1 and 4). The MPF method involves an extraction of mobile metal from soil where the concentration of the trace element is described relative to the amount of organic carbon (% C) as Me/C.

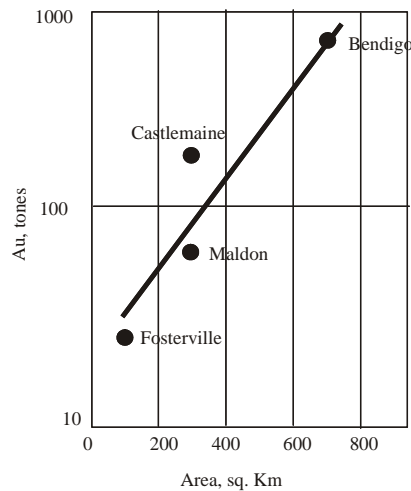


Fig. 3. Correlation between area of depletion zones in sq. km and proven resources of Au in tonnes for deposits in Bendigo region. Victoria. Australia.

The cumulative curve of Au/C% identifies 3 populations: I) $< 0.04 \cdot 10^{-4}\%$ (constitutes a depletion zone), II) $> 0.04 \cdot 10^{-4}\%$ and $< 0.2 \cdot 10^{-4}\%$ corresponds to background and III) $> 0.2 \cdot 10^{-4}\%$ to $1.35 \cdot 10^{-4}\%$ corresponds to a zone of enrichment. The distribution of Au/C% in the area is characterized by a clear zoning, represented by spatially related zones of depletion and enrichment. There are two large geochemical systems in the area, namely Ballarat and Mount Rothwell (I and II, respectively on Fig. 4). The Mount Rothwell geochemical system covers approximately 2300 km² with an enrichment zone (nucleus of the system) covering an area of 150 km². The size of the Mount Rothwell geochemical system is comparable to the geochemical depletion and enrichment zones in the Bendigo area (Fig. 2). Spatially these anomalies, according to the model of geochemical polar systems, could be united in single systems.

CONCLUSIONS

Regional geochemical surveying with a sampling density of 1 point per 25 km² was carried out in the gold-ore province of Victoria over an area of 12 000 km². The distribution of mobile organic forms of gold in soils was investigated using the MPF

method.

The aim of the investigation was to outline the most promising areas for gold exploration in Ordovician host rock lying under more recent basalts. According to preliminary data, the thickness of the basalt cover is between 100 and 300 m.

Using the phase geochemistry method, areas were identified in the soils with anomalously high concentrations of gold (enrichment zones). It has been shown in many works, including our own data (Antropova *et al.* 1972, Goldberg *et al.* 1997), that such anomalies of mobile forms of metals at the surface largely reflect the distribution of ore metals in underlying host rocks. This is so even when the apparent source is deeply buried, or concealed under very thick overburden be it consolidated or unconsolidated.

For the first time, in the case of this territory, areas have been identified with anomalously low concentrations of gold (depletion zones) which stand out clearly on the cumulative statistical gold-distribution graphs. Anomalous areas of low gold concentrations are spatially associated with areas of high concentrations. As can be seen from the data presented, the structure of such systems is polar and similar to the structure of geochemical systems in host rocks and akin to the geochemical systems identified in rocks hosting the gold-ore deposits of Bendigo and other deposits.

Mapping of geochemical systems, including enrichment and depletion zones of metals mobile forms in covered areas, could be a key criterion for assessing a favourable region.

Nevertheless, the genesis of such geochemical systems superimposed onto surficial sediment is still not well enough understood; therefore, the interpretation of the geochemical mapping data remains complicated.

REFERENCES

- ANTROPOVA, L.V., GOLDBERG I.S., VOROSHILOV N.A., & RYSS JU.S. 1992. New methods of regional exploration for blind mineralisation:

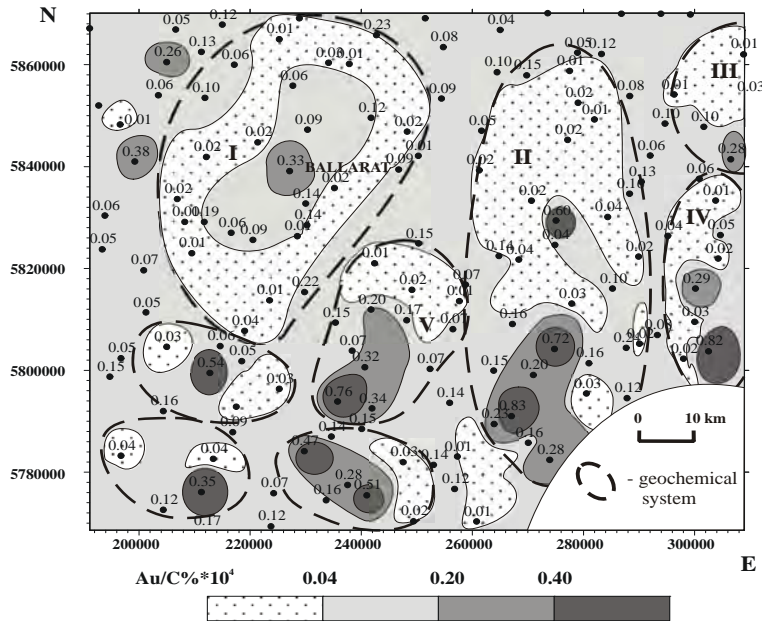


Fig. 4. Distribution of gold in soil (MPF) and geochemical systems in southern part of Bendigo–Ballarat Zone. Victoria, Australia. The area of this figure is outlined by box B on Fig.1.

application in the USSR. *Journal Geochemical Exploration*, **43**, 157-166.

GOLDBERG, I.S., ABRAMSON, G.J., & LOS, V.L. 2003. Depletion and enrichment of *primary* haloes: their importance in the genesis of and exploration for mineral deposits: *Geochemistry: Exploration, Environment, Analysis*, **3**, 281-293.

GOLDBERG, I.S. ABRAMSON, G.Y., HASLAM, C.O., & Los, V.L.. 1997. Mobile form of elements: their use in geochemical mapping and exploration: *Proceeding of Exploration 97:Fourth Decennial International Conference on Mineral Exploration*, 365-370.

GOLDBERG, I.S. ABRAMSON, G.Y., HASLAM, C.O., & Los, V.L. 2007. Depletion and enrichment

zones in the Bendigo gold field. A possible source of gold and implications for exploration: *Economic Geology*, **102**, 745-753.

MORAND, V.J., RAMSAY, W.R.H., HUGHES, M., & STANLEY, J.M. 1995. The southern Avoca Fault Zone: site of newly identified 'greenstone' belt in western Victoria. *Australian Journal of Earth Sciences*, **42**, 133-143.

VANDENBERG, A. 1974. Melbourne Sheet S1 55-1. Geological Map. Scale: 1:63,360. Lower half of Melbourne (7822) 30x30 minute Quadrangle. *Geological Survey of Victoria*.

The application of quantitative automated mineralogy in enhancing geochemical data interpretation in mineral exploration and metallurgical processes

Chris Gunning¹, Hugh de Souza¹, & Tassos Grammatikopoulos¹,

¹Advanced Mineralogy Facility, SGS Minerals Services, 185 Concession Street, Lakefield, ON, K0L 2H0 CANADA
(e-mail: chris.gunning@sgs.com)

ABSTRACT: Complete mineralogical and geochemical analyses of rocks have always been a key to improve understanding of the mineral deposits, their genesis and evolution. Furthermore, mineralogy can be applied to predict metallurgical and environmental responses of the ore. Advances in methods of geochemical analysis have had a distinct advantage over mineralogical studies in that they generate high volumes of data for a wide range of elements at low cost. However, over the past few years, significant technical developments in instrumentation for mineralogical analysis can now produce large amounts of mineralogical data quickly. Although these instruments still cannot match the throughput of commercial XRF or ICP-MS, these advances have made significant strides in providing high volume, unbiased, reproducible, and cost effective mineralogical analyses, which yield reliable data on ore samples with relatively low mineral/elemental concentrations.

Mineralogical data can improve interpretation of geochemical data, thus adding value to mineral exploration programs. Combined geochemical and mineralogical analyses can lead to ore delineation, resource estimation and definition of geological domains characterized by specific metallurgical parameters.

KEYWORDS: *automated mineralogy, QEMSCANTM, geometallurgy, ExplominTM*

INTRODUCTION

The new generation of automated mineralogy instruments is based on a fully automated Scanning Electron Microscope (SEM) platform, with high speed Energy Dispersive Spectrometers (EDS) and sophisticated software – fully integrated systems available on the market include the QEMSCANTM (Butcher *et al.* 2007, Reid 2007) and the Mineral Liberation Analyzer (MLA) (Gu 2003). Equipped with large SEM chambers that accommodate up to 16 sections for unattended sample analysis, along with digital control and monitoring of electron beam functions, these systems allow a higher volume of samples to be analyzed at lower cost. In general, only the backscattered electron (BSE) image is used as it allows phases to be discriminated on the basis of their average atomic number. The latest EDS systems are Peltier-cooled, high speed detectors that are capable of high count rates (c. 100 000 cps) with minimal dead time. This is critical because it permits the

real time collection of higher resolution X-ray based mineralogical maps and phase chemistry to complement the BSE image. The technological core of the system is the image acquisition and analysis software that, in addition to fully controlling the instruments, allows rapid image acquisition and processing and graphical output of data. The mineralogist's input is critical in setting the criteria for mineral recognition (on the basis of BSE signal and phase chemistry) and for interpretation of the output.

The advantages of using SEM based automated mineralogy instruments over conventional mineralogical techniques are three-fold. (1) Ten to hundreds of thousands (on average) of data points (or X-Ray chemistries) are collected within a single sample. This is in order of magnitudes greater than traditional optical microscopy. (2) The detection limits for low concentration minerals are superior compared to X-Ray Diffraction (XRD) analysis (cf. Berry *et al.* 2008). XRD will

likely not discern the Cu-bearing minerals for a 0.5% Cu sample, especially if there are more than two Cu phases, but QEMSCAN™ will be able to resolve this with relative ease. (3) Low level deleterious elements, e.g., Pb and As, can be mineralogically speciated, that is As can occur as arsenopyrite and/or, lollingite etc, or Pb as galena or cerrusite.

Over the past decade SGS has utilized QEMSCAN™ to focus primarily on the mineral processing sector for plant optimization, flow sheet development, and prefeasibility and feasibility studies which required High Definition Mineralogy™. Samples types used in these studies include drill-core, hand specimens, crushed reject material, feeds, concentrates, leached and smelter products. However, exploration programs do not require all of the detail associated with these studies - the Explomin™ analysis uses a standardized methodology to provide modal data (including deleterious & advantageous minerals at trace levels), mineral associations & liberation, particle & grain sizes, and elemental deportment. For these programs it is advisable to sample the coarsely crushed reject portion of the drill core for QEMSCAN™ analysis for best correlation with the geochemical data. The Explomin™ output replaces classical petrographic descriptions with mineral and textural maps of the entire section that are more complete and easier to comprehend.

CASE STUDIES

The QEMSCAN™ mineralogical applications, in conjunction with geochemistry can be applied to a variety of different ore bodies and commodities as illustrated below.

Case-1: Porphyry-type: Cu assays and mineral abundances were measured at 3 meter intervals through a Cu–Au porphyry. Figure 1 displays the sample depth vs. the total clay content vs. the Cu-Sulfide content (chalcopyrite and secondary Cu-sulfides such as bornite and covellite). Based on the mineral abundances, three distinct zones are recognized; leached, supergene and hypogene zones, each

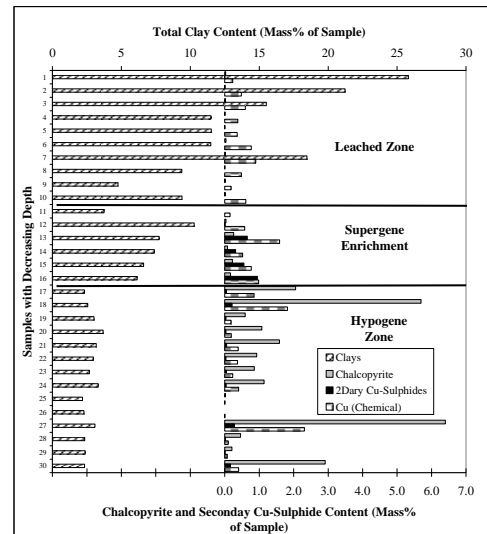


Fig. 1. An example of a Cu-Porphyry defining the leached, supergene and hypogene enriched zone from the mineral abundances of a typical figure.

geometallurgically distinct. There is a significant increase in clay content from the hypogene to the leached zone. The supergene zone is characterized by a greater abundance of secondary Cu-Sulfides to chalcopyrite. Clay content in the hypogene zone is generally less than 4% and chalcopyrite is the predominant Cu mineral. It should be noted that Cu occurs in low concentrations within clay minerals.

Case-2: Iron oxide copper gold deposits (IOCG): Tables 1 and 2 display a geochemical and mineralogical comparison, respectively, of composite samples from two different IOCG ores. The data are based on the analysis of hundreds of samples, necessary to understand the variability of each deposit. The comparison illustrates the obvious geochemical and mineralogical differences in major element chemistry that are reflected in the mineral distributions. Thus, the high LOI in IOCG-A is attributed to the higher abundance of hydrous minerals and carbonates. IOCG-A is composed predominately of Fe-oxides, and olivine and serpentine, whereas IOCG-B is composed of Fe-oxides, pyroxene, amphibole, quartz and

Table 1. Major element geochemistry for IOCG A & B.

Assay	IOCG	IOCG
	Deposit A	Deposit B
SiO ₂ %	10.4	28.2
Al ₂ O ₃ %	1.00	4.20
Fe ₂ O ₃ %	65.4	50.3
MgO %	15.70	4.46
CaO %	0.62	9.20
Na ₂ O %	<0.05	1.26
K ₂ O %	0.03	0.42
TiO ₂ %	0.11	0.19
P ₂ O ₅ %	0.14	0.12
MnO %	0.14	0.20
Cr ₂ O ₃ %	<0.01	0.01
V ₂ O ₅ %	<0.01	0.01
LOI %	5.42	0.64
Sum %	99.0	99.2
S %	2.56	2.71
Cu %	0.15	0.26
Au g/t	0.03	0.21
Fe %	45.7	35.2

feldspars.

The two IOCG ores have similar S and Cu contents, but different mineralogical expression (Table 2). Vallerite is the main Cu-bearing mineral within IOCG A, and chalcopyrite within IOCG-B. Additionally, the pyrrhotite content has mineral processing implications. Thus, if pyrrhotite is monoclinic (magnetic), it would significantly elevate the S content during magnetic separation of the magnetite concentrate, and therefore affect its saleability. Although QEMSCANTM cannot distinguish between monoclinic and hexagonal pyrrhotite, the pyrrhotite to pyrite ratio can be used to help determine the maximum S content from the pyrrhotite in a concentrate (assuming all of the pyrrhotite is monoclinic). Based on the mineral distributions, IOCG-A will be more problematic than IOCG-B because pyrrhotite is more abundant in the former. Pyrrhotite and pyrite account for ~6% and 7%, of the total Fe, in IOCG-A and B, respectively. However, there is a significant difference in gangue Fe distribution whereby IOCG-B has significantly more Fe bearing silicate.

Case-3: Rare Earth Mineral (REE) Deposits. The Thor Lake rare metals deposits are hosted by the peralkaline Blachford Lake intrusion, an Aphebian ring complex emplaced in Archean-supracrustal rocks of the Yellowknife

Table 2. Mineral distribution between IOCG A & B.

Mineral	IOCG	IOCG
	Deposit A	Deposit B
Abundances		
Fe-Oxides	66.2	48.4
Pyrite	1.22	2.29
Pyrrhotite	4.26	3.22
Chalcopyrite	0.02	0.77
Vallerite	0.81	N/A
Other Sulphides	0.04	0.27
Quartz	0.11	2.18
Feldspar	0.03	6.93
Pyroxene	0.33	21.7
Amphiboles	3.02	9.19
Serpentine	13.57	N/A
Olivine	6.27	0.64
Chlorite	2.02	1.02
Epidote	0	0.25
Mica/Clays	0.16	2.40
Other Silicates	0	0.06
Carbonates	1.36	0.18
Apatite	0.15	0.18
Other	0.48	0.31
Total	100	100
Py/Po Ratio	3.5	1.4

Supergroup. The principal rock-types in the intrusion are syenites, granites and gabbros, and associated pegmatitic bodies hosting rare metal mineralization. Five distinct zones of rare metal mineralization have been identified as potentially economic. The Lake Zone is one of them and is characterized by its enrichment in the more valuable HREE (Eu, Tb, and Dy), relative to light rare earths (LREE, i.e., La and Ce) (Palmer & Broad 2007).

Geochemical data can generally provide little quantitative information on the mineralogical distribution of the host REE minerals in any deposit. Many REE deposits can contain a number of REE phases with significant variations in light REE (LREE) and the heavy REE (HREE). Understanding this is important for mineral processing and estimating mineral resources. A combination of QEMSCANTM on drill core samples, reject material and size by size analysis, and electron microprobe analyses of a large number of samples have quantified the REM (rare earth minerals) and the REE distribution among the REM. Thus, Figure 2 illustrates an example of the distribution of LREE and HREE and Y. The diagram shows that zircon (ZrSiO₄) and fergusonite ((Y, HREE)NbO₄) account for most of the

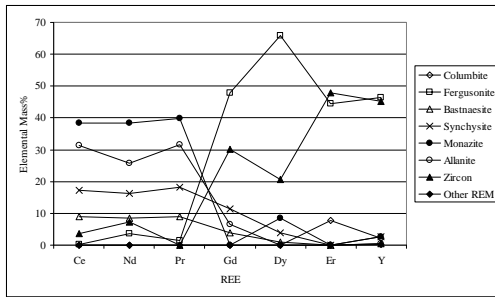


Fig. 2. LREE and HREE and Y distribution within the Lake Zone REM.

HREE & Y, whereas monazite, allanite, synchysite and bastnaesite contain most of the LREE. Based on quantitative data approximately half of the fergusonite mass% is associated mainly with zircon, and <2% of the zircon with fergusonite (i.e., reflecting mass distribution differences in the samples). Therefore, in order to recover the HREE, both minerals must be processed and recovered together. The LREE carriers can be recovered as a group.

CONCLUSIONS

The value of basic geological and geochemical information from mapping, sampling and assaying, and, diverse drillhole-logging methods is enhanced if accompanied by quantitative mineralogical data on mineralization as can be provided by automated mineralogy (QEMSCANTM).

The geological work coupled with the quantitative, statistically representative and complete mineralogical data and input into a geometallurgical framework provides a strong foundation for the development of any project.

Mineralogical variations, among the different ore zones in deposits, are critical in establishing a detailed geological context for delineating the limits of the

deposits and for bulk metallurgical testing.

QEMSCANTM studies are performed according to the needs of the project at different stages and it is currently the sole avenue for quantitative mineralogical studies. They can help in the recognition of the lithology, petrography, and alteration assemblages, that can define geometrical patterns and dimensions of exploration targets and mineralization, but most importantly that can provide metallogenic and metallurgical information.

ACKNOWLEDGMENTS

We thank SGS Lakefield Research for logistical support for this paper. We thank Volta Resources Inc, Northland Resources Inc., Avalon Ventures Ltd., and Rare Metals Inc. for permission to publish parts of data.

REFERENCES

- BERRY, R.F., HUNT, J.A., & MCKNIGHT S.W. 2008. Estimating mineralogy in bulk samples. *GeM^{III} (Amira P843) Technical Report 1 - February*.
- BUTCHER, A. BENEDICTUS, A. CROPP, A., & GOTTLIEB, P. 2007. Improving Process Efficiencies by Linking Macro-, Meso-, and Micro-Features Obtained from Automated Mineralogical Techniques. *SME '07, Denver, Colorado, Feb 26-28*.
- GU, Y. 2003. Automated scanning electron microscope based mineral liberation analysis. An introduction to JKMR/FEI mineral liberation analyzer. *Journal of Minerals & Materials Characterization & Engineering*, **2**, 33-41.
- PALMER, K. & BROAD, P. 2007. Avalon Ventures Ltd, Technical Report on the Thor Lake Rare Metals Project, NT. *Wardrop*, 97 p.
- REID, A. 2007. QEM*SEM® to QEMSCAN® 1974 – 2007. *iUG07, September 2007, Brisbane Australia*.

Provenance of the Upper Carboniferous sedimentary rocks, Maritime Basin, New Brunswick, Canada: a sedimentary geochemical approach

M.M.N. Islam, David R. Lentz, & David G. Keighley

*University of New Brunswick, 2 Bailey Dr., Box 4400, Fredericton, NB, E3B 5A3 CANADA
(e-mail: z1x61@unb.ca)*

ABSTRACT: A sedimentary geochemical approach is adopted to assess provenance in the Upper Carboniferous of New Brunswick. Data for this study is compiled from the mineral occurrence database of the provincial Department of Natural Resources. Studied drill core is composed of sandstone and claystone with minor conglomerate and coal. Mainly grey to red, very fine- to coarse-grained sandstone can be classified as litharenite based on major oxide analysis. Chemical Index of Alteration (CIA) values range from 63.91 to 73.77, suggesting a moderate to relatively high degree of alteration (weathering) in the source area. Major- and trace-element concentrations in the rocks of the studied sandstone indicate that sediments were derived from felsic to mixed felsic/basic and quartzose sedimentary source.

KEYWORDS: *Carboniferous Sedimentary Rock, Litharenite, Provenance, Weathering, New Brunswick*

INTRODUCTION

The chemical composition of clastic sedimentary rocks is a function of a multifaceted association of a number of variables, including the nature of the source rocks, source area weathering, and diagenesis (McLennan *et al.* 1993). However, the provenance of the sedimentary basins has been considered as the dominant control on the composition of sedimentary rocks (McLennan *et al.* 2003). Though weathering and diagenesis can alter the composition of basin sediments, there often remains a potent geochemical signature of the original source terrain which reflects the nature of the exposed continental crust (Roser & Korsch 1988). Literature provides many examples of the use of discrimination diagrams based on the relationship of major- and trace-elements to interpret sedimentary rock provenance (e.g., Roser & Korsch 1988; Armstrong-Altrin *et al.* 2004). As the major elements can be mobile under conditions of diagenesis (Zimmermann & Bahlburg 2003), less mobile elements (i.e., Ti, Cr, Co, Th, Y, Th, Zr, Hf, Nb, and Sc), are more reliable for discrimination of provenance (Taylor & McLennan 1985; Bhatia & Crook 1986; Asiedu *et al.* 2000).

The study area is located within in the eastern tip of the Indian Mountain Deformed Zone, southeastern New Brunswick, Canada. The area is underlain by Upper Carboniferous sedimentary rock and bounded by the Smith Creek and Berry Mills faults to the north and south, respectively (St. Peter 2006). These sedimentary rocks are dominantly grey to red, very fine- to coarse-grained sandstone, and variable red grey/green claystone with minor conglomerate and coal fragments. The study was conducted, based on MacDougall SB-3 (W 64° 39' 25.0", N 46° 16' 28.7) drill core samples. The geochemical data for this investigation was taken from a New Brunswick Department of Natural Resources Minerals Policy and Planning Division, Mineral Assessment Report (# 476200).

CLASSIFICATION OF SANDSTONE

For geochemical classification of sandstone, most of the recent literature (Armstrong-Altrin *et al.* 2004; Spalletti 2008) uses the classification schemes of Pettijohn (1972) and Herron (1988). The geochemical classification diagram presented in Fig. 1 shows that samples used in this study (Table 1) fall in the

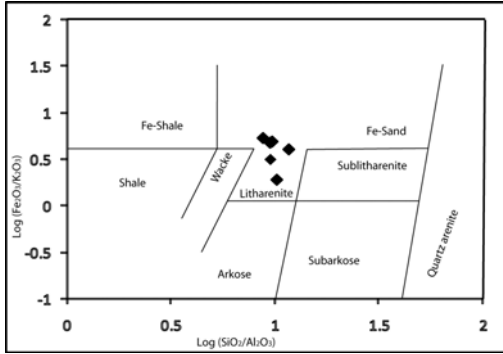


Fig. 1. Chemical classification of sandstone samples from the MacDougall SB-3 drill hole (Table 1). Field boundaries are from Herron (1988).

Table 1. Chemical composition of the selected samples.

Sample No.	S-1	S-2	S-3	S-4	S-8
Major Oxide (wt%)					
SiO ₂	80.19	81.68	73.83	75.22	73.74
Al ₂ O ₃	6.84	7.95	7.56	7.88	8.35
Fe ₂ O ₃	5.08	2.81	7.3	6.85	7.41
MgO	0.42	0.77	0.6	0.57	0.81
CaO	1.29	0.88	0.27	1.36	0.57
Na ₂ O	1.23	1.31	1.25	1.71	1.07
K ₂ O	1.21	1.43	1.43	1.38	1.33
TiO ₂	0.23	0.78	0.44	0.34	0.51
P ₂ O ₃	0.06	0.08	0.07	0.07	0.11
MnO	0.08	0.08	0.04	0.09	0.08
Cr ₂ O ₃	0.002	0.004	0.003	0.003	0.005
Trace elements (ppm)					
La	18.6	27.8	25.5	22.1	29.4
Th	4.1	8.3	5.8	7.1	5.5
Sc	4	7	5	5	7
Hf	2.8	8.4	5.9	6.1	4.8
Co	5.4	7.3	11.6	7.8	19.5

litharenite class, reflecting the mineralogical submaturity of these sediments.

SOURCE AREA WEATHERING

The most common method of measuring the degree of chemical weathering is to calculate the chemical index of alteration (CIA = [Al₂O₃/(Al₂O₃ + CaO + Na₂O + K₂O) × 100]; Nesbitt & Young 1982). High CIA values (64.7, 68.7, 71.9, 63.9, and 73.8) indicate a high degree of alteration of the source rocks. The average CIA values for the samples used in this study are 68.6. Most of the data used in this study plot

between idealized plagioclase (CIA = 50) and shale (CIA = 70-75), indicating that the weathering is dominantly the conversion of plagioclase to clay (Fig. 2). Yet, the high value of CIA suggests transportation and recycling from sources located distal to the depositional basin (Nesbitt & Young 1982), which is consistent with a provenance from the stable craton interior or recycled orogen (Dickinson *et al.* 1983). Also, the SiO₂/Al₂O₃ ratios for the samples are high (average 10.0), and indicate a high degree of maturity of the sediments (Asiedu *et al.* 2000).

PROVENANCE

In order to determine the source composition of sediments using trace elements, it is necessary to ascertain that the element is immobile under conditions of diagenesis and weathering (Spalletti 2008). Several ratios and plots may be used to define the source rocks. The felsic source rock compositions are found in the Co/Th vs. La/Sc diagram (Fig. 3; Table 1). Other trace element characteristics of sedimentary rocks also place some constraints on the nature of the source rock. Floyd & Leveridge (1987) used a La/Sc vs. Hf plot to discriminate between different source compositions. In this plot, most data fall in the felsic source to mixed felsic/basic source field (Fig. 4; Table 1).

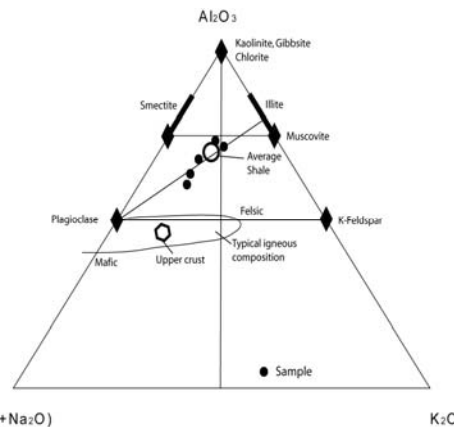


Fig. 2. Ternary plot of Al₂O₃–(Na₂O + CaO)–K₂O (CIA) for the studied sample (after Gu *et al.* 2002). Black filled circles are samples used in this study.

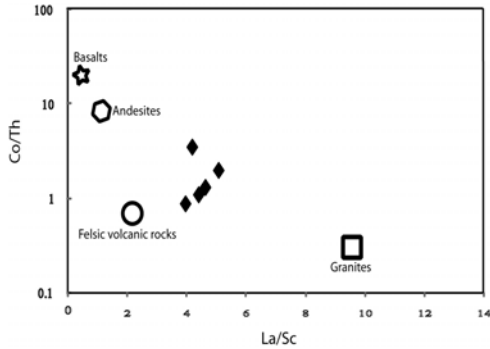


Fig. 3. Co/Th vs. La/Sc source rock discrimination diagram (after Gu *et al.* 2002) illustrating the distribution of samples from MacDougall SB-3 (black diamond symbol).

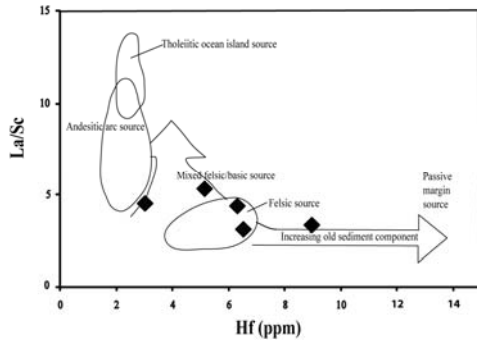
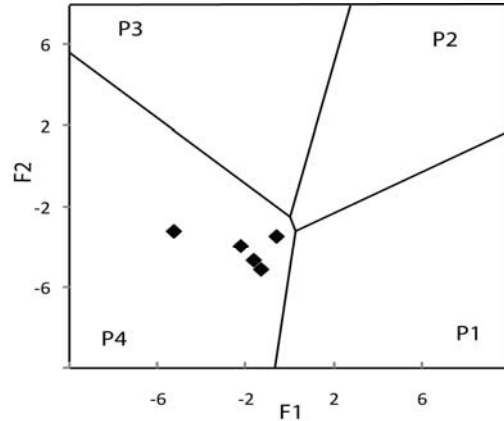


Fig. 4. La/Sc vs. Hf source rock discrimination diagram (after Floyd and Leveridge 1987) illustrating the distribution of samples from MacDougall SB-3 (black diamond symbol).

High contents of Fe₂O₃ and high Al₂O₃/TiO₂ ratios indicate continentally derived sediments (Fyffe & Pickerill 1993). Presences of greater than 70% SiO₂ implies the sandstones are rich in quartz from quartz-rich crystalline provenance (Potter 1978). In the discrimination diagrams for sedimentary provenance, samples used in this study plot in the quartzose recycled fields (Fig. 5).

CONCLUSIONS

The geochemical classification using major oxides shows that the samples used in this study plot in the litharenite field, and, implies that they are mineralogically submature. Major-element concentrations point to significant weathering effect in the source area of the sample set. Provenance analyses, based on major- and trace-element compositions suggest



P1 = Mafic, First-Cycle basaltic and lesser andesitic detritus.
 P2 = Intermediate dominantly andesitic detritus.
 P3 = Felsic-acidic plutonic and volcanic detritus.
 P4 = Recycled mature polycyclic quartzose detritus.

Fig. 5. Provenance discriminant function diagram from Roser & Korsch (1988). F1= 1.773 TiO₂+0.607 Al₂O₃+ 0.76 Fe₂O₃-1.5 MgO+ 0.616 CaO+ 0.509 Na₂O- 1.224 K₂O-9.09; F2=0.445 TiO₂+ 0.07 Al₂O₃- 0.25 Fe₂O₃-1.142 MgO+ 0.438 CaO+ 1.475 Na₂O+1.426 K₂O-6.861.

the sandstones were derived from felsic to mixed felsic/basic and quartzose sedimentary source.

ACKNOWLEDGEMENTS

The authors would like to thank ValeInco for the funding of this research. Thanks are also extended to New Brunswick Department of Natural Resources-Minerals, Policy and Planning Division.

REFERENCES

ARMSTRONG-ALTRIN, J.S., YONG, I.L., VERMA, S.P., & RAMASAMY, S. 2004. Geochemistry of sandstones from the Upper Miocene kudankulam formation, southern india: implications for provenance, weathering, and tectonic setting. *Journal of Sedimentary Research*, **74**, 285-297.
 ASIEDU, D.K., SUZUKI, S., & SHIBATA, T. 2000. Provenance of sandstones from the Lower Cretaceous Sasayama Group, Inner Zone of Southwest Japan. *Sedimentary Geology*, **131**, 9-24.
 BHATIA, M.R. & CROOK, K.A.W. 1986. Trace element characteristics of graywackes and tectonic setting discrimination of sedimentary basins. *Contributions to Mineralogy and Petrology*, **92**, 181-193.
 DICKINSON, W.R. *et al.* 1983. Provenance of North American Phanerozoic sandstone in

- relation to tectonic setting, *Geological Society of America Bulletin*, **94**, 222-235.
- FLOYD, P.A. & LEVERIDGE, B.E. 1987. Tectonic environment of the Devonian Gramscatho basin, south Cornwall: framework mode and geochemical evidence from turbiditic sandstones. *Journal of the Geological Society of London*, **144**, 531-542.
- FYFFE, L.R. & PICKERILL, R.K. 1993. Geochemistry of Upper Cambrian – Lower Ordovician black shale along a northeastern Appalachian transect. *Geological Society of America Bulletin*, **105**, 897-910.
- GU, X.X., LIU, J.M., ZHENG, M.H., TANG, J.X., & QI, L. 2002. Provenance and tectonic setting of the Proterozoic turbidites in Hunan, South China: Geochemical Evidence. *Journal of Sedimentary Research*, **72**, 393-407.
- HERRON, M.M. 1988. Geochemical classification of terrigenous sands and shales from core or log data. *Journal of Sedimentary Petrology*, **58**, 820-829.
- MCLENNAN, S.M., BOCK, B., HEMMING, S.R., HUROWITZ, J.A., LEV, S.M., & MCDANIEL, D.K. 2003. The role of provenance and sedimentary processes in the geochemistry of sedimentary rock. In: Lentz, D.R. (ed.), *Geochemistry of Sediments and Sedimentary Rocks: Evolutionary Considerations to Mineral Deposits-Forming Environments*: Geological Association of Canada, Geotext, **4**, 121-133
- MCLENNAN, S.M., HEMMING, S., MCDANIEL, D.K., & HANSON, G. N. 1993. Geochemical approaches to sedimentation, provenance, and tectonics. In: JOHNSON, M.J. & BASU, A. (eds.), *Processes Controlling the Composition of Clastic Sediments*. Geological Society of America. Special Paper, **284**, 21-40.
- NESBITT, H.W. & YOUNG, G.M. 1982. Early Proterozoic climates and plate motions inferred from major element chemistry of lutites. *Nature*, **299**, 715-717.
- PETTIJOHN, F.J., POTTER, P.E., & SIEVER, R. 1972. *Sand and Sandstone*. Springer-Verlag, New York.
- POTTER, P.E. 1978. Petrology and chemistry of modern Big River sands. *Journal of Geology*, **86**, 423-449.
- ROSER, B.P. & KORSCH, R.J. 1988. Provenance signatures of sandstone-mudstone suites determined using discriminant function analysis of major-element data. *Chemical Geology*, **67**, 119-139.
- SPALLETTI, L.A., MERODIO, J.C., & MATHEOS, S.D. 2008. Sedimentary petrology and geochemistry of siliciclastic rocks from the upper Jurassic Tordillo Formation (Neuquén Basin, western Argentina): Implications for provenance and tectonic setting. *Journal of South American Earth Sciences*, **25**, 440-463.
- ST. PETER, C. 2006. Geological relationship between the Cocagne Subbasin and Indian Mountain Deformed Zone, Maritime Basin, New Brunswick. In: MARTIN, G.L. (ed.), *Geological Investigations in New Brunswick for 2005*. New Brunswick Department of Natural Resources, Mineral Policy and Planning Division, Mineral Resource Report **2006-3**, 103-183.
- TAYLOR S.R. & MCLENNAN S.M. 1985. *The Continental Crust: Its Composition and Evolution*. Blackwell Science Publisher, Oxford.
- ZIMMERMANN, U. & BAHLBURG, H. 2003. Provenance analysis and tectonic setting of the Ordovician clastic deposits in the southern Puna Basin, NW Argentina. *Sedimentology*, **50**, 1079-1104.

Spatial geochemical trends of beach and dune sands from the Northeastern coast of Mexico: implications for provenance

Juan Jose Kasper-Zubillaga¹, John S. Armstrong-Altrin¹, & Arturo Carranza Edwards¹

¹ Instituto de Ciencias del Mar y Limnología, Universidad Nacional Autónoma de México, Circuito Exterior s/n, Coyoacan, México DF, MÉXICO 04510 (e-mail: kasper@icmyl.unam.mx)

ABSTRACT: A geochemical analysis of major, trace and rare earth elements was carried out in beach sands collected from the Northeastern coast of Mexico in order to observe the spatial trends along three different beaches. Results show that major elements patterns along the beaches are controlled by heavy minerals and plutonic and sedimentary input towards the coast. In addition, trace elements tendencies indicate that the beach sands are influenced by the presence of magnetite. Finally, the differences in Eu anomalies indicate a mix of felsic to mafic and intermediate rocks and feldspar weathering.

KEYWORDS: *beach, sand, provenance, Mexico*

INTRODUCTION

Beach and dune sediments are compositionally controlled by physical, chemical and mechanical factors such as waves, wind, and long shore currents, climate, relief, source composition, transport and river discharges among others (Folk 1974, Ibbeken & Schleyer, 1991; Carranza-Edwards *et al.* 1994; Critelli *et al.* 1997; Carranza-Edwards *et al.* 1998; Armstrong-Altrin *et al.* 2003; Armstrong-Altrin *et al.* 2004; Kasper-Zubillaga & Carranza-Edwards 2005; Kasper-Zubillaga *et al.* 2008a). A wide range of techniques are used for geochemical determinations to investigate the compositional differences of the beach and dune sediments. Such techniques are defined by major, trace and rare earth elements analyses. Furthermore, these techniques allow to understanding the multi-factorial roles that control the composition of coastal sediments. In this paper we focus our attention in showing the spatial trends of geochemical data obtained during the dry season in the northeastern coast of the Gulf of Mexico to discuss the provenance implications.

STUDY AREA

The study area is located in the coastal

area of the state of Tamaulipas, Mexico (22°10' 24°00'W; 98°00'N). The sampling was carried out in three main localities: Playa Miramar, Boca del Tordo and La pesca (Figs. 1 & 2). Main rivers discharging in each site are Panuco, Carrizal and Soto La Marina.

The geology of the study area comprises mainly: limestones, shales, alluvial deposits, and basic extrusive and intrusive rocks.

MATERIALS AND METHODS

Sand samples were dried at 110 °C and treated with lithium meta- and tetraborate to make pressed powder pellets. They were analysed using an X-ray fluorescence Siemens SRS 3000 equipment for major and trace elements. For major and trace elements precision is valued in terms of relative standard deviation being < 1% (Sutarno & Steger 1985).

The REE analysis was carried out in 22 sand samples by using 0.1 g of dried sample (mesh 200) and digested with strong acid. Digestion was performed in teflon vessels using 4 ml of HCl O₄ and 10 ml HF. This mixture was heated and residue dissolved in distilled water.

Residue was incorporated to a volumetric flask. Determinations of REE

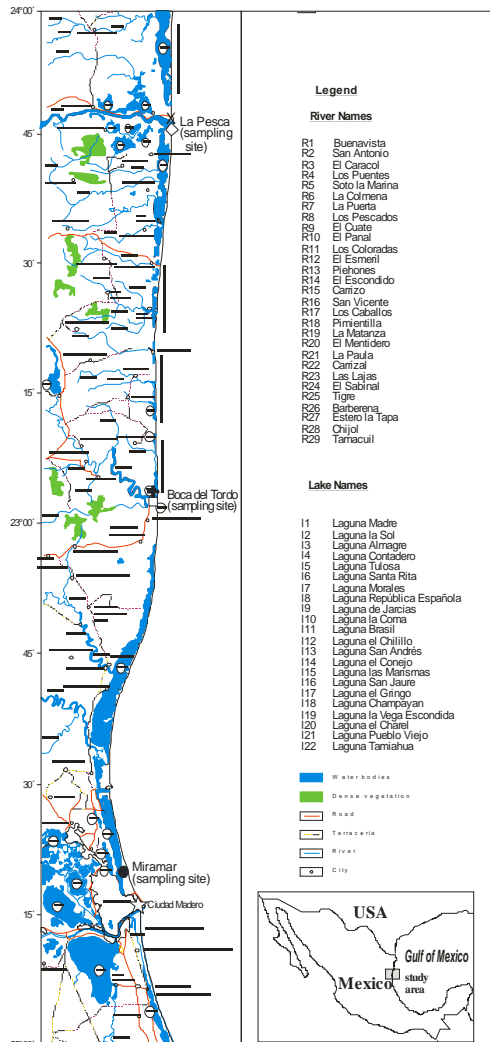


Fig. 1. Study area and sampling sites.

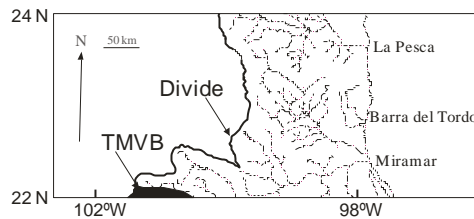


Fig. 2. Map showing the Trans-Mexican Volcanic Belt (TMVB) near the study area.

were carried out with an ICP mass spectrometer VG Elemental model PQ3. Detection limits were calculated as the concentration equivalent to three times the standard deviation of five replicates of the blank solution. It was better than 200 ppt for all elements determined. Calibration of

the apparatus was done with a 0.1, 1 10 and 100 ppb multi elemental standard solution (SPEX- High Purity) and a blank solution of de-ionized water all containing HNO_3 at 2%. Results were observed for international standards (JG-2). The validity of the analytical procedure was assessed by means of accuracy and precision tests. They were calculated by comparing measured and reference values (JA-2). All elements determined had a better than 10 % relative standard deviation (RSD) precision. Data resulted for BCU-3 or “in house standard indicated good agreement with the certified values.

Chondrite-normalized REE patterns were based on values by Evensen *et al.* (1978) averaging the samples firstly determined in ppm for each site.

RESULTS & DISCUSSION

From Figure 3 it can be observed that among the major element trends Ti shows various peaks from localities 10 to 22 that correspond to some beach areas from Playa Miramar, the whole area of Boca del Tordo and one sample from the La Pesca. This suggests that this area might have influenced by heavy minerals and plutonic and sedimentary outcrops as it has previously reported in dune sands from Mexico (Kasper-Zubillaga *et al.* 2008a). The rest of the major elements do not show differences in their trends along the coast. However, Ca shows a dynamic behavior represented by oscillations along the coast probably produced by the amount of biogenic debris.

Trace elements show that V exhibit high peaks in Boca del Tordo beach probably associated with the presence of some heavy minerals like magnetite (Kasper-Zubillaga *et al.* 2008a).

Rare earth elements patterns show differences in Eu anomalies for the samples studied from Boca del Tordo (Fig. 5) that can be attributed to the mix of felsic and mafic sources. This variation can also be explained due to the impoverishment of feldspars due to weathering (Kasper-Zubillaga *et al.* 2008b). Also Boca del Tordo concentrates more rare earth elements especially in samples 16 and 18,

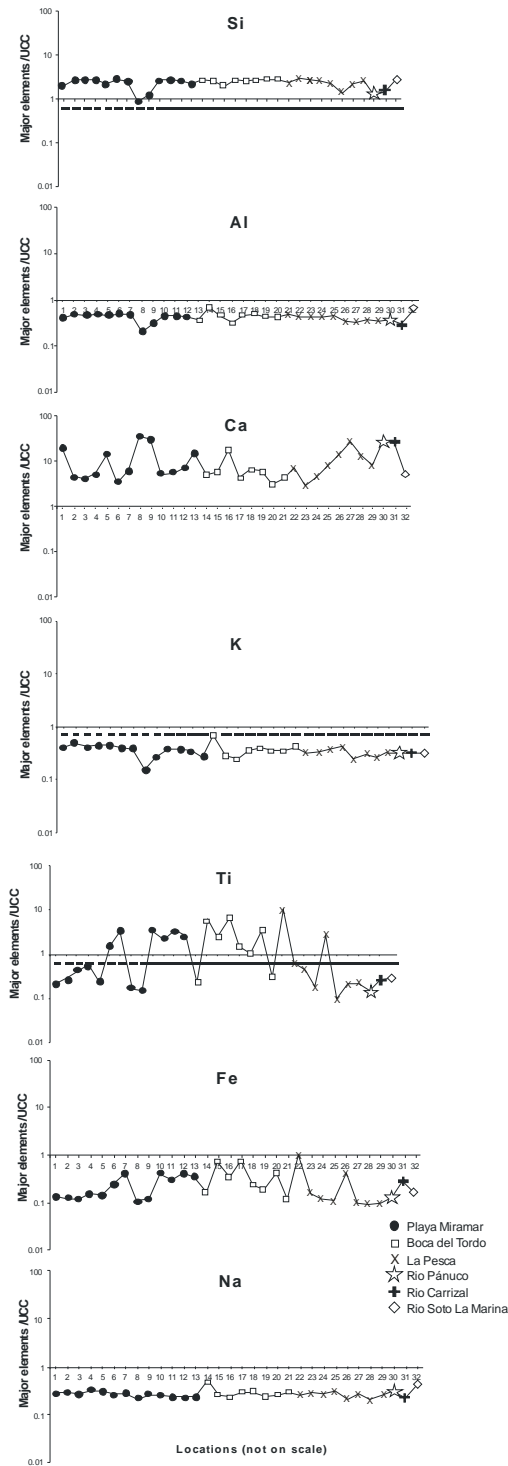


Fig.3. Spatial trends of major elements at beach and dune sands from the northeastern coast of Mexico.

which is probably due to the presence of some heavy minerals that are potential

carriers of rare earth elements (Kasper-Zubillaga *et al.* 2008b). The possible source of volcanic is mainly through the Panuco River that intersects volcanic from the Trans-Mexican Volcanic Belt.

CONCLUSIONS

- (1) Major element trends show that Northeastern Mexican beaches are influenced by heavy minerals and plutonic and sedimentary outcrops.
- (2) Trace element tendencies suggest that the Boca del Tordo beach is more influenced by the presence of magnetite than other beaches.
- (3) Rare earth element trends show negative and positive Eu anomalies in some samples studied from the Northeastern beaches suggesting a mix of felsic and mafic source rocks and feldspar weathering.

ACKNOWLEDGMENTS

We are indebted to Rufino Lozano and Ofelia Morton for the geochemical analyses carried out at the Instituto de Geología and Instituto de Geofísica, respectively, from the Universidad Nacional Autónoma de México, México.

REFERENCES

ARMSTRONG-ALTRIN, J.S., VERMA, S.P., MADHAVARAJU, J., LEE, Y.I., & RAMASAMY, S. 2003. Geochemistry of upper Miocene Kudankulam limestones, southern India. *International Geological Review*, **45**, 16-26.

ARMSTRONG-ALTRIN, J.S., LEE, Y.I., VERMA, S.P., & RAMASAMY, S. 2004. Geochemistry of sandstones from the Upper Miocene Kudankulam Formation, Southern India: implications for provenance, weathering and tectonic setting. *Journal of Sedimentary Research*, **74**, 285-297.

CARRANZA-EDWARDS, A., ROSALES-HOZ, L., & SANTIAGO-PÉREZ, S. 1994. Provenance memories and maturity of holocene sands in Northwest Mexico. *Canadian Journal of Earth Sciences*, **31**, 1550-1556.

CARRANZA-EDWARDS, A., BOCANEGRA-GARCIA, G., ROSALES-HOZ, L. & DE PABLO GALÁN, L. 1998. Beach sands from Baja California Peninsula, México. *Sedimentary Geology*, **119**, 263-274.

CRITELLI, S., LE PERA, E., & INGERSOLL, R.V. 1997. The effects of source lithology,

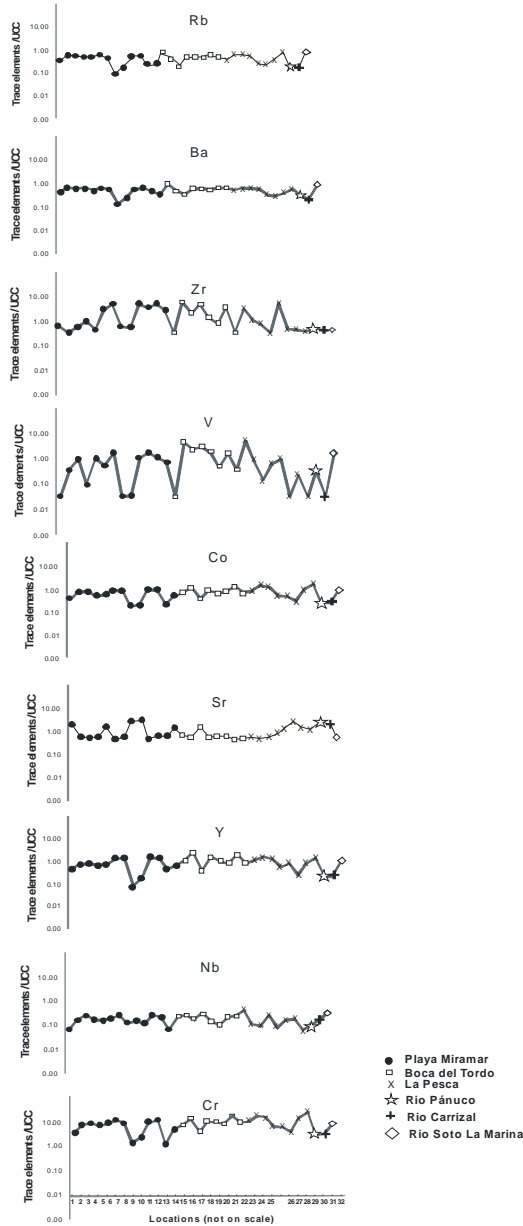


Fig.4. Trace elements tendencies along the northeastern coast of Mexico.

transport, deposition and sampling scale on the composition of southern California sand. *Sedimentology*, **44**, 653-671.

EVENSEN, M.N., HAMILTON, P.J., & ONIONS, P.K., 1978. Rare earth abundance in chondrite meteorites. *Geochimica et Cosmochimica Acta*, **42**, 1199-1212.

FOLK, R. L., 1974. *Petrology of Sedimentary Rocks*. Hemphill Publishing Co., Austin, TX.

IBBEKEN, H. & SCHLEYER, R., 1991. *Source and Sediment*. Springer Verlag, Berlin.

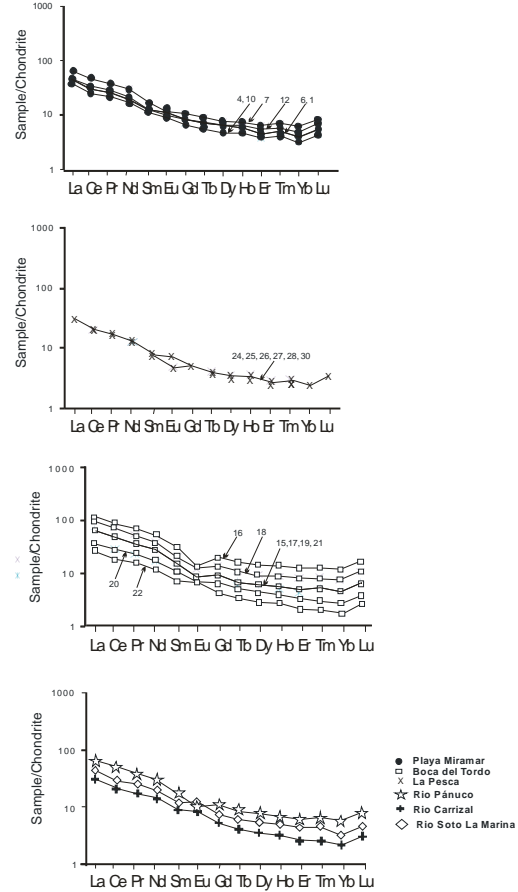


Fig.5. Rare earth elements in the northeastern coast of Mexico.

KASPER-ZUBILLAGA, J.J. & CARRANZA-EDWARDS, A., 2005. Grain size discrimination between sands of desert and coastal dunes from northwestern Mexico. *Revista Mexicana de Ciencias Geológicas*, **22**, 383-390.

KASPER-ZUBILLAGA, J.J., ACEVEDO-VARGAS, B., MORTON-BERMEA, O., & ORTIZ-ZAMORA, G., 2008a. Rare earth elements of the Altar Desert dune and coastal sands, Northwestern Mexico. *Chemie Der Erde Geochemistry*, **68**, 45-69.

KASPER-ZUBILLAGA, J.J., CARRANZA-EDWARDS, A., & MORTON-BERMEA, O. 2008b. Heavy minerals and rare earth elements in coastal and inland dunes of El Vizcaino Desert Baja California Peninsula, Mexico. *Marine Georesources and Geotechnology*, **26**, 172-188.

SUTARNO, R. & STEGER, H.F., 1985. The use of certified reference materials in the verification of analytical data and methods. *Talanta*, **32**, 439-445.

The Chemistry of black shale and exploration for VHMS, Mount Read Volcanics, Western Tasmania

Andrew W. McNeill¹

¹CODES, University of Tasmania, Private Bag 79, Hobart, TAS 7001 AUSTRALIA
(e-mail: andrew.mcneill@utas.edu.au)

ABSTRACT: Black shales in the hanging wall to the Pb-Zn VHMS deposits of the Mount Read Volcanics may have been altered by the underlying hydrothermal systems and the signature of such alteration may provide vectors to mineralisation. The major and trace element chemistry of the Rosebery Hanging wall Shale and the trace element chemistry of the pyrite and pyrrhotite that it contains have been investigated. Preliminary results indicate that a whole-rock Sb and TI 'halo' at the base of the shale unit is not as extensive as has previously been suggested. The elevated Co, Zn, As and Mo contents and Co/Ni of 'early' pyrite, proximal to the orebody may provide vectors to underlying mineralisation.

KEYWORDS: *Exploration, Shale, VHMS, pyrite, geochemistry*

INTRODUCTION

The geochemical signature of footwall alteration of the major Pb-Zn VHMS deposits of the Mt Read Volcanics (MRV) is well constrained (Large *et al.* 2001b), and vectors such as elevated TI have been used successfully (e.g., discovery of Y lens at the Rosebery Mine; McNeill, unpublished).

However, the characteristics of any hanging wall alteration, particularly in the black shales that overly Rosebery and Hellyer, the two major Pb-Zn VHMS deposits in the MRV, are not as well constrained. Previous studies of the well developed hanging wall alteration zone at Hellyer have defined its whole-rock geochemical signature (Sinclair 1994; Gemmell & Fulton, 2001) while studies of the sulfide trace element signature are ongoing (Layton-Matthews *et al.* 2008).

At Rosebery, studies of the hanging wall alteration by Large *et al.* (2001a) indicated that, based on a limited dataset, whole-rock TI, Sb, and Ba were all elevated in shale above the orebody, while characterisation of the trace element signature of sulfides is limited to two analyses of Co and Ni in pyrite by Loftus-Hills and Solomon (1967).

In this contribution I present the preliminary results of an investigation into the alteration signature of the Rosebery Hanging wall shale, using an expanded whole-rock chemical dataset and trace element analyses of pyrite and pyrrhotite, the major sulfide minerals in the shale.

METHODS

Rosebery Hanging-wall Shale samples were selected from drill core in proximal (<120m from ore), medial (~1000m) and distal (>4km) locations.

Whole-rock compositions were determined by XRF and solution ICP-MS using the methods outlined by Yu *et al.* (2001) and Robinson (2003).

LA-ICPMS analyses of pyrite and pyrrhotite in both spot and imaging mode (for 32 and 22 elements respectively) were completed on a New Wave 213nm solid-state laser microprobe coupled to an Agilent 4500 quadrupole ICPMS using the procedures of Large *et al.* (*submitted*).

WHOLE-ROCK GEOCHEMISTRY

Vertical sections through the Rosebery Hanging wall shale were sampled in drill holes from proximal and medial locations and results compared with those from

distal locations, including shale units stratigraphically higher and lower in the sequence.

Preliminary results indicate that base and precious metal, As, and Ba contents of shale in proximal and medial locations are within the range of shale samples from distal locations. Only Sb, up to 23 ppm, and Tl, up to 9 ppm, in the lower 10-15m of the hanging wall shale are significantly higher than in medial and distal samples, with <8 ppm Sb and <1.4 ppm Tl.

SULFIDE MINERAL CHEMISTRY

Pyrrhotite

Anhydrous pyrrhotite, from <10-200 μm in diameter, occurs in the matrix and in veins in all but one of the analysed samples. Visually the pyrrhotite appears to be inclusion-free, but Rare Pb- and Zr+REE-rich inclusions were found during analysis and it was noted that pyrrhotite in contact with pyrite generally has lower Co contents than other grains (3 ppm vs 280ppm, respectively, in samples from one drill hole) and have not been used for interpretation.

Trace elements, in order of decreasing abundance are Ni, Co, Se, Pb, Sb, Ag and Bi. The only statistically significant difference in composition between pyrrhotite from proximal and distal samples is the lower Co contents of the latter.

Pyrite

Three textural types of pyrite occur in all samples examined; 1) early framboids or irregular masses, 2) isolated euhedra, and 3) pyrites with massive cores and 'spongy' or porous rims (Fig. 1). Types 2 and 3 occur in both shale and cross-cutting to bedding parallel veins, whereas type 1 occurs in shale only.

Compositional variations among all textural types are obvious (Fig. 1) and a comparison of type 1 pyrite in proximal and distal locations is shown in Fig. 2 (Note that data have not been included for elements where a large proportion [>40%] of results were below detection limit).

The elevated Zn, As, Co and Mo which appear to distinguish proximal from distal

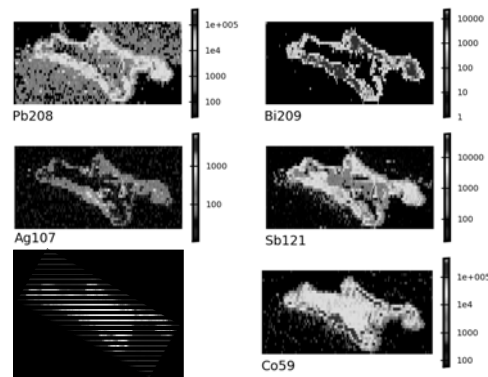


Fig. 1. LA-ICPMS maps of trace element variations in pyrite from a bedding parallel quartz-carbonate vein. The two textural types are a "spongy" discontinuous rim with higher Pb, Bi, Ag, Sb and Co contents than the 'massive' core.

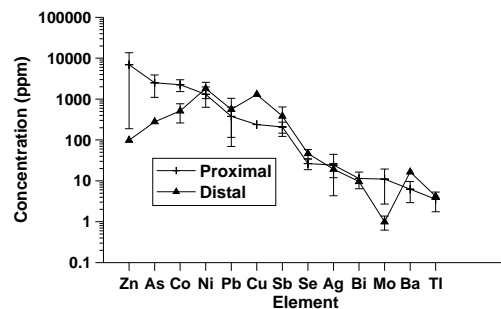


Fig. 2. Trace element variations in type 1 pyrite. Average values for pyrite in proximal (n=10) and distal (n=5); bars indicate 1 σ . Note log scale.

type 1 pyrite result from the presence, interpreted from the time-integrated LA-ICPMS signal profile, of inclusions and micro-inclusions in the case of Zn and predominantly lattice substitution, as indicated by generally smooth profiles, in the case of Mo, Co and As.

The Co/Ni of type 1 pyrite from distal samples is 0.15-0.5 compared with 1.0-4.0 in proximal samples, consistent with the results of Loftus-Hill and Solomon (1967) who recorded ratios of 0.03-0.4 and 0.8 respectively (note that the 'distal' samples in this earlier study are largely from shale units closer to the Hellyer orebody).

CONCLUSIONS

Preliminary results indicate that the alteration signature of shales in the Hanging wall of the Rosebery orebody is characterised by:

- (1) Elevated Co in pyrrhotite.
- (2) Elevated Zn, As, Co and Mo and Co/Ni in early (type 1) pyrite.
- (3) Elevated Sb and Tl in whole-rock samples from the lower 10-15m of the shale unit proximal (<120m) to the orebody.

These represent potential vectors to mineralisation that may be applied in exploration drill programs.

ACKNOWLEDGEMENTS

I thank Zinifex Limited (now Oz Minerals) for financial support and for permission to present these results. D. Hicks, C. Archer and M. Skirka (Zinifex) and M. Jacobson (MRT) facilitated access to drill core and other data. P. Robinson, K. McGoldrick and S. Gilbert completed the XRF and solution ICPMS analyses and S. Gilbert provided assistance and advice on LA-ICPMS analyses.

REFERENCES

- GEMMELL, J.B. & FULTON, R.L. 2001. Geology, genesis and exploration implications of the footwall and hanging-wall alteration associated with the Hellyer volcanic-hosted massive sulfide deposit, Tasmania, Australia. *Economic Geology*, **96**, 1003-1035.
- LARGE, R.R. *et al.* Submitted. Gold and trace element zonation in pyrite using a laser imaging technique; implications for the timing of gold in orogenic and Carlin-style

sediment-hosted deposits. *Economic Geology*.

- LARGE, R.R., ALLEN, R.L., BLAKE, M.D., & HERRMANN, W. 2001a. Hydrothermal alteration and volatile element haloes for the Rosebery K Lens volcanic-hosted massive sulfide deposit, Western Tasmania. *Economic Geology*, **96**, 1055-1072.
- LARGE, R.R., MCPHIE, J., GEMMELL, J.B., HERRMANN, W., & DAVIDSON, G.J. 2001b. The spectrum of ore deposit types, volcanic environments, alteration halos and related exploration vectors in submarine volcanic successions: some examples from Australia. *Economic Geology*, **96**, 913-938.
- LAYTON-MATTHEWS, D., GEMMELL, J.B., LARGE R.R., & PETER J. 2008. Trace-element budget of the Que River shale: exploration implications of hanging-wall modification of sulfide minerals at the Hellyer deposit, Tasmania, *Abstract. 33rd International geological Congress, Oslo*.
- LOFTUS-HILLS, G & SOLOMON, M. 1967. Cobalt, Nickel and Selenium in sulphides as indicators of ore genesis. *Mineralium Deposita*, **2**, 228-242.
- ROBINSON, P. 2003. XRF analysis of flux-fused discs. *Abstract. Geoanalysis 2003, Finland*.
- SINCLAIR, B.J. 1994. *Geology and geochemistry of the Que River Shale, western Tasmania*. BSc (Hons.) Thesis, University of Tasmania, Hobart.
- YU, Z, ROBINSON, P., & MCGOLDRICK, P. 2001. An evaluation of methods for the chemical decomposition of geological materials for trace element determination using ICP-MS. *Geostandards Newsletter*, **25**, 199-217.

Weathering-related rare earth element patterns in the regolith of the Cobar region, western New South Wales

K.G. McQueen

Faculty of Applied Science, University of Canberra, ACT, 2601
AUSTRALIA (e-mail: Ken.McQueen@canberra.edu.au)

ABSTRACT: Analysis of REE distributions through weathered profiles on siliclastic metasedimentary rocks in the Cobar region indicates that older profiles (60-20 Ma), beneath Paleocene lake sediments and Early Miocene lava flows, commonly show depletion of light rare earths (LREE) in the upper saprolite. Cerium which is depleted in the upper saprolite can be markedly enriched near the base. Younger profiles formed after erosional stripping in the Miocene (<20 Ma) and under drier climatic conditions do not show LREE fractionation (flat pattern) and either have REE abundances similar to the unweathered parent rock or show some overall REE enrichment due to profile leaching, collapse and concentration of host resistate minerals. These various patterns reflect different climatic and weathering regimes in the long history of sub-aerial exposure of the Cobar terrain. The REE patterns could be used to identify weathering profiles of different ages and different degrees of chemical leaching.

KEYWORDS: REE, fractionation, weathering, climate, geochemistry

INTRODUCTION

The Rare Earth Elements (REE-Lanthanides and Y) are commonly used to unravel rock-forming processes because of their similar chemical properties, typically low solubilities and assumed resistance to fractionation in crustal and surface environments. However, under some weathering conditions REE are significantly mobilised and fractionated (e.g., Nesbitt 1979; Duddy 1980; Sharma & Rajamani 2000).

REE patterns have been investigated down a series of weathered profiles formed under different weathering regimes in the Cobar region of western New South Wales. The patterns vary and appear to reflect the weathering history of individual profiles, providing a means for recognising different weathering regimes and the associated processes of leaching and element dispersion. This knowledge could assist geochemical exploration in regolith dominated terrains.

GEOLOGICAL SETTING

The Cobar region is underlain by Palaeozoic rocks of the central Lachlan Orogen of eastern Australia. It contains

mainly siliclastic metasedimentary rocks (originally turbiditic shales, siltstones and quartzites), some mafic to felsic volcanic rocks and granites. The region is a major metallogenic province for base metal and gold deposits, with more than 12 mined deposits and active exploration. The bedrocks and contained mineral deposits have had a long history (>65 Ma) of sub-aerial exposure and weathering under contrasting climatic regimes. Weathering, erosion and deposition have produced an extensive regolith with both *in situ* and transported components that renders mineral exploration difficult.

WEATHERING HISTORY

The climatic and weathering history of the Cobar region has been established using a combination of palynological records, palaeomagnetic dating of ferruginous weathering zones, $^{40}\text{Ar}/^{39}\text{Ar}$ dating of manganese oxides, $\delta^{18}\text{O}$ characteristics of weathering clays and relative dating techniques (Fig. 1). In broad terms, climatic conditions were warm and humid from the Late Cretaceous to the Early Miocene with some cooler periods. The climate then became predominately cooler, drier and more seasonal through

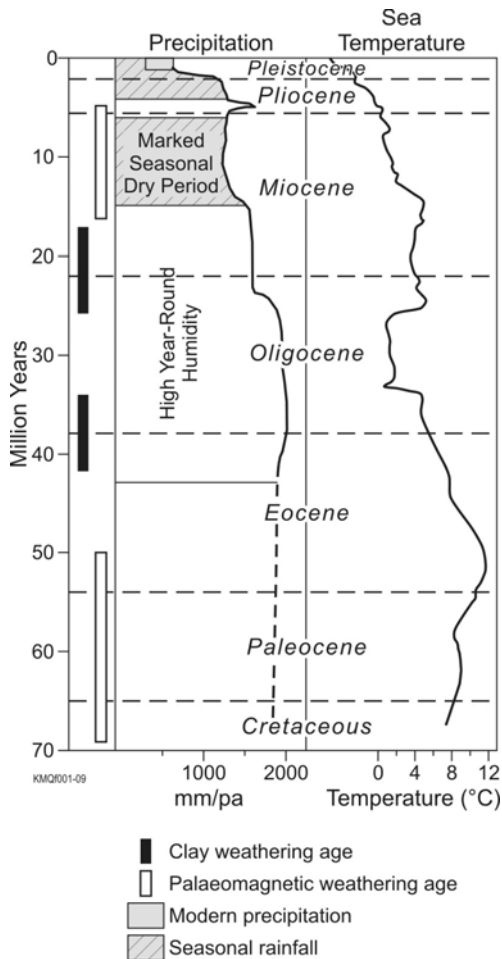


Fig. 1. Climate chart for SE Australia for the Cenozoic with dated weathering features from the Cobar region. Estimated precipitation from palynological records (Martin 1991), ocean water temperature (Zachos *et al.* 2001), hematite fixation and clay weathering ages (McQueen *et al.* 2002, 2007; Smith 2006).

the later Cenozoic, but with a significant short warmer and wetter period in the Late Miocene. Palaeomagnetic dating indicates periods of intense oxidation and possible drying of profiles after prolonged weathering in the Late Cretaceous to Paleocene (ca. 60±10 Ma) and the Early Miocene (15±5 Ma).

METHODS

Most of the samples for this study were collected by air-core drilling through the regolith. Samples were 1 kg splits taken with a sample spear from larger bulk

samples representing 1 m intervals. One exposed weathered profile preserved beneath a Miocene leucitite lava flow was sampled in outcrop. Sub-samples from the homogenised and pulverised samples were analysed by fusion disc X-ray fluorescence (XRF) for major elements. REE and other trace elements were analysed by inductively coupled plasma mass spectrometry (ICP MS) following multi-acid digestion of the fusion discs.

RARE EARTH ELEMENT PATTERNS

Four weathered profiles in different landscape settings and of different ages were examined. All profiles were developed on siliclastic metasedimentary rocks (siltstone-sandstone).

The oldest profile (CBAC 215) was preserved beneath Paleocene lake sediments. The least weathered saprock in this profile (59 m beneath the unconformity) has a REE pattern very similar to North American shale composite (NASC). The light REE show marked relative depletion in the upper part of the profile and enrichment near the weathering front. Cerium shows marked enrichment at depth (Fig. 2).

The second profile is Early Miocene in age and preserved beneath a leucitite lava flow dated at 17.1±0.2 Ma. The ferruginised upper part of the profile has been palaeomagnetically dated at 15±5Ma (McQueen *et al.* 2007). This profile also shows light REE depletion in the upper part, but not as marked as in the older profile (Fig. 3). There is also slight, relative enrichment in the heavy REE in the upper part of the profile.

A third profile (BRAC 1) was examined beneath Late Miocene alluvial sands and ferruginous gravels. This profile is considered to be mid Cenozoic in age and has been partly eroded. The upper part of this profile below the unconformity has a similar REE pattern to NASC. Deeper in the profile there is relative enrichment in all the REE, but slightly more marked in the light REE (Fig. 4).

The fourth weathering profile is in an area of post Miocene erosion, which has exposed areas of saprock. This profile

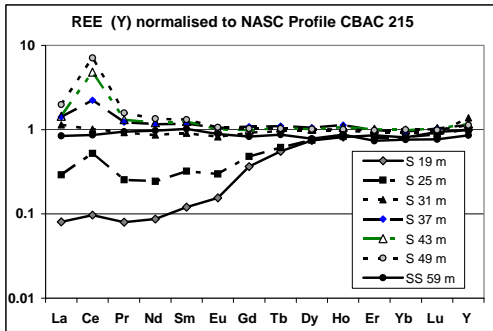


Fig. 2. REE pattern in a Late Cretaceous to Paleocene weathering profile preserved beneath Paleocene lake sediments. S is saprolite, SS is saprock.

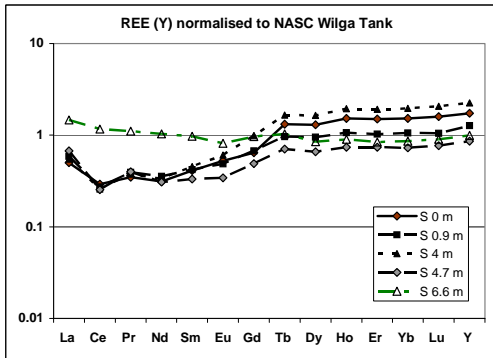


Fig. 3. REE pattern in Miocene profile preserved beneath leucitite lava flow at Wilga Tank. S is saprolite.

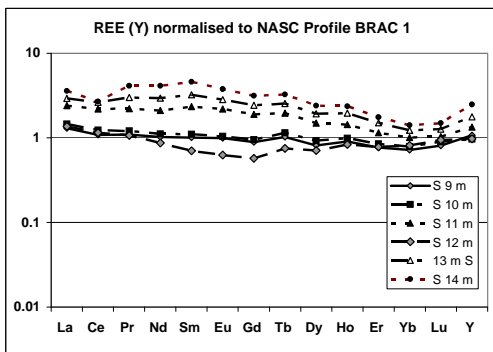


Fig. 4. REE pattern in a partly eroded mid Cenozoic weathering profile beneath Late Miocene alluvial sediments. S is saprolite.

was sampled above the current water table and weathering front. It shows a REE pattern for all samples very similar to NASC, with no significant depletion or enrichment (Fig. 5).

DISCUSSION

The various differences in the REE patterns reflect both the regolith-landform setting and the timing of profile formation within the long history of weathering that has occurred under contrasting climatic regimes. The main control on REE patterns is the varying stability of accessory REE host minerals (particularly apatite, monazite, titanate and zircon) under the different weathering regimes. Oxidation of Ce^{3+} to Ce^{4+} and precipitation of CeO_2 is a likely mechanism for Ce concentration deeper in profiles at redox boundaries. Interestingly, Ce has also been concentrated in carbonates within saprolite surrounding the New Cobar sulfide deposit. This deposit was exposed and weathered through the Cenozoic. Residual concentration and mechanical transfer of residual resistate minerals during profile compaction and collapse have probably also affected REE abundances, particularly the overall enrichment in profile BRAC 1.

The different REE patterns provide a technique for identifying weathered profiles formed under particular climatic and weathering regimes at different stages of the Cobar weathering history. This would be very useful at sites where there are no other age constraints. REE fractionation also provides a means of recognising *in situ* regolith that has been subjected to intense and prolonged chemical weathering and element leaching. Identifying strongly leached regolith has important implications for sampling and anomaly detection during geochemical exploration.

CONCLUSIONS

REE patterns in weathered siliclastic metasedimentary rocks in the Cobar region vary depending on the stage and conditions of weathering.

- (1) Older profiles formed under warm and humid climates show depletion of LREE in the upper saprolite and enrichment (particularly for Ce) towards the base
- (2) Post Miocene profiles show little fractionation, but in some cases have been residually enriched in all the REE.
- (3) REE can be significantly mobilised

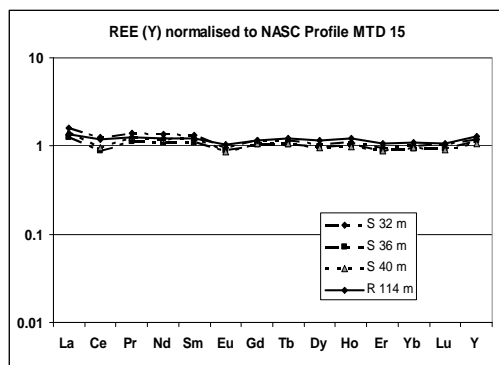


Fig. 5. REE pattern in a post Miocene weathering profile. S is saprock/saprock, R fresh rock.

during intense and prolonged weathering depending on the stability of their host minerals.

ACKNOWLEDGEMENTS

The work reported here was supported by the Australian Government Cooperative Research Centre Program within CRC LEME. The regolith drilling was carried out by the NSW Department of Primary Industries and by Cobar Management Pty Ltd. Sample analyses were performed at Geoscience Australia with the assistance of Bill Papas. I thank my many colleagues in CRC LEME for their help in sampling.

REFERENCES

DUDDY, I.R. 1980. Redistribution and fractionation of rare-earth and other

elements in a weathering profile. *Chemical Geology*, **30**, 363-381.

MARTIN, H.A. 1991. Tertiary stratigraphic palynology and palaeoclimate of the inland river systems in New South Wales. In: WILLIAMS, M.A.I., DE DEKKER, P., & HERSHAW, A.P. (eds.), *The Cainozoic in Australia: A reappraisal of the evidence*. Geological Society of Australia Special Publication, **18**, 181-194.

MCQUEEN, K.G., GONZALEZ, O.R., ROACH, I.C., PILLAND, B.J., DUNLAP, W.J., & SMITH M.L. 2007. Landscape and regolith features related to Miocene leucite lava flows, El Capitan northeast of Cobar, NSW, Australia. *Australian Journal of Earth Sciences*, **54**, 1-17.

MCQUEEN, K.G., PILLANS, B.J., & SMITH, M.L. 2002. Constraining the weathering history of the Coare region, western NSW. In: PREISS, V.P. (ed.), *Geoscience 2002: Expanding Horizons, Abstracts of the 16th Australian Geological Convention, Adelaide, 1-5 July 2002*, **67**, 246.

NESBIT, H.W. 1979. Mobility and fractionation of rare earth elements during weathering of a granodiorite. *Nature*, **279**, 206-210.

SHARMA, A. & RAJAMANI, V. 2000. Major element, REE and other trace element behaviour in amphibolite weathering under semiarid conditions in southern India. *The Journal of Geology*, **108**, 487-496.

SMITH, M.L. 2006. *Towards a geochronology for long-term landscape evolution of northwestern New South Wales, Australia*. Ph.D thesis, Australian National University.

ZACHOS, J. PAGANI, M., SLOAN, L., THOMAS, E. & BILLUPS, K. 2001. Trends, rhythms, and aberrations in global climate 65 Ma to present. *Science*, **292**, 686-693.

Lithogeochemical vectors to ore: a study of the Elura Zn-Pb-Ag deposit, Cobar, NSW, Australia

K.G. McQueen¹ & M.A.I. Whitbread²

*1Faculty of Applied Science, University of Canberra, ACT, 2601 AUSTRALIA
(e-mail: Ken.McQueen@canberra.edu.au)*

2Io Geochemistry, PO Box 433, Sumner Park BC, QLD, 4074 AUSTRALIA

ABSTRACT: Hydrothermal alteration around the Elura Zn-Pb-Ag sulfide deposit has produced detectable and systematic chemical changes that are also reflected in subtle mineralogical features. Iron carbonate development accompanied by potassic alteration, the destruction of albite and absence of chlorite are the dominant mineral alteration effects in the surrounding host rocks. Key elements enriched in the primary dispersion zone are Zn, Pb, Ag, As, Rb, Tl, and particularly Sb. Sodium is strongly depleted. Cryptic alteration and primary dispersion can be detected up to 300 m from the ore body below the weathering front. Pearce Element Ratio (PER) and General Element Ratio (GER) techniques more clearly identify and quantify this alteration and could assist in vectoring towards high intensity alteration adjacent to ore during exploration drilling.

KEYWORDS: *lithogeochemistry, exploration, hydrothermal, alteration, drilling*

INTRODUCTION

Mineral exploration for blind ore systems is increasingly dependant on better methods of vectoring to mineralisation during drilling. Lithogeochemical features in and around ore deposits, particularly recognition of cryptic alteration and primary dispersion zoning, can indicate relative proximity to ore and provide tools to navigate within the ore system. This study of the Elura Zn-Pb-Ag deposit has defined the key lithogeochemical features developed around a sediment-hosted, structurally controlled, hydrothermal ore system. The approach used for detecting cryptic alteration could be applied in exploration for similar deposits.

NATURE OF THE ELURA DEPOSIT

The Elura deposit (45 Mt @ 8.5% Zn, 5.3% Pb, 69 ppm Ag) is located 43 km north-northwest of Cobar in western New South Wales (Lorrigan 2005). The deposit is hosted by weakly metamorphosed and deformed turbiditic sedimentary rocks of the Early Devonian Cobar Basin. It consists of a series of vertical, pipe-like sulfide concentrations composed of varying proportions of pyrrhotite, pyrite, sphalerite, galena and accessory sulfide

minerals. The sulfide-rich pods are discreet entities aligned along a NNW trend. They are connected along strike, attaining a sheet-like morphology to the north. The outer part of the ore system consists of enveloping low-grade vein and stringer mineralisation (Lawrie & Hinman 1998; Schmidt 1990). The main sub-cropping pod was discovered by its magnetic signature and near surface geochemical expression in the regolith, and by drilling. The deeper northern pods were not detected until after mining of the main pod had commenced.

METHODS

The primary dispersion halo and wallrock alteration around the Elura deposit was established from integrated petrographic, mineralogical and geochemical (major-, minor- and trace-element) analysis of diamond drill core samples. Seventy eight samples of variably altered and unaltered host rocks, as well as 67 near-surface weathered equivalents, were analysed for major elements using fusion disc, X-ray fluorescence analysis (XRF). Trace elements were determined by pressed powder XRF analysis. Carbonate carbon

and absorbed and structural H₂O were determined by LECO analysis.

A key aspect of the study was the separate investigation of the silt-sand and clay dominant components of the turbiditic host rocks. The Pearce Element Ratio (PER) technique was used to avoid closure effects in the compositional data for variably altered rocks around the ore system, and to assess element changes (Pearce 1968; Stanley & Medeisky 1995). As a second step in the data analysis the General Element Ratio (GER) technique was applied to test the likely mineral assemblages in unaltered, altered and weathered rocks and to explore changes in these assemblages caused by alteration and subsequent weathering.

RESULTS

Preliminary analysis of the geochemical data indicated that Ti and Nb, significantly concentrated in fine-grained rutile-anatase, were the most conserved elements during hydrothermal alteration and weathering. Due to its greater abundance and lower relative analytical error, Ti was selected as the conserved denominator element in the PER analysis. Changes in PER values for major- and trace-elements with distance from ore are listed in Table 1.

Key indicators of alteration and proximity to ore are: increased K₂O (particularly in the shale component); near complete loss of Na₂O; increased FeO (particularly in the siltstone-sandstone component); and increased CO₂ in shale. These changes reflect the development of iron carbonate (siderite and ankerite) by carbonate introduction and some alteration of existing calcic carbonate in siltstone-sandstone samples. Destruction of albite, absence of chlorite and increased abundance of muscovite due to potassic alteration, are the other major mineral alteration effects in the altered host rocks. Trace elements enriched in the primary dispersion zone are Zn, Pb, Ag, Sb, As, Rb, and Tl. Antimony provides the most consistent and extensive trace element dispersion halo around the deposit and is also preserved in most of

Table 1. Summary of PER changes in altered host rocks with distance from the Elura orebody. Sst = siltstone-sandstone component.

<i>Element/ oxide</i>	<i>PER variations (E/TiO₂) with distance from orebody.</i>
Ag	Increased up to 80 m.
As	Increased but poor resolution.
Ba	Increased but poor resolution.
Pb	Spot highs, unreliable.
Rb	Increased up to 120 m in shale 80 m in sst.
Sb	Increased up to 200 m.
Tl	Increased up to 40 m in shale.
Zn	Spot highs unreliable.
CaO	No systematic difference.
CO ₂	Increased in shale.
FeO	Increased up to 100 m in sst.
K ₂ O	Increased up to 130 m in shale 70 m in sst.
MgO	Loss in shale, gain in sst
Na ₂ O	Near complete loss >250 m.

the weathered alteration zone rocks. Figures 1-3 illustrate key element variation patterns within the cryptic alteration zone around the Elura deposit.

GER analysis incorporating element combinations designed to reflect the main minerals of the unaltered, altered and weathered rocks reveals clear separation of these different compositions and explains the mineralogical changes during alteration (Fig. 4). Unaltered shale compositions cluster toward the muscovite/ankerite node of the muscovite/ankerite-chlorite/albite/calcite assemblage, whereas unaltered siltstone-sandstone samples cluster towards the chlorite/albite/calcite node. The altered equivalents plot closer to the muscovite/ankerite node and most of the altered shale lies beyond this node, consistent with the presence of significant non-calcic carbonate (e.g., siderite). This provides a method for clearly defining the altered rocks around the Elura deposit. The compositions of weathered rocks from both unaltered and altered precursors define a clear trend towards the goethite/hematite/kaolinite node. This trend is explained by the initial weathering breakdown of calcite-albite and most

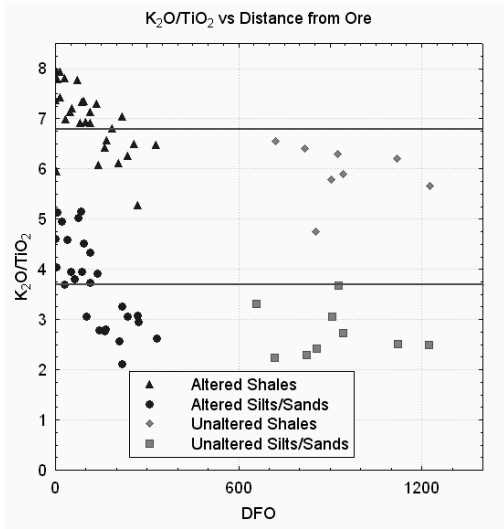


Fig. 1. Variation in K_2O/TiO_2 with distance (m) from the Elura ore deposit.

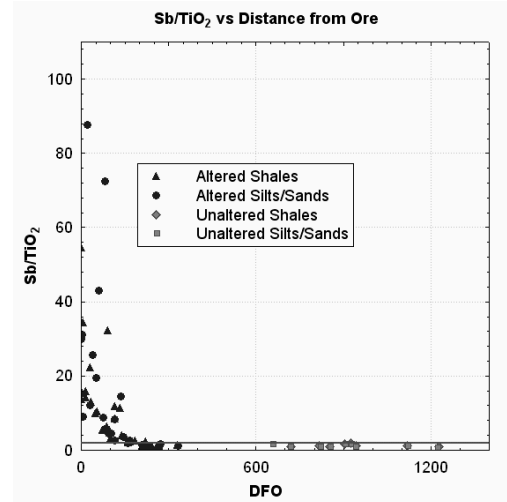


Fig. 3. Variation in Sb/TiO_2 with distance from ore (DFO) in metres at the Elura ore deposit.

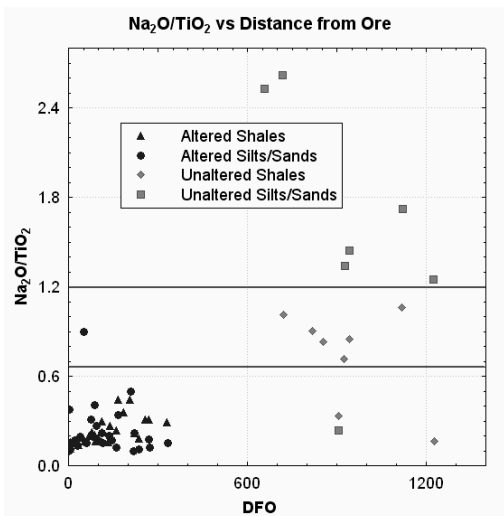


Fig. 2. Variation in Na_2O/TiO_2 with distance (m) from the Elura ore deposit.

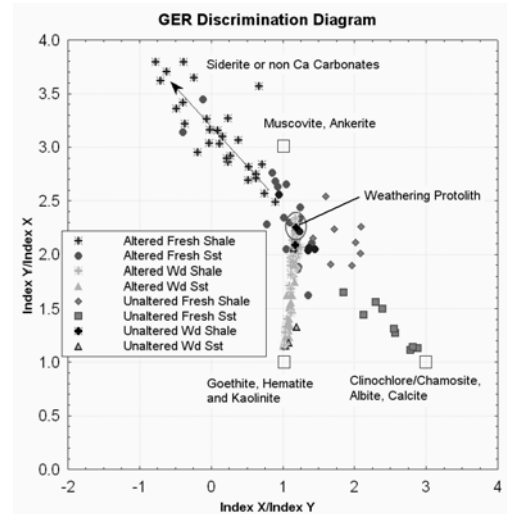


Fig. 4. GER discrimination diagram for unaltered, altered and weathered rocks around the Elura ore deposit. Also shown are the nodal positions of major minerals in the various rocks and their weathered equivalents.

chlorite to produce an assemblage dominated by relict muscovite and some kaolinite-goethite and then a progressive increase in goethite-hematite-kaolinite with further chemical weathering. Unfortunately any distinction between altered and unaltered precursor rocks is largely lost during the weathering.

DISCUSSION

Hydrothermal alteration associated with the formation of the Elura deposit has produced visible mineralogical changes in

a narrow zone around the deposit. These include an inner irregular zone of silicification with some sericitization and a surrounding zone 5-70 m wide of carbonate spotting.

Lithogeochemical analysis can detect the cryptic alteration that extends around the visible alteration zone out to 300 m from the orebody. The key major element features are: increased K_2O content; increased FeO in carbonates; increased

CO₂, most obvious in shale; and depletion of Na. Many ore-related elements show primary dispersion (up to 300 m in the case of Zn), but their distribution is patchy or inconsistent. Antimony provides the most consistent primary dispersion pattern for the trace elements.

Pearce Element Ratios provide a clearer indication of the chemical alteration effects and the true change in intensity with proximity to ore. The technique can be applied in both visibly and cryptically altered rocks with a very high degree of success in classifying alteration in unweathered rocks. General Element Ratios (GERs) are also useful in separating unaltered, altered and weathered rock compositions and in understanding the mineralogical controls involved.

This study has shown that there are important differences in the alteration effects observed in the fine and coarse fractions of the host turbidite units. It is critical to examine and analyse these end members separately as many of the key lithogeochemical features of the alteration would be obscured in bulk samples.

The very prolonged weathering of the Cobar terrain under a wide range of climatic conditions has destroyed most of the key lithogeochemical features in the resulting regolith. However, indications are variably provided by molar K/Al ratios and preserved relative enrichment in some trace elements (Sb, Tl, Ag, and patchy Pb).

CONCLUSIONS

Hydrothermal alteration related to formation of the Elura deposit can be detected in the host rocks up to 300 m from ore using lithogeochemical techniques. The effects can be reliably quantified within 250 m of the ore.

Proximity to ore is best indicated by PER values of:

- (1) Molar K vs Al in shale;
- (2) Molar K vs (Al-Na) in sandstone-siltstone;
- (3) Molar Ca vs carbonate C in shale; and
- (4) Sb in both rock types.

ACKNOWLEDGEMENTS

We thank the management and staff of Pasminco Exploration for initiating and assisting with research on the Elura deposit. The work was conducted as part of a CRC LEME PhD project. MW acknowledges the support of a CRC LEME scholarship. Sample analyses were performed by INAX Services, Australian National University.

REFERENCES

- LAWRIE, K.C. & HINMAN, M.C. 1998. Cobar-style polymetallic Au-Cu-Ag-Pb-Zn deposits. *AGSO Journal of Australian Geology and Geophysics*, **17**, 169-187.
- LORRIGAN, A.N. 2005. Elura Zn-Pb-Ag deposit, Cobar district, NSW. In: BUTT, C.R.M., ROBERTSON, I.D.M., SCOTT, K.M., & CORNELIUS, M. (eds), *Regolith Expression of Australian Ore Systems*. CRC LEME, Perth, 143-145.
- PEARCE, T.H. 1968. A contribution to the theory of variation diagrams. *Contributions to Mineralogy and Petrology*, **19**, 142-157.
- SCHMIDT, B.L. 1990. Elura zinc-lead-silver deposit, Cobar. In: HUGHES, F.E. (ed.), *Geology of the Mineral Deposits of Australia and Papua New Guinea*. The Australasian Institute of Mining and Metallurgy, Melbourne, **2**, 1329-1326.
- STANLEY, C.R. & MADEISKY, H.E. 1995. Pearce element ratio analysis in lithogeochemical exploration. *17th International Geochemical Exploration Symposium, Association of Exploration Geochemists, Annual Meeting, Short Course*, Townsville, Queensland, Australia, May, 96 p.

Lithogeochemistry of the Quebrada Blanca Porphyry Cu Deposit, Atacama Desert, Northern Chile

Tamara Moss & Cliff Stanley

Dept. of Earth & Environmental Science, Acadia University, Wolfville, Nova Scotia, CANADA B4P 2R6
(e-mail: 091163m@acadiau.ca)

ABSTRACT: Despite intense weathering, the geology of the supergene and leached cap zones at the Quebrada Blanca (QB) porphyry Cu deposit, northern Chile, can be understood using major oxide lithogeochemical data. Five supergene and four hypogene drill cores from a NS cross-section across the QB open pit were logged, and samples from the hypogene zone were examined mineralogically and petrographically. Pre-existing major oxide lithogeochemical data, mostly from drill cores through the supergene zone (n = 7540), and new petrological and lithogeochemical data (n = 178) from deep drill cores through the hypogene zone, were evaluated. Lithologies at QB include Carboniferous diorite intruded by Late Eocene equigranular granodiorite, and then by quartz-feldspar porphyry dykes associated with mineralization. In general, weak to moderate potassic alteration in these three lithologic units is locally overprinted by strong phyllic alteration. Weathering processes significantly affect the supergene rocks, but do not impede recognition of lithology or hydrothermal alteration style and intensity in the supergene and leached cap zones.

KEYWORDS: *Quebrada Blanca, Collahuasi district, porphyry Cu deposit, lithogeochemistry, molar element ratio, supergene weathering, Chile.*

INTRODUCTION

The Quebrada Blanca (QB) porphyry Cu deposit (21°24' S, 68°55' W) is located 1,500 km north of Santiago in the Tocopilla Province, Chile (Region 1). Located at 4,300 m elevation in the Atacama Desert, QB is less than 10 km west of the Rosario and Ujina porphyry Cu deposits, which together with QB make up the Collahuasi porphyry Cu district. QB is also located east of the West Fissure within the Domeyko fault system, a major crustal structure controlling the location of large economic porphyry Cu deposits, including the Chuquibambilla porphyry Cu deposit located ~150 km south of QB.

To date, only the supergene enrichment zone at QB has been mined. Unfortunately, intense weathering has impeded a thorough understanding of the geology of this zone. This research attempts to advance knowledge of the geology at QB by investigating: (a) the igneous rocks that host mineralization, (b) the nature of hydrothermal alteration that has affected these rocks, (c) how host rock compositions control the resulting

alteration mineral assemblages, and (d) how weathering processes have affected hypogene rocks.

METHODS

Two lithogeochemical datasets were investigated to advance understanding of the lithologies, mineralization, and hydrothermal alteration at QB. The first dataset consists of 7540 samples from historic NQ core and RC chips mostly from the supergene enrichment and leached cap zones (the 'supergene dataset'). These were analyzed for major oxides and some trace elements by XRF at several laboratories in Chile. The second dataset was smaller (n = 178), but consists only of recent NQ drill core samples from the hypogene zone (the 'hypogene dataset'). These were analyzed for major oxide and a more extensive suite of trace elements by fusion or aqua regia/ICP-OES or ICP-MS at Acme Analytical Laboratories, Canada.

Geological control for data interpretation was provided by detailed logging of nine drill cores through the QB supergene

(DDH098, 023, 112, 115, 125) and hypogene (DDH313, 275, 259, 270) zones. The drill cores are from the 19,600 m E cross-section through the open pit. Samples from the hypogene cores were collected and examined via thin section petrography, Na-cobaltinitrate staining, electron microprobe analysis, scanning electron microscopy, and x-ray diffraction analysis. Results provide constraints to interpret the characteristics of both supergene and hypogene lithogeochemical datasets.

Molar element ratio (MER) analysis was carried out on both lithogeochemical datasets because of its ability to avoid closure and isolate the impacts of different geochemical processes using projective geometry. Because weathering did not affect the hypogene dataset, the unweathered samples provided the geological control necessary to interpret results from the supergene dataset.

PETROLOGY

Three intrusions occur in the QB open pit and drill core. These consist of: (i) Carboniferous diorite that was intruded by (ii) Late Eocene granodiorite, and (iii) later quartz-feldspar porphyry dykes of granodiorite composition.

Diorite is medium grey, equigranular and composed of plagioclase (cgr, anh, 50 - 80 %) and biotite (fgr, anh, 20 - 50 %), probably after clinopyroxene. Equigranular granodiorite (formerly known as quartz monzonite) is light to medium grey and composed of quartz (fgr to cgr, anh, 20 - 75 %), plagioclase (fgr to mgr, anh, 10 - 60 %), biotite (fgr to cgr, in clusters, 5 - 25 %), and chlorite after biotite (vfgr to cgr, in clusters, 2 - 10). Quartz-feldspar porphyry (QFP; formerly known as feldspar porphyry or plagioclase porphyry) is white to dark grey and composed of plagioclase (mgr to cgr, euh, porphyritic, 30 - 60 %), quartz (fgr to mgr, porphyritic, partially resorbed 'eyes' & some square section cristobalite, 2 - 40 %), biotite (vfgr to cgr, porphyritic, subh, 3 - 15%), chlorite (cgr, partially replacing biotite, 5 %) in a very fine grained groundmass of biotite and subordinate quartz (Fig. 1).

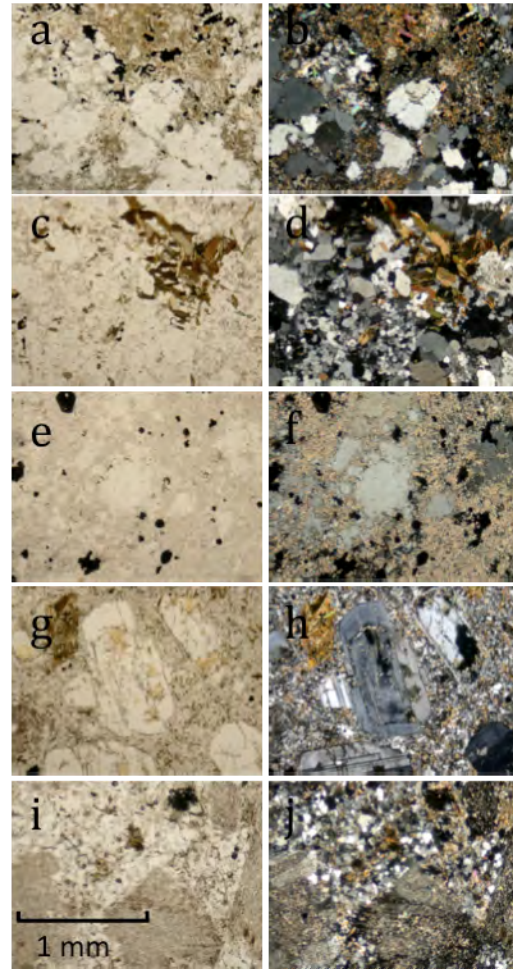


Fig. 1. Phyllically altered diorite in (a) PPL and (b) XPL; fresh granodiorite in (c) PPL and (d) XPL; phyllically altered granodiorite in (e) PPL and (f) XPL; fresh QFP in (g) PPL and (h) XPL; phyllically altered QFP in (i) PPL and (j) XPL. All samples are from hypogene drill cores and are un-weathered.

LITHOGEOCHEMICAL ANALYSIS

Hypogene Dataset

A conserved element scatterplot of the hypogene lithogeochemical dataset (Fig. 2) illustrates that Zr/TiO₂ ratios can be used to identify QB intrusive rocks.

Furthermore, a Pearce element ratio (PER) scatterplot testing feldspar compositional control (Fig. 3) illustrates that some hypogene rocks have compositions controlled by feldspar (primary igneous or potassic alteration),

whereas others are controlled by muscovite (phyllic alteration). Lastly, diorite samples have lower Al/Ti ratios than granodiorite samples, which in turn have lower Al/Ti ratios than QFP samples.

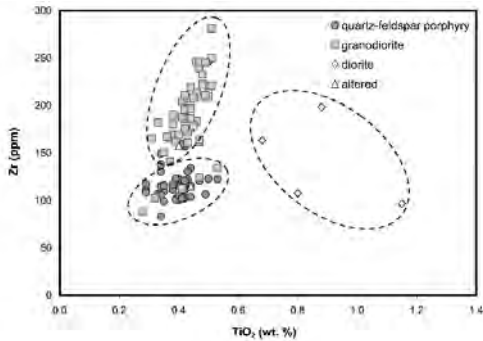


Fig. 2. A conserved element scatterplot of TiO₂ vs. Zr can be used to classify the hypogene data.

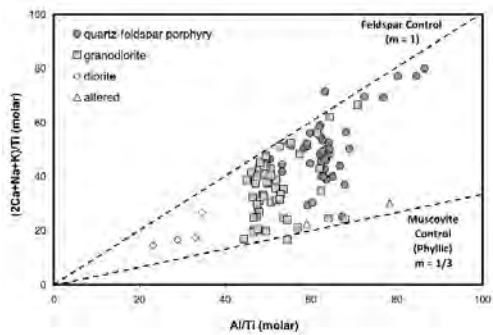


Fig. 3. PER scatterplot of hypogene data testing feldspar (fresh igneous or potassic alteration) and muscovite (phyllic alteration) compositional controls.

A MER scatterplot (Fig. 4) illustrates that most of the intensely phyllically altered samples within the hypogene dataset are granodiorite. Additionally, Figure 5 illustrates that hypogene samples can be compositionally described as mixtures of muscovite (phyllic alteration) and albite, andesine, or oligoclase (fresh igneous plagioclase). Many QFP samples are fresh or have only minor propylitic alteration. Less altered samples contain An₁₀ (in the granodiorite) or An₁₀ to An₃₅ (in the QFP). Figure 6 illustrates that the hypogene dataset does not contain strongly potassically-altered samples.

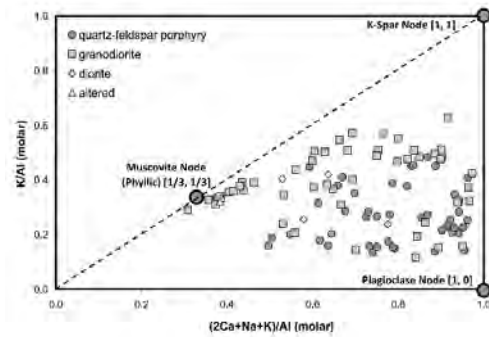


Fig. 4. MER scatterplot of hypogene data identifying which samples have muscovite (phyllic alteration) compositional control.

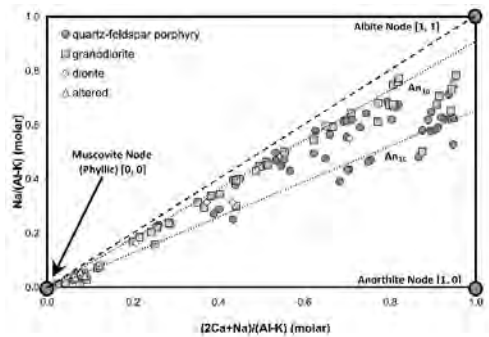


Fig. 5. MER scatterplot of hypogene data capable of determining plagioclase compositions in un-altered rocks using the trends away from muscovite.

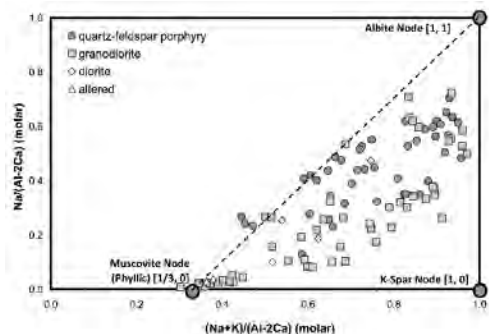


Fig. 6. MER scatterplot of hypogene data capable of detecting and quantifying the intensity of potassic alteration.

Supergene Dataset

The above investigation of QB hypogene litho-geochemistry provides insight into the overlying supergene enrichment zone. In the following plots, supergene data has been expressed using shaded point densities because the large number of samples causes significant overlap. Most

of the same MER diagrams used to investigate the hypogene dataset have been plotted below using the supergene dataset.

A scatterplot of TiO₂ vs. Zr (Fig. 7) illustrates that three distinct modes are present in the supergene dataset (granodiorite, QFP, and diorite).

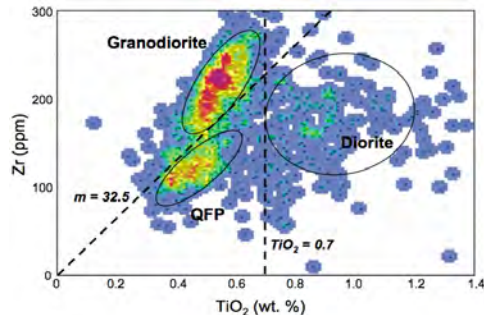


Fig. 7. Conserved element scatterplot of supergene data identical to Figure 2.

The PER diagram of Figure 8 illustrates that intense phyllic alteration affected most supergene rocks. The Al/Ti ratios in this supergene dataset also discriminate between diorite, granodiorite and QFP, just like the hypogene dataset.

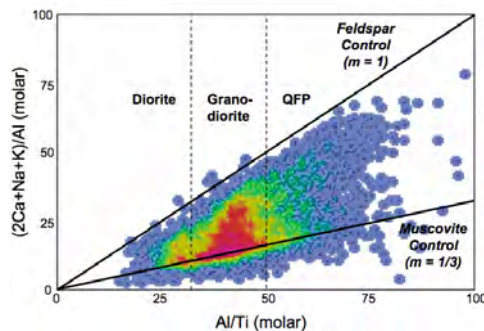


Fig. 8. PER scatterplot of supergene data identical to Figure 3.

MER scatterplot diagrams of the supergene dataset (Figs. 9 & 10) illustrate that most samples are phyllically altered. Similar to the hypogene dataset, supergene samples contain An₁₀ to An₃₅ plagioclase compositions, and do not contain samples that are strongly potassically altered.

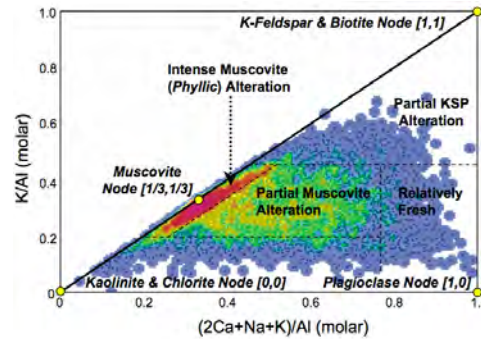


Fig. 9. MER of supergene data identical to Figure 4.

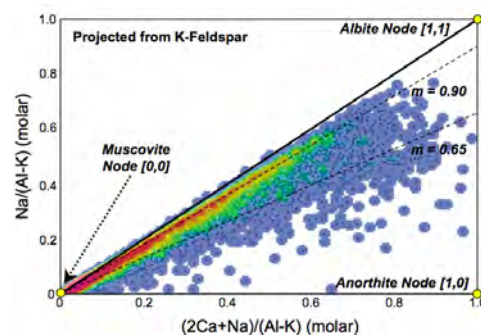


Fig. 10. MER scatterplot of supergene data identical to Figure 5.

CONCLUSIONS

Diorite, granodiorite, and QFP can be discriminated using TiO₂ concentrations and Zr/TiO₂ mass and Al/Ti molar ratios. Granodiorite with An₁₀ plagioclase was intruded by QFP with up to An₃₅ plagioclase. Granodiorite is intensely phyllically altered whereas QFP is commonly less altered. Potassic alteration is not well expressed in this lithochemical dataset.

Supergene lithochemical results are similar to hypogene results. Thus, supergene lithochemistry can be used to understand the lithologies and hydrothermal alteration of intensely weathered rocks.

ACKNOWLEDGEMENTS

This research was supported by Compañia Minera Quebrada Blanca S.A. and a National Science & Engineering Research Council Discovery Grant # 220302-217290 to C.R. Stanley.

Classification of Igneous Rocks Using Lithogeochemistry Data, Essential Rock Mineralogy, and Projective Geometry in a Streckeisen Ternary Diagram Approach

Cliff Stanley

Dept. of Earth & Environmental Science, Acadia University, Wolfville, Nova Scotia, B4P 2R6
(e-mail: cliff.stanley@acadiau.ca)

ABSTRACT: A rigorous yet adaptable method for the classification of igneous rocks uses numerical manipulation of major oxide lithogeochemical data instead of modal petrographic estimates. Essential mineralogy constraints and projective geometry are employed in a classification procedure that involves: (i) conversion of weight percent oxide concentrations to molar element quantities through division by gram formula weights, (ii) calculation of independent geochemical parameters describing the amount of each mineral used in classification, (iii) conversion of these quantities to volume modes through multiplication by the appropriate molar volumes, and finally (iv) standardization to a sum of unity to allow plotting on Streckeisen ternary diagrams and subsequent classification. These procedures can be employed to classify igneous rocks using any ternary diagram and the presence of minerals not used in classification does not impact the results. Such lithogeochemical classifications exhibit excellent correspondence with petrologically defined classifications, but are more representative, accurate and precise than conventional results, because, provided that adequate sample preparation methods and modern analytical procedures are used, they avoid human visual estimation errors and sample mass representativity problems introduced by thin section or slab point count or image analysis procedures.

KEYWORDS: *igneous rocks, petrographic classification, lithogeochemistry, projective geometry, Streckeisen ternary diagrams.*

INTRODUCTION

Plutonic rock classification by petrologic means is a simple procedure involving the use of Streckeisen ternary diagrams. Unfortunately, classification suffers from modal estimation errors involving visual estimates, or representativity issues from point counts or image analysis procedures applied to thin sections or slabs of insufficient size.

In contrast, volcanic rock classification by petrologic means is generally difficult because complete crystallization is not achieved, making it impossible to use the modal rock petrography as a classification criterion. As a result, classification of volcanic rocks has historically relied on lithogeochemistry, and the most successful approaches have employed conserved, trace element concentration ratios. These have been used as proxies for petrology to empirically classify volcanic rocks. Unfortunately, these trace elements are imperfect proxies for rock

petrology, and represent only a small proportion of the rock mass, allowing their concentrations to be modified by even subtle geological processes. Thus, igneous rock classification can pose substantial challenges to the geoscientist.

Below, a numerical method for igneous rock classification is described that uses representative, accurate and precise lithogeochemical major oxide data to obtain independent geochemical parameters that describe the volume proportions of the three minerals defining any Streckeisen ternary diagram. This approach is analogous to classical Streckeisen petrological classification procedures, and thus can be compared with petrologic-based classification results to determine how similar the two methods are. Furthermore, because this approach uses major oxide concentrations and is constrained by the essential petrology of the rocks, it can be used to classify

volcanic rocks, and may provide better results than conserved trace elements.

METHOD

Lithochemical concentrations can be used to classify igneous rocks by first converting the wt. % concentration data into un-standardized molar element quantities through division of the gram formula weight of the oxide or element. For di-cationic oxides (e.g., Al_2O_3 , K_2O), dividing by one half the gram formula weight converts the oxide mass concentration into the appropriate molar (cation) element quantity.

Then, the compositions of the essential (> 5 volume %) minerals in the rocks to be classified are defined in a 'composition matrix' (C) and used, in conjunction with a second matrix (T) defining what minerals are employed in classification (the 'classifying minerals'; e.g., quartz, plagioclase, alkali feldspar), to obtain a third matrix (W) containing a set of independent vectors containing major element coefficients. When multiplied by the un-standardized molar element quantities, they produce un-standardized molar classifying mineral quantities that are un-affected by the presence of non-classifying minerals in the rocks.

These quantities are then multiplied by their associated molar volumes to convert them into volume classifying mineral quantities. After standardization to a unit sum, these become volume proportions than can be plotted on Streckeisen ternary diagrams for classification.

EXAMPLE CALCULATION

If one considers a granitoid rock containing essential amounts of quartz (QZ), plagioclase (AN, AB), alkali feldspar (KS) and biotite (BT) that requires classification, an appropriate composition matrix (C), where $FM = Fe+Mg$, is:

	Si	Al	FM	Ca	Na	K	OH
QZ	1	0	0	0	0	0	0
AN	2	2	0	1	0	0	0
AB	3	1	0	0	1	0	0
KS	3	1	0	0	0	1	0
BT	3	1	3	0	0	1	2

Classification of such a rock would employ the quartz (QZ)-plagioclase (PL)-alkali feldspar (AF) Streckeisen ternary diagram, and so geochemical parameters describing the proportions of quartz, plagioclase and alkali feldspar can be obtained using the T matrix:

	V_{QZ}	V_{PL}	V_{AF}	V_{BT}
QZ	1	0	0	0
AN	0	1	0	0
AB	0	1	0	0
KS	0	0	1	0
BT	0	0	0	1

Attaching these matrices side by side ($D = [C \ T]$) and then employing a Gauss-Jordan elimination procedure converts this (5 × 11) matrix into a new matrix consisting of a (5 × 5) identity sub-matrix on the left and a (5 × 6) sub-matrix of coefficients on the right. After discarding the identity matrix, the coefficient sub-matrix is further sub-divided into two sub-matrices. A (2 × 2) negative identity matrix is then appended to the bottom of the (5 × 2) left coefficient sub-sub-matrix and a (2 × 4) zero matrix is appended to the (5 × 4) right coefficient sub-sub-matrix, yielding a (7 × 6) solution matrix (W):

	O_N	O_M	V_{QZ}	V_{PL}	V_{AF}	V_{BT}
Si	0	0	1	0	0	0
Al	1	0	-3	0	1	0
FM	0	2/3	0	0	-1/3	1/3
Ca	-2	0	4	1	-2	0
Na	-1	0	0	1	-1	0
K	-1	0	0	0	0	0
OH	0	-1	0	0	0	0

The last four columns of this matrix contain coefficients that can be used to determine the volume proportions of quartz, plagioclase, alkali feldspar and biotite in the rock to be classified using its major element composition, as described above. The first two columns of this matrix can be added in any linear combination to any of the last four vectors to produce alternative coefficients that yield the same independent measures of the classifying mineral proportions.

For example, a granitoid rock from the Sloggett pluton, Oberon batholith, New South Wales, Australia (Glen *et al.* 2006)

plots as a grey circle on Fig. 1 using the V_{QZ} , V_{PL} , and V_{AF} vectors from the above W matrix. Because the biotite volume proportion determined from V_{BT} in W is 2 %, this granitoid rock would be classified as a leucomonzogranite.



Fig. 1. Classification of a Sloggett pluton sample by two different means on a Streckeisen 'QAP' ternary diagram using major oxide lithogeochemical concentrations (data from Glen et al. 2006).

Note that in W , zero coefficients exist for OH in vectors V_{QZ} , V_{PL} , V_{AF} , and V_{BT} , making this classification appropriate when structural water (H_2O^+) is not analyzed. However, if this rock was affected by a material transfer process that modified its composition, say cut by calcite veins too small to be physically removed during sampling, classification could be negatively impacted. Fortunately, alternative classifications (e.g., matrix W') can be obtained by adding linear combinations of the V_N and V_M vectors to V_{QZ} , V_{PL} , and V_{AF} , in this case to produce new vectors with zero Ca coefficients. These vectors are unaffected by the presence of the calcite veins, and thus will provide an accurate classification. The alternative classification using these vectors plots as a grey diamond on Fig. 1. This plots very close to the first classification, and also indicates that this rock is a leucomonzogranite.

PETROLOGIC VALIDATION

Plutonic rocks from the Emerald Lake pluton, Yukon, comprise four phases: (i) augite syenite, (ii) hornblende quartz

	$V_{QZ} + 2V_N$	$V_{PL} + 1/2V_N$	$V_{AF} - V_N$	V_{BT}
Si	1	0	0	0
Al	-1	1/2	0	0
FM	0	0	-1/3	1/3
Ca	0	0	0	0
Na	-2	1/2	0	0
K	-2	0	1	0
OH	0	0	0	0

syenite, (iii) hornblende quartz monzonite, and (iv) biotite granite (classified based on field observations; Smit 1984). Contacts between these units are generally intrusive, except for the contact between phases (ii) and (iii), which is transitional because they are likely related via fractional crystallization.

Image analysis of stained slabs (Duncan 1999) indicates these rocks should probably be referred to as: (i) augite syenite, (ii & iii) hornblende quartz syenite, and (iv) biotite syenogranite (from mean petrographic classification; Fig. 2).

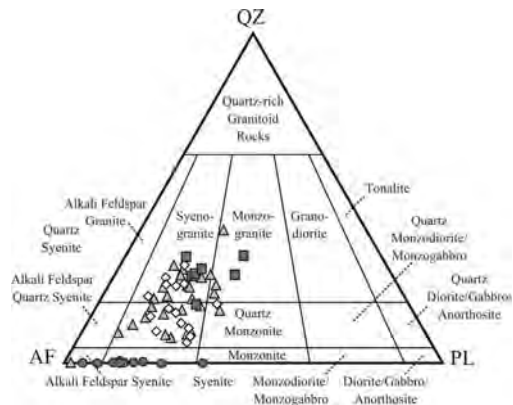


Fig. 2. Classification Emerald Lake pluton samples on a Streckeisen 'QAP' ternary diagram using stained slab image analysis results (data from Duncan 1999).

Unfortunately, these rock textures are relatively coarse compared to the size of the slabs used in classification (Duncan 1999). Thus, representativity is low, likely explaining why these image analysis results exhibit high scatter in Fig. 2.

Lithogeochemical classification of these same rocks was undertaken to provide an alternative classification. This was done using three different essential mineral suites (with different C and T matrices) because: (a) the augite syenite contains

alkali feldspar, plagioclase, and augite, (b) the hornblende quartz syenite and hornblende quartz monzonite contain alkali feldspar, plagioclase, quartz and hornblende, and (c) the biotite granite contains quartz, plagioclase, alkali feldspar, and biotite (note that the classification calculations undertaken for this last phase are identical to the Sloggett pluton example, above). Results are plotted on a Streckeisen diagram (Fig. 3).



Fig. 3. Classification of Emerald Lake pluton samples on a Streckeisen 'QAP' ternary diagram using major oxide lithogeochemical concentrations (data from Duncan 1999).

These lithogeochemical classification results are similar to the petrographic classifications of Fig. 2. Nevertheless, they do suggest that the four units should actually be referred to as: (i) augite quartz syenite, (ii & iii) hornblende syenogranite, and (iv) biotite monzogranite. Furthermore, these lithogeochemical classification results exhibit much less scatter than the petrographic data, principally because the samples used to obtain the lithogeochemical concentrations used in the calculations have a much larger volume than the stained slabs used in image analysis.

CONCLUSIONS

Classification of igneous rocks can be undertaken using: (i) major oxide lithogeochemical concentrations, (ii) knowledge of the essential mineralogy of the rock, (iii) matrix algebra procedures and (iv) Streckeisen ternary classification diagrams. Results are generally consistent

with petrographic classifications, but are likely more accurate, precise and representative. This is because lithogeochemical classification is based on quantitative data with high accuracy and precision derived from samples that typically have larger mass than the stained slabs or thin sections used in point counting or image analysis. The flexibility of the approach allows accurate classification of igneous rocks that are not entirely fresh, and can be used for volcanic rocks if the essential mineral assemblage can be identified/postulated.

ACKNOWLEDGEMENTS

This research was supported by NSERC Discovery Grant # 220302-217290 to the author.

REFERENCES

- DUNCAN, R.A. 1999. *Physical and Chemical Zonation in the Emerald Lake Pluton, Yukon Territory*. M.Sc. thesis, Inv. of B.C., Vancouver.
- GLEN, R.A., DAWSON, M.W., COLQUHOUN, G.P. 2006. Eastern Lachlan Orogen Geoscience Database (on DVD-ROM) Version 2, NSW Department of Primary Industries – Minerals, Geol. Surv. of NSW, Maitland, NSW, Australia.
- SMIT, H. 1984. *Petrology, chemistry, age, and isotope study of the high potassium Emerald Lake pluton, eastern Yukon Territory*. B.Sc. thesis, Univ. of B.C., Vancouver.
- STRECKEISEN, A., ZANETTIN, B.A., LE BAS, M.J., BONIN, B., BATEMAN, P., BELLINI, G., DUDEK, A., EFREMOVA, S., KELLER, J., LAMEYRE, J., SABINE, P.A., SCHMID, R., SORENSEN, H., WOOLLEY, A.R. 2002. *Igneous rocks; a classification and glossary of terms; recommendations of the International union of Geological Science Subcommittee on the Systematics of Igneous Rocks*. Cambridge University Press, Cambridge, U.K., 800 p.

Distal exhalative manganese enriched stratigraphy to carbonate-hosted zinc deposits, Adirondack Lowlands, New York State, U.S.A.

Alex Tolson¹ & Norm Duke²

¹Exploration Geologist Consultant, 56-C Medhurst Dr., Ottawa, ON, K2G 4V2 CANADA
(e-mail: alextolson@hotmail.com)

²Economic Geology Professor, University of Western Ontario, Rm 118-A Biology & Geology Bldg. University of Western Ontario, London, ON, N6A 5B7 CANADA

ABSTRACT: The Arnold Pit is an industrial talc/tremolite deposit near Gouverneur, New York. The mine is located in the Balmat-Edwards Mining District in the Adirondack Lowlands of the Grenville Province. The Balmat-Edwards SEDEX-type zinc deposits, hosted within a metamorphosed evaporitic carbonate sequence, are located within a few kilometres of the Arnold Pit. This pit exposes a manganese-rich unit overlying stromatolitic marble and calc-silicate gneisses and is capped by talc-dominated schists. Electron microprobe analysis together with bulk rock major- and trace-element geochemistry confirms manganese enrichment in oxide, carbonate, and silicate phases; up to 13% Mn, 5.9% Fe, 192 ppm Zn, and 13700 ppm Ba are preserved in the metamorphic assemblage. Spessartine garnets, tirodite, tephroite, and kutnohorite are intergrown with Mg-rich staurolites, trace pyrolusite is intergrown with sphalerite. The depositional setting is a distal exhalative environment to the zinc ore and such Mn-enrichments may be utilized for targeting stratiform base-metal mineralization even in high-grade metamorphic terranes.

KEYWORDS: *Manganese, SEDEX, Balmat-Edwards, Distal exhalative, Adirondack Lowlands*

INTRODUCTION

The Arnold Talc Mine, near the town of Gouverneur, New York, is located in the Balmat-Edwards Mining District within the Frontenac-Adirondack Terrane of the Grenville Province. The district hosts SEDEX-type zinc deposits, and these occur within a few km of the Arnold pit. A significant manganese-rich unit is exposed in the pit and its relationship to the ore has not been determined. Twenty-five samples were collected from the Arnold Pit in September of 2005 to study the stratigraphic position and geochemistry of the Mn-subunit in detail. Qualitative microprobe analyses determined manganese in several silicate, carbonate and oxide phases. Bulk rock major- and trace-element geochemistry of six samples provide quantitative evidence for the enrichment of an elemental suite consistent with being distal products of an exhalative hydrothermal system.

REGIONAL GEOLOGICAL SETTING

The Mesoproterozoic Grenville Province

extends from Labrador to Texas (Rivers 2005). The province has been subdivided into terranes, based on lithology, structure, and metamorphic ages (Easton 2005). The main divisions within the Ontario/New York segment are: the Central Gneiss Belt to the northwest, the Central Metasedimentary Belt, and the Central Granulite Terrane to the southeast. The Balmat-Edwards district is located within the Frontenac-Adirondack Terrane, specifically within the Adirondack Lowlands of the Central Metasedimentary Belt (DeLorraine & Carl 1993). The Adirondack Lowlands is a supracrustal gneissic terrane noted for its extensive marble that hosts the stratiform zinc deposits (Chiarenzelli *et al.* 1993). The Lowlands stratigraphy includes pelitic schists, metavolcanic gneisses and two major marble units (Whelan *et al.* 1990). It underwent upper amphibolite to granulite facies metamorphism during the 1190-1140 Ma Shawinigan Orogeny (Rivers 2005). Metamorphic conditions in the Lowlands reached peak pressure and

temperatures of >6 Kbars and 625°C (Charenzelli *et al.* 1993).

The Balmat-Edwards District is underlain by four main stratigraphic divisions (DeLorraine & Carl 1993). The basal Hyde School Gneiss is composed of leucogneisses with thin concordant amphibolite layers. This is overlain by the Lower Marble Formation which is dominated by graphite-phlogopite-calcite marble containing disseminated tourmaline. The Popple Hill Gneiss, in tectonic contact above the Lower Marble, is a variably migmatitic gneiss of dacitic composition. The Upper Marble capping the regional stratigraphy hosts the zinc mineralization and has an inferred age between 1150 to 1300 Ma (Whelan *et al.* 1990). The Upper Marble is further subdivided into 16 distinct stratigraphic units of relatively pure and variably dolomitic limestone interbedded with calc-silicate units after impure marlstone (DeLorraine & Carl 1993). The interbedded dolomitic and calc-silicate marble members indicate shallow basin margin environments. Original evaporative conditions are clearly indicated by the presence of thick (up to 15 m) gypsum/anhydrite in Unit 13. Extensive dolomitization is common in evaporative basins (Warren 1990). Sulfur and oxygen isotope studies on the gypsum support evaporative deposition from seawater and protracted hydrothermal activity related to the nearby base-metal mineralization may be involved in sulfate reduction (Whelan *et al.* 1990).

LOCAL STRATIGRAPHY EXPOSED IN THE ARNOLD PIT

The Arnold Pit is on the steeply dipping, overturned limb of the Sylvia Lake Syncline, the structural hanging wall is the stratigraphic footwall. Commercial talc occurs in Unit 13 near the contact with Unit 14 of the Upper Marble from the metamorphism or impure evaporative dolomite. The upper section of Unit 13 grades from tremolite-rich talc ore into a pure talc schist up section. Unit 12 is a white massive dolomitic marble with convolute bands of grey and orange to

purple calc-silicate marble. A metre thick lens of stromatolitic marble, occurring just below the base of Unit 13, suggests a shallow subtidal to supratidal sabkha environment (Whelan *et al.* 1990). This is stratigraphically overlain by banded quartz diopside gneiss. The manganiferous subunit of this study directly overlies the pyritic quartz diopside gneiss and has a calc-silicate hanging wall rich in talc and tremolite, i.e., the Mn-rich member underlies Unit 14, the host of the Balmat-Edwards zinc deposits. It has an apparent thickness of about 2 to 3 m in width and is concordant with the local stratigraphy. Both upper and lower contacts are sharp and distinct. It is very dense and black to dark brown in colour. Internal compositional banding is visible in outcrop. The subunit contains carbonate, as well as brownish to yellowish bands of coarse grained manganese-bearing silicates. Petrographic study of samples from the Mn unit identified several Mn-bearing phases including spessartine garnets, tirodite, tephroite, and kutnohorite. Pyrolusite was found intergrown with sphalerite. The mineralogy is a direct reflection of the amphibolite facies overprint of an original Mn-rich sediment.

GEOCHEMICAL RESULTS

Six samples were analyzed by C. Wu at the University of Western Ontario for major and trace-element bulk rock litho geochemistry using X-Ray Fluorescence (XRF) and Induced Coupled Plasma Atomic Emission Spectrometry (ICP-AES). The results of the analyses are shown in Tables 1 and 2, respectively.

Significant Zn, Pb, Ba, and Sr is detected in sample 07A from the base of the manganese subunit. Sample 07B, collected higher in stratigraphy than 07A, is dominantly comprised of kutnohorite and Mn-bearing amphiboles, and this has the highest amount of manganese (13.03 %) determined. Sample 07B also has anomalous base metals as well as the greatest Ba enrichment of all the analyzed samples at 13700 ppm. The 1140 ppm value for sulfur reflects barite content.

Table 1. Major Element Oxides (in wt %) (recalculated to 100%).

Sample	SiO ₂	TiO ₂	Al ₂ O ₃	Fe ₂ O ₃	MnO	MgO	CaO	K ₂ O	Na ₂ O	P ₂ O ₅	L.O.I.	Total
04	76.77	0.10	1.64	0.85	0.66	10.61	5.46	0.10	0.88	0.03	2.32	99.43
07A	54.39	0.05	0.73	1.97	9.10	21.56	6.67	0.02	0.49	0.05	4.31	99.33
07B	43.73	0.02	0.84	1.33	13.03	20.46	5.79	0.04	0.16	0.09	12.47	97.97
08A	42.81	1.28	10.50	5.90	0.42	22.42	5.91	0.93	0.63	0.89	7.56	99.24
10A-S	52.03	0.60	6.59	4.28	11.78	16.88	2.79	0.06	0.68	0.06	3.49	99.26
10A-G	46.33	0.22	2.24	2.73	12.66	19.96	5.06	0.01	0.33	0.06	9.56	99.16

Table 2. Trace Element Analyses (in ppm).

Sample	Nb	Zr	Y	Sr	Rb	Ba	Mo	Pb	Zn	Cu	Ni	Co	Cr	V
04	98	181	28	590	< 50	728	128	357	< 25	< 30	< 25	< 25	< 25	82
07A	62	120	22	135	< 50	200	102	247	153	< 30	< 25	< 25	< 25	141
07B	55	152	21	119	< 50	13700	900	243	72	< 30	< 25	< 25	< 25	57
08A	91	199	128	835	110	207	975	258	192	36	309	105	146	467
10A-S	68	169	22	131	< 50	936	104	283	29	< 30	25	63	< 25	575
10A-G	60	158	42	436	< 50	175	884	221	131	38	26	53	< 25	78

Sample 10A was divided into Mg-staurolite dominated “S” and a garnet dominated “G”. Sample 10A-S has ~6 % Al₂O₃ and significant SiO₂ (~52%), Fe (~4.3%), MgO (16.88%), MnO (11.78%), and lesser CaO (2.79%), consistent with the staurolite-amphibole-dominated assemblage. This sample contains low Zn (29 ppm), although trace disseminated sphalerite was identified. It has 283 ppm lead and significant (970 ppm) Ba enrichment. Sample 10A-G has significant SiO₂, MgO, MnO (~12 %), and CaO. The garnet-rich nature of the sample 10A-G accounts for its Y enrichment, containing double the amount detected in the other samples. The trace-element analysis shows minor enrichments in Zn (131 ppm) consistent with observed sphalerite, as well as elevated Pb (221 ppm), Ba (175 ppm), and Cu (38 ppm) values. Sample 04 is from the quartz diopside gneiss adjacent to the Mn unit and sample 08A from an ultramafic boudin from the pit.

DISCUSSION

Irish-type SEDEX deposits are carbonate-hosted stratiform to stratabound sulfide deposits that occur as syngenetic exhalative to early diagenetic replacement bodies (Coleman *et al.* 1989). Many SEDEX deposits have formed in Proterozoic intracontinental rifts and Phanerozoic deposits occur in similar

environments (Lydon 1996). Evaporite dissolution provides Cl⁻ ions to complex with base metals to promote hydrothermal solubility (Warren 1990). The presence of evaporite minerals or their pseudomorphs, as well as stromatolites, indicate the stratiform zinc deposits of the Balmat-Edwards District occur in a hydrothermally active evaporite setting (Warren 1990; Goodfellow 2004). Manganese is not associated with typical evaporite mineral assemblages especially in the significant concentration observed. However, in hydrothermal systems there is well documented geochemical zonation from proximal to distal facies relative to the original hydrothermal feeder zone (Lydon 1996). There is a shift from reduced Cu-, Pb- and Zn-rich sulfide facies to Ba-, Fe- and Mn-rich oxide facies away from the zone of hydrothermal discharge (Lydon 1996). Ba and Mn are typically distal elements. Distal hydrothermal products are characterized by deposition of chert, barite with minor sphalerite and pyrite and notable manganese enrichment (Lydon 1996).

Most SEDEX deposits are not precipitated directly adjacent to their feeder zone (Sangster 2002) therefore the geochemical zonation of distal products provides a valuable exploration tool. Manganese halos have been well documented for the Tynagh mine in

Ireland (Russell 1983), as well as the HYC and Lady Loretta deposits in Australia (Large & McGoldrick 1998; Large *et al.* 2000). Manganese associated with these hydrothermal systems is found in carbonates and oxides, as well as in spessartine garnets in metamorphosed terranes (Lydon 1996). Manganese halos have survived the effects of amphibolite to granulite facies metamorphism in the Proterozoic Zn-Pb deposits of South Africa such as the Gamsberg mine (Stalder & Rozendaal 2005). The manganese enrichment has been found several kilometres from known deposits (Lydon 1996).

The Mn-subunit exposed in the Arnold pit contains up to 13% Mn and 13700 ppm Ba with associated elements consistent with distal hydrothermal products. Microprobe analysis determined barite to be present as inclusions within and on the margins of pyrolusite, demonstrating Mn and Ba deposition from the same fluid. Such anomalous enrichments are atypical of basinal settings other than those receiving input from hydrothermal discharge.

CONCLUSIONS

The Balmat-Edwards District in the Adirondack Lowlands contains several carbonate-hosted stratiform base-metals deposits hosted within a metamorphosed evaporite sequence. The nearby Gouverneur Talc Mine's Arnold Pit exposes stratigraphy distal to the zinc mines. Manganese is concentrated in a well defined stratigraphic subunit of calc-silicate gneiss in Unit 13 underlying Units 14, host to the zinc ores. The upper amphibolite facies metamorphic overprint caused the units to undergo prograde recrystallization, while retaining primary chemical composition at the micro-scale. The manganese partitioned into various carbonate, silicate, and oxide phases. Enrichment in Ba, Fe, and Zn is typical of distal facies of well documented SEDEX hydrothermal systems. There is therefore a direct genetic relationship between the chemical anomaly in the Arnold Pit and the base-metals deposits. The

manganese is related to hydrothermal mineralizing brine that carried the mobile elements to a distal redox boundary where they were precipitated as exhalative sediments. When targeting SEDEX mineralization, one must consider such distal geochemical signatures. This is especially true in high-grade metamorphosed terranes where original stratigraphy has become obscure. Enrichment of manganese is of particular interest for regional target generation and as a vector for more detailed follow-up exploration. The stratigraphy, petrography, and geochemistry of the manganiferous unit at the Arnold Pit strongly support a link to direct hydrothermal input. The geochemical anomaly of Mn, Zn, Pb, and Ba is a clear demonstration that such distal exhalative products are preserved even under high-grade metamorphic conditions.

ACKNOWLEDGEMENTS

We thank Mr. John Kreider of the Gouverneur Talc Company for graciously granting access to the mine to collect samples during production.

REFERENCES

- CHIARENZELLI, J.R. *et al.* 1993. Proterozoic rocks east and southeast of the Grenville front. In: RANKIN, D.W. (ed.), *Precambrian: Conterminous U.S.* The Geological Society of America.
- COLEMAN, T.B., JONES, D.G., PLANT, J.A., & SMITH, K. 1993. In: PLANT, J.A. & JONES, D.G. (eds.), *Metallogenic models and exploration criteria for buried carbonate-hosted ore deposits – a multidisciplinary study in eastern England.* The Institution of Mining and Metallurgy, British Geological Survey.
- DELORRAINE, W.F. & CARL, J.D. 1993. Precambrian Geology of the northwest Adirondack Lowlands: a Stratigraphic Viewpoint. In: BURSNALL, J.T. (ed.), *New York Geological Association Field Trip Guidebook*, 1-51.
- EASTON, M. 2005. The Grenville Province in Ontario, what you need to know for effective mapping and exploration. In: *Geology and Mineral Deposits of the Grenville Province.* University of Western Ontario, Society of Economic Geologists Student Chapter, Short Course Manual.

- GOODFELLOW, W.D. 2004. *Sediment-hosted Lead-Zinc Sulphide Deposits*. Narosa Publishing, 367p.
- LARGE, R.R. & MCGOLDRICK, P.J. 1998. Lithochemical halos and geochemical vectors to stratiform sediment hosted Zn-Pb-Ag deposits; Part 1. Lady Loretta Deposit, Queensland. *Journal of Geochemical Exploration*, **63**, 37-56.
- LARGE, R.R., BULL, S.W., & MCGOLDRICK, P.J. 2000. Lithochemical halos and geochemical vectors to stratiform sediment hosted Zn-Pb-Ag deposits; Part 2. HYC deposit, McArthur River, Northern Territory. *Journal of Geochemical Exploration*, **68**, 105-126.
- LYDON, J.W. 1996. Sedimentary exhalative sulphides (Sedex). In: ECKSTRAND, O.R., SINCLAIR, W.D., & THORPE, R.I. (eds.), *Geology of Canadian Mineral Deposit Types*. Geological Survey of Canada, Geology of Canada, **8**, 130-152.
- RIVERS, T. 2005. Architecture and tectonic evolution of the Grenville Province: Part of a long-lived hot wide orogen on the southeastern margin of Laurentia. In: *Geology and Mineral Deposits of the Grenville Province*. University of Western Ontario, Society of Economic Geologists Student Chapter, Short Course Manual.
- RUSSELL, M.J. 1983. Major Sediment-Hosted Exhalative Zinc + Lead Deposits: Formation From Hydrothermal Convection Cells That Deepen During Crustal Extension. In: SANGSTER, D.F. (ed.), *MAC Short Course in Sediment-hosted stratiform lead-inc deposits*.
- SANGSTER, D.F. 2002. The role of dense brines in the formation of vent-distal sedimentary-exhalative (SEDEX) lead-zinc deposits: field and laboratory evidence. *Mineralium Deposita*, **37**, 149-157.
- STALDER, M. & ROZENDAAL, A. 2005. Distribution and geochemical characteristics of barite and barium-rich rocks associated with the Broken Hill-type Gamsberg Zn-Pb deposit, Namaqua Province, South Africa. *South African Journal of Geology*, **108**, 35-50.
- WARREN, J.K. 1989. *Evaporite Sedimentology*. Prentice Hall.
- WHELAN, J.F., RYE, R.O., DELORRAINE W., & OHMOTO, H. 1990. Isotopic Geochemistry of a Mid-Proterozoic Evaporite Basin: Balmat, New York. *American Journal of Science*, **290**, 396-424

Lithogeochemical analysis through the deformed volcanosedimentary sequence hosting the Boomerang massive sulfide deposits, Tulks Belt, Central Newfoundland

Ryan M. S. Toole¹ & David R. Lentz¹

*1University of New Brunswick, Department of Geology, P.O. Box 4400, Fredericton, NB, E3B 5A3 CANADA
(e-mail: ryan.toole@unb.ca)*

ABSTRACT: A detailed study of 8 drill cores through the Cambrian to middle Ordovician rocks hosting the 1.3 Mt Boomerang massive sulfide deposit in the Tulks Volcanic Belt, Central Newfoundland, attempts to unravel the complicated stratigraphy and enhance belt-scale correlations. Rock types include Greenschist facies felsic, intermediate, and mafic volcanoclastic rocks (ash, lapilli-tuff, agglomerate), mafic to intermediate dykes and sills, and sedimentary rocks (greywacke, siltstone, graphitic shale, and carbonaceous phyllite). Using immobile elements, the hanging wall (HW) volcanoclastic rocks are divided into four units (HW1, HW2, HW3, HW4), whereas footwall (FW) volcanoclastic rocks are divided into five units (FW1, FW2, FW3, FW4, FW5). Compositionally these units span a range from basalt (HW2, HW3, FW3, FW4, FW5), to basaltic andesite (HW4, FW2), to andesite (FW1), to rhyodacite (HW1), shown by immobile element ratios (TiO_2/Zr and Al_2O_3/TiO_2). Four populations of fine grained dykes (D1, D2, D3, D4) have been compositionally identified (two basalts (D1, D2), andesite (D3), and rhyolitic dacite (D4)), based on discrimination diagrams, TiO_2 and $Na_2O + K_2O$.

KEYWORDS: *Chemostratigraphy, Volcanoclastics, VMS, Newfoundland, Discrimination plots*

INTRODUCTION

The Boomerang Zn-Pb-Cu-Ag-Au massive sulfide deposit, which was discovered by Messina Minerals in 2004, is located in the Tulks Volcanic Belt (TVB) of the Victoria Lake Supergroup approximately 20km southwest of Red Indian Lake (Fig. 1). Grading 7.09% Zn, 3.00% Pb, 0.51% Cu, with 110.43 g/t Ag and 1.66 g/t Au, Boomerang has an estimated reserve tonnage of 1.36 Mt with another 278 100 tonnes inferred grading 6.72% Zn, 2.88% Pb, 0.44% Cu, with 96.53 g/t Ag, & 29 g/t Au (Messina Minerals press release, June 21st, 2007).

During the summer of 2006, 200 petrographic and lithogeochemical samples were collected from the rocks that host the Boomerang massive sulfide deposit. In order to characterize the different rock types sampled ICP-AES and XRF analysis of these samples was completed by ALS Chemex (Sudbury Ontario), and Memorial University of Newfoundland, respectively.

GEOLOGICAL SETTING

Regional Geology

The Victoria Lake Supergroup (Evans & Kean 2002) is divided into northern and southern terranes, separated by the Rogerson Lake Conglomerate. The northern terrane consists of the Tally Pond Belt, the Diversion Lake Group, the Long Lake Belt, the Harbour Round Belt, the Harpoon Brook Belt and the TVB whereas the southern terrane contains the Point of the Woods Belt (Fig. 1; Evans & Kean 2002). The northern terrane is bounded by the Red Indian Line to the north and the Rogerson Lake Conglomerate to the south and consists predominantly of a volcano-sedimentary rocks. The southern terrane is bounded by the Rogerson Lake Conglomerate to the north and the Noel Paul's Line to the south and consists of a volcano-sedimentary sequence intruded by Siluro-Devonian biotite granite (Evans & Kean 2002).

Geology of the Tulks Volcanic Belt

The TVB extends for 65 km from Victoria

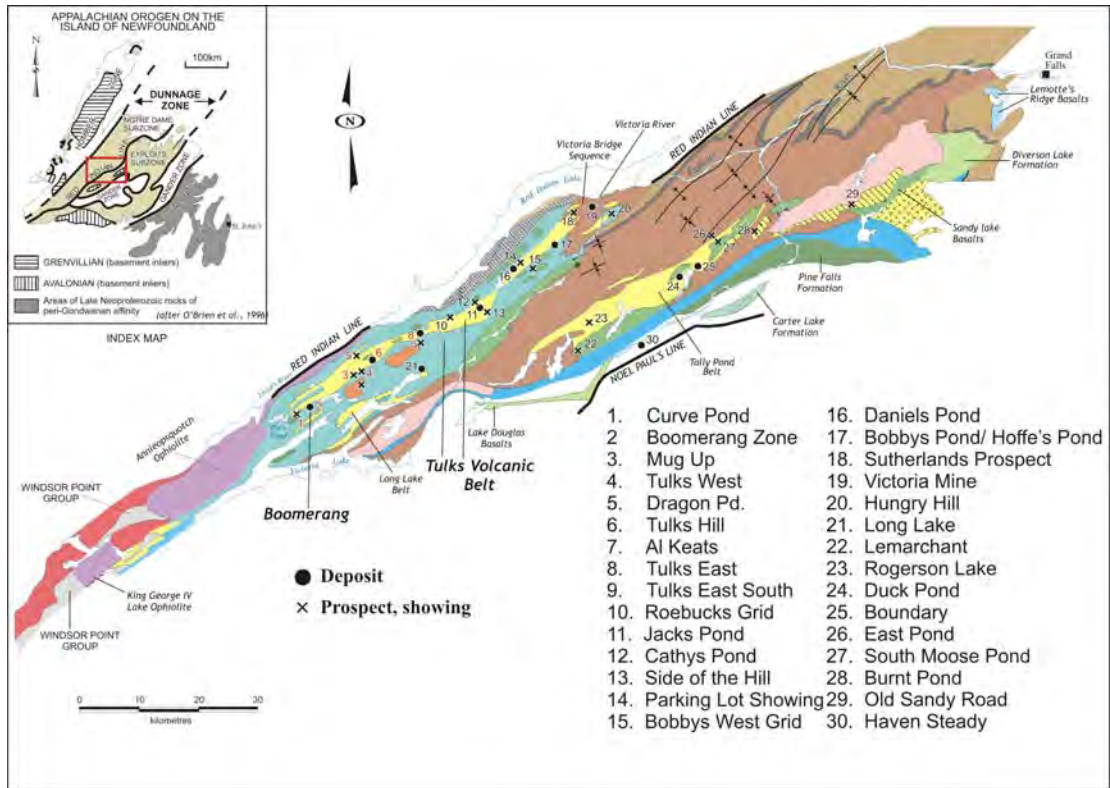


Fig 1. Regional geology map of the Victoria Lake Supergroup showing the Tulks Volcanic Belt occurring from the south west to the north central part of the map area. Also shown are the other volcanogenic massive sulfide deposits (modified from Hinchey 2007).

Lake to just south of where the Victoria River empties into Red Indian Lake (Fig. 1). Light grey-green to white, dacitic to rhyolitic quartz-feldspar-porphyrific pyroclastic flow deposits with 1 to 6 mm crystals, crystal-tuff breccia, ash tuff, flow banded rhyolite, and small subvolcanic quartz-feldspar porphyritic intrusions are included in the TVB (Evans & Kean 2002; Rogers & van Staal 2002). Mafic volcanic rocks of the TVB include tuff, lapilli tuff, volcanic breccia, and minor amygdaloidal pillow lava and breccia. Sedimentary rocks within the TVB include volcanogenic wacke, siltstone, and limestone (Evans & Kean 2002; Rogers & van Staal 2002).

There are twenty-one significant VMS deposits in the TVB with recent discoveries by Messina Minerals adding to this total (Evans & Kean 2002). These deposits include Daniels Pond, Jacks Pond, Bobbys Pond, Long Lake, Tulks East, Tulks Hill, Victoria Mine, Long Lake,

Curve Pond Zone, and Boomerang all hosted within felsic volcanic rocks and spatially associated with black, locally graphitic shale and chert. (McKenzie *et al.* 1993; Evans & Kean 2002; Rogers & van Staal 2002, Squires & Moore 2004); however, the Boomerang deposit is spatially associated with significant volumes of volcanoclastic rocks of intermediate composition.

DISCUSSION

The volcanoclastic rocks hosting the Boomerang massive sulfide show a wide range of petrographic and chemical compositions. Petrographically the HW volcanoclastic rocks show increasing fine-grained white mica (muscovite/sericite) development with proximity to the mineralized horizon. The abundance of these phyllosilicates enhances the development of more intense foliation in

the vicinity of the deposit. Relative to the HW, the FW volcanoclastic rocks are typically more fine-grained and show increased chlorite, fine white micas, and a stronger foliation.

The HW volcanoclastic rocks have been divided into four units (HW1, n=35; HW2, n=4; HW3, n=7; HW4, n=36), based on immobile elements and immobile element ratios. All hanging wall rocks have dominantly volcanic arc signatures. Based on the Nb/Y vs Zr/TiO₂ discrimination diagram by Winchester & Floyd (1977), later revised by Pearce (1996), HW 1 has a rhyodacitic composition, HW2 has a basaltic andesite composition, whereas HW3 and HW4 have basaltic compositions (Fig 2). To further distinguish between the hanging wall rocks, TiO₂/Zr was plotted against TiO₂/Y and Al₂O₃/TiO₂. A positive correlation between TiO₂/Zr and TiO₂/Y is consistent with more mafic rocks. A negative correlation between TiO₂/Zr and Al₂O₃/TiO₂ is consistent with more mafic rocks having increased TiO₂/Zr affinities and decreased Al₂O₃/TiO₂ affinities.

The footwall volcanoclastic rocks are divided into five units (FW1, n=34; FW2, n=15; FW3, n=2; FW4, n=3; FW5, n=4), based on the same parameters used for the hanging wall rocks. All of the footwall rocks have volcanic arc signatures based on the fields of Pearce *et al.* (1984). Based on the Nb/Y vs Zr/TiO₂ discrimination diagram (Winchester and Floyd 1977 and revised by Pearce 1996), FW1 shows an andesitic composition, FW2 shows a basaltic andesite composition, and FW3, FW4, and FW5 show basaltic compositions (Fig. 3). To further distinguish between the HW populations, TiO₂/Zr was plotted against TiO₂/Y and Al₂O₃/TiO₂ resulting in the same correlation trends as found in the HW volcanoclastic rocks.

The intermediate and felsic dykes associated with the host volcanoclastic rocks are believed to postdate the youngest metamorphic event in the TVB, In contrast the mafic dykes post date all but the latest folding event. The dykes have been divided into 4 populations (D1,

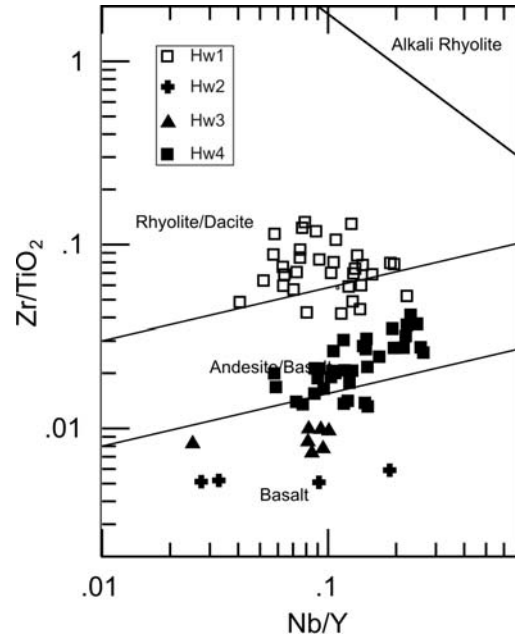


Fig. 2. Nb/Y vs Zr/TiO₂ discrimination diagram showing distribution of hanging wall tuff samples. Field boundaries are from Pearce (1996).

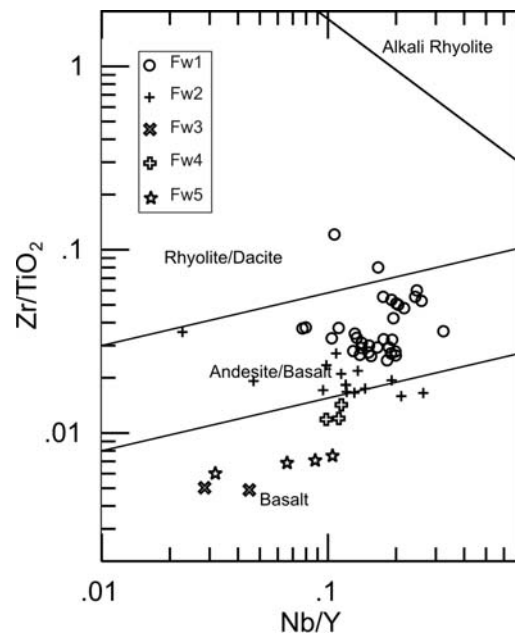


Fig. 3. Nb/Y vs Zr/TiO₂ showing the distribution of footwall tuff samples. Field boundaries are from Pearce (1996).

n=27; D2, n=4; D3, n=8; D4, n=17), based on mobile and immobile elements and their element ratios, as they are believed to have minimal alteration effects. Much like

the HW and FW volcanoclastic rocks, the dykes and sills have volcanic arc signatures. Based on the Zr/TiO₂ vs SiO₂ discrimination diagram (Winchester and Floyd's 1977), D1 and D2 have basaltic compositions, D3 is andesitic and D4 is rhyolitic dacite composition. On the SiO₂ vs Na₂O + K₂O discrimination diagram both D3 and D4 have a dominantly alkaline affinity, whereas D1 and D2 are subalkaline.

Although faulting and thrusting has complicated the distribution of rocks types one key aspect within 5 of 8 drill holes remains consistent. All HW volcanoclastic samples in direct contact with the ore horizon belong to HW4 and all FW volcanoclastic samples in direct contact with the ore horizon belong to FW1.

ACKNOWLEDGEMENTS

Thank you to Messina Minerals for allowing us to work such an interesting project and to all of their staff, specifically Gerry Squires for all his advice and input.

REFERENCES

- EVANS, D.T.W. & KEAN, B.F. 2002. The Victoria Lake Supergroup, central Newfoundland – Its definition, setting, and volcanogenic massive sulfide mineralization. Government of Newfoundland and Labrador, Department of Mines and Energy, Geological Survey Branch, *Open File NFLD/2790*, 68 p.
- HINCHEY, J.G. 2007. Volcanogenic Massive Sulfides of the Southern Tulls Volcanic Belt, Central Newfoundland: Preliminary Findings and Overview of Styles and Environments of Mineralization. In: Current Research, Newfoundland and Labrador Department of Natural Resources, Geological Survey Branch, *Report 07-1*, 117-143.
- MCKENZIE, C.B., DESNOYERS, D.W., BARBOUR, D., & GRAVES, R.M. 1993. Contrasting volcanic-hosted massive sulfide styles in the Tulls Belt, Central Newfoundland. *Exploration and Mining Geology*, **2**, 73-84.
- PEARCE, J.A. 1996. Sources and Settings of Granitic Rocks. *Episodes*, **19**, 120-125.
- PEARCE, J.A., HARRIS, NIGEL, B.W., & TINDLE, A.G. 1984. Trace element Discrimination Diagrams for the Tectonic Interpretation of Granitic Rocks. *Journal of Petrology*, **25**, 956-983.
- ROGERS, N. & VAN STAAL, C. 2002. Toward a Victoria Lake Supergroup: A provisional stratigraphic revision of the Red Indian to Victoria Lakes Area, Central Newfoundland. In: Current Research, Newfoundland Department of Mines and Energy, Geological Survey Branch, *Report 02-1*, 185-195.
- SQUIRES, G.C. & MOORE, P.J. 2004. Volcanogenic massive sulfide environments of the Tally Pond volcanics and adjacent area: geological, lithogeochemical and geochronological results. In: Current Research, Newfoundland Department of Mines and Energy, Geological Survey Branch, *Report 04-1*, 63-91.
- WINCHESTER, J.A. & FLOYD, P.A. 1977. Geochemical Discrimination of Different Magma Series and their Differentiation Products using Immobile Elements. *Chemical Geology*, **20**, 325-343.

Stratigraphic and geochemical interpretation of the Early Silurian Woodstock ferromanganese deposits, New Brunswick, Canada

Bryan C. Way¹, David R. Lentz, & David G. Keighley

¹University of New Brunswick, 2 Bailey Dr., Box 4400,
Fredericton, NB, E3B 5A3 CANADA (e-mail: bryan.way@unb.ca)

ABSTRACT: The Woodstock Fe-Mn deposits are a series of Early Silurian manganese banded iron formations (BIFs) that are hosted in the Late Ordovician to Early Silurian White Head Formation and the conformably overlying Silurian Smyrna Mills Formation. Six major lenticular-shaped Fe-Mn bodies were initially identified by gravimetric surveys (circa 1954) that followed southwest along the strike of the bedrock from Jacksontown to Green Road in western New Brunswick. These assemblages were identified within the Plymouth deposit as a series of manganese oxide and manganese carbonate-silicate-oxide units commonly in sharp contact with layers of red shale, green shale and (or) alternations of the two. Regional and local sedimentologic studies indicate these units as a transgression-regression wedge in a shallow marine basin under rapidly changing redox conditions. Litho-geochemical data from drill cores within the Plymouth deposit display strong inverse correlations between Al_2O_3 in relation to Fe_2O_3 and MnO, depletions of Eu, and high ratios of Ce/La (2.5 ± 0.2) suggesting that the source of Fe and Mn was from multiple sources (i.e., oceanic and terrestrial Fe-Mn) without direct volcanic or hydrothermal input as a source of Fe^{+2} and Mn^{+2} .

KEYWORDS: *Woodstock, Manganese, Banded Iron Formations, Plymouth Deposit.*

INTRODUCTION

The Woodstock area of western New Brunswick hosts a series of manganese banded iron formations (BIFs) that collectively constitute one of the largest manganese resources in North America (approximately 194 000 000 tonnes). This Woodstock deposits were exploited for iron from 1848 to 1884. It was during these Fe mining operations that high concentrations of Mn were first recognized. The Mn potential of the Woodstock deposits was reevaluated in the early 1900's (Sidwell 1957).

The Mn deposits are large lenticular bodies readily identified by gravimetric surveys (circa 1954). Six major ferromanganese zones were initially identified southwest along the strike from Jacksontown to Green Road, New Brunswick, with other occurrences found within similar strata in parts of eastern Maine (Sidwell 1957; Roberts & Prince 1990). Expansion of highway Route 95 from Houlton, ME to Woodstock, New Brunswick (Fig. 1) has exposed several new outcrops of the White Head and the

Smyrna Mills formations that were unmappable until recently.

The purpose of this study is to examine and document the sedimentology and stratigraphy of the newly exposed section on highway Route 95. This work together with a compilation and reinterpretation of archived mineralogical data from the Plymouth Fe-Mn deposit will be used to aid in formulating a genetic model explaining the origin of the Woodstock Fe-Mn deposits.

REGIONAL GEOLOGY

The ferromanganese-rich units associated with the Woodstock deposits are hosted within the Late Ordovician to Early Silurian White Head Formation and the conformably overlying Silurian Smyrna Mills Formation (Fig. 1). The Fe-Mn mineralization was deposited during the Taconic Orogeny by precipitation of Fe, Mn, and Si within a shallow marine transgression-regression wedge (Roberts & Prince 1990; Force & Maynard 1991). Laminations in the BIFs are attributed to seasonal fluctuations of Fe, Mn, and Si

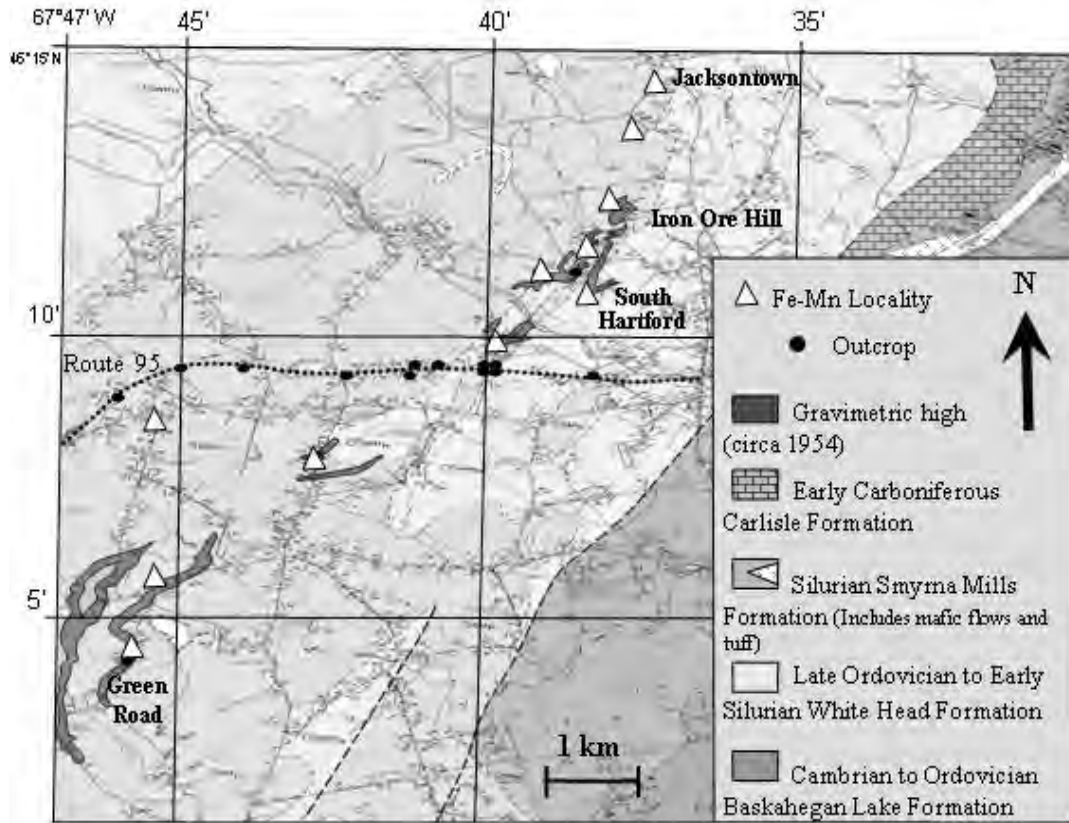


Fig. 1 Geologic map of the Woodstock area in western New Brunswick adapted from Smith and Fyffe (2006) displaying Fe-Mn deposits from Jacksontown to Green Road, NB.

within a shallow marine environment. The distribution of bedrock units is controlled by F1 and F2 folds that have northeast striking axial planes. The host sequence was metamorphosed to greenschist facies during the Acadian Orogeny (middle Devonian).

SEDIMENTOLOGY

The strata hosting the ferromanganese deposits were assigned by Roberts and Prince (1990) to the Late Ordovician–Early Silurian Cary Mills Formation and Silurian Smyrna Mills Formation in Maine and New Brunswick. However, in New Brunswick the sequence hosting the BIFs has been assigned to the Silurian Smyrna Mills Formation of the Perham Group and lies conformably on top of the Late Ordovician–Early Silurian White Head Formation associated with the Matapedia Group (Fig.1; Smith & Fyffe 2006).

The White Head Formation consists of dark grey to bluish fine-grained argillaceous limestone with interbedded calcareous shale. The Smyrna Mills Formation is composed of dark grey noncalcareous silty shale with minor layers of green and red mudstone, and associated ferromanganiferous siltstone (Smith & Fyffe 2006). The great variation in shale and/or siltstone in the Smyrna Mills Formation suggest that ocean redox conditions were highly variable during deposition of the host sequence. Manganiferous BIFs (i.e., Plymouth, Iron Ore Hill, South Hartford, Green Road) are commonly in sharp contact with units of red or green shale, or a combination of the two (Sidwell 1957). The lenticular shape and compositional variation in the Woodstock BIFs (Roberts & Prince 1990) indicates that these are stratigraphically separate Mn deposits.

The Fe-Mn zone within the Plymouth ore body was described as an assemblage of manganese oxide and manganese carbonate-silicate-oxide that formed within a shallow marine basin, an interpretation supported by the presence of asymmetrical ripple marks within the surrounding strata (Roberts & Prince 1990). Gross (1996) initially described the Plymouth Fe-Mn BIF as a series of sedimentary-volcanic ferromanganese units; however, alternative hypotheses suggest the Fe-Mn could possibly have originated from a variety of sources including oceanic Fe-Mn hydroxides and (or) the weathering of terrestrial bedrock.

GEOCHEMICAL COMPOSITION

Archived litho-geochemical data was obtained from four diamond drill holes (DDH) in the Plymouth Fe-Mn deposit. The Fe/Mn ratios from these cores were found to decrease sharply at the lower contacts between the Mn siltstone and surrounding strata. A strong inverse correlation between Al_2O_3 and $Fe_2O_3 + MnO$ occurs within the manganiferous siltstone (Fig. 2).

Rare earth elements (REEs) displayed an average value of 140 ± 23 ppm for Σ REEs within the Mn-BIFs (Roberts & Prince 1990). REE data displayed a negative Eu anomaly within the Mn-BIF and the barren host rocks DDH 87-2 suggestive of no volcanic input associated with the Mn-BIFs (Fig. 3). Positive Eu anomalies commonly occur with Fe-Mn-bearing sediments associated with igneous systems (Mishra *et al.* 2007). If low ratios of Cerium and Lanthanum (i.e., Ce/La ratios of ≤ 0.12) occur in manganiferous BIF then the Fe and Mn are likely derived from ocean water. In Mn-BIFs the Ce/La ratio increases with an increase in carbonate, biogenic, and with increasing terrigenous Fe and Mn (Jiancheng *et al.* 2006). The high Ce/La ratios (2.5 ± 0.2) returned from in DDH 87-2 of at the Plymouth deposit suggests that the Fe and Mn may not be entirely sourced from marine Fe-Mn hydroxides.

CONCLUSIONS

The presence of Silurian mafic volcanic

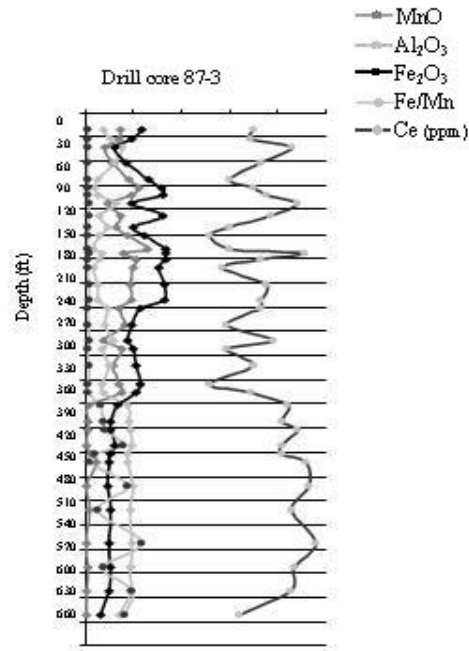


Fig. 2. Displaying the correlation between MnO, Fe_2O_3 , Al_2O_3 , Fe/Mn, and Ce contents within DDH 87-3

rocks in the Smyrna Mills Formation suggests the possibility that the Mn-BIFs might be sedimentary-volcanic in origin. However, the negative Eu anomalies associated with the host rocks suggest that there was no volcanic and (or) hydrothermal input associated with the formation of the manganiferous BIFs. High average Ce/La ratios of (2.5 ± 0.2) associated within DDH 87-2 suggests the Fe and Mn within the Woodstock are not purely from oceanic Fe-Mn hydroxides. It is probable that the Fe and Mn are derived from multiple sources contributing to the overall composition of the deposit.

ACKNOWLEDGEMENTS

Funding is from the New Brunswick Department of Natural Resources-Minerals. Thanks also to Chris Roberts (GEODAT).

REFERENCES

- FORCE, E.R. & MAYNARD, J.B. 1991. Manganese: Syngenetic Deposits on the Margins of Anoxic Basins. In: FORCE, E.R., EIDEL, J.J., & MAYNARD, J. B. (eds.), *Sedimentary and Diagenetic Mineral*

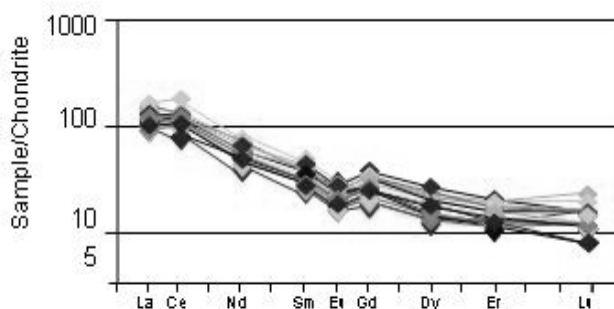


Fig. 3. Chondrite-normalized REE data from DDH-87-2 displaying depletions and anomalies of Ce. There is also a strong depletion in Eu within the drill core.

- Deposits: A Basin Analysis Approach to Exploration*, Society of Economic Geologists, *Reviews in Economic Geology*, **5**, 147-157.
- GROSS, G.A. 1996. Stratiform iron. In: ECKSTRAND, O.R., SINCLAIR, W.D., & THORPE, R.I. (eds.), *Geology of Canadian Mineral Deposit Types*. Geological Survey of Canada, **8**, 41-54.
- JIANCHENG, X., YANG, X., JIANGUO, D., & WEI, X. 2006. Geochemical Characteristics of Sedimentary Manganese Deposit of Guichi, Anhui Province, China. *Journal of Rare Earths*, **24**, 374-380.
- MISHIRA, P.P., MOHAPATRA, B.K., & SINGH, P.P. 2007. Contrasting REE Signatures on Manganese Ores of Iron Ore Group in North Orissa, India. *Journal of Rare Earths*, **25**, 749-758.
- ROBERTS, C.G. & PRINCE, J.D. 1990. Further Characterization of Plymouth Mn Deposit, New Brunswick. Department of Natural Resources and Energy Division, *Open File Report 90-4*.
- SIDWELL, K.O.J. 1957. The Woodstock, N.B., Iron – Manganese Deposits. *Transactions: Canadian Institute of Mining & Metallurgy*, **50**, 411-416.
- SMITH, E.A. & FYFFE L. R. (Compilers) 2006. Bedrock Geology of the Woodstock Area (NTS 21J/04) Carleton county, New Brunswick, New Brunswick *Department of Natural Resources, Minerals, Policy and Planning Division*, *Plate 2006-5*.

Lithogeochemistry of the Meguma Supergroup, Nova Scotia, Canada: petrographic constraints, depositional environments and alteration haloes about sediment hosted hydrothermal mineral deposits

Chris E. White¹ & Clifford R. Stanley²

¹Mineral Resources Branch, Dept. of Natural Resources, 1701 Hollis Street, Halifax, NS, B3J 3M8 CANADA
(email: whitece@gov.ns.ca)

²Dept. of Earth & Environmental Science, Acadia University, Wolfville, NS, B4P 2R6 CANADA

ABSTRACT: A lithogeochemical evaluation of Meguma Supergroup metasedimentary rocks from Nova Scotia has: (i) identified mineral suites that control the various rock compositions, (ii) provided clues about the paleo-environmental seafloor and basin conditions during sedimentation, (iii) detected previously unknown alteration zones, and (iv) established element concentration backgrounds. Variations in the amounts of quartz, albite, illite, smectite, chlorite and kaolinite control the sedimentary rock compositions and allow identification of cryptic stratigraphic boundaries that assist in establishing stratigraphic level within the basin. In addition, Mn, Fe, and P concentration patterns indicate that the basin became progressively more reducing with time, allowing identification of strata that could host sediment-hosted massive sulfide mineralization. Finally, alteration halos about saddle reef gold deposits and primary dispersion haloes in sedimentary rocks adjacent to Sn greisen deposits can be readily identified, providing useful exploration criteria.

KEYWORDS: *Meguma Supergroup, lithogeochemistry, stratigraphy, alteration haloes, sedimentary environment.*

INTRODUCTION

Stratigraphic correlation in flysch sequences is difficult because these thick, monotonous piles of proximal and distal turbidites contain a range of interbedded sedimentary rocks. As a result, locating prospective strata hosting mineral deposits and identifying hydrothermally altered rocks within these sequences represents a significant challenge.

Nevertheless, thorough evaluation of lithogeochemical data collected from such flysch successions, when coupled with careful mapping and correlation, can provide valuable information that benefits mineral exploration programs.

STRATIGRAPHY

The Late Neoproterozoic/Cambrian Meguma Supergroup of Nova Scotia is a flysch sequence that contains the metasandstone-dominated Goldenville Group and the overlying slate-dominated Halifax Group (White 2008a). Mapping indicates that three spatially distinct

stratigraphic sequences exist in the supergroup: the Eastern, South, and French Shore stratigraphies (Fig. 1).

The South Shore Meguma stratigraphy is best known (White 2008b). The basal Goldenville Group comprises, from bottom to top: (i) the Moses Lake Formation, an 800 m thick package of grey metawacke, green metasiltstone, and carbonaceous pyritic and magnetitic slate; (ii) the Green Harbour Formation, a 4,830 m thick, thick-bedded metawacke; (iii) the Government Point Formation, a 1750 m thick, thin-bedded metawacke, green metasiltstone, and multicoloured slate; and (iv) the Moshers Island Formation, a 300 m thick sequence of green and grey, laminated Mn-rich slate and metasiltstone with minor interbedded metawacke. The overlying Halifax Group comprises: (v) the Cunard Formation, a 2250 m thick grey to black slate containing pyrite, pyrrhotite, and arsenopyrite beds; overlain by (vi) the Feltzen Formation, a 2000 m thick grey slate and metasiltstone.

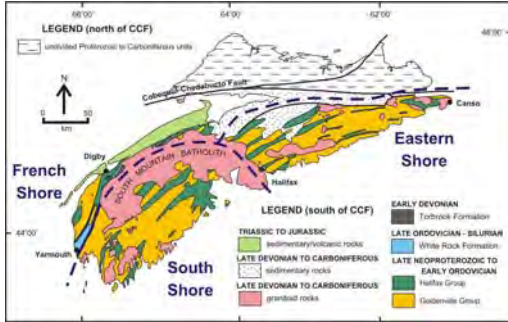


Fig. 1. Map of Nova Scotia illustrating the location of the Meguma Supergroup.

LITHOGEOCHEMISTRY

A 499 sample major oxide- and trace-element lithogeochemical database was assembled from fourteen different sources to further investigate the South Shore Meguma Supergroup stratigraphy. These relatively un-weathered samples represent all formations within the Halifax ($n = 71$) and Goldenville groups ($n = 428$). After pulverization, major oxides and some trace elements were analyzed by fusion-XRF or ICP-OES, whereas other trace elements were analyzed by four acid or aqua regia digestions, with AAS or ICP-MS finish, at the St. Mary's University Regional Geochemical Laboratory, Halifax, N.S. or at ACME Analytical Laboratories Ltd., Vancouver, B.C.

A molar element ratio (MER) analysis was undertaken to gain insight into the diversity and compositional controls on these rocks, and to identify stratigraphy hosting alteration zones and potential mineral deposits.

SEDIMENT COMPOSITIONS

Three MER diagrams (Figs. 2, 3, & 4) collectively illustrate the mineralogical controls observed in each of the Meguma Supergroup formations. Because these metamorphosed rocks derive from proximal and distal flysch sediments, they likely once contained: quartz, K-feldspar, albite, muscovite, illite, smectite (montmorillonite-beidellite), chlorite (clinochlore/chamosite), Al-chlorite (sheridanite/daphnite), and (or) kaolinite. These minerals (Table 1) could be used to interpret the geochemical results on these

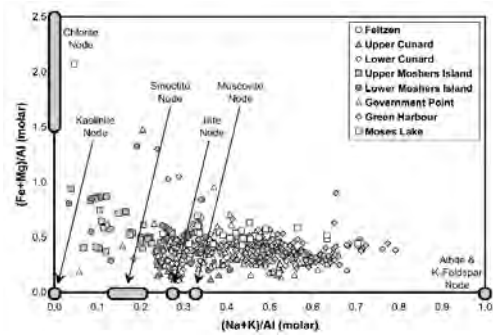


Fig. 2. Whole-rock compositions plotted on an (Na+K)/Al versus (Fe+Mg)/Al MER diagram.

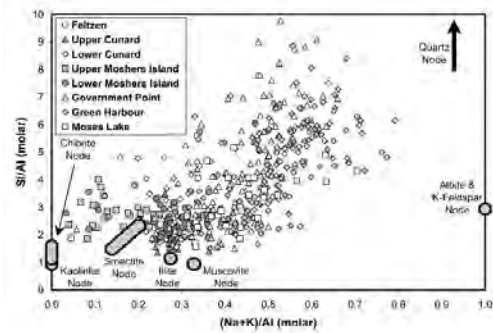


Fig. 3. Whole rock compositions plotted on an (Na+K)/Al versus Si/Al MER diagram.

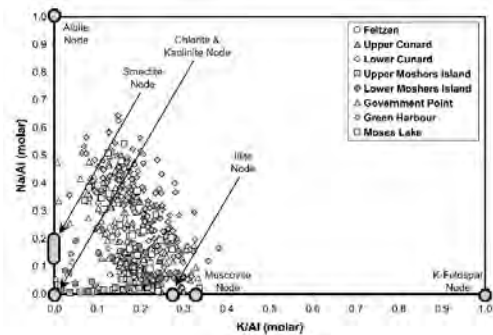


Fig. 4. Whole-rock compositions plotted on a K/Al versus Na/Al MER diagram.

diagrams because metamorphism rarely affects major oxides (with the exception of volatiles: H₂O, CO₂, & S₂), ensuring that the original precursor (pre-metamorphic) mineralogical controls are preserved.

Overall, Meguma Supergroup slate samples are relatively homogeneous, whereas metawackes tend to exhibit more compositional variation, probably because of their fining-upward textures.

In the Halifax Group, the Cunard

Formation has compositionally distinct upper and lower members. Both can be explained by illite-smectite mixtures, but Lower Cunard slates also contain quartz. Like the Lower Cunard rocks, the Feltzen Formation has compositions explained by mixtures of illite, smectite and quartz.

In the Goldenville Group, the Moshers Island Formation also has two compositional members: an upper one explained by mixtures of chlorite, kaolinite illite, and smectite, and a lower one explained by only illite and smectite.

In contrast, metawackes in the Government Point, Green Harbour, and Moses Lake formations (Goldenville Group) have compositions explained by mixtures of illite, albite, and quartz, but each of these formations differ slightly in terms of the amounts of quartz and feldspar they contain, relative to illite. In addition, the Moses Lake Formation contains significant amounts of chlorite.

DEPOSITIONAL ENVIRONMENTS

Stratigraphy-MER scatterplots illustrate that background Mn/Ti and Fe/Ti ratios (Figs. 5 & 6) are elevated throughout the Moshers Island Formation. Very anomalous Mn/Ti ratios also occur sporadically in this formation, and the upper part of the Government Point Formation. These anomalies are associated with pink or black spessartine-bearing coticles possibly related to hydrothermal brine expulsion onto the seafloor that might be associated with sediment-hosted massive sulfide (SHMS) mineralization. In contrast, the elevated background Mn/Ti and Fe/Ti ratios are likely products of redox cycling associated with a change from suboxic pore water chemistry during deposition of the Moses Lake, Green Harbour, and Government Point metawackes, to anoxic pore water

Table 1. Ideal clay mineral formulae controlling Meguma Supergroup rock compositions.

Chlorite	$(\text{Fe,Mg})_{10}\text{Al}_4\text{Si}_6\text{O}_{20}(\text{OH})_{16}$
Al-Chlorite	$(\text{Fe,Mg})_9\text{Al}_5\text{Si}_6\text{O}_{20}(\text{OH})_{16}$
Montmorillonite	$\text{Na}_{2/3}(\text{Fe,Mg})_{2/3}\text{Al}_{10/3}\text{Si}_8\text{O}_{20}(\text{OH})_4$
Beidellite	$\text{Na}_{2/3}\text{Al}_{14/3}\text{Si}_{22/3}\text{O}_{20}(\text{OH})_4$
Illite	$\text{K}_{3/2}\text{Al}_{11/2}\text{Si}_{13/2}\text{O}_{20}(\text{OH})_4$
Kaolinite	$\text{Al}_2\text{Si}_2\text{O}_5(\text{OH})_4$

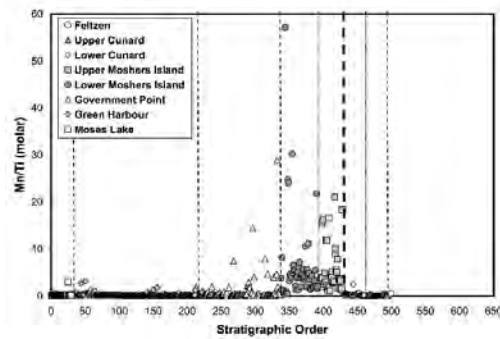


Fig. 5. Molar Mn/Ti ratios plotted versus stratigraphic order.

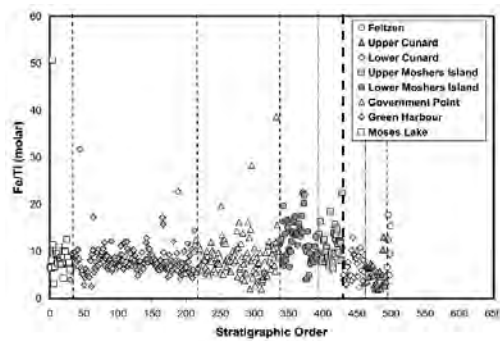


Fig. 6. Molar Fe/Ti ratios plotted versus stratigraphic order.

chemistry during deposition of the Moshers Island slates.

Subtly low Fe/Ti (Fig. 6) and P/Ti (not pictured) MER's in the overlying Cunard Formation are thus likely a result of the absence of pelagic sedimentation of Fe-oxo-hydroxides, with adsorbed seawater phosphate, as redox conditions became even more anoxic (low enough to reduce Fe^{+3} to Fe^{+2}). Thus, evidence for a significant drop in the redox state of pore waters exists in the lower part of the Halifax Group and the upper part of the Goldenville Group, indicating that these sedimentary rocks are likely prospective for SHMS mineralization that may be responsible for the high Pb concentrations (> 700 ppm) observed in the Moshers Island Formation (Fig. 7).

HYDROTHERMAL ALTERATION

Stratigraphy-element concentration scatterplots illustrate that anomalous Zn (Fig. 8), Cu, and Rb (not pictured) exist in the lower part of the Green Harbour

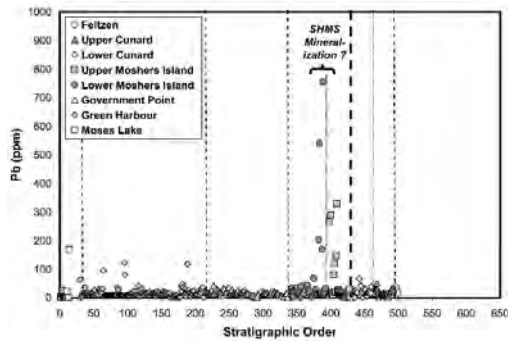


Fig. 7. Pb concentrations (ppm) plotted versus stratigraphic order.

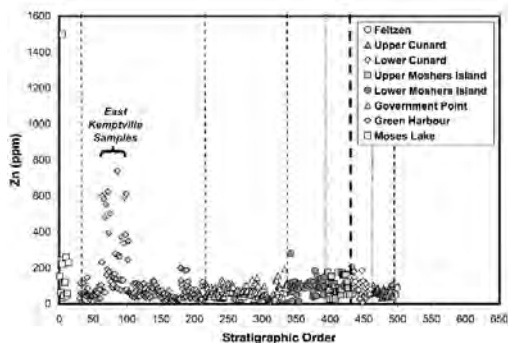


Fig. 8. Zn concentrations (ppm) plotted versus stratigraphic order.

Formation, proximal to the East Kemptville Sn greisen deposit. Given that this deposit contains accessory sphalerite and chalcopyrite, and has significant amounts of muscovite gangue, these anomalous concentrations, observed in rocks that are not visibly altered, likely comprise the geochemical expression of a cryptic primary dispersion halo about the deposit. The stratigraphy-MER scatterplot of Figure 9 illustrates that a bimodal distribution of (Na+K)/Ti ratios (two circles) exist in metawackes that are not visibly altered near the North Brookfield saddle reef gold deposit. These low (Na+K)/Al ratios are likely the result of hydrothermal alteration of feldspar to muscovite by hydrothermal fluids associated with auriferous quartz vein precipitation via reaction involving a net Na+K loss:

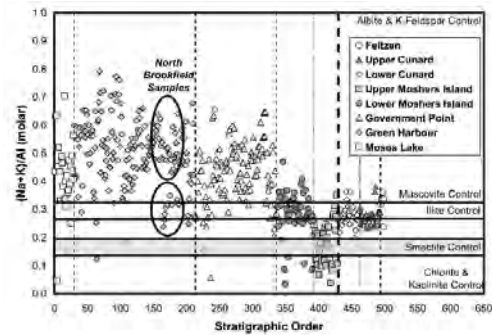
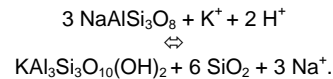


Fig. 9. Molar (Na+K)/Al ratios plotted versus stratigraphic order.



CONCLUSIONS

Major oxide- and trace-element geochemistry of sedimentary rocks can provide significant information critical to exploration for sediment hosted mineral deposits. Lithochemical evaluation of the Meguma Supergroup has facilitated stratigraphic correlation, contributed to an understanding of the marine environment of deposition, and detected the presence of hydrothermal alteration zones associated with sediment hosted massive sulfide mineralization, saddle reef Au, and greisen Sn deposits.

REFERENCES

- WHITE, C.E. 2008a. Defining the stratigraphy of the Meguma Supergroup in southern Nova Scotia: where do we go from here? In: *Atlantic Geoscience Society 34th Colloquium and Annual Meeting, Program and Abstracts, February 1-2, 2008, Dartmouth, Nova Scotia*, 58 p.
- WHITE, C.E. 2008b. Preliminary bedrock geology of the New Germany map sheet (NTS 21A/10), southern Nova Scotia. In: D.R. MACDONALD (ed.), *Mineral Resources Branch, Report of Activities 2007. Nova Scotia Department of Natural Resources, Report ME 2008-1*, 113-124.

**NEW AND OLD DISCOVERIES: GEOCHEMICAL EXPLORATION CASE
STUDIES**

EDITED BY:

**HUGH DESOUZA
MARK ARUNDELL
DAVE HEBERLEIN**

Using regional geochemistry, geology, aeromagnetics, Landsat, and digital elevation models (DEM) to define favourable areas for porphyry-style mineralization in southwestern Alaska

Eric D. Anderson¹, Robert G. Eppinger¹, & Karen D. Kelley¹

¹United States Geological Survey, Denver, CO USA (e-mail: ericanderson@usgs.gov)

ABSTRACT: The Late Cretaceous (90 Ma) Pebble Cu-Au-Mo porphyry deposit is located within the southern Kahiltna terrane, which is comprised of the Chilikadrotna Greenstone and the Koksetna River sequence. Near the Pebble deposit, the Chilikadrotna Greenstone marks the northwest border of the southern Kahiltna terrane, and the Koksetna River flysch sequence is the host for mineralization at Pebble. Throughout the world, porphyry deposits are found in clusters associated with multiple intrusive events, typically, if not always, subduction-related, thereby suggesting the southern Kahiltna terrane is potentially favourable for other porphyry occurrences. Our integration of multiple geoscientific data layers has revealed that the world-class Pebble deposit may similarly be accompanied by additional porphyry-style mineralization elsewhere in the southern Kahiltna terrane. Delineation of watersheds, derived from processing of digital elevation data, provided an effective framework for predicting favourable areas for mineralization. Beyond analysis of individual data layers of geochemistry, geology, geophysics, and remote sensing, geographic information systems (GIS) applications facilitated an integrated approach that provided a more refined and detailed process to locate potential mineralization within those watersheds. Preliminary results suggest 23 watersheds contain favourable geochemical, geological, and geophysical signatures for Pebble-like porphyry-style mineralization.

KEYWORDS: *Pebble, Porphyry Cu-Au-Mo, Regional Targeting, Southwest Alaska, Kahiltna Terrane*

INTRODUCTION

Regional-scale spatial data are readily available from numerous United States Geological Survey (USGS) websites. The individual datasets can be processed and enhanced to help identify areas of particular geologic phenomena, in this case mineralization. Individually, these enhanced products provide clues to the underlying geology, but when integrated in a geographic information system (GIS), they allow a more detailed interpretation that can delineate favourable areas for porphyry-style mineralized rock.

The Pebble Cu-Au-Mo porphyry deposit (Fig. 1) contains one of the largest resources of copper and gold in the world (NDM 2009). Porphyry deposits typically occur in clusters within subduction-related magmatic belts, suggesting the possibility of multiple occurrences of porphyry-style mineralization near the Pebble deposit, within the southern Kahiltna terrane. In this study, we use USGS spatial data to

locate additional highly favourable areas for porphyry-style mineralization around the Pebble deposit. Such datasets include, but are not limited to, geochemistry, geology, aeromagnetics, Landsat imagery, and Digital Elevation Models (DEM).

GEOLOGICAL SETTING

Regional Geology

The Late Cretaceous Pebble deposit is located within the southern part of the Late Jurassic to Early Cretaceous Kahiltna terrane, which is bounded to the southeast by the Peninsular terrane (Late Triassic to Late Jurassic) and to the northwest by flysch of the Kuskokwim Group (middle to Late Cretaceous) (Fig. 1). The southern Kahiltna terrane consists predominately of Jurassic to Cretaceous turbidite deposits and can be divided into two major lithologic units: the Koksetna River sequence and the Chilikadrotna Greenstone (Wallace *et al.* 1989). The

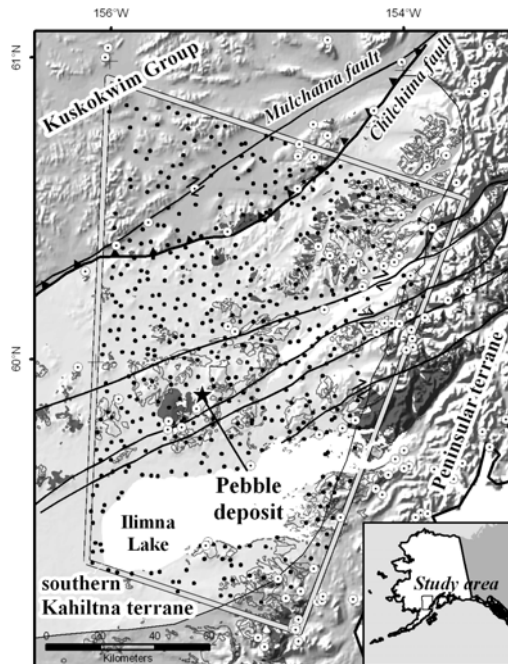


Fig. 1. Index map showing the location of the study area (double line). The southern Kahiltna terrane is located between the Kuskokwim Group and the Peninsular terrane. The localities of 485 regional geochemistry samples are shown as black dots. Generalized geologic structures are shown as black lines. Late Cretaceous-Tertiary intrusions shown in dark gray. Tertiary-specific rocks are outlined in gray. Reported mineral occurrences are shown as white circles.

deformed, interbedded volcanoclastic turbidites. The sediments of the Koksetna River sequence are mainly derived from the Peninsular terrane. These sedimentary rocks host the porphyry-style mineralization at Pebble. The Chilikodrotna Greenstone (Bundtzen *et al.* 1979) occurs near the northwestern boundary of the southern Kahiltna terrane and is comprised mainly of massive altered basalt. The contact between rocks of the Chilikodrotna Greenstone and the Kuskokwim Group is the steeply NW-dipping Chilkina fault, which merges with the subparallel Mulchatna fault to the northwest (Wallace *et al.* 1989). The southern Kahiltna terrane is progressively covered towards the southeast by unconformably-overlying, mostly latest Cretaceous to Paleocene volcanic rocks

of the Alaska Range (Wallace *et al.* 1989; Wallace & Engebretson 1984).

Local Geology

The Pebble district is comprised of gently folded rocks of the Koksetna River sequence that have been cut by diorite sills (Rebagliati & Lang 2008). Magmatism in the district includes a pre-hydrothermal ca. 96 Ma group of alkalic and subalkalic intrusions, and a ca. 90 Ma group of granodiorites which includes the Kaskanak batholith and plutons associated with the deposit. Hydrothermal mineralization at Pebble has a Re-Os date of ca. 90 Ma (Lang *et al.* 2008). Also in the district a later pulse of hydrothermal activity associated with an epithermal Au-Ag prospect occurred at ca. 46 Ma (Lang *et al.* 2008).

Hydrothermal alteration at Pebble consists of a central, strong K-silicate assemblage with sparse magnetite, and peripheral sericitic alteration that overprints the deposit, with propylitic and illite assemblages present locally (Rebagliati & Lang 2008).

METHODS

Multidisciplinary spatial datasets have been downloaded from USGS websites. Each dataset has been processed to enhance the signature of porphyry-style mineralization within and proximal to the southern Kahiltna terrane.

Geochemical data consist of analyses of 485 pond sediment samples collected as part of the 1970s National Uranium Resource Evaluation (NURE) program (<http://tin.er.usgs.gov/geochem/>).

Elements chosen from the limited NURE multi-element geochemical packages that may be pathfinders for porphyry-style deposits (Lefebure & Ray 1995) include Ba, Co, Cu, Mn, Pb, Ti, V, and Zn. Under the NURE program, two analytical techniques were used: energy dispersive x-ray fluorescence (Cu and Pb) and neutron activation (Ba, Co, Mn, Ti, V, and Zn). Single element plots and element association plots were generated. Geochemical data for pond sediments collected over the Pebble deposit in 2008

are pending and will be evaluated and used in the favourability modelling.

Geology of the studied area was derived from 1:250,000 scale geologic maps of the Lake Clark and Iliamna quadrangles (Wilson *et al.* 2006). These data contain attribute information that identifies lithologic units and their ages. Subsets were made of all igneous rock types from Late Cretaceous through Tertiary.

Regional aeromagnetic data (Connard *et al.* 1999) are useful for mapping the distribution of magnetic minerals, mainly magnetite. The analytic signal transformation (Nabighian 1972) was used to simplify the complexities associated with depth to source and remnant magnetization. The result is a map where high values suggest relatively high concentrations of magnetic minerals.

Landsat imagery was downloaded from the GloVis viewer (<http://glovis.usgs.gov/>). The data were atmospherically and geometrically corrected. Band ratios were used to map the presence of iron oxides, hydroxides, and hydrous minerals, possibly associated with porphyry-style hydrothermally altered and mineralized rocks.

Elevation (DEM) (<http://agdc.usgs.gov/>) and hydrologic data (<http://nhd.usgs.gov/>) were merged and processed to delineate individual watersheds for the 485 geochemistry samples. A watershed can be thought of as an area that would drain into a single point (geochemical sample location) as defined by the DEM. The watersheds tend to be 1 – 10 km². Inaccuracies in location of the geochemistry samples were taken into account by creating proximity zones around each location using a 150 metre search radius. The resulting watersheds were used as a framework for interpretation of the multidisciplinary datasets.

RESULTS

Igneous activity that occurred between Late Cretaceous and Early Tertiary time shows a strong northeast-southwest trend, which is also evident in the regional aeromagnetic data. The aeromagnetic

data define the boundary between rocks of the Kuskokwim Group and the southern Kahiltna terrane, thus marking the northwestern edge of favourable terrain for Pebble-age porphyry-style occurrences. Ninety watersheds show elevated (>95th percentile) values of one or more pathfinder elements and 63 of these are in areas characterized by a favourable geophysical signature. Of these 63 watersheds, 23 contain intrusive rocks of favourable age for Pebble-like porphyry-style mineralization. In general, relatively elevated copper concentrations (>47 ppm) are found in the more mountainous terrain north and east of Pebble. There is a spatial correlation between the elevated copper concentrations and Late Cretaceous and Early Tertiary igneous rocks. The Landsat data further refine the location of favourable watersheds by suggesting the presence of iron oxides, hydroxides, and hydrous minerals.

CONCLUSIONS

Preliminary results suggest that the integration of multidisciplinary data is crucial in locating favourable areas for porphyry-style mineralization. This contribution can be summarized as follows:

- (1) Clipping the datasets using boundaries of watersheds reduced overall spatial coverage from 19,000 km² to 2,400 km² within the study area and allowed a more focused area for data interpretation, this is useful considering a porphyry target typically being less than 15 km². However, this may in turn, exclude areas where mineralized rock is present and detectable in datasets other than the regional geochemistry.
- (2) NURE geochemical samples were not collected over the concealed Pebble deposit making it difficult to directly define the mineralization signature in the regional geochemical database. New pending pond sediment data will help rectify this.
- (3) Patterns within the multidiscipline datasets can be queried against each other to further refine favourable areas.

(4) Proper watershed delineation provided an effective framework for interpretation and analysis of multidisciplinary data and relies on the quality of the original DEM. In the flat, vegetated lowlands, the resultant watersheds tend to be small, whereas in the alpine areas they are larger and more favourable to the detection of hydrothermal minerals by the Landsat imagery because of sparse vegetation.

(5) Without additional absolute dating of the intrusive bodies, or further geochemical analysis of the igneous rocks, differentiating between Pebble-aged igneous activity and later Alaska Range magmatic activity is problematic.

ACKNOWLEDGEMENTS

We thank the Pebble Limited Partnership for site access and background information, as well as Rich Goldfarb and Greg Lee for their helpful comments.

REFERENCES

- ALASKA GEOSPATIAL DATA CLEARINGHOUSE (AGDC) 30/05/08, <http://agdc.usgs.gov>; e-mail: ascweb@usgs.gov
- BUNDTZEN, T.K., GILBERT, W.G., & BLODGETT, R.B. 1979. The Chilikadrotna Greenstone, an Upper Silurian metavolcanic sequence in the central Lake Clark quadrangle, Alaska: *Alaska Division of Geological and Geophysical Surveys Geologic Report*, **61**, 31-35.
- CONNARD, G.W., SALTUS, R.W., HILL, P.L., CARLSON, L., & BILICEVIC, B. 1999. Alaska Digital Aeromagnetic Database Description. *USGS Open-File Report* **99-503**.
- LANG, J.R., REBAGLIATI, C.M., & ROBERTS, K. 2008. The Pebble copper-gold-molybdenum

porphyry deposit, south-west Alaska, USA. *Proceedings, PACRIM 2008, AUSIMM*, 27-32.

- LEFEBURE, D.V. & RAY, G.E. 1995. Selected British Columbia Mineral Deposits Profiles: Metallics and Coal. *BCMEMP Open File* **1995-20**, 1.

MINERAL RESOURCES ON-LINE SPATIAL DATA (MRDATA) 12/12/08, <http://tin.er.usgs.gov/geochem/>; e-mail: pschweitzer@usgs.gov

NABIGHIAN, M.N. 1972. The analytic signal of two-dimensional magnetic bodies with polygonal cross-section: its properties and use for automated anomaly interpretation. *Geophysics*, **37**, 507-517.

NATIONAL HYDROGRAPHY DATASET (NHD) 13/08/08, <http://nhd.usgs.gov>; e-mail: ask@usgs.gov

NORTHERN DYNASTY MINERALS, INC. 2009. <http://www.northerndynastyminerals.com>

REBAGLIATI, M., & LANG, J. 2008. Geology and exploration history of the super-giant Pebble copper-gold-molybdenum porphyry deposit, Alaska. *International Geology Congress*, **33**.

USGS GLOBAL VISUALIZATION VIEWER (GLOVIS), 12/08/08, <http://glovis.usgs.gov>; e-mail: custserv@usgs.gov.

WALLACE, W.K. & ENGBRETSON, D.C. 1984. Relationships between plate motions and Late Cretaceous to Paleocene magmatism in southwestern Alaska. *Tectonics*, **3**, 295-315.

WALLACE, W.K., HANKS, C.L., & ROGERS, J.F. 1989. The southern Kahiltna terrane; Implications for the tectonic evolution of southwestern Alaska. *Geological Society of America Bulletin*, **101**, 1389-1407.

WILSON, F.H., MOHADJER, S., LABAY, K.A., & SHEW, N. 2006. Preliminary Integrated Geologic Map Databases for the United States. *USGS Open-File Report* **2006-1303**.

Termitaria: its application as sample media to gold exploration-a case study in northern Ghana

Emmanuel Arhin

University for Development Studies, P. O. Box 24, Navrongo, Upper East Region GHANA.
(e-mail: eaarthin@yahoo.com)

ABSTRACT: Extensive lateritization and widespread sheetwash and alluvial deposits characterized the savannah regions of northern Ghana. The presence of these materials affects geochemical gold response during surficial gold exploration. Anomaly detection thus becomes very difficult perhaps due to gold grain encrustation during lateritization and anomaly dilution by sheet wash deposits. The use of termite mounds sampling in areas of transported overburden and laterite cap has shown to be a successful way of locating buried anomalies. Termite mounds samples analyzed for Au using Fire Assay was able to define anomalous zones in northern Ghana. Size fractions consisting of -125 μ m, +125 μ m, -500 μ m and + 500 μ m were analyzed for Au. The statistical analyzes between the results from -125 μ m and +125 μ m size fractions showed insignificant change in assay results but there were significant change when sub- samples were re-analyzed from the different size fractions. Au content repeatability was greater in -125 μ m size fraction and decreases as the grain size become coarser, confirming the conclusion of the statistical analysis. The study showed that termite mound can be used as a geochemical sample media to support the conventional soil survey especially in areas under cover and that -125 μ m size fraction is the most appropriate size fraction.

KEYWORDS: *Termite, mound, size fraction, northern Ghana. Geochemical field*

INTRODUCTION

Termite mounds are common in savannah regions of northern Ghana, though some are in southern Ghana. These mounds had significant uses in mineral exploration especially in areas under cover (Gleeson & Poulin 1989) but its application in Ghana became known when the studies by Affam & Arhin (2004) and Roquin *et al.* (1991), indicated that termites play an important role in the remobilization of the laterite weathering profiles. In reality, the termite mound building activity results in an upward transfer of clay, silts, fine Au grains, and sand particles to the ground surface; a process opposite to leaching. Also as a result of environmental stress and climate changes Termitaria collapse under different climatic condition and are subsequently eroded, transported and deposited in low-lying areas of the landscape influencing chemical element contents in the geochemical fields. This process of mechanical dispersion and formation of silty – clay soil cover is evident in most part of the study area,

making conventional geochemical survey difficult to define anomalous targets.

The day to day geochemical surveys for gold often begin with soil surveys. But areas with in-situ soils and outcrops had all been explored; leaving behind an environment with complex regolith-generally masked by laterite caps and transported covers. Materials collected in these areas as samples generally do not bear relationship to the bedrock mineralization. Butt & Zeegers (1992) and Arhin & Nude (2008) found out that these materials on the landscape may be residual or transported in character. Their implication is the many False Au geochemical anomalies that are delineated in areas under cover. The research used termite mound as sample medium to support the conventional soil surveys. The results from termite mound samples gave gold results that were site specific and are considered as “Poor Man’s Drill hole”. The False anomalies were checked by results obtained from the

termite mounds; reducing time and money on following non-existing anomalies.

GEOLOGICAL SETTING

The area is underlain by Birimian meta-volcanic and meta-sedimentary rocks that have been intruded by granites. The meta-volcanic rocks are of basaltic and gabbroic compositions and most have been altered to various schists. The metasedimentary rocks consist of sandstones, siltstones, tuffs, carbonaceous phyllites, tuffaceous phyllites, cherts and manganese rocks (Leube *et al.* 1990).

METHODS

Termitaria were sampled over an area of 10 km² with a regular density of 100 m x 50 m corresponding to soil sampling grid of a previous geochemical survey. The density of sampling was five (5) termite mounds over 1 km². Composite samples were collected at areas with termite mound clusters i.e. about ten (10) termite mounds on a km² area. Total of 240 samples were taken from cluster of termite mounds from different anomalous areas which were in close proximity to known illicit mining area. The 240 samples collected comprised of 60 samples each from the four size fractions i.e. -125 µm, +125 µm - 500 µm and +500 that were used as media for gold analyses. Five quality care (QA/QC) samples were inserted in each batch of size fractions that were sent to a commercial laboratory for gold analysis.

RESULTS

The gold contents (in ppb) in the various size fractions from the termite mounds are presented in Table 1 and the geochemical distribution of gold in the various size fractions were compared with the gold content in -125µm fractions as that appeared to be the size fractions used in gold exploration surveys especially in Ghana and West Africa.

For the purpose of comparison, gold content in -125µm was compared with +125µm, -500µm and +500µm respectively and the outcome summarised in figure 1. The results from the

comparative studies show that the four size fractions appear to have similar gold distribution patterns defining the same anomalous zones. Conversely, -125µm size fraction from termite mound sample analysed registered relatively higher gold values than the other size fractions use in the study (Fig. 1). To add to that the gold content in -125µm size fraction appears reasonably consistent when sub-samples were re-analysed. The re-analyses of the other sub- samples collected from +125 µm, - 500 µm and + 500 µm lack precision (Table 1). It is probable that the assay values obtained in the coarser size fractions perhaps were due to some detrital Au grains that were picked up in the first or original analyses. The implication is that if coarser size fractions are selected as sample media, disregarding sample reproducibility, then critical assessment would be required as a single coarse gold grain in the sample could introduce nugget effect.

The two size fractions of -125 µm and +125 µm have similar gold geochemical patterns from the plots of the original assays but had different anomalous patterns when repeat samples were analysed. The variation in -125 µm sub samples was generally insignificant but the variations in +125 µm sub – samples were very significant. For example, a sample that originally registered gold value of 523 ppb returned assay of 200 ppb from the repeat analyses. Similarly 200 ppb sample from + 125 µm also returned assay value of 21 ppb in the repeat analyses. The lack of precision between the original analysed samples to the repeat samples make it impractical to use it as an appropriate size fraction for geochemical assay when nugget effect can lead to serious lost of time and money in exploration. The lack of precision escalates even more when coarser materials such as -500 µm and + 500 µm size fractions are analysed for gold. For instance 511 ppb Au obtained from analysing gold in - 500 µm size fraction from termite mound returned 56 ppb Au when sub-sample of the same sample was analyzed. The imprecision increases

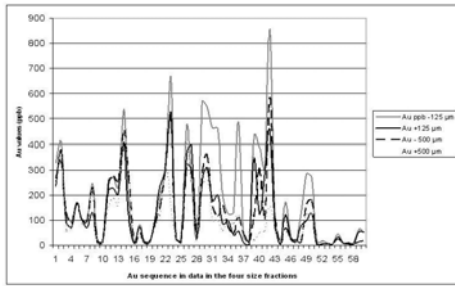


Fig. 1. Comparisons of Au in different size fractions.

as coarser samples are analysed.

Despite the lack of precision associated with the coarser size fractions, all the four size - fractions defined the same areas but confidence of finding potential mineralization appeared associated with the -125 µm size fraction. It is apparent that termite mound survey thus be used as a supplementary grassroots' exploration tool to enhance the conventional exploration methods especially in areas under cover.

CONCLUSIONS

The conventional soil surveys conducted in the study area often returned tricky results, with isolated high point anomalies that were not followed up with the anxiety that they were not real. The current study using termite mound as sample medium, however, isolated the real anomalies from the false anomalies. The sampled materials came from in-situ materials representing bedrock mineralization; making gold results from Termitaria more dependable than the surficial soils. It is concluded from the study that termite mound geochemical surveys provided cost effective method of defining prospective anomalous areas especially in areas covered by transported overburden and laterite caps. More so as termites can burrow beyond depths exceeding 10 m chasing the water table to get materials to build the mounds, sampled materials from them can be considered as 'Poor Man's Drill hole" during Greenfield exploration. Above all gold value precision in -125 µm size fraction was better in terms of grade and reproducibility during re-analyses than

Table 1. Comparisons of gold in different size fractions in termite mounds

Au ppb - 125 µm	Au ppt - 125µm	Au +125 µm	Au ppt- 125 µm	Au - 500 µm	Au ppt - 500 µm	Au +500 µm	Au ppt +500 µm
327	328	238	120	269	50	231	15
406		377		335		366	
114		97		134		59	
95		71		86		63	
172		167		169		162	
104		104		103		84	
99		71		93		102	
247	200	131	90	232	25	126	67
16		16		12		9	
15		16		12		10	
298		216		239		150	
271		227		276		167	
230		205		254		155	
539	534	408	512	455	390	437	12
184		104		277		252	
13		10		10		10	
82		74		49		32	
17		9		14		8	
15	13	12	10	17	12	12	5
100		109		91		74	
196		237		154		118	
302		302		312		318	
664	661	523	200	511	56	139	45
27		34		33		27	
18		12		14		32	
473		361		318		404	
281		391		296		233	
29		39		27		33	
570		260		294		221	
545		309		360		258	
464	451	178	50	154	12	100	5
460	450	200	21	114	15	98	9
195		85		159		58	
126		100		73		98	
130		40		47		85	
490		56		112		120	
30		10		44		44	
20		5		17		52	
435		349		114		19	
390		123		308		49	
310	300	290	59	106	13	58	23
855		456		588		154	
104		70		106		58	

the other size fractions used in the study, hence -125 µm size fraction could be used in all Greenfield exploration in savanna regions of Ghana as well as all areas under cover in West Africa.

REFERENCES

AFFAM, M. & ARHIN, E. 2004. Termite Mound - a supplementary geochemical gold sampling medium in complex regolith terrains. *Ghana Mining Journal*, **8**, 1- 7.

ARHIN, E. & NUDE, P.M. 2008. Significance of regolith mapping and its implication for gold exploration in northern Ghana: a case study at Tinga and Kunche. *Geochemistry: Exploration, Environment, and Analysis*, **9**, 1- 8.

BUTT, C.R.M. & ZEEGERS, H. 1992. *Handbook of exploration geochemistry Regolith Exploration geochemistry in Tropical and Subtropical terrains*. Elsevier, New York, **4**, 607 p.

D'OREY, F.C.C. 1975. Combination of termite mound to locating hidden Copper Deposit. *Transactions of the Institute of Mineral and Metallurgy - Applied Earth Science*, **84**, 150-156.

GLEESON, C.F. & POULIN, R. 1989. Gold exploration in Niger using soil and

- Termitaria. *Journal of Geochemical Exploration*, **31**, 253-283.
- LEUBE, A., HIRDES, W., MAUER, R., & KESSE, G. O. 1990. The early Proterozoic Birimian Super group of Ghana and some aspects of its associated gold mineralization. *Precambrian Research*, **46**, 139-165.
- ROQUIN, C., FREYSSINET, PH., NOVIKOFF, A., & TARDY Y. 1991. Geochemistry of Termitaria and soils covering ferricrete. Application to gold exploration in Western Africa. *European Network on tropical laterite and global Environment*, Eurolat **91**, 133-137.

Exploration history and discovery of a new mineralization style, Freegold Mountain area, Dawson Range, Yukon Territory, Canada

Thierry Bineli Betsi¹, Fabrizio Colombo², & David R. Lentz¹

¹Department of Geology, University of New Brunswick, 2 Bailey Drive, Fredericton NB, E3B 5A3 Canada
(e-mail: drlentz@unb.ca)

² Northern Freegold Resources Ltd. 900-475 Howe Street, Vancouver, BC, Canada V6C2B3
(e-mail: fcolumbo@northernfreegold.com)

ABSTRACT: The Dawson Range Cu-Au-(Mo) Belt portion of the Tintina Au Province had been explored for decades through geological mapping, trenching, diamond and rotary drilling, and geochemical and geophysical surveys, all leading to the mining of a few claims, such as Laforma, Mt. Nansen and Minto. Gold-rich pyrrhotite veins (up to 113 g/t Au), Au-bearing sulphides in granitoids (up to 410 g/t Au), as well as Au-bearing pyroxene-actinolite-(biotite)-pyrite-pyrrhotite assemblage (1.15 g/t Au) have been newly discovered in the Nucleus zone of the Freegold Mountain Project of Northern Freegold Resources (NFR). Due to the presence of reduced minerals (pyrrhotite & pyroxene), and the abundance of Au relative to Cu, the Nucleus zone shares similarities with “reduced porphyry Cu-Au” and “intrusion-related pyrrhotite vein” systems.

KEYWORDS: Dawson Range Cu-Au-(Mo) Belt, Tintina Gold province, reduced porphyry

INTRODUCTION

The Dawson Range, in the Yukon Territory hosts several types of mineral occurrence that belong to the Dawson Cu-Au-(Mo) Belt portion of the the Tintina Au Province. The Tintina Au Province spans Alaska and Yukon and contains significant Au deposits, such as True North and Fort Knox in Alaska, and Dublin Gulch and Brewery Creek in Yukon (Fig. 1). The Dawson Range Cu-Au-(Mo) hosts minerals deposit of four main types: porphyries, epithermal veins, skarns, and transitional varieties associated with brecciation and porphyry dyke emplacement (Carlson 1987). Mineralization throughout the district has a spatial association with hypabyssal felsic porphyry stocks and dykes intruding Paleozoic Yukon Tanana metamorphic rocks and Mesozoic granitic rocks.

Mineralization in the Dawson Range is related either to the Middle Cretaceous Mount Nansen and Late Cretaceous Carmacks magmatic events (Mortensen *et al.* 2003) or only to the Late Cretaceous Carmacks magmatic event (Smuk *et al.* 1997; Selby & Creaser 2001).

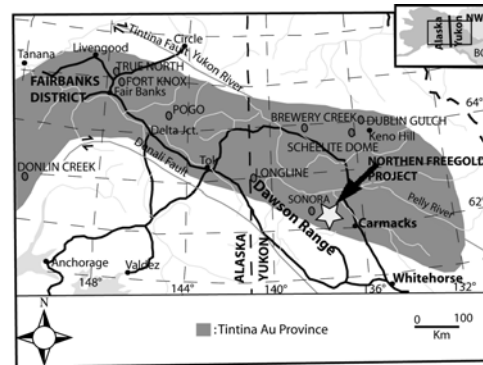


Fig.1. Location of the Dawson Range within the Tintina Au Province that extends from Alaska to Yukon and hosts significant gold deposits (after Tucker & Smith 2000).

Major mineral occurrences within the Dawson Range NW-SE trending Cu-Au belt as observed from the northwest to the southeast include: Casino, Cockfield, Sonora, Tad, Cash, Minto, Northern Freegold project mineral occurrences, Laforma, Carmacks, and Mount Nansen (Fig. 2).

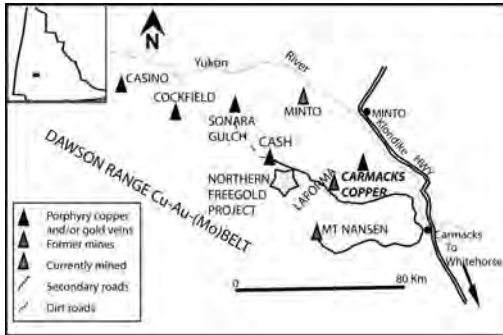


Fig. 2. Northern Freegold Project and other major mineral occurrences within the NW-SE trending Dawson Range Cu-Au-(Mo) Belt.

Mt. Nansen (Au-Ag) & Laforma (Au-bearing quartz vein systems) have been mined in the past and Minto (Cu-Au) is currently mined. This paper portrays the exploration history in the NFR Freegold Mountain project and highlights new discoveries recently made by NFR.

EXPLORATION HISTORY

The Freegold Mountain project of NFR extends 35 km along strike within the Dawson Range Cu-Au-(Mo) Belt. It covers 12000 hectares and comprises the following properties from northwest to southeast: Nitro, Big, Golden Revenue, Happy, Seymour, Glen, Rage, Goldstar, Goldy, and Tinta Hill (Fig. 3).

Nitro

The property first staked as Klazan in 1966 by Coranex Ltd. was later restaked as Nitro. Exploration on the property includes: geological reconnaissance, bulldozer trenching, grid soil sampling, magnetic survey, diamond drilling, and mapping. Nitro shows a strong gossan with anomalous Mo, Cu, Pb, Zn, Ag, and Au Cu-Mo-(Au-Ag) values.

Big: Au anomaly

This property consists of just one claim also referred to as Big. The Big property underwent only a few grid soil geochemistry studies.

Golden Revenue: Cu-Au

The Golden Revenue property is

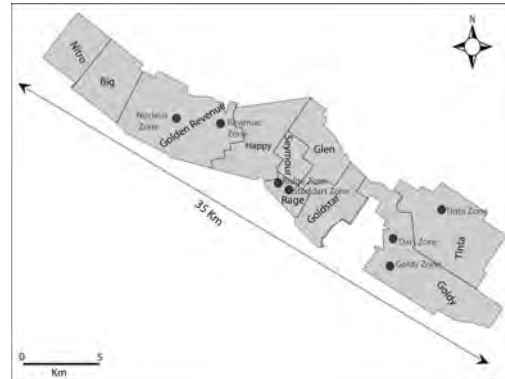


Fig. 3. Different properties and zones extending over 35 km at the Freegold Mountain NFR project.

composed of two zones: Revenue and Nucleus with each zone made up of several claims. The first claim in the Golden Revenue property was registered in 1950 by P.F. Guder as the Discovery zone and staked as Revenue. Exploration on the Golden Revenue property has involved EM, VLF-EM, resistivity, magnetic, and IP geophysical surveys, geochemical surveying, hand and bulldozer trenching, diamond (50296 m) and RAB (8582 m) drilling, grid soil sampling, reverse circulation or percussion drilling (3557 m), and geological mapping.

Happy

In 1954, P.F. Guder found gold-bearing quartz float and staked a claim on the Happy zone. The actual Happy property restaked as Happy by B. Harris in 2001 is made up of Guder's original Happy claims that have been tied to the east to the Luck claim (of Shawack Exploration) and to the north to the Angus claim of the Big Creek Joint Venture. So far, Happy underwent successively hand trenching, geological mapping, soil and rock sampling, minor blast trenching, line-cutting, grid work, magnetometer and VLF-EM surveying.

Seymour

The Seymour claims were staked in 1981. Nevertheless, exploration started much earlier in the area and the claims staked ceased thereafter. The Seymour showing

consists of a weak potassic alteration? core surrounded by phyllic (with 5% pyrite and trace of chalcopyrite) and argillic zones. Exploration in the area involved mapping, grid soil and rock geochemistry, magnetic and VLF-electromagnetic surveys, hand and mechanized trenching.

Glen

The Glen property is centred on 2 showings: (1) the (Ag-Pb-Zn ± Au) quartz vein of the Red Fox showing first staked in 1931 by P.F. Guder and later restaked as Vindicator, and, (2) the Cu ± Ag Castle claims first staked as the Sun claim in 1969. Exploration in the area has involved mapping, rock and soil geochemistry, magnetic survey, hand and bulldozer trenching, and diamond drilling (317.6 m).

Rage

The Rage property contains 2 main zones: Ridge and Stoddart. The area was first staked as Low in 1969 by R. McKamey and afterwards restaked as Ag, Au, Seymour, May, and Rag. The property underwent hand and bulldozer trenching, geological mapping, rock and grid soil geochemistry, diamond drilling (4763 m), and magnetic and IP geophysical surveys.

Goldstar

The original discovery in the Freegold Mountain area was made on this property in 1930 by P.F. Guder who staked the first claim (Augusta). The discovery consisted of a gold-bearing magnetite vein in which free gold was found in the oxidized magnetite. Guder subsequently acquired a property that included the Liberty, Augusta, Margarete, Peerless, and Gold Star claims. The actual Goldstar property includes the original Guder's claims and the Pauline claims. The Goldstar property had been explored by hand and bulldozer trenching, pitting, grid geochemical survey, VLF-EM and magnetometer geophysical surveys, and diamond (1058.6m) and rotary (304.8m) drilling.

Goldy

The Goldy property is made up of 2 main zones: Dart and Goldy. Dart is

represented by quartz-barite-Sb-Au vein occurrences at Emmon Hill, discovered in the early 1930's by T. Bee and W. Renworth. Before being restaked as Dart, it had been staked as Ant, Bill, Darb, Free, Joe, and Moon. The Goldy zone comprises the Whale claim (blue-gray quartz vein containing very fine-grained sulphides and gold) staked in 1933 by J.H. Carpenter and W. Forbes and the Forbes Creek showing. The property had been explored by hand and bulldozer trenching, geological mapping, geochemical rock, soil and stream sediment studies, line cutting, EM and IP surveying, diamond drilling (3920 m) and 12 reverse circulation drill holes (468 m).

Tinta Hill

In 1930, the original Tinta Hill showing made up of a quartz rich vein with galena, sphalerite, and, minor tetrahedrite and chalcopyrite was discovered, and a claim was subsequently staked in 1931 by George McDade and partners. Since 1931 the claim has been restaked as Tinta, May, June, and Sno. Exploration of Tinta Hill since 1930 has involved bulldozer trenching, underground development (939 m), diamond drilling (10493 m), rock and soil geochemistry, and VLF-EM surveying.

NEW DISCOVERIES

The 2007 & 2008 NFR diamond drilling campaign highlighted new mineralization styles at the Nucleus and Stoddart zones.

New discoveries at Nucleus were made following up Au-As-Bi soil anomaly zone, and they consist of (1) massive pyrrhotite veins with minor chalcopyrite, (2) calc-silicate (grossular-pyroxene-actinolite)-pyrite-pyrrhotite lenses or skarn and (3) massive sulphide replacement in granitoid. Interestingly, these new mineralized bodies are highly enriched in Au. For instance, some massive pyrrhotite veins grade up to 113 g/t Au, while sulphide-rich granitoids samples range up to 410 g/t Au, but the hydrogrossular-pyroxene-actinolite-pyrite-pyrrhotite assemblages grade, 1.15 g/t. Because of the predominance of reduced minerals (pyrrhotite & pyroxene), as well as the

importance of Au relative to Cu, the Golden Revenue property shares similarities with intrusion-related pyrrhotite vein and reduced porphyry Cu-Au systems described by Rowins (2000), such as the Rosslund and 17 Mile Hill deposits in British Columbia and Western Australia respectively. Field observations show that dykes, as well as granite of the Dawson Range Batholith, crosscut the mineralized calc-silicate. This suggests that mineralization may be older than the Dawson Range Batholith (Early Cretaceous) and that may extend the age of mineralization in the Dawson Range to even earlier than the Cretaceous as suggested by Bineli & Lentz (2009).

In Stoddart zone, 2 holes have been drilled to test the historical Au, Mo, & Cu soil anomaly, coincident with airborne magnetic survey anomaly. The drill holes revealed for the first time the occurrence of porphyry-style Cu-Mo mineralization in the Freegold Mountain area. Mineralization occurs as either quartz-chalcopyrite-molybdenite veins and microstockworks, or chalcopyrite & molybdenite disseminations.

CONCLUSIONS

This study shows that:

- (1) The Dawson Range and especially the Freegold Mountain area have been extensively explored for about 80 years, but only a few discoveries have been mined;
- (2) New discoveries at the Golden Revenue property of NFR testify not only to the great wealth in Au in the Freegold Mountain area, but provide new evidence that suggests that the Golden Revenue is a reduced-porphyry system that does not display features typical of the classical oxidized porphyry Cu deposits.

ACKNOWLEDGEMENTS

We thank Yukon Geological Survey, NFR, and a NSERC Discovery grant to DL for funding & logistical support.

REFERENCES

- CARLSON, G.G. 1987. Geology of Mount Nansen (115-1/3) and Stoddart Creek (115-1/6) map areas Dawson Range, Central Yukon. *Indian and Northern Affairs Canada, Northern Affairs*, Yukon Region, Open File **1987-2**.
- MORTENSEN, J.K., APPEL, V., & HART, J.R. 2003. Geological and U-Pb constraints on base and precious metal vein systems in the Mount Nansen area, eastern Dawson Range, Yukon. *Yukon Exploration and Geology* **2002**, 165-174.
- PAUTLER, J. 2006. Evaluation Report on the Freegold Project, NTS 115I/3, 6 & 7, Latitude 62°18'N, Longitude 137°12'W, Whitehorse Mining District, Yukon, 108 p.
- SELBY, D. & CREASER, R.A. 2001. Late and mid-Cretaceous mineralization in the northern Canadian Cordillera: Constraints from Re-Os molybdenite dates. *Economic Geology*, **96**, 1461-1467.
- ROWINS, M.S. 2000. Reduced porphyry copper-gold deposits: a new variation on an old theme. *Geology*, **28**, 491-494.
- SMUK, K.A., WILLIAMS-JONES, A.E., & FRANCIS, D. 1997. The Carmacks hydrothermal event: an alteration study in the southern in the southern Dawson Range, In: *Yukon Geology 1996*, Exploration and Geological Services Division, Yukon Region, Indian and northern Affairs, Canada, 92-106.
- SMITH, M.T., THOMPSON, J.F., MOORE, K.H., BRESLER, J.R., MORTENSEN, J.K., ABE, I., & TAKAOKA, H. 2000. The Liese zone, Pogo property: a new high grade gold deposit in Alaska, in Tucker, T.L. & Smith, M.T., eds: the Tintina Gold Belt: concepts, exploration and discoveries. BC-Yukon Chamber of Mines, Cordilleran Round up special 2, 131-134.
- BINELI-BETSI, T. & LENTZ, D.R. 2009. Petrogenesis of dykes related to Cu-Au & base-metal-Au-Ag occurrences, Mt. Freegold area, Dawson Range, Yukon Territory, Canada. Extended conference abstract, 24th IAGS meeting, Fredericton, NB, Canada.

Evidence of 25-m of Vertical Metal Migration Over the High-Grade Perseverance Zinc Ore Body, Matagami, Quebec

Lynda Bloom¹ & Charles Beaudry²

¹ *Analytical Solutions Ltd, 1214-3266 Yonge St., Toronto, ON, CANADA, M4N 2L6;*
(e-mail: lynda@explorationgeochem.com)

² *IAMGOLD Corporation, 401 Bay St, Toronto, ON M5H 2Y4*

ABSTRACT: The CAMIRO 3D Geochem project (2002-2004) conducted a detailed geochemical survey over the high-grade zinc Perseverance Main Lens (14% zinc) that subcrops with a footprint of high grade sphalerite (approximately 25% zinc) over approximately 25 m. The sulphide lens subcrops beneath 25m of transported Quaternary sediments composed of glacial till, outwash gravel and varved lacustrine clay. Samples were collected at 80 sites, generally at 25 to 50 m spacings, and over 100 variables were measured including MMI, Enzyme LeachTM, aqua regia digest-ICPMS, pH, conductivity, etc. Very closely-spaced sampling (5 m spacings) was undertaken overlying the subcropping area of the massive sulphides (25 by 40 meters). Low pH and strong conductivity readings directly over subcropping mineralization, combined with subtle aqua regia-ICPMS ("AR-ICPMS") responses, are compelling evidence of vertical metal migration. A supplementary verification sampling program was undertaken by C. Beaudry in 2006 to confirm the results of the CAMIRO study and, in particular to extend sampling further into the background area to the south. A total of 34 samples were collected. The elements Zn, Cu, Co, Ti, V, Mn and Fe show significant responses over the deposit. Even with many other elements which do not show significant anomalous values over the deposit the results often show much higher variance in the target area compared to the graben or background samples.

KEYWORDS: *soil geochemistry, partial extraction, selective extraction, Matagami, Perseverance zinc deposit.*

INTRODUCTION

The high grade Perseverance Deposit, located in the historic Matagami mining district in northern Quebec, is composed of high grade massive sulphides that subcrop beneath about 25 m of transported Quaternary sediments composed of glacial till, outwash gravel and varved lacustrine clay. As such it is an excellent candidate test case for the study of non-conventional geochemical analyses since the transported cover sediments and in particular the lacustrine clays precludes the use of conventional soil sampling.

This study covers the results of deposit-scale sampling by Bloom in 2004 for CAMIRO Project 01-02-002 and supplementary soil sampling by Beaudry in 2006.

PERSEVERANCE ZINC DEPOSIT

The Perseverance property is located approximately 10km west of the town of Matagami, Quebec. The Perseverance

deposit has been drilled off at close spacing but the actual surface expression of the deposit remains relatively undisturbed except for previous logging activities. The terrain is mixed coniferous and deciduous forest in a relatively flat topography with generally poor drainage.

The Perseverance deposit is comprised of three small volcanogenic massive sulphide (VMS) deposits, namely the Perseverance, Perseverance West and the Equinox deposits that, together are estimated to contain 5.1 M Tonnes (measured and indicated) grading 14.2% Zn, 1.1% Cu, 30 gpt Ag and 0.4 gpt Au. The Perseverance deposit itself is composed of the Main Zone with 1.12 M Tonnes at 17.07% Zn, 1.20% Cu, 26 gpt Ag and 0.3gpt Au and the smaller, 200,000 Tonnes Lens 2 Zone grading 13.74% Zn, 1.94% Cu, 24 gpt Ag and 0.4 gpt Au.

The Perseverance Main Zone deposit forms a compact mass of high grade massive sulphides approximately 175 m

long, 24 m thick and 120 m down dip. The lenses have been at least partly eroded and outcrop beneath the overburden on their eastern limit. They plunge towards the west beneath the hanging wall Dumagami rhyolite and end at a depth of approximately 130 m.

The three Perseverance deposits are located in a graben structure bounded by two major NW-SE trending faults. The Perseverance block was down dropped to its current, near horizontal, position. Although there is clear evidence of late orogenic movement along these faults the similarities with other VMS environments in the Matagami district support the interpretation that these were originally syn-volcanic faults that focused hydrothermal fluid flow into the graben structure.

The Perseverance deposits are only weakly conductive because of the high sphalerite content of the massive sulphides and the general paucity of sulfides in the underlying pipe alteration zones. The Perseverance Main Zone was originally detected by a ground TEM survey in the early 80's but a drill hole failed to intersect the deposit (missed the east end by a few meters). It was the combination of the recently developed airborne MEGATEM system along with three-component borehole TEM technology that led to the discovery of the Perseverance Zone in 2000 and shortly afterwards to the other deposits at Perseverance.

GLACIAL HISTORY

The Matagami area was covered by the Labrador ice sheet during the last ice age which deposited several till layers and fluvio-glacial sediments. During the final deglaciation the Labrador ice sheet was split into two distinct entities separated by the Harricanna Moraine located approximately 50km west of Matagami. Glaciofluvial, glaciolacustrine, and, intertill organic deposits underlie the uppermost Cochrane till, and these are in turn underlain by older tills that were deposited by at least three distinct ice flows. The Cochrane advance deposited sandy,

carbonate-rich till within the evolving glacial lake Barlow-Ojibway. As the lake slowly receded in response to isostatic rebound, poor drainage and cold weather resulted in the region being covered by forest and peat bogs, depositing up to several meters of organic material.

CAMIRO 2004 3D GEOCHEM PROJECT

The objective of the 2002 – 2004 CAMIRO 3D Geochem project was to study the dispersion of elements in overburden overlying known mineralization. The Perseverance project sampling focused primarily on measuring the geochemical response over the Perseverance Main Lens that subcrops with a footprint of high grade sphalerite over approximately 25 m. Samples were collected at 80 sites, generally at 25 to 50 m spacings, and over 100 variables were measured. Very closely-spaced sampling (5 m spacings between 15040 to 15100N and along several short east-west cross lines) was undertaken overlying the subcropping area of the massive sulphides (25 by 40 meters).

Low pH and strong conductivity readings directly over subcropping mineralization, combined with subtle aqua regia-ICPMS ("AR-ICPMS") elemental responses, are compelling evidence of vertical metal migration. Commercially available partial extractions, including targets in all cases; however, the threshold was manually selected to maximize the number of anomalous samples over the target and minimize the total number of anomalous samples. The following elements show significant responses over the deposit: Zn, Cu, Co, Ti, V, Mn and Fe. Even with many other elements that do not show significant anomalous values over the deposit, the results often display much higher variance in the target area compared to the graben or background samples.

2006 SUPPLEMENTARY SAMPLING

A supplementary verification sampling program was undertaken by C. Beaudry in June 2006 to confirm the results of the CAMIRO study and, in particular to extend

sampling further into the background area to the south. A total of 34 samples were collected including 6 field duplicates. A series of samples were sent to Actlabs in Ancaster, Ontario for Enzyme Leach™ analysis and another to SDP in Australia for Soil Desorption Analysis (SDP). Only results for Enzyme Leach™ are reported here.

Samples were classified by location; over the deposit, within the Perseverance Graben or in background areas. Except for the effects of the deposit there does not appear to be any difference between samples over the graben and those in the background. Samples were also classified for underlying lithology namely Watson Lake Rhyolite (footwall) or Dumagami Rhyolite; in this case the differences were important, at least for some elements and in particular Ca and Mg.

The surface trace of the Perseverance Main and its small satellite deposit is identified over approximately 200 m along the sampling line by elevated values for a number of elements, some of which were expected, but others were surprising. All the profiled responses were tested using the hypergeometric function hypothesis tests using an alpha risk of 0.05. The same sample locations were presumed targets in all cases; however, the threshold was manually selected to maximize the number of anomalous samples over the target and minimize the total number of anomalous samples. The following elements show significant responses over the deposit: Zn, Cu, Co, Ti, V, Mn and Fe. Even with many other elements that do not show significant anomalous values over the deposit, the results often display much higher variance in the target area compared to the graben or background samples.

CONCLUSIONS

The CAMIRO and Beaudry surveys at Perseverance demonstrate that a geochemical signature can be measured where mineralization is buried under 30 m

of complicated and stratified overburden. The low conductivity of the sphalerite-rich ore appears to have still been sufficient to generate electrochemical processes capable of generating surface geochemical responses, including changes in pH, conductivity and some AR-ICPMS variables. The interpretation of partial leach anomalies requires a systematic approach to classifying anomalous values and evaluating data for both single peak and “rabbit ear” anomalies.

ACKNOWLEDGEMENTS

We would like to thank the corporate sponsors of the CAMIRO 3D Project and Noranda-Falconbridge Inc., especially Grant Arnold, the chief geologist at Matagami at the time.

REFERENCES

- CARON, S. 2004. Overburden Pionjar Percussion Drilling on the Perseverance Property, Matagami, Quebec.
- CHAUVIN, L. 1977. Géologie des dépôts meubles de la région de Joutel-Matagami; Ministère des Richesses naturelles, Dossier public 539, 106 p.
- CHAUVIN, L. & LASALLE, P. 1978. Forage dans les sédiments meubles de la région de Joutel-Matagami. Ministère des Richesses naturelles, Dossier public 560, 38 p.
- GEOCON 2002. Rapport de forage sur la propriété Persévérance.
- PASTAKIA, N. 2004. Report to Sponsors: Analytical Methods and Quality Control for the 3D Geochem Projects 2002-2004. 3D Geochem Internal Report.
- VEILLETTE, J.J. 1986. Former southwesterly ice flows in the Abitibi-Timiskaming region: implications for the configuration of the late Wisconsinan ice sheet. *Canadian Journal of Earth Sciences* 23: 1724-1741.
- VEILLETTE, J.J. 1989. Ice movements, till sheets and glacial transport in Abitibi-Timiskaming, Quebec and Ontario; *In* Drift Prospecting, ed. R.N.W. DiLabio and W.B. Coker; Geological survey of Canada Paper 89-20, 139-154.
- VEILLETTE, J.J. 1994. Evolution and paleohydrology of glacial lakes Barlow and Ojibway. *Quaternary Sciences Reviews*, 13, 945-971.

Exploration stream sediment geochemistry of the Otago region, New Zealand

Anthony B. Christie¹, & Richard Carver²

¹GNS Science, P O Box 30-368, Lower Hutt, New Zealand (e-mail: t.christie@gns.cri.nz)

²GCXplore Pty Ltd, 67 Chelmsford Road, Mt Lawley, WA 6050, Australia (e-mail: richard.carver@gcxplore.com)

ABSTRACT: New Zealand open file mining company exploration stream sediment geochemical survey data are compiled in the REGCHEM (Regional Exploration Geochemistry) database managed by GNS Science (<http://maps.gns.cri.nz/website/minmap>). Data for the Otago region include more than 2000 stream sediment samples from 19 surveys, more than 800 BLEG (bulk leach extractable gold) samples from 14 surveys and a few pan concentrate samples. The stream sediment samples were typically analysed for Au and As, and in many cases for other elements including Cu, Pb, Zn, Sb, W and Mo. The BLEG samples were analysed for Au and occasionally for As. The main exploration target was orogenic Au±W±Sb deposits in the Otago Schist, although Au deposits associated with the Dunedin volcanic complex and W deposits in the schist were also targeted. Geochemically, the orogenic Au deposits are characterised by anomalous As and Au, with some also characterised by anomalous W and/or Sb. These four elements are the best pathfinders in stream sediment geochemical surveys and the anomalous values identified were associated with known deposits. Lower Au detection limits in the more recent stream sediment, and in the BLEG surveys, enables the use of this element as the primary pathfinder for orogenic gold deposits.

KEYWORDS: *stream sediment, BLEG, geochemistry, orogenic gold deposits, Otago*

INTRODUCTION

Mining companies have carried out stream sediment sampling as part of their exploration of mineralised provinces in New Zealand. These mining company data are the only stream sediment data with any significant geographic coverage in New Zealand. There have been no systematic geochemical surveys by Government agencies and the only research data are for localised areas. Results of the mining company surveys are reported to government (Crown Minerals, Ministry of Economic Development) as a condition of the prospecting and exploration permits. Much of the archived data has been compiled in digital form in the REGCHEM (Regional Geochemistry) database (Warnes & Christie 1995) and is publicly accessible via the MinMap interface at <http://maps.gns.cri.nz/website/minmap/>.

This study describes the REGCHEM data for the Otago region (Fig. 1), an area

highly prospective for orogenic gold deposits (Crown Minerals 1982).

REGIONAL GEOLOGY AND MINERAL DEPOSITS

A large part of the Otago region is characterised by basin and range topography, with ranges of Mesozoic schist (Haast Schist Group) and basins of Cenozoic sedimentary rocks. Greyschist (sandstone and mudstone) is the predominant form of schist, although there are local areas of greenschist (volcanics).

The schist belt formed between the early Jurassic and mid Cretaceous during terrane collision beneath a fore-arc region. It hosts orogenic Au±W±Sb deposits (Fig. 1), typically lensoidal quartz veins localised along single or multiple parallel shear zones. Disseminated Au mineralisation is also present in several shear zones, including the 25 km-long Hyde-Macraes Shear Zone that hosts the Macraes deposit, currently mined by open

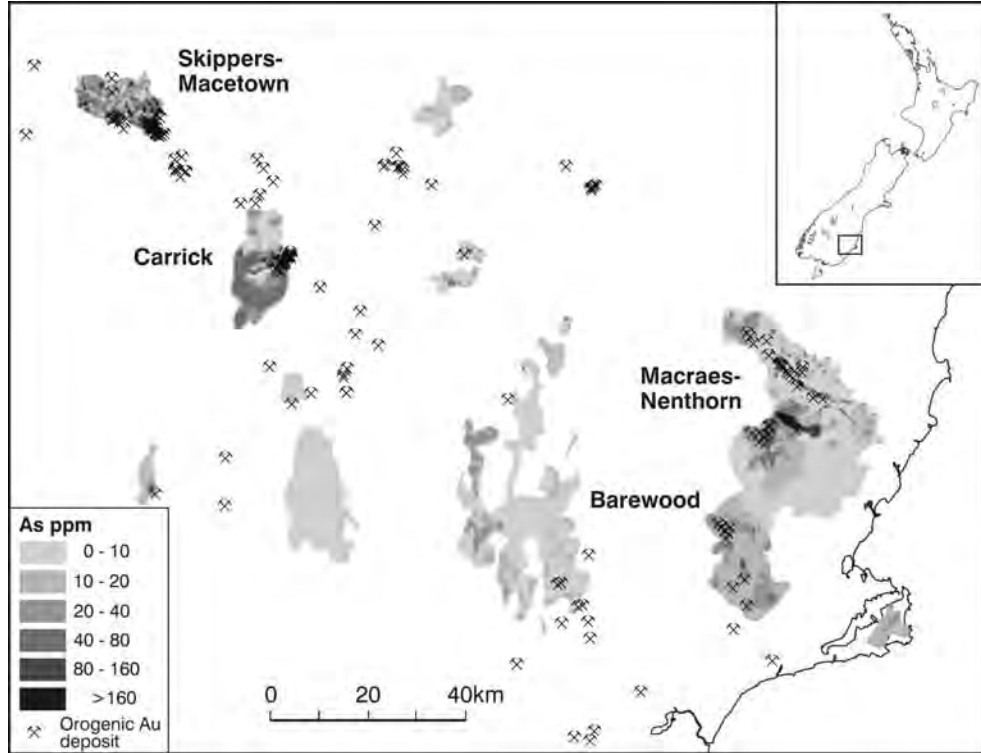


Fig. 1. As in stream sediments, and orogenic gold deposits in the Otago region.

pit and underground methods and producing 5000 kg (160,000 oz) Au annually.

The sedimentary basins contain schist and greywacke gravels eroded from the ranges, and some coal measures. Many of the alluvial gravel units and the modern river channels host placer gold deposits that have produced approximately 8 Moz Au.

Cenozoic volcanism produced the Dunedin volcanic complex, and several isolated cones of basalt are now preserved capping hills in eastern Otago.

STREAM SEDIMENT GEOCHEMISTRY

Mineral exploration stream sediment geochemical survey data for the Otago region includes more than 2000 standard stream sediment samples from 19 surveys, more than 800 BLEG (bulk leach extractable gold) samples from 14 surveys and a few pan concentrate samples (MR reports). The stream sediment samples were typically analysed for Au and As, and

in many cases for other elements including Ag, Cu, Pb, Zn, Sb, W and Mo. The BLEG samples were analysed for Au and in some cases also for As. The main exploration target was orogenic gold deposits in the Otago Schist, although one survey of the Otago Peninsula targeted potential gold deposits associated with the Dunedin volcanic complex, and several surveys sought tungsten deposits, in addition to gold.

Samples with high detection limits (e.g. 10 and 50 ppb Au) have been discarded in the following analysis. Figures 1-3 show contour maps for As, Au and W, and Table 1 lists summary statistics for some elements.

Background values between different surveys have been assessed in relation to the geology, and sample groups with elevated background values have been levelled.

Anomalous values identified for Au and As are all associated with known orogenic gold deposits (Figs 1 and 2). Arsenic has

Table 1. Percentile statistics for stream sediment samples.

El ppm	As	Cu	Pb	Sb	W	Zn
N	2226	1907	1283	572	1524	1731
Mean	23.8	22.6	19.3	15.5	25.0	63.6
P10	<10	6.0	8.0	0.4	<1	38.0
P50	10.0	15.5	13.0	1.0	2.0	59.0
P90	50.0	34.0	18.0	3.1	7.0	79.0
P97.5	130	47.0	21.0	8.0	30.0	89.0
Con	13.0	3.0	1.6	8.0	15.0	1.5

been used in some exploration surveys at the prospect scale to help define extensions of known shear zones. The orogenic gold deposits at Skippers-Macetown, Macraes and in the Waipouri-Lammerlaw Range area exhibit anomalous W values (Fig. 3). Additionally, strong W anomalies, probably related to quartz vein and stratiform W deposits, are present in the Kakanui-Waitaki area and in the Pomahaka River area west of Roxburgh. Anomalous values of Sb are

present in the Waipouri area, where stibnite has been reported associated with the orogenic Au-bearing quartz veins. Copper anomalies are present only in the Waipouri-Lammerlaw Range area, although some elevated values are present at Skippers-Macetown and Ophir. There are no Pb anomalies exhibited in the stream sediment data.

CONCLUSIONS

Geochemically, the orogenic gold deposits in Otago are delineated by anomalous Au and As, with some also characterised by anomalous W and Sb, and these four elements are the best pathfinders in stream sediment geochemical surveys. Lower Au detection limits in the more recent stream sediment surveys (e.g. 0.05 ppb Au for BLEG) enables the use of this element as the primary pathfinder for orogenic gold deposits. The Otago stream sediment data also exhibit W anomalies that are associated with W vein deposits and stratiform W deposits.

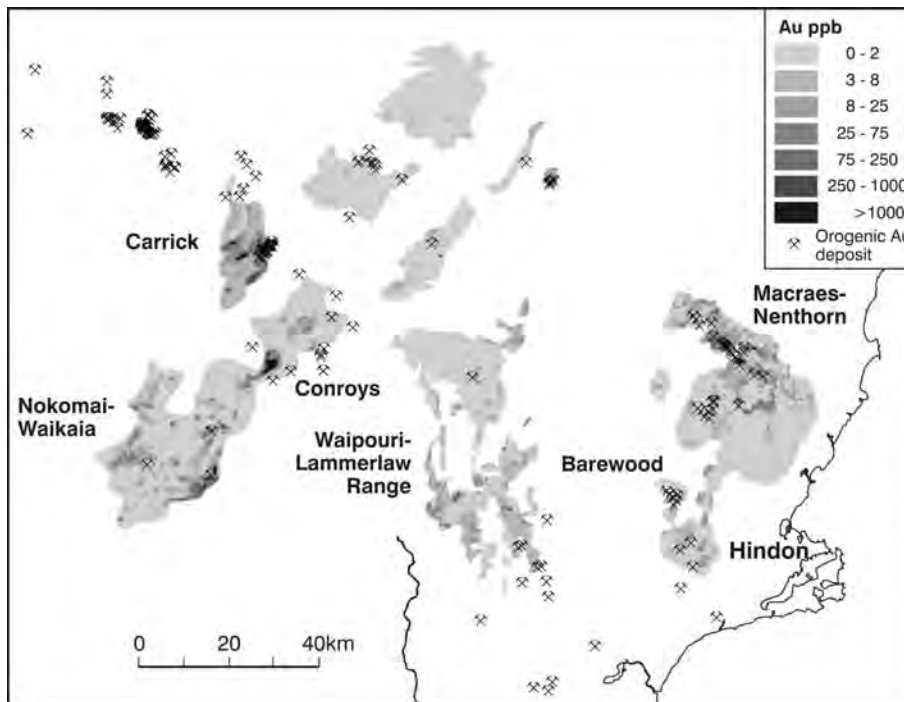


Fig. 2. Au in stream sediments (including BLEG data), and orogenic gold deposits.

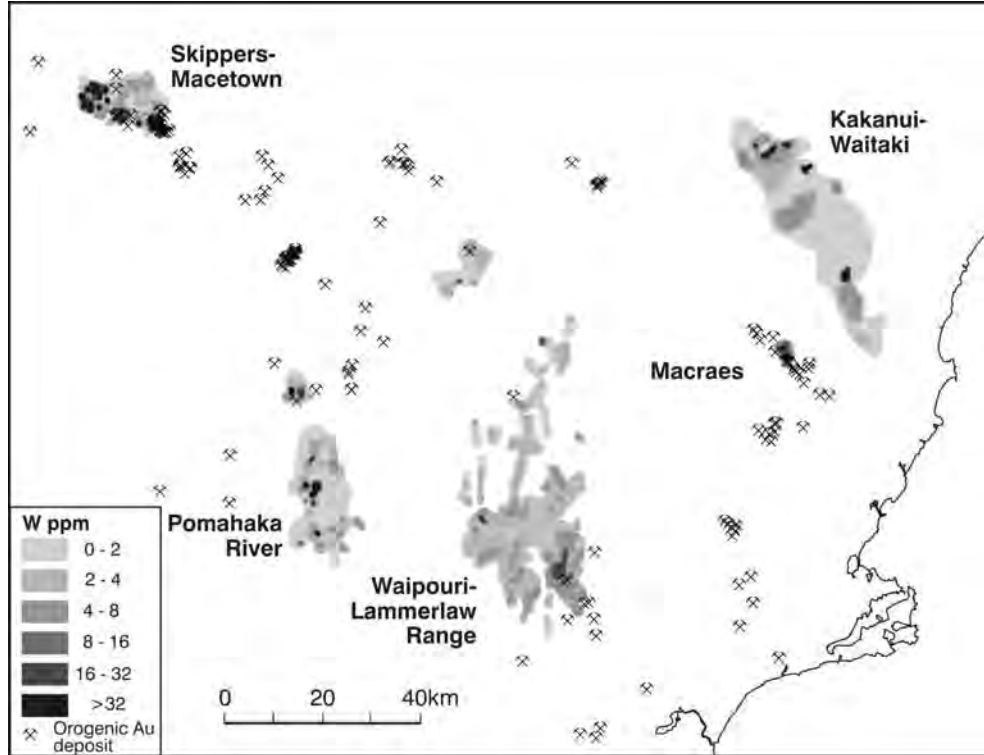


Fig. 3. W in stream sediments, and orogenic gold deposits.

ACKNOWLEDGEMENTS

Data were compiled during the GNS and Crown Minerals mesothermal gold prospectivity project (Crown Minerals 2002), and subsequently by Kenex Knowledge Systems for HPD (supplied courtesy of Glass Earth Gold Ltd) and Joe Coyle at GNS Science. Hugh de Souza reviewed and improved the paper.

REFERENCES

CROWN MINERALS 2002. Mesothermal gold in New Zealand: GIS data package and prospectivity modelling. Crown Minerals, Ministry of Economic Development and Institute of Geological and Nuclear Sciences.

MR REPORTS. Publicly available mining company exploration reports 1818, 1837, 1853, 1855, 1957, 1991, 2005, 2006, 2007, 2010, 2119, 2126, 2515, 3052, 3080, 3083, 3094, 3140, 3150, 3236, 3302, 3332, 3333, 3335, 3338, 3339, 3375, 3376, 3377, 3392, 3395, and 3465 available from https://data.crownminerals.govt.nz/MEDMG_UEST/system/mainframe.asp.

WARNES, P.N. & CHRISTIE, A.B. 1995. Regional stream sediment geochemistry database (REGCHEM) for selected regions of New Zealand. *The Australasian Institute of Mining and Metallurgy Publication Series 9/95*, 611-616.

A Hydrogeochemical Exploration Study at the Pebble Deposit, Alaska

R.G. Eppinger¹, D.L. Fey¹, K.D. Kelley¹, S.M. Smith¹, & S.A. Giles¹

¹USGS, PO Box 25046, MS 973, Denver, CO 80225, USA, (e-mail eppinger@usgs.gov)

ABSTRACT: A hydrogeochemical study using high resolution ICP-MS (HR-ICPMS) was undertaken at the giant Pebble porphyry Cu-Au-Mo deposit and we show that it is a powerful new tool in the search for concealed deposits. Surface and ground water samples were collected from regional background and the deposit areas. Rigorous quality control confirms consistent results at low parts per trillion (ppt) levels. Overall, pH varies from 3.6 to 8.2, with values below 5.1 from ponds at Pebble West, where sulphide-bearing rubble crop is thinly covered. Anomalous SO_4^{2-} and F^- are present in waters from Pebble West. Silver distribution (maximum 61 ppt) reveals a cluster of anomalous spring and pond samples in a ~10 km² area centred on Pebble. Nearly the entire upper quartiles of both Ag and Mo data fall within this area. The widespread areal extent of Mo, Ag, and several other elements in ponds and their presence in springs and boreholes are evidence that the elements are present in shallow and deep groundwater systems. Anomalous elements around Pebble West (thin cover) include Cu, Ni, Re, the REE, and Tl. Anomalous elements over both Pebble West and Pebble East (thick cover) include Ag, Mo, Sb, Th, U, V, W, and Zn.

KEYWORDS: porphyry Cu, exploration, hydrochemistry, high resolution ICP-MS, Alaska

INTRODUCTION

The U.S. Geological Survey (USGS) began exploration-oriented geochemical and geophysical studies in 2007 at the giant Pebble porphyry Cu-Au-Mo deposit, 320 km west of Anchorage, Alaska. The research is still underway. Presented here are initial findings from hydrogeochemical studies in and around Pebble.

Cations were determined by high-resolution inductively coupled plasma-mass spectrometry (HR-ICPMS), relatively new analytical instrumentation with a large dynamic range and detection limits (DLs) in the low (1-50) parts per trillion (ppt) for most elements. The exceedingly low DLs allow for recognition of elemental variations that are not possible with traditional analytical methods for water.

In 2007, regional water samples were collected along with local waters where present, along an east-west soil transect across the deposit (46 samples). In 2008, these were augmented with 83 more water samples, mostly from ponds over and around the deposit area, for a combined total of 129 water samples (Fig 1). Pond sediments were collected as well and geochemical analysis is underway.

GEOLOGICAL SETTING

As summarized by Lang *et al.* (2007), regionally, upright Jura-Cretaceous argillite, siltstone, and wacke of the Kahiltna terrane are cut by a diverse suite of intrusions that occupy a northeast-trending structural corridor, likely related to the crustal-scale Lake Clark translational fault. At Pebble, subalkalic granodiorite bodies (91-89 Ma; satellites to the Kaskanak Batholith) appear to be genetically related to mineralization.

Unconsolidated cover at Pebble consists of 0-50 m of a variety of glacial deposits over Pebble West, where the deposit is partially exposed. At Pebble East, the deposit was partially eroded and is unconformably overlain by an eastward thickening wedge of post-mineralization Late Cretaceous to Eocene volcano-sedimentary rocks, up to 600 m in thickness, which in turn are overlain by the glacial deposits.

Mineralization is present mostly in strong K-silicate altered rocks dominated by K-feldspar, and in multi-generational stock works of quartz-carbonate-sulphide veins. Laterally extensive sericite-altered rocks are peripheral to and overprint the

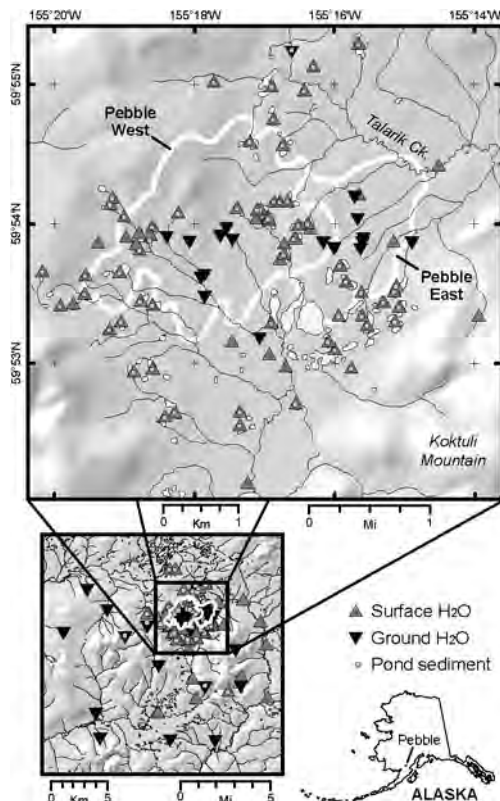


Fig. 1. Location and sample site map.

margins of the deposit; propylitic and illite assemblages are locally developed. Dominant ore minerals are chalcopyrite, molybdenite, and native gold, the latter mostly within chalcopyrite. High-grade, bornite-bearing mineralization was discovered at Pebble East in 2006.

The Pebble Cu-Au-Mo porphyry deposit contains one of the largest resources of Cu and Au in the world. The deposit consists of two zones: Pebble West, discovered by Cominco America in 1989, and Pebble East, discovered in 2005 by Northern Dynasty Minerals Inc. (NDM), who began exploring the area in 2001. In 2007, NDM and Anglo American formed the Pebble Limited Partnership. The West and East zones contain a combined resource of 72 billion pounds of Cu, 94 million ounces of Au, and 4.8 billion pounds of Mo (NDM 2009).

METHODS

Water samples were collected from ponds (78), springs (24), streams (18), and from

rare deposit area borehole seeps (9), from numerous sites in a 20-km² area around Pebble, and from background sites in a 300-km² surrounding region (Fig. 1). A thorough description of collection, analysis, and quality control (QC) procedures, and a listing of the 2007 data is presented in Fey *et al.* (2008); a similar report for 2008 analytical data will be completed in 2009.

Water samples were collected in mid-summer, precipitation-free periods, following protocols of Ficklin & Mosier (1999). On-site measurements include pH, specific conductance, alkalinity, acidity, dissolved oxygen, turbidity, and water temperature. Samples were collected in 1-litre polypropylene bottles and filtered on-site (0.45 µm) with disposable filters. Sub-samples for cation analysis were placed in acid-rinsed polypropylene bottles and acidified with ultra-pure HNO₃. Filtered, unacidified sub-samples for anion analysis were refrigerated until analyzed. In 2007, samples for Hg analysis were collected; no Hg was detected at detection limits of 0.02 µg/L, precluding collection in 2008.

Determination of 63 cations by HR-ICPMS was done on filtered/acidified samples by Activation Laboratories Ltd., using a Finnegan Mat ELEMENT 2 instrument. Anions were determined by ion chromatography and Fe²⁺ and dissolved organic carbon (DOC) by spectrophotometry in USGS labs.

A QC assessment was done for all samples. De-ionized water field blanks were collected on seven different days to evaluate process contamination. Site duplicates were taken at eight sites to evaluate repeatability and site variation. Instrumental precision was constrained by analysis of laboratory duplicate solutions, and is typically less than 5%. Finally, standard reference material (SRM) water standards were analyzed with sample batches, to assess instrumental accuracy.

All aspects of the QC assessment yielded impressive results. There was no contamination by sample processing. In blanks, very low concentrations (<5 ppb) of some major elements were detected and most trace elements were not

detected at low ppt levels. Comparison of site duplicate pairs showed agreement within 20% for most, and within 10% for some elements, even at low ppt levels. Comparison of the SRMs with accepted values showed that almost all elements were analyzed with an accuracy of ±10%.

RESULTS

Median, minimum, maximum, and upper quartile values are given in Table 1. The 7 sites with pH values below 5.1 are all from ponds in the Pebble West area, concentrated where sulphide-bearing rubble crop is exposed or under thin cover. All but two of the 32 sites with pH values below 5.88 (lower quartile) are from surface and ground water samples in and adjacent to the Pebble deposit. Borehole seeps are all circum-neutral.

Many surface waters are extremely dilute (low tens of µS/cm). The lowest specific conductance values are from ponds peripheral to or outside the deposit area. Samples with specific conductance above 89 µS/cm (upper quartile) are from ponds and ground waters within or close to the deposit area. The highest values are from borehole seeps that probably reflect a deeper ground water source.

For the major anions, the waters range from HCO₃⁻ to SO₄²⁻ dominant; the SO₄²⁻

dominant waters are from low-pH ponds in the Pebble West area (Fig. 2). The major cations are Ca dominant, with a few ponds that have stronger Na + K components. Not surprisingly, springs and borehole seeps have the highest major ion concentrations. The highest SO₄²⁻ and F⁻ concentrations occur in ground waters and lower pH ponds at Pebble West. The ratio of Fe²⁺/Fe³⁺ (median, 4.1) indicates that most waters are reduced; the more reduced waters are highest in dissolved organic carbon.

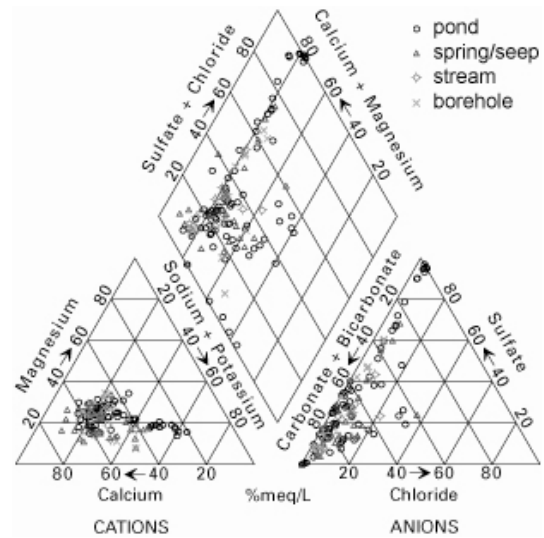


Fig. 2. Piper diagram showing major ion composition (Piper, 1944). Values for ions are in percent milli-equivalents per litre.

Table 1. Statistics for selected variables.

Variable	Min	Max	Median	Qrt ¹	unit
pH	3.6	8.2	6.4	5.88	
Sp Con ²	4	390	48	89	µS/cm
Ag	<2	60.5	<2	2.55	ppt
Cu	0.081	661	0.659	2.22	ppb
F ⁻	<0.08	2.6	<0.08	0.1	mg/L
Mo	7	18300	202	436	ppt
Ni	<0.05	19	0.138	0.379	ppb
Re	<0.1	158	0.93	5.49	ppt
ΣREE	15.8	1820	139	219	ppt
Sb	6/67	281	18.9	29.1	ppt
SO ₄ ²⁻	<0.08	84.8	3.9	11.8	mg/L
Th	0.02	21.5	0.678	1.33	ppt
Tl	0.147	122	2.3	3.73	ppt
U	0.428	967	3.1	6.63	ppt
V	5.82	3420	167	269	ppt
W	<1	18600	1.97	7.04	ppt
Zn	0.709	93	3.11	5.63	ppt

¹ Qrt is the upper quartile value for all variables except pH, where it is the lower quartile value

² Sp Con, specific conductance

The HR-ICPMS cation analytical results are a robust dataset that is remarkably free of data qualifiers for 32 of the 63 cations analyzed; an additional 14 cations have <20% censored data. Further, the low-level data have consistent map distribution patterns that make sense geologically. Described below are patterns for several possible porphyry-related elements.

Gold was not detected at the 7 ppt DL. About 59% of the samples have censored values for Ag (DL = 2 ppt) and the maximum Ag concentration is 61 ppt. Nevertheless, the distribution pattern for Ag reveals a cluster of anomalous spring and pond samples in a ~10-km² area that is centred on the Pebble deposit. The area

of anomalous Ag overlaps with that for Mo. Nearly the entire upper quartile of both Ag and Mo data falls within this area. Anomalous Ag and Mo in borehole seeps indicate that they are likely present in the deeper ground water system. However, the widespread areal extent of Mo and Ag in ponds and their presence in springs are evidence that they are also present in the shallow groundwater system, a pattern repeated for other elements.

Copper, Ni, Re, the rare earth elements (REE), and Tl exhibit similar distributions with the upper quartile of data from samples centred about Pebble West. These elements occur in ponds, springs, and borehole seeps, but are highest in the low-pH ponds. Curiously, elevated values of Cu and REE are not present in borehole seeps (circum-neutral pH).

Elements anomalous in waters over both Pebble West (thin cover) and Pebble East (thick cover) include Ag, Mo, Sb, Th, U, V, W, and Zn, occurring in all sample types. Anomalous W concentrations are confined to the deposit area, with highest concentrations in springs and boreholes.

CONCLUSIONS

- (1) The low-level HR-ICPMS data exhibit good QC at ppt levels and consistent map patterns that appear to relate to mineralization.
- (2) For pond and spring waters, nearly the entire upper quartiles of both Ag and Mo data fall within a ~10-km² area centred on the Pebble deposit.
- (3) Anomalous elements around Pebble West (thin cover) include Cu, Ni, Re, the rare earth elements (REE), and Tl.
- (4) Anomalous elements over both Pebble West and Pebble East (thick cover) include Ag, Mo, Sb, Th, U, V, W, and Zn.

(5) Hydrogeochemical exploration using HR-ICPMS delineates the variably concealed Pebble deposit and is a powerful new tool in the search for concealed deposits.

ACKNOWLEDGEMENTS

We thank Pebble Limited Partnership, particularly Jim Lang, Mark Rebagliati, Keith Roberts, Lena Brommeland, Robin Smith, Gernot Wober, and Sean Magee for logistical and scientific support for this work. Eric Hoffman and Activation Laboratories, Ltd. are thanked for contributing the HR-ICPMS analyses.

REFERENCES

- FEY, D.L., GRANITTO, M., GILES, S.A., SMITH, S.M., EPPINGER, R.G., & KELLEY, K.D. 2008. Geochemical data for samples collected in 2007 near the concealed Pebble porphyry Cu-Au-Mo deposit, SW Alaska. *U.S. Geological Survey Open-File Report, 2008-1132*, 153.
- FICKLIN, W.H. & MOSIER, E.L. 1999. Field methods for sampling and analysis of environmental samples for unstable and selected stable constituents. *Society of Economic Geologists, Reviews in Economic Geology*, **6A**, 249-264.
- LANG, J., PAYNE, J., REBAGLIATI, M., ROBERTS, K., OLIVER, J. & McLAUGHLIN, J. 2007. The super-giant Pebble copper-gold-molybdenum porphyry deposit, southwest Alaska. *Arizona Geological Society, Ores & Orogenesis*, 120-121.
- NORTHERN DYNASTY MINERALS 2009. <http://www.northerndynastyminerals.com>; email: receptionist@pebblepartnership.com
- PIPER, A.M. 1944. A graphic procedure in the geochemical interpretation of water analyses. *American Geophysical Union Transactions*, **25**, 914-923.

Spectral, geochemical, and petrographic spatial analysis of the Maze Lake orogenic gold exploration project, Nunavut

Anna Fonseca¹, Patrick Lengyel², & Cameron Rennie³

¹Krystallos Petrographic Consulting, 804 Wood St., Whitehorse YT, Y1A 2G5 CANADA
(e-mail: afonseca@northwestel.net)

²Laurentian Goldfields Ltd., 1400-625 Howe St., Vancouver, BC, V6C 2T6 CANADA

³Cameron Rennie Consulting, P.O. Box 62014, 104 Regent Ave. East, Winnipeg, MB, R2C 5G1 CANADA

ABSTRACT: The Maze Lake orogenic gold exploration project is located in the Tavani Segment of the Central Hearne Supracrustal Belt, Hearne Province. The area is underlain primarily by massive mafic volcanic and volcanoclastic rocks, with subordinate felsic volcanic flows and siliciclastic units, and intruded by synvolcanic gabbroic dykes and sills, granitoid plutons, quartz-feldspar porphyry dykes, syenites, and lamprophyre dykes and sills. Three main exploration targets were identified on the basis of till and water geochemistry and airborne magnetic surveys. Haputilik-Dogleg, the northernmost target has the most advanced exploration database, including infrared spectra and multi-element geochemical analyses of eight drill holes. A careful re-examination of the geochemical and infrared spectroscopic data from Haputilik-Dogleg, aided by transmitted light petrographic analyses allowed for re-interpretations of lithology, structure, and hydrothermal alteration. Gold mineralization in the Haputilik-Dogleg zone is associated with iron sulfides in quartz-carbonate veins, with strongly anomalous silver, tungsten, molybdenum, copper, and tellurium. Mineralization envelopes have illite with high degree of crystallinity, low water content, and high Al-OH absorption feature wavelengths, and chlorite with high Mg-OH absorption feature wavelengths. The geochemical and spectral parameters that best correlate with gold were used to identify areas of high exploration potential beyond the drilled zone.

KEYWORDS: *infrared spectroscopy, transmitted light petrography, illite crystallinity index, 4-acid digestion ICP-MS, orogenic gold*

INTRODUCTION

A careful re-examination of the Maze Lake data set, including 1,357 infrared spectral feature extraction data points, 82 samples described in detail through transmitted light petrography and infrared spectroscopic analyses, and 2,200 gold fire assay plus 48-element ICP-MS analyses obtained using 4-acid digestion for nearly complete extraction of most elements allowed for an educated re-interpretation of lithological units, structure, hydrothermal alteration, and mineralization, and highlighted prospective, undrilled targets.

GEOLOGICAL SETTING

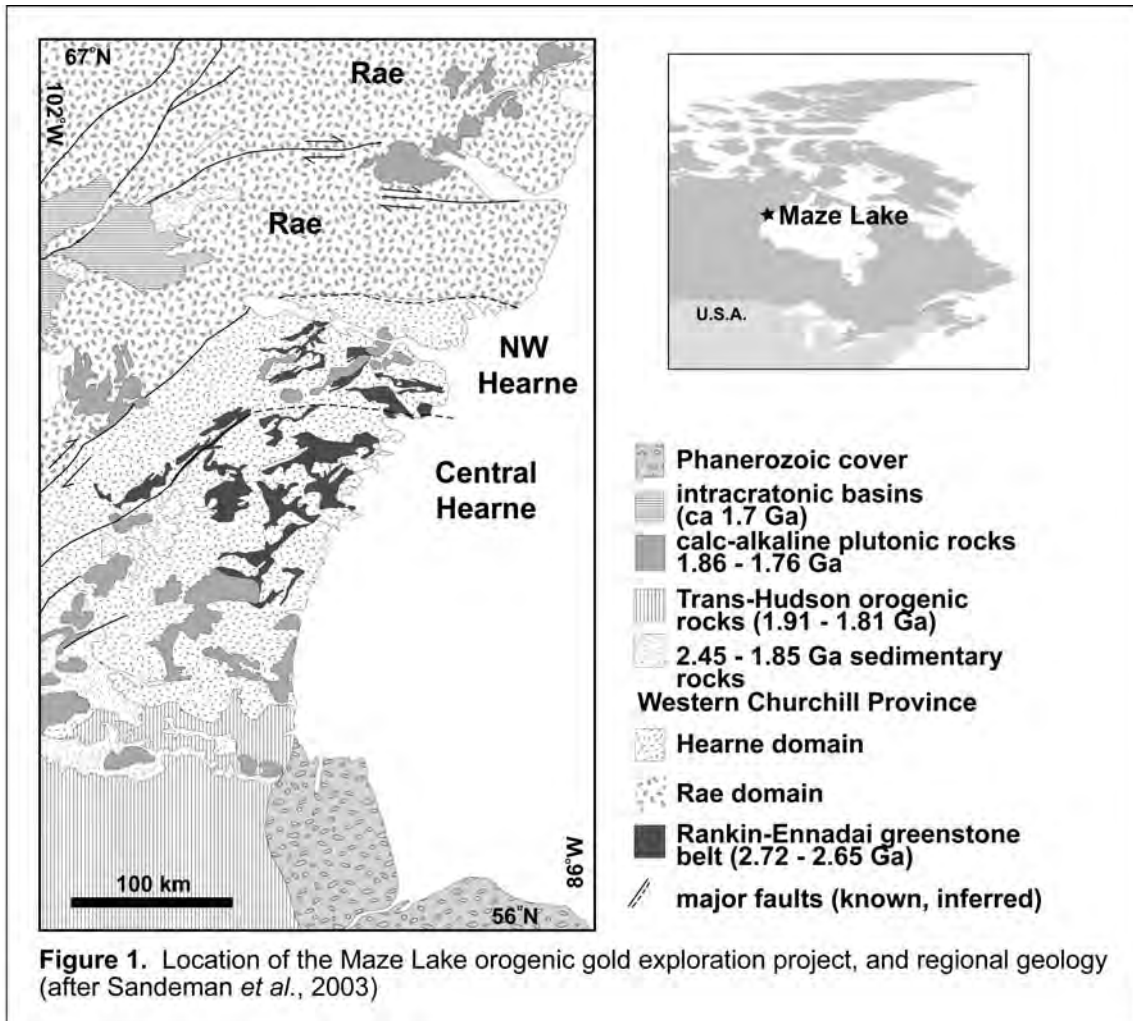
Regional Geology

The Maze Lake orogenic gold exploration project is located in the Tavani Segment of the Central Hearne Supracrustal Belt, Hearne Province (Park & Ralser 1992; Martel *et al.* 2007). The area is underlain

by Archean supracrustal rocks comprising two volcanic assemblages that are unconformably overlain by Timiskaming-type sediments, and intruded by three igneous suites. The rocks underwent deformation and greenschist facies metamorphism towards the end of each depositional sequence. The second deformation event appears to be associated with the emplacement of gold mineralization. The Archean rocks are unconformably overlain by Paleoproterozoic Hurwitz Group siliciclastic and lesser carbonate rocks, which are currently distributed as erosional remnants of regional scale synforms.

Local Geology

Park & Ralser (1992) and Tella *et al.* (2005) mapped the southern half of the Maze Lake area as part of the Geological Survey of Canada's Tavani 1:100,000



scale mapping project. They defined the stratigraphy as belonging to Kasigialik Group, which is divided into two main Archean volcanic formation (Atungag and Akliqnaktuk) and an Archean sedimentary formation (Evitruktuk). Kasigialik Group is unconformably overlain by the Archean dominantly sedimentary Taiulik formation, which is in turn unconformably overlain by Paleoproterozoic Hurwitz Group's Kinga and Tavani formations. Sikaman Resources and Placer Dome Inc. conducted geological mapping of the Maze Lake area in the 1980s and in 2003-2004, respectively.

The Maze Lake area is underlain primarily by massive mafic volcanic flows and lesser pillowed, and amygdaloidal flows and tuffaceous rocks in the southern and central portions of the property, and along the extreme northern edge. Minor

felsic to intermediate volcanic flows and siliciclastic units occur in the northern and southern ends of the property, and banded iron formations are inferred from aeromagnetic data. The volcano-sedimentary sequence is intruded by synvolcanic gabbroic dykes and sills, granitoid plutons, quartz-feldspar porphyry dykes, diorite, syenite, and lamprophyric dykes. The main exploration targets are Haputilik-Dogleg in the north, Anomaly 1 in the south, and Anomaly 2 in the centre of the property. Haputilik-Dogleg and Anomaly 1 were drilled by Placer Dome Inc. and by Laurentian Resources Ltd.

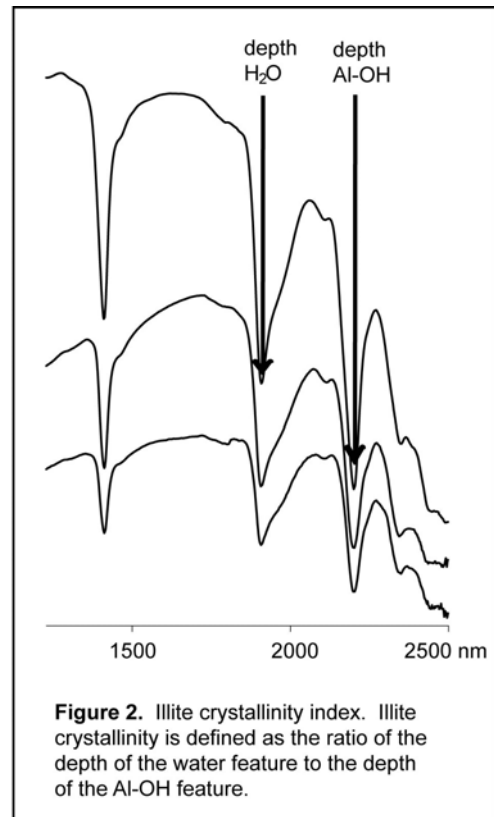
ALTERATION & MINERALIZATION

Variably texture-destructive carbonate alteration is ubiquitous throughout the Maze Lake property, and often precludes conclusive lithological identification in

hand specimen and in petrographic samples. The alteration hosting mineralized veins is dominantly potassic, though carbonate alteration is present as an early pervasive phase and as late veinlets in mineralized areas. Proximal potassic alteration consists of mosaic orthoclase replacing primary feldspar phenocrysts and fine-grained feldspars in the groundmass, very fine-grained biotite-carbonate replacing mafic phenocrysts and lithic clasts, and trace clusters of very fine-grained leucoxene. Elevated magnetic susceptibility associated with mineralized areas suggests that magnetite forms part of the potassic alteration assemblage.

Throughout the Maze Lake property, gold shows moderate positive correlation with illite crystallinity indices and with higher wavelengths for the Al-OH absorption features extracted from infrared spectroscopic analyses of drill core. Illite crystallinity index is defined as the ratio between the depth of the Al-OH spectral absorption feature centered around 2200 nm and the depth of the water feature centered around 1905 nm (Fig. 2). Gold has a weaker positive correlation with increasing Al-OH band wavelength, and a modest negative correlation with the depth of the white mica water absorption features. The spectral feature analysis suggests that gold mineralization is associated with white micas containing low structural water content and high degree of crystallinity, and with the Fe-rich chloritic end-member. Automated mineral identifications using The Spectral Geologist software is biased towards the most abundant phyllosilicates that define tectonic foliations, namely chlorite and muscovite, and therefore has limited use in characterizing alteration zones and defining new targets in the Maze Lake property. However, automated mineral identifications proved useful in the re-interpretation of lithological units. Manual mineral identifications of limited available infrared spectra indicates the presence of phengite adjacent to mineralized intervals, whereas the automated mineral identifications show a negative correlation between gold and presence of phengite.

Gold mineralization in the Haputilik-Dogleg zone is often emplaced near the contacts of lamprophyre and shonkonite intrusions, and hosted dominantly by volcanoclastic rocks, and less commonly by gabbro and quartz-feldspar porphyry dykes. Lamprophyric and shonkonitic dykes are characterized by high magnetic susceptibility, elevated HFSE and variably elevated LILE, P, and Li, and are inferred from geochemical striplogs in cases where they were not logged. Limited petrographic analyses suggest that some of what is logged as gabbroic rocks hosting mineralized veins likely consist of mafic syenite (shonkonite). Elevated sodium geochemistry coincident with intense



chloritic alteration interpreted from infrared spectroscopic automated mineral identifications of bleached drill core units logged as aplite are interpreted as propylitic alteration in a volcanic and volcanoclastic host. This interpretation allows for a simpler structural and

lithological model for Haputilik-Dogleg zone.

Mineralized intervals in drill holes of the Haputilik-Dogleg zone show correlations between gold and Ag, W, Mo, Cu, and Te. A spatial analysis using geochemical analyses for those elements and K and spectral features highlights undrilled anomalous target areas at the far east, northwest, and southwest Haputilik zone, as well as anomalous areas in Anomaly 1 zone.

CONCLUSIONS

An integrated analysis of automated spectral mineral identifications and spectral feature extractions using The Spectral Geologist software combined with multi-element ICP-MS geochemistry using 4-acid digestion, and assisted by transmitted light petrography provides an efficient and affordable means to interpret the geology and characterize the alteration of orogenic gold style deposits.

Automated feature extraction using The Spectral Geologist provides a fast means to obtain abundant and valuable data pertaining to mineral alteration. However, the automated spectral mineral identifications of foliated rocks proved strongly biased towards the phyllosilicates that define tectonic foliations, and were not sufficient to model hydrothermal mineral alteration zoning.

In spite of limitations in the dissolution of certain immobile and mobile elements, 4-acid digestion ICP-MS analyses combined

with petrographic observations provides an affordable means to track and model major oxide mobility in the Maze Lake orogenic gold property.

ACKNOWLEDGEMENTS

We thank Laurentian Goldfields Inc., and Terrane Metals Corp. for making the Maze Lake database available, and for allowing us to publish and present our findings.

REFERENCES

- MARTEL, E., VAN BREEMEN, O., BERMAN, R.G. & PEHRSSON, S. 2007. Geochronology and tectonometamorphic history of the Snowbird Lake area, Northwest Territories, Canada: New insights into the architecture and significance of the Snowbird tectonic zone. *Precambrian Research*, in press.
- PARK, A.F. & RALSER, S. 1992. Precambrian Geology of the Southwestern Part of the Tavani Map Area, District of Keewatin, Northwest Territories. *Geological Survey of Canada Bulletin*, **416**.
- SANDEMAN, H.A., HANMER, S., DAVIS, W.J., RYAN, J.J., & PETERSON, T.D. 2004. Whole-rock and Nd isotopic geochemistry of Neoarchean granitoids and their bearing on the evolution of the Central Hearne supracrustal belt, Western Churchill Province, Canada. *Precambrian Research*, **134**, 143-167.
- TELLA, S., PAUL, D., DAVIS, W.J., BERMAN, R.G., SANDEMAN, H.A., PETERSON, T.D., PEHRSSON, S.J., & KERSWILL, J.A. 2005. Bedrock geology compilation and regional synthesis, parts of Hearne domain, Nunavut. *Geological Survey of Canada, Open File* **4729**.

Porphyry Copper Indicator Minerals (PCIMs) in glacial till samples from the giant Pebble porphyry Cu-Au-Mo deposit: exploration significance

Karen D. Kelley¹, Robert G. Eppinger¹, Steven M. Smith¹, & David L. Fey¹

¹U.S. Geological Survey, Box 25046, MS 973, Denver, CO 80225 USA
(e-mail: kdkelley@usgs.gov)

ABSTRACT: Porphyry Cu indicator minerals (PCIMs) are mineral species in clastic sediments that indicate the presence of mineralization and hydrothermal alteration associated with porphyry Cu deposits. PCIMs from glacial till samples near the giant Pebble Cu-Au-Mo deposit in southwest Alaska include visible gold and jarosite. All samples including those up-ice from the deposit, contain some gold. However, tills immediately west and down-ice of Pebble contain more abundant gold, and the overall number of grains decreases fairly systematically in the down-ice direction. Furthermore, all samples in the immediate vicinity of Pebble contain more than 30% pristine grains compared to mostly re-shaped grains in distal samples. Most gold in the deposit is contained in chalcopyrite; therefore, the pristine nature of the grains likely reflects liberation during *in situ* weathering of transported chalcopyrite grains. Jarosite is also abundant (up to 25%) in samples adjacent to and up to 7 km down-ice from the deposit. Most jarosite grains have a detrital morphology (variably worn) suggesting the jarosite formed prior to glaciation. Overall, the results indicate that PCIMs in till samples may be useful for exploration of porphyry deposits in southwest Alaska.

KEYWORDS: *porphyry Cu, indicator minerals, glacial till, exploration, Alaska*

INTRODUCTION

Indicator mineralogy has been developed as an exploration tool for a variety of base metal sulfide deposits (Averill 2001, 2007). Grain abundance and morphology are among the characteristics that may be diagnostic. Indicator minerals are heavy (>2.8 S.G.) and thus concentratable, readily identifiable, and chemically stable in weathered surficial sediments. The suite of porphyry Cu indicator minerals (PCIMs) were initially determined for deposits in arid regions but have more recently been applied to those in humid areas (Averill 2007). PCIMs typically produce strong anomalies in surficial sediments due to the large size of mineralized porphyry systems (Averill 2001). PCIMs that have been used successfully include diaspore, tourmaline, FeCaMn garnet, alunite, rutile, and jarosite (Averill 2007). As part of an orientation study, the PCIM method was applied to the Pebble porphyry Cu-Au-Mo deposit, located ~320 km southwest of Anchorage, Alaska (Fig. 1). Twenty six glacial till samples were collected up- and

down-ice from the deposit. Several minerals were identified that target the deposit, suggesting that PCIMs may be useful in exploration for concealed porphyry deposits in southwest Alaska.

REGIONAL AND LOCAL GEOLOGY

The Pebble porphyry deposit contains one of the largest resources of copper and gold in the world. The deposit consists of the Pebble West and Pebble East Zones,

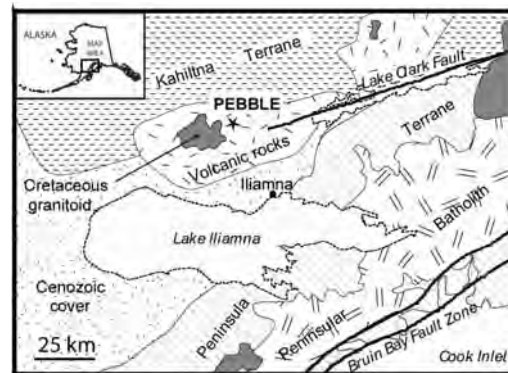


Fig. 1. Location of Pebble with major geologic and tectonic features (from Wallace *et al.* 1989).

containing a combined resource of 72 billion pounds of copper, 94 million ounces of gold, and 4.8 billion pounds of molybdenum (NDM 2009).

The Pebble deposit is located in the Kahiltna terrane, near the boundary between two lithologic packages: Jurassic and older magmatic-metamorphic rocks to the southeast, and an assemblage of Mesozoic volcanoclastic and sedimentary rocks overlain by Tertiary volcanic rocks, to the northwest. The Lake Clark fault trends northeast and is coincident with the change in lithologic packages (Haeussler & Saltus 2004; Fig. 1).

The Pebble district comprises Jura-Cretaceous andesitic argillite, siltstone and wacke, cut by diorite sills (Bouley *et al.* 1995). Diverse intrusions occupy a northeast-trending structural corridor. Subalkalic granodiorite intrusions (91-89 Ma) include the Kaskanak Batholith and smaller satellite bodies that are genetically related to Cu-Au-Mo mineralization (Lang *et al.* 2007).

The Pebble West Zone extends from surface to ~500 m depth. The East Zone, which extends to at least 1700 m depth, was partially eroded and is concealed by an eastwardly thickening wedge of Late Cretaceous to Eocene volcanic and sedimentary rocks (Bouley *et al.* 1995; Lang *et al.* 2007). Mineralization occurs in strong K-silicate alteration zones, and in multi-generational stockworks of quartz-carbonate-sulfide veins. Ore minerals include chalcopyrite, molybdenite, and native gold found mostly within chalcopyrite. High-grade, bornite-bearing mineralization occurs in the core of the East Zone (Lang *et al.* 2007).

Quaternary Geology

The Pebble area was affected by Pleistocene-age glaciers from two sources: one flowed southwestward down the Lake Clark structural trough, and the other overflowed westward from Cook Inlet. At various times, these glaciers blocked each of the three major drainages in the Pebble project area – Upper Talarik Creek and the North and South Forks of the Kuktuli River. The resulting ice-

dammed lakes filled lowlands in headward parts of each drainage (Fig. 2).

The glacial till deposits consist of poorly sorted to unsorted, nonstratified till ranging from muddy gravel to sandy coarse gravel. Pebbles and small cobbles are dominant. Surface morphology commonly includes morainal ridges, dry and water-filled kettle depressions, and meltwater channels (Hamilton 2007).

RESULTS AND DISCUSSION

Till samples (about 8 kg of material) were collected up- and down-ice from the deposit, over a total distance of about 20 km (Fig. 2). The samples were put through a shaking table (<2 mm) and gold grain counts were reported. Sieving and heavy liquid (S.G. 2.8-3.2 and >3.2) separation followed. The PCIMs were identified in the 0.25-0.5 mm fraction.

The most effective indicator minerals for targeting the Pebble deposit are gold and jarosite. Sulfide minerals (pyrite or chalcopyrite) are rare in the tills, in spite of their abundance in the deposit. Possible explanations for this are explored in the following discussion.

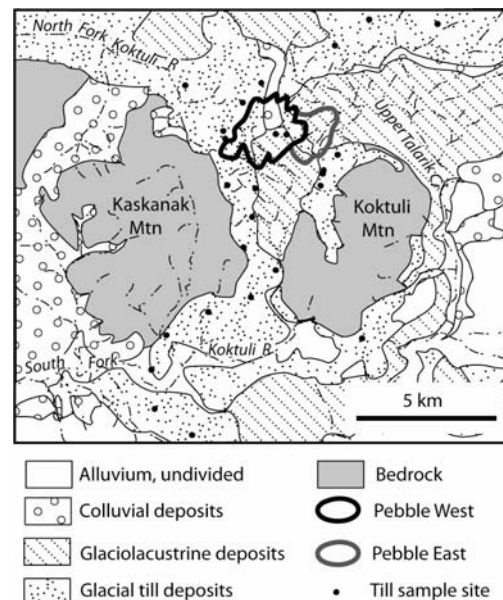


Fig. 2. Quaternary geology of the Pebble area showing sample locations (modified from Hamilton 2007).

Gold Morphology and Distribution

Gold grain abundance and shape show interesting patterns (Fig. 3). All samples contain some gold (avg. size 75 μm); even samples 8 km up-ice contain 5-10 grains. There are many possible sources of gold in the region, including porphyry, skarn, and epithermal deposits in the Lake Clark quadrangle northeast of Pebble (Bickerstaff 1998) and in the Pebble district (Hawley 2004). However, tills immediately adjacent to Pebble West contain 12 times the number of gold grains in samples up- or down-ice, and the overall number of grains decreases in the down-ice direction (Fig. 3).

Also important is the morphology (degree of rounding, polishing, bending and flatness) of the gold grains which may provide information about the transport mechanism (Averill 1988; McClenaghan 2005). All samples in the immediate vicinity of Pebble West contain 30% or more pristine grains whereas those at greater distance down-ice or up-ice contain almost exclusively re-shaped grains. The transport history of pristine grains may be interpreted in two ways: (1) gold grains were eroded from a bedrock source nearby and transported to the site with little or no surface modification (short transport distance), and (2) gold grains were liberated from rock fragments during *in situ* weathering of transported sulfide grains containing gold (Coker & Shilts 1991; McClenaghan 2005). Because most gold in the Pebble deposit is contained in chalcopyrite (Lang *et al.* 2007), the second option is the most likely, and it implies that post-glacial oxidation of the till was nearly completely sulfide destructive.

Jarosite

The distribution of jarosite in till samples is even more compelling than that for gold. Except for three samples with trace amounts, the most abundant jarosite (from 1 to 25% of the grains in the heavy mineral fraction) occurs in samples adjacent to and within 7 km down-ice from the deposit (Fig. 4). Most jarosite grains have a detrital morphology (variably

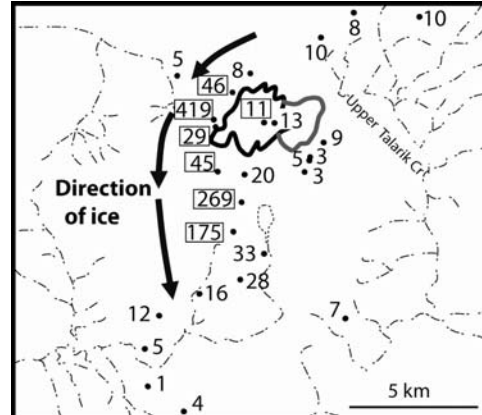


Fig. 3. Distribution of gold in till samples. The number refers to number of grains. Boxes around numbers signify >30% of gold grains are pristine.

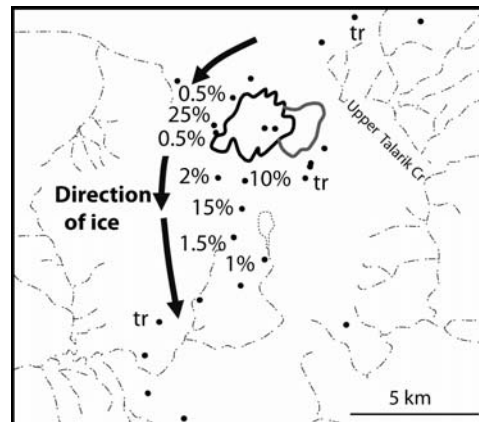


Fig. 4. Distribution of jarosite in till samples. The number refers to percent abundance.

worn), suggesting the jarosite formed prior to glaciation. Jarosite occurs in porphyry systems that have extensive supergene enrichment zones, having formed from acidic weathering of pyrite in fluctuating arid/semi-arid conditions (intermittent periods of wetness in an arid climate) (Hartley & Rice 2005). The upper portion of the Pebble West Zone is oxidized, and much of it is underlain by supergene mineralization. The Pebble East Zone lacks such supergene development. Either it was not developed there or it has been completely eroded away; in many glaciated areas (i.e., areas with till), the level of bedrock erosion is below the level of the main oxide cap development (Averill

2001). Further studies are planned to date the jarosite and identify when it formed.

CONCLUSIONS

The primary PCIMs in till samples from the Pebble deposit are visible gold and jarosite. Summary points include:

- (1) The abundance of visible gold in samples is highest adjacent to and immediately down-ice from the deposit
- (2) Within the deposit, gold occurs mostly within chalcopyrite. The pristine nature of gold in the tills suggests that it was liberated during *in situ* weathering of transported chalcopyrite grains
- (3) The presence of jarosite in tills is a good vector to mineralization.

ACKNOWLEDGEMENTS

We thank the Pebble Limited Partnership, particularly Jim Lang, Mark Rebagliati, Keith Roberts, Lena Brommeland, Robin Smith, Gernot Wober, and Sean Magee for logistical and scientific support for this work. Stu Averill (Overburden Drilling Management Limited) offered helpful discussions.

REFERENCES

AVERILL, S.A. 2001. The application of heavy indicator mineralogy in mineral exploration with emphasis on base metal indicators in glaciated metamorphic and plutonic terrains. In: MCCLENAGHAN, M.B. BOBROWSKY, P.T., HALL, G.E.M., & COOK, S. (eds.), *Drift Exploration in Glaciated Terrain. Geological Society of London, Special Publication 185*, 69-81.

AVERILL, S.A. 2007. Recent advances in base metal indicator mineralogy. *Explore*, **134**, 2-6.

BICKERSTAFF, D. 1998. Alaska resource data file, Lake Clark quadrangle, Alaska. *U.S. Geological Survey Open-File Report 1998-359*, 109 p.

BOULEY, B.A., ST. GEORGE, P., & WETHERBEE, P.K. 1995. Geology and discovery at Pebble Copper, a copper-gold porphyry system in southwest Alaska, In: SCHROEDER, T.G. (ed.), *Porphyry deposits of the northwest Cordillera of North America: Canadian Institute of Mining, Metallurgy, and Petroleum, Special Volume 46*, 422-435.

COKER, W.B. & SHILTS, W.W. 1991. Geochemical exploration for gold in glaciated terrain. In: FOSTER, R.P. (ed.), *Gold Metallogeny and Exploration*. Chapman & Hall, London, 336-359.

HAEUSSLER, P.J. & SALTUS, R.W. 2004. 26 KM of offset on the Lake Clark Fault since Late Eocene time. *U.S. Geological Survey Professional Paper 1709A*, 4.

HAMILTON, T. 2007. Surficial geologic map of the Pebble Limited Partnership's Pebble Project, *Report Series C*, <http://www.pebblepartnership.com/pages/environment/environment-pre-permitting.php>.

HARTLEY, A.J. & RICE, C.M. 2005. Controls on supergene enrichment of porphyry copper deposits in the Central Andes: A review and discussion. *Mineralium Deposita*, **40**, 515-525.

HAWLEY, C. 2004. Alaska resource data file, Iliamna quadrangle, Alaska. *U.S. Geological Survey Open-File Report 2004-105*, 118 p.

LANG, J., PAYNE, J., REBAGLIATI, M., ROBERTS, K., OLIVER, J., & MCLAUGHLIN, J. 2007. The super-giant Pebble copper-gold-molybdenum porphyry deposit, southwest Alaska. *Arizona Geological Society, Ores and orogenesis*, 120-121.

MCCLENAGHAN, M.B. 2005. Indicator mineral methods in mineral exploration. *Gechemistry: Exploration, Environment, Analysis*, **5**, 233-245.

NORTHERN DYNASTY MINERALS, INC. 2009. <http://www.northerndynastyminerals.com>

WALLACE, W.K., HANKS, C.L., & ROGERS, J.F. 1989. The southern Kahiltna terrane: Implications for the tectonic evolution of southwestern Alaska. *Geological Society of America Bulletin*, **101**, R1389-1407.

Geochemical and mineralogical exploration of sandstones in the Lublin Carboniferous Basin, SE Poland

Aleksandra J. Kozłowska¹ & Katarzyna L. Jarmolowicz-Szulc¹

¹Polish Geological Institute, Rakowiecka 4, 00-975, Warsaw POLAND
(e-mail: aleksandra.kozłowska@pgi.gov.pl)

ABSTRACT: Geochemical and mineralogical studies were performed on sandstones drilled in the Lublin Coal Basin to characterize minerals and cements. The sandstones studied are mostly arenites and subarkose and quartz wackes (rare sublithic, sporadic lithic and arkose). Quartz is the main component with subordinate feldspars, micas (muscovite and biotite) and chlorites. The diagenetic processes observed in the sandstones are: dissolution, alteration, replacement and mechanical compaction. Different types of cements are present such as clay, quartz and carbonate cements. Kaolinite (vermicular and blocky), illite and dickite are the main components of clay cements. Quartz and carbonate cements (siderite, Fe-dolomite, ankerite and Fe-calcite) are significant. The carbonates display different isotopic and fluid inclusion characteristics. The $\delta^{13}\text{C}$ data suggest that siderite and ankerite formed in the zone of microbiological methane genesis. The organic matter of the Carboniferous deposits mainly represents the humus type and R_o indices point to a maximum palaeotemperature of about 120°C. The K/Ar dating suggests that the crystallization age of diagenetic illite is from 286.5±3.4 Ma to 278±3.4 Ma.

KEYWORDS: *geochemistry, mineralogy, Carboniferous, sandstones, diagenesis*

INTRODUCTION

Rocks from 27 boreholes from the Lublin Carboniferous Basin (LCB) were analysed to characterize their mineralogy and diagenetic history (Fig. 1).

The top of the Carboniferous deposits occurs there at the depth of 2528 m in the Potycz 1 borehole and decreases towards SE in the Terebin 1 borehole.

The analysed sandstones with accompanying mudstones, claystones and subordinate conglomerates are of fluvial origin and interlayered with marine and deltaic deposits (Waksmundzka 2008).

GEOLOGICAL SETTING

The Lublin Coal Basin is the Carboniferous basin situated in SE Poland. It is located in the south-eastern part of the Polish Lowlands, close to the Teisseyre -Tornquist zone, which divides the whole territory of Poland to the Palaeozoic - Mesozoic and Precambrian platforms. The Lublin graben is an elongated NW-SE structural unit. The base of the Carboniferous in the basin is of Namurian age. The thickness of the

Carboniferous deposits increases towards the SE from about 370 m to over 1600 m.

ANALYTICAL METHODS

Standard microscopic analysis was performed on thin sections. Quantitative mineralogical and porosity data were derived by point counting. Samples were stained with Evamy's solution (calcite became purple, ankerite – blue, dolomite

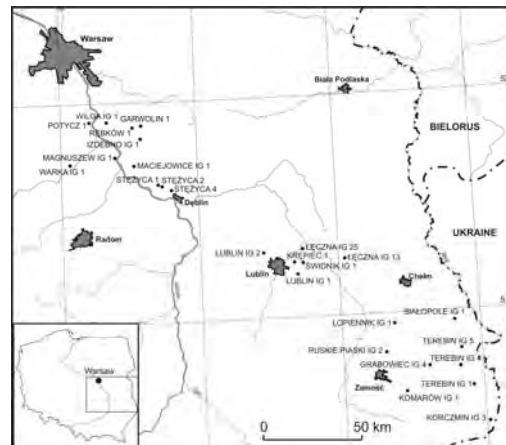


Fig. 1. Boreholes locations in the Lublin Carboniferous Basin (LCB).

and siderite – remain unstained), and analyzed using cathodoluminescence (CL) and energy dispersive x-rays (EDS). Clay minerals were determined by XRD. Fluid inclusions were analysed in the different cement types. Homogenisation temperatures of two phase inclusions (T_h) were measured on quartz, calcite and ankerite (Fig. 2), and freezing experiments performed as well. Oxygen and carbon isotopic analyses were conducted on carbonates. The fibrous illite was dated by the K/Ar method.

RESULTS AND DISCUSSION

Petrological Characteristics

Microlithofacial classification of the sandstones is based on Dott's classification modified by Pettijohn *et al.* (1972). They are mostly arenites and subarkose and quartz wackes (rare sublithic, sporadically lithic and arkosic). Quartz is the main component of the sandstones (about 60-70 vol. percent). Feldspars (6 vol. percent) are mostly represented by potassium feldspars with plagioclases in lesser amounts. Some micas (muscovite and biotite) and chlorites are observed. Mica content of arenites reaches 3 vol. %, but is higher in the wackes. Heavy minerals present include zircon, sphene, rutile and apatite. Magmatic rocks (volcanic more than plutonic) are predominant among lithoclasts (about 2 vol. %), but some metamorphic and sedimentary clasts being present too.

The detrital material is most frequently semi rounded and well sorted. It is rather loosely arranged in the arenites - the indicator of grain contacts in the sediment may be estimated at about 2.0. Point contacts are few, or absent in the wackes.

The diagenetic processes observed in the sandstones are: dissolution, alteration, replacement and mechanical compaction.

Main Components of Cements

The sandstones studied contain different types of cements, such as clay, quartz and carbonate cements. Clay cements are often a mixture of allo- and authigenic minerals. Kaolinite is the main component

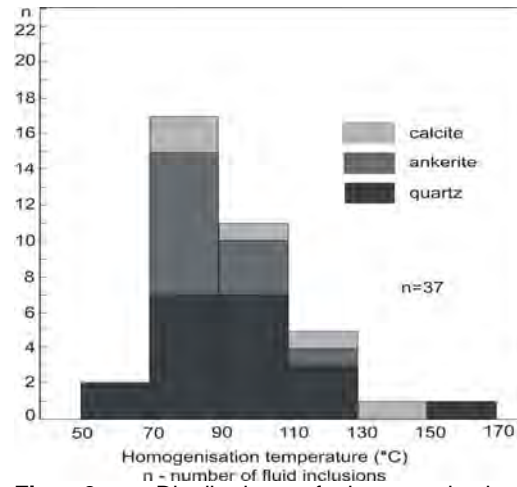


Fig. 2. Distribution of homogenisation temperatures in different cements

with a volume percentage from 4 to maximum of 19.3%. Two morphological types of kaolinite - vermicular and blocky kaolinites were observed in the Carboniferous sandstone profile. The higher amounts of the vermicular kaolinite occur in the upper parts of profiles. Dickite is present in the <2 μm and 2-10 μm fractions (XRD). Illite occurs in form of very fine plates. It coats detrital grains and fills intergranular space. K/Ar dating indicates that the crystallization age of diagenetic illite changes from 286.5 ± 3.4 Ma in the Komarow IG 1 to 278 ± 3.4 Ma in the Grabowiec IG 4 boreholes (Kozłowska 2006). Chlorite, mostly ferruginous, is developed as overgrowths and filling pore space. The presence of mixed-layered minerals illite/smectite, with over 90% illite, was indicated by XRD. Quartz, a significant component of the cements, occurs either as quartz dust mixed with clay minerals, or forms authigenic regeneration rims over the quartz grains. The percentage of quartz cement ranges from 1 to 10 vol.%, locally exceeding 20%. Fluid inclusion studies in the quartz cement revealed mostly one phase inclusions that may point to cement formation below 50°C (Roedder 1984; Goldstein & Reynolds 1994). In two phase inclusions, the homogenization temperatures fall in the interval from 58°C to 160°C.

Carbonate cement content in the studied rocks varies from 0 to 45 vol. %, mostly forming the pore filling. The following carbonates were observed (Kozłowska 2004): siderite, Fe-dolomite, ankerite and Fe-calcite. The term “siderite” corresponds to minerals from the isomorphous group $\text{FeCO}_3\text{--MgCO}_3$ with 60–100 mol percent FeCO_3 . Most siderites fall into the interval siderite – sideroplesite (Fig. 3).

Two siderite generations have been distinguished: early and late (Kozłowska 2004). Sideroplesite or siderite represent the early generation. The minerals mostly occur as finely crystalline grains or spherulites, rarely as massive forms. The $\delta^{18}\text{O}_{\text{PDB}}$ values for the siderite are in the interval from -18.37 to -4.30‰ , while the $\delta^{13}\text{C}_{\text{PDB}}$ range from -8.52 to 3.63‰ . The $\delta^{13}\text{C}$ data point to siderite formation in the zone of microbiological methane genesis (Morad 1998). The late siderite generation displays a higher MgCO_3 content, while the chemical composition corresponds to sideroplesite, and occasionally to pistomesite. These minerals often crystallize in form of rhombohedrons filling empty pore space or replacing the earlier siderite generation. Fe-dolomite and ankerite most frequently occur as isolated euhedral crystals or form massive spar cement. Two phase fluid inclusions homogenize in temperatures between 70°C and 117°C (Jarmolowicz-Szulc 1999). The $\delta^{18}\text{O}_{\text{PDB}}$ values for ankerite range from -15.11 to -7.47‰ , while the $\delta^{13}\text{C}_{\text{PDB}}$ are in the interval from -8.77 to 3.74‰ . The $\delta^{13}\text{C}$ data suggest ankerite formation in the zone of microbiological methane genesis (Morad 1998). Fe-calcite forms the pore cement, filling the inter- and intra-grain space. The fluid inclusions in calcite homogenized at temperatures from 84°C to 138°C . The $\delta^{18}\text{O}_{\text{PDB}}$ values for Fe-calcite lie in the interval from -19.35 to -3.48‰ , while the $\delta^{13}\text{C}_{\text{PDB}}$ values vary between -19.45 and 1.39‰ . The $\delta^{13}\text{C}$ data suggest Fe-calcite formation in the zone of microbiological methane genesis and of thermal decarboxilation of the organic matter (Morad 1998).

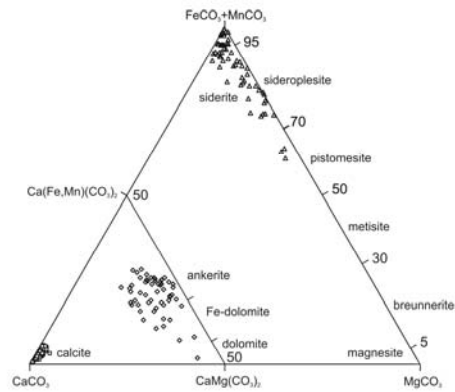


Fig. 3. Classification triangle for carbonates

Other types of cements include anhydrite, barite, pyrite, iron hydroxides haematite, albite and apatite and are subordinate.

The whole diagenetic sequence of the rocks drilled in the boreholes in LCB may be shown diagrammatically as in Fig. 4.

Organic matter in the Carboniferous deposits mainly represents the humus type with vitrinite as a main component. The R_o index measured on the authigenic vitrinite increases towards the bottom of the deposits from 0.49 to 1.15% (Grotek 2005). These data point to a maximum palaeotemperature of about 120°C .

The sandstone porosity in thin sections oscillates from below 1 to 22.3 vol. % of rock (average 8 % vol.) Primary porosity dominates over secondary porosity in the sandstones.

CONCLUSIONS

The following conclusions may be drawn from the present contribution:

- (1) The Carboniferous sandstones in the boreholes in LCB are represented by arenites and wackes, mainly quartz, subarkose and sublithic;
- (2) Space between the detrital grains is filled in, totally or partly, by matrix and/or different types of cement;
- (3) Clay minerals, quartz and carbonates predominate among the cements;

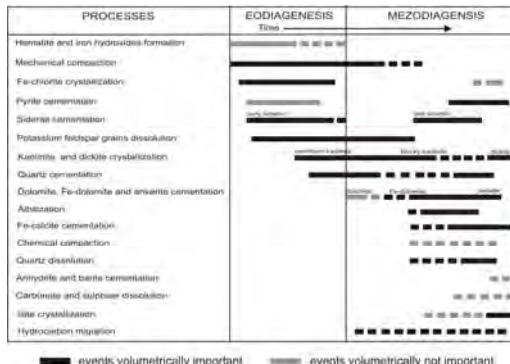


Fig. 4. Diagenetic sequence for studied rocks.

(4) The porosity (primary and secondary) of the sandstones ranges from below 1% to 22.3 vol. %.

(5) During their diagenesis, the Carboniferous deposits were subjected to temperatures up to a maximum of 120°C.

(6) The Carboniferous deposits reached their maximum temperatures at the end of the Carboniferous, while the diagenetic processes carried on until the Early Permian.

ACKNOWLEDGEMENTS

The present research was performed with a grant of the Polish Ministry of Science and High Education to A. Kozłowska.

REFERENCES

GOLDSTEIN, R.H. & REYNOLDS, T.J. 1994. Systematics of fluid inclusions in diagenetic

minerals. *SEPM Short Course*, **31**.

GROTEK, I. 2005. Variability of coalification degree of the dispersed organic matter in the Carboniferous deposits along the margin of the East European Platform. *Polish Geological Institute Bulletin*, **413**, 5-80.

JARMOŁOWICZ-SZULC, K. 1999. Fluid inclusion systematics in the filling of the pore space of Paleozoic sedimentary rocks in the Polish Lowlands. *Przegląd Geologiczny*, **47**, 542-546.

KOZŁOWSKA, A. 2004. Diagenesis of the Upper Carboniferous deposits at the margin of the Lublin graben and the Warsaw block. *Polish Geological Institute Bulletin*, **411**, 5-70.

KOZŁOWSKA, A. 2006. K-Ar dating of authigenic illite from sandstones and thermal history of the Lublin Carboniferous basin (SE Poland). *Sediment 2006. Göttingen, Abstracts*, **106**.

MORAD, S. 1998. Carbonate cementation in sandstones: distribution patterns and geochemical evolution. *Special Publications of International Association of Sedimentologists*, **26**, 1-26.

PETTIJOHN F.J., POTTER P.E., & SIEVER, R. 1972. *Sand and sandstone*. New York, Springer Verlag.

ROEDDER, E. 1984. Fluid inclusions. *Reviews in Mineralogy, Mineralogical Society of America*, **2**.

WAKSMUNDZKA, M.L. 2008. Correlation And Genesis Of The Carboniferous Sandstones On The Basis Of Sequence Stratigraphy and Their Hydrocarbon Potential In: *NW And Central Parts of the Lublin Graben. Polish Geological Institute Bulletin*, **429**, 215-224.

Target delineation by Fuzzy Logic approach at East-Kahang Porphyry Cu-Mo deposit, Central Iran

Ahmad R. Mokhtari¹, Hooshang Asadi-Haroni¹,
Seyed-Hassan Tabatabaei¹, & Somayeh Akbar¹

¹Department of Mining Engineering, Isfahan University of Technology, Isfahan IRAN
(e-mail: ar.mokhtari@cc.iut.ac.ir)

ABSTRACT: Mineral potential mapping in a GIS environment is becoming a common practice at different exploration scales. In this study information synthesis, by using a knowledge-based Fuzzy Logic method, has been examined on four multiclass maps extracted from detailed exploration data from the East-Kahang porphyry Cu-Mo deposit. Integration of geochemical data, mapped lithological/alteration units and structural controls, that could be associated with porphyry copper mineralization, are used to rate high potential areas for further drilling. This is achieved by validating the data integration model against elevated values of copper from previously drilled holes.

KEYWORDS: Information Synthesis, Fuzzy Logic, Data Integration, Porphyry Copper, Iran

INTRODUCTION

Data integration methods, within a Geographic Information System (GIS), are largely used to delineate mineral exploration targets on a regional scale (Asadi & Hale 2000; de Quadros *et al.* 2006). In this study, a Fuzzy Logic method is employed to integrate surface exploration data over the 1 Km² East-Kahang porphyry Cu-Mo deposit in order to predict potential hidden mineralized zones on a local scale.

The Kahang deposit is in the central part of the Urumieh Dokhtar belt, the main volcanic arc of Iran (Fig. 1). Kahang was discovered in 2002 by mapping hydrothermal alteration using Landsat-TM satellite imagery data. In the Kahang area, there are three separate mineralized zones (East, Central and West) within a 16 km² porphyry type alteration system. The exploration activities, completed in the East-Kahang, include detailed geological mapping and systematic geochemical and geophysical surveying, which have led to deep drilling. Three out of five bore holes, drilled at East-Kahang, intersected a number of relatively deep Cu-Mo mineralized zones. In order to design the best borehole locations for the next phase of drilling, an integrated

analysis of the surface exploration data is employed using a Fuzzy Logic technique.

GEOLOGY OF THE AREA

The major rock units in the East-Kahang are made up of andesite, volcanic breccia, dacite, quartz-diorite, diorite and locally mineralized hydrothermal breccia (Fig. 2). Eocene andesite and volcanic breccias showing propylitic alteration are the oldest units in the area. They have been intruded by dacite, mostly showing phyllic alteration associated with weak copper mineralization. Quartz-diorite and dioritic



Fig. 1. The location of Kahang deposit in the Urumieh Dokhtar Volcanic Arc.

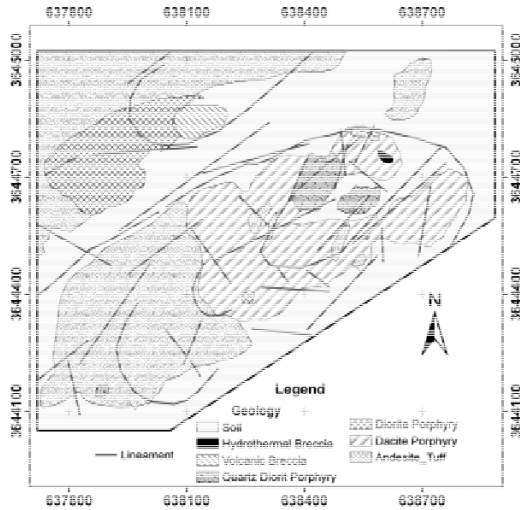


Fig. 2. Input lithological units and structures in the Fuzzy Logic model.

stocks with phyllic and propylitic alterations have intruded into dacite and andesites, causing alteration of older units and Cu-Mo mineralization (Fig. 3). The structural controls consist of linear and semi-circular features, some of which associated with Cu-Mo mineralization.

PRINCIPALS OF FUZZY DATA FUSION

Fuzzy Logic is a knowledge driven technique that works in mineral exploration on the basis of assigned weights to the different memberships/input layers, possibly associated with certain mineralization. Fuzzy membership values need to be determined by expert knowledge. The assigned weights for the memberships are then integrated, using different Fuzzy operators, for production of the final mineral prospectivity map. The Fuzzy operators applied in this study are as follows:

Fuzzy OR:

$$W_{Combination} = MAX(W_A, W_B, W_C, \dots) \quad (1)$$

Where W_A , W_B and W_C are weights of different memberships, associated with Cu-Mo mineralization.

Fuzzy PRODUCT:

$$W_{Combination} = \prod_{i=1}^n W_i \quad (2)$$

Where n is the number of memberships and W_i is the given weight for each certain membership.

Fuzzy SUM:

$$W_{Combination} = 1 - (\prod_{i=1}^n (1 - W_i)) \quad (3)$$

and,

Fuzzy GAMMA:

$$\mu_{Combination} = (Fuzzy\ Algebraic\ Sum)^{\gamma} * (Fuzzy\ Algebraic\ Product)^{1-\gamma} \quad (4)$$

Based on the importance of Fuzzy Product or Fuzzy Sum, Gamma values could be changed between 0 to 1.

INPUT LAYERS

Input map layers into Fuzzy Logic Operators include lithologies and hydrothermal alteration plus their ranges of influence (buffer zone), lineament density maps and multiplicative geochemical maps. Input map layers are explained in the following sections.

Lithology and Alteration

The lithological and hydrothermal alteration units from the geological map of the area (1:1000 scale) are converted to an appropriate format for information synthesis. By considering the conceptual models for porphyry copper deposits and

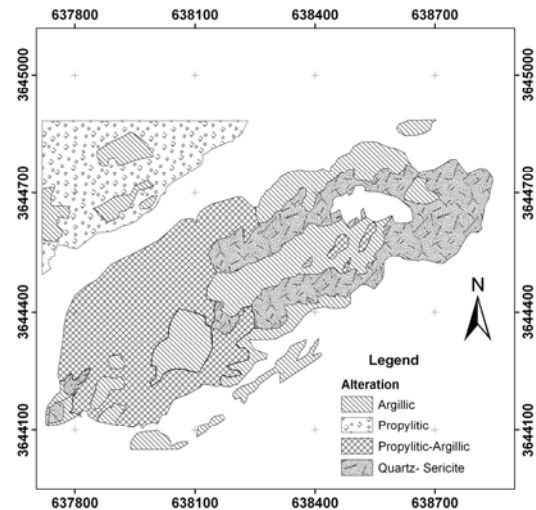


Fig. 3. Input hydrothermal alteration units in the Fuzzy Logic model.

characteristics of the mineralisation at East-Kahang, and based on expert knowledge, weights between 0.3 – 0.9 are assigned to appropriate lithological units and hydrothermal alteration (Tables 1 & 2).

Lineaments

The structural layer input is prepared by mapping linear and semi-circular structures from high resolution multi spectral Quick Bird satellite images as well as by digitizing them from the 1:1000 geological map of the area. These structures could control the migration of hydrothermal fluids and formation of porphyry copper mineralization. Using all lineaments and semi-circular structures, a lineament density map is prepared and weights are accordingly given to each structural density unit. The lineament density map is prepared by computing the magnitude per unit cell from linear/circular features in a given radius (30 m). The allocated weights are shown in Table 3.

GEOCHEMISTRY

Seventy soil samples were systematically collected over the East-Kahang area in a 150 by 150 m grid. The samples were analysed for 44 elements by ICP-MS at Amdel Limited lab in Australia. Using statistical techniques, it was decided to produce a multiplicative Cu*Mo map, as better defined anomalies can be achieved by multiplicative haloes (Beus & Grigorian 1977). The Cu*Mo map is then classified into four classes for final data integration (Fig. 4). Multiplicative Cu*Mo geochemical classes and their assigned weights are shown in Table 4.

FUZZY INTEGRATION MODEL

In order to prepare the final multi-class predictor map, the input weighted layers are fused using various Fuzzy operators (Fig. 5). Figure 6 is a reclassified final Fuzzy map, predicting the high potential areas for further drilling at East-Kahang. To validate the accuracy of the Fuzzy model, the projected Cu values of the completed drill holes are overlain on the final predictive map. The results show

Table 1. Fuzzy weights assigned to lithological units and their 20 m buffered zones.

Lithology Layer		Weight
Rock Type	Hydrothermal Breccia	0.9
	Dacite Porphyry	0.8
	Quartz-Diorite-Porphyry	0.8
	Volcanic Breccia	0.7
	Diorite Porphyry	0.5
	Andesite - Tuff	0.5
	Soil	0.5
Rock Buffer	Hydrothermal Breccia	0.9
	Dacite Porphyry	0.8
	Quartz-Diorite-Porphyry	0.8
	Volcanic Breccia	0.6

Table 2. Fuzzy weights assigned to alteration units and their 20 m buffered zones.

Alteration Layer		Weight
Alteration	Quartz-Sericite	0.9
	Argillic	0.7
	Propylitic-Argillic	0.4
	Propylitic	0.3
Buffer	Quartz-Sericite	0.8

Table 3. Lineament density classes and their Fuzzy weights.

Class		Weight
Lineament Density	>45	0.9
	45	0.6
	35	0.3
	<15	0

Table 4. Multiplicative geochemical classes and their weights.

Class		Weight
Geochemistry (Cu*Mo) ppm ²	>3500	0.9
	1000-3500	0.7
	500-1000	0.5
	<500	0.1

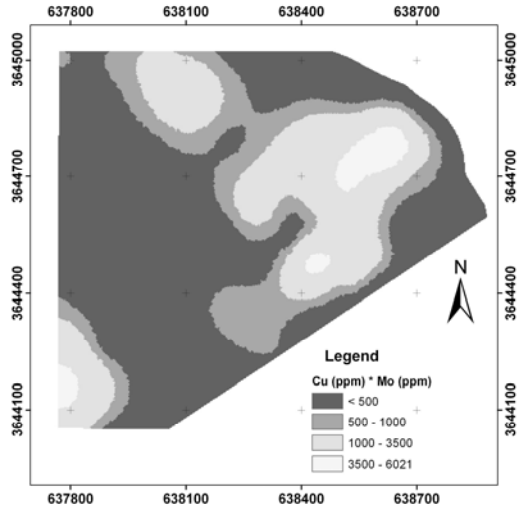


Fig. 4. Input Cu*Mo geochemical map in the Fuzzy Logic Model.

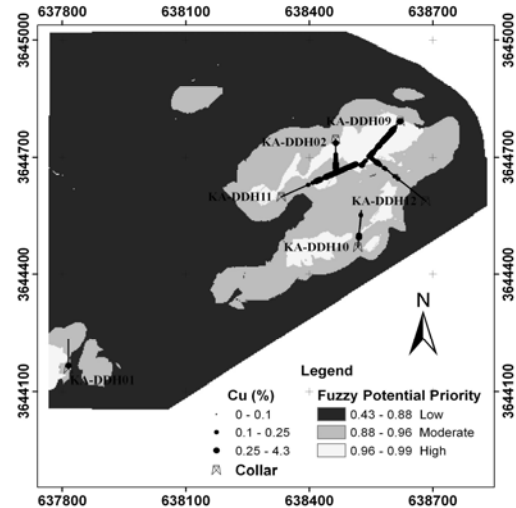


Fig. 6. Fuzzy potential priority map at East-Kahagn deposit.

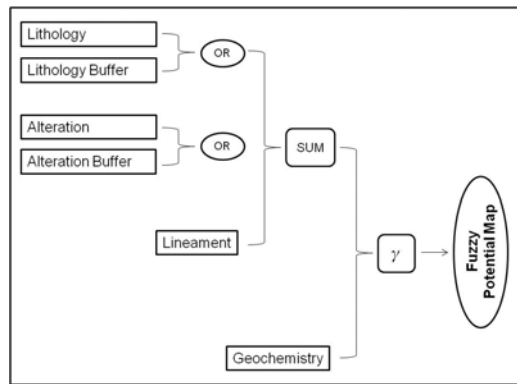


Fig. 5. Flow chart of the input data integration method in Fuzzy potential mapping.

relatively significant correlation between the high and moderate potential areas with the elevated Cu values in the boreholes.

CONCLUSION AND RECOMMENDATIONS

Although, methods of data integration for target detection are mostly used on a regional scale, in this study the Fuzzy

approach is successfully employed on a local scale in the East-Kahang Cu-Mo deposit to map high potential areas, for further drilling.

It is recommended to use data fusion techniques such as the Fuzzy approach or other methods like the Neuro-Fuzzy on surface data to locate the most promising sites for drilling.

REFERENCES

- ASADI, H.H. & HALE, M. 2000. A predictive GIS model for mapping potential gold and base metal mineralization in Takab area, Iran. *Computer & Geosciences*, **27**, 901-912.
- BEUS, A.A. & GRIGORIAN, S.V. 1977. Geochemical exploration methods for mineral deposits. *Applied Publishing Ltd. Illinois, USA*.
- DE QUADROS, T.F.P., KOPPE, J.C., STRIEDER, A.J., & COSTA, J.F.C.L. 2006. Mineral-Potential Mapping: A Comparison of Weights-of-Evidence and Fuzzy Methods. *Natural Resources Research*, **15**, 49-65.

Carlin-type gold geochemical patterns delineated by different-density data

Lanshi Nie^{1,2,3} & Xueqiu Wang^{2,3}

¹China University of Geosciences, 29 Xueyuan Rd, Beijing, 100083 CHINA
(e-mail: nielanshi@igge.cn)

²Institute of Geophysical and Geochemical Exploration, Langfang, 065000, Hebei CHINA

³Key Laboratory of Applied Geochemistry, CAGS, Langfang, 065000, Hebei CHINA

ABSTRACT: The world's second largest Carlin-type gold province occurs in southwest China. The RGNR project covering the total area of the metallogenic province provides an excellent opportunity for insight into the multi-scale geochemical patterns using different data densities. The results show that local geochemical anomalies delineated by 1 datum/4km² can define individual ore deposits, regional anomalies delineated by 1 datum /16 km² reveal ore clusters, while geochemical provinces delineated by 1 datum/100 km² show the metallogenic province and the large deposit clusters.

KEYWORDS: *Carlin-type gold deposit, geochemical pattern, data density, ore cluster*

INTRODUCTION

Carlin-type gold deposits are currently being targeted and mined in Nevada, USA and in the southwest of China. The deposits are characterized by decarbonation, argillization, sulfidation, and silicification of typically calcareous sedimentary rocks (Hofstra & Cline 2000).

Many detailed studies have focused on local-scale geochemical anomalies for ore deposits. Limited attention has been paid to the regional geochemical patterns related to gold ore clusters or provinces. In this paper, we use different densities of data to display multi-scale geochemical patterns related to ore deposits, deposit clusters and metallogenic provinces of the Carlin-type gold deposits in the southwest of China.

GEOLOGICAL SETTING

The world's second largest Carlin-type gold province next to that in Nevada, USA is located in the boundary region of Guizhou, Yunnan and Guangxi provinces, with a total area of approximately 150,000km², and a central area of approximately 20,000 km² in Guizhou (Fig. 1).

Tectonically, it is situated in the western

part of the South China Fold Belt adjacent to the north Yangtze Platform (Nie 1997). The outcropping rocks consist mainly of graywacke, siltstones, claystones, carbonates, argillites, carbonaceous slates, and siliceous rocks of Devonian, to Triassic age (Fig. 1). Gold mineralization occurs mainly in Devonian and Triassic strata as veins and as lenticular or layer-like bodies hosted by carbonaceous slate, siltstone, sandstone, argillite and carbonate (Nie 1997). Over 30 gold deposits have been discovered and 68 prospects have been identified, with total gold reserves of over 300 tons. The large deposits include Lannigou, Zimudang, Getang, Bangi, Jinya, etc. (Fig. 1).

METHODOLOGY FOR DELINEATION OF GEOCHEMICAL PATTERNS

A large Carlin-type gold deposit named Lannigou was found by a regional geochemical survey, as a part of the RGNR project (Xie 1997), in 1986 at a scale of 1: 200,000 in the Anlong map sheet of Guizhou (Wang & Xie 2000; Wang *et al.* 2007). Since then the RGNR project using -60 mesh fraction stream sediment samples has covered all of the Carlin-type gold province in the southwest of China. The project data provide an

excellent opportunity for insight into the different-scale geochemical patterns using different data densities.

The database of the RGNR project consists of 1 datum per 4 km². In this paper three densities of data were used to delineate the different-scale geochemical patterns.

(1) An average value taken from a grid of 10 × 10 km, i.e. 1 datum per 100 km², is used to produce a 1:1,000,000 scale geochemical map.

(2) An average value taken from a grid of 4 × 4 km, i.e. 1 datum per 16 km², is used to produce a 1:500,000 scale geochemical map.

(3) One datum taken from a grid of 2 × 2 km, i.e. one per 4 km², is used to produce a 1:200,000 scale geochemical map.

Smoothed contour surface maps (contour maps where the areas between the isolines are filled with colours) were produced.

RESULTS

Figures 2, 3, and 4 show geochemical patterns delineated by densities of 1 datum/ 100km², 1 datum/16km² and 1 datum/4km² respectively.

The results show that: (1) the general distribution area and direction of gold geochemical anomalies are very consistent for the three data densities, (2) geochemical anomalies delineated by the three density data coexist in the central area of the Carlin-type gold province containing large gold deposit clusters in Guizhou (Zimudang-Yanshang and Lanigou-Banqi clusters), (3) 1 datum per 100km² can only delineate large geochemical anomalies and miss small anomalies, for example a small gold cluster of the Dachang-Lamo is not delineated by this density (Fig. 2), (4) 1 datum per 16km² can delineate all the gold clusters (Fig. 3), (5) 1 datum per 4km² can not only delineate regional anomalies produced by deposit clusters

but also delineate local anomalies produced by single deposits (Fig.4).

CONCLUSIONS AND DISCUSSION

Geochemical patterns are related to choice of map scale, which depends on densities of data. What map scale and data density used mainly depends on the size of the surveyed area and the purpose of the mapping study.

The preferred map scales and data densities for delineation of different scale geochemical patterns are as follows.

(1) Geochemical provinces related to Carlin-type metallogenic provinces can be delineated by the 1: 1,000,000 map at a density of one datum per 100 km².

(2) Regional geochemical anomalies related to Carlin-type deposit clusters can be delineated by the 1: 500,000 map at a density of one datum per 16 or 25 km².

(3) Local geochemical anomalies related to ore deposits can be delineated by the 1: 200,000 map at a density of one datum per 4 km² or by higher densities of data.

ACKNOWLEDGEMENTS

We would like to thank the Ministry of Science and Technology and the Ministry of Finance for financial support (projects: 2007CB411406 and Sinoprobe04).

REFERENCES

- HOFSTRA, A.H. & CLINE, J.S. 2000. Characteristics and models for Carlin-type gold deposits. *Reviews in Economic Geology*, **13**, 163–220.
- NIE, F.J. 1997. An overview of the gold resources of China. *International Geology Review*, **39**, 55-81.
- WANG, X.Q. & XIE, X.J. 2000. *Exploration Geochemistry of Gold*. Shandong Science Publishing House, Jinan.
- WANG, X.Q., ZHANG, Q., & ZHOU, G.H. 2007. National-scale geochemical mapping in China. *Journal of Geostandards and Geoanalytical Research*, **31**, 311-320.
- XIE, X.J. MU, X.Z., & REN, T.X. 1997. Geochemical mapping in China. *Journal of Geochemical Exploration*, **60**, 99-113.

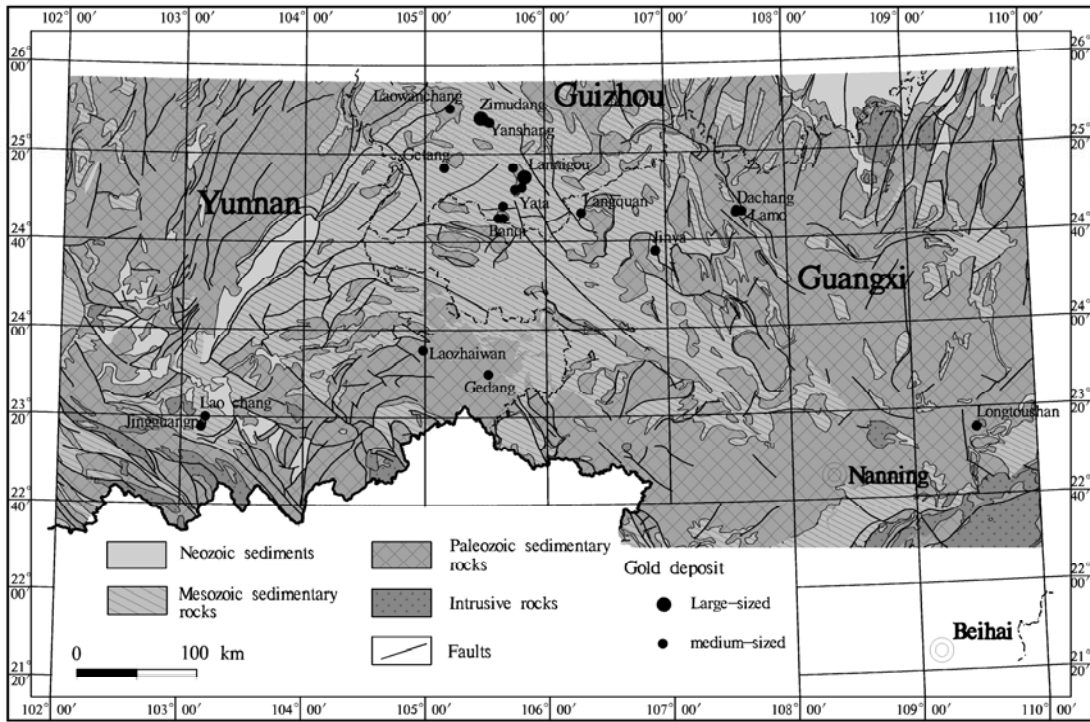


Fig. 1. Geological map with Carlin-type gold deposits in southwest China.

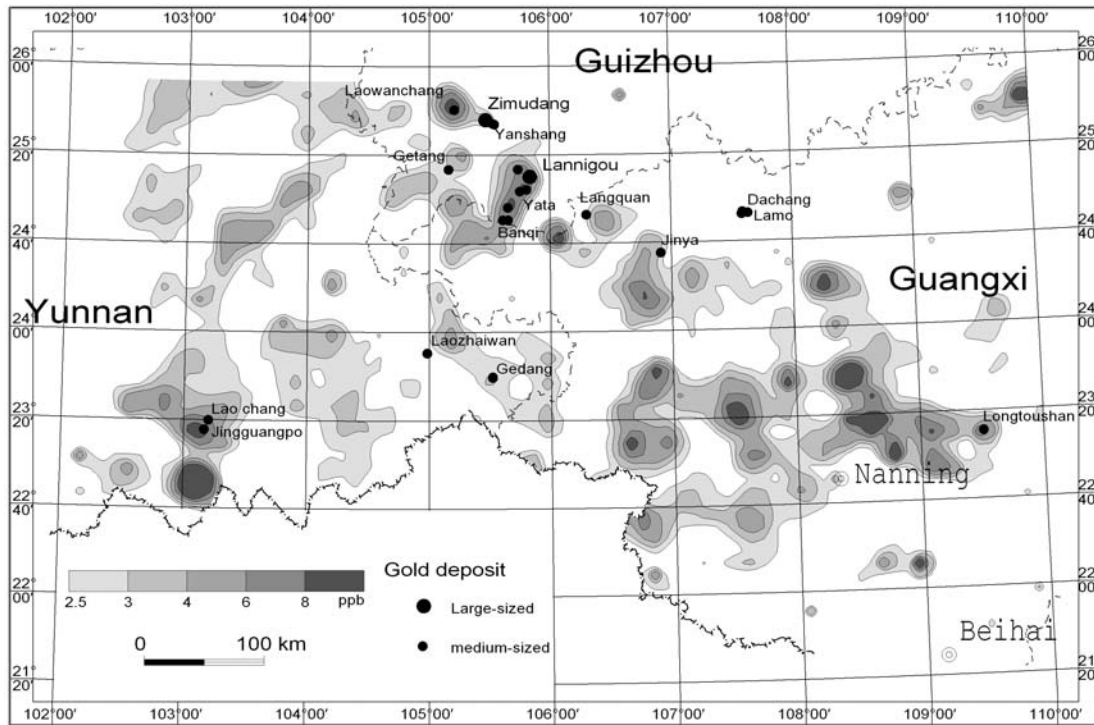


Fig. 2. Gold geochemical pattern delineated by 1 datum per 100 km².

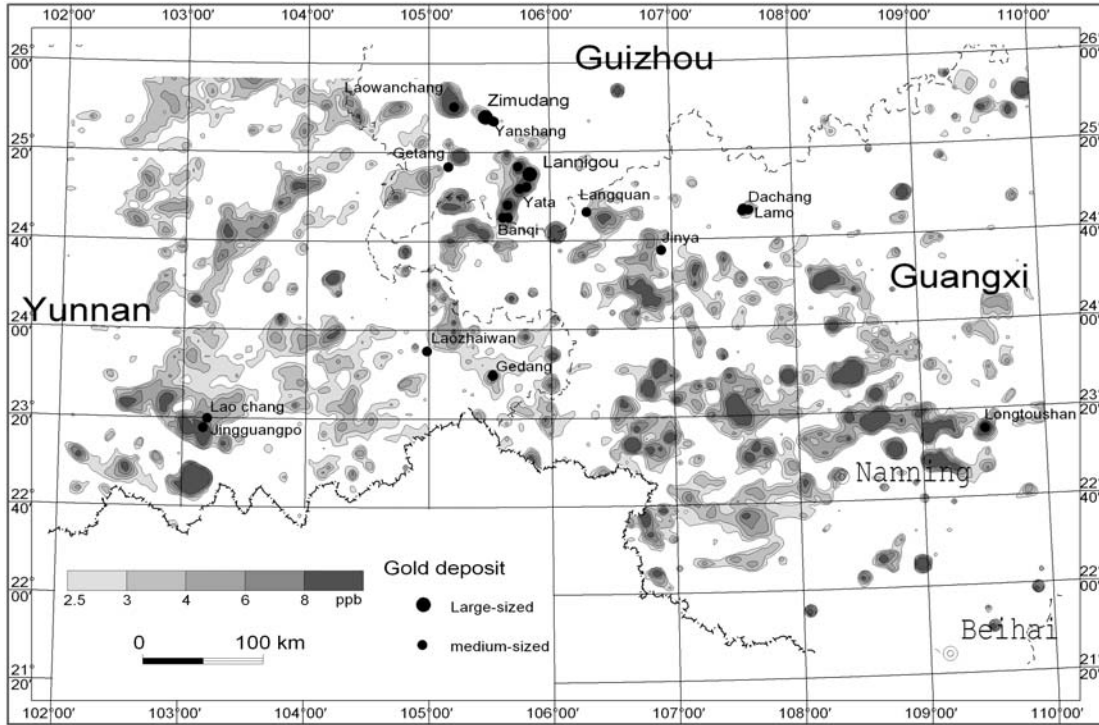


Fig. 3. Gold geochemical pattern delineated by 1 datum per 16 km².

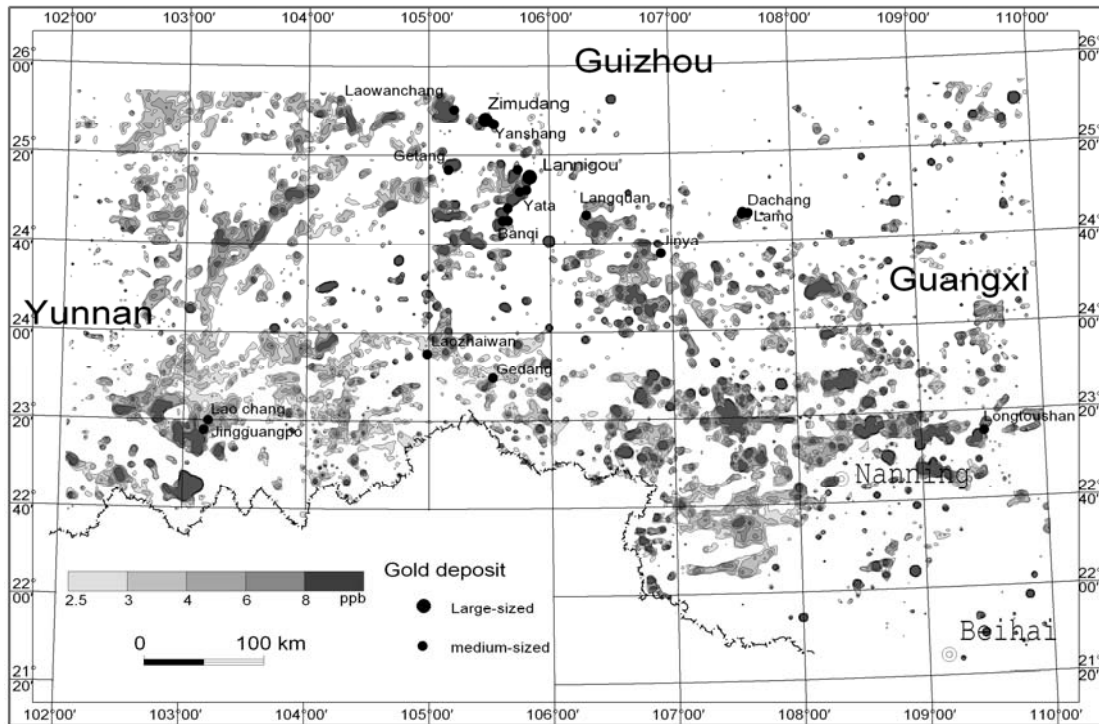


Fig. 4. Gold geochemical pattern delineated by 1 datum per 4 km².

Organic and inorganic surface expressions of the Lisbon and Lightning Draw Southeast oil and gas fields, Paradox Basin, Utah, USA

David M. Seneshen¹, Thomas C. Chidsey, Jr.²,
Craig D. Morgan², & Michael D. Vanden Berg²

¹Vista Geoscience, 130 Capital Drive, Suite C, Golden, CO, 80401 USA
(e-mail: dseneshen@vistageoscience.com)

²Utah Geological Survey, 1594 West North Temple, Salt Lake City, UT, 84114 USA

ABSTRACT: Exploration for Mississippian Leadville Limestone-hosted oil and gas reservoirs in the Paradox Basin is high risk in terms of cost and documented low success rates (~10% based on drilling history). This study was therefore initiated to evaluate the effectiveness of low-cost, non-invasive, organic and inorganic surface geochemical methods for predicting the presence of underlying Leadville hydrocarbon reservoirs. Lisbon field was chosen for testing because it is the largest Leadville oil and gas producer in the Paradox Basin, and the recently discovered Lightning Draw Southeast field, with its almost original reservoir pressure, is also available for comparison. In comparison with Lisbon field, Lightning Draw Southeast field, San Juan County, Utah, is smaller, with more carbon dioxide, nitrogen and helium, and has productive intervals in the overlying Ismay zone of the Pennsylvanian Paradox Formation.

The main conclusion of this study is that hydrocarbon-based surface geochemical methods can discriminate between productive and non-productive oil and gas reservoir areas. Variables in surface soils that best distinguish productive from non-productive areas are ethane, *n*-butane and heavy (C₂₄₊) aromatic hydrocarbons. Heavy metals (U, Mo, Cd, Hg, Pb) are possibly indirect indicators of hydrocarbon microseepage, but they are more difficult to link with the reservoirs.

KEYWORDS: *Lisbon field, hydrocarbons, microseeps, metals, exploration*

INTRODUCTION

Previous work has shown the potential of remote-sensing techniques for locating kaolinite-enriched, bleached redbed Triassic Wingate sandstones over productive parts of Lisbon field, San Juan County, Utah (Fig. 1) (Conel & Alley 1985; Segal *et al.* 1986). These studies used Landsat Thematic Mapper (TM) data to identify kaolinite as well as reduced iron (i.e., bleached redbed sandstones). Other than this work, there are no published surface geochemical studies in the Lisbon field area. The Utah Geological Survey (UGS), therefore, initiated this study to test the effectiveness of several conventional and unconventional surface geochemical methods in the Lisbon area. The main objective for testing these techniques is to find effective geochemical exploration methods to pre-screen large areas of the Paradox Basin, for follow-up geophysical surveys and lease

acquisitions targeting the Leadville Limestone oil and gas reservoirs.

The premise behind surface geochemical exploration for petroleum is that light volatile hydrocarbons (i.e., C₁-C₅) from a pressured reservoir, ascend rapidly to the surface along water-filled fractures, joints, and bedding planes, as buoyant colloidal-size "microbubbles" (Klusman 1993; Saunders *et al.* 1999). In some cases, liquid C₅₊ hydrocarbons also ascend to surface along faults, to produce oil seeps at surface. Partial aerobic and anaerobic bacterial consumption of the ascending hydrocarbons produces carbon dioxide and hydrogen sulfide that can significantly alter the chemical and mineralogical composition of overlying sediments and soils (Schumacher 1996). Changes include decreased iron and potassium concentration and increased silica, carbonate, magnetic minerals and uranium.

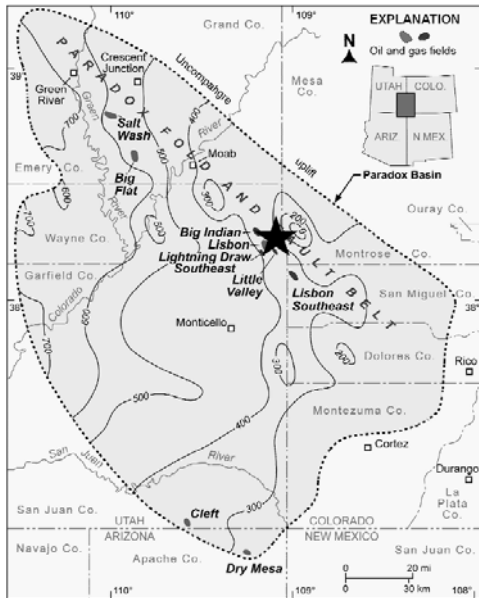


Fig. 1. Location of the Lisbon and Lightning Draw Southeast fields in the Paradox Basin of eastern Utah.

Both direct and indirect methods were tested in the Lisbon area. Direct methods include the assessment of hydrocarbon compositional signatures in surface soils, outcrop fracture-fill soils and mosses, and 6-ft (2 m) deep free-gas samples. Indirect methods use the major and trace element chemistry of soils to look for alteration effects resulting from hydrocarbon microseepage.

HYDROCARBON ANOMALIES IN SOILS

Soil samples were collected at 200 to 500 m intervals over the Lisbon and Lightning Draw fields and analyzed for thermally desorbed C₁ to C₁₂ alkanes by Flame Ionization Detection Gas Chromatography (GC-FID) and solvent-extractable C₆ to C₃₆ aromatics by UV-fluorescence spectrophotometry.

Aromatic hydrocarbon anomalies are evident in soils over both fields (Fig. 2). The anomalous 4-, 5-, and 6-ring aromatic hydrocarbons, which correspond with the 395 nm, 431 nm and 470 nm fluorescence peaks suggest the presence of heavy oil seeps at surface. Light alkanes (ethane and *n*-butane) are the most important

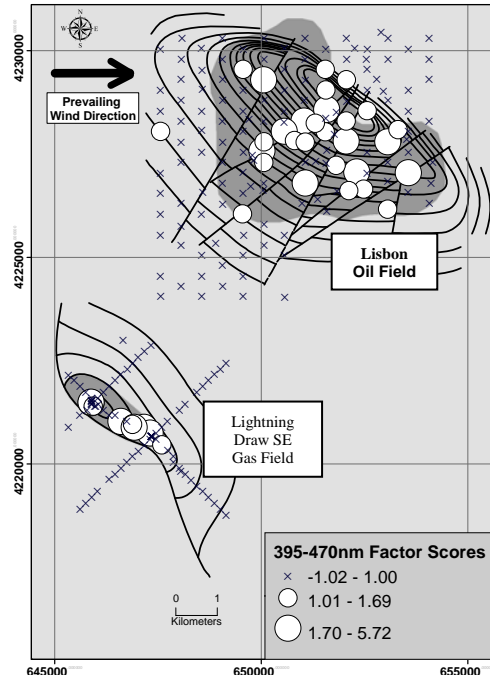


Fig. 2. Distribution of 395 to 470 nm factor scores in soils over the Lisbon and Lightning Draw Southeast fields, which correspond to high correlation with 4- to 6-ring aromatic hydrocarbons.

variables for discriminating between the productive fields and down-dip water-legs.

FREE GAS ANOMALIES

Free gas samples were collected at a 2 m depth with a GeoProbe drill, at 50 m intervals over Lightning Draw Southeast. The samples were analyzed for C₁ to C₆ hydrocarbons by GC-FID and fixed gases (He, H₂, CO₂, CO, O₂, N₂, Ne, and Ar) by Thermal Conductivity Detection Gas Chromatography (GC-TCD). The gas produced from the Leadville Formation is particularly rich in CO₂ and He, and thus these are key variables for identifying microseepages (Fig. 3). Light alkanes (C₂-C₆), H₂ and CO₂ are anomalous over the Lightning Draw field, but He is only anomalous off-structure to the southeast and over the water-leg of Lisbon (Fig. 3).

HEAVY METAL ANOMALIES IN SOILS

Soil samples were analyzed for 53 aqua regia extractable elements by Inductively Coupled Plasma Mass Spectrometry and

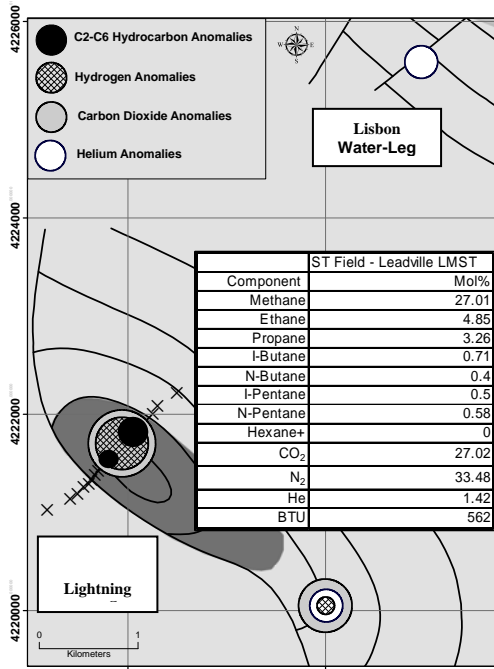


Fig. 3. Distribution of alkanes, H₂, CO₂ and He anomalies in 2 m deep free gas over the Lightning Draw Southeast field.

Emission Spectroscopy (ICP-MS-ES). Cadmium, uranium and molybdenum are anomalous over part of the Lisbon field and most of the Lightning Draw Southeast field (Fig. 4). Mercury, lead and organic carbon are also anomalous over both fields.

DISCUSSION

Light alkane and heavy aromatic anomalies over the Lisbon and Lightning Draw Southeast fields suggest that both volatile and liquid hydrocarbons are ascending to surface from the Leadville Limestone reservoir. The free gas C₂ to C₆, CO₂ and H₂ anomalies over the crest of the Lightning Draw Southeast field also provide evidence for the ascent of volatiles from the reservoir. In the case of Lightning Draw Southeast, however, there is also historic oil production from the stratigraphically higher Ismay Zone, and some of the hydrocarbon microseepage may be therefore partially or entirely from this reservoir. The higher CO₂ in free gas over the field suggests that there is leakage also from the lower CO₂-rich

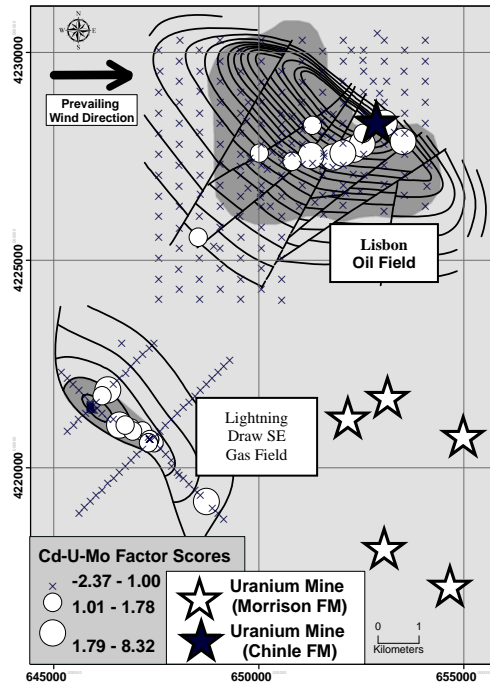


Fig. 4. Distribution of aqua regia extractable Cd-U-Mo factor scores in soils over the Lisbon and Lightning Draw Southeast fields.

The heavy metal anomalies over both fields are interesting, but more difficult to explain in terms of leakage from the reservoir. The Cd-U-Mo anomalies over Lisbon can be explained by outcropping uranium mineralization in the Chinle Formation (Fig. 4), but there are no outcrops of Chinle exposed at Lightning Draw Southeast. An alternative explanation could be that uranium mineralization eroded from Morrison Formation deposits to the southeast (Fig. 4) is being “fixed” by the hydrocarbon microseepage at Lightning Draw Southeast. The anomalies would, therefore, be an indirect indication of hydrocarbon microseepage. The mercury and lead anomalies observed over both fields may be derived from the oil seeping to surface.

CONCLUSIONS

The main conclusion from this study is that hydrocarbon- and fixed gas-based geochemical exploration methods in the Paradox Basin are cost-effective tools for pre-screening large areas for subsequent

lease acquisition and seismic surveys for oil and gas exploration. Heavy metal anomalies are more difficult to link to the reservoir.

ACKNOWLEDGEMENTS

The Utah Geological Survey and the US Department of Energy are acknowledged for providing funding and logistical support for this study.

REFERENCES

- CONEL, J.E. & ALLEY, R.E. 1985. Lisbon Valley, Utah uranium test site report. In M. J. Abrams, J. E. Conel, H. R. Lang, & H. N. Paley (Eds.), *The joint NASA Geosat test case project – final report: AAPG Special Publication*, pt. 2, **1**, 8-1-8-158.
- KLUSMAN, R.W. 1993. *Soil gas and related methods for natural resource exploration*. Chichester, John Wiley & Sons, 483 p.
- SAUNDERS, D. F., BURSON, K.R., & THOMPSON, C.K. 1999. Model for hydrocarbon microseepage and related near-surface alterations: *AAPG Bulletin*, **83**, 170-185.
- SCHUMACHER, D. 1996, Hydrocarbon-induced alteration of soils and sediments. In: D. SCHUMACHER, & M. A. ABRAMS (eds.), *Hydrocarbon migration and its near-surface expression: AAPG Memoir* 66, 71-89.
- SEGAL, D.B., RUTH, M.D., & MERIN, I.S. 1986. Remote detection of anomalous mineralogy associated with hydrocarbon production, Lisbon Valley, Utah. *The Mountain Geologist*, **23** (2), 51-62.

An orientation soil survey at the Pebble Cu-Au-Mo porphyry deposit, Alaska

Steven M. Smith¹, Robert G. Eppinger¹, David L. Fey¹,
Karen D. Kelley¹, & S.A. Giles¹

¹USGS, PO Box 25046, MS 973, Denver, CO, 80225 USA (e-mail: smsmith@usgs.gov)

ABSTRACT: Soil samples were collected in 2007 and 2008 along three traverses across the giant Pebble Cu-Au-Mo porphyry deposit. Within each soil pit, four subsamples were collected following recommended protocols for each of ten commonly-used and proprietary leach/digestion techniques. The significance of geochemical patterns generated by these techniques was classified by visual inspection of plots showing individual element concentration by each analytical method along the 2007 traverse. A simple matrix by element versus method, populated with a value based on the significance classification, provides a method for ranking the utility of methods and elements at this deposit. The interpretation of a complex multi-element dataset derived from multiple analytical techniques is challenging. An example of vanadium results from a single leach technique is used to illustrate the several possible interpretations of the data.

KEYWORDS: *porphyry Cu, soil, analytical methods, exploration, Alaska*

INTRODUCTION

Soil sampling surveys are routinely used to explore for concealed mineral deposits. The giant Pebble Cu-Au-Mo porphyry deposit, located 320 km southwest of Anchorage, Alaska, provides an opportunity to test various sampling and analytical methods commonly used by the exploration community.

As part of an orientation study, the U.S. Geological Survey (USGS) collected soils along traverses across the Pebble deposit area. In 2007, soil samples were collected from 78 sites along a 7.8-km east-west traverse over the Pebble East and Pebble

West zones (Fig. 1). Eight additional soil sites were collected outside of the deposit area to determine background concentrations. A north-south traverse (4.5 km, 44 sites) across the Pebble East zone and a short east-west traverse within the Pebble West zone (1.4 km, 12 sites) were sampled in 2008. The soil samples were submitted to USGS and five cooperating laboratories for analysis by ten leach/digestion methods.

GEOLOGIC SETTING

The Pebble deposit is located in the Kahiltna terrane, near the boundary between two lithologic packages: Jurassic and older magmatic-metamorphic rocks to the southeast, and an assemblage of Mesozoic volcanoclastic and sedimentary rocks overlain by Tertiary volcanic rocks, to the northwest. An extended discussion of the regional geology is given in Kelley *et al.* (this volume).

Above the bedrock are tundra-covered unconsolidated deposits from two episodes of Pleistocene glaciation. These glacial deposits consist of poorly sorted to unsorted, non-stratified compact till ranging from muddy gravel to sandy

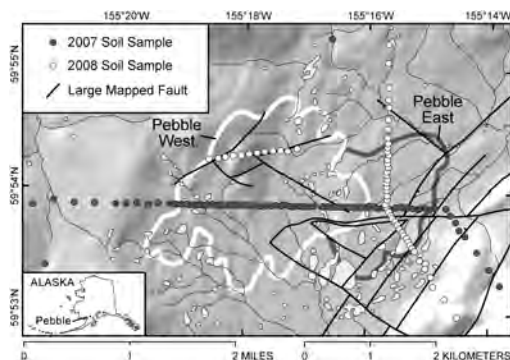


Fig. 1. Study location and soil sample map showing the 2007 and 2008 traverses.

coarse gravel. Small cobbles and pebbles dominate. Surface morphology commonly includes morainal ridges, dry and water-filled kettle depressions and meltwater channels (Hamilton 2007).

The Pebble Cu-Au-Mo porphyry deposit contains one of the largest resources of copper and gold in the world. The Pebble West Zone, partially covered by glacial deposits up to 50 m thick, extends from the surface to ~500 m depth (Lang *et al.* 2007). The East Zone, which extends to at least 1700 m depth, was partially eroded and is concealed by an eastwardly thickening wedge (300-600 m thick) of Late Cretaceous to Eocene volcanic and sedimentary rocks (Bouley *et al.* 1995; Lang *et al.* 2007).

METHODOLOGY

Soil samples were collected along three traverses crossing different extents of the Pebble deposit. At each site, a pit about 0.5 m wide and 0.7 m deep was dug through the tundra. Four different soil subsamples were collected following recommended protocols of the commercial laboratories for the respective methods as described in Fey *et al.* (2008).

The subsamples were split and sent to different laboratories to be subjected to ten commonly-used and proprietary leach/digestion techniques: (a) aqua regia partial digestion method at Acme Analytical Laboratories; (b) sodium pyrophosphate and cold hydroxylamine leaches at ALS Chemex; (c) enzyme and TerraSol leach methods at Skyline Labs; (d) Bioleach and soil gas hydrocarbon analyses at Activation Laboratories; (e) Mobile metal ion (MMI) extraction at SGS Minerals; (f) 4-acid near-total and sodium peroxide sinter total digestions (under the USGS contract) at SGS Minerals; and (g) de-ionized water leach at the USGS laboratories.

For most of the laboratories, additional quality control (QC) samples were inserted within each batch of samples sent. These included sample site duplicates, sample splits for analytical duplicates, a suite of USGS-prepared standard reference materials (SRMs), and

two Pebble project soil standards, created in USGS labs specifically for this project by compositing and homogenizing excess minus-80 mesh material derived from processing all of the soil samples from the 2007 field season.

The analytical data for soil, water, and vegetation samples from the 2007 field season plus an evaluation of QC samples are found in Fey *et al.* (2008). A similar publication for 2008 data will be completed in 2009.

DISCUSSION

Evaluation of Multiple Methods

The ten leach/digestion procedures range in intensity from a very weak, simple de-ionized water leach to complete digestions. Applying extractions of varying strengths targets the release of pathfinder elements from different phases within the soil: ion-exchangeable phases, carbonates, sulfides, or even biogenically derived phases. The purpose of applying less-than-total extractions is to determine whether geochemical anomalies (and therefore patterns) are better indicated by the weakly-bound ions than data from total digestions.

A subjective technique was used to evaluate the performance of the ten analytical procedures. Single element traverse plots were created for every element by every method, plotting them over the known spatial limits of the ore zone. Then each plot was visually evaluated to determine whether the geochemical response pattern could be related to background or the underlying deposit. Patterns for each element/method combination were classified as "significant", "possibly significant", or "no apparent relationship." A simple matrix of analytical methods and elements was created from this information. By assigning values to each classification and then summing the values by row and by column, the matrix could be sorted to give an indication of the relative performance of analytical methods and to list elements that were classified as significant by the most methods. The most significant elements for the 2007 soil traverse were

Ag, As, Au, Cu, Mo, Re, Sb, Tl, U, and V. The highest ranking analytical methods were enzyme leach, cold hydroxylamine hydrochloride leach, and MMI. It should be noted that this matrix method did not take into account the added value of creating ratios (such as to total Fe or organic carbon) between related elements. The use of ratios may change the rank of evaluated analytical methods. Also, the soil gas hydrocarbons technique was treated separately, since the analyses are for organic compounds, rather than for the inorganic elements of the other methods.

Based on the results of this matrix evaluation, cold hydroxylamine leach and enzyme leach methods were chosen for use in subsequent field seasons.

Preliminary Interpretations

Some analytical results are still pending and interpretation of the large volume of analytical results is only partially completed. Thus, data for just two elements, determined by enzyme leach, are discussed here.

The Pebble Limited Partnership has provided drill core geology and rock chemistry, which were used to create a geologic and geochemical cross sections along the line of the 2007 soil traverse – a

valuable third dimension to this orientation study. Figure 2 displays vanadium data from the drill core rock analyses and illustrates possible corresponding V concentrations in soils from the 2007 traverse. High V is noted in the soils over the near-surface Pebble West zone, but there is also an indication of high V over the deeply buried Pebble East zone. These anomalies appear to correspond with dense fracture networks and major faults that cut the overlying volcanic cover. This same general pattern is noted along the 2007 traverse line for As, Cl, Cr, K, Mo, Pb, Re, S, Sb, Sc, & U. High values of Ag, Au, & Cu only seem to be primarily associated with the shallow Pebble West zone.

Based in part on the above results, soils in 2008 were collected along a north-south traverse over the Pebble East zone to confirm the influence of large faults on surface geochemistry in the deeper portions of the deposit. The early results from the 2008 N-S traverse show a broad zone of high values. Figure 3 shows the distribution of molybdenum in a plan view from the combined 2007 and 2008 data. Enzyme leach values for Ag, As, Br, Ca, Cl, Mg, Re, S, Sb, Se, Tl, V, & W show similar distribution patterns in the N-S

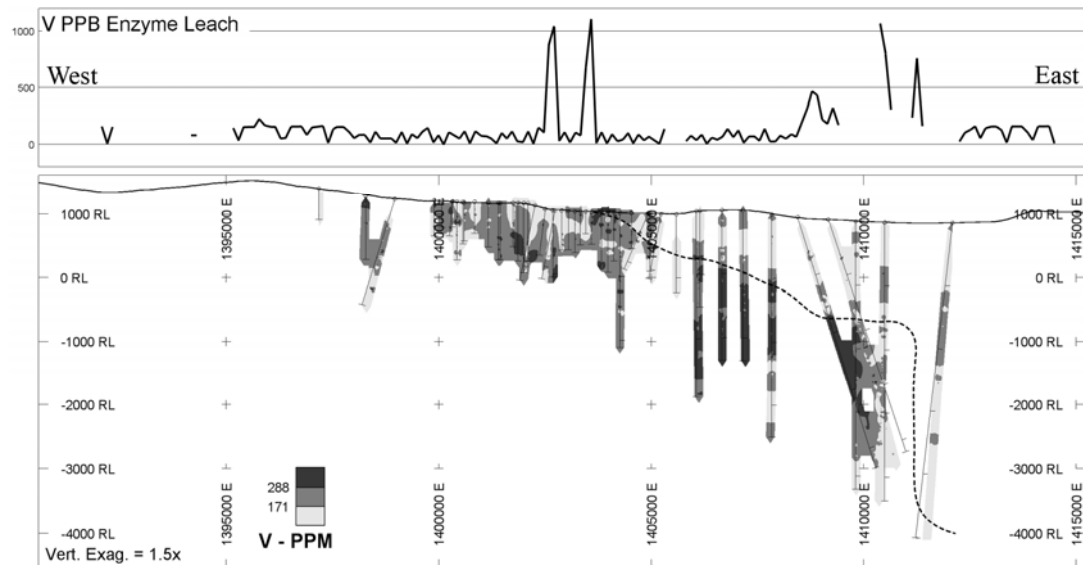


Fig. 2. West to east plot of vanadium by enzyme leach in soils on top of a cross section showing vanadium in drill core. Dashed line shows the subcrop of Cretaceous, granitic rock of Pebble East beneath the Palaeozoic/Eocene volcanic and sedimentary rock cover.

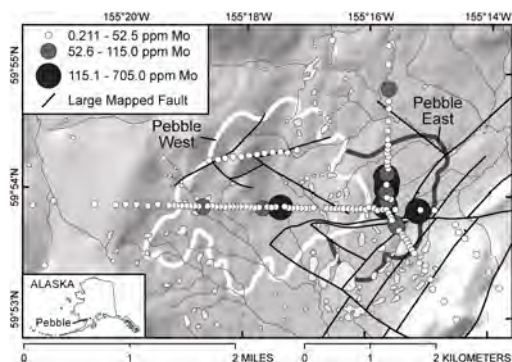


Fig. 3. Distribution of Mo in soil samples analyzed by the enzyme leach method.

traverse.

Because the underlying geology for the 2008 soil traverses is not yet available, hypotheses relating higher concentrations of specific elements to fault structures cannot be confirmed.

Hydrogeochemical anomalies for some elements reported by Eppinger *et al.* (this volume) show coincident anomalies with soils over the shallow Pebble West zone. A general lack of surface and spring water along the soil traverses over the deeper Pebble East zone make it difficult to see similarities.

CONCLUSIONS

- (1) All ten of the analytical methods used show element patterns in soils over the Pebble West and Pebble East zones.
- (2) The most significant patterns were seen for Ag, As, Au, Cu, Mo, Re, Sb, Tl, U, & V for the 2007 soil traverse.
- (3) Early interpretations suggest that soil anomalies above the deeper Pebble East may be related to faulting. Incorporation of drill core geology for this traverse is underway to confirm this hypothesis.

ACKNOWLEDGEMENTS

We thank the Pebble Limited Partnership,

particularly Jim Lang, Mark Rebagliati, Keith Roberts, Lena Brommeland, Robin Smith, Gernot Wober, and Sean Magee for logistical and scientific support for this work. Nicola Struyk and Lindsey Kleppin assisted us with soil sampling.

Under a cooperative agreement, J. Robert Clark, Skyline Assayers and Laboratories; S. Mary Doherty and Brenda Caughlin, ALS Chemex; John Gravel, Acme Analytical Laboratories, Ltd; Eric Hoffman, Activation Laboratories, Ltd.; and Pierrette Prince, SGS Minerals Services contributed analytical services.

REFERENCES

- BOULEY, B.A., ST. GEORGE, P., & WETHERBEE, P.K. 1995. Geology and discovery at Pebble Copper, a copper-gold porphyry system in southwest Alaska, In: SCHROEDER, T.G. (ed.), *Porphyry deposits of the northwest Cordillera of North America: Canadian Institute of Mining, Metallurgy, & Petroleum Special Volume*, **46**, 422-435.
- FEY, D.L., GRANITTO, M., GILES, S.A., SMITH, S.M., EPPINGER, R.G., & KELLEY, K.D. 2008. Geochemical data for samples collected in 2007 near the concealed Pebble porphyry Cu-Au-Mo deposit, southwest Alaska. *U.S. Geological Survey Open-File Report 2008-1132*, <http://pubs.usgs.gov/of/2008/>.
- HAMILTON, T. 2007. Surficial geologic map of the Pebble Limited Partnership's Pebble Project, *Report Series C*, <http://www.pebblepartnership.com/pages/environment/environment-pre-permitting.php>
- LANG, J., PAYNE, J., REBAGLIATI, M., ROBERTS, K., OLIVER, J., & MCLAUGHLIN, J. 2007. The super-giant Pebble copper-gold-molybdenum porphyry deposit, southwest Alaska: *Arizona Geological Society, Ores & Orogenesis*, 120-121.

Ore deposit simulation and reserve estimation in Masjeddaghi epithermal gold mineralization – Azerbaijan - Iran

Payam Soodishoar¹ & Maryam Hashemi²

¹Geological Survey of IRAN, Exploration Dep. IRAN
(email: payam_soodishoar@gsi.org.ir ; payam_soodishoar@yahoo.com),
²Geological Survey of IRAN, Geomatics Dep. IRAN

ABSTRACT: Ore deposit simulation and reserve estimation is the most important part of an exploration project. This part is a good guide to evaluate all done work and shows the certification level of data. MASJED DAGHI, the area that was studied is well known for gold mineralization and some evidence of porphyry copper was reported in a limited area. Several exploration activities have been done on this area but most of them focused on a quartz vein. Ore deposit Simulation would provide a suitable atmosphere for work and shows the shape and extension of the ore body. To recognize the behaviour of the elements that are associated with gold mineralization, statistical processing was done. These studies revealed three different types of elements' parageneses whereas one of them had not been found before. The last processing on this study was GEOSTATISTIC studies. These studies lasted to block kriging estimation, which shows the amount of gold in each block as well as the variance of estimation. To recap, this study ends to show the amount of gold is much less than what was previously suppose to be in this quartz vein. However, this vein could be enough for a small local economic activity but switching the exploration activity from gold to porphyry copper, has been suggested.

KEYWORDS: *Epithermal Gold, Porphyry Copper, Geostatistic, Enrichment Blanket, Reserve Estimation*

INTRODUCTION

MASJEDDAGHI area is located in northwest of Iran and in the north of East Azerbaijan province adjacent to the boundary between Iran and Azerbaijan. The area's latitude is between 38° 52' 03" and 38° 53' 22" and its longitude is in the range of 45° 56' 05" and 45° 58' 29". Its total area is about 8 Km². The access road is JOLFA – SIAH RUD asphalted road. The highest elevation is 950 m from sea level. Weather in this region is hot in the summer and cold in the winter.

GEOLOGICAL SETTING

The geological history of this area seems started by sedimentary units of Mesozoic – Cenozoic age which contains Fylisch and Limestone. These units were influenced by intrusion of volcanic and sub volcanic rocks in Miocene – Oligocene age. These igneous rocks mainly contain dacite, trachyandesite and andesite. These young volcanic units exposed in KIAMACCI Mountain vastly and their

outcrop continues to QAREDAGH Mountain in south and southwest of studied area. Metallic mineralization in whole of this area seems to be associated with QAREDAGH plutonic unit, which influenced a vast area and has made a couple of porphyry mines in Azerbaijan Country. Volcanic units in this area show a hilly morphology and the highest one is 950 meter above sea level. Different and varied types of volcanic rocks in studied area, show evidences of strato volcano of old composite volcano. Based on detail geology map of this area, geological units are pyroclastics, subareal tuff, flows, dykes and small outcrops of shallow intrusive rocks. Pyroclastic and tuff units are mostly found in high lands and intrusive units are located near the river.

Different types of alterations were reported in this area. Silicification is the most usual alteration whole over the area. Argillitic alteration was observed in two types, indogenic, which has extended around mineralization zone and exogenic,

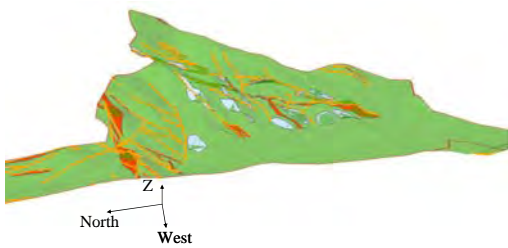


Fig. 1. 3D view of quartz veins and intrusive outcrops in Masjed daghi Area.

that was reported around sulfide (pyrite) zones. Two small exposed location of potassic alteration around river were reported. Phyllic alteration was reported around potassic alteration and sometimes destroyed it.

Mineralization is a little complex on this area and can be divided into two main types. The first one, which led explorers to this area, is Low Sulfide Quartz Gold vein. This vein has more than 700m length and its average width is 5 m. It can be classified to epithermal category. Another mineralization, which has just two small limited outcrops on the surface, is a porphyry copper – gold mineralization, which has identified with potassic zone. These two mineralizations have a significant difference in age and epithermal veins are much younger than the porphyry system and have ascended through the faults.

To recap, the argillic alteration, which has a vast extension on the surface, mainly was produced by epithermal system and over print on the other alterations, those associated with porphyry systems. The host rock is a Trachyandesite, whereas a porphyry Diorite had intruded in it and made a Copper – Gold mineralization in it as a porphyry system. Then after long time and maybe because of another intrusion system in depth (much deeper than the present porphyry mineralization) huge amount of silica came up trough the faults and brought gold in itself from an unknown source (present porphyry system or another source) and made an extension alteration that over printed on existing alteration. Nowadays, we see some quartz

veins, include gold, that cross a copper porphyry system.

ORE BODY SIMULATION

Simulation of ore shape is the first step for 3d studies and provide a base for not only reserve estimatin but also for study on geochemical distribution of elements. For this purpose, all available data have been used that contain geological and topography map, results of 12 trenches with the volume of 200 m², 10 boreholes with about 2000 m accumulate lenght and all the samples that have beeb taken from trenched and boreholes. Simulation of MASJED DAGHI quartz gold vein shows the reasonable volume of porphyry copper system, rather than quartz vein (Fig.3). In addition, by study on the trend of oxidized zone it has revealed the boreholes logs and descriptions need a review. That's not a regular shape (Fig. 2) and though the sulfide zone for these sort of small resources, is not economic to mine, this boundary has a critical role in defining the resource.

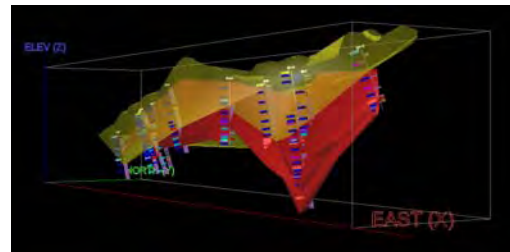


Fig. 2. 3D view of quartz veins (Red) and oxidized atmosphere around it (Yellow).

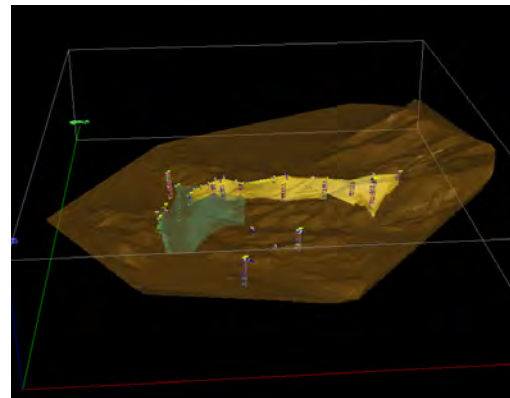


Fig. 3. 3D view of quartz veins (yellow) and porphyry body (Cyan).

GEOSTATISTICAL PROCESSING

Geostatistical processing is one of the most useful and practical methods for evaluation and estimation of a resource. Its BLUE (Best Linear Unbiased Estimator) Kriging not only can indicate the distribution and amount of ore in a resource, but also, based on variance and error of Kriging can identify some parts of ore body, that have lack of data and need more exploration. For a routine Geostatistical processing some issues should be considered:

- (1) Kind of Mineralization and its basics and principals in ore forming and associated structure.
- (2) Primary statistics processing
- (3) Statistics parameters
- (4) Correlations and trends of elements
- (5) Outlier values and samples
- (6) Specifics of populations
- (7) Defining the estimation space for ore body
- (8) Variograms
 - o Effective structures in ore forming
 - o Composite
 - o Non directional Variograms
 - o Directional Variograms
 - o Spatial structure of elements' distribution
 - o Anisotropic ellipsoid
 - o Cross validation
- (9) Estimation
 - o Defining the type of the estimation based on essence of mineralization and available data.
 - o Determining size of blocks, based on type of mineralization and its specifics.
 - o Creating block model for ore body
 - o Kriging Estimation and its associated errors
 - o Ore reserve estimation and its Grade – Tonnage diagram
- (10) Variograms: Variograms are powerful tools to determine the structure and pattern of distribution of ore, based on analytical results. Actually, Variograms are basics of Geostatistic methods and all other calculations would be done base on

introduced model in Variograms. Although Variograms can work easily in disseminated and mass form mineralization, they could also work in vein type ore bodies if they consider the specifications and conditions of mineralization. In the MASJED DAGHI quartz vein gold resource, because of several types of mineralization, recognizing the suitable Variograms to use is a little complicated. A rich zone of gold and copper in host rock, which is very similar to an "Enrichment Blanket" could have a negative effect in Variograms (Fig. 4). On the other hand, because of the essence of mineralization, the directions of anisotropic ellipsoid's axes are approximately known but variograms can help us to find out the range of influence of elements inside the vein.

(11) After finding any structure in non directional variogram, the next step is looking for azimuth and dip of structure or structures of ore body. For this purpose, it is necessary to make directional variograms. All data of MASJED DAGHI were used to make these variograms. Variograms for all horizontal directions, from zero to 180 degrees, all vertical sections from zero to 90 degrees, and different Lag distances were made and studied. The three best of them were chosen for deducing the structure of gold distribution in the vein. Table 3, shows the quality and specifications of some of the variograms, and examples are shown in figure 5.

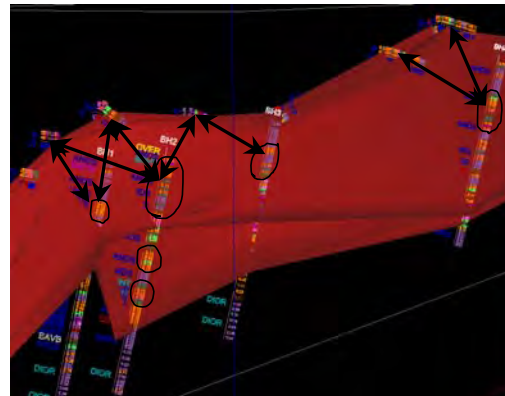


Fig. 4. Negative effect of Enrichment Blanket on Variograms.

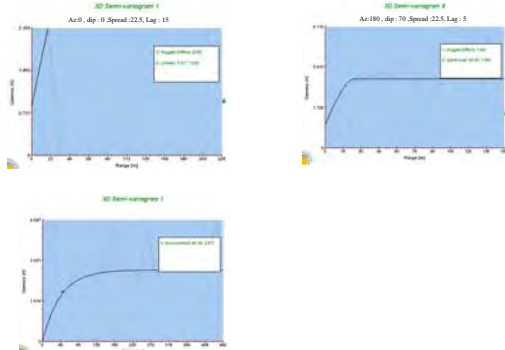


Fig. 5. Geostatistical Model for Estimation in Quartz Vein

(12) Model Fitting: When experimental variograms reveal the structure and distribution pattern in an ore body then for any further estimation, it is necessary to fit a mathematical model to experimental variograms, which are called theoretical variograms. These mathematical models will be used in Kriging estimation. Several predefined models (Linear, Spherical, Gaussian, etc.).

Three parameters are necessary for each model; Sill, Range and Nugget Effect. Each one has a specific meaning and has important effect on a Theoretical variograms for used data are as follow:

(1) For the present data, after replacing outlier values with 4 (ppm, equal to the value of 97% of Au population in data) the relationship between estimated data and reported ones is about 0.6, which make sense, though the amount of data is not enough at all.

(2) Space for estimation: Estimation is a mathematical process whereas the main constraint on the orebody is the geological condition. Therefore, it is necessary to introduce the spatial limits of mineralization. For this project mineralization is not only limited by the vein but also it will be limited by the oxidized zone so that, the estimated space is that part of vein, which is located in oxidized atmosphere (Figure 6).

Block Estimation Kriging: Kriging is an unbiased estimator and due to the conditions of mineralization, it has several different methods. On this project, "Simple Kriging" is used. The sizes of blocks are

1x1x1 m and if half a block contains mineralization, it will be involved in estimation. The results of Kriging will show the distribution of Au throughout the vein and Error of estimation as well. Therefore, not only the amount and volume of gold is ready for any further decision, but also it will be clear which parts of vein need more information and where the existing data is not useful for estimating those parts. The shape of estimated blocks, which have more than one gram per ton gold are shown in Figure 7.

To recap, after estimation, that was obtained total amount of gold in vein 3 is about 450 kg, that's not interesting for any mining sector. The tonnage – grade diagram has shown in Figure 8.

CONCLUSIONS

This project had targeted gold, but the results show there is little hope of obtaining much gold in this area. The thickness of the oxidized zone, the size of

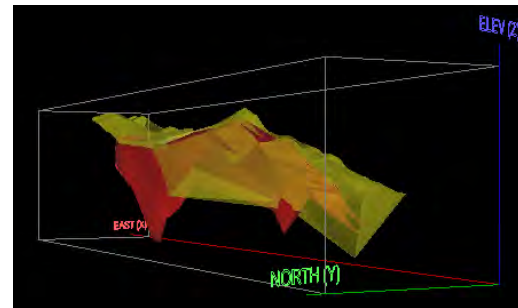


Fig. 6. State of Quartz Vein (Red) inside of Oxidized Zone (Yellow).

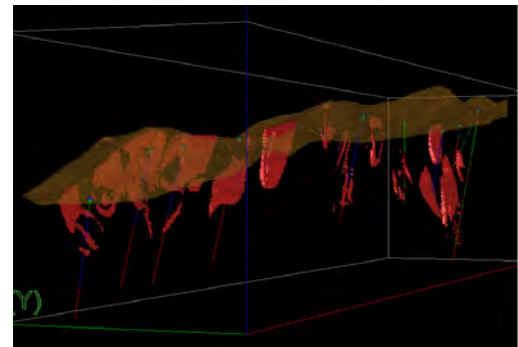


Fig. 7. Parts of Quartz Vein with grade more than one gram per tone gold.

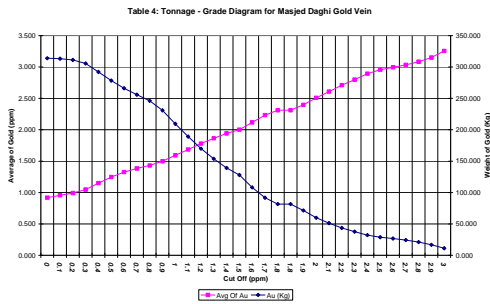


Fig. 8: Tonnage – Grade diagram of Gold in Quartz Vein.

vein and grades of gold could not justify defining this vein as a small gold resource. Therefore, my suggestion was to change the aim of exploration activities from epithermal gold to porphyry copper, which is laid down beneath the river as identified by some borehole results.

Of course, based on government policy for increasing employment in this part of the country and avoiding emigration from these parts to big cities, and as there are several veins like the studied one available in this area, country people can be guided to exploit veins like this and sell the ore to a central gold extraction refinery.

Some important issues for any other exploration for gold in this area are as follows:

- (1) Due to fluctuation of gold assay, the distance between surface channel sampling, should be less than 25 m.
- (2) All the samples should be analyzed for 40 elements (by ICP-MS) as well as gold (Fire assay) and the results should be cross checked by several methods.
- (3) The thickness of the oxidized zone is not very great in this area, so it is necessary to establish a plant for extracting gold from sulfide zone.
- (4) Drilling should be designed to cross the vein at a depth less than 30 meter because of oxidized zone thickness.

ACKNOWLEDGEMENTS

We thank Mr. Mohammad Taghi Korehei, Chief of Geological Survey of Iran, Mr. Abedian, Deputy of Exploration Dep. Mr. Borna Exploration Manager and Mr. Behzad Mohammadi, project geologist.

The application of lithogeochemistry for VMS exploration in the Sherridon Complex, northern Manitoba

Sean A. Timpa¹, Lynda Bloom², & Johan D. Krebs³

¹Halo Resources Ltd., 54 Main Street, Suite #2, Flin Flon, MB, R8A 1J6 CANADA
(e-mail: stimpa@halores.com)

²Halo Resources Ltd., 25 King St. West, Suite 2900A, Toronto, ON, M5L 1G3 CANADA

³Halo Resources Ltd., 54 Main Street, Suite #2, Flin Flon, MB, R8A 1J6 CANADA

ABSTRACT: The Sherridon complex in northwestern Manitoba is part of the Flin Flon – Snow Lake metavolcanic belt and hosts several economic Cu-Zn sulfide deposits. Deformation and metamorphism to upper amphibolite facies has erased primary igneous textures, obscured stratigraphic relationships and metamorphosed VMS-related alteration to higher grade assemblages. Lithogeochemistry has been employed to resolve these issues and improve exploration targeting. Analysis of immobile trace element patterns has been used to identify major lithologies and establish the relationships between them. As a consequence, the Sherridon complex has been shown to be a felsic-dominated bimodal arc suite. High-resolution geochemical sampling has been used on key sequences to identify stratigraphic units and aid structural models. This has helped reveal a previously obscured F₁ doubling of stratigraphy and the prospective ore horizon. Interpretation of major elements has led to the identification, characterization and quantification of VMS-related metasomatism, factors vital in targeting new deposits.

KEYWORDS: *chemostratigraphy, alteration indices, VMS exploration, Sherridon complex, Manitoba*

INTRODUCTION

Terranes that have been subjected to high-grade metamorphism or high strain pose significant challenges for volcanogenic massive sulfide (VMS) exploration. Volcanic textures that are used in less deformed VMS settings may be obscured or obliterated by transposition and recrystallization. These processes can make stratigraphy more difficult to interpret, especially if early generations of deformation are overprinted by later ones. Likewise, alteration assemblages that are typical of VMS deposits are metamorphosed to higher grade assemblages and may be overlooked or misinterpreted.

The Sherridon complex in northwest Manitoba is host to the Sherritt Gordon Cu-Zn mines that collectively produced some 8 million tonnes grading approximately 2% Cu and 5% Zn, as well as six other smaller unexploited Cu-Zn sulfide deposits. Correlation between the Sherridon complex and the Flin Flon – Snow Lake metavolcanic belt (Zwanzig

1999) make it a good prospect for VMS exploration. The Sherridon complex has experienced upper amphibolite grade metamorphism and deformation resulting in elongation of 10:1 or more. Primary igneous textures are not preserved, early structures are obscured by subsequent deformation, and alteration minerals such as chlorite, sericite are present solely as retrograde phases.

Lithogeochemical analysis has been employed in the Sherridon complex in an attempt to better understand the geological setting and to target mineralization. The complex has been shown to be a felsic-dominated bimodal arc suite, lacking either sedimentary protoliths or igneous protoliths of intermediate composition. Orthogneiss with apparent intermediate composition has been shown to be either derived from metasomatized felsic volcanic rocks or are unrelated to the primary arc magmatism. Alteration indices have been established in an attempt to penetrate the effects of upper amphibolite facies metamorphism

and vector toward mineralization.

GEOLOGICAL SETTING

Regional Geology

The Sherridon complex is one of several arc terranes that form the south flank of the Kiseynew Domain (Fig. 1), a metasedimentary terrane that is part of the Paleoproterozoic Trans-Hudson Orogen. The Kiseynew Domain is dominated by Burntwood Group metasedimentary rocks and flanked by arc terranes, notably the Lynn Lake Belt to the north and the Flin Flon Belt on the southern flank (Fig. 1).

The Flin Flon Belt is composed of the metavolcanic Amisk Group and the metasedimentary Missi Group. Recent work (Zwanzig 1999) has shown that the metavolcanic rocks of the Sherridon Complex correlate well with the Amisk Group metavolcanics and the surrounding Nokomis Group metasedimentary rocks are correlated with the Missi Group.

Local Geology

The Sherridon complex was initially interpreted as a sedimentary basin. This was due primarily to the abundance of metapelites and to the exceptional strike length of the deposits (>4 km). More recently, the complex has been reinterpreted as an antiform dominated by metavolcanic lithologies (Zwanzig 1999). The Sherridon complex is dominated by leucocratic quartz - feldspar - biotite gneiss derived from felsic volcanic rocks (Fig. 2). Amphibolites are also present, but less common, accounting for ~10% of sampled lithologies. Aluminous biotite - quartz - feldspar - garnet ± hornblende ± sillimanite ± cordierite gneiss is also common. All of these lithologies may have reacted with various amounts of carbonate to form calc-silicates and in a few instances marble and dolomite are observed. All lithologies are cut by a variety of different pegmatites.

Structural studies by Zwanzig (1999) identified five episodes of deformation in the south flank of the Kiseynew Domain, four of which are evident in the Sherridon Complex. An episode of F₁ isoclinal folding has been recently hypothesized

based on the repetition of stratigraphy in the Sherridon Complex, but is largely obscured by subsequent deformation. The F₂ event deformed the complex into a large sheath fold with a shallow plunge to the east. This was followed by F₃ isoclinal folding that bent the complex into its distinctive hooked shape (Fig. 2). Lastly, the F₄ episode of brittle faulting cut across the center of the complex.

CHEMOSTRATIGRAPHY

Lithochemochemistry was initially applied to the rocks from the Sherridon complex in an attempt to help clarify the stratigraphy of the volcanic sequence. To date, the major- and trace-element compositions of 1964 samples of drill core and 751 outcrop samples have been analysed by



Fig. 4. Regional setting of the Sherridon complex within the Flin Flon Belt (Zwanzig 1990).

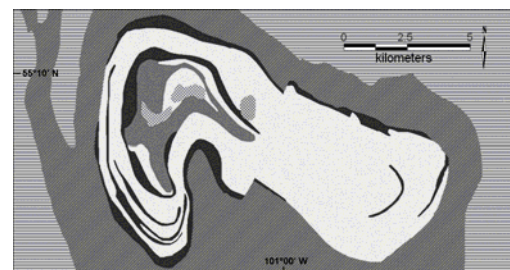


Fig. 5. Geological map of the Sherridon Complex (after Froese & Goetz, 1981). Felsic gneisses are in light grey, intermediate gneisses in medium grey and amphibolites in dark grey. The complex is surrounded by the Missi Group metasedimentary rocks (medium grey with diagonal lines) and Burntwood Group metasedimentary rocks (light grey with horizontal lines) and intruded by gabbro and pyroxenite (cross-hatched).

lithium metaborate fusion followed by ICP-MS. Drill core is typically sampled every ten meters. Outcrop sampling is limited by exposure, but is typically between 25 and 50 meters where exposure is good.

Protoliths have been inferred using the patterns of the immobile trace elements Th, Nb, P, Zr, Ti, Y, Lu and the rare earth elements. This met with limited success with respect to improving the stratigraphy due to the similarity of the trace element patterns of the protoliths and the extreme attenuation of the strata resulting from deformation. However, several key lithologies were identified and their affinities determined. The majority of the samples (63%) are felsic orthogneiss derived from a juvenile arc and are interpreted to be the felsic component of the VMS system. Two types of amphibolites have been identified. The first has a trace element pattern consistent with a mafic protolith derived from a juvenile arc and has been interpreted to be the mafic component of the VMS system. The second variety of amphibolite has an enriched mid-ocean ridge basalt (E-MORB) affinity and is considered to have been emplaced as younger dykes and sills. A large unit of intermediate gneiss has trace element patterns indicative of a more mature arc setting and is unrelated to the VMS system. Highly aluminous lithologies previously identified as metapelites have proven to have trace element patterns that are identical to the felsic orthogneiss and are interpreted to have been metasomatized prior to metamorphism. None of the lithochemical samples collected showed evidence of sedimentary protolith.

Higher resolution chemostratigraphic sampling of drill core has been used to recognize structurally induced repeats of stratigraphy. This effort has successfully demonstrated repetition of the stratigraphy in the immediate vicinity of the F₁ fold hinge.

ALTERATION

The metasomatic alteration that is characteristic of most VMS systems has been all but unrecognized in the Sherridon

complex as the typical hydrothermal alteration minerals, i.e. chlorite and sericite, occur solely as minor retrograde phases. In the last decade it was realised that anthophyllite-cordierite pods at Sherridon represented zones of intense alteration (Froese & Goetz 1981); however, these pods are widely scattered and have not as yet provided an obvious vector to new deposits.

With the recognition that rocks with aluminous intermediate chemistry originated as altered felsic volcanic rocks it is now possible to use these more broadly distributed rocks to target new deposits.

CONCLUSIONS

Lithochemistry has proven to be a vital tool for VMS exploration in high grade metamorphic terranes. Analysis of immobile trace element patterns has allowed the identification of several major lithologies despite metasomatism and subsequent upper amphibolite facies metamorphism. Identification of key stratigraphic units by their trace element patterns has aided the creation and testing of structural models. Analysis of major elements has led to the identification of zones of metasomatism and reveals the nature and degree of alteration, factors vital in targeting new deposits.

ACKNOWLEDGEMENTS

We would like to thank Bill Barclay, Herman Zwanzig (Manitoba Geological Survey) and Doug Tinkham (Laurentian University) for their insights. Sampling, analyses and support for this project was provided by Halo Resources Ltd. as part of an ongoing exploration programme in the Sherridon Complex.

REFERENCES

- FROESE, E. & GOETZ, P.A. 1981. Geology of the Sherridon Group in the vicinity of Sherridon, Manitoba. *Geological Survey of Canada Paper 80-21*.
- ZWANZIG, H.V. 1990. Kisseynew gneiss belt in Manitoba: stratigraphy, structure, and tectonic evolution. In: LEWRY, J.F. &

- STAUFFER, M.R. (eds.), *The Early Proterozoic Trans-Hudson Orogen of North America*. Geological Association of Canada, Special Paper, **37**, 95-120.
- ZWANZIG, H.V. 1999. Structure and stratigraphy of the south flank of the Kisseynew Domain in the Trans-Hudson Orogen, Manitoba: implications for 1.845-1.77 Ga collision tectonics. *Canadian Journal of Earth Sciences*, **36**, 1859-1880.

Orientation survey results at the Tameapa property in Sinaloa, Mexico

Todd W. Wakefield¹

¹AMEC E&C Services, 780 Vista Blvd. Suite 100, Sparks, NV, 89434 USA
(e-mail: todd.wakefield@amec.com)

ABSTRACT: In late 2008, soil and stream sediment orientation surveys were carried out to provide optimized field and analytical procedures for use in property and regional-scale exploration programs on MinCore's Tameapa property in Sinaloa Mexico. The property is host to two advanced mineral prospects named Pico Prieto (copper-molybdenum porphyry) and Venado (molybdenum-copper structurally controlled porphyry) that were first explored in detail by Las Cuevas during the 1970s and early 1980s.

A total of 80 soil samples and 30 stream sediment samples were collected in the vicinity of known mineralization and analyzed for 36 elements in four size fractions. Orientation results indicate that soil samples should be collected from the near-surface soil horizon on a 100 by 200 m grid pattern, and sieved to the coarse, -8+35 mesh fraction prior to analysis. Stream sediment samples should be collected at a sample density of approximately 1 sample per 1 km² and sieved to the fine, -150 mesh fraction. As expected, copper and molybdenum show the strongest response to copper-molybdenum mineralization at both Pico Prieto and Venado; in addition, the following elements are also associated with mineralization at Tameapa: Au, Ag, Pb, Zn, V, W, Ni, As, Sb, Bi, Se, Sr, and Ba.

KEYWORDS: *geochemical exploration, copper, molybdenum, porphyry, Mexico*

INTRODUCTION

MinCore Inc., a private mineral exploration company based in Toronto, Canada, is currently exploring the Tameapa property in Sinaloa Mexico, that contains two advanced mineral prospects separated by 2.5 km, named Pico Prieto (copper-molybdenum porphyry) and Venado (structurally-controlled porphyry molybdenum-copper). MinCore is focused on advancing these two prospects to a scoping level, and exploring the property for additional mineralization.

In October 2008, MinCore commissioned AMEC, a global engineering services company, to conduct soil and stream sediment geochemical orientation surveys at Tameapa. The primary purpose of these surveys was to define the optimal field and assay parameters for the regional soil and stream sediment surveys, planned for 2009. The results of these surveys are the subject of this paper.

GEOLOGICAL SETTING AND HISTORY

Copper and molybdenum mineralization at

Tameapa are spatially associated with a Laramide-age batholith that intrudes a sequence of coeval interbedded volcanic and sedimentary rocks. Mineralized zones typically occur near the contacts of the batholith and are often associated with late stage, Tertiary-age, felsic porphyritic intrusive bodies. Pico Prieto is interpreted as a classic, porphyry copper-molybdenum system consisting of a leached cap, and underlying supergene copper, and hypogene copper (\pm molybdenum) mineralization. Oxide copper mineralization is mostly absent at Pico Prieto. Venado is a structurally controlled zone of molybdenum-copper mineralization along the eastern contact of a lower grade molybdenum mineralized quartz-feldspar porphyry body. Mineralization occurs within several rock types, including hydrothermal and contact breccia zones, that contain volcanic and intrusive fragments, and are cemented by molybdenum-rich quartz veins, quartz feldspar porphyry, and hornfels (Cargill 2007).

Detailed exploration of the 5,000 ha

Tameapa property has been confined to the 12 km² area surrounding the Pico Prieto and Venado prospect areas. Exploration by MinCore and previous operators has included geologic mapping, geochemical and geophysical surveys, and 43,000 m of drilling in 144 diamond drill holes. MinCore plans to systematically explore the entire property area during the 2009 and 2010 field seasons.

SOIL ORIENTATION SURVEY

Design and Collection

The soil orientation survey consisted of three east-west traverses across the known areas of mineralization on the property at Pico Prieto and Venado; and three soil profiles in the Venado area. The primary purpose of the soil traverses was to determine the spacing required to find a deposit of similar dimensions and style of mineralization, and to determine the optimum soil size fraction and pathfinder elements for these styles of mineralization. The purpose of the soil profile samples was to determine whether metal concentrations vary with soil horizon and depth.

A total of 72 samples were collected from the three soil orientation traverses, including three field duplicate samples. Samples were collected every 50 m along each traverse. A single pit was dug at each site to between 50 and 60 cm in depth. Soil was collected from the bottom of the hole, and sieved to 100% passing 8 mesh on site.

Eight samples were also collected from three vertical soil profiles. At each profile site, the soil exposed in a road-cut was first cleaned to remove possible contamination, and samples were collected from two distinct soil horizons between the surface and 1.2 m in depth.

All soil samples were sieved into four size fractions and analyzed for 36 elements by aqua regia digestion/ICP-MS finish. The size fractions included a coarse size (-8+35 mesh), a medium size (-35+80 mesh), a fine size (-80+150 mesh), and a very fine size (-150 mesh). The coarse and medium size fractions were pulverized to 70% passing 150 mesh prior

to analysis, and the fine and very fine size fractions were analyzed as is.

Results

Evaluation of the soil profile results indicates that there is a strong partitioning of copper and molybdenum into the near-surface soil horizon. Copper and molybdenum concentrations are significantly greater in the near-surface (0 to 30 cm) B horizon soils than in the deeper C horizon soils (Fig. 1). More work is required to determine the reason for the preferential partitioning of metals into the B horizon.

Overall, copper and molybdenum show the best anomaly-to-background contrast in the coarse, -8+35 mesh, size fraction. Copper response is strongest in the coarse (-8+35 mesh) and very fine (-150 mesh) size fractions. Molybdenum response is generally strongest in the coarse size fractions, though in some places, the very fine, -150 mesh, fraction yields the highest values. Where molybdenum response is subdued, the coarse fraction often returns the lowest values, thus providing the best anomaly-to-background contrast ratios.

Anomalous patterns of copper and molybdenum suggest a maximum sample spacing of 100 m and line spacing of 200 m is required to adequately delineate areas of interest. This spacing is primarily aimed at adequately defining the

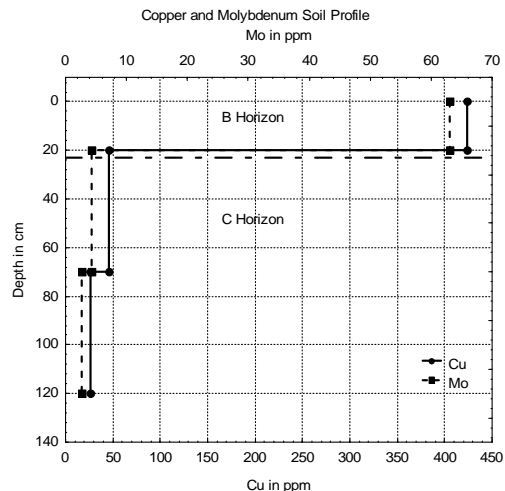


Fig. 1. Partitioning of Copper Near-surface B Soil Horizon (-8+35# fraction shown).

structurally controlled molybdenum mineralization at Venado. The Pico Prieto porphyry-style target would support a much wider sample spacing, say 200 to 250 m, without increasing the risk of missing significant mineralization.

The following elements are associated with copper-molybdenum mineralization in soils at Tameapa: Cu, Mo, Au, Ag, Pb, Zn, V, W, Ni, As, Sb, Bi, and Se. As expected, copper and molybdenum show the strongest response to copper-molybdenum mineralization at both Pico Prieto and Venado.

STREAM SEDIMENT ORIENTATION SURVEY

Design and Collection

The Tameapa stream sediment orientation survey consisted of 30 sample sites situated down-stream from the Pico Prieto and Venado prospect areas. The primary purpose of the stream sediment orientation survey was to determine optimum sampling and assaying parameters for use in the regional stream sediment survey.

A total of 31 stream sediment samples were collected from dry and flowing drainages, including one field duplicate sample. Sediment was collected from 2 to 4 sites along 30 to 100 m of drainage length, and sieved in the field to 100% passing 12 mesh. Stream sediment samples were processed in the same way as soil samples. Each sample was sieved into four size fractions (-8+35, -35+80, -80+150, and -150) and analyzed for 36 elements by aqua regia digestion of a 15 gram sub-sample with ICP-MS finish. The coarse and medium size fractions were pulverized to 70% passing 150 mesh prior to analysis, and the fine and very fine size fractions were analyzed as is.

Results

Analysis of down-stream single element profile maps indicates the very fine, -150 mesh, size fraction provides the best response to Tameapa copper-molybdenum mineralization and thus is the optimal size fraction for use in the

regional stream sediment survey. This fraction provides the best anomaly-to-background contrast for both copper and molybdenum.

Copper and molybdenum concentrations are anomalous for nearly 18 km downstream from mineralization, though there are several sources of mineralization along the drainage (Fig. 2). The anomalous response is diluted sharply when the main stream reaches a confluence with other significant streams that are not draining mineralization. Anomaly to background contrast for both copper and molybdenum is about 3:1.

The following elements are associated with copper-molybdenum mineralization in stream sediments at Tameapa: Cu, Mo, Au, Sr, Sb, and Ba. Copper and molybdenum are clearly the most useful pathfinder elements for copper-molybdenum mineralization at Tameapa, but other elements may prove useful in delineating anomalous areas during the regional survey where copper and molybdenum concentrations are not anomalous.

CONCLUSIONS AND RECOMMENDATIONS

The results of the orientation surveys indicate that both soil and stream sediment geochemical methods are effective for the exploration of copper-molybdenum mineralization on the Tameapa property.

Results from the soil orientation survey suggest that soil samples should be

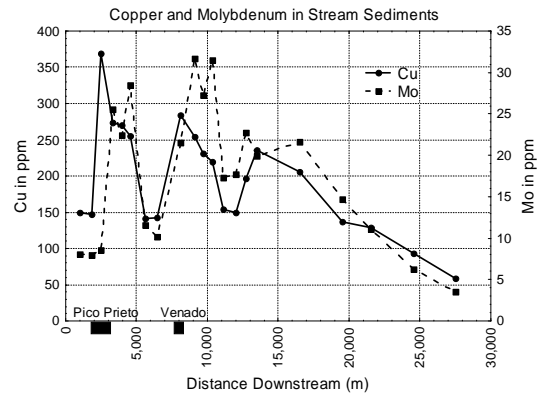


Fig. 2. Copper and Molybdenum Response in Stream Sediment Samples.

collected on 100 m spaced stations on lines spaced 200 m apart. This spacing is the maximum grid spacing recommended to allow discovery of Tameapa-style copper-molybdenum mineralization in the regional soil survey. Further, between 0.5 and 1.0 kg of -12 mesh soil should be collected from the near-surface B horizon (0-30 cm) at each soil site. The soil samples collected from vertical profiles show that the B horizon response is strongest and will provide greater anomaly contrast than the C horizon. At the assay laboratory, all soil samples should be sieved to the -8+35 mesh, coarse size fraction and analyzed by aqua regia digestion/ICP-MS finish. The coarse size fraction was shown to provide the best anomaly-to-background contrast for copper and molybdenum in soil samples.

Results from the stream sediment orientation survey indicate that stream

sediment samples should be collected at a sample density of approximately 1 sample per 1 km². This is the optimal sample spacing determined from the downstream dispersion patterns in the orientation survey. About 1.5 kg of -8 mesh, sediment from the current stream channel should be collected from three or more locations along 20 to 100 m of drainage at each sample site. Samples should be sieved to the very fine, -150 mesh size fraction, and analyzed by aqua regia digestion/ICP-MS finish. The very fine size fraction was shown to provide the best anomaly-to-background contrast for copper and molybdenum in stream sediment samples.

REFERENCES

CARGILL, D.G. 2007. Technical Report on the Tameapa Project, Sinaloa Mexico. Report for NI 43-101 prepared for MinCore Inc.

Gold dispersion under pediplanation in desert terrains

Bimin Zhang^{1,2,3}, Xueqiu Wang^{1,3}, Qinghua Chi^{1,3}, & Qingtian Lü²

¹Institute of Geophysical and Geochemical Exploration, CAGS, Langfang, Hebei, 065000 CHINA
(e-mail: zhangbimin@igge.cn)

²Institute of Mineral Resources, CAGS, Beijing, 100037 CHINA

³Key Laboratory of Applied Geochemistry, CAGS, Beijing, 100037 CHINA

ABSTRACT: Some desert terrains in northern and northwestern China are peneplains formed by a long period of erosion. A concealed gold deposit was selected for study of gold dispersions in the process of pediplanation by using overburden drilling sampling. The results show that (1) gold tends to be concentrated in the top and bottom of the vertical profile over the ore body, (2) gold is enriched in the fine-grained fractions of soils with clay-rich horizons at surface or near surface and the largest gold anomalies occur in fine-grained samples (-100 mesh) over the ore body, (3) gold distribution in different size fractions of soils at the bottom of the weathering regolith display no obvious difference but tend to be anomalously enriched in bedrock troughs. This indicates that gold was concentrated in the lowest places by erosion and transportation during the process of pediplanation. Vertical migration to the soil surface and entrapment by clays and amorphous Fe-Mn oxides leads to the formation of geochemical anomalies directly over the ore body.

KEYWORDS: desert terrains, gold deposit, ARC drilling, pediplanation, dispersion

INTRODUCTION

A large, contiguous desert terrain, totalling c. $2 \times 10^6 \text{ km}^2$, covers most of northern and northwestern China (Wang *et al.* 2007). Much of this region has not been explored or under-explored by effective geochemical methods due to peneplains formed during a long period of erosional and depositional cycles, and weathering regolith concealing mineral deposits. To search for mineral deposits using geochemical methods, it is critical to have an understanding of geochemical dispersion during pediplanation. Many researchers have been trying to understand the process of geochemical dispersion in the desert peneplain since the 1990s (Wang *et al.* 2003; Ye 2004; Wang 2005; Wang *et al.* 2007). In this paper, the authors will describe gold dispersion in the process of pediplanation based on sampling by Air Reverse Circulation (ARC) drilling.

GEOLOGICAL SETTING

The study area, Jinwozi gold field, is located at the boundary of Xinjiang and Gansu provinces in northwestern China

and is a typical peneplain. There are two NE-trending mineralized belts (Fig. 1).

In the northern belt, ore bodies are associated with quartz veins, occurring at

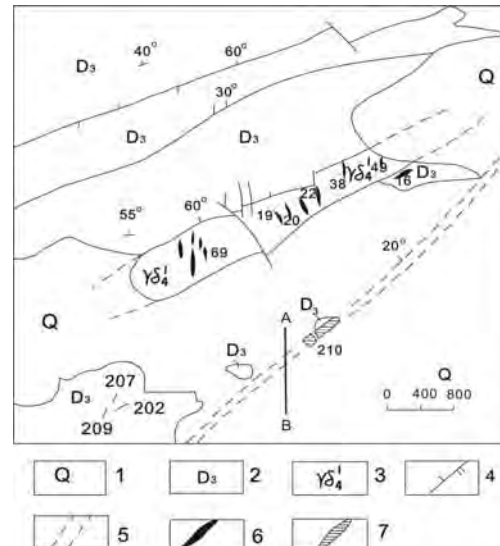


Fig. 1. Geological outline of Jinwozi gold deposit with drilling profile A-B 1 Quaternary; 2 Clastolite and volcanoclastic rocks of upper Devonian; 3 Biotite granodiorite; 4 Fault; 5 Ductile alteration zone; 6 Auriferous quartz vein; 7 Auriferous altered rocks.

the contact between granodiorite and Devonian sequences. The average Au grade is 7g/t. In the southern belt, the ore bodies occur in a ductile alteration fault within a Devonian sequence, which is composed of metamorphic tuff, carbonaceous tuff, sandstone and volcanoclastic rocks intruded by Carboniferous granodiorite or biotite adamellite granite (Zhao 2004). The average Au grade is 4 g/t.

The northern belt is situated in an outcropping area of relatively high relief. The southern belt is located in an area covered by regolith composed of windblown sand, alluvium and residuum. The depth of cover varies from 4 to 20m.

SAMPLING AND ANALYSIS

Sampling

An ARC drilling program was conducted along Profile A-B across the southern concealed gold belt (Fig. 1). 23 bore holes were drilled at a spacing of 50-100 m. Samples were collected every metre from the surface to bedrock. They were split into three fractions: +40, 40-100, and -100 mesh by sieving in the field. Sample types (transported materials, weathered rock, and bedrock) can be recognized based on changes in sample colour, granularity and mineral composition.

Analysis

All the samples were ground to -200 mesh (75µm) for analysis. A 10.0 g sample was digested in aqua regia and analysed for Au and Ag by graphite furnace atomic absorption spectrometry (GF-AAS). A 0.5 g sample was used for As and Hg analysis by hydride generation atomic fluorescence spectrometry (HG-AFS) after an aqua regia digest. A 0.25 g sample was digested in a mixture of HF+HNO₃+HClO₄ and aqua regia. ICP-MS was used for the determination of Ba, Cu, La, Pb, Sb, Sr, Th, U and Zn, and ICP-OES was employed for the determination of P₂O₅, Li, MnO, TiO₂, Al₂O₃, Fe₂O₃, MgO, CaO, Na₂O, and K₂O. Standard reference samples of the GSS series (Xie *et al.* 1985) were used to monitor analytical quality.

RESULTS

Figure 2 shows the variations of gold and mercury contents in the fine fraction (-100 mesh) in drill hole (JWZZK8W) over the gold ore body (Fig. 3). Gold in the fine-grained fraction tends to concentrate in the top and in the bottom of the vertical profile over the ore body. This fact implies that fine-grained gold and similarly mercury could penetrate through the Tertiary and Quaternary sequences and be transported up to the surface.

Figure 3 shows gold distribution in different fractions (+40, 40-100, -100 mesh) along A-B profile. The top part of the figure is drawn by using results from the top sample in each drill hole and the bottom part of the figure from the interface samples between regolith and bedrock. Gold is enriched in the fine-grained fractions of soils with clay-rich horizons at surface or near surface and the greatest gold anomaly contrasts occur in fine-grained samples (-100 mesh) over the ore body. The gold distribution in different grain size fractions of soils at the bottom of the weathering regolith display no obvious difference but anomalies tend to be enlarged in the lowest places at the bedrock interface

DISCUSSION OF GOLD DISPERSION

From the Devonian to the Quaternary period, the study area experienced a complicated geological and weathering history (Fig. 4). Granodiorite or biotite adamellite granite intruded Devonian tuff

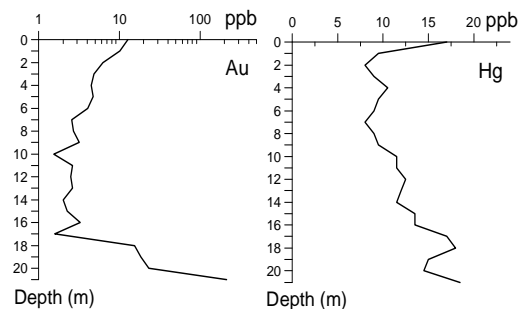


Fig. 2. Variations of Au and Hg from top to bottom in the vertical profile over the ore body.

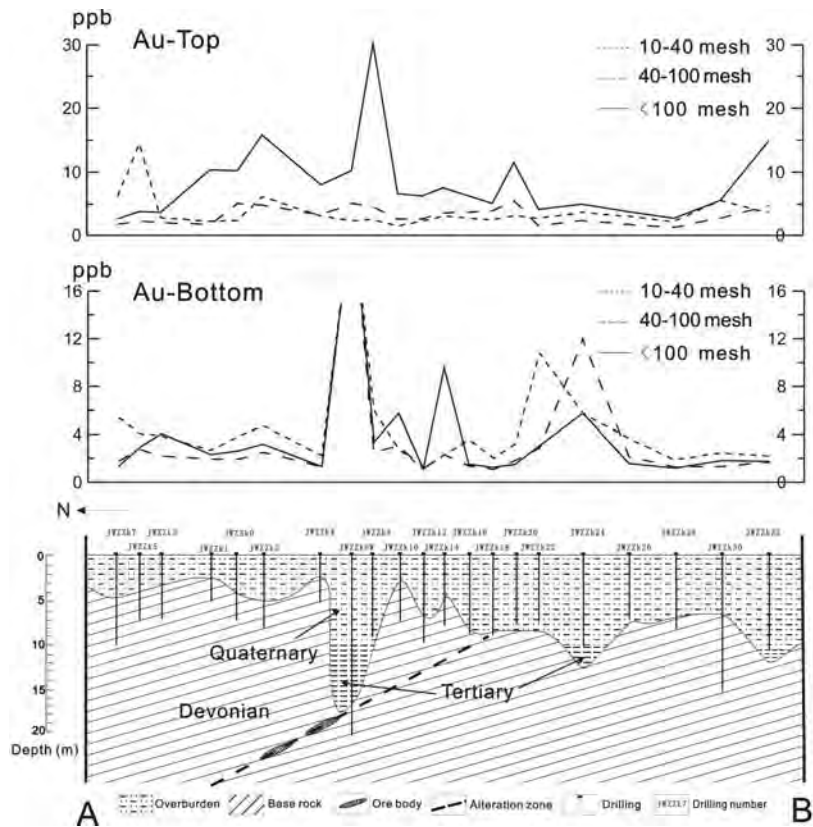


Fig. 3. Gold variations in different fractions at the top and bottom of the profile.

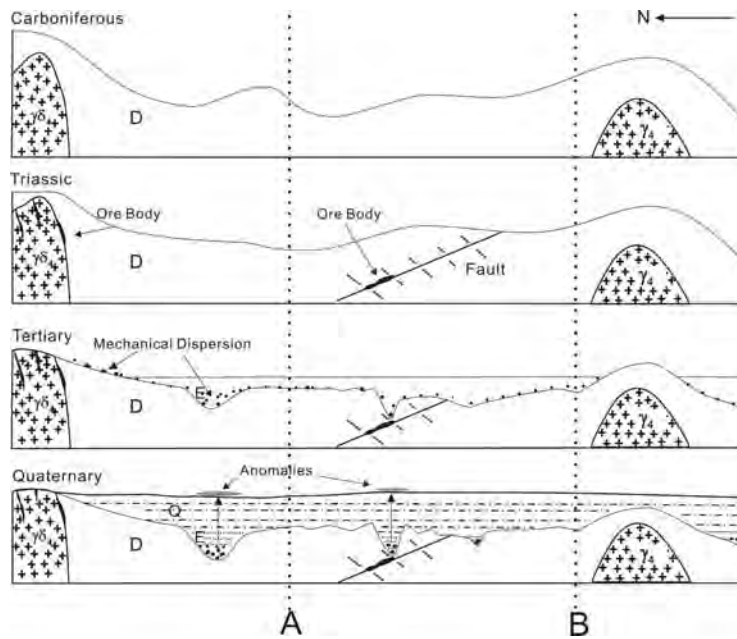


Fig.4. Model showing formation of Au anomalies during pediplanation.

and volcanoclastic sequences in the Carboniferous. Gold deposits were formed in the Triassic (Zhao 2004). The rocks have been under continuous pediplanation since the Tertiary period (Fig. 4). The eroded gold mineralized rocks were mechanically transported and deposited in the Tertiary in topographic lows to form gold anomalies at Drill hole 8 and Drill hole 24 JWZZK8W and JWZZK24 (Fig. 4).

Coarse gold grains are stable in weathered rocks in or near the ore bodies, whereas fine and ultra-fine grains of gold are mobile, so they can be easily dispersed and migrate a long way vertically, penetrating through cover to the surface (Wang *et al.* 1995, 2007). Arriving at the surface, gold may be trapped on clay surfaces and by amorphous manganese and iron oxides.

ACKNOWLEDGEMENTS

We thank the Ministry of Science and Technology of the People's Republic of China and the China Geological Survey for the financial support (projects: 2007AA06Z133, 2006AA06Z135, Sinoprobe04).

REFERENCES

LUO, L. 1999. Geology and Geochemistry of the Jinwozi Gold Mine in Gansu, (in Chinese). *Geological Exploration for Non-ferrous Metals*, **8**, 522-525 (in Chinese with English abstract).
 WANG, X. Q. 2005. Conceptual model of deep-penetrating geochemical migration. *Geological Bulletin of China*, **24**, 892-896 (in

Chinese with English abstract).
 WANG, X.Q., CHI, Q.H., LIU, H., NIE, L.S., & ZHANG, B.M. 2007. Wide-spaced sampling for delineation of geochemical provinces in desert terrains, northwestern China. *Geochemistry: Exploration, Environment, Analysis*, **7**, 153-161.
 WANG, X.Q., LIU Z.Y., YE, R., CHENG, Z.Z., & FU, Y.H. 2003. Deep-penetration geochemistry: a comparative study in the Jinwozi gold ore district, Xinjiang. *Journal of Geophysical and Geochemical Exploration*, **27**, 247-254 (in Chinese with English abstract).
 WANG, X.Q., WEN, X.Q., YE, R., LIU Z.Y., SUN, B.B., ZHAO, S.D., SHI, S.J., & WEI, H.L. 2007. Vertical variation and dispersion of elements in arid desert regolith: a case study from the Jinwozi gold deposit, northwestern China. *Geochemistry: Exploration, Environment, Analysis*, **7**, 163-171.
 WANG, X.Q., XIE, X.J., & YE, S. 1995. Concepts for an exploration based on the abundance and distribution of ultrafine Au. *Journal of Geochemical Exploration*, **55**, 93-102.
 XIE, X.J. YAN, M.C., LI, L., & SHEN, H. 1985. Usable values for Chinese standard reference samples of stream sediments, soils and rocks: GSD9-12, GSS1-8 and GSR1-6. *Geostandards Newsletter*, **5**, 277-280.
 YE, R. 2004. Study on deep-penetrating geochemical methods for Jinwozi gold deposit in desert regions. *Geology and Exploration*, **40**, 65-70 (in Chinese with English abstract).
 ZHAO, Y. 2004. Geological characteristic and exploration indication of Jinwozi Gold Deposit. *Journal of Xinjiang Nonferrous Geology*, **2004**, 18-21 (in Chinese with English abstract)

Structure and stratigraphy of the Key Anacon Main Zone and East Zone massive sulfide deposits, Bathurst Mining Camp, NB, Canada

Joseph D.S Zulu¹, David. R. Lentz¹, & James A.Walker²

¹Department of Geology, University of New Brunswick, Fredericton, NB, E3B 5A3 CANADA
(email: dlentz@unb.ca)

²New Brunswick Department of Natural Resources, Geological Surveys Branch, PO Box 50, Bathurst, NB, E2A 3Z1 CANADA

ABSTRACT: The Middle Ordovician stratigraphy of Key Anacon consist of graphitic shale and quartzose wacke of the Miramichi Group that occur at the base of the stratigraphic section, and are disconformably overlain by the Tetagouche Group volcanic, volcanoclastic, and sedimentary rocks that are composed of fine-grained tuffs, quartz crystal tuffs, and quartz-feldspar crystal tuffs belonging to the Nepisiguit Falls Formation. Rhyolite flows of the Flat Landing Brook Formation and basaltic and sedimentary rocks of the Little River Formation overlie the exhalative (sulfides and iron-formation) horizon.

The felsic rocks have negative Sr and Eu anomalies suggesting plagioclase fractionation. Zr/Al₂O₃ appears to be the best criteria for the discrimination of volcanic rocks and related volcanoclastic sedimentary rocks, because the rocks have been hydrothemally altered; Al₂O₃ is the most conserved. The mafic rocks are dominantly of transitional alkaline to calc-alkaline affinity with high Cr and Ni contents.

The Key Anacon Main Zone and East Zone massive sulfide deposits occur on the eastern limb of the large-scale Portage River Anticline, and are locally concentrated in the hinges of parasitic F₂ folds. Local variations in plunge of F₁ are due to generation of sheath-type fold structures during progressive D₁ deformation, or F₁/F₂ interference folding.

KEYWORDS: Massive sulfide deposit, geochemistry, chemostratigraph, structural geology

INTRODUCTION

The Key Anacon Main Zone has approximately 785000 t grading 0.34% Cu, 3.07% Pb, 7.65% Zn, and 120 g/t Ag. This deposit is located 20 km south of Bathurst and 11 km east-northeast of the Brunswick No. 6 deposit, with the smaller Key Anacon East Zone located approximately 1.5 km to the northeast of the Main Zone (Irrinki 1992, Fig. 1).

The Key Anacon deposits lie on the eastern limb of the Portage River Anticline and are hosted by an autochthonous sequence of Middle Ordovician felsic and mafic volcanics and related sedimentary rocks of the Tetagouche Group. The Tetagouche Group is underlain by sedimentary rocks of the Miramichi Group (van Staal & Williams 1984). The stratigraphy hosting the east Zone is unconformably overlain by Carboniferous sedimentary rocks.

This study was undertaken to document the geometry, stratigraphic position of sulfide mineralization, and litho-geochemistry of felsic and mafic volcanic rocks of the sequence hosting the Key Anacon deposits.

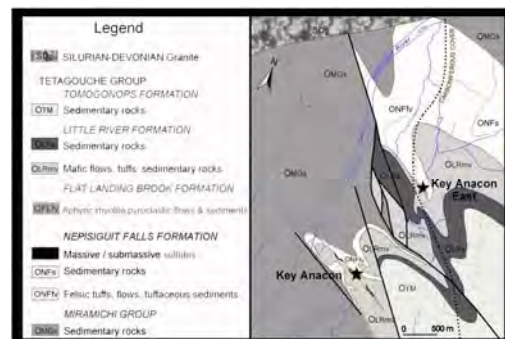


Fig. 1. Geological map of Key Anacon Main Zone and East Zone deposits, northeastern New Brunswick (Canada).

GEOLOGICAL SETTING

The rocks of the Bathurst Mining Camp are assigned to five groups, only two of which occur in the Key Anacon area, namely: the Cambro-Ordovician Miramichi Group and the Middle Ordovician Tetagouche Group (van Staal *et al.* 2003). The Miramichi Group is dominated by a mature quartzose sedimentary sequence, which becomes progressively finer grained and more graphitic towards its upper contact with the Tetagouche Group (van Staal & Williams 1984; Lentz 1996). Rice & van Staal (1992) interpreted the graphitic shale and quartzose wackes of the Miramichi Group as having been formed on an abyssal plain.

Conformably to locally disconformably overlying the Miramichi Group rocks are the bimodal volcanic and sedimentary rocks of the Tetagouche Group. The Tetagouche Group is divided into four all of which occur in the study area; in ascending stratigraphic order they are: Nepisiguit Falls (NF), Flat Landing Brook (FLB), Little River (LR), and Tomogonops formations.

The NF consists of the quartz- and quartz-feldspar-phyric felsic volcanoclastic and minor associated sedimentary rocks. This formation has been interpreted as a pyroclastic sequence dominated by crystal-rich ash flow tuffs, reworked tuffites, and related sedimentary (van Staal *et al.* 2003).

Aphyric to sparsely feldspar-phyric rhyolite flows, associated breccias and related hyalotuffaceous sedimentary rocks of the FLB Formation, and basaltic and related sedimentary rocks of the LR Formation immediately overlie the exhalative (sulfides and iron-formation) horizon of the Key Anacon East and the Key Anacon Main Zones, respectively (van Staal *et al.* 2003).

A sequence of younger calcareous sedimentary rocks belonging to the Tomogonops Formation overlies the LR rocks at the Main Zone, and these are more calcareous than the LR sedimentary rocks.

LITHOGEOCHEMISTRY

Both Key Anacon deposits have large, well-developed footwall and hanging wall alteration halos. Therefore, major- and immobile trace-element data are used to help discriminate rock types.

The felsic rocks of NF are predominantly rhyodacite, whereas the FLB rocks are more evolved with compositions ranging from rhyodacite to rhyolite. The LR mafic rocks have a dominantly alkali to subalkaline basalt signature. The basalts have low Zr/Al_2O_3 (<0.0025) suggesting that the parent magmas had relatively low Zr content. In contrast, Ti, V, Cr, and Ni are high in the basalts due to source characteristics and subsequent fractionation of olivine, pyroxene, Fe-Ti oxides, and glass prior to eruption (Fig. 2).

The positive correlation between TiO_2 and Zr is also characteristic of alkali basalts, and is interpreted to reflect mantle partial melting and fractionation of more mafic parent rocks, as Zr and Ti are both incompatible in primitive melts. Zr remains incompatible up to the felsic end-members (≥ 67 wt. % SiO_2), whereupon it becomes compatible and crystallizes as zircon. This explains the increase of Zr from rhyodacitic through to rhyolitic melts in the NF and FLB formations (Fig. 2). The Y/Al_2O_3 - TiO_2/Al_2O_3 plots show two distinct populations of the LR mafic rocks, and the NF and FLB felsic rocks (Fig. 3). The Y/Al_2O_3 - Zr/Al_2O_3 plot (Fig. 4) shows a scatter trend of the NF and FLB felsic volcanic rocks indicative of magma mixing with the crustal sequence during eruption. Zr/Al_2O_3 vs. Y/Al_2O_3 plots show a similar distinct genetic trend for the FLB rhyolite

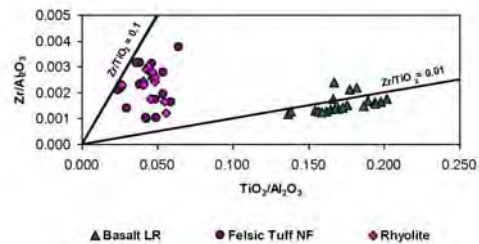


Fig. 2. TiO_2/Al_2O_3 vs. Zr/Al_2O_3 plot of mafic and felsic volcanic rocks of the Key Anacon area.

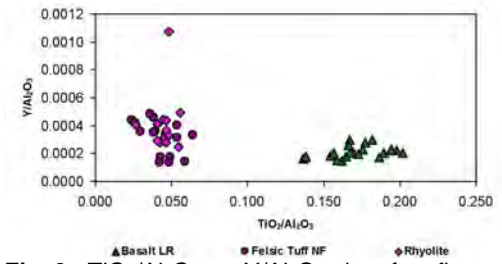


Fig. 3. TiO_2/Al_2O_3 vs. Y/Al_2O_3 plot of mafic and felsic volcanic rocks of the Key Anacon area.

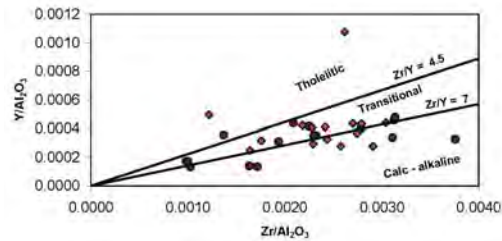


Fig. 4. Zr/Al_2O_3 vs. Y/Al_2O_3 scatter trend of felsic volcanic rocks of the Key Anacon area. Symbols as in Figure 3.

and NF tuffs, suggesting similar magma types as the source of the volcanic rocks. The Zr versus Al_2O_3 diagram is used to quantify the degree of alteration, with rocks having the same magmatic affinity falling on a straight line, whereas mass changes due to alteration show a deviation from the fractionation curve. The LR mafic rocks have moderate variation in Al_2O_3 content (12-16.4 wt %) which is compatible with the moderately altered samples from the hanging-wall, whereas footwall NF felsic rocks and the FLB hanging-wall rocks have variation in Al_2O_3 content (11.5-22.1 wt %) suggesting strong mass change during alteration.

The primitive mantle-normalized trace-element spider diagram of felsic rocks shows negative Sr and Eu anomalies that are indicative of either plagioclase restite or plagioclase fractionation resulting from a combination of the partial melting and fractional crystallization processes (Fig. 5), and later changed by hydrothermal alteration.

STRUCTURAL GEOLOGY

The structural history of the Key Anacon Main and the East Zones is the same as

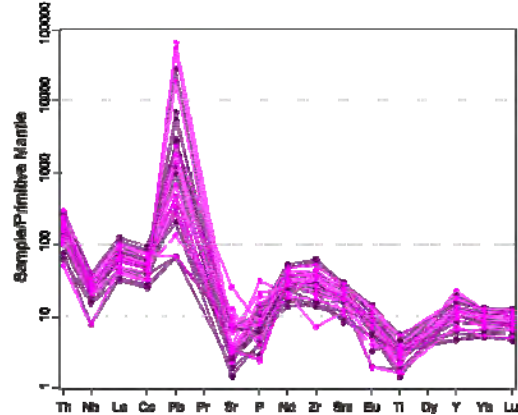


Fig. 5. Primitive Mantle-normalized spider diagram for the NF felsic tuffs and the FLB rhyolite of the Key Anacon area.

rest of the Bathurst Mining Camp, i.e. five phases of regionally developed penetrative deformation (D_1 - D_5 , van Staal & Williams 1984). Saif *et al.* (1978) and Irrinki (1992) recognised at least four deformational events (D_1 - D_4) in the study area. During the course of this study mesoscopic and microstructural evidence of overprinting relations has identified 4 phases of penetrative deformation that are consistent with those of the previous authors.

The four phases are: D_1 thrust-related tight to isoclinal (F_1) folds and associated axial planar schistosity (S_1). D_2 tight-to-isoclinal folds (F_2), with S_2 , are interpreted as high strain deformation with F_1/F_2 fold interference structure (Fig. 6) resulting in the development of S_1/S_2 composite fabric elements. D_3 are recumbent and best developed in the west part of the BMC, and D_4 are represented as kink-folds.

The Key Anacon Main and East Zones are located along the east limb of the Key Anacon syncline, which is a very-tight steeply-plunging, F_2 fold with a well developed axial-planar (S_2) cleavage, and on the west limb of the adjacent moderately south-plunging F_2 anticline, respectively (Irrinki 1992). This interpretation is consistent with observations by van Staal & Williams (1984) who attributed the F_1/F_2 fold interference as having a significant role in the overall structure of the Mining Camp.

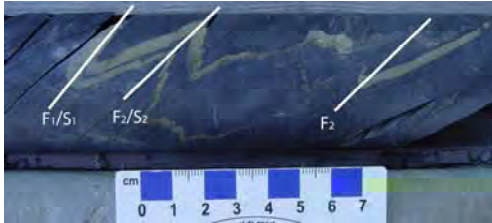


Fig. 6. Photograph of F_1/F_2 fold structures with axial planar S_1/S_2 fabric in shale (KA61-125 m).

Garnet and cordierite blastesis post-dating S_1/S_2 fabric contain inclusion trails of quartz, biotite and phengitic micas and indicate the influence of a late thermal overprint due to intrusion of the Pabineau Granite.

CONCLUSIONS

This contribution can be summarized in a number of points below:

- (1) The F_1/F_2 folds are the dominant structure and control the distribution of rock-types with mineralization concentrated in the noses of the F_2 parasitic folds.
- (2) Zr/Al_2O_3 ratio appears to be the best chemostratigraphic index for discrimination among felsic volcanic rocks in the Key Anacon area.
- (3) Primitive mantle-normalized data show negative Eu and Sr in the felsic volcanic rocks. These negative anomalies are attributed to plagioclase fractionation and/or feldspar destructive hydrothermal alteration and removal of Eu during deposit formation.
- (4) Low Nb and Ti in the felsic rocks are due to fractionation of Ti-bearing phases during calc-alkaline differentiation or during crustal partial melting.

ACKNOWLEDGEMENTS

We thank the Department of Natural Resources-Geologic Surveys Branch, Bathurst Office for providing logistical support during field work. S.R. McCutcheon is thanked for discussions on the petrogenesis of volcanics rocks.

REFERENCES

IRRINKI, R.R. 1992. Key Anacon sulfide deposit, Gloucester County, New Brunswick. *Exploration Mining Geology*, **1**, 121-129.

- LENTZ, D.R. 1996. Trace-element systematics of felsic volcanic rocks associated with massive-sulphide deposits in the Bathurst Mining Camp: petrogenetic, tectonic and chemostratigraphic implications for VMS exploration. In: WYMAN, D.A. (ed.), *Trace Element Geochemistry of Volcanic Rocks: Applications for Massive Sulphide Exploration*: Geological Association of Canada, Short Course Notes, **12**, 359-402.
- RICE, R.J. & VAN STAAL, C.R. 1992. Sedimentological Studies in the Ordovician Miramichi, Tetagouche, and Fournier groups in the Bathurst camp and the Belledune-Elmtree Inlier, northern New Brunswick. In: *Current Research, Geological Survey of Canada*, Paper **92-1D**, 257-264.
- SAIF, S.I., MCALLISTER, A.L., & MURPHY, W.L. 1978. Geology of the Key Anacon mine area, Bathurst, New Brunswick. *Canadian Institute of Mining and Metallurgy Bulletin*, **71**, 161-168.
- VAN STAAL, C.R. & WILLIAMS, P.F. 1984. Structure, origin, and concentration of the Brunswick 12 and 6 orebodies. *Economic Geology*, **79**, 1669-1692.
- VAN STAAL, C.R., WILSON, R.A., ROGERS, N., FYFFE, L.R., LANGTON, J.P., MCCUTCHEON, S.R., MCNICOLL, V., & RAVENHURST, C.E. 2003. Geology and Tectonic History of the Bathurst Supergroup, Bathurst Mining Camp, and Its Relationships to Coeval Rocks in Southwestern New Brunswick and Adjacent Maine-A Synthesis. In: Goodfellow, W.A., McCutcheon, S.R., & Peter, J.M. (Eds.) *Massive Sulfide Deposits of the Bathurst Mining Camp, New Brunswick, and Northern Maine*. *Economic Geology Monograph* **11**, 37-60.

**URANIUM DEPOSITS: GEOCHEMICAL EXPLORATION TECHNIQUES TO
CASE STUDIES**

EDITED BY:

**DAVID QUIRT
ROBERT BOWELL
DAVID LENTZ**

Fraser Lakes Zones A and B, Way Lake Project, Saskatchewan: geological, geophysical, and geochemical characteristics of basement-hosted uranium mineralization

Irvine R. Annesley¹, Carol Cutford¹, Dave Billard¹, Richard T. Kusmirski¹, Ken Wasyluk¹, Terrance Bogdan¹, Ken Sweet², & Chris Ludwig³

¹JNR Resources Inc., 204 – 315 22nd St. East, Saskatoon, SK S7K 0G6 CANADA (e-mail: jnrirvine@sasktel.net)

²WMC Kenco Minerals, 7420 South Upham St., Littleton, CO 80128 UNITED STATES OF AMERICA

³Geophysical Consultant, Denver, CO 80112 UNITED STATES OF AMERICA

ABSTRACT: The Fraser Lakes uranium showings (Fraser Lakes Zones A and B) were identified in 2008 by ground prospecting of airborne geophysical targets in the southern half of JNR Resources Inc.'s Way Lake property in northern Saskatchewan, Canada. The mineralized zones are proximal to a 5-kilometre-long folded electroromagnetic (EM) conductor comprised of Wollaston Group graphitic pelitic gneisses and uraniumiferous granitic pegmatites; some five kilometres east of the main Walker Lake EM conductive trend. Outcrop grab samples returned from 0.038 to 0.453% U₃O₈ and drill core samples returned mineralized sections with values from 0.012 to 0.552% U₃O₈.

KEYWORDS: U-Th-REE mineralization, basement-hosted, unconformity-type, Hudsonian granitoids, Fraser Lakes

INTRODUCTION

The Fraser Lakes uranium showings, part of JNR's Way Lake Project, are situated circa 25 km southeast of the southeastern margin of the Athabasca Basin, northern Saskatchewan, Canada (Fig. 1). These uranium showings (Fraser Lakes Zones A and B) were identified recently in 2008 by ground prospecting of airborne geophysical targets within the southern half of the Way Lake property. An ongoing drilling program is focusing on the widespread outcrops of uranium mineralization, referred to as the Fraser Lakes uranium showings.

The purpose of this paper is to document the occurrence, geology, geophysics, and geochemistry of the Fraser Lakes uranium showings.

GEOLOGICAL SETTING

Regional Geology

The Fraser Lakes uranium showings are located SE of the Athabasca Basin in the eastern Wollaston Domain, part of the eastern sub-Athabasca basement complex (Fig. 1).

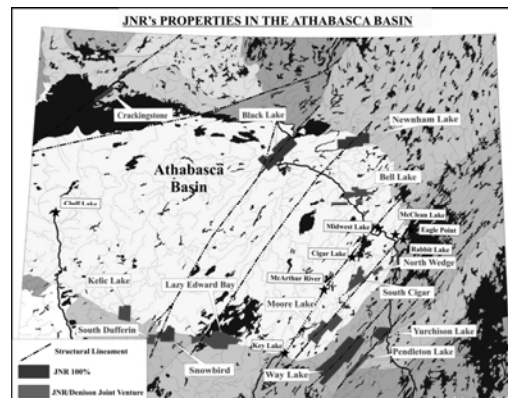


Fig. 1. Location of JNR's properties in the Athabasca Basin, including its Way Lake property on the SE margin (courtesy of JNR Resources Inc. Home Page).

The Athabasca Basin occurs within the southwestern part of the Churchill Structural Province of the Canadian Shield. The 100,000 km² basin is filled by an unmetamorphosed clastic sequence of the Mesoproterozoic (Helikian) Athabasca Group. The basin is underlain by an Archean/Paleoproterozoic basement complex that was strongly deformed and metamorphosed during the Hudsonian

Orogeny (Lewry & Sibbald 1977, 1980; Annesley *et al.* 1997, 1999, 2005).

The Wollaston and Mudjatik domains form two of the major subdivisions of the Cree Lake Zone (Lewry & Sibbald 1977), and also the eastern part of the western foreland of the Paleoproterozoic Trans-Hudson Orogen (i.e., part of the Hearne Province; Hoffman 1989, 1990; Bickford *et al.* 1990; Lewry & Collerson 1990). The present tectonic configuration resulted from the oblique collision of the Superior Province into the accreted Reindeer Zone and Hearne Province during the Hudsonian Orogeny (Fig. 2).

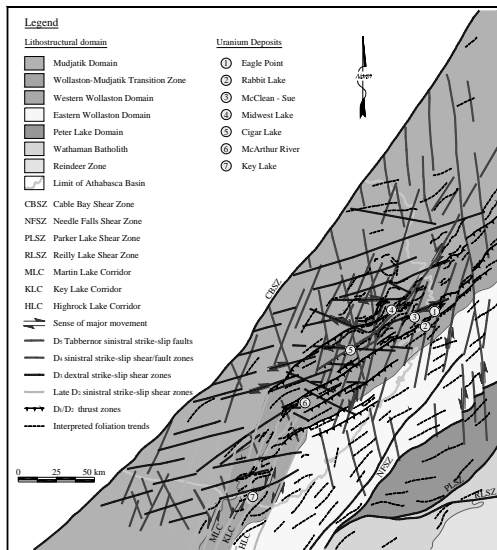


Fig. 2. Geological framework of the basement to the eastern Athabasca Basin, including the location of the major unconformity-type uranium deposits, from Annesley *et al.* (2005).

Local Geology

The Way Lake uranium project of JNR Resources Inc. is located 55 kilometres east of the Key Lake uranium mine in the Athabasca Basin of northern Saskatchewan. The property is underlain by a steeply-dipping, northeast-trending, highly folded sequence of intercalated Paleoproterozoic Wollaston Group metasediments and underlying Archean orthogneisses. In 2006, high-grade uranium mineralization was obtained from a previously identified massive pitchblende vein, now called the Hook

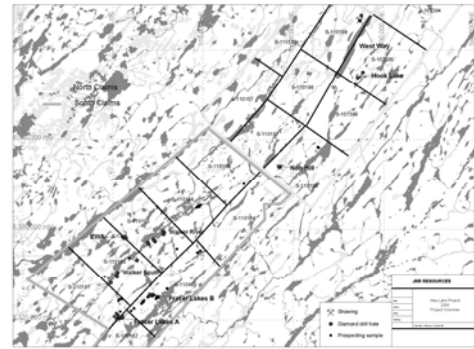


Fig. 3. The major uranium showings within the northern and southern parts of the Way Lake property, including the newly discovered Fraser Lakes zones A and B.

Lake showing (Fig. 3), where two grab samples yielded 40.1% and 48% U_3O_8 with significant Pb, REE, and Th enrichment, and anomalous B, Co, and V.

Within the Walker Lake area (Fig. 3, south-western part of the property), two major uranium showings (now called Fraser Lakes Zones A and B) were identified by airborne geophysics and ground prospecting. These mineralized zones are proximal to a 5-kilometre-long, folded EM conductor comprised of Wollaston Group graphitic pelitic gneisses and uraniumiferous granitic pegmatites and leucogranites.

A major prospecting campaign during the summer of 2008 identified significant uranium, thorium, and REE mineralization in several outcrops of granitic pegmatites and leucogranites, coincident with this conductive EM trend. These outcrops are estimated to be ~200-250 meters below a glacially eroded Athabasca/basement unconformity. The radioactive granitic pegmatites and leucogranites occur within a highly tectonized contact zone between Archean granitoids and basal Wollaston Group metasediments. This crustal melt shear zone (decollement) is folded around Archean granitic domes and is thickest within NE-plunging synformal and antoformal noses. These fold noses are interpreted to have been dilation zones with potential for brittle reactivation and associated fluid flow, alteration, and

mineralization after deposition of the Athabasca sandstones. The radioactive quartz-feldspar-biotite granitic pegmatites and leucogranites contain minor to trace amounts of uraninite, U-Th-REE-rich monazite, molybdenite, chalcopryrite, pyrite, and ilmenite. Locally, dark smoky quartz segregations and veins are noted.

The Fraser Lakes Zone B (Figs. 4 & 5) comprises numerous outcrop showings along the northern extent of this folded EM conductor, and is currently the more prospective of the two mineralized zones. Nearly 70 individual mineralized outcrop sites were identified over a 500-metre-wide by 1.5-kilometre-long area within an antiformal fold nose cut by an E-W dextral ductile-brittle cross-structure and younger NNW- and NNE-trending brittle faults. Over 70% of the grab samples taken from these sites assayed from 0.038 to 0.453% U₃O₈.

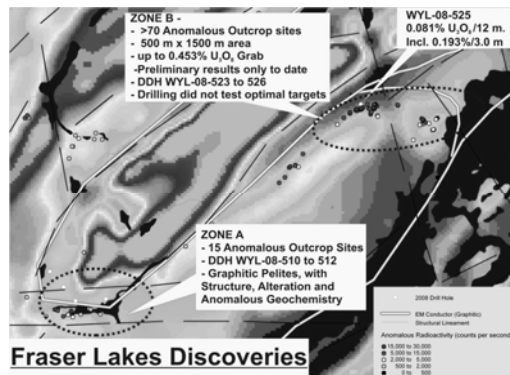


Fig. 4. Some highlights and details of the Fraser Lakes discoveries shown superimposed on the total field aeromagnetic image and a surface trace of the complexly folded EM conductor.

The B zone was tested by three drill holes (WYL-08-524 to 526) at the end of the 2008 program (Figures 4 and 5). Although they could not test the optimum target, namely the graphitic pelitic gneiss/granitic pegmatite contact that occurs beneath muskeg, all three intersected uranium and thorium mineralization, accompanied by rare-earth element enrichment and anomalous levels of pathfinder elements. The best results were from drill hole WYL-08-525, which

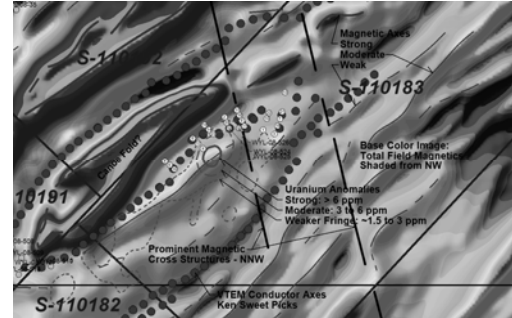


Fig. 5. Location of Zone B 2008 and 2009 drill holes (numbered dots) superimposed on the total field aeromagnetic image, airborne radiometric anomalies (contoured), and EM conductor picks (dark dots). Note the highly disrupted nature of the EM conductor picks in the vicinity of Zone B.

intersected numerous uraniumiferous intervals, mainly within granitic pegmatite. Of particular note was a 12.0-metre intersection from 77.50 to 89.50 metres down hole that returned 0.081% U₃O₈; including a 3.0-metre intercept of 0.193% U₃O₈ (true widths cannot be reliably estimated at this time).

Fraser Lakes Zone A uranium showings occur within a reactivated NE-plunging synformal fold nose, associated with Wollaston Group graphitic pelitic gneisses and leucogranites at the southern end of the EM conductor (Figs. 3 & 4). Seven holes (WYL-08-508 to 514) were drilled in this area, three of which intersected broad zones of significantly altered and structurally disrupted graphitic pelitic gneisses accompanied by anomalous levels of pathfinder elements, particularly copper, nickel, vanadium, bismuth, and zinc. Outcrop samples in the area contained up to 0.042% U₃O₈.

DISCUSSION AND CONCLUSIONS

The main results of this contribution can be summarized as follows:

- (1) The Fraser Lakes uranium showings (Fraser Lakes Zones A and B) were identified in 2008 by ground prospecting of airborne geophysical targets, and show characteristics typical of basement-hosted uranium deposits.
- (2) Outcrop radiometrics of the granitic pegmatites and leucogranites correlate

well with a high-resolution magnetic /radiometric survey over the Fraser Lakes and surrounding area.

(3) The large aerial extent of the airborne anomalies and the presence of U and Th in outcrop and within several boreholes clearly show that the Fraser Lakes area has a very high potential and likelihood of further uranium discoveries, including high-grade root zones.

In summary, the Fraser Lakes district has numerous similarities to nearby basement-hosted uranium deposits, such as Eagle Point and Millennium, and to U-Th-REE deposits found in the Grenville Province (Lentz 1991) and the Erzgebirge -Fichtelgebirge region, Germany (Förster 1998).

ACKNOWLEDGEMENTS

We thank JNR Resources Inc. for permission to publish.

REFERENCES

- ANNESLEY, I.R., MADORE, C., & PORTELLA, P. 2005. Geology and thermotectonic evolution of the western margin of the Trans-Hudson Orogen: evidence from the eastern sub-Athabasca basement. *Canadian Journal of Earth Sciences*, **42**, 573-597.
- ANNESLEY, I.R., MADORE, C., SHI, R., & KROGH, T.E. 1997. U-Pb geochronology of thermotectonic events in the Wollaston Lake area, Wollaston Domain: A summary of 1994-1996 results. *Summary of Investigations 1997*, Saskatchewan Geological Survey, Saskatchewan Energy and Mines, Miscellaneous Report **97-4**, 162-173 plus map.
- ANNESLEY, I.R., MADORE, C., KROGH, T.E., KWOK, Y.Y., & KAMO, S.L. 1999. New U-Pb zircon and monazite geochronological results for Archean and Paleoproterozoic basement to the southeastern part of the Athabasca Basin, Saskatchewan. *Summary of Investigations 1999*, Saskatchewan Geological Survey, Saskatchewan Energy and Mines, Miscellaneous Report **99-4.2**, 90-99.
- BICKFORD, M.E., COLLERSON, K.D., LEWRY, J.F., VAN SCHMUS, W.R., & CHIARENZELLI, J.R. 1990. Proterozoic collisional tectonism in the Trans-Hudson Orogen, Saskatchewan. *Geology*, **18**, 14-18.
- FÖRSTER, H.-J. 1998. The chemical composition of REE-Y-Th-U-rich accessory minerals in peraluminous granites of the Erzgebirge-Fichtelgebirge region, Germany, Part I: The monazite-(Ce)-brabantite solid solution series. *American Mineralogist*, **83**, 259-272.
- HOFFMAN, P.F. 1989. Precambrian geology and tectonic history of North America. In: Bally, A.W. & Palmer, A.R. (eds) *The Geology of North America - An Overview*. Geological Society of America, **A**, 447-512.
- HOFFMAN, P.F. 1990. Subdivision of the Churchill province and extent of the Trans-Hudson Orogen. In: Lewry, J.F. & Stauffer, M.R. (eds) *Early Proterozoic Trans-Hudson Orogen of North America*. Geological Association of Canada, Special Paper, **37**, 15-39.
- LENTZ, D. 1991. U-, Mo-, and REE-bearing pegmatites, skarns and veins of the Grenville Province, Ontario and Quebec. *Canadian Journal of Earth Sciences*, **28**, 1-12.
- LEWRY, J.F. & COLLERSON, K.D. 1990. The Trans-Hudson Orogen: Extent, subdivision and problems. In: Lewry, J.F. & Stauffer, M.R. (eds) *Early Proterozoic Trans-Hudson Orogen of North America*. Geological Association of Canada, Special Paper, **37**, 1-14.
- LEWRY, J.F. & SIBBALD, T.I.I. 1977. Variation in lithology and tectonometamorphic relationships in the Precambrian basement of northern Saskatchewan. *Canadian Journal of Earth Sciences*, **14**, 1453-1467.
- LEWRY, J. & SIBBALD, T. 1980. Thermotectonic Evolution of the Churchill Province in Northern Saskatchewan. *Tectonophysics*, **68**, 45-82.

Geochemical controls on uranium precipitation in calcrete palaeochannel deposits of Namibia

R.J. Bowell¹, A. Barnes, J. Grogan, & M. Dey

¹SRK Consulting, Churchill House, Churchill Way, Cardiff CF102HH, Wales (e-mail: bowell@srk.co.uk)

ABSTRACT: Palaeo-river channels containing calcrete are important potential hosts for economic uranium mineralization in many parts of southern Africa particularly Namibia. The main feature of these deposits are the dominance of the mineral Carnotite $[K_2(UO_2)_2(VO_4)_2 \cdot 3(H_2O)]$ as the main uranium host in these channels. However other phases such as andersonite $(Na_2K_3UO_3(CO_3)_3(H_2O)_6)$, liebigite $(Ca_2UO_2(CO_3)_3(H_2O)_{10})$, rutherfordine (UO_2CO_3) , swartzite $(CaMgUO_2(CO_3)_3(H_2O)_{12})$, tyuyamunite $(Ca(UO_2)_2(VO_4)_2 \cdot 5-8H_2O)$, and urancalcarite $[Ca(UO_2)_3(CO_3)(OH)_6 \cdot 6H_2O]$ are also present in minor amounts. These minerals are associated with epigenetic calcite, dolomite, gypsum, palygorskite, and strontianite. Typically a complex stratigraphy of calcite as transported and epigenetic calcite can be observed in the deposits. Uranium precipitation can occur more than once in the paragenesis indicating carnotite can be dissolved and re-precipitated in the palaeochannel possibly in response to fresh alkaline groundwater. Clear evidence exists that carbonates, gypsum, and uranium minerals are precipitated interstitially in the granite dominated detrital that fills the channel. Grade in these channels is typically higher at shallow depth with often the highest grade being at surface indicating that evaporation may play a role in precipitating uranium. Mineral equilibrium calculations, based on known mineralogy and groundwater chemistry have been used to construct geochemical models to understand ore genesis and assist exploration for carnotite hosted calcrete deposits. Multiple phases of calcite and carnotite formation are indicated in mineral paragenesis and an explanation for this may be that there has been frequent re-working of the deposit by inflowing groundwater. In addition, high evaporation in the near surface environment generate conditions for another mechanism for carnotite formation. Species activities and mineral saturation have been determined. These demonstrate that for many of the deposits carnotite is close to saturation or is only weakly undersaturated demonstrating that recent or even seasonal dissolution and re-mobilization of uranium may occur in these deposits leading to wide hydrogeochemical halos for trace levels of uranium in groundwater around these deposits. However inherent difficulties in the analysis of trace levels of metals in high salinity groundwater typical of palaeochannels may limit application in exploration.

KEYWORDS: *uranium, hydrogeochemistry, geochemical modelling, Namibia*

INTRODUCTION

The discovery of the calcrete hosted surficial uranium deposits of Namibia demonstrated the presence of widespread uranium in calcrete filled palaeochannels (Hambleton-Jones 1984) and similar mineral deposits have been observed elsewhere in Southern Africa, USA and Australia (Carlisle 1978; Hambleton-Jones 1978; Mann & Deutscher 1978). The host rocks are typically lenticular bodies of alluvium, soil or detritus material cemented by calcite, gypsum, palygorskite, and other mineral phases. Uranium mineralogy is dominated by the mineral Carnotite $[K_2(UO_2)_2(VO_4)_2 \cdot 3(H_2O)]$ as the main mineral in these channels. However other phases such as andersonite $(Na_2K_3UO_3(CO_3)_3(H_2O)_6)$, liebigite $(Ca_2UO_2(CO_3)_3(H_2O)_{10})$,

rutherfordine (UO_2CO_3) , swartzite $(CaMgUO_2(CO_3)_3(H_2O)_{12})$, tyuyamunite $(Ca(UO_2)_2(VO_4)_2 \cdot 5-8H_2O)$, and urancalcarite $[Ca(UO_2)_3(CO_3)(OH)_6 \cdot 6H_2O]$ are also present in minor amounts (Bowell *et al.* 2008). In Namibia the presence of authigenic gypsum in the surface calcrete increases with proximity to the Atlantic Ocean and this has been identified as an important factor in considering genesis of these deposits (Hambleton-Jones & Toens 1978). The genesis of carnotite-hosted calcrete deposits has been studied in both Namibia and in Australia and several mechanisms have been invoked; including evaporative controls weakening uranyl-carbonate species and decreasing pH close to the groundwater table (Mann & Deutscher 1978; Carlisle 1978), physical and chemical attenuation through

common ion effect and interaction with clay minerals and capillary driven diffusion mechanism similar to chemical dilatancy (Cameron *et al.* 2002). In order to determine the major geochemical controls on these deposits and the implications this may have for regional exploration geochemical modelling has been undertaken using groundwater chemistry from four deposits in Namibia.

GEOLOGY

The Namib Desert is underlain by bedrock complex of Late Proterozoic Damaran Belt unconformably overlying a 2 billion year old (Giga-annum or Ga) Mesoproterozoic basement complex of granite-gneiss (Kukla *et al.* 1991). The Damaran beds consist of metamorphosed arsenites and argillites of the Nosib Group overlain by pelitic rocks of the Swakop Group. Folding combined with regional granite intrusions occurred in the Pan African Orogeny (800 to 500 million years ago). Some of these orogenic granites are uraniferous. The sequence was intruded by both late to post tectonic 528Ma granites and most importantly by a series of post Karoo age (124-137Ma), anorogenic, peralkaline, slightly peraluminous, and topaz bearing granites with moderately elevated background uranium counts (e.g., Rössing; Basson & Greenway 2004). The latter younger granites (Spitzkoppe) are related to the break up of Gondwanaland (130 – 80Ma) and constitute the ultimate source rocks for Trekkopje Project mineralization, with background contents of 20-30ppm uranium in places.

Between 80 Ma and 50 Ma, the Namib rocks were eroded to a smooth peneplain (the Namib Unconformity). Namib Group Tertiary and Quaternary sedimentary debris was deposited in east-west to southwest trending paleochannels incised into Karibib marbles and schists on that Cretaceous age unconformity. From mid Tertiary to present, the central Namib region has maintained profoundly arid climatic conditions for the last 50 or more million years. Uplift initiated the post African erosion surface that filled valleys and channels with poorly sorted angular

material, with little evidence of chemical weathering or organic debris. Host rocks are paleo-channel deposits of cobbles, gravels, and local sands composed of the regional rock types. Calcrete formation is widespread throughout the region particularly in alluvium channels and paleoriver beds. The major calcrete channels in central western Namibia are shown in Figure 1.

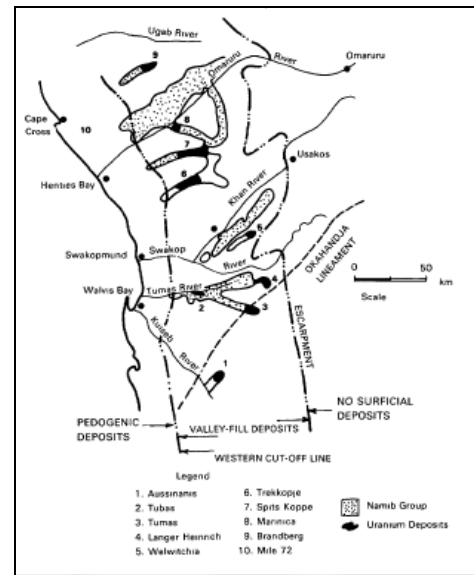


Fig. 1. Distribution of calcrete-hosted carnotite deposits in central Namibia (from Hambleton-Jones 1984).

HYDROGEOCHEMISTRY OF CARNOTITE HOSTED CALCRETE DEPOSITS

Data has been obtained from published sources and listed data held in the library of the Geological Survey of Namibia. This data has been used to assess the geochemical environment in the vicinity of channel fill and pedogenic uranium-bearing calcrete deposits. The data has been analysed by various methods and laboratories so direct comparison of the data has to be treated with caution. A summary table of the geochemistry of waters from each of the deposits is given in Table 1.

The deposit with the highest salinity is Mile 72, followed by Tubas, Trekkopje, and Langer Heinrich. The reason behind

Table 1. Hydrogeochemistry of representative groundwater analysis, Calcrete Uranium deposits, Namibia (average of available data).

Element	Trek-kopje	Langer Heinrich	Tubas	Mile 72
pH	6.62	7.8	7.57	7.81
Eh, mV	64	107	137	455
Carbonate mg/L	174	473	575	88.3
Sulfate mg/L	2090	2240	3250	1270
Chloride mg/L	6750	3000	6580	6790
Sodium mg/L	4110	970	2640	3070
Potassium mg/L	121	387	822	1160
Calcium mg/L	665	429	1460	890
Uranium mg/L	0.212	0.316	0.182	0.019
Vanadium mg/L	0.038	0.121	0.061	<0.005

this obviously can be related to distance from the sea with Trekkopje and Langer Heinrich the furthest from the coast, Tubas being 40 km and Mile 72 at the coast. Uranium is present in many of the groundwaters (Table 1). In terms of a correlation, a positive correlation can be observed for uranium with redox potential (Eh), high carbonate and lower sulfate and chloride, pH, and potassium in groundwaters (Fig. 2).

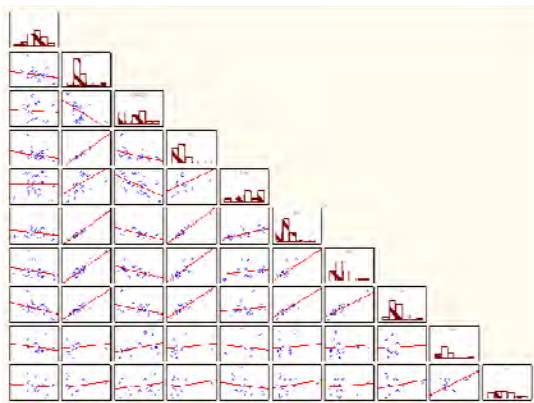


Fig. 2. Matrix plot for key groundwater parameters, calcrete-hosted carnotite deposits, Namibia.

GEOCHEMICAL CONTROLS

The speciation of uranium and vanadium has been determined for groundwaters from the calcrete-hosted carnotite deposits. These were completed in Geochemists Workbench v.7 using in-

program database supplemented by additional data from Gorman-Lewis *et al.* (2008). The chemistry of groundwater for Namibian calcretes promotes the stabilization of the species, $UO_2(CO_3)_2^-$ (Fig. 3) and for vanadium, $VO_2(OH)_4^-$.

The uranyl dicarbonate species is extremely stable in aqueous solutions but by evaporation can become sufficiently concentrated by evaporation to generate the low solubility mineral carnotite in the pH range 6 to 8, the natural range of pH values in the Namibian groundwaters.

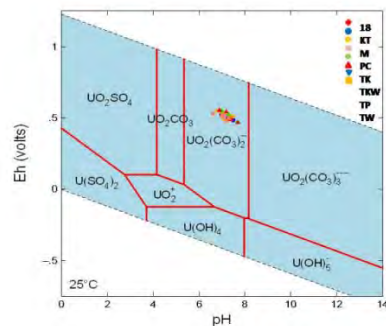


Fig. 3. Eh-pH diagram for the system U-H-O-S-Cl-C at 298 K.

At the prevailing pH in the Namibian groundwaters, the predicted solubility of carnotite is low and close to saturation. From one hole in the Tubas deposit, carnotite saturation is close to 0 and predicted to be over saturated around the water-table zone and in the near-surface upper 2m of the gypcrete. Where Eh is positive carnotite is predicted to be near-saturation. This indicates that carnotite accumulation at or above the regional water-table can occur by upward diffusion of uranyl carbonate species with possible precipitation due to nucleation on clay minerals or gypsum, as evidenced in the Tubas River.

MECHANISMS OF FORMATION

Understanding the formation of carnotite in calcrete is important with respect to not just understanding the formation of the deposits but also has implications for exploration of such deposits (Nash *et al.* 1981; Hambleton-Jones *et al.* 1984). A

number of mechanisms have been proposed to explain the precipitation of Carnotite in calcrete formations (Boyle 1984). These include reduction, sorption, uranyl complex dissociation, changes in redox state of constituent metals, evaporation, variation in CO₂ partial pressure, pH, mixing of different groundwaters and colloidal precipitation.

The source of uranium mineralization is erosion of uraniferous granites in the region followed by transportation of uranium in mildly oxidizing saline alkaline groundwater solutions in constricted drainages to semi-closed basins with variable evaporative conditions. The Quaternary erosion cycle was marked by uplift of coastal areas and marine regression with planation and incision of the post African erosion surface, with river valleys becoming younger towards the coast (Nash & McLaren 2003). This regional uplift across the Southern African subcontinent resulted in renewal of deposition of coarse sedimentary debris into incised drainage ways, creating the current drainage channels (Ringrose *et al.* 2005). Precipitation fluctuations in this period are believed to have effected uranium deposition, dissolution, and re-deposition.

In the fluvial-type deposits, such as Langer Heinrich or Trekkopje, most likely high carbonate fluids are responsible to mobilize uranium as uranium (VI) and deposition is in response to changes in a_{HCO₃}, pH, or redox similar to mechanisms proposed for Australian calcrete hosted carnotite deposits (Mann & Deutscher 1978b; Hartleb 1988). This form of carnotite is primarily due to remobilization of carnotite "upstream" and to de-complexing of uranyl-carbonates in waters of higher salinity. Uranium analyses and solubility indices suggest that the carnotite up stream is at present re-dissolving and that a different mechanism was primarily responsible for its original precipitation. The slow moving and upward welling groundwater undergo chemical and redox (reduction/oxidation state) changes allowing for precipitation of uranium as carnotite near surface. Carnotite occurs

within the margins of the "chemical delta" formed as the drainage system forms, as observed for trace-element distribution in modern inland deltas (Ringrose *et al.* 2005).

In zones close to or at the water table the primary driver for remobilization appears to be high salinity and evaporative driven chemical dilatancy such as in the shallow calcrete deposits, for example Mile 72. A possible comparative mechanism has been proposed by Cameron *et al.* (2002) to explain the development of surface geochemical anomalies in areas with a thick vadose zone. Results of soil and groundwater analyses from an integrated study at the Spence porphyry copper deposit in northern Chile, which is buried beneath 50 to 100 m of Miocene gravels, are consistent with the vertical movement of saline metal-rich groundwater along fractures (Cameron *et al.* 2002). Copper in groundwater is restricted to the mineralised area due to the tendency of Cu²⁺ released by oxidation of sulfides to adsorb to Fe hydroxide colloidal particles and coatings, whereas elements that dissolve as anions (e.g., As, Mo, Se, and Re), are dispersed widely. Field measurement of the conductivity of soil-water slurries showed two zones of salt (NaCl) enrichment, one directly over the deposit and the other 1 km away. Trenching of the soils in these zones revealed vertical fractures in the gravels, whereas trenching in a background area showed no fractures. The fracture zones appear to have formed by reactivation of basement faults. Elements present in the soils above the fracture zones are the same as those enriched in ground-water near the deposit and indicate redistribution of elements by ground-water movement to the surface during earthquakes, followed by evaporation and further redistribution by rain.

The correlation to calcrete-gypcrete deposits is that saline groundwater may mobilize uranium both laterally and vertically through cyclic diffusion and pumping in a similar, albeit on a smaller scale. This may occur in response to

recent marine transgression-regression episodes or even seasonally high salinity incursions in coastal groundwater.

Field measurements in sedimentary fluvial-type calcrete deposits also suggest that present-day groundwater in these areas may also display potential to both dissolve and precipitate uranium in the near surface. Chemical dilatancy and evaporation-driven diffusion that promote de-complexing, diffusion, and re-precipitation mechanisms are seen to play integral parts in the continued chemical re-working and modification of these calcrete-hosted carnotite deposits.

IMPLICATIONS FOR EXPLORATION

The development of relatively large, but weak geochemical halos associated with calcrete-hosted carnotite deposits can be utilized on a regional scale through the application of aerial radiometric surveys and in more detailed prospect level evaluation by direct geochemical analysis of groundwater coupled with borehole geology and down hole radiometric surveys. The proximity to such superficial deposits of uranium can be gauged by groundwater uranium content. In addition for blind deposits the development of a Carnotite Saturation Index has been applied in Australia as a more sensitive approach based on several parameters (Mann & Deutscher 1978). This index can be defined as;

$$CSI = \log \frac{[U][V][K]}{1.13 \times 10^4 [HCO_3]^{-2}}$$

Where uranium and vanadium concentrations are in µg/L and potassium and bi-carbonate are in mg/L. Where the CSI is equal to zero then groundwater chemistry and carnotite saturation are in equilibrium and the mineral has the potential to be present. The assessment of groundwater chemistry in the vicinity of calcrete-hosted carnotite deposits indicates that a wide geochemical halo exists and that this halo can be identified during exploration. In Australia direct analysis of groundwater and the CSI have been demonstrated as suitable methods for exploration. In Namibia, in reality although the approach may be useful for

higher grade deposits, such as Langer Heinrich, in reality the low uranium and vanadium chemistry in most groundwaters in proximity to calcrete-hosted carnotite deposits and difficulties in detecting trace levels of these metals will limit application. In addition for many of the Namibian deposits direct surface mapping of carnotite is possible for most of the known deposits so surface radiometrics and geological mapping will continue to provide a more cost-effective and reliable method of exploration for this class of deposit in Namibia and throughout Southern Africa.

REFERENCES

- ARAKEL, A.V. 1988. Carnotite mineralization in inland drainage areas of Australia. *Ore Geology Reviews*, **3**, 289-311.
- BOWELL, R.J., BOOYSENS, M., PEDLEY, A., CHURCH, J., & MORAN, A. 2008. Characterization of carnotite uranium deposit in calcrete channels, Trekkopje, Namibia. In: *Proceedings of Africa Uncovered: Mineral Resources for the future*. SEG-GSSA 2008 Conference, 7th-10th July 2008, 114-121.
- BOYLE, D.R. 1984. The genesis of surficial uranium deposits. In: TOEN, P.D. (ed) *Surficial Uranium Deposits*. IAEA-Tecdoc-322. Vienna, 45-52.
- CAMERON, E.M., LEYBOURNE, M.I., & KELLEY, D.L. 2002. Exploring for deeply covered mineral deposits: formation of geochemical anomalies at the Spence copper porphyry deposit, Chile. *Geology*, **30**, 1007-1010.
- CARLISLE, D. 1978. The distribution of calcretes and gypcretes in the southwestern United states and their uranium favourability. Grand Junction, *Dept. Energy Report*, GJBX-29-78, 274 p.
- GORMAN-LEWIS, D., BURNS, P.C., & FEIN, J.B. 2008. Review of uranyl mineral solubility measurements. *Journal of Chemical Thermodynamics*, **40**, 335-352.
- HAMBLETON-JONES, B.B., & TOEN, P.D. 1978. The geology and geochemistry of calcrete/gypcrete uranium deposits in duricrust, Namib desert, South West Africa. *Economic Geology*, **73**, 1407-1408.
- HAMBLETON-JONES, B.B. 1984. Surficial uranium deposits in Namibia. In: TOEN, P.D.(ed) *Surficial Uranium Deposits*. IAEA-Tecdoc-322, Vienna, 205-216.
- HAMBLETON-JONES, B.B., HEARD, R.G., & TOEN, P.D. 1984. Exploration for surficial uranium deposits. In: TOEN, P.D. (ed) *Surficial*

- Uranium Deposits*. IAEA-Tecdoc-322, Vienna, 61-64.
- Hartleb, J.W.O. 1988. The Langer Heinrich Uranium Deposit: Southwest Namibia. *Ore Geology Reviews*, **3**, 277-287.
- LEROY, J.L. & TURPIN, L. 1988. REE, Th and U behaviour during hydrothermal and supergene processes in a granitic environment. *Chemical Geology*, **68**, 239-251.
- MANN, A.W. & DEUTSCHER, R.L. 1978. Genesis principles for the precipitation of Carnotite in calcrete drainages in Western Australia. *Economic Geology*, **73**, 1724-1737.
- NASH, J.T., GRANGER, H.C., & ADAMS, S.S. 1981. Geology and concepts of genesis of important types of uranium deposits. *Economic Geology*, 75th Anniversary Volume, 63-116.
- NASH, D.J. & MCLAREN, S.J. 2003. Kalahari valley calcretes: Their nature, origins and environmental significance. *Quaternary International*, **111**, 3-22.
- PAGEL, M. 1984. Petrology, mineralogy and geochemistry of surficial uranium deposits. In: TOEN, P.D.(ed), *Surficial Uranium Deposits*. IAEA-Tecdoc-322, Vienna, 37-44.
- RINGNOSE, S., HUNTSMAN-MAPILA, P., KAMPUNZU, A.B., DOWNEY, W., COETZEE, S., VINK, B., MATHESON, W., & VANDERPOST, C. 2005. Sedimentological and geochemical evidence for palaeo-environmental change in the Makgadikgadi subbasin, in relation to the MOZ rift, Botswana. *Palaeogeography, Palaeoclimatology and Palaeoecology*, **217**, 265-287.

Variability of U and some trace elements in ferromanganese nodules of the Clarion-Clipperton zone (Pacific Ocean) and mechanism of their formation

V. M. Gulyi¹ & O. M. Tysiachna¹

¹Ukrainian State Geological Research Institute, 78 Avtozavods'ka str., Kyiv, 04114 UKRAINE
(e-mail: vgul@ukr.net)

ABSTRACT: Marine geological exploration is able to provide accurate assessments of the metal content in seabed mineral deposits, which are considered as a new industrial type. Besides the relatively well-studied elements (Mn, Fe, Co, Ni, Cu, Zn, Pb, etc.), a number of economically important trace elements occur in deep-sea ferromanganese nodules, but they have been poorly studied in the past. Characteristic of U, Th, Ra, and Sr distributions in ferromanganese nodules, as well as adjacent bottom sediments from the Clarion-Clipperton region are given in this paper to get knowledge on their economic interest. These elements are not associated with the iron and manganese phases in ferromanganese precipitates and it is important to know possible mechanism of their concentration. The ferromanganese nodules have been formed in an open physicochemical system from an unsaturated ore components environment and only electrochemical mechanisms are possibly powerful enough to form these ore components at industrial scales.

KEYWORDS: *ferromanganese nodules, uranium, ore deposits*

INTRODUCTION

The ferromanganese nodules commonly are regarded as a new industrial kind of ore deposits due to high concentrations of Mn, Fe, Co, Ni, Cu, Zn, and Pb. In the recent past, we are seeing an increasing interest in the nodules as a possible source of many other elements, especially trace metals important for modern technologies. Many of the trace elements have been poorly studied in the past, due to analytical problems and lack of economic interest. For the element U, Th, Ra, and Sr only a few data are available, with mostly overestimated contents, caused by insufficient analytical capabilities and deficient sample treatments. We have therefore studied the distribution of these elements in the nodules and adjacent bottom sediments in order to estimate their possible source, relationship with common metals of the nodules, and assess their industrial importance. For these purposes we used our previous investigation (Gulyi & Tysiachna 2008) of distribution and peculiarities of typical nodule components,

as well as their economic evaluation (Koschinsky 2008).

GEOLOGICAL SETTING

Regional Geology

The nodules studied have been dredged from a number of sites of the Clarion-Clipperton area of the Pacific Ocean floor between long. 137° and 138° W and lat. 12° and 13° N (Fig. 1). The Fe-Mn deposits are located between two famous faults – Clarion and Clipperton and they were the objects of several studies by a number of investigators.

Local Geology and Samples

The geology, textural characteristics of the nodules and bottom sediments, and descriptions of the substratum are summarized on site (Gulyi 2004). Samples have been studied for its dimension, and mineralogical and chemical composition in accordance with their space distribution as well as age differences.

The nodules rest as a mono-disperse layer of potato-like balls on unconsolidated pelagic sediments down to 5500 m water depth.



Fig. 1. Location of studied area.

They have diameters of 2 to more than 8 cm. The substratum of the nodules is shark teeth, basalts, andesites, and more rare varieties of weathered volcanic rocks.

Nodules have an average population density of 12 kg/m² in high-quality fields, crust of 4 to 5 cm thickness show local coverages of 15 to 25 kg/m².

We studied two sites of samples. Firstly, the element's distribution in the ferromanganese nodules and adjacent bottom sediments has been investigated after undisturbed sampling by grabs. Secondly, dimension distribution of discoid, plate, and ellipsoid nodules, as well its fragments and crusts discovered after seagoing dredged samples.

Uranium, thorium, radium, and strontium spatial distribution within studied area turn out to be different: 1) a relatively similar pictures of U, Th, and Ra distributions (Fig. 2 – 4), and 2) a clear difference of distribution for Sr (Fig. 5). The greatest features in the spatial distributions of U, Th, and Ra appear in the northern-western and southern-eastern parts of the region (see Fig. 2 – 4).

Clear differences in spatial distribution of U, Th, Ra and Sr can reflect general differences in nature of these elements in the nodules.

We determined also another pictures of spatial distributions of U, Th, Ra and Mn, which are supported by negative values of correlation coefficients for these elements and Mn. At the same time, positive values of correlation coefficients for these elements and Fe (**rFe-U= 0.45**, **rFe-Th=**

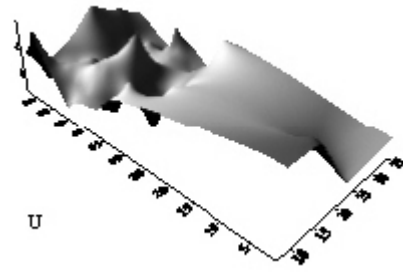


Fig. 2. Spatial distribution of U.

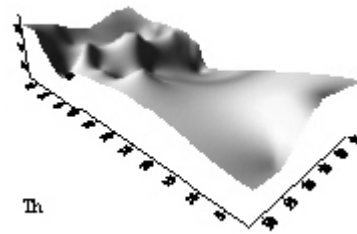


Fig. 3. Spatial distribution of Th.

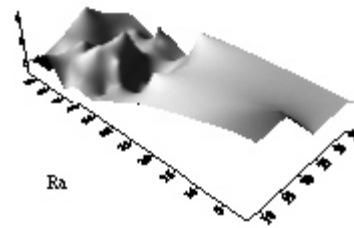


Fig. 4. Spatial distribution of Ra.

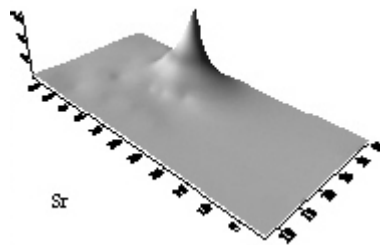


Fig. 5. Spatial distribution of Sr.

0.53, **rFe-Ra= 0.17**) give to us evidence of the close genetic relationships between these elements and Fe phases.

The characters of each element's distribution in ferromanganese nodules and adjacent sediments are different and

reflect differences in nature of ore components concentration. In general, according to obtained average compositions and calculated dispersions, the nodule matter is richer in uranium, thorium, and radium than the adjacent bottom sediment.

The ferromanganese nodules show a marked increase (up to 10 – 100 times) in manganese, cobalt, nickel, zinc, and copper concentrations (Guliy 2004). In contrast, the U and Th contents in the nodules show a weak increase (less than 2 times). Manganese, iron, cobalt, nickel, zinc, lead, and copper in the nodules are subdivided on the basis of character of their correlation into two main groups: Mn, Ni, Zn, Cu and Fe, Pb, and Co. However, our results do not show any strong correlation between these elements and U, Th, and Ra.

The main evidence for a different origin of the same components from the ferromanganese nodules and sediments is their marked difference in correlation coefficients for these materials. As we know from investigation of separate parts of sediments, the upper part of the sediment (darker) is rich in almost every metal due to a lot of small nodules. But, taking into consideration much lower concentration levels of metals in ocean water and sediments we can't accept two major hypotheses of nodule formation: (1) precipitation directly from ocean water, and (2) precipitation from pore solution during diagenesis. From this example we can see a paradoxical situation when from significantly metal-undersaturated solutions precipitate phases rich in some metals. So, the U, Th, and Mn, Fe, Ni, Co, Cu, Zn, and Pb contents and patterns in ferromanganese nodules and sediments studied lead to the idea that an electro-geochemical mechanism (adsorption & absorption) for ore component concentration.

CONCLUSIONS

This contribution can be summarized in such ways:

(1) Analysis of ferromanganese nodules from the Clarion-Clipperton zone show

contents of U, Th, Ra, and Sr similar to that from continental rocks.

(2) Results of U determinations show maximum values of U, Th, and Ra in the nodules, i.e., there is a chance to use these elements as additional economic components during future mining of seabed ferromanganese deposits.

(3) Obtained data show that the ferromanganese nodules have been formed in open physicochemical ore forming system from unsaturated seawater components. Ore elements could concentrate in solid phases in case if near bottom natural galvanic elements have been originated. It is suggested that electrochemical mechanisms are the main possible mechanism to enhance adsorption and absorption creating conditions for enhancing these important elements in seabed Mn-Fe nodules on a very scale.

ACKNOWLEDGEMENTS

We would like to thank P. Piven' and V. Gordienko for analytical support in this study.

REFERENCES

- GULIY, V. 2004. Peculiarities of morphology and composition of ferromanganese nodules and possible mechanism of their formation. *Geologist of Ukraine*, **3**, 61-71.
- GULIY, V. & TYSIACHNA, O. 2008. Peculiarities of morphology and composition of the ferromanganese nodules of Clarion-Clipperton region, Pacific Ocean, and possible mechanism of their formation. / International Symposium "Shaping the Future -- Deep-Sea Minerals and Mining, (March 9-12, 2008), RWTH Aachen University. Abstracts, p. 2 – 3.
- KOSCHINSKY, A. 2008. Ferromanganese Nodule Deposits: Distribution, Composition and Origin / International Symposium "Shaping the Future -- Deep-Sea Minerals and Mining, (March 9-12, 2008), RWTH Aachen University. Abstracts, pp. 17 – 20.

Mineralogical, geochemical, and geochronological constraints in the Double S Zone uranium deposit, Lac Turgeon Granite, north shore of the St. Lawrence Seaway, Quebec, Canada

Susan Kingdon¹, David Lentz¹, & Douglas Hall²

¹Department of Geology, University of New Brunswick, Fredericton, New Brunswick, E3B 5A3 CANADA
(email: Susan.Brodie@unb.ca)

²Microscopy & Microanalysis Facility, University of New Brunswick, Fredericton, New Brunswick, E3B 5A3 CANADA

ABSTRACT: The Main Double S Zone is a system of uraniferous granite and granitic pegmatites occurring within the late tectonic Grenvillian Lac Turgeon granitic intrusion, which is hosted by metasedimentary units of the Grenvillian Wakeham Bay Group. Several episodes of U mineralization occur within this leucogranite and crosscutting pegmatitic dykes. The host leucogranite is similar to the pegmatite dykes in petrology, composition, and age. SEM-BSE images show uraninite and thorite/uranothorite are the major U-bearing minerals and are usually surrounded by chloritic minerals associated with radiation damage of the host phase with alteration. These uraniferous minerals also occur as inclusions in xenotime, monazite, and zircon and are associated with magnetite, rutile, and allanite. Some U minerals are secondary (non-magmatic) occurring within fractures. The granite has Rb (66-369 ppm), Nb (1.2-35 ppm), and Y (3.4-130 ppm) typifying syn-collisional, peraluminous (ASI = 1.15-1.26) granitic intrusions of S-type affinity, coupled with extensive fractionation into the (crustal) A-type granite field. Earlier dating by U-Pb concordia intercept indicates an age of primary U mineralization between 980 and 1000 Ma. The U-Th-Pb chemical monazite dating yield ages of 1028 ± 6 Ma and 981 ± 7 Ma, respectively for the granite and pegmatite.

KEYWORDS: uranium, granitic pegmatite, Lac Turgeon, Grenville Province, Quebec

INTRODUCTION

The uraniferous Main Double S Zone is located within the Lac Turgeon Granite, on the north shore of the St. Lawrence Seaway (North Shore Property) in eastern Quebec, approximately 9 km northwest of the town of Baie Johan Beetz.

Currently, Uracon Resources Limited owns claims to the Main Double S Zone, as well as two other mineralized zones (Middle Zone and TJ Zone) within the North Shore Property. These three zones combined contain a total inferred resource estimate of 154.9 million tonnes at an average grade of 0.012% U₃O₈ and contain 18.48 million kilograms (40.73 million pounds) of uranium using a 0.009% cut off (Uracon website). These resources outcrop at surface, are open at depth and along strike.

The deposit is also host to rare earth element mineralization, and porphyritic granitoids are noted to carry copper-gold and copper-molybdenum (Uracon).

GEOLOGICAL SETTING

Regional Geology

The uraniferous granitic pegmatites occur within the late tectonic Lac Turgeon granitic intrusion, which is hosted by metasedimentary units of the Grenvillian Wakeham Bay Group (Fig. 1).

The Wakeham Group (1.6-1.5 Ga) is the largest remnant of the sedimentary basins formed on the southeastern margin of Laurentia in Mesoproterozoic time. The Wakeham Bay Group consists of a north-trending synclinal basin about 3,885 km² in size of quartzites, schists, phyllites, marbles, and aluminous bands interlayered with metagabbro sills. Gabbroic and granitic rocks, such as the Turgeon Lake Granite have intruded and incorporated these units as xenoliths (Fig. 1). These volcanic rocks have a continental arc magmatic signature. The Grenville (1.08-0.98 Ga) orogeny is a major collisional event. It is associated with extensive crustal thickening and

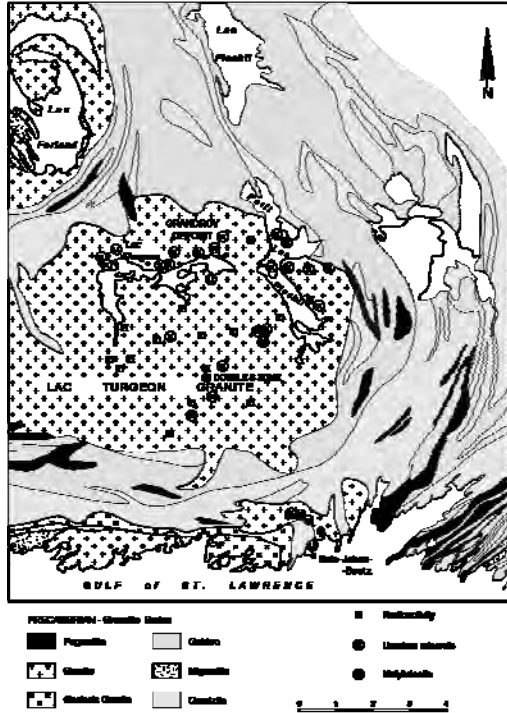


Fig. 1. Geology map of the Lac Turgeon Granite, Quebec. The Main Double S zone is indicated, along with several U occurrences, and the Grandroy deposit (modified from Cooper 1957).

tectonic extrusion, and led to widespread high-grade metamorphism (Ludden & Haynes 2000).

Local Geology

The mineralized Double S zone is a sequence of granitic pegmatite dykes and adjacent coarse-grained granites. At the surface, high radiometric signatures (1500-9000 c/s) in pegmatites and the surrounding granite are used to delineate the zone. The pegmatites range from low to very high radiometric signatures, and can have similar or distinct signatures from their host.

PETROLOGY

The granite outcrops are medium- to coarse-grained and have a hypidiomorphic granular texture dominated by rounded or interlocking quartz grains, and laths of pink, white, and perthitic feldspars.



Fig. 2. Photograph of a pegmatite dyke in host granite (SB-2670). The pencil tip points North.

Biotite and magnetite are also usually present and visible in hand specimen, muscovite may be present, and more rarely other oxides may be seen. Field estimates of modes ranged from 20-35 vol.% quartz, 15-35 vol.% plagioclase, 30-50 vol.% potassium feldspar, and 1-10 vol.% biotite. Accessory minerals include magnetite, muscovite, monazite, xenotime, zircon, apatite, epidote, ilmenite, titanite, allanite, molybdenite, and galena. The major U and Th minerals are uraninite and uranothorite.

The granitic pegmatites are composed largely of alkali feldspar, and to lesser amounts, quartz and plagioclase feldspar, and minor amounts of biotite and magnetite. The pegmatite bodies intrude the granite as dykes, lenses, and pods. The contact may be diffuse; the grain size may gradually grade into the other unit, making the contact difficult to determine. In sample SB-2670, the contact is sharp, but the granite coarsens at the contact and the pegmatite fines at the contact (Fig. 2). The contact may also be very distinct and it may be easy to trace to the edge of the outcrop or to where the intrusion terminates.

The layered quartzite occurs as xenoliths in the granite. The contact between the two units is sharp and discordant, and is locally undulatory. The xenoliths have rounded edges and range in size; xenoliths are very rare within the Main Double S Zone and do not contain U mineralization (e.g., 250-300 c/s).

MINERALIZATION

Uraninite is a common accessory mineral in the texturally homogeneous unzoned granitic pegmatite and peraluminous granite, and is present in both rock types in the Main Double S Zone.

Uraninite is associated with the following minerals: zircon, monazite, carbonaceous material (thucolite?), mica, feldspar, and with rare-earth-bearing minerals. It occurs in small distinct crystals or may be massive. Some grains are discoloured, especially in the centre, metamict, and fractured.

Although the general formula of uraninite is UO_{2+x} the naturally occurring mineral is partly oxidized ($x < 0.25-0.3$) and contains additional elements (Palache *et al.* 1944). The structural formula,

$(U^{4+}_{1-x-y-z}U^{6+}_xREE^{3+}_yM^{2+}_zV)_O_{2+x-0.5y-z-2v}$, shows the common nonstoichiometric uraninite. The composition of the uraninite in the Double S zone ranges as follows: 63.88-81.15 wt% UO_2 , 5.2-9.74 wt% ThO_2 , 7.6-12.36 wt% PbO , 0.58-6.04wt% CaO , and 1.44-6.49 wt% Y_2O_3 , as well as up to 2.64 wt% rare-earth elements (REE) in its structure, with other trace elements.

GEOCHEMISTRY

The pegmatites of the Main Double S zone are classified as Mirolitic-REE class, NYF-A type pegmatites (Černý & Ercit 2005). The granites and pegmatites have a granitic composition (72-73 wt%

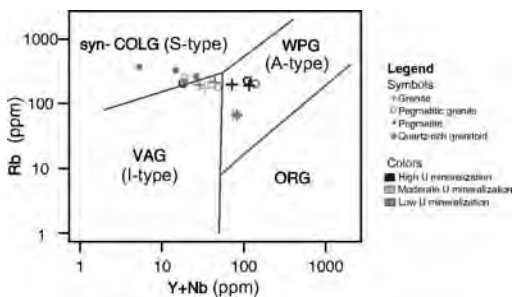


Fig. 3. Tectonic discrimination diagram of Rb versus Y + Nb from Pearce *et al.* (1984) and modified by Christiansen and Keith (1996) for syn-collision granites (syn-COLG), volcanic arc granites (VAG), within plate granites (WPG), and ocean ridge granites (ORG). The diagram suggests the granites and pegmatite were contaminated by a crustal component.

SiO_2), range from ferroan to magnesian (Fe^* of 0.71 to 0.91), mainly alkali-calcic (MALI of 2.26 to 10.75), and weakly peraluminous (ASI of 1.15 to 1.26).

Thorium (4 to 226 ppm) and U values (5 to 787 ppm) vary widely. Their U/Th ratios range from 0.14 to 23, but are typically < 4 .

Large variations in Zr/Hf (1.55 to 79.11), Nb/Y (0.04 to 0.97), and Nb/Ta (0.85 to 84.97) ratios, and moderate Rb/Sr (1.21 to 2.90) ratio reflect low-T crystal fractionation. The granite has Rb (66-369 ppm), Nb (1.2-35 ppm), and Y (3.4-130 ppm) typifying syn-collisional, peraluminous granitic intrusions of S-type affinity, with extensive fractionation into the (crustal) A-type granite field. This is consistent with their age and geologic setting.

GEOCHRONOLOGY

The Lac Turgeon Granite was previously dated at > 980 Ma, based on a U-Pb concordia intercept (Rimšaitė 1982), and 948 ± 23 Ma from a whole-rock Rb-Sr isochron. It has an initial $^{87}Sr/^{86}Sr$ of 0.7090 ± 0.0043 (Fowler & Doig 1983); it is relatively young suggesting it has been partially reset or remained open.

Polished thin sections of the host mineralized granite, SB-2671, and pegmatite with minor mineralization, SB-2670B, were selected for U-Th-Pb chemical monazite dating using to the method of Montel *et al.* (1996).

Forty-nine analyses were taken of the

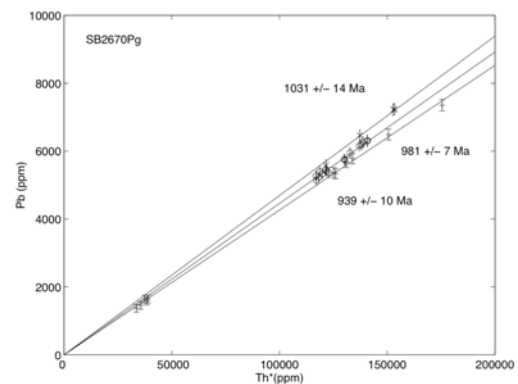


Fig. 4. Pb versus Th^* graph of a pegmatite intrusion (sample SB-2670) showing three age populations.

granite, SB-2671, showing two age populations: P1 of 1028 ± 6 Ma (n=23) and P2 of 946 ± 6 Ma (n=26). The populations can also be defined chemically; P1 has U>2500 ppm and P2 has U<2500 ppm. Although there is some overlap between the populations in Y, P1 generally has greater Y than P2.

Thirty-one analyses were taken of the pegmatite, SB-2670, showing three age populations: P3 of 981 ± 7 Ma (n=16), P4 of 939 ± 10 Ma (n=11), and P5 of 1031 ± 14 Ma (n=4, Fig. 4).

P1 and P5 represent the age of the granite, and agree with previous dating (Rimšaitė 1982). P3 represents the age of the pegmatite. P2 and P4 overlap and represent an event that reset monazite in both the granite and pegmatite, and corresponds to the age that Fowler & Doig (1983) obtained by whole-rock Rb-Sr methods.

Other pegmatites dating around the Grenville Orogeny are older, ranging from ca. 1000 to 1080 Ma (Easton 1986). Even with geologic constraints on the geochronologic data, pegmatites in the southwestern Grenville Province are dated to ca. 1020 to 1060 Ma (Lentz 1996).

CONCLUSIONS

The Lac Turgeon granite was generated at depth due to anatexis of the Wakeham Group, and is associated with high-grade metamorphism tectonically late in the Grenvillian orogeny. Since its age is younger than peak metamorphism, it likely corresponds to a period of adiabatic uplift. The pegmatites were likely derived from the same source as the Lac Turgeon granite, but represent a later stage of melt. Both display characteristics of an A-type source that has been generated from crust.

ACKNOWLEDGEMENTS

I thank Marc Simpson (Uracan) who helped with the sample collection, and provided Main Double S zone maps. Consul-Teck Exploration Incorporated hired me to do field work in the Double S zone. Funding for this project was

provided by Uracan Resources Limited and a NSERC Discovery grant to DL.

REFERENCES

- ČERNÝ, P. & ERCIT, T.S. 2005. The classification of granitic pegmatites revisited. *The Canadian Mineralogist*, **43**, 2005-2026.
- COOPER, G.E. 1957. *Johan Beetz area, Quebec*. Quebec Department of Mines, Geological report, 74 p.
- EASTON, R.M. 1986. Geochronology of the Grenville Province. In: DAVIDSON, A. & BAER, A.J. (eds) *The Grenville Province*. Geological Association of Canada Special Paper, **31**, 271-280.
- FOWLER, A. D. & DOIG, R. 1983. The age and origin of the Grenville Province uraniferous granites and pegmatites. *Canadian Journal of Earth Sciences*, **20**, 92-104.
- LENTZ, D. 1996. U, Mo, and REE mineralization in late-tectonic granitic pegmatites, southwestern Grenville Province, Canada. *Ore Geology Reviews*, **11**, 197-227.
- LUDDEN, J. & HYNES, A. 2000. The Lithoprobe Abitibi-Grenville transect: two billion years of crust formation and recycling in the Precambrian Shield of Canada. *Canadian Journal of Earth Sciences*, **37**, 459-476.
- MONTEL, J.M., FORET, S., VESCHAMBRE, M., NICOLLET, C., & PROVOST, A. 1996. Electron microprobe dating of monazite. *Chemical Geology*, **131**, 37-53.
- RIMŠAITE, J. 1982. Mineralogical and petrochemical properties of heterogeneous granitoid rocks from radioactive occurrences in the Grenville structural province, Ontario and Quebec. In: MAURICE, Y.T. (ed) *Uranium in Granite*. Geological Survey of Canada, **81-23**, 19-30.

Exploration strategies for Uranium deposits

**Kurt Kyser, Paul Alexandre, Paul Polito, Merline Djouka-Fonkwe,
Majdi Geagea, & Yulia Uvarova**

*Department of Geological Sciences & Geological Engineering, Queen's University, Kingston, ON CANADA
(e-mail: kyser@geol.queensu.ca)*

ABSTRACT: Although exploration strategies for uranium differ slightly for each deposit type, radiometrics, geophysics, and drilling are the major tools used. However, certain aspects common to all uranium deposits should be exploited to refine exploration. These include the timing of alteration and mineralizing systems, the nature of the fluids involved in each, the likely source of uranium, and the precipitation mechanism for the ore and alteration minerals. How these can be integrated into exploration is exemplified by comparing and contrasting results from unconformity-related and sandstone-hosted deposits.

KEYWORDS: *uranium, geochronology, basins, exploration, geochemistry*

INTRODUCTION

Exploration strategies for various types of U deposits vary depending on the type of deposit, but there are some general aspects critical to all types of U deposits. Although often considered academic, these should be part of advanced exploration efforts and include; (1) timing of the mineralizing and alteration processes, (2) nature of the fluids involved, (3) source of the U, and (4) the nature of an effective trapping mechanism. These aspects are often overlooked or trivialized relative to more classical aspects such as tectonic or structural setting.

(1) Timing of the mineralizing and alteration events is required in exploration so that the geologic, chemical and physical environment conducive to mineralization at the critical time in the evolution of an environment can be realized. Determining the age of U deposits is not straightforward (e.g., Chipley *et al.* 2005), but precise dating of uranium minerals and associated gangue minerals of known paragenesis, and integration of age data with other geologic factors render interpretation of geochronological data meaningfully for exploration. Without an idea of both the relative and absolute age of the mineralization, and both the alteration and

the host, strategies cannot evolve beyond prospector-driven exploration.

Effective exploration in any deposit requires detailed knowledge of the time-space relationships. For example, magmatic-related deposits form after advanced differentiation of peralkaline, post-orogenic parent magmas to allow extreme U enrichment in the latest magma intrusions and related magmatic fluids. In collision zones, U deposits related to peraluminous leucogranites require melting of the crust, which is facilitated by crustal thickening at an appropriate time during convergence. Metasomatic U deposits are associated with metamorphism during rapid uplift of an orogen, almost exclusively during the Proterozoic. Unconformity-related deposits require 75-100 m.y. after basin formation to allow chemical and thermal evolution of the fluids.

The timing of events that have subsequently affected the ores can also reveal when elements such as radiogenic Pb have been mobilized from the deposits and moved into the surrounding environment. These elements would elevate element concentrations in the surrounding environment, with gradients in concentrations as vectors to the deposits (Holk *et al.* 2003, Kister *et al.* 2004).

(2) Knowledge of the nature of the fluids involved, particularly their origin, temperature, pressure, oxygen fugacity, and chemical composition, is needed to identify the correct environment in which to explore. For example, most highly evolved alkaline intrusives do not host U deposits because they do not evolve to concentrate U in the last fluids, thereby necessitating evolution to magmatic fluids rich in U. Most areas of albitization do not host deposits because there was no reductant to trap the U. Diagenetic brines are involved in the genesis of unconformity-related uranium deposits, but most areas in basins with the appropriate geology and structure conducive to the ore-forming process are devoid of any significant U mineralization because reducing fluids were not present at the appropriate times in these areas. Most sandstone-hosted deposits occur in meanders of paleostreams where organic detritus could accumulate, but most such areas do not host ore because groundwaters either did not flow or did not carry U. Understanding why barren areas that should have ore, but do not, requires knowledge of the physical, chemical, and temporal characteristics of the fluids required to form various types of U deposits.

(3) The source of the U for many deposits is in units that have aberrantly high U contents, such as in volcanic glasses in the case of tabular deposits or in highly differentiated alkaline intrusions in the case of some magmatic-type deposits. Enrichment of U in the source region of basin-hosted deposits certainly increases the probability that a deposit could form (e.g., McNeal *et al.* 1981), as does the availability of U in the source region. Uraninite represents the most easily leachable U (sourced by oxidized fluids). Further, U is unlikely to be released from refractory minerals such as zircon unless they become metamict, which requires time. In sandstone-hosted deposits, unstable volcanic glasses with high U contents, mainly of peralkaline composition, make ideal sources because the U can be effectively mobilized.

(4) Trapping of U is a critical process for the generation of a deposit, with gradients in redox environments a necessity. For example, roll-front deposits best exemplify the gradients that occur in U mobilization and fixation. Deposits in the Paleoproterozoic Franceville Basin have characteristics very similar to unconformity-related deposits, but they occur at a redox boundary between oxidized sandstone and black shales within the basin. Unconformity-related deposits are normally associated with graphite, sulfide or a reducing fluid from the basement. For high temperature environments, such as the Rössing deposit, redox boundaries are represented by graphite-sulfide-rich metasediments. In these and other deposits, carbon appears to be an effective reductant, but there are alternatives such as sulfides and ferrous iron. Graphite, which is intimately associated with most unconformity-related deposits, is geochemically inert and therefore is unlikely to be an effective reductant unless it is modified to a more reactive form.

Although specific tectonic environments, structural settings and lithologies are required for all U deposit types, none of these are definitive indicators of mineralization because most of these settings, structures and lithologies do not host deposits. Thus, they are required for the deposits to form, but are not definitive indicators of mineralization. In effect, the only definitive indicators are geochemical, both in terms of U concentration and in the associated elements.

EXPLORATION STRATEGIES

With few exceptions, there is a paucity of published examples of exploration strategies for U, especially during the past 40 years. This would suggest that either there has been minimal advancement in exploration techniques or that this knowledge is resident in the geologists or companies that survived the drought in uranium exploration. The latter is unlikely given the time and personnel that have passed, and there have been advances in exploration for U other than drilling, but

these have been largely unnoticed. Differences and similarities in exploration strategies are conveniently illustrated by comparing how exploration is normally done for unconformity-related and sandstone-hosted deposits.

Unconformity-related deposits

Exploration for unconformity-related deposits is based firstly on Proterozoic red-bed basins overlying basement complexes and source regions characterized by high U contents. Given this criteria alone, there are nearly 200 basins that would qualify. Graphitic metasedimentary units within the basement complex are desirable, but not necessary, as exemplified by the Nabarlek deposit in the Northern Territory, Australia (Polito *et al.* 2004). Repeated brittle reactivations of ductile structures, normally from far field tectonic events, that may offset the basal unconformity and were foci for fluid flow are required.

Lithogeochemical and mineralogical haloes around unconformity-type uranium deposits can expand the size of drill targets (e.g. Quirt 1985). The ratio K_2O/Al_2O_3 can be useful in delineating hydrothermal illite distribution in the sandstone, and anomalously high boron haloes, corresponding to dravite alteration are also characteristic of these deposits, although dravite is not paragenetically related with the ore-forming process. Uranium, Ni, As, and Co are generally of more limited use because their haloes are restricted to a few tens of metres. The complexity of the basement lithology inhibits the use of individual elements as alteration guides other than in the intensely altered zone (Sopuck *et al.* 1983).

Clay minerals are ubiquitous up to hundreds of metres from hydrothermal U mineralization, and often there is zoning in the type of alteration minerals (Hoeve & Quirt 1984). These can be mapped with remote sensing that can detect in the visible and the middle-infrared sections of the electromagnetic spectrum (Earle *et al.* 1999). The two oxidation states of U and Fe have been proposed to map bleached

alteration zones associated with uranium mineralization using multispectral sensors like Landsat ETM+ (Rajesh 2008).

Lake water and sediment geochemistry and radiometric prospecting are significant tools in early regional exploration for U deposits in Canada (Cameron 1980). The development of anomalies in lakes is a two-stage process wherein U-rich detritus is transported down-ice from the mineralized source and then the metal is dispersed in solution from this detritus into the lakes. Ground-water samples collected from boreholes tens of metres from unconformity-related uranium mineralization have high levels of U, Ra, Rn, and He (Earle & Drever 1983). However, Rn and He distributions can be greatly affected by variations in permeability of the rocks and are frequently ineffective tools to detect buried mineralization (Butt & Gole 1985).

Biogeochemistry has been developed for uranium exploration during the 1980s (Dunn 2007). For example, spruce twigs indicate that tree roots can extract anomalous U from ground water and reflect deposits at 300m depth.

The mainstay of exploration geophysics for all types of U deposits is gamma-ray spectroscopy used in airborne surveys, down hole logging and on outcrops using hand held units. The former is normally collected as part of airborne magnetic surveys with magnetics used to reveal the general geology. Airborne gamma-ray spectrometry directly measures K, eU, and eTh, but only in near surficial material.

Improved magnetotelluric methods have detected deep conductors and shallow alteration zones in the search for deep unconformity-related deposits (Farquharson & Craven 2008). Clay-rich, quartz-corroded quartz-arenite has relatively low resistivity, whereas quartz-rich silicified zones are characterized by high resistivity. Although expensive, 3D seismic has been used to image details of basement topology and more favourable areas for drilling.

Sandstone-hosted deposits

Uranium ore deposits in the Grants

Mineral Belt, New Mexico, occur in fluvial sandstones in the Jurassic Morrison Formation where U is concentrated by dark gray to black humate derived from decaying vegetation. The ores vary greatly in size and shape, generally occur in clusters, and often are difficult targets for drilling. Exploration is done primarily by drilling, delineating favourable ground on a wide-spacing and then using closely spaced drilling in mineralized areas. Criteria for favourable areas includes the presence of a host sandstone, anomalous U contents, dark colour of host rock, presence of carbonaceous matter, and position of an area with respect to mineralized trends (Fitch 1979).

Analysis of groundwater can be a useful strategy for regional exploration for U in the reduced sediments in palaeochannels, although multi-element data are required. Lead isotopes can be used to confirm the groundwater interpretations (Dickson & Giblin 2007). If reduction of U by bacteria is an effective mechanism for formation of U deposits in palaeochannels, then microbial induced geochemical signals, such as carbon isotopes or enhanced mobile metals, should indicate favourable areas.

Geochemical detection of uranium deposits in sandstone-type deposits depends on the geochemical behavior of U and pathfinder elements (Rose & Wright 1980). Uranium is dispersed under oxidizing conditions but is immobile under reducing conditions. Adsorption on freshly precipitated Fe-oxides and certain types of organic matter also limits dispersion unless high concentrations of CO_3^{2-} or other complexers are present. Thorium accompanies U in most plutonic processes, but the two elements are separated under oxidizing conditions. Possible pathfinder elements associated with U in sandstone-type deposits include S, V, Mo, Se, As and at some deposits Cu, Ag, Cr, Pb, Zn, Ni, Co, Re, Be, P, Mn, and rare earths, plus He, Rn, and other radioactive decay products.

Most uranium deposits in sedimentary rocks are associated with geochemical provinces enriched in U and Th or with U-

rich intrusives or volcanic rocks, although the deposits may be separated by tens of kilometres from these U-rich source rocks. Weak regional U and Th anomalies in sediments containing U deposits may be present. Anomalies in U, Se, Mo, V, As, He, Rn, and other pathfinder elements in rock and in ground and surface waters can furnish geochemical guides to ore, as can thermoluminescence (Hochman & Ypma 1984), Pb, S and C isotopes, and textures of Fe and Ti oxides.

CONCLUSIONS

Because U deposits are geochemical anomalies, they are best discovered using strategies that integrate geochemistry as a significant part of the exploration repertoire. Exploration for U deposits, as with any type of deposit, requires the integration of geology, geophysics and geochemistry and must embrace new technologies and research results to be effective and competitive. Although "serendipity" will always be a factor, exploration must be more purposeful, especially as the need to find deposits undercover becomes more urgent. The last boom period was witness to limited success and in predominately brownfield areas. We should prepare ourselves for the next boom by refining models and finding key factors that promote formation of large deposits and the physical and chemical indicators of areas where deposits reside.

REFERENCES

- BUTT, R.M. & GOLE, M.J. 1985. Helium in soil and overburden gas as an exploration pathfinder — an assessment. *Journal of Geochemical Exploration*, **24**, 141-173.
- CAMERON, E.M. 1980. Geochemical exploration for uranium in northern lakes; geochemical exploration for uranium. *Journal of Geochemical Exploration*, **13**, 221-250.
- CHIPLEY, D., POLITO, P.A., & KYSER, T.K. 2007. Measurement of U-Pb ages of uraninite and davidite by Laser Ablation-HR-ICP-MS. *American Mineralogist*, **92**, 1925-1935.
- DICKSON, B.L. & GIBLIN, A.M. 2007. Effective exploration for uranium in South Australian palaeochannels; Geology of uranium deposits. *Transactions - Institution of Mining*

- and Metallurgy. Section B: Applied Earth Science*, **116**, 50-54.
- DUNN C.E. 2007. Biogeochemistry in Mineral Exploration. *Handbook of Exploration and Environmental Geochemistry*, **9**, 1-460.
- EARLE, S.A.M. & DREVER, G.L. 1983. Hydrogeochemical exploration for uranium within the Athabasca Basin, northern Saskatchewan. *Journal of Geochemical Exploration*, **19**, 57-73.
- EARLE, S., WHEATLEY, K., & WASYLIUK, K. 1999. Application of reflectance spectroscopy to assessment of alteration mineralogy in the Key Lake area. *MinExpo '96 Symposium - Advances in Saskatchewan geology and mineral exploration*, Saskatoon, November 21, 22, 1996, Proceedings, 109-123.
- FARQUHARSON, C.G. & CRAVEN, J.A. 2008. Three-dimensional inversion of magnetotelluric data for mineral exploration: An example from the McArthur River uranium deposit, Saskatchewan, Canada. *Journal of Applied Geophysics*, in press.
- FITCH, D.C. 1979. Exploration for uranium deposits in grants mineral belt, New Mexico. *AAPG Bulletin*, **63**, 688.
- HOCHMAN, M.B.M. & YPMA P.J.M. 1984. Thermoluminescence as a tool in uranium exploration. *Journal of Geochemical Exploration*, **22**, 315-331.
- HOEVE, J. & QUIRT, D.H. 1984. Mineralization and Host Rock Alteration in Relation to Clay Mineral Diagenesis and Evolution of the Middle- Proterozoic, Athabasca Basin, northern Saskatchewan, Canada. *Saskatchewan Research Council, SRC Technical Report 187*, 187 p.
- HOLK, G.J., KYSER, T.K. DON CHIPLEY, HIATT, E.E., & MARLATT, J. 2003. Mobile Pb-isotopes in Proterozoic sedimentary basins as guides for exploration of uranium deposits. *Journal of Geochemical Exploration*, **80**, 297-320.
- KISTER P., CUNEY M., GOLUBEV V.N., ROYER J.J., LE CARLIER DE VESLUD C., & RIPPERT J.C. 2004. Radiogenic lead mobility in the Shea Creek unconformity-related uranium deposit (Saskatchewan, Canada): migration pathways and Pb loss quantification. *Comptes Rendus Geosciences*, **336**, 205-215.
- MCNEAL, J.M., LEE, D.E., & MILLARD, JR. H.T. 1981. The distribution of uranium and thorium in granitic rocks of the basin and range province, Western United States. *Journal of Geochemical Exploration*, **14**, 25-40.
- POLITO, P.A., KYSER, T.K., MARLATT, J., ALEXANDRE, P., BAJWAH, Z., & DREVER, G. 2004. Significance of alteration assemblages for the origin and evolution of the Proterozoic Nabarlek unconformity-related uranium deposit, Northern Territory, Australia. *Economic Geology*, **99**, 111-139.
- QUIRT, D.H. 1985. Lithochemistry of the Athabasca Group: Summary of sandstone data. In: *Summary of Investigations 1985: Saskatchewan Geological Survey, Saskatchewan Energy and Mines*, Miscellaneous Report **85-4**, 128-132.
- RAJESH, H.M. 2008. Mapping Proterozoic unconformity-related uranium deposits in the Rockhole area, Northern Territory, Australia using landsat ETM+. *Ore Geology Reviews*, **33**, 382-396.
- ROSE, A.W. & WRIGHT, R.J. 1980. Geochemical exploration models for sedimentary uranium deposits; geochemical exploration for uranium. *Journal of Geochemical Exploration*, **13**, 153-179.
- SOPUCK, V.J., CARLA, A. DE, WRAY, E.M., & COOPER, B. 1983. The application of lithochemistry in the search for unconformity-type uranium deposits, Northern Saskatchewan, Canada. *Journal of Geochemical Exploration*, **19**, 77-99.

Basement-hosted uranium oxides from Athabasca Basin: mineralogy, U/Pb dating, major and Rare Earth Element (REE) concentrations: comparison with U-oxides from deposits located in the vicinity of the unconformity

Julien Mercadier¹, Michel Cuney¹, & David Quirt²

¹G2R, Nancy-Université, CNRS, CREGU, boulevard des aiguillettes, B.P. 239, F-54506 Vandoeuvre lès Nancy
(e-mail: julien.mercadier@g2r.uhp-nancy.fr)

²Areva Resources Canada Inc, 817 45th St W, Saskatoon, SK S7L 5X2 CANADA

ABSTRACT: The basement of the Athabasca Basin (Saskatchewan, Canada) is currently strongly explored for finding basement-hosted uranium deposits comparable to the Eagle Point deposits. However, few data are available on this type of deposit to compare them with deposits located in the vicinity of the unconformity. Recent results obtained by *in situ* analysis on three basement-hosted deposits are presented: the Millennium, Eagle Point, and P-Patch deposits. U/Pb isotopic ages of the best preserved uranium oxides are similar to ages obtained on deposits located in the vicinity of the unconformity (1340 Ma, 1275-1210 Ma, 1100 Ma, 770 Ma and 280 Ma) and they both have the same major-element composition. The Rare Earth Elements (REE) in basement-hosted uranium oxides have bell-shaped chondrite-normalized patterns, similar to those of the deposits located in the vicinity of the unconformity like McArthur River or Cigar Lake deposits. These results suggest that similar processes are involved for the formation of the two types of deposits (basement-hosted deposits and located at the unconformity).

KEYWORDS: Athabasca, uranium deposits, U-Pb dating, REE, basement-hosted

INTRODUCTION

Unconformity-type uranium deposits from the Athabasca Basin (Saskatchewan, Canada) represent the world-richest uranium ores with the McArthur River deposit as a prime example. They are mainly located close to the unconformity between a Paleo- to Meso-Proterozoic sedimentary basin, the Athabasca Basin, and an Archean to Paleoproterozoic metamorphic to plutonic basement. For several years, a new type of uraniferous mineralization, entirely located in the basement, has been drilled in the South-Eastern part of the basin. Few data are available for this type of deposit, limiting the comparison of their characteristics and possible genetic links with deposits located at the unconformity.

Hoeve & Quirt (1984) proposed two models for the dynamic of fluid circulation associated with the formation of unconformity-related deposits : (i) an "Ingress" type model for basement-hosted

deposits with the infiltration of a basin-derived U-bearing oxidized fluid into graphite-rich basement structure and precipitation of U by reaction with reduced basement lithologies, (ii) an "Egress" type model for unconformity-located deposits with the injection into the basin of a reduced basement-derived fluid precipitating uranium by mixing with the basin-derived U-bearing oxidized fluid. The REE patterns obtained for the uranium oxides from both deposits by Fayek & Kyser (1997) tend to support these two models.

The aim of this work is to further characterize the different generations of uranium oxide from three basement-hosted deposits: the Millennium, Eagle Point, and P-Patch with multiple micro-scale analysis techniques. The results will be compared to those previously obtained on uranium oxides from deposits located in the vicinity of the unconformity to evaluate the previously proposed ore formation models.

GEOLOGICAL SETTING

Regional Geology

The basement of the Athabasca Basin comprises Archean and Paleoproterozoic (Aphebian) rocks belonging to two structural provinces (Rae and Hearne) separated by the northeast-trending Snowbird tectonic zone (Hoffman 1990; Fig. 1). The two provinces consist of Archean granitoid gneisses, Aphebian platform metasedimentary rocks and mafic to felsic plutons (Annesley *et al.* 2005).

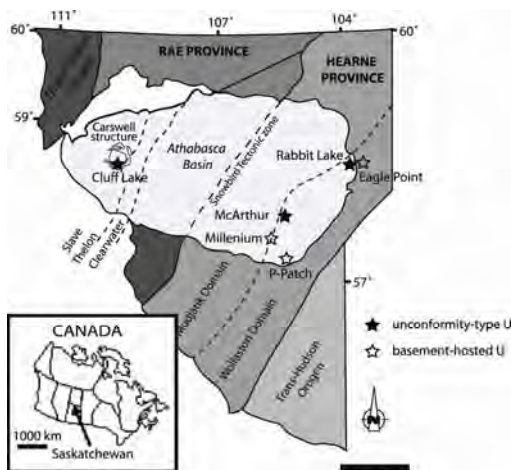


Fig. 1. Location of the Millennium, Eagle Point, P-Patch, and some of the main unconformity-type uranium deposits in Athabasca Basin (modified from Card *et al.* 2007)

The Athabasca sedimentary Basin consists of Helikian polycyclic, mature fluvial to marine quartz-rich sandstone deposited in a near-shore shallow shelf environment (Ramaekers 1990) with an estimated filling beginning at about 1700 to 1750 Ma (Armstrong & Ramaekers 1985). The estimate maximum thickness of the basin was 5 to 6 km from fluid inclusion studies (Pagel 1975).

RESULTS

Isotopic U/Pb dating of basement-hosted uranium oxides

For each deposit, the uranium oxides were carefully studied by SEM and EPMA to separate the different generations and

to select the less altered zones for isotopic U/Pb analysis.

Several U/Pb isotopic ages were determined by ion microprobe (Cameca IMS-3f) for the Millennium and Eagle Point deposits: 1340 Ma, 1275-1210 Ma, 1100 Ma, 770 Ma from Concordia diagrams (Fig. 2) and 278 Ma ($^{207}\text{Pb}/^{206}\text{Pb}$ age).

Similar ages were obtained on Athabasca Basin deposits for mineralizations located in the vicinity of the unconformity or partly in the basement (McArthur River or Cigar Lake for example). The oldest ages obtained on uranium oxides from several deposits (i.e. Alexandre *et al.* 2009) have not been obtained in the present study. Such a feature could be linked either to lack of uranium deposition in the basement during this period or to the dissolution of the first U-oxides generations by later fluid circulation events.

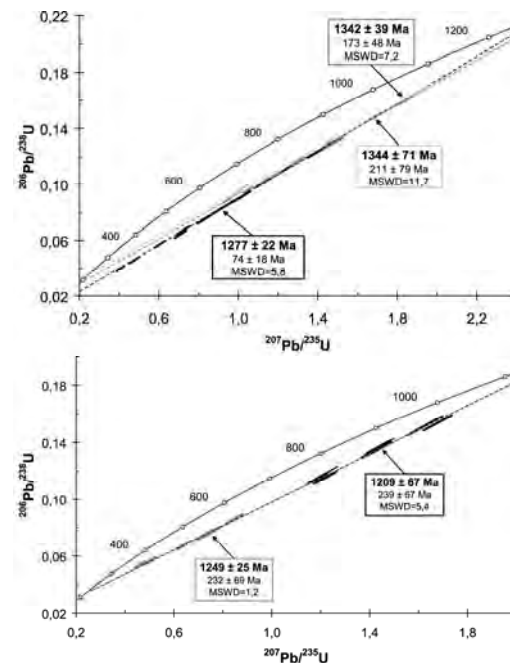


Fig. 2. U/Pb isotopic dating of different generations of uranium oxides from the Millennium (upper part) and Eagle Point (lower part) deposits.

REE abundances for basement-hosted mineralizations

Most uranium oxide generations which have been dated were also analyzed for

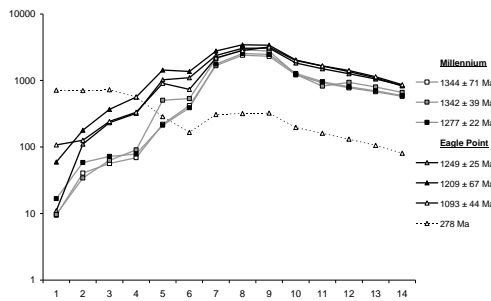


Fig. 3. Chondrite-normalized mean REE patterns of different generations of uranium oxides from the Millennium (square) and Eagle Point (triangle) deposits with their corresponding U-Pb isotopic age.

their REE contents by ion microprobe (Cameca IMS-3f) (Fig. 3).

The uranium oxides from the Eagle Point and Millennium deposits have bell-shaped REE patterns centred on Tb or Dy, typical of unconformity-related deposits (Pagel *et al.* 1987; Fayek & Kyser 1997; Bonhoure *et al.* 2007). All uranium oxides, from both deposits, presenting the oldest U/Pb ages (1340 Ma, 1275-1210 Ma, and 1100 Ma) have identical Heavy Rare Earth Elements (HREE) fractionation and abundance. Light Rare Earth Element (LREE) concentrations are identical between the different uranium oxide generations, from each deposit, whatever their U/Pb age but the LREE abundances differ between the two deposits. This difference is considered as reflecting the variability of the basement lithologies. However, the youngest uranium oxide generation (280 Ma) is strongly enriched in the lightest REE, but with the same bell-shaped pattern defined by the HREE.

REE abundance in uranium oxides from basement versus basin deposits

Uranium oxides studied by in-situ methods (Bonhoure 2007), Bonhoure *et al.* (2007), this study), from deposits located in the vicinity of the unconformity (Fig. 4) or in the basement have nearly identical REE abundance and fractionation (HREE/LREE>1).

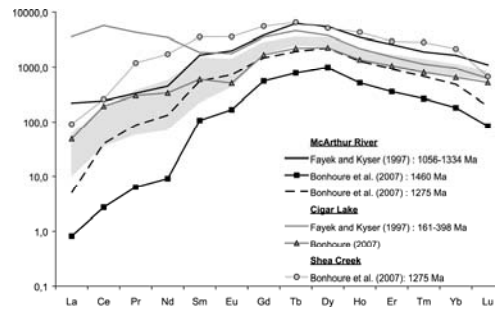


Fig. 4. Chondrite-normalized mean REE patterns of uranium oxides from deposits located near the unconformity (McArthur River, Cigar Lake and Shea Creek) and from basement deposits (grey zone, this study). Fayek & Kyser (1997): chemical age; Bonhoure (2007) and Bonhoure *et al.* (2007): U/Pb isotopic age.

For an equal isotopic age, and at the Athabasca Basin scale, uranium oxides located at the unconformity or in the basement have similar REE abundances.

CONCLUSION

This study has permitted us to obtain a large and systematic database of the geochemical characteristics and the ages of the different generations of uranium oxides from several basement-hosted deposits from Athabasca Basin.

The isotopic ages obtained for basement-hosted uranium oxides are identical to those published for uranium oxides located at the unconformity, indicating that the same fluid circulations, at a large scale, existed in both environments.

The chondrite-normalized REE patterns for basement-hosted uranium oxides are similar, except for a small variation of LREE abundances, indicating identical physico-chemical deposition conditions (T, pH, fluid composition) for the Eastern part of the Athabasca Basin basement. The previous REE distinction made between “Ingress” and “Egress” deposits (Fayek & Kyser 1997) is not confirmed by the present study, because both types have similar REE abundance and fractionations, indicating the similarity of the sources and the processes for both deposit types. Thus, these results suggest

reconsidering the previously “Ingress” and “Egress” models.

ACKNOWLEDGEMENTS

We thank Areva Resources Canada Inc and CAMECO for their assistance and for authorizing us to sample the mine sites. Areva NC is acknowledged for its financial support.

REFERENCES

- ALEXANDRE, P., KYSER, K., THOMAS, D., POLITO, P., & MARLAT, J. 2009. Geochronology of unconformity-related uranium deposits in the Athabasca Basin, Saskatchewan, Canada and their integration in the evolution of the basin. *Mineralium Deposita*, **44**, 41-59.
- ANNESLEY, I.R., MADORE, C., & PORTELLA, P. 2005. Geology and thermotectonic evolution of the western margin of the Trans-Hudson Orogen: evidence from the eastern sub-Athabasca basement, Saskatchewan. *Canadian Journal of Earth Sciences*, **42**, 573-597.
- ARMSTRONG, R.L. & RAMAEKERS, P. 1985. Sr isotopic study of Helikian sediment and diabase dikes in the Athabasca Basin, northern Saskatchewan. *Canadian Journal of Earth Sciences*, **22**, 399-407.
- BONHOURE, J., KISTER, P., CUNEY, M., & DELOULE, E., 2007. Methodology for rare earth element determinations of uranium oxides by ion microprobe. *Geostandards and Geoanalytical Research*, **31**, 209-225.
- BONHOURE, J. 2007. *Géochimie des éléments de terres rares et du plomb dans les oxydes d'uranium naturels*. Ph.D Thesis, INPL, Nancy, France, 390 p.
- CARD, C.D., PANA, D., PORTELLA, P., THOMAS, D.J., & ANNESLEY, I.R. 2007. Basement rocks to the Athabasca Basin, Saskatchewan and Alberta. In: JEFFERSON, C.W. & DELANEY, G. (eds) EXTECH IV: Geology and Uranium EXploration TEChnology of the Proterozoic Athabasca Basin, Saskatchewan and Alberta. *Geological Survey of Canada. Bulletin*, **588**, 69-87.
- FAYEK, M. & KYSER, T.K. 1997. Characterization of multiple fluid-flow events and rare-earth-element mobility associated with formation of unconformity-type uranium deposits in the Athabasca Basin, Saskatchewan. *Canadian Mineralogist*, **35**, 627-658.
- HOEVE, J. & QUIRT, D. 1984. Mineralization and host rock alteration in relation to clay mineral diagenesis and evolution of the middle Proterozoic Athabasca basin, northern Saskatchewan, Canada. *Saskatchewan Research Council Technical Report 187*, 187 p.
- HOFFMANN, P. 1990. Subdivision of the Churchill province and extend of the Trans-Hudson Orogen. *Geological Association of Canada Special Paper*, **37**, 15-39.
- PAGEL, M. 1975. Détermination des conditions physico-chimiques de la silicification diagénétique des grès Athabasca (Canada) au moyen des inclusions fluides. *Comptes Rendus Académie Sciences Paris*, **280**, 2301-2304.
- PAGEL, M., PINTE, G. & ROTACH-TOULHOAT, N. 1987. The rare earth elements in natural uranium oxides. *Monograph Series on Mineral Deposits*, **27**, 81-85.
- RAMAEKERS, P. 1990. Geology of the Athabasca Group (Helikian) in northern Saskatchewan. *Saskatchewan Geological Survey, Saskatchewan. Mineral. Resources Technical Report*, **1950**, 49 p.

Two contrasted types of Uranium mineralization in the "Cage" Uranium district, Nunavik, Quebec, Canada

Jérémy Neto¹, Christian Marignac¹, Michel Cuney¹,
Claude Caillat², & Jean Luc Lescuyer²

¹G2R, Nancy Université, CNRS, CREGU, BP239, F54506, Vandoeuvre les Nancy FRANCE
(e-mail: netojeremy@g2r.uhp-nancy.fr)

²AREVA NC, Tour AREVA, 1, Place Jean Millier, 92 084 Paris La Défense Cedex FRANCE

ABSTRACT: The CAGE district discovered in 2005 is located to the Northeast of the Canadian Shield, along the eastern margin of the Ungava Bay. The uranium showings are hosted by the Lake Harbour Group, a Paleoproterozoic metasedimentary sequence intruded by several pegmatoid generations at the end of the Torngat Orogen (1.87 – 1.77 Ga). Two contrasted types of uranium mineralization have been distinguished according to their geological setting, and mineralogical and geochemical characteristics, but both give the same U-Pb isotopic age on uraninite (1790 ±10 Ma):

(i) The first type occurs in impure dolomitic marbles and skarnoids. The mineralization consists in pure uraninite associated with enrichments in Ba, V, Zn, Pb, and S. REE patterns of uraninite present no or a positive Eu anomaly and a low global REE abundance. Organic matter and sulfides may have represented the initial uranium traps.

(ii) The second type is hosted by calc-silicate rocks (skarnoids or primary skarns) located in close vicinity of pegmatoid injections associated spatially with tremolite, scapolite, phlogopite, and calcite in veins. The mineralization consists in Th-rich uraninite and uranothorianite, characterized by REE patterns typical of magmatic uraninite. It is probably related to magmatic fluids expelled from pegmatites during a transtensive event at the end of the Torngat tectonic-magmatic cycle.

KEYWORDS: *Cage, marble, skarnoid, primary skarn, REE pattern*

INTRODUCTION

The Cage district was discovered during an exploration survey made in summer 2005 in northern Québec, by Claude Caillat (AREVA) and Serge Genest (Omegalpa). Two contrasted types of U mineralization have been recognized and are associated with marbles and "skarns s.l." of Lake Harbour Group: one is represented by Th-bearing uraninite and uranothorianite; the other by Th-free uraninite.

The aim of this study is to use mineralogical and geochemical tools for characterization of both types of uranium mineralization and possible identification of the U source(s).

GEOLOGICAL SETTING

The Cage district is located to the North-East of the Canadian Shield, along the eastern side of the Ungava Bay (Fig.1).

The Cage district belongs to the Core Zone of the south-eastern Churchill Province. This province represents a central terrane of reworked Archean gneiss and Paleoproterozoic intrusives and supracrustal rocks sandwiched between the Archean Nain and Superior cratons during Paleoproterozoic oblique collisions. The Torngat Orogen which welds the Core Zone to the Nain Craton in the East (1.87-1.82 main stage; 1.8-1.77 uplifting and associated pegmatites) and the New Quebec Orogen which welds the core zone to the Superior craton in the West (1.82-1.77) are formed during these collisions (Wardle et al., 2002).

REGIONAL GEOLOGY

The Core zone is divided into four lithostratigraphic units (Verpaelst *et al.* 2000):

1) the Kangiqsualujuaq Complex,

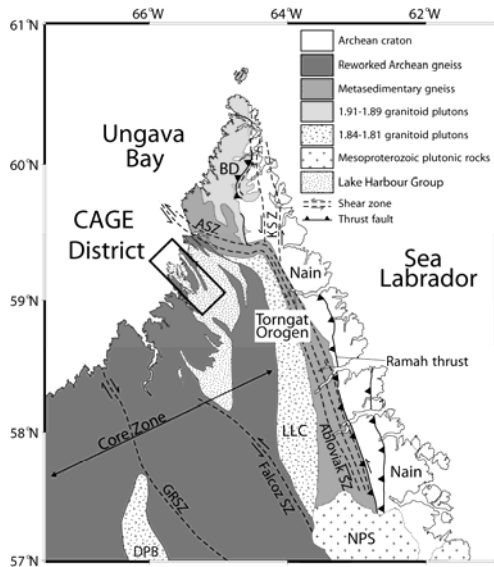


Fig. 1. Location map of the Cage District in northern Quebec within the Core Zone of the Churchill Province. KSZ-Komaktorvik Shear Zone; GRSZ-George River Shear Zone; NPS-Nain Plutonic Suite; DPB-De Pas Batholith; BD-Burwell Domain; LLC-Lac Lomier Complex (modified from Wardle *et al.* 2002).

comprising tonalitic and granitic orthogneisses crosscut by Archean granitoid plutons and dykes, remobilized during the Paleoproterozoic.

2) the Baudan Complex, corresponding to Archean granitic gneisses and diatexites, remobilized during the Paleoproterozoic.

3) the Lake Harbour Group, a Paleoproterozoic platform sequence of approximately 1 km thickness represented by calcitic and dolomitic marbles, paragneisses, calc-silicates rocks, quartzites, and metabasalts injected by several generations of pegmatites. The stratigraphic polarity is still not defined. Possible evaporites are proposed as the source for a Lapis Lazuli mineralization in extension of this Group in the Baffin Island (Hogarth & Griffin 1978).

4) the Nuvulialuk Mafic Suite, consisting in Proterozoic ultramafics and gabbros intruded as dykes and sills in the Lake Harbour Group.

Most U showings in the Cage District are located in marbles and “skarns s.l.” belonging to the Lake Harbour Group.

Tectono-magmatic evolution

The tectonic study of the Cage district suggests that a continuum deformation linked to the Torngat Orogen is developed in the Lake Harbour Group and its Archean basement from early syn-foliation recumbent folds to late plurikilometric symmetric folds. N130°E is the average strike of these structures.

Towards the end of this tectonic evolution, a transtensive deformation (N130° dextral) is accompanied by the generation of U-Th enriched pegmatites along the marble/paragneiss contact, which apparently postdates a first generation of non radiogenic pegmatites associated with primary skarn.

URANIUM TH-FREE MINERALIZATION

This type of U mineralization is hosted in dolomitic marbles and skarnoids with Ca/Mg cationic ratios comprised between 0.7 and 1.1, without direct relationship with the pegmatite intrusions. Marbles are made of dolomite and variable amounts of forsterite and phlogopite, rarely K-feldspar. The skarnoids bear diopside and tremolite as major minerals and K-Feldspar, quartz, and scapolite (40%<Me<60%) as minors components. Skarnoids form elongated boudins within marbles bands, which can be followed over several kilometres along strike. In the dolomitic marbles and skarnoids, U mineralization is represented by very fine (<200µm) euhedral uraninite crystals as inclusions within carbonates and silicates, often rimmed by molybdenite.

High U contents are consistently associated with high Ba (as barite, Ba-rich K-feldspar and Ba-phlogopite, celsian, kampfite $Ba_{12}(Si_{11}Al_5)O_{31}(CO_3)_8Cl_5$), V (as coulsonite $Fe_{2+}V_{3+}2O_4$, V-Pyroxene), Zn (as sphalerite), S (as pyrite, pyrrhotite), Cu (as chalcopyrite), As (as arsenopyrite), and Sb (as ullmanite $NiSSb$). Non radiogenic galena cements this mineral assemblage. Graphite associated with uraninite has been identified in one marble occurrence.

REE patterns of the uranium oxides present a decreasing fractionation from the light to the heavy REE, with no or a

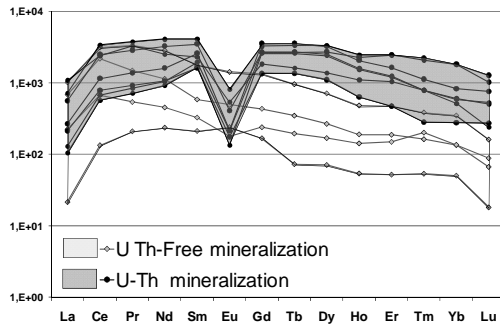


Fig. 2. Chondrite-normalized REE spectra measured on U-minerals of Cage district.

slightly positive Eu anomaly and a low global abundance of the REE (Fig. 2).

U-TH MINERALIZATION

The U-Th showings are located in primary skarn and skarnoid (diopsidite) developed at the contact with pegmatite injections or late migmatitic granite segregations, which are crosscut by infiltration skarns linked to late pegmatite injections at the end of the tectonic-magmatic cycle. Veins of tremolite, scapolite, and phlogopite are spatially associated with the U-Th mineralization, both being related to a late fluid infiltration. The U-Th mineralization seems associated with Fe-enrichment in host rocks.

The U-Th minerals are large (>mm) anhedral crystals of Th-rich uraninite or uranothorianite with lobate contours. High Y₂O₃ contents (0.56±0.1 wt%) are also distinctive of the U-Th mineralization.

REE patterns of Th-rich uraninite and uranothorianite, are characterized by the high REE contents, a weak global fractionation, and a marked negative Eu anomaly (Fig.2), that are typical for magmatic uraninite, in particular those of the Rössing alaskite (Bonhoure 2007).

DISCUSSION

The most distinctive characteristics of the Cage district ore showings are the two contrasted types of uranium mineralization. Th concentration is one of the key geochemical parameters to discriminate both types of mineralization.

In marbles and skarnoids, the consistent U-Ba-Mo-Pb-V-Zn association and absence of Th, the rare occurrence of graphite, and the REE patterns in uraninite are evidences for a possible synsedimentary and/or diagenetic origin of the uranium and associated metals. This primary metal stock located in impure dolostone with possible evaporitic layers (as indicated by the presence of scapolite and kampfite in skarnoids) would have been more or less remobilized during regional metamorphism and tectonics.

Non-metamorphic equivalents of this Th-free mineralization may be sought in some rare limestone-hosted U-occurrences, such as the Jurassic Todilto lacustrine formation in the Grant Uranium Belt (Rawson & Richard 1980), the Cretaceous Toolebuc marine formation in Eromanga Basin (Ramsden 1982), the Mesoproterozoic Vempale marine formation in Cuddapah Basin (Sinha *et al.* 1989), and the Cretaceous Probeer marine formation in the Huab deposit (Hartleb 1988).

A late-metamorphic origin is proposed for the U-Th mineralization because of its spatial association with late pegmatites, its high contents in Th, REE, and Y contents and the typical magmatic REE patterns of the U minerals.

In terms of U-Th mineralogy and host rocks, the U-Th mineralization shares numerous similarities with U-Th-Mo-REE skarns of the Central Metasedimentary Belt of the Grenville Province (Lentz 1998) and uranothorianite rich Tranamaro pyroxenite of Madagascar (Moine *et al.* 1985). In these deposits the U-Th mineralization is related to hydrothermal fluids derived from pegmatite or granite intrusion related to syn-metamorphic partial melting. The different types of skarns could result either from recrystallization of impure siliceous limestones or marls recrystallization during regional metamorphism or from metasomatic reactions between the marbles and a hydrothermal fluid or magmatic intrusion.

The same U-Pb isotopic ages have been obtained for both types of Cage

mineralization at 1790±10 Ma, which corresponds to the uplift phase of the Torngat orogen (Wardle *et al.* 2002).

CONCLUSIONS

The two distinct types of mineralization at Cage could reflect the evolution of uranium from the initial trapping in epicontinental platform sediments to the remobilization by metamorphic processes in a collisional orogen:

1) Primary Ba-Mo-Pb-V-Zn and U-enrichment during sedimentary and (or) diagenetic phase possibly linked to reduction by organic matter.

2) During metamorphism, partial melting of metasediments, and possibly of the basement led to the formation of U-Th-rich anatectic melts and fluids, which have been trapped in “skarns s.l.” forming the second type of U-Th mineralization. During this event (1790±10Ma), local redistribution of the primary mineralization may also occur.

ACKNOWLEDGEMENTS

The authors acknowledge AREVA for the technical and the financial support of this study. We warmly thank all the Cage staff for its assistance during the field work.

REFERENCES

BONHOURE, J. 2007. *Géochimie des éléments de terres rares et du plomb dans les oxydes d'uranium naturels*. PhD Thesis, Université Henri Poincaré.

HARTLEB, J.W.O. 1988. The Langer Heinrich uranium deposit, Southwest Africa/Namibia. *Ore Geology Reviews*, **3**, 277-287.

HOGARTH, D.D. & GRIFFIN, W.L. 1978. Lapis lazuli from Baffin Island - a Precambrian meta-evaporite. *Lithos*, **11** (1), 37-60.

LENTZ, D.R. 1998. Late-tectonic U-Th-Mo-REE skarn and carbonatite vein-dyke system in the southwestern Grenville Province: a pegmatite related pneumatolytic model linked to marble melting (limestone syntexis). In: Mineralized Intrusion-Related Skarn System. Association of Canada Short Course **26**, 519-657.

MOINE, B. *ET AL.* 1985. Les pyroxénites à uranothorianite du sud-est de Madagascar: conditions physico-chimique de la metasomatose. *Bulletin de Mineralogie*, **108**, 325-340.

RAMSDEN, A.R. *ET AL.* 1982. Origin and significance of the Toolebuc gamma-ray anomaly in parts of the Eromanga Basin. *Journal Geological Society of Australia*, **29**, 285-296.

RAWSON, R. & RICHARD, R. 2002. Uranium in Todilto Limestone (Jurassic) of New Mexico – Example of a sabkha-like deposit. *Memoir - New Mexico Bureau of Mines and Mineral Resources*, 304-331.

SINHA, P.A. *ET AL.* 1989. Crystalline magnesite associated with Vempalle dolomites of Cuddapah Basin, Andhra Pradesh. *Journal - Geological Society of India*, **33**, 183-185.

VERPAELST, P. *ET AL.* 2000. *Geology of the Koroc River area and part of the Hébron area*. Rapport RG 2000-2 du Ministère des Ressources naturelles du Québec.

WARDLE, R.J. *ET AL.* 2002. The southeastern Churchill Province: Synthesis of a Paleoproterozoic transpressional orogen. *Canadian Journal of Earth Sciences*, **39**, 639-663.

Applying Pb isotopes in unconformity-type uranium exploration

David Quirt¹

¹ AREVA Resources Canada Inc., P.O. Box 9204, Saskatoon, SK S7K 3X5 CANADA
(email: david.quirt@areva.ca)

ABSTRACT: Lead isotopes have been proposed as indicators of the fluid evolution of sedimentary basins and as guides for exploration of uranium deposits. In uranium exploration, the Pb isotope ratios provide information on timing of mineralization and element remobilization, and presence and timing of U and Pb migration on a regional basis and at drill hole scale. Sandstone distal to known uranium deposits has dominantly non-radiogenic Pb isotope ratios, while sandstone in the region around the uranium deposits often displays radiogenic Pb isotope ratios unsupported by the amount of U in the sandstone. Plots using the $^{206}\text{Pb}/^{204}\text{Pb}$, $^{207}\text{Pb}/^{204}\text{Pb}$, $^{208}\text{Pb}/^{204}\text{Pb}$, and $^{207}\text{Pb}/^{206}\text{Pb}$ ratios show systematic trends useful in unconformity-type uranium exploration. Raw $^{206}\text{Pb}/^{204}\text{Pb}$ downhole plots do not provide information on 'excess Pb' content superimposed upon the original sedimentary/diagenetic Pb, but $^{206}\text{Pb}/^{204}\text{Pb}$ downhole plots adjusted for U content highlight those isotopic values that are unsupported by the amount of U in the sandstone.

KEYWORDS: Pb isotopes, unconformity-type uranium, sandstone, exploration

INTRODUCTION

Uranium oxides easily lose their radiogenic Pb and, in unconformity-type U deposits, part of this Pb has migrated significant distances from the deposits. Thus, the detection and interpretation of radiogenic Pb anomalies may be useful in exploration for these deposits. In particular, the Pb isotope ratios allow discrimination between potential sources of U, such as between U mineralization and background country rock. Several reports concerning the use of Pb isotopes in exploration for unconformity-type uranium deposits have been written since the late 1970s (Robbins & Gupta 1979; Kister, 2003; Holk *et al.* 2003; Kister *et al.* 2004; Carr & Rutherford 2005; Annesley *et al.* 2005).

This report concerns the application of Pb isotope geochemistry in the exploration for unconformity-type uranium deposits in the Athabasca Basin of northern Saskatchewan (Fig. 1). 2006 Pb isotope data from a number of current projects, several with U mineralization, will be discussed (Cigar Lake East, Close Lake, Midwest A, Wolly/McCleen Lake, Cree-Zimmer project, and Shea Creek).



Fig. 1. Location map of deposits in the Athabasca Basin, northern Saskatchewan.

GEOLOGICAL SETTING

These unconformity-type deposits are located around the unconformity between the Helikian Athabasca Group sandstones and underlying Archean to early Proterozoic metamorphic basement (Hoeve & Sibbald 1978; Hoeve & Quirt 1984). The present sandstone cover ranges from 0 to ~1500 m in thickness and is dominantly composed of mature coarse-grained quartz arenite with a kaolin-illite clay matrix.

The deposits are localized at fault intersections, are associated with breccia zones, and are within clay mineral and silicification/desilicification host-rock alteration haloes. Mineralization can be found up to 40 m above and (or) below the unconformity. Basement-hosted mineralization can occur up to 200 m below the unconformity. The high-grade mineralization consists of massive to botryoidal pitchblende/uraninite replacements, veins, and impregnations, with varying amounts of Ni-Co-Fe arsenides, sulfarsenides, and sulfides.

ANALYSES

Approximately 100 g of each drill core sample of sandstone was crushed to -2 mm in a steel jaw crusher and ground to ~150 mesh in a motorized agate grinder.

Each sample was leached/digested using three methods:

1. Weak-acid partial leach - 0.5 g of ground sample material leached for 2 hours in 5 ml of 2% HNO₃ then diluted 10x with weak acid.
2. Aqua Regia partial digestion - 0.5 g of ground sample material digested in 2.25 ml of a 9:1 mixture of concentrated HNO₃:HCl then diluted 15x with deionized water.
3. Total digestion - 0.125 g of ground sample digested in a mixture of concentrated HF/HNO₃/HClO₄ until dry. Residue redissolved in dilute HNO₃ then diluted 8x with deionized water.

All leachates were analysed for ²³⁸U, ²⁰⁴Pb, ²⁰⁶Pb, ²⁰⁷Pb, ²⁰⁸Pb, and ²³²Th using a Perkin Elmer Sciex Elan DRCII ICP-Mass Spectrometer.

Corrections were made on the ²⁰⁴Pb data for ²⁰⁴Hg interference using ²⁰²Hg, and a

procedural blank was analysed. Detection limits for the isotopes were 0.01 ppm for ²³⁸U, ²⁰⁶Pb, ²⁰⁷Pb, ²⁰⁸Pb, and ²³²Th, and 0.001 ppm for ²⁰⁴Pb.

RESULTS

Systematic trends in ²⁰⁶Pb/²⁰⁴Pb, ²⁰⁷Pb/²⁰⁴Pb, ²⁰⁸Pb/²⁰⁴Pb, and ²⁰⁷Pb/²⁰⁶Pb ratios are observed in the data. The shallow uraniumogenic Pb trend in the ²⁰⁶Pb/²⁰⁴Pb-²⁰⁸Pb/²⁰⁴Pb plot (Fig. 2), with high ²⁰⁶Pb/²⁰⁴Pb ratio values, is consistent with elevated U/Th values, suggesting the presence of a high-priority target. This diagram also shows the effects of detrital Th-bearing minerals (e.g., Eastern Athabasca heavy mineral beds) on the Pb data and total gamma count data.

The features on the ²⁰⁷Pb/²⁰⁴Pb-²⁰⁶Pb/²⁰⁴Pb plot (Fig. 3) can be related to the timing of primary U mineralization and later remobilization.

Strongly anomalous ²⁰⁷Pb/²⁰⁶Pb ratio values correspond to elevated U values, but some samples do display low ratio values, suggestive of radiogenic signature, along with low U contents (Fig. 4).

Sandstone around the uranium deposits typically has radiogenic ²⁰⁶Pb/²⁰⁴Pb isotope ratios (>30) (Fig. 5), with Pb isotopic compositions that are unsupported by the amount of U in the sandstone. This is consistent with the introduction of this Pb

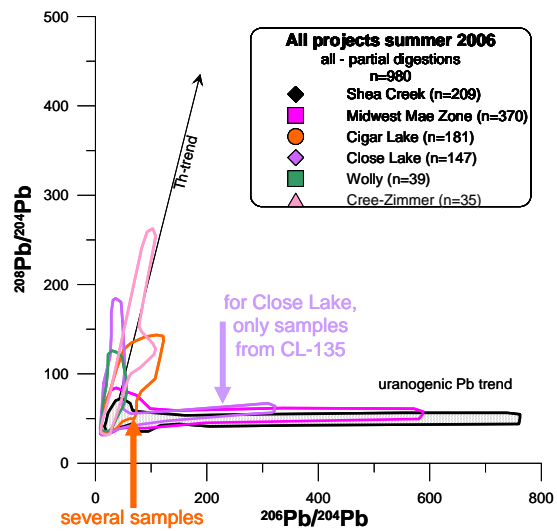


Fig. 2. ²⁰⁶Pb/²⁰⁴Pb-²⁰⁸Pb/²⁰⁴Pb plot.

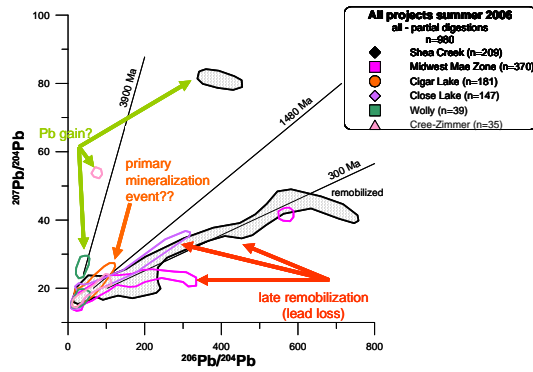


Fig. 3. $^{207}\text{Pb}/^{204}\text{Pb}$ - $^{206}\text{Pb}/^{204}\text{Pb}$ plot.

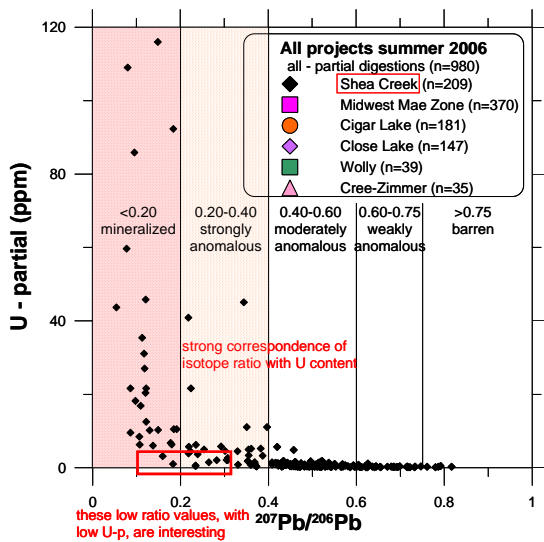


Fig. 4. $^{207}\text{Pb}/^{206}\text{Pb}$ ratio versus U-partial.

from the U deposits during post-mineralization fluid events. The presence of these radiogenic $^{206}\text{Pb}/^{204}\text{Pb}$ ratios show that the sandstone was permeable to late fluids.

The raw $^{206}\text{Pb}/^{204}\text{Pb}$ downhole plots (Fig. 6) illustrate the variations in the original Pb isotope data with depth down the drill hole. But they do not provide information on 'excess Pb' content superimposed upon the original sedimentary/diagenetic amounts by movement/transport of mineral deposit-related U through the sediments.

The adjusted $^{206}\text{Pb}/^{204}\text{Pb}$ downhole plots highlight those isotopic values that are unsupported by the amount of U in the sandstone, consistent with the introduction of these daughter isotopes from the U deposits during post-mineralization fluid

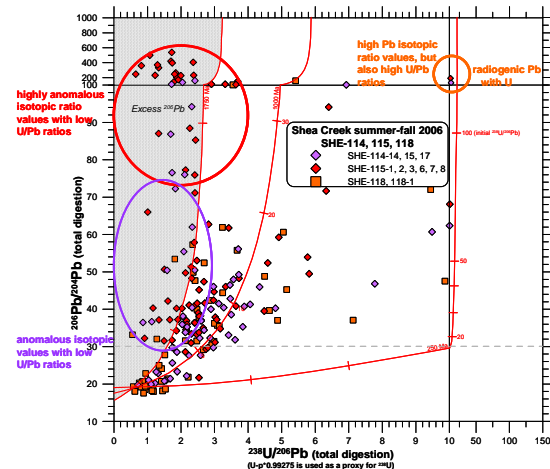


Fig. 5. $^{206}\text{Pb}/^{204}\text{Pb}$ ratio versus U/Pb ratio.

events.

CONCLUSIONS

Plots using the $^{206}\text{Pb}/^{204}\text{Pb}$, $^{207}\text{Pb}/^{204}\text{Pb}$, $^{208}\text{Pb}/^{204}\text{Pb}$, and $^{207}\text{Pb}/^{206}\text{Pb}$ ratios show systematic trends useful in unconformity-type uranium exploration.

$^{206}\text{Pb}/^{204}\text{Pb}$ versus U/Pb plots provide information on Pb isotopic compositions that are supported or unsupported by the amount of U in the sandstone. This information is used in $^{206}\text{Pb}/^{204}\text{Pb}$ downhole plots to reflect 'excess Pb' contents.

Raw $^{206}\text{Pb}/^{204}\text{Pb}$ downhole plots do not provide information on 'excess Pb' content, but adjusted $^{206}\text{Pb}/^{204}\text{Pb}$ downhole plots highlight these unsupported isotopic values.

REFERENCES

- ANNESLEY, I.R., MCCREADY, A.J., HOLSTEN, A., KUSMIRSKI, R., BILLARD, D., & HOCHSTEIN, R. 2005. Lead isotopes as a tool for examining palaeoplumbing in unconformity-type uranium mineralization systems: What are they telling us at Moore Lakes? Abstracts, **30**, Geological Association of Canada-Mineralogical Association of Canada, Joint Annual Meeting, Halifax, May 2005.
- CARR, G. & RUTHERFORD, N. 2005. U exploration using Pb isotopes: Opportunities in partial extraction geochemistry. 22nd International Geochemical Exploration Symposium (IGES 2005), Perth, Australia, September 2005.
- CUNEY, M.I. 2007. Évolution récente des recherches sur la métallogénèse de l'uranium. *Géologues*, **152**, 52-62.

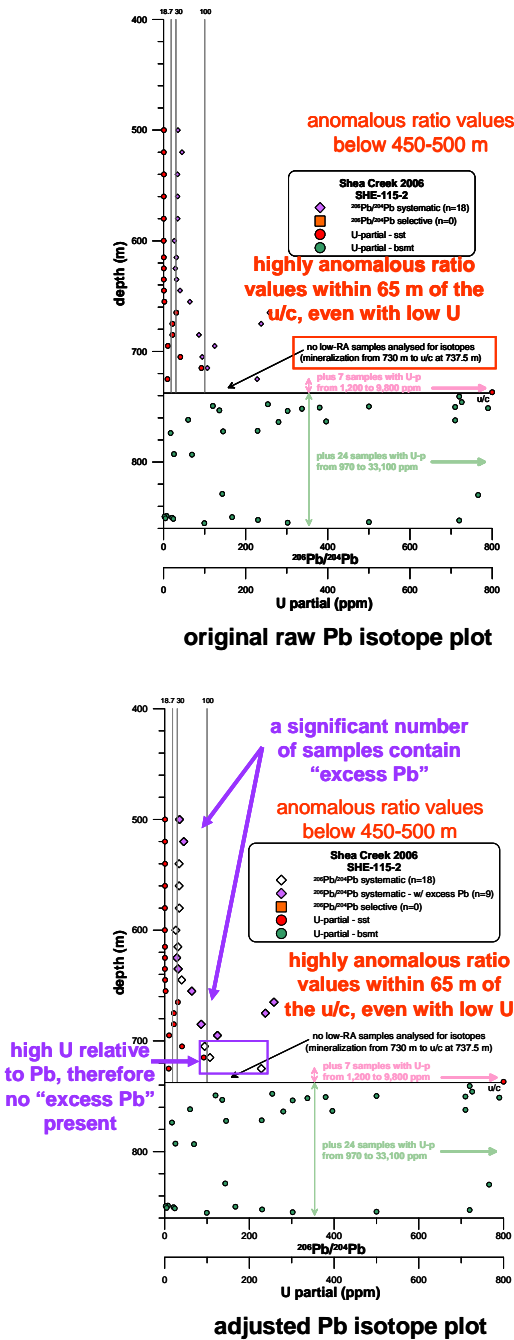


Fig 6. $^{206}\text{Pb}/^{204}\text{Pb}$ downhole plots - raw versus adjusted.

CUNEY, M., CHABIRON, A., KISTER, P., GOLUBEV, V., & DELOULE, E. 2002. Chemical versus ion microprobe isotopic dating (Cameca IMS 3f) of the Shea Creek unconformity type uranium deposit (West Athabasca, Saskatchewan, Canada). *Program and Abstracts*, **27**,

Geological Association of Canada-Mineralogical Association of Canada, Joint Annual Meeting, Saskatoon, May 2002.

FAURE, G. 1986. *Principles of isotope geology*. John Wiley & Sons Inc., 2nd edition, 589 p.

HOEVE, J. & SIBBALD, T.I.I. 1978. On the genesis of Rabbit Lake and other unconformity-type uranium deposits northern Saskatchewan, Canada. *Economic Geology*, **73**, 1451-1473.

HOEVE, J. & QUIRT, D.H. 1984. Mineralization and host rock alteration in relation to clay mineral diagenesis and evolution of the middle Proterozoic Athabasca Basin, northern Saskatchewan, Canada. Saskatchewan Research Council, Technical Report, **187**, 187 p.

HOLK, G.J., KYSER, T.K., CHIPLEY, D., HIATT, E.E., & MARLATT, J. 2003. Mobile Pb-isotopes in Proterozoic sedimentary basins as guides for exploration of uranium deposits. *Journal of Geochemical Exploration*, **80**, 297–320.

KISTER, P. 2003. *Mobilité des éléments géochimiques dans un bassin sédimentaire clastique, du Protérozoïque à nos jours: le bassin, Athabasca (Saskatchewan, Canada)*. Unpublished PhD Thesis, Institut National Polytechnique de Lorraine, Nancy, France.

KISTER, P., CUNEY, M., GOLUBEV, V.N., ROYER J.J., LE CARLIER DE VESULD, C., & RIPPERT, J.C. 2004. Radiogenic lead mobility in the Shea Creek unconformity-related uranium deposit (Saskatchewan, Canada): migration pathways and Pb loss quantification. *Comptes Rendus Geosciences*, **336**, 205-215.

ROBBINS, J. & GUPTA, B.K. 1979. Lead isotope measurements in uranium exploration. Paper no. 60, CIMM AGM, Quebec City, April 1979.

Timing, chemistry, and implication of fluids in Canadian and Australian unconformity-related uranium deposits

Antonin Richard, Michel Cathelineau, Michel Cuney, Marie-Christine Boiron,
Donatienne Derome, & Cécile Fabre

Nancy Université, UMR CNRS-7566 G2R, CREGU, BP239, 54506 Vandœuvre les Nancy cedex FRANCE
(email: antonin.richard@g2r.uhp-nancy.fr)

ABSTRACT: World class unconformity-related U deposits occur in the Proterozoic McArthur Basin (Northern Territory, Australia) and Athabasca Basin (Saskatchewan, Canada). Widespread pre- to post-ore silicifications in the vicinity of the deposits, allow proper observation of paragenetically well-characterized fluid inclusions. We used a combination of microthermometry, Raman microspectroscopy and Laser Induced Breakdown Spectroscopy (LIBS), to establish the physical-chemical characteristics of the main fluids having circulated at the time of U mineralization. The deduced salinities, cation ratios (Na/Ca, Na/Mg) and P-T conditions, led to the detailed characterization of a NaCl-rich brine, a CaCl₂-rich brine and a low-salinity fluid, and to the identification of mixing processes that appear to be key factors for U mineralization.

KEYWORDS: *uranium deposits, unconformity, silicifications, fluid inclusions, fluid mixing*

INTRODUCTION

Unconformity-related U deposits account for more than 33% of the world uranium resource due to their tremendous grade and tonnage. Most of them occur in the McArthur Basin (Northern Territory, Australia) and in the Athabasca Basin (Saskatchewan, Canada). The ore is commonly found close to the interface between Archaean to lower Proterozoic metamorphic and plutonic rocks, and unconformably overlying Proterozoic sandstones. Basement-rooted graphitic reverse faults are also important structural controls.

The most widely accepted models for the formation of unconformity-related U deposits involve the interaction of oxidizing diagenetic brines with a basement-derived reducing fluid, or alternatively with reduced basement lithologies (Hoeve & Sibbald 1978; Kotzer & Kyser 1995; Fayek & Kyser 1997). Uranium is thought to be leached by oxidizing diagenetic brines from accessory minerals either in the basin, or in the basement, or both, but evidence of U leaching are only found in the basement (Hecht & Cuney 2000).

Although fluids were described in previous fluid inclusion studies in Australian (Ypma and Fuzikawa, 1980; Wilde *et al.* 1989) and Canadian deposits (Pagel *et al.* 1980; Kotzer & Kyser 1995), no detailed fluid compositions are available and the following questions still remain: i) How many fluids have occurred in the vicinity of the unconformity-type U deposits? ii) At what P-T conditions have they circulated? iii) What are their major elements compositions? iv) Do they show evidence of mixing? v) What are their chronological and genetic relationships to U deposits?

METHODOLOGY

The precise determination of the composition of individual fluid inclusions in the H₂O-NaCl-(Ca,Mg)Cl₂ system from low temperature microthermometry is often limited by the difficulties in observing the melting of salt hydrates and by their common metastable behaviour. To add, the liquid phase can fail to nucleate any ice or hydrate during cooling down to -190°C.

Thus, when such problems appeared, we used Raman microspectrometry to identify the salt hydrates and to measure

the chlorinity of the aqueous phase (Dubessy *et al.* 2002), and Laser Induced Breakdown Spectroscopy (LIBS) to determine cation ratios Na/Ca and Na/Mg (Fabre *et al.* 1999).

FLUIDS FROM AUSTRALIAN DEPOSITS

The above methods were applied to fluid inclusions from the Jabiluka, Nabarlek, Caramal, South Horn and Ranger deposits. The results are presented in Derome *et al.* (2003) and Derome *et al.* (2007) and summarized here.

These studies revealed the occurrence of three distinct fluids: i) a NaCl-rich brine with about 10-19 wt.% NaCl, 4-11 wt.% CaCl₂, and 0-6 wt.% MgCl₂, ii) a calcium-rich brine with about 1-8 wt.% NaCl, 14-23 wt.% CaCl₂ and almost no detectable MgCl₂ iii) a low-salinity fluid with about 3-13 wt.% NaCl, 1-13 wt.% CaCl₂, and 0-0.6 wt.% MgCl₂.

Both NaCl and CaCl₂-rich brines are thought to have circulated at the base of the sandstones at minimal P-T conditions of 150 ± 20°C and 1250 ± 250 bars. The low-salinity fluid is slightly warmer and is thought to have circulated at depth before being injected at the base of the sandstones. The two brines and the low-salinity fluid were mixed and trapped at the favour of pressure decrease from lithostatic to hydrostatic regime at the time of U deposition.

FLUIDS FROM CANADIAN DEPOSITS

The above methods were applied to fluid inclusions from the McArthur River deposit. The results are presented in Derome *et al.* (2005) and summarized here.

This study revealed the occurrence of three distinct fluids: i) a NaCl-rich brine with about 25 wt.% NaCl, up to 14 wt.% CaCl₂, and up to 1 wt.% MgCl₂, ii) a CaCl₂-rich brine with about 5-8 wt.% NaCl, 20 wt.% CaCl₂, and up to 11 wt.% MgCl₂, iii) a low-salinity fluid with 6-9% NaCl, 2.5-5% CaCl₂ and 0-0.1% MgCl₂.

The NaCl-rich brine is thought to have circulated at P-T conditions of 220 ± 30°C and 1350 ± 150 bars, while the CaCl₂-rich brine is thought to have circulated at P-T

conditions of 110 ± 30°C and 700 ± 200 bars. Mixing between the two brines occurred during the pre-ore stage at 700 ± 200 bars after a pressure decrease from lithostatic to near hydrostatic conditions. The low-salinity fluid doesn't mix with brines and appears to be post-ore.

Ongoing studies on the Rabbit Lake, Shea Creek, Millennium, P-Patch and Eagle Point deposits give similar results. NaCl-rich, CaCl₂-rich brines and mixing trends between the two end-members are found in all deposits. Strictly basement-hosted deposits (Millennium, Eagle Point and P-Patch) share comparable fluid characteristics with classical unconformity-hosted deposits.

CONCLUSIONS

These studies identify three types of fluids in the Australian and Canadian deposits. In both cases, the NaCl- and CaCl₂-rich brines mixed with each other. The main differences between the two cases, is the mixing of the brines with a low-salinity fluid, which took place only in Australian deposits.

In both cases, the CaCl₂-rich brine is thought to have evolved from the NaCl-rich brine after fluid-rock interactions in the basement. The fault zones and the breccia bodies at the base of the basins represent active drainage zones where different fluid reservoirs were connected, and thus a highly favourable location for fluid mixing. Temperature and pressure changes, combined with the effects of fluid mixing, appear to be key-factors in the main stages of quartz cementation and U deposition in both Australian and Canadian deposits.

ACKNOWLEDGEMENTS

We gratefully thank the AREVA NC company for financial support and both the AREVA NC and CAMECO companies for providing samples.

REFERENCES

DEROME D., CUNEY M., CATHELINEAU M., FABRE C., DUBESSY J., BRUNETON P., & HUBERT A. 2003. A detailed fluid inclusion study in silicified breccias from the Kombolgie

- sandstones (Northern Territory, Australia): inferences for the genesis of middle-Proterozoic unconformity-type uranium deposits. *Journal of Geochemical Exploration*, **80**, 259-275.
- DEROME, D., CATHELIN, M., CUNEY, M., FABRE, C., LHOMME, T., & BANKS, D.A. 2005. Mixing of sodic and calcic brines and uranium deposition at McArthur River, Saskatchewan, Canada. A raman and laser-induced breakdown spectroscopic study of fluid inclusions. *Economic Geology*, **100**, 1529-1545.
- DEROME D., CATHELIN M., FABRE C., BOIRON M.-C., BANKS D.A., LHOMME T., & CUNEY M. 2007. Paleo-fluid composition determined from individual fluid inclusions by Raman and LIBS: Application to mid-proterozoic evaporitic Na-Ca brines (Alligator Rivers Uranium Field, northern territories Australia). *Chemical Geology* **237**(3-4), 240-254.
- DUBESSY, J., LHOMME, T., BOIRON, M.-C., & RULL, F. 2002. Determination of chlorinity in aqueous fluids using Raman spectroscopy of the stretching band of water at room temperature: application to fluid inclusions. *Applied Spectroscopy*, **56**, 99-106.
- FABRE, C., BOIRON, M.-C., DUBESSY, J., & MOISSETTE, A. 1999. Determination of ions in individual fluid inclusions by laser ablation optical emission spectroscopy: development and applications to natural fluid inclusions. *Journal of Analytical Atomic Spectrometry*, **14**(6), 913-922.
- FAYEK, M. & KYSER, T.K. 1997. Characterization of multiple fluid-flow events and rare-earth-element mobility associated with formation of unconformity-type uranium deposits in the Athabasca Basin, Saskatchewan. *Canadian Mineralogist*, **35**, 627-658.
- HECHT, L. & CUNEY, M. 2000. Hydrothermal alteration of monazite in the Precambrian crystalline basement of the Athabasca Basin (Saskatchewan, Canada): Implications for the formation of unconformity-related uranium deposits. *Mineralium Deposita*, **35**, 791-795.
- HOEVE, J. & SIBBALD T.I.I. 1978. On the genesis of the Rabbit Lake and other unconformity-type uranium deposits in Northern Saskatchewan, Canada. *Economic Geology* **73**, 1450-1473.
- KOTZER, T.G. & KYSER, T.K. 1995. Petrogenesis of the Proterozoic Athabasca Basin, Northern Saskatchewan, Canada, and its relation to diagenesis, hydrothermal uranium mineralization and paleohydrogeology. *Chemical Geology*, **120**, 45-89.
- PAGEL, M., POTY, B., & SHEPPARD, S.M.F. 1980. Contribution to some Saskatchewan uranium deposits mainly from fluid inclusion and isotopic data. *International Uranium Symposium on the Pine Creek Geosyncline*, Sydney, 639-654.
- WILDE, A.R., MERNAGH, T.P., BLOOM, M.S., & HOFFMANN, C. 1989. Fluid inclusion evidence on the origin of some Australian unconformity-related uranium deposits. *Economic Geology*, **84**, 1627-1642.
- YPMA, P.J.M. & FUJIKAWA, K. 1980. Fluid inclusion isotope studies of the Nabarlek and Jabiluka uranium deposits, Northern Territory, Australia. *International Uranium Symposium on the Pine Creek Geosyncline*, Sydney, 375-395.

Petrological, geochemical, and isotopic evaluation of the Grenvillian uraniumiferous pink and white granitic pegmatites, Fort-Coulonge, Quebec

Caroline Richer¹ & David R. Lentz¹

¹Department of Geology, University of New Brunswick, PO Box 4400, Fredericton, NB E3B 5A3 CANADA
(e-mail: c.richer@unb.ca)

ABSTRACT: The pink and white U- and Th-bearing granitic pegmatites of Fort-Coulonge Quebec were studied using petrology, geochemical analysis, and oxygen isotopes of quartz, feldspar, and biotite. Both pegmatites show some characteristics of NYF-type pegmatite and A-type granite, such as low CaO, MgO, and high Zr. For the oxygen isotope study, 21 mineral separates were obtained picking from 8 rock samples. The $\delta^{18}\text{O}$ values for the analysed minerals are within the general range of pegmatitic rocks, and the order of enrichment of ^{18}O quartz > feldspar > biotite is preserved in most cases. $\delta^{18}\text{O}$ values from quartz vary between 11.3-14.3‰, feldspar between 10.4-11.9‰, and biotite 7.0-8.3‰. The observed wide range of Δ quartz–biotite (+3 to +6‰) and Δ quartz–feldspar values (-0.6 to +3‰) could be the result of isotope exchange between minerals and magmatic fluids in an open system or of infiltration of a small quantity of external fluids.

KEYWORDS: uranium, pegmatite, oxygen isotope, Grenville Province, Quebec

INTRODUCTION

To date no economically viable uranium deposits have been identified in the Pontiac area of Quebec, although is noted for its high airborne radiometric background and presence of several occurrences of low-grade uranium mineralization. Therefore, a petrological and geochemical study of the uranium- and thorium-rich white to pink granitic pegmatites in the Fort-Coulonge area in southwestern Quebec, Canada was initiated to help build a better overview of the characteristics of these uraniumiferous pegmatitic systems.

GEOLOGICAL SETTING

The Grenville Province is a major structural province included within the Canadian Shield. The first two units of this Province are semi continuous, stacked belts: the Parautochthonous belt (PB) and the structurally overlying Allochthonous Polycyclic belt (APB) (Fig. 1). The Allochthonous Polycyclic belt and the Allochthonous Monocyclic belt (AMB) are two allochthonous units. After Carr *et al.* (2000) and Tollo *et al.* (2004), the Allochthonous Monocyclic belt is divided into three separate units: the Wakeham

terrane, the Composite Arc Belt, and the Frontenac-Adirondack-Morin Belt. The Composite Arc Belt is included in the Central Metasedimentary Belt in the tectonic subdivision of Wynne-Edwards (1972).

The Fort Coulonge area is located in the Central Metasedimentary Belt (CMB) in the western part of the Grenville Province about 100 km northwest of Ottawa, Canada. The Central Metasedimentary Belt consists of five units: Bancroft terrane, Elzevir terrane, Mont Laurier terrane, Frontenac terrane, and Adirondack Lowlands. The study area is located within the Mont Laurier terrane that is characterized by metasedimentary and metavolcanic rocks. Granitic, pegmatitic, tonalitic, or gabbroic intrusions of various dimensions and with variable degrees of metamorphism are common throughout the Mont Laurier terrane.

PETROLOGY

Two types of late orogenic granitic pegmatites are found in Fort-Coulonge, intruding ductily deformed and high-grade metamorphic rocks formed during the Proterozoic Grenvillian orogeny. The pink pegmatites are locally sheared, foliated or

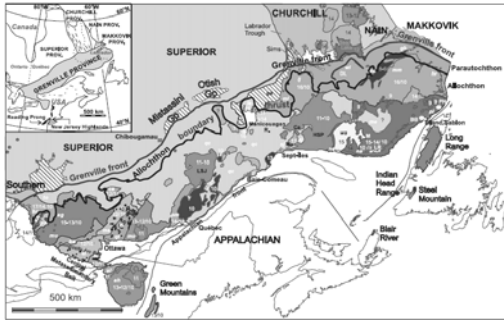


Fig. 1. Map of the geological subdivisions of the Grenville Province (modified after Corriveau *et al.* 2007).

zoned and are mainly quartz, two feldspars, biotite (5-10%), and magnetite (1-5%). Their grain sizes vary from aplitic to pegmatitic (2-5 cm). Hornblende is observed close to the mineralized zones and shows chlorite alteration. Graphic (Fig. 2) and granophyric quartz and K-feldspar intergrowths are common (Madore *et al.* 1994; Lentz 1996). The mineralized zones are mainly represented by uranothorite and zircon. The white pegmatites are unzoned (Fig. 3), vary in grain size from aplitic to pegmatitic (2-5 cm) and locally show graphic or granophyric texture. They contain mainly plagioclase and K-feldspar, both white, quartz, and biotite. Locally, the white pegmatites contain molybdenite or tourmaline as accessory minerals. The mineralized zones rich in U and Th of the white pegmatites contain uraninite, uranothorite or thorite usually located in biotite, K-feldspar, or rarely in apatite. Other accessory minerals that may contain U or Th are monazite, zircon, allanite, and xenotime.

GEOCHEMISTRY & GEOCHRONOLOGY

The pegmatites of the Fort-Coulonge area are classified as NYF pegmatite, AB-U subclass (Černý & Ercit 2005). The two types of pegmatite are peraluminous indicated by an $A/CNK > 1$ and have low CaO, MgO, TiO₂, and P₂O₅ (Fig. 4). All pegmatite samples contain high silica and alkali contents, with SiO₂ ranging from 63-80 wt.% and total K₂O+Na₂O varying from 5.1-10.2 wt.%. Thorium values (10-468 ppm) and U values (<1-613 ppm) vary

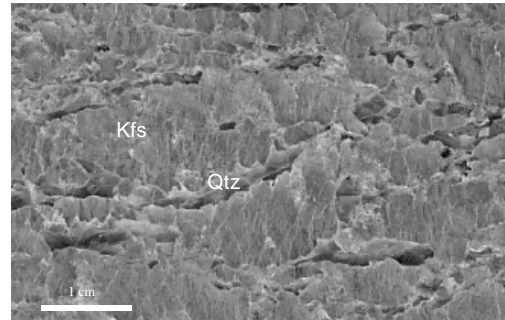


Fig. 2. Photograph of sample FC07-TJCR-258 showing graphic texture in the pink pegmatite.

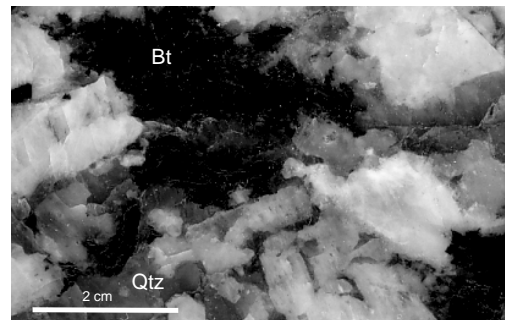


Fig. 3. Photograph of sample FC07-CR-Ch1 showing a pegmatitic texture in an unzoned white pegmatite.

widely. Their Th/U ratios range from 0.77 to 25, but are typically between 2 to 4 indicative of both extensive fractionation and magmatic hydrothermal processes. A total of six samples, four from the pink pegmatite and two from the white pegmatite show enrichment in total REE, with values between 530-712 ppm. Some mineralized white pegmatites have a very high La/Lu between 6280-8360, but with a mode closer to 300. The La/Lu ratio of the pink pegmatite is usually moderate to low, around 150. The white pegmatite has lower Sr values (155-254 ppm) compared to the pink pegmatite (199-659 ppm). The magma shows important crustal contamination, evident from the Rb-Ba-Sr systematics, where these pegmatites fall in the anomalous granite field. Their Nb-Y-Rb contents suggests that they are most likely to be of collisional origin and this is in agreement with them being associated with late orogenic processes (Lentz 1996) such as partial melting, magmatic coalescence, and quartz-

feldspar crystal fractionation leading to U-Th enrichment.

The multiphase pegmatitic intrusions were generated at depth due to anatexis associated with late high-grade metamorphism during the Grenvillian Orogeny. The pegmatites of the western part of the Grenville previously dated at 937 to 980 Ma using whole-rock Rb-Sr isochrons and at 1010 to 1060 Ma using U-Pb zircons, which are 30 to 80 Ma younger than the peak metamorphism at this level of the Ottawa phase of the Grenville orogeny and probably correspond to an uplift period. Recently, sample FC07-CR-Ch1, a white pegmatite was dated using CHIME U-Th-Pb on monazite. The weighted mean age is 1060 +/- 5 Ma and is similar to the ones obtained with previous U-Pb zircon dating.

OXYGEN ISOTOPE

Whole-rock $\delta^{18}\text{O}$ values can be acquired from homogenized rock samples, or from separates of individual rock-forming minerals. When $\delta^{18}\text{O}$ data of individual minerals are available, the oxygen isotope systematics of the rock-forming minerals can be evaluated in δ vs. δ plots (Gregory & Criss 1986).

For this study a total of 21 mineral separates were obtained by hand picking from 8 rock samples. Oxygen isotope analyses were measured using a DELTA^{plus}XP Stable Isotope Ratio Mass Spectrometer. The $\delta^{18}\text{O}$ values for the analysed minerals are within the general range of pegmatitic rocks, and the order of enrichment of ^{18}O quartz > feldspar > biotite is preserved in most cases. Only one sample shows a noticeable disequilibrium conditions with feldspar having $\delta^{18}\text{O}$ value higher than quartz and one sample shows apparent enrichment in $\delta^{18}\text{O}$.

In the δ - δ diagrams, plotted with a mineral which exchanges oxygen relatively slowly (quartz) on the horizontal axis and a mineral which exchanges oxygen relatively rapidly (feldspar, biotite) on the vertical axis, the data from the pink pegmatites shows vertical trends which is usually caused by open-system hydro-

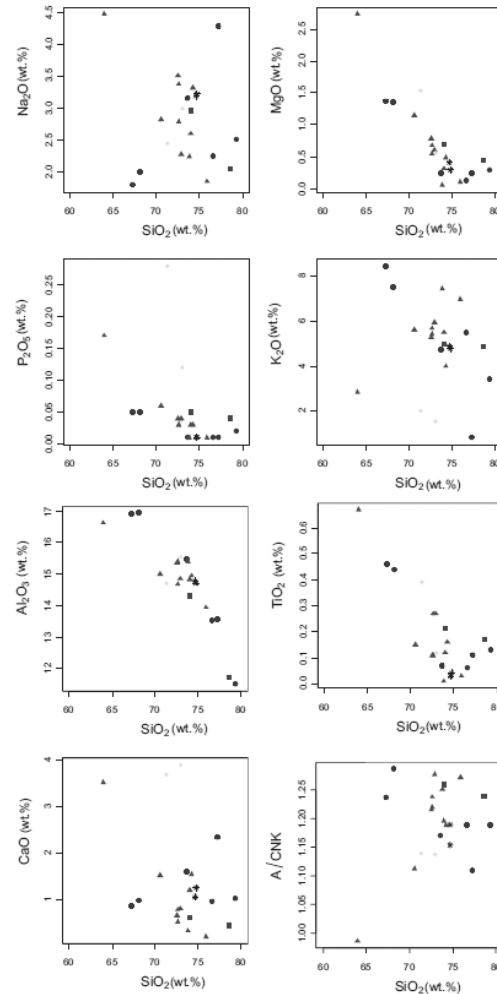


Fig. 4. Harker plots of SiO₂ wt.% vs Na₂O, MgO, Al₂O₃, P₂O₅, K₂O, CaO, TiO₂, and A/CNK. The symbols are: square for host rock, circle for white pegmatite, triangle for pink pegmatite, diamond for mineralized samples, and star for altered pegmatite.

thermal alteration (Gregory *et al.* 1989). The data from the quartz-feldspar diagram of the white pegmatites shows an array with a constant per mil difference (Δ) between the two minerals, indicative of constant temperature crystallization of minerals of different $^{18}\text{O}/^{16}\text{O}$ ratio (Harris *et al.* 1997). The observed wide range of $\Delta_{\text{quartz-biotite}}$ (from +3‰ to +6‰) and $\Delta_{\text{quartz-feldspar}}$ values (from -0.6‰ to +3‰) could be the result of isotope exchange between minerals and magmatic fluids in a system opened to fluid, or of infiltration of a small quantity of

external fluids. Harris *et al.* (1997) used the $\delta^{18}\text{O}$ data of quartz for distinguishing between S-type and I-type (or A-type) granites, as this mineral is generally less sensitive to alteration. The observed quartz $\delta^{18}\text{O}$ values from the Fort-Coulonge pegmatites range between 11.3 and 14.3‰, which is a bit higher than S-type granites. This is probably due to contamination with metasediments or hydrothermal alteration with a fluid having a high $\delta^{18}\text{O}$ value.

CONCLUSIONS

The geochemical analyses showed that the Grenvillian granitic white and pink pegmatites of Fort-Coulonge were affected by crustal contamination, which is characterized by high Rb and Th contents. Furthermore, the oxygen isotope data from the pink pegmatites shows vertical trends, which is usually caused by open-system hydrothermal alteration and the data from the quartz-feldspar diagram of the white pegmatites shows an array with a constant per mil difference (Δ) between the two minerals, indicative of constant temperature crystallization of minerals of different $^{18}\text{O}/^{16}\text{O}$ ratio. This supports the hypothesis that the pink and the white pegmatites of Fort-Coulonge haven't been influenced by the same fluids.

ACKNOWLEDGEMENTS

We thank Aldershot Resources Ltd. for providing funding for analyses and field work. This study was also financed through a NSERC Discovery grant to DL.

REFERENCES

CARR, S.D. *et al.* 2000. Geologic transect across the Grenville Orogen of Ontario and New York. *Canadian Journal of Earth Sciences*, **37**, 193-216.

ČERNÝ, P. & ERCIT, T.S. 2005. The classification of granitic pegmatites revisited. *The Canadian Mineralogist*, **43**, 2005-2026.

CORRIVEAU, L. *et al.* 2007. Prospective metallogenic settings of the Grenville Province. In *Mineral Deposits of Canada: A synthesis of major deposit-types, district metallogeny, the evolution of geological provinces, and exploration methods:*

Geological Association of Canada, Special Publication, **5**, 819-847.

GREGORY, R.T & CRISS, R.E. 1986. Isotopic exchange in open and closed systems. In *Stable isotopes in high temperature geological processes*. Reviews in Mineralogy **16**, Mineralogical Society of America, Washington, 91-127.

GREGORY, R.T., *et al.* 1989. Oxygen isotope exchange kinetics of mineral pairs in closed and open systems: application to problems of hydrothermal alteration of igneous rocks and Precambrian iron formations. *Chemical Geology*, **75**, 1-42.

HARRIS, C., *et al.* 1997. Oxygen and hydrogen isotope chemistry of S- and I-type granitoids: the Cape granite suite, South Africa. *Chemical Geology*, **143**, 95-114.

LENTZ, D. 1996. U, Mo, and REE mineralization in late-tectonic granitic pegmatites, southwestern Grenville Province, Canada. *Ore Geology Reviews*, **11**, 197-227.

MADORE, L. *et al.* 1994. Synthèse géologique de la région de Fort-Coulonge (SNCF 31F). Ministère des Ressources naturelles du Québec, MB 94-39.

TOLLO, R.P. *et al.* 2004. Proterozoic tectonic evolution of the Grenville orogen in North America: An introduction. In: *Proterozoic tectonic evolution of the Grenville orogen in North America*. Geological Society of America, Memoir **197**, 1-18.

WYNNE-EDWARDS, H.R. 1972. The Grenville Province. In *Variations in tectonic styles in Canada*. Geological Association of Canada, Special Paper **11**, 263-334.

Role of geochemistry in the search for Uranium deposits

Samuel B. Romberger¹

¹Department of Geological Engineering, Colorado School of Mines, Golden, Colorado, 80401
UNITED STATES OF AMERICA (e-mail: sromberg@mines.edu)

ABSTRACT: The behaviour of uranium, associated trace elements, and radon in surface and near-surface aqueous environments is discussed as it applies to the exploration for uranium deposits. Elemental dispersion and zoning will depend on composition, Eh, and pH of surface and near surface waters. Mobility is favored by oxidized conditions while uranium will be fixed under reducing conditions. Certain elements show a consistent zoning in deposits and can serve as pathfinders, however, because of its mobility under oxidizing conditions, uranium distribution in rocks, soils, and waters also can be used as vectors for deposits. Dispersion patterns will depend on hydrology, which is controlled by local structure and host rock porosity and permeability. Geochemical and radiometric exploration techniques can be useful as guides to ore when combined with mineral and alteration zoning, structural geology, and geophysical techniques.

KEYWORDS: *uranium, aqueous chemistry, redox equilibria, radon, hydromorphic dispersion*

INTRODUCTION

Exploration models applied to uranium deposits must be cost-effective and timely in order to be useful in the present day competitive environment. Economic uranium deposits take a wide range of forms in a variety of geologic terrains, and methods used must take into account the types of deposits sought. Geochemical methods should be just one component of a well-integrated exploration program, which includes geology, geophysics and radiometric surveys, both on a local and regional scale.

URANIUM GEOCHEMISTRY

The understanding of the geochemistry of uranium and its daughter elements, as well as useful pathfinder elements, in surface and near surface aqueous systems is paramount in the design of exploration models for economically recoverable deposits. This understanding should consider: 1) the mechanisms of uranium transport and deposition, and thus the petrogenesis of the deposits; 2) alteration assemblages typical of various types of deposits, and important in field recognition of mineralization; and 3) the hydromorphic dispersion of uranium and associated elements during secondary

processes, the interpretation of which is the focus of geochemical exploration.

In surface and near surface low temperature aqueous environments the behaviour of uranium is strongly controlled by the oxidation state, pH and the chemical composition of the solution because of its: 1) variable oxidation state (U^{4+} , and U^{6+} as UO_2^{2+}); 2) tendency to hydrolyze to dissolved species such as UO_2OH^+ ; 3) ability to form a large number of aqueous complexes (40) with a number of major and minor anions (OH^- , CO_3^{2-} , Cl^- , SO_4^{2-} , F^- , PO_4^{3-}); 4) tendency to adsorb on organic material and various oxyhydroxides; and 5) ability to form a large number of primary and secondary minerals (145). The latter may contain arsenic, selenium, vanadium, copper, molybdenum, and phosphate as essential components, and therefore some of these elements may serve as important pathfinders. These systems will be chemically open, therefore minor changes in pH and oxidation state will result in competition for uranium between solid phases, resulting in either precipitation or adsorption, and the aqueous phase, resulting in various soluble complexes.

Uranium most commonly is mobile in oxidized groundwaters as the uranyl

carbonate complex, and immobile in reduced fluids as the uranous state (Fig. 1). However, even under oxidized conditions, in the presence of As, Se, P, or V, uranium may be immobilized by the precipitation of various secondary minerals near neutral pH's as shown in Figure 2 for carnotite, $K_2(UO_2(VO_4)_2 \cdot 3H_2O$. These secondary minerals have characteristic spectral behaviour and thus constitute first order visual criteria in recognizing the presence of uranium mineralization. Interpretation of uranium dispersion patterns must consider the possibility of episodic changes in solution chemistry and aquifer composition, resulting in the progressive enrichment or depletion of uranium in space and time.

Figure 1 illustrates that in reduced aquifers uranium would not be mobile. It also shows that uranium can be precipitated well into the field of stability of hematite under oxidizing conditions. This common association between uranium mineralization and hematite needs to be taken into account in any exploration program.

INTERPRETATION

Geochemical data may be collected from the analysis of solids, both primary and secondary, the aqueous phase, either groundwater or streams, or in the case of decay products, the vapor phase. Sampling and analytical procedures should follow protocols typical of any survey employing geochemical methods, with attention paid to proper quality assurance and control issues. The design of a viable geochemical exploration program must include local background and threshold studies, particularly in areas where known uranium geochemical provinces occur.

Characteristics that complicate the interpretation of geochemical and radiometric data for uranium deposits include: 1) variable oxidation state of uranium and associated elements; 2) the variety of aqueous species possible; 3) the tendency for soluble uranium and

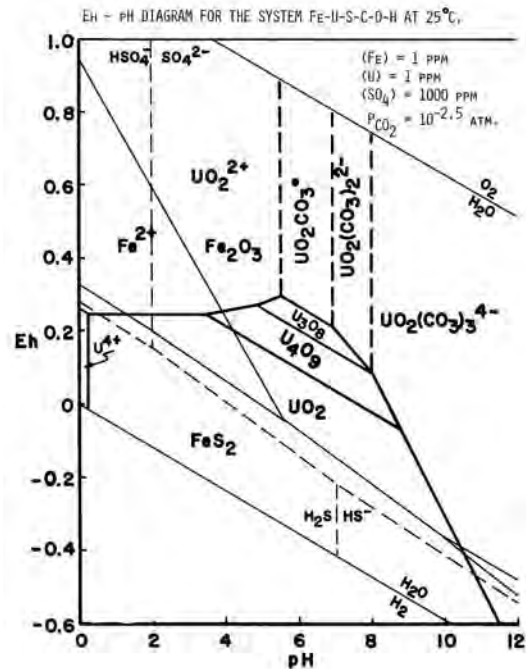


Fig.1. Eh-pH diagram for the system Fe-U-S-C-H₂O at 25 °C showing the mobility of uranium under oxidizing conditions, the relative stability of iron minerals, and the distribution of aqueous sulfur species. Heavy line represents the boundary between soluble uranium (above), and insoluble conditions (below), assuming 1 ppm uranium in solution.

associated elements to adsorb onto various oxides and clays; and 4) the contrasting behavior of uranium and decay products in the secondary environment. Eh, pH and fluid composition are important parameters in geochemical exploration programs. Additionally, the type of deposit targeted will also be important in the interpretation of geochemical data. For example, structurally-controlled deposits such as vein and unconformity-type will produce a dispersion pattern quite different from a sandstone-hosted deposit.

Depending on type, uranium deposits exhibit characteristic primary alteration and trace element zoning patterns, the latter commonly including, but are not limited to, elements exhibiting changes in oxidation state such as vanadium, selenium, molybdenum, arsenic, cobalt, and nickel (Fig. 3). It can be shown that

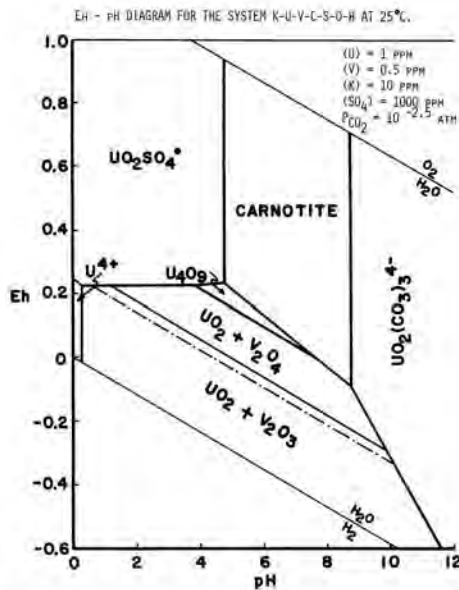


Fig. 2. Eh-pH diagram for the system K-U-V-C-S-H₂O at 25 °C showing the stability of secondary carnotite.

the order in which the elements occur away from the oxidized tongue is directly related to the order in which they precipitate as a result of decrease in Eh (reduction). Analytical data including anomalous amounts of more than one of these elements showing consistent spatial patterns may be useful in determining the type of deposit and the nature of dispersion.

Alteration assemblages may include primary chlorite, illite, smectites, and/or kaolinite, and various primary and secondary iron oxides, carbonates, and sulfides (Fig.1), any one of which may serve as indicators of fluid composition. Lithologic geochemical surveys rely on an understanding of these patterns to vector towards uranium deposits. The interpretation of hydromorphic geochemical surveys, including lake and stream sediment, and soil, depends on the mobility of uranium and associated elements in the surface and near surface environment.

RADIOMETRIC METHODS

The radioactive nature of uranium and associated daughter elements adds an additional dimension to geochemical

methods not typically available for other metallic commodities. The interpretation of radiometric surveys is affected by the degree of disequilibrium between uranium and decay products, which, in turn, depends on the relative mobility of parent and daughter nuclides and their half lives, such as helium, radium, radon, bismuth and lead. Radon and helium will be mobile and most easily detected in the vapor state. However, interpretation can be troublesome. The solubility of all gases in water will be directly proportional to pressure and inversely proportional to temperature. Therefore, interpretation of aqueous gas data will need to take into account both seasonal and diurnal atmospheric conditions. Because of the very low solubility of noble gases such as radon and helium in surface waters, they will be particularly sensitive to meteoric variations. During degassing of natural waters, as a result of groundwater discharge (during the sampling of wells) or in turbulent streams, trace gases will be quantitatively scavenged into the bubbles and pass out into the atmosphere.

Radon probably rarely reaches saturation in groundwater because of its transient nature. Radon (²²²Rn) is the decay product of radium (²²⁶Ra) with a half life of 3.8 days, which decays to polonium (²¹⁸Po, t_{1/2} = 3 min) and ultimately to lead, through alpha decay. The general rule is that after 10 half lives in a closed system the parent radon will be gone (38 days), so the parents of radon, radium or uranium, must be recharged in an open system. Even though radium has a significant half-life of 1600 years, it is very immobile under near surface conditions because it forms insoluble compounds. However, it probably does not reach aqueous saturation because it is readily adsorbed or co-precipitated with various secondary oxides, and may rarely migrate far from the site of uranium decay unless physically transported by stream flow. The contrasting mobility of uranium and these daughter elements suggests relying on total gamma eU determinations for estimation of uranium concentrations may

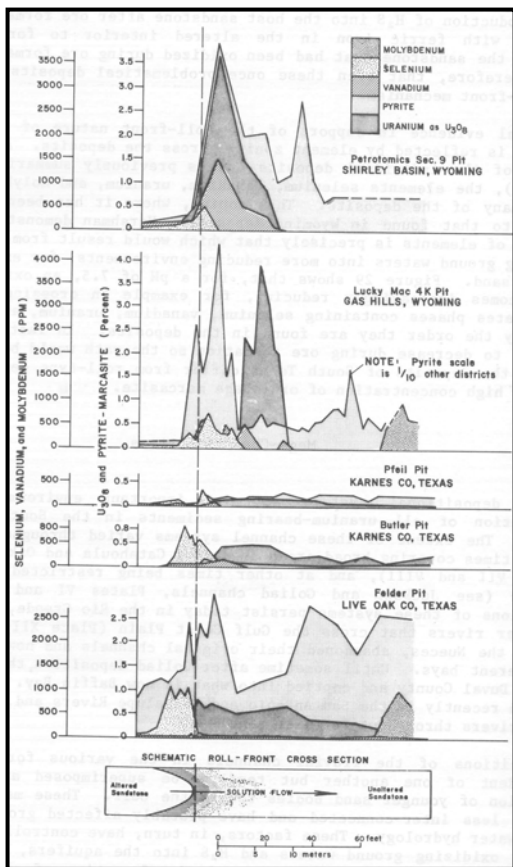


Fig. 3. Elemental and mineral zoning exhibited by selected roll-front uranium deposits. From Adams & Smith (1981) adapted from Harshman (1974).

be suspect, and more up-to-date instrumentation employing wavelength-specific techniques should be used.

Indirect methods have been suggested as viable exploration tools for uranium deposits by investigating radiation damage in minerals produced by radioactive decay processes. Botis *et al.* (2006) described the cathodoluminescence (CL) spectra in quartz in association with uranium mineralization in the Athabasca Basin of Saskatchewan. Hu *et al.* (2008) described the application of electron paramagnetic resonance (EPR) to investigate radiation damage in quartz also in the Athabasca Basin. They showed that radiation-damaged quartz occurred in alteration haloes surrounding known uranium deposits.

CONCLUSIONS

Because of the high mobility of uranium and daughter elements in surface and near surface environments, geochemical methods can be very useful in exploration programs for uranium deposits. However, geochemical surveys should not be used alone, but in conjunction with detailed geology, including, primary lithology, alteration zoning and structure, both pre- and post-mineralization. In hydrologic systems fluid flow is important and structures commonly define pathways that control element distribution during both primary mineralization and secondary dispersion. Pathfinder elements may be useful if their distribution is more widespread than uranium, particularly in hydrothermal deposits. However, because of its high mobility in the oxidizing environment, uranium and its daughter products may exhibit a wider secondary dispersion than associated trace elements, and therefore it may be best to analyze for uranium directly using chemical and/or radiometric methods using wavelength-specific instrumentation.

REFERENCES

- ADAMS, S.S. & SMITH, R.B. 1988. Geology and recognition criteria for sandstone uranium deposits in mixed fluvial-shallow marine sedimentary sequences, South Texas. *Bendix Field Engineering Corporation, Grand Junction*, Colorado NURE Report GJBX-4(81), 146 p.
- BOTIS, S.M., PAN, Y., BONLI, T., XU, Y., SOPUCK, V., & NOKHRIN, S. 2006. Natural radiation-induced damage in quartz. II. Implications for uranium mineralization in the Athabasca Basin. *Canadian Mineralogist*, **44**, 1387-1402.
- HU, B., PAN, Y., BOTIS, S., ROGERS, B., KOTZER, T., & YEO, G. 2008. Radiation-induced defects in drusy quartz, Athabasca Basin, Canada: A new aid to exploration of uranium deposits. *Economic Geology*, **103**, 1571-1580.
- HARSHMAN, E.N. 1974. Distribution of elements in some roll-type uranium deposits. In: *Formation of Uranium Ore Deposits*. International Atomic Energy Agency, Athens, 169-183.

Mobility of Uranium and Radon associated with uranium roll front occurrences in the Horton Group of the Windsor area, Nova Scotia, Canada

R.J. Ryan¹, A.M. O'Beirne-Ryan², D. Finlayson², & A. Parsons²

¹ Nova Scotia Department of Natural Resources, Box 698, Halifax, NS B3J 2T4 CANADA

² Department of Earth Science, Dalhousie University, Halifax NS CANADA

(Email: Rjryan@gov.ns.ca, amryan@dal.ca)

Abstract: There are numerous uranium occurrences in the basin fill units of the Maritimes Basin and in the adjacent crystalline basement rocks in Atlantic Canada. The uranium occurrences in the Carboniferous Horton Group sedimentary strata are sandstone-hosted uranium roll fronts. Recent recognition of deeply weathered granitoids below the unconformity of the Horton Group on the Late Devonian South Mountain Batholith suggests a possible genetic link to regolith-related unconformity deposits as well. The roll fronts in the Horton Group sandstones are known primarily from drill core, however there is an excellent exposure of mineralized sandstone at Green Street, near Windsor, Nova Scotia. The rate and quantity of uranium and radon contributed to surface and groundwater by mineralized outcrops has been poorly documented in the past. Leaching experiments were undertaken using the mineralized sandstones and siltstones from the Green Street occurrence. All of the samples revealed significant uptake of uranium and radon into both distilled water and in samples mixed with natural rain water. These leaching experiments have important implications for the mobility of these elements in the environment and dispersion patterns in regards to geochemical exploration. Although this paper deals primarily with uranium and radon from occurrences in the Windsor area of Nova Scotia, the regional nature the Horton Group strata throughout eastern Canada would seem to imply that environmental issues related to the uranium mineralization might exist throughout the Maritimes Basin. This may be of particular note in areas that have elevated uranium occurrences within granitoid basement rocks adjacent to the Carboniferous basin fill.

Keywords: *uranium, radon, roll fronts, saprolites, mobility, Nova Scotia*

INTRODUCTION

The rate and quantity of radon and uranium contributed to waters exposed to mineralized outcrops and the subsequent mobility of these elements in the present day environment has not been previously documented. This paper presents the results from leaching experiments carried out on uranium-enriched Horton Group sandstones in the Windsor area of Nova Scotia. Understanding of these processes is important both to environmental and exploration geochemistry.

GENERAL GEOLOGY

The rocks and saprolites referred to in this paper are located primarily in southern Nova Scotia (Fig.1). Southern Nova Scotia forms the Meguma Terrane of the northern portion of the Appalachian

Orogen (Williams 1995). The Meguma Terrane is made up primarily of Cambro-Ordovician metasedimentary rocks of the Meguma Group and approximately one third of the terrane has been intruded by Late Devonian granitoid batholiths, the largest of which is the South Mountain Batholith (MacDonald 2001). These basement rocks are overlain by the sedimentary rocks of the Maritimes Basin.

The general stratigraphy of the Maritimes Basin consists of a late Devonian redbed and volcanic sequence referred to as the Fountain Lake Group, Mississippian clastic fluvial-lacustrine rocks of the Horton Group, Mississippian marine evaporite, clastic-carbonate sequence of the Windsor Group, the fine terrestrial clastics of the Mabou Group, the coal measures of the Cumberland Group, and the late

Carboniferous to Permian redbeds of the Pictou Group (Bell 1929). In the area surrounding the Bay of Fundy, there was also a Jurassic-Triassic sedimentary basin (Fundy Group) developed in which sandstones, shales, basalts and minor limestone were deposited. During the Cretaceous fluvial quartz sands and kaolin of the Chaswood Formation were deposited throughout the Maritimes, but only a few outliers have been preserved (Stea & Pullan 2001).

The Horton Group rocks of the Maritimes Basin are hosts to the best documented uranium occurrences (Quarch *et al.* 1981). The Horton Group can be divided into the upper arkosic Cheverie Formation and the lower Horton Bluff Formation.

URANIUM MINERALIZATION

The presence of anomalous levels of uranium, radium, and radon in the Carboniferous-aged Horton Group and underlying basement rocks of Atlantic Canada has been known for many years (Quarch *et al.* 1991; Fig. 1). The exploration model applied on the sandstone-hosted occurrences was that of a uranium roll-front similar to the deposits found in Texas and the western United States. However the recognition of deeply weathered granitoids below the unconformity of the Horton Group on the South Mountain Batholith suggests a genetic link to regolith-related unconformity deposits such as the Athabaska Basin of Saskatchewan may also be applicable.

There is no doubt of the presence of roll fronts in the Horton Group sandstones, however the source of the uranium within the system may be related to the weathered horizons beneath the Horton Group rocks and not exclusively the result of diagenetic change within the sandstones (Ryan & O'Beirne-Ryan 2007).

The granitoid rocks of the South Mountain Batholith in Nova Scotia contain numerous uranium deposits and occurrences. These deposits are interpret-

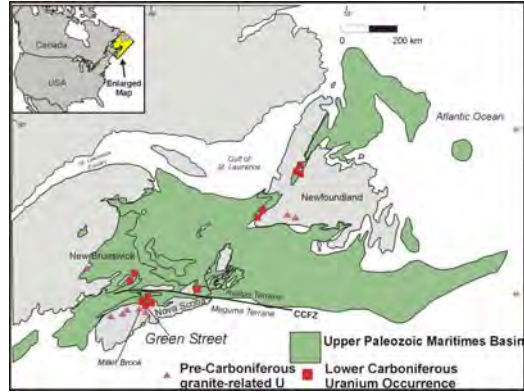


Fig. 1. Location of uranium occurrences in granitoids and the Horton Group in Atlantic Canada.

ed as having been formed due to fluid migration in the late stages of the granitoid emplacement and occur within shear and fracture zones of altered rocks either within the granitoids or as peribatholithic occurrences in the metasedimentary Meguma Group country rocks (Chatterjee 1983). These occurrences exhibit mineralogical evidence that they have been deeply weathered (Chatterjee 1983).

The uranium liberated by weathering of the granitic region must have been incorporated in the surface water and subsequently entered, as uranium-enriched groundwater, into the permeable sandstone and conglomerate aquifers of the Horton Group. Upon entering the sandstones of the Horton Group, the uranium-enriched oxygenated waters caused diagenetic reddening of the sandstone therefore liberating additional uranium into the water that travelled down dip until it reached a reduction-oxidation boundary where the uranium was deposited.

Uranium mineralization in the Windsor area is a typical sandstone roll-front type. The Green Street occurrence that is the focus of this study occurs in thick arkosic sandstones, siltstones, and pebbly conglomerates of the Cheverie Formation (Fig. 2). The occurrence is a remnant tail of a uranium roll front that has subsequently migrated down dip from the outcropping (Ryan & O'Beirne-Ryan 2007).

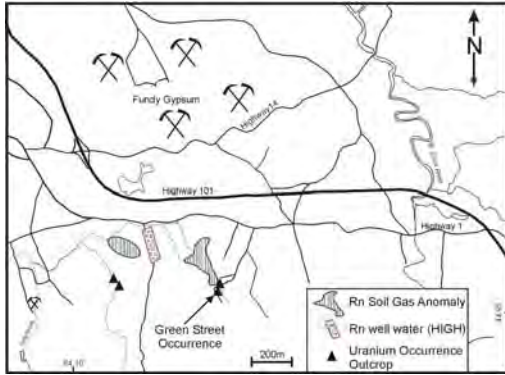


Fig. 2. Location of Green Street Occurrence and related radon soil gas and well water anomalies.

MOBILITY OF URANIUM AND RADON

The initial exploration and subsequent drilling in the Windsor area was sparked by the discovery of radon anomalies in the soil gas and well waters in the area (Quarch *et al.* 1981; Fig. 2). In addition, uranium and radium in well waters were weakly anomalous in the area. It is therefore not difficult to infer that these geochemical techniques are useful exploration tools for deposits of this type and that there are environmental issues related to uranium occurrences in the Horton Group.

A series of leaching experiments were carried out on mineralized sandstone and siltstone from the Green Street Occurrence (Parsons 2007). The samples were poorly consolidated and easily broken apart by hand and placed into the waters. The samples were placed in distilled water, stream water, and rain water at temperatures ranging from 5 to

Table 1. Total uranium in water analyses, leaching experiments using rainwater, Green Street Occurrence, near Windsor Nova Scotia (after Parsons, 2007).

Time	Mineralized sandstone	Mineralized siltstone
8 days	83,000 Bq/m ³	422,000 Bq/m ³
10 days	796,000 Bq/m ³	558,000 Bq/m ³
12 days	>1,000,000 Bq/m ³	>1,000,000 Bq/m ³

20⁰C. In addition to unshaken samples, duplicate samples were agitated at regular intervals for varying lengths of time and subsequently analyzed for uranium and radon. All of the samples demonstrated significant uptake of uranium into the water (Table 1; Parsons 2007). The uranium content of the water from the siltstone sample exceeded the Canadian Drinking Water Quality Guidelines of 20 µg/L. There are no guidelines for Radon in drinking water however the concentrations in the waters exceeded 1,000,000 Bq/m³ (Table 2; Finlayson 2008). Whereas the radon and uranium can easily be incorporated into the surface and groundwater and transported down slope (to the north) the anomalous radon in soil and well waters in the area can be attributed to the mineralized outcrops (Fig. 2).

Table 2. Radon uptake in unshaken distilled water at 20⁰C from mineralized Green Street samples (after Finlayson 2008).

Sample AP06-01	Sample AP06-04
Mineralized Sandstone	Mineralized Siltstone
16 µg/L Uranium	24 µg/L Uranium

Although this paper deals primarily with uranium and radon from occurrences in the Windsor area of Nova Scotia, the areal extent of the Horton Group strata throughout eastern Canada would seem to imply that environmental issues related to the Horton Group uranium mineralization might exist throughout the Maritimes Basin.

ACKNOWLEDGEMENTS

Funding for this project was provided by the Nova Scotia Department of the Environment and Labour and the Nova Scotia Department of Natural Resources.

REFERENCES

BELL, W.A. 1929. Horton-Windsor district, Nova Scotia: Geological Survey of Canada Memoir 155, 268 p.
 CHATTERJEE, A.K. 1983. Mineral deposit studies: contrasting granophile (Sn, W, Mo, Cu, Li) deposits of Nova Scotia. Nova Scotia

- Department of Mines and Energy, Mines and Minerals Branch, Report **83-1**, 49-51.
- FINLAYSON, D. 2008. *Potential for the presence of radon in water from weathered outcrops of uranium-bearing strata of southern Nova Scotia*. BSc Honours Thesis, Earth Sciences, Dalhousie University.
- MACDONALD, M.A. 2001. Geology of the South Mountain Batholith, southwestern Nova Scotia. Nova Scotia Department of Natural Resources, Minerals and Energy Branch Open File Report ME **2001-2**, 281 p.
- PARSONS, A. 2007. *Potential for Uranium mobilization from weathered outcrops of uranium-bearing sedimentary strata, southern Nova Scotia*. BSc Honours Thesis, Earth Sciences, Dalhousie University.
- QUARCH, H., RIKEIT, K., RYAN, R.J., & ADAMS, G.C. 1981. Report on drilling, Hants and Kings Counties, Nova Scotia: Saarberg Interplan Canada Limited. Nova Scotia Department of Mines and Energy Assessment Report, **81-019**.
- RYAN, R.J. & O'BEIRNE-RYAN, A.M. 2007. Preliminary report on the origin of Uranium Occurrences in the Horton Group of the Windsor area, Nova Scotia. *In: Mineral Resources Branch, Report of Activities 2006, Edited by D.R. MacDonald*. Nova Scotia Department of Natural Resources, Report **2007-1**, 137-157.
- SCHENK, P. 1995. Meguma Zone. *In: Geology of the Appalachian-Caledonian Orogen in Canada and Greenland. Edited by H. Williams. Geological Survey of Canada, Geology of Canada, 6*, 261-277.
- STEA, R.R. & PULLAN, S.E. 2001. Hidden Cretaceous basins in Nova Scotia. *Canadian Journal of Earth Science, 38*, 1335-1354.
- WILLIAMS, H. 1995. Introduction, Chapter 1. *In: Geology of the Appalachian-Caledonian Orogen in Canada and Greenland. Edited by H. Williams: Geological Survey of Canada, Geology of Canada, 6*, 1-19.

QA/QC, verification and integration of multisource data for the Novoveska Huta and Kuriskova deposits in Eastern Slovakia

Ravi Sharma

¹*Tournigan energy Ltd. 15782, Marrine Dr.- Unit 1, White Rock, BC, V4B1E6 CANADA
(e-mail: rsharma@tournigan.com)*

ABSTRACT: Novoveska Huta (NVH) and Kuriskova are uranium deposits in eastern Slovakia. They are located at the western end of the Carpathian Mountains. The Western Carpathian Mountain range of Eastern Europe is the result of the Variscan and Alpine multi-cycle collision orogenies and they host a number of uranium deposits. Kuriskova is near the town of Kosice in eastern Slovakia and NVH is approximately 65 kilometres west of Kuriskova. While Kuriskova has been explored since 1980, NVH has a much longer history including uranium production from open pit and underground mining. Uranium mineralization at both of these deposits is similar in style and character, occurring along the contact of meta-volcanic rocks and underlying meta-sedimentary rocks.

These deposits are currently being explored by Tournigan Energy Ltd. The NVH deposit has large amounts of historical data available. The challenge for the Tournigan team was to implement an efficient approach and method for data compilation and verification for integrating all of the different data types and to implement strict QA/QC procedures for more recent data collection and assaying. This paper summarizes the different types of historical data and the procedures and the QA/QC system that Tournigan adopted.

KEYWORDS: *Kuriskova, Novoveska Huta, Historical data, QAQC, Tournigan*

INTRODUCTION

The objective of data validation and verification, along with strict QA/QC procedures, is to ensure the quality of data for reliable mineral resource estimates.

Data collected, stored and validated is of no use unless it is stored in a meaningful way to ensure easy retrieval and presentation. Tournigan Energy Ltd. implemented these QA/QC procedures at an early stage on their projects, before stepping into detailed exploration and mineral resource estimates.

This paper highlights the procedures, QA/QC, and database management system implemented by Tournigan to ensure a reliable and secure data set. The effective QA/QC by Tournigan also helped to establish that Pressed Pellet and Borate Fusion XRF are a more accurate assaying method compared to ICP.

PROJECT GEOLOGY

The Kuriskova Uranium Deposit is located in the Kjsovska Hola region of the Volovec

Hills, which are a component of the Western Carpathian Range. The mountain range at Kuriskova is composed of mesozonal to epizonal metamorphic rocks known as the Gemericum tectonic unit of the Carpathian belt. There is a nearly continuous, 0.5 to 6.0 km wide and 80 km long zone of Permian rocks along the northern periphery of the tectonic unit in which there are numerous uranium occurrences.

The Novoveska Huta and surrounding area are part of the North Gemeric Syncline, which belongs to the Gemericum tectonic unit. The deposit itself is hosted in folded and faulted Permian age rocks. Active exploration in the area continues and is extending the limits of known mineralization.

EVOLUTION OF INDUSTRY STANDARDS

Prior to 1997, only a few QA/QC guidelines existed, and monitoring programs were not commonly conducted by mining companies. In 1997, the Toronto Stock Exchange and the Ontario

Securities Commission established the Mining Standards Task Force. One of the key recommendations, a Qualified Person (QP) concept, was developed.

In 2000, the CIMM adopted “Definitions and Guidelines” for “Standards on Mineral Resources and Reserves, which included a “Checklist for the Estimation of Mineral Resources” and “Exploration Best Practice Guidelines”. In early 2001, new mining disclosure standards were introduced by the Canadian Securities Administrators (CSA) under NI 43-101 (Standards of Disclosure for Mineral Projects), and its Companion Policy 43-101CP, and Technical Report Form 43-101F1.

DATA TYPES AND SOURCE

While Kuriskova has been explored since 1980, Novoveska Huta has information dating back to 1950. Kuriskova information is mainly older historical drill holes and the more recent holes drilled by Tournigan Energy Ltd. The Novoveska Huta data set includes channel samples from underground workings, underground drilling samples, surface drilling results (between 1950- 1990) and Tournigan drill holes from 2007 onwards.

Drill Holes information types			Number of holes	Year
Drill holes LH-NH-1 - 13 (Tournigan holes)			13	2006-2008
Historic holes	surface		106	1950-1990
Historic holes	underground	HP-xx (core)	20	1975-1982
		UP holes (no core)	167	1982-1986
Historic holes	underground	Down holes (core)	184	1982-1986
		composite	2010	1982-1986
Radiometric channel	composite		71	1982-1986
			2571	

DATA VERIFICATION AND COMPILATION

The key tasks in working with historical data was

1. To verify the information was of good quality before proceeding.
2. Compilation of the data in one standard format, which can be imported into Datamine Studio for resource modelling
3. Creation of a secure database for preservation of historical data and storage of future data. The database needed to be easily accessible through the Internet for company personnel.

4. Verify disequilibrium.
5. Document QA/QC procedures for radiometric and geochemical analysis. Implement these procedures. Conduct internal audits to ensure procedure are in place and record actions taken for data that failed the checks.
6. Documenting of standard operating procedures for sampling, chain of custody, QA/QC, survey, logging, and data verification.

To start with, twinning of historical holes and underground raises was carried out to verify the reliability of geology, mineralization and survey information.

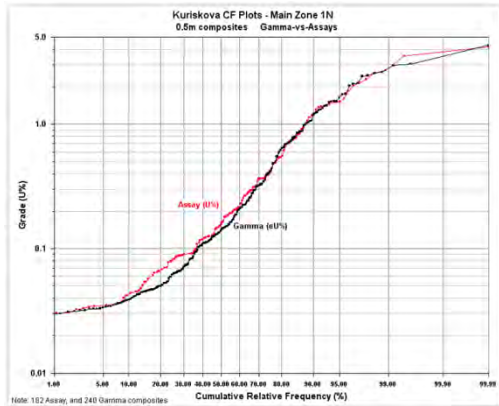
The documentation of all the available types of data in the archives was done and tabulated to decide which information could be verified. Tournigan incorporated only those holes in the database which could be verified from original documentation.

For the historical drill holes that have gamma-only eU data, Tournigan has verified the gamma log conversion data. This was done by randomly selecting 6 drill holes. Graphical logs were re-digitizing and then re-tabulated to create a data table of 0.1m eU% data. This was compared with data from the original 0.1m interval eU% data – essentially a double entry check of the data. For the historical gamma-only holes that have only graphical logs, all logs were digitized and output as 0.1m data tables, then re-plotted graphically and checked against the original plots.

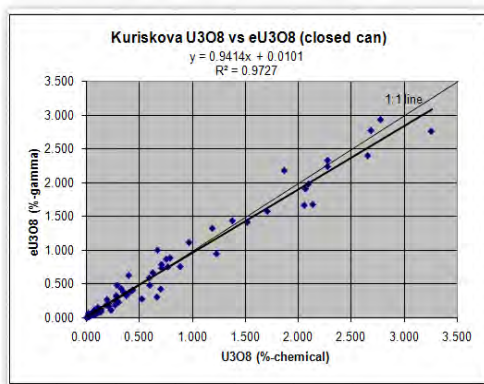
The recent drilling campaigns have essentially validated the mineralization reported by historical workers.

Documentation of radiometric calibration procedure from historical time until recent was discussed reviewed and documented. The results of parameters and software used in the past were verified by reproducing results.

Tournigan carried out closed can analysis to study the comparison of gamma versus assay data for Kuriskova. The general comparative distribution is shown in following CF plot.



Closed can analysis results in the following graph shows disequilibrium analysis done at Energy Lab (US) to verify disequilibrium.



Disequilibrium is the difference in grades, expressed as a ratio, of chemical U_3O_8 to gamma derived eU_3O_8 , as determined for the same sample volume.

Disequilibrium in uranium deposits relates to the chemical dissolution and re-deposition (usually by groundwater) of uranium prior to the time required for that uranium to generate the radiometric daughter products from the natural decay of uranium isotopes (U-238 and U-235)

The gamma logging procedure is indirect measurement of uranium and can be misleading if uranium has been remobilized and there has not been enough time at the original site of deposition for development of daughter products. The results of closed can analysis established the accuracy of

gamma data for historical as well as current drilling.

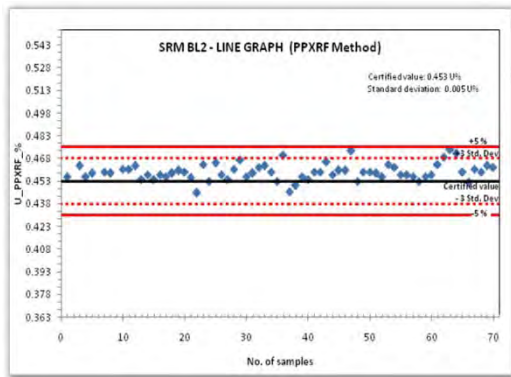
QA/QC FOR ASSAY DATA AND GAMMA DATA

In August 2007, Tournigan instituted a rigorous QA/QC program that is summarized in their corporate project reference manual (Tournigan Energy, 2007). The reference manual enumerates the sampling steps, chain-of-custody (sample management), QA/QC procedures performed, and reporting procedures. Once the samples are delivered to the labs, a dedicated Tournigan geologist tracks the samples, and reports all assay data completed as it is received.

Once initial analyses are completed, random samples are sent from SGS to ActLabs for check assays, to establish precision (repeatability) and analytical bias. Additionally, coarse sample rejects are chosen at random and sent to ActLabs for preparation and analysis, to check the accuracy and repeatability of the original sample preparation. A further check on SGS Lab precision is conducted by renumbering pulps and re-submission from ActLab to SGS for analysis. Tournigan monitors quality assurance by plotting and analyzing the data, as received, and activates re-assaying of sample batches that do not meet pre-determined standards.

Tournigan has done a sufficient amount of analyses by multiple methods ICP, pressed pellet-XRF (PP-XRF), and borate fusion bead and XRF (bf-XRF), to determine that pp-XRF provides the most accurate and precise analyses for uranium.

The following line graph on PP XRF and ICP demonstrate that PP XRF is a better method for the Novoveska Huta and Kuriskova ore types. As part of QA/QC for gamma data, two open holes are used for gamma relogging to obtain duplicate readings. The same drill holes are also relogged to establish accuracy of gamma measurement.



CREATION OF IN-HOUSE ONLINE DATABASE

Instead of implementing standard database packages, Tournigan decided to create their own database system based on .Net framework and SQL server. The salient features of this database are online remote access, multiple level security, documentation of any changes made to the database, compatibility with Datamine for easy updating and reduction of human entry errors, ease of use, inbuilt validations, automatic QC sample insert flags, automated QA graphs, no acceptance of assay data unless it passes QA/QC, automated e-mails to concerned parties in case of delays and the setting of flags for verified holes to be used in Datamine.

CONCLUSIONS

Integration of multi-type and multisource data is useful for any program using historical data. Integration and validation of all the available data types provides a number of real benefits including having a better understanding of the deposit with the more complete database. It also saves costs if historical data can be used rather than re-acquiring the data.

Strict QA/QC in each batch established PP XRF and BF XRF are the best means of sample analysis for the Kuriskova and Novoveska Huta deposits.

The result of all these processes and procedures creates a quality database which can be used to determine a reliable mineral estimate.

REFERENCES

- Kuriskova 43-101 mineral resource report, August 2008.
- Tournigan procedures manual
- Internal memo to Tournigan on disequilibrium by Allan Moran, principle Geologist, SRK, Tucson
- QA/QC at Oyu Tolgoi Cu-Au Project South Gobi, Mongolia - Ivanhoe Mines Mongolia Inc. Meeting and Exceeding Technical Disclosure Requirements Dale A. Sketchley

A U-bearing hydrothermal vein system related to the strongly peraluminous, high heat producing North Pole Stream granitic suite, north-central New Brunswick Canada

David A. Shinkle¹, David R. Lentz¹, & Steven R. McCutcheon²

¹*Department of Geology, University of New Brunswick, Fredericton, NB E3B 5A3 CANADA (email: dlentz@unb.ca)*

²*Geological Surveys Branch, New Brunswick Department of Natural Resources, Bathurst, NB E2A 3Z1 CANADA*

ABSTRACT: The Siluro-Devonian North Pole Stream Granitic suite (NPSG) is located in north-central New Brunswick and is cut by a late regional-scale wrench fault system. Magmatic fractionation produced at least four comagmatic differentiates, namely: biotite granite (oldest phase); biotite-muscovite granite; muscovite granite; and late quartz-feldspar porphyry (QFP) granitic dikes that crosscut all other phases of the pluton. Petrochemical data for the NPSG suggest that the muscovite granite is the most evolved phase in that it has A/CNK = 1.3-1.4, and very low TiO₂, Fe₂O₃T, MgO, CaO (0.04, 0.93, 0.12, 0.39 wt.%, respectively), Sr, Ba, Zr, Hf, Y and Σ REE (8, 22, 21, 1.2, 4, and 9.8 ppm, respectively); however, it is enriched in Rb, Sn, Nb, and Ta (546, 31, 50, and 8.6 ppm, respectively). The K (4.11 wt.%), U (30 ppm), and Th (5 ppm) contents are consistent with a high-heat producing (HHP) granite. Convection cells established in the NPSG and surrounding country rock near the HHP granite resulted in late fluid circulation and U leaching from the enriched granite, and localization of U vein formation in the adjacent wrench fault system.

KEYWORDS: *uranium, high-heat producing, specialized granite, Long Lake*

INTRODUCTION

The North Pole Stream granitic suite (NPSG) is located 31 kilometers northeast of Plaster Rock and underlies an area of approximately 500 km² in north central New Brunswick. This plutonic suite is a Siluro-Devonian, intrusive complex that was emplaced discordantly into Cambro-Ordovician metasedimentary rocks of the Miramichi Terrane (Fig. 1). The NPSG is crosscut by steeply-dipping wrench faults related to the Middle Devonian Acadian orogeny. All the wrench faults in the area postdate the oldest of the Devonian granites, and are truncated by younger Devonian and Carboniferous intrusions (Ruitenbergh & McCutcheon 1982).

The granitic rocks of the NPSG are the youngest granitic rocks in the Long Lake area and are associated with several styles of mineralization: an early base metal (Zn, Cu, Pb) and granophile element (Mo, Sn, W, In) polymetallic vein system is associated with the emplacement of the NPSG (Fyffe & Pronk 1985), and later uranium vein mineralization, that resulted from

circulating meteoric fluids leaching uranium from the granites is associated with a late steeply-dipping wrench fault beneath Long Lake (Fig. 1).

GEOLOGY OF THE NORTH POLE STREAM GRANITIC SUITE

The NPSG mainly consists of four comagmatic differentiates, namely: biotite granite (oldest phase); biotite-muscovite granite; muscovite leucogranite; and late quartz-feldspar porphyry (QFP) granitic dikes (youngest phase). These phases are attributed to assimilation and fractional crystallization processes that modified an inward propagating solidification front and the dikes represent late stage magma that was intruded into the solidified carapace. The uranium and polymetallic styles of vein mineralization are genetically related to the muscovite leucogranite and QFP granitic dikes, respectively.

The NPSG primarily consists of biotite granite (Whalen 1993), that is generally pink to white, fine- to coarse-grained, and equigranular to K-feldspar porphyritic.

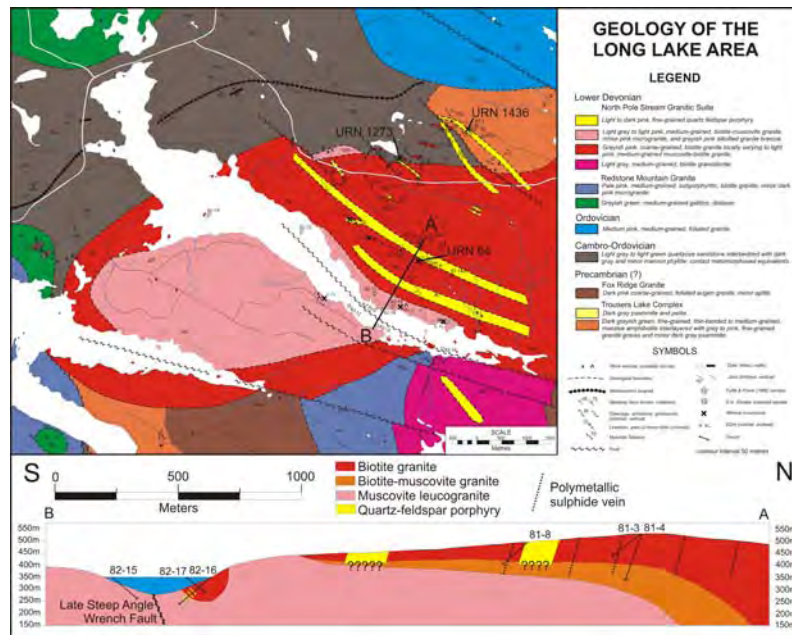


Fig. 6. General geology, mineral occurrences, and diamond drillhole locations in the Long Lake area with a cross section corresponding to the line A-B, illustrating the general geology beneath the surface (modified from Fyffe & Pronk 1985).

Biotite forms approximately 1 to 2 % of the rock, and is partly altered to chlorite.

The biotite-muscovite granite is a transitional phase between the biotite granite and the muscovite leucogranite. This two-mica granite is light-grey to light-pink, medium-grained, and equigranular; biotite and muscovite together account for approximately 3 to 4 % of the rock.

The muscovite leucogranite is found at the core of the pluton and, petrochemically, is the most differentiated. The leucogranite is pink, medium-grained, and equigranular with muscovite accounting for approximately 2 to 3 % of the rock.

The QFP granitic dikes are the youngest phase and crosscut the biotite granite. The polymetallic sulfide veins and mineralized breccias are parallel to the contacts of the QFP dikes and the biotite granite, implying that the sulfide mineralization and the QFP dikes are cogenetic. The dykes are green to pink and are comprised of subhedral to euhedral quartz, K feldspar, plagioclase, and minor biotite phenocrysts in an aphanitic quartzofeldspathic matrix. The

phenocrysts range from 2 to 3 mm and constitute approximately 50% of the rock.

AGE OF EMPLACEMENT OF THE NORTH POLE STREAM GRANITIC SUITE

A sample of biotite granite from 500 meters south of the study area has yielded a U-Pb monazite age of 417 ± 1 Ma, which has been interpreted as the emplacement age of the NPSG (Bevier & Whalen 1990a). Recent CHIME dating of monazite from the biotite-muscovite granite has yielded two dates, an older age of 421 ± 6 Ma (n=8) from U-, Y-, and Ca-rich monazite inclusions in quartz, and a younger age of 399 ± 16 Ma (n=12) from accessory U-, Y-, and Ca-poor monazite associated with zircon, apatite, and xenotime aggregates. In addition to monazite age dating, Ar-Ar dating of primary muscovite in the muscovite leucogranite has yielded an age of 406.1 ± 1.87 Ma (Fig. 2).

The quartz-hosted monazite inclusions pre-date the muscovite leucogranite and are in the same range as Bevier & Whalen's (1990a) U-Pb monazite age

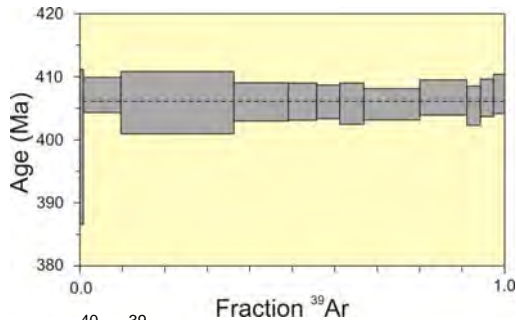


Fig. 2. $^{40}\text{Ar}/^{39}\text{Ar}$ release spectra of primary muscovite from the muscovite leucogranite phase of the NPSG.

from the biotite granite, implying that the inclusions are inherited from an earlier phase in the crystallization history. The younger monazite age and the Ar-Ar age overlap, implying that the muscovite leucogranite crystallized much later than other parts of the pluton, i.e., during the terminal stages of crystallization of the NPSG.

GEOCHEMISTRY OF THE NORTH POLE STREAM GRANITIC SUITE

Existing petrochemical data for the NPSG suggest that it is a strongly peraluminous ($A/CNK = 1.3-1.4$), evolved 'I-Type to 'S-Type' granite, derived from a low degree of partial melting of supracrustal sedimentary rocks. With increasing magmatic fractionation, the NPSG shows increases and decreases in a number of major and trace elements (Table 1). Early monazite, xenotime, zircon, and apatite fractionation, due to the low solubility of these minerals in peraluminous low-temperature melts, resulted in strong Zr, Y, Hf, Th, and REE depletion. Increases in SiO_2 , Al_2O_3 , Na_2O , P_2O_5 , Rb, Nb, Ta, and U are due to fractional crystallization, and late-stage assimilation of the surrounding country rock by a melt derived from a very low degree of partial melting.

The two-mica granite and the muscovite leucogranite phases of the NPSG fall in the field of specialized granites on a Rb-Sr-Ba ternary variation diagram for granitic intrusions (Fig. 3). Based on the elevated uranium contents in these two phases, it is likely that the uranium at Long Lake was derived predominantly from them.

URANIUM MINERALIZATION

The two-mica granite and the muscovite leucogranite of the NPSG can be considered high-heat producing granites since they are abnormally enriched in the radioactive elements U (24 and 30 ppm, respectively), K (4.36 and 4.11 K_2O wt.%, respectively), and, to a lesser degree, Th (4 and 5 ppm, respectively). Fehn *et al.* (1978) showed that a granite of radius 17 km and a depth of 6.25 km, with a

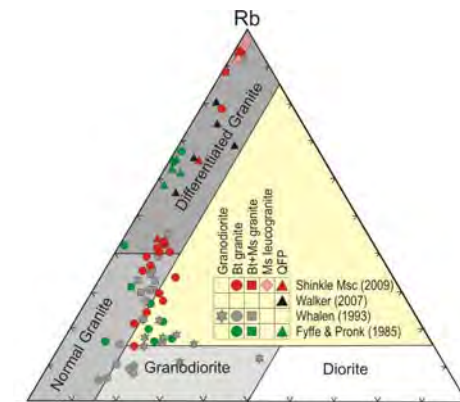


Fig. 3. Rb-Sr-Ba ternary variation diagram for rocks of the NPSG (after El Bouseily & El Sokkary 1975).

permeability of 0.5 mD and containing 15 ppm U, 57 ppm Th, and 4.0 wt.% K_2O could develop a U vein deposit of 10,000 tons in 2 Ma via heat generation from these radioactive elements and their daughter products producing local fluid convection of sufficient magnitude to develop hydrothermal uranium deposits long after cooling of the intrusion.

The uranium mineralization in the Long Lake area has been primarily intersected adjacent to a large northwesterly-trending wrench fault that underlies Long Lake. It is postulated that, post-crystallization of the NPSG, radiogenically-driven hydrothermal convection cells established in the NPSG and surrounding country rock drove oxidized meteoric fluids that leached uranium from the surrounding granites via the oxidation of uranium-rich phases such as uraninite and monazite. Post-oxidation, U was easily transported in

Table 1. Average concentration of selected elements for various phases of the NPSG

Element	Bt granite (n=16)	Bt-Ms granite (n=4)	Ms Leuco granite (n=5)	QFP granite (n=2)
SiO ₂ wt. %	75.12	77.12	76.68	75.87
Al ₂ O ₃ wt. %	16.01	16.21	17.14	17.77
TiO ₂ wt. %	0.25	0.06	0.04	0.16
Fe ₂ O ₃ T wt. %	2.01	0.97	0.93	1.73
MgO wt. %	0.72	0.13	0.12	0.64
CaO wt. %	1.28	0.69	0.39	0.32
Na ₂ O wt. %	3.35	3.91	4.28	0.75
K ₂ O wt. %	4.91	4.36	4.11	6.82
P ₂ O ₅ wt. %	0.09	0.25	0.28	0.04
Rb (ppm)	219	414	546	368
Sr (ppm)	75	5	8	47
Y (ppm)	25	5	4	27
Zr (ppm)	127	22	21	74
Nb (ppm)	19	37	50	25
Ba (ppm)	339	29	23	270
Hf (ppm)	3.6	1.0	1.2	2.2
Ta (ppm)	2.4	5.8	8.6	2.5
Th (ppm)	15	4	5	23
U (ppm)	9	24	30	13
ΣREE (ppm)	154.4	14.3	9.8	111.1

these circulating meteoric fluids and summarily deposited as pitchblende and hydrothermal uraninite after the hydrothermal fluids became reduced by sulfides formed along the wrench fault beneath Long Lake.

CONCLUSIONS

The muscovite leucogranite represents the upper part of a highly-fractionated magma chamber that underwent segregation into an upper phenocryst-poor residual liquid and a lower phenocryst-rich melt prior to its terminal stage of crystallization. A late, steeply-dipping

wrench fault crosscut and tilted the oldest granitic phase and brought the deep highly-evolved part of the NPSG into contact with the sulfide mineralization associated with the QFP dikes. High levels of heat generation from residual thermal energy and the decay of radiogenic elements and their daughter products established post-crystallization convection cells in the NPSG and surrounding country rock. Late-stage fluid circulation of oxygen-rich meteoric fluids along these convection cells resulted in leaching of uranium from the NPSG via the oxidation of uraninite and monazite, followed by deposition of pitchblende and hydrothermal uraninite along the wrench fault beneath Long Lake after the U-rich fluids were reduced by a fault-hosted sulfide mineralization.

REFERENCES

- BEVIER, M.L. & WHALEN, J.B. 1990a. U-Pb geochronology of Silurian granites, Miramichi terrane, New Brunswick. In: Radiogenic Age and Isotopic Studies: Report 3. *Geological Survey of Canada Paper*, **89-2**, 93-100.
- EL BOUSEILY, A.M. & EL SOKKARY, A.A. 1975. The relation between Rb, Ba and Sr in granitic rocks. *Chemical Geology*, **16**, 207-219.
- FEHN, U., CATHLES, L.M., & HOLLAND, H.D. 1978. Hydrothermal convection and uranium deposits in abnormally radioactive plutons. *Economic Geology*, **73**, 1556-1566.
- FYFFE, L.R. & PRONK, A.G. 1985. Bedrock and surficial geology, rock and till geochemistry in the Trousers Lake area, Victoria County, New Brunswick. *New Brunswick Department of Natural Resources Report of Investigation*, **20**, 74 p.
- WHALEN, J.B. 1993. Geology, petrography and geochemistry of Appalachian granites in New Brunswick and Gaspésie, Quebec. *Geological Survey of Canada Bulletin*, **436**, 124 p.

Diverse uranium mineralization in the Central Mineral Belt of Labrador, Canada: multiple styles and multiple questions

Greg W. Sparkes¹ & Andrew Kerr¹

¹Geological Survey of Newfoundland and Labrador, Department of Natural Resources, PO Box 8700, St. John's, NL CANADA A1B 4J6 (e-mail: gregsparkes@gov.nl.ca)

ABSTRACT: Strong commodity prices in the last few years have led to a remarkable renaissance of uranium exploration in Labrador, focused in a complex and geologically diverse region known as the Central Mineral Belt (CMB). Potentially economic epigenetic U deposits are mostly hosted by supracrustal rocks of Paleoproterozoic and Mesoproterozoic age, and are difficult to place in the traditional pantheon of uranium deposit types. Recent exploration work implies that structural controls are important in some examples, but the relationships between mineralization and deformation remain far from clear. Geochronological data imply at least three periods of uranium mineralization between 1900 and 1650 Ma. It seems likely that the Labrador CMB represents a region in which U (and other lithophile elements) were repeatedly and sequentially concentrated by hydrothermal processes. The current exploration boom lends impetus for systematic research studies that may ultimately lead to refined genetic models that may be applicable elsewhere.

KEYWORDS: *Uranium, Labrador, Exploration, Epigenetic, Hydrothermal*

INTRODUCTION

Since 2005, Labrador has become an important area for uranium exploration in the Canadian Shield, second only to the Athabasca Basin of Saskatchewan. The unusual Michelin deposit is the largest undeveloped Canadian uranium deposit outside Saskatchewan, and one of the ten largest undeveloped uranium deposits in the world. The renewed exploration of the last few years led to new ideas and new discoveries, and views on the nature and genesis of mineralization are constantly changing. This contribution provides an historical overview, highlights the most significant exploration results, and discusses the known (or suspected) geological context of deposits, with emphasis on new geochronological results. The most recent overview of uranium mineralization in the CMB is provided by Sparkes & Kerr (2008).

GEOLOGICAL SETTING

Labrador (Fig. 1) contains sections of the Superior and North Atlantic Archean cratons, separated by a wide tract of Paleoproterozoic rocks assigned to the

Churchill Province. These are all bounded to the south by Paleoproterozoic and Mesoproterozoic orogenic belts of the Makkovik and Grenville Provinces. Uranium occurs in many parts of the territory, in a wide range of environments, but the most important examples are all located within the Central Mineral Belt (CMB), a loosely-defined area at the intersection of the Nain, Churchill, Makkovik and Grenville provinces (Fig. 1).

The CMB is defined mostly in terms of several Paleoproterozoic and Mesoproterozoic supracrustal sequences containing low-grade sedimentary and volcanic rocks, but it also includes voluminous plutonic suites and older (largely Archean) basement rocks. The CMB has a very complex evolutionary history and the timing of some important deformational and magmatic events lacks precise definition. Figure 2 provides a general summary of its geology and the setting of contained U mineralization.

The oldest supracrustal rocks are mafic volcanics and sedimentary rocks of the 2100-2000 Ma Moran Lake and Post Hill groups, believed to have formed as a

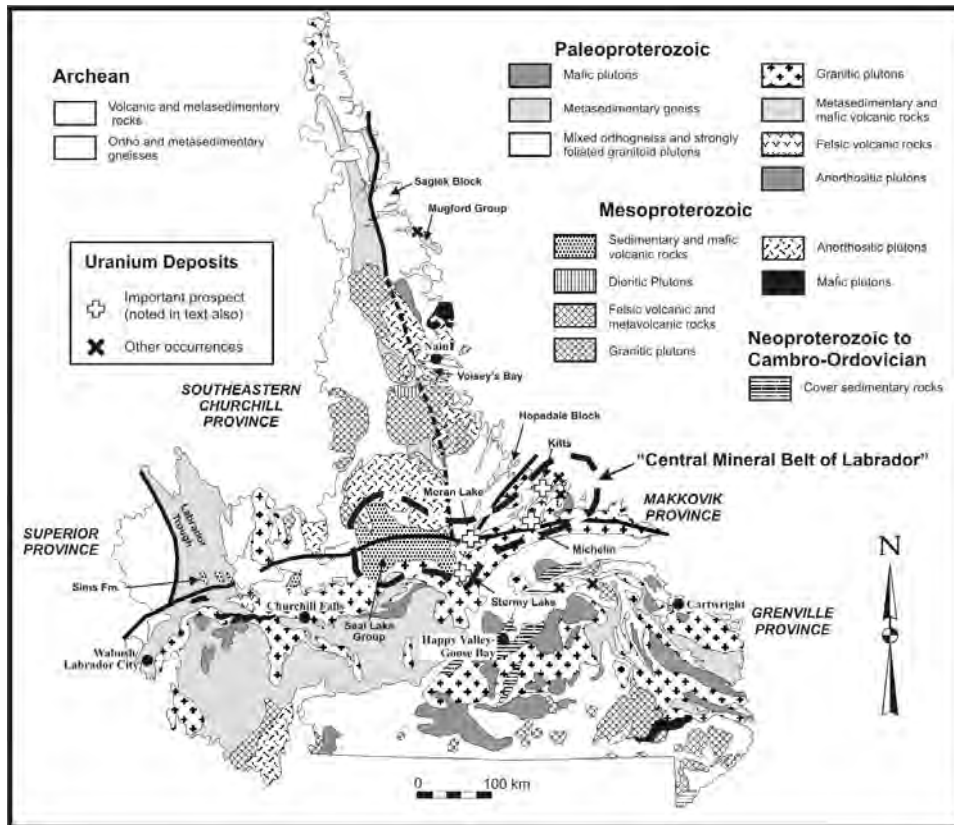


Fig. 1. The Central Mineral Belt of Labrador and its principal uranium occurrences.

passive margin sequence following rifting. These were variably deformed, and intruded by granitoid rocks prior to the deposition of the 1880 Ma – 1850 Ma Aillik Group, which is dominated by felsic volcanic and volcanoclastic rocks. Strong deformation during the main phase of the ca. 1800 Ma Makkovikian Orogeny affected all of the above, and this event also generated large volumes of syn- and post-tectonic granites. More local granitoid magmatism occurred ca. 1720 Ma. Voluminous magmatism occurred throughout the CMB at ca. 1650 Ma, forming the Trans-Labrador Batholith (TLB). The sedimentary and volcanic rocks of the Bruce River Group unconformably overlie the older Moran Lake Group, and their ca. 1650 Ma age implies that they are in part a carapace to the TLB. The youngest supracrustal sequences in the CMB are the ca. 1330 Ma alkaline volcanic rocks of the Letitia

Lake Group, and the overlying Seal Lake Group (ca. 1270 Ma), which includes varied (terrestrial) sedimentary rocks and mafic volcanics. The Seal Lake Group is well-known for its numerous Cu occurrences, and the Letitia Lake Group contains some rare-metal (Zr, Be, REE) occurrences. The southwestern portion of the CMB lies within the Grenville Province, and was affected by distal deformation related to the 1000-900 Ma Grenvillian orogenic event.

URANIUM MINERALIZATION

Uranium occurs throughout the CMB, but the most significant deposits are hosted by supracrustal sequences, notably in the Post Hill, Aillik and Bruce River Groups (Fig. 2).

In the Post Hill Group, the Kitts Deposit (~0.2 Mt at 0.7% U₃O₈) and related zones are hosted by graphitic to ferruginous, pelitic metasedimentary rocks. The same

unit locally hosts syngenetic (but barren) massive sulphides. Early models viewed the U as a syngenetic component of the protolith shales (Gandhi 1978), but subsequent work suggests that it is of epigenetic hydrothermal origin (Evans 1980). Reduction of fluids by carbon and sulphides provided a quasi-stratigraphic control on U precipitation. The relatively ductile host rocks lie within an important shear zone for which the timing of deformation relative to the mineralization is less clear. U-Pb ages from cross-cutting dykes, interpreted to be post-mineralization, indicate that uranium was deposited prior to ca. 1880 Ma, indicating that Kitts formed in a separate event from the ore-forming episode at Michelin.

In the Aillik Group, the most important uranium mineralization is hosted by felsic metavolcanic rocks. The largest deposit is Michelin, in which low grades (0.1 to 0.2% U₃O₈) are compensated by large size (44.5 Mt), continuity and structural predictability. The deposit as a whole is conformable with compositional layering, and was traditionally thought of as broadly syngenetic (Evans 1980; Gower *et al.* 1982). The mineralized zone has a remarkably consistent dip and plunge, and is now recognized to be part of an important regional shear zone. This has led to alternative models in which uranium is suggested to have been introduced syntectonically, connected with the development of the shear zone. However, the relationships between mineralization and deformation remain unclear.

Alteration at Michelin is dominated by intense soda metasomatism and potash depletion, coupled with locally intense hematization; much of the mineralization consists of fine-grained uraninite within sodium-rich silicates such as aegirine and arfvedsonite. The recently discovered Jacques Lake deposit, which is an important resource in its own right (about 17 million pounds U₃O₈), has many similarities to Michelin, although its metavolcanic host rocks are compositionally distinct. The age of the uranium mineralization in these deposits is

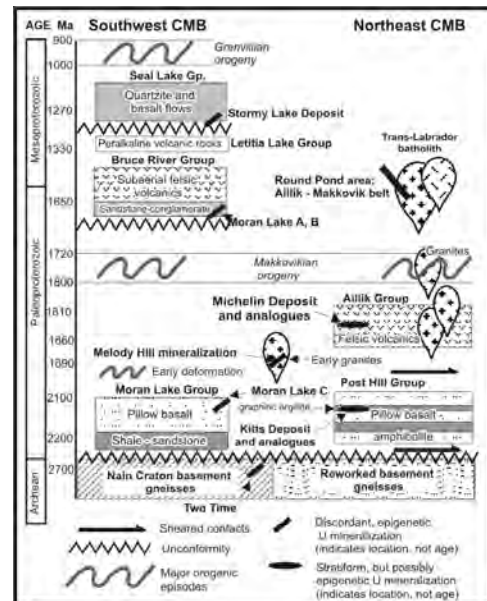


Fig.2. Simplified stratigraphic chart showing the settings of uranium deposits in the Central Mineral Belt of Labrador.

constrained by the age of the host rocks (ca. 1860 Ma) and the age of cross-cutting quartz-feldspar porphyry dykes (ca. 1800 Ma). Many aspects of the Michelin deposit are reminiscent of so-called “albitite” or “metasomatite” or “episyenite” deposits described from Europe, although it is considerably larger than any of these possible analogues.

Uranium deposits in the Moran Lake area present a different set of problems, in that they are hosted by two sequences differing in age by at least 150 Ma. The most widespread mineralization is hosted by mafic metavolcanic rocks of the Moran Lake Group, where it is associated with the development of iron carbonate-rich breccias and strong hematitic alteration. Unlike Kitts and Michelin, which essentially contain uranium alone, mineralization at Moran Lake contains associated Cu, V and Ag. The Fe-enrichment, coupled with the associated metals, invites comparison with IOCG-type settings, although these Labrador examples are uranium-rich rather than copper-rich. However, uranium mineralization is also present in closely

adjacent terrestrial sedimentary rocks of the ca. 1650 Ma Bruce River Group, which sits structurally below the older Moran Lake Group. This style of mineralization, hosted by sandstones and conglomerates, appears to be associated with redox boundaries in the sedimentary rocks, and it may have affinities with much younger sandstone-type uranium deposits. The relationships between these closely adjacent styles of uranium mineralization remain unknown, as do their absolute and relative ages; however, mineralization in the Bruce River Group must be younger than 1650 Ma. Uranium is also hosted by similar iron-rich breccia zones developed in Late Archean granodiorites, although these may be much younger than their host rocks. This deposit, known as Two Time, is one of the few truly new discoveries from the second wave of exploration in Labrador.

In addition to the examples listed above, uranium mineralization occurs in several other geological settings in and around the CMB, including within granitoid plutonic rocks and as possible syngenetic mineralization in felsic volcanic rocks of both the Aillik and Bruce River groups. Pegmatite-hosted uranium mineralization is also known in deeper-level reworked Archean basement terranes.

CONCLUSIONS

Uranium mineralization in the CMB is characterized by a diversity of style and host rocks, and it is naïve to suppose that a single genetic model can explain all its variations. Like many metallogenic provinces in which incompatible (or "lithophile") elements are important, the CMB of Labrador seems to represent an area in which U has been repeatedly and perhaps sequentially concentrated, and

then locally redistributed. The new geochronological data from the region indicate that there are at least three, and possibly four, periods of uranium deposition between about 1900 Ma and 1650 Ma. Much remains to be learnt about the timing and genetic origins of individual deposits, and the possibly connections between different styles of mineralization. The current exploration boom has reawakened interest in this area and its numerous metallogenic questions, and it is hoped that a growing research database from corporate data, university research projects and government geoscience will clarify some of these problems in the years to come.

REFERENCES

- EVANS, D. 1980. *Geology and petrochemistry of the Kitts and Michelin uranium deposits and related prospects, Central Mineral Belt, Labrador*. PhD thesis, Queens University, Kingston, ON.
- GANDHI, S.S. 1978. Geological setting and genetic aspects of uranium occurrences in the Kaipokok Bay – Big River area, Labrador. *Economic Geology*, **73**, 1492-1522.
- GOWER, C. F., FLANAGAN, M. J., KERR, A., & BAILEY, D. G. 1982. Geology of the Kaipokok Bay – Big River area, Central Mineral Belt Labrador. *Newfoundland Department of Mines and Energy*, Mineral Development Division, Report **82-7**.
- SPARKES, G. W. & KERR, A. 2008. Diverse styles of uranium mineralization in the Central Mineral Belt of Labrador: An overview and preliminary discussion. *Newfoundland and Labrador Department of Natural Resources*, Geological Survey, Report **2008-1**, 193-229.
- WILTON, D.H.C. 1996. Metallogeny of the Central Mineral Belt and adjacent Archean basement, Labrador. *Newfoundland Department of Mines and Energy*, Geological Survey, Mineral Resource Report **8**.

Harvey: a volcanic-hosted Uranium occurrence at the edge of the Maritimes Basin

José M. Texidor Carlsson¹ & Neil E. Downey¹

¹Tripple Uranium Resources Inc., 108-F Trider Crescent, Dartmouth, NS B3B 1R6 CANADA
(e-mail: josefc@turinc.com neild@turinc.com)

ABSTRACT: The late Devonian-early Carboniferous volcanic units of the Harvey Group west of Fredericton have received less attention than similar volcanic areas regarding their volcanic characteristics and potential for metallic mineral occurrences. Previous research and mineral exploration activity between the 1950s and 1980s typically focused on the search for Uranium mineralization and improved knowledge of the local volcanic stratigraphy.

Tripple Uranium Resources Inc. commissioned an airborne geophysical survey of the Harvey mineral property (including the Manners-Sutton occurrence) in early 2007 and identified several radiometric targets and geological structures, which were checked during the summer of 2007. Mapping during fieldwork led to a better understanding of the local geology and resulted in the identification of several substantially anomalous radiometric locations. These locations were further tested by commissioning a diamond drilling program during the fall of 2007.

Study of the drill-core, bore-hole geophysical data and IPC-MS multi-element geochemical assaying were combined with the airborne geophysics and historical work to produce a better understanding of the local geology and a model that would explain the various episodes of hydrothermal alteration observed at surface and on drill-core. The results of the study indicate that the geology in the drilling area is stratigraphically consistent yet characterized by multiple and overlapping hydrothermal alteration events.

KEYWORDS: *Harvey Group, Uranium, ignimbrite, volcanic centre, hydrothermal fluid*

INTRODUCTION

The wedge-shaped southwestern border of the Carboniferous age Maritimes Basin near Fredericton is rimmed to the south and to the west by late Devonian (and early Carboniferous?) volcanic units of the Harvey and Piskahegan groups. The southern edge volcanic and sedimentary rocks of the Piskahegan Group associated to the Mount Pleasant Caldera have been the subject of several studies and host the well known W-Mo and Sn-In Mount Pleasant Mine. However, less attention has been paid to the study of the predominantly volcanic rocks of the Harvey Group southwest of Fredericton, which may have a similar potential to Piskahegan Group to host economic mineral deposits. The Harvey Group hosts the Manners Sutton, York Mills, Harvey Station-Cherry Hill and Harvey Mountain-Acton mineral occurrences.

Previous exploration projects that took place between the 1950s and 1970s were

attracted by radon anomalies and anomalous Uranium concentrations in groundwater. These early projects identified hydrothermal alteration features in volcanic rocks, but were not thorough enough to identify the full potential of the local mineral occurrences and indicated that the presumed but as-of-then undiscovered Uranium mineralization style might be of the unconformity- or vein-type mineralization styles. Recent magnetic and radiometric airborne survey data combined with drill-core and geochemical analysis indicate that a more descriptive mineralization model is needed.

A magnetic and radiometric aerial survey was commissioned by Tripple Uranium Resources Inc. in early 2007 to gain a better understanding of the Harvey Group. Analysis and interpretation of the aerial survey results identified structural features and strong radiometric anomalies, which were prospected and mapped through the summer of 2007 and

resulted in the identification of several drill targets near the Manners Sutton mineral occurrence. During the fall of 2007 ten diamond drill-holes recovered 2,881m of drill-core, from which several hundred rock samples were taken and assayed by ICP-MS for major oxides and trace elements in order to study the rocks of the Harvey Group.

Analysis of drill-core combined with bore-hole logging and geochemical assay results point to the presence of several hydrothermal events, and that local stratigraphy of the Harvey Group consists of extensive laterally contiguous units which can be divided into 1) an upper assemblage of four ignimbritic and two volcanoclastic units and 2) a lower assemblage of mudstone with minor intermediate composition flow units. Assayed Uranium concentrations and radiometric bore-hole data indicate that Uranium is widely distributed in all units of the upper assemblage.

GEOLOGICAL SETTING

Regional Geology

The geology of the area consists of rocks from three time periods (Fig. 1): Silurian (Kingsclear Group), Devonian (Harvey Group) and Carboniferous (Mabou Group).

Kingsclear Group

This Silurian Group (418-424 Ma) has two formations associated with the Harvey area, Burtt's Corner Formation and Flume Ridge formation, both consisting predominantly of deep marine facies. The Burtt's Corner Formation is characterized by grey lithic wacke interstratified with dark grey, locally graptolite-bearing, siltstone and shale. The Flume Ridge formation consists of calcareous-argillaceous sandstone, siltstone, and shale.

Harvey Group

The Devonian (383-355 Ma) Harvey Group is approximately 200 metres thick and forms a narrow belt 16 km long by about 2 km wide (Beaudin *et al.* 1980). The Harvey Group consists primarily of

felsic volcanic rocks thrust over red conglomerate, sandstone and siltstone of the Early Carboniferous Shin Formation to the west and is unconformably overlain by the same rocks to the east (St. Peter 2000). The Harvey Group unconformably overlies the Late Silurian Kingsclear Group.

The Harvey Group consists of three units: Harvey Mountain, Cherry Mountain, and York Mills Formations. The upper Harvey Mountain formation consists of felsic volcanic rocks, typically flow-banded massive rhyolitic lava accompanied by ash-fall tuff. Rocks of the middle Cherry Mountain formation are characterized by the predominance of ash-fall and ash-flow tuffs at the top and volcanogenic sedimentary rocks at the base. The lower York Mills formation is a sequence of interbedded clastic, volcanogenic and minor volcanic rocks, that latter consisting of felsic volcanic-clast conglomerate, volcanogenic sandstone, siltstone and shale, felsic crystal lithic lapilli tuff and flow-banded rhyolite.

Mabou Group

The Shin Formation of the Mabou Group is Early Carboniferous in age and shows a fining-upward sequence of pebble to boulder conglomerate. The Minto Formation of the Pictou Group is from the Late Carboniferous and contains cross- and horizontal-bedded feldspathic and quartzose arenite and pebble arenite.

Local Geology

The earliest detailed description of the Harvey Group was by Kuan (1970), who proposed a twofold subdivision. Later descriptions by van de Poll (1972) and Pajari (1973) helped Beaudin *et al.* (1980) redefine the stratigraphic sequence in light of detailed mapping that was undertaken by Seru Nucleaire Limited as part of a Uranium exploration program on the Manners Sutton claims. Seru Nucleaire proposed that the Harvey Formation should be elevated to a group and suggested that it could be divided into three formations.

Payette & Martin (1986a, 1986b) described the chemistry and mineralogy of the volcanic rocks and of melt inclusions within the quartz-feldspar porphyry. Fyffe & Barr (1986) gave one chemical analysis for the Harvey volcanics in their comparative study of Carboniferous volcanic rocks in New Brunswick, and indicated that the analyzed Harvey sample is a subalkalic rhyolite of calc-alkalic affinity.

Diamond drilling of the Harvey area by Tripple Uranium Resources Inc. indicates that the local stratigraphy is characterized by extensive laterally continuous units, which can be divided into a 250 to 300 metres thick 'upper assemblage' of stacked ignimbritic and volcanoclastic units, and a 'lower assemblage' with approximately 130 metres of recovered core but unknown thickness (base not observed), consisting of red and grey mudstone with lenses of intermediate extrusive volcanic rocks. Identification and discrimination of distinct ignimbritic units near the top of the 'upper assemblage' was challenging due to sub-surface

weathering and also as a result of multiple, irregularly distributed episodes of hydrothermal alteration, including fluoridization, argillization, hematization, carbonatization and silicification. Positive field identification of ignimbritic units was aided by relatively consistent stratigraphy, the presence of distinct 'marker' lithological units and by analysis of the down-hole conductivity and background gamma radiation data from each borehole.

The ignimbrite units of the 'upper assemblage' are texturally very similar and display blocky textures and glass shards, indicating quick cooling at the basal depositional contact and at the exposed top, with a warmer 'core' that contains characteristic flattened pumice fragments. The base of one of the ignimbrite units is characterized by a distinct quenching texture with very well formed spherulitic nodules up to 10cm wide.

The alteration sequence in the ignimbrite units is assumed to have started with an early introduction of

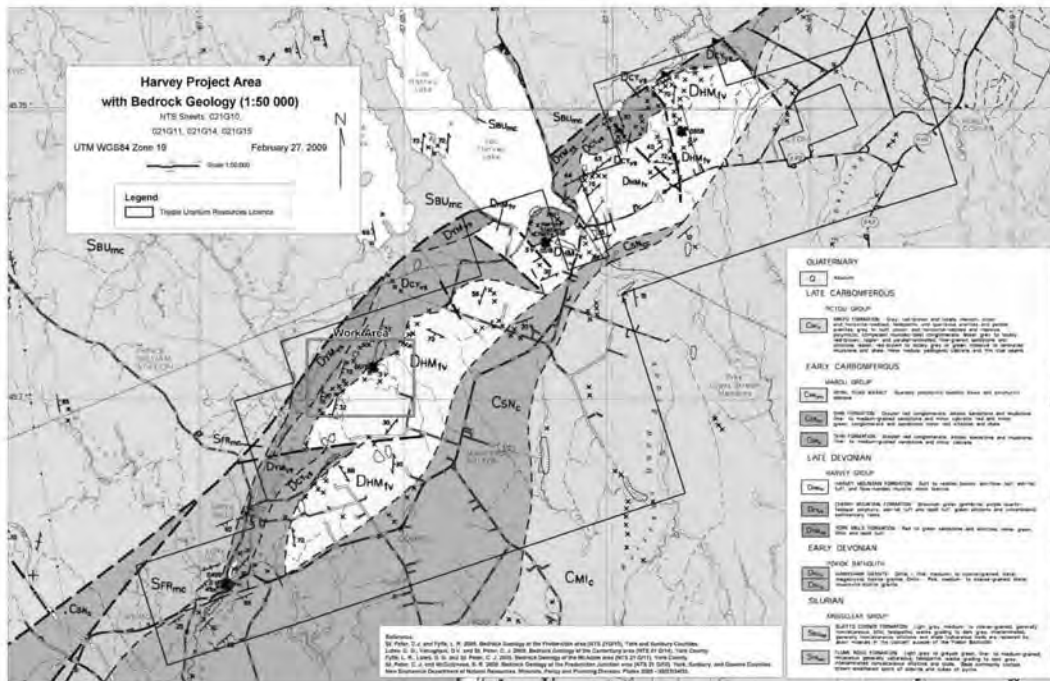


Fig. 1. Geological setting of the Harvey area.

fluorine-rich hydrothermal fluid that created the fluorite crystals, later altered to clay in places by subsequent, apparently multiple argillization +/- hematization +/- silicification events, and a late distinct siliceous alteration, which likely produced the widespread glassy appearance overprinting fluorite, clay and hematite observed in most of the drill-core. Strong localized silicification of the ignimbrite may be a result of interaction between meteoric/ground-water fluid and cooling of the pyroclastic unit.

The 'lower assemblage' consists predominantly of red mudstone, with narrow sections (5-20 cm) of reduction spots and entire sections (0.5 to 2 m) of grey reduced and pyritic mudstone becoming more common towards the base. Narrow (0.5 to 5 m) intermediate extrusive volcanic flows become more common towards the base of this assemblage, and display basal textures indicating that moisture and mudstone rip-clasts were acquired into the flow and that heat was supplied to the underlying mudstones, which produced narrow (< 5 cm) contact metamorphism bands of recrystallized mudstone.

Several sections of economic Uranium mineralization (>0.1% U₃O₈) were identified in drill-core. These appear to be associated to discrete stratigraphic horizons and to fault zones, of which the latter are strongly suspected to have acted as conduits of hydrothermal fluids.

CONCLUSIONS

Diamond-drilling of the Manners Sutton occurrence has substantially increased knowledge of the Harvey Formation stratigraphy and identified several distinct ignimbritic and volcanoclastic units. Analysis of drill-core and geochemical analysis of samples have supplied evidence for the presence of multiple hydrothermal alteration episodes. Ongoing analysis of data from geochemical assays and the airborne geophysical surveys will

help produce a hydrothermal alteration model and a better understanding on local Uranium mineralization.

ACKNOWLEDGEMENTS

We thank Steve McCutcheon and Malcolm McLeod of the New Brunswick Department of Natural Resources for their comments and suggestions, and Kathryn MacFarlane of Tripple Uranium Resources Inc. for GIS assistance.

REFERENCES

- BEAUDIN, J., LEGALLAIS, C., & SCHIMANN, K. 1980. Final report of the 1979 campaign, Manners Sutton claim group, Project 24-147, York County, New Brunswick. Report prepared for Seru Nucleaire Canada Limited. New Brunswick Department of Natural Resources & Energy, Minerals and Energy Division, Assessment Report 472589.
- FYFFE, L.R. & BARR, S.M. 1986. Petrochemistry and tectonic significance of Carboniferous volcanic rocks in New Brunswick. *Canadian Journal of Earth Sciences*, **23**, 1243-1256.
- KUAN, S. 1970. *The geology of Carboniferous volcanic rocks in the Harvey area, New Brunswick*. Unpublished M.Sc. thesis, University of New Brunswick, Fredericton, New Brunswick, 78 p.
- PAJARI, G.E., JR. 1973. The granitic rocks of southwestern New Brunswick. In N. Rast (ed) *Geology of New Brunswick, New England Intercollegiate Geological Conference, Field Guide to Excursions*. Department of Geology, University of New Brunswick, Fredericton, New Brunswick, p. 12-20.
- PAYETTE, C. & MARTIN, R.F. 1986a. The Harvey volcanic suite, New Brunswick. I. Inclusions of magma in quartz phenocrysts. *Canadian Mineralogist*, **24**, 557-570.
- PAYETTE, C. & MARTIN, R.F. 1986b. The Harvey volcanic suite, New Brunswick. II. Postmagmatic adjustments in the mineralogy and bulk composition of a high-fluorine rhyolite. *Canadian Mineralogist*, **24**, 571-584.
- ST. PETER, C. 2000a. *Carboniferous geology of the southwestern New Brunswick platform (Maugerville Subbasin)*. New Brunswick Department of Natural Resources and Energy, Mineral Resources, Plate 2000-16.

Deep-penetrating geochemical exploration for hidden sandstone-type uranium deposits in the Turpan-Hami basin, northwestern China

Xueqiu Wang^{1,2}, Shanfa Xu^{1,2}, Qinghua Chi^{1,2}, Bimin Zhang^{1,2}, & Lanshi Nie^{1,2}

¹ Institute of Geophysical and Geochemical Exploration (IGGE), 84 Golden Rd., Langfang, Hebei 065000, CHINA (e-mail: wangxueqiu@igge.cn)

² Key Laboratory of Applied Geochemistry, CAGS, 84 Golden Rd., Langfang, Hebei 065000, CHINA

ABSTRACT: The Turpan-Hami basin, covering an area of approximately 50 000 km² in northwestern China, has very good potential for sandstone-type uranium deposits. Recently, a sandstone-type uranium deposit was discovered at a depth of 300 m hosted in a Jurassic sequence composed of sandstone, mudstone, and coal beds. Conventional geochemical methods, based on coarse soil fraction sampling to avoid windblown sand dilution, are not effective to indicate the hidden deposits due to overburden concealing prospective bedrock sequences. A deep-penetration geochemical procedure, based on fine fraction sampling and selective partial leaching is effective to give signals from the hidden deposits and wide-spaced sampling of fine-fraction soils can provide a cost-effective powerful tool for delineation of regional targets of sandstone-type uranium in the basin. A wide-spaced sampling survey at a sampling density of approximately 1 / 100 km² was carried out throughout the whole basin. Samples were processed for analysis of 30 elements by ICP-MS. Three large geochemical anomalies have been delineated across the whole basin. One of the anomalies is consistent with the explored uranium deposit, and a new big deposit has been discovered by a follow-up exploration program at one of the delineated geochemical anomalies.

KEYWORDS: *deep-penetration, geochemistry, exploration, sandstone-type, uranium deposits*

INTRODUCTION

Traditional exploration for sandstone-type uranium deposits has centered on genetic models and radiometric methods (Morse 1969; Harshman 1970; Rubin 1970). However, these methods have become prohibitive for sandstone-type uranium deposits hidden at a depth of hundreds of metres (Riese *et al.* 1978). Radioactivity detectors are ineffective in regions where there is a relatively thin inactive overburden (Bowie *et al.* 1970).

Conventional regional soil geochemical surveys based on coarse fractions of soils (>20 mesh) to avoid windblown sand dilution for elemental contents failed to delineate uranium geochemical anomalies for blind sandstone-type uranium deposits in desert basin terrains in China.

The authors have set out to attempt to use deep-penetrating geochemical methods, based on fine-grained fraction sampling and selective leaching in exploration for hidden sandstone-type

uranium deposits and to delineate potential targets in large unexplored basins.

GEOLOGICAL SETTING

The Turpan-Hami basin covers an area of approximately 50 000 km² in Xinjiang, northwestern China. The west part of the basin, located in Turpan, is the lowest area of China mainland, with an elevation of -154 m. The region is extremely arid with the average annual rainfall of less than 15 mm.

The region is substantially covered by regolith sediments, which conceal prospective bedrock sequences. The regolith sediments include windblown sand, alluvial gravels, and caliche horizons. Commonly, the vertical profile of the regolith sediments consists of surface lag or loosely windblown sand underlain by weakly cemented sands and dense caliche-cemented sediments with gypsum.

Miocene sandstone overlying Jurassic sedimentary rocks occur in the Turpan-Hami Basin. Sandstone-type uranium

Table 1. Concentrations and percentage of various uranium forms in regolith over Shihongtan Uranium deposit, Xinjiang

Samples	contents (ppb)					Percentage(%)			
	WEM	AEM	OCM	FMM	T	WEM/T	AEM/T	CM/T	FMM/T
SHT34P0	53.8	954.6	381.3	35.5	2392.5	2.3	39.9	15.9	1.5
SHT34P1	26.7	407.9	228.4	26.4	1712.2	1.6	23.8	13.3	1.5
SHT32P0	57.8	976.9	378.2	47.7	2444.3	2.4	40.0	15.5	1.9
SHT32P1	22.2	331.7	203.4	28.3	1856.8	1.2	17.9	10.9	1.5
Average	40.1	667.8	297.8	34.5	2101.5	1.9	30.4	13.9	1.6

WEM-water extractable U, AEM-adsorbed and exchangeable U, OCM-U occluded in carbonate, FMM-U adsorbed in coatings of Fe-Mn oxides (FMM), T-total U.

deposits are hosted in the Jurassic sandstone rocks.

SAMPLING AND CHEMICAL ANALYSIS

Samples were collected from the weakly cemented sandy clay-rich horizon of soils at a depth of 15-30cm and sieved to -120 mesh in the field.

The samples were ground to a grain size less than 200 mesh (74 μ m) by using high-alumina ceramic or agate mills. The samples were processed for total analysis by 4 acids and selective leaching of water extractable metals (WEM), adsorbed and exchangeable metals (AEM) in clays, occluded metals in carbonate (OCM), and adsorbed metals in coatings of Fe-Mn oxides (FMM) (Wang 1998). Elements are determined by ICP-MS.

RESULTS

Variations of uranium over the deposit

Table 1 shows that Uranium is largely present as adsorbed and exchangeable forms in clays, which make up average 30.4% of the total contents in the soils over a known uranium deposit, Xinjiang.

Figure 1 shows that concentrations of U and associated elements such as Mo, La, Ce, Au, and Th tend to increase in fine fraction of soils over the uranium deposit. This is due to the fact that U complexes $[UO_2]^{2+}$ are easily adsorbed by clays.

Figure 2 shows that U and Mo in -120 mesh fraction of soils give good indication to uranium deposit at the depth of 300m.

Fine fraction samples can give very good indications to concealed uranium deposits.

Regional geochemical survey

Wide-spaced sampling was carried out in an area of approximately 150 000 km² at density of one sample per 100 km² (Wang *et al.* 2007). Soil samples were collected from the weakly cemented sandy horizon at a depth of 20-30cm. The soil samples were subjected to total analysis and selective leaching of mobile metals. Elements were determined by ICP-MS.

Three geochemical provinces of U and Mo were delineated in the Turpan-Hami Basin (Fig. 3). The westernmost one contains the Shihongtan large sandstone-type uranium deposit. Sandstone-type uranium deposits are characteristic by coexisting U and Mo anomalies. The east one at Hami area is was selected for follow-up exploration and a big deposit was found by drilling program.

CONCLUSIONS

(1) The uranium tends to concentrate in the fine fractions of soils in which clays can adsorb uranium complex compounds $[UO_2]^{2+}$ transported from uranium deposits.

(2) Sandstone-type uranium deposits are characteristic by coexisting uranium and molybdenum anomalies.

(3) Sampling of fine-grained fractions of soils (-120 mesh) from the cemented clay-rich horizon at a depth of 15-30 cm are

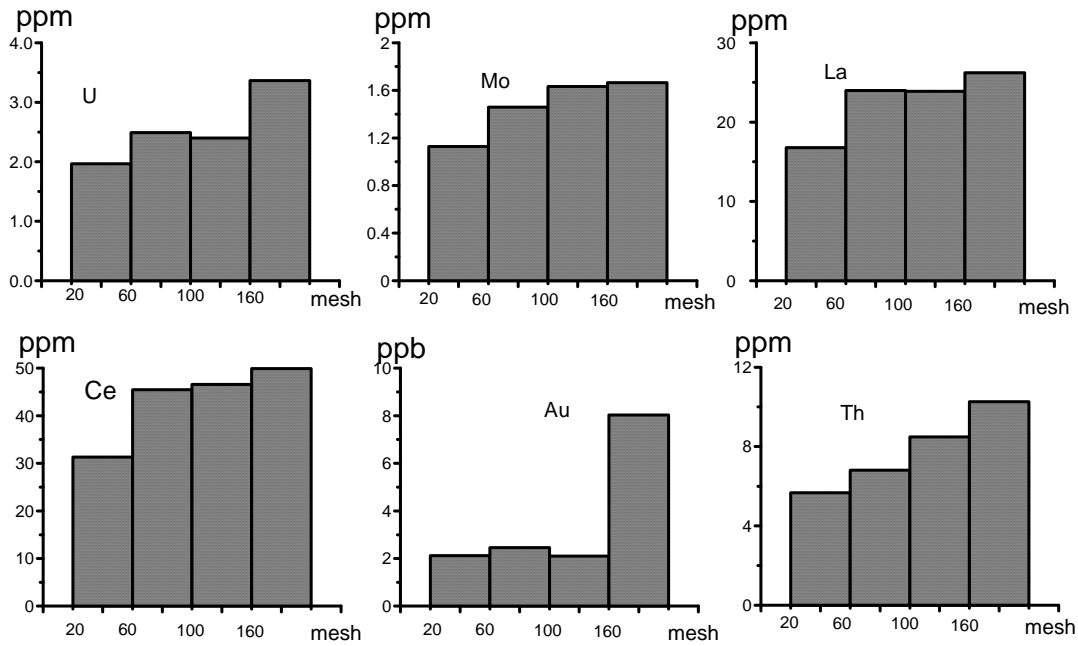


Fig. 1. Bar graphs showing the concentrations of various elements in different size fractions of soil over the Shihongtan sandstone-type uranium deposit.

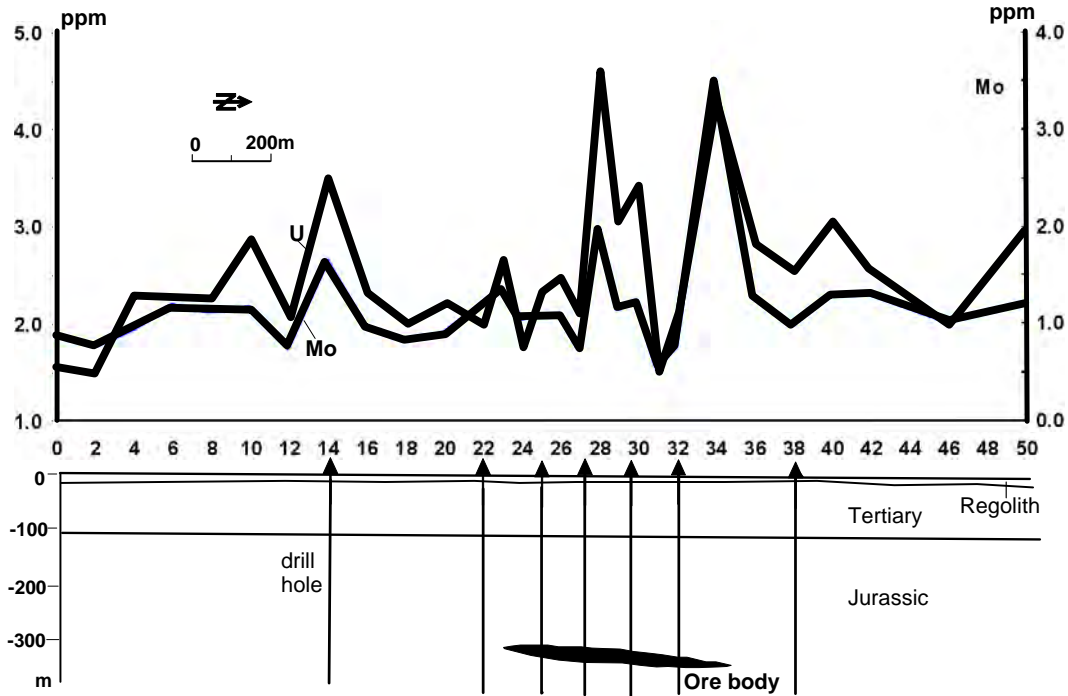


Fig. 2. Uranium and molybdenum anomalies over the Shihongtan uranium deposit.

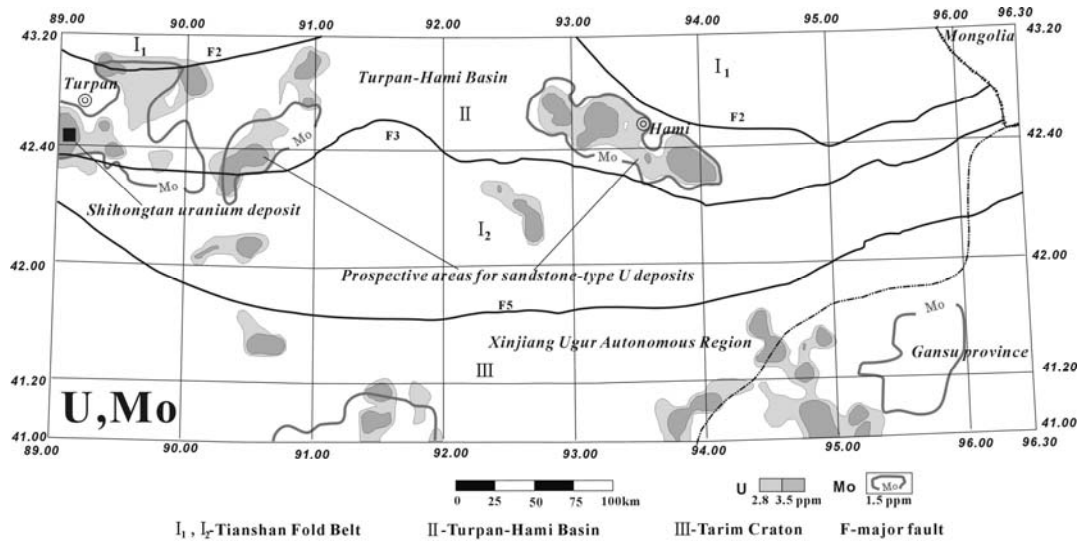


Fig. 3. Uranium geochemical provinces delineated by wide-spaced sampling.

effective both in local and regional exploration for sandstone-type uranium deposits in desert basins.

ACKNOWLEDGEMENTS

Thanks are given to the Ministry of Science and Technology of the People's Republic of China and the China Geological Survey for the financial support (projects Sinoprobe04, 2007AA06Z133, and 2007CB411406).

REFERENCES

BOWIE, S.H.U., BALL, T.K., OSTLE, D. ALPERS, C.N. & BRIMHALL, G.H. 1970. Geochemical methods in the detection of hidden uranium deposits. In: BOYLE, R.W. (ed) *Geochemical Exploration, Proceeding*, 3rd International Geochemical Exploration Symposium. Toronto, Canada, 103-111.

HARSHMAN, E. N. 1970. Uranium ore rolls in the United States. In: *Uranium Exploration Geology*. Vienna: International Atomic Energy Agency, 219-232.

MORSE, R.H. 1969. Radium geochemistry applied to prospecting for uranium. *Canadian Mining Journal*, 75-76.

RIESE, W. C., LEE, M. J, BROOKINS, D, G, AND DELLA VALLE, R. 1978. Application of trace element geochemistry to prospecting for sandstone-type uranium deposits. In: WATTERSON, J.R. AND THEOBALD, P. K. (ed.), *Geochemical Exploration 1978, Proceedings of the Seventh International Geochemical Exploration Symposium*. The Association of Exploration Geochemists, Rexdale, Ontario, Canada, 47-64.

RUBIN, B. 1970. Uranium roll front zonation in the southern Powder River Basin, Wyoming. *Earth Science Bulletin [M]*, Wyoming Geological Association, 5-12.

WANG, X.Q. 1998. Leaching of mobile forms of metals in overburden: development and applications. *Journal of Geochemical Exploration*, **61**, 39-55.

WANG, X. Q., CHI, Q. H., LIU, H. Y., NIE, L. S. AND ZHANG. B. M. 2007. Wide-spaced sampling for delineation of geochemical provinces in desert terrains, northwestern China. *Geochemistry: Exploration, Environment, Analysis*, **7**,153-161.

Vectoring potential of multi-element chemistry in unconformity-associated uranium deposits: major and trace element signatures of the McArthur River Uranium Deposit, Saskatchewan, Canada.

Donald M. Wright

Cameco Corporation, 2121 11th St. West, Saskatoon, SK S7M 1J3 CANADA (e-mail: donald_wright@cameco.com)

ABSTRACT: McArthur River, the world's largest high-grade uranium deposit discovered to date, is located in the Athabasca Basin, Saskatchewan, Canada. Multidisciplinary investigations of the McArthur River deposit have identified key features of the unconformity uranium deposit model from which ongoing exploration has benefitted. Historically, geochemical investigations of this area has been typically restricted in the past to drill core analysis of a suite of five "pathfinder" elements (U, Pb, Ni, Cu, and B), and to the use of short-wave infrared identification of dominant clay species. These investigations have identified broad anomalous uranium halos and refined the known distribution of clay species around this deposit. However, the identification of zones of economic mineralization within these relatively large halos remains problematic. Modern multielement geochemical analysis methods have been recently applied in an attempt to further refine our geochemical models of these deposits and improve our targeting of economic mineralization. Exploration-relevant results of this study have included the identification of 1) multielement signatures associated with mineralization and alteration and 2) the relative spatial distribution of these elements for application in exploration for unconformity-associated uranium deposits.

KEYWORDS: *uranium, geochemistry, unconformity-associated, Athabasca Basin.*

INTRODUCTION

The McArthur River Uranium Deposit, located in northern Saskatchewan, Canada, is the largest high-grade uranium deposit found to date, and is arguably the most valuable deposit of any type or commodity in the world. Exploration for unconformity-associated deposits like McArthur River has utilized geological, geophysical, and geochemical models and techniques to assist with targeting prospective areas. Multielement geochemistry techniques have been recently adopted in the McArthur River area, and have displayed potential for refining the exploration model for unconformity-associated uranium deposits.

GEOLOGICAL SETTING

The McArthur River Uranium Deposit lies in the eastern portion of the Athabasca Basin and within the Churchill Structural Province of the Canadian Shield. The deposit straddles the unconformity between the quartz arenite - rich Late Paleoproterozoic Athabasca Group and

Early Paleoproterozoic metasedimentary/ Archean granitoid basement rocks of the Wollaston Domain. The deposit is also spatially associated with a post-Athabasca Group reverse fault (known as the P2 fault), a feature that occurs within and sub-parallel to a group of graphite-bearing Early Paleoproterozoic metasedimentary units.

The deposit currently consists of eight significant zones of mineralization occurring at vertical depths ranging from 500 to 600 metres. As of December 31, 2007, the deposit contains publically quoted uranium proven (486,500 metric tonnes at 17.38%) and probable reserves (280,000 metric tonnes at 26.33%) totalling 766,500 metric tonnes of ore at an average grade of 20.66% U₃O₈ (Cameco 2008 Business Review).

CURRENT EXPLORATION

METHODOLOGIES

Current exploration for unconformity-associated uranium deposits in the Athabasca Basin rely upon the integration

and comparison of geological, geophysical, and geochemical information relative to the unconformity-associated exploration model (e.g., Jefferson *et al.* 2007).

Key components of the model used in exploration for these deposits include: 1) the presence of an angular unconformity between a Paleoproterozoic sandstone basin and older graphite-bearing metasedimentary and plutonic basement rocks, 2) post-Athabasca Group structural disruption, and 3) the presence of mineralization and mineralization-related hydrothermal alteration.

Due to a lack of outcrop, an abundance of transported overburden, and significant target depths, past exploration has relied heavily on diamond drilling to test electromagnetic conductors. These EM conductors are presumed to have been caused by faulted graphitic basement units at and beneath the Athabasca Group-Basement unconformity. Once the EM conductors have been intersected by drilling, follow-up geological evaluation, clay alteration speciation, and trace-element chemistry of drill core is typically utilized to assist with vectoring exploration towards the location of potential mineralization.

Clay speciation analysis, dominated by the use of short-wave infrared techniques, highlights variations in the clay alteration associated with these deposits. The presence of a key species, such as illite, may be locally significant, but absolute amounts of each clay relative to alteration intensity are typically unattainable from these types of analyses.

The historic use of trace-element geochemistry around the McArthur River Uranium Deposit has primarily focussed on a limited suite of elements, including uranium, lead, nickel, copper, and boron. At McArthur River, uranium is distributed around the main deposit to significant distances (100's of meters) in the overlying Athabasca Group (McGill *et al.* 1993), yet variations in the uranium content of this halo is typically restricted to 1-3 parts per million with little spatial variation, restricting one's ability to vector

into the deposit. Lead is a product of the radioactive decay of uranium, and typically displays a similar distribution to that of uranium. Nickel and copper are common components of unconformity-associated uranium deposits, but their distribution is usually restricted proximally to the main deposits. Boron contents confirm the presence of dravite, an alteration phase that often shows a general spatial association with uranium deposits.

Multielement Geochemical Modelling

In order to refine the geochemical model for unconformity-uranium deposits, whole-rock multielement geochemistry was determined in drill holes from the north end of the McArthur River Uranium Deposit. These data were used to assist with refining the geochemical signatures of mineralization and alteration associated with the deposit, and to define the spatial distribution of these features to assist with deposit vectoring. As a result of this review, several basic geochemical associations related to uranium through a series of geochemical processes have been identified and spatially modelled.

Reduction-oxidation processes, which are the dominant control for uranium mobility and deposit formation, are also responsible for elevated molybdenum and vanadium contents observed associated with mineralization.

Radioactive decay of the two main isotopes of uranium produces significant contents of the lead isotopes ²⁰⁶Pb and ²⁰⁷Pb. The total amount and age of uranium combined with the differences in decay rate of the two uranium isotopes leads to the production of distinct ²⁰⁷Pb/²⁰⁶Pb lead isotope ratios uniquely related to mineralization (e.g., Gulson 1986; Holk *et al.* 2003).

Several elements from the multielement suite are associated with alteration and clay chemistry. Due to the relative cleanliness of the Athabasca Group sandstones, anomalous contents of aluminium, magnesium, potassium, lithium, and boron, along with loss-on-ignition, provide measures of the amount and type of alteration present. These data

can also assist with refining our understanding of the spectral clay results in these areas.

The relative spatial distribution of the mineralization- and alteration-related geochemical signatures can be useful in vectoring toward uranium mineralization (Fig. 1).

A distal uranium halo (1 ppm) extends over 500 metres from the deposit towards surface, indicating the presence of mineralization. Significant changes in the uranium content are not observed until within approximately one hundred metres of mineralization, where partial digest uranium values begin to increase significantly.

Anomalous values of lithium, ²⁰⁷Pb/²⁰⁶Pb, and molybdenum (and other process-related elements) are observed within the distal uranium halo, and appear to represent intermediate and perhaps proximal halos enveloping mineralization. Local enrichments are also observed associated with structural features distal or intermediate to the main zone of mineralization, the trend of which may be useful for vectoring into the deposit.

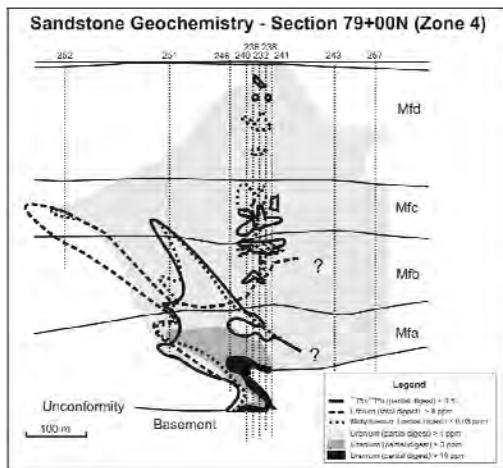


Fig. 1. Cross-sectional distribution of uranium, molybdenum, lithium, and ²⁰⁷Pb/²⁰⁶Pb lead isotope ratios around mineralization at Zone 4, P2 North, McArthur River.

CONCLUSIONS

Exploration for unconformity-associated uranium deposits is dependent upon the effective integration of geological,

geophysical, and geochemical information as well as exploration models. The McArthur River Uranium Deposit is one of the most economically significant examples of an unconformity-associated uranium deposit, and is an ideal model for the review of the multielement chemistry associated with such a deposit. Several major and trace element signatures associated with alteration and mineralization have been identified (e.g., Li, Mo, ²⁰⁷Pb/²⁰⁶Pb), and the relative distribution of these signatures may be integrated with geological and geophysical information to highlight the presence and location of uranium mineralization in unconformity-associated uranium deposits.

ACKNOWLEDGEMENTS

Cameco Corporation, AREVA Resources Canada, and UEM Inc. are gratefully acknowledged for their support of this work and their permission to present it here. Numerous members of the Cameco Exploration team contributed to the collective product, and the staff of the McArthur River Exploration Team are especially thanked for their logistical assistance in the collection of the material analyzed.

REFERENCES

- GULSON, B.L. 1986. *Lead Isotopes in Mineral Exploration*. Developments in Economic Geology, Volume 23, Elsevier, 245 p.
- HOLK, G.J., KYSER, T.K., CHIPLEY, D., HIATT, E.E., & MARLATT, J. 2003. Mobile Pb-isotopes in Proterozoic sedimentary basins as guides for exploration of uranium deposits. *Journal of Geochemical Exploration*, **80**, 297–320.
- JEFFERSON, C.W., THOMAS, D.J., GANDHI, S.S., RAMAEKERS, P., DELANEY, G., BRISBIN, D., CUTTS, C., QUIRT, D., PORTELLA, P., & OLSON, A. 2007. Unconformity-Associated Uranium Deposits of the Athabasca Basin, Saskatchewan and Alberta. In: W.D. Goodfellow (ed) *Mineral Deposits of Canada: A Synthesis of Major Deposit-Types, District Metallogeny, the Evolution of Geological Provinces, and Exploration Methods*. Geological Survey of Canada, Mineral Deposits Division, Special Publication No. 5, 273-305.

MCGILL, B.D., MARLATT, J.L., MATTHEWS, R.B.,
SOPUCK, V.J., HOMENIUK, L.A., & HUBREGTSE,
J.J. 1993. The P2 North Uranium Deposit,

Saskatchewan, Canada. *Exploration and
Mining Geology*, **2**, 321-331.

Broad-based physicochemical paragenetic aspects of primordial uranium deposits of endogenic origin

Igor A. Zotov¹ & Maksim V. Seredkin²

¹ORAS, IGE M RAS, Staromonetny per. 15, Moscow, 119017, Russia (e-mail: olimpus16@yandex.ru)

²Publ. Corporation "Atomredmetzoloto", Drovyanoi Lane 22 B, Moscow, 109004 Russia
(e-mail: seredkin.m.v.@armz.ru)

ABSTRACT: Many U deposits have an endogenic origin connected with magmas of a very wide in composition from nepheline-normative and carbonatite to different granitoid types. We concluded that all U-bearing granitoids belong to alkali magmatic types whose transmagnetic fluids (Korzhinskii's term) participate in formation of U-containing and proper U ore deposits. These fluids extract U from crustal and terrigenous rocks by oxidation into transportable complexes. At the same time crustal rocks fuse giving rise granitic magmas of alkalic affinity specialized in both U and rare metals. The generally oxidizing nature of transmagnetic fluids result in the mobility of U (and other metals) and subsequent precipitation occurring at reducing barriers, such as rocks containing graphite, free carbon, sulfides, and quartz-rich rocks.

KEYWORDS: *alkali magmas, transmagnetic fluids, endogenic deposits, uranium*

INTRODUCTION

It is well known that the overwhelming majority of U deposits form as the result of two key processes – first endogenic (hypogene hydrothermal) and later supergene enrichment ones. We'll only view the processes of the former group.

PRINCIPLE METHOD OF OUR POINT OF VIEW

We base on progress of Korzhinskii's ideas of physicochemical analysis of mineral parageneses of natural rocks (Korzhinskii 1959) and participation of transmagnetic fluids (dense superheated gases and solutions) in magmatism (Korzhinskii 1952) and other endogenic processes. The active role of these fluids in endogenic ore formation is developed by I.A. Zotov (1980, 1989; Korzhinskii *et al.* 1984) and A.A. Marakushev (1999) (e.g., Marakushev *et al.* 2006).

MAIN FACTORS CONTROLLING FORMATION OF PRIMODIAL ENDOGENIC U-MINERALIZATION OF DEPOSITS

Magmatic factor

Many U deposits indisputably are

connected to alkalic magmas of re-activated tectonic structures (often depressions) of ancient platforms. The typical high relative Th and U concentrations of such magmatic rocks support such point of view. Nevertheless some U deposits probably have maternal granitic magmas, which have no obvious signs of high alkalinity like the presence of alkalic dark colour minerals. But some granites of this group, such as charnockites and rapakivi varieties, contain mineral parageneses (K-spar+hypersthene in the former and K-spar+olivine in the latter) of high alkali conditions according to Korzhinskii's criteria (Korzhinskii 1946). Often U productive granitic complexes of unclear alkalinity contain leucogranite and alaskite (mono-spar) phases and facies, which are also indicators of magma evolution in high alkali environments (Zotov 2006). By the way early connection of U deposits with alkali magmatism was proposed by A.A. Marakushev (1999, p. 205-215).

Transmagnetic fluids

The reason for the similarity of Th-U and rare-metal ore mineralization between silica-undersaturated (nepheline-

normative) and silica-saturated (granitic family) magmas is not simple, since the former group magmas are generated in mantle conditions and granitoid magmas – in the crust. Straightforward relations between them are not known, but the latter ones obviously are generated under influence of the heat of the mantle magmas. Alkali basalt magmas possibly are parental for both groups of magmas. The exact mechanism of transfer of rare-metal specialization of alkali basalts to spatially and temporally associated (bimodal) granitoid magmas remains enigmatic, but questions of volatile transfer mechanisms are needed. The radical change in understanding of the role of volatiles was developed by D.S. Korzhinskii (1952), who formulated the concept of transmagmaic fluid flow that naturally develops from crystallizing magmas; he postulated that such fluids can percolate into and even through magmatic liquids (melts) as free supercritical overheated gases. Since transmagmaic fluids would be in chemical equilibrium with the parental magmas and eventually evolve from those consolidating magmas, the evidence for these fluids can typically be found in the exocontacts of these magmatic bodies. The magmatic fluids chemically and thermally react with the wall rocks causing metasomatic and metamorphic changes in them. This *magmatic stage* metasomatism differs from the more widespread post-magmatic metasomatism in that the former does not react with the parental magmatic rocks, whereas the derivative metasomatites are cut by magmatic veins that contain their xenoliths. During 1954-1984 in Russia there have been comprehensive studies of magmatic stage metasomatites of all natural magma types, which completely confirms Korzhinskii's concept. At the same time it was found that although all magmatic bodies always contained evidence of transmagmaic fluid flow, their activity (or better fluid volumes) was greatly variable not only from one magmatic massif and complex to another, but even within one magmatic body; the later regularity is evidence that there is

fluid movement through crystallizing magmas. These studies also show that the great majority of magmatic massifs are characterized by minimal fluid flow such that they do not influence magma evolution. Fluid flow interaction is only most evident in ore-bearing intrusions (Korzhinskii 1962). Korzhinskii (1952) noted the sublithospheric source of transmagmaic fluid, which probably originates in the athenosphere (Zotov 1989).

Later (Zotov 1980, 1989; Korzhinskii *et al.* 1984; Marakushev *et al.* from 2002 up to 2006), it was shown that transmagmaic fluids are able to transport ore metals whose portion may be predominant in endogenic deposits as for example in Pt-Pd-Cu-Ni sulfide deposits (same ref.), apatite deposits of alkali (Zotov 1989) and alkali-carbonatite (Seredkin *et al.* 2004) magmatic massifs. This concept is essentially useful as an application for understanding of genesis of big endogenic ore deposits (Zotov 1980).

The role of transmagmaic fluids in genesis of U endogenic deposits

It was proposed above that endogenic U deposits seem to be produced by a wide variety of alkalic magmas, which are usually accompanied by active (great volume) reaction of transmagmaic fluids. Additional evidence of it is the widespread occurrence of apatite in amounts up to 60 vol.% in many deposits. Our early studies of different types of primary apatite deposits (Zotov 1989; Seredkin *et al.* 2004) have shown that they indisputably were formed by transmagmaic fluids of alkali magmas, which serve as good conductors for K-P compounds of the fluids producing K-metasomatism (finitization) of exocontact rocks. Ca-rich lithofacies of the latter play a role as barriers for P mobility resulting in deposition as apatite mineralization. Thus apatite mineralization of many U deposits confirms participation of transmagmaic fluids of alkali magmas in their formation.

At the same time it is quite obvious that most mantle material cannot be the source of uranium, because it was not

found in critical amounts in any mantle xenoliths. Hence transmagnetic fluids sequester their uranium from the crust. Transmagnetic fluids derived from alkalic magmas are good solutions for leaching uranium from crustal rocks, via transformation into transportable oxidized uranyl complexes. This is related to the relatively high oxidation environment in alkali magmas (nepheline-normative and carbonatitic ones) at depth and remain incompatible in these magmas with oxidized iron contained in rock-forming minerals – aegerine and alkali amphiboles. Most likely, complexing is related to high activity of fluorine and not just oxygen fugacity, although transmagnetic fluids must also be characterized by high oxidation potential.

It is obvious that the action of such fluids on crustal rocks invoke oxidation of uranium transforming it in mobile complexes. At the same time uraniumiferous terrigenous rocks may partially melt giving rise to derivative crustal anorogenic granitoid magmas of alkalic affinity that may accompany contamination (including U) of primary mantle alkalic magmas, which initiated these crustal fusion processes.

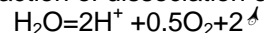
Formation of Primary Endogenic U Concentrations of the Deposits

The high oxidized character of U-bearing magmatic ore-forming systems determines both their metallogenic specialization and conditions of deposition of their ore load including U.

The ore mineralization should be deposited in or near U-bearing intrusion. According to the concepts described, ore productive magmatic bodies are to be characterized by active action of transmagnetic fluids, which should be expressed by wide-spread metamorphism, magmatic stage metasomatism, and magmatic replacement phenomena along intrusion exocontacts. Contamination by wall rock materials is also a typical feature of such intrusions.

The ore formation itself is connected with the oxidation state of ore-bearing fluids for which reducing mediums are

favourable as chemical reaction barriers for ore precipitation. Such a reductant role can be associated with graphitic, free carbon, sulfidic, and other reduced iron-rich rocks. Quartz-rich rocks also show reducing properties under hydrothermal influence due to oxidation-reduction interaction of components of hydrothermal solutions and the rocks (Korzhinskii, 1963). Reaction of dissociation of water



show inverse dependence of acidity ($\text{pH} = -\log[\text{H}^+]$), and reduction potential (μ) at constant oxygen fugacity ($f(\text{O}_2)$), which is reliable for leucocratic or quartz-rich rocks. Dilution of silica of the latter provoke decrease of activity of all acids due to lowering of activity coefficient (ν) of acidic components. Hence when hydrothermal fluids come in to quartz-rich rocks, the reduction potential is supposed to increase causing precipitation of U and high-charged ore elements, especially rare metals.

These factors of U ore deposition can be demonstrated by the following examples. In deposits of "Unconformity" type from the Athabasca basin, the uranium localizes in graphite-containing layers, which are used as favourable prospecting signs as at the MacArthur River deposit. In deposits of the El'kon U ore region spreading of brannerite streaks is limited by zones of pyrite-containing K-spar metasomatites. We should be reminded that the giant Olympic Dam U deposit initially was prospected and explored as copper-sulfide sandstone. Lastly, there is the enormous group of Proterozoic deposits where U-TR and Au-U mineralization is localized in quartz-pebble conglomerate layers (Dahlkamp 1991) and Witwatersrand with its mineralized conglomerate-like polymictic breccia with quartz rounded fragments (70-80 vol.%) and pyrite is between them. Some U deposits (including the big Tulukai one) of Strel'tsovskoe ore field (Russia) are localized in Si-rich felsites.

CONCLUSIONS

This contribution is summarized as

follows:

- (1) primary uranium mineralization of endogenic U deposits are related to the production of a wide variety of alkalic magmas;
- (2) transmagnetic fluids (first supposed by D.S. Korzhinskii in 1952) derived from mantle alkalic magmas are postulated to be involved in the leaching and (or) melting of U; the derivative alkalic crustal affinity of the granitic magmas are a related product of heat advection from advecting mantle magmas;
- (3) the oxidized state of the U-bearing transmagnetic fluids under discussion explains the typical precipitation of U in the reducing rocks with graphite, free carbon, sulfide, other reduced Fe-rich rocks, and quartz-rich rock varieties;
- (4) such conditions and origin of U-containing fluids can also explain the valuable rare-metal components typifying many U deposits.

ACKNOWLEDGEMENTS

We express our gratitude to D.S. Korzhinskii, who supported the research developed here from the first steps.

REFERENCES

DAHLKAMP F.J. 1991. *Uranium ore deposits*. N.Y. Springer, 460 p.

KORZHINSKII, D.S. 1952. Granitization as magmatic replacement. Academy of Sciences of USSR. *Geological seria*, No. 4. 56-69. (In Russian)

KORZHINSKII, D.S. 1959. *Physicochemical basis of the analysis of the paragenesis of minerals*. Consultant bureau, Inc. N.Y., 142 p.

KORZHINSKII, D.S. 1962. Problems of physicochemical theory of petrological processes. *Izvestiya of Academy of Sciences of USSR. Geological seria*. No. 1. 10-25. (In Russian)

KORZHINSKII, D.S. 1963. Correlation between activity of oxygen, oxidity and reduction potential in endogenic mineral formation. *Izvestiya of Academy of Sciences of USSR. Geological seria*. No. 3. 54-61. (In Russian)

KORZHINSKII, D.S., PERTSEV, N.N., & ZOTOV, I.A. 1984. Transmagnetic fluids and magmatogenic ore deposits: A problem of mantle ore sources. *Proc. Siths quadren. IAGOD symp. Stuttgart*: Nagele und Obermiller, 131-138.

MARAKUSHEV, A.A. 1999. *Origin of the Earth and nature of its' endogenic activity*. "Nauka" publ. house. Moscow. 255 p.(In Russian)

MARAKUSHEV, A.A., ZOTOV, I.A., & PANEYAKH, N.A. 2006. Paragenetic systematization of platinum metal deposits and its' genetic significance. *"Understanding the genesis of ore deposits to meet the demand of the 21st century."* 12th Quadren. IAGOD symposium. Extended abstracts. CD. No. 117.

SEREDKIN, M.V., ZOTOV, I.A., & KARCHEVSKII, P.I. 2004. Geological and genetic model for the formation of the Kovdor massif and the accompanying apatite-magnetite deposit. *Petrology*, 12, 519-539 (Transl. from Rus.)

ZOTOV, I.A. 1980. About role of transmagnetic fluids in genesis of magmatogenic ore deposits. *Soviet Geology*, No. 1, 45-57. (In Russian)

ZOTOV, I.A. 1989. *Transmagnetic fluids in magmatism and ore formation*. Moscow. "Nauka" publishing house, 215 p.(In Russian)

ZOTOV, I.A., 2006. The problem of ore metal sources of granite magmatism: the rare metal mineralized alaskite-leucogranite magmatic associations are taken as an example. *"Understanding the genesis of ore deposits to meet the demand of the 21st century"* 12th Quadren. IAGOD symposium. Extended abstracts. CD. No. 071.

NORTH ATLANTIC MINERALS SYMPOSIUM

EDITED BY:

**ANDREW KERR
GERRY STANLEY
LAWRENCE WINTER
STEVE McCUTCHEON**

Mass change constraints and hydrothermal alteration of felsic volcanic rocks that host the Restigouche Volcanogenic Massive Sulfide Deposit, Bathurst Mining Camp, New Brunswick, Canada

Amanuel Bein¹ & David R. Lentz¹

¹Department of Geology, University of New Brunswick, 2 Bailey Drive, Fredericton, New Brunswick, E3B 5A3 CANADA (e-mail: u3x30@unb.ca)

ABSTRACT: An immobile-element lithochemical study of the volcanic rocks that host the Restigouche volcanogenic massive sulfide (VMS) deposit in the Bathurst Mining Camp (BMC) discriminated seven geochemical units (A, B, C, D, E, F, and G). The units are stratigraphically in ascending order and the massive sulfide horizon occurs between units A-D and A-E. Hydrothermal alteration of these tholeiitic, transitional, and transitional-calc-alkaline volcanic rocks is characterized by general additions of MnO, MgO, Fe₂O₃, LOI (H₂O), Zn, Ga, and Pb, and loss of Na₂O, SiO₂, and Ba. K₂O, and CaO are leached from the footwall sequence, but CaO is enriched in the hanging wall. Using constant Al₂O₃ with the isocon method of Grant (1986), the study demonstrates the immobile nature of TiO₂, Zr, Nb, Y, Nd, and Th. Net mass loss in units B, C, D, F, and G and mass addition in the sulfide horizon between A and E are consistent with hydrothermal alteration and mineralization processes that formed the Restigouche VMS deposit. Also, compositional additions and losses of various components are attributed to chlorite, sericite, and carbonate alterations of the host rocks.

KEYWORDS: *Restigouche, massive sulfide, immobile elements, Isocon method, hydrothermal alteration*

INTRODUCTION

The Restigouche massive sulfide deposit is located in the northwestern part of the Bathurst Mining Camp (BMC), 60 km west of the city of Bathurst, northern New Brunswick. The property is currently controlled by Blue Note Mining and the company reports show that the deposit has an estimated reserve of 1.3 Mt grading 6.53% Zn, 5.05% Pb, and 99.6g/t Ag as of 2007 (Art Hamilton, pers. communication).

The present study was commenced in order to define the geological and lithochemical characteristics of the volcanic rocks hosting the Restigouche deposit. Using lithochemical techniques, the first phase of this study discriminated hydrothermally altered volcanic rocks that host the Restigouche deposit into 7 geochemical groups, with chemostratigraphic significance (Bein & Lentz 2009). The second part of this lithochemical study involved mass

change calculations for 92 samples from the 7 geochemical groups.

GEOLOGICAL SETTING

The Ordovician felsic volcanic pile that hosts the Restigouche massive sulfide deposit in the BMC is composed of 7 geochemically distinct groups; A, B, C, D, E, F, and G (Bein & Lentz 2009). The units A, B, C, D, E, and F are in stratigraphically ascending order and each group consists of hydrothermally altered effusive and volcanoclastic rhyodacitic-dacitic rocks of tholeiitic, transitional, transitional-calc-alkaline magmatic nature. The massive sulfide lens occurs between footwall unit A and hanging wall units D and E. Finlow-Bates & Stumpfl (1981) described that the felsic volcanic rocks that host the Restigouche VMS deposit are intensely altered to levels, where the normally immobile element Nb acted as a mobile component.

HYDROTHERMAL ALTERATION

Methodology

XRF lithochemical analysis of 124 diamond drill core samples was performed at the Department of Geology, University of Ottawa. Accuracy and precision of the analysis is demonstrated by 9 runs for selected major and trace elements in a rhyolitic standard (RHY-94, Lentz 1995). The first step was selection of a least-altered sample for each of the 7 geochemical units. Least-altered samples were selected based on comparison of the lithochemical data of samples from the Restigouche deposit and composition of fresh felsic volcanic rocks. Based on arguments provided by Leitch & Lentz (1994) and coinciding syngenetic hydrothermal and post-hydrothermal metamorphic conditions of the Restigouche deposit, Al₂O₃ is considered as the most immobile component. Also, Al₂O₃ shows high Pearson Product correlation coefficients ($r > 0.90$) with TiO₂, Zr, and Nb and thus it can be considered as an immobile component. Thus the constant Al₂O₃ Isocon method of Grant (1986) is used to demonstrate immobility of immobile elements and compositional changes of the hydrothermally altered volcanic rocks. Relation between compositional and mass changes is demonstrated using the procedures Barrett and Maclean (1999) used for a rhyolite unit that host the Phelps Dodge VMS deposit in Matagami, Quebec.

Immobile Elements

Isocon plot and mass balance calculations of altered samples from the Restigouche deposit demonstrated that TiO₂, Zr, Nb, Y, Nd, and Th are immobile. Isocon plot of selected samples from the 7 geochemical units from the study area are shown in Figures 1-7. Yttrium, Nd, and Th show slight mobility in some samples, but considering the accuracy and precision parameters of the analysis they can still be considered as immobile components. Gallium shows some mobility, whereas La and Ce are moderately mobile. SiO₂, Fe₂O₃, MnO, MgO, CaO, Na₂O, K₂O, and LOI are extremely mobile, and they are

either added or leached. P₂O₅ is moderately mobile with strong affinity of immobility in some samples (Figs. 3-7). Zn, Rb, Sr, Ba, and Pb are also mobile components.

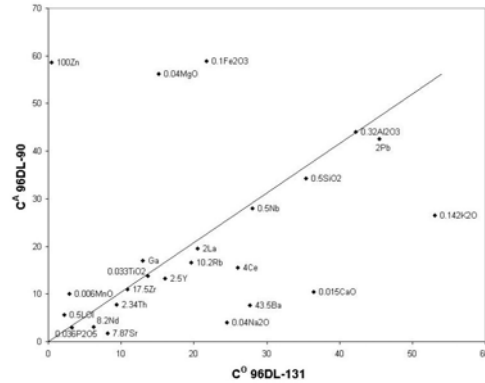


Fig. 1. Scaled Isocon plot of sample 96DL-90 from unit A.

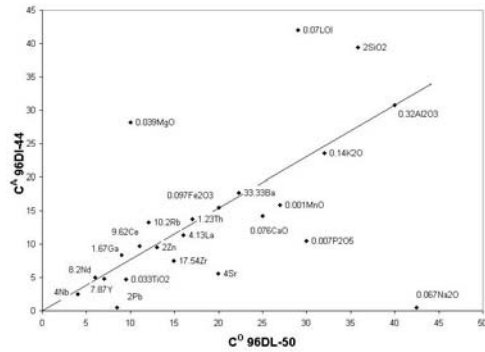


Fig. 2. Scaled Isocon plot of sample 96DL-44 from unit B.

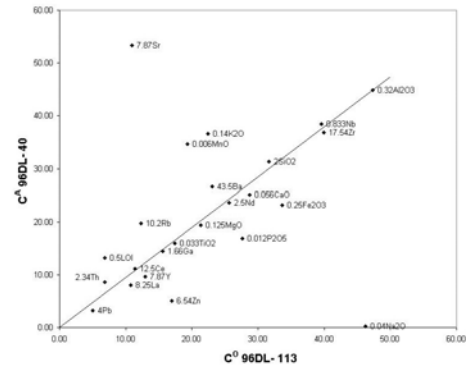


Fig. 3. Scaled Isocon plot of sample 96DL-40 from unit C.

respectively. Some samples from unit C and D show Pb enrichment on the levels of 22-228 and 601-705 ppm. Prominent leaching of SiO₂ and Na₂O characterize all the 7 geochemical units except that substantial samples from unit A show 5-32 wt.% SiO₂ enrichment and unit G show 0.02-1.1 wt.% addition of Na₂O. 4-8, 6-23, 9-24, 7-35, 9-41, 3-42, and 4-38 wt.% losses of SiO₂ in units A, B, C, D, E, F, and G and 0.6-1.3, 0.02-2.8, 0.8-1.84, 0.2-2.7, and 0.4-8 wt.% loss of Na₂O in units A, B, C, D, E, and F, are observed. General loss of Ba is also characteristic in units A, B, D, E, F, and G where 428-1024, 115-285, 16-792, 158-865, 67-719, and 529-1716 ppm Ba leaching is observed. However, 55-573 ppm Ba enrichment in unit C is noted. 0.74-5.6, 0.2-2.9, 0.13-2.63, and 0.7-3.2 wt.% K₂O is lost from units A, B, D, and G. 0.1-3 wt.% K₂O is added to unit C and K₂O is both added and lost in samples of units E and F where enrichment can reach as much as 0.7-1.3 and 0.03-1.2 wt.% respectively. 0.1-0.5, 0.5-1.2, and 0.13-1 wt.% CaO losses in the footwall units A, B, C and D and on the other hand 0.1-1.8 and 0.01-2.5 wt.% CaO additions in the hanging wall units E and F are also marked.

CONCLUSIONS

This study has revealed that;

- (1) Despite the intense hydrothermal alteration of the volcanic rocks that host the Restigouche VMS deposit, immobility of TiO₂, Zr, Nb, Y, Nd, and Th is demonstrated using the Isocon method of Grant (1986).
- (2) Both the hanging wall and footwall volcanic rocks are altered and it is confirmed that MnO, MgO, Fe₂O₃, LOI (H₂O), Zn, Ga, and Pb are generally added to the rocks, whereas Na₂O, SiO₂, and Ba are leached. Leaching of Na₂O from units A, B, C, D, E, and F and of CaO from footwall units A, B, and C, and addition of MgO to A, B, D, E, and F, Fe₂O₃ to footwall units A and B, and K₂O to units C, E, and F can be attributed to breakdown of feldspar and sericitization

and chloritization of the volcanic rocks. Besides, leaching of K₂O and CaO from the footwall units accompanied by their respective addition in the hanging wall units is consistent with sericitization and carbonitization of the rocks which is reported in Bein and Lentz (2009). Fe₂O₃ enrichment to the sulfide horizon between unit A and E and the hanging wall units E and F is related to chloritization of the footwall and siderite (carbonate) alteration of the hanging wall.

ACKNOWLEDGEMENTS

We acknowledge Blue Note Mining and NB Department of Natural Resources for their assistance and support during the course of the study.

REFERENCES

- BARRETT, T.J. & MACLEAN, W.H. 1999. Volcanic Sequences, Lithogeochemistry, and Hydrothermal Alteration in Some Bimodal Volcanic-Associated Massive Sulfide Systems. *Reviews in Economic Geology*, **8**, 101-131.
- BEIN, A. & LENTZ, D.R. 2009. Immobile Element Lithogeochemistry of felsic volcanic rocks hosting the Restigouche Volcanogenic Massive Sulfide Deposit, Bathurst Mining Camp, New Brunswick Canada. Proceedings of IAGS 2009.
- FINLOW-BATES, T & STUMPFL, E.F. 1981. The Behaviour Of So-Called Immobile Elements In Hydrothermally Altered Rocks Associated With Volcanogenic Submarine-Exhalative Ore Deposits. *Mineralium Deposita*, **11**, 319-328.
- GRANT, J.A. 1986. The Isocon Diagram-A Simple Solution To Gresens' Equation For Metasomatic Alteration. *Economic Geology*, **81**, 1976-1982.
- LEITCH, C.H.B. & LENTZ, D.R. 1994. The gresen approach to mass balance constraints of alteration systems: methods, pitfalls, examples, In: LENTZ, D.R., (ed) *Alteration and Alteration processes associated with Ore-forming systems*, Geological Association of Canada, Short Course Notes, **11**, 161-192.
- LENTZ, D.R. 1995. Preliminary evaluation of six in-house rock geochemical standards from the Bathurst Camp, New Brunswick. *New Brunswick Department of Natural Resources and Energy*, Minerals and Energy Division, Miscellaneous Report **18**, p. 81-89.

Results of 2008 exploration program Mount Pleasant Property: geochemistry, mineralogy, and deposit modeling of Sn-In and WO₃-MoS₂ zones

Trevor Boyd¹ & Gustaaf Kooiman¹

¹Adex Mining Inc., Suite 1402, 67 Yonge St., Toronto, Ontario, Canada
(e-mail: tboyd@adexmining.com)

ABSTRACT: During 2008, the Mount Pleasant Mine Property owned by Adex Mining Inc. underwent a major exploration program comprising extensive diamond drilling plus the additional re-sampling of material stored on-site from previous drill programs on the property. In addition, samples of the multi-metal porphyry mineralization from different zones on the property were chosen for quantitative mineralogical characterization.

The geochemical analyses generated from this program were compiled and incorporated into a computer database with the purpose of generating regulatory compliant physical deposit models and resource estimates of the mineralized bodies for both the Sn-In-Zn-Cu and WO₃-MoS₂-Bi zones on the property. In this presentation, Adex Mining discusses the results of the program and its context with respect to better understanding and integrating the geochemical and mineralogical variations within and among the zones. The purpose is to update and improve the evolving economic geology model of the polymetallic mineralization hosted on the property.

KEYWORDS: tungsten, tin, indium, quantitative mineralogy, porphyry mineralization

INTRODUCTION

The Mount Pleasant Mine Property is located in Charlotte County, southwestern New Brunswick, Canada. The mineralization is divided into two main groups consisting of porphyry-type tungsten-molybdenum deposits, and vein and replacement-type tin polymetallic bodies. The deposits at Mount Pleasant are described in some detail in Kooiman *et al.* (1986) and Sinclair *et al.* (2006). Their petrogenetic character is discussed in Yang *et al.* (2003), Inverno & Hutchinson (2006) and Sinclair *et al.* (2007).

This presentation is an updated review of the economic geology at Mount Pleasant based upon our recent exploration results. There has been a resurgence of interest in these deposit types with the recent recovery of W, Mo, and Sn metal prices. Economic interest in the Mount Pleasant deposits has been heightened due to its hosting of metals that are increasingly important in high technology applications and medicine, such as indium and bismuth.

GEOLOGICAL SETTING

The mineralized area lies within the Appalachian Orogen at the southwest margin of a Devonian caldera structure associated with the emplacement of multiple granitic intrusions (see Figure 1). The caldera rocks were emplaced in an anorogenic or post-collisional setting following the Acadian Orogeny and are bounded by highly deformed Ordovician and Silurian metasedimentary rocks and a late Silurian to Devonian granitic batholith (McLeod 1990).

Within the Mount Pleasant Mine Property, there are at least three stages of high-level, fine-grained to porphyritic intrusions. The granitic bodies and related mineral deposits are found at three main areas referred to as the Fire Tower Zone, North Zone, and between them the Saddle Zone, which are aligned along a northerly direction for two kilometres. There is evidence that the three zones are joined along a single continuously mineralized trend.

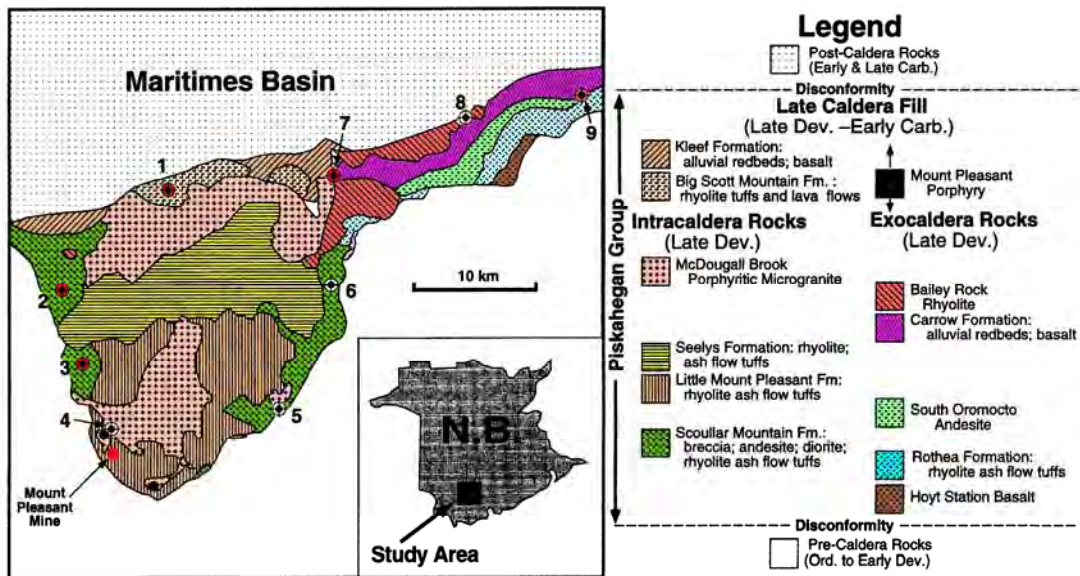


Fig. 1. Location of the Mount Pleasant W-Mo and Sn-Zn-In deposit, within the Late Devonian Caldera, southwestern New Brunswick (after McCutcheon 1990).

The W-Mo mineralization containing significant Bi, but negligible amounts of indium, is hosted by the early Granite I intrusion. The later Granite II intrusion hosts polymetallic tin mineralization that has indium grades of at least equal metal value to the Sn content, plus significant concentrations of Zn, Cu and Bi. The earlier Granite I episode of mineralization mainly focused within the Fire Tower Zone. This zone was mined for tungsten from 1983 to 1985 by Billiton Canada. The later Granite II episode occurs predominantly within the North Zone, although both types are found throughout the mineralized trend. The youngest Granite III episode underlies the other two at depths of greater than 450 metres and remains largely unexplored.

DISCUSSION

During 2008, 13,300 metres of diamond drilling and greater than 5,200 analyses of the core and historical samples were completed for WO₃, MoS₂, Sn, In, Zn, Cu, Pb, Bi, and As. An additional 1900 historical samples were analysed for Indium only (Boyd 2008). Seven samples obtained from a wide variety of

mineralization types throughout the property underwent quantitative mineralogical characterization including QEMSCAN analysis and semi-quantitative XRD. In addition, EPMA was carried out on selected sulfide and oxide minerals to quantify the distribution of indium within the deposit (Prout *et al.* 2008).

Geochemical analyses from approximately 1500 drill holes were entered into separate GEMCOM 3-D wireframe computer models for the Fire Tower Zone and North Zone and used to generate regulatory compliant mineral resource estimates broken down into sub zones for both types of the mineralized bodies. To date, the Fire Tower Zone reports an indicated resource of 13,489,000 tonnes at 0.33 wt.% WO₃, 0.21 wt.% MoS₂, 0.06 wt.% Bi, and 0.57 wt.% As (Dunbar & El-Rassi 2008). The modelling and resource estimation results for the North Zone remain pending. Most mineralized bodies require more delineation drilling to fully outline their limits and remain open laterally for exploration.

CONCLUSIONS

Final interpretations of the 2008 program remain pending depending upon the completion of the deposit modelling and release of geochemical and mineralogical analyses. The following tentative conclusions are presented, which largely support and build upon earlier work completed on the property.

The geochemistry and setting of the mineralization varies with respect to depth, as well as with host rock type and intrusive episode. For the Granite I type deposits, there is considerable compositional variation among separate sub-zones, however, overall the mineralization is zoned with the MoS₂ content and MoS₂/WO₃ ratio increasing and As content decreasing with depth from 200 to 450 metres, especially within the Fire Tower Zone.

For the Granite II type deposits, the deeply (300–450 metres) emplaced Sn-bearing mineralization is largely controlled by the primary fracturing of the host granitic rocks. The deposits at these levels are Sn rich with relatively low indium and base-metal contents. Toward the surface, the setting of the Sn mineralization changes, becoming increasingly controlled and confined by erratically emplaced replacement-type narrow veins or “lodes”. However, indium and base-metal contents of the mineralization also significantly increase and occur as well within the highly brecciated wall-rocks to the lodes.

The result is that at shallow depths, the Sn-In-Zn-Cu-Bi-bearing mineralization (although lower grade in comparison to the deeper deposits) is more widespread than originally believed, and its lateral extent is in part controlled by the rough layering of the brecciated zones. The discovery of significant indium values within this widespread low-grade near surface mineralized halo presents the possibility of open pit exploitation opportunities at Mount Pleasant.

ACKNOWLEDGEMENTS

We thank Adex Mining Inc. and CEO Kabir Ahmed for financial support and for

permission to present this paper. We acknowledge that our understanding of these mineral deposits draws upon the contribution of many workers over the past 50 years who have built and studied Mount Pleasant.

REFERENCES

- BOYD, T. 2008. Results Of 2008 Exploration program and GemCom modelling of Sn-In-Zn-Cu and WO₃-MoS₂-Bi zones on the Mount Pleasant Mine Property, Charlotte County, southwestern New Brunswick (Oral Presentation). *Exploration, Mining and Petroleum, New Brunswick Open House, Fredericton*.
- DUNBAR, P. & EL RASSI, D. 2008. A Technical Review of the Mount Pleasant Property, Including an Updated Mineral Resource Estimate on the Fire Tower Zone, Southwestern New Brunswick. 43-101 Report to Adex Mining Inc. by Watt, Griffiths and McQuat Limited (available on SEDAR), 149p.
- INVERNO, C.M.C. & HUTCHINSON, R.W. 2006. Petrochemical discrimination of evolved granitic intrusions associated with Mount Pleasant deposits, New Brunswick, Canada. *Applied Earth Science (Trans Inst. Min. Metall. B)*, **116**, B23-39.
- KOOIMAN, G.J.A., MCLEOD, M.J., & SINCLAIR, W.D. 1986. Porphyry Tungsten-Molybdenum Orebodies, Polymetallic Veins and Replacement Bodies, and Tin-Bearing Greisen Zones in the Fire Tower Zone, Mount Pleasant, New Brunswick. *Economic Geology*, **81**, 1356-1373.
- MCCUTCHEON, S.R. 1990. *The Late Devonian Mount Pleasant caldera complex: stratigraphy, mineralogy, geochemistry and the geologic setting of a Sn-W deposit in southwestern New Brunswick*. Unpublished Ph.D. thesis, Dalhousie University, Halifax.
- MCLEOD, M.J. 1990. Geology, Geochemistry, and Related Mineral Deposits of the Saint George Batholith, Charlotte, Queens, and Kings Counties, New Brunswick. *Natural Resources and Energy, Mineral Resources, Mineral Resource Report*, **5**, 169 p.
- PROUT, S., GRAMMATIKOPOULOS, T., YEUNG, B., & MCKEEN, T. 2008. Quantitative characterisation of a multi-metal porphyry ore by automated mineralogy from the Mount Pleasant Mine, New Brunswick, Canada. *Winter Meeting of Mineral Deposit Studies Group/Applied Mineralogy Group, Mineralogical Society (UK)*.

SINCLAIR, W.D., KOOIMAN, G.J.A., MARTIN, D.A., & KJARSGAARD, I.M. 2006. Geology, Geochemistry and Mineralogy of Indium Resources at Mount Pleasant, New Brunswick, Canada. *Ore Geology Reviews*, **28**, 123-145.

SINCLAIR, W.D., KOOIMAN, G.J.A., & TAYLOR, R.P. 2007. Letter to the Editor: Petrochemical discrimination of evolved granitic intrusions associated with Mount Pleasant deposits, New Brunswick, Canada,

by C.M.C. Inverno, and R.W. Hutchinson. *Applied Earth Science (Trans Inst. Min. Metall. B)*, **116**, B23-39.

YANG, X-M, LENTZ, D.R., & MCCUTCHEON, S.R. 2003. Petrochemical evolution of subvolcanic granitoid intrusions within the late Devonian Mount Pleasant Caldera, southwestern New Brunswick, Canada: comparison of Au versus Sn-W-Mo-polymetallic mineralization systems. *Atlantic Geology*, **39**, 97-121.

The Nash Creek Zn–Pb–Ag deposit, Tobique –Chaleurs Zone, New Brunswick, Canada

Derek Brown¹ & James Walker²

¹SLAM Exploration Ltd. Miramichi NB (e-mail: explore@slamexploration.com)

²New Brunswick Department of Natural Resources, Geological Surveys Branch, P.O. Box 50, Bathurst New Brunswick, E2A 3Z1, Canada, (e-mail jim.walker@gnb.ca)

ABSTRACT: Nash Creek is the largest Zn–Pb deposit in the Tobique–Chaleurs Zone, and contains indicated and inferred resources of 7.8 Mt grading 2.72% Zn, 0.55% Pb and 18.26 g/t Ag and 1.2 Mt grading 2.66% Zn, 0.52% Pb and 18 g/t Ag, respectively. The deposit is hosted by Early Devonian bimodal volcanic and minor interlayered sedimentary rocks that were deposited in a trans-pressional rift. The host rocks sequence includes the Archibald Settlement Formation (rhyolite flows domes and related rocks), and the Sunnyside Formation (mafic lava flows and interlayered volcanoclastic and sedimentary rocks).

The deposit, which is divided into the Hayes and Hickey zones, lies near the western fault-bound limb of the Jacquet River Syncline and consists of sparsely disseminated to locally massive sulfide veins and replacements. Mineralization occurs in at least two phases; 1) early massive sulfide veins and replacement zones, and 2) late carbonate–quartz–sulfide veins. Drilling indicates that within the deposit mineralization is concentrated along steeply dipping structures that strike between 314 and 326°.

Alteration is spatially associated with, and extends beyond, mineralization and consists of v-fine-grained mixture of Fe-carbonate, Fe-oxide, sericite, calcite and minor chlorite. Additional clay alteration is controlled by faulting and is spatially related to sulfide emplacement.

KEYWORDS: *base metals, New Brunswick, Nash Creek, sulfides, VMS*

INTRODUCTION

The Nash Creek Zn–Pb–Ag deposit is located approximately 50 Km northwest of the city of Bathurst, New Brunswick. This is the largest of several syngenetic sulfide deposits within the Tobique–Chaleurs Zone (Fig. 1), and contains an Indicated resource of 7.8 Mt grading 2.72% zinc, 0.55% lead and 18.26 g/t Ag and an additional Inferred resource of 1.2 Mt grading 2.66% Zn, 0.52% Pb and 18 g/t Ag. The deposit was discovered by AMEX during follow-up work on silt geochemical anomalies in 1954 (Moorhouse, 1955)

Previous drilling programs undertaken by Falconbridge and Texasgulf focused on the Hayes Zone where the Bulk of the resources have been outlined. The latest drilling program focused on expanding the Hickey Zone north and has added 52.5% to the total indicated tonnage

GEOLOGICAL SETTING

Northern New Brunswick and the adjacent

Gaspé Peninsula in Quebec are divided into four north- to northeasterly-trending tectono-stratigraphic belts of Palaeozoic rocks. The Nash Creek deposit occurs in the Tobique–Chaleurs Zone (TCZ), the youngest of these belts (Walker and McCutcheon, 1995) that is interpreted to have formed in transpressional rift (Dostal et al. 1989). In the study area, the TCZ is divided into two groups. At the base, early to middle Silurian sedimentary and volcanic rocks of the Chaleur Group are in unconformable or fault contact with Ordovician rocks. The Chaleurs Group is disconformably to unconformably overlain by Early Devonian rocks of the Dalhousie Group.

The distribution of stratigraphic units in this part of the TCZ is controlled by the Km-scale, north-south trending, doubly plunging Jacquet River Syncline (JRS). Chaleurs group rocks exposed on the east limb of this JRS are vertical to eastward-overturned, whereas the disconformably overlying Dalhousie Group is shallowly to

moderately west dipping. On the west limb of the JRS Chaleurs Group rocks are not exposed, and very gently east-dipping Dalhousie Group rocks are in fault contact (Black Point–Arleau Brook Fault) with a structural block that contains northeast- to north-striking Ordovician (Matapedia Group) and Silurian (Chaleurs Group) rocks to the west (Fig. 2).

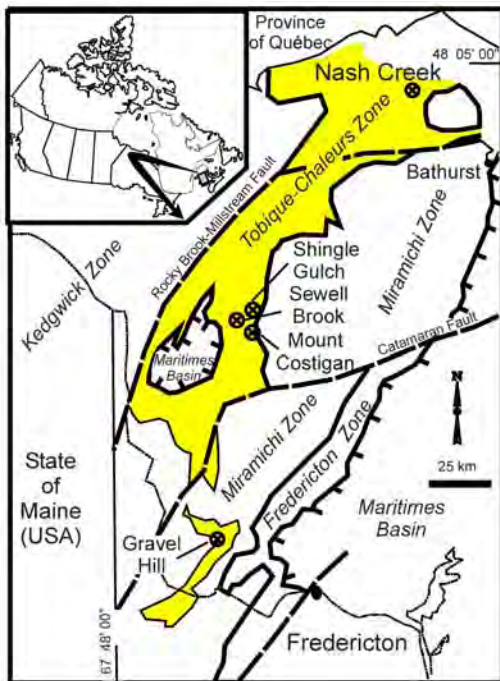


Fig. 1. Location of the Nash Creek, and other Zn–Pb deposit (circled X symbol) in the TCZ. Modified from (Walker 2005).

In the JRS the Dalhousie Group is divided into five formations (Walker and McCutcheon 1995). Only the upper three; Archibald Settlement, Sunnyside and Big Hole Brook formations (described below), are exposed in the vicinity of Nash Creek. The Archibald Settlement Formation is the lowermost of these and consists of massive flows and domes of orange to red, aphyric, commonly flow-layered rhyolite. Up section massive flows are interlayered with fine- to coarse-grained volcanoclastic rocks including heterolithic lapilli-tuff and agglomerate, as-well-as volumetrically minor feldspar-phyric rhyodacite. A U/Pb zircon age of 415.6 +/- 0.4 Ma has been returned from rhyolite of

the Archibald Settlement Formation collected at the Nash Creek deposit (Wilson and Kamo 2008).

The upper part of the Archibald Settlement Formation is conformably overlain, and in part interlayered with, the Sunnyside Formation. The base of the Sunnyside Formation consists of generally thin (< 10m) massive to amygdaloidal basalt flows and minor interbedded fine- to coarse-grained clastic and minor carbonate-bearing sedimentary rocks. Higher in this unit more massive mafic flows, hyaloclastite and tuff predominate (Fig. 2). Some of the clastic units near the base of the Sunnyside Formation locally contain abundant orange rhyolite clasts indicating that Archibald Settlement rocks were being eroded at the time the Sunnyside was being deposited.

The Big Hole Brook Formation is the uppermost Formation in the Dalhousie Group and conformably overlies the Sunnyside Formation. The Big Hole Brook Formation consists of green-grey, micaceous, locally calcareous fine-grained thin- to thick-bedded sandstone and siltstone (Fig. 2). North of the deposit the Big Hole Brook Formation is unconformably overlain by clastic rocks of the Carboniferous Bonaventure Formation (Fig. 2).

MINERALIZATION

Four distinct zones of base metal sulfide accumulation have been identified on the Nash Creek property. All four are fracture controlled sub-parallel conduits striking between 314 and 326°.

The calculated resources are contained within two of these zones. The Hayes Zone, in the south hosts the largest tonnage, It consists of discontinuous to semi-continuous pods of sulfide mineralization over a strike length of 585 m. This zone is open to the southeast, and has been intersected over widths up to 55 m. The Hickey Zone consists of at least ten sub-parallel, steeply-dipping, discontinuous zones that range in length from 140 to 450 m. The thickest Zn-Pb accumulations are subparallel (implying a possible structural control), and occur

within a laterally extensive typically flat lying lower grade halo of mineralization. The Hickey Zone strikes to the north for 840 m. The mineralized structures are open in all horizontal directions. Limited

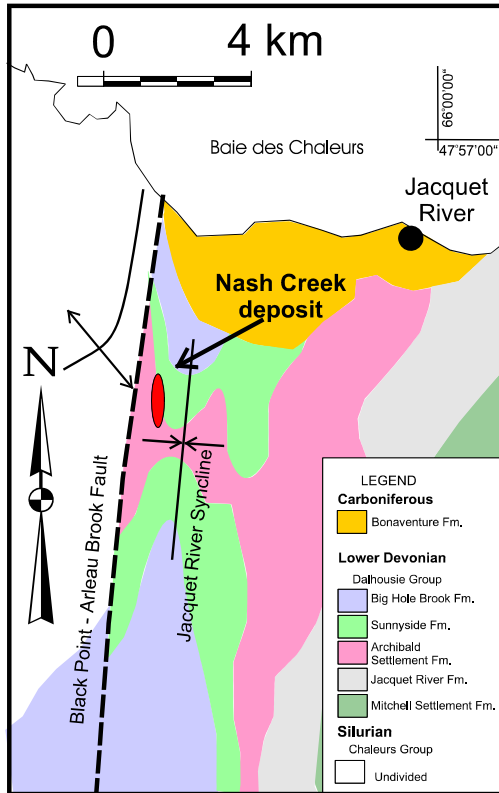


Fig. 2. North end of the Jacquet River Syncline showing position of Nash Creek deposit with respect to Dalhousie Group Stratigraphy.

deep drilling (up to 500m vertical) indicates that additional base metal sulfide bearing lenses occur below the extensively explored near surface zones.

The Hickey and Hayes zones occur within a larger envelop of Zn–Pb–Ag–Fe sulfide mineralization that lies more or less along a north-south line straddling the contacts between the upper most flows and clastic rocks associated with the Archibald Settlement and bounding Sunnyside formations. Specifically, it is concentrated between and adjacent to subvertical, north–south striking faults that parallel the Black Point–Arleau Brook Fault.

A small dextral east-west offset in the geological units occurs between the Hickey and Hayes zones resulting in an apparent offset of the deposit. It is unclear whether this is a tectonic dismemberment and subsequent offset of a single mineralized zone or a reflection of the control on mineralization exerted by differences in rock type in a replacement type deposit.

In both the Hayes and Hickey zones mineralization occurs in three forms; Type I mineralization consists of massive (> 90%) sulfide veins that range from 1 to 5 cm in width. These veins are for the most part restricted to the massive rhyolite of the Archibald Settlement Formation. However, where Type I veins intersect carapace-breccias or marginal zones of flows characterized by zones of contorted flow-layering and/or auto-breccia development, sulfides fill and cement the interstices such that rhyolite appears to be cemented by sulfide.

Type II mineralization is replacement type mineralization occurring in the fragmental tops of mafic flows, within the Sunnyside Formation near its lower contact with the Archibald Settlement Formation. Type II Veins and veinlets are commonly intricately banded with zones of early rhythmically-layered amorphous silica and later sulfide commonly displaying framboidal textures.

Type III mineralization consists of late carbonate ± quartz veins with minor sulfides (≈ 20%). These veins cross cut Type I mineralization.

Hydrothermal alteration is laterally extensive and manifest as Fe-carbonate, Fe-oxide (supergene?), sericite, calcite and minor chlorite. Clay alteration is so pervasive that much of the core disintegrates via clay hydration processes after very short exposure to the atmospheric conditions. Although limited XRD work has not shown the presence of swelling clays sericite which is abundant does have the capacity to swell (Eberl et al. 1987). Additional intense clay alteration is controlled by faulting and is spatially related to sulfide emplacement.

DISCUSSION AND CONCLUSIONS

The genesis of the Nash Creek deposit has been problematic as it does not fit easily into any one genetic model. The salient points to consider when formulating a model for this deposit are:

1. The rift setting in which the host sequence was deposited.
2. The absence of synvolcanic intrusions other than rhyodacite dikes
3. Sedimentary rocks in the section (calcareous shale, and sandstone), and volcanoclastic layers are rarely mineralized.
4. Porphyritic rhyodacite (dykes or flows?) are spatially related to base metal sulphide mineralization.
5. Mineralization appears concentrated along northwest trending zones with mineralization migrating outward along permeable horizons ultimately forming a laterally extensive area of alteration with disseminated sulfide.
6. The alteration zone has a significant clay component that expands when exposed to surface weathering conditions.

Based on the points outlined above Nash Creek best fits a VMS style deposit, and appears to have characteristics of the "Stratal Model". The deposit appears to be "Stratabound", dominantly Zn+Pb sulfide with variable amounts of pyrite.

Sufficient information is now available to consider the following in future studies: 1) relationship of grade with host rock, 2) SG in relation to mineralization and lithology, 3) possible relationship of Ag with the alteration halo, 4) Zn to Pb ratios as a predictive measure for late phase quartz-carbonate veining, 5) effective use of blank, standard, duplicate and split samples in delineation drilling.

REFERENCES

- DOSTAL, J., WILSON, R.A., & KEPPIE, J.D. 1989. Geochemistry of Siluro-Devonian Tobique belt in northern and central New Brunswick (Canada). Tectonic Implications. *Canadian Journal of Earth Sciences*, **26**, 1282–1296.
- EBERL, D.D., ŚRODOŃ, J., LEE, M., NADEAU, P.H., & NORTHROP, H.R. 1987. Sericite from the Silverton caldera, Colorado: Correlation among structure, composition, origin and particle thickness. *American Mineralogist*, **72**, 914–934.
- MOOREHOUSE, W.W., 1955. Report of work on the Nash Creek option. New Brunswick Department of Natural Resources; Minerals, Policy and Planning Division, Assessment Report # 47197.
- WALKER, J.A. 2005. *Petrogenesis and tectonic setting of Devonian volcanic and related rocks and their control on mineralization at the Shingle Gulch East Zn–Pb–Ag sulfide deposit, northwest New Brunswick*. Unpublished Ph.D. thesis, University of New Brunswick, Canada, p. 430.
- WALKER, J. A. & McCUTCHEON, S.R., 1995. Siluro-Devonian stratigraphy of the Chaleurs Bay Synclinorium, northern New Brunswick. In Merlini, S.A.A. ed., *Current Research 1994*. New Brunswick Department of Natural Resources, Minerals, Policy and Planning Division, Miscellaneous Report **18**, 225–244.
- WILSON, R.A. & KAMO, S.L. 2008. New U-Pb ages from the Chaleurs and Dalhousie Groups: Implications for regional correlations and tectonic Evolution of Northern New Brunswick. In *Geological investigations in New Brunswick for 2007*. Edited by G.L. Martin. New Brunswick Department of Natural Resources: Minerals, Policy, and Planning Division, Mineral Resource Report 2005-1, 167–212.

The Williams Brook gold discovery – northern New Brunswick

Heather Campbell¹ & Art Hamilton¹

¹Blue Note Mining Inc., 9361 Route 180, P.O. Box 26, Bathurst NB, E2A 3Z1 CANADA
(e-mail: ahamilton@bluenotemining.ca, hcampbell@bluenotemining.ca)

ABSTRACT: Recent diamond drilling has confirmed significant gold mineralization on the Williams Brook Property, held by Blue Note Mining Inc. in northern New Brunswick. Two types of mineralization occur on the property; 1) sulfides in massive quartz veins with gold values of 11.16 g/t over 2.8 meter core length, including a 0.5 meter section grading 24.1 g/t Au and 2) disseminated pyrite and sulfide veinlets with gold values of 0.91 g/t Au over 28.0 meters (23.3 m estimated true width) including a 1.0 meter section grading 5.44 g/t Au. Mineralization occurs within potassically altered rhyolite and massive quartz veins that intrude the altered rhyolite. No mineralization is found in the drill holes in zones of unaltered rhyolite. Preliminary investigations of the geochemistry of drill hole WB08-11 reveals significant Spearman rank correlations between Au and As, Cu, Sb and Mo. Drill holes WB08-03 to WB08-06 show correlations between Au and Ag, Mo and S. Observations of alteration, mineralogy and element associations suggest that the gold is part of an epithermal system. These preliminary observations of the drill core along with the differing correlations in trace elements between the drill holes indicate that there may be two events contributing to mineralization in the Williams Brook property.

KEYWORDS: *gold, correlations, Devonian, trace element, geochemistry*

INTRODUCTION

The Williams Brook gold property is located about 100m west of Bathurst and north of Highway 180 (Fig. 1) Significant gold mineralization in angular float was found by prospector David O'Neil who staked three claim blocks on the property which were later optioned by Blue Note Mining in 2006.

GEOLOGICAL SETTING

Regional Geology

The study area is situated in the Tobique–Chaleurs Zone, (TCZ) which contains early to middle Silurian sedimentary and volcanic rocks (Chaleurs group) that are disconformably overlain by Lower Devonian volcanic and sedimentary rocks of the Dalhousie and Tobique groups (Wilson 2004) and is bounded by the Rocky Brook–Millstream Fault to the northeast and the Mackenzie Gulch Fault to the north (Fig.1). The McCormack Brook Fault (a splay of the Rocky Brook–Millstream Fault) lies to the north of the

study area. Several Au showings east of the present study area are coincident with these large scale faults. These occurrences; Jonpol, Mulligan Gulch, Dalhousie Road, Simpson's Field, McCormack, Ramsay Brook, and Upsalquitch Forks, have returned assays of up to 12.4 g/t Au in rocks and 20 g/t Au in heavy metal concentrates in till (Rose & Johnson 1990).

Local Geology

The Williams Brook area is underlain by the Wapske Formation (Tobique Group), that contains mafic and felsic volcanic rocks interlayered with fine-grained sedimentary rocks. Mineralization at Williams Brook is hosted within and/or is spatially related to red to pink rhyolites. The rhyolites were unknown in this area prior to the 2008 exploration program, but are tentatively assigned to the Wapske Formation. The Wapske Formation is conformably overlain by the Early Devonian Greys Gulch Formation that

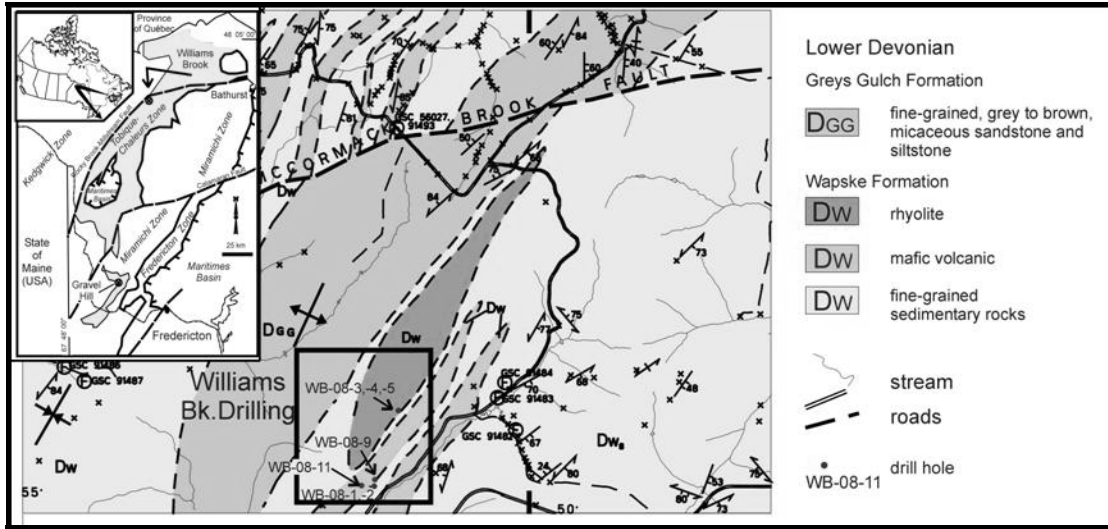


Fig. 1. The Williams Brook property is located within the Tobique–Chaleurs Zone (inset-shaded), approximately 100 km west of Bathurst, NB. Locations of some of the drill holes are indicated by the boxed area.

consists of brown micaceous sandstones. Primary textures such as spherulites, pumice clasts, flow-layering and monomict breccias are common and are taken as evidence of autoclastic processes that are consistent with an effusive emplacement for these rocks. The host rhyolite is commonly salmon coloured, possibly reflecting potassic alteration, and is cut by micro-brecciated quartz and pyrite veinlets with sericite, occurring sub parallel to the main foliation. Large (≈ 2 mm diameter) euhedral pyrite grains are observed overprinting the flow layering. Later stage milky, vuggy quartz veins crosscut flow layering and contain small (sub mm scale) gold grains in DDH-WB-08-11 (Fig. 2).

The rocks in the study have undergone zeolite facies regional metamorphism but locally intense penetrative fabrics are recognized in areas adjacent major faults.

MINERALOGY

Preliminary work has shown that mineralization at Williams Brook includes the sulfide phases pyrite and honey-brown sphalerite. Oxide phases including magnetite and hematite are prevalent throughout the core and heavily concentrated in the first 10 m of the drill

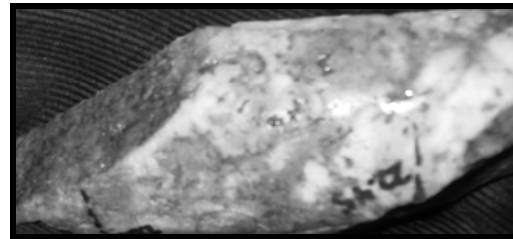


Fig. 2. Quartz vein with visible gold. Sample is from DDH WB-8-11 @ 22.43 m.

cores, thus implying possible supergene alteration.

ASSAYS

Trace element geochemical values for the Williams Brook project were obtained using INAA (Au), and Fire Assay (FA). Standards and blanks were typically submitted with every 20 samples. Correlation between FA and INAA was good ($r_s=0.87$) except for isolated erratic values in some samples.

Significant assays include 11.16 g/t Au over 2.8 meter core length, including 0.5 meter grading 24.1 g/t Au in WB-08-11 and 0.91 g/t over 28.0 m core length (23.3 m true width) including 5.44 g/t over 1.0 m (0.8 m true width) in WB-08-04.

Assays from the 2.8m section of WB-08-11 were rerun using FA gravimetric metallic screen analysis because of erratic and high Au concentrations. One kg samples were run through 100 mesh sieves; the coarse (> 149 micron) and fine (< 149 micron) fractions were analyzed using gravimetric analysis. The < 149 micron portion was split and analyzed to provide replicate data. Results from this analysis indicate that 41% of the gold in the 2.8 m section is over 149 micron.

GEOCHEMISTRY

Trace element geochemical values for the Williams Brook project were obtained using INAA (Au) ICP-OES-4 acid (total) digestion. Both geochemical packages are exploration grade. The alkali contents of the rock samples are relatively high; K₂O values are up to 9.3 wt.% (average 4.09), whereas Na₂O values up to 6.97 wt.% (average 3.65) with (Na₂O+K₂O) up to 13.7wt.% (average 7.7). Variations in gold and selected trace elements in DDH-WB08-04 are shown in Figs. 3 to 6. Higher concentrations of Au and Ag are seen in the highly altered rhyolites.

Trace element contents in rocks intersected by drill holes WB-08-03 to WB-08-06 are associated with altered rhyolite; Spearman rank correlation coefficients for Ag, Mo and S with Au are moderate to high. Correlation coefficients for Au with As, Cu, Sb and Mo in drill hole WB08-11 (vuggy quartz) are moderate to high. These element correlations suggest that mineralization may be related to an epithermal system (Panteleyev 1995).

CONCLUSIONS

The Williams Brook property has yielded high gold assays. Preliminary work presents evidence suggesting that Au mineralization occurs in two forms: 1) as refractory Au in mm scale massive sulfide (dominantly pyrite) and disseminated veins that cut potassically altered rocks, and 2) as vuggy quartz veins as fine-grained (≤ mm) free gold. Trace element correlations indicate that Au may be related to epithermal mineralization as there are good correlations of Au with Ag,

Sb, and As. Likewise, the presence of vuggy (subsequently brecciated) open space quartz veins support this. High gold contents (41%) in the > 149 micron portion of the crushed core indicate that coarse gold may be a factor in variability in duplicate results.

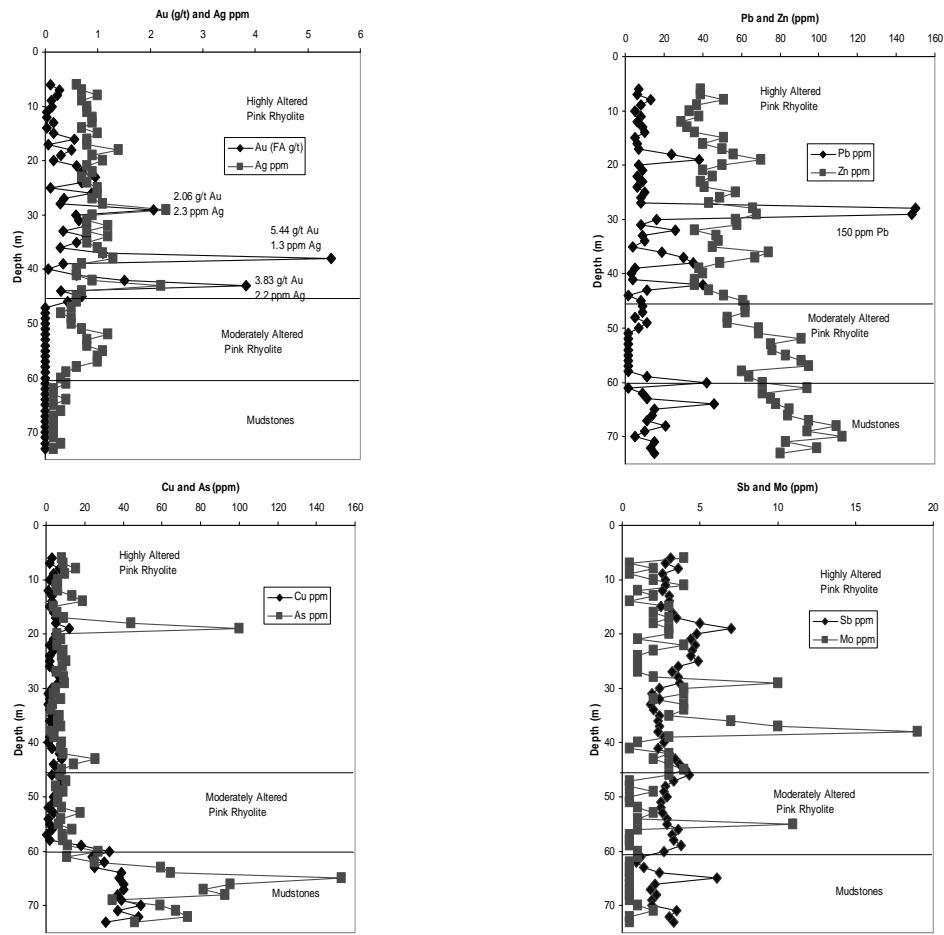
Further work is necessary to determine whether Au mineralization was emplaced in a single pulse or as multi pulses of mineralization. Detailed research including thin sections and whole rock geochemistry will provide better insight into the timing and nature of Au mineralization on the Williams Brook property and the extent of gold mineralization in the Williams Brook Property.

ACKNOWLEDGEMENTS

We would like to acknowledge the New Brunswick Department of Natural Resources - Geological Surveys Branch for their assistance in reviewing the data and discussions on geology and geochemical results.

REFERENCES

- MOORE, C. & LENTZ, D. 1995. Copper-Skarn associated felsic intrusive rocks in the MacKenzie Gulch area (NTS 21 O/10), Restigouche County, New Brunswick. In: CARROLL, B.M.W. (ed) Current Research, 1995. New Brunswick Department of Natural Resources, Minerals and Energy Division, Mineral Resource Report, **96-1**, 121-153.
- PANTELEYEV, A. 1995. Epithermal AU-AG-CU: In: Mineral Deposit Profile Tables - Listed by Deposit Group and Lithological Affinities; B.C. Ministry of Energy, Mines and Petroleum Resources, Open File 1995-8.
- ROSE, D. & JOHNSON, S. 1990. New Brunswick computerized mineral occurrence database. New Brunswick Department of Natural Resources, Minerals and Energy Division, Mineral Resource Report Energy, Mines and Petroleum Resources, Mineral Resource Report 3.
- WILSON, R., BURDEN, E., BERTRAND, R., ASSELIN, E., & MCCracken, A. 2004. Stratigraphy and tectono-sedimentary evolution of the Late Ordovician to Middle Devonian Gaspé Belt in northern New Brunswick: evidence from the Restigouche area. *Canadian Journal of Earth Science*, **41**, 527-551.



Figs. 3-6. Gold and trace element geochemical concentrations with depth in DDH-WB-08-04. Values are not corrected for mass loss or gains. Higher values of Cu, Zn and As exist in the mudstones underlying the rhyolites in hole WB-08-04.

Current geological survey, academic research and exploration activity is focused on improving geological understanding both regionally and internationally.

GEOLOGICAL BACKGROUND

The Tyrone Igneous Complex extends over an area of approximately 350km² of counties Tyrone and Londonderry in Northern Ireland. It is comprised of the Tyrone Plutonic Group and overlying Tyrone Volcanic Group (Cooper 2004). Together, they structurally overlie sillimanite-grade paragneisses of the Tyrone Central Inlier which, based on detrital zircon age profiling, appear to be of Upper Dalradian Laurentian affinity (Chew *et al.* 2008). The Tyrone Igneous Complex and Tyrone Central Inlier are pinned together by a suite of arc-related tonalitic-granitic intrusives.

The Tyrone Plutonic Group comprises a basic igneous association of layered, isotropic and pegmatitic gabbros, doleritic sheeted dykes and rare basaltic pillow lavas first recognized as ophiolitic by Hutton *et al.* (1985).

The Tyrone Volcanic Group sequence comprises basaltic pillow lavas, tuffs of basic to intermediate composition, rhyolites, cherts, siltstones and dark grey mudstones representing up to three volcanic cycles. From base to top of each cycle and through the sequence as a whole, the Tyrone Volcanic Group becomes progressively more acidic in composition.

GEOCHEMISTRY

Though limited, the geochemistry presented herein serves to show the broad compositional differences (Fig. 2a) between the ophiolitic, normal-type MORB (Fig. 2b) and the volcanic arc-related granitoids (Fig. 2c). Current geochemical research, targeted towards the location of potential VMS mineralization, will expand and improve this area of investigation.

BIOSTRATIGRAPHY

Graptolites from close to the top of the

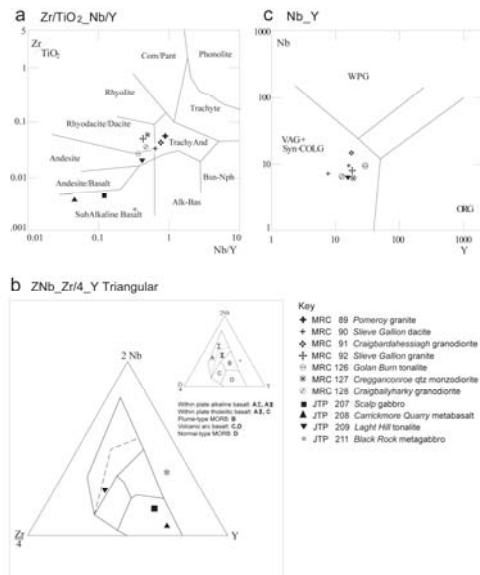


Fig. 2. (a-c). Geochemical plots for Tyrone Plutonic and Volcanic Groups.

Tyrone Volcanic Group on Slieve Gallion (Fig. 1b – ST) have been assigned (Cooper *et al.* 2008) to the *Isograptus victoriae lunatus* Zone of the Australasian graptolite succession (VandenBerg & Cooper 1992), and to the lowest Ca1 subdivision of the Castlemainian Stage, which is now taken internationally to represent the base of the Middle Ordovician (Cooper 1999). In terms of the British succession, this horizon is approximately equivalent to a level at the top of the Whitlandian Stage of the Arenig.

U-Pb ZIRCON ISOTOPIC AGES

Until now the age of Tyrone Igneous Complex has been based on a magma mixing relationship between gabbro and tonalite at Craigherrillagh. The tonalite has been dated at 472 ± 4 Ma, and was taken as evidence for the age of the ophiolite and for the timing of obduction (Hutton *et al.* 1985). Although their mixing with gabbro is clear, the tonalites have a volcanic arc geochemical signature and geological scenario would therefore require obduction of contemporaneous ophiolite and an active volcanic arc.

Presented herein are eight U-Pb zircon ages from the Tyrone Volcanic Group and

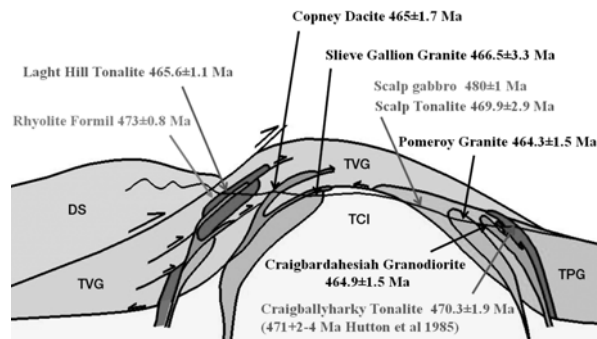


Fig. 3. (a) Schematic cross section through Tyrone Central Inlier (TCI), Tyrone Plutonic Group (TPG) and Tyrone Volcanic Group (TVG) indicating the U-Pb zircon ages. Dalradian Supergroup (DS).

arc-related intrusive suite, which range from 473 - 464 Ma (Fig. 3). The 473 ± 0.8 Ma age is from a high-level rhyolite from Formil (Fig 1b – FH), which occurs at a similar level within the Tyrone Volcanic Group to the biostratigraphical correlation close the base of the Middle Ordovician.

A U-Pb zircon age of 480 ± 1 Ma from layered gabbros at Scalp (Fig 1b – SC) provides the only direct age for the ophiolitic Tyrone Plutonic Group so far. This age date negates the need for the obduction of contemporaneous ophiolite and an active volcanic arc and simplifies the tectonomagmatic evolution.

The difference in age between the ophiolitic Tyrone Plutonic Group (c. 480 Ma) and Tyrone Volcanic Group (c. 473 - 464 Ma) allows time for northwards directed obduction (c. 475 Ma) of the Tyrone Plutonic Group related to southwards directed subduction (Fig. 4c), followed by the establishment of northwards directed subduction and the development of the Tyrone Volcanic Group arc (Fig. 4d).

CONCLUSIONS

A U-Pb zircon age of 480 ± 1 Ma provides the first direct isotopic age for the ophiolitic Tyrone Plutonic Group.

The isotopic age range of the Tyrone Volcanic Group is c. 473 - 464 Ma and is based on eight U-Pb zircon dates.

The 473 ± 0.8 Ma age is from a high-level rhyolite that occurs at a similar level within the Tyrone Volcanic Group to a

biostratigraphical correlation close the base of the Middle Ordovician.

The difference in age between the ophiolitic Tyrone Plutonic Group and Tyrone Volcanic Group allows time for northwards directed obduction of the Tyrone Plutonic Group related to southwards directed subduction, followed by the establishment of northwards directed subduction and the development of the Tyrone Volcanic Group arc.

REFERENCES

- CHEW, D.M., FLOWERDEW, M.J., PAGE, L.M., CROWLEY, Q.G., DALY, J.S., COOPER, M.R., & WHITEHOUSE, M.J. 2008. The tectonothermal evolution and provenance of the Tyrone Central Inlier, Ireland: Grampian imbrication of an outboard Laurentian microcontinent? *Journal of the Geological Society, London*, **165**, 675-685.
- COOPER, M.R. & MITCHELL, W.I. 2004. Midland Valley Terrane. In: *The Geology of Northern Ireland-Our Natural Foundation*, Mitchell, W. I. (ed). (Second Edition) Geological Survey of Northern Ireland, Belfast.
- COOPER, M.R., CROWLEY, Q.G. & RUSHTON, A.W. A. 2008. New age constraints for the Ordovician Tyrone Volcanic Group, Northern Ireland. *Journal of the Geological Society, London*, **165**, 333-339.
- COOPER, R. A. 1999. The Ordovician time scale – calibration of graptolite and conodont zones. *Acta Universitatis Carolinae – Geologica*, **43** (1/2), 1-4.
- GOODFELLOW, W. D. & MCCUTCHEON, S. R. 2003. Geologic and Genetic Attributes of Volcanic Sediment-Hosted Massive Sulfide Deposits of the Bathurst Mining Camp,

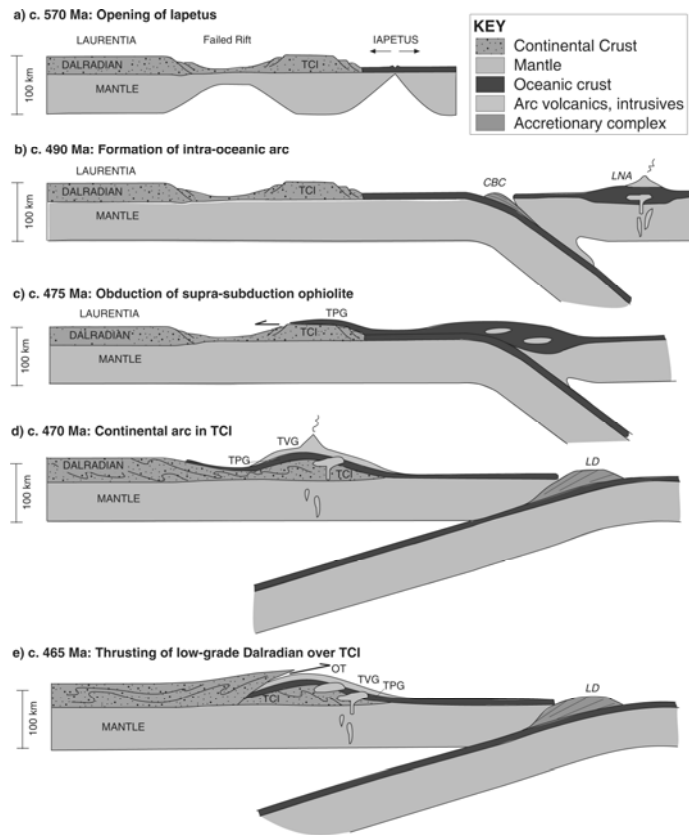


Fig.4 . Schematic reconstruction of the Late Neoproterozoic–Early Palaeozoic tectonic evolution of the Tyrone Central Inlier. TCI, Tyrone Central Inlier; TPG, Tyrone Plutonic Group; TVG, Tyrone Volcanic Group; OT, Omagh Thrust; CBC, Clew Bay Complex; LD, Longford–Down terrane; LNA, Lough Nafoe Arc (from Chew *et al.* 2008).

Northern New Brunswick – A Synthesis. *Economic Geology Monograph*, **11**, 245-301.

HUTTON, D.H.W., AFTALION, M., & HALLIDAY, A. N. 1985. An Ordovician ophiolite in County Tyrone, Ireland. *Nature*, **315**, 210-212.

VAN DEN BERG, A. H. M. & COOPER, R. A. 1992. The Ordovician Graptolite Sequence of Australasia. *Alcheringa*, **16**, 33-85.

VAN STAAL, C.R., DEWEY, J.F., MAC NIOCAILL, C.,

& MCKERROW, W.S. 1998. The Cambrian–Silurian tectonic evolution of the northern Appalachians and British Caledonides: history of a complex, west and southwest Pacific-type segment of Iapetus. In Blundell, D.J. and Scott, A. C. (eds) *Lyell: The Past is the Key to the Present*. Geological Society, London, Special Publications, **143**, 199-242.

Molybdenum and tungsten mineralization associated with late-stage granitoid magmatism in the Appalachian Orogen of Newfoundland: an overview and a summary of recent developments

Andrew Kerr¹, Tim van Nostrand¹, Lawson Dickson¹, & Edward Lynch²

¹*Geological Survey of Newfoundland and Labrador, Department of Natural Resources, PO Box 8700, St. John's, NL, A1B 4J6 CANADA (e-mail: andykerr@gov.nl.ca)*

²*Department of Earth Sciences, National University of Ireland, Galway, Ireland.*

ABSTRACT: Molybdenum mineralization was first discovered in Newfoundland in the 1880s, and tungsten mineralization has been known for over 50 years. Molybdenum is best-known in the Devonian Ackley Granite, where it forms syngenetic, endocontact, disseminated deposits in evolved granitoid rocks, close to the original roof of the magma chamber. Locally, these occurrences have high grades (up to 0.5% Mo), but are of limited extent. However, buried extensions of the Ackley Granite may exist, and these could be associated with both endocontact and exocontact mineralization. In the Grey River area, a potentially significant, bulk-tonnage Mo deposit consists of epigenetic, sheeted to stockwork-style quartz veins in an older (unrelated) granitoid pluton. This is considered to be a porphyry-style deposit. Although grades are relatively low (<0.1% Mo), this is a large system that also contains Cu mineralization. The vein system is probably linked to a subsurface granite pluton that locally forms sheets and dykes within the deposit. These veins contain disseminated syngenetic molybdenite, suggesting a close genetic and temporal relationship. Widespread molybdenum mineralization recently delineated in south-central Newfoundland is also associated with sheeted and stockwork-style quartz veining, and may have similar origins, although such genetic connections remain to be established. Vein-style tungsten mineralization is also best known in the Grey River area, where one such deposit contains a significant resource. It seems probable that this mineralization is genetically connected to the same buried pluton implicated for nearby Mo mineralization, and associated base-metal (\pm Au, Ag) veins may also be part of a larger zoned hydrothermal system. Skarn-type W mineralization is uncommon, but it occurs in central Newfoundland, spatially associated with a large leucogranite pluton.

KEYWORDS: *Tungsten, Molybdenum, Granites, Newfoundland, Mineral Deposits*

INTRODUCTION

The increased interest in Mo and W due to commodity price increases since 2006 has created a need for a synthesis of information on known deposits and potential exploration environments within the province of Newfoundland and Labrador. This review is drawn from the historical database of exploration and scientific studies, but it also provides some essential geological information concerning recent exploration developments in Newfoundland. Further information is provided in a recent article by Kerr *et al.* (2009). Molybdenum mineralization also occurs in Precambrian granites in Labrador, but these deposits presently lie within Inuit lands that are

currently closed to exploration and are not discussed here.

GEOLOGICAL SETTING

The formation of Mo and W deposits in Newfoundland is linked to its plutonic history, which has a much looser link to its accretionary tectonics. Although granites in Newfoundland range in age from Neoproterozoic to Devonian, the most abundant (at least in terms of areal extent) formed during the Silurian and the Devonian (Kerr 1997). The major pulse of magmatism postdates both the accretion of peri-Laurentian and peri-Gondwanan arcs to Laurentia, and the final collision of Laurentia and Ganderia. The youngest Devonian plutonic rocks also postdate any

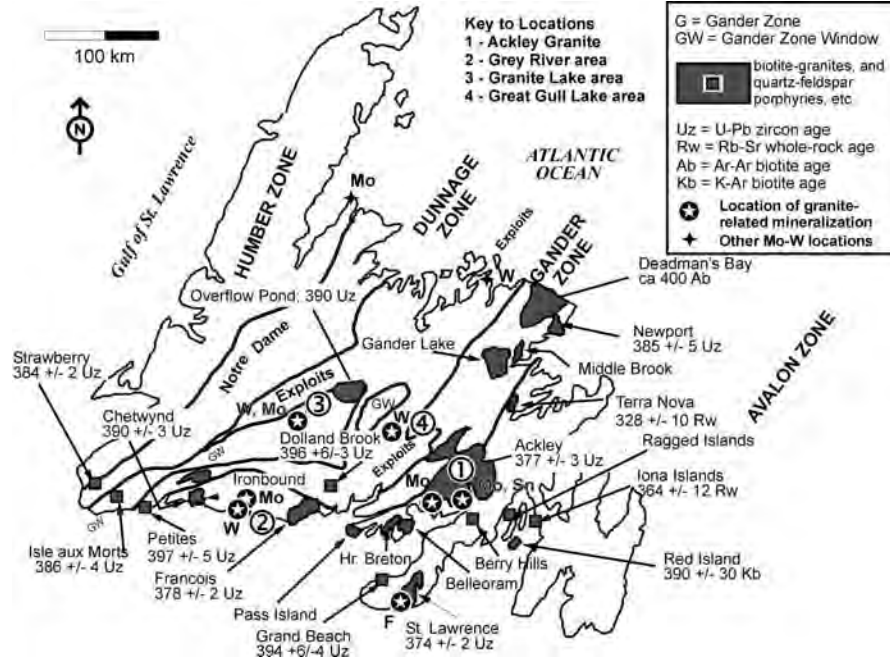


Fig. 1. Locations of late-stage granitoid plutons and related mineralization in Newfoundland. Numbers refer to locations discussed in text.

later juxtaposition of Ganderia and Avalonia, because they intrude the boundary between these regions. The plate-tectonic setting of the widespread Silurian-Devonian plutonic suites is keenly debated, and the divergent viewpoints reflect contrasting interpretations of Ganderia–Avalonia relationships. In some models, these granitoid suites are viewed as ‘distal’ manifestations of subduction-zone magmatism (e.g., van Staal 2007), whereas in others they are interpreted as post-collisional and largely ensialic (e.g., Kerr 1997).

The distribution of Devonian plutonic suites is indicated in Figure 1, together with the locations of the main occurrences of granite-related mineralization, including tungsten and molybdenum. Available data indicate a gradual southeastward shift in the locus of magmatic activity through time (Kerr 1997). The youngest granites have a much more restricted distribution; most are located along the south coast of the island, and on both sides of the Gander–Avalon boundary. This broad northwest to southeast age progression could be interpreted in terms of subduction rollback, or attributed to

propagating lithospheric delamination, or could even be viewed as migration of conjoined Laurentian and Gondwanan blocks across a relatively static thermal anomaly (Kerr 1997).

MOLYBDENUM

Molybdenum mineralization is widely distributed in Newfoundland, but the most significant examples are located on or near to the south coast of the island.

The Ackley Granite (Fig. 1) is a large polyphase granitic batholith in which high-level, evolved phases representing its fossil roof are preserved. In several areas, disseminated molybdenite is associated with alaskitic rocks adjacent to its contact with Precambrian country rocks. The grades in some of these deposits are interesting (~ 0.5% Mo), and there were some early attempts at mining them, but the tonnages appear to be small. Regional geological considerations suggest that evolved granites (and possible cupolas) may exist in the shallow subsurface south of the main part of the pluton, and there is direct evidence for these in the form of mineralization associated with a small plug on an offshore island. The Ackley

Granite was previously dated at 377 ± 3 Ma (U-Pb zircon) and recent Re-Os determinations at three prospects indicate an age of 380 ± 2 Ma, indicating that mineralization is indeed syngenetic (Lynch *et al.* 2009).

In the Grey River area on the south coast of Newfoundland, exploration in the 1990s located widespread molybdenite and chalcopyrite-bearing quartz veins within foliated and altered granodiorites of presumed Silurian age. It was recognized at the time that such mineralization was extensive, but it was not delineated in detail. This deposit, known as "Moly Brook", is now the subject of an advanced exploration program aimed at defining a large-tonnage, low-grade target. The style of mineralization consists of sheeted to stockwork-like quartz veins developed over a wide area, and the system extends to considerable depths. The grades are generally low (<0.1 % Mo), but the true size of the zone has yet to be established. Most holes have ended in mineralization, and the longest intersection to date was 360 m of 0.07% Mo. The mineralization is considered to be epigenetic and to have no direct relationship to its altered host rocks. The latter contain a widespread regional alteration of broadly propylitic type, and zones of intense veining and mineralization are commonly associated with potassic (argillic) alteration, which is superimposed on the regional alteration. Initial results of alteration studies using visible-infrared reflectance spectroscopy (VIRS) confirm this general pattern, but also hint at the complexity of its details. Rare examples of fine-grained granite dykes that contain disseminated molybdenite are considered to represent apophyses from a buried pluton. The nearest pluton of strongly evolved character is the François Granite, dated at 378 ± 2 Ma (U-Pb zircon), and this is a possible correlative for the largely hidden source of mineralizing fluids. The precise age of the mineralization remains unknown but is presently under investigation using both U-Pb and Re-Os techniques.

In the Granite Lake area of south-central Newfoundland, disseminated and vein-style molybdenum and tungsten mineralization has been known since the 1980s, but no significant deposits were outlined. Recent exploration has now documented more widespread molybdenite associated with a swarm of quartz veins present to vertical depths of some 100 m. The style of mineralization in this deposit resembles that observed at Moly Brook and, not surprisingly, it has been christened "Moly Hill". On a regional scale, molybdenite is present in at least three granitoid units of different inferred ages, and it may not have a genetic relationship to any of them. However, there is presently no direct evidence for a buried pluton, nor are there any direct constraints on the age of the mineralization.

+

TUNGSTEN

Tungsten mineralization in Newfoundland is more restricted in distribution than molybdenum. The best known deposit is in the Grey River area (Fig. 1) and is very close to the Moly Brook deposit (see above). However, it lies within a different package of host rocks, dominated by late Precambrian metasedimentary and metavolcanic rocks.

Wolframite-bearing veins were initially discovered in the 1950s, and two such veins were explored in detail. The largest of these can be traced for about 2 km, and was assessed via underground exploration, but considered too small for commercial development. Its average width is about 1 m. The deposit is now again under assessment and a resource estimate completed in 2007 indicates about 850,000 tonnes at 0.86% WO₃. The tungsten-bearing veins appear to be some of the youngest elements of the local geology. Their paragenesis is complex, with an initial stage containing molybdenite, followed by the main W-bearing veins (Higgins 1985). The later stages consist of other base-metal sulfides (e.g., galena, sphalerite and pyrite and are locally gold-rich) followed by veins containing fluorite, calcite, and barite

(Higgins 1985). Although it may not be especially large, the Grey River deposit was once described as “one of the largest typical wolframite-quartz deposits in Canada”, and it is possibly indicative of much wider potential for W in the general area.

The timing of mineralization at Grey River is not well constrained. K–Ar data from muscovites in greisen zones, suggests that they formed between 387 and 370 Ma (Higgins 1985). The concept of a hidden plutonic body that provided the fluids was outlined many years ago, and local leucocratic granite veins were correlated with the nearby 378 Ma François Granite. The relationship between the numerous W-bearing veins, base-metal veins and the nearby Mo-bearing vein system at Moly Brook is a subject of some interest, and it is hard to believe that all are coincidentally associated.

Tungsten mineralization of possible skarn affinity is located in central Newfoundland, where it is associated with calc-silicate horizons in siliciclastic sedimentary rocks. The mineralized units are generally thin, and contain variable amounts of scheelite, clinopyroxene, garnet, and chlorite. The grades range up to 2.7% WO₃, but are more commonly < 1% WO₃. The host rocks show signs of contact metamorphism, and are cut by leucocratic granite veins and pegmatites, possibly related to the nearby Middle Ridge Granite, dated at ca. 410 Ma. Scheelite and fluorite mineralization is also locally present in tourmaline-bearing granite veins that cut the sedimentary rocks. A link to magmatic fluids derived from the Middle Ridge Granite is suspected.

Other tungsten occurrences in Newfoundland are minor in extent, and most of these represent veins, some of which also contain minor gold mineralization.

CONCLUSIONS

There is a long history for these commodities in Newfoundland, dating

back to the 1880s for molybdenum and to the 1950s for tungsten. Although none of these examples have ever produced metals, recent exploration work is encouraging both in terms of resources, and in terms of the wider potential for new discoveries in the region. Ongoing research work by the NL Geological Survey and by other agencies will hopefully provide better age constraints and geochemical references that will allow plutonic suites of specific ages and compositions to be targeted.

ACKNOWLEDGEMENTS

We thank Tenajon Resources and Playfair Mining for hospitality in the field and for many interesting geological discussions. Edward Lynch acknowledges support from the Ireland-Newfoundland partnership and a scholarship from SEG.

REFERENCES

- HIGGINS, N.C. 1985. Wolframite deposition in a hydrothermal vein system: The Grey River tungsten prospect. *Economic Geology*, **80**, 1297-1397.
- KERR, A. 1997. Space-time-composition relationships amongst Appalachian-cycle plutonic suites in Newfoundland. *Geological Society of America*, Memoir **191**, 193-220.
- KERR, A., VAN NOSTRAND, T., DICKSON, L., & LYNCH, E. 2009. Molybdenum and tungsten in Newfoundland: An overview and a summary of recent exploration developments. *Geological Survey of Newfoundland and Labrador, Report 2009-1*, 43-80.
- LYNCH, E., SELBY, D., FEELY, M., & WILTON, D. 2009. New constraints on the timing of molybdenite mineralization in the Devonian Ackley Granite suite, southeastern Newfoundland: Preliminary results of Re-Os geochronology. *Geological Survey of Newfoundland and Labrador, Report 2009-1*, 225-234.
- VAN STAAL, C. 2007. Pre-Carboniferous tectonic evolution and metallogeny of the Canadian Appalachians. *Geological Association of Canada, Mineral Deposits Division, Special Publication 5*, 793-818.

Distribution and geochemistry of Cu-rich massive sulfides at the Brunswick No. 12 Deposit, Bathurst Mining Camp, New Brunswick.

Sean H. McClenaghan¹, David R. Lentz², & Erin M. Powe²

¹Geological Surveys Branch, New Brunswick Department of Natural Resources, P.O. Box 50, Bathurst, NB E2A 3Z1 CANADA (e-mail: Sean.McClenaghan@qnb.ca)

²Department of Geology, University of New Brunswick, Fredericton, NB E3B 5A3 CANADA

ABSTRACT: The super-giant Brunswick No.12 volcanogenic massive sulfide deposit is largely syngenetic in origin with 329 Mt of Zn–Pb–Cu–Ag-type pyritic sulfides forming an intimate relationship with a laterally extensive Algoma-type iron formation. Development of a large replacement-style basal sulfide facies, confined between an exhalative Zn–Pb-rich banded sulfide facies and an underlying stringer sulfide zone, is characterized by an increased modal abundance of chalcopyrite, pyrrhotite, and native bismuth. Analyses from the basal sulfide facies reveal an enrichment in Co (avg. 475 ppm), Bi (16 ppm), Se (21 ppm), and Cu (1.3%) with values reaching up to 3.4%. The composition of sphalerite from the basal sulfide facies (avg. 8.8 wt.% Fe) is similar to compositions reported for the exhalative banded sulfide facies, indicating a common vent-proximal origin. Remnant masses of sphalerite exhibiting chalcopyrite disease, suggest that the basal sulfide facies likely represents an exhalative sulfide facies that has undergone hydrothermal recrystallization (zone refining) by high-temperature Cu-bearing hydrothermal fluids.

KEYWORDS: *Copper, Brunswick No. 12, Main Zone, Bathurst Mining Camp, Volcanogenic Massive Sulfide*

INTRODUCTION

The Brunswick No. 12 volcanogenic massive sulfide (VMS) deposit is presently host to the world's largest underground Zn mine and is the fourth-largest Zn producer, worldwide. Since production began in 1964, over 124 Mt of ore grading 8.8% Zn, 3.5% Pb, 0.36% Cu, 103 g/t Ag, and 0.6 g/t Au have been extracted from the Brunswick No. 12 Mine. Additional low-grade massive sulfides with elevated Cu contents are distributed throughout the deposit, and are generally concentrated in a basal Cu zone. This potential Cu resource could be exploited as incremental ore, extending mining production, which is currently expected to end in 2011.

GEOLOGICAL SETTING

The Bathurst Mining Camp (BMC) occurs within a Middle-Ordovician bimodal volcanic and sedimentary sequence in the northern Appalachians of New Brunswick. Volcanic rocks were emplaced within an intra-continental back-arc basin inboard of

the Popelogan–Victoria volcanic arc at the eastern margin of the proto-Atlantic (Iapetus) Ocean (van Staal *et al.* 2003). Closure of the back-arc basin by northwest-directed subduction from the Late Ordovician to Silurian led to polyphase deformation and associated greenschist facies metamorphism (van Staal & Williams 1984).

The oldest rocks in the BMC consist of a continentally derived Cambro–Ordovician turbidite sequence of quartz wacke, siltstone, and black shale of the Miramichi Group. These rocks are conformably to disconformably overlain by pyroclastic rocks of the Nepisiguit Falls Formation, comprising quartz–feldspar crystal tuff and tuffaceous sedimentary rocks. These rocks form the footwall to Brunswick No. 12 (Fig. 1) and are overprinted by stringer sulfide mineralization and a large alteration halo, resulting from hydrothermal fluid circulation during VMS formation (Luff *et al.* 1992; Lentz & Goodfellow 1996). Massive sulfides are for the most part syngenetic, with the bulk

of the sulfides occurring in a Zn–Pb-rich banded sulfide facies that, in the vicinity of Brunswick No. 12 (Fig. 1), forms an intimate relationship with a laterally extensive Algoma-type iron formation, and defines the Brunswick Horizon. The Nepisiguit Falls Formation is overlain by more effusive felsic volcanic rocks of the Flat Landing Brook Formation and the mafic dominated Little River Formation (upper Tetagouche Group).

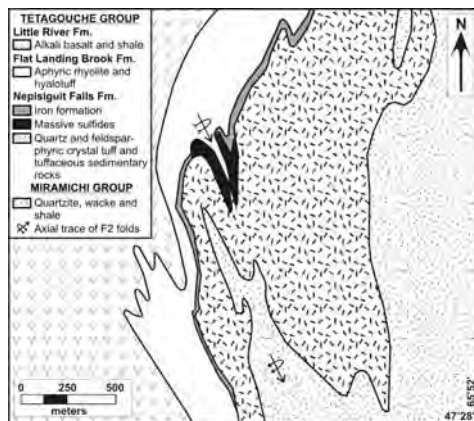


Fig. 1. Geological map of Brunswick No. 12 (after van Staal & Williams 1984).

BRUNSWICK NO. 12

The geometry of the Brunswick No. 12 deposit has been affected by syn-metamorphic polyphase deformation (heterogeneous) with a large amount of strain accommodated by exhalative sedimentary rocks. As a result, massive sulfides dominated by ductile sulfides (sphalerite, galena, chalcopyrite, and pyrrhotite) are commonly attenuated along limbs of folds and thickened in fold noses. The most prominent folds seen in the mine sequence consist of tight to isoclinal asymmetrical F2 folds, which overprint an overturned north-facing F1 synform (Fig. 1) and define a sheath structure extending to deeper levels to the south (van Staal & Williams 1984). The massive sulfide body bottoms out at a depth of 1125 m (below surface) with altered footwall rocks fully enveloping the basal keel of the deposit (Fig. 2). Despite the deformation, metals exhibit zonation from a Cu-rich footwall to overlying Zn–Pb-rich massive sulfides and

iron formation that indicates younging to the northwest (van Staal & Williams 1984; Luff *et al.* 1992).

The Brunswick No. 12 deposit can be broadly divided into four key ore zones: the Main, West, East, and V2 zones (Luff *et al.* 1992), which merge at depth in the nose of an F2 structure (Fig. 1), and represent a dismembered, but originally continuous sulfide body (van Staal & Williams 1984). The Main Zone (Fig. 2) contains the bulk of the deposit, whereas the West Zone is smaller but has somewhat higher grades in base metals. Massive sulfides total 329 Mt; of which, 163 Mt are distributed amongst 10 principal ore lenses with an average grade of 10.4% Zn, 4.2% Pb, 0.34% Cu, and 115 g/t Ag. The remaining 166 Mt of low-grade sulfides (1.7% Zn, 0.54% Pb, 0.71% Cu and 41 g/t Ag) occur in six massive pyrite (+/- pyrrhotite) lenses, of which 5.4 Mt grade 1.5% Cu (Powe 2008).

PETROLOGY

Based on mineralogy and stratigraphic relationships, massive sulfides can be divided into two principal facies: 1) a layered Zn–Pb-rich banded (bedded) sulfide facies, containing most of the resources recovered to date; and 2) a Cu-rich basal sulfide facies, sometimes referred to as the basal Cu-zone or vent complex. The Zn–Pb-rich banded sulfide facies is composed of pyrite, sphalerite, and galena with minor chalcopyrite and

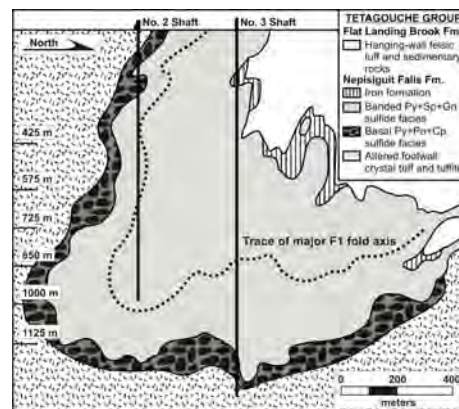


Fig. 2. Longitudinal section of the Main Zone, coincident with an F2 axial trace (after van Staal & Williams 1984).

tetrahedrite, and locally contains sub-economic sections of barren pyrite.

In stratigraphically lower parts of the sequence, Cu-rich massive sulfides (pyrite, pyrrhotite, chalcopyrite, and sphalerite) form a basal keel (Fig. 2) to the Zn–Pb-rich banded sulfide facies and are best developed towards the south end of the Main Zone. The abundance of Cu is primarily a function of chalcopyrite with lesser amounts of chalcocite, bornite, stannite, and Cu-bearing sulfosalts. Other trace phases recognized in the basal sulfide facies include arsenopyrite, magnetite, galena, and cassiterite. Overall, chalcopyrite occurs chiefly as free grains (anhedral) with only minor amounts occurring as inclusions in sphalerite. Sphalerite contents are low, with <10% of the total sphalerite grains exhibiting chalcopyrite disease (Fig. 3), a texture that is unique only to the basal sulfide facies. Average Fe contents for diseased (8.2 wt.% Fe) and non-diseased (9.9 wt.% Fe) varieties of sphalerite are consistent with electron microprobe (EPMA) compositions reported for the Main zone (Lentz 2002).

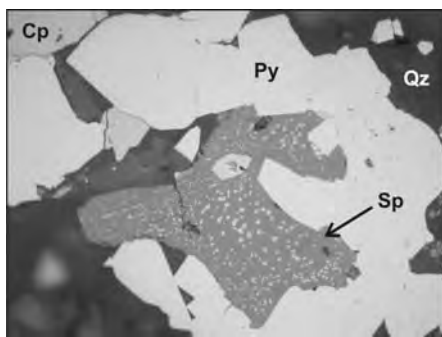


Fig. 3. Sphalerite mass exhibiting chalcopyrite disease, basal sulfide facies, 1125m level, Main Zone.

Pyrite has undergone variable degrees of recrystallization during metamorphism with porphyroblast development facilitated in sections with increased contents of pyrrhotite and gangue minerals (quartz and carbonate) in the matrix. Pyrrhotite and chalcopyrite exhibit extensive recrystallization and plastic flow features, with pyrrhotite-rich sections exhibiting durchbewegung textures. Pyrrhotite in the

Cu zone is abundant (up to 40%) and dominantly monoclinic, with lesser hexagonal forms also present suggesting incomplete retrograde equilibration. Analyses of pyrrhotite by EPMA revealed elevated contents of Co and Se accounting for their enrichment in the basal sulfide facies.

GEOCHEMISTRY

Bulk geochemical analyses reveal two distinct trace-element associations that are consistent with recognized sulfide facies (McClenaghan *et al.* 2009). The banded sulfide facies commonly exhibits enrichment in Zn, Pb, Ag, Sb, As, Au, Sn, In, and Tl; whereas the basal sulfide facies is comparably enriched in Cu, Bi, Co, and Se. These associations have been documented throughout the BMC (Goodfellow & McCutcheon 2003; MacLellan *et al.* 2006), and are consistent with a zone refining model (see Large 1977).

Hydrothermal recrystallization has resulted in higher Fe contents (avg. 44.0% Fe₂O_{3T}) - a result of an increased modal abundance of pyrite, pyrrhotite, and chalcopyrite, and lesser sphalerite and galena. Massive sulfides (n=78) from the basal Cu-zone (1125m level) average 1.1% Zn, 0.28% Pb, 1.3% Cu, with notable contents of As (0.4%), Bi (0.03%), and Co (0.08%). Ratios of Pb/Zn average 0.4, equivalent to those from the banded sulfide facies. However the basal sulfide facies exhibits considerable enrichment in Cu (Fig. 4) with values as high as 3.4%, and accompanied by increased contents of Bi (avg. 16 ppm), Co (475 ppm), and Se (21 ppm). Enrichment of Cu, Bi, Co, and Se are accompanied by concomitant depletions in Zn, Pb, Ag, Au, Sb, Sn, and In, which characterize the banded sulfide facies. Contents of As average 0.14% reflecting the arsenian nature of pyrite and the presence of arsenopyrite, the most abundant trace-sulfide phase in the Main Zone.

CONCLUSIONS

The high-temperature hydrothermal signature (Cu–Co–Bi–Se) characterizing the basal sulfide facies of the Brunswick No.

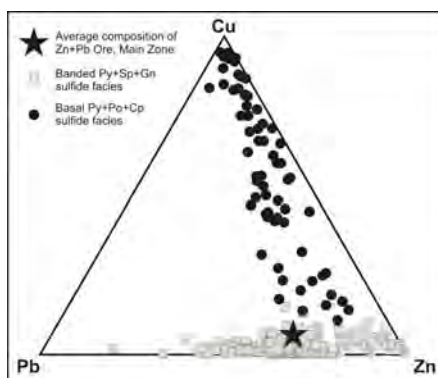


Fig. 4. Cu-Pb-Zn plot displaying metal ratios for the Brunswick No. 12 deposit.

12 deposit is consistent with its occurrence above a stringer sulfide zone; the proximity of the basal Cu zone to the vent is common to both the Brunswick No. 12 and No. 6 exhalative deposits. This distribution of metals within the deposit is interpreted to reflect an exhalative sulfide zone that has undergone extensive hydrothermal recrystallization (replacement) during zone refining. This is corroborated by the high abundance of chalcopyrite, arsenopyrite, and native bismuth all of which have higher temperature sensitive solubilities than sphalerite and galena, resulting in elevated ratios of Cu/Zn and Cu/Pb within the basal sulfide facies.

Although the Brunswick No. 12 deposit is mined primarily for Zn and Pb in the banded sulfide facies, significant Cu resources exist in the basal sulfide facies. The predominance of free chalcopyrite grains, recoverable during the milling process, may allow for its exploitation as an incremental ore.

ACKNOWLEDGMENTS

Electron-microprobe analyses were conducted by Douglas Hall (UNB). Funding was provided by Xstrata Canada Corp. and the NB Museum. Thanks to P. Bernard, T. Babin, B. Drolet, S. Wells, and A. Huard for access to the Brunswick No. 12 Mine.

REFERENCES

GOODFELLOW, W.D. & McCUTCHEON, S.R. 2003. Geologic and genetic attributes of volcanic

sediment-hosted massive sulfide deposits of the Bathurst Mining Camp, northern New Brunswick – a synthesis. *Economic Geology Monograph*, **11**, 245–302.

LARGE, R.R. 1977. Chemical evolution and zonation of massive sulfide deposits in volcanic terrains. *Economic Geology*, **72**, 549–572.

LENTZ, D.R. 2002. Sphalerite and arsenopyrite at the Brunswick No. 12 massive-sulfide deposit, Bathurst Camp, New Brunswick: constraints on P–T evolution. *Canadian Mineralogist*, **40**, 19–31.

LENTZ, D.R. & GOODFELLOW, W.D. 1996. Intense silicification of footwall sedimentary rocks in the stockwork alteration zone beneath the Brunswick No. 12 massive sulphide deposit, Bathurst, New Brunswick. *Canadian Journal of Earth Sciences*, **33**, 284–302.

LUFF, W.M., GOODFELLOW, W.D., & JURAS, S. 1992. Evidence for a feeder pipe and associated alteration at the Brunswick No. 12 massive sulphide deposit. *Exploration and Mining Geology*, **1**, 167–185.

MACLELLAN, K.L., LENTZ, D.R., & McCLENAGHAN, S.H. 2006. Petrology, geochemistry, and genesis of the copper zone at the Brunswick No. 6 volcanogenic massive sulfide deposit, Bathurst Mining Camp, New Brunswick, Canada. *Exploration and Mining Geology*, **15**, 53–76.

McCLENAGHAN, S.H., LENTZ, D.R., MARTIN, J., & DIEGOR, W.G. 2009. Gold in the Brunswick No. 12 volcanogenic massive sulfide deposit, Bathurst Mining Camp, Canada: Evidence from bulk-ore analysis and laser-ablation ICP–MS data on sulfide phases. *Mineralium Deposita*, in press.

POWE, E.M. 2008. *Petrology, geochemistry and distribution of the copper zones at the Brunswick No. 12 volcanogenic massive sulfide deposit, Bathurst Mining Camp, New Brunswick*. BSc Thesis, University of New Brunswick, Fredericton, New Brunswick.

VAN STAAL, C.R. & WILLIAMS, P.F. 1984. Structure, origin and concentration of the Brunswick 12 and 6 orebodies. *Economic Geology*, **79**, 1669–1692.

VAN STAAL, C.R., WILSON, R.A., ROGERS, N., FYFFE, L.R., LANGTON, J.P., McCUTCHEON, S.R., McNICOLL, V., & RAVENHURST, C.E. 2003. Geology and tectonic history of the Bathurst Supergroup, Bathurst Mining Camp and its relationship to coeval rocks in southwestern New Brunswick and adjacent Maine—a synthesis. *Economic Geology Monograph*, **11**, 37–60.

Lithogeochemistry of Ordovician Sedimentary Rocks: Implications for VMS Exploration in the Bathurst Mining Camp (BMC), Canada

Steven R. McCutcheon¹ & James A. Walker¹

¹New Brunswick Geological Surveys Branch, P.O. Box 50, Bathurst, NB E2A 3Z1, CANADA
(e-mail: steve.mccutcheon@gnb.ca)

ABSTRACT: Volcanic-hosted massive sulfide deposits of the BMC formed during the early stage of back-arc basin development (circa 470 Ma). The pre-existing volcanic arc is represented by volcanoclastic sedimentary rocks that overlie Cambro-Ordovician, continental-margin flysch. The sulfide deposits are within the felsic volcanic pile that overlies these “older” sedimentary rocks. The felsic rocks give way up-section to mafic volcanic rocks that are capped by post-volcanic (circa 460 Ma), deep-water shale and chert, i.e., “younger” sedimentary rocks. Evolution from a continental margin to a back-arc basin setting is reflected in the lithogeochemistry. Most “older” sedimentary rocks can be distinguished from “younger” ones by a line of slope $y/x = 0.2$ on a V/Nb versus Zr/Cr diagram; older rocks have higher Zr/Cr and younger ones have higher V/Nb. Sedimentary rocks intercalated with the felsic volcanic pile plot with the older population indicating that the old-young transition is stratigraphically higher than previously thought. Log Fe_2O_3^T versus log MnO, Al versus Si, and Si versus Zr diagrams do not effectively discriminate older and younger rocks.

KEYWORDS: Bathurst, VMS, Ordovician, sedimentary (or sediment) lithogeochemistry

INTRODUCTION

The volcanic-sediment-hosted massive sulfide (VMS) deposits of the Bathurst Mining Camp (BMC) formed during the initial stage of opening of the Tetagouche – Exploits back-arc basin, which developed behind a volcanic arc on the Ganderian (peri-Gondwanan) continental margin of the northern Appalachians. This basin began to form during the Middle Ordovician (circa 470 Ma) as a result of westward migration of the ensialic arc. Felsic volcanism predominated in the early stage of basin development but gave way to mafic volcanism in the later stages of rifting, ultimately producing oceanic crust (van Staal *et al.* 2003a).

Volcanic rocks in this basin are conformably underlain by, intercalated with, and gradationally overlain by sedimentary rocks that can provide broad constraints on the depositional setting of VMS deposits within the volcanic pile. Goodfellow *et al.* (2003) suggested that anoxic shale from beneath the volcanic pile can be distinguished from oxidized shale within the pile on the basis of lithogeochemistry, i.e., using Si/Al, Zr/Si,

and $\text{MnO}/\text{Fe}_2\text{O}_3^T$ ratios. Furthermore, Rogers *et al.* (2003) proposed that the sedimentary rocks beneath the pile (“older” group) can generally be distinguished from those within and above the pile (“younger” group) on the basis of their V/Nb versus Zr/Cr ratios. If such geochemical discriminants work, they have practical application in poorly exposed and complexly deformed terrain, such as the BMC, where it is difficult to assign a particular sedimentary rock to the correct formation on the basis of its appearance. Because the nomenclature and correlation of rock units in the BMC were still in a state of flux when the above authors collected their samples in the 1990s, a re-evaluation of their rock-unit assignments was undertaken. Also, a comparison of their data to others from stratigraphically well constrained samples was made to test the utility of their proposed discriminants.

STRATIGRAPHY

In the BMC, sedimentary rocks underlying the volcanic pile are assigned to the Miramichi Group (MG), whereas those

within and overlying the pile are assigned to the Bathurst Supergroup (van Staal *et al.* 2003a), which comprises the California Lake (CLG), Fournier (FG), Sheephouse Brook (SBG), and Tetagouche (TG) groups (Fig. 1).

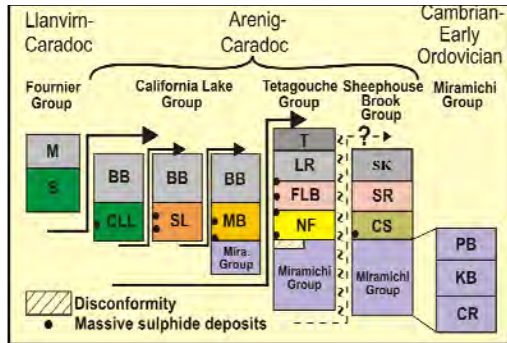


Fig. 1. Schematic tectonostratigraphy of the Bathurst Mining Camp showing inferred positions of known deposits. Formations as follows: BB-Boucher Brook, CLL-Canoe Landing Lake, CR-Chain of Rocks, CS-Clearwater Stream, FLB-Flat Landing Brook, KB-Knights Brook, LR-Little River, M-Millstream, MB-Mount Brittain, NF-Nepisiguit Falls, PB-Patrick Brook, S-Sormany, SK-Slacks Lake, SL-Spruce Lake, SR-Sevogle River, T-Tomogonops.

From apparent base to top, the MG comprises the CR, KB, and PB formations that collectively are referred to as “older sediments” (Fig. 1). The CR Formation consists of thickly bedded, greenish grey, quartz wacke with minor shale. The KB Formation is similar compositionally to the CR, but the rocks are dark grey, and shale is more voluminous. The PB Formation generally has more shale than the KB Formation; it also contains minor dark grey, quartz wacke (\pm volcanic quartz) and coarse-grained, feldspathic wacke. The PB Formation, unlike the CR and KB, reflects two sediment sources, one from the continental margin and the other from the volcanic arc.

Sedimentary rocks within the lower (mainly felsic) part of the volcanic pile are highly variable and not voluminous. Greenish grey to dark grey mudrocks and volcanoclastic rocks occur locally in the FLB, MB, NF, SL and SR formations (Fig.

1). Some of them look lithologically similar to those of the PB Formation.

Sedimentary rocks in the upper (mainly mafic) part of the pile are predominantly mudrocks, but they have an exhalative component. Maroon shale and chert are present in the BB, LR, and SK formations (Fig. 1). Notably, maroon shale and chert are abundant in the CLL Formation and also occur locally near the top of the FLB and SR formations. Caradocian black shale and pelagic chert of the BB, LR, and SK formations mark the end of volcanic activity in the BMC. In places, these rocks grade upward into flysch of the M or T formations (Fig. 1).

LITHOGEOCHEMISTRY

Data and Methods

In total, 590 analyses were used in our evaluation of sedimentary rocks of the BMC, including 234 from Goodfellow *et al.* (2003), 133 from Rogers *et al.* (2003), and 108 from various reports of the NB Geological Surveys Branch. All of these data were collected during the federal-provincial EXTECH-II Project (1994-1998); an additional 115 samples, acquired subsequently, were analysed at Activation Laboratories Ltd. using their lithium metaborate/tetraborate fusion ICP whole rock package (Code 4B) and trace element ICP-MS package (Code 4B2).

Each reported sample location was cross referenced with the 1:100,000 scale geological map of the BMC (van Staal *et al.* 2003b) to determine if the given rock unit matched the one on the map, or subsequent revisions to it. This resulted in the re-assignment of 52 samples to other formations. The resulting dataset (n = 590) comprises 87 BB, 19 CLL, 16 FLB, 40 KB, 54 LR, 61 M, 8 MB, 60 NF, 138 PB, 13 SK, 71 SL, 3 SR, and 20 T samples. All samples were plotted on the proposed discrimination diagrams and the results inspected and interpreted. The data were then filtered as follows: BB, LR, M, and T samples with V/Nb > 8; CR, KB, PB, and NF samples with Zr/Cr > 5; and all samples with Al/(Al+Fe+Mn) < 0.45 were removed from the dataset, leaving only the most problematic samples to

discriminate. The remaining 282 samples (37 BB, 18 CLL, 9 FLB, 19 KB, 5 LR, 12 M, 7 MB, 45 NF, 57 PB, 1 SK, 69 SL, 3 SR, and 0 T) were then re-plotted and interpreted.

Results

On a V/Nb versus Zr/Cr diagram, a line ($y/x = 0.2$) passing through the origin separates most of the “older” group (CLL, KB, MB, NF, PB, SR, and SL formations) from the “younger” ones (BB, LR, M, SK, and T formations). Specifically, it correctly discriminates 145/178 MG, 132/150 TG, 105/185 CLG, 6/16 SBG, and 50/61 FG samples, which represents success rates of 82%, 88%, 56%, 38%, and 82%, respectively. In the MG, 30 PB samples plot with the younger group, which is not surprising considering that this formation received erosional detritus from the Popelogan Arc (van Staal *et al.* 2003a). In the TG, 11 NF samples plot with the younger group but 8 of them come from one area suggesting that these samples were assigned to the wrong formation. In the CLG, 45 BB samples plot with the older group and 28 SL samples plot with the younger one, yielding a low success rate (56%). However, these two formations are everywhere tectonically interleaved and the sedimentary rocks in both look much alike. This low success rate may reflect incorrect assignment of samples to each formation. The success rate for the SBG is the lowest (38%), but the sample population ($n = 16$) is small.

A binary $Al/(Al+Fe+Mn)$ versus Fe/Ti plot reveals that 57/590 samples have $Al/(Al+Fe+Mn) < 0.45$ and $Fe/Ti > 20$, i.e., in the “hydrothermal field” of Böstrom (1973). Notably, 33 of them are PB samples, all but three of which come from drill cores in the vicinity of the Brunswick No.12 mine, no doubt reflecting addition of iron to the footwall rocks. Surprisingly, only 24/412 samples from the Bathurst Supergroup plot in this hydrothermal field as follows: TG (2 NF, 3 FLB, 2 LR), CLG (1 CLL, 1 SL, 8 BB), and SBG (7 SK).

Ternary diagrams (Sc-Th-Zr/10 and Th-La-Sc) show that the majority of the samples plot in or near the “continental

island arc” field of Bhatia & Crook (1986). Notably, the MG samples show the same distribution on these diagrams as those from the Bathurst Supergroup.

On a $\log Fe_2O_3^T$ versus $\log MnO$ binary diagram, most formations show a similar distribution, with samples clustering along a line ($y/x = 0.9$) that passes through 1.5 log units on the x-axis. Samples from the KB, FLB, MB, NF, and T formations plot towards the bottom end (0.01-0.2 MnO) of this line, whereas SK samples plot towards the top end (1-10); samples from the BB, CLL, LR, M, PB, and SL formations span the length of the line.

On an Al versus Si binary diagram, most of the data plot along a line ($y/x = -1.7$) that passes through 18 wt.% Al. A number of samples from the BB, CLL, LR, M, NF, PB, SK, SL, and T formations plot below this line, but virtually none plot above it. Samples from individual formations generally span the entire length of the line. Goodfellow *et al.* (2003) indicated that a line of slope 5 ($Si/Al = 5$), passing through 3 wt.% Al, separates BB, CLL and LR shales from those of the PB and SL formations; however, there is no indication of this from our data.

These authors also suggest that a Si versus Zr binary diagram can be used to help distinguish BB, CLL, and LR shales from PB and SL shales, i.e., the former rocks generally have lower Zr/Si ratios than the latter. Our data cluster along two broad trends: one ($y/x = -8$) that passes through 45 wt.% Si and another ($y/x = 40$) that passes through 25 wt.% Si. Most BB, LR, M, SK, and T samples have < 250 ppm Zr and plot along the first trend, but the CLL, FLB, MB, PB, and SL samples plot along both trends.

Examination of the filtered dataset reveals additional information. On a V/Nb versus Zr/Cr binary diagram, most of the samples that do not plot where expected are from the BB (31/37), LR (4/5), M (8/12), NF (11/45), PB (15/57), SL (20/69), and SR (3/3) formations. Of the 31 BB samples that are not classified correctly, 23 of them have a “hydrothermal” component and 5 others could be from the SL Formation. Similarly, 2/4 LR samples

could be from the SL Formation. Of the 8 samples from the M Formation, 3 have a hydrothermal component. Of the 11 NF samples, 7 are from one area and may reflect incorrect unit assignment. Of the 15 PB samples, 8 are from drill cores near the Brunswick No.12 mine. Of the 20 SL samples, 11 could be from the BB and LR formations.

CONCLUSIONS

Our re-evaluation of geochemical data (n=590) from sedimentary rocks of the BMC indicates the following: 1) A line ($y/x = 0.2$) passing through the origin on a V/Nb versus Zr/Cr diagram discriminates most “older” sedimentary rocks from “younger” sedimentary rocks. 2) The transition between older and younger appears to be near the top of the felsic volcanic pile, not near the bottom as reported by Rogers *et al.* (2003). 3) Overall, this discriminant is most effective for the TG (88%), followed by the MG (82%), and FG (81%); it is least effective for the CLG and SBG (56%). 4) Low percentages for the BB (49%) and SL (60%) formations reduce the overall total for the CLG; this probably reflects incorrect assignment of samples to these two formations. 5) Over half of the 57 “metalliferous sediments” in the dataset come from the PB Formation, specifically from drill cores near Brunswick No. 12, suggesting that iron was added to the footwall rocks during hydrothermal alteration. 6) Log $Fe_2O_3^T$ versus log MnO, Al versus Si, and Si versus Zr binary diagrams do not effectively discriminate older and younger rocks of the BMC.

REFERENCES

- BHATIA, M.R. & CROOK, K.A.W. 1986. Trace element characteristics of greywackes and tectonic setting discrimination of sedimentary basins. *Contributions to Mineralogy and Petrology*, **92**, 181–193.
- BÖSTROM, K. 1973. The origin and fate of ferromanganoan active ridge sediments. *Stockholm Contributions to Geology*, **27**, 147–243.
- GOODFELLOW, W.D., PETER, J.M., WINCHESTER, J.A., & VAN STAAL, C.R. 2003. Ambient marine environment and sediment

provenance during formation of massive sulphide deposits in the Bathurst Mining Camp: importance of reduced bottom waters to sulphide precipitation and preservation. In: GOODFELLOW, W.D., McCUTCHEON, S.R., & PETER, J.M. (eds), *Massive sulphide deposits of the Bathurst Mining Camp, New Brunswick, and northern Maine*, Economic Geology Monograph **11**, 129–156.

- ROGERS, N., VAN STAAL, C.R., WINCHESTER, J.A., & FYFFE, L.R. 2003. Provenance and chemical stratigraphy of the sedimentary rocks of the Miramichi, Tetagouche, California Lake, and Fournier groups, northern New Brunswick. In: GOODFELLOW, W.D., McCUTCHEON, S.R., & PETER, J.M. (eds), *Massive sulphide deposits of the Bathurst Mining Camp, New Brunswick, and northern Maine*, Economic Geology Monograph **11**, 111–128.

- VAN STAAL, C.R., WILSON, R.A., ROGERS, N., FYFFE, L.R., GOWER, S.J., LANGTON, J.P., McCUTCHEON, S.R., & WALKER, J.A. 2003b. A new geologic map of the Bathurst Mining Camp and surrounding areas – a product of integrated geological, geochemical and geophysical data. In: GOODFELLOW, W.D., McCUTCHEON, S.R., & PETER, J.M. (eds), *Massive sulphide deposits of the Bathurst Mining Camp, New Brunswick, and northern Maine*, Economic Geology Monograph **11**, 61-64.

- VAN STAAL, C.R., WILSON, R.A., ROGERS, N., FYFFE, L.R., LANGTON, J.P., McCUTCHEON, S.R., McNICOLL, V., & RAVENHURST, C.E. 2003a. Geology and tectonic history of the Bathurst Supergroup, Bathurst Mining Camp, and its relationships to coeval rocks in southwestern New Brunswick and adjacent Maine – a synthesis. In: GOODFELLOW, W.D., McCUTCHEON, S.R., & PETER, J.M. (eds), *Massive sulphide deposits of the Bathurst Mining Camp, New Brunswick, and northern Maine*, Economic Geology Monograph **11**, 37–60.

Evaluating Bromine Geochemistry as a Prospecting Tool For Potash in Western Newfoundland

Jackie O' Driscoll¹, Robert Boehner², Lawrence Winter¹ & Roland Butler¹

¹Altius Resources Inc., P.O. Box 385, St. John's, Newfoundland, A1C 5J9 CANADA
(e-mail: jodriscoll@altiusminerals.com)

²P.O. Box 1365, Montague, Prince Edward Island, C0A 1R0 CANADA

ABSTRACT: Salt deposits of Early Carboniferous age (~325-335 Ma) Windsor Group are known throughout the Atlantic Provinces. These marine evaporite sequences were precipitated from seawater in a series of restricted basins, which formed in the larger Maritimes Basin. Intermittent exploration work including mapping, diamond drilling, and geophysical surveys in the St. George's Bay area of western Newfoundland over the last sixty years has resulted in the recognition of salt and potash, analogous to those evaporite sequences of New Brunswick and Nova Scotia. Altius currently holds mineral claims covering 46,250 hectares in the St. George's Bay area, which are currently being evaluated for the potential to host economic potash deposits.

Previous geochemical bromine profiling of Eastern Canadian salt deposits and occurrences has illustrated the usefulness of this technique in this region (Baar 1965). Several salt intersections from previous drilling in the St. George's Bay area were sampled for a bromine geochemical study. Geochemical data are pending at the time of writing. The presentation will summarize the results and compare the data to representative profiles from Nova Scotia and New Brunswick.

KEYWORDS: *Evaporite, Potash, Bromine, Carboniferous, Codroy Group*

INTRODUCTION

The Carboniferous sediments of the Maritimes Basin were originally deposited as red-green interstratified continental to marginal siliciclastics, marine limestone, dolostone, gypsum, anhydrite, halite, and locally, potash. The salt deposits vary from stratified, with only minor structural complications, to those that have been tectonized into pillows, anticlines (e.g., Penobscus Deposit) and diapirs or domes. In the latter cases, structural complexities make the stratigraphic position of many of these deposits uncertain.

The St. George's Bay Sub-basin of western Newfoundland is contained within the Carboniferous Maritimes Basin (Fig. 1) and hosts sedimentary rocks assigned to the Codroy Group. The Codroy Group is equivalent to the Windsor Group, which hosts potash deposits and occurrences in Nova Scotia and New Brunswick, including Potash Corporation's Penobscus Mine in Sussex. Annual production from this deposit comprises 0.7



Fig. 1. Regional map of Atlantic Canada outlining the known limits the Maritimes Basin.

million tonnes KCl and 0.6 million tonnes of salt (Moore *et al.* 2008).

Altius currently holds mineral licenses covering 46,250 hectares in the St. George's Bay area, which hosts several potash prospects (Fig. 2). This area has established infrastructure, excellent road access, and is adjacent to deep water port facilities currently being utilized for shipping base metal concentrate.

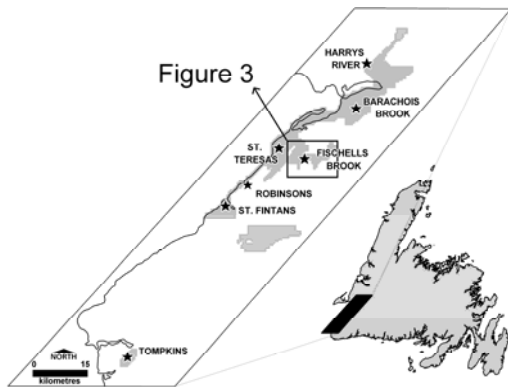


Fig. 2. Property location map with Altius claims shaded and potash prospects shown as stars.

The potash occurrences within the St. George's Bay area consist mainly of halite (NaCl) with variable siliciclastics and potash minerals including sylvite (KCl) and carnallite ($\text{KMgCl}_3 \cdot 6\text{H}_2\text{O}$).

Phase I exploration work by Altius included a compilation of all publicly available data from previous diamond drill holes, petroleum exploration wells, and geophysical surveys (gravity and seismic) for incorporation into an integrated 3D model. Phase II of the work program is currently ongoing and consists of a new ground gravity survey, re-assessment and re-sampling of previous drill core, and assessment of previous seismic data. This presentation will summarize the exploration methodology and focus on the use of bromine as a geochemical vector for potash.

GEOLOGICAL SETTING

Regional Geology

The St. George's Bay area is located within the Humber Zone of western Newfoundland; the westernmost tectono-stratigraphic subdivision of the Newfoundland Appalachians. The Humber Zone represents the ancient continental margin of eastern North America (Williams 1995) and is partly bounded to the east by the Cabot Fault.

The "Maritime Disturbance" refers to tectonic activity that mainly occurred within the basin areas of the Late Paleozoic

overstep sequence. The Appalachian basement fragmented resulting in subsidence and uplift creating areas for deposition of Carboniferous sediments. Deformation caused local and regional compression represented by broad open folds, reverse and normal faulting, and salt tectonism (Williams 1995).

The St. George's Bay Sub-basin formed as a strike-slip successor basin adjacent to, and west of, the northeasterly trending Long Range Fault. This fault is a major strike-slip structure that is part of the Hercynian Cabot Fault system in western Newfoundland. Dextral strike-slip movements began in Middle or Late Devonian time and ended in the Early Carboniferous. The sub-basin comprises a 22 kilometre wide zone between St. George's Bay and the Long Range Mountains, extending 125 kilometres from the coast near Codroy Valley, north-east to the vicinity of Stephenville, covering an area totalling 2700 square kilometres (Knight 1983).

Local Geology

The rocks of the St. George's Bay Sub-basin are divided into three groups: the Anguille, Codroy, and Barachois Groups, which are correlated to the Horton, Windsor, and Canso (Mabou) Groups, respectively, in Nova Scotia and New Brunswick (Knight 1983). The Anguille Group is a sequence of non-marine siliciclastic rocks defining the oldest strata in the basin. It is conformably overlain by a series of marine evaporite and carbonate rocks and locally dominant non-marine clastic rocks comprising the Codroy Group. The Codroy Group is conformably overlain by a variably interbedded sequence of non-marine sandstone, siltstone and shale of the Barachois Group (Knight 1983). The Carboniferous sedimentary rocks in the St. George's Sub-basin lie upon anorthosite and mafic and felsic orthogneiss of the Late Proterozoic Long Range Complex.

The marine sedimentary rocks of the Codroy Group host the evaporite sequence of interest and are divided in ascending order into the Ship Cove

Formation, the Journois Pond Formation, the Woodville Formation, the Jeffrey's Village Formation, and the Highlands Formation.

The lower limestone, gypsum, and anhydrite units of the Ship Cove and Journois Pond Formations are overlain by a 200-1000 metre thick sequence of salt and grey shale of the Woodville Formation. The Woodville Formation has been subdivided into four members: Basal, Middle and Upper Halite Members, and an overlying shale member with pseudomorphs of halite and gypsum veinlets.

The potash units occur within the rock salt sequences of the Woodville Formation. Sylvite is disseminated or occurs as distinct sylvinite beds within the upper portion of the Middle Halite. The lower portion of the unit consists of fine-grained metallic copper-red disseminated carnallite and vug fillings. Minor potash-bearing intervals are also found in the Upper Halite, typically with interbedded clays.

EXPLORATION HISTORY

Previous exploration circa late 1940's demonstrates the area's high potential for potash deposits. However, there has been limited sustained exploration in this region, emphasized by the presence of gravity lows throughout the area, which have not been extensively tested. Moreover, recent salt or potash intersections discovered during drilling of petroleum exploration wells (e.g., Flat Bay-101-1 and Captain Cook-1) further illustrate the potash potential of the region. These were not expected, and are not associated with gravity lows. Potash assays up to 20.4% K₂O were reported from Captain Cook-1 in 2008 (Vulcan 2008).

Historical exploration has highlighted the Fischell's Brook salt/potash prospect as a possible analog to the Sussex deposits in southern New Brunswick. The prospect is located approximately 15 kilometres south of the Town of St. George adjacent to and underlying the Trans-Canada Highway. The deposit is associated with a gravity anomaly that is approximately 10.5 x 8.5

kilometres in size. Historical drilling of this gravity anomaly has identified a significant body of salt.

In the 1968 discovery hole (Hooker-1; Hooker Chemical Inc.), approximately 750 metres of salt was intersected with the hole terminating in salt at 1099 metres. Sylvite was intersected at a vertical depth of 381.0 to 402.3 metres and assayed up to 15.1% K₂O with insoluble content up to 11.6%.

PRINCIPLES OF BROMINE

GEOCHEMISTRY

Bromine (Br) is the most important genetic trace element for potash within salt deposits. Bromide minerals do not form during the crystallization of salts from seawater; rather bromine tends to accumulate with increasing brine concentration and occurs only as a trace in solid solution as a substitute for chlorine in the precipitating chloride minerals.

Bromine has an ionic radius of 1.96 Å and thus easily substitutes for chlorine (1.81 Å) in the halite crystal lattice as well as in the other chloride salts. The distribution coefficients for bromine in chloride salts deposited from seawater is less than 1 (Warren 2006).

The bromine content of halite is characteristic for each sequence of the evaporitic strata. The bromide level in a halite crystal also increases with increases in parent brine temperature and with the speed of crystallization (Warren 2006).

Typical marine water contents of Br are 65 ppm. The first chloride salt precipitated in an evaporite basin is halite (70-75 ppm Br). Bromine content of halite increases to >230 ppm Br as the first potassium mineral crystallizes (Valyashko 1956).

Thus, the trends of Br content in halite sampled systematically in profiles of salt sequences may be used as a guide to:

- 1) saline evaporite mineral depositional history and stratigraphic trends,
- 2) remnant high Br indicative of former high order evaporite deposition (potash salts),
- 3) salt sequence anomalies including potential structural repetition or dissolution intervals,

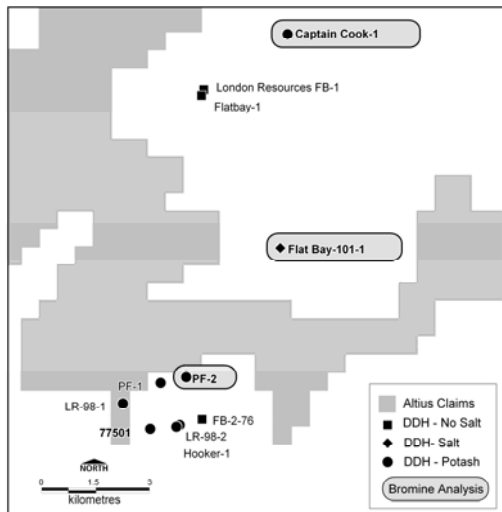


Fig. 3. Location of drill holes in the Fischells Brook and Flat Bay areas illustrating salt and potash intercepts and highlighting PF-2, Flat Bay-101-1 and Captain Cook-1, selected for the current bromine geochemistry study.

- 4) regional basin correlation and comparison to areas with economic deposits, and
- 5) post depositional alteration/diagenesis of these highly soluble rocks.

2009 BROMINE GEOCHEMISTRY STUDY

Altius' current bromine geochemical study utilizes core samples from holes PF-2, Flat Bay-101-1 and Captain Cook-1 (Fig. 3). This study was undertaken to establish baseline bromine profiles for the St. Georges Bay region.

The data will assist in evaluating the potash potential in each area, especially where structural complexities present challenges with stratigraphic interpretations.

CONCLUSIONS

- (1) The St. Georges Sub-basin is considered prospective but underexplored for potash deposits.
- (2) Bromine geochemistry has been proven as a useful prospecting tool for potash mineralization in various regions.
- (3) Ongoing exploration work by Altius Resources, including bromine geochemistry, will further our understanding of the potash mineralization in western Newfoundland.

REFERENCES

- BAAR, C.A. 1965. Bromine investigations on eastern Canada salt deposits. In: RAU, J.L. (ed) *Second Symposium on Salt*. Northern Ohio Geological Society, 276-292.
- KNIGHT, I. 1983. *Geology of the Carboniferous Bay St. George sub-basin, western Newfoundland*. Mineral Development Division, NDME, Memoir 1, 358 p.
- MOORE, G. et al. 2008. *National Instrument 43-101 Technical Report on Penobsquis & Picadilly Potash Deposits, Kings County, New Brunswick, Canada*. Potash Corporation of Saskatchewan Inc., 83 p.
- VALYASHKO, M.G. 1956. Geochemistry of bromine in the processes of salt deposition and the use of the bromine content as a genetic and prospecting criterion. *Geochemistry*, 6, 570-589.
- VULCAN MINERALS INC., 2008. "Potash Assays up to 20.4% K₂O", news release Sept 25, 2008.
- WARREN, J.K. 2006. *Evaporites. Sediments, Resources and Hydrocarbons*, 1035 p.
- WILLIAMS, H. 1995. *Geology of the Appalachian-Caledonian Orogen in Canada and Greenland*. Geological Survey of Canada, Geology of Canada Series, 6, 944 p.

Mesothermal, auriferous quartz veins of the Golden Promise deposit, central Newfoundland: their setting and the nature of wall rock alteration

Hamish Sandeman¹, Heather Rafuse¹, David Copeland² and Jeff Morgan³

¹Geological Survey of Newfoundland and Labrador, Department of Natural Resources, PO Box 8700, St. John's, NL, A1B 4J6 CANADA (e-mail: hamishsandeman@gov.nl.ca)

²Paragon Minerals Corporation, 85 Thorburn Road, Suite 202, St. John's, NL, A1B 3M2 CANADA

³Crosshair Exploration and Mining Corporation, Suite 202, Kenmount Business Centre, 66 Kenmount Road, St. John's, NL, A1B 3V7 CANADA

ABSTRACT: The Golden Promise gold deposit is located ca. 10 km southwest of the community of Badger in central Newfoundland within the Exploits sub-zone of the Appalachian orogen. The deposit is poorly exposed and comprises a series of likely en-echelon, ENE-trending auriferous quartz veins hosted in shales and greywackes of the Upper Victoria Lake Supergroup. Native Au occurs in association with pyrite, arsenopyrite and rare galena within cockscomb-textured and stylolitic quartz veins. Alteration associated with the mineralization comprises visibly bleached zones proximal to the veins with bleached spotted zones up generally ≤ 10 m outward from the veins. Close spatial overlap between a suite of E-W trending intermediate dykes, the quartz veins and the characteristic spot-texture and widespread alteration of the dykes themselves, obfuscates petrogenetic-paragenetic relationships. Preliminary VIRS spectrometry, petrographic analysis and EDS electron microprobe studies indicate that the alteration assemblage is dominated by Fe-chlorite+sericite+CaCO₃. Two generations of quartz veins are observed, an early series of coarse cockscomb quartz veins are cut by a younger series of apparently thinner, mosaic-textured fine-grained quartz. Visible Au and economic mineralization appears to accompany early, coarse-grained veins.

KEYWORDS: *gold, infrared spectrometry, alteration, mineralization*

INTRODUCTION

The Golden Promise deposit was discovered by prospector William Mercer in 2002 after a forest fire razed thick brush in heavily drift covered areas immediately south of the community of Badger. The initial discovery consisted of coarse-grained, comb-textured and stylolitic quartz boulders exposed on sub-cropping, bedrock-cored ridges. A composite sample from ~10 of these boulders assayed ca. 30 g/t Au. The deposit was immediately optioned by Rubicon Minerals Corporation in 2002 and has since been explored under a number of joint venture projects involving Rubicon Minerals Corporation, Paragon Minerals Corporation, Placer Dome Ltd., and Crosshair Exploration & Mining Corporation. Since 2002, the property has been subjected to intense scrutiny including: the completion of 8,250 line

kilometres of airborne magnetic and electromagnetic surveys; a regional soil sampling program that included ca. 6000 B-horizon samples; intensive prospecting and mapping and; 98 near-surface (<314 m) NQ drill holes totalling 15,310 m. A NI-43-101F1 resource calculation on the deposit (Pilgrim & Giroux 2008) outlines a total of 921,000 tonnes averaging 3.02 g Au/t (89,500 contained ounces of gold), with a cut-off grade of 1 g/t Au. Golden Promise therefore represents the first significant gold resource in this part of central Newfoundland, wherein low metamorphic grade sedimentary rocks were previously considered non-prospective for mineralization.

REGIONAL SETTING

The Golden Promise deposit lies within the Exploits subzone of the Dunnage Zone of the Appalachians, ca. 8 km east of the

Red Indian Line. Within the Dunnage zone, rocks of the Exploits subzone lie to the east of the Red Indian Line and are considered to have peri-Gondwanan affinities. In contrast, rocks of the Notre Dame subzone, which are of peri-Laurentian affinity, lie to the west of the Red Indian Line (Williams 1995). In the Exploits subzone, rocks of the Cambrian-Ordovician Victoria Lake Group (now Supergroup; cf., Evans & Kean 2002; Rogers & van Staal 2002) comprise at least three volcanic-rock dominated sequences that are stratigraphically and structurally intercalated with marine sedimentary rocks consisting of vari-coloured shales along with volcanoclastic sandstones and wackes. Many of these, particularly those of the study area, have recently been assigned to the Stanley Waters Formation by Rogers *et al.* (2005). Collectively, rocks of the Victoria Lake Supergroup are conformably(?) overlain by polymictic conglomerates, medium-grained quartz-rich sandstones, and sparse shaley horizons constituting the continentally-derived, overlap, Ordovician-Silurian Badger Group considered to have been deposited in restricted oceanic basins during closure of Iapetus Ocean (Williams & O'Brien, 1991; Williams 1995).

Historical geological maps (e.g., Kean & Jaysinghe 1982) suggest that the host rocks of the Golden Promise veins belong to the subsequently defined Badger Group (cf., Williams 1995). In this area of poor exposure, however, modern, airborne magnetic and resistivity studies (Copeland & Newport 2005) have significantly improved our knowledge of the 3-D architecture of the rocks of the region. These investigations have outlined persistent and continuous magnetic and conductive *versus* poorly-magnetic and non conductive horizons within the rocks of the study area. In conjunction with key, but rare, well exposed bedrock outcrops, the geophysical surveys have led to a more sound and informed subdivision of the distribution of rock-types and, in particular, has led to more accurate delineation of the drift-covered contacts between the Victoria Lake Supergroup

and the Badger Group. The recent detailed field work and regional geophysical surveys have yielded new interpretive maps (Copeland & Newport 2005) that clearly indicate that the auriferous quartz veins of the Golden Promise Deposit are hosted by upward-fining marine clastic sedimentary rocks of the Upper Victoria Lake Supergroup rather than the siliciclastic flysch sequences of the Badger Group (Williams & O'Brien, 1991; Pilgrim & Giroux 2008).

LOCAL GEOLOGY AND MINERALIZATION

The host rocks to the Golden Promise vein systems are very poorly exposed. A number of the ridge-crests in the immediate area of the main Jaclyn veins (Fig. 1) host broken, angular boulders that may represent possible subcrop. Perhaps the best bedrock exposure in the area is that at Little Red Indian Falls, ca. 7 km to the SW of the deposit on the Exploits River. There, a ca. 300m long section preserves, vari-coloured, dm-scale bedded siltstones grading upwards into grey and black mudstones and into black, pyritic Caradocian shales capping the Victoria Lake Supergroup. The upward fining nature, the scale of bedding and the character of the sedimentary rocks are identical to those observed in the upper stratigraphic sections of drill core from the Golden Promise Deposit.

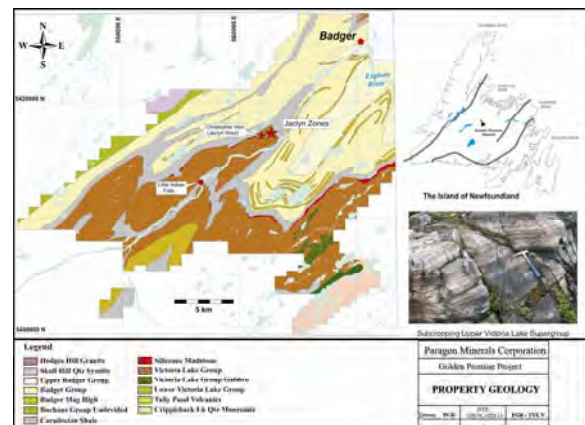


Fig. 1. Regional setting and geology of the Golden Promise Deposit, Newfoundland.

Trenches excavated across the veins are typically flooded by surface water; however, three partially flooded trenches have exposed bedrock. From small ($\leq 5\text{m}^2$) outcrops exposed in three of the trenches, it is apparent that the average grain size of the clastic sedimentary rocks and the abundance of coarse-grained detritus, increases from NE to SW away from the buried Caradocian shale, with arkosic sandstone most abundant in the SW near the Christopher vein. An extensive array of 98 drill holes provides excellent downhole, 3-D control on our understanding of the geology.

Collectively the field, drillcore, and regional data yield a number of first order conclusions.

1) The deposit is hosted by fining-upwards, right-way-up clastic sedimentary units that are dominated by plagioclase-rich intermediate to mafic volcanic and fine-grained pelagic sedimentary debris. These are distinctly different in composition from quartzose conglomerates, sandstones and shales of the proximal Badger Group.

2) The deposit lies in the core of a 2-3 km wavelength, tight, shallow to moderate Northeast-plunging anticline that folds the Upper Victoria Lake Supergroup, the black, pyritic Caradocian shale, and the Badger Group.

3) Two distinct styles of veining are recognized: stratigraphy discordant veins dominant at the Jaclyn Main and Christopher deposits, and stratigraphy parallel veins dominating at the Jaclyn North vein system. These have been inferred to represent: 1) vein systems developed roughly axial planar to regional anticlinal axes, and; 2) saddle-reef style veins developed along bedding surfaces in the limbs of the same regional folds.

4) Upright veins cross-cut bedding in the host sedimentary rocks at a high angle, trend $075-090^\circ$ and dip ca. $70-80^\circ\text{S}$. Jaclyn North veins roughly parallel bedding, similarly trend $075-090^\circ$ and dip $35-45^\circ\text{N}$.

5) Upright veins are subparallel to two distinct suites of dykes that exhibit well-defined chill margins; a) typically fine-

grained, flow-aligned basaltic andesite dykes with abundant saussuritized plagioclase, and; b) medium-grained clinopyroxene+plagioclase gabbro dykes that are commonly fresh.

6) Strong bleaching and alteration of host siltstones only occurs proximal ($\leq 2\text{m}$) to the veins, whereas spot-bleaching occurs more distally (\leq ca. 10m) and is commonly not spatially associated with quartz veining. Alteration in coarse-grained sedimentary rocks is subtle and is accompanied by an increase in sulfides (typically pyrite) along with chlorite+sericite (white mica) and carbonate.

7) Quartz veined, high-grade zones range up to 4 m but individual veins are typically $< 1\text{m}$ in thickness. These stylonitic and massive comb-textured veins containing abundant free gold and pyrite along with trace arsenopyrite, pyrrhotite, sphalerite and galena.

VIRS (VISUAL AND INFRARED SPECTROMETRIC ANALYSIS)

We have examined a range of selected drill core and outcrop samples using VIRS in conjunction with petrography. In drill hole GP07-86, unaltered host rocks generally reveal low reflectance, whereas spotty alteration is marked by spectra indicating the presence of sericite and iron-rich chlorite. With increasing depth, towards the quartz veins, there is a marked increase in iron as well as an increase in the amounts of illite and other clay minerals. Proximal to the quartz veining, spectra indicate carbonate alteration in the adjacent altered host rocks as well as within the veins. Moreover, the relative VIRS response of iron-rich chlorite increases significantly, however, only 1 m below the quartz veins, the host rocks are much less altered, and show little to no reflectance in the VIRS range.

In drill hole GP07-92, a strong VIRS response to sericite and chlorite occurs in host rocks up to 15 m structurally above a quartz vein intercept, whereas a sample of lithic greywacke, 5 m below a ca. 3 m wide quartz veined zone (22.2-25.9 m) yields

no VIRS response. This pattern is similar to that seen in GP07-86. A sample of similar greywacke (at a depth of ca. 44 m) having no proximal quartz veining, however, shows a sericite and chlorite VIRS signature comparable to that observed in rocks from immediately above the quartz veins. Clearly, detailed and systematic VIRS analysis of a number of representative drill holes may help clarify the nature and extent of the alteration and may provide a vector towards further hidden quartz veins.

LITHOGEOCHEMISTRY

Although preliminary in nature, lithogeochemical studies help to provide insight into the extent and nature of the alteration associated with mineralization. Quartz veins and their immediate altered wall-rocks, as well as having elevated Au, are typically enriched in As, Sb, Pb and Ag relative to visually unaltered rocks. Closer integration between VIRS, petrographic and electron microprobe analysis and lithogeochemistry may help elucidate the relative elemental variations associated with veining and alteration.

CONCLUDING STATEMENT

Field, drill hole, and limited petrographic information suggest that the mineralized systems at Golden Promise are comparable to turbidite-hosted gold mineralization of the Meguma Zone in Nova Scotia and those of southeastern Australia. Future work will incorporate ⁴⁰Ar-³⁹Ar geochronology, extensive regional and down-hole lithogeochemistry, mineral geochemistry, fluid inclusion and stable isotopic studies. These investigations will examine the relationships between the vein systems (mineralization), alteration and the two generations of cospatial mafic dykes. Significant attention will be directed to the origin and distribution of the notable "spotty" alteration in the host rocks, which may provide a vector towards such Au mineralization.

ACKNOWLEDGEMENTS

We thank Paragon Minerals Corporation and Crosshair Exploration & Mining Corporation for access to their drill holes and databases. Andy Kerr graciously reviewed an earlier version of this contribution.

REFERENCES

- COPELAND, D.A. & NEWPORT, A. 2005. Supplementary 2nd year assessment report on soil sampling, prospecting, geological mapping, trenching and diamond drilling on the Golden Promise Property, central Newfoundland NFLD/2910.
- EVANS, D.T.W. & KEAN, B.F. 2002. The Victoria Lake Supergroup, central Newfoundland - its definition, setting and volcanogenic massive sulphide mineralization. Open File NFLD/2790, 80 p.
- KEAN, B.F. & JAYASINGE, N.R. 1982. *Geology of the Badger Map area (12A/16), Newfoundland*. Newfoundland Department of Mines and Energy, Mineral Development Division, Report **81-2**, 37 p.
- PILGRIM, L.R. & GIROUX, G.H. 2008. *Form 43-101F1 technical report for the Golden Promise, south Golden Promise and Victoria Lake properties Badger, Grand Falls, Buchans and Victoria Lake areas (NTS 12a/06, 09, 10, 15, 16 and 02d/13), Newfoundland and Labrador*. SEDAR filing.
- ROGERS, N. & VAN STAAL, C. 2002. Toward a Victoria Lake Supergroup: a provisional stratigraphic revision of the Red Indian to Victoria Lakes area, Central Newfoundland. In: Current Research, Newfoundland Department of Mines and Energy Geological Survey, Report **02-1**, 185-195.
- ROGERS, N., VAN STAAL, C., & MCNICOLL, V.J. 2005. *Geology, Badger, Newfoundland and Labrador*; Geological Survey of Canada, Open File 4546, scale 1:50,000.
- WILLIAMS, S. H. & O'BRIEN, B. H. 1991. Silurian graptolites from the Bay of Exploits, north-central Newfoundland and their geological significance. *Canadian Journal of Earth Sciences* **28**, 1534-1540.
- WILLIAMS, H. 1995. Chapter 4 – Middle Paleozoic rocks. In: WILLIAMS, H. (ed) *Geology of the Appalachian-Caledonide Orogen in Canada and Greenland*. Geological Survey of Canada, Geology of Canada Series No. **6**, 315-446.

Cathodoluminescence: A tool to discriminate the tectonic history in gold-bearing veins in the Brunswick Subduction Complex, Canada

Sabine Schwarz¹, David Lentz¹, & James Walker²

¹*University of New Brunswick, Department of Geology, Fredericton, NB, E3B 5A3 CANADA
(e-mail: s.vetter@unb.ca)*

²*Geological Surveys Branch, Department of Natural Resources-Minerals, Bathurst, NB, E2A 3Z1 CANADA*

ABSTRACT: Transmitted light microscopy in combination with cathodoluminescence (CL) can be a useful tool for determining the tectonic history of hydrothermal veins. The Elmtree and Guitard Brook Au deposits that occur in the poly-deformed Ordovician sedimentary and volcanic rocks of the Elmtree Inlier, and its Silurian sedimentary cover sequence (northern New Brunswick), are the subject of this study. These occurrences are located on minor fault zones that contain at least four generations of quartz-calcite-sulfide veining. These veins contain pyrite, arsenopyrite, and chalcopyrite with small gold inclusions or refractory gold, as well as later base-metal veins with galena, sphalerite, and chalcopyrite. In this study, cathodoluminescence imaging using the Gatan Chroma-CL system in combination with the scanning electron microscope was applied to examine quartz veins from these two deposits.

Results indicate that in both deposits early quartz with growth textures outlined by blue/red CL colors likely formed during the Salinic Orogeny. Subsequently, these veins were brecciated and partly dissolved during the exhumation/ongoing orogeny resulting in metamorphic quartz (red-brown CL colors) in microfractures and microshear zones or as mantles on early quartz. Finally, late-stage quartz (bright yellow CL), occurring in veinlets and cutting earlier quartz, is likely related to hydrothermal intrusion-related base-metal quartz-carbonate veining.

KEYWORDS: *cathodoluminescence, Brunswick Subduction Complex, hydrothermal, orogenic gold, Elmtree Inlier*

INTRODUCTION

The Elmtree Inlier (EI) hosts more than 85 mineral occurrences or deposits, the majority of which can be linked to hydrothermal orogenic or intrusion-related systems. Two of these, the Elmtree deposit (ED) and the Guitard Brook occurrence (GB), are the most significant in terms of gold mineralization with best grades up to 23 g/t Au and 12 g/t Au, respectively. Mineralization at both deposits is hosted within shear zones and both display characteristics typical of hypozonal- to epizonal-orogenic gold systems. Late intrusion-related base-metal veins also occur at both the ED and GB.

The purpose of this study is to determine the relative timing of Au mineralization in the context of the regional tectonic history. This was accomplished by using cathodoluminescence to study gangue quartz in auriferous sulfide-quartz-carbonate veins.

GEOLOGICAL SETTING

The EI consists of mafic intrusive and extrusive rocks and related sedimentary rocks of the Fournier Group that were deposited in the Middle Ordovician Tetagouche-Exploits back-arc basin (Fig.1). Closure of the back-arc basin in the Late Ordovician to Early Silurian, resulted in the accretion of these rocks to Laurentia (Salinic Orogeny). The EI is the polydeformed imbricated thrust stack that resulted from obduction of the Fournier Group. The Fournier Group is divided into the Devereaux, Pointe Verte, and the Elmtree formations (van Staal & Fyffe 1991; Langton 1993; Fig. 1). The Belledune River Mélange (BRM) also occurs within the EI and is a tectonic unit that marks the thrust contact between the Elmtree and Pointe Verte formations (Fig. 1). The units are unconformably overlain by the Silurian Chaleurs Group sedimentary rocks (Fig. 1). Major and

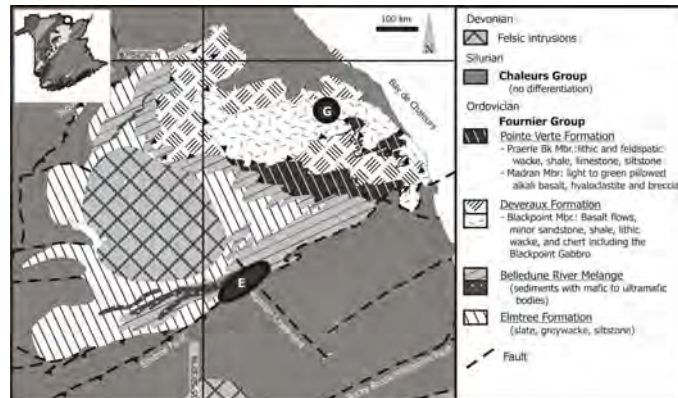


Fig. 4. Geological map of the Elmtree Inlier showing the Elmtree (ED) and Guitard Brook deposit (GB) located near faults (NBDNRE, 2005).

minor faults, such as the Elmtree and the Nigadoo lineament cut through the area. Late tectonic felsic intrusions are related to the accretion of the Avalonian microcontinent during the Acadian Orogeny in the Middle Devonian.

DEPOSITS

The ED, located in the southern EI, is divided into West Gabbro, Discovery, and South Gold zones that are hosted by the BRM, the Elmtree Formation, and/or by the Chaleurs Group. The Discovery Zone (DZ) consists of several zones of poly-metallic base-metal veins, whereas the South Gold Zone and WGZ consists of fine-grained disseminated sulfides and very minor base-metal veins.

The Guitard Brook deposit (GB) located in the northeast EI is hosted by tholeiitic basalt and gabbro of the Devereaux Formation, specifically the Black Point Gabbro and associated trondhjemitic, diabasic dykes, and basaltic flows (Langton, 1993).

The GB mineralization is characterized by narrow veins concentrated in several larger zones each approximately 50 cm wide and 60 m long, all of which occur within a larger shear zone.

METHODS AND RESULTS

Cathodoluminescence activates electrons in the mineral, which then emit characteristic light rays of distinct wavelengths that can be collected with the CL system. CL imaging is used to

recognize subtle variation (i.e., growth zoning) in quartz (and other phases) as defined by crystal defects and/or minor variation in trace element contents all of which result in variation in CL color. This method can be used to determine mineral paragenesis and link various stages of mineralization (i.e., different pulses of mineralizing fluid) with different stages in the regional tectonic history.

This study relied on a combination of transmitted light- and scanning electron-microscopy (SEM) and cathodoluminescence (CL) imaging in order to determine textural relationships that are indiscernible using normal (visible spectrum) light microscopy or with the backscattered SEM alone. The SEM used in this study was equipped with a Gatan Chroma-Cathodo-luminescence mirror operating at 15nA and a current of 15kV. The CL was captured live and mixed into color images using DigiScan software.

The CL images and colors were compared to literature (Table 1). Normally hydrothermal quartz shows short-lived green to blue or yellow (high temperature related) colors whereas red and intense blue CL colors stand for volcanic related quartz. Brown to red CL imaging quartz is related to metamorphism.

Work concentrated on gangue quartz in main gold-bearing sulfides veins, and in late stage intrusion-related (?) base-metal veins. Polished sections were first investigated by transmitted and reflected light microscopy to find suitable samples

Table 1. Cathodoluminescence colors of quartz (and inferred geologic environment) from the Elmtree Deposit (ED) and Guitard Brook occurrence (GB).

CL color	Environment	Seen in	Ref.
Intense blue	Igneous, volcanic	ED	1, 2, 3
red to red brown	metamorphic	ED, GB	1, 2, 3
Red	volcanic	GB	1, 3
Transient blue	alpha-quartz in aqueous solutions	ED, GB	1, 3
Short lived green/blue	hydrothermal, pegmatitic	ED, GB	2, 3
Yellow	hydrothermal	ED, GB	3

1) Boggs & Krinsley (2006), 2) Zinknagel (1978), 3) Goetze *et al.* (2005)

containing different phases of veining and (or) gold grains.

Five different vein phases (Types I to V) are recognized at both deposits, all have variable amounts of carbonates and quartz gangue. Type I veins contain only brecciated quartz and carbonate minerals and at ED are spatially associated with disseminated arsenopyrite, chalcopyrite, pyrrhotite, and pyrite in the mafic host rock. Type II veins in both deposits are partly brecciated and contain 5-80% sulfides of dominantly pyrite, arsenopyrite, and at GB chalcopyrite. Type III veins are quartz–calcite–tetrahedrite–bismuthinite microveins that cut both Types I and II veins. The fine-grained sulfides replace and enclose arsenopyrite and pyrite in Type II veins and are also visible in microfractures within the Type II sulfides. Type IV veins are base-metal rich and characterized by galena, sphalerite, chalcopyrite, pyrite, and stibnite with a maximum width of 20 cm. The Type V veins are late barren-carbonate veins cutting all previous veins and textural features.

In both deposits, refractory gold occurs in arsenopyrite and pyrite of Type II veins analyzed by EPMA. At GB, gold is also located in chalcopyrite as electrum microinclusions.

At ED, Type I and Type II veins contain primary quartz cores that have blue to green CL colors, which define subtle

growth zoning. The early quartz was brecciated, partially dissolved and mantled by a matrix of fine-crystalline metamorphic quartz (brown CL; Table 1). The metamorphic quartz contains small crystals of apatite with bright blue CL colors. Bright yellow CL colored quartz veinlets cutting Type II veins are a sign of later hydrothermal fluid, likely related to late brittle-ductile deformation and infilling of fractures by fluids. Similar CL features are observed in quartz from Type IV base-metal veins. Here unbrecciated quartz (blue CL), with growth zoning mantles sulfides. Dark blue CL quartz from Type IV veins is in contact with quartz and red luminescent calcite from the Type II veins and is characterized by less brecciation than the Type II vein quartz. A later hydrothermal quartz veinlet (yellow CL), fills a fracture that developed during tectonic stress between quartz and sulfide.

Cathodoluminescence images from the GB deposit show primary quartz of Type II veins (blue CL), with visible growth zoning in CL. These are crosscut by later hydrothermal Type III vein quartz that exhibits growth textures in short-lived blue and red CL colors. Both Type-II and -III veins are weakly to moderately brecciated and are overprinted by later fluids that modified the primary quartz to red and/or yellow hydrothermal quartz characteristic of higher temperature and likely reflects

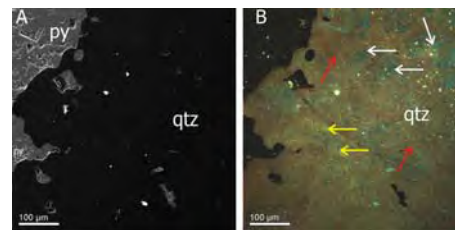


Fig. 5. (A) Backscattered SEM image of quartz (qtz) and pyrite (py) from the ED showing no textures, (B) CL imaging of area in (A) showing blue-green growth textures in primary quartz (top right, white arrows) surrounded by fine-grained metamorphic brown quartz (red arrows). Hydrothermal quartz veinlets (yellow CL) cut through the section (yellow arrows). Sample is from DDH DZ-2006-05 at 61.00 m.

interaction with a fluid of volcanic hydrothermal origin (Fig. 3; Table 1). This is also visible in quartz from Type II veins that are overprinted by metamorphic quartz with red-brown luminescence. Later hydrothermal quartz (bright yellow CL) also occurs at GB as thin fractures in and between the early and metamorphic quartz (red-brown CL).

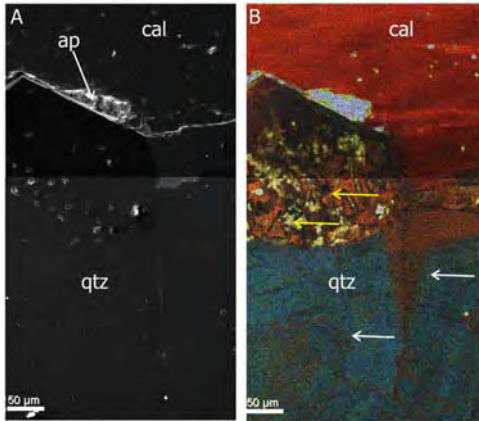


Fig. 6. (A) Backscattered SEM image of quartz (qtz) from GB, (B) CL imaging of (A) showing green-blue to red growth textures (white arrows), and a red calcite (cal). The contact is marked by yellow and red hydrothermal quartz (yellow arrows) Sample is from DDH HM-2003-08 at 53.04 m.

CONCLUSIONS

The results of the CL study for the ED and GB deposits are summarized as follows:

- (1) Hydrothermal euhedral quartz (blue-green/red CL colors), of Type II veins exhibit growth textures and are related to sulfide mineralization during early Salinic Orogeny.
- (2) The microbrecciation and dissolution of primary quartz in Type II and IV veins and subsequent overprinting by metamorphic quartz (red-brown CL), is attributed to the ongoing Salinic Orogeny and exhumation of the Brunswick Subduction Complex.
- (3) Later volcanic/hydrothermal base metal-containing quartz-carbonate bearing Type IV veins are recognized as thin veinlets with bright yellow CL color. These are likely related to epizonal mineralization during the emplacement of middle Devonian felsic intrusions.

ACKNOWLEDGEMENTS

We thank the Department of Natural Resources for funding this project and for logistical support. Additional funding was provided with a NSERC Discovery grant to DL.

REFERENCES

- BOGGS, S. & KRINSLEY, D. 2006. *Application of cathodoluminescence imaging to the study of sedimentary rocks*, Schweizerbart'sche Verlagsbuchhandlung, 165p.
- GOETZE, J., PLOETZE, M., & TRAUTMANN, T., 2005. Structure and luminescence characteristics of quartz from pegmatites. *American Mineralogist*, **90**, 13-21.
- LANGTON, J. P. 1993. *Stratigraphy, structure, and geochemistry of the ophiolitic inlier, Northern New Brunswick*. Unpublished MSc thesis, Queen's University.
- NBDNRE 2005. Bedrock Geology of New Brunswick, Map NR-3, Scale 1:20000, New Brunswick Department of Natural Resources and Energy.
- VAN STAAL, C.R., WHALEN, J.B., MCNICOLL, V.J., PEHRSSON, S.J., LISSEBERG, C.J., ZAGOREVSKI, A., VAN BREEMEN, O., & JENNER, G.A., 2007. The Notre Dame arc and the Taconic Orogeny in Newfoundland. In: Hatcher, Jr., Carlson, M.P., McBride, J.H. and Martínez Catalán, J.R. (ed), *The 4D Framework of Continental Crust*, Geological Society of America Special Paper, **200**, 511-552.
- ZINKNAGEL, U. 1978. *Cathodoluminescence of quartz and its application to sandstone petrology*. Contributions to Sedimentology, 65 p.

Ireland's historic mine sites inventory

Gerry Stanley¹, Eibhlin Doyle¹, Vincent Gallagher¹,
Fionnuala Ni Mhairtin¹, & Jane Brogan²

¹Geological Survey of Ireland, Beggars Bush, Haddington Road, Ballsbridge, Dublin 4, Ireland
(e-mail: gerry.stanley@gsi.ie)

²Environmental Protection Agency, PO Box 3000, Johnstown Castle Estate, Co. Wexford, Ireland

ABSTRACT: Ireland has a long history of mining dating back to the Bronze Age. The main commodities exploited included Cu, Au, Pb, Zn and coal. Many of the early mines consisted of small vein type deposits, whereas more recent mining (20th century) has included exploitation of VMS and Irish Type Zn/Pb deposits using modern mining and processing techniques at industrial scales. Many of these historic mines were abandoned or closed with little or no remediation. The Historic Mine Site Inventory project aimed to compile a comprehensive list of all past mining sites which are now abandoned or closed. One of the principal drivers for this project was Directive 2006/21/EC of the European Parliament and of the Council on the management of waste from the extractive industries. A relative scoring system was developed which used the source, pathway, receptor paradigm. Over one hundred individual mine sites were assessed, in some cases mine sites were grouped into districts where appropriate resulting in 27 mine sites/districts. This paper will present the scoring system that was developed and the overall results of the project.

KEYWORDS: *Ireland, closed mines, environment, risk categorization*

INTRODUCTION

The European Union passed the 'Extractive industries waste directive' in 2006. The full title of the directive is:

'Directive 2006/21/EC of the European Parliament and of the Council on the management of waste from extractive industries and amending Directive 2004/35/EC'

Most of the directive deals with how extractive industry waste is to be dealt with in the future within Member States. However, one article addresses legacy waste facilities by requiring Member States to draw up an inventory of such facilities. The text of Article 20 is:

'Member States shall ensure that an inventory of closed waste facilities, including abandoned waste facilities, located on their territory which cause serious negative environmental impacts or have the potential of becoming in the medium or short term a serious threat to human health or the environment is drawn up and periodically updated. Such an inventory, to be made available to the public, shall be carried out by 1

May 2012, taking into account the methodologies as referred to in Article 21, if available.'

The reference to Article 21 relates to the methodology to be used in drawing up the inventory. Specifically:

'Such methodologies shall allow for the establishment of the most appropriate risk assessment procedures and remedial actions having regard to the variation of geological, hydrogeological and climatological characteristics across Europe.'

A waste facility is defined in the directive as:

'waste facility" means any area designated for the accumulation or deposit of extractive waste, whether in a solid or liquid state or in solution or suspension.

Such facilities are deemed to include any dam or other structure serving to contain, retain, confine or otherwise support such a facility, and also to include, but not be limited to, heaps and ponds, but excluding excavation voids into which waste is replaced, after

extraction of the mineral, for rehabilitation and construction purposes’.

For practical purposes this means any tailings facility or rock tip or heap – whether either is contained or not.

The GSI (Geological Survey of Ireland) and the EPA (Environmental Protection Agency (of Ireland)) embarked upon creating this inventory in 2006 for those waste facilities associated with closed or abandoned metal, industrial mineral and coal mines. The project was completed in early 2009 and is known as the Historic Mine Site – Inventory and Risk Categorization project or HMS for short.

SITE PRE-SELECTION

The known number of mineral deposits worked in Ireland runs to several hundred. It would be impractical to include every site in the inventory, especially as the inventory has to include aggregate and stone operations as well. Indeed, another Member State (Italy) has records of over 20,000 stone operations and over 3,000 metal mines.

As a starting point the GSI, like most geological surveys, has a mineral locality database. The database contains records for some 5,000 individual sites ranging in size from the recordings of field geologist of outcrop description of sphalerite occurrences to the largest zinc mine in Europe – the Navan deposit in Co. Meath operated by Boliden Tara mines Limited. Also in the database are records relating to aggregates quarries and sand and gravel pits. Below is a list of the locality type and the number of locations within each category.

The entries shaded are candidate sites for inclusion in the inventory giving a total of 460 (mine and tip heap/spoil) plus the unknown category (511 locations) giving a total of some 971 sites.

Next ‘expert knowledge’ was used to reduce further the number of sites to be included in our investigations. This involved GSI staff with knowledge of mining in Ireland assessing the 971 localities and from their knowledge of the sites determining whether the site was

Locality Type	No.
Borehole	206
Coastal section	6
Float.....	30
Man-made excavation	32
Mine.....	456
Natural exposure	1,916
Other.....	35
Pit	554
Quarry.....	1,297
Sub outcrop	16
Temporary exposure	2
Tip heap/Spoil	4
Unknown	511
Well.....	6
Total.....	5,071

sufficiently significant for inclusion. Significance was determined by reference to the mineral worked at the site and the size of the operation. This resulted in some 106 individual sites being visited in the field.

Several of these sites occur in clusters and for ease of working a District name was given to these. This was especially the case for the coalfields. A number of the sites did not warrant inclusion in the inventory as all evidence of mining has been removed and any waste at the sites either removed for other uses nearby, such as filling in subsidence features caused by the former mine activity or had been completely remediated and in either case the waste material is indistinguishable from the surrounding countryside. When both of these factors are taken into account 27 mine districts and individual mines were include in the inventory with reports generated for some 82 sites.

ASSESSMENT METHODOLOGY

The HMS Project created an inventory of closed mine waste facilities on a risk basis. However, it is emphasized that this is NOT a risk assessment of the sites. Rather the sites have been ranked on a risk basis so as to determine a relative ranking.

At each mine site all waste heaps, tailings facilities and discharges are

identified and scores assigned based on the parameters to be measured.

In order to carry out the field work a systematic method was needed so a Generalized Conceptual Model was developed. This guided data collection in the field but would not be so rigid as to prevent the recoding of features unique to any one site. Later a conceptual model may assist with the identification of remedial strategies.

Conceptual Model

The conceptual model uses the Source – Pathway – Receptor Paradigm. The paradigm requires that each of the parameters within the model are documented, estimated, measured or recorded. The model identifies the source of any contamination; identifies who or what is affected (the receptor); and identifies how the source may reach the receptor (pathway). The collection of field data, observations and estimates confirms whether a linkage exists between the source and receptor.

Sources are the origin of contaminants that may issue from an historic mine site. The cause or source of the contamination is identified as well as its location. The possible sources of contamination are:

Liquid (water): - Adit discharges and Seeps.

Solids: - Waste piles, Tailings impoundments and Stream sediments.

Receptors are those elements of the paradigm that are affected by the potential contamination emanating from the various sources via the different pathways. A receptor is any person, animal, plant, ecosystem, waterbody, protected site, or property. Receptors, in the context of the Historic Mine Site project include:

People: - Local inhabitants, Workers and Visitors to the site

Farm animals: Livestock

Ecosystems and waterbodies: -

Rivers, Estuaries and Groundwater.

Protected areas: - National Parks, National Heritage Areas (NHAs), Special Protection Areas (SPAs),

Special Areas of Conservation (SACs) and Nature Reserves

Five pathways were assessed during the project: Groundwater, Surface water, Air pathway, Direct contact, and Stream sediments.

Scoring System

Each of the inputs to the paradigm is scored. In the first instance a hazard score is developed for each source. The hazard score is determined from the amount of contaminants, the relative toxicity of these contaminants and the volume (or area) within each source.

Next the **Likelihood of release**, of a contaminant, from a waste pile or discharge is considered. It is an assessment of whether there have been releases of contaminants to the environment in the past and addresses whether the waste pile or discharge is in any way contained. The former determines whether there have been releases of the contaminants from the mine site in the past while the latter issues may affect whether there is likely to be releases from the source in the future. In all cases any contaminant must be attributable to the mine site.

The individual waste facilities are characterised so that a **Hazard** number is developed. This is then modified by the **Likelihood of release** and **Receptor** factors for each Pathway. Once the final score for the mine site is obtained it is assigned to one of the following groups (Table 1)

RESULTS

Of the 27 individual districts/sites investigated, three are classified in the Group I, one in Group II, two in Group III, five in Group IV and the remaining 16 as Group V (Table 2).

ACKNOWLEDGEMENTS

We would like to thank Roger Olsen, Jim Lavelle, Paul Nathanail, Jimmy McLaughlin, and Tessa Grealley for useful discussions in the development of the scoring system.

Table 1. Groups into which the closed mine sites are classified.

Group	Score	Description
I	>2,000	Sites which should have a full site specific risk assessment carried out.
II	1,000 – 2,000	Sites requiring general monitoring of most or all waste piles, discharges or stream sediments on an annual basis.
III	300 – 1,000	Sites requiring general monitoring of most or all waste piles, discharges or stream sediments on a biennial basis.
IV	100 – 300	Sites requiring specific monitoring on particular waste piles, discharges or stream sediments on a five yearly basis.
V	<100	Sites not requiring any specific monitoring.

Table 2. Closed Irish mine sites classified in this study.

Mine / District	No. of Sites	Total Score	Group
Silvermines	6	2,884	I
Tynagh	4	2,712	I
Avoca	7	2,439	I
Glendalough /Glendasan	8	1,122	II
Caim	1	559	III
Glenmalure	2	335	III
Ballycorus	1	244	IV
Connaught Coalfield	7	189	IV
Gortdrum	1	157	IV
Leinster Coalfield	7	133	IV
Slieve Ardagh Coalfield	10	118	IV
Clements (Connemara Pb)	1	97	V
Kilbricken (Clare Pb)	1	89	V
Allihies	6	76	V
Abbeytown	1	70	V
Tassan (Monaghan Pb)	1	44	V
Ballyvergin (Clare Pb)	1	43	V
Ballyhickey (Clare Pb)	1	19	V
Keeldrum (Donegal Pb)	1	18	V
West Cork Cu-Ba	8	17	V
Doolin (Clare Phosphate)	1	15	V
Bunmahon	1	14	V
Hope (Monaghan Pb)	1	13	V
Clontibret (Monaghan Pb)	1	12	V
Glentogher (Donegal Pb)	1	6	V
Benbulbin	1	5	V
Hollyford (Tipperary)	1	4	V

Metallogeny of the gold-enriched Cambro-Ordovician rocks in the Annidale area, south-central New Brunswick, Canada

Kathleen G. Thorne¹, Susan C. Johnson²,
Malcolm J. McLeod², & Leslie R. Fyffe¹

¹New Brunswick Department of Natural Resources, Geological Surveys Branch, PO Box 6000, Fredericton, NB E3B 5H1 CANADA (e-mail: kay.thorne@gnb.ca)

²New Brunswick Department of Natural Resources, Geological Surveys Branch, PO Box 5040, 207 Picadilly Road, Sussex, NB E4E 5L2 CANADA

ABSTRACT: Gold occurrences are prolific throughout the Cambro-Ordovician volcanic, sedimentary, and intrusive rocks of the Annidale area in south-central New Brunswick. The majority of gold occurrences are structurally controlled by regional northeast-trending thrusts related to telescoping of the stratigraphic succession, subsequent strike-slip faulting (and associated shear zones), and late, north- to northwest-trending normal faults that generated relatively minor displacements along the northeast-trending structures. A spatial association with rhyolite dome complexes is established for some of the gold occurrences. The characteristics of gold mineralization vary, depending on the host rocks, structural setting, and proximity to felsic intrusions. Stable isotope studies (O, Pb, S) indicate that the majority of occurrences have features typical of orogenic gold systems derived from metamorphic fluids whereas others are clearly derived from magmatic fluids, which is consistent with field observations. Timing of these mineralizing events has been constrained to Late Cambrian to Middle Ordovician time, with possible remobilization into the later north- to northwest-trending structures.

KEYWORDS: *gold, Annidale, New Brunswick, Ganderia, stable isotopes*

INTRODUCTION

In the Annidale area in south-central New Brunswick, 37 metallic mineral occurrences/prospects are concentrated within a 50 km long northeast-trending belt of Early Cambrian to Middle Ordovician volcano-sedimentary and intrusive rocks. The majority of these occurrences contain gold, in some cases significant quantities, in addition to base-metals, antimony, and/or silver. Mineralization spans the entire length of the belt and is primarily located along major structural features and/or situated peripheral to felsic dome complexes or intrusions within the Annidale Group. We propose that gold-enriched fluids were focussed into favourable depositional environments during mineralizing events associated with episodic tectonic and magmatic activity throughout the belt. This paper will provide a brief overview of the geological setting of the Annidale area, the various styles of gold mineralization present, and provide

isotopic constraints on the mineralizing conditions and source(s) of the fluids.

GEOLOGICAL SETTING

Regional Geology

Neoproterozoic to Early Paleozoic rocks of the Annidale area are interpreted to mark the southeastern margin of Ganderia in the New Brunswick segment of the northern Appalachians (Johnson *et al.* 2009). The area is underlain by Late Cambrian to Early Ordovician rocks of the Annidale Group and Late Neoproterozoic to Early Cambrian rocks of the Belleisle Bay Group, which are juxtaposed along a major tectonic boundary marked by the Taylor Brook Fault (Fig. 1).

Volcanic rocks of the Annidale Group are mostly arc type but an unusual group of high-Mg, high-Cr basalts with geochemical characteristics typical of normal mid-ocean ridge basalts (MORB) and within-plate types are also

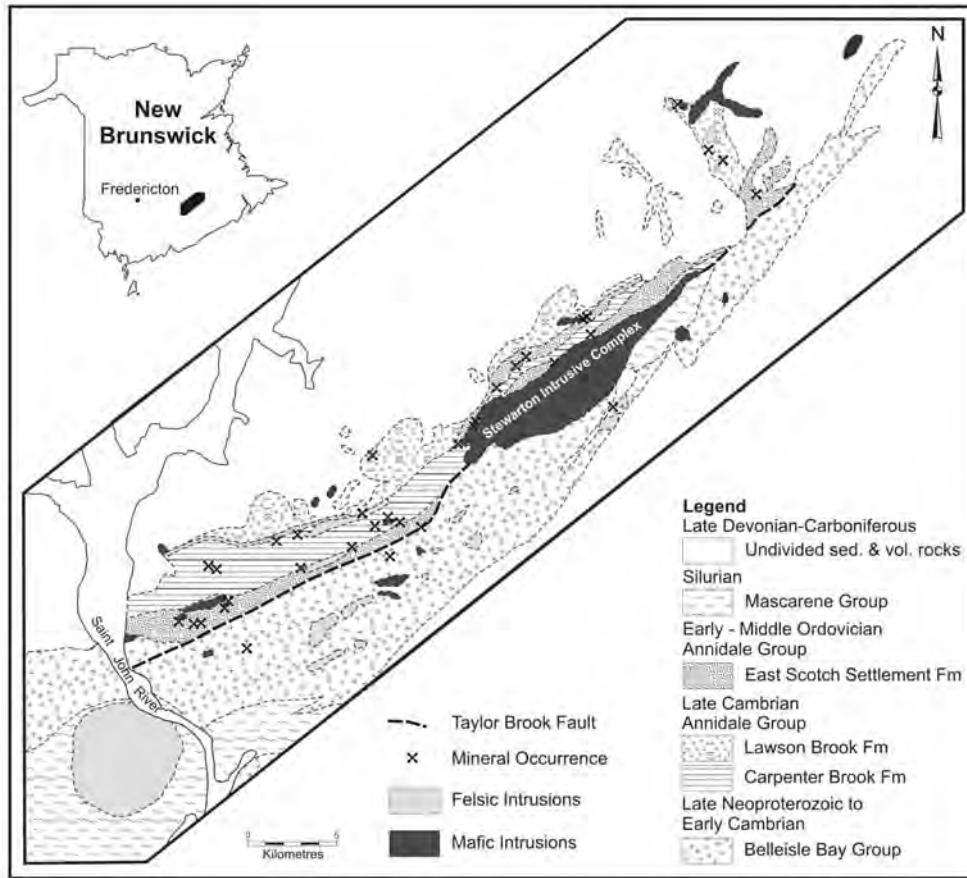


Fig. 1. Geology of the Annidale area showing the distribution of mineral occurrences throughout the belt (Johnson *et al.* 2009).

present (McLeod *et al.* 1994; Johnson *et al.* 2009). The mixed MORB and arc signature is consistent with deposition in a back-arc basin tectonic setting, with the MORB rocks indicating possible closure of a small ocean basin (McLeod *et al.* 1994; Johnson *et al.* 2009). The volcanic rocks of the Belleisle Bay Group primarily exhibit within-plate characteristics (Johnson & Barr 2004).

Local Geology

Bedrock in the Annidale area is dismembered into several northwesterly transported thrust panels that contain stratigraphic packages, which differ in lithology, age, and intensity and style of deformation. Three formations comprise the Annidale Group (from oldest to youngest): the Carpenter Brook, Lawson

Brook, and East Scotch Settlement formations (Johnson *et al.* 2009). The Carpenter Brook Formation consists of sedimentary and volcanoclastic rocks intercalated with felsic flows and lapilli tuffs, and associated microgranite. The Lawson Brook Formation comprises mafic volcanic rocks, felsic flows and tuffs, and associated microgranite with subordinate black shale and siltstone. The East Scotch Settlement Formation consists of mafic volcanic rocks and black shales. Telescoping of the stratigraphic succession produced an imbricated assemblage consisting of numerous thrust faults, many of which have been later reactivated into steeply dipping strike slip faults. A number of felsic and mafic intrusions were emplaced into the sequence between Late Cambrian to

Silurian time, the largest of which is the Stewarton Gabbro (Fig. 1). A latest Arenig (Ordovician) age for the Stewarton Gabbro constrains the timing of tectonic interleaving of the Annidale Group and its juxtaposition with the Belleisle Bay Group to the Early Ordovician.

METALLOGENY

Mining activity in the Annidale area has been restricted to limited copper and silver extraction from the Annidale Mine in the early 1900's. Exploration was sporadic until the late 1980's-early 1990's when several mining companies were actively exploring for gold and base-metals. Several significant gold discoveries were encountered during that time, the most notable being a grab sample that yielded >200 g/t Au at the Devil Pike Brook occurrence (PGE Resources Corporation 1993). Chip and grab samples from the East Scotch Settlement - BP (BP Resources 1991) and Grant Brook West (Brunswick Mining and Smelting 1992) occurrences also contained >1 oz/t Au. Subsequent trenching and drilling programs were implemented throughout the belt; however, falling metal prices shortly thereafter hampered further exploration efforts in the area.

The composition and competence of the host rocks, structural setting, and in some cases, proximity to felsic intrusions appear to be the main factors controlling gold mineralization. The majority are structurally controlled by northeast-trending thrust and strike-slip faults within the highly deformed panels containing the East Scotch Settlement and Carpenter Brook formations (i.e., Taylors Brook, East Scotch Settlement - BP, and Grant Brook West). To a lesser degree, occurrences are associated with later north- to northwest-trending normal faults (i.e., Sheba Pit and Devil Pike Brook) that locally offset the northeast-trending faults. A few select occurrences are situated peripheral to (and appear to be associated with) felsic dome complexes (i.e., Jones Creek and Grant Brook Central).

Gold mineralization manifests itself as shear zone-hosted quartz (\pm carbonate)

veins and/or disseminated mineralization mainly within altered wall rocks. Pyrite and arsenopyrite are commonly associated with the mineralized zones but base-metal sulfides, stibnite, and silver-bearing minerals may be present as well. Alteration assemblages broadly consist of some combination of quartz, carbonate, sericite, fuchsite, and/or leucoxene.

The gold occurrences can generally be classified into two different categories based on their mode of occurrence: those with characteristics typical of orogenic mesothermal lode gold systems and those that have an obvious genetic association with felsic dome complexes. However the alteration assemblages for either deposit type are not diagnostic because of the complexity of the hosting bedrock geology, which ultimately controls the resulting alteration assemblage.

ISOTOPE STUDIES

In an attempt to establish the fluid and metal sources and to help constrain a genetic model, stable isotope studies (O, Pb, S) were conducted on selected occurrences. Oxygen isotope analysis of quartz vein material from eight separate occurrences yielded $\delta^{18}\text{O}$ values of 10.9-16.0‰. Assuming equilibrium between quartz and the hydrothermal fluid, the $\delta^{18}\text{O}$ values calculated for the mineralizing fluids, at temperatures between 300-400°C, range between 4.0 and 11.9‰. This overlaps accepted values for both magmatic and metamorphic fluids.

Based on contrasting common lead isotope signatures from five Pb-bearing occurrences (East Scotch Settlement - BP, Scotch Mountain, South Fuchsite Zone, Grant Brook West, and Taylors Brook), it is apparent that the mineralized fluids are compositionally distinct for each occurrence. For the most part, the sources of lead appear to be derived from a variety of reservoirs, which is likely a reflection of the heterogeneity amongst the hosting lithologies for each occurrence.

Results of $\delta^{34}\text{S}$ analyses obtained for 12 sulfide separates ranged between -3.90‰ and +12.00‰. Samples with $\delta^{34}\text{S}$ values that clustered around 0‰ are presumed to

contain S from an igneous source (i.e., a direct magmatic source or the leaching of S from preexisting igneous rocks). Those with more enriched $\delta^{34}\text{S}$ values are inferred to have S leached from the local sedimentary country rocks by metamorphic fluids. For the most part, the S isotope results thus broadly delineate two groupings, which confirms the presence of two gold deposit types (intrusion-related and mesothermal orogenic).

DISCUSSION

The Taylor Brook Fault is thought to have played a major role in focusing fluids into subsidiary structures during stacking and dehydration of the stratigraphic sequences thus generating the various orogenic gold systems. Overprinting of these systems by younger intrusion-related gold systems is possible to some extent. Because of the complexity of alteration and sulfide assemblages observed in the field, isotope studies combined with mode of occurrence are key to distinguishing between the two deposit types. Gold mineralization located along late northwest-trending faults may represent younger mineralizing systems or possible remobilization of older deposits.

CONCLUSIONS

Gold occurrences within the Annidale area:

- (1) were deposited along structural features during episodic orogenic and magmatic activity between 490 and 478 Ma;
- (2) are characterized by quartz-carbonate veining and/or replacement styles of mineralization;
- (3) can be categorized as mesothermal orogenic or intrusion-related gold systems

based on mode of occurrence and isotopic signature.

ACKNOWLEDGEMENTS

We thank Greg Dunning (Memorial University of Newfoundland.) and Jonathan LaFontaine (student) for their assistance.

REFERENCES

- BP RESOURCES 1991. Report on prospecting, trenching, channel and soil sampling for the Stewarton claims. New Brunswick Department of Natural Resources Assessment File 474057.
- BRUNSWICK MINING AND SMELTING 1992. Report of Work, Annidale Property – Project 4247, Queens County, New Brunswick. New Brunswick Department of Natural Resources Assessment File 474233.
- JOHNSON, S.C., MCLEOD, M.J., FYFFE, L.R., & DUNNING, G.R. 2009. A Penobscottian arc system along the margin of Ganderia: evidence from geochemistry and U-Pb zircon dating of the Annidale Group in southern New Brunswick. *Atlantic Geoscience Society 35th Colloquium, Program and Abstracts*, 18.
- JOHNSON, S.C. & BARR, S.M. 2004. New geochemical data from Neoproterozoic-Cambrian igneous rocks in the Long Reach area, southern New Brunswick. New Brunswick Department of Natural Resources, MRR 2004-4, p. 75-94.
- MCLEOD, M.J., WINCHESTER, J.A., & RUITENBERG, A.A. 1994. Geochemistry of the Annidale Group: implications for the tectonic setting of Lower Ordovician volcanism in southwestern New Brunswick. *Atlantic Geology*, **30**, 87-95.
- PGE RESOURCES CORPORATION 1993. Report of work Devil Pike property Kings County, New Brunswick. New Brunswick Department of Natural Resources, Assessment File 474299.

Early Devonian felsic volcanic rocks and associated Zn–Pb mineralization, Tobique–Chaleurs Zone, New Brunswick, Canada

James A. Walker¹

¹New Brunswick Department of Natural Resources, Geological Surveys Branch,
P.O. Box 50, Bathurst, New Brunswick, E2A 3Z1 CANADA (e-mail: jim.walker@qnb.ca)

ABSTRACT: Early Devonian felsic volcanic rocks of the Tobique–Chaleurs Zone (TCZ) are host to several syngenetic to epigenetic Zn–Pb ± Cu and Ag deposits that span a wide range of size and grade. The largest deposit is Nash Creek (3.2 Mt grading 4.67% Zn, 0.80% Pb, and 27.8 g/t Ag), whereas the smallest and highest grade deposit is at Sewell Brook (≈ 0.5 Mt with grades locally >40 wt.% Zn+Pb). With the exception of Sewell Brook, which has a small Cu-rich zone, these deposits have Zn/Pb ratios ≥ 4 and have low Cu. All of the deposits are spatially associated with high SiO₂ (≥ 70 wt.%) aphyric to sparsely feldspar-phyric rhyolite flows or domes, and at least two are spatially associated with rocks of more intermediate (rhyodacite) composition.

The rocks of the TCZ are interpreted to have erupted in a transtensional continental rifting environment in the Late Silurian to Middle Devonian. In this tectonic environment A-type granites are expected, and indeed the relatively high Zr, Nb, and Y content in these rocks support this. However, many other geochemical aspects of these rocks, i.e., high Ba, Rb, Th and K, are more typical of the I-type magmas that commonly occur in collisional settings.

KEYWORDS: *Zn-Pb sulfide, VMS, I-type granites, New Brunswick*

INTRODUCTION

The Siluro-Devonian Tobique–Chaleurs Zone (TCZ) of New Brunswick is host to several relatively small Zn–Pb ± Cu–Ag sulfide deposits and occurrences that are all spatially associated with Early Devonian felsic volcanic and related sedimentary rocks (Fig. 1). The sulfide mineralization occurs as veins, veinlets and replacements of rock units that had high primary permeability (e.g., flow top breccias). Massive bedded sulfides that are typical of many modern and ancient VMS deposits are not present; however, their absence is not surprising given the relatively shallow oxidizing marine conditions at that time; therefore, the TCZ deposits belong to that part of the VMS family formed beneath the seafloor. This study was undertaken to assess the nature of the felsic volcanic host rocks and their control on mineralization.

GEOLOGICAL SETTING

The TCZ extends from the Gaspé Peninsula of Québec in the northeast to the State of Maine (USA) in the

southwest, and is dominated by bimodal volcanic and interlayered fine- to coarse-grained sedimentary rocks. In New Brunswick the TCZ is divided into northern and southern parts by the Rocky Brook–Millstream Fault (Fig. 1).

In the northern part of the TCZ, the Chaleurs Group comprises subaerially deposited, Late Silurian bimodal volcanic rocks that overlie early Silurian shallow marine fine- to coarse-grained clastic and carbonate sedimentary rocks. The Chaleurs Group is overlain disconformably by bimodal volcanic rocks and interlayered sandstones and siltstones of the Dalhousie Group.

In the southern TCZ only Early Devonian rocks are exposed, and all of them are assigned to the Tobique Group. The Tobique and Dalhousie groups are in part coeval and are similar in terms of rock types. The depositional environment for the Tobique Group is, for the most part, thought to be outer shelf or slope based on sedimentary bed forms and ichnofauna and the presence of abundant pillow lava and hyaloclastite in mafic volcanic units. In

contrast, the Dalhousie Group was deposited in a shallow marine to locally subaerial setting.

There are three common Acadian structural elements in the TCZ; 1) north-northeast trending, doubly-plunging shallow folds of km-scale amplitude, which control the distribution of rock units; 2) east-west striking, normal to oblique faults at high angles to regional stratigraphy; and 3) north-northeast striking, belt-parallel faults. Throughout the TCZ the level of erosion is generally shallow, an interpretation that is supported by the low metamorphic grade (zeolite facies) and absence of coeval plutons; however, limited vitrinite reflectance data from the northern TCZ suggests variable degrees of thermal alteration.

The volcanic rocks of the TCZ are interpreted to have erupted in a continental rift setting. Rifting was triggered by transpression resulting from oblique collision of the Miramichi Zone (Ganderia), with the North American Plate (Laurentia), during the final stages of closure of the Iapetus Ocean, including the Tetagouche–Exploits back-arc basin (Dostal *et al.* 1989).

MINERALIZATION

Within the TCZ there are five significant Zn–Pb sulfide deposits/occurrences. These vary greatly in terms of grade and size. The largest is Nash Creek (≈ 3.2 M tonnes grading 4.67% Zn, 0.80% Pb, and 27.8 g/t Ag), The other deposits are Mount Costigan (7.1% Zn, 2.13% Pb, and 16.32g/t Ag over 7.5 m), Sewell Brook ($\approx 25,000$ t grading 20% Zn+Pb), Gravel Hill (best assays $\approx 10\%$ Zn+Pb), and Shingle Gulch East (large tonnage, low grade ($< 2\%$ Zn+Pb)). Interestingly, all five of these deposits are spatially associated with Lower Devonian felsic volcanic rocks, in particular high SiO₂ (>70 wt.%) rhyolite. At Nash Creek there are also minor volumes of more intermediate lavas (rhyodacite) whereas, the host sequence at Sewell Brook is dominated by rhyodacite.

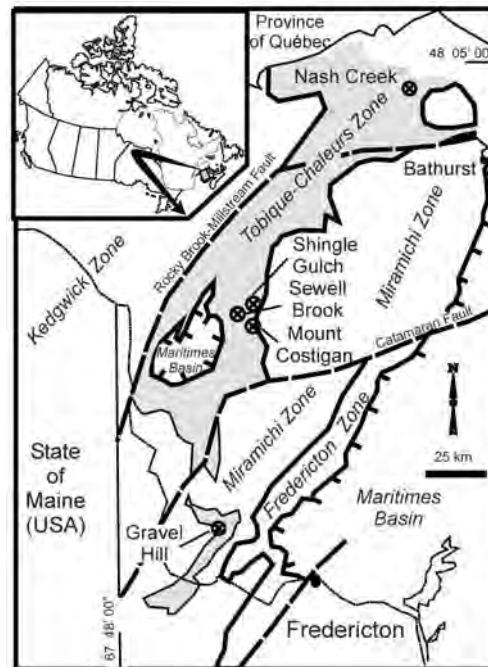


Fig. 1. The Tobique–Chaleurs Zone of New Brunswick with the location of significant Zn–Pb sulfide deposits or occurrences (modified from Walker 2005).

These deposits are generally simple in terms of their mineralogy, with sphalerite dominant over galena with Zn/Pb ranging between 2 and 5. Significant chalcopryite occurs only at the Sewell Brook deposit. All of the deposits are marked by low (20–50 volume % of sulfide) pyrite, and an absence of pyrrhotite. Marcasite has been identified in the Nash Creek deposit, implying low-pressure conditions, consistent with shallow level of emplacement. Non-sulfide phases occurring in veins are generally subordinate to sulfides and consist of calcite, siderite and minor quartz. Sericite or K-feldspar (adularia) and (or) chlorite vary in abundance adjacent to sulfide accumulations and are attributed to hydrothermal alteration processes.

GEOCHEMISTRY

The submarine depositional setting inferred for most Early Devonian volcanic rocks in part explains the highly variable alkali contents. Specifically, many have generally low Na₂O (< 3 wt.%) and high

K₂O (up to 14 wt.%). Such a signature may, in part be explained by low-temperature seawater alteration (Galley 1995); however, unmineralized rocks may also have high K₂O, implying that some of the K is a function of primary magmatic processes.

The highly variable Zr/Ti and Zr/Hf ratios of felsic rocks along the belt are not likely a function of crystal fractionation in large magma chambers. Rather, these variations are interpreted to reflect differences in small-batch felsic melts that erupted along the belt at the same time. These data also show elevated Ba, Rb, and Th (Fig. 2) and anomalously low Nb, Sr, Ti, and Eu. The chondrite-normalized major element and REE diagram (Fig. 2) shows that these rocks have profiles that, in many respects, are similar to I-type granites. This is problematic as I-type intrusions are not normally associated with rift-settings; rather, they tend to occur in subduction settings (Christiansen & Keith 1996). The negative Nb anomalies in these rocks (Fig. 2) are consistent with a subduction-related setting, as Nb tends to be sequestered in the down-going slab rather than passing into the overlying mantle wedge via metasomatic fluids (Green 1995). However, absolute values of Nb and to a lesser degree the Nb/Ta ratio, are somewhat higher than the upper limit of I-type granite (Fig. 3). The higher Nb+Y of these rocks was interpreted by Lentz (1998) to represent an A-type affinity.

The rhyolites hosting the deposits in the TCZ are aphyric to very sparsely feldspar-phyric. Most have high SiO₂ (commonly ≥ 70 wt. %), and negative Eu anomalies that are indicative of feldspar fractionation in the source magma. These characteristics are typical of relatively highly fractionated magmas. Locally, the rhyolites can be divided into low-Zr (250 to 350 ppm) and high-Zr (400 to ≥ 900 ppm) types; with maximum Zr contents in excess of 1100 ppm have been recorded. In some areas, e.g. Nash Creek, relatively low Zr/Hf indicate extensive fractionation. A few of the very high Zr samples collected by previous workers have been classified as

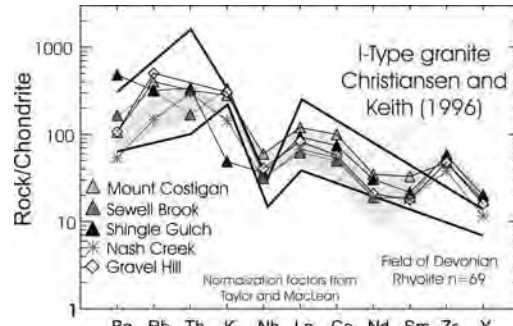


Fig. 2. Chondrite-normalized major and REE data for host felsic volcanic rocks from various deposits in the TCZ.

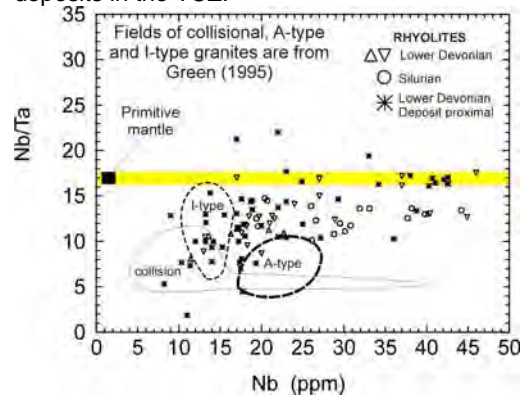


Fig. 3. Nb vs. Nb/Ta discrimination diagram with TCZ rhyolites plotted with respect to fields for A-, I-, and collision-type granites.

peralkaline (R. Wilson pers. comm. 2008). The relatively high Ga and Ga/Al of many of these rocks suggest an affinity with A-type granites.

Volcanic rocks of more intermediate composition are rare in the TCZ but are present at both the Nash Creek and Sewell Brook deposits. At Nash Creek, feldspar-phyric rhyodacite containing 500 ppm Zr immediately overlies low-Zr rhyolite and likely reflects draw-down in a small, zoned magma chamber. At Sewell Brook, most of the volcanic rocks in the immediate vicinity of the deposit are rhyodacitic in composition.

CONCLUSIONS

The volcanic rocks of the TCZ were erupted in a shallow marine basin developed during trans-tensional rifting (Dostal *et. al* 1989). These lavas exhibit some of the geochemical characteristics typical of magmas generated in rift

settings, e.g., the bimodal nature of the magmatism. With respect to the felsic volcanic rocks, elevated K, Zr, Y, Ga, and Ga/Al ratios are consistent with A-type felsic rocks. However, these felsic rocks also display characteristics typical of I-type (subduction-related) magmas, such as high Ba and Nb.

Undoubtedly, the source material for the melts that generated these rhyolites and related sulfide mineralization developed from a heterogeneous mantle source (Dostal *et al.* 1989) with a complex history including subduction, and mantle heterogeneity. At higher crustal levels contamination, magma segregation (magma chamber zoning), and crystal fractionation process probably added additional complications.

In terms of exploration vectoring, the following physicochemical criteria are most likely to lead to successful targeting of Zn-Pb mineralization in the TCZ.

(1) High K₂O, low Na₂O compositions indicate zones of deposit-related hydrothermal alteration.

(2) Rocks of more intermediate (rhyodacite) composition, as based on Zr/TiO₂, may indicate proximity to intrusions that have undergone crystal-fractionation and subsequent development of metal-laden hydrothermal fluids.

(3) Rocks with high primary permeability (flow-top breccia, etc.) are the preferred traps for sulfide minerals.

ACKNOWLEDGEMENTS

Thanks to Reg Wilson for supplying some unpublished geochemical data, and to S.R. McCutcheon for editorial comments.

REFERENCES

- CHRISTIANSEN E.H. & KEITH, J.D. 1996. Trace element systematics in silicic magmas: A metallogenic perspective. In: Wyman, D.A. (ed), Trace Element Geochemistry of Volcanic Rocks: Applications for Massive Sulphide Exploration: *Geological Association of Canada, Short Course Notes*, **12**, 115–151.
- DOSTAL, J., WILSON, R.A., & KEPPIE, J.D. 1989. Geochemistry of Siluro-Devonian Tobique belt in northern and central New Brunswick (Canada): Tectonic Implications. *Canadian Journal of Earth Sciences*, **26**, 1282–1296.
- GALLEY, A.G. 1995. Target vectoring using lithochemochemistry: Applications to the exploration for volcanic hosted massive sulphide deposits. *CIM Bulletin*, **88**, 15-27.
- GREEN, T.H. 1995. Significance of Nb/Ta as an indicator of geochemical processes in the crust-mantle system. *Chemical Geology*, **120**, 347–359.
- LENTZ, D.R. 1998. Petrogenetic evolution of felsic volcanic sequences associated with Phanerozoic volcanic-hosted massive sulphide systems: the role of extensional geodynamics. *Ore Geology Reviews*, **12**, 289–327.
- WALKER, J.A. 2005. *Petrogenesis and tectonic setting of Devonian volcanic and related rocks and their control on mineralization at the Shingle Gulch East Zn–Pb–Ag sulfide deposit, northwest New Brunswick*. Unpublished PhD thesis, University of New Brunswick, Fredericton, NB, Canada, 430 p.

Sulfide petrology and geochemistry of the Key Anacon Main Zone and East Zone massive sulfide deposits, Bathurst Mining Camp, NB, Canada

Joseph D.S. Zulu¹, David. R. Lentz¹, & James A.Walker²

¹Department of Geology, University of New Brunswick, Fredericton, NB, E3B 5A3 CANADA (e-mail: dlentz@unb.ca)

²New Brunswick Department of Natural Resources, Geological Surveys Branch, PO Box 50, Bathurst, New Brunswick E2A 3Z1 CANADA

ABSTRACT: The Key Anacon Zn-Pb-Cu-Ag massive sulfide deposits contain more than two Mt of 0.22% Cu, 3.47% Pb, 8.41% Zn, and 111 g/t Ag. These deposits occur in the hinges of parasitic F₂ folds of Middle Ordovician felsic volcanic rocks. Zone refining of massive sulfide deposits (Cu-rich footwall to the Zn-Pb rich hanging wall) is controlled by temperature, pressure, metal ion concentrations, stabilities of soluble complex ions during transport, multiple hydrothermal episodes and mixing, and mineral free energies.

Zinc strongly correlates with Pb ($r^2=0.97$) reflecting similar paragenesis, determined by free energies of sphalerite and galena, and the degree of saturation. In contrast, the absence of correlation between Cu and Ag ($r^2=0.11$) or Zn ($r^2=0.34$) is attributed to non-cogenetic deposition. Silver exhibits strong positive Spearman's Rank correlations with Pb ($r^2=0.91$); associated with tetrahedrite- and galena-rich assemblages), Zn ($r^2=0.86$), Cd ($r^2=0.86$), and Sb ($r^2=0.63$). Mineral growth zoning in arsenopyrite and pyrite support multiple injections of fluids during mineralization and the order of crystallization is deduced from entrapped inclusion trails of other sulfides. The sulfide compositions are influenced by the discharge of hydrothermal elements (Eu, Fe, Mn, Zn, Cu, Pb, Cd, Au, Ag, Sr, Ba, Ca, P, and CO₂) on the sea floor.

KEYWORDS: massive sulfide deposit, silver, Key Anacon, New Brunswick

INTRODUCTION

The calculated reserve for the Key Anacon Main Zone is 1.11 Mt of 0.22% Cu, 3.47% Pb, 8.41% Zn, and 111 g/t Ag (Irrinki 1992). No reserves are reported for the Key Anacon East Zone; however, twelve drill intersections were reported in a Northern Miner press release dated August 11th, 1993, with the best intersection of 82.3 m of low- to high-grade massive-sulfide lens at 350 m vertical depth in (DDH KA 93-42). The two zones are approximately 1.5 km apart, and located 20 km south of Bathurst and 11 km east-northeast of the Brunswick No. 6 deposit (Fig. 1).

The Key Anacon deposits lie on the eastern limb of the Portage River Anticline (Fig.1). They are hosted by an autochthonous sequence of Middle Ordovician felsic and mafic volcanic rocks and related sedimentary rocks of the Tetagouche Group, and overlie sedimentary rocks of the Miramichi Group,

which includes the Patrick Brook, Knights Brook and Chain of Rocks formations (van Staal & Williams 1984).

This study documents sulfide petrology and the chemical behaviour of various

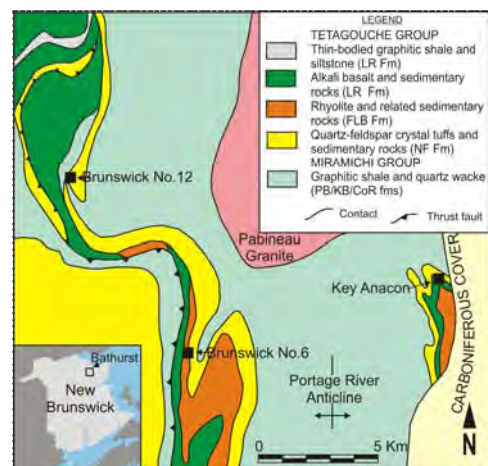


Fig. 1. A Geological map with location of the Key Anacon Main Zone deposit, New Brunswick, Canada (modified after van Staal & Williams 1984).

metals within the massive sulfides, with emphasis on Ag and on the factors controlling mineral zonation in this volcanogenic massive sulfides system.

SULFIDE PETROLOGY

The Key Anacon Main and East zones occur at or near the upper contact of the felsic volcanic rocks of the Nepisiguit Falls Formation (Tetagouche Group). These exhalative deposits formed in a reducing ocean. Three sulfide facies, based on the predominant mineralogy, are recognized: 1) pyrite–chalcopyrite, 2) pyrite–sphalerite–galena, and 3) pyrrhotite–sphalerite–galena (Jambor 1979). These three assemblages have distinct textural and microstructural characteristics, metal grades, and spatial distribution (Jambor 1979; Irrinki 1992).

The pyrite–chalcopyrite–pyrrhotite assemblage contains up to 1% Cu, and consists of disseminated to massive pyrite, pyrrhotite, with subordinate remobilized chalcocopyrite filling the intragranular fractures in pyrite and interstitial spaces between highly strained and brecciated Fe-sulfides (Saif 1983; Fig. 2).

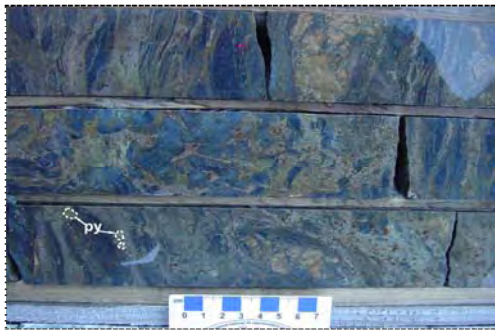


Fig. 2. Pyrrhotite-chalcopyrite breccia from footwall of the Key Anacon East zone. Note pyrite porphyroblasts (arrow). Sample from DDH KA61-921m.

The pyrrhotite–sphalerite–galena assemblage occurs mainly as disseminated fine- to medium-grained pyrrhotite and sphalerite, and fine- to coarse-grained pyrite, with arsenopyrite occurring as inclusions in pyrrhotite and sphalerite (consistent with observations made by Lentz 2002). Arsenopyrite occurs mostly as euhedral porphyroblasts enclosed in pyrite.

The pyrite–sphalerite–galena facies is typically fine- to medium-grained and consists of disseminated to banded massive sulfides, containing brecciated clasts of pyrite. Locally, minor amounts of chalcocopyrite, galena, and pyrrhotite occur as fracture fillings or as inclusions in pyrite.

The distribution of sulfide lenses at the Key Anacon Main Zone is the result of folding with sulfides thickened in the hinge zones of F_1/F_2 folds and attenuated on the limbs (Fig. 3). The S_1 fabric is transposed parallel to S_2 on the fold limbs, resulting in a composite S_1/S_2 fabric. In contrast S_1 is at a high angle to S_2 near the noses of F_2 folds (van Staal & Williams 1984).

Evidence from drill core and microstructure studies indicate that euhedral, zoned arsenopyrite grains tend to be clustered, and mantled by pyrite (Fig. 4), and their distribution is structurally controlled. These textures are interpreted to represent pressure solution as the main deformation mechanism during D_1 . This interpretation is supported by serrated pyrite boundaries (Fig. 4) and pyrite-bearing veins. However, locally unstrained euhedral pyrite porphyroblasts overprint D_1 and D_2 structures, implying a late-stage post- D_2 growth (Fig. 4).

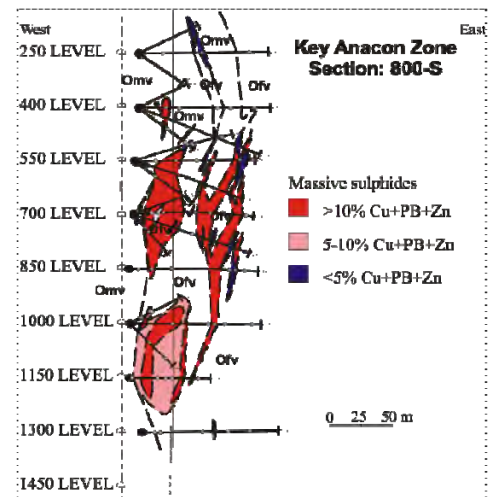


Fig. 3. A vertical projection indicating geology and zonal distribution of sulfides in Key Anacon Main No. 2 zone, Section 800 S (from Rennie & Irrinki 1986).

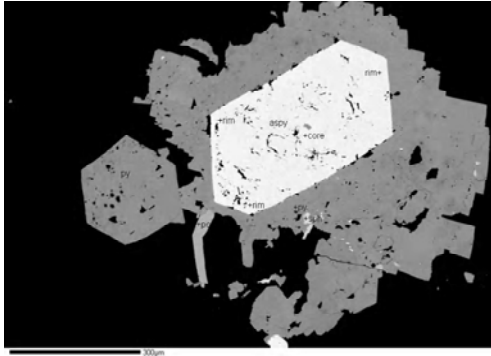


Fig. 4. Photomicrograph of a SEM-BSE image showing arsenopyrite enclosed in a serrated pyrite porphyroblast from the Key Anacon Main zone. Note: The euhedral and serrated pyrite contain inclusions of sphalerite and pyrrhotite (DDH KA64-712.8 m).

GEOCHEMISTRY OF MASSIVE SULFIDE

Metal contents of the sulfide samples collected from the Key Anacon deposits have been classified using the Cu and Zn ratios (Fig. 5). The majority of the massive sulfide samples plot in the Zn–Pb–Cu type (cf. Large 1992; Fig. 5); however, the semi-massive to disseminated sulfides in the footwall are enriched in Cu, Co, and Bi and lower in Zn and Pb, typical of stringer zone mineralization. These plots in the Cu type field and one sample contains enough zinc to be placed in the Zn-Cu group (Fig. 5).

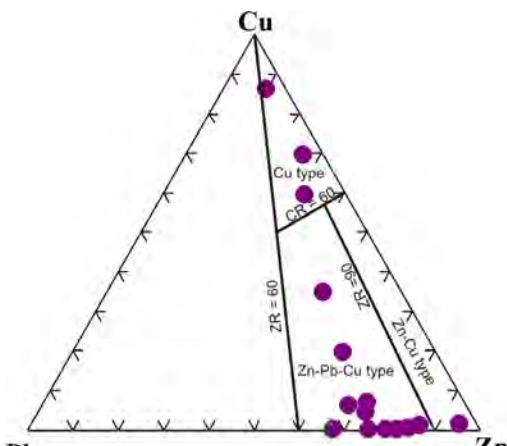


Fig. 5. The Pb-Cu-Zn, discrimination diagram for massive sulfide samples collected during this study. Field boundaries are from Large, 1992. $ZR = (100 \text{ Zn}/(\text{Zn}+\text{Pb}))$, $CR = 100 \text{ Cu}/(\text{Cu}+\text{Zn})$.

The binary plots of selected metals along with Spearman Rank coefficients are presented in Figure 6. Cobalt correlates strongly with Bi ($r'=0.90$) and both are concentrated with Cu in basal sulfides or in the stringer zone. Deposition of sulfides belonging to this same class (Susak & Crerar 1982) are determined solely by the free energies of the mineral species (chalcopyrite, bismuthinite, arsenopyrite), corresponding dissolved metal species, and by the degree of saturation.

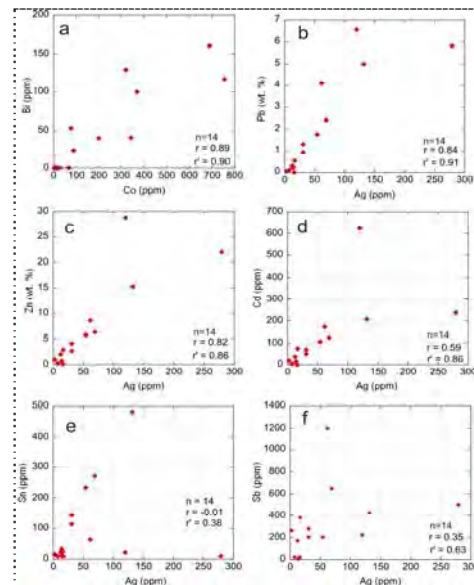


Fig. 6. Binary plots of metal contents of massive sulfides, showing spearman rank correlation coefficients (r') of: **a)** Co vs Bi ($r'=0.90$), **b)** Ag vs Pb ($r'=0.91$), **c)** Ag vs Zn ($r'=0.86$), **d)** Ag vs Cd ($r'=0.86$), **e)** Ag vs Sn ($r'=0.38$), and **f)** Ag vs Sb ($r'=0.63$). Note: r , is the Pearson's product-moment coefficient of linear correlation.

Silver exhibits a strong Spearman's Rank correlation with Pb ($r'=0.91$) reflecting its original syngenetic substitution for Pb in galena and/or micro-inclusions of other Ag-Pb phases. There is a slightly lower correlation of Ag with Zn ($r'=0.86$), and Cd ($r'=0.86$). In contrast, Ag correlates poorly with Au, and Cu suggesting that the high Ag/Pb ratio is from substituted Ag, and that tetrahedrite has little control on the Ag/Pb ratios. The positive correlation of Ag with Sb ($r'=0.63$) is attributed to

tetrahedrite. Cadmium correlates well with Zn ($r'=0.99$), indicating substitution of Cd for Zn in the sphalerite structure. Tin does not correlate with Ag or with Zn.

ORE GENESIS DISCUSSION

The Key Anacon deposits are exhalative deposits with metal zonation grading from a pyrite-chalcopyrite-pyrrhotite zone in the footwall, through a pyrite-sphalerite zone in the main parts of the deposits, to pyrite-sphalerite-galena zone in the upper and vent-distal parts of the system (cf. Petruk 2000). At the base, these deposits consist of structurally attenuated and dismembered stockwork veins and disseminations of chalcopyrite and pyrrhotite, in a matrix of chlorite.

The pyrite-sphalerite zone contains mono-mineralic bands of sphalerite- and galena that wrap around brecciated and rotated pyrite. These textures reflect variation in the response to deformation of sulfides of varying ductility. Evidence supporting this metal zonation is evident at microscopic scale where the crystallization sequence of ore minerals is explained by zone refining processes due to progressive changes in the solution chemistry, temperature, and the f_{O_2} and f_{S_2} as the rising hydrothermal solution mixed with sea water (Large 1977).

CONCLUSIONS

This contribution can be summarized in a number of points:

- (1) The F_1/F_2 sheath-like fold structures control the distribution of sulfide mineralization in the noses of the F_2 parasitic folds.
- (2) Ag exhibits a strong Spearman's Rank correlation with Pb, Zn, Cd, and Sb reflecting its cogenetic nature with these elements as they are controlled by free energies, dissolved metal species, and degree of saturation.
- (3) Metal zonation in massive sulfides is controlled by progressive changes in the solution chemistry, temperature, and the f_{O_2} and f_{S_2} as ascending hydrothermal solution interacts with the massive sulfide lens and with sea water.

- (4) The sulfide compositions are dictated by hydrothermal elements such as Eu, Fe, Mn, Zn, Cu, Pb, Cd, Au, Ag, Sr, Ba, Ca, P, CO_2 , and S, precipitated on the sea floor from discharged hydrothermal solutions.

ACKNOWLEDGEMENTS

The Department of Natural Resources, Geologic Surveys Branch, is thanked for the logistical support during field work. Steven R. McCutcheon is thanked for discussions on the petrogenesis of massive sulfides.

REFERENCES

- JAMBOR, J.L. 1979. Mineralogical Evaluation of Proximal-Distal features in New Brunswick Massive-Sulfide Deposits. *Canadian Mineralogist*, **17**, 649-664.
- IRRINKI, R.R. 1992. Key Anacon sulfide deposit, Gloucester County, New Brunswick. *Exploration Mining Geology*, **1**, 121-129.
- LARGE, R.R. 1992. Australian volcanic-hosted massive sulfide deposits: features, styles and genetic models. *Economic Geology*, **87**, 471-510.
- LARGE, R.R. 1977. Chemical Evolution and Zonation of Massive Sulfide Deposits in Volcanic Terrains. *Economic Geology*, **72**, 549-572.
- LENTZ, D.R. 2002. Sphalerite and Arsenopyrite at the Brunswick No. 12 Massive-Sulfide Deposit, Bathurst Camp, New Brunswick: Constraints on P-T Evolution. *The Canadian Mineralogist*, **40**, 19-31.
- PETRUK, W. 2000. Applied Mineralogy in the Mining Industry. *Elsevier, Netherlands*, 268 p.
- RENNICK, P.M. & IRRINKI, R.R. 1986. Geology and zonal distribution of Sulfides at Key Anacon No. 2 zone. Internal unpublished Report. *New Brunswick, Department of Natural Resources and Energy, Minerals and Energy Division*.
- SAIF, S.I. 1983. Petrographic and geochemical investigation of iron formation and other iron-rich rocks in Bathurst District, New Brunswick. In: *Current Research, Geological Survey of Canada*, **80-1A**, 309-317.
- SUSAK, N.J. & CRERAR, D.A. 1982. Factors Controlling Mineral Zoning in Hydrothermal Ore Deposits. *Economic Geology*, **77**, 476-482.
- VAN STAAL, C.R. & WILLIAMS, P.F. 1984. Structure, origin, and concentration of the Brunswick 12 and 6 orebodies. *Economic Geology*, **79**, 1669-1692.



Sponsors



Symposium bags sponsor



Platinum sponsors



ANGLO AMERICAN

Gold sponsors



Silver sponsors



Bronze sponsors

